Mohamed A. Elsawy *Editor*

Peptide Bionanomaterials

From Design to Application

Springer

Peptide Bionanomaterials

Mohamed A. Elsawy

Editor

Peptide Bionanomaterials

From Design to Application

Editor
Mohamed A. Elsawy
Leicester School of Pharmacy, Leicester
Institute for Pharmaceutical Innovation
De Montfort University
Leicester, UK

Preface

Molecular self-assembly has been exploited by nature for developing the higher functional macromolecular structures of both the genome and proteome. Inspired by nature, there has been a surge of research, in the last two decades, for the molecular engineering of peptide-based self-assembling nanostructures, adopting the bottom-up design approach. This book gives the reader an overview on the design rules for de novo self-assembling peptide and reviews the diverse range of bioinspired peptide nanostructures such as β-sheet and β-hairpin, α-helical and coiled coil, self-assembling short peptides and peptidomimetics, collagen-based and elastin-like peptides, silk peptides, peptide amphiphiles, peptides co-polymers, and others. Characterization of peptide-based nanomaterials over the length scale, in silico prediction of assembly into hierarchical nanostructures, and advanced manufacturing of these materials are discussed. The book also covers the wide variety of responsive and functional biomaterials that have been innovated based on those structures for various applications ranging from tissue engineering, therapeutics, and drug delivery to antimicrobial nanomaterials and biointerfaces. Also, the book discusses the peptide bionanomaterials global market and the future of the emerging industry.

Leicester, UK   Mohamed A. Elsawy

Contents

Chapter 1
Design Rules for Self-Assembling Peptide Nanostructures

Abdulwahhab Khedr, Mohamed A. N. Soliman, and Mohamed A. Elsawy

Abstract Self-assembling peptides represent a versatile chemical toolbox for the development of discrete nanostructures that can be tailored for a variety of biomedical applications. Rational design of a peptide building block involves wise selection from the amino acids pool to create a primary sequence capable of adopting a bioinspired secondary structure stabilized by a combination of non-covalent and/or covalent interactions in response to external stimuli. Herein, we focus on the basic molecular design rules for self-assembling peptides as the building units for supramolecular nanomaterials formation through a bioinspired bottom-up design strategy. We look at the physicochemical nature of different amino acids and their proposed sequence arrangements needed to guide the molecular assembly into higher-order structures governed by certain types of intra- and/or intermolecular interactions and to give insights into how the materials' structural and functional properties can be fine-tuned to satisfy different application needs. We will discuss the structural features of biosynthesized protein nanomaterials (such as collagen, elastin-like, silk-elastin-like, keratin, and resilin) and how they inspired the development of mimetic self-assembling polypeptide analogues of shorter length, while keeping the inherent material properties of the parent designs. In addition, design rules of de novo short peptides which assemble into higher bioinspired structures (β-sheets,

---

A. Khedr
Leicester School of Pharmacy, Leicester Institute for Pharmaceutical Innovation, De Montfort University, Leicester, UK

Department of Pharmaceutics and Industrial Pharmacy, Faculty of Pharmacy, Zagazig University, Zagazig, Egypt

M. A. N. Soliman
Leicester School of Pharmacy, Leicester Institute for Pharmaceutical Innovation, De Montfort University, Leicester, UK

Department of Pharmaceutics and Industrial Pharmacy, Faculty of Pharmacy, Cairo University, Cairo, Egypt

M. A. Elsawy (✉)
Leicester School of Pharmacy, Leicester Institute for Pharmaceutical Innovation, De Montfort University, Leicester, UK
e-mail: mohamed.elsawy@dmu.ac.uk

β-hairpins, α-helices and amphiphiles assembly), as well as unconventional peptide designs (short aromatic and cyclic peptides), are also explained. This is an introductory chapter that gives a comprehensive overview of the basic design rules for the main classes of self-assembling peptides, which are discussed in more details in the relevant chapter for each class.

Keywords Self-assembling · Peptides · Nanostructures · Biomedical · Bioinspired

1.1   Nature: Source of Inspiration

Nature never stops amazing us with the meticulous functional nanostructures developed in the cellular environment, which construct organelles, membranes, and cytoskeleton leading to formation of integrated biological system. A "chemical toolbox" of versatile but simple molecules, such as amino acids, nucleic acids, lipids, and sugars, is manipulated to engineer building blocks that self-assemble into biological nanostructures (Whitesides and Boncheva 2002; Whitesides and Grzybowski 2002; Tu and Tirrell 2004). Self-assembly involves spontaneous molecular recognition and organization of these building blocks into stable, ordered nanostructures with well-defined properties under equilibrium (Han et al. 2010), which is controlled by the balance between both intra- and intermolecular attractive and repulsive forces (Lehn 2002). Feynman was the first to propose the molecular "self-assembly" concept, in 1959, describing the formation process of well-organized supramolecules through a bottom-up approach by combining the individual building blocks (Feynman 1959).

Inspired by nature, biomaterials engineers have adopted the bottom-up design approach using biomimetic molecules to develop functional nanostructures. In the last three decades, there has been a surge of research in designing such molecules, particularly synthetic peptides that have drawn a significant attention among other biomolecular self-assembling building blocks. Peptides are simple structures formed of short chains of amino acids, which enable flexibility of designing versatile sequences providing a wide range of different self-assembling nanostructures such as nanofibers (Wychowaniec et al. 2020; Dong et al. 2008; Behanna et al. 2005; Webber et al. 2013; Hartgerink et al. 2001; Gao et al. 2017), nanotubes (Reches and Gazit 2003; Vauthey et al. 2002; Santoso et al. 2002; Zhan et al. 2005; Gao et al. 2006; Ghadiri et al. 1993; Ghadiri et al. 1994; Chapman et al. 2012; Hartgerink et al. 1996; Montenegro et al. 2013; Sun et al. 2015; Kol et al. 2005; Reches and Gazit 2006; Yemini et al. 2005), ribbons (Aggeli et al. 2001), nanospheres (Capes et al. 2010; Chen et al. 2009; Mandal et al. 2013), micelles (Hüttl et al. 2013; Shi et al. 2018; Perinelli et al. 2019) . . .etc. (Fig. 1.1). In addition, peptides are functional and sustainable materials that can be easily chemically functionalized and feasibly synthesized on large scale, using high-throughput automated synthesizers. Besides, peptide-based nanostructures are immensely useful for developing biomimetic materials, thanks to their biocompatibility and biodegradability (Zhao et al. 2010; Hauser and Zhang 2010a; Hamley 2011).
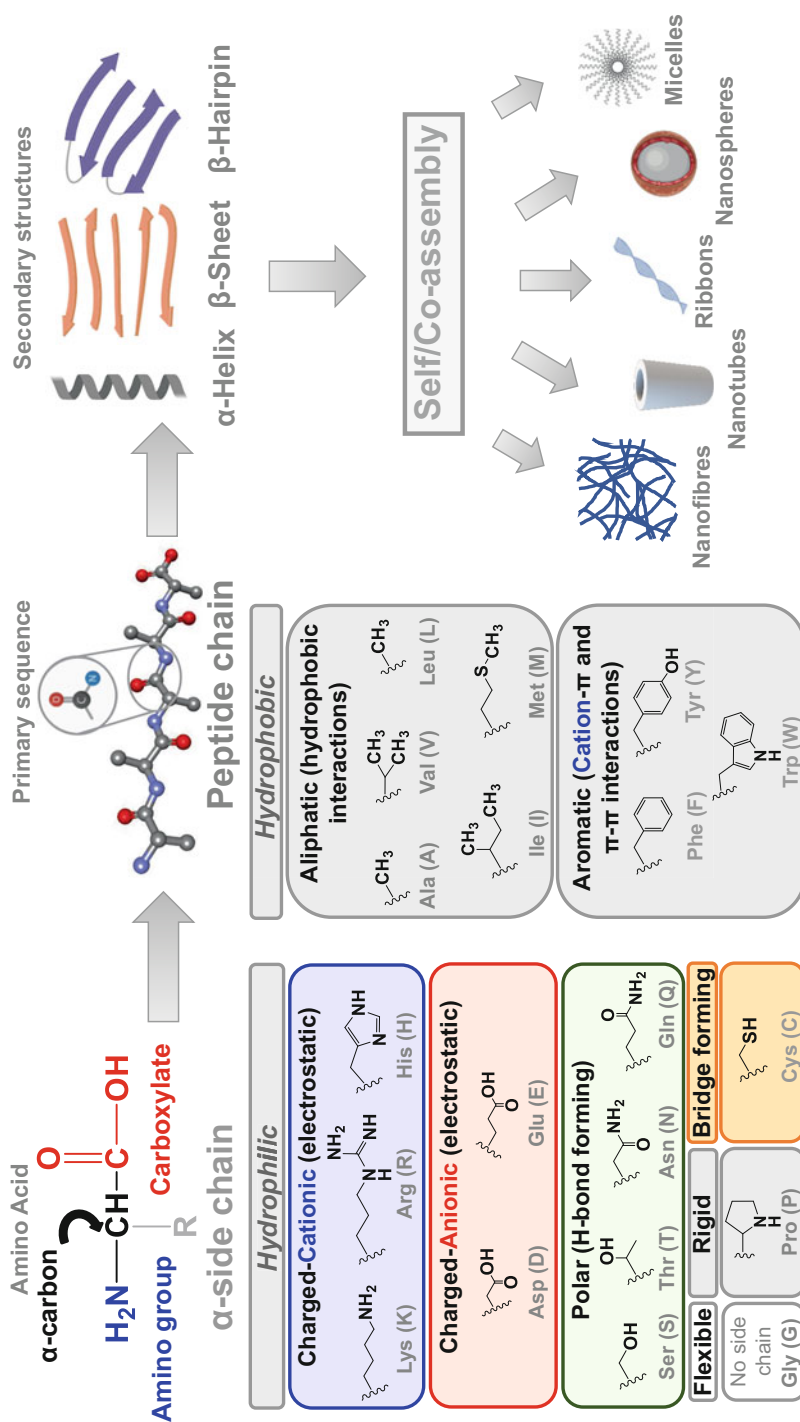
Fig. 1.1 Showing structure of α-amino acid, the building unit of peptide chains. The various functionalities of Cα-side chains define the physicochemical properties of the peptide molecule and dictate the formation of secondary structures and self/co-assembly into higher nanostructures, mainly via non-covalent interactions. Structures of Cα-side chains with relevant structural features and non-covalent interactions are demonstrated

The focus of this chapter is on the molecular design rules for self-assembling peptide-based building blocks that govern nanostructure formation through a bottom-up design strategy. We aim to provide insights into how natural proteins have been an inspiration for the design of such biomimetic self-assembling peptides and how it provided the design bases for bioinspired nanostructures. Understanding molecular design rules is a crucial prerequisite not only for fine tuning nanostructure formation but also for tailoring material properties to meet application needs.

1.2 Amino Acids: The Building Units

For better understanding of design rules of self-assembling peptides, the chemical nature of the basic building units – amino acids – should be first explained. A peptide is formed of a primary sequence of amino acids linked via amide bond formation between the amino and carboxylic acid groups of each two successive residues in the sequence (Fig. 1.1). This forms the amide backbone of the peptide, which is normally involved in a particular pattern of either inter- or intra-chain hydrogen bonding (H-bonding), stabilizing the formation of secondary structures. The physicochemical properties, chirality, and sequence arrangement of amino acids will guide self-assembly and nanostructure formation, based on their ability to perform specific intra- and/or inter-chain interactions. These interactions are determined by the type of chemical functionality of the alpha-carbon (Cα) side chain (Fig. 1.1).

For instance, hydrophilic charged residues both cationic (such as H, K, and R) and anionic (such as D and E) can undergo either electrostatic attraction forming salt bridges between countercharges aiding assembly or repulsion between similar charges hindering the assembly process (Fig. 1.1) (King et al. 2016; Wester et al. 2020; Wong et al. 2020; Caplan et al. 2000). The pKa of these residues will determine charge status depending on the pH of surrounding media, a property that has been widely exploited to trigger assembly/disassembly of charged peptides (Caplan et al. 2000). Uncharged hydrophilic polar residues can build hydrogen bonds (H-bonds) via hydroxyl (–OH) groups of side chains of S and T, as well as for the amide (–CONH) groups of N and Q residues (Fig. 1.1).

On the other hand, hydrophobic aliphatic residues (including A, V, L, I, and M) provide a hydrophobic environment, which can drive and stabilize assembly in aqueous media to shield hydrophobic areas from thermodynamically unfavored interactions with water (Fig. 1.1) (Bowerman et al. 2009; Mu and Yu 2014). Additionally, hydrophobic aromatic residues (F, Y, and W) are involved in aromatic interactions through π–π stacking of aromatic rings by overlapping *p*-orbitals (Fig. 1.1) (Uyaver et al. 2018; Bera et al. 2020; Lee et al. 2018). They can also undergo cation-π attraction with cationic residues (Chen et al. 2011a). Aromatic interactions have been commonly utilized to stabilize self-assembly and nanostructure formation of short synthetic peptides (Wychowaniec et al. 2020; Madhusudan Makwana and Mahalakshmi 2015).

Some amino acids have unique chemical characteristics, which can be used to imbue self-assembling peptides with certain structural or functional properties. The C residue, for example, provides the peptide molecule with a unique chemical reactivity governed by the thiol (-SH) functionality of the side chain, which is often targeted for chemical modification and inter-/intramolecular crosslinking through the formation of disulfide bridge stabilizing assembly (Fig. 1.1) (Tanrikulu and Raines 2014; Galloway et al. 2021). Another unique residue is P, which is a secondary amine with the Cα-side chain covalently linked to the amino group giving rise to a locked ring conformation (Fig. 1.1). This constrained conformation offers a structural rigidity to the peptide chain and creates a "kink" in the chain backbone, a feature that has been widely used to introduce β-turns in self-assembling peptides (Schneider et al. 2002) and to mimic helical structures of collagen-like peptides (Luo and Kiick 2013; Engel 2005). Conversely, G can offer a higher degree of flexibility to the peptide chain, as it is lacking the Cα-side chain, which imparts both steric hindrance and chirality to other residues (Fig. 1.1).

Chirality of amino acids and hence peptides plays a critical role in the design of self-assembling nanomaterials of tailored structural, physicochemical, mechanical, and biological properties (Melchionna et al. 2016). Naturally, biological systems utilize L-amino acids for the development of supramolecular structures through "like-like" intermolecular interactions, a criterion which makes the use of homochiral peptides crucial for guiding molecular recognition and self-assembly (Basak et al. 2017). However, incorporation of non-natural D-amino acids into heterochiral peptides was found to introduce some unexpected effects on self-assembly behavior (Zheng et al. 2021), secondary structure conformation (Melchionna et al. 2016), supramolecular morphology (Clover et al. 2020), enzymatic stability (Tugyi et al. 2005), and even therapeutic activity (Gelain et al. 2021). For example, D-proline used in the central turn sequence of β-hairpin-forming peptides was found to be a key feature in stabilizing the conformation of the adopted secondary structure, leading to the formation of hydrogels (Schneider et al. 2002; Struthers et al. 1996). In addition, heterochiral cyclic peptides of alternating D- and L-amino acids were found to self-assemble into hollow nanotubes of various pharmaceutical and biomedical applications (Ghadiri et al. 1993; Ghadiri et al. 1994; Chapman et al. 2012). Moreover, the heterochiral peptide sequences [D]VFF, [D]FFV, and [D]LFF showed rapid self-assembly into antiparallel β-sheets, forming different morphological nanostructures such as nanotapes, twisted fibers, and thick bundles, respectively, which then developed self-supporting hydrogels. On the other hand, their homochiral L-analogues did not show gel formation at the same conditions (Marchesan et al. 2012a; Marchesan et al. 2012b).

Collectively, amino acid sequence of peptides can be purposely designed to manipulate some of the inter-/intramolecular interactions mentioned above, to stabilize specific hierarchical arrangement into supramolecular nanostructures. While we have discussed examples of genetically encoded amino acids, there is a wide range of available residues, both natural and unconventional, providing an enormous chemical toolbox of these building units allowing flexibility of molecular design. A significant progress has been made in this area, and the main design rules have now

become disclosed, which can guide biomaterials engineers for developing self-assembling peptides with tailored structural and functional properties. In the following sections, we will introduce the different classes of bioinspired self-assembling peptides and will shed the light on recent advances in the molecular design of these building blocks.

1.3 Molecular Design of Self-Assembling Peptides: The Building Blocks

The basic amino acid building units can be rationally arranged in a chain-like sequence to form self-assembling peptide "building blocks," which assemble in hierarchical constructs to form higher nanostructures. In this section, we will give an overview on the main two arms of these peptide building blocks: the biosynthetic polypeptides and the de novo synthetic short peptides.

1.3.1 Biosynthetic Polypeptides

Self-assembling polypeptides are long peptide chains (~20–50 amino acid residues) designed to mimic structural protein domains. This class has emerged as an alternative to structural proteins, to overcome limitations of protein-based biomaterials including batch-to-batch variations, insufficient purity, low stability, potential immunogenicity, risk of transinfections, high production cost, etc. (Collier and Segura 2011). Most of these polypeptides are biosynthesized using bacterial gene expression and recombinant technology (Kyle et al. 2009). With the recent advances in solid phase peptide synthesis and click chemistry, the chemical synthesis of some of these polypeptides was made possible with acceptable yields and purities (Palomo 2014). The synthesis of these polypeptides provides the opportunity of generating biomaterials of tailored properties through functionalization or simple modification of the native peptide sequence in order to improve biological, physicochemical, and mechanical characteristics. Biosynthetic polypeptides are classified into collagen-like, elastin-like, silk-elastin-like, keratin-like, and resilin-like polypeptides; the structural features of which are discussed in this section.

1.3.1.1 Collagen-Like Polypeptides

Collagen is a functional protein found as a main component of the extracellular matrix, articular and bone tissues (Gelse et al. 2003; Aigner and Stöve 2003; Ramachandran and Kartha 1955). Collagen comprises a family of fibrous proteins responsible for the proper mechanical functioning of the body and falls under
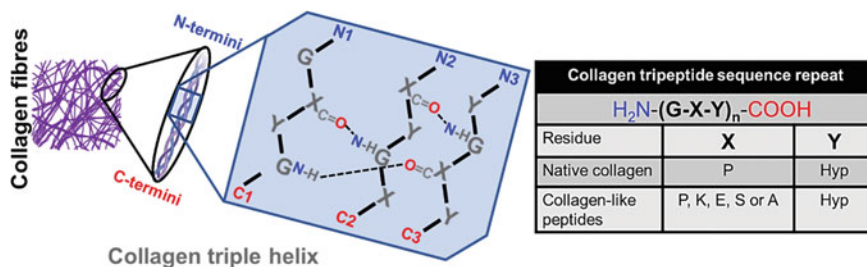
Fig. 1.2 H-bonding pattern between the basic tripeptide sequence repeat (G-X-Y) of collagen, which stabilizes triple helix formation (left). Table showing different amino acid residues used at positions X and Y to design collagen-like peptides (right)

28 different types with various structures and functionalities (Gelse et al. 2003; Aigner and Stöve 2003; Ramachandran and Kartha 1955). The main structural element of collagen is the proline-rich triple helix bundles which consist of the basic tripeptide sequence repeat (G-X-Y), where X and Y positions are usually filled with proline (P) and hydroxyproline (Hyp) amino acid residues (Fig. 1.2) (Luo and Kiick 2013; Engel 2005). The abundance of P residues is crucial for pre-organizing the individual strands into a polyproline type II (PPII) helical conformation, which then form interstrand "amide-amide" H-bonding with G residues, resulting in tight packing and folding of collagen at a decreased entropic cost (Fig. 1.2) (Cram 1988; Shoulders and Raines 2009). In addition, the presence of Hyp residues was found to increase thermal stability of the collagen triple helix through formation of water-mediated hydrogen bonds which tightly pack the folded structure (Shoulders and Raines 2009; Berg and Prockop 1973; Sakakibara et al. 1973; Suzuki et al. 1980).

Collagen-based proteins have been widely used for tissue engineering purposes (Kyle et al. 2009; Aigner and Stöve 2003). However, due to the limitations associated with the use of natural collagen such as poor reproducibility, thermal instability, and microbial contamination, collagen-like peptides have been developed with sequence similarity to that of natural collagen, to address these limitations (Fallas et al. 2012; Persikov et al. 2005; Boudko and Engel 2004). Collagen-like polypeptide analogues with the bioinspired basic sequence repeat (G-X-Hyp), where X has been occupied by K, E, S, A, or P, have been used to develop higher-order fibrillar structures (Fig. 1.2) (Hu et al. 2010). Assembly into these fibrillar structures is stabilized through a combination of π–π (Hu et al. 2010; Cejas et al. 2007), cation-π (Chen et al. 2011a), electrostatic (Gauba and Hartgerink 2007; Rele et al. 2007; Jiang et al. 2014), and hydrophobic interactions (Cejas et al. 2008), as well as H-bonding (Rele et al. 2007; O'Leary et al. 2011). Metal-triggered assembly was used to attain supramolecular structures of distinct morphologies controlled by precise definition of the chemical composition of triple helices and the number of sequence repeats (Pires and Chmielewski 2009; Pires et al. 2012; Przybyla et al. 2013; He et al. 2016; Hsu et al. 2012).

Interestingly, collagen mimetic peptides capable of self-assembling into triple helical structures which aggregate into nanofibers and further to hydrogels have been

designed by Hartgerink and co-workers, using "sticky end" approach (O'Leary et al. 2011). They have designed the triblock peptide, KOD (36 residues) of the amino acid sequence (P**K**G)$_4$(**PO**G)$_4$(**D**OG)$_4$ which incorporates the main structural repeating unit of collagen (POG) in the central domain, where O refers to Hyp. In addition, the presence of the countercharge amino acids, K and D in the peripheral domains, stabilizes the formation of a sticky-ended triple helix through interstrand salt-bridge hydrogen bonding. Sticky-ended triple helices act as nuclei for nanofiber formation through end-to-end elongation governed by the unpaired K and D residues (O'Leary et al. 2011). The formed nanofibers further entangle into hydrogels which show similar properties to those created from natural collagen. KOD self-assembled nanofibrous hydrogel has been used as a biomimetic matrix for adhering and activating platelets, demonstrating its potential for use as a hemostat (Kumar et al. 2014).

1.3.1.2 Elastin-Like Polypeptides

Elastin is a structural protein found in the extracellular matrix providing it with the required elasticity and tensile strength for proper functioning (Fig. 1.3) (Jia and Kiick 2009). It also plays a crucial role in the regulation of intercellular and cellular-extracellular matrix interactions (Rodgers and Weiss 2005). As a natural protein, it has a limited use in biomedical applications due to lack of purity which can lead to immunological responses. On the other hand, elastin-like polypeptides have been biosynthesized by genetic engineering of tropoelastin-derived peptides and were used instead of elastin for construction of self-assembling multifunctional biomaterials (Fig. 1.3) (Betre et al. 2002; Deming 2012). These polypeptides have several advantages including elasticity, deformation flexibility, biocompatibility, biodegradability, and thermal sensitivity (Eskandari et al. 2017; Wang et al. 2014; Raucher et al. 2008; Huang et al. 2016).

Basically, the structure of elastin-like polypeptides (ELPs) is inspired by the natural elastin and composed of the pentapeptide sequence repeat (VPGXG)$_n$, where X position can be occupied by any natural amino acid residue other than P (Fig. 1.3) (Bessa et al. 2010). The polarity of the amino acid at position X is responsible for determination of the transition temperature of the peptide leading to the formation of peptides with thermo-responsive hydrogelation property (Wang et al. 2017). At low temperatures, the ELP is present in solution form adopting random coil conformations due to hydration of hydrophobic residues with ordered water. Above the peptide's transition temperature, the surrounding water loses its ordered and bulky structure. As a result, the peptide undergoes transition from the random coil structure to the self-assembled cylindrical micelles stabilized by β-sheet formation which further aggregate to form a hydrogel (Fig. 1.3) (Shi et al. 2014; Kumar et al. 2011; Haider et al. 2004). ELPs can undergo self-assembly into various nanostructures depending on the molecular design of the building blocks. These nanostructures include spherical, cylindrical, and worm-like micelles, nanofibers, and rod-like and vesicular structures (Fig. 1.3) (Saha et al. 2020).
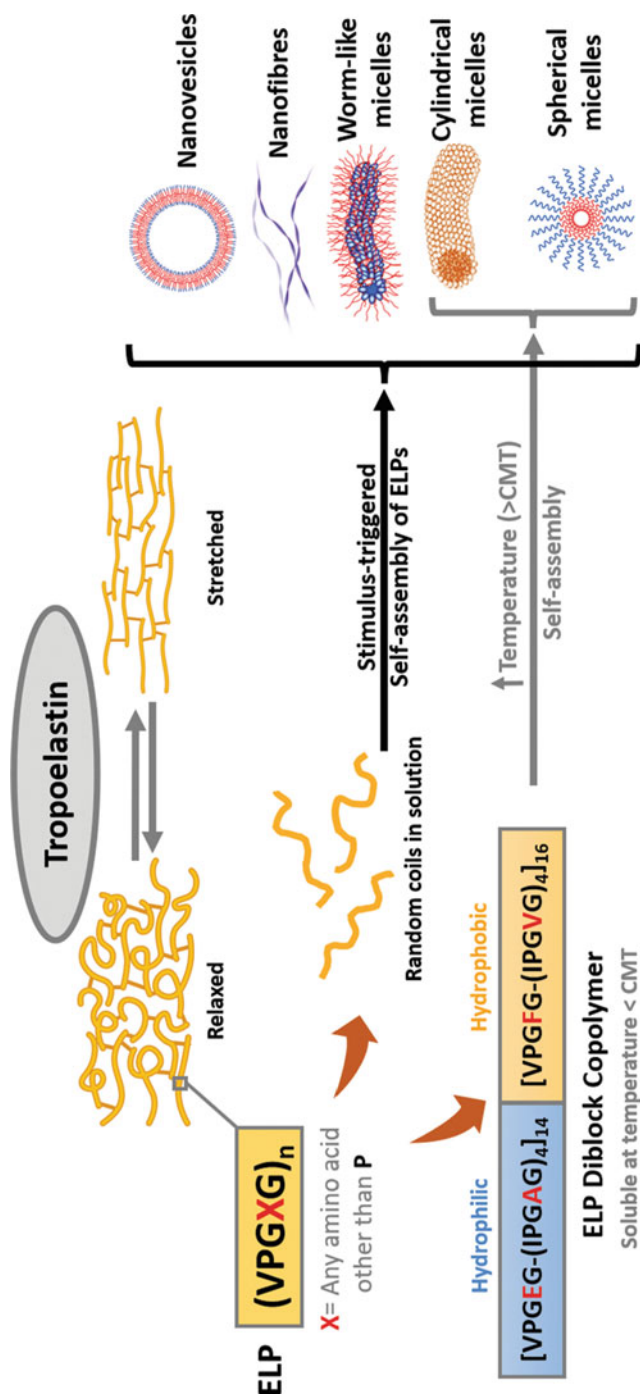
Fig. 1.3 A schematic showing the general peptide sequence of elastin-like polypeptides (ELPs), an example of ELP diblock copolymers, and their different stimulus-triggered self-assembled nanostructures

An example of ELPs is $(VPAVG)_n$, in which the X position is occupied with a V residue and the central glycine residue is replaced by an A residue. This polypeptide self-assembles into spherical nanoparticles and has been studied for the use in bone tissue engineering as a delivery carrier for the bone morphogenetic proteins (BMP-2 and BMP-14). These proteins play an important role in bone formation by triggering stem cell differentiation. The polypeptide $(VPAVG)_n$ has been found to successfully release the BMPs which enhanced cellular mineralization (Bessa et al. 2010). In another study for bone regeneration, elastin mimetic peptides based on the repetitive pentapeptides VPGIG and VPGKG were designed to incorporate the cell adhesion motif (RGDS) or the mineralization promotor sequence (DDDEEKFLRRIGRFG) or both, for mesenchymal stem cell adhesion, mineralization, and both cell adhesion and mineralization, respectively (Saha et al. 2020). In addition, ELP block copolymers have been extensively used for the development of self-assembling micelles. ELP diblocks containing both a hydrophilic and a hydrophobic block, through incorporation of a hydrophilic and a hydrophobic guest residue, are amphiphilic and can undergo self-assembly into spherical micelles at a temperature above the critical micelle temperature (CMT) (Fig. 1.3) (Roberts et al. 2017). The first ELP diblock copolymer capable of undergoing temperature-triggered micelle self-assembly was developed by Conticello research group (Lee et al. 2000). This ELP diblock copolymer consisted of the hydrophilic block $[VPGEG\text{-}(IPGAG)_4]_{14}$ having the guest residues E and A and the hydrophobic block $[VPGFG\text{-}(IPGVG)_4]_{16}$ having the guest residues F and V. These amphiphilic diblock copolymers showed temperature-triggered self-assembly into spherical and cylindrical micelles depending on the pH which was used to control the micellar size and shape (Fig. 1.3). The pH sensitivity of these ELP diblock copolymers was gained from the presence of the ionizable E residue (Lee et al. 2000).

1.3.1.3 Silk-Elastin-Like Polypeptides

Similar to collagen and elastin, silks are structural proteins which are naturally produced by insects such as spiders and worms. Silk fibroin is the fibrous silk protein produced by the silkworm *Bombyx mori*. This protein is composed of two protein structures: fibroin and sericins (Fig. 1.4) (Gamo et al. 1977). Fibroin is a fibrous protein composed of both light and heavy polypeptide chains in a 1:1 ratio and linked together through a disulfide bridge between Cys-c20 and Cys-172 residues of the heavy and light fibroin chains, respectively (Tanaka et al. 1999). The formation of intermolecular disulfide bonds is essential for silk fibroin secretion in vivo from the silk gland (Mori et al. 1995). Fibroin is surrounded by the glue-like sericins which comprise amorphous soluble hydrophilic proteins (Fig. 1.4). Fibroin is mainly composed of the G, A, S, and Y amino acids in the hydrophobic repeating amino acid sequence pattern $(GAGAGS/Y)_n$ and the repeating dipeptide Gly-Ala/Ser/Tyr in the heavy chain, which gives silk fibroin its β-sheet forming propensity (Fig. 1.4). β-strands containing G residues at one face and the side chains of non-G residues at the other face are alternately packed to form stable antiparallel β-sheets crystallites
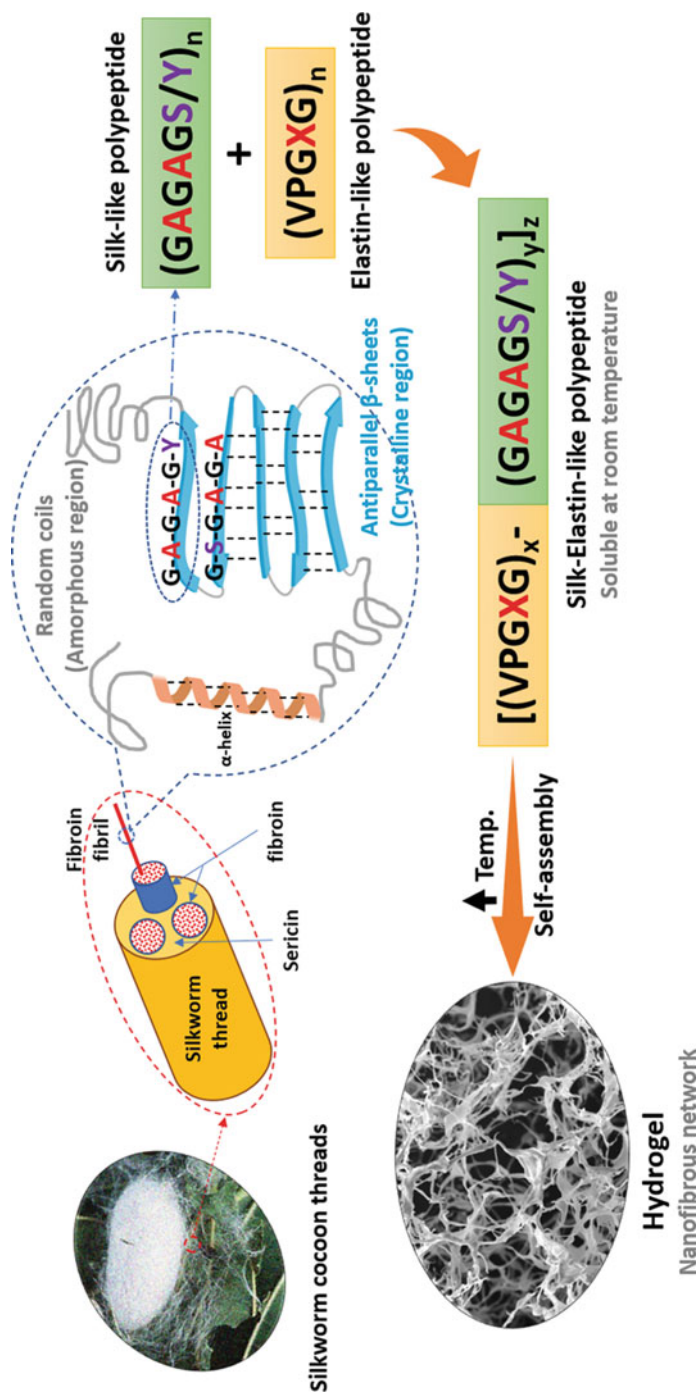
Fig. 1.4 Schematic presentation of the hierarchical structure of silkworm threads, showing fibroin secondary structures (random coils, α-helix, β-sheet) and the general peptide sequence of the self-assembling silk-like polypeptides (SLPs) and silk-elastin-like polypeptides (SELPs)

through H-bonding between G/G and non-G/non-G interfaces (Fig. 1.4) (Zhou et al. 2001; Mita et al. 1994; Qi et al. 2017). On the other hand, the light chain amino acid sequences are non-repetitive, being more hydrophilic and relatively elastic than the heavy chain (Qi et al. 2017).

Silk-elastin-like polypeptides (SELPs) have been synthesized with silk-like and elastin-like peptides to benefit from the combined features of both components (Fig. 1.4). These polypeptides have shown to be chemically and thermally stable owing to the silk-like component which enhances the formation of β-sheet crystals stabilized by H-bonding leading to hydrogel formation. On the other hand, the polypeptide's flexibility and aqueous solubility are provided by the elastin-like component. At room temperature, these SELPs materials are liquid, but at higher temperatures, they undergo gelation. These thermo-responsive polypeptides can be designed with different silk-like to elastin-like component ratios, component lengths, and sequences in order to attain hydrogels with tunable properties (Megeed et al. 2002).

An example of a SELP showing sensitivity to changes in pH and temperature is that synthesized by Nagarsekar et al. (Nagarsekar et al. 2002; Nagarsekar et al. 2003) The repeating silk-like sequence (GAGAGS) and the elastin-like sequence (VPGVG) were used for constructing the polypeptide of the general structure [(GVGVP)$_4$-GXGVP-(GVGVP)$_4$-GAGAGS]$_{11}$, where X position can be occupied by either V or E residues. These protein polymers have shown a transition from the solution state to turbidity upon elevating the temperature (Nagarsekar et al. 2002; Nagarsekar et al. 2003). In a different study, Zeng et al. investigated the self-assembly of SELPs into nanofibers. Different peptide sequences were designed based on repetitive units; each is composed of several blocks of the silk-like GAGAGS and elastin-like GVGVP sequences, in addition to one block of the charged modified elastin-like G**K**GVP or G**E**GVP sequences and the non-repetitive head and tail units. Peptide self-assembly into nanofibers was initiated by preexisting fiber nuclei through electrostatic interactions between the oppositely charged K and E residues in the head and tail units which then undergo folding into β-rolls stabilized by hydrophobic interactions governed by the hydrophobic A residues exposed at the surface (Zeng et al. 2014). More recently, Narayan et al. developed a genetically engineered photo-responsive SELP of the general sequence [(GVGVP)$_4$(G**Y**GVP)$_1$(GVGVP)$_3$(GAGAGS)$_1$], which self-assembles into hydrogels triggered by polymerization with the C-terminal adenosylcobalamin (AdoB$_{12}$)-binding domain (CarH$_C$) in the presence of AdoB$_{12}$ and dark. The self-assembled hydrogel showed dis-assembly and gel-sol transition upon exposure to visible light (Narayan et al. 2021).

1.3.1.4 Keratin and Keratin-Like Polypeptides

In addition to the aforementioned protein-like nanomaterials, keratin is another structural protein which has been interestingly exploited as a biopolymer template for the design of polypeptide-based nanostructures for biomedical applications.

Keratins are the main structural components of both mammalian and avian cytoplasmic epithelial and epidermal appendages including hairs, nails, skin, wools, fur, horns, feathers, and claws (Rouse and Van Dyke 2010). It constitutes more than 80% of the mammalian hair and the avian feathers and plays a vital protective role against external harassment (Reddy et al. 2021).

Keratins are insoluble proteins rich in C residues and can be classified into two main types depending on their structure and function: "hard" keratins and "soft" keratins. "Hard" keratins are the primary constituent of tough epidermal structures, formed of ordered intermediate filament (IF) bundles embedded in a cysteine-rich protein matrix. On the other hand, "soft" keratins known as "hair" keratins are the main component of soft tissues such as hairs and wools and formed of loosely packed cytoplasmic IF bundles, imparting a mechanical resilience to epithelial tissues (Fig. 1.5) (Moll et al. 1982; Fraser et al. 1986; Coulombe et al. 2000). Both types of keratin are composed of two different protein chains (types I and II), varying in molecular weight and composition, while sharing the presence of a central domain of an alpha-helical structure and terminal non-helical domains. Both type I and type II keratin chains which are acidic and neutral-basic, respectively, pack into coiled-coil dimers stabilized by intermolecular disulfide bridges, which in turn undergo lateral association through disulfide cross-linking into IFs (Fig. 1.5). Although the secondary structures of both types of keratin are closely related, they have different structural properties related to different amino acid sequences, where the non-helical domains of the "soft" hair keratin are richer in C residues and thus forming fibrous structures of higher toughness and durability through formation of intermolecular disulfide bonds (Fraser et al. 1986; Moll et al. 2008; Yu et al. 1993). Furthermore, keratin is characterized by the presence of specific amino acid sequences such as the cell adhesion motifs, RGD, and LDV which binds to the cell surface vitronectin integrin receptors that are overexpressed by different tumor cells (Xu et al. 2013).

As the overall physicochemical and biological properties of self-assembling keratin-based nanomaterials are dependent on keratins' key properties, these have been used for different biomedical applications (Rouse and Van Dyke 2010). Self-assembly of keratin solutions into different porous structures such as nanoparticles (Ferroni and Varchi 2021), films (Reichl 2009; Fujii and Ide 2004), sponges or scaffolds (Tachibana et al. 2002; Tachibana et al. 2005; Tachibana et al. 2006), and fibers (Aluigi et al. 2007; Aluigi et al. 2008; Katoh et al. 2004; Wrześniewska-Tosik et al. 2007) has been widely studied (Fig. 1.5). For example, Yi et al. studied the self-assembly of epigallocatechin-functionalized human hair keratin to develop spherical nanoparticles of a diameter of 50 nm to be used as an antioxidant and a free radical scavenger (Yi et al. 2021). In addition, Xiao-Zhou et al. reported the co-assembly of the hydrophilic GY-rich keratin and the hydrophobic casein into complex nanomicelles through electrostatic and hydrophobic interactions. The developed keratin/casein composite nanomicelles were less than 100 nm in diameter, showing high water solubility and structural stability, in addition to good drug loading capacity (Xiao-Zhou et al. 2014).
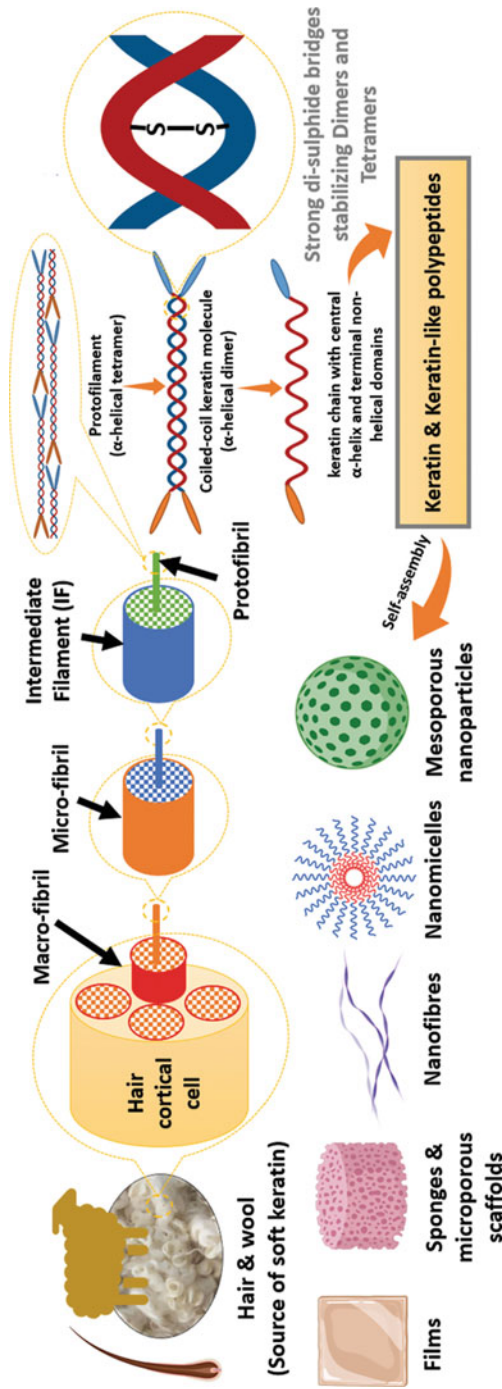
Fig. 1.5 Hierarchical structure of "soft" hair keratin and the different nanostructures developed from keratin-like polypeptides self-assembly

1.3.1.5 Resilin-Like Polypeptides

Resilin is another structural protein found in the exoskeletons of insects, mainly in the flight and jumping organs (Fig. 1.6) (Chen et al. 2013; Elvin et al. 2005; Qin et al. 2009). It is an insoluble thermostable protein of an outstanding resilience and considered one of the most efficient elastic proteins of an elastic modulus reaching 600–2000 kPa (Su et al. 2014; Gosline 1980). It can be stretched up to threefolds of its original length before breaking and immediately reforms to its original shape even after weeks of stretching (Elvin et al. 2005; Qin et al. 2009). These outstanding elastic properties of resilin have introduced it as a promising candidate for biomaterials fabrication.

Resilin is biosynthesized in an uncross-linked form known as "pro-resilin" which then undergoes enzyme-triggered cross-linking to form di- and tri-tyrosine cross-linked hydrogels (Coles 1966). Resilin's peptide structure contains about 60% hydrophobic amino acid residues with both glycine and proline residues constituting about 45% which contribute to resilin's high elasticity (Andersen 1964). The amino acid sequence of resilin identified in the fruit fly *Drosophila melanogaster* involves three domains; N-terminal exon-1 domain composed of the sequence repeats (GGRPSDSYGAPGGGN)$_{18}$ adopting β-turn structure and the C-terminal exon-3 domain (GYSGGRPGGQDLG)$_{11}$ of polyproline type II (PPII) helical conformation, with the middle domain exon-2 composed of the unorganized chitin-binding random coil sequence (Fig. 1.6) (Qin et al. 2009; Ardell and Andersen 2001; Bochicchio et al. 2008). The PPII conformations adopted by the proline-rich sequences have a key role in determining the elasticity of resilins. Furthermore, the high resilience of resilin-mimetics is believed to depend on the co-existence of both β-turn and PPII conformations (Bochicchio et al. 2008; Tamburro et al. 2010; Rauscher et al. 2006).

Resilin-like polypeptides (RLPs) have been widely studied for self-assembly into nanostructures. For example, Tamburro et al. designed the bioinspired resilin-like polypeptide RES50 of the amino acid sequence (PGGGN)$_{10}$, which is a repetitive sequence derived from the β-turn forming N-terminal exon-1 domain of *D. melanogaster* resilin protein (Fig. 1.6) (Tamburro et al. 2010). Interestingly, RES50 demonstrated self-assembly into β-turn structures similar to that adopted by the parent protein domain and can further organize into higher hierarchical nanofibrous networks (Fig. 1.6) (Tamburro et al. 2010). RLPs have also been studied for different stimuli-triggered self-assembly including pH and temperature and were found to have multi-stimuli responsiveness, in addition to their capability to incorporate cell adhesion motifs for tissue engineering and different biomedical applications (Su et al. 2014; Balu et al. 2021).
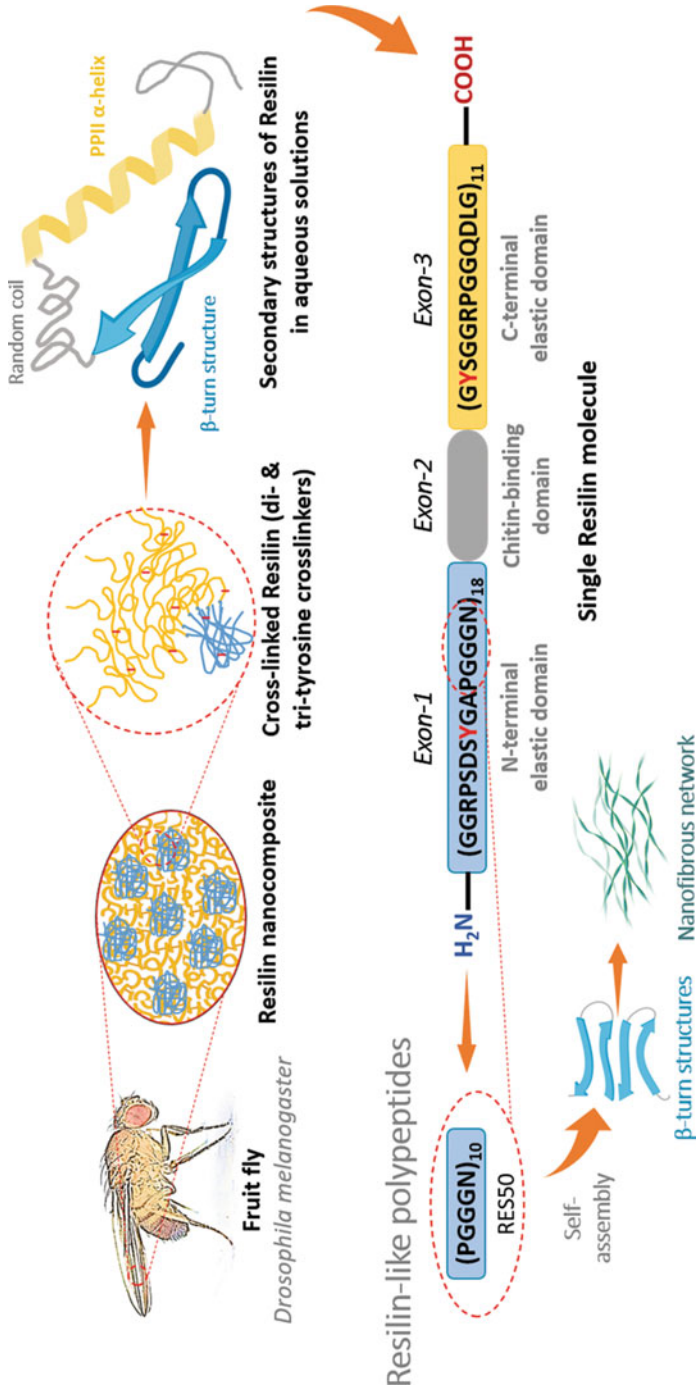
Fig. 1.6 Schematic presentation of resilin structure in the fruit fly *Drosophila melanogaster* showing the primary peptide sequence of a single resilin molecule, its secondary structures with N-terminal exon-1 adopting β-turn structure (blue color), C-terminal exon-3 acquiring PPII α-helix conformation (orange color), both connected via the unstructured chitin-binding exon-2 domain (grey color). The figure also shows the self-assembly of the exon-1 derived peptide sequence (PGGGN)$_{10}$ into β-turn structures forming nanofibrous networks, as an example of resilin-like polypeptides

1.3.2   De Novo Synthetic Short Peptides

De novo self-assembling short peptides are shorter sequences than polypeptides (~< 30 amino acid residues), chemically synthesized, with the sequence design inspired by short fragments of protein domains. Hence, simple design rules for these peptides are implemented through native sequence mimicry to adopt naturally existing protein secondary structures including β-sheets and β-turns, α-helices, and coiled coil. Beside bioinspired sequences, other unnatural self-assembling short peptides were innovated, which are covalently conjugated to either hydrophobic alkyl groups forming amphiphiles or aromatic groups allowing assembly through π–π stacking. Cyclic peptides have also been designed to develop tubular nanostructures. In essence, de novo short peptides follow simpler design rules in comparison to polypeptides, form thermodynamically stable nanostructures, and are thus cost-effective. In this section, we will give an overview on this important class of self-assembling peptides.

1.3.2.1   β-Sheet Forming Peptides

β-sheet structures, either parallel or antiparallel, represent one type of the natural proteins secondary structures, first identified in the early 1950s by Pauling, Corey, and others (Pauling and Corey 1951). In general, a β-sheet structure consists of a "ladder-like" arrangement of extended peptide chains, also known as strands, assembled via H-bonding between the backbone amides (Fig. 1.7a). Parallel β-sheet structures are formed when the C-termini of all peptide chains are oriented at one end of the sheet, while antiparallel structures have alternating N and C termini. It is well known that β-sheets have the ability to undergo a higher level of association into extended long fibrous structures and protein aggregates, which is believed to be the main etiology for many protein misfolding diseases involving amyloidosis such as Alzheimer's and Parkinson's diseases (Chiti and Dobson 2006; Hamley 2012).

   In the early 1990s, Zhang and co-workers were the first to design a β-sheet forming short peptide, EAK16 or (AEAEAKAK)$_2$, based on the ionic self-complementary sequence pattern identified in Z-DNA binding protein Zuotin; a nuclear protein of the baker's yeast *Saccharomyces cerevisiae* (Fig. 1.7a) (Zhang et al. 1992; Zhang et al. 1993; Zhang et al. 1994). The sequence of such peptides is composed of ~8–16 residues and exhibits alternation of hydrophobic (A) and hydrophilic charged (B) amino acids: (ABAB)$_n$, where n is the number of the pattern repeats (e.g., (RADA)$_4$, (AEAEAKAK)$_2$, (FEFK)$_2$, etc.) (Zhang et al. 1994). Different design patterns of charge distribution on the hydrophilic side of β-sheet structures have been reported and can be classed into four main moduli as the mostly used ones: modulus I (-+-+-+), modulus II (--++--++), modulus III (---+++), and modulus IV (----++++) (Zhang 2003). Peptides self-assembly is triggered by masking sequence charge to reduce electrostatic repulsion between peptide chains, which can be achieved by adding electrolytes or changing pH, allowing for

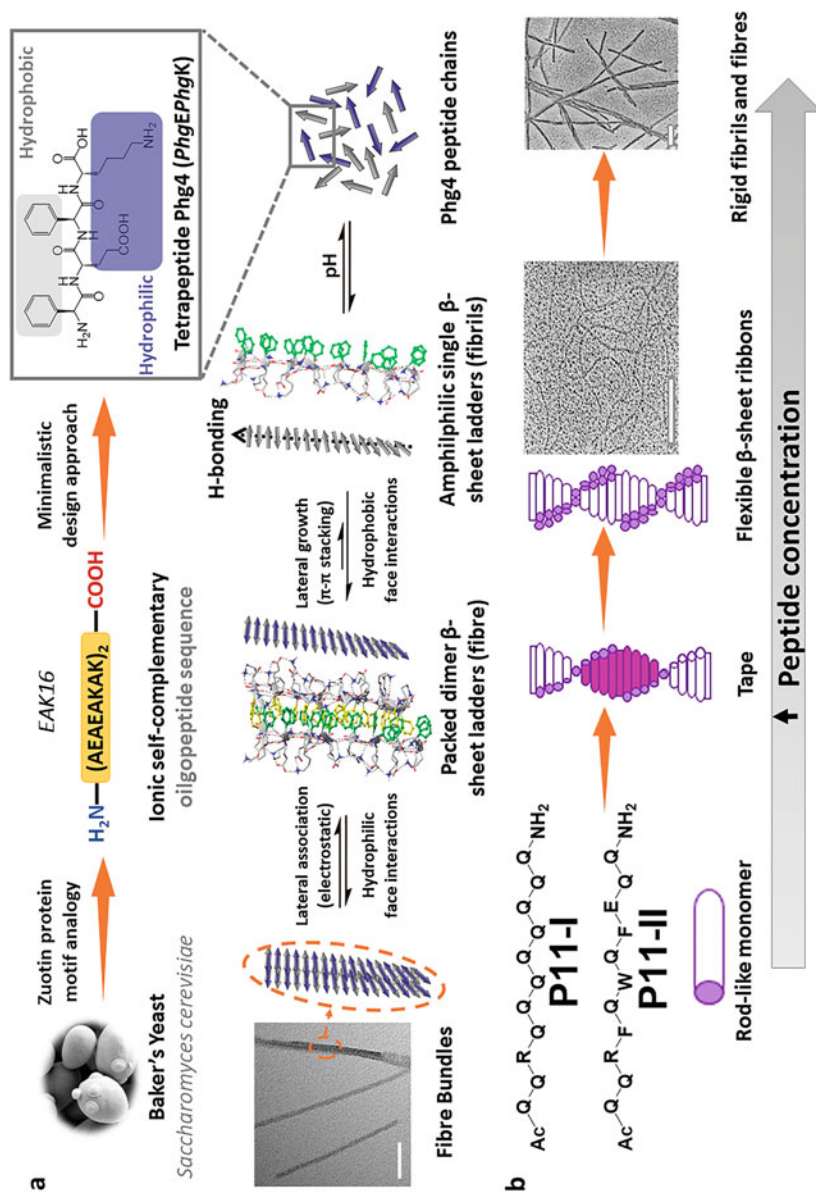**Fig. 1.7** (**a**) Schematic illustration of self-assembly of ionic self-complementary peptides, inspired from the baker's yeast Zuotin protein, into amphiphilic β-sheet single ladder form, which pack into dimers through hydrophobic interaction/π-stacking of the aromatic rings alongside the intermolecular H-bonding

consequent inter-chain H-bonding between backbone amides within single β-strands (Fig. 1.7a) (Caplan et al. 2000). Lateral hydrophobic interactions occur to shield the hydrophobic faces from the surrounding aqueous media while forming β-sheets (Fig. 1.7a). The resulting β-sheet bilayers, either parallel or antiparallel, then form fibrils via lateral intermolecular electrostatic interactions (Fig. 1.7a) (Zhang et al. 1994; Zhang 2003; Caplan et al. 2002; Hauser and Zhang 2010b; Yokoi et al. 2005). The hierarchical structure formation depends on the number of sheets laterally associated together to create the final structure, which can be fibrils, fibers, ribbons, or tapes (Fig. 1.7b) (Aggeli et al. 2001; Mandal et al. 2014). The formation of these higher-order assemblies can be controlled by peptide concentrations, where increasing the concentration results in the formation of higher-level structures. Recently, many studies involving systematically designed peptide sequences have been carried out for identification of key physicochemical and structural features controlling the ionic self-complementary peptide assembly and hydrogelation (Wychowaniec et al. 2020; Gao et al. 2017; Elsawy et al. 2016; Guilbaud et al. 2010; Guilbaud et al. 2013; Swanekamp et al. 2012; Bowerman and Nilsson 2012; Betush et al. 2018).

As the assembly of these systems depends on minimizing electrostatic repulsion, thus salt concentration can play an important role in the assembly process by masking charges involved in multiple β-sheets interactions (Hong et al. 2005; Dai et al. 2013). For instance, Chen and co-workers found that at low concentration of peptide EAK16-II or (AEAEAKAK)$_2$, NaCl prevents random interactions at "critical salt concentration" and promotes assembly of fibers by only allowing favorable interactions to occur as these become stronger, while at higher peptide concentration, this effect is reduced (Aluigi et al. 2008). Charge interactions and assembly can as well be controlled by adjusting aqueous medium pH (Wychowaniec et al. 2020; Boothroyd et al. 2013; Ye et al. 2008). Elsawy and co-workers showed that molecular self-assembly, surface activity, and sol-gel-sol transitions for Phg4 or *Phg*E*Phg*K (where *Phg* is phenylglycine) can be finely tuned at a wide range of pH values (Wychowaniec et al. 2020). Molecular assembly into β-sheet structures, nanofiber formation, emulsification, and hydrogelation have all occurred only at pH values where the overall charge of Phg4 peptide chain was neutral (Wychowaniec et al. 2020). In addition to electrostatics, hydrophobic interactions play a crucial role in stabilizing assembly of ionic self-complementary peptides (Betush et al. 2018; Senguen et al. 2011; Doran et al. 2012). In order to explore

---

Fig. 1.7 (continued) between backbone amides along the fiber axis. Further lateral growth through electrostatic interactions leads to the formation of thicker fiber bundles. Minimalist design approach led to the development of the shortest ionic self-complementary peptide, the tetrapeptide Phg4, which self-assemble into thermodynamically stable β-sheet fibrous structures. Adapted from (Wychowaniec et al. 2020), with copyrights permission from the American Chemical Society published under Creative Commons Attribution 4.0 International license. (**b**) Concentration dependent hierarchical self-assembly of chiral rod-like P11-I and P11-II peptide units. Adapted from (Aggeli et al. 2001), with copyrights permission from the National Academy of Science

the hydrophobicity threshold at which peptides can effectively self-assemble, Nilsson's group has studied the assembly behavior of different peptide sequences derived from $(AKAE)_2$ which failed to self-assemble compared to the more hydrophobic analogue $(FKFE)_2$, which rapidly assembled into β-sheet bilayer nanoribbons under similar conditions (Betush et al. 2018). The replacement of two A residues with a variety of more hydrophobic residues led to obvious changes in tendency and rate of self-assembly of the developed analogues, where substitution pattern has only a moderate effect on the rate of self-assembly and fibril morphology, while hydrophobicity has a much more significant impact on promoting self-assembly (Betush et al. 2018). No doubt that H-bonding is the key interaction for stabilization of β-sheet formation, which is significantly affected by the peptide chain length. Mostly, the peptide chain length threshold for successful assembly of ionic complementary peptides is ∼6–8 residues, i.e., at least 2 repeats of the $(ABAB)_n$ sequence pattern ($n = 2$) is essential for assembly to occur (Wychowaniec et al. 2020). Ulijn, Saiani, Miller, and co-workers have reported the inability of tetrapeptide FEFK to self-assemble ($n = 1$), which was only possible via reverse hydrolysis into octapeptides ($n = 2$) upon incubation with thermolysin (Guilbaud et al. 2010; Guilbaud et al. 2013). The shortest ionic self-complementary peptide reported to successfully self-assemble and form hydrogels is the tetrapeptide Phg4 (*PhgEPhgK*), which was designed by Elsawy and co-workers to stabilize assembly via π–π stacking of the constrained aromatic *Phg* residues, alongside an average of ∼3 inter-chain H-bonds (Fig. 1.7a) (Wychowaniec et al. 2020). This was inspired by the exploitation of π–π interactions for the stabilization of self-assembly of ultra-short peptides, which will be discussed under Sect. 1.3.2.5.

The design of a β-sheet-forming peptide of minimal complexity capable of self-assembly into uniform reproducible hierarchical nanostructures is challenging indeed. Overall, the basic requirements for hierarchical self-assembly include (a) presence of attractive forces between peptide side chains within the strand including H-bonding, hydrophobic, and electrostatic interactions, (b) presence of recognition sites between adjacent β-strands to direct their lateral growth into one dimension and to avoid randomly associated β-sheet structures, and (c) the ability of solvent to strongly adhere to β-sheet surface to control solubility (Aggeli et al. 1997).

Following the above design rules for β-sheet nanostructure formation, Aggeli and co-workers have developed the β-sheet-forming peptides P11-I (QQRQQQQQEQQ) and P11-II (QQRFQWQFEQQ) (Aggeli et al. 2001), which do not follow the $(ABAB)_n$ pattern, but rather inspired by the polyglutamine (PolyQ) amyloid-like fibril formation, which is believed to be the etiology of several neurodegenerative diseases, such as Huntington's disease (Perutz et al. 1994; Chen et al. 2002). These two peptides successfully assemble into twisted β-sheet tapes as well as hydrogels due to their amphiphilic nature (Fig. 1.7b). P11-I sequence is rich in glutamine (Q) residues which interact strongly in water through their side chains via hydrophobic and H-bonding interactions. R and E residues at the third and the ninth positions, respectively, can act as molecular recognition sites between adjacent antiparallel β-strands aggregating in tape-like form through electrostatic interactions (Fig. 1.7b). The combined intermolecular interactions between side chains and

H-bonding between peptide backbones promoted the assembly into β-sheet tapes (Aggeli et al. 2001; Aggeli et al. 1997).

1.3.2.2 β-Hairpin-Forming Peptides

The β-hairpin (β-turn or β-ribbon) is another secondary structure of proteins consisting of two short H-bonded β-strands oriented in an anti-parallel direction and linked together by a "kink" forming sequence (Fig. 1.8) (Fersht 1999; Berg et al. 2012). Pochan, Schneider, and co-workers designed a series of de novo β-hairpin-forming short peptides possessing on-demand self-assembly and folding in response to external triggers, resulting in hydrogel formation (Schneider et al. 2002; Ozbas et al. 2004; Pochan et al. 2003; Haines et al. 2005; Rajagopal et al. 2009).

These β-hairpin-forming peptides share the presence of a central tetrapeptide (-V^{D}PPT-) as a turn-forming sequence. The unconventional D-enantiomeric form of proline (^{D}P) permanently forces the formation of type II′ turn structure, to avoid *cis*-prolyl bond formation that could result in assembly of heteroconformers (Fig. 1.8). This turn sequence is flanked between two short extended chains (~ 8 amino acid residues) of a typical β-sheet forming structure with alternating hydrophobic and hydrophilic amino acids (Schneider et al. 2002; Ozbas et al. 2004; Pochan et al. 2003; Haines et al. 2005; Rajagopal et al. 2009). This design allows such amphiphilic sequences to undergo folding to "hairpin" structure, stabilized by β-sheet formation via intra-chain H-bonding (Fig. 1.8). Individual hairpins can subsequently assemble at the hydrophobic faces together through lateral interactions to form higher-order structures, i.e., nanofibers, and further to nanofibrous networks forming self-supporting hydrogels (Fig. 1.8) (Kretsinger et al. 2005).

As earlier mentioned, these peptides have been designed to undergo folding and self-assembly triggered by external stimulus such as change in pH, ionic strength, temperature, or in response to light (Schneider et al. 2002; Ozbas et al. 2004; Pochan et al. 2003; Haines et al. 2005; Rajagopal et al. 2009; Kretsinger et al. 2005; Haines-Butterick et al. 2007). From these peptides, MAX1 was the first designed sequence with 20 amino acids (VKVKVKVK-V^{D}PPT-KVKVKVKV-NH$_2$), containing V as the hydrophobic residue and K as the hydrophilic residue. At low pH, the peptide is unfolded and fully soluble, attaining random coil conformation in solution, but after raising the pH to a basic value (pH 9) or the ionic strength by salt addition, it forms an amphiphilic β-hairpin structure which self-assembles into branched clusters of well-defined nanofibrils, further associating to form a hydrogel of a fibrous network structure (Fig. 1.8a) (Schneider et al. 2002; Haines et al. 2005; Yucel et al. 2008). MAX1 hydrogels have been used for tissue engineering where the cell culture growth media can act as an external stimulus for β-hairpin folding and hydrogel formation upon addition to the aqueous peptide solution. Many analogues of MAX1, like MAX8, for instance, were developed and successfully formed nanofibrous hydrogels (Fig. 1.8a) (Pochan et al. 2003; Kretsinger et al. 2005; Haines-Butterick et al. 2007; Branco et al. 2009). A photo-responsive analogue of MAX1 was also engineered, MAX7CNB, which is the C16-analogue of MAX1 (MAX7:
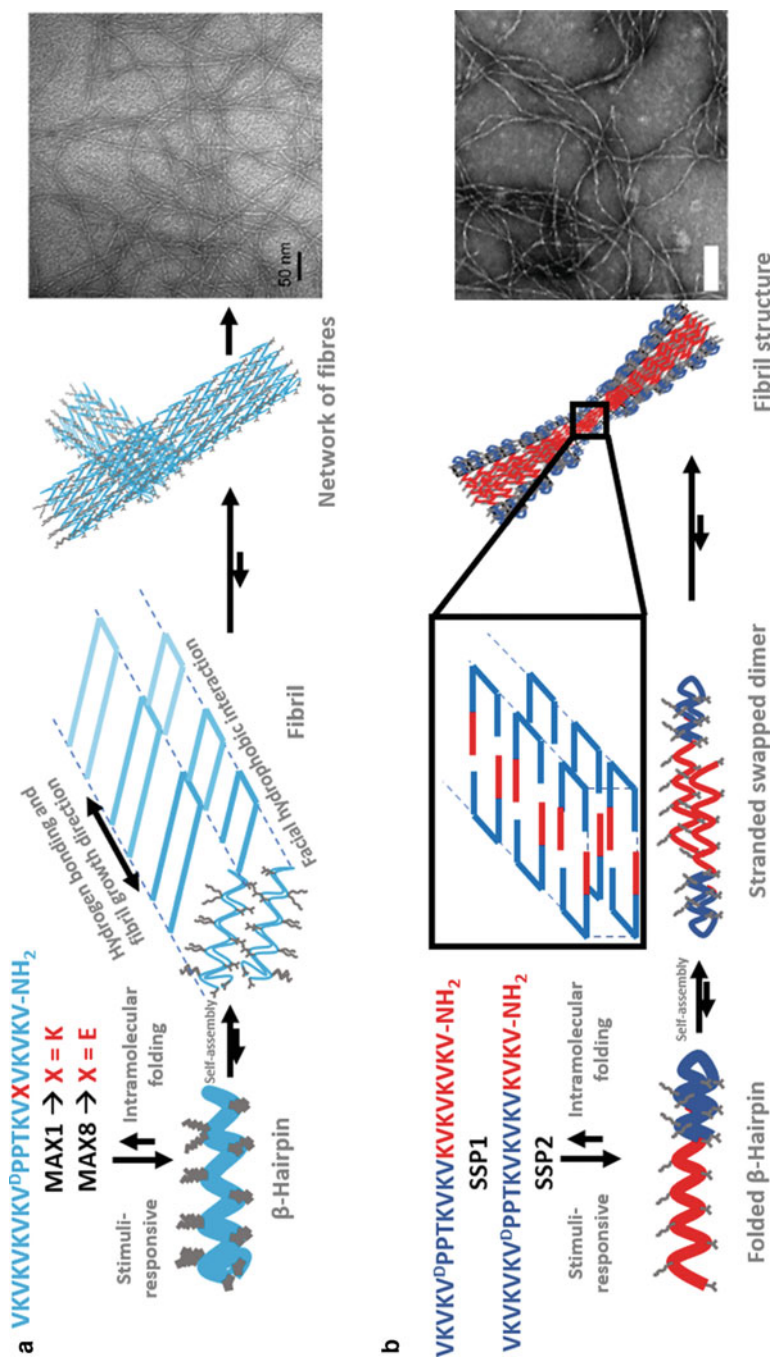
Fig. 1.8 Schematic illustration of (**a**) the self-assembly mechanism of MAX1 and MAX8 β-turn structures into fibrils through lateral hydrophobic interactions and H-bonding along the fibril axis. Further growth and entanglement of fibrous structures leads to network formation. Adapted from (Ozbas et al. 2004), with copyrights permission from the American Chemical Society, (**b**) the proposed self-assembly mechanism of β-turn forming strand-swapping peptides into fibrillar structures. Adapted from (Nagarkar et al. 2008), with copyrights permission from the American Chemical Society

VKVKVKVK-V^{D}PPT-KVK**C**KVKV-NH$_2$) conjugated to the photo-labile group *ortho*-Nitrobenzyl (*o*-NB) at C16 forming a photocage (Haines et al. 2005). MAX7CNB remains unfolded in solution and unable to self-assemble, but upon UV irradiation, the peptide is uncaged yielding MAX7 that undergoes folding, self-assembly, and hydrogelation (Haines et al. 2005). Pochan and Schneider have also introduced another subclass of β-hairpin-forming peptides, the so-called strand-swapping peptides (SSP), in which the two β-strand domains linked to the β-turn sequence are of different lengths. These peptides undergo self-assembly and hydrogel formation through thermally triggered β-strand swapping (Fig. 1.8b) (Nagarkar et al. 2008; Hule et al. 2009).

1.3.2.3   α-Helix/Coiled-Coil-Forming Peptides

Like β-sheets and β-turns, α-helices and helical coiled-coils are naturally occurring self-assembling systems, which are inspired from secondary structural elements and folding patterns in proteins (Pollard and Earnshaw 2008; Whitford 2005). Based on the self-assembling behavior of these systems into high-order fibrous structures, α-helix-forming peptides have been designed by copying nature and used to develop a number of biomaterials as first described by Pauling, Corey, and Crick (Crick 1953; Pauling and Corey 1953).

The structure of a typical α-helix comprises a repeating motif of seven amino acid residues designated as a, b, c, d, e, f, and g, constituting what is referred to as "heptad." The peptide backbone of each heptad undergoes twisting into two helical turns with 3.6 amino acid residues being involved per turn. This helical structure is stabilized by intramolecular H-bonding between the carbonyl group (–C=O) of each residue (*i*) and the amide (–NH–) group of the following fourth residue (*i* + 4) along the helical chain. Additional structure stabilization can be gained through hydrophobic and electrostatic interactions resulting from packing of at least two α-helices to constitute what is known as a coiled coil (Fig. 1.9a). Coiled coils either right- or left-handed are very common in naturally occurring systems, from which the design rules of coiled-coil-forming peptides are inspired (Adamson et al. 1993; Oas and Endow 1994; Hodges 1996; Lupas 1996; Kohn et al. 1997; Kohn and Hodges 1998; Yu 2002; Xu et al. 2002).

Designing helical peptide sequences that can associate into coiled coils involves hydrophobic residues, usually aliphatic, located at the first (a) and fourth (d) positions of the heptad to form the hydrophobic face of α-helix (Fig. 1.9a). Packing of two helices forms a coiled-coil dimer, where the hydrophobic face is shielded forming an inter-helical hydrophobic core that results in stabilization of the coiled-coil structure. Selectivity of association can be further controlled by incorporating a hydrophilic residue in the hydrophobic core, which can specifically interact with a counterpart hydrophilic residue in the other helix via specific co-complementary interactions (for instance, H-bonding between 2 N residues) (Banwell et al. 2009). Complementary charge patterns between the two facing helices forming the coiled-coil dimer have also been exploited to stabilize structure
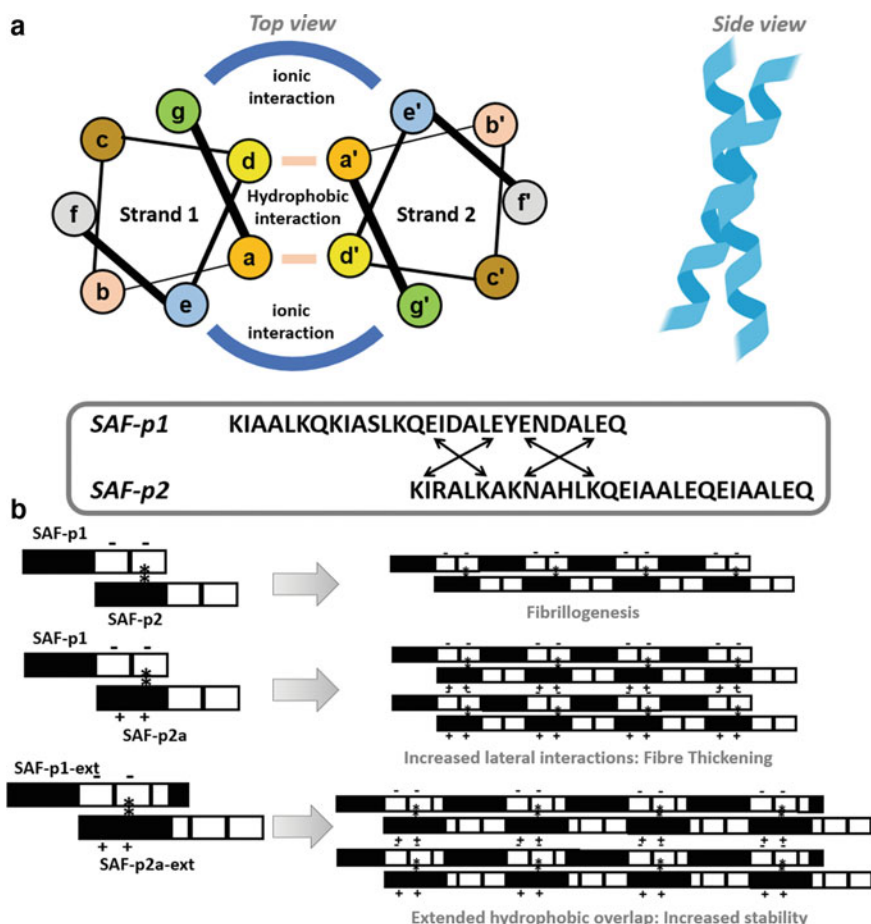
Fig. 1.9 (**a**) α-helix and coiled-coil assembled structure. Left panel showing top view of the coiled-coil core hydrophobic interactions and ionic interactions between countercharge residues. Right panel showing side view of the dimeric coiled coil. (**b**) Amino acid sequences of coiled-coil-based self-assembling fiber (SAF) peptides (SAF-p1 and SAF-p2) and their redesign into sticky ended dimers to form longer fibrils and increase fiber thickening and fiber stability. Black blocks represent heptads with positively charged K residues at the coiled-coil interfacial e and g, while white blocks represent heptads with negatively charged E residues at the e and g sites; "–" and "+" represent the charged D and R residues, respectively, on the surfaces of the peptides; and "*" represents complementary buried (N) residues. Adapted from (Smith et al. 2006), with copyrights permission from John Wiley and Sons

through electrostatic attraction and provide association specificity among helices (Fig. 1.9a) (Petka et al. 1998).

Woolfson and co-workers have designed nanofibrous systems based on self-assembly of helical structures into coiled coils using "sticky end" approach (Fig. 1.9b) (Banwell et al. 2009; Pandya et al. 2000). For example, two 28-residue

α-helix-forming peptides were designed to co-assemble into a dimeric coiled coil with complementary sticky ends (Fig. 1.9b) (Ryadnov and Woolfson 2003; Papapostolou et al. 2007). The self-assembling fibers, SAF-p1 and SAF-p2, were designed based on the heptad design rules discussed above, to form a parallel coiled-coil heterodimer with a staggered hydrophobic interface (Fig. 1.9a). The peptides contain the hydrophobic residues I and L at positions (a) and (d) of the heptad repeats, respectively. The cationic K and anionic E residues were located at positions (e) and (g) with complementary distribution patterns in the heptad repeats (Fig. 1.9b). Such peptide design ensures the co-assembly into coiled-coil dimers with sticky ends which further associate laterally and longitudinally propagating the structure into larger α-helical coiled-coil fibrils (Fig. 1.9b) (Pandya et al. 2000). An R residue was incorporated replacing one A in the peptide SAF-p2 allowing for salt bridge formation with D residue at the coiled-coil interface (Fig. 1.9b). This modification resulted in fibers with higher stability (Smith et al. 2006). Bundles of 3-helices have also been developed using "sticky end" association (Ogihara et al. 2001). Other approaches were used to design coiled-coil structures without "sticky ends," with design rules closely similar to those used for "sticky end" approach (Dong et al. 2008).

By combining the use of bioinformatics in structural analysis of thousands of natural coiled coils and the design studies, Woolfson and co-workers rationally designed self-assembling coiled coils based on parallel dimers, trimers, and tetramers which are either homo- or heteromeric (Woolfson 2017; Dawson et al. 2021). Moreover, they have designed α-helical barrels with central channels composed of 5–9 α-helices which can be exploited for different applications (Woolfson 2017; Dawson et al. 2021). For example, based on the number and the position of both hydrophobic (h) and polar (p) residues in the self-assembling sequence repeats, different self-assembling patterns can be developed. A sequence pattern of *hpphppp* can direct the self-assembly of α-helices into dimeric to tetrameric bundles. However, larger α-helical barrels can be produced by changing pattern to *hpphhph* (Dawson et al. 2021). Higher coiled-coil structures are discussed in more details in Chap. 3.

1.3.2.4 Amphiphilic Peptides

Another class of self-assembling peptides capable of forming well-defined supramolecular nanostructures through amphiphilicity, the presence of both hydrophilic and hydrophobic regions, is referred to as "amphiphilic peptides." Such peptides are rationally designed inspired by the structure of naturally occurring molecules such as phospholipids which have important functions in living organisms such as composing cell membranes and acting as signal transduction initiators through protein–protein and protein–lipid interactions (Hinterding et al. 1998; Löwik and van Hest 2004). Self-assembly of amphiphilic peptides is mainly controlled by hydrophobic interactions which result in molecular arrangement into assemblies that shield hydrophobic regions in response to exposure to surrounding aqueous environment.

In addition, other different non-covalent interactions such as electrostatic interactions between counter charged amino acid residues and H-bonding aid the formation of stable assemblies with various morphologies, depending on the physicochemical and architectural properties of molecules (such as peptide sequences, charges, concentration, size, and shape) (Antonietti and Forster 2003; Huang et al. 2011; Liu et al. 2011). As such, the self-assembled structures can be in the form of nanofibers, nanotubes, nanovesicles, micelles, nanotapes, and nanosheets. Self-assembling peptide-based amphiphiles can be classed depending on their structure into two main classes: (a) those purely composed of only amino acids, referred to as "amphiphilic peptide sequences," and (b) those composed of peptide-hydrocarbon conjugates, referred to as "lipidated peptides," which are summarized in Table 1.1 and discussed in this section.

Amphiphilic Peptide Sequences

Amphiphilic peptides of pure amino acid sequences are composed of both hydrophilic and hydrophobic domains giving rise to their amphipathic properties. These peptides fall under two subclasses: one of them is mimicking the structure of typical surfactants and consists of a hydrophobic amino acid block composing the surfactant's tail connected to a hydrophilic amino acid sequence composing the head, while the other subclass consists of peptide sequences with alternating hydrophilic and hydrophobic residues. Surfactant-like peptides have been largely designed with various sequences (Vauthey et al. 2002; Santoso et al. 2002; von Maltzahn et al. 2003). Basically, the tail of the amphiphilic molecule is composed of a number of hydrophobic amino acids, while only one or two hydrophilic amino acids usually compose the hydrophilic head. Following this basic rule, a wide range of surfactant-like peptides with different chemical and physical properties can be freely designed based on proper selection of both hydrophilic and hydrophobic amino acids. Generally, the tail of these peptides consists of six hydrophobic amino acid residues such as G, A, V, L, I, and F, which have different degrees of hydrophobicity, thus giving the opportunity to control the overall hydrophobicity of the molecule. The six amino acid tail gives the whole peptide molecule a similar length to that of a natural phospholipid (2–3 nm long), however, the tail length can be designed with varying number of hydrophobic amino acids. Zhang and co-workers designed an amphiphilic peptide (Ac-GAVILRR-NH$_2$) with a hydrophobic tail of five residues, where both the hydrophobicity and amino acid size gradually decrease in the direction of the tail forming a cone-shaped peptide strand. Above a critical aggregation concentration (CAC), the cone-shaped peptide chains self-assemble into micelles and then grow to form nanopipes and eventually nanodoughnuts (Khoe et al. 2009) (Fig. 1.10a). In general, tails with 4–10 residues have been proven to form peptides which self-assemble in similar behaviors forming either spherical micelles or nanotubes/cylinders (Fig. 1.10b), while those with longer tails form more polydisperse nanostructures (Santoso et al. 2002). On the other hand, the amphiphilic head is composed of hydrophilic amino acids which are either negatively charged like D

Table 1.1 Summary of the main classes of self-assembling amphiphilic peptides

Amphiphilic peptides class		Peptide sequence	Morphology of self-assembled structures	Reference
Amphiphilic peptide sequences	Surfactant-like peptides	GAVIL-RR Cone-shaped peptide	(>CAC) Micelles → nanopipes → nanodoughnuts	Liu et al. (2011)
		V6D	Nanotubes	von Maltzahn et al. (2003)
		I2-K2E2N2 I2-E2N2D2	Nanospheres through β-sheet formation	Capes et al. (2010)
	Diblock peptides	K_xL_y, E_xL_y K_xV_y	Hydrogelating α-helical and crystalline β-sheet assemblies	Cui et al. (2014)
	Bolaamphiphilic peptides	K-A6-K	Nanospheres and short nanofibers	Chen et al. (2009)
		K-GAV-K	Extremely long nanofibers	Chen et al. (2009)
	β-Sheet forming peptides	Phg4 (*PhgEPhgK*)	β-Sheet nanofibers and hydrogel	Wychowaniec et al. (2020)
		Ac-(AAAK)₃-NH₂ Ac-(AAAK)₄-NH₂	β-Sheet nanofibers and hydrogel	Qiu et al. (2008), Kisiday et al. (2002), and Measey and Schweitzer-Stenner (2006)
	β-Hairpin forming peptides	MAX peptides	Nanofibers and hydrogel	Schneider et al. (2002), Fersht (1999), Berg et al. (2012), Ozbas et al. (2004), Pochan et al. (2003), Haines et al. (2005), Rajagopal et al. (2009), and Kretsinger et al. (2005)
Lipidated peptides	Bolaamphiphiles	A-(CH₂)ₙ-A, H-(CH₂)ₙ-H	Nanovesicles and nanofibers ($n = 10, 12$), Nanofibers and hydrogel ($n = 20$)	Jang et al. (2009)
	Gemini amphiphiles	Two N-decyloxybenzyl	Nanospheres and	Menger and Littau (1991)

<div align="right">(continued)</div>

Table 1.1 (continued)

Amphiphilic peptides class		Peptide sequence	Morphology of self-assembled structures	Reference
		Valine residues linked through a spacer	nanofibrous hydrogel	
	Peptides with multi-structural domains	Hydrocarbon tail –β-sheet-forming polymerizable tetracysteine –triglycine flexible spacer-Hydrophilic head with bio-functionality	Cylindrical micelles	Rubio et al. (2012), Cui et al. (2014), and Harrington et al. (2006)

and E, or positively charged like K, H, and R, creating either anionic or cationic amphiphilic peptides, respectively. In addition, the hydrophilic head can be designed to attach to the hydrophobic tail at either its N-terminal or C-terminal, forming amphiphilic peptides with different charge distribution, but self-assemble in a similar way (von Maltzahn et al. 2003).

Based on these simple design rules, various amphiphilic surfactant-like peptides have been designed such as A6D, V6D, A6K, KA6, V6D2, L6K2, G4D2, G6D2, and G8D2, which spontaneously self-assemble in aqueous solutions into ordered nanostructures upon reaching the CAC; for instance, V6D has shown to spontaneously self-assemble into stable nanotubes (Fig. 1.10c) (Vauthey et al. 2002; von Maltzahn et al. 2003; Hosseinkhani et al. 2013). In general, these simple surfactant-like peptide-based amphiphiles composed of 1–2 hydrophilic amino acids in the polar head and 4–8 hydrophobic amino acids in the non-polar tail have been found to form hollow nanovesicles and closed-end nanotubes (Fig. 1.10b and c) (Vauthey et al. 2002; Santoso et al. 2002; von Maltzahn et al. 2003). In addition, amphiphilicity does not necessarily require the hydrophilic domain to construct the head nor the hydrophobic domain to construct the tail. Structural components of both the head and the tail can be shifted. For example, Capes et al. investigated the self-assembly of two amphiphilic surfactant-like peptides (I2-K2E2N2 and I2-E2N2D2), in which two isoleucine residues formed the hydrophobic head, while the hydrophilic tail was structured from six hydrophilic amino acid residues. These peptides have been found to form nanospheres through β-sheet formation upon decreasing the medium pH (Capes et al. 2010). Moreover, Deming and co-workers have investigated the self-assembly of amphiphilic peptides in which the hydrophilic and the hydrophobic domains are connected in a diblock or triblock fashion (Deming 2005; Nowak et al. 2002; Nowak et al. 2003; Pochan et al. 2002; Holowka et al. 2005; Nowak et al. 2006; Li and Deming 2010; Breedveld et al. 2004). The diblock peptides (K_xL_y, K_xV_y, and E_xL_y) containing the highly hydrophilic amino acid domains, poly(L-lysine) or poly(L-glutamate), were found to form hydrogelating α-helical and crystalline β-sheet assemblies when connected to the hydrophobic
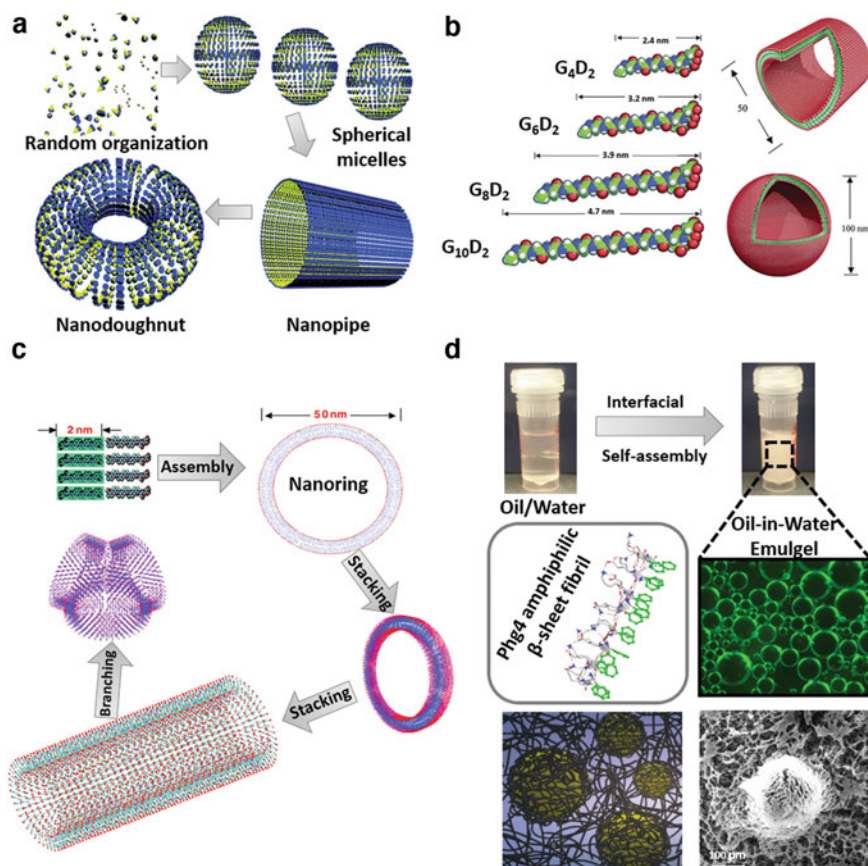
Fig. 1.10 (**a**) Self-assembly of the cone-shaped amphiphilic peptide Ac-GAVILRR-NH2 into nanodoughnut structure, where at low concentration peptide chains are unstructured and randomly organized. Increasing peptide concentration above the CAC progressively led to the formation of spherical micelles, nanopipes, and eventually nanodoughnut structures. Adapted from (Khoe et al. 2009), with copyrights permission from the American Chemical Society. (**b**) Structure of peptides of negatively charged heads and 4–10 glycine residues tail (left) which self-assemble in similar behaviors into either nanotubes (top right) or nanovesicles (bottom right). Color code: red, negatively charged aspartic acid heads; green, non-polar glycine tail. Adapted from (Santoso et al. 2002), with copyrights permission from the American Chemical Society. (**c**) V6D peptide self-assembly into nanorings progressively stacking into nanotubes. Three nanotubes connected through three-way junction similar to lipid microtubule structure. Adapted from (Vauthey et al. 2002), with copyrights permission from the National Academy of Science. (**d**) Interfacial self-assembly of Phg4 at Oil/Water interface into amphiphilic β-sheet fibril structures (top), forming nanofibrous microcages encapsulating oil droplets within the continuous nanofibrous network of the aqueous phase (bottom), forming stable emulgels. Adapted from (Wychowaniec et al. 2020), with copyrights permission from the American Chemical Society published under Creative Commons Attribution 4.0 International license

domains, poly(L-leucine) and poly(L-valine), respectively (Katchalski and Sela 1958).

Unlike conventional amphiphiles designed with structural similarities to those of traditional surfactants which are composed of only one hydrophilic head and a hydrophobic tail, bolaamphiphilic peptides are designed by mimicking the structure of a special surfactant group known as bolaamphiphilic surfactants. The molecular structure of these peptides involves two hydrophilic peptide-based heads linked together through a hydrophobic stretch which can be either a peptide sequence or an alkyl chain (Claussen et al. 2003). These peptides could self-assemble into a variety of nanostructures such as nanotubes, nanovesicles, helical ribbons, and membrane-mimetic films which have shown promising biomedical applications (Zhan et al. 2005; Gao et al. 2006; Sun et al. 2006; Song et al. 2002; Cameron et al. 2002; Gaucheron et al. 2001; Weissig and Torchilin 2000). A series of bolaamphiphilic peptides (such as K-A4-K, K-A6-K, K-A8-K, and K-GAV-K) have been designed using the hydrophobic residues, G, A, and V as the hydrophobic stretch, and the charged hydrophilic residues, K and D as the amphiphilic head (Qiu et al. 2008). Peptide assemblies of different structures can be generated by adjusting the length and the overall hydrophobicity of molecules through changing the number of both hydrophilic and hydrophobic amino acids. The peptide (K-A6-K) can self-assemble into nanospheres as well as short nanofibers, which undergo dynamic transformation to each other. On the other hand, the peptide (K-GAV-K) undergoes homogenous self-assembly into extremely long nanofibers (Chen et al. 2009).

In the other subclass of amphiphilic peptides based on pure amino acid sequences, amphiphilicity originates from the formation of both hydrophilic and hydrophobic faces upon self-assembly of peptides which are structured with alternating hydrophilic and hydrophobic amino acid residues. These peptides include the β-sheet-forming ionic self-complementary peptides pioneered by Zhang and co-workers (discussed earlier in Sect. 1.3.2.1) (Zhang et al. 1993; Zhang et al. 1994). Such peptides contain hydrophilic charged residues with alternating distribution between cationic and anionic side chains, which self-assemble into stable β-sheet structures forming amphiphilic nanofibers through charge neutralization upon addition of electrolytes (Fig. 1.7a). These nanofibers further undergo networking into self-supporting hydrogels at low peptide concentrations (Wychowaniec et al. 2020; Zhang et al. 1992; Zhang et al. 1993; Zhang et al. 1994; Zhang 2003; Caplan et al. 2002; Hauser and Zhang 2010b; Yokoi et al. 2005; Mandal et al. 2014; Elsawy et al. 2016; Kisiday et al. 2002). Elsawy and co-workers reported that the tetrapeptide Phg4 (*PhgEPhgK*) self-assemble into amphiphilic β-sheet nanofibers that are not only capable of hydrogel formation in aqueous medium but can also act as nanoemulsifier and stabilized oil-in-water emulsions in biphasic media (Figs. 1.7a and 1.10d) (Wychowaniec et al. 2020). The amphiphilic nanofibrils are exhibiting a hydrophobic face of stacked aromatic rings of *Phg* residue and a hydrophilic face decorated with the polar side chains of E and K residues (Fig. 1.10d). Amphiphilic β-sheet fibrils adsorbed at the oil/water interface forming nanofibrous microspheres stabilize oil droplets in the aqueous continuous hydrogel phase forming emulgels (Fig. 1.10d). Another type of β-sheet-forming amphiphilic peptides reported by

Schweitzer-Stenner et al. such as Ac-(AAAK)$_3$-NH$_2$ and Ac-(AAAK)$_4$-NH$_2$ have shown to self-assemble into β-sheet structures and further to hydrogels at particularly low concentrations (Jang et al. 2009; Measey and Schweitzer-Stenner 2006; Measey et al. 2010). Also, β-hairpin-forming peptides reported by Pochan, Schneider, and co-workers that were discussed earlier in Sect. 1.3.2.2 show amphiphilic properties arising from the alternating sequence repeats of the hydrophobic valine (V) and the hydrophilic lysine (K) residues (Schneider et al. 2002; Ozbas et al. 2004; Pochan et al. 2003; Haines et al. 2005; Rajagopal et al. 2009; Kretsinger et al. 2005; Haines-Butterick et al. 2007; Yucel et al. 2008).

Lipidated Peptides

On the other hand, lipidated peptides are depending on the hydrophobicity of the alkyl chain-containing tail attached to the hydrophilic peptide head to gain their amphiphilic properties. As a result, their self-assembly is facilitated by the more hydrophobic interactions provided by the alkyl chain leading to the formation of stable nanostructures such as micelles and bilayered assemblies. Depending on peptide concentration, these assemblies can further aggregate to form nanofibers or nanotubes capable of networking into hydrogels. Basically, a linear hydrophobic alkyl group of 12–16 carbons composing the tail is attached to the hydrophilic head of a short peptide sequence at either the N- or C-terminus. In aqueous solutions, these molecules undergo self-assembly into micellar structures with a hydrophobic core that is stabilized by hydrophobic interactions and a hydrophilic surface composed of the radially exposed peptides adopting a β-sheet conformation that is stabilized by H-bonding with different orientations (straight, twisted, or perpendicular to the nanostructure Z-axis) and electrostatic interactions (Fig. 1.11a) (Behanna et al. 2005). The formation of β-sheet structures within the peptide core, in a close proximity to the alkyl chain, can be regarded as a self-assembly key feature of amphiphilic peptides. Careful examination of the self-assembling behavior of a number of N-methylated amphiphilic molecules has concluded that the formation of intermolecular H-bonding between the first four amino acid residues following the alkyl chain is essential for the formation of self-supporting hydrogels with good mechanical resistance; otherwise, spherical micelles are formed. On the other hand, a little effect on the molecular structure and hydrogel formation has been observed from prevention of H-bonding between the outer amino acid residues in the amphiphilic molecules. This indicates that peptides assemble into helical ribbons with the outer amino acids capable of adopting different configurational structures, only if the inner residues are sufficiently close to each other allowing for H-bonding (Paramonov et al. 2006). Collectively, these findings indicate that self-assembly is driven by a combination of both hydrophobic interactions and H-bonding between the alkyl tails and the peptide heads, respectively. Lipidated peptides can be subclassed based on the number of hydrophilic heads and hydrophobic tails into three main subclasses: (a) bolaamphiphiles, (b) gemini amphiphiles, and (c) other lipidated peptides with multi-structural domains.
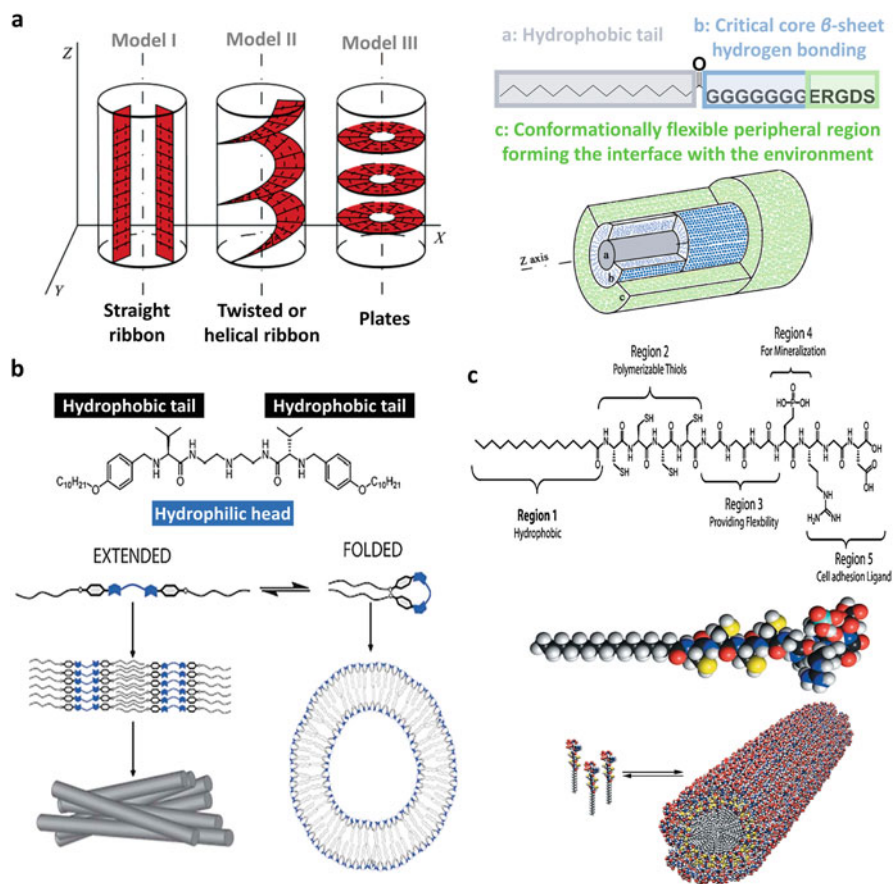
Fig. 1.11 (**a**) Peptide amphiphile (PA) nanofiber: (Left) Schematic representation of the proposed β-sheet-type interactions along the PA nanofiber. Model I: H-bonding occurs in the planes oriented along the nanofiber Z axis. Model II: H-bonding takes place in a helical fashion of a variable pitch. Model III: H-bonding resides in the plates perpendicular to the nanofiber Z axis. (Right): representation of PA nanofiber regions. Adapted from (Paramonov et al. 2006), with copyrights permission from the American Chemical Society. (**b**) Chemical structure of gemini amphiphile and schematic representation of the proposed assembly of extended or folded conformations into fibers and vesicles, respectively. Adapted from (Rubio et al. 2012), with copyrights permission from the Royal Society of Chemistry. (**c**) Top panel: Chemical structure of multi-structural domain peptide amphiphile, highlighting five key structural features. Middle panel: Molecular model of the PA showing the overall conical shape of the molecule going from the narrow hydrophobic tail to the bulkier peptide region. Color scheme: C, black; H, white; O, red; N, blue; P, cyan; S, yellow. Bottom panel: Schematic showing the self-assembly of PA molecules into a cylindrical micelle. Adapted from (Hartgerink et al. 2001), with copyrights permission from the American Association for the Advancement of Science

Lipidated bolaamphiphiles are structurally similar to the previously discussed bolaamphiphilic peptides except that their hydrophobic regions are formed of alkyl chains instead of peptide sequences. Franceschi et al. have studied the self-assembly of a series of hydrogelating bolaamphiphiles with terminal carboxylic acids including the peptides, A-$(CH_2)_n$-A and H-$(CH_2)_n$-H, where $n = 10$, 12, and 20 (Franceschi et al. 1999). Depending on the length of the alkyl linker, different self-assembling nanostructures have been shown including micellar, vesicular, and fibrous structures. In a concentration-dependent fashion, the self-assembled nanovesicles generated from molecules with linkers of shorter lengths undergo transition to nanofibers. Only molecules with the longest methylene linkers ($n = 20$) showed hydrogel formation (Franceschi et al. 1999). In addition, bolaamphiphiles in which the head groups are composed of dipeptides with terminal carboxylic acids and connected by alkyl chain linkers of different methylene lengths ($n = 8$ or 10) have been thoroughly explored by Shimizu and co-workers (Kogiso et al. 1998). These molecules have shown different aggregation behaviors in response to pH changes and different pKa values depending on the linker length.

Gemini amphiphiles are another group of lipidated peptides which are structured with two hydrophilic head groups separated by a spacer, and each is attached to a terminal hydrophobic alkyl tail (Menger and Littau 1991; Menger and Keiper 2000). Although there is a wide range of gemini surfactants capable of self-assembly into hydrogels, there is only one study involving a peptide-based gemini amphiphile (Fig. 1.11b) (Rubio et al. 2012). Initially, Luis et al. had designed and studied the aggregation behavior of a series of simple gemini-like pseudopeptides structured from two amino acids connected at their C-termini by a flexible spacer, and each amino acid is tailed with a terminal hydrophobic alkyl chain (Rubio et al. 2012). Further self-assembly studies involved the synthesis of a more water-soluble derivative by incorporation of an N-atom in the middle of the spacer's structure. The head group is composed of a V residue which is N-substituted with decyloxybenzyl moiety. The spacer is responsible for the peptide's folding-unfolding patterns depending on the polarity of the medium. In a highly polar medium, the molecules undergo folding and self-assembly into bilayered vesicular structures where the spacers are exposed to water, and the hydrophobic tails are buried within the bilayer (Fig. 1.11b). The molecules have shown water-triggered self-assembly through van der Waals interaction between the hydrophobic tails. On the other hand, the extended peptide conformation preferably directed the self-assembly into fibrous nanostructures through intermolecular H-bonding driven by the centrally located polar pseudopeptidic spacer (Fig. 1.11b).

Another class of lipidated amphiphilic peptides with multi-structural domains comprises those designed by Stupp and co-workers (Webber et al. 2013; Hartgerink et al. 2001; Cui et al. 2014). Generally, the peptide amphiphilic molecule contains four basic structural segments (Fig. 1.11c). The first domain comprises a single long alkyl chain as the amphiphile's tail, which is connected to the N-terminus of the peptide and provides the hydrophobic nature of the molecule. The second domain comprises a β-sheet-forming peptide sequence driving the molecular cross-linking and self-assembly. The third domain is a peptide linker composed of three glycine

residues and provides flexibility to the hydrophilic part of the molecule against the rigidity of the cross-linked part. The fourth segment of the molecule comprises the hydrophilic head of amphiphile which acts as a target section for further functionalization such as binding to a cell targeting motif for biological applications. As the hydrophilic head has the largest cross-sectional area of the molecule, it is considered a key feature for self-assembly, giving the assembling unit its cone shape and thus leading to the formation of cylindrical micelles (Fig. 1.11c). Also, the same amphiphilic molecule can be functionalized with different epitopes through embranchment of the peptide's C-terminus using lysine dendron (Harrington et al. 2006; Guler et al. 2006; Guler et al. 2005). Moreover, the peptide amphiphile can be modified in the hydrophobic tail region by attaching more than one alkyl chain (Chen et al. 2011b) or replacing the alkyl tail by a cholesteryl group (Chen et al. 2011b; Hwang et al. 2002). One of the most widely studied examples of these peptides contains a cysteine stretch in the second part of the molecule which forms intermolecular disulfide bridges upon oxidation resulting in polymerization of the self-assembled structure (Fig. 1.11c). In addition, the hydrophilic head group in the fourth region is composed of a phosphorylated serine residue which is designed with the aim of directing mineralization through strong interaction with calcium ions. Furthermore, the hydrophilic head is functionalized with the cell adhesion RGD motif for biological applications, composing the fifth structural region of the molecule (Fig. 1.11c) (Hartgerink et al. 2001).

1.3.2.5 Short Aromatic Peptides

The use of short aromatic peptides for formation of higher-order self-assembled nanostructures has been bioinspired from the structure of amyloid fibrils which self-assemble and accumulate in response to various characteristic diseases including Alzheimer's and Parkinson's diseases and many others (Glabe 2006). It has been demonstrated that diphenylalanine comprises the core sequence of the β-sheet-forming amyloid peptides, and it can undergo self-assembly into stable hollow nanotubes on its own (Reches and Gazit 2003). It has been proposed that self-assembly is triggered by both intermolecular H-bonding between backbone amides and π–π stacking of the F aromatic rings (Reches and Gazit 2003). The self-assembled nanotubes showed significant rigidity and appear as a nanoforest of needles upon evaporation of the solvent (Fig. 1.12a) (Kol et al. 2005; Reches and Gazit 2006; Song et al. 2004). Also, diphenylglycine, the simpler analogue of diphenylalanine, can self-assemble into nanospheres in aqueous solutions (Reches and Gazit 2004). Moreover, diphenylalanine nanotubular self-assembly can be modified by introducing a thiol group into FF to form the tripeptide CFF through incorporation of a cysteine residue. This modified peptide has shown self-assembly into nanovesicles instead of nanotubes (Martin and Kohli 2003).

On the other hand, short peptides can gain aromaticity and self-assembling behavior through π–π stacking by capping the peptide with an aromatic group. For example, N-terminal conjugation of the peptide to an aromatic moiety such as
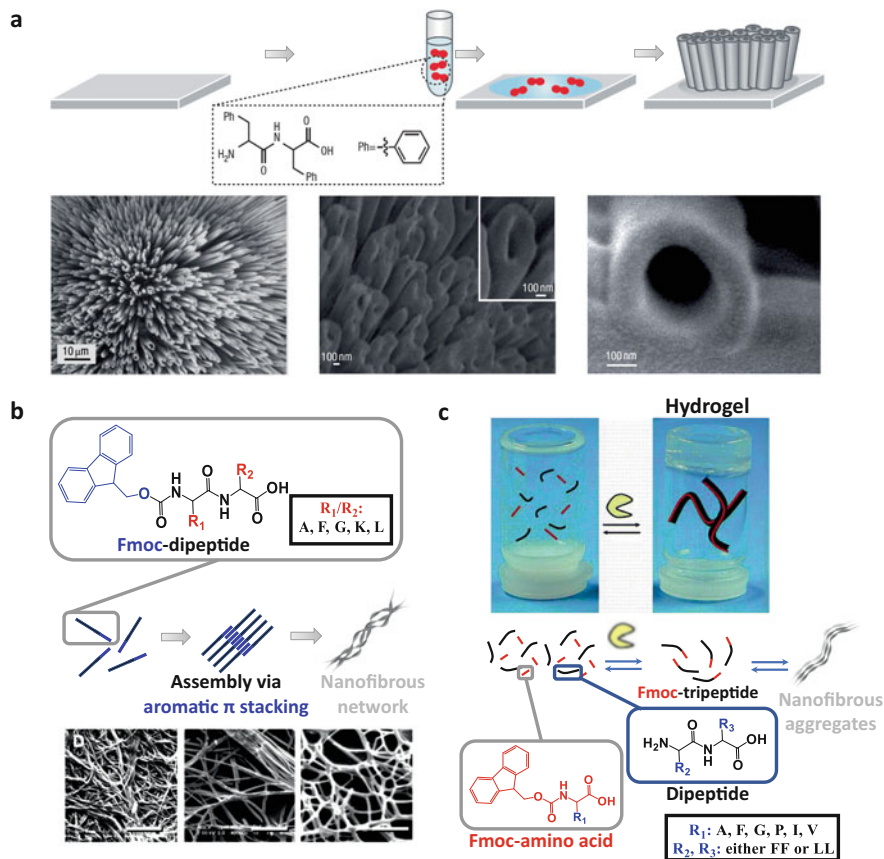
Fig. 1.12 (**a**) Vertically aligned diphenylalanine-based nanotubes self-assembled into a peptide nanoforest, the possible model for their formation and SEM photomicrographs. Adapted from (Reches and Gazit 2006), with copyrights permission from Springer Nature. (**b**) Molecular structure of Fmoc dipetides and their proposed self-assembly mechanism via aromatic π stacking of Fmoc groups into molecular stacks that further assemble to form nanofibers as shown in SEM. Adapted from (Jayawarna et al. 2006), with copyrights permission from John Wiley and Sons. (**c**) Proposed mechanism to form Fmoc tripeptides that self-assemble to higher-order aggregates by coupling Fmoc amino acids (red) to dipeptides (black) by a protease enzyme. Adapted from (Toledano et al. 2006), with copyrights permission from the American Chemical Society

fluorenylmethoxycarbonyl (Fmoc), naphthalene (Nap), or carbobenzyloxy (Cbz) has been shown to form stable and self-supporting hydrogels (Fig. 1.12b) (Yang et al. 2004; Jayawarna et al. 2006). The class of aromatic short peptides comprises a diverse group of peptide derivatives capable of self-assembly into various shaped and sized nanostructures depending both on the mechanism of self-assembly and the physicochemical properties of the peptide building units (Reches and Gazit 2003; Reches and Gazit 2006; Jayawarna et al. 2006; Smith et al. 2008; Toledano et al. 2006). Gazit et al. and Ulijn et al. have reported that (Fmoc) protection of

diphenylalanine led to its self-assembly in aqueous solutions into nanofibrillar structures which further network into a hydrogel (Fig. 1.12b) (Yemini et al. 2005; Jayawarna et al. 2006; Smith et al. 2008; Toledano et al. 2006; Cherny and Gazit 2008; Findeis et al. 1999; Soto et al. 1998; Mahler et al. 2006). The formed hydrogel has shown to behave in a similar rheological pattern to that of solid-like gel materials and exhibit a significant stability against a wide range of pH values and temperatures (Smith et al. 2008). This model peptide, Fmoc-FF, self-assembles into antiparallel β-sheet structures stabilized through π–π interactions between Fmoc groups on alternating sides. As such, Fmoc groups can be regarded as a zipper which packs the adjacent sheets together in a twisted shape generating the characteristic cylindrical structure (Fig. 1.12b) (Smith et al. 2008). Other dipeptides with N-terminal Fmoc protection have been reported by Vegners et al. (Vegners et al. 1995). These anionic peptides including Fmoc-AD, Fmoc-LD, and Fmoc-ID have showed hydrogel formation and were used for incorporation of antiviral drug derivatives (Cherny and Gazit 2008). Also, as reported by Zhang et al., hydrogels can be formed with high efficiency from other Fmoc-protected dipeptides such as Fmoc-^{D}A^{D}A, Fmoc-AA, Fmoc-GG, Fmoc-G^{D}A, and Fmoc-GS (Zhang et al. 2003). Interestingly, these peptide hydrogels have showed a biological specificity towards ligand-receptor interactions where they showed different binding affinities and sensitivities to vancomycin.

Interestingly, enzyme-triggered self-assembly of short peptides has been exploited via reverse hydrolysis. Hydrolytic proteases such as thermolysin, which has a catalytic preference on the *N*-terminal hydrophobic/aromatic residues, was used to couple the non-gelling Fmoc-capped non-polar amino acids with dipeptides to form Fmoc-tripeptides, capable of self-assembling into higher-order structures stabilized by aromatic stacking of Fmoc groups (Toledano et al. 2006). For example, Fmoc-capped amino acids (such as A, V, F, L) and FF dipeptides were coupled through thermolysin-triggered reverse hydrolysis to form Fmoc-AFF, Fmoc-VFF, Fmoc-FFF, and Fmoc-LFF which self-assembled into nanofibrous hydrogels above a critical concentration (Cherny and Gazit 2008). Similarly, lipase enzyme was used to trigger the self-assembly of Fmoc-F and FF through the formation of the gelling peptide Fmoc-FFF via a reverse hydrolysis process (Chronopoulou et al. 2010).

Collagen-like short peptides capped with aromatic moieties have also been developed as self-assembling hydrogelators. For instance, hydrogelation was attained with G-X-Hyp short collagen-based sequences capped with a naphthyl (Nap)-group (e.g., Nap-G-F-F-Y-G-G-**X**-Hyp) (Hu et al. 2010). This is attributed to the stabilization of assembly through π–π stacking, governed by the aromatic moieties conjugated at the C- and N-termini of the individual helical strands (G-P-Hyp)$_n$ which enhance the head-to-tail assembly of triple-helical subunits (Cejas et al. 2007). Nap-capped short peptides have shown to undergo hydrogelation in phosphate-buffered saline with the strongest hydrogel seen from the K-containing peptide, which has also shown to be the best cell scaffold out of the investigated sequences (Hu et al. 2010). This is attributed to the cationic K residues which introduced anchoring points for attachment of negatively charged cell membranes (Hu et al. 2010). Moreover, an ultrashort collagen-like peptide sequence,

Nap-FFGSO was designed to undergo co-assembly in the presence of short laminin mimetic peptides into composite hydrogel scaffolds to simulate the structure of extracellular matrix. Self-assembly of the inherently non-gelling Nap-FFGSO peptide into nanofibrous hydrogel was triggered by laminin-like peptides which act as nuclei for nanofibers formation and growth (Jain and Roy 2019).

In addition to short aromatic peptides, aromatic structures as short as a single amino acid can undergo self-assembly leading to hydrogel formation. A phenylalanine protected with a cinnamoyl group can be regarded as the smallest studied hydrogelator so far. Also, phenylalanine and tyrosine with N-terminal protection have shown efficient self-assembly and hydrogelation at low concentrations ranging 0.1–2 wt% (Shi et al. 2011). The self-assembling behavior of single amino acids with Fmoc-protection has been studied by Xu and co-workers who were the first to report the ability of these molecules to form fibrillar structures and subsequent hydrogels. For example, a mixture of Fmoc-K and Fmoc-V has shown co-assembly and hydrogel formation at basic pH values (Shi et al. 2011).

Self-assembling systems based on aromatic short peptides have been widely investigated for formation of different nanostructures and generation of self-supporting hydrogels with tunable mechanical and physicochemical properties through de novo synthesis of many peptide derivatives and aromatic substitutions which have been involved in various biomedical applications.

1.3.2.6 Cyclic Peptides

In the early 1970s, cyclic peptides composed of alternating D- and L-amino acids were theoretically identified to undergo self-assembly into tubular nanostructures (De Santis et al. 1974). However, these self-assembling peptides had not found their way from theory to practicality till the early 1990s, when Ghadiri and co-workers synthesized the first self-assembling cyclic peptide capable of forming nanotubes (Ghadiri et al. 1993). The synthesized peptide sequence of cyclo-$(^LQ^DA^LE^DA)_2$ was capable of forming extended hollow cylindrical structures through β-sheet-like assembly upon stacking to one another (Fig. 1.13a and Table 1.2) (Ghadiri et al. 1993; Ghadiri et al. 1994).

Basically, the monomers of cyclic peptides have shown to adopt a planar ring conformation with their amides and carbonyls positioned perpendicular to the ring, while the peptide side chains are directed outward (Chapman et al. 2012). These monomeric rings act as the basic building units which by stacking undergo self-assembly into nanotubes with antiparallel β-sheet structures stabilized through intermolecular H-bonding (Fig. 1.13a) (Chapman et al. 2012; Fernandez-Lopez et al. 2001).

Interestingly, the physical and chemical properties of the self-assembled nanotubes can be efficiently tailored by controlling the peptide sequence and length. Both H-bonding pattern and diameter of nanotubes are controlled by the type of amino acids used in the sequence, which could be α-amino acids with alternating D- and L-isomers, β-amino acids, alternating α- and β-amino acids, alternating α- and
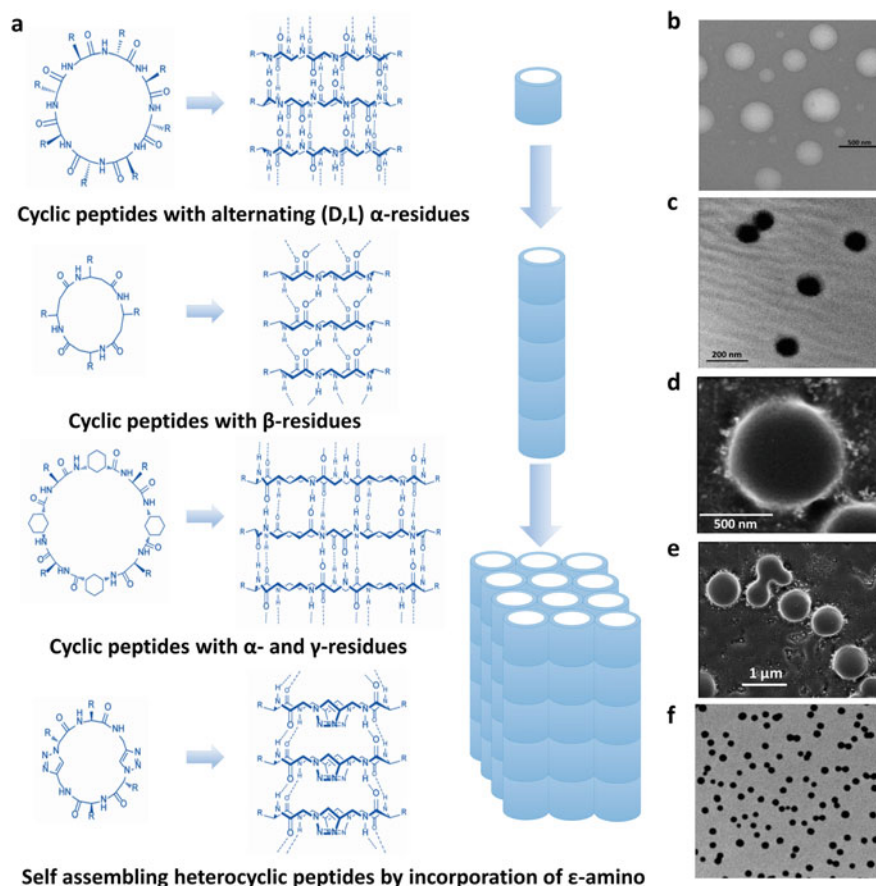
Fig. 1.13 (**a**) Cyclic peptides assembly into nanotubes and nanotube arrays through inter-chain H-bonding between backbone amides. Left panel showing H-bonding patterns adopted with different types of amino acid residues used. Right panel depict hierarchical growth of cyclic peptides into nanotubes and nanotube arrays. Adapted from (Chapman et al. 2012), with copyrights permission from the Royal Society of Chemistry. (**b**) TEM images of self-assembled structures of [WR]4 in water after 2 weeks (without negative staining). (**d**) and (**e**) FE-SEM image of self-assembled structure of [WR]5 (2 mM) in water after 20 days. (**c**) TEM images of self-assembled structures of [WR]3 in water after 14 days (without negative staining). (**f**) TEM images of self-assembled structures of [WR]5 in water after 14 days (without negative staining). Microscopy images (**b**–**f**) are adapted from (Tu and Tirrell 2004), with copyrights permission from the Royal Society of Chemistry

γ-amino acids, δ-amino acids, and oligoureas (Fig. 1.13a) (Chapman et al. 2012; Montenegro et al. 2013; Ishihara and Kimura 2010; Guerra et al. 2012). Also, nanotube diameter can be precisely controlled through changing the number of amino acid residues per peptide. As such, increasing the peptide's length from 4 to 12 amino acid residues could result in a corresponding increase in the peptide's

Table 1.2 Gives an overview of the main self-assembling cyclic peptides reported and the morphology of the formed self-assembling structures

Cyclic peptide	Peptide sequence	Morphology of self-assembled structures	Reference
α-Amino acids with alternating D- and L-isomers	c-$(^LQ^DA^LE^DA)_2$	–Nanotubes (7–8°A diameter), assemble into rod-like crystals –Nanoparticles	Hartgerink et al. (1996) and Sun et al. (2015)
L-amino acids	c-[WR]4	Nanospheres (550 nm diameter)	Mandal et al. (2013)
	c-[WR]3	Nanospheres (100 nm diameter)	Mandal et al. (2013)
	c-[WR]5	Nanospheres (930 nm diameter)	Mandal et al. (2013)

internal diameter from 2 to 13°A (Whitesides and Grzybowski 2002; Chapman et al. 2012; Hartgerink et al. 1996). However, peptides with an even number of amino acid residues are hypothesized to show a low-energy planar ring conformation. Nanotubes of varying functions can be formed from peptides of different chemical properties though modification of the peptide side chains (Chapman et al. 2012).

The parent peptide of this class, the octapeptide cyclo-$(^LQ^DA^LE^DA)_2$, undergoes spontaneous self-assembly in acidic media into nanotubular structures of an internal diameter ranging 7–8°A, which further aggregate to form rod-like crystals resulting from tight packing of hundreds of nanotubes (Hartgerink et al. 1996). Moreover, this cyclic peptide can also self-assemble into nanoparticles through the use of different methods and tunable self-assembly parameters (Sun et al. 2015). It has been found that the morphology and the size of the self-assembled nanostructures were greatly affected by the changes in peptide concentration and pH values, modification of peptide's side chains, different reaction and sonication times, and stirring intensity (Sun et al. 2015).

In essence, cyclic peptides can also undergo self-assembly into spherical nanostructures. For example, cyclic peptides containing alternating W and R residues have been reported to form nanospherical assemblies (Lim et al. 2007). Namely, the L-amino acids-based cyclic octapeptide c-[WR]4 has shown self-assembly into nanospheres in aqueous solutions at room temperature. The peptide's self-assembly has been found to occur through a combination of the hydrophobic interactions governed by the high hydrophobic nature of the tryptophan's indole ring in addition to their π–π stacking and intermolecular H-bonding between the positively charged guanidine groups of R residues (Mandal et al. 2013). As indicated by TEM, this peptide has shown nanospherical structures with a diameter of 550 nm (Fig. 1.13b and Table 1.2). However, for investigating the effect of ring size on self-assembly, a shorter and a longer peptide sequence of the same peptide has been designed including the hexapeptide c-[WR]3 and the decapeptide c-[WR]5, respectively. Both peptides have shown self-assembly into spherical nanostructures of varying sizes (Fig. 1.13c–f and Table 1.2). The peptide c-[WR]3 has formed

nanospheres sized 100 nm after an incubation period of 14 days (Fig. 1.13c), while in case of the peptide *c*-[WR]5 nanospherical structures sized 930 nm have been observed (Fig. 1.13d–f and Table 1.2) (Mandal et al. 2013).

1.4 Summary

Nature is undoubtedly the main source of inspiration for designing self-assembling peptides capable of forming a wide range of functional nanostructures such as nanofibers, nanotubes, ribbons, nanospheres, micelles, etc. Mimicry of protein domains combined with deep understanding of both physicochemical and structural features of amino acid building units and how these features govern the involvement of these residues in both covalent and non-covalent interactions are all crucial for the rational design of such peptide-based nanomaterials. Also, understanding of higher levels of hierarchical organization is key for fine-tuning the molecular, nanoscopic/ mesoscopic, and bulk material properties. Combining this knowledge enables bio-materials engineers to fully control the peptidic nanomaterials over the length scale and thus facilitates tailoring fit for purpose materials that can meet the desired biomedical application needs.

References

Adamson JG, Zhou NE, Hodges RS (1993) Structure, function and application of the coiled-coil protein folding motif. Curr Opin Biotechnol 4(4):428–437

Aggeli A, Bell M, Boden N, Keen JN, McLeish TCB, Nyrkova I, Radford SE, Semenov A (1997) Engineering of peptide β-sheet nanotapes. J Mater Chem 7:1135–1145

Aggeli A, Nyrkova IA, Bell M, Harding R, Carrick L, McLeish TCB, Semenov AN, Boden N (2001) Hierarchical self-assembly of chiral rod-like molecules as a model for peptide beta-sheet tapes, ribbons, fibrils, and fibers. Proc Natl Acad Sci U S A 98(21):11857–11862

Aigner T, Stöve J (2003) Collagens—major component of the physiological cartilage matrix, major target of cartilage degeneration, major tool in cartilage repair. Adv Drug Deliv Rev 55(12): 1569–1593

Aluigi A, Varesano A, Montarsolo A, Vineis C, Ferrero F, Mazzuchetti G, Tonin C (2007) Electrospinning of keratin/poly(ethylene oxide) blend nanofibers. J Appl Polym Sci 104:863–870

Aluigi A, Vineis C, Varesano A, Mazzuchetti G, Ferrero F, Tonin C (2008) Structure and properties of keratin/PEO blend nanofibres. Eur Polym J 44:2465–2475

Andersen SO (1964) The cross-links in resilin identified as dityrosine and trityrosine. Biochim Biophys Acta 93:213–215

Antonietti M, Forster S (2003) Vesicles and liposomes: a self-assembly principle beyond lipids. Adv Mater Deerfeld 15(16):1323–1333

Ardell DH, Andersen SO (2001) Tentative identification of a resilin gene in *Drosophila melanogaster*. Insect Biochem Mol Biol 31(10):965–970

Balu R, Dutta NK, Dutta AK, Choudhury NR (2021) Resilin-mimetics as a smart biomaterial platform for biomedical applications. Nat Commun 12(1):149

Banwell EF, Abelardo ES, Adams DJ, Birchall MA, Corrigan A, Donald AM, Kirkland M, Serpell LC, Butler MF, Woolfson DN (2009) Rational design and application of responsive alpha-helical peptide hydrogels. Nat Mater 8(7):596–600

Basak S, Singh I, Ferranco A, Syed J, Kraatz HB (2017) On the role of chirality in guiding the self-assembly of peptides. Angew Chem Int Ed Engl 56(43):13288–13292

Behanna HA, Donners JJ, Gordon AC, Stupp SI (2005) Coassembly of amphiphiles with opposite peptide polarities into nanofibers. J Am Chem Soc 127(4):1193–1200

Bera S, Xue B, Rehak P, Jacoby G, Ji W, Shimon LJW, Beck R, Král P, Cao Y, Gazit E (2020) Self-assembly of aromatic amino acid enantiomers into supramolecular materials of high rigidity. ACS Nano 14(2):1694–1706

Berg JM, Tymoczko JL, Stryer L (2012) Biochemistry, 7th edn. W. H. Freeman, New York, pp 42–43

Berg RA, Prockop DJ (1973) The thermal transition of a non-hydroxylated form of collagen. Evidence for a role for hydroxyproline in stabilizing the triple-helix of collagen. Biochem Biophys Res Commun 52(1):115–120

Bessa PC, Machado R, Nürnberger S, Dopler D, Banerjee A, Cunha AM, Rodríguez-Cabello JC, Redl H, van Griensven M, Reis RL, Casal M (2010) Thermoresponsive self-assembled elastin-based nanoparticles for delivery of BMPs. J Control Release 142(3):312–318

Betre H, Setton LA, Meyer DE, Chilkoti A (2002) Characterization of a genetically engineered elastin-like polypeptide for cartilaginous tissue repair. Biomacromolecules 3(5):910–916

Betush RJ, Urban JM, Nilsson BL (2018) Balancing hydrophobicity and sequence pattern to influence self-assembly of amphipathic peptides. Biopolymers

Bochicchio B, Pepe A, Tamburro AM (2008) Investigating by CD the molecular mechanism of elasticity of elastomeric proteins. Chirality 20(9):985–994

Boothroyd S, Millerb AF, Saiani A (2013) From fibres to networks using self-assembling peptides. Faraday Discuss 166:195–207

Boudko SP, Engel J (2004) Structure formation in the C terminus of type III collagen guides disulfide cross-linking. J Mol Biol 335(5):1289–1297

Bowerman CJ, Nilsson BL (2012) Review self-assembly of amphipathic β-sheet peptides: insights and applications. Pept Sci 98:69–184

Bowerman CJ, Ryan DM, Nissan DA, Nilsson BL (2009) The effect of increasing hydrophobicity on the self-assembly of amphipathic beta-sheet peptides. Mol BioSyst 5(9):1058–1069

Branco MC, Nettesheim F, Pochan DJ, Schneider JP, Wagner NJ (2009) Fast dynamics of semiflexible chain networks of self-assembled peptides. Biomacromolecules 10(6):1374–1380

Breedveld V, Nowak AP, Sato J, Deming TJ, Pine DJ (2004) Rheology of block copolypeptide solutions: hydrogels with tunable properties. Macromolecules 37:3943–3953

Cameron LM, Fyles TM, Hu C (2002) Synthesis and membrane activity of a bis(metacyclophane)-bolaamphiphile. J Org Chem 67(5):1548–1553

Capes JS, Kiley PJ, Windle AH (2010) Investigating the effect of pH on the aggregation of two surfactant-like octapeptides. Langmuir 26(8):5637–5644

Caplan MR, Moore PN, Zhang S, Kamm RD, Lauffenburger DA (2000) Self-assembly of a beta-sheet protein governed by relief of electrostatic repulsion relative to van der Waals attraction. Biomacromolecules 1(4):627–631

Caplan MR, Schwartzfarb EM, Zhang S, Kamm RD, Lauffenburger DA (2002) Control of self-assembling oligopeptide matrix formation through systematic variation of amino acid sequence. Biomaterials 23(1):219–227

Cejas MA, Kinney WA, Chen C, Leo GC, Tounge BA, Vinter JG, Joshi PP, Maryanoff BE (2007) Collagen-related peptides: self-assembly of short, single strands into a functional biomaterial of micrometer scale. J Am Chem Soc 129(8):2202–2203

Cejas MA, Kinney WA, Chen C, Vinter JG, Almond HR Jr, Balss KM, Maryanoff CA, Schmidt U, Breslav M, Mahan A, Lacy E, Maryanoff BE (2008) Thrombogenic collagen-mimetic peptides: self-assembly of triple helixc-based fibrils driven by hydrophobic interactions. Proc Natl Acad Sci U S A 105(25):8513–8518

Chapman R, Danial M, Koh ML, Jolliffe KA, Perrier S (2012) Design and properties of functional nanotubes from the self-assembly of cyclic peptide templates. Chem Soc Rev 41(18): 6023–6041

Chen CC, Hsu W, Kao TC, Horng JC (2011a) Self-assembly of short collagen-related peptides into fibrils via cation-π interactions. Biochemistry 50(13):2381–2383

Chen J-X, Wang H-Y, Li C, Han K, Zhang X-Z, Zhuo R-X (2011b) Construction of surfactant-like tetra-tail amphiphilic peptide with RGD ligand for encapsulation of porphyrin for photodynamic therapy. Biomaterials 32(6):1678–1684

Chen Q, Liang S, Thouas GA (2013) Elastomeric biomaterials for tissue engineering. Prog Polym Sci 38:584–671

Chen S, Berthelier V, Hamilton JB, O'Nuallain B, Wetzel R (2002) Amyloid-like features of polyglutamine aggregates and their assembly kinetics. Biochemistry 41(23):7391–7399

Chen Y, Qiu F, Lu Y, Shi Y-K, Zhao X (2009) Geometrical shape of hydrophobic section determines the self-assembling structures of peptide detergents and bolaamphiphilic peptides. Curr Nanosci 5(1):69–74

Cherny I, Gazit E (2008) Amyloids: not only pathological agents but also ordered nanomaterials. Angew Chem Int Ed Engl 47(22):4062–4069

Chiti F, Dobson CM (2006) Protein misfolding, functional amyloid, and human disease. Annu Rev Biochem 75:333–366

Chronopoulou L, Lorenzoni S, Masci G, Dentini M, Togna AR, Togna G, Bordi F, Palocci C (2010) Lipase-supported synthesis of peptidic hydrogels. Soft Matter 6(11):2525–2532

Claussen RC, Rabatic BM, Stupp SI (2003) Aqueous self-assembly of unsymmetric peptide bolaamphiphiles into nanofbers with hydrophilic cores and surfaces. J Am Chem Soc 125(42):12680–12681

Clover TM, O'Neill CL, Appavu R, Lokhande G, Gaharwar AK, Posey AE, White MA, Rudra JS (2020) Self-assembly of block heterochiral peptides into helical tapes. J Am Chem Soc 142(47): 19809–19813

Coles GC (1966) Studies on resilin biosynthesis. J Insect Physiol 12(6):679–691

Collier JH, Segura T (2011) Evolving the use of peptides as components of biomaterials. Biomaterials 32(18):4198–4204

Coulombe PA, Bousquet O, Ma L, Yamada S, Wirtz D (2000) The 'ins' and 'outs' of intermediate filament organization. Trends Cell Biol 10(10):420–428

Cram DJ (1988) The design of molecular hosts, guests, and their complexes. Science 240(4853): 760–767

Crick FHC (1953) The packing of α-helices: simple coiled-coils. Acta Crystallogr 6:689–697

Cui H, Cheetham AG, Pashuck ET, Stupp SI (2014) Amino acid sequence in constitutionally isomeric tetrapeptide amphiphiles dictates architecture of one-dimensional nanostructures. J Am Chem Soc 136(35):12461–12468

Dai B, Kang SG, Huynh T, Lei H, Castelli M, Hu J, Zhang Y, Zhou R (2013) Salts drive controllable multilayered upright assembly of amyloid-like peptides at mica/water interface. Proc Natl Acad Sci U S A 110(21):8543–8548

Dawson WM, Martin FJO, Rhys GG, Shelley KL, Brady RL, Woolfson DN (2021) Coiled coils 9-to-5: rational de novo design of α-helical barrels with tunable oligomeric states. Chem Sci 12(20):6923–6928

De Santis P, Forni E, Rizzo R (1974) Conformational analysis of DNA-basic polypeptide complexes: possible models of nucleoprotamines and nucleohistones. Biopolymers 13(2):313–326

Deming T (2012) Peptide-based materials. Springer Science &. Business Media, Berlin, p 310

Deming TJ (2005) Polypeptide hydrogels via a unique assembly mechanism. Soft Matter 1:28–35

Dong H, Paramonov SE, Hartgerink JD (2008) Self-assembly of alpha-helical coiled coil nanofibers. J Am Chem Soc 130(41):13691–13695

Doran TM, Kamens AJ, Byrnes NK, Nilsson BL (2012) Role of amino acid hydrophobicity, aromaticity, and molecular volume on IAPP (20-29) amyloid self-assembly. Proteins 80(4): 1053–1065

Elsawy MA, Smith AM, Hodson N, Squires A, Miller AF, Saiani A (2016) Modification of β-sheet forming peptide hydrophobic face: effect on self-assembly and gelation. Langmuir 32(19): 4917–4923

Elvin CM, Carr AG, Huson MG, Maxwell JM, Pearson RD, Vuocolo T, Liyou NE, Wong DC, Merritt DJ, Dixon NE (2005) Synthesis and properties of crosslinked recombinant pro-resilin. Nature 437(7061):999–1002

Engel J (2005) In: Brinckmann J, Notbohm H, Muller PK (eds) Collagen: primer in structure, processing and assembly, vol 247. Springer-Verlag, Berlin, p 7

Eskandari S, Guerin T, Toth I, Stephenson RJ (2017) Recent advances in self-assembled peptides: implications for targeted drug delivery and vaccine engineering. Adv Drug Deliv Rev 110-111: 169–187

Fallas JA, Dong J, Tao YJ, Hartgerink JD (2012) Structural insights into charge pair interactions in triple helical collagen-like proteins. J Biol Chem 287(11):8039–8047

Fernandez-Lopez S, Kim HS, Choi EC, Delgado M, Granja JR, Khasanov A, Kraehenbuehl K, Long G, Weinberger DA, Wilcoxen KM, Ghadiri MR (2001) Antibacterial agents based on the cyclic D, L-alpha-peptide architecture. Nature 412(6845):452–455

Ferroni C, Varchi G (2021) Keratin-based nanoparticles as drug delivery carriers. Appl Sci 11(20): 9417

Fersht A (1999) Structure and mechanism in protein science: a guide to enzyme catalysis and protein folding. Freeman, New York

Feynman RP (1959) There's plenty of room at the bottom. Caltech Eng Sci 23(5):22–36

Findeis MA, Musso GM, Arico-Muendel CC, Benjamin HW, Hundal AM, Lee JJ, Chin J, Kelley M, Wakefield J, Hayward NJ, Molineaux SM (1999) Modified-peptide inhibitors of amyloid beta-peptide polymerization. Biochemistry 38(21):6791–6800

Franceschi S, Viguerie N, Riviere M, Lattes A (1999) Synthesis and aggregation of two-headed surfactants bearing amino acid moieties. New J Chem 23(4):447–452

Fraser RD, MacRae TP, Parry DA, Suzuki E (1986) Intermediate filaments in alpha-keratins. Proc Natl Acad Sci U S A 83(5):1179–1183. Erratum in: Proc Natl Acad Sci U S A 1986;83(17):6664

Fujii T, Ide Y (2004) Preparation of translucent and flexible human hair protein films and their properties. Biol Pharm Bull 27(9):1433–1436

Galloway JM, Bray HEV, Shoemark DK, Hodgson LR, Coombs J, Mantell JM, Rose RS, Ross JF, Morris C, Harniman RL, Wood CW, Arthur C, Verkade P, Woolfson DN (2021) De novo designed peptide and protein hairpins self-assemble into sheets and nanoparticles. Small 17(10): e2100472

Gamo T, Inokuchi T, Laufer H (1977) Polypeptides of fibroin and sericin secreted from the different sections of the silk gland in Bombyx mori. Insect Biochem 7(3):285–295

Gao J, Tang C, Elsawy MA, Smith AM, Miller AF, Saiani A (2017) Controlling self-assembling peptide hydrogel properties through network topology. Biomacromolecules 18(3):826–834

Gao P, Zhan C, Liu M (2006) Controlled synthesis of double- and multiwall silver nanotubes with template organogel from a bolaamphiphile. Langmuir 22(2):775–779

Gauba V, Hartgerink JD (2007) Self-assembled heterotrimeric collagen triple helices directed through electrostatic interactions. J Am Chem Soc 129(9):2683–2690. Erratum in: J Am Chem Soc. 2007 Jul 18;129(28):8921

Gaucheron J, Santaella C, Vierling P (2001) In vitro gene transfer with a novel galactosylated spermine bolaamphiphile. Bioconjug Chem 12(4):569–575

Gelain F, Luo Z, Rioult M, Zhang S (2021) Self-assembling peptide scaffolds in the clinic. NPJ Regen Med 6(1):9

Gelse K, Pöschl E, Aigner T (2003) Collagens—structure, function, and biosynthesis. Adv Drug Deliv Rev 55(12):1531–1546

Ghadiri MR, Granja JR, Buehler LK (1994) Artificial transmembrane ion channels from self-assembling peptide nanotubes. Nature 369(6478):301–304

Ghadiri MR, Granja JR, Milligan RA, McRee DE, Khazanovich N (1993) Self-assembling organic nanotubes based on a cyclic peptide architecture. Nature 366(6453):324–327

Glabe CG (2006) Common mechanisms of amyloid oligomer pathogenesis in degenerative disease. Neurobiol Aging 27(4):570–575

Gosline JM (1980) The elastic properties of rubber-like proteins and highly extensible tissues. Symp Soc Exp Biol 34:332–357

Guerra A, Brea RJ, Amorin M, Castedo L, Granja JR (2012) Self-assembling properties of all gamma-cyclic peptides containing sugar amino acid residues. Org Biomol Chem 10(44): 8762–8766

Guilbaud JB, Rochas C, Miller AF, Saiani A (2013) Effect of enzyme concentration of the morphology and properties of enzymatically triggered peptide hydrogels. Biomacromolecules 14(5):1403–1411

Guilbaud JB, Vey E, Boothroyd S, Smith AM, Ulijn RV, Saiani A, Miller AF (2010) Enzymatic catalyzed synthesis and triggered gelation of ionic peptides. Langmuir 26(13):11297–11303

Guler MO, Hsu L, Soukasene S, Harrington DA, Hulvat JF, Stupp SI (2006) Presentation of RGDS epitopes on self-assembled nanofbers of branched peptide amphiphiles. Biomacromolecules 7(6):1855–1863

Guler MO, Soukasene S, Hulvat JF, Stupp SI (2005) Presentation and recognition of biotin on nanofbers formed by branched peptide amphiphiles. Nano Lett 5(2):249–252

Haider M, Megeed Z, Ghandehari H (2004) Genetically engineered polymers: status and prospects for controlled release. J Control Release 95(1):1–26

Haines LA, Rajagopal K, Ozbas B, Salick DA, Pochan DJ, Schneider JP (2005) Light-activated hydrogel formation via the triggered folding and self-assembly of a designed peptide. J Am Chem Soc 127(48):17025–17029

Haines-Butterick L, Rajagopal K, Branco M, Salick D, Rughani R, Pilarz M, Lamm MS, Pochan DJ, Schneider JP (2007) Controlling hydrogelation kinetics by peptide design for three-dimensional encapsulation and injectable delivery of cells. Proc Natl Acad Sci U S A 104(19):7791–7796

Hamley IW (2011) Self-assembly of amphiphilic peptides. Soft Matter 7(9):4122–4138

Hamley IW (2012) The amyloid beta peptide: a chemist's perspective. Role in Alzheimer's and fibrillization. Chem Rev 112(10):5147–5192

Han TH, Oh JK, Lee G-J, Pyun S-I, Kim SO (2010) Hierarchical assembly of diphenylalanine into dendritic nanoarchitectures. Colloids Surf B: Biointerfaces 79(2):440–445

Harrington DA, Cheng EY, Guler MO, Lee LK, Donovan JL, Claussen RC, Stupp SI (2006) Branched peptide-amphiphiles as self-assembling coatings for tissue engineering scaffolds. J Biomed Mater Res A 78(1):157–167

Hartgerink JD, Beniash E, Stupp SI (2001) Self-assembly and mineralization of peptide-amphiphile nanofibers. Science 294(5547):1684–1688

Hartgerink JD, Granja JR, Milligan RA, Ghadiri MR (1996) Self-assembling peptide nanotubes. J Am Chem Soc 118(1):43–50

Hauser CA, Zhang S (2010a) Designer self-assembling peptide nanofiber biological materials. Chem Soc Rev 39(8):2780–2790

Hauser CAE, Zhang S (2010b) Designer self-assembling peptide materials for diverse applications. Macromol Symp 295(1):30–48

He M, Wang L, Wu J, Xiao J (2016) Ln^{3+} −mediated self-assembly of a collagen peptide into luminescent banded helical nanoropes. Chemistry 22(6):1914–1917

Hinterding K, Alonso-Díaz D, Waldmann H (1998) Organic synthesis and biological signal transduction. Angew Chem Int Ed Engl 37(6):688–749

Hodges RS (1996) *De novo* design of alpha-helical proteins: basic research to medical applications. Biochem Cell Biol 74(2):133–154

Holowka EP, Pochan DJ, Deming TJ (2005) Charged polypeptide vesicles with controllable diameter. J Am Chem Soc 127(35):12423–12428

Hong Y, Pritzker MD, Legge RL, Chen P (2005) Effect of NaCl and peptide concentration on the self-assembly of an ionic-complementary peptide EAK16-II. Colloids Surf B Biointerfaces 46(3):152–161

Hosseinkhani H, Hong PD, Yu DS (2013) Self-assembled proteins and peptides for regenerative medicine. Chem Rev 113(7):4837–4861

Hsu W, Chen YL, Horng JC (2012) Promoting self-assembly of collagen-related peptides into various higher-order structures by metal-histidine coordination. Langmuir 28(6):3194–3199

Hu Y, Wang H, Wang J, Wang S, Liao W, Yang Y, Zhang Y, Kong D, Yang Z (2010) Supramolecular hydrogels inspired by collagen for tissue engineering. Org Biomol Chem 8(14):3267–3271

Huang RL, Qi W, Su RX, Zhao J, He ZM (2011) Solvent and surface controlled self-assembly of diphenylalanine peptide: from microtubes to nanofbers. Soft Matter 7(14):6418–6421

Huang W, Tarakanova A, Dinjaski N, Wang Q, Xia X, Chen Y, Wong JY, Buehler MJ, Kaplan DL (2016) Design of multistimuli responsive hydrogels using integrated modeling and genetically engineered silk-elastin-like proteins. Adv Funct Mater 26(23):4113–4123

Hule RA, Nagarkar RP, Hammouda B, Schneider JP, Pochan DJ (2009) Dependence of self-assembled peptide hydrogel network structure on local fibril nanostructure. Macromolecules 42(18):7137–7145

Hüttl C, Hettrich C, Miller R, Paulke BR, Henklein P, Rawel H, Bier FF (2013) Self-assembled peptide amphiphiles function as multivalent binder with increased hemagglutinin affinity. BMC Biotechnol 18(13):51

Hwang JJ, Iyer SN, Li L-S, Claussen R, Harrington DA, Stupp SI (2002) Self-assembling biomaterials: liquid crystal phases of cholesteryl oligo(l-lactic acid) and their interactions with cells. Proc Natl Acad Sci U S A 99(15):9662–9667

Ishihara Y, Kimura S (2010) Nanofiber formation of amphiphilic cyclic tri-beta-peptide. J Peptide Sci 16(2):110–114

Jain R, Roy S (2019) Designing a bioactive scaffold from coassembled collagen–laminin short peptide hydrogels for controlling cell behaviour. RSC Adv 9:38745–38759

Jang S, Yuan JM, Shin J, Measey TJ, Schweitzer-Stenner R, Li FY (2009) Energy landscapes associated with the self-aggregation of an alanine-based oligopeptide (AAKA)4. J Phys Chem B 113(17):6054–6061

Jayawarna V, Ali M, Jowitt TA, Miller AE, Saiani A, Gough JE, Ulijn RV (2006) Nanostructured hydrogels for three-dimensional cell culture through self-assembly of fluorenylmethoxycarbonyl-dipeptides. Adv Mater 18:611–614

Jia X, Kiick KL (2009) Hybrid multicomponent hydrogels for tissue engineering. Macromol Biosci 9(2):140–156

Jiang T, Xu C, Liu Y, Liu Z, Wall JS, Zuo X, Lian T, Salaita K, Ni C, Pochan D, Conticello VP (2014) Structurally defined nanoscale sheets from self-assembly of collagen-mimetic peptides. J Am Chem Soc 136(11):4300–4308

Katchalski E, Sela M (1958) Synthesis and chemical properties of poly-alpha-amino acids. Adv Protein Chem 13:243–492

Katoh K, Shibayama M, Tanabe T, Yamauchi K (2004) Preparation and properties of keratin-poly (vinyl alcohol) blend fiber. J Appl Polym Sci 91:756–762

Khoe U, Yang Y, Zhang S (2009) Self-assembly of nanodonut structure from a cone-shaped designer lipid-like peptide surfactant. Langmuir 25(7):4111–4114

King PJ, Giovanna Lizio M, Booth A, Collins RF, Gough JE, Miller AF, Webb SJ (2016) A modular self-assembly approach to functionalised β-sheet peptide hydrogel biomaterials. Soft Matter 12(6):1915–1923

Kisiday J, Jin M, Kurz B, Hung H, Semino C, Zhang S, Grodzinsky AJ (2002) Self-assembling peptide hydrogel fosters chondrocyte extracellular matrix production and cell division: implications for cartilage tissue repair. Proc Natl Acad Sci U S A 99(15):9996–10001

Kogiso M, Hanada T, Yase K, Shimizu T (1998) Intralayer hydrogen-bond-directed self-assembly of nano-fibers from dicarboxylic valylvaline bolaamphiphiles. Chem Commun 17:1791–1792

Kohn WD, Hodges RS (1998) *De novo* design of alpha-helical coiled coils and bundles: models for the development of protein-design principles. Trends Biotechnol 16:379–389

Kohn WD, Mant CT, Hodges RS (1997) Alpha-helical protein assembly motifs. J Biol Chem 272(5):2583–2586

Kol N, Adler-Abramovich L, Barlam D, Shneck RZ, Gazit E, Rousso I (2005) Self-assembled peptide nanotubes are uniquely rigid bioinspired supramolecular structures. Nano Lett 5(7):1343–1346

Kretsinger JK, Haines LA, Ozbas B, Pochan DJ, Schneider JP (2005) Cytocompatibility of self-assembled beta-hairpin peptide hydrogel surfaces. Biomaterials 26(25):5177–5186

Kumar P, Pillay V, Modi G, Choonara YE, du Toit LC, Naidoo D (2011) Self-assembling peptides: implications for patenting in drug delivery and tissue engineering. Recent Pat Drug Deliv Formul 5(1):24–51

Kumar VA, Taylor NL, Jalan AA, Hwang LK, Wang BK, Hartgerink JD (2014) A nanostructured synthetic collagen mimic for hemostasis. Biomacromolecules 15(4):1484–1490

Kyle S, Aggeli A, Ingham E, McPherson MJ (2009) Production of self-assembling biomaterials for tissue engineering. Trends Biotechnol 27(7):423–433

Lee J, Ju M, Cho OH, Kim Y, Nam KT (2018) Tyrosine-Rich peptides as a platform for assembly and material synthesis. Adv Sci (Weinh) 6(4):1801255

Lee TAT, Cooper A, Apkarian RP, Conticello VP (2000) Thermo-reversible self-assembly of nanoparticles derived from elastin-mimetic polypeptides. Adv Mater 12:1105

Lehn JM (2002) Toward complex matter: supramolecular chemistry and self-organization. Proc Natl Acad Sci U S A 99(8):4763–4768

Li Z, Deming TJ (2010) Tunable hydrogel morphology via self-assembly of amphiphilic pentablock copolypeptides. Soft Matter 6(11):2546–2551

Lim YB, Lee E, Lee M (2007) Controlled bioactive nanostructures from self-assembly of peptide building blocks. Angew Chem Int Ed Engl 46(47):9011–9014

Liu L, Busuttil K, Zhang S, Yang Y, Wang C, Besenbachera F, Dong M (2011) The role of self-assembling polypeptides in building nanomaterials. Phys Chem Chem Phys 13(39):17435–17444

Löwik DW, van Hest JC (2004) Peptide based amphiphiles. Chem Soc Rev 33(4):234–245

Luo T, Kiick KL (2013) Collagen-like peptides and peptide-polymer conjugates in the design of assembled materials. Eur Polym J 49(10):2998–3009

Lupas A (1996) Coiled coils: new structures and new functions. Trends Biochem Sci 21(10):375–382

Madhusudan Makwana K, Mahalakshmi R (2015) Implications of aromatic-aromatic interactions: from protein structures to peptide models. Protein Sci 24(12):1920–1933

Mahler A, Reches M, Rechter M, Cohen S, Gazit E (2006) Rigid, self-assembled hydrogel composed of a modified aromatic dipeptide. Adv Mater 18(11):1365–1370

von Maltzahn G, Vauthey S, Santoso S, Zhang S (2003) Positively charged surfactant-like peptides self-assemble into nanostructures. Langmuir 19(10):4332–4337

Mandal D, Nasrolahi Shirazi A, Parang K (2014) Self-assembly of peptides to nanostructures. Org Biomol Chem 12(22):3544–3561

Mandal D, Tiwari RK, Shirazi AN, Oh D, Ye G, Banerjee A, Yadav A, Paranga K (2013) Self-assembled surfactant cyclic peptide nanostructures as stabilizing agents. Soft Matter 9(39)

Marchesan S, Easton CD, Kushkaki F, Waddington L, Hartley PG (2012a) Tripeptide self-assembled hydrogels: unexpected twists of chirality. Chem Commun (Camb) 48(16):2195–2197

Marchesan S, Waddington L, Easton CD, Winkler DA, Goodall L, Forsythe J, Hartley PG (2012b) Unzipping the role of chirality in nanoscale self-assembly of tripeptide hydrogels. Nanoscale 4(21):6752–6760

Martin CR, Kohli P (2003) The emerging field of nanotube biotechnology. Nat Rev Drug Discov 2(1):29–37

Measey TJ, Schweitzer-Stenner R (2006) Aggregation of the amphipathic peptides (AAKA)n into antiparallel beta-sheets. J Am Chem Soc 128(41):13324–13325

Measey TJ, Schweitzer-Stenner R, Sa V, Kornev K (2010) Anomalous conformational instability and hydrogel formation of a cationic class of self-assembling oligopeptides. Macromolecules 43(18):7800–7806

Megeed Z, Cappello J, Ghandehari H (2002) Genetically engineered silk-elastin-like protein polymers for controlled drug delivery. Adv Drug Deliv Rev 54(8):1075–1091

Melchionna M, Styan KE, Marchesan S (2016) The unexpected advantages of using D-amino acids for peptide self- assembly into nanostructured hydrogels for medicine. Curr Top Med Chem 16(18):2009–2018

Menger FM, Keiper JS (2000) Gemini Surfactants. Angew Chem Int Ed Engl 39(11):1906–1920

Menger FM, Littau CA (1991) Gemini-surfactants: synthesis and properties. J Am Chem Soc 113(4):1451–1452

Mita K, Ichimura S, James TC (1994) Highly repetitive structure and its organization of the silk fibroin gene. J Mol Evol 38(6):583–592

Moll R, Divo M, Langbein L (2008) The human keratins: biology and pathology. Histochem Cell Biol 129(6):705–733

Moll R, Franke WW, Schiller DL, Geiger B, Krepler R (1982) The catalog of human cytokeratins: patterns of expression in normal epithelia, tumors and cultured cells. Cell 31(1):11–24

Montenegro J, Ghadiri MR, Granja JR (2013) Ion channel models based on self-assembling cyclic peptide nanotubes. Acc Chem Res 46(12):2955–2965

Mori K, Tanaka K, Kikuchi Y, Waga M, Waga S, Mizuno S (1995) Production of a chimeric fibroin light-chain polypeptide in a fibroin secretion-deficient naked pupa mutant of the silkworm *Bombyx mori*. J Mol Biol 251(2):217–228

Mu Y, Yu M (2014) Effects of hydrophobic interaction strength on the self-assembled structures of model peptides. Soft Matter 10(27):4956–4965

Nagarkar RP, Hule RA, Pochan DJ, Schneider JP (2008) *De novo* design of strand-swapped beta-hairpin hydrogels. J Am Chem Soc 130(13):4466–4474

Nagarsekar A, Crissman J, Crissman M, Ferrari F, Cappello J, Ghandehari H (2002) Genetic synthesis and characterization of pH- and temperature-sensitive silk-elastin-like protein block copolymers. J Biomed Mater Res 62(2):195–203

Nagarsekar A, Crissman J, Crissman M, Ferrari F, Cappello J, Ghandehari H (2003) Genetic engineering of stimuli-sensitive silk-elastin-like protein block copolymers. Biomacromolecules 4(3):602–607

Narayan OP, Mu X, Hasturk O, Kaplan DL (2021) Dynamically tunable light responsive silk-elastin-like proteins. Acta Biomater 121:214–223

Nowak AP, Breedveld V, Pakstis L, Ozbas B, Pine DJ, Pochan D, Deming TJ (2002) Rapidly recovering hydrogel scaffolds from self-assembling diblock copolypeptide amphiphiles. Nature 417(6887):424–428

Nowak AP, Breedveld V, Pine DJ, Deming TJ (2003) Unusual salt stability in highly charged diblock co-polypeptide hydrogels. J Am Chem Soc 125(50):15666–15670

Nowak AP, Sato J, Breedveld V, Deming TJ (2006) Hydrogel formation in amphiphilic triblock copolypeptides. Supramol Chem 18:423–427

O'Leary LE, Fallas JA, Bakota EL, Kang MK, Hartgerink JD (2011) Multi-hierarchical self-assembly of a collagen mimetic peptide from triple helix to nanofibre and hydrogel. Nat Chem 3(10):821–828

Oas TG, Endow SA (1994) Springs and hinges: dynamic coiled coils and discontinuities. Trends Biochem Sci 19(2):51–54

Ogihara NL, Ghirlanda G, Bryson JW, Gingery M, DeGrado WF, Eisenberg D (2001) Design of three-dimensional domain-swapped dimers and fibrous oligomers. Proc Natl Acad Sci U S A 98(4):1404–1409

Ozbas B, Kretsinger J, Rajagopal K, Schneider JP, Pochan DJ (2004) Salt-triggered peptide folding and consequent self-assembly into hydrogels with Tunable modulus. Macromolecules 37(19): 7331–7337

Palomo JM (2014) Solid-phase peptide synthesis: an overview focused on the preparation of biologically relevant peptides. RSC Adv 4:32658–32672

Pandya MJ, Spooner GM, Sunde M, Thorpe JR, Rodger A, Woolfson DN (2000) Sticky-end assembly of a designed peptide fiber provides insight into protein fibrillogenesis. Biochemistry 39(30):8728–8734

Papapostolou D, Smith AM, Atkins ED, Oliver SJ, Ryadnov MG, Serpell LC, Woolfson DN (2007) Engineering nanoscale order into a designed protein fiber. Proc Natl Acad Sci U S A 104(26): 10853–10858

Paramonov SE, Jun HW, Hartgerink JD (2006) Self-assembly of peptide-amphiphile nanofibers: the roles of hydrogen bonding and amphiphilic packing. J Am Chem Soc 128(22):7291–7298

Pauling L, Corey RB (1951) Configurations of polypeptide chains with Favored orientations around single bonds: two new pleated sheets. Proc Natl Acad Sci U S A 37(11):729–740

Pauling L, Corey RB (1953) Compound helical configurations of polypeptide chains: structure of proteins of the alpha-keratin type. Nature 171(4341):59–61

Perinelli DR, Campana M, Singh I, Vllasaliu D, Doutch J, Palmieri GF, Casettari L (2019) PEGylation affects the self-assembling behaviour of amphiphilic octapeptides. Int J Pharm 25(571):118752

Persikov AV, Ramshaw JA, Brodsky B (2005) Prediction of collagen stability from amino acid sequence. J Biol Chem 280(19):19343–19349

Perutz MF, Johnson T, Suzuki M, Finch JT (1994) Glutamine repeats as polar zippers: their possible role in inherited neurodegenerative diseases. Proc Natl Acad Sci U S A 91:5355–5358

Petka WA, Harden JL, McGrath KP, Wirtz D, Tirrell DA (1998) Reversible hydrogels from self-assembling artificial proteins. Science 281(5375):389–392

Pires MM, Chmielewski J (2009) Self-assembly of collagen peptides into microflorettes via metal coordination. J Am Chem Soc 131(7):2706–2712

Pires MM, Lee J, Ernenwein D, Chmielewski J (2012) Controlling the morphology of metal-promoted higher ordered assemblies of collagen peptides with varied core lengths. Langmuir 28(4):1993–1997

Pochan DJ, Pakstis L, Ozbas B, Nowak AP, Deming TJ (2002) SANS and Cryo-TEM study of self-assembled diblock copolypeptide hydrogels with rich nano- through microscale morphology. Macromolecules 35:5358–5360

Pochan DJ, Schneider JP, Kretsinger J, Ozbas B, Rajagopal K, Haines L (2003) Thermally reversible hydrogels via intramolecular folding and consequent self-assembly of a de novo designed peptide. J Am Chem Soc 125(39):11802–11803

Pollard TD, Earnshaw WC (2008) Cell biology, 2nd edn. Saunders Elsevier, Philadelphia

Przybyla DE, Rubert Pérez CM, Gleaton J, Nandwana V, Chmielewski J (2013) Hierarchical assembly of collagen peptide triple helices into curved disks and metal ion-promoted hollow spheres. J Am Chem Soc 135(9):3418–3422

Qi Y, Wang H, Wei K, Yang Y, Zheng R-Y, Kim IS, Zhang K-Q (2017) A review of structure construction of silk fibroin biomaterials from single structures to multi-level structures. Int J Mol Sci 18(3):237

Qin G, Lapidot S, Numata K, Hu X, Meirovitch S, Dekel M, Podoler I, Shoseyov O, Kaplan DL (2009) Expression, cross-linking, and characterization of recombinant chitin binding resilin. Biomacromolecules 10(12):3227–3234

Qiu F, Chen Y, Tang C, Zhou Q, Wang C, Shi Y, Zhao X (2008) De novo design of a bolaamphiphilic peptide with only natural amino acids. Macromol Biosci 8(11):1053–1059

Rajagopal K, Lamm MS, Haines-Butterick LA, Pochan DJ, Schneider JP (2009) Tuning the pH responsiveness of beta-hairpin peptide folding, self-assembly, and hydrogel material formation. Biomacromolecules 10(9):2619–2625

Ramachandran GN, Kartha G (1955) Structure of collagen. Nature 176(4482):593–595

Raucher D, Massodi I, Bidwell GL (2008) Thermally targeted delivery of chemotherapeutics and anti-cancer peptides by elastin-like polypeptide. Expert Opin Drug Deliv 5(3):353–369

Rauscher S, Baud S, Miao M, Keeley Fred W, Pomès R (2006) Proline and glycine control protein self-organization into elastomeric or amyloid fibrils. Structure 14:1667–1676

Reches M, Gazit E (2003) Casting metal nanowires within discrete self-assembled peptide nanotubes. Science 300(5619):625–627

Reches M, Gazit E (2004) Formation of closed-cage nanostructures by self-assembly of aromatic dipeptides. Nano Lett 4:581–585

Reches M, Gazit E (2006) Controlled patterning of aligned self-assembled peptide nanotubes. Nat Nanotechnol 1(3):195–200

Reddy CC, Khilji IA, Gupta A, Bhuyar P, Mahmood S, Al-Japairai KAS, Chua GK (2021) Valorization of keratin waste biomass and its potential applications. J Water Process Eng 40: 101707

Reichl S (2009) Films based on human hair keratin as substrates for cell culture and tissue engineering. Biomaterials 30(36):6854–6866

Rele S, Song Y, Apkarian RP, Qu Z, Conticello VP, Chaikof EL (2007) D-periodic collagen-mimetic microfibers. J Am Chem Soc 129(47):14780–14787

Roberts S, Costa S, Schaal J, Simon JR, Dzuricky M, Quiroz FG, Chilkoti A (2017) In: Healy K, Hutmacher DW, Grainger DW, Kirkpatrick CJ (eds) Comprehensive biomaterials II, vol 2. Elsevier, Amsterdam, pp 90–108

Rodgers UR, Weiss AS (2005) Cellular interactions with elastin. Pathol Biol (Paris) 53(7):390–398

Rouse JG, Van Dyke ME (2010) A review of keratin-based biomaterials for biomedical applications. Materials 3(2):999–1014

Rubio J, Alfonso I, Burguete MI, Luis SV (2012) Interplay between hydrophilic and hydrophobic interactions in the self-assembly of a gemini amphiphilic pseudopeptide: from nano-spheres to hydrogels. Chem Commun (Camb) 48(16):2210–2212

Ryadnov MG, Woolfson DN (2003) Engineering the morphology of a self-assembling protein fibre. Nat Mater 2(5):329–332

Saha S, Banskota S, Roberts S, Kirmani N, Chilkoti A (2020) Engineering the architecture of elastin-like polypeptides: from unimers to hierarchical self-assembly. Adv Ther (Weinh) 3(3): 1900164

Sakakibara S, Inouye K, Shudo K, Kishida Y, Kobayashi Y, Prockop DJ (1973) Synthesis of (Pro-Hyp-Gly) n of defined molecular weights. Evidence for the stabilization of collagen triple helix by hydroxypyroline. Biochim Biophys Acta 303(1):198–202

Santoso S, Hwang W, Hartman H, Zhang S (2002) Self-assembly of surfactant-like peptides with variable glycine tails to form nanotubes and nanovesicles. Nano Lett 2(7):687–691

Schneider JP, Pochan DJ, Ozbas B, Rajagopal K, Pakstis L, Kretsinger J (2002) Responsive hydrogels from the intramolecular folding and self-assembly of a designed peptide. J Am Chem Soc 124(50):15030–15037

Senguen FT, Doran TM, Anderson EA, Nilsson BL (2011) Clarifying the influence of core amino acid hydrophobicity, secondary structure propensity, and molecular volume on amyloid-β 16-22 self-assembly. Mol BioSyst 7(2):497–510

Shi J, Gao Y, Yang Z, Xu B (2011) Exceptionally small supramolecular hydrogelators based on aromatic-aromatic interactions. Beilstein J Org Chem 7:167–172

Shi P, Gustafson JA, MacKay JA (2014) Genetically engineered nanocarriers for drug delivery. Int J Nanomedicine 9:1617–1626

Shi Y, Lin R, Cui H, Azevedo HS (2018) Multifunctional self-assembling peptide-based nanostructures for targeted intracellular delivery: design, physicochemical characterization, and biological assessment. Methods Mol Biol 1758:11–26

Shoulders MD, Raines RT (2009) Collagen structure and stability. Annu Rev Biochem 78:929–958

Smith AM, Banwell EF, Edwards WR, Pandya M, Woolfson DN (2006) Engineering increased stability into self-assembled protein fibers. Adv Funct Mater 16(8):1022–1030

Smith AM, Williams RJ, Tang C, Coppo P, Collins RF, Turner ML, Saiani A, Ulijn RV (2008) Fmoc-diphenylalanine self assembles to a hydrogel via a novel architecture based on π–π interlocked β-sheets. Adv Mater 20(1):37–41

Song J, Cheng Q, Stevens RC (2002) Morphological manipulation of bolaamphiphilic polydiacetylene assemblies by controlled lipid doping. Chem Phys Lipids 114(2):203–214

Song Y, Challa SR, Medforth CJ, Qiu Y, Watt RK, Peña D, Miller JE, van Swolab F, Shelnutt JA (2004) Synthesis of peptide-nanotube platinum-nanoparticle composites. Chem Commun (Camb) 9:1044–1045

Soto C, Sigurdsson EM, Morelli L, Kumar RA, Castaño EM, Frangione B (1998) Beta-sheet breaker peptides inhibit fibrillogenesis in a rat brain model of amyloidosis: implications for Alzheimer's therapy. Nat Med 4(7):822–826

Struthers MD, Cheng RP, Imperiali B (1996) Design of a monomeric 23-residue polypeptide with defined tertiary structure. Science 271(5247):342–345

Su RS, Kim Y, Liu JC (2014) Resilin: protein-based elastomeric biomaterials. Acta Biomater 10(4): 1601–1611

Sun L, Fan Z, Wang Y, Huang Y, Schmidt M, Zhang M (2015) Tunable synthesis of self-assembled cyclic peptide nanotubes and nanoparticles. Soft Matter 11(19):3822–3832

Sun X-L, Biswas N, Kai T, Dai Z, Dluhy RA, Chaikof EL (2006) Membrane-mimetic films of asymmetric phosphatidylcholine lipid bolaamphiphiles. Langmuir 22(3):1201–1208

Suzuki E, Fraser RDB, MacRae TP (1980) Role of hydroxyproline in the stabilization of the collagen molecule via water molecules. Int J Biol Macromol 2:54–56

Swanekamp RJ, DiMaio JT, Bowerman CJ, Nilsson BL (2012) Coassembly of enantiomeric amphipathic peptides into amyloid-inspired rippled β-sheet fibrils. J Am Chem Soc 134(12): 5556–5559

Tachibana A, Furuta Y, Takeshima H, Tanabe T, Yamauchi K (2002) Fabrication of wool keratin sponge scaffolds for long-term cell cultivation. J Biotechnol 93(2):165–170

Tachibana A, Kaneko S, Tanabe T, Yamauchi K (2005) Rapid fabrication of keratin-hydroxyapatite hybrid sponges toward osteoblast cultivation and differentiation. Biomaterials 26(3):297–302

Tachibana A, Nishikawa Y, Nishino M, Kaneko S, Tanabe T, Yamauchi K (2006) Modified keratin sponge: binding of bone morphogenetic protein-2 and osteoblast differentiation. J Biosci Bioeng 102(5):425–429

Tamburro AM, Panariello S, Santopietro V, Bracalello A, Bochicchio B, Pepe A (2010) Molecular and supramolecular structural studies on significant repetitive sequences of resilin. Chembiochem 11(1):83–93

Tanaka K, Kajiyama N, Ishikura K, Waga S, Kikuchi A, Ohtomo K, Takagi T, Mizuno S (1999) Determination of the site of disulfide linkage between heavy and light chains of silk fibroin produced by *Bombyx mori*. Biochim Biophys Acta 1432(1):92–103

Tanrikulu IC, Raines RT (2014) Optimal interstrand bridges for collagen-like biomaterials. J Am Chem Soc 136(39):13490–13493

Toledano S, Williams RJ, Jayawarna V, Ulijn RV (2006) Enzyme-triggered self-assembly of peptide hydrogels via reversed hydrolysis. J Am Chem Soc 128(4):1070–1071

Tu RS, Tirrell M (2004) Bottom-up design of biomimetic assemblies. Adv Drug Deliv Rev 56(11): 1537–1563

Tugyi R, Uray K, Iván D, Fellinger E, Perkins A, Hudecz F (2005) Partial D-amino acid substitution: improved enzymatic stability and preserved ab recognition of a MUC2 epitope peptide. Proc Natl Acad Sci U S A 102(2):413–418

Uyaver S, Hernandez HW, Habiboglu MG (2018) Self-assembly of aromatic amino acids: a molecular dynamics study. Phys Chem Chem Phys 20(48):30525–30536

Vauthey S, Santoso S, Gong H, Watson N, Zhang S (2002) Molecular self-assembly of surfactant-like peptides to form nanotubes and nanovesicles. Proc Natl Acad Sci U S A 99(8):5355–5360

Vegners R, Shestakova I, Kalvinsh I, Ezzell RM, Janmey PA (1995) Use of a gel-forming dipeptide derivative as a carrier for antigen presentation. J Pept Sci 1(6):371–378

Wang H, Zhu D, Paul A, Cai L, Enejder A, Yang F, Heilshorn SC (2017) Covalently adaptable elastin-like protein–hyaluronic acid (ELP–HA) hybrid hydrogels with secondary thermoresponsive crosslinking for injectable stem cell delivery. Adv Funct Mater 27(28): 1605609

Wang Q, Xia X, Huang W, Lin Y, Xu Q, Kaplan DL (2014) High throughput screening of dynamic silk-elastin-like protein biomaterials. Adv Funct Mater 24(27):4303–4310

Webber MJ, Berns EJ, Stupp SI (2013) Supramolecular nanofibers of peptide amphiphiles for medicine. Isr J Chem 53(8):530–554

Weissig V, Torchilin V (2000) Mitochondriotropic cationic vesicles: a strategy towards mitochondrial gene therapy. Curr Pharm Biotechnol 1(4):325–346

Wester JR, Lewis JA, Freeman R, Sai H, Palmer LC, Henrich SE, Stupp SI (2020) Supramolecular exchange among assemblies of opposite charge leads to hierarchical structures. J Am Chem Soc 142(28):12216–12225

Whitesides GM, Boncheva M (2002) Beyond molecules: self-assembly of mesoscopic and macroscopic components. Proc Natl Acad Sci U S A 99(8):4769–4774

Whitesides GM, Grzybowski B (2002) Self-assembly at all scales. Science 295(5564):2418–2421

Whitford D (2005) Proteins: structure and function. Wiley, Chichester

Wong KM, Wang Y, Seroski DT, Larkin GE, Mehta AK, Hudalla GA, Hall CK, Paravastu AK (2020) Molecular complementarity and structural heterogeneity within co-assembled peptide β-sheet nanofibers. Nanoscale 12(7):4506–4518

Woolfson DN (2017) Coiled-coil design: updated and upgraded. Subcell Biochem 82:35–61

Wrześniewska-Tosik K, Wawro D, Ratajska M, Stęplewski W (2007) Novel composites with feather keratin. Fibres Text East Eur 15:157–162

Wychowaniec JK, Patel R, Leach J, Mathomes R, Chhabria V, Patil-Sen Y, Hidalgo-Bastida A, Forbes RT, Hayes JM, Elsawy MA (2020) Aromatic stacking facilitated self-assembly of ultrashort ionic complementary peptide sequence: β-sheet nanofibers with remarkable gelation and interfacial properties. Biomacromolecules 21(7):2670–2680. Epub 2020 May 29

Xiao-Zhou S, Hong-Ru W, Mian H (2014) Characterization of the casein/keratin self-assembly nanomicelles. J Nanomater 2014:183815

Xu C, Joss L, Wang C, Pechar M, Kopecek J (2002) The influence of fusion sequences on the thermal stabilities of coiled coil proteins. Macromol Biosci 2(8):395–401

Xu S, Sang L, Zhang Y, Wang X, Li X (2013) Biological evaluation of human hair keratin scaffolds for skin wound repair and regeneration. Mater Sci Eng C Mater Biol Appl 33(2):648–655

Yang ZM, Gu HW, Zhang Y, Wang L, Xu B (2004) Small molecule hydrogels based on a class of antiinflammatory agents. Chem Commun 2:208–209

Ye Z, Zhang H, Luo H, Wang S, Zhou Q, Du X, Tang C, Chen L, Liu J, Shi YK, Zhang EY, Ellis-Behnke R, Zhao X (2008) Temperature and pH effects on biophysical and morphological properties of self-assembling peptide RADA16-I. J Pept Sci 14(2):152–162

Yemini M, Reches M, Rishpon J, Gazit E (2005) Novel electrochemical biosensing platform using self-assembled peptide nanotubes. Nano Lett 5(1):183–186

Yi Z, Cui X, Chen G, Chen X, Jiang X, Li X (2021) Biocompatible, antioxidant nanoparticles prepared from natural renewable tea polyphenols and human hair keratins for cell protection and anti-inflammation. ACS Biomater Sci Eng 7(3):1046–1057

Yokoi H, Kinoshita T, Zhang S (2005) Dynamic reassembly of peptide RADA16 nanofiber scaffold. Proc Natl Acad Sci U S A 102(24):8414–8419

Yu J, Yu DW, Checkla DM, Freedberg IM, Bertolino AP (1993) Human hair keratins. J Invest Dermatol 101(1 Suppl):56S–59S

Yu YB (2002) Coiled-coils: stability, specificity, and drug delivery potential. Adv Drug Deliv Rev 54(8):1113–1129

Yucel T, Micklitsch CM, Schneider JP, Pochan DJ (2008) Direct observation of early-time hydrogelation in beta-hairpin peptide self-assembly. Macromolecules 41(15):5763–5772

Zeng L, Jiang L, Teng W, Cappello J, Zohar Y, Wu X (2014) Engineering aqueous fiber assembly into silk-elastin-like protein polymers. Macromol Rapid Commun 35(14):1273–1279

Zhan C, Gao P, Liu M (2005) Self-assembled helical spherical-nanotubes from an l-glutamic acid based bolaamphiphilic low molecular mass organogelator. Chem Commun 4(4):462–464

Zhang S (2003) Fabrication of novel biomaterials through molecular self-assembly. Nat Biotechnol 21(10):1171–1178

Zhang S, Holmes T, Lockshin C, Rich A (1993) Spontaneous assembly of a self-complementary oligopeptide to form a stable macroscopic membrane. Proc Natl Acad Sci U S A 90(8): 3334–3338

Zhang S, Lockshin C, Cook R, Rich A (1994) Unusually stable beta-sheet formation in an ionic self-complementary oligopeptide. Biopolymers 34(5):663–672

Zhang S, Lockshin C, Herbert A, Winter E, Rich A (1992) Zuotin, a putative Z-DNA binding protein in Saccharomyces cerevisiae. EMBO J 11(10):3787–3796

Zhang Y, Gu H, Yang Z, Xu B (2003) Supramolecular hydrogels respond to ligand-receptor interaction. J Am Chem Soc 125(45):13680–13681

Zhao X, Pan F, Xu H, Yaseen M, Shan H, Hauser CAE, Zhang S, Luab JR (2010) Molecular self-assembly and applications of designer peptide amphiphiles. Chem Soc Rev 39(9):3480–3498

Zheng Y, Mao K, Chen S, Zhu H (2021) Chirality effects in peptide assembly structures. Front Bioeng Biotechnol 22(9):703004

Zhou CZ, Confalonieri F, Jacquet M, Perasso R, Li ZG, Janin J (2001) Silk fibroin: structural implications of a remarkable amino acid sequence. Proteins 44(2):119–122

Chapter 2
β-Sheet and β-Hairpin Peptide Nanomaterials

Elena Quigley and Bradley L. Nilsson

Abstract Supramolecular peptide assemblies have emerged as promising next-generation nanomaterials for applications in medicine, tissue engineering, and energy. Peptide assemblies composed of β-sheet and β-hairpin peptides have been the subject of extensive development and study. The purpose of this chapter is to present advances in the design, characterization, and application of supramolecular β-sheet materials in the context of key foundational studies and selected innovative examples that build upon this foundational work.

Keywords Peptide self-assembly · β-Sheet · Nanomaterials · Biomaterials

2.1 Introduction

Nature provides many examples of proteins and peptides that self-assemble into β-sheet fibers. Amyloid assemblies associated with protein misfolding disorders such as Alzheimer's disease, Parkinson's disease, prion encephalopathies, and type II diabetes are among the most commonly studied examples of these β-sheet assemblies (Sadigh-Eteghad et al. 2015; Irwin et al. 2013; Milardi et al. 2021; Knowles et al. 2014; Ke et al. 2017). Functional amyloid assemblies that serve structural (bacterial curli), storage (mammalian hormones), and information carrying (yeast HET-s prion) purposes are also found in both prokaryotes and eukaryotes (Van Gerven et al. 2015; Deshmukh et al. 2018; Bergman et al. 2016; Otzen and Riek 2019). Naturally occurring amyloid systems have inspired the development of engineered supramolecular β-sheet assemblies as functional next-generation materials (Knowles and Mezzenga 2016; Wang et al. 2015; Park et al. 2019; Li et al. 2014; Lopez-Silva and Schneider 2021). These biomaterials have been used for diverse applications that include regenerative medicine, drug delivery, light harvesting, and electron transfer (Hu et al. 2020; Varanko et al. 2020; Najafi et al.

E. Quigley · B. L. Nilsson (✉)
University of Rochester, Department of Chemistry, Rochester, NY, USA
e-mail: bradley.nilsson@rochester.edu

2021; Lai et al. 2021; Zhang et al. 2021). In this chapter, we present a discussion of key historical findings in the field of self-assembled β-sheet materials and provide recent examples of key innovations in the development of β-sheet and β-hairpin assemblies as functional nanomaterials.

2.2 Early Investigations of β-Sheet Peptide Assemblies as Materials

In the early 1950s, Pauling and Corey investigated the molecular architecture of silk fibroin and β-keratin assemblies (Pauling and Corey 1951; Pauling and Corey 1953; Marsh et al. 1955). These protein assemblies, known for their structural and mechanical properties, are among the first materials identified which are composed of assembled β-sheets. They proposed that amphipathic proteins and peptides, those which had alternating hydrophilic and hydrophobic residues, could be arranged into β-sheets wherein the β-strands were in either parallel or anti-parallel conformations (Marsh et al. 1955). Today, these types of structures are referred to as cross-β assemblies, a term that originated in the amyloid field (Fig. 2.1). Cross-β assemblies are composed of pleated β-sheets (parallel or antiparallel) that assemble into one-dimensional fibrils in which the amino acid side chain groups are oriented perpendicular to the fibril axis. An interstrand hydrogen bond network that is oriented perpendicular to the fibril axis stabilizes the β-sheets, which form face-to-face laminates with other β-sheets in the mature assemblies. The nature of the self-assembling peptide defines the number of laminate sheets within the fibrils.

Early efforts to correlate amphipathic peptide sequence to β-sheet secondary structure were undertaken by Walton and coworkers (Anderson et al. 1972; Bippon et al. 1973). They characterized polydisperse assemblies of model $(AG)_n$ and $(SG)_n$ repeat peptides using circular dichroism (CD), infrared (IR) spectroscopy, and
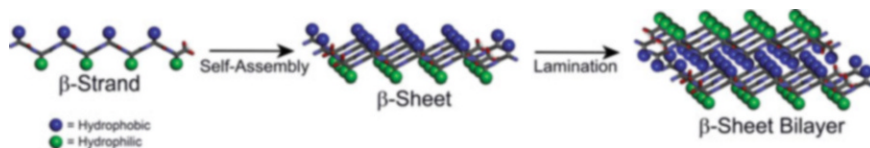
Fig. 2.1 An idealized structural representation of self-assembled amphipathic cross-β-peptide fibrils. Hydrophobic amino acid side chains are represented as blue spheres; hydrophilic amino acid side chains as green spheres. Side chains are oriented perpendicular to the fibril axis, which is defined by an interstrand hydrogen bond network that is parallel to the fibril axis. Note that in this figure, the fibril axis extends perpendicular to the plane of the page (extending into and out of the page). The example shown is consistent with the structure proposed by Brack and Orgel (1975) for self-assembled β-sheet bilayer fibrils formed by amphipathic β-sheet peptide fibrils with alternating hydrophobic and hydrophilic amino acid sequence patterns. In these fibrils, the pattern of hydrophobic and hydrophilic amino acids results in a nanoribbon assembly with two laminated β-sheets. Peptides with different sequence patterns have been found to form fibrils with varying numbers of laminated β-sheets

electron microscopy (EM) and confirmed that assemblies formed by these peptides adopt an arrangement rich in β-sheet secondary structure (Anderson et al. 1972). The $(AG)_n$ and $(SG)_n$ repeat systems, which are neutral, were subsequently compared to assemblies of $(KX)_n$ systems (X = Phe, Val, Leu, Tyr, Ser) (Anderson et al. 1972; Brack and Caille 1978; Seipke et al. 1974; Brack and Orgel 1975; St. Pierre et al. 1978; Seipke et al. 1980; Kubota et al. 1983). Inclusion of lysine in these peptide sequences provided a charge center which could be used to influence the assembly of the peptides as a function of solution pH or ionic strength. At low pH values, the lysine residues were protonated and thereby repelled each other due to their like charges. This correlated to the observed increase in β-sheet signal as the pH or salt concentration was increased in systems with this sequence pattern (Anderson et al. 1972; Seipke et al. 1974; Brack and Orgel 1975; Seipke et al. 1980; Kubota et al. 1983). X-ray scattering data showed reflections at both 4.7 Å and 9 Å, with the 4.7 Å reflection indicative of strand-strand distances within a β-sheet and the 9 Å reflections indicative of the sheet-to-sheet interlaminar distances (Anderson et al. 1972; Brack and Orgel 1975). Brack and Orgel suggested that the β-sheet peptides were arranged into a bilayer which allowed the hydrophobic sidechains to form a core, leaving the hydrophilic amino acids exposed to solvent (Fig. 2.1) (Brack and Orgel 1975). The effect of charge on self-assembly into β-sheets was further studied using both cationic and anionic peptides (Anderson et al. 1972; Brack and Orgel 1975). These foundational studies established that peptides with alternating hydrophobic and hydrophilic residues readily assemble into β-sheets and higher-order structures.

The aforementioned studies relied on uncontrolled polymerization of amino acid dimers, trimers, and tetramers to form mixtures of amphipathic peptides with polydisperse sequence lengths (Brack and Caille 1978). The introduction of solid-phase peptide synthesis methodology enabled the preparation of peptides of specific sequences and lengths (Osterman et al. 1984; Osterman and Kaiser 1985; Ono et al. 1990). Osterman and Meredith were interested in determining the shortest amphipathic peptide sequence length that would undergo self-assembly into an ordered structure (Osterman et al. 1984; Osterman and Kaiser 1985). They prepared H_2N-$(VEV(Orn))_n$-CO_2H (Orn = ornithine and n = 1, 2, 3) peptides to characterize peptide self-assembly propensity as a function of length. They found that only the peptide with length repeat of $n = 3$ efficiently self-assembled; however when the ornithine amines were modified with trifluoroacetate to eliminate positive charge, the resulting peptides assembled into β-sheet materials at both $n = 2$ and $n = 3$ sequence lengths (Osterman et al. 1984; Osterman and Kaiser 1985). These early efforts in peptide design established key principles for the development of supramolecular β-sheet nanomaterials. In the following section, we present peptides that build upon these early foundational studies.

2.3 Short Amphipathic β-Sheet Peptides

2.3.1 Ionic Self-Complementary Peptides: EAK16 and RAD16

Zhang et al. subsequently demonstrated that amphipathic β-sheet fibril assemblies can form entangled hydrogel networks (Zhang et al. 1993; Zhang 2018; Zhang 2002; Caplan et al. 2002a; Yokoi et al. 2005; Luo et al. 2008; Zhang et al. 2011; Gelain et al. 2020; Zhang and Altman 1999). In a study of the yeast DNA-binding protein, zuotin, they were intrigued by a repeated amino acid sequence and initiated studies of a peptide made up of that sequence, Ac-(AEAEAKAK)$_2$-NH$_2$ (EAK16-II, Table 2.1) (Zhang et al. 1992). They made the serendipitous discovery that EAK16-II formed dense membranes consisting of β-sheet fibrils that exhibited emergent hydrogel properties (Zhang et al. 1993; Zhang et al. 1994). They also showed that similar sequences with shorter lengths had reduced self-assemble propensities (Zhang et al. 1993; Zhang et al. 1994). The self-assembly of EAK16-II was found to occur under various ionic strength, pH, and temperature conditions, indicating the potential of these types of peptides for biomaterial applications (Zhang et al. 1993; Zhang et al. 1994). The EAK16-II sequence was systematically modified to provide additional amphipathic sequences in which the sequence order of the charged amino acids was altered (Zhang et al. 1994; Zhang et al. 1995; Holmes et al. 2000). Included in these sequences was Ac-(RARADADA)$_2$-NH$_2$ (RAD16-II) (Fig. 2.2), which was shown to have enhanced functional properties compared to EAK16 derivatives. Specifically, the RAD16 and EAK16 peptides were shown to assemble under physiological conditions to produce materials capable of acting as cell matrices for several mammalian cell lines (Zhang et al. 1993; Zhang et al. 1994; Zhang et al. 1995). In these efforts, the RAD16 assemblies typically exhibited improved biochemical properties that facilitated hydrogels with improvements in cellular adhesion and proliferation.

Comparison of the biophysical characteristics of the peptide assemblies listed in Table 2.1 has provided insight into the relationship between sequence, assembly propensity, and emergent properties. The critical aggregation concentration (CAC) for formation of hydrogels of EAK16-II was determined to be 0.1 mg mL^{-1} (Fung et al. 2003). EAK16-II was found to self-assemble at concentrations lower than the

Table 2.1 Sequences of peptides in the EAK16 and RAD16 families

Name	Sequence	Reference
EAK16-I	Ac-(AEAK)$_4$$^-NH_2$	Zhang et al. (1993)
EAK16-II	Ac-(AEAEAKAK)$_2$-NH$_2$	Zhang et al. (1992)
EAK16-IV	Ac-(AE)$_4$(AK)$_4$-NH$_2$	Zhang and Altman (1999)
RAD16-I	Ac-(RADA)$_4$-NH$_2$	Zhang and Altman (1999)
RAD16-II	Ac-(RARADADA)$_2$-NH$_2$	Zhang et al. (1994)
RAD16-IV	Ac-(RA)$_4$(DA)$_4$-NH$_2$	Zhang and Altman (1999)
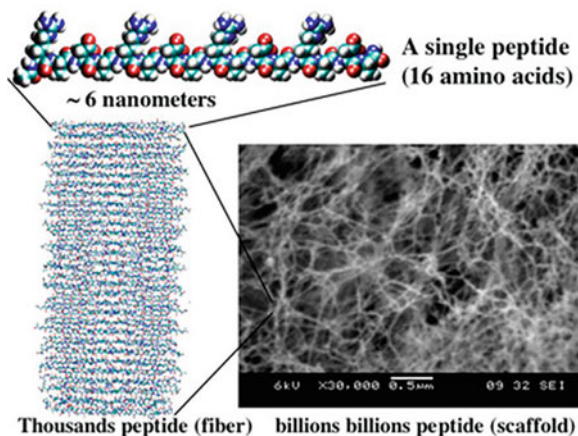
Fig. 2.2 Proposed model of fibrillar hydrogel assemblies of the RAD16-I peptide along with an SEM image that illustrates the entangled network that gives rise to hydrogel properties. Reproduced with permission from (Gelain et al. 2020). Copyright 2020 American Chemical Society

CAC, but these assemblies failed to form stable hydrogel networks. While the assembly of EAK16-II was not a dependent solution pH, EAK16-IV formed globular assemblies at pH values between 6.5 and 7.5 and fibrillar assemblies at pH values below 6.5 or above 7.5 (Hong et al. 2003). These sequence-dependent differences in assembly properties were hypothesized to be due to the tendency of EAK16-IV to adopt a charge-templated β-hairpin structure, while EAK16-I and EAK16-II assemble into extended β-strands (Jun et al. 2004). This hypothesis was supported by subsequent molecular dynamics simulations performed by Emamyari et al. (2015) RAD16 sequences without N-terminal acetyl groups also exhibited increased pH sensitivity for self-assembly due to the basicity of the unmodified N-terminal amine (Bagrov et al. 2016). Sun et al. extended these studies by analyzing how the attachment of functional peptide motifs that impart specific cell-interaction properties to these sequences, including the promotion of neurogenesis (Farrukh et al. 2017) and cell adhesion (Huettner et al. 2018), affected the self-assembly properties of the resultant peptides (Sun et al. 2016a). As would be expected, the self-assembly of the modified peptides was sensitive to the acid/base and hydrophilic/hydrophobic properties of the appended peptide motif sequences.

Zhang's RAD16 and EAK16 β-sheet assemblies have been pivotal for the demonstration of supramolecular hydrogel materials for biomedical applications. These assemblies have been frequently used as scaffolds for the display of biologically relevant signal motifs that promote interactions of the network with cells. The biocompatibility of these systems has allowed them to be used for tissue engineering (Zhang and Altman 1999; Zhang et al. 1994; Zhang et al. 1995; Sieminski et al. 2008; Kisiday et al. 2002; Horii et al. 2007; Yang et al. 2018; Cho et al. 2012), to promote neurite outgrowth in neural tissue (Holmes et al. 2000; Ellis-Behnke et al. 2006a; Gelain et al. 2006; Wu et al. 2017a; Lu et al. 2018), for hemostasis (Ellis-
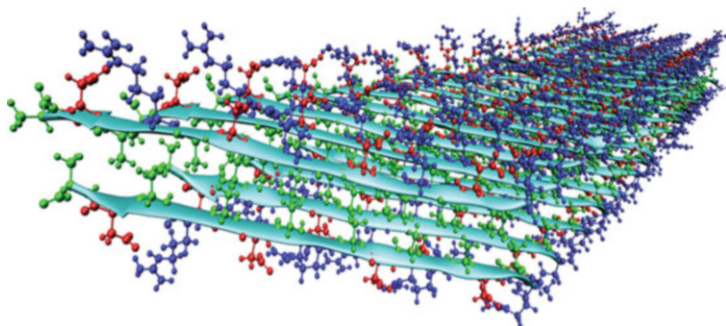
Fig. 2.3 Molecular model of RAD16-II fibrils based on ssNMR constraints. The structural data is consistent with a β-sheet bilayer composed of parallel pleated β-sheets with the Ala side chains (green) occupying the interior core of the bilayer and the Arg (blue) and Asp (red) side chains positioned on the exterior solvent-exposed faces of the fibrils. Reproduced with permission from (Cormier et al. 2013). Copyright 2013 American Chemical Society

Behnke et al. 2006b; Luo et al. 2011; Taghavi et al. 2018; Wei et al. 2020), for drug delivery (Gelain et al. 2010; Koutsopoulos et al. 2009; Wu et al. 2017b; Zhou et al. 2016), and as injectable matrices for cell delivery in tissue regeneration applications (Luo et al. 2008; Horii et al. 2007; Luo et al. 2011; Wang et al. 2008; Davis et al. 2006; Genove et al. 2005; Wu et al. 2017c; Tajima et al. 2015). Since their discovery more than two decades ago, these peptide assemblies are still under active development as next-generation biomaterials.

Recently, efforts have been made to understand how the atomic structure of these materials correlate to the emergent properties of the β-sheet assemblies. Defining the high-resolution structure of β-sheet assemblies has not been possible using typical X-ray crystallographic or solution NMR methods. Except in rare circumstances, these one-dimensional fibrils are non-crystalline, and the molecular weight of the assemblies is far too large to obtain useful information from solution NMR. Additionally, the assembled state of these fibrils can limit molecular motion and decrease signal intensity, further limiting the application of solution NMR to these materials. Solid-state NMR (ssNMR) has emerged as a useful tool for understanding the molecular structure of β-sheet assemblies. Paravastu and coworkers have interrogated the structure of RAD16-II fibrils using a variety of ssNMR techniques (Cormier et al. 2013). The structural data supports the predicted β-sheet bilayer architecture with the Ala residue side chains forming the core of the bilayer and the Arg/Asp side chains exposed on the exterior solvent-exposed faces of the fibrils (Fig. 2.3). Interestingly, the proposed models for this peptide before applying ssNMR techniques predicted that the neighboring β-strands would be arranged in antiparallel pleated β-sheet structures. Instead, it was found that the strands were aligned in parallel pleated β-sheets.

2.3.2 (FKFE)$_n$ and Related Amphipathic Peptide Sequences from the EAK/RAD Family

Zhang's discovery of the EAK and RAD families of self-assembling β-sheet peptides was followed soon thereafter by studies in which peptides with hydrophobic residues other than Ala were incorporated into the sequences (Table 2.2). Among the first of these sequences to be reported was the Ac-(FKFE)$_n$-NH$_2$ peptide system (Caplan et al. 2002a; Caplan et al. 2002b). Lauffenburger et al. first reported that,

Table 2.2 A selection of peptides derived from the original (FKFE)$_n$ sequence

Name	Sequence	Reference
(FKFE)$_3$	Ac-FKFEFKFEFKFE-NH$_2$	Caplan et al. (2002a, 2002b)
(FKFE)$_2$	Ac-FKFEFKFE-NH$_2$	Caplan et al. (2002a)
(FKFQ)$_3$	Ac-FKFQFKFQFKFQFKFQ-NH$_2$	Caplan et al. (2002a)
(FKFE)$_4$	Ac-FKFEFKFEFKFEFKFE-NH$_2$	Caplan et al. (2002a)
[(FE)$_2$(FK)$_2$]$_2$	Ac-FEFEFKFKFEFEFKFK-NH$_2$	Zhang and Altman (1999) and Wang et al. (2005)
(IKIE)$_3$	Ac-IKIEIKIEIKIE-NH$_2$	Caplan et al. (2002a)
(VKVE)$_3$	Ac-VKVEVKVEVKVE-NH$_2$	Caplan et al. (2002a)
(AKAE)$_2$	Ac-AKAEAKAE-NH$_2$	Bowerman et al. (2009)
(VKVE)$_2$	Ac-VKVEVKVE-NH$_2$	Bowerman et al. (2009)
(LKLE)$_2$	Ac-LKLELKLE-NH$_2$	Bowerman et al. (2009)
[(Cha)K(Cha)E]$_2$	Ac-(Cha)K(Cha)E(Cha)K(Cha)E-NH$_2$	Bowerman et al. (2009)
F9	H$_2$N-FEFKFEFKK-COOH	Elsawy et al. (2016)
FC9-BM	H$_2$N-FEFKC(BM)EFKK-COOH	Elsawy et al. (2016)
FEFK	H$_2$N-FEFK-COOH	Guilbaud et al. (2010) and Guilbaud et al. (2013)
VEK1	H$_2$N-VEVEVKVE-COOH	Guilbaud et al. (2013) and Roberts et al. (2012)
VEK2	H$_2$N-VEVKVEVK-COOH	Roberts et al. (2012)
VEK3	H$_2$N-VKVKVEVK-COOH	Roberts et al. (2012)
(RVQV)$_3$	Ac-RVQVRVQVRVQV-COOH	Zhang et al. (2017)
(RVEV)$_3$	Ac-RVEVRVEVRVEV-NH$_2$	Zhang et al. (2017)
(RV)$_6$	Ac-RVRVRVRVRVRV-COOH	Zhang et al. (2017)
(RVQV)$_3$-Am	Ac-RVQVRVQVRVQV-NH$_2$	Zhang et al. (2017)
OVA-Z1	H$_2$N-SIINFEKL-SGSG-RVQVRVQVRVQV-COOH	Zhang et al. (2017)
(FEFK)$_2$	H$_2$N-FEFKFEFK-COOH	Wychowaniec et al. (2020a) and Gao et al. (2017)
K(FEFK)$_2$K	H$_2$N-KFEFKFEFKK-COOH	Wychowaniec et al. (2020a) and Gao et al. (2017)
Cyclic (FKFE)$_2$	Ac-CFKFEFKFECG-NH$_2$	Bowerman and Nilsson (2010)

similar to EAK and RAD peptides, $(FKFE)_3$ underwent self-assembly and hydrogelation at characteristic coagulation concentrations that were dependent on the valence of counterions in the assembly solutions (Caplan et al. 2000) They subsequently explored the effects of varying sequence length ($(FKFE)_2$ and $(FKFE)_4$), replacement of Phe residues with Ile or Val ($(IKIE)_3$ and $(VKVE)_3$), and the Glu residue with Gln ($(FKFQ)_3$) (Caplan et al. 2002a). These studies revealed that increased side chain hydrophobicity decreased the required concentration of NaCl needed to promote gelation of the self-assembled network. These observations illustrate that peptide hydrophobicity can be exploited to tune the properties of assembled materials as a function of their environment.

Additional variations of these amphipathic peptides have been explored in pursuit of further insight into structure-function correlation between sequence, self-assembly propensity, and emergent properties. Muller and coworkers modified the charge distribution with $[(FE)_2(FK)_2]_2$ as the basis peptide and replaced selected Phe residues with Gly, Ala, Val, Leu, and Ile (Wang et al. 2005). Each of these variant peptides formed β-sheet assemblies with the exception of one sequence where there was substitution for three Gly residues (Ac-IEAEGKGKIEGEAKIK-NH$_2$). The lack of β-sheet formation for the peptide with high Gly content was attributed to the increased backbone flexibility of this sequence (Wang et al. 2005). The peptide sequence order and the steric bulk of the hydrophobic amino acids both impacted the morphology of these β-sheet assemblies. This work provided understanding of the scope and limitation of sequences that self-assemble into β-sheet materials.

The $(FKFE)_2$ peptide has since emerged as a commonly studied peptide to explore various facets of supramolecular β-self-assembly. For example, Marini et al. found that at low pH the $(FKFE)_2$ peptide initially formed left-handed helical tapes with a 7 nm diameter and a 20 nm helical pitch (Marini et al. 2002). It was observed that after 90 min these helices were no longer the dominant morphology, instead presenting flat tapes with a 7 nm diameter and no helical pitch. These "flat tapes" have subsequently been shown to be nanotubes (Wang et al. 2021). Initial molecular modeling suggested that the observed $(FKFE)_2$ assemblies were composed of antiparallel β-sheets in which the strand alignment leaves the terminal Phe residue offset. The 7 nm diameter correlates to two laminated sheets aligned edge to edge (Hwang et al. 2003). Nilsson and coworkers have observed similar helical ribbon and nanotube structures (Fig. 2.4), though the helical species persisted for several weeks before nanotubes were observed to dominate the assembled structures (Bowerman et al. 2009).

Nilsson and coworkers adopted Ac-$(XKXE)_2$-NH$_2$ as a sequence template to study the role of varying hydrophobicity and aromaticity in promotion of β-sheet self-assembly (Bowerman et al. 2009). In this study, the hydrophobic amino acid, X, was Ala, Val, Leu, Phe, or cyclohexylalanine (Cha), listed in order of increasing peptide hydrophobicity. Ac-$(AKAE)_2$-NH$_2$ failed to undergo self-assembly under the concentrations used in the study. The remaining peptides were all found to assemble into β-sheet structures, with only Ac-$(FKFE)_2$-NH$_2$ forming helical ribbons and nanotubes, likely due to steric constraints imposed by the aromatic Phe sidechains (Bowerman et al. 2009; Betush et al. 2018). The remaining peptide

Fig. 2.4 Transmission electron micrograph of (FKFE)₂ β-sheet assemblies showing both the helical and nanotube structures. Adapted with permission from (Bowerman et al. 2009). Copyright 2009 Royal Society of Chemistry
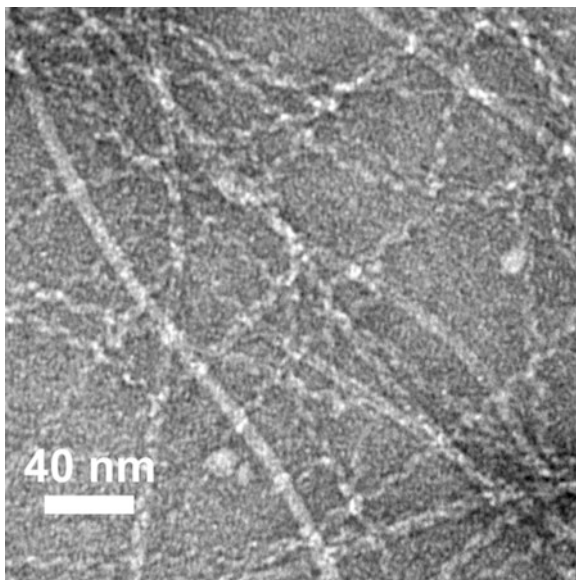
sequences formed morphologically distinct assemblies as a function of hydrophobic amino acid identity. Moreover, the hydrophobicity of the nonpolar amino acids correlated to general fibril density in the samples. Saiani et al. also compared the assembly properties of (FEFK)₂ and (FE)₂(FK)₂ peptides with (AEAK)₂ and (AE)₂(AK)₂ peptides (Mohammed et al. 2007; Saiani et al. 2009). The Ala-containing peptides required significantly higher concentrations to undergo assembly, consistent with the data previously reported by Nilsson et al. In addition, the capacity of these Ac-(XKXE)₂-NH₂ β-sheet bilayer assemblies to accommodate bulky hydrophobic amino acids in the hydrophobic core has been assessed (Jones et al. 2021). Peptides in which X is Phe, homophenylalanine (Hph), Trp, 1-naphthylalanine (1-Nal), 2-naphthylalanine (2-Nal), or biphenylalanine (Bip) (in order of increasing steric profile) were assessed. It was found that all the peptides effectively self-assemble into β-sheet bilayer fibrils, with the rate of assembly increasing as the peptide hydrophobicity increases. The identity of amino acid X also impacted the morphology of the assembled β-sheet structures. Saiani and Miller also investigated the effect of alterations to the hydrophobic face by comparing two peptides: F9 and FC9-BM, the latter peptide being identical save for the replacement of the third phenylalanine residue with a cysteine which was then conjugated to bromomaleimide (Table 2.2) (Elsawy et al. 2016). This change in sequence resulted in the partial loss of the extended β-sheet conformation of these peptide assemblies and significantly affected fibril morphology, indicating that the hydrophobic interactions play a significant role in the self-assembly of these peptides (Elsawy et al. 2016). Collectively, these studies demonstrate the impressive capacity for self-assembling amphipathic peptides to accommodate sequence changes that affect the self-assembly process.

Nilsson and coworkers also studied the impact of amino acid aromaticity and hydrophobicity on β-sheet assembly using cationic Ac-(XK)$_4$-NH$_2$ peptides (Bowerman et al. 2011). In these studies, X was Val, Ile, Phe, pentafluorophenylalanine (^{F5}F), or Cha in order of increasing hydrophobicity. This family of peptides fails to undergo self-assembly in simple aqueous solutions due to charge repulsion from the cationic Lys residues; self-assembly was triggered by increasing the ionic strength of the solution through addition of NaCl, which effectively screens repulsive charge effects (Bowerman et al. 2011) With the exception of Ac-(VK)$_4$-NH$_2$, which failed to undergo self-assembly under the conditions examined, each of the other peptides effectively formed β-sheet assemblies. As the hydrophobicity of the peptide increased, the amount of salt required to promote self-assembly decreased. Interestingly, these assemblies also formed hydrogel networks, and those assemblies that contained aromatic amino acids provided hydrogels with higher viscoelasticity, suggesting the possible presence of aromatic interactions that further stabilized the entangled β-sheet network (Bowerman et al. 2011).

The effect of length and sequence order on β-sheet self-assembly has also been investigated within this type of amphiphilic peptide (Guilbaud et al. 2010; Guilbaud et al. 2013; Wychowaniec et al. 2020b; Lee et al. 2013a; Lee et al. 2013b). The assembly of Ac-(FKFE)$_2$-NH$_2$, an octamer, was also compared to the assembly of two shorter heptamer peptides: Ac-FKFEFKF-NH$_2$ and Ac-KFEFKFE-NH$_2$ (Lee et al. 2013b). It was found that at acidic pH, Ac-FKFEFKF-NH$_2$ self-assembled into β-sheet tapes that were distinct from the Ac-(FKFE)$_2$-NH$_2$ helical ribbons and nanotubes. At acidic pH, Ac-KFEFKFE-NH$_2$ showed no evidence of self-assembly at the concentrations studied. At neutral pH, all three peptides effectively self-assembled, although each peptide formed β-structures with distinctive morphologies. Ulijn, Saiani, and Miller made use of the tetrapeptide FEFK (Table 2.2) to investigate enzymatically triggered synthesis and assembly of amphipathic β-sheet peptides (Guilbaud et al. 2010; Guilbaud et al. 2013). In the concentration range studied (up to 300 mg mL^{-1}), the tetrapeptide did not undergo self-assembly. The subsequent addition of thermolysin to the peptide solution triggered formation of a hydrogel (Guilbaud et al. 2010). Initially, thermolysin partially hydrolyzed the peptides into dipeptides; however, eventually new peptides were formed as a result of reverse hydrolysis. Given enough time, the main products of these reverse hydrolysis reactions were octapeptides composed of four Phe residues, two Glu residues, and two Lys residues, indicating that these were the thermodynamically favored products (Guilbaud et al. 2010). Elsawy et al. were also intrigued by the FEFK tetrapeptide and sought to rationally modify it and improve its self-assembly properties (Wychowaniec et al. 2020b). By replacing the phenylalanine residues with phenylglycine (Phg), which is significantly more rigid, the aromatic sidechains were locked in a position which favored aromatic interactions. This change yielded a short peptide which self-assembled into a hydrogel at 20 mg/mL. Additionally, this peptide was able to act as an emulsifier, further broadening its potential biomaterial applications (Wychowaniec et al. 2020b). Roy and coworkers also modified the FEFK sequence in order to access a self-assembling material. Their rational design involved the conjugation of napthoxyacetic acid to the N-terminus of the peptide

(Kaur et al. 2020). The addition of this aromatic group allowed the peptide to assemble into a variety of nanostructures, dependent on the pH at which it was assembled (Kaur et al. 2020). These nanostructures resulted in materials with different physical properties, broadening the scope of materials formed by tetrapeptides of this class. The ability of these gels to form at physiological pH led Roy and coworkers to test their biocompatibility with a range of cells and demonstrated successful adhesion and growth with fibroblasts as well as several neuronal cell lines (Kaur et al. 2020).

The self-assembly of peptides with identical amino acid composition but different sequence patterning was also studied: Ac-(FKFE)$_2$-NH$_2$, Ac-(FK)$_2$(FE)$_2$-NH$_2$, Ac-KEFFFFKE-NH$_2$, Ac-(KFFE)$_2$-NH$_2$, and Ac-FFKEKEFF-NH$_2$ (Lee et al. 2013a). It was found that Ac-(FKFE)$_2$-NH$_2$ and Ac-(FK)$_2$(FE)$_2$-NH$_2$ effectively self-assembled, although the latter formed fibrils as opposed to the nanoribbons and nanotubes formed by Ac-(FKFE)$_2$-NH$_2$. In contrast, Ac-KEFFFFKE-NH$_2$ formed distinct β-sheet nanotapes with three times the width of the thinner structures formed by Ac-(FKFE)$_2$-NH$_2$ and Ac-(FK)$_2$(FE)$_2$-NH$_2$. Ac-(KFFE)$_2$-NH$_2$ assembled into mixtures of nanoribbons and spherical micelles, and IR spectra of the amide I region suggested that the major secondary structure was not β-sheet, but rather random structures. Ac-FFKEKEFF-NH$_2$ failed to self-assemble under the conditions explored in this study. Together, these works indicate that both sequence length and sequence pattern exert strong effects on self-assembly pathways in the formation of β-sheet assemblies.

The effect of charge as well as the distribution of charge has also been investigated for peptides which fall within this peptide family. Saiani and Miller investigated the role of net charge on β-sheet assembly of three peptides, VEK1, VEK2, and VEK3 (Table 2.2) (Roberts et al. 2012). At pH 7, these peptides have a −2, 0, and +2 charge, respectively. Interestingly, they found that the critical gelation concentration was directly dependent on the charge modulus at the pH of assembly (Roberts et al. 2012). As the charge modulus decreased, there were fewer observed lateral interactions between peptide fibrils, which may explain this observation. Furthermore, these peptide hydrogels were loaded with two different hydrophilic molecules to act as model drugs: naphthol yellow and Martius yellow. The release of these molecules showed a rate of diffusion which was dependent on the charge of the peptide as well as the molecule that was being released, but independent of the gelator concentration and mechanical properties of the hydrogel. This suggested that rate of diffusion for these systems could be directly controlled by manipulating the ratio of charge between the hydrogel network and the molecule to be released (Roberts et al. 2012). Woodrow and coworkers made a small library of peptides (Table 2.2) to investigate salt-triggered hydrogels (Zhang et al. 2017). First they compared the assembly propensity of several peptides, (RVQV)$_3$, (RVQV)$_3$-Am, and (RV)$_6$, in both water and dilute PBS. (RVQV)$_3$, (RVQV)$_3$-Am, and (RV)$_6$ all had net charges which were high enough to prevent self-assembly into fibers due to electrostatic repulsion. In contrast, (RVEV)$_3$ whose net charge in water is 1 formed well-defined nanofibrils (Zhang et al. 2017). In PBS, which has an increased ionic strength, (RVQV)$_3$ formed a dense fibril network. (RVQV)$_3$-Am and (RV)$_6$ had
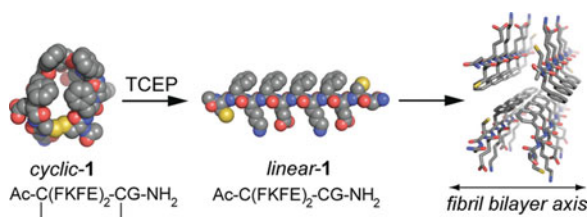
Fig. 2.5 A schematic representation of the stimulus-responsive self-assembly of cyclic (FKFE)$_2$ peptide. Nitrogen atoms are blue, oxygen atoms are red, carbons are gray, and sulfur atoms are yellow. Addition of the TCEP-reducing agent facilitates cleavage of the disulfide bond and subsequent relaxation of the constrained cyclic structure to β-strands that undergo rapid β-sheet self-assembly. Reproduced with permission from (Bowerman and Nilsson 2010). Copyright 2010 American Chemical Society

some assembly but were still hindered by charge repulsions. Interestingly, a fraction of (RVEV)$_3$ formed particles in PBS due to self-complementarity (Zhang et al. 2017). Due to its ability to remain a solution in water, but to form a hydrogel when the ionic strength was high enough, Woodrow and coworkers chose (RVQV)$_3$ as a scaffold and conjugated it to a biological motif, OVA$_{257-264}$, producing the peptide OVA-Z1 (Table 2.2). This bioconjugated peptide was able to enhance CD8$^+$ T-cell activation in vitro (Zhang et al. 2017).

The self-assembled β-sheet fibrils formed from peptides in this class have three major structural features: the hydrophobic core, the hydrophilic surface, and the fiber edges where the hydrophobic residues may be exposed. Saiani and Miller have studied the role of these fiber edges and their interactions in modulating network topology and physical properties of the emergent hydrogels (Wychowaniec et al. 2020a; Gao et al. 2017). The importance of sheet-edge interactions was clearly demonstrated by the comparison of (FEFK)$_2$ and K(FEFK)$_2$K peptide assemblies. The addition of lysine residues to the edges of the peptides did not affect the ability of the peptide to assemble into β-sheet fibrils, but did decrease the lateral aggregation into fibril bundles as compared to (FEFK)$_2$ (Wychowaniec et al. 2020a). This change in network topology also produced materials with significantly weaker mechanical properties, indicating that the lateral interactions between fibrils are paramount to the emergent properties of peptide materials within this class (Wychowaniec et al. 2020a).

The Nilsson group also modified this family of β-sheet peptides to create sequences that undergo stimulus-responsive self-assembly under reducing conditions (Bowerman and Nilsson 2010). Specifically, (FKFE)$_2$ peptides were prepared in which the assembly motif was flanked by a Cys residue at each terminus. These Cys residues facilitate cyclization of the peptides by disulfide bond formation (Fig. 2.5). The peptide did not assemble in cyclic form since it could not adopt the requisite β-sheet orientation. However, upon addition of a reducing agent, the disulfide bond breaks and β-sheet assembly occurs rapidly (Bowerman and Nilsson 2010). Amphipathic peptides with alternating hydrophobic/hydrophilic amino acid

sequence patterns self-assemble extremely rapidly in aqueous solutions. Thus, peptide cyclization provides a convenient strategy to exert control over the self-assembly of these types of materials as a function of the chemical environment.

As stated previously, determination of the precise molecular structure of β-sheet assemblies has been exceptionally challenging. Solid-state NMR has been a valuable tool in defining the structure of self-assembled β-sheet nanomaterials, though like most techniques it has limits. Recently, Conticello, Egelman, and coworkers have reported near-atomic resolution structures of the polymorphic left-handed helical ribbons and nanotubes formed by the $(FKFE)_2$ peptide using cryo-EM methods (Wang et al. 2021). In a stunning finding, Egelman and Conticello discovered that the exterior β-sheets of these nanoribbons and nanotubes are *antiparallel* pleated β-sheets and that the interior β-sheets are *parallel* β-sheets (Fig. 2.6)! This remarkable level of peptide orientational polymorphism within the assembled structures was completely unanticipated. This work illustrates that our current understanding of the structure of self-assembled β-sheet nanomaterials does not reflect the level of complexity that likely to exists in many of these types of materials. In the coming decades, structural analysis using high-resolution methods such as ssNMR and cryo-EM must be critical elements in the study of β-sheet assemblies in order to increase our ability to accurately design these materials.

2.3.3 *P11 Peptides and Related Sequences*

Nature has motivated the design of many β-sheet supramolecular materials. In one example, Aggeli and Boden drew inspiration from the IsK protein transmembrane segment in the design of the K24 peptide (Table 2.3) as a self-assembling β-sheet peptide (Aggeli et al. 1997). They demonstrated that the 24-amino acid K24 peptide formed tape-like structures composed of β-sheet bilayer assemblies (Aggeli et al. 1997). In pursuit of a shorter self-assembling peptide, Aggeli and Boden took some inspiration from Lysβ-21 (Table 2.3) a domain which forms a three stranded β-sheet in hen egg white lysozyme. They also drew inspiration from the huntingtin protein, a poly-Gln repeat protein implicated in Huntington's disease. They experimented with various short poly-Gln-containing peptides, including the 11-amino acid $P_{11}-1$ and P_{11} peptide derivatives (Table 2.3) (Aggeli et al. 1997; Fishwick et al. 2003; Berryman et al. 2009; Carrick et al. 2005; Aggeli et al. 2003; Kayser et al. 2004; Carrick et al. 2007). The $P_{11}-1$ peptide formed short β-sheet nanotapes approximately 300 nm in length, whereas $P_{11}-2$ formed β-sheet fibrils greater than a micron in length (Fishwick et al. 2003; Nyrkova et al. 2000). Computational simulations suggested that aromatic interactions from the Phe and Trp residues which reside in the hydrophobic core of the $P_{11}-2$ β-sheet bilayer (Fig. 2.7) account for the longer persistence length of these assemblies compared to the shorter $P_{11}-1$ nanotapes (Fishwick et al. 2003; Kayser et al. 2004). In addition, it was shown that
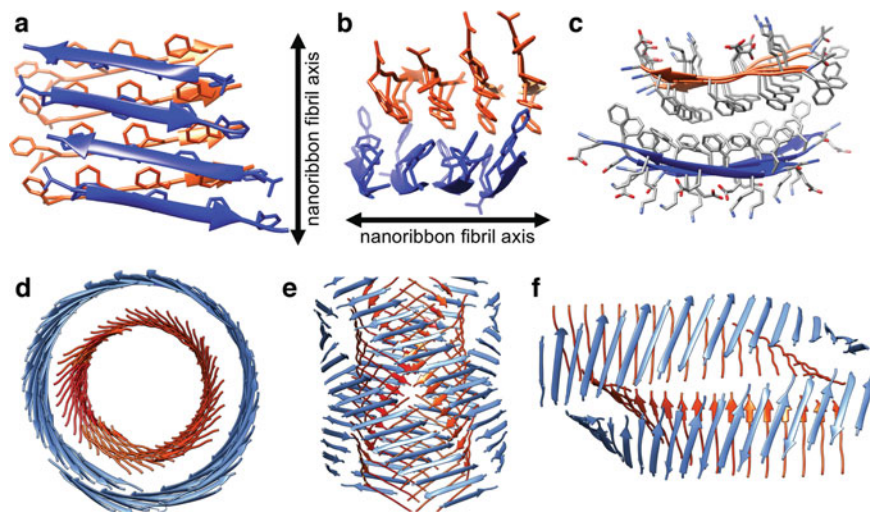
Fig. 2.6 Selected structural representations of the β-sheet structure of (FKFE)$_2$ nanotubes and nanoribbons determined by cryo-EM. (**a**) An illustration of the pleated β-sheet bilayer structure formed by self-assembled (FKFE)$_2$ (constructed from PDB 7LQE). The orange and blue strands differentiate between the interior and exterior sheets in the bilayer, respectively. The external β-sheet (blue) is composed of antiparallel β-sheets, and the interior sheet (orange) is composed of parallel β-sheets. (**b**) An edge view of the β-sheet bilayer structure of (FKFE)$_2$ shown in panel (**a**) (PDB 7LQE). (**c**) A 90-degree rotation of the β-sheet bilayer structure of (FKFE)$_2$ shown in panel (**a**) (PDB 7LQE). (**d**) A top view of an (FKFE)$_2$ β-sheet nanotube (PDB 7LQE). (**e**) A 90-degree rotation of the image shown in panel (**d**) that shows two helical β-sheet protofilaments each composed of two side-by-side bilayers of L-Ac-(FKFE)$_2$-NH$_2$ β-sheets that entwine to form the mature nanotube (PDB 7LQE). (**f**) A representation of a section of a single isolated protofilament from the nanotube structures shown in panels (**d**) and (**e**). The exterior β-sheets (blue) are antiparallel β-sheets and the interior β-sheets (orange) are parallel β-sheets (PDB 7LQE). Structures shown are constructed from PDB files that originated in (Wang et al. 2021)

incorporation of ionizable amino acids on the hydrophilic face of the assembly (see P$_{11}$4–P$_{11}$9, Table 2.3) imparts pH sensitivity to the self-assembly of these sequences (Fishwick et al. 2003; Carrick et al. 2007). The effect of sequence length on the self-assembly properties of these sequences has been studied using P_x^{-2} peptides, in which x is the length of the peptide (Davies et al. 2017). It was found that shorter sequences have higher CACs, providing another tool to modulate the supramolecular properties of these materials (Davies et al. 2017).

This series of peptides and related sequences have been widely used for a variety of biomaterial applications (Cai et al. 2020; Al-Halifa et al. 2019). Peptides from this 11 amino acid sequence family and related sequences (such as the Q11 peptide developed by Collier and Messersmith) (Collier and Messersmith 2003; Collier and Messersmith 2004) have been used as 3D tissue culture matrices (Maude et al. 2011; Jung et al. 2009; Jung et al. 2008; Kyle et al. 2012; Gasiorowski and Collier 2011; Tian et al. 2011; Hainline et al. 2019) (injectable lubricants for osteoarthritis (Bell

Table 2.3 A selection of peptide sequences from the P11 peptide family

Name	Sequence	Reference
K24	H_2N-KLEALYVLGFFGFFTLGIMLSYIR-CO_2H	Aggeli et al. (1997)
Lysβ-21	Ac-QAYNRNYRGSTDYGILQINSR-NH_2	Aggeli et al. (1997)
P_{11}–1	Ac-QQRQQQQQEQQ-NH_2	Fishwick et al. (2003)
P_{11}–2 (DN1)	Ac-QQRFQWQFEQQ-NH_2	Aggeli et al. (1997)
P_{11}–3	Ac-QQRFQWQFQQQ-NH_2	Aggeli et al. (2003)
P_{11}–4	Ac-QQRFEWEFEQQ-NH_2	Aggeli et al. (2003)
P_{11}–5	Ac-QQOFOWOFEQQ-NH_2	Aggeli et al. (2003)
P_{11}–8	Ac-QQRFOWOFEQQ-NH_2	Carrick et al. (2007)
P_{11}–9	Ac-SSRFOWOFESS-NH_2	Carrick et al. (2007)
Q11	Ac-QQKFQFQFEQQ-NH_2	Carrick et al. (2007) and Collier and Messersmith (2003)

et al. 2006), and treatment of early caries lesions(Brunton et al. 2013) an5d for immunotherapy (Mora-Solano et al. 2017; Si et al. 2018). Collier and Messersmith have developed a modified peptide in this class, Q11, that has also been used as a functional biomaterial scaffold for a wide range of applications (Collier and Messersmith 2003; Collier and Messersmith 2004). Many of these applications rely on the self-assembled β-sheet materials as a scaffold that is used to present a multivalent display of functional motifs, including cell signaling peptides and immunogenic epitopes (Distaffen et al. 2021) The biocompatibility of these supra-molecular assemblies makes them outstanding candidates as next-generation biomaterials.

2.3.4 Multidomain Peptides

Hartgerink et al. developed a class of multidomain peptides with an ABA motif pattern to investigate the balance between noncovalent forces that promote β-sheet assembly with the frustrating forces of charge repulsion (Table 2.4) (Dong et al. 2007; Aulisa et al. 2009). In these systems, the B block is the amphipathic segment with alternating hydrophobic and hydrophilic residues, and the A block contains a variable number of charged amino acids (Fig. 2.8) (Dong et al. 2007) Initial studies were conducted using two systems, where they perturbed either the A or B blocks within the motif: Ac-$K_n(QL)_6K_n$-NH_2 (with n = 0–4) and Ac-$K_2(QL)_mK_2$-NH_2 (m = 2–6). The variation of the B block yielded peptides with a range of self-assembly behaviors. Ac-$K_2(QL)_2K_2$-NH_2, Ac-$K_2(QL)_3K_2$-NH_2, and Ac-$K_2(QL)_4K_2$-NH_2 remained random coil in structure and formed only amorphous aggregates. Ac-$K_2(QL)_5K_2$-NH_2 showed weak β-sheet structure accompanied by the observation of spherical aggregates and short, 5 nm wide fibrils. The $K_2(QL)_6K_2$ peptide formed β-sheet fibers which were 120 nm long, 6 nm wide, and 2 nm in
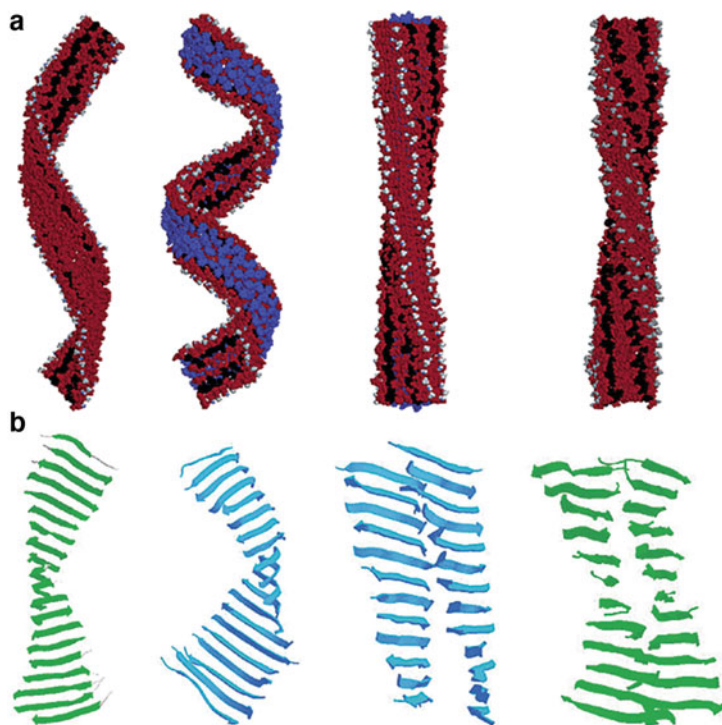
Fig. 2.7 (**a**) Molecular models of $P_{11}-1$ and $P_{11}-2$ tapes (left) and ribbons (right). Aromatic residues are highlighted in blue. (**b**) Side views of β-sheet assemblies from molecular dynamic simulations for 100 ps time periods. Reprinted with permission from (Fishwick et al. 2003). Copyright 2003, American Chemical Society

Table 2.4 A selection of multi-domain peptide sequences

Name	Sequence	Reference
$K_2(QL)_6K_2$	Ac-KKQLQLQLQLQLQLKK-NH$_2$	Dong et al. (2007)
$E(QL)_6E$	Ac-EQLQLQLQLQLQLE-NH$_2$	Aulisa et al. (2009)
$K_2(SL)_6K_2$	Ac-KKSLSLSLSLSLSLKK-NH$_2$	Aulisa et al. (2009)
$E(SL)_6E$	Ac-ESLSLSLSLSLSLE-NH$_2$	Aulisa et al. (2009)
$K_2(QFQL)_3K_2$	Ac-KKQFQLQFQLQFQLKK-NH$_2$	Bakota et al. (2013)
$K_2(QF)_6K_2$	Ac-KKQFQFQFQFQFQFKK-NH$_2$	Bakota et al. (2013)
$K_2(QW)_6K_2$	Ac-KKQWQWQWQWQWQWKK-NH$_2$	Bakota et al. (2013)
$K_2(QY)_6K_2$	Ac-KKQYQYQYQYQYQYKK-NH$_2$	Bakota et al. (2013)
$O_5(SL)_6O_5$	Ac-OOOOOSLSLSLSLSLSLOOOOO-NH$_2$ (O is hydroxyproline)	Lopez-Silva et al. (2019)

Fig. 2.8 (**a**) Summary of the molecular assemblies formed by the varying K$_2$ and (QL)$_6$ peptides. (**b**) Proposed model of assembly for these K$_2$ and (QL)$_6$ peptides. Reproduced with permission from (Dong et al. 2007). Copyright 2007 American Chemical Society
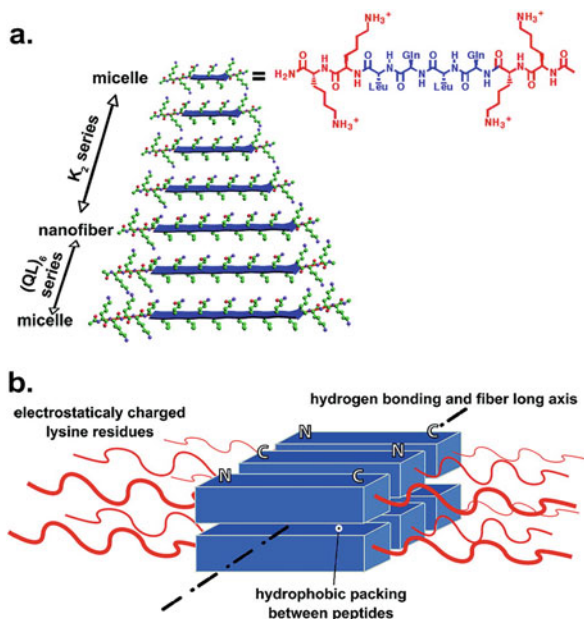
height. This was the first example of length-controlled fibrils in amphipathic β-sheet peptide assembly (Dong et al. 2007; Aulisa et al. 2009) Within the Ac-K$_n$(QL)$_6$K$_n$-NH$_2$ series of peptides, Ac-(QL)$_6$-NH$_2$ and Ac-K(QL)$_6$K-NH$_2$ were poorly soluble in water. Adding greater than two Lys residues in the A blocks (Ac-K$_3$(QL)$_6$K$_3$-NH$_2$ and Ac-K$_4$(QL)$_6$K$_4$-NH$_2$) resulted in peptides that assembled weakly or not at all. The culmination of these systems indicated that Ac-K$_2$(QL)$_6$K$_2$-NH$_2$ was the most promising peptide to use as a starting point in further experimentation.

Changes to the charged amino acid patterns in β-sheet self-assembling peptides have been found to alter their emergent properties. The use of Glu in place of Lys in the flanking regions resulted in a peptide, E(QL)$_6$E (Table 2.4), that required only a single amino acid in the A blocks to maintain peptide and fibril solubility as opposed to Lys, which required at least two residues in each A block (Aulisa et al. 2009). The use of Glu also facilitated the use of divalent cations to promote assembly by coordinating neighboring negatively charged carboxylates (Aulisa et al. 2009). The replacement of Gln with Ser (K$_2$(SL)$_6$K$_2$, Table 2.4) yielded significantly longer fibrils that enabled formation of a shear-responsive hydrogel network, ideal for biological applications which require injection (Aulisa et al. 2009). Hartgerink et al. also investigated the effect of incorporation of aromatic amino acids in the hydrophobic core (K$_2$(QFQL)$_3$K$_2$, K$_2$(QF)$_6$K$_2$, K$_2$(QW)$_6$K$_2$, and K$_2$(QY)$_6$K$_2$, Table 2.4). Interestingly, they observed morphology changes as well as a preference for arrangement into parallel β-sheets rather than antiparallel for the peptides where Leu was replaced with Tyr and Trp (Bakota et al. 2013). Finally, they also studied peptides with hydroxyproline (Hyp, O) in the A block positions (O$_n$(SL)$_6$O$_n$) to

determine the effects of neutral residues in these flanking positions (Lopez-Silva et al. 2019). Hyp had the ideal combination of hydrophilicity and steric bulk in the flanking positions due to the tendency for poly-Hyp sequences to form polyproline type II helices. Of the peptides tested in this series, $O_5(SL)_6O_5$ self-assembled into β-sheet fibrils that were prone to hydrogelation (Lopez-Silva et al. 2019). These hydrogels were shown to support the viability of fibroblasts cultured within the matrix without inducing inflammatory responses. These combined properties demonstrate the potential of these materials for biological applications.

Multidomain peptide β-sheet assemblies have been validated for use in a range of biomaterial applications. Many of these involve the assembly of multidomain peptides that incorporate functional motifs at the surface of the fibrils to facilitate desired interactions with the biological environment. Kumar et al. have used multidomain peptide assembly domain for a range of applications that include an antiangiogenic scaffold and a delivery system for EPep2–8 to regulate lipoprotein homeostasis and for the controlled release of naloxone (Nguyen et al. 2018; Harbour et al. 2020; Crowe et al. 2020). Dong and coworkers have demonstrated that multidomain β-sheet assemblies can be applied for drug delivery, as antimicrobial agents which selectively kill bacteria without becoming cytotoxic to mammalian cells, and for cell penetrating applications (Yang et al. 2014; Jiang et al. 2015; Xu et al. 2015a; Chen et al. 2019a; Chen et al. 2019b; Xu et al. 2015b; Yang and Dong 2020). Related assemblies modified with appropriate functional elements have been used as in vitro tissue culture matrices,(Bakota et al. 2011) as antimicrobial materials,(Jiang et al. 2015; Xu et al. 2015a; Chen et al. 2019a; Chen et al. 2019b) to promote gene transfection,(Xu et al. 2015b; Yang and Dong 2020) as materials for the controlled release and delivery of drugs,(Crowe et al. 2020; Yang et al. 2014; Bakota et al. 2011; Kumar et al. 2015a; Li et al. 2016; Moore and Hartgerink 2017) as materials for dental pulp tissue engineering,(Galler et al. 2012; Kang et al. 2014) to regulate of lipoprotein homeostasis,(Harbour et al. 2020) to promote angiogenesis,(Kumar et al. 2015b; Wickremasinghe et al. 2015) to elicit anti-angiogenic effects,(Nguyen et al. 2018) to promote nerve regeneration,(Lopez-Silva et al. 2021) and to accelerate wound healing (Carrejo et al. 2018).

2.4   β-Hairpin Self-Assembling Peptides

Schneider and Pochan designed β-hairpin peptides in pursuit of further diversifying self-assembling peptide materials. These hairpin peptides are composed of strands of alternating charged residues (Lys) and hydrophobic residues separated by a D-Pro-L-Pro (^{D}PP) motif that promotes type II′ hairpin formation (Ozbas et al. 2004a). Their first reported hairpin peptide, MAX1 (Table 2.5), remains unassembled in aqueous solution, but undergoes β-hairpin folding and self-assembly in response to changes in pH (Schneider et al. 2002), temperature (Pochan et al. 2003), and/or ionic strength (Ozbas et al. 2004b). The resulting β-hairpin fibrils efficiently form entangled hydrogel networks. These MAX1 self-assembled

Table 2.5 A selection of β-hairpin self-assembling peptide sequences

Name	Sequence	Reference
MAX1	H_2N-VKVKVKVKV^{D}PPTKVKVKVKVKV-NH_2	Schneider et al. (2002)
MAX4	H_2N-KVKVKVKVK^{D}PPSVKVKVKVKVK-NH_2	Rajagopal et al. (2006)
MAX5	H_2N-VKVKVKVKV^{D}PPSKVKVKVKVKV-NH_2	Rajagopal et al. (2006)
MAX8	H_2N-VKVKVKVKV^{D}PPTKVEVKVKV-NH_2	Haines-Butterick et al. (2007)
MAX-X	H_2N-XKXKXKXKV^{D}PPTKXKXKXKX-NH_2	Micklitsch et al. (2015)
HLT2	H_2N-VLTKVKTKV^{D}PPTKVEVKVLV-NH_2	Medina et al. (2015)
SSP1	H_2N-VKVKV^{D}PPTKVKVKVKVKVKV-NH_2	Nagarkar et al. (2008)
SSP2	H_2N-VKVKVKV^{D}PPTKVKVKVKVKVKV-NH_2	Nagarkar et al. (2008)
TSS1	H_2N-VKVKVKVKV^{D}PPTKVKVKVKVK^{D}PPKVKVKVKV-NH_2	Rughani et al. (2009)
SVS-1	H_2N-KVKVKVKV^{D}PPTKVKVKVK-NH_2	Sinthuvanich et al. (2012) and Gaspar et al. (2012)

hydrogels were shown to be cytocompatible and to support fibroblast proliferation within the hydrogel matrix (Kretsinger et al. 2005). MAX1 fibrils also displayed inherent antibacterial activity (Salick et al. 2007).

MAX1 is a peptide designed to make use of lateral hydrophobic interactions. Variants of the MAX1 peptide, MAX4 and MAX5 (Table 2.5), were designed to probe the importance of these lateral hydrophobic interactions in the self-assembly process. MAX4 was designed to inhibit some of these interactions by changing the position of the charged residues and hydrophobic residues. MAX5 was a control peptide used to ensure that the change from threonine to serine was not responsible for any of the observed changes in self-assembly (Rajagopal et al. 2006). It was concluded based on CD spectroscopy, rheology, and TEM that the hydrophobic interactions aid the kinetics of assembly and contribute to the rigidity of resultant hydrogels (Rajagopal et al. 2006). The influence of the hydrophobic sidechains on assembly and gelation was further interrogated using MAX-X peptides (Table 2.5) in which X represented Val, aminobutyric acid, norvaline, norleucine, Phe, or Ile (Micklitsch et al. 2015). The identity of the amino acid in the X position in these peptides was not found to significantly change the local morphology of the assembled fibrils, but did affect the higher-order assembly as evidenced by changes in mechanical rigidity and rate of gelation (Micklitsch et al. 2015).

Changes in the parent MAX1 peptide were found to tune the properties of the resultant hydrogel assemblies for specific biological applications. The MAX8 peptide differs from MAX1 by a single Lys to Glu substitution (Table 2.5) (Haines-Butterick et al. 2007). Assemblies of MAX8 were found to have improved properties for assembly and gelation in complex tissue culture media, including DMEM. These hydrogels were able to homogenously suspend cells in the media throughout the gel due to the rapid gelation time, as well as support the viability and proliferation of these cells within the hydrogel matrix. They also exhibited the thixotropic

shear-response properties that are necessary for injectable hydrogels (Yan et al. 2010). In cellular tests, MAX1 and MAX8 showed no macrophage activation in vitro that would be consistent with an inflammatory response, suggesting that these gels were excellent candidates for in vivo delivery of cells (Haines-Butterick et al. 2008; Yan et al. 2012). MAX1-derived hydrogels were also shown to release molecular cargo by diffusion at rates that support the potential of these materials for sustained and localized drug delivery (Branco et al. 2009; Branco et al. 2010; Altunbas et al. 2011; Lindsey et al. 2015; Nagy-Smith et al. 2016; Sun et al. 2016b). Both MAX1 and MAX8 assemblies were effective as templates for silica precursors used to mimic biosilification, providing a high fidelity template for inorganic materials (Altunbas et al. 2010). Finally, MAX1, MAX8, and the derivative HLT2 self-assembled β-hairpins were demonstrated to be effective plasmid DNA transfection agents that enhanced the immunostimulatory activity of the delivered genes (Medina et al. 2015).

Encouraged by the wide range of applications that the MAX1 family of β-hairpin peptides had exhibited, several more selective applications were explored. Inspired by cadherin dimerization by swapping of N-terminal EC1 β-strand domains (Vendome et al. 2011), they designed a set of strand swapped β-hairpin peptides, SSP1 and SSP2 (Table 2.5) (Nagarkar et al. 2008). These β-hairpin peptides have asymmetric structures with SSP1 containing an eight residue exchangeable β-strand domain and SSP2 having a four residue exchangeable domain (Nagarkar et al. 2008). These peptides underwent thermally triggered self-assembly into β-hairpin assemblies in which the longer strand retains unpaired amino acids that are available to form strand-swapped β-sheet structures. SSP1 assembled into twisted fibrils and SSP2, which had a longer strand-swapped segment, assembled into fibrils which were not twisted (Nagarkar et al. 2008). Subsequently, Pochan and Schneider also designed a three stranded peptide which contained two hairpin turns, TSS1 (Table 2.5) (Rughani et al. 2009). As with other peptides in the MAX1 series, these TSS1 double β-hairpin hydrogels were also shown to assemble into cytocompatible, shear thinning materials (Rughani et al. 2009).

Another β-hairpin peptide, SVS-1, was designed for anticancer activity (Sinthuvanich et al. 2012; Gaspar et al. 2012; Medina and Schneider 2015). It remained unfolded in solution due to charge repulsion of the cationic residues, but folded and assembled when it encountered the surface of cancer cells, thereby disrupting the membrane. This interaction was designed to be driven by the interaction between the negatively charged membrane surface on cancer cells and the peptides themselves. It showed activity against a wide range of cancer cells, but low cytotoxicity to noncancerous cells which have different lipid membrane compositions, making it a promising nanomaterial (Sinthuvanich et al. 2012). Additionally, the SVS-1 peptide is shorter than other peptides within this class, making it more cost-effective for therapeutic applications. In contrast to the mechanism of action that most antimicrobial peptides use, this anticancer peptide did *not* need to fully neutralize the membrane charge in order to kill the cells, as shown by zeta potential analyses (Gaspar et al. 2012). The folding activity of SVS-1 was also used
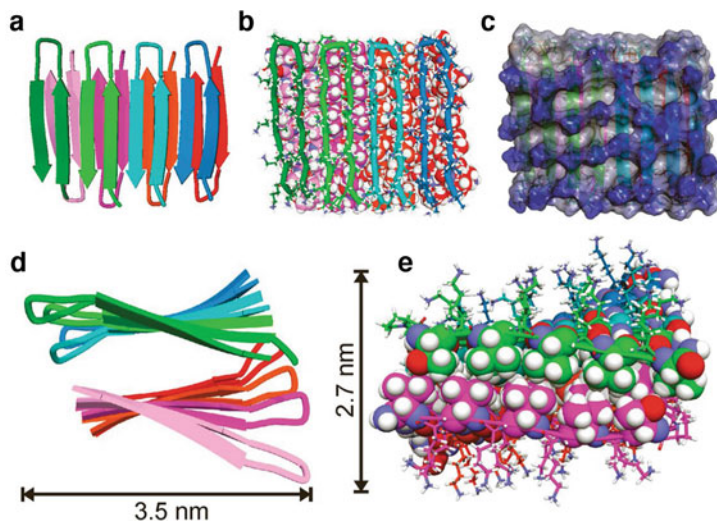
Fig. 2.9 Representations of the structural models for MAX1 self-assembly. (**a**) A cartoon schematic which is viewed perpendicularly to the fibril growth axis. (**b**) The same view as in A, but with the upper layer of monomers shown as tubes, and the lower layer of monomers shown as a CPK representation. (**c**) The same view a third time, represented with an interpolated charge surface. The positive charge produced by the Lysine residues is shown in blue. (**d**) A view along the fibril growth access, shown as a cartoon representation, which shows the left-handed β-sheet twist. (**e**) The same view as in (**d**), where the lysine and proline residues are shown as stick models, and the valine and threonine residues are CPK representations. Reproduced with permission from (Nagy-Smith et al. 2015)

to enhance drug delivery across the membrane, further improving its anticancer activity (Medina and Schneider 2015).

The structure of MAX1 self-assembly has been studied in depth using ssNMR to refine the strand alignment model (Nagy-Smith et al. 2015). The self-assembled structure is composed of a β-sheet bilayer structure as proposed, with the hydrophobic amino acids found in the core of the bilayer and the hydrophilic amino acids found at the exterior exposed surface of the fibrils. In addition, these studies confirmed that MAX1 formed a β-hairpin structure which is *syn* within each individual β-sheet layer and adopts an *anti*-orientation between layers (Fig. 2.9) (Nagy-Smith et al. 2015). Structural models were calculated using restraints from ssNMR data as potential energy functions. These models also showed that a left-handed twist develops along the fibril axis (Nagy-Smith et al. 2015). Most importantly, MAX1 formed a network of homogenous structures, suggesting that the assembly occurs at a thermodynamic minimum. The structural analysis of these materials has been of critical importance to understand precise alignment of the monomeric units within the assembled β-hairpins. In addition, these studies provide confidence that the design principles for these materials are based on sound understanding of the underlying assumptions regarding the structure-function

relationships that correlate peptide sequence to assembly structure and the resulting emergent properties.

2.5 Surfactant-Like Peptide Assemblies

Zhang and coworkers designed another class of self-assembling peptides inspired by surfactants in an effort to broaden the scope of self-assembling peptide nanomaterials. These peptides are composed of a charged head group at the C-terminus with a chain of nonpolar amino acids which end at an acetylated N-terminus (Table 2.6). These novel peptides (A_6D, V_6D, A_6D_2, and V_6D_2) self-assembled into ordered vesicles and, in the case of V_6D and A_6D, also formed hollow nanotubes with open ends (Vauthey et al. 2002). These assemblies were found to have secondary structures that did not appear entirely β-sheet or α-helical, possibly due to the dynamic nature of the assemblies. While these materials may not be strictly "β-sheet," they share enough characteristics with this class of material that we have chosen to discuss them here. Zhang et al. subsequently assessed the assembly characteristics of a series of related peptides in which the hydrophobic region was composed entirely of Gly (G_4D_2, G_6D_2, G_8D_2, $G_{10}D_2$, Table 2.6) (Santoso et al. 2002). They found that the assembled nanostructures of these peptides

Table 2.6 A selection of surfactant-like peptide sequences

Name	Sequence	Reference
A_6D	Ac-AAAAAAD-COOH	Vauthey et al. (2002)
V_6D	Ac-VVVVVVD-COOH	Vauthey et al. (2002)
V_6D_2	Ac-VVVVVVDD-COOH	Vauthey et al. (2002)
A_6D_2	Ac-AAAAAADD-COOH	Vauthey et al. (2002)
G_4D_2	Ac-GGGGDD-COOH	Santoso et al. (2002)
G_6D_2	Ac-GGGGGGDD-COOH	Santoso et al. (2002)
G_8D_2	Ac-GGGGGGGGDD-COOH	Santoso et al. (2002)
$G_{10}D_2$	Ac-GGGGGGGGGGDD-COOH	Santoso et al. (2002)
V_6K_2	Ac-VVVVVVKK-NH$_2$	von Maltzahn et al. (2003)
L_6K_2	Ac-LLLLLLKK-NH$_2$	von Maltzahn et al. (2003)
A_6K	Ac-AAAAAAK-NH$_2$	von Maltzahn et al. (2003)
V_6H	Ac-VVVVVVH-NH$_2$	von Maltzahn et al. (2003)
V_6K	Ac-VVVVVVK-NH$_2$	von Maltzahn et al. (2003)
H_2V_6	H$_2$N-HHVVVVVV-NH$_2$	von Maltzahn et al. (2003)
KV_6	H$_2$N-KVVVVVV-NH$_2$	von Maltzahn et al. (2003)
$A_{12}R_2$	(Me)$_2$N-AAAAAAAAAAAARR-COOH	Hamley et al. (2013a)
A_6R	H$_2$N-AAAAAAR-COOH	Hamley et al. (2013b)
A_6D	H$_2$N-AAAAAAD-COOH	Hamley et al. (2016)
A_9R	H$_2$N-AAAAAAAAAR-COOH	Castelletto et al. (2019)

Fig. 2.10 Molecular models of structures formed by surfactant-like peptides. The negatively charged heads are colored red and the nonpolar tail is colored green. The top image shows a peptide nanotube 50 nm in diameter, the bottom image shows a nanovesicle with diameter of 100 nm. Reproduced with permission from (Santoso et al. 2002). Copyright 2002 American Chemical Society
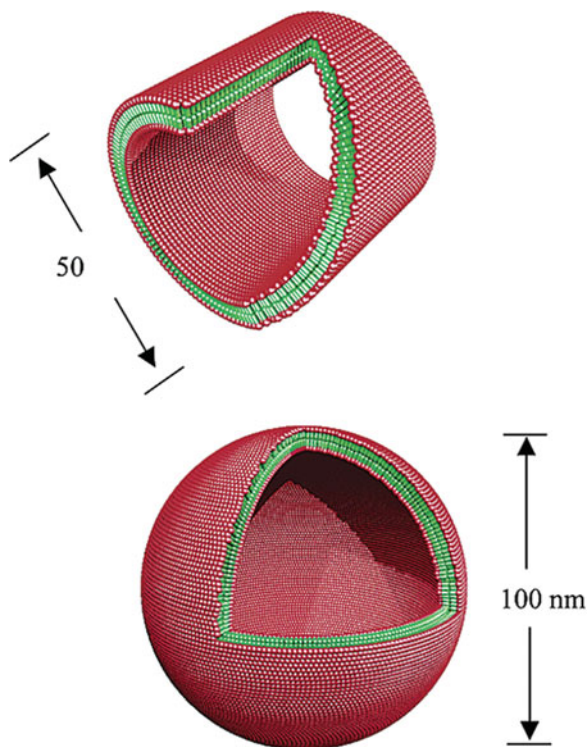
became more polydisperse as the glycine tail increased in length (Fig. 2.10) (Santoso et al. 2002). These initial groups of surfactant-like peptides all featured negatively charged head groups. Positively charged head groups with amidated C-termini to mask the negative charge of the carboxylate were subsequently assessed (von Maltzahn et al. 2003). Two classes of cationic peptides were considered: C-terminal charged head groups (V_6K_2, L_6K_2, A_6K, V_6H, V_6K, Table 2.6) and N-terminal charged head groups (H_2V_6 and KV_6, Table 2.6) (von Maltzahn et al. 2003). Like the anionic peptides, these peptides assembled into dynamic vesicles and nanotubes when below the isoelectric point (pI) of the peptide. Interestingly, when above the pI, the peptides instead formed membranous sheets (von Maltzahn et al. 2003).

Hamley et al. have also explored self-assembling surfactant-like peptides. They designed the $A_{12}R_2$ peptide (Table 2.6), which self-assembled into fibrils which contained both β-sheet and α-helical characteristics (Hamley et al. 2013a). The resulting fibrils were described as ultra-thin, with diameters around 5–6 nm (Hamley et al. 2013a). They found that shortening the length of the charged head group and hydrophobic segment by half (A_6R, Table 2.6) resulted in self-assembly into nanosheets that, over time, wrap into nanotubes (Hamley et al. 2013b). These assemblies were initially ultra-thin free floating sheets, which did not display β-sheet character, but as the concentration of peptide increased, so did the β-sheet
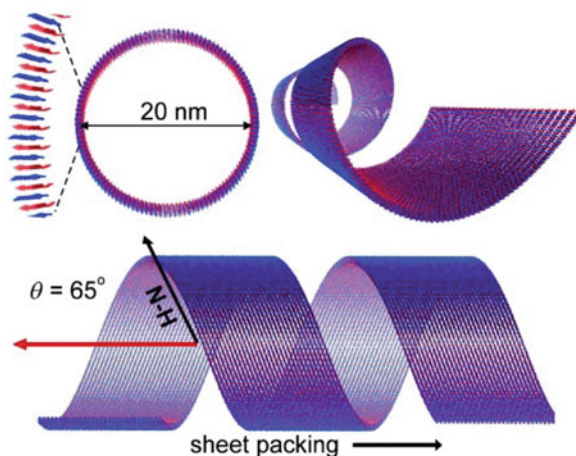
Fig. 2.11 Molecular model of the nanotube structure formed by the A_6K peptide illustrating the tilt angle of 65 degrees. Reproduced with permission from (Middleton et al. 2013). Copyright 2013 Wiley

character (Hamley et al. 2013b). In order to gain understanding of the structural basis for the formation of tubes in these assemblies, Hamley et al. applied ssNMR and FTIR to interrogate the structure of A_6K assemblies (Middleton et al. 2013). They were able to determine the tilt angle of the peptide hydrogen bonding network within the nanotube which enabled the construction of structural models that are consistent with the available structural data (Fig. 2.11) (Middleton et al. 2013).

Further exploration of the formulation of these surfactant-like peptide assemblies enabled the use of the materials for a range of biological applications. Self-assembly of the A_6D peptide (Table 2.6) was modulated by the addition of varying amounts of hexamethylenediamine, which varied the type of nanostructure depending on the ratio of the two components (Hamley et al. 2016). Nanosheet, nanotape, and platelet structures were formed, with the nanotape and platelet assemblies being observed for the first time in surfactant-like peptide assemblies (Hamley et al. 2016). Hamley et al. also used a peptide in this class, A_9R to stabilize oil-water emulsions that exhibited antimicrobial activity (Castelletto et al. 2019). They also showed that self-assembly and de-emulsification can both be triggered by biocatalysis wherein the enzyme elastase breaks down the peptide assembly. This suggests that this system has potential as a stimulus-responsive release material (Castelletto et al. 2019). Assemblies of surfactant-like peptides have also been used for applications in tissue culture (Castelletto et al. 2014) and as antimicrobials agents to prevent infections during wound healing (Castelletto et al. 2019; Castelletto et al. 2018; Chen et al. 2010). Collectively, these studies illustrate that surfactant-like self-assembling peptides occupy a unique structural and application space relative to the related supramolecular β-sheet and β-hairpin assemblies.

2.6 Conclusion

Our understanding of β-sheet assemblies has significantly expanded since Pauling and Corey first defined the structure of the β-sheet motif. Nature has inspired the development of a wide range of supramolecular materials derived from β-sheet assemblies for a broad range of applications. Deeper understanding of the relationships between peptide sequence order, length, and amino acid properties (hydrophobicity, charge, etc.) and the self-assembly propensity and emergent properties of the assembled material has been critical for the rational design of β-sheet nanomaterials. This understanding does not, however, always inform rational design in a predictable manner. Recent structural characterization of self-assembled β-sheet materials has demonstrated that these assemblies form under chaotic conditions that often result in a striking degree of polymorphism within the assembled structures (Wang et al. 2021). Emerging tools for high-resolution structural analysis of β-sheet assemblies will facilitate even greater understanding of the structure and mechanisms of assembly for these materials. This understanding will enable the more confident design of next-generation β-sheet materials in which properties can be predictably tuned for the selected application.

References

Aggeli A, Bell M, Boden N, Keen JN, McLeish TCB, Nyrkova IA, Radford SE, Semenov AN (1997) Engineering of peptide ß-sheet nanotapes. J Mater Chem 7:1135–1145

Aggeli A, Bell M, Carrick LM, Fishwick CW, Harding R, Mawer PJ, Radford SE, Strong AE, Boden N (2003) pH as a trigger of peptide beta-sheet self-assembly and reversible switching between nematic and isotropic phases. J Am Chem Soc 125(32):9619–9628

Al-Halifa S, Babych M, Zottig X, Archambault D, Bourgault S (2019) Amyloid self-assembling peptides: potential applications in nanovaccine engineering and biosensing. Pept Sci 111(1): 1–11

Altunbas A, Lee SJ, Rajasekaran SA, Schneider JP, Pochan DJ (2011) Encapsulation of curcumin in self-assembling peptide hydrogels as injectable drug delivery vehicles. Biomaterials 32(25): 5906–5914

Altunbas A, Sharma N, Lamm MS, Yan C, Nagarkar RP, Schneider JP, Pochan DJ (2010) Peptide—silica hybrid networks: biomimetic control of network mechanical behavior. ACS Nano 4(1):181–188

Anderson JM, Chen HH, Rippon WB, Walton AG (1972) Characterization of three sequential polydipeptides containing glycine. J Mol Biol 67(3):459–468

Aulisa L, Dong H, Hartgerink JD (2009) Self-assembly of multidomain peptides: sequence variation allows control over cross-linking and viscoelasticity. Biomacromolecules 10(9): 2694–2698

Bagrov D, Gazizova Y, Podgorsky V, Udovichenko I, Danilkovich A, Prusakov K, Klinov D (2016) Morphology and aggregation of RADA-16-I peptide studied by AFM, NMR and molecular dynamics simulations. Biopolymers 106(1):72–81

Bakota EL, Sensoy O, Ozgur B, Sayar M, Hartgerink JD (2013) Self-assembling multidomain peptide fibers with aromatic cores. Biomacromolecules 14(5):1370–1378

Bakota EL, Wang Y, Danesh FR, Hartgerink JD (2011) Injectable multidomain peptide nanofiber hydrogel as a delivery agent for stem cell secretome. Biomacromolecules 12(5):1651–1657

Bell CJ, Carrick LM, Katta J, Jin Z, Ingham E, Aggeli A, Boden N, Waigh TA, Fisher J (2006) Self-assembling peptides as injectable lubricants for osteoarthritis. J Biomed Mater Res, Part A 78(2):236–246

Bergman P, Roan NR, Romling U, Bevins CL, Munch J (2016) Amyloid formation: functional friend or fearful foe? J Intern Med 280(2):139–152

Berryman JT, Radford SE, Harris SA (2009) Thermodynamic description of polymorphism in Q- and N-rich peptide aggregates revealed by atomistic simulation. Biophys J 97(1):1–11

Betush RJ, Urban JM, Nilsson BL (2018) Balancing hydrophobicity and sequence pattern to influence self-assembly of amphipathic peptides. Biopolymers:1–13

Bippon WB, Chen HH, Walton AG (1973) Spectroscopic characterization of poly(Glu-Ala). J Mol Biol 75(2):369–375

Bowerman CJ, Liyanage W, Federation AJ, Nilsson BL (2011) Tuning beta-sheet peptide self-assembly and hydrogelation behavior by modification of sequence hydrophobicity and aromaticity. Biomacromolecules 12(7):2735–2745

Bowerman CJ, Nilsson BL (2010) A reductive trigger for peptide self-assembly and hydrogelation. J Am Chem Soc 132(28):9526–9527

Bowerman CJ, Ryan DM, Nissan DA, Nilsson BL (2009) The effect of increasing hydrophobicity on the self-assembly of amphipathic beta-sheet peptides. Mol BioSyst 5(9):1058–1069

Brack A, Caille A (1978) Synthesis and beta-conformation of copolypeptides with alternating hydrophilic and hydrophobic residues. Int J Pept Protein Res 11(2):128–139

Brack A, Orgel LE (1975) Beta structures of alternating polypeptides and their possible prebiotic significance. Nature 256(5516):383–387

Branco MC, Pochan DJ, Wagner NJ, Schneider JP (2009) Macromolecular diffusion and release from self-assembled beta-hairpin peptide hydrogels. Biomaterials 30(7):1339–1347

Branco MC, Pochan DJ, Wagner NJ, Schneider JP (2010) The effect of protein structure on their controlled release from an injectable peptide hydrogel. Biomaterials 31(36):9527–9534

Brunton PA, Davies RP, Burke JL, Smith A, Aggeli A, Brookes SJ, Kirkham J (2013) Treatment of early caries lesions using biomimetic self-assembling peptides--a clinical safety trial. Br Dent J 215(4):1–6

Cai Y, Ran W, Zhai Y, Wang J, Zheng C, Li Y, Zhang P (2020) Recent progress in supramolecular peptide assemblies as virus mimics for cancer immunotherapy. Biomater Sci 8(4):1045–1057

Caplan MR, Moore PN, Zhang S, Kamm RD, Lauffenburger DA (2000) Self-assembly of a beta-sheet protein governed by relief of electrostatic repulsion relative to van der Waals attraction. Biomacromolecules 1(4):627–631

Caplan MR, Schwartzfarb EM, Zhang S, Kamm RD, Lauffenburger DA (2002a) Control of self-assembling oligopeptide matrix formation through systematic variation of amino acid sequence. Biomaterials 23(1):219–227

Caplan MR, Schwartzfarb EM, Zhang S, Kamm RD, Lauffenburger DA (2002b) Effects of systematic variation of amino acid sequence on the mechanical properties of a self-assembling, oligopeptide biomaterial. J Biomater Sci Polym Ed 13(3):225–236

Carrejo NC, Moore AN, Lopez Silva TL, Leach DG, Li IC, Walker DR, Hartgerink JD (2018) Multidomain peptide hydrogel accelerates healing of full-thickness wounds in diabetic mice. ACS Biomater Sci Eng 4(4):1386–1396

Carrick L, Tassieri M, Waigh TA, Aggeli A, Boden N, Bell C, Fisher J, Ingham E, Evans RM (2005) The internal dynamic modes of charged self-assembled peptide fibrils. Langmuir 21(9): 3733–3737

Carrick LM, Aggeli A, Boden N, Fisher J, Ingham E, Waigh TA (2007) Effect of ionic strength on the self-assembly, morphology and gelation of pH responsive β-sheet tape-forming peptides. Tetrahedron 63(31):7457–7467

Castelletto V, Barnes RH, Karatzas KA, Edwards-Gayle CJC, Greco F, Hamley IW, Rambo R, Seitsonen J, Ruokolainen J (2018) Arginine-containing surfactant-like peptides: interaction with lipid membranes and antimicrobial activity. Biomacromolecules 19(7):2782–2794

Castelletto V, Edwards-Gayle CJC, Hamley IW, Barrett G, Seitsonen J, Ruokolainen J (2019) Peptide-stabilized emulsions and gels from an arginine-rich surfactant-like peptide with anti-microbial activity. ACS Appl Mater Interfaces 11(10):9893–9903

Castelletto V, Gouveia RM, Connon CJ, Hamley IW, Seitsonen J, Nykanen A, Ruokolainen J (2014) Alanine-rich amphiphilic peptide containing the RGD cell adhesion motif: a coating material for human fibroblast attachment and culture. Biomater Sci 2(3):362–369

Chen C, Pan F, Zhang S, Hu J, Cao M, Wang J, Xu H, Zhao X, Lu JR (2010) Antibacterial activities of short designer peptides: a link between propensity for nanostructuring and capacity for membrane destabilization. Biomacromolecules 11(2):402–411

Chen W, Li S, Renick P, Yang S, Pandy N, Boutte C, Nguyen KT, Tang L, Dong H (2019b) Bacterial acidity-triggered antimicrobial activity of self-assembling peptide nanofibers. J Mater Chem B 7(18):2915–2919

Chen W, Yang S, Li S, Lang JC, Mao C, Kroll P, Tang L, Dong H (2019a) Self-assembled peptide nanofibers display natural antimicrobial peptides to selectively kill bacteria without compromising cytocompatibility. ACS Appl Mater Interfaces 11(32):28681–28689

Cho H, Balaji S, Sheikh AQ, Hurley JR, Tian YF, Collier JH, Crombleholme TM, Narmoneva DA (2012) Regulation of endothelial cell activation and angiogenesis by injectable peptide nanofibers. Acta Biomater 8(1):154–164

Collier JH, Messersmith PB (2003) Enzymatic modification of self-assembled peptide structures with tissue transglutaminase. Bioconjug Chem 14(4):748–755

Collier JH, Messersmith PB (2004) Self-assembling polymer–peptide conjugates: nanostructural tailoring. Adv Mater 16(11):907–910

Cormier AR, Pang X, Zimmerman MI, Zhou HX, Paravastu AK (2013) Molecular structure of RADA16-I designer self-assembling peptide nanofibers. ACS Nano 7(9):7562–7572

Crowe KM, Siddiqui Z, Harbour V, Kim K, Syed S, Paul R, Roy A, Naik R, Mitchell K, Mahajan A, Sarkar B, Kumar VA (2020) Evaluation of injectable naloxone-releasing hydrogels. ACS Appl Bio Mater 3(11):7858–7864

Davies RPW, Liu B, Maude S, Carrick LM, Nyrkova I, McLeish TC, Harris SA (2017) Peptide strand length controls the energetics of self-assembly and morphology of beta-sheet fibrils. Biopolymers:1–12

Davis ME, Hsieh PC, Takahashi T, Song Q, Zhang S, Kamm RD, Grodzinsky AJ, Anversa P, Lee RT (2006) Local myocardial insulin-like growth factor 1 (IGF-1) delivery with biotinylated peptide nanofibers improves cell therapy for myocardial infarction. Proc Natl Acad Sci U S A 103(21):8155–8160

Deshmukh M, Evans ML, Chapman MR (2018) Amyloid by design: intrinsic regulation of microbial amyloid assembly. J Mol Biol 430(20):3631–3641

Distaffen HE, Jones CW, Abraham BL, Nilsson BL (2021) Multivalent display of chemical signals on self-assembled peptide scaffolds. Pept Sci 113(2):1–137

Dong H, Paramonov SE, Aulisa L, Bakota EL, Hartgerink JD (2007) Self-assembly of multidomain peptides: balancing molecular frustration controls conformation and nanostructure. J Am Chem Soc 129(41):12468–12472

Ellis-Behnke RG, Liang YX, Tay DK, Kau PW, Schneider GE, Zhang S, Wu W, So KF (2006b) Nano hemostat solution: immediate hemostasis at the nanoscale. Nanomedicine 2(4):207–215

Ellis-Behnke RG, Liang YX, You SW, Tay DK, Zhang S, So KF, Schneider GE (2006a) Nano neuro knitting: peptide nanofiber scaffold for brain repair and axon regeneration with functional return of vision. Proc Natl Acad Sci U S A 103(13):5054–5059

Elsawy MA, Smith AM, Hodson N, Squires A, Miller AF, Saiani A (2016) Modification of beta-sheet forming peptide hydrophobic face: effect on self-assembly and gelation. Langmuir 32(19):4917–4923

Emamyari S, Kargar F, Sheikh-Hasani V, Emadi S, Fazli H (2015) Mechanisms of the self-assembly of EAK16-family peptides into fibrillar and globular structures: molecular dynamics simulations from nano- to micro-seconds. Eur Biophys J 44(4):263–276

Farrukh A, Ortega F, Fan W, Marichal N, Paez JI, Berninger B, Campo AD, Salierno MJ (2017) Bifunctional hydrogels containing the laminin motif IKVAV promote neurogenesis. Stem Cell Rep 9(5):1432–1440

Fishwick CWG, Beevers AJ, Carrick LM, Whitehouse CD, Aggeli A, Boden N (2003) Structures of helical β-tapes and twisted ribbons: the role of side-chain interactions on twist and bend behavior. Nano Lett 3(11):1475–1479

Fung SY, Keyes C, Duhamel J, Chen P (2003) Concentration effect on the aggregation of a self-assembling oligopeptide. Biophys J 85(1):537–548

Galler KM, Hartgerink JD, Cavender AC, Schmalz G, D'Souza RN (2012) A customized self-assembling peptide hydrogel for dental pulp tissue engineering. Tissue Eng Part A 18(1–2): 176–184

Gao J, Tang C, Elsawy MA, Smith AM, Miller AF, Saiani A (2017) Controlling self-assembling peptide hydrogel properties through network topology. Biomacromolecules 18(3):826–834

Gasiorowski JZ, Collier JH (2011) Directed intermixing in multicomponent self-assembling bio-materials. Biomacromolecules 12(10):3549–3558

Gaspar D, Veiga AS, Sinthuvanich C, Schneider JP, Castanho MA (2012) Anticancer peptide SVS-1: efficacy precedes membrane neutralization. Biochemistry 51(32):6263–6265

Gelain F, Bottai D, Vescovi A, Zhang S (2006) Designer self-assembling peptide nanofiber scaffolds for adult mouse neural stem cell 3-dimensional cultures. PLoS One 1:1–11

Gelain F, Luo Z, Zhang S (2020) Self-assembling peptide EAK16 and RADA16 nanofiber scaffold hydrogel. Chem Rev 120(24)

Gelain F, Unsworth LD, Zhang S (2010) Slow and sustained release of active cytokines from self-assembling peptide scaffolds. J Control Release 145(3):231–239

Genove E, Shen C, Zhang S, Semino CE (2005) The effect of functionalized self-assembling peptide scaffolds on human aortic endothelial cell function. Biomaterials 26(16):3341–3351

Guilbaud JB, Rochas C, Miller AF, Saiani A (2013) Effect of enzyme concentration of the morphology and properties of enzymatically triggered peptide hydrogels. Biomacromolecules 14(5):1403–1411

Guilbaud JB, Vey E, Boothroyd S, Smith AM, Ulijn RV, Saiani A, Miller AF (2010) Enzymatic catalyzed synthesis and triggered gelation of ionic peptides. Langmuir 26(13):11297–11303

Haines-Butterick L, Rajagopal K, Branco M, Salick D, Rughani R, Pilarz M, Lamm MS, Pochan DJ, Schneider JP (2007) Controlling hydrogelation kinetics by peptide design for three-dimensional encapsulation and injectable delivery of cells. Proc Natl Acad Sci U S A 104(19):7791–7796

Haines-Butterick LA, Salick DA, Pochan DJ, Schneider JP (2008) In vitro assessment of the pro-inflammatory potential of beta-hairpin peptide hydrogels. Biomaterials 29(31):4164–4169

Hainline KM, Gu F, Handley JF, Tian YF, Wu Y, de Wet L, Vander Griend DJ, Collier JH (2019) Self-assembling peptide gels for 3D prostate cancer spheroid culture. Macromol Biosci 19(1): 1–9

Hamley IW, Dehsorkhi A, Castelletto V (2013b) Self-assembled arginine-coated peptide nanosheets in water. Chem Commun 49(18):1850–1852

Hamley IW, Dehsorkhi A, Castelletto V, Seitsonen J, Ruokolainen J, Iatrou H (2013a) Self-assembly of a model amphiphilic oligopeptide incorporating an arginine headgroup. Soft Matter 9(19):4794–4801

Hamley IW, Hutchinson J, Kirkham S, Castelletto V, Kaur A, Reza M, Ruokolainen J (2016) Nanosheet formation by an anionic surfactant-like peptide and modulation of self-assembly through ionic complexation. Langmuir 32(40):10387–10393

Harbour V, Casillas C, Siddiqui Z, Sarkar B, Sanyal S, Nguyen P, Kim KK, Roy A, Iglesias-Montoro P, Patel S, Podlaski F, Tolias P, Windsor W, Kumar V (2020) Regulation of lipoprotein homeostasis by self-assembling peptides. ACS Appl Bio Mater 3(12):8978–8988

Holmes TC, de Lacalle S, Su X, Liu G, Rich A, Zhang S (2000) Extensive neurite outgrowth and active synapse formation on self-assembling peptide scaffolds. Proc Natl Acad Sci U S A 97(12):6728–6733

Hong Y, Legge RL, Zhang S, Chen P (2003) Effect of amino acid sequence and pH on nanofiber formation of self-assembling peptides EAK16-II and EAK16-IV. Biomacromolecules 4(5): 1433–1442

Horii A, Wang X, Gelain F, Zhang S (2007) Biological designer self-assembling peptide nanofiber scaffolds significantly enhance osteoblast proliferation, differentiation and 3-D migration. PLoS One 2(2):1–9

Hu B, Lian Z, Zhou Z, Shi L, Yu Z (2020) Reactive oxygen species-responsive adaptable self-assembly of peptides toward advanced biomaterials. ACS Appl Bio Mater 3(9):5529–5551

Huettner N, Dargaville TR, Forget A (2018) Discovering cell-adhesion peptides in tissue engineering: beyond RGD. Trends Biotechnol 36(4):372–383

Hwang W, Marini DM, Kamm RD, Zhang S (2003) Supramolecular structure of helical ribbons self-assembled from a β-sheet peptide. J Chem Phys 118(1):389–397

Irwin DJ, Lee VM, Trojanowski JQ (2013) Parkinson's disease dementia: convergence of alpha-synuclein, tau and amyloid-beta pathologies. Nat Rev Neurosci 14(9):626–636

Jiang L, Xu D, Sellati TJ, Dong H (2015) Self-assembly of cationic multidomain peptide hydrogels: supramolecular nanostructure and rheological properties dictate antimicrobial activity. Nanoscale 7(45):19160–19169

Jones CW, Morales CG, Eltiste SL, Yanchik-Slade FE, Lee NR, Nilsson BL (2021) Capacity for increased surface area in the hydrophobic core of beta-sheet peptide bilayer nanoribbons. J Pept Sci 27(9):1–13

Jun S, Hong Y, Imamura H, Ha BY, Bechhoefer J, Chen P (2004) Self-assembly of the ionic peptide EAK16: the effect of charge distributions on self-assembly. Biophys J 87(2):1249–1259

Jung JP, Jones JL, Cronier SA, Collier JH (2008) Modulating the mechanical properties of self-assembled peptide hydrogels via native chemical ligation. Biomaterials 29(13):2143–2151

Jung JP, Nagaraj AK, Fox EK, Rudra JS, Devgun JM, Collier JH (2009) Co-assembling peptides as defined matrices for endothelial cells. Biomaterials 30(12):2400–2410

Kang MK, Colombo JS, D'Souza RN, Hartgerink JD (2014) Sequence effects of self-assembling multidomain peptide hydrogels on encapsulated SHED cells. Biomacromolecules 15(6): 2004–2011

Kaur H, Sharma P, Patel N, Pal VK, Roy S (2020) Accessing highly tunable nanostructured hydrogels in a short ionic complementary peptide sequence via pH trigger. Langmuir 36(41): 12107–12120

Kayser V, Turton DA, Aggeli A, Beevers A, Reid GD, Beddard GS (2004) Energy migration in novel pH-triggered self-assembled beta-sheet ribbons. J Am Chem Soc 126(1):336–343

Ke PC, Sani MA, Ding F, Kakinen A, Javed I, Separovic F, Davis TP, Mezzenga R (2017) Implications of peptide assemblies in amyloid diseases. Chem Soc Rev 46(21):6492–6531

Kisiday J, Jin M, Kurz B, Hung H, Semino C, Zhang S, Grodzinsky AJ (2002) Self-assembling peptide hydrogel fosters chondrocyte extracellular matrix production and cell division: implications for cartilage tissue repair. Proc Natl Acad Sci U S A 99(15):9996–10001

Knowles TP, Mezzenga R (2016) Amyloid fibrils as building blocks for natural and artificial functional materials. Adv Mater 28(31):6546–6561

Knowles TP, Vendruscolo M, Dobson CM (2014) The amyloid state and its association with protein misfolding diseases. Nat Rev Mol Cell Biol 15(6):384–396

Koutsopoulos S, Unsworth LD, Nagai Y, Zhang S (2009) Controlled release of functional proteins through designer self-assembling peptide nanofiber hydrogel scaffold. Proc Natl Acad Sci U S A 106(12):4623–4628

Kretsinger JK, Haines LA, Ozbas B, Pochan DJ, Schneider JP (2005) Cytocompatibility of self-assembled beta-hairpin peptide hydrogel surfaces. Biomaterials 26(25):5177–5186

Kubota S, Ikeda K, Yang JT (1983) Conformation of sequential polypeptides of (Lysi-Leuj), (Lysi-Serj), and (Lys-Gly) in sodium dodecyl sulfate solution. Biopolymers 22(10):2237–2252

Kumar VA, Shi S, Wang BK, Li IC, Jalan AA, Sarkar B, Wickremasinghe NC, Hartgerink JD (2015a) Drug-triggered and cross-linked self-assembling nanofibrous hydrogels. J Am Chem Soc 137(14):4823–4830

Kumar VA, Taylor NL, Shi S, Wang BK, Jalan AA, Kang MK, Wickremasinghe NC, Hartgerink JD (2015b) Highly angiogenic peptide nanofibers. ACS Nano 9(1):860–868

Kyle S, Felton SH, McPherson MJ, Aggeli A, Ingham E (2012) Rational molecular design of complementary self-assembling peptide hydrogels. Adv Healthc Mater 1(5):640–645

Lai Y, Li F, Zou Z, Saeed M, Xu Z, Yu H (2021) Bio-inspired amyloid polypeptides: from self-assembly to nanostructure design and biotechnological applications. Appl Mater Today 22:1–23

Lee NR, Bowerman CJ, Nilsson BL (2013a) Effects of varied sequence pattern on the self-assembly of amphipathic peptides. Biomacromolecules 14(9):3267–3277

Lee NR, Bowerman CJ, Nilsson BL (2013b) Sequence length determinants for self-assembly of amphipathic beta-sheet peptides. Biopolymers 100(6):738–750

Li D, Jones EM, Sawaya MR, Furukawa H, Luo F, Ivanova M, Sievers SA, Wang W, Yaghi OM, Liu C, Eisenberg DS (2014) Structure-based design of functional amyloid materials. J Am Chem Soc 136(52):18044–18051

Li IC, Moore AN, Hartgerink JD (2016) "Missing tooth" multidomain peptide nanofibers for delivery of small molecule drugs. Biomacromolecules 17(6):2087–2095

Lindsey S, Piatt JH, Worthington P, Sonmez C, Satheye S, Schneider JP, Pochan DJ, Langhans SA (2015) Beta hairpin peptide hydrogels as an injectable solid vehicle for neurotrophic growth factor delivery. Biomacromolecules 16(9):2672–2683

Lopez-Silva TL, Cristobal CD, Edwin Lai CS, Leyva-Aranda V, Lee HK, Hartgerink JD (2021) Self-assembling multidomain peptide hydrogels accelerate peripheral nerve regeneration after crush injury. Biomaterials 265:1–12

Lopez-Silva TL, Leach DG, Li IC, Wang X, Hartgerink JD (2019) Self-assembling multidomain peptides: design and characterization of neutral peptide-based materials with pH and ionic strength independent self-assembly. ACS Biomater Sci Eng 5(2):977–985

Lopez-Silva TL, Schneider JP (2021) From structure to application: progress and opportunities in peptide materials development. Curr Opin Chem Biol 64:131–144

Lu J, Sun X, Yin H, Shen X, Yang S, Wang Y, Jiang W, Sun Y, Zhao L, Sun X, Lu S, Mikos AG, Peng J, Wang X (2018) A neurotrophic peptide-functionalized self-assembling peptide nanofiber hydrogel enhances rat sciatic nerve regeneration. Nano Res 11(9):4599–4613

Luo Z, Wang S, Zhang S (2011) Fabrication of self-assembling D-form peptide nanofiber scaffold d-EAK16 for rapid hemostasis. Biomaterials 32(8):2013–2020

Luo Z, Zhao X, Zhang S (2008) Self-organization of a chiral D-EAK16 designer peptide into a 3D nanofiber scaffold. Macromol Biosci 8(8):785–791

von Maltzahn G, Vauthey S, Santoso S, Zhang S (2003) Positively charged surfactant-like peptides self-assemble into nanostructures. Langmuir 19(10):4332–4337

Marini DM, Hwang W, Lauffenburger DA, Zhang S, Kamm RD (2002) Left-handed helical ribbon intermediates in the self-assembly of a β-sheet peptide. Nano Lett 2(4):295–299

Marsh RE, Corey RB, Pauling L (1955) An investigation of the structure of silk fibroin. Biochim Biophys Acta 16:1–34

Maude S, Miles DE, Felton SH, Ingram J, Carrick LM, Wilcox RK, Ingham E, Aggeli A (2011) De novo designed positively charged tape-forming peptides: self-assembly and gelation in physiological solutions and their evaluation as 3D matrices for cell growth. Soft Matter 7(18): 8085–8099

Medina SH, Li S, Howard OM, Dunlap M, Trivett A, Schneider JP, Oppenheim JJ (2015) Enhanced immunostimulatory effects of DNA-encapsulated peptide hydrogels. Biomaterials 53:545–553

Medina SH, Schneider JP (2015) Cancer cell surface induced peptide folding allows intracellular translocation of drug. J Control Release 209:317–326

Micklitsch CM, Medina SH, Yucel T, Nagy-Smith KJ, Pochan DJ, Schneider JP (2015) Influence of hydrophobic face amino acids on the hydrogelation of beta-hairpin peptide amphiphiles. Macromolecules 48(5):1281–1288

Middleton DA, Madine J, Castelletto V, Hamley IW (2013) Insights into the molecular architecture of a peptide nanotube using FTIR and solid-state NMR spectroscopic measurements on an aligned sample. Angew Chem Int Ed Engl 52(40):10537–10540

Milardi D, Gazit E, Radford SE, Xu Y, Gallardo RU, Caflisch A, Westermark GT, Westermark P, Rosa C, Ramamoorthy A (2021) Proteostasis of islet amyloid polypeptide: a molecular perspective of risk factors and protective strategies for type II diabetes. Chem Rev 121(3): 1845–1893

Mohammed A, Miller AF, Saiani A (2007) 3D networks from self-assembling ionic-complementary octa-peptides. Macromol Symp 251(1):88–95

Moore AN, Hartgerink JD (2017) Self-assembling multidomain peptide nanofibers for delivery of bioactive molecules and tissue regeneration. Acc Chem Res 50(4):714–722

Mora-Solano C, Wen Y, Han H, Chen J, Chong AS, Miller ML, Pompano RR, Collier JH (2017) Active immunotherapy for TNF-mediated inflammation using self-assembled peptide nanofibers. Biomaterials 149:1–11

Nagarkar RP, Hule RA, Pochan DJ, Schneider JP (2008) De novo design of strand-swapped beta-hairpin hydrogels. J Am Chem Soc 130(13):4466–4474

Nagy-Smith K, Moore E, Schneider J, Tycko R (2015) Molecular structure of monomorphic peptide fibrils within a kinetically trapped hydrogel network. Proc Natl Acad Sci U S A 112(32):9816–9821

Nagy-Smith K, Yamada Y, Schneider JP (2016) Protein release from highly charged peptide hydrogel networks. J Mater Chem B 4(11):1999–2007

Najafi H, Jafari M, Farahavar G, Abolmaali SS, Azarpira N, Borandeh S, Ravanfar R (2021) Recent advances in design and applications of biomimetic self-assembled peptide hydrogels for hard tissue regeneration. Biodes Manuf:1–22

Nguyen PK, Sarkar B, Siddiqui Z, McGowan M, Iglesias-Montoro P, Rachapudi S, Kim S, Gao W, Lee EJ, Kumar VA (2018) Self-assembly of an antiangiogenic nanofibrous peptide hydrogel. ACS Appl Bio Mater 1(3):865–870

Nyrkova IA, Semenov AN, Aggeli A, Boden N (2000) Fibril stability in solutions of twisted -sheet peptides: a new kind of micellization in chiral systems. Eur Phys J B 17(3):481–497

Ono S, Lee S, Mihara H, Aoyagi H, Kato T, Yamasaki N (1990) Design and synthesis of basic peptides having amphipathic β-structure and their interaction with phospholipid membranes. Biochim Biophys Acta Biomembr 1022(2):237–244

Osterman D, Mora R, Kedzy FJ, Kaiser ET, Meredith SC (1984) A synthetic amphiphilic/3-strand tridecapeptide: a model for apolipoprotein B. J Am Chem Soc 106:6845–6847

Osterman DG, Kaiser ET (1985) Design and characterization of peptides with amphiphilic beta-strand structures. J Cell Biochem 29(2):57–72

Otzen D, Riek R (2019) Functional amyloids. Cold Spring Harb Perspect Biol 11(12):1–30

Ozbas B, Kretsinger J, Rajagopal K, Schneider JP, Pochan DJ (2004b) Salt-triggered peptide folding and consequent self-assembly into hydrogels with tunable modulus. Macromolecules 37(19):7331–7337

Ozbas B, Rajagopal K, Schneider JP, Pochan DJ (2004a) Semiflexible chain networks formed via self-assembly of beta-hairpin molecules. Phys Rev Lett 93(26 Pt 1):1–4

Park J, Moon H, Hong S (2019) Recent advances in melanin-like nanomaterials in biomedical applications: a mini review. Biomater Res 23:1–10

Pauling L, Corey RB (1951) Configurations of polypeptide chains with favored orientations around single bonds: two new pleated sheets. Proc Natl Acad Sci U S A 37(11):729–740

Pauling L, Corey RB (1953) Two rippled-sheet configurations of polypeptide chains, and a note about the pleated sheets. Proc Natl Acad Sci U S A 39(4):253–256

Pochan DJ, Schneider JP, Kretsinger J, Ozbas B, Rajagopal K, Haines L (2003) Thermally reversible hydrogels via intramolecular folding and consequent self-assembly of a de novo designed peptide. J Am Chem Soc 125(39):11802–11803

Rajagopal K, Ozbas B, Pochan DJ, Schneider JP (2006) Probing the importance of lateral hydrophobic association in self-assembling peptide hydrogelators. Eur Biophys J 35(2):162–169

Roberts D, Rochas C, Saiani A, Miller AF (2012) Effect of peptide and guest charge on the structural, mechanical and release properties of beta-sheet forming peptides. Langmuir 28(46):16196–16206

Rughani RV, Salick DA, Lamm MS, Yucel T, Pochan DJ, Schneider JP (2009) Folding, self-assembly, and bulk material properties of a de novo designed three-stranded beta-sheet hydrogel. Biomacromolecules 10(5):1295–1304

Sadigh-Eteghad S, Sabermarouf B, Majdi A, Talebi M, Farhoudi M, Mahmoudi J (2015) Amyloid-beta: a crucial factor in Alzheimer's disease. Med Princ Pract 24(1):1–10

Saiani A, Mohammed A, Frielinghaus H, Collins R, Hodson N, Kielty CM, Sherratt MJ, Miller AF (2009) Self-assembly and gelation properties of α-helix versus β-sheet forming peptides. Soft Matter 5(1):193–202

Salick DA, Kretsinger JK, Pochan DJ, Schneider JP (2007) Inherent antibacterial activity of a peptide-based beta-hairpin hydrogel. J Am Chem Soc 129(47):14793–14799

Santoso S, Hwang W, Hartman H, Zhang S (2002) Self-assembly of surfactant-like peptides with variable glycine tails to form nanotubes and nanovesicles. Nano Lett 2(7):687–691

Schneider JP, Pochan DJ, Ozbas B, Rajagopal K, Pakstis L, Kretsinger J (2002) Responsive hydrogels from the intramolecular folding and self-assembly of a designed peptide. J Am Chem Soc 124(50):15030–15037

Seipke G, Arfmann HA, Wagner KG (1974) Synthesis and properties of alternating poly(Lys-Phe) and comparison with the random copolymer poly(Lys 51, Phe 49). Biopolymers 13(8): 1621–1633

Seipke G, Arfmann H-A, Wagner KG (1980) Conformation of sequential and random lysine-phenylalanine copolypeptides. Biopolymers 19(1):189–201

Si Y, Wen Y, Kelly SH, Chong AS, Collier JH (2018) Intranasal delivery of adjuvant-free peptide nanofibers elicits resident CD8(+) T cell responses. J Control Release 282:120–130

Sieminski AL, Semino CE, Gong H, Kamm RD (2008) Primary sequence of ionic self-assembling peptide gels affects endothelial cell adhesion and capillary morphogenesis. J Biomed Mater Res, Part A 87(2):494–504

Sinthuvanich C, Veiga AS, Gupta K, Gaspar D, Blumenthal R, Schneider JP (2012) Anticancer beta-hairpin peptides: membrane-induced folding triggers activity. J Am Chem Soc 134(14): 6210–6217

St. Pierre S, Ingwall RT, Verlander MS, Goodman M (1978) Conformational studies of sequential polypeptides containing lysine and tyrosine. Biopolymers 17(8):1837–1848

Sun JE, Stewart B, Litan A, Lee SJ, Schneider JP, Langhans SA, Pochan DJ (2016b) Sustained release of active chemotherapeutics from injectable-solid beta-hairpin peptide hydrogel. Biomater Sci 4(5):839–848

Sun Y, Zhang Y, Tian L, Zhao Y, Wu D, Xue W, Ramakrishna S, Wu W, He L (2016a) Self-assembly behaviors of molecular designer functional RADA16-I peptides: influence of motifs, pH, and assembly time. Biomed Mater 12(1):1–11

Taghavi L, Aramvash A, Seyedkarimi MS, Malek Sabet N (2018) Evaluation of the hemocompatibility of RADA 16-I peptide. J Biomater Appl 32(8):1024–1031

Tajima A, Liu W, Pradhan I, Bertera S, Bagia C, Trucco M, Meng WS, Fan Y (2015) Bioengineering mini functional thymic units with EAK16-II/EAKIIH6 self-assembling hydrogel. Clin Immunol 160(1):82–89

Tian YF, Devgun JM, Collier JH (2011) Fibrillized peptide microgels for cell encapsulation and 3D cell culture. Soft Matter 7(13):6005–6011

Van Gerven N, Klein RD, Hultgren SJ, Remaut H (2015) Bacterial amyloid formation: structural insights into curli biogensis. Trends Microbiol 23(11):693–706

Varanko A, Saha S, Chilkoti A (2020) Recent trends in protein and peptide-based biomaterials for advanced drug delivery. Adv Drug Deliv Rev 156:133–187

Vauthey S, Santoso S, Gong H, Watson N, Zhang S (2002) Molecular self-assembly of surfactant-like peptides to form nanotubes and nanovesicles. Proc Natl Acad Sci U S A 99(8):5355–5360

Vendome J, Posy S, Jin X, Bahna F, Ahlsen G, Shapiro L, Honig B (2011) Molecular design principles underlying beta-strand swapping in the adhesive dimerization of cadherins. Nat Struct Mol Biol 18(6):693–700

Wang F, Gnewou O, Wang S, Osinski T, Zuo X, Egelman EH, Conticello VP (2021) Deterministic chaos in the self-assembly of beta sheet nanotubes from an amphipathic oligopeptide. Matter 4(10):3217–3231

Wang K, Keasling JD, Muller SJ (2005) Effects of the sequence and size of non-polar residues on self-assembly of amphiphilic peptides. Int J Biol Macromol 36(4):232–240

Wang X, Horii A, Zhang S (2008) Designer functionalized self-assembling peptide nanofiber scaffolds for growth, migration, and tubulogenesis of human umbilical vein endothelial cells. Soft Matter 4(12):2388–2395

Wang X, Li Y, Zhong C (2015) Amyloid-directed assembly of nanostructures and functional devices for bionanoelectronics. J Mater Chem B 3(25):4953–4958

Wei S, Chen F, Geng Z, Cui R, Zhao Y, Liu C (2020) Self-assembling RATEA16 peptide nanofiber designed for rapid hemostasis. J Mater Chem B 8(9):1897–1905

Wickremasinghe NC, Kumar VA, Shi S, Hartgerink JD (2015) Controlled angiogenesis in peptide nanofiber composite hydrogels. ACS Biomater Sci Eng 1(9):845–854

Wu G, Cao Z-Z, Luo X-L, Wang X-X, Wang S-H, Wang D-L (2017c) Fabrication and characterization of a PDLSCs/BMP-2-PLGA-NP/RADA peptide hydrogel composite for bone repair. J Biomater Tissue Eng 7(5):379–391

Wu H, Zhou T, Tian L, Xia Z, Xu F (2017b) Self-assembling RADA16-I peptide hydrogel scaffold loaded with tamoxifen for breast reconstruction. Biomed Res Int 2017:1–10

Wu X, He L, Li W, Li H, Wong WM, Ramakrishna S, Wu W (2017a) Functional self-assembling peptide nanofiber hydrogel for peripheral nerve regeneration. Regen Biomater 4(1):21–30

Wychowaniec JK, Patel R, Leach J, Mathomes R, Chhabria V, Patil-Sen Y, Hidalgo-Bastida A, Forbes RT, Hayes JM, Elsawy MA (2020b) Aromatic stacking facilitated self-assembly of ultrashort ionic complementary peptide sequence: beta-sheet nanofibers with remarkable gelation and interfacial properties. Biomacromolecules 21(7):2670–2680

Wychowaniec JK, Smith AM, Ligorio C, Mykhaylyk OO, Miller AF, Saiani A (2020a) Role of sheet-edge interactions in beta-sheet self-assembling peptide hydrogels. Biomacromolecules 21(6):2285–2297

Xu D, Dustin D, Jiang L, Samways DS, Dong H (2015b) Designed filamentous cell penetrating peptides: probing supramolecular structure-dependent membrane activity and transfection efficiency. Chem Commun 51(59):11757–11760

Xu D, Jiang L, Singh A, Dustin D, Yang M, Liu L, Lund R, Sellati TJ, Dong H (2015a) Designed supramolecular filamentous peptides: balance of nanostructure, cytotoxicity and antimicrobial activity. Chem Commun 51(7):1289–1292

Yan C, Altunbas A, Yucel T, Nagarkar RP, Schneider JP, Pochan DJ (2010) Injectable solid hydrogel: mechanism of shear-thinning and immediate recovery of injectable beta-hairpin peptide hydrogels. Soft Matter 6(20):5143–5156

Yan C, Mackay ME, Czymmek K, Nagarkar RP, Schneider JP, Pochan DJ (2012) Injectable solid peptide hydrogel as a cell carrier: effects of shear flow on hydrogels and cell payload. Langmuir 28(14):6076–6087

Yang H, Hong N, Liu H, Wang J, Li Y, Wu S (2018) Differentiated adipose-derived stem cell cocultures for bone regeneration in RADA16-I in vitro. J Cell Physiol 233(12):9458–9472

Yang M, Xu D, Jiang L, Zhang L, Dustin D, Lund R, Liu L, Dong H (2014) Filamentous supramolecular peptide-drug conjugates as highly efficient drug delivery vehicles. Chem Commun 50(37):4827–4830

Yang S, Dong H (2020) Modular design and self-assembly of multidomain peptides towards cytocompatible supramolecular cell penetrating nanofibers. RSC Adv 10(49):29469–29474

Yokoi H, Kinoshita T, Zhang S (2005) Dynamic reassembly of peptide RADA16 nanofiber scaffold. Proc Natl Acad Sci U S A 102(24):8414–8419

Zhang H, Park J, Jiang Y, Woodrow KA (2017) Rational design of charged peptides that self-assemble into robust nanofibers as immune-functional scaffolds. Acta Biomater 55:183–193

Zhang L, Lu JR, Waigh TA (2021) Electronics of peptide- and protein-based biomaterials. Adv Colloid Interf Sci 287:1–14

Zhang S (2002) Emerging biological materials through molecular self-assembly. Biotechnol Adv 20(5–6):321–339

Zhang S (2018) Discovery of the first self-assembling peptide, study of peptide dynamic behaviors, and G protein-coupled receptors using an Aviv circular dichroism spectropolarimeter. Biopolymers 109(8):1–12

Zhang S, Altman M (1999) Peptide self-assembly in functional polymer science and engineering. React Funct Polym 41(1–3):91–102

Zhang S, Holmes T, Lockshin C, Rich A (1993) Spontaneous assembly of a self-complementary oligopeptide to form a stable macroscopic membrane. Proc Natl Acad Sci U S A 90(8):3334–3338

Zhang S, Holmes TC, DiPersio CM, Hynes RO, Su X, Rich A (1995) Self-complementary oligopeptide matrices support mammalian cell attachment. Biomaterials 16(18):1385–1393

Zhang S, Lockshin C, Cook R, Rich A (1994) Unusually stable beta-sheet formation in an ionic self-complementary oligopeptide. Biopolymers 34(5):663–672

Zhang S, Lockshin C, Herbert A, Winter E, Rich A (1992) Zuotin, a putative Z-DNA binding protein in Saccharomyces cerevisiae. EMBO J 11(10):3787–3796

Zhang Y, Kuang Y, Gao Y, Xu B (2011) Versatile small-molecule motifs for self-assembly in water and the formation of biofunctional supramolecular hydrogels. Langmuir 27(2):529–537

Zhou A, Chen S, He B, Zhao W, Chen X, Jiang D (2016) Controlled release of TGF-beta 1 from RADA self-assembling peptide hydrogel scaffolds. Drug Des Devel Ther 10:3043–3051

Chapter 3
α-Helix and Coiled-Coil Peptide Nanomaterials

Franziska Thomas

Abstract Good synthetic access to peptide materials with controllable morphology holds great promise for medical applications, but also for the development of biomimetic devices. α-Helical peptides can be designed to self-assemble into biomimetic materials with highly diverse morphologies and that with precise control at the molecular level. Most α-helical peptide material designs to date have been derived from the α-helical coiled coil, as the sequence-structure relationships are well understood and designs for most of the described coiled-coil assemblies are readily available. In general, α-helical peptide materials can be fibrous, tubular, or cage-like, or can assemble into geometric figures or highly ordered crystalline arrays. This chapter provides a comprehensive overview of research activities on materials constructed from α-helical peptides. In addition to coiled-coil materials, which account for the majority of reported designs, peptide materials made from other α-helical building blocks are also included. We discuss the design strategies that have been used to produce the various forms of materials and briefly outline intended applications where applicable.

Keywords Coiled coil · α-Helical peptide fibers · α-Helical peptide nanotubes · α-Helical peptide cages · α-Helical peptide networks and crystals

3.1 Scope of This Chapter

Materials based on α-helical proteins are widespread in nature. For example, α-keratin, actin filaments, or the silk proteins of some insects consist of long α-helical proteins and exhibit impressive mechanical stability (Fraser et al. 1962; Djinović-Carugo et al. 1999; Sutherland et al. 2010). This has even inspired scientists to extract these materials from nature and modify their structure to create new

---

F. Thomas (✉)
Institute of Organic Chemistry, Heidelberg University, Heidelberg, Germany

Heidelberg University, Heidelberg, Germany
e-mail: franziska.thomas@oci.uni-heidelberg.de

materials with, for example, shape memory (Fu et al. 2015; Cera et al. 2021). It is therefore not surprising that many efforts have been made to design biomimetic materials with similar or even completely new properties from easily accessible α-helical peptides. This chapter reviews the research efforts in this field. Several recent reviews highlight progress in the design of α-helical peptide materials to some extent (Mondal and Gazit 2016; Conticello et al. 2017; Beesley and Woolfson 2019; Park 2020; Sinha et al. 2021); however, we have seen a surge of very recent reports on new design approaches of α-helical peptide materials in the last 2 years. These reports are included in this comprehensive review, as are longer-known design approaches. This should give a thorough overview of the field of α-helical peptide materials.

With the exception of a few examples, most α-helical peptide materials are designed from the well-understood α-helical coiled coil (Lupas et al. 2017; Woolfson 2017). The straightforward sequence-structure relationships, the versatility of coiled-coil structures, and the available peptide designs make the coiled coil an ideal building block for the modular design of materials with very different morphologies. Coiled coils have been designed to self-assemble into extended fibrous structures, nanotubes, arrays, networks, and cages, or have been used as oligomerization domains for protein cage assemblies, all with high precision. This diversity is due not only to the aforementioned easy access to well-defined coiled-coil building blocks but also to the robustness of the coiled-coil structure to covalent modification of the outer surface and the N and C termini. We therefore begin our review with a brief overview of the general design rules for the coiled coils that have been used as building blocks in the materials described here. We then continue with the design of α-helical peptide fibers, which is followed by the design of α-helical peptide nanotubes. Fourth, we give an overview of design strategies on α-helical peptide cages. This includes a short section on coiled-coil protein origami, as amazing geometries of α-helical coiled-coil nanostructures can be obtained using this approach. In another section, the design of α-helical peptide networks and arrays is discussed. This section is divided into amorphous assemblies and crystalline structures. Finally, we give a summary and also critically discuss new possibilities in the field.

3.2 De Novo Design of α-Helical Coiled Coils

Coiled coils are probably the best understood protein folding motifs and are thus widely explored in terms of formulating easy-to-apply design rules. Therefore, they are attractive building blocks for synthetic biological applications and, more relevant to this chapter, for the design of biomimetic materials. One relatively recent review provides an excellent and detailed overview about the structure and design of coiled coils (Woolfson 2017). However, we feel that to better understand the design underlying each coiled-coil material, a brief overview of the topic should be provided.

The sequence-to-structure relationships are straightforward and can best be described as a heptad repeat pattern of hydrophobic (**h**) and polar (**p**) residues in a **hpphppp** sequence for the classical coiled coils (Fig. 3.1a). The heptad repeat is formally referred to as an ***abcdefg*** register (Lupas et al. 2017). Peptides exhibiting such a sequence pattern fold into amphiphilic α-helices, with the *a* and *d* residues pointing to one side and the polar *b*, *c*, *e*, *f*, *g* residues to the other side. Driven by the hydrophobic effect, such α-helices associate via their hydrophobic *a-d* faces and wrap around each other to form a left-handed supercoil structure. The supercoiling is caused by a slightly offset helix packing that results from a combination of the sequence pattern with seven residues and the 3.6 residues per turn of the helix. The residues at the coiled-coil interface, involving not only the *a* and *d* residues but also the corresponding *e* and *g* residues, are tightly packed in a so-called knobs-into-holes manner (Crick 1953). The ideal coiled coil can be described by geometric parameters such as the pitch in Å, i.e., the distance required for a 360° rotation of the superhelix; the radius in Å measured from the superhelical axis to the center of an α-helix of the coiled coil; the pitch angle, i.e., the angle of a helix relative to the superhelical axis; or the helix crossing angle, which is the angle between two adjacent helices (Fig. 3.1b) (Lupas and Gruber 2005).

Although the sequence pattern appears simple at first, coiled coils exist in a variety of homomeric or heteromeric oligomeric states and in parallel and antiparallel orientations (Testa et al. 2009). Many of these structures are accessible by de novo design. A list of representative coiled coils from dimer to heptamer together with their pitch and radii is given in Fig. 3.1c. The design rules are shown in Fig. 3.1d–g and are summarized as follows: The oligomeric state of a coiled-coil assembly is mainly controlled by the residues at the *a* and *d* positions (Harbury et al. 1993; Fletcher et al. 2012). Due to the different knobs-into-holes packing modes in coiled-coil dimers, coiled-coil trimers, and coiled-coil tetramers, amino acid residues with different steric demands can be accommodated at these positions in the respective assemblies. It has been experimentally found that an isoleucine-leucine core, with the isoleucine residues occupying the *a* positions and the leucine residues occupying the *d* positions, leads to the formation of a coiled-coil dimer. That said, an asparagine residue at a central *a* position of a coiled-coil is advantageous to increase the specificity for a dimeric assembly (Fletcher et al. 2012). This is often referred to as a negative design because the asparagine residues are structurally destabilizing; however, in coiled-coil dimers, the asparagine residues face each other in the hydrophobic core and form a dynamic hydrogen bond that partially compensates for the loss of structural stability (Thomas et al. 2017). Coiled-coil trimers can be obtained by introducing only isoleucine residues into the hydrophobic core, and coiled-coil tetramers usually have a leucine residue at the *a*-position and an isoleucine residue at the *d* position.

Charged residues at the *e* and *g* positions flanking the hydrophobic seam contribute significantly to the orientation of the coiled-coil assembly and the specificity for homo- versus hetero-assembly (Lumb and Kim 1995; Lavigne et al. 1996; Lumb and Kim 1996). In homomeric coiled coils, the *e* and *g* positions are populated with oppositely charged residues that stabilize the assembly through attractive charge
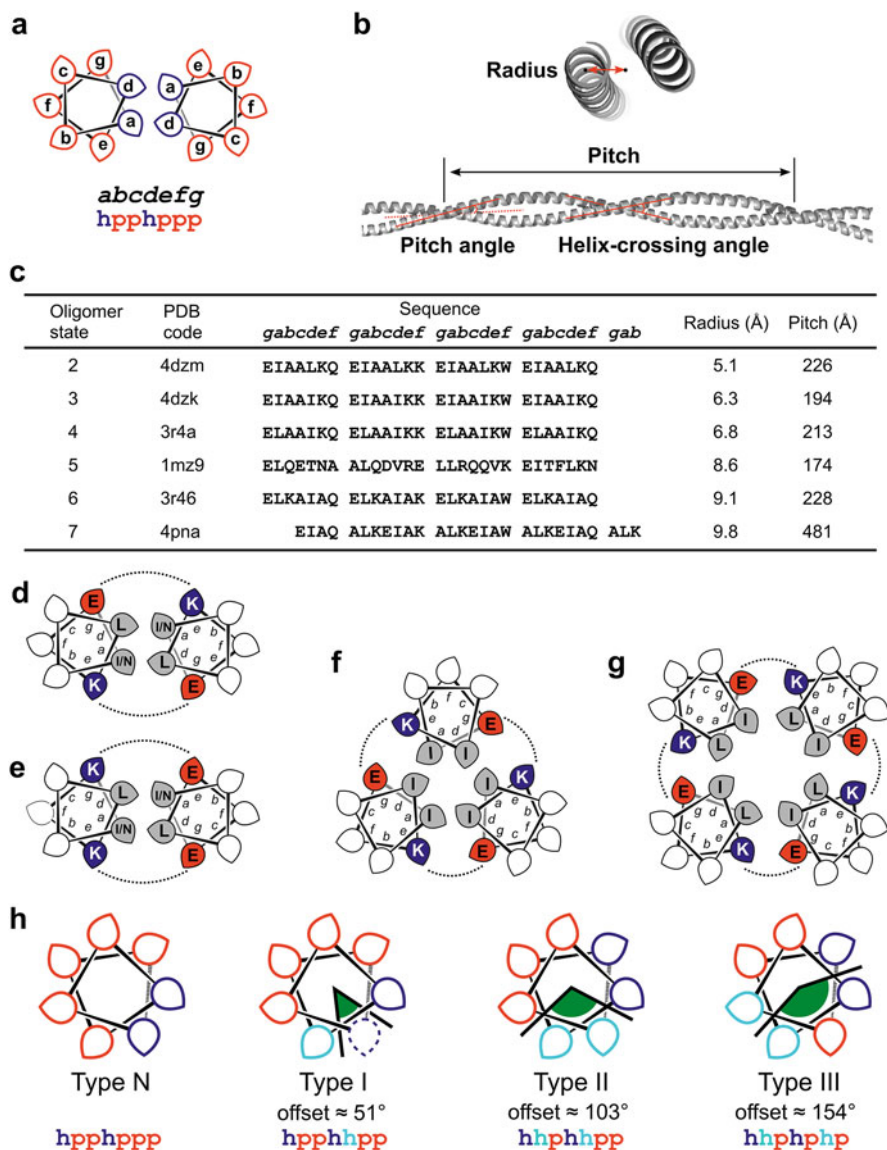
Fig. 3.1 Structure and de novo design of coiled-coil peptides. (**a**) General helix-wheel representation and *abcdefg* register of the heptad repeat of a coiled-coil dimer with hydrophobic residues typically located at positions *a* and *d*, and polar residues occupying positions *b*, *c*, *e*, *f*, *g*. (**b**) Geometric parameters of a coiled-coil dimer (Pitch: Distance required for an α-helix to complete a 360° turn; radius: distance from the superhelical axis to the center of an α-helix of the assembly; pitch angle: angle of a helix relative to the superhelical axis; helix-crossing angle: angle between two adjacent helices). (**c**) Overview of example coiled coils of different oligomer states with the respective pitches and radii (Thomson et al. 2014; Wood et al. 2014). (**d–g**) Helical-wheel representations of the heptad repeat sequence pattern of (**d**) a parallel homodimeric coiled coil, (**e**) a parallel heterodimeric coiled coil, (**f**) a homotrimeric coiled coil, and (**g**) a homotetrameric coiled coil. (**d–g**) The sequence positions are assigned to an *abcdefg* register. Hydrophobic residues are displayed in gray, positively charged residues in blue, and negatively charged residues in red.

interactions (Fletcher et al. 2012). In heteromeric coiled coils, on the other hand, the charge pattern at these positions is such that homomeric assemblies are significantly destabilized compared to heteromeric assemblies due to charge repulsion (Lumb and Kim 1995). In the simplest case of a heterodimeric coiled coil, one strand is fully positively charged, with lysine residues occupying positions *e* and *g*, while the other strand is negatively charged and carries glutamic acid residues at these positions (Litowski and Hodges 2002; Thomas et al. 2013; Groth et al. 2018). Similar design strategies have been used for coiled-coil heterotrimers (Nautiyal et al. 1995) and coiled-coil heterotetramers (Root et al. 2009). By using more complex charge patterns in combination with negative design, i.e., the introduction of asparagine residues at different *a* positions in the hydrophobic cores, it is possible to design the so-called orthogonal heterodimeric coiled coils that interact with very high specificity (Bromley et al. 2009; Gradišar et al. 2013; Fletcher et al. 2017).

In higher-order coiled coils, the *a* and *d* positions are occupied by leucine and isoleucine residues, which is also the case in coiled-coil tetramers; therefore, core-packing arguments cannot be used to explain folding discrimination between tetrameric coiled coils or higher-order coiled-coil assemblies. This is where the classical **hpphppp** sequence pattern reaches its limits. For higher-order coiled coils, different heptad repeat patterns have to be considered (Walshaw and Woolfson 2003; Woolfson 2017). This led to a classification of coiled coils into four groups (Fig. 3.1h) (Woolfson et al. 2012): Type N coiled coils are based on the classical **hpphppp** pattern and in their purest form mainly comprise coiled-coil dimers. Coiled-coil trimers and tetramers are often better described with an **hpphhpp** sequence pattern, as peripheral residues (e.g., *g* positions) are occasionally part of the hydrophobic core. These coiled coils are referred to as Type I. In higher-order coiled coils with four to seven α-helices, we see two hydrophobic seams that interact independently with the respective adjacent α-helix, thus including *e* and *g* residues in the knobs-into-holes packing. These Type II coiled coils exhibit a **hhphhpp** heptad repeat. Coiled-coil peptides with eight or more α-helices as well as coiled-coil tapes are based on an **hhphphp** sequence pattern, which is referred to as Type III.

Compared to parallel coiled-coil designs, antiparallel coiled-coil design rules are more difficult to formulate and are mostly reported for coiled-coil dimers (Woolfson 2017). Many of the designs are based on buried polar residues that direct the structure towards a parallel or antiparallel orientation (Oakley and Kim 1998; Oakley and Hollenbeck 2001). Furthermore, electrostatic interactions in antiparallel coiled coils are found between the *e* and *e'* or *g* and *g'* residues of the respective coil strands, while in parallel coiled coils, such interactions exist between *e* and *g'* residues. This can be exploited to promote the antiparallel orientation (McClain

---

Fig. 3.1 (continued) The dotted lines indicate potential electrostatic interactions. The leaf shape of the Cα atom of each residue represents the orientation of the Cα to the Cß atom. (**h**) Helical wheel representations and heptad repeat patterns of Type N, Type I, Type II, and Type III coiled coils. Residues involved in knobs-into-holes packing are shown in dark and light blue. Polar residues are shown in red

et al. 2001). By applying computational design, it was possible to create orthogonal antiparallel heterodimeric coiled coils (Hadley et al. 2008; Steinkruger et al. 2012; Negron and Keating 2014). Antiparallel coiled-coil designs beyond dimers are usually tailor-made or found by accident (Lombardi et al. 1996; Ogihara et al. 1997). An example is a steric matching approach for antiparallel coiled-coil trimers (Schnarr and Kennan 2004). Antiparallel coiled-coil tetramers based on a Type I heptad repeat pattern were designed by DeGrado and co-workers (Betz and DeGrado 1996). A peptide that is also relevant to this review is an antiparallel coiled-coil hexamer that has been explored in the design of self-assembling fibers with long-range electronic conductivity (vide infra) (Spencer and Hochbaum 2016).

3.3 α-Helical Peptide Fibers

The first class of materials to be made accessible via biomimetic design approaches from α-helical peptides were fibrous materials. Kojima et al. were the first to describe an α-helical fibrous peptide material based on the self-assembly of a tetrameric 3-heptad coiled coil (Kojima et al. 1997). Most of the reported designs are based on staggered α-helical coiled coils, but more recently, α-helical fibrous materials based on self-assembly of blunt-ended coiled-coil building blocks have also been reported.

Fibers Based on Staggered Coiled-Coil Assembly Among the first fibrous α-helical materials, coiled-coil-based designs were predominant, in which the individual monomer units self-assembled in a staggered arrangement. This was seen as a prerequisite to promote longitudinal self-assembly and thus fiber formation. One of the first designs was based on a 5-heptad coiled-coil peptide, with the fifth heptad shortened by one amino acid to allow self-assembly into a five-stranded α-helical bundle (Potekhin et al. 2001). The sequence pattern showed an extended hydrophobic core with leucine residues at the *a* and *d* positions and alanine residues at the *e* positions to accommodate more than two α-helices. Glutamic acid and arginine residues were incorporated at the *f* and *g* positions to promote *f-g'* attractive electrostatic interactions as observed in natural five-stranded coiled coils (Fig. 3.2a). Based on these design rules, peptides were obtained that self-assembled into fibrous structures at acidic pH. At neutral pH, the structure dissembled into more vesicle-like arrangements. A five-stranded α-helical bundle was proposed as the most likely filamentous architecture, with the individual α-helices arranged parallel to the helix axis.

Based on the design rules for parallel heterodimeric coiled coils, the Woolfson group designed sticky-ended coiled-coil dimers that self-assembled into extended α-helical fibers (Fig. 3.2b). Two complementary four-heptad peptides were designed such that, based on the charge pattern, blunt-ended assembly would lead to repulsion of the two α-helical peptides, while assembly shifted by two heptads promoted self-association due to attractive charge interactions. To support this staggered assembly,
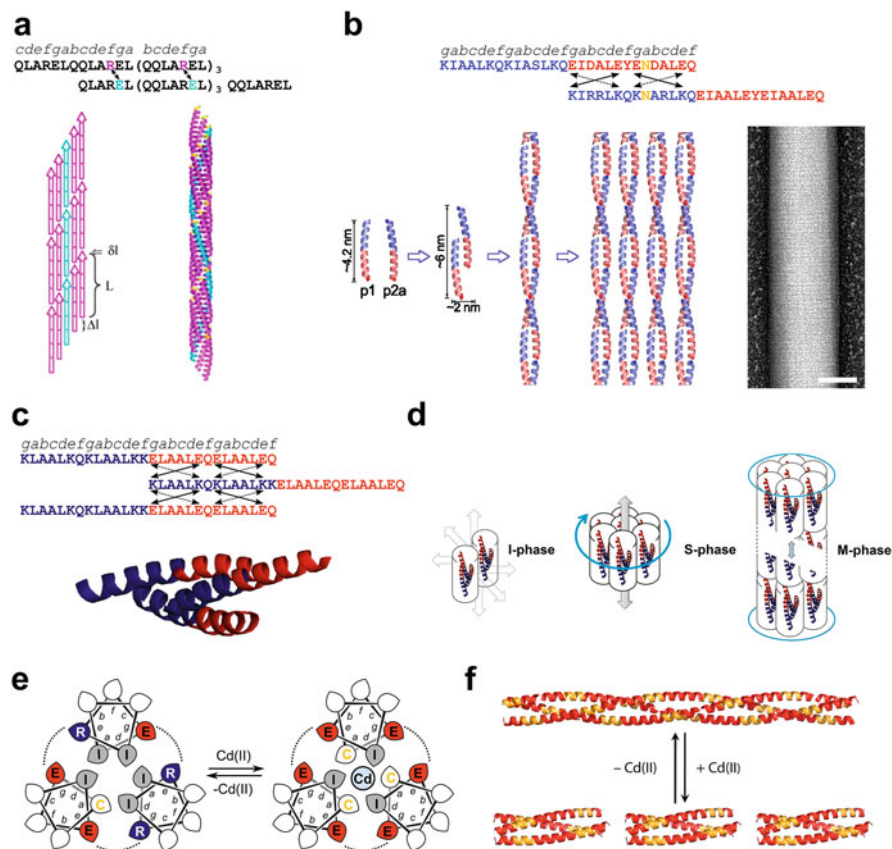
Fig. 3.2 α-Helical fibers from staggered coiled coils. (**a**) Schematic representation of self-assembling α-helical fibers based on staggered five-stranded coiled-coil subunits (Reprinted from (Potekhin et al. 2001), with permission from Elsevier. (**b**) FiM self-assembling fibers from sticky-ended heterodimeric coiled coils and transmission electron micrograph from paracrystalline hexagonally packed SAFs (Reprinted from (Sharp et al. 2012), with permission from the National Academy of Science); (**c**) Conceptional design of a self-assembling sticky-ended heterotrimeric coiled-coil; (**d**) Schematic representation of the three-phase assembly of the sticky-ended coiled-coil trimer (Figs. **c–d** reprinted with permission from (Bella et al. 2014), copyright © Angelo Bella et al.; please note that the schematics in (**e**) have been realigned for formatting reasons); (**f–g**) Cd (II) responsive α-helical fibers. (**e**) Helical-wheel representations indicate the reversible register shift upon the addition of Cd(II); (**f**) Schematic representation of the Cd(II)-induced disassembly of the α-helical fibrous material (Reprinted with permission from (Anzini et al. 2013), Copyright © 2013 American Chemical Society)

core asparagine residues were introduced at the **a** positions of the last and second heptads, respectively (see Fig. 3.2b, asparagine residues highlighted in yellow). This design scheme resulted in the formation of extended self-assembling fibers (SAFs) that were several micrometers long and additionally showed lateral assembly

(Pandya et al. 2000). Based on the residues at the f positions, the morphology of the fibers could be controlled. Glutamine residues on the f positions resulted in stiff, paracrystalline, hexagonally packed fibers of more than 50 nm width (Papapostolou et al. 2007; Sharp et al. 2012). In contrast, when alanine and tryptophan residues were incorporated at the f positions, a hydrogel was formed whose utility in tissue engineering could be demonstrated (Banwell et al. 2009). In addition to lateral assembly, Ryadnov et al. were also able to control longitudinal assembly in SAFs by designing fiber-shaping peptides that were able to associate with the sticky-ended fiber-forming heterodimers and, because they contained two two-heptad units connected by a β-alanine linker either head-to-head or tail-to-tail, introduce kinks into the fibrous assemblies (Ryadnov and Woolfson 2003). Furthermore, De Santis et al. found the length of SAF-like fibrous systems to be correlated with the length of the peptide subunit. Interestingly, shorter subunits (four heptads) resulted in longer fibril formation which was found to be due to a synergistic interplay between charge and cooperative fiber formation (De Santis et al. 2014).

A staggered parallel coiled-coil trimer with an all-leucine core (FiM – fibrillogenesis imaging model) was investigated for its propensity to self-assemble into elongated α-helical fibers in real time (Fig. 3.2c). A three-phase assembly mechanism was proposed and monitored by electron microscopy (Fig. 3.2d): the initiation phase (I) describing the seeding phase of the monomeric subunits, the stabilization phase (S) involving the stabilization of the seeds by lateral self-assembly, and the maturation phase (M) describing longitudinal growth, with lateral growth arrested (Bella et al. 2014). This model was used to develop a FiM-like system that formed discrete fibrils without thickening by maturation. The staggered coiled-coil trimer was modified with tryptophan residues at the f positions every second heptad repeat at a regular spacing of 1.63 Å to promote tryptophan zippering of the coiled coils into discrete, elongated fibrils or fibrillar bundles without undesired thickening (De Santis et al. 2015).

The ultimate control over the self-assembly of fibers based on coiled coils would be achieved with a switch system that allows a conformational change of the α-helical subunits from unfolded or blunt-ended arrangements to staggered arrangements, thus initiating fiber formation. The Conticello group designed trimeric coiled coils that changed conformation in response to an external trigger. The first system described was pH sensitive and harbored histidine residues at every other d position in a peptide with six heptads (Zimenkov et al. 2006). At neutral pH, the peptide formed extended fibers with high aspect ratios; however, at pH values approximately equal to or lower than the pK_a of the histidine side chains, protonation of the imidazole moieties led to charge repulsion and thus disassembly of the fibrous coiled-coil arrangement. Even more sophisticated was the design of a six-heptad metal-responsive coiled-coil trimer that harbored cysteine residues at the a positions of heptads two and five (Anzini et al. 2013). The charge pattern of the residues at the e and g positions promoted staggered self-assembly and thus the formation of elongated α-helical fibers. The addition of cadmium ions, which were strongly coordinated by the cysteine residues, led to a shift in the coiled-coil register and thus to blunt-ended trimeric coiled coils that could not form fibrillar architectures.
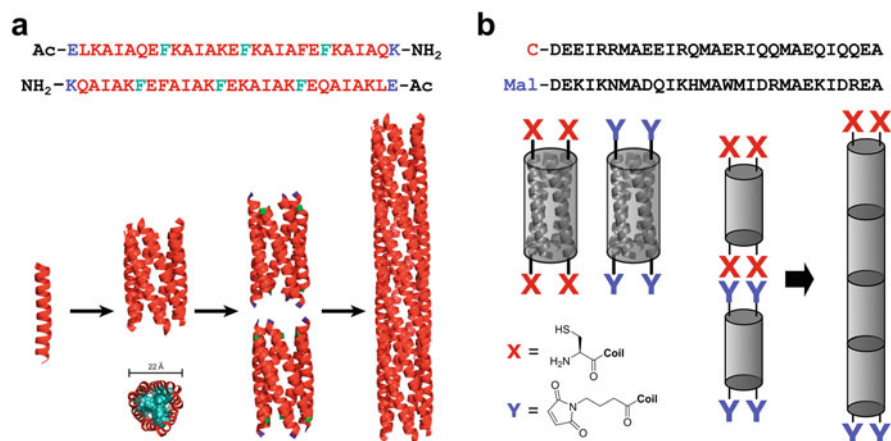
Fig. 3.3 α-Helical fibers from blunt-ended coiled coils. (**a**) Schematic representation of blunt-ended self-assembly of the antiparallel coiled-coil hexamer ACC-Hex. The phenylalanine residues are shown in turquoise and the charged termini in blue. The sequence of ACC-Hex is shown twice to emphasize the antiparallel arrangement (Ac - acetyl) (Reprinted with permission from (Ing et al. 2018). Copyright © 2018 American Chemical Society); (**b**) Schematic representation of the covalent assembly of coiled-coil tetramers using maleimide-cysteine ligation (Mal – maleimide)

This process was reversed by the addition of ethylenediaminetetraacetic acid (EDTA, Fig. 3.2e–f).

Blunt-Ended Coiled-Coil-Based Fibrous Materials Compared to the variety of α-helical fibrous assemblies based on staggered coiled-coil subunits, fibrous systems of blunt-ended coiled coils are rarely described. The first to report an α-helical fibrous system based on blunt-ended coiled-coil subunits were Dong et al. (Dong et al. 2008). They designed three-heptad peptides in which the hydrophobic core promoted dimeric assembly but which contained only glutamic acid residues at the *e* and *g* positions. This allowed precise control over fiber assembly, which would only occur at acidic pH, as the glutamic acid residues were protonated. This stopped the structure-destabilizing charge repulsion and allowed the formation of structure-stabilizing hydrogen bonds. Furthermore, the morphology of the fibrils formed could be influenced by the introduction of charged or aromatic residues in *b*, *c*, or *f* positions. Charged residues such as lysine led to a hydrogelating material of long and thin fibers. Aromatic residues, on the other hand, lead to shortened or no fibrillar arrangements if too many were introduced into the peptide sequence.

While investigating the self-assembly of uncapped α-helical barrels, Burgess et al. also examined the longitudinal self-assembly of uncapped coiled coils CC-Di-F, CC-Tri-F, and CC-Tet2-F, which were coiled-coil dimers, trimers, and tetramers (vide infra) (Burgess et al. 2015). With the exception of CC-Di-F, all formed α-helical fibrous assemblies, although the fibrils of CC-Tri-F were relatively short. An interesting but similar approach was described by Spencer and Hochbaum (Fig. 3.3a). They designed an antiparallel coiled-coil hexamer (ACC-Hex) whose

feature was the isoleucine-phenylalanine zipper of the hydrophobic core (Spencer and Hochbaum 2016; Spencer and Hochbaum 2017). The bulky phenylalanine and isoleucine residues completely fill the interior of the assembly; hence ACC-Hex is not tubular. The self-assembly of this peptide into extended α-helical fibers was promoted by electrostatic interactions between charged residues – N-terminal glutamic acid and C-terminal lysine amide – and resulted in a material with unique long-range electronic conductivity explained by the supramolecular order and α-helicity of the subunits, both of which are crucial for the observed electronic properties (Ing et al. 2018).

Besides self-assembling systems, a covalent approach can also be used to create coiled-coil-based biomimetic materials. Coiled-coil tetramers, for example, were modified with maleimide (mal) or thiol moieties and could be covalently linked in such a way to obtain an α-helical fibrous material with high mechanical stability (Fig. 3.3b) (Wu et al. 2019). The physical properties such as stiffness and morphology could be controlled by the linkers applied for the system. For example, linking a flexible thiol-modified organic molecule instead of the thiol-functionalized coiled-coil tetramer and the maleimide-functionalized α-helical bundles resulted in a flexible fibrous material. Recently, it has also been shown that this system is suitable for electrospinning, producing nanofibers with high control of structure over multiple length scales (Kim et al. 2021).

3.4 α-Helical Peptide Nanotubes

Self-assembly of α-helical peptides into peptide nanotubes (PNTs) has been reported for coiled-coil α-helical barrels (Gunasekar et al. 2009; Burton et al. 2013; Xu et al. 2013), surfactant-like peptides (Castelletto et al. 2020), and α-helical peptide hairpins and coiled coils that form ribbon-like assemblies (Egelman et al. 2015; Hughes et al. 2019; Wang et al. 2021). PNTs from α-helical barrels describe longitudinal arrangements of more or less closed cylindrical subunits, whereas PNTs from peptide amphiphiles result from an exclusively lateral arrangement of linear α-helical subunits. The α-helical peptide building blocks in ribbon-like nanotubes have two hydrophobic faces that promote lateral assembly and a charged head and tail that allow axial or cross self-assembly. Since the nature of self-assembly is very different for these three classes of PNTs, they are discussed individually in this chapter.

α-Helical PNTs from Cylindrical Subunits α-Helical barrels are cylindrically shaped assemblies of five to nine α-helices that show a knobs-into-holes packing and can therefore be classified as coiled coils (Thomson et al. 2014; Dawson et al. 2021). The inner channel is usually flanked by hydrophobic residues, but is accessible to small molecules (Burton et al. 2013; Thomas et al. 2018). Most of the known arrangements form blunt-ended barrels, but some show a lock washer-like arrangement (Liu et al. 2006). The first α-helical barrel engineered to self-assemble into

elongated PNTs was the lock-washer-like seven-helix coiled-coil GCN4-pAA, which was engineered from the well-studied leucine zipper GCN4-1p by replacing the charged residues at positions *e* and *g* with alanine residues (Fig. 3.4a and c) (Liu et al. 2006). To generate GCN4-pAA-based PNTs, the Conticello lab redesigned GCN4-pAA to obtain 7HSAP1 (Fig. 3.4c), which was further stabilized by attractive charge interactions between the *b* and *c* positions and contained uncapped termini to promote axial self-assembly showing single fibrils and paracrystalline assemblies resulting from lateral self-assembly (Fig. 3.4e) (Xu et al. 2013).

A similar strategy for elongated PNTs, but from completely de novo designed α-helical peptide building blocks, was presented by Burgess et al. (Burgess et al. 2015). They used blunt-ended coiled-coil trimers to heptamers (CC-Tri-F, CC-Tet2-F, CC-Pent-T, CC-Hex-T, and CC-Hept-T) with uncapped termini and investigated longitudinal self-assembly (Fig. 3.4b and d (sequence CC-Hex-T)). Interestingly, all oligomeric states resulted in fibrillar or tubular assemblies driven by the electrostatic interactions between the respective termini (see exemplarily for CC-Hex-T Fig. 3.4f). While the CC-Tri-F-based assemblies were relatively short and thin, all other coiled coils showed extensive longitudinal and lateral self-assembly, indicating that this simple engineering approach, uncapped termini, can be considered a generic strategy for initiating longitudinal self-assembly in coiled-coil peptides. Similar to 7HSAP1, highly paracrystalline structures were observed for CC-Tet2-F and CC-Hex-T after the peptide suspensions were subjected to thermal treatment (Fig. 3.4i). Cryo-EM studies and x-ray fiber diffraction allowed the conclusion of a square-packed model for CC-Hex-T.

All of the abovementioned examples of longitudinally assembled PNTs were accompanied by significant lateral assembly, which strictly speaking resulted in PNT arrays. This array formation is sensitive to pH changes, at least for CC-Hex-T (Thomas et al. 2016). At acidic pH, glutamate residues on the outside of CC-Hex-T are protonated, resulting in a strongly positively charged surface. As a result, the CC-Hex-T lattices break down, leaving fibrils corresponding to individual PNTs. Based on this observation, Thomas et al. designed CC-Hex-T+ with a lysine-rich outer surface (Fig. 3.4d). This peptide showed exclusively longitudinal self-assembly (Fig. 3.4g and j). To stabilize this assembly, covalent linkage of individual CC-Hex-T+co building blocks via native chemical ligation was also attempted (Fig. 3.4h). In this way, individual short PNTs of up to 100 nm in length could be generated, which corresponds to 25 covalently attached CC-Hex-T + co units (Fig. 3.4k). The hydrophobic interior of all de novo designed α-helical barrel-based PNTs proved to be accessible to hydrophobic environmentally sensitive dyes such as Prodan or 1,6-diphenylhexatriene.

In addition to the de novo designed α-helical barrel-based PNTs, a remodeled α-helical barrel that was based on the parallel pentameric coiled-coil domain of the cartilage oligomeric matrix protein (COMP$_{CC}$) (Gunasekar et al. 2009) was used to generate elongated PNTs by longitudinal self-assembly also driven by attractive charge interactions between the termini of adjacent barrels (Hume et al. 2014). Fibrils of 3.5 nm diameter were obtained, which also assembled laterally into thickened fiber bundles. Similar to the systems of Conticello et al. and Woolson
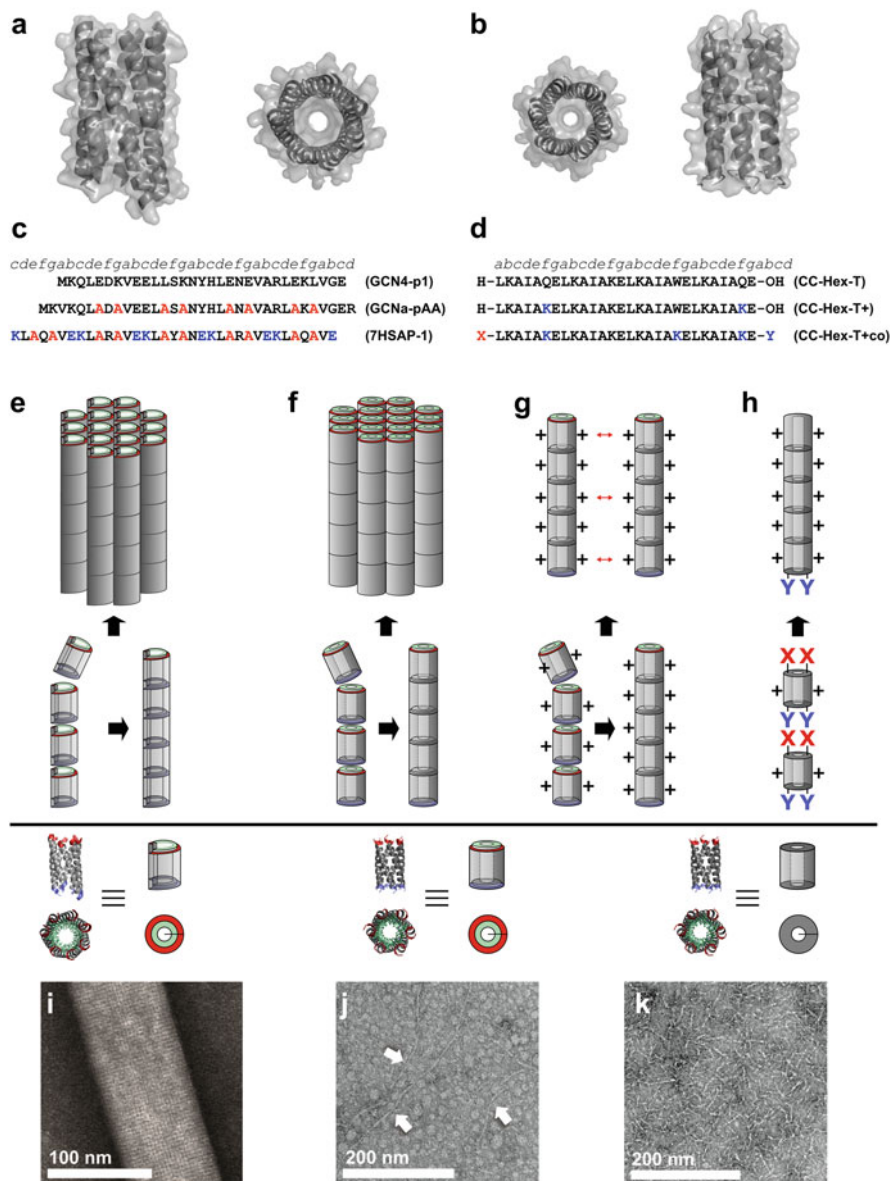
Fig. 3.4 PNTs from α-helical barrels. Space filling models of the x-ray crystal structures of (**a**) GCN4-pAA (left – parallel view, right – orthogonal view; pdb: 2HY6 (Liu et al. 2006)); (**b**) CC-Hex (left – parallel view, right – orthogonal view; pdb: 3R3K (Zaccai et al. 2011)). (**c**) Peptide sequences of GCN4-p1, GCN4-pAA and 7HSAP1 showing the stepwise engineering process. Mutations from GCN4-p1 to GCN4-pAA are shown in red. Mutations from GCN4-pAA to 7HSAP1 are shown in blue. (**d**) Peptide sequences of CC-Hex-T, CC-Hex-T+ and CC-Hex-T +co. Lysine mutations are shown in blue. (**e–h**) Schematic representation of PNT assembly: (**e**) Self-assembly of broadened PNTs from 7HSAP1 (represented packing mode is only symbolic for the formation of paracrystalline fibrils); (**f**) self-assembly of broadened PNTs from CC-Hex-T; (**g**) self-assembly of single PNTs from CC-Hex-T+; (**h**) covalent assembly of CC-Hex-T+co (X and Y

et al., the interior of the porous material was accessible to small molecules, in this case curcumin. The properties of the material were further developed into hydrogels that allow the release of small molecules upon an external trigger (Hill et al. 2019; Meleties et al. 2021).

PNTs from α-Helical Peptide Surfactants Surfactant-like α-helical peptides have been shown to self-assemble into different nanostructures depending on the pH (Castelletto et al. 2020; Castelletto et al. 2021). The reported peptides consist of a cationic arginine head group and a leucine tail. Driven by the hydrophobic effect, peptide membranes form from antiparallel peptide dimers lying perpendicularly in the membrane wall with a membrane thickness consistent with the length of a peptide dimer subunit. This nanotube architecture is also referred to as "cross-α" (Tayeb-Fligelman et al. 2017). The charged arginine head groups are located on the surface of the nanostructures, which is thus strongly positively charged. In aqueous dilution, the formation of tubular structures was observed (Castelletto et al. 2020). However, this was pH-dependent. At pH 4 to pH 2, only tubular structures were observed, whereas at very acidic pH, these tubular structures are transformed into tubular networks. Such networks were also detected at neutral and slightly basic pH. At pH 12–13, which corresponds approximately to the pK_a of the arginine side chains, the arginine head groups are deprotonated. This changes the surface charge and leads to vesicle-like structures with phase-separated domains, which was explained by the coexistence of disordered peptides forming the vesicles and α-helical peptide compartments (Castelletto et al. 2021).

Ribbon-Like PNTs Self-assembly into ribbon-like architectures has been reported for designed α-helical peptide hairpins and coiled-coil peptides that exhibit a Type III heptad repeat pattern of **hphhphp** (vide supra). Both PNT designs were described by the Conticello group (Egelman et al. 2015; Hughes et al. 2019; Wang et al. 2021).

The self-assembling PNTs from α-helical peptide hairpins are based on natural tandem repeat proteins such as the leucine-rich repeat variant (LRV) (Peters et al. 1996) and the phycobilisome lyase HEAT (PBS_HEAT) (Urvoas et al. 2010). These proteins form superhelical assemblies and were therefore identified as suitable starting points for the design of ribbon-like PNTs. Based on the consensus sequences of LRV and PBS-HEAT, two peptides, the 23 amino acid LRV_M3Δ1 and the 31 amino acid HEAT_R1, were designed that self-assembled into highly ordered PNT filaments with high aspect ratios in a pH range of 5 to 8 and with highly uniform diameters (Fig. 3.5a) (Hughes et al. 2019). High-resolution structural analyses revealed a ribbon-like assembly with laterally arranged peptides in both cases (Fig. 3.5b–c) and inner diameters of about 30 Å and 35 Å, respectively. Interestingly, LRV_M3Δ1 is a left-handed superhelix with 17.4 monomer peptides per turn and a pitch of 20 Å, while HEAT_R1 describes a right-handed superhelix

---

Fig. 3.4 (continued) present thiol and thioester moieties that react in a native chemical ligation); (**i**–**k**) negative stain TEM images of (**i**) CC-Hex-T; (**j**) CC-Hex-T+; (**k**) CC-Hex-T+co after 7 days (**d**–**i** were adapted from Thomas et al. (2016), copyright © Franziska Thomas et al., published under a CC BY 4.0 license)
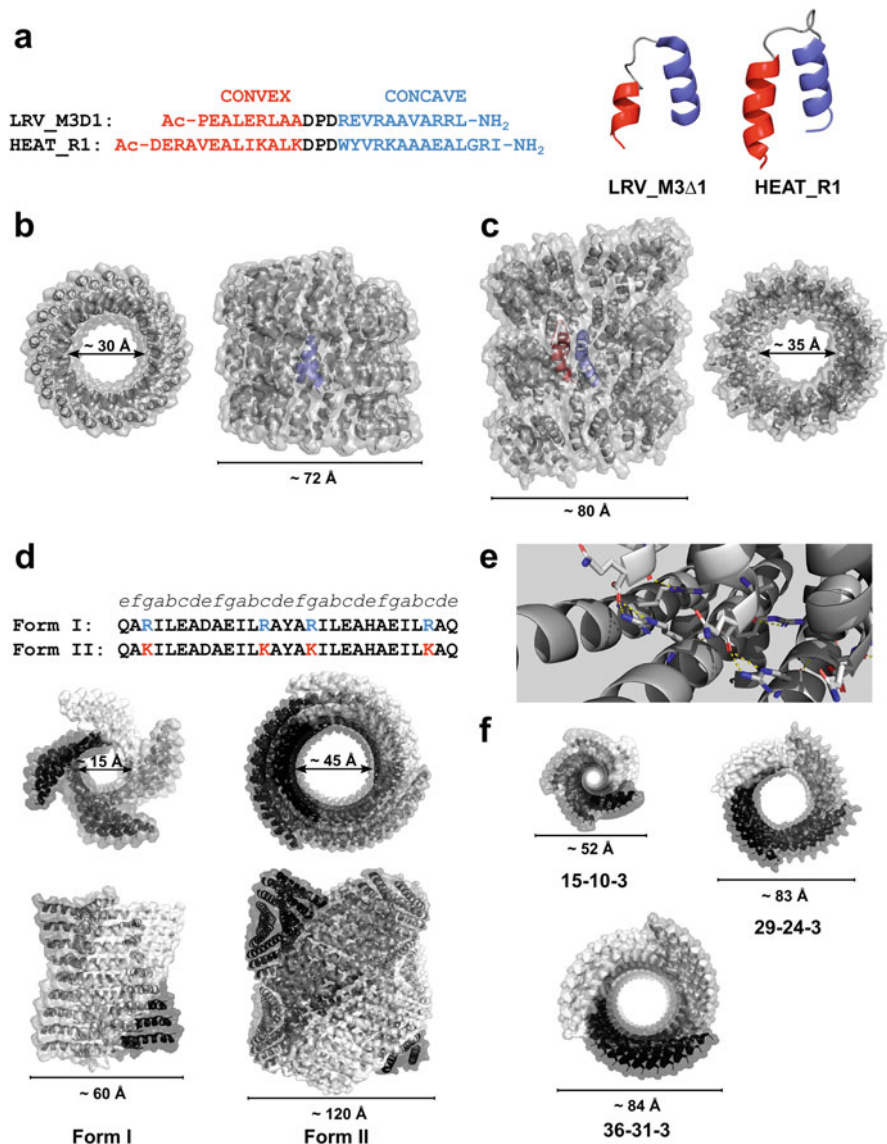
Fig. 3.5 Ribbon-like PNTs. (**a**) Sequences and cartoon representations of the LRV_M3Δ1 and HEAT_R1 monomer units (pdb: 6HQE, 6MK1, Ac - acetyl) (Hughes et al. 2019). (**b**, **c**) Space filling models of the high-resolution Cryo EM structures of (**b**) LRV_M3Δ1 (left – orthogonal view, right – parallel view; pdb: 6HQE (Hughes et al. 2019); hairpin subunit is depicted in blue); (**c**) HEAT_R1 (left – parallel view, right – orthogonal view; pdb: 6MK1 (Hughes et al. 2019); dimeric subunit is depicted in red and blue); (**d**) sequences and space filling models of Form I (29-17-3) (top – orthogonal view, bottom – parallel view; pdb: 3 J89 (Egelman et al. 2015)) and Form II (top – orthogonal view, bottom – parallel view; pdb: 6WL8 (Wang et al. 2021)); (**e**) arginine clasp in Form I (29-17-3) PNTs: Arginine residues form an extended hydrogen-bond network and promote a side-to-end helical interaction between adjacent α-helical stacks; (**f**) Orthogonal views of high-resolution Cryo EM structures of Form I (15-10-3), Form I (29-24-3), and Form I (36-31-3) (pdb: 6WKX, 6WKY, 6WL1 (Wang et al. 2021)). Pore diameters shown in this figure are obtained from the respective pdb files

with 10.3 dimeric subunits per turn and a pitch of 31 Å. The unexpected dimerization of the HEAT_R1 subunits is due to planar π-stacking between anti-oriented tryptophan residues of two monomers. This results in only one peptide being aligned on the superhelical axis and the other being slightly tilted. In LRV_M3Δ1, arginine clusters and electrostatic interactions, which are also conserved in nature, promote the axial assembly and almost parallel arrangement of the subunits to the PNT axis, thus stabilizing the superhelical structure.

Based on a model by Walshaw and Woolfson (Walshaw and Woolfson 2003), Egelman et al. designed bifacetted α-helical coiled coils that self-assembled laterally into tubular structures in a cross-α arrangement and with diameters ≥5 nm (Egelman et al. 2015). These peptides showed a Type III heptad repeat pattern ***abcdefg*** of hydrophobic and polar residues of **hphhphp**, with the two hydrophobic faces offset by one amino acid residue (Fig. 3.1g) (Woolfson et al. 2012). To promote larger diameter PNTs, the hydrophobic positions were populated by small alanine residues for positions ***a*** and ***f*** on the outer surface and more sterically demanding isoleucine and leucine residues for positions ***c*** and ***d*** on the inner surface of the helix-helix interface. Charged residues, lysine or arginine and glutamate, were introduced at positions ***b*** and ***e*** to favor α-helical assembly and suppress β-amyloid formation by repulsive electrostatic interactions between the ***b*** and ***e*** interstrand positions. Interestingly, the nature of the positively charged residues significantly influenced the final architecture of the respective PNTs. Arginine residues lead to the so-called Form I PNT, an almost square arrangement in which four stacks of α-helices were intertwined, each forming a four-start helix (Fig. 3.5d). Replacing the arginine residues with lysines resulted in a dramatic change of quaternary structure. The formed PNTs revealed a diameter twice as large as the Form I PNTs (Fig. 3.5d). This Form II arrangement was circular and consisted of an inner and an outer layer of three stacks each of laterally arranged coiled coils forming a three-start helix. The reason for the different arrangements is the ability of the central arginine side chains Arg 13 and Arg 17 to interact with the C-terminal glutamine residues of the adjacent stack of α-helical peptides to form a hydrogen-bond network (Fig. 3.5e). This interaction was recently characterized by high-resolution cryo-EM and named the arginine clasp or RXXXR motif (Wang et al. 2021). The two arginine residues are arranged as i, $i + 4$ within the sequence and form a so-called side-to-end helical interaction motif (Ghosh et al. 2009). This is unique and has not been found in nature before. Although this interaction is probably weak, multivalence effects lead to a significant stabilization of the supramolecular arrangement.

Based on this analysis, a series of different peptides containing the RXXXR motif was designed (Fig. 3.5f) (Wang et al. 2021). Depending on the distance of the RXXXR motif relative to the C-terminus, PNTs with five to three α-helical stacks were rationally designed, with the number of α-helical protofilaments increasing with shorter distance from the C-terminus and shorter length. The RXXXR motif was localized in the N-terminal heptad repeat at positions ***e*** and ***b***, respectively. The peptide length thereby determined the symmetry of the respective cross-α-PNTs through the number and relative orientation of the protofilaments, which enabled the

maintenance of the structurally critical cohesive interactions at the axial and lateral interfaces.

3.5   α-Helical Peptide Cages and Protein Origami

The self-assembly of α-helical peptides and proteins into defined three-dimensional objects has recently received a boost, mainly due to advances in computer-assisted protein design. However, even before that, peptide cages were designed from scratch based on symmetry considerations. This chapter focuses on the design of cages based on α-helical coiled coils; however, since coiled coils have also been successfully used as oligomerization domains in protein-cage design, this is also covered. Finally, we will summarize recent progress in the field of coiled-coil-based protein origami. Although there are many fine examples of computationally designed protein cages from α-helical proteins (Padilla et al. 2001; Hsia et al. 2016; Sasaki et al. 2017; Cannon et al. 2020), this is not covered in this paragraph as we think it is beyond the scope of this book chapter.

α-Helical Peptide Cages from Coiled-Coil Self-Assembly The first self-assembling peptide cages (SAGEs) generated entirely from de novo designed coiled-coil peptides were presented by the Woolfson Lab (Fletcher et al. 2013). The basic design included de novo designed coiled-coil building blocks, the parallel coiled-coil homotrimer CC-Tri, and the parallel coiled-coil heterodimer CC-Di-AB, linked by a disulfide bond such that each strand of CC-Tri was linked to either CC-Di-A or CC-Di-B leaving the hydrophobic seams of CC-Di-A and CC-Di-B solvent-exposed (Fig. 3.6a and b). To obtain the SAGEs, the two modified CC-Tri species were first assembled into the respective CC-Tri-CC-Di-A or CC-Tri-CC-Di-B hubs, which were then mixed to assemble into extended hexagonal arrays that closed into α-helical peptide cages (Fig. 3.6c). These cages have been shown to be robust to modification and have been explored as a platform for vaccine design and as a drug delivery system (Beesley et al. 2018; Morris et al. 2019). The closure of the hexagonal array in SAGEs was recently investigated by double conformationally constraining the CC-Tri-CC-Di building blocks via the disulfide bond and a flexible loop, resulting in a peptide hairpin structure (Galloway et al. 2021). The position of the disulfide bond was placed either distal or proximal to the loop. It was found that the proximal disulfide bond allowed splaying of the α-helices, resulting in closure of the hexagonal arrays into spherical objects. In contrast, distal disulfide pinning resulted in rigid peptide hairpins that self-assembled into flat hexagonal lattices.

Using a trifaceted coiled-coil helix, virus-like particles were obtained based on self-assembly (Noble et al. 2016). The basic design idea mimics the typical C_n-fold rotational symmetry of virus particles, where n is 3 or 5. The peptide design included a coiled-coil dimer covalently linked by an N-terminal disulfide bridge (Fig. 3.6e). In addition to the dimer interface, each individual helix was able to interact specifically with identical neighbors via two polar interaction sites, promoting the formation of a
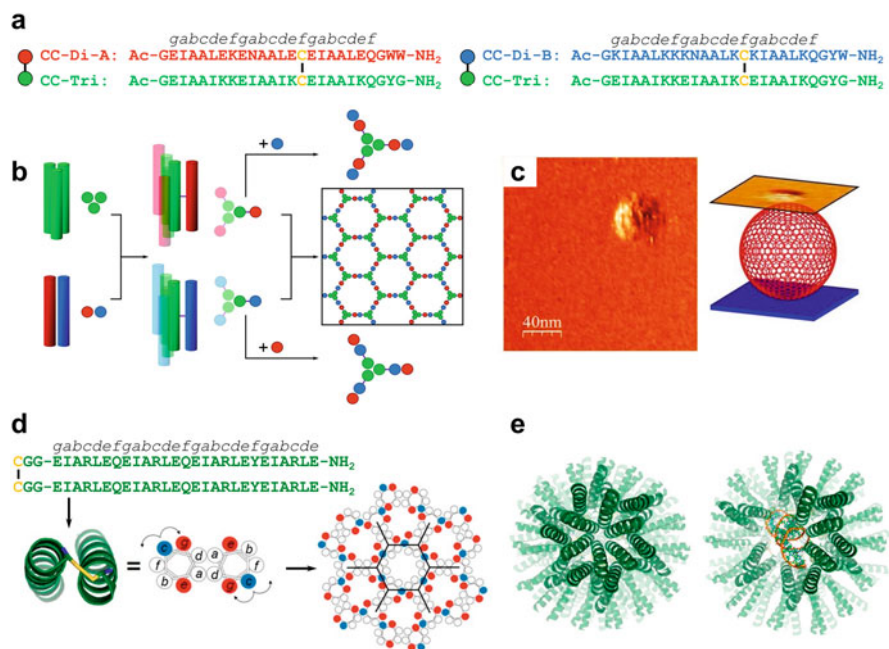
Fig. 3.6 α-Helical peptide cages from coiled-coil self-assembly. (**a**) Sequences of the monomer building blocks of the self-assembling cages (SAGEs, Ac – acetyl); (**b**) schematic representation of the formation of coiled-coil self-assembling cages (SAGEs) from coiled-coil homotrimers and coiled-coil heterodimers with the individual chains of the coiled-coil heterodimer being covalently linked to a chain of the coiled-coil homotrimer, respectively, giving hetero self-assembling hubs that form hexagonal arrays (From (Fletcher et al. 2013) Reprinted with permission from AAAS.); (**c**) atomic force micrograph of the surface of a SAF (From (Fletcher et al. 2013) Reprinted with permission from AAAS.); (**d**) schematic representation of the self-assembly of coiled-coil virus-like particles from covalently linked trifaceted coiled-coil dimers; (**e**) virus-like particles from self-assembling trifaceted coiled coils without cargo (left) and with sequestered single-stranded RNA (right); (**d**–**e** adapted with permission from Noble et al. (2016). Copyright © 2016 American Chemical Society)

dendritic virus-like structure with a very uniform morphology due to the highly symmetrical hexagonal arrangement. The particles are hollow and have been shown to sequester nucleic acids and deliver them into human cells (Fig. 3.6e).

Protein Cages from Coiled-Coil Fusion Proteins Since the oligomerization state in coiled coils is easy to control and many coiled-coil building blocks have been made accessible by de novo design, they were often used as oligomerization domains to fuse proteins together into artificial cages. Very often, symmetry considerations played a key role in the design of such cages. For example, an octahedral protein cage was designed from a trimeric esterase (Fig. 3.7a) (Sciore et al. 2016). An octahedron has C_3- and C_4-rotational symmetry, with the C_3-symmetry axes passing through the faces and the C_4-rotational symmetry axes passing through the corners. Consequently, the esterase with C_3-fold rotational symmetry would form

Fig. 3.7 Protein cages from coiled-coil fusion proteins. (**a**) Self-assembling protein octahedron from a C_3-symmetric esterase and a C_4-symmetric coiled-coil tetramer (Reprinted from Sciore et al. (2016), with permission from the National Academy of Science); (**b**) self-assembling protein icosahedra from a C_3-symmetric esterase and a C_5-symmetric coiled-coil pentamer (Reprinted

the faces of the protein octahedron, which would be oligomerized by coiled-coil homotetramers, thus forming the corners of the cage. In a follow-up report,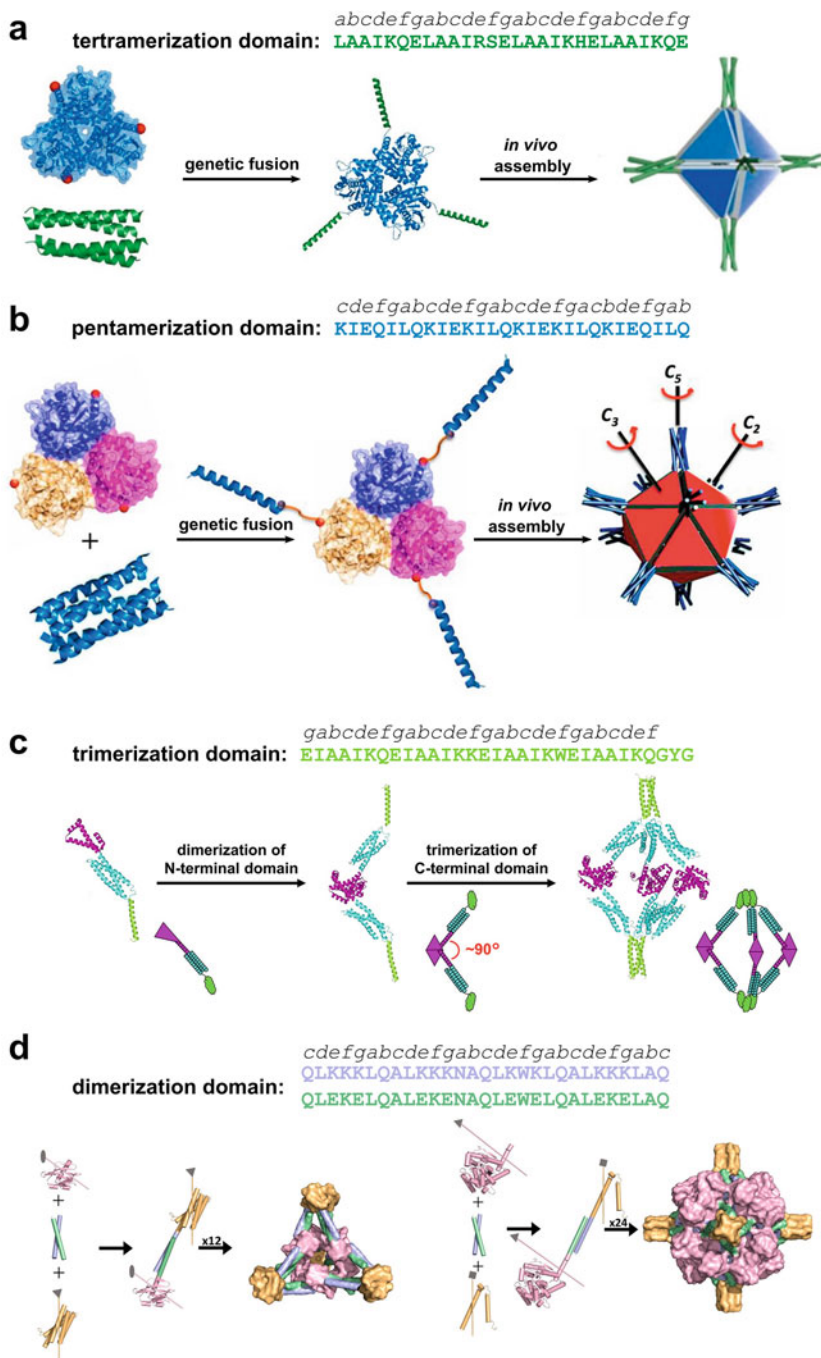 it was shown that additional proteins can be fused to the coiled-coil oligomerization domains to create protein-decorated protein cages (Cristie-David et al. 2018). This symmetry approach has been shown to be universally applicable. For example, using a homotrimeric coiled coil instead of a homotetrameric coiled coil resulted in a protein tetrahedron, with the esterase again forming the C_3-rotationally symmetric faces and the coiled-coil homotrimer forming the corners (Badieyan et al. 2017). An icosahedral protein cage was achieved in a similar approach by combining the C_3-rotationally symmetric esterase with a C_5-symmetric coiled-coil pentamer (Fig. 3.7b) (Cristie-David et al. 2019).

A slightly different approach to α-helical cages was taken by Hirota et al. They designed fusion proteins with a central three-helix bundle fused N-terminally with an α-helical dimerization domain to give a rigid V-shaped structure after dimerization (Fig. 3.7c) (Miyamoto et al. 2019). The C-terminus of this fusion protein was either modified with another dimerization domain to obtain a square-like assembly or with a de novo designed coiled-coil homotrimer to obtain a cage-like hexamer that can be most closely described geometrically as an octahedron. By combining computational design and symmetric considerations, Yeates et al. designed heterodimeric coiled-coil fusion proteins in which one of the coiled-coil components was modified with a different α-helical oligomerization domain, respectively (Fig. 3.7d) (Laniado et al. 2021). The key to the design was fusion via continuous α-helical linkers to give rigidity to the system. The coiled coils were either fused with a dimerization and trimerization domain, resulting in a tetrahedral cage, or with a trimerization and tetramerization domain, resulting in an octahedral protein cage.

Coiled-Coil-Based Protein Origami Heterodimeric coiled coils can be designed to interact with high specificity. This can be achieved by the charge pattern of the *e*- and *g*-positions of the coiled-coil interface or by negative design, e.g., by introducing polar amino acid residues such as asparagine into the hydrophobic core (Bromley et al. 2009; Thomas et al. 2017). These so-called orthogonal coiled-coil peptides have been used and further developed to fold into defined polyhedral structures when concatenated into a single protein chain (Fig. 3.8) (Lapenta et al. 2018). This engineering approach is commonly referred to as coiled-coil protein origami (CCPO). The very first example was the design of a coiled-coil tetrahedron consisting of three pairs of parallel orthogonal coiled-coil heterodimers, two pairs
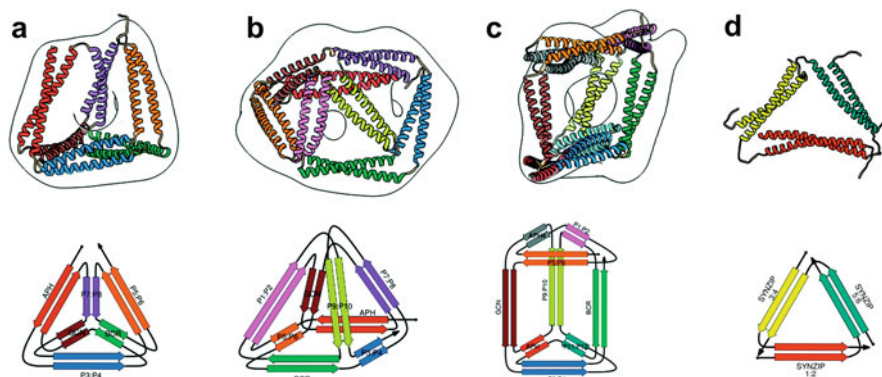
Fig. 3.8 Coiled-coil protein origami. Models of (**a**) a single chain CCPO tetrahedron; (**b**) a single chain CCPO square pyramid; (**c**) a single chain CCPO triangular prism; (**d**) a CCPO trimer with (**a**–**c**) superimposed to volumes obtained by EM negative stain single-particle reconstruction. (Figures reprinted with permission from Lapenta et al. (2018), copyright © Fabio Lapenta et al., published under a CC BY 3.0 license; please note that in this Figure content of two figures from the original publication are merged for clarity reasons)

of antiparallel coiled-coil homodimers, and one parallel coiled-coil homodimer, with each coiled-coil dimer forming one edge of the tetrahedron (Fig. 3.8a) (Gradišar et al. 2013). Since then, the toolbox of coiled-coil dimers that can be used for CCPO has been expanded. In addition, detailed studies of the folding pathway within a CCPO tetrahedron revealed a sequential stepwise construction of the polyhedral structure that allows identical coiled-coil pairs on several edges of the cage structure (Aupič et al. 2021). These two facts enabled the design of a number of different polyhedral structures, including a square pyramid (Fig. 3.8b), a triangular prism (Fig. 3.8c), and a trigonal bipyramid (Ljubetič et al. 2017; Lapenta et al. 2021). The CCPO polyhedra have been shown to be stable to functionalization with nanobodies (Majerle et al. 2021), paving the way to applications in biomaterial design, for example. Interestingly, the less complex CCPO triangles appeared to be less accessible at first. In the meantime, however, two designs of CCPO triangles have been described (Fig. 3.8d) (Park et al. 2017; Božič Abram et al. 2021).

3.6 α-Helical Peptide Networks and Arrays

α-Helical peptides have been used to design two- and three-dimensional peptide networks or highly ordered paracrystalline arrays. In this chapter, the term network is used to describe amorphous, largely disordered two- or three-dimensional arrangements, while arrays describe highly ordered two- and three-dimensional peptide assemblies with paracrystalline properties. The tendency of coiled coils with their C_n-rotational symmetry to self-assemble into highly ordered paracrystalline

structures has already been discussed in the context of coiled-coil fibers and coiled-coil nanotubes. Certain analogies to α-helical networks can also be found in the construction of α-helical cages, as networks are often created by covalently linking the α-helical subunits. However, there are many reports of two- and three-dimensional peptide materials that are neither fibrillar, tubular, or cage-like, but simply exist as networks. We have divided this chapter into amorphous α-helical peptide networks and paracrystalline α-helical arrays according to the morphology of the arrangement obtained.

Amorphous α-Helical Peptide Networks An amorphic peptide network based on covalently linked α-helical coiled coils was presented by the Horne Lab (Staples et al. 2012; Oshaben and Horne 2014). The basic design comprised homodimeric coiled coils derived from the GCN4 leucine zipper, modified with a cysteine residue at a central f position to allow covalent linkage via flexible or rigid acetamide linkers (Fig. 3.9a). Coiled-coil stability was adjusted by replacing valine residues at the a-positions with isoleucine residues. In general, rigid linkers resulted in more extended polymer formation, independent of coiled-coil stability.

An extended peptide network was obtained when asymmetric coiled-coil helices designed according to the typical heterodimeric design scheme were forced into a non-self-associating antiparallel arrangement by cyclisation (Fig. 3.9b) (Faruqui et al. 2014). This resulted in the coiled-coil interfaces still being accessible and allowing specific interaction with further coiled-coil cyclopeptides. The sequence pattern of the individual coiled-coil domains of such a cyclopeptide comprised either two positively charged and one negatively charged heptad or two negatively charged and one positively charged heptad, favoring different heptad overlaps between the individual coiled-coil cyclic peptides, eventually leading to an extended network with a high nanoscale order. It was shown that this material allowed proliferation of mammalian cells and showed resistance to bacterial colonization.

An electrogelling material was obtained by linking pH-sensitive coiled-coil domains, i.e., ambiguously oligomerizing coiled coils, with spider silk glue that naturally had a high glutamic acid content and thus enabled anionic electrophoretic transport (Lin et al. 2017). Coiled-coil assembly occurred only below a defined pH trigger point of 5.3. Above this pH, a glutamic acid residue within the hydrophobic core of the coiled-coil oligomerization domain was negatively charged, thus promoting coiled-coil disassembly. When a current was applied in an electrochemical cell, a pH gradient was induced, with the anode acidic and the cathode basic (Fig. 3.9c). The peptides moved to the anode due to the high glutamic acid content of the spider silk glue domains, where coiled-coil formation induced the electrogelation process. This process was reversible when the current was reversed.

Another interesting approach towards an amorphous peptide network was the synthesis of a cross-linked and zinc-responsive coiled-coil polyethylene glycol (PEG) material (Tunn et al. 2019). The individual helices of a coiled-coil heterodimer were cross-linked with maleimide-functionalized star-shaped PEG (star-PEG) via their cysteine-functionalized N- or C-termini, forming hubs that self-assembled into gelling peptide-PEG networks upon mixing (Fig. 3.9d). The coiled-coil domains were modified with histidine residues to allow coordination to

a

stability

gabcdefgabcdefgabcdefgabcdefgabcd
Ac-RMKQLEDKVEELLCKNYHLENEVARLKKLVGER-NH$_2$
Ac-RMKQLEDKIEELLCKNYHLENEVARLKKLVGER-NH$_2$
Ac-RMKQLEDKIEELLCKNYHLENEIARLKKLVGER-NH$_2$
Ac-RMKQLEDKIEELLCKNYHLENEIARLKKLIGER-NH$_2$

Coil–S—NH HN—S–Coil

Coil–S—N N—S–Coil

b

edcbagfedcbagfedcbag
GELAAIEQKLAAIKQKLAAIK**G**
G **G**
GEIAALEQEIAALEYKIAALK**G**
gabcdefgabcdefgabcde

c pH-sensitve coiled coil

abcdefgabcdefgabcdefgabcdefg
IAALEAENEALKAEIAELKAEIAAEKAE

Electrochemical gelation ⇌ Electrochemical dissolution

pH ≤ pKa   pH > pKa

Anode   Cathode

e-gel

d metal-resposive coiled-coil dimer

gabcdefgabcdefgabcdefgabcdef
CGG EIAALEHEIAALEHENAALEHEIAALEQ GG
GG KIAALKHKIAALKHKNAALKHKIAALKQ GGC

Coiled coil   Star-PEG   Zn(II)

Fig. 3.9 Amorphous α-helical peptide networks. (**a**) One-dimensional assembly of thioether linked coiled-coil dimers. The stability of the coiled-coil oligomerization domain was tailored by engineering the hydrophobic core (Ac – acetyl) (Figure adapted with permission from (Oshaben and Horne 2014). Copyright © 2014 American Chemical Society); (**b**) schematic representation of a self-assembling peptide network that forms from asymmetric cyclized coiled-coil dimers (Figure adapted with permission from (Faruqui et al. 2014). Copyright © 2014 American Chemical Society); (**c**) schematic representation of the electrogelation in a pH-sensitive coiled-coil-spider silk material. The amino acid residues highlighted in blue promote disassembly at high pH, while the amino acids highlighted in red stabilize the coiled-coil oligomers at low pH (Figure reprinted with permission from (Lin et al. 2017). Copyright © 2017 American Chemical Society); (**d**) Zn(II)-responsive coiled-coil-star-PEG material. The histidine residues at the f-positions of the coiled-coil heterodimer strands coordinate to Zn(II). The cysteine residues highlighted in yellow allow conjugation to maleimide residues (Figures reprinted with permission from (Tunn et al. 2019), copyright © Isabell Tunn et al. published under a CC BY 4.0 license; please note that the schematics in (**d**) have been realigned for formatting reasons)

zinc ions. The material was self-healing, and the addition of zinc ions allowed the change from a viscoelastic to an elastic material.

Paracrystalline α-Helical Peptide Arrays A computational approach was applied to design a polar, layered three-dimensional protein crystal with space group P6 (Lanci et al. 2012). The computational design approach involved the creation of an
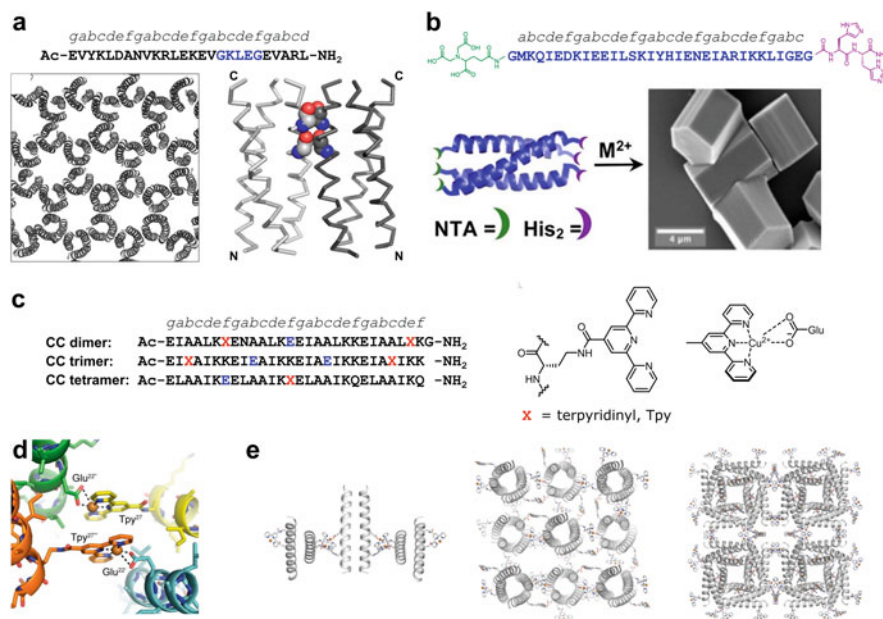
Fig. 3.10 Coiled-coil protein crystals. (**a**) Sequence and crystalline structure of the coiled-coil peptide P6-d. The key to the design is a GX_3G motif (highlighted in blue in the sequence) that enables close van der Waals contacts (Ac- acetyl). The dimer (right) shows the glycine residues of the GX_3G motifs of the two interacting coiled-coil trimers in close contact (**a**) produced from pdb 4DAC (Lanci et al. 2012) using PyMol). (**b**) NTA-His₂-tag modified coiled-coil trimer assembling into crystalline hexagonal prismatic morphologies (Figure reprinted with permission from Nepal et al. (2016). Copyright © 2016 American Chemical Society); (**c**) sequences of coiled-coil dimers to tetramers modified with Tpy amino acids to mediate self-assembly into highly ordered peptide arrays by Cu(II) coordination (left). The Tpy structure and mode of metal complexation (right). (**d**) Terpyridinyl-Cu(II)-Glu-linkage between coiled-coil dimers; (**e**) one-dimensional assembly of coiled-coil dimers induced by Cu(II) coordination via the terpyridinyl moieties and Glu side chains (left), two-dimensional coiled-coil array formation induced by metal coordination (middle), and three-dimensional metal-induced self-assembly of coiled-coil tetramers (right) (**d–g** reprinted with permission from Tavenor et al. (2017). Copyright © 2017 American Chemical Society)

ensemble of crystalline structures that possessed the target symmetry, the identification of designable peptide candidates within the created ensemble, and the experimental characterization of these peptides. A coiled-coil trimer (P6-d) was identified as a suitable subunit that was able to crystallize in the manner described above, forming a porous crystalline array that exhibited a honeycomb-like structure with hexagonal channels spanning the crystal (Fig. 3.10a). Key to the design was a GlyX₃Gly motif in which the glycine residues occupy the **b** and **f** positions of the third heptad of the four-heptad peptide, allowing van der Waals contact of adjacent coiled-coil trimers within the crystal (Fig. 3.10a).

Metal coordination has been used to generate paracrystalline peptide assemblies. One example included a coiled-coil homotrimer modified with metal-coordinating ligands, more specifically, with nitrolotriacetic acid (NTA) and two histidine

residues at the N- and C-termini, respectively (Nepal et al. 2016). This allowed metal-induced head-to-tail self-assembly of the coiled-coil peptides (Fig. 3.10b). Several transition metals were found to promote self-assembly into paracrystalline superstructures, for example, a hexagonal prismatic morphology was obtained in the presence of divalent zinc, cobalt, or copper ions. Nickel ions, on the other hand, promoted the formation of spherical morphologies. Another example of metal-induced formation of coiled-coil crystals involved side-chain modification of coiled-coil dimers to tetramers with terpyridine moieties that promoted copper(II)-induced self-assembly based on specific terpyridine-copper(II)-glutamic acid inter-actions (Fig. 3.10c–d) (Tavenor et al. 2017). Based on the coiled-coil oligomer state and the placement of the coordinating ligands, highly ordered one-dimensional coordination polymers, two-dimensional lattices, or three-dimensional arrays were obtained (Fig. 3.10e).

A highly interesting example of the formation of a paracrystalline α-helical material is Pro-Phe-Phe (Bera et al. 2019). This tripeptide, which was expected to form β-like assemblies, in fact self-assembled into a highly ordered assembly, in which it exhibited an α-helical secondary structure. The self-assembly was promoted by (1) electrostatic interactions between the uncapped termini and (2) aromatic interactions between the phenylalanine side chains. In this case, the phenylalanine residues were in an aromatic zipper arrangement.

3.7 Conclusions

In this Chapter, we have discussed the different materials that can be designed or constructed from α-helical peptides. The materials available from α-helical peptide building blocks are very versatile and range from fibers and nanotubes to cages and highly ordered arrays. Many of the designed materials have proven robust to modification and custom engineering and are therefore promising candidates for the development of biomimetic materials that can be used in electronics (Ing et al. 2018), tissue engineering (Faruqui et al. 2014; Mehrban et al. 2014; Mehrban et al. 2015), drug or biomaterial delivery (Noble et al. 2016; Beesley et al. 2018), or vaccine development (Pimentel et al. 2009; Morris et al. 2019; Majerle et al. 2021). A comprehensive review of progress in the use of coiled coils and coiled-coil materials in the development of drug delivery strategies was recently presented by Utterström et al. (2021). However, most applications of coiled-coil materials are still more or less proof of concepts and not real-world applications. This final obstacle could be overcome by the development of materials that are not only responsive to pH or metals but also to other environmental factors such as temperature, light, or enzymes, or the development of peptide hybrid materials that are easier to fabricate, e.g., by electrospinning or direct laser writing.

Although materials from α-helical peptide surfactants and α-helical peptide hairpins have also been presented, the majority of materials have been derived from α-helical coiled-coil building blocks. This is mainly due to the diversity of

accessible coiled coils and their ease of design, as the influences of the relationship between the amino-acid sequence and the resulting three-dimensional structure are well understood (Woolfson 2017). Coiled coils can highly reliably be designed as parallel or antiparallel homo- and heterodimers, heterotrimers, and heterotetramers, as well as α-helical coiled-coil barrels with five to nine helices and coiled-coil tapes based on Type III coiled-coil interfaces. This versatility is reflected in the materials obtained, in which the coiled coils either mark the material scaffold or are used as oligomerization domains, e.g., in engineering or protein cages. In addition, the coiled-coil scaffold can be modified at the termini and helical backbone to allow covalent cross-linking or fusion with other proteins. Coiled coils can largely be designed from scratch without computational support, making them an attractive building block for the construction of pure coiled-coil or coiled-coil hybrid materials. Moreover, the encodability of heterodimeric coiled-coil interactions enables the design of complex assemblies such as the coiled-coil protein origami nanostructures (Lapenta et al. 2018). An overview of the coiled-coil sequences and the materials that are derived thereof is given in Tables 3.1 and 3.2.

The predominant use of coiled-coils in α-helical peptide design emphasizes an unbalance in the field. The secondary structural motif α-helix is more than just the α-helical coiled coil and is found in many more protein folding motifs such as the α-helical peptide hairpin or the EF hand, a short calcium(II) binding helix-loop-helix motif (Gifford et al. 2007). However, design rules for these peptides are difficult to establish and often require computational methods. Easily applicable design rules for further α-helical protein folding motifs would expand the scope of shapes of α-helical peptide materials and, above all, also mean a higher diversity of α-helical functional materials.

Table 3.1 Overview of blunt-ended coiled coils used in the design of peptide materials

Blunt-ended coiled coils – de novo design

oligomer statev	orientationv	subunits	sequence gabcdef gabcdef gabcdef gabcdef gabcdef gabcd	materials
2	parallel	homomer	EIAALKx ENxALKx EIAxLKx EIAAxKx	pH-sensitive coiled coil-spider silk material, fibres driven by Cu(II) complexation via Tpy moieties
2	parallel	homomer	EIARLEQ EIARLEQ EIARLEY EIARLE	self-assembling virus-like particles (trifacial coiled coils)
2	parallel	heteromer	EIAALEx ENAALEx EIAALEx EIAALEx / KIAALKx KNAALKx KIAALKx KIAALKx	self-assembling cages (SAGEs, heterodimerization domain, x_2 = C), Zn(II)-responsive coiled-coil-star-PEG material (x_{1-3} = H)
2	parallel	heteromer	QLEK ELQALEK ENAQLEW ELQALEK ELAQ / QLKK KLQALKK KNAQLKW KLQALKK KLAQ	tetrahedral and octahedral protein cages (dimerization domain)
3	parallel	homomer	EIxAIKx EIxAIKx EIAxIKx EIAxIKx	self-assembling cages (SAGEs, trimerization domain), octahedral protein cage (trimerization domain)
4	parallel	homomer	ELAAIKx ELAAIKx ELAAIKx ELAAIKx	octahedral protein cages (oligomerization domain)
4	parallel	homomer	NILQ EVKNILK EVKNILW EVKNILQ EVK	self-assembling fibres (electrostatic interactions between termini)
5	parallel	homomer	KIEQ ILQKIEK ILQKIEx ILQKIEQ ILQ	self-assembling nanotubes (electrostatic interactions between termini), icosahedral protein cages (oligomerization domain)
6	parallel	homomer	LKAIAx ELKAIAx ELKAIAx ELKAIAx E	self-assembling nanotubes (electrostatic interactions between uncapped termini); covalent nanotubes (amide bond)
6	antiparallel	homomer	ELKAIAQ EFKAIAK EFKAIAF EFKAIAQ K	self-assembling fibres (electrostatic interactions between termini; blue: positively charged, red: negatively charged)
7	parallel	homomer	EIAQ ALKEIAK ALKEIAW ALKEIAQ ALK	self-assembling nanotubes (electrostatic interactions between termini; blue: positively charged, red: negatively charged)

Blunt-ended coiled coils – engineering of natural coiled coils

oligomer statev	orientationv	subunits	sequence gabcdef gabcdef gabcdef gabcdef gabcdef gabcd	materials
2	parallel	homomer	RMKQLED KVEELLC KNYHLEN EVARLKK LVGER	self-assembling fibres (thioether linkage via *f* postion)
3	parallel	homomer	GMKQIED KIEEILS KIYHIEN EIARIKK LIGEG	paracrystalline hexagonal prisms (head-to-tail metal complexation)

Table 3.2 Overview of staggered coiled-coil assemblies used in the design of peptide materials

Staggered coiled coils – de novo design

oligomer statev	orientationv	subunits	sequence							materials
			gabcdef	*gabcdef*	*gabcdef*	*gabcdef*	*gabcdef*	*gabcdef*	*ga*	
2	parallel	heteromer	KIAALKQ	KIASLKQ	EIDALEY	ENDALEQ				self-assembling fibres (SAFs, driven by sticky ends, charge interactions and N-N hydrogen bond; blue: – positively charged, red: negatively charged, yellow: hydrogen bond)
			KIRRLKQ	KNARLKQ	EIAALEY	EIAALEQ				
3	parallel	homomer	EIAQIEE	ECQAIEE	RIAQIEY	RIQAIEE	KCAQIKE	KIQAIK		self-assembling fibres (driven by sticky ends and charge interactions); dissembly of the fibres upon metal complexation via C residues (yellow); blue: positively charged, red: negatively charged
3	parallel	homomer	KLAALKQ	KLAALKK	ELAALEQ	ELAALEQ				self-assembling fibres (driven by sticky ends and charge interactions; blue: positively charged, red: negatively charged)
			KLAALKQ	KLAALKK	ELAALEQ	ELAALEQ				
			KLAALKQ	KLAALKK	ELAALEQ	ELAALEQ				
5	parallel	homomer	QLAR	ELQQLAK	ELQQLAK	ELQQLAK	EL			self-assembling fibre, tape-like assembly (driven by electrostatic interactions; blue: positively charged, red: negatively charged)
			QLAR	ELQQLAK	ELQQLAK	ELQQLAK	EL			
-	parallel	homomer	QA	RILEADA	EILRAYA	RILEAHE	EILRAIQ			tape-like self-assembling nanotubes; Form I
-	parallel	homomer	QA	KILEADA	EILKAYA	KILEAHE	EILKAIQ			tape-like self-assembling nanotubes; Form II

Staggered coiled coils – engineering of natural coiled coils

oligomer statev	orientationv	subunits	sequence							materials
			gabcdef	*gabcdef*	*gabcdef*	*gabcdef*	*gabcdef*	*gabcdef*	*ga*	
7	parallel	homomer	KIAQ	AVEKLAR	AVEKLAY	ANEKLAR	AVEKLAQ	AVE		self-assembling nanotubes (electrostatic interactions between termini; blue: positively charged, red: negatively charged)

References

Anzini P, Xu C, Hughes S, Magnotti E, Jiang T, Hemmingsen L, Demeler B, Conticello VP (2013) Controlling self-assembly of a peptide-based material via metal-ion induced registry shift. J Am Chem Soc 135:10278–10281

Aupič J, Strmšek Ž, Lapenta F, Pahovnik D, Pisanski T, Drobnak I, Ljubetič A, Jerala R (2021) Designed folding pathway of modular coiled-coil-based proteins. Nat Commun 12:1–12

Badieyan S, Sciore A, Eschweiler JD, Koldewey P, Cristie-David AS, Ruotolo BT, Bardwell JCA, Su M, Marsh ENG (2017) Symmetry-directed self-assembly of a tetrahedral protein cage mediated by de novo-designed coiled coils. Chembiochem 18:1888–1892

Banwell EF, Abelardo ES, Adams DJ, Birchall MA, Corrigan A, Donald AM, Kirkland M, Serpell LC, Butler MF, Woolfson DN (2009) Rational design and application of responsive α-helical peptide hydrogels. Nat Mater 8:596–600

Beesley JL, Baum HE, Hodgson LR, Verkade P, Banting GS, Woolfson DN (2018) Modifying self-assembled peptide cages to control internalization into mammalian cells. Nano Lett 18:5933–5937

Beesley JL, Woolfson DN (2019) The de novo design of α-helical peptides for supramolecular self-assembly. Curr Opin Biotechnol 58:175–182

Bella A, Shaw M, Ray S, Ryadnov MG (2014) Filming protein fibrillogenesis in real time. Sci Rep 4:1–6

Bera S, Mondal S, Xue B, Shimon LJW, Cao Y, Gazit E (2019) Rigid helical-like assemblies from a self-aggregating tripeptideNat Mater 18:503–509

Betz SF, DeGrado WF (1996) Controlling topology and native-like behavior of de novo-designed peptides: design and characterization of antiparallel four-stranded coiled coils. Biochemistry 35:6955–6962

Božič Abram S, Gradišar H, Aupič J, Round AR, Jerala R (2021) Triangular in vivo self-assembling coiled-coil protein origami. ACS Chem Biol 16:310–315

Bromley EHC, Sessions RB, Thomson AR, Woolfson DN (2009) Designed α-helical tectons for constructing multicomponent synthetic biological systems. J Am Chem Soc 131:928–930

Burgess NC, Sharp TH, Thomas F, Wood CW, Thomson AR, Zaccai NR, Brady RL, Serpell LC, Woolfson DN (2015) Modular design of self-assembling peptide-based nanotubes. J Am Chem Soc 137:10554–10562

Burton AJ, Thomas F, Agnew C, Hudson KL, Halford SE, Brady RL, Woolfson DN (2013) Accessibility, reactivity, and selectivity of side chains within a channel of de novo peptide assembly. J Am Chem Soc 135:12524–12527

Cannon KA, Park RU, Boyken SE, Nattermann U, Yi S, Baker D, King NP, Yeates TO (2020) Design and structure of two new protein cages illustrate successes and ongoing challenges in protein engineering. Protein Sci 29:919–929

Castelletto V, Seitsonen J, Ruokolainen J, Hamley IW (2021) Alpha helical surfactant-like peptides self-assemble into pH-dependent nanostructures. Soft Matter 17:3096–3104

Castelletto V, Seitsonen J, Ruokolainen J, Piras C, Cramer R, Edwards-Gayle CJC, Hamley IW (2020) Peptide nanotubes self-assembled from leucine-rich alpha helical surfactant-like peptides. Chem Commun 56:11977–11980

Cera L, Gonzalez GM, Liu Q, Choi S, Chantre CO, Lee J, Gabardi R, Choi MC, Shin K, Parker KK (2021) A bioinspired and hierarchically structured shape-memory material. Nat Mater 20:242–249

Conticello V, Hughes S, Modlin C (2017) Biomaterials made from coiled-coil peptides. In: Parry DAD, Squire JM (eds) Fibrous proteins: structures and mechanisms. Springer International Publishing, Cham, pp 575–600

Crick FHC (1953) The packing of alpha-helices - simple coiled-coils. Acta Crystallogr 6:689–697

Cristie-David AS, Chen J, Nowak DB, Bondy AL, Sun K, Park SI, Banaszak Holl MM, Su M, Marsh ENG (2019) Coiled-coil-mediated assembly of an icosahedral protein cage with extremely high thermal and chemical stability. J Am Chem Soc 141:9207–9216

Cristie-David AS, Koldewey P, Meinen BA, Bardwell JCA, Marsh ENG (2018) Elaborating a coiled-coil-assembled octahedral protein cage with additional protein domains. Protein Sci 27: 1893–1900

Dawson WM, Martin FJO, Rhys GG, Shelley KL, Brady RL, Woolfson DN (2021) Coiled coils 9-to-5: rational: de novo design of α-helical barrels with tunable oligomeric states. Chem Sci 12: 6923–6928

De Santis E, Castelletto V, Ryadnov MG (2015) Interfacial zippering-up of coiled-coil protein filaments. Phys Chem Chem Phys 17:31055–31060

De Santis E, Faruqui N, Noble JE, Ryadnov MG (2014) Exploitable length correlations in peptide nanofibres. Nanoscale 6:11425–11430

Djinović-Carugo K, Young P, Gautel M, Saraste M (1999) Structure of the α-actinin rod: molecular basis for cross-linking of actin filaments. Cell 98:537–546

Dong H, Paramonov SE, Hartgerink JD (2008) Self-assembly of α-helical coiled coil nanofibers. J Am Chem Soc 130:13691–13695

Egelman EH, Xu C, DiMaio F, Magnotti E, Modlin C, Yu X, Wright E, Baker D, Conticello VP (2015) Structural plasticity of helical nanotubes based on coiled-coil assemblies. Structure 23: 280–289

Faruqui N, Bella A, Ravi J, Ray S, Lamarre B, Ryadnov MG (2014) Differentially instructive extracellular protein micro-nets. J Am Chem Soc 136:7889–7898

Fletcher JM, Bartlett GJ, Boyle AL, Danon JJ, Rush LE, Lupas AN, Woolfson DN (2017) N@a and N@d: oligomer and partner specification by asparagine in coiled-coil interfaces. ACS Chem Biol 12:528–538

Fletcher JM, Boyle AL, Bruning M, Bartlett GJ, Vincent TL, Zaccai NR, Armstrong CT, Bromley EHC, Booth PJ, Brady RL, Thomson AR, Woolfson DN (2012) A basis set of de novo coiled-coil peptide oligomers for rational protein design and synthetic biology. ACS Synth Biol 1:240–250

Fletcher JM, Harniman RL, Barnes FRH, Boyle AL, Collins A, Mantell J, Sharp TH, Antognozzi M, Booth PJ, Linden N, Miles MJ, Sessions RB, Verkade P, Woolfson DN (2013) Self-assembling cages from coiled-coil peptide modules. Science 80(340):595–599

Fraser RDB, Macrae TP, Rogers GE (1962) Molecular organization in alpha-keratin. Nature 193: 1052–1055

Fu J, Guerette PA, Miserez A (2015) Self-assembly of recombinant hagfish thread keratins amenable to a strain-induced α-helix to β-sheet transition. Biomacromolecules 16:2327–2339

Galloway JM, Bray HEV, Shoemark DK, Hodgson LR, Coombs J, Mantell JM, Rose RS, Ross JF, Morris C, Harniman RL, Wood CW, Arthur C, Verkade P, Woolfson DN (2021) De novo designed peptide and protein hairpins self-assemble into sheets and nanoparticles. Small 17:1–11

Ghosh TS, Chaitanya SK, Sankararamakrishnan R (2009) End-to-end and end-to-middle interhelical interactions: new classes of interacting helix pairs in protein structures. Acta Crystallogr Sect D Biol Crystallogr 65:1032–1041

Gifford JL, Walsh MP, Vogel HJ (2007) Structures and metal-ion-binding properties of the $Ca2+-$ binding helix–loop–helix EF-hand motifs. Biochem J 405:199–221

Gradišar H, Božič S, Doles T, Vengust D, Hafner-Bratkovič I, Mertelj A, Webb B, Šali A, Klavžar S, Jerala R (2013) Design of a single-chain polypeptide tetrahedron assembled from coiled-coil segments. Nat Chem Biol 9:362–366

Groth MC, Rink WM, Meyer NF, Thomas F (2018) Kinetic studies on strand displacement in de novo designed parallel heterodimeric coiled coils. Chem Sci 9:4308–4316

Gunasekar SK, Asnani M, Limbad C, Haghpanah JS, Hom W, Barra H, Nanda S, Lu M, Montclare JK (2009) N-terminal aliphatic residues dictate the structure, stability, assembly, and small molecule binding of the coiled-coil region of cartilage oligomeric matrix protein. Biochemistry 48:8559–8567

Hadley EB, Testa OD, Woolfson DN, Gellman SH (2008) Preferred side-chain constellations at antiparallel coiled-coil interfaces. Proc Natl Acad Sci 105:530–535

Harbury P, Zhang T, Kim P, Alber T (1993) A switch between two-, three-, and four-stranded coiled coils in GCN4 leucine zipper mutants. Science 80(262):1401–1407

Hill LK, Meleties M, Katyal P, Xie X, Delgado-Fukushima E, Jihad T, Liu CF, O'Neill S, Tu RS, Renfrew PD, Bonneau R, Wadghiri YZ, Montclare JK (2019) Thermoresponsive protein-engineered coiled-coil hydrogel for sustained small molecule release. Biomacromolecules 20: 3340–3351

Hsia Y, Bale JB, Gonen S, Shi D, Sheffler W, Fong KK, Nattermann U, Xu C, Huang PS, Ravichandran R, Yi S, Davis TN, Gonen T, King NP, Baker D (2016) Design of a hyperstable 60-subunit protein icosahedron. Nature 535:136–139

Hughes SA, Wang F, Wang S, Kreutzberger MAB, Osinski T, Orlova A, Wall JS, Zuo X, Egelman EH, Conticello VP (2019) Ambidextrous helical nanotubes from self-assembly of designed helical hairpin motifs. Proc Natl Acad Sci 116:14456–14464

Hume J, Sun J, Jacquet R, Renfrew PD, Martin JA, Bonneau R, Gilchrist ML, Montclare JK (2014) Engineered coiled-coil protein microfibers. Biomacromolecules 15:3503–3510

Ing NL, Spencer RK, Luong SH, Nguyen HD, Hochbaum AI (2018) Electronic conductivity in biomimetic α-helical peptide nanofibers and gels. ACS Nano 12:2652–2661

Kim K, Kloxin CJ, Saven JG, Pochan DJ (2021) Nanofibers produced by electrospinning of Ultrarigid polymer rods made from designed peptide bundlemers. ACS Appl Mater Interfaces

Kojima S, Kuriki Y, Yoshida T, Yazaki K, Miura K (1997) Fibril formation by an amphipathic alpha-helix-forming polypeptide produced by gene engineering. Proc Jpn Acad Ser B 73:7–11

Lanci CJ, MacDermaid CM, Kang SG, Acharya R, North B, Yang X, Qiu XJ, DeGrado WF, Saven JG (2012) Computational design of a protein crystal. Proc Natl Acad Sci U S A 109:7304–7309

Laniado J, Cannon KA, Miller JE, Sawaya MR, McNamara DE, Yeates TO (2021) Geometric lessons and design strategies for nanoscale protein cages. ACS Nano 15:4277–4286

Lapenta F, Aupič J, Strmšek Ž, Jerala R (2018) Coiled coil protein origami: from modular design principles towards biotechnological applications. Chem Soc Rev 47:3530–3542

Lapenta F, Aupič J, Vezzoli M, Strmšek Ž, Da Vela S, Svergun DI, Carazo JM, Melero R, Jerala R (2021) Self-assembly and regulation of protein cages from pre-organised coiled-coil modules. Nat Commun 12:1–12

Lavigne P, Kay CM, Sönnichsen FD, Hodges RS, Lumb KJ, Kim PS (1996) Interhelical salt bridges, coiled-coil stability, and specificity of dimerization. Science 271:1136–1138

Lin Y, An B, Bagheri M, Wang Q, Harden JL, Kaplan DL (2017) Electrochemically directed assembly of designer coiled-coil telechelic proteins. ACS Biomater Sci Eng 3:3195–3206

Litowski JR, Hodges RS (2002) Designing heterodimeric two-stranded α-helical coiled-coils. J Biol Chem 277:37272–37279

Liu J, Zheng Q, Deng Y, Cheng C-S, Kallenbach NR, Lu M (2006) A seven-helix coiled coil. Proc Natl Acad Sci 103:15457–15462

Ljubetič A, Lapenta F, Gradišar H, Drobnak I, Aupič J, Strmšek Ž, Lainšček D, Hafner-Bratkovič I, Majerle A, Krivec N, Benčina M, Pisanski T, Veličković TĆ, Round A, Carazo JM, Melero R, Jerala R (2017) Design of coiled-coil protein-origami cages that self-assemble in vitro and in vivo. Nat Biotechnol 35:1094–1101

Lombardi A, Bryson JW, DeGrado WF (1996) De novo design of heterotrimeric coiled coils. Biopolymers 40:495–504

Lumb K, Kim P (1995) Measurement of interhelical electrostatic interactions in the GCN4 leucine zipper. Science 268:436–439

Lumb KJ, Kim PS (1996) Response: how much solar radiation do clouds absorb? Science 271: 1137–1138

Lupas AN, Bassler J, Dunin-Horkawicz S (2017) The structure and topology of $α$-helical coiled coils. In: Parry DAD, Squire JM (eds) Fibrous proteins: structures and mechanisms. Springer International Publishing, Cham, pp 95–129

Lupas AN, Gruber M (2005) The structure of α-helical coiled coils. Adv Protein Chem 70:37–38

Majerle A, Hadzi S, Aupič J, Satler T, Lapenta F, Strmšek Ž, Lah J, Loris R, Jerala R (2021) A nanobody toolbox targeting dimeric coiled-coil modules for functionalization of designed protein origami structures. Proc Natl Acad Sci U S A 118

McClain DL, Woods HL, Oakley MG (2001) Design and characterization of a heterodimeric coiled coil that forms exclusively with an antiparallel relative helix orientation. J Am Chem Soc 123: 3151–3152

Mehrban N, Abelardo E, Wasmuth A, Hudson KL, Mullen LM, Thomson AR, Birchall MA, Woolfson DN (2014) Assessing cellular response to functionalized α-helical peptide hydrogels. Adv Healthc Mater 3:1387–1391

Mehrban N, Zhu B, Tamagnini F, Young FI, Wasmuth A, Hudson KL, Thomson AR, Birchall MA, Randall AD, Song B, Woolfson DN (2015) Functionalized α-helical peptide hydrogels for neural tissue engineering. ACS Biomater Sci Eng 1:431–439

Meleties M, Katyal P, Lin B, Britton D, Montclare JK (2021) Self-assembly of stimuli-responsive coiled-coil fibrous hydrogels. Soft Matter (26)

Miyamoto T, Hayashi Y, Yoshida K, Watanabe H, Uchihashi T, Yonezawa K, Shimizu N, Kamikubo H, Hirota S (2019) Construction of a quadrangular tetramer and a cage-like hexamer from three-helix bundle-linked fusion proteins. ACS Synth Biol 8:1112–1120

Mondal S, Gazit E (2016) The self-assembly of helical peptide building blocks. ChemNanoMat 2: 323–332

Morris C, Glennie SJ, Lam HS, Baum HE, Kandage D, Williams NA, Morgan DJ, Woolfson DN, Davidson AD (2019) A modular vaccine platform combining self-assembled peptide cages and immunogenic peptides. Adv Funct Mater 29:1–12

Nautiyal S, Woolfson DN, King DS, Alber T (1995) A designed heterotrimeric coiled coil. Biochemistry 34:11645–11651

Negron C, Keating AE (2014) A set of computationally designed orthogonal antiparallel homodimers that expands the synthetic coiled-coil toolkit. J Am Chem Soc 136:16544–16556

Nepal M, Sheedlo MJ, Das C, Chmielewski J (2016) Accessing three-dimensional crystals with incorporated guests through metal-directed coiled-coil peptide assembly. J Am Chem Soc 138: 11051–11057

Noble JE, De Santis E, Ravi J, Lamarre B, Castelletto V, Mantell J, Ray S, Ryadnov MG (2016) A de novo virus-like topology for synthetic virions. J Am Chem Soc 138:12202–12210

Oakley MG, Hollenbeck JJ (2001) The design of antiparallel coiled coils. Curr Opin Struct Biol 11: 450–457

Oakley MG, Kim PS (1998) A buried polar interaction can direct the relative orientation of helices in a coiled coil. Biochemistry 37:12603–12610

Ogihara NL, Weiss MS, Degrado WF, Eisenberg D (1997) The crystal structure of the designed trimeric coiled coil coil-VaLd: implications for engineering crystals and supramolecular assemblies. Protein Sci 6:80–88

Oshaben KM, Horne WS (2014) Tuning assembly size in peptide-based supramolecular polymers by modulation of subunit association affinity. Biomacromolecules 15:1436–1442

Padilla JE, Colovos C, Yeates TO (2001) Nanohedra: using symmetry to design self assembling protein cages, layers, crystals, and filaments. Proc Natl Acad Sci U S A 98:2217–2221

Pandya MJ, Spooner GM, Sunde M, Thorpe JR, Rodger A, Woolfson DN (2000) Sticky-end assembly of a designed peptide fiber provides insight into protein fibrillogenesis. Biochemistry 39:8728–8734

Papapostolou D, Smith AM, Atkins EDT, Oliver SJ, Ryadnov MG, Serpell LC, Woolfson DN (2007) Engineering nanoscale order into a designed protein fiber. Proc Natl Acad Sci U S A 104: 10853–10858

Park WM (2020) Coiled-coils: the molecular zippers that self-assemble protein nanostructures. Int J Mol Sci 21

Park WM, Bedewy M, Berggren KK, Keating AE (2017) Modular assembly of a protein nanotriangle using orthogonally interacting coiled coils. Sci Rep 7:1–10

Peters JW, Stowell MHB, Rees DC (1996) A leucine-rich repeat variant with a novel repetitive protein structural motif. Nat Struct Biol 3:991–994

Pimentel TAPF, Yan Z, Jeffers SA, Holmes KV, Hodges RS, Burkhard P (2009) Peptide nanoparticles as novel immunogens: design and analysis of a prototypic severe acute respiratory syndrome vaccine. Chem Biol Drug Des 73:53–61

Potekhin SA, Melnik TN, Popov V, Lanina NF, Vazina AA, Rigler P, Verdini AS, Corradin G, Kajava AV (2001) De novo design of fibrils made of short α-helical coiled coil peptides. Chem Biol 8:1025–1032

Root BC, Pellegrino LD, Crawford ED, Kokona B, Fairman R (2009) Design of a heterotetrameric coiled coil. Protein Sci 18:329–336

Ryadnov MG, Woolfson DN (2003) Engineering the morphology of a self-assembling protein fibre. Nat Mater 2:329–332

Sasaki E, Böhringer D, Van De Waterbeemd M, Leibundgut M, Zschoche R, Heck AJR, Ban N, Hilvert D (2017) Structure and assembly of scalable porous protein cages. Nat Commun 8:1–10

Schnarr NA, Kennan AJ (2004) Strand orientation by steric matching: a designed antiparallel coiled-coil trimer. J Am Chem Soc 126:14447–14451

Sciore A, Su M, Koldewey P, Eschweiler JD, Diffley KA, Linhares BM, Ruotolo BT, Bardwell JCA, Skiniotis G, Marsh ENG (2016) Flexible, symmetry-directed approach to assembling protein cages. Proc Natl Acad Sci U S A 113:8681–8686

Sharp TH, Bruning M, Mantell J, Sessions RB, Thomson AR, Zaccai NR, Brady RL, Verkade P, Woolfson DN (2012) Cryo-transmission electron microscopy structure of a gigadalton peptide fiber of de novo design. Proc Natl Acad Sci U S A 109:13266–13271

Sinha NJ, Langenstein MG, Pochan DJ, Kloxin CJ, Saven JG (2021) Peptide design and self-assembly into targeted nanostructure and functional materials. Chem Rev 121:13915–13935

Spencer RK, Hochbaum AI (2016) X-ray crystallographic structure and solution behavior of an antiparallel coiled-coil hexamer formed by de novo peptides. Biochemistry 55:3214–3223

Spencer RK, Hochbaum AI (2017) The Phe-Ile zipper: a specific interaction motif drives antiparallel coiled-coil hexamer formation. Biochemistry 56:5300–5308

Staples JK, Oshaben KM, Horne WS (2012) A modular synthetic platform for the construction of protein-based supramolecular polymers via coiled-coil self-assembly. Chem Sci 3:3387–3392

Steinkruger JD, Bartlett GJ, Hadley EB, Fay L, Woolfson DN, Gellman SH (2012) The d′-- d -- d′ vertical triad is less discriminating than the a′-- a -- a′ vertical triad in the antiparallel coiled-coil dimer motif. J Am Chem Soc 134:2626–2633

Sutherland TD, Young JH, Weisman S, Hayashi CY, Merritt DJ (2010) Insect silk: one name, many materials. Annu Rev Entomol 55:171–188

Tavenor NA, Murnin MJ, Horne WS (2017) Supramolecular metal-coordination polymers, nets, and frameworks from synthetic coiled-coil peptides. J Am Chem Soc 139:2212–2215

Tayeb-Fligelman E, Tabachnikov O, Moshe A, Goldshmidt-Tran O, Sawaya MR, Coquelle N, Colletier J-P, Landau M (2017) The cytotoxic Staphylococcus aureus PSMα3 reveals a cross-α amyloid-like fibril. Science 355:831–833

Testa OD, Moutevelis E, Woolfson DN (2009) CC+: a relational database of coiled-coil structures. Nucleic Acids Res 37:D315–D322

Thomas F, Boyle AL, Burton AJ, Woolfson DN (2013) A set of de novo designed parallel heterodimeric coiled coils with quantified dissociation constants in the micromolar to sub-nanomolar regime. J Am Chem Soc 135:5161–5166

Thomas F, Burgess NC, Thomson AR, Woolfson DN (2016) Controlling the assembly of coiled-coil peptide nanotubes. Angew Chem Int Ed Engl 55:987–991

Thomas F, Dawson WM, Lang EJM, Burton AJ, Bartlett GJ, Rhys GG, Mulholland AJ, Woolfson DN (2018) De novo -designed α-helical barrels as receptors for small molecules. ACS Synth Biol 7:1808–1816

Thomas F, Niitsu A, Oregioni A, Bartlett GJ, Woolfson DN (2017) Conformational dynamics of asparagine at coiled-coil interfaces. Biochemistry 56:6544–6554

Thomson AR, Wood CW, Burton AJ, Bartlett GJ, Sessions RB, Brady RL, Woolfson DN (2014) Computational design of water-soluble α-helical barrels. Science 346:485–488

Tunn I, Harrington MJ, Blank KG (2019) Bioinspired histidine-Zn2+ coordination for tuning the mechanical properties of self-healing coiled coil cross-linked hydrogels. Biomimetics 4:25

Urvoas A, Guellouz A, Valerio-Lepiniec M, Graille M, Durand D, Desravines DC, van Tilbeurgh H, Desmadril M, Minard P (2010) Design, production and molecular structure of a new family of artificial alpha-helicoidal repeat proteins (αRep) based on thermostable HEAT-like repeats. J Mol Biol 404:307–327

Utterström J, Naeimipour S, Selegård R, Aili D (2021) Coiled coil-based therapeutics and drug delivery systems. Adv Drug Deliv Rev 170:26–43

Walshaw J, Woolfson DN (2003) Extended knobs-into-holes packing in classical and complex coiled-coil assemblies. J Struct Biol 144:349–361

Wang F, Gnewou O, Modlin C, Beltran LC, Xu C, Su Z, Juneja P, Grigoryan G, Egelman EH, Conticello VP (2021) Structural analysis of cross α-helical nanotubes provides insight into the designability of filamentous peptide nanomaterials. Nat Commun 12:407

Wood CW, Bruning M, Ibarra AA, Bartlett GJ, Thomson AR, Sessions RB, Brady RL, Woolfson DN (2014) CCBuilder: an interactive web-based tool for building, designing and assessing coiled-coil protein assemblies. Bioinformatics 30:3029–3035

Woolfson DN (2017) Coiled-coil design: updated and upgraded. Subcell Biochem 82:35–61

Woolfson DN, Bartlett GJ, Bruning M, Thomson AR (2012) New currency for old rope: from coiled-coil assemblies to α-helical barrels. Curr Opin Struct Biol 22:432–441

Wu D, Sinha N, Lee J, Sutherland BP, Halaszynski NI, Tian Y, Caplan J, Zhang HV, Saven JG, Kloxin CJ, Pochan DJ (2019) Polymers with controlled assembly and rigidity made with click-functional peptide bundles. Nature 574:658–662

Xu C, Liu R, Mehta AK, Guerrero-Ferreira RC, Wright ER, Dunin-Horkawicz S, Morris K, Serpell LC, Zuo X, Wall JS, Conticello VP (2013) Rational design of helical nanotubes from self-assembly of coiled-coil lock washers. J Am Chem Soc 135:15565–15578

Zaccai NR, Chi B, Thomson AR, Boyle AL, Bartlett GJ, Bruning M, Linden N, Sessions RB, Booth PJ, Brady RL, Woolfson DN (2011) A de novo peptide hexamer with a mutable channel. Nat Chem Biol 7:935–941

Zimenkov Y, Dublin SN, Ni R, Tu RS, Breedveld V, Apkarian RP, Conticello VP (2006) Rational design of a reversible pH-responsive switch for peptide self-assembly. J Am Chem Soc 128:6770–6771

Chapter 4
Ultra-Short Peptide Nanomaterials

Demetra Giuri, Paolo Ravarino, and Claudia Tomasini

Abstract In the analysis of the materials formed by short peptides, we need to define what we mean by short, as the determination of "short peptide" has not been given so far (Apostolopoulos et al. Molecules 2021, 26, 1–45). In the literature, we can find contradictory information, with fewer than 30 or 100 residues. On the other hand, ultra-short peptides were precisely defined as peptides consisting of up to seven amino acids (Hauser et al. Proc Natl Acad Sci U S A. 2011, 108, 1361–1366; Seow and Hauser. Mater Today 2014, 17, 381–388; Makovitzki et al. Proc Natl Acad Sci USA 2006, 103, 15997–16002).

4.1 Introduction

4.1.1 Definition of Ultra-Short Peptide

In the analysis of the materials formed by short peptides, we need to define what we mean by short, as the determination of "short peptide" has not been given so far (Apostolopoulos et al. 2021). In the literature, we can find contradictory information, with fewer than 30 or 100 residues. On the other hand, ultra-short peptides were precisely defined as peptides consisting of up to seven amino acids (Hauser et al. 2011; Seow and Hauser 2014; Makovitzki et al. 2006).

Ultra-short peptides are ideally suited for the formation of nanomaterials because naturally occurring amino acids hold a wide range of distinct physical properties (Jayawarna et al. 2006). This diversity allows for rational incorporation of noncovalent interactions including electrostatic (acidic and basic amino acids), hydrophobic, π-stacking (aromatic amino acids), hydrogen bonding (polar amino

D. Giuri · P. Ravarino · C. Tomasini (✉)
Dipartimento di Chimica Giacomo Ciamician, Università Di Bologna, Bologna, Italy
e-mail: claudia.tomasini@unibo.it

acids), as well as steric contributions. While individually these interactions are quite weak, collectively they can give rise to very stable structures. Nevertheless, each of these interactions depend in different ways on environmental conditions such as ionic strength, pH, and temperature. Thus, it is crucial to find the trigger that is more suitable to initiate the process of self-assembly leading to the formation of a strong nanomaterial.

In this chapter, we will present different materials that may be obtained by self-aggregation of ultra-short peptides, both in the protected and in the unprotected form. This includes also materials obtained by self-aggregation of single amino acids.

4.1.2 A Brief History of Short and Ultra-Short Peptide Nanomaterials

Zhang and colleagues serendipitously discovered several self-assembling peptide sequences about 30 years ago (Zhang et al. 1993), as they found out that a 16-residue peptide was water soluble, with a characteristic β-sheet circular dichroism spectrum, but, upon the addition of salt, the peptide spontaneously assembled to form a macroscopic membrane that does not dissolve in heat or in acidic or alkaline solutions, nor upon addition of a variety of proteolytic enzymes. The analysis of the membrane by scanning EM revealed a network of interwoven fragments of 10–20 nm in diameter.

At the beginning of the twenty-first century, General and Antonietti demonstrated that the simple complexation of a model oligopeptide with appropriate surfactants leads to species soluble in organic solvents (General and Antonietti 2002). These molecules, by a combination of polarity effects, packing, and the formation of hydrogen-bonding bridges, further aggregate to complicated, but well-defined super-structures and lyotropic phases (Fig. 4.1).

In the same period, Ghadiri et al. presented an open-ended hollow tubular structure based on hydrogen-bond-directed self-assembly of a chimeric cyclic peptide subunit comprised of alternating α- and a novel 1,4-disubstituted-1,2,3-triazole ε-amino acid that acts as peptide backbone surrogate (Horne et al. 2003). The cyclic peptide self-assembly has been studied in solution by ^{1}H NMR and mass spectrometry, and the resulting tubular ensemble is characterized in the solid state by X-ray crystallography (Fig. 4.2).

Since then, this research field flourished, and a *plethora* of new self-aggregating ultra-short peptides have been reported by several research groups, with the aim of producing smart nanomaterials obtained by self-organisation of very small molecules (Yanlian et al. 2009). Their idea was to follow the forecast of the Nobel laureate physicist Richard Feynman, who gave the lecture titled "There's plenty of room at the bottom" for the American Physical Society annual banquet in 1959 in Pasadena. During the lecture, he said: "What I wanted to talk about is the problem of
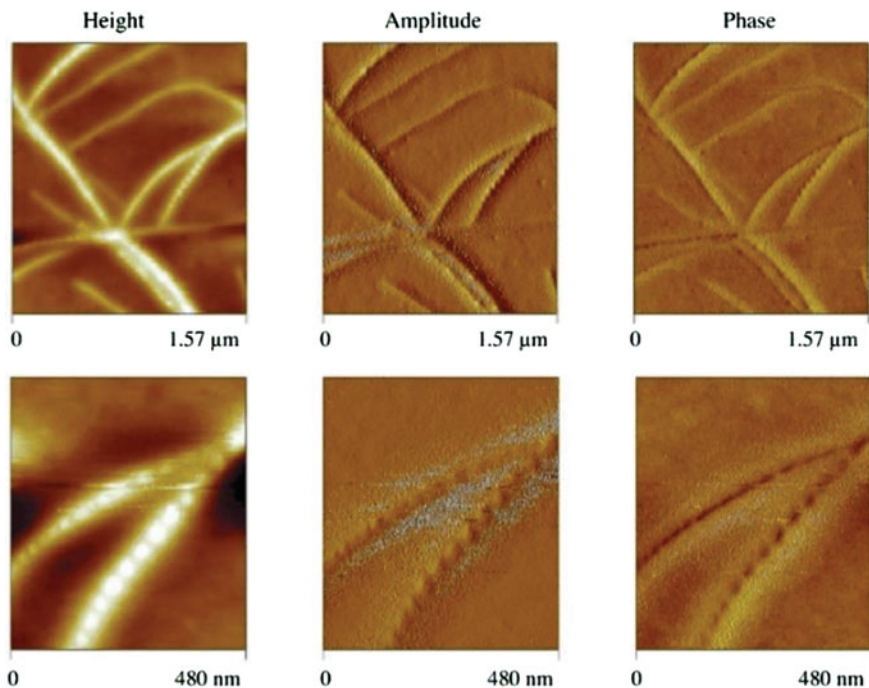
Fig. 4.1 Tapping-AFM pictures of the GSSG–lecithin complex, different views of two selected areas; the aggregates are left-handed spirals. Image from (General and Antonietti 2002)
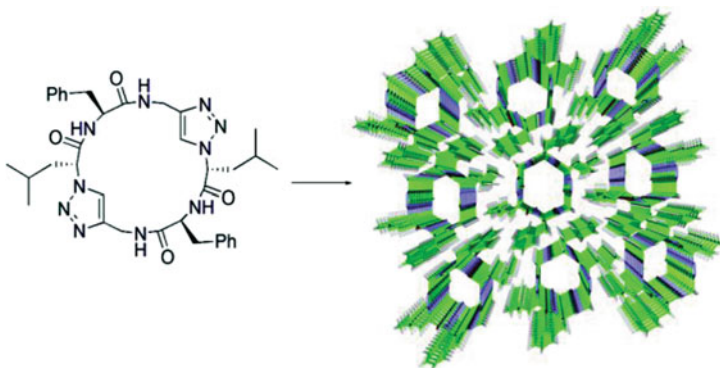
Fig. 4.2 Chemical and X-rays structure of the cyclic peptide self-assembly synthesized by Ghadiri. Image adapted from (Horne et al. 2003)

manipulating and controlling things on a small scale. In the year 2000, when they look back at this age, they would wonder why it was not until the year 1960 that anybody began seriously to move in this direction." (Feynman 1959).
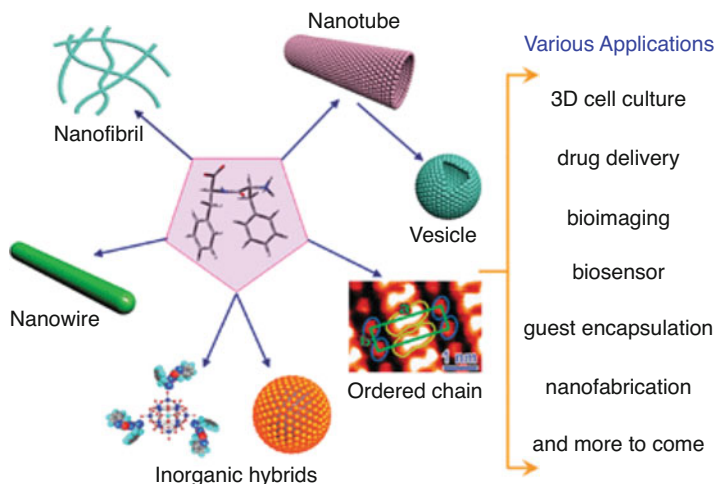
Fig. 4.3 Schematic representation of various nanostructures formed by self-assembly of Phe-Phe-based building blocks and their potential applications. Image adapted from (Yan et al. 2010)

A very successful example is all the work done on the study of self-assembly of the dipeptide Phe-Phe (Yan et al. 2010). The use of this small dipeptide has been suggested by the pathogenic process that is triggered by Alzheimer's disease. Indeed Phe-Phe is extracted from Alzheimer's β-amyloid polypeptide as the core recognition motif for molecular self-assembly (Reches and Gazit 2003). Since the emergence of Phe-Phe as a self-assembling building block, many studies have been made to organize the Phe-Phe-based building blocks into various functional nanostructures such as nanotubes, spherical vesicles, nanofibrils, nanowires, and ordered molecular chains (Fig. 4.3). We will describe some of those studies later in this chapter.

4.1.3 General Mechanism of Self-Aggregation

Molecular self-assembly is a process of formation of ordered structures under thermodynamic and kinetic conditions that occurs spontaneously as a consequence of local interactions of the molecules (Lehn 2009; Whitesides and Grzybowski 2002). We can list two different kinds of self-assembly: the static and the dynamic one. Static self-assembly involves systems that are at equilibrium and do not dissipate energy: molecular crystals are a good example of aggregation formed by static self-assembly. In dynamic self-assembly, the interactions responsible for the formation of the supramolecular structures only occur if the system is dissipating energy (Fig. 4.4).

With inspiration from biology, a wide range of nanomaterials have been constructed via dynamic self-assembly (Sanchez et al. 2005; Aizenberg and Fratzl 2009). This process relies on a combination of noncovalent interactions, including
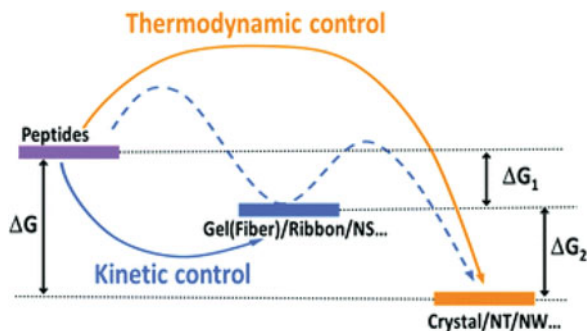
hydrogen bonds, electro–static interactions, π–π stacking, hydrophobic forces, non-specific Van der Waals forces, and chiral dipole–dipole interactions.

Although all noncovalent interactions are relatively weak, they can govern the self-assembly of molecular building blocks into superior and ordered structures, when they are combined as a whole. As the individual forces are of a similar magnitude compared to thermal forces, a small variation of parameters enables variations of structures, thus affecting the material properties. A wide range of self-assembled nanomaterials may be obtained by self-assembly of ultra-short peptides, such as nanoparticles, fibres, nanotubes, gels, and adhesives. As they are composed by self-assembled building blocks through noncovalent interactions, their formation is reversible and have excellent responsiveness to different stimuli, such as pH, light, enzyme, ions, temperature, ultrasound, and mechanical strength.

In this chapter, we will show an overview of some nanomaterials that may be readily obtained by dynamic self-aggregation of ultra-short peptides, mentioning also some applications.

4.2 Nanotubes

Nanotubes (NTs) are hollow tube-like structures with nanometre dimensions. The unique properties of these tubular architectures derive not only from the chemical composition and functional groups of the starting units but also from the geometry of the tube (diameter, length, wall type, chirality) that ensures a confined space and selectivity based on the compartment size. These features make nanotubes suitable structures for a variety of applications in chemistry, biochemistry, and materials science, being useful to mimic biological channels and porous structures, fabricate new catalysts, or design novel optical, electronic, and energy storage devices.

The possibility to achieve such architectures using peptides was first conjectured by Lipnick et al. (Lipnick and Garbisch 1973) and then tentatively assigned by Tomasic's group (Tomasic and Lorenzi 1987). Then, Ghadiri et al. reported in their pioneering work the rational design of an eight-residue cyclic polypeptide, *cyclo*[−(D-Ala-Gln-D-Ala-Glu)₂], alternating D- and L-amino acids (Reza Ghadiri et al.
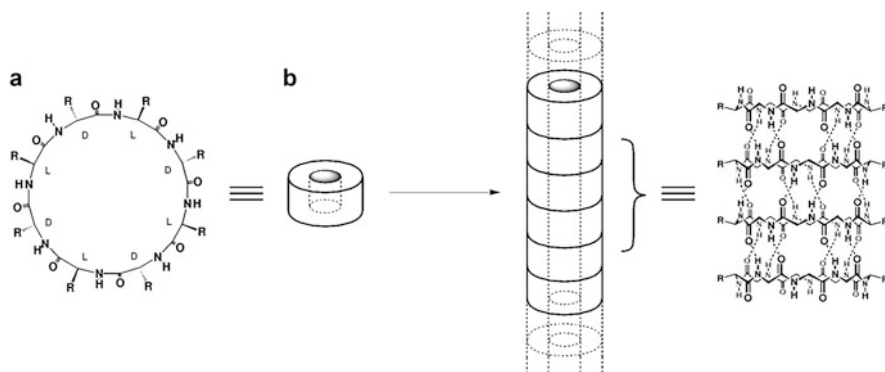
Fig. 4.5 (**a**) Two-dimensional representation of the chemical structure of the cyclic peptide subunit, with indication of the amino acid chirality (D or L). (**b**) Peptide subunits shown in a self-assembled tubular configuration emphasizing the antiparallel stacking and the intermolecular hydrogen-bonding interactions. Image adapted from (Bong et al. 2001)

1994). The resulting tubular structures were hundreds of nanometres long, with internal diameters of 7–8 Å. They demonstrated with a number of techniques (electron microscopy, electron diffraction, Fourier-transform infrared spectroscopy, and molecular modelling) that the formation of peptide nanotubes (PNTs) derived from the flat ring conformation adopted by antiparallel stacks of subunits, stabilized by intermolecular hydrogen bonds between the amide functionalities (Fig. 4.5). These results also inspired the investigation on the structural features and the electronic properties of the tubular self-assembly, through DFT-based calculations (Carloni et al. 1997), and opened the way for the following works in the field.

The same group demonstrated the possibility to rigorously control the dimension of the PNT, such as the inner diameter, by simply changing the size of the peptide ring (Khazanovich et al. 1994). For example, the dodecapeptide cyclo[−(L-Gln-D-Ala-L-Glu-D-Ala)$_n$] ($n = 3$), the analogue of the previously described compound, which had n = 2, can assemble in nanotubes with uniform diameter of 13 Å.

Cyclic D,L-α-peptides with 6 and 8 residues were used as selective antibacterial agents, acting preferentially on Gram-positive or Gram-negative bacteria compared to mammalian cells (Fernandez-Lopez et al. 2001).

The same cyclic peptide was further modified, introducing 1,4-disubstituted-1,2,3-triazole ε-amino acids in the backbone (Horne et al. 2003), resulting in a heterocyclic peptide ring. In this way, they produced a modification in the physical properties of the nanotube interior, compared to the previously reported peptide, that assembles into solvent-filled nanotubes.

Other peptides with nanotubular assembly were reported by Zhang and collaborators, which exploited surfactant-like peptides with 7–8 residues. The formation of the tubular structures can be easily followed through dynamic light scattering (DLS) experiments. These peptides usually bear a hydrophilic head, composed of aspartic acid, and a lipophilic tail made of hydrophobic amino acids (such as valine, alanine,

and leucine) (Vauthey et al. 2002). Similarly to what happens in lipids and fatty acids, when dissolved in water, the negatively charged carboxylic acids tend to self-assemble forming a polar interface that isolates the lipophilic tail from contact with water. This type of structures can be further modified adding functionalities that allow, for example, to bind the self-assembled tubes on different substrates, including inorganic surfaces (Zhang et al. 2002; Scott et al. 2016; Bai et al. 2014; Moreira et al. 2016). The wide variety of functions offered by naturally occurring amino acids can be also extended introducing non-natural residues, thus resulting in an increased design flexibility depending on the final application.

A much simpler and shorter peptide, Phe-Phe, was serendipitously found to be able to assemble into nanotubes by Gazit and Reches (Reches and Gazit 2003) while studying the formation of amyloid fibrils associated to Alzheimer's disease. This assembly is probably due to the aromatic moieties of the dipeptide and shares to some extent morphological similarities with the surfactant-like compounds previously described. These PNTs have several advantages: biocompatible, water-soluble, inexpensive, and easy to manufacture, form under mild conditions (dissolution in 1,1,1,3,3,3-hexafluoro-2-propanol, HFP), can assemble very efficiently (<1% of amorphous aggregates), and have thermal and chemical stability.

The diphenylalanine motif can also act as a mould for the formation of silver nanowires in the inner part of the peptide hollow tube. Then, it can be removed by proteolysis, thus leaving free individual silver nanowires (Reches and Gazit 2003).

The same architecture can be employed where enzymatically stable nanotubes are desired, like in the fabrication of biosensors (Reches and Gazit 2003). For this purpose, D-Phe-D-Phe is prepared replacing L amino acids with the D analogues. It forms enantiomeric nanotubes with the same morphology but completely insensitive to incubation in proteinase K.

March et al. used Monte Carlo simulations to predict the nanotubes self-assembly (Song et al. 2004), and they predicted that it is possible to obtain porous lamellar layers, just changing the peptide concentration. This way, they were able to grow Pt nanoparticles on the walls of the nanotubes exploiting their porosity and opened the way for the formation of novel nanocomposites, such as Pt catalysts and Au nanoparticles (Maity et al. 2014; Ramasamy et al. 2009), where peptide nanotubes served as templates.

Gazit et al. expanded the study on diphenylalanine-based nanostructures and found a method to determine the mechanical properties of peptide nanotubes based on indentation experiments performed with the tip of an Atomic Force Microscope (AFM) (Kol et al. 2005). They calculated the nanotubes stiffness, which has an average value of around 160 N/m, not affected by the diameter dimension, and an estimated Young's modulus of about 19 GPa, much higher than other biological nanostructures.

Another amazing result from this group was the successful formation under mild conditions of aligned nanoforests (a dense array of nanotube assemblies) with controlled vertical or horizontal patterns (Fig. 4.6) (Reches and Gazit 2006). From the SEM images, it appeared clearly the multiwalled nature of the nanotubes for the difference between inner and outer diameters.
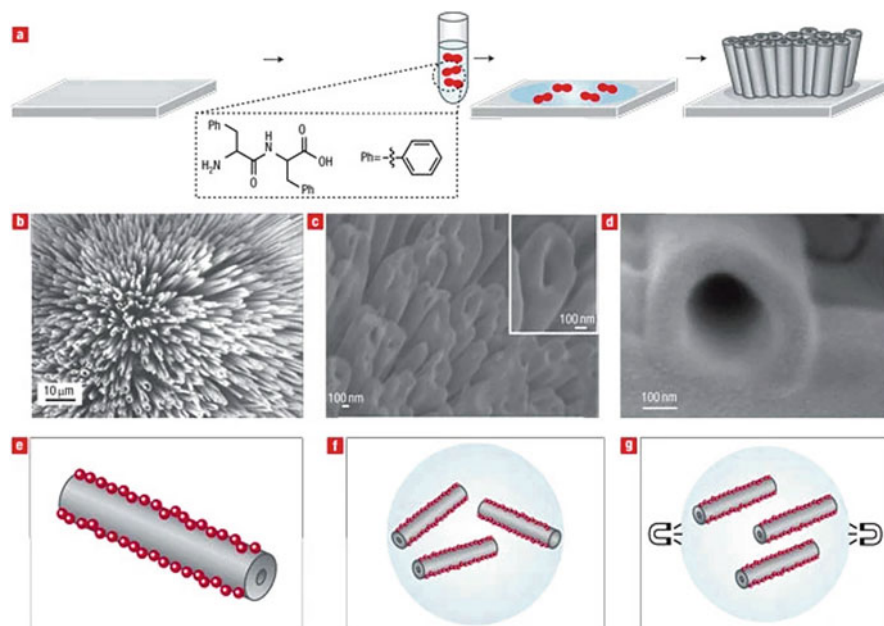
Fig. 4.6 (**a**) A possible model for the formation of the aligned peptide nanotubes array. (**b**) SEM analysis of the vertically aligned peptide nanotubes. (**c, d**) Cold field-emission gun high-resolution scanning electron microscope (CFEG-HRSEM) analysis of the nanotubes array. (**e**) Schematic representation of the self-assembly process of the peptide nanotubes in the presence of magnetic nanoparticles before (**f**) and after (**g**) the application of the magnetic field. Image adapted from (Reches and Gazit 2006)

To understand the principles leading to this molecular assembly, the behaviour of several Phe-Phe analogues with different electrostatic charges was studied. This way, the authors demonstrated the importance of repulsive electrostatic interactions in the stabilisation of ordered self-assembled nanostructures. To achieve a horizontal alignment of the tubes, the dipeptide was assembled in presence of magnetic nanoparticles that adhered on the walls of the tubes through hydrophobic interactions. The nanotubes covered with nanoparticles adopted random orientations on the surface, but rapidly aligned with high yield when the magnetic field was applied, responding to its direction (Fig. 4.6).

These results represent a milestone in the preparation of PNTs, as well-defined and aligned nanostructures with exceptional chemical and thermal stability were obtained, using mild conditions and a simple biocompatible building block (Zhang 2006; Adler-Abramovich et al. 2006; Bera et al. 2019). Several studies demonstrated that the surface that directs the assembly and the concentration of the dipeptide both play a key role in the formation of nanotubes and that dilutions can lead to spontaneous formation of vesicles (Yan et al. 2007; Yan et al. 2008; Huang et al. 2011). Moreover, the solvent modification can lead to the self-assembly of these
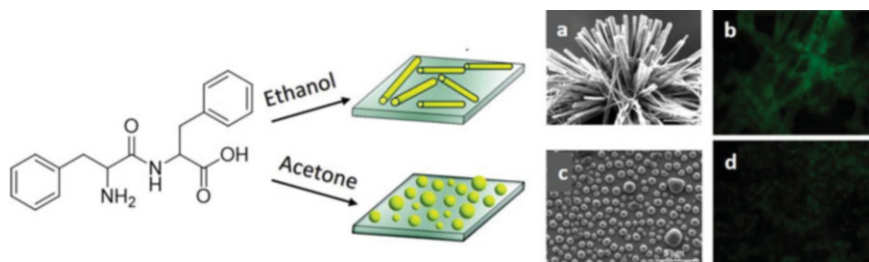
Fig. 4.7 (Left) Phe-Phe dipeptide assembling in tubes or vesicles depending on the solvent used. (Right) SEM image of the nanotubes (**a**) and vesicles (**c**) formed. Fluorescence microscopy images of BSA-FITC-adsorbed PPX-coated dipeptide tubes (**b**) and vesicles (**d**). Adapted from (Demirel et al. 2010)

peptides in different tubular or vesicular structures (Fig. 4.7). The differences in this case can be attributed to the different dielectric constants of the solvent (Demirel et al. 2010) that should be also taken into account in the formation of supramolecular structures. The structural stability of tubes and vesicles can be improved with protective coatings, as suggested by Demirel et al., that used poly-(chloro-*p*-xylylene) (PPX) and achieve proteolytic stability of their peptide assembly. The thickness of the PPX coating also allows to control protein adsorption onto the biomaterial surface, expanding the application of both tubes and vesicles in drug or gene delivery and tissue engineering.

PNTs self-assembling can be controlled varying the preparation conditions. The mechanism of formation of the nanostructures can be highly influenced with the nature of the additive, such as electroluminescent species (Ribeiro et al. 2019), resulting in the formation of different nanostructures. The tubes can also be externally functionalized, for example, with electron donor/acceptors (Tu et al. 2011), polymers or small molecules (Matsumura et al. 2005), and integration of reduced graphene oxide decorated by nickel nanoparticles (Ivanov et al. 2018).

In addition, a new class of *cis*-3-aminocyclo hexanecarboxylic acid (γ-Ach) residues alternated with D-α-amino acids was proposed, with the resulting nanotubes having hydrophobic cavities, able to act as channels that conduce alkaline cations (Amorín et al. 2003; Amorín et al. 2005; García-Fandiño et al. 2012). Cyclic peptides have also been functionalised or coated with polymers that can influence the solubility and aggregation of the nanotubes. Among the examples, polymer-conjugated PNTs able to respond to a pH switch were prepared, as well as multi-shell nanotubes and thin films with subnanometer aligned channels (Chapman et al. 2013a; Chapman et al. 2013b; Xu et al. 2011).

From the three main classes of peptide nanotubes presented here (cyclic peptides, surfactant-like and dipeptides), several works described the possible chemical modifications, decoration, and applications of these versatile nanomaterials, in the following years and until now (Hamley 2021; Du et al. 2021; Tarvirdipour et al. 2020; Zou et al. 2020).

4.3   Hydrogels

Hydrogels are materials consisting primarily of water, although they have solid-like properties (Adams 2011; Smith 2010), due to the presence of a fibre network which immobilises the liquid phase. Traditionally, this network is prepared by the cross-linking of polymer chains (Peppas et al. 2000), as the cross-linked poly (hydroxyethyl methacrylate), that was originally used for contact lenses. Alternatively, to improve biodegradability, hydrogels have been prepared using a biopolymer matrix. For example, some polysaccharides dissolve in water at high temperature and form a gel on cooling (Peppas et al. 2000).

Aggregation and disaggregation are central phenomena in nature. In this context, the formation of fibres through self-assembly is of particular interest, as common building principles are found in both living and non-living systems (Binder and Smrzka 2006). Many organic motifs such as steroids (Svobodová et al. 2012; Knudtson and Dias 2019), peptides (Adams and Topham 2010), ureas (Yamanaka 2013), amides (Estroff and Hamilton 2004), sugars (Morris et al. 2021; Davidovich-Pinhas 2019), dendrimers (Sapra et al. 2019; Ge et al. 2021), and π-conjugated molecules (Rao and Sun 2013; Zhang et al. 2017; Cao et al. 2018) have been designed and developed as gelators. Among them, Zhang pioneered the use of peptides with alternating hydrophobic and charged amino acids (Zhang 2003).

Most of these molecules need to be synthesized by tedious procedures, while ultra-short peptides are readily available molecules that may be obtained in large scale. These molecules are called low molecular weight gelators (LMWG) (Raeburn et al. 2015; Chivers and Smith 2019), as they have a molecular weight < 1000 Da and self-assembles in water to form long, fibrous structures (Binder and Smrzka 2006). The self-aggregation of small gelator molecules leads to the formation of entangled Self-Assembled Fibrillar Networks (SAFINs) through a combination of noncovalent interactions like H-bonding, π–π stacking, donor–acceptor interactions, metal coordination, solvophobic forces (hydrophobic forces for gels in water), and van der Waals interactions (Sangeetha and Maitra 2005; Angelici et al. 2008; Shin et al. 2012; Frederix et al. 2015). These fibres form a three-dimensional network that immobilises the water, thus behaving as a supramolecular cross-linked polymer in the hydrogel formation (Draper and Adams 2017). Since these networks involve weak interactions, the gel-to-sol transition is facile (and usually rapid) as compared to polymeric gelators, so they can be readily transformed to a fluid (sol) by heating and are generally thermally reversible.

The mechanical properties of a gel are usually studied with a rheometer, which is an apparatus with a mechanical arm, named shaft, consisting in a rod attached either to a round plate, a cone, or four tiny vanes. As it comes in contact with the gel, it starts rotating to probe the resistance opposed by the gel network. This resistance is expressed in terms of G', which represents the storage modulus, namely the "solid behaviour," and G", which represents the loss modulus or "liquid behaviour" of the gel, both measured in Pa. The rheological analysis allows the determination of a large amount of information, including the time required for the gel to form, the

stiffness of the gel network, its breaking point, and whether the gel is thixotropic or not, i.e. if the gel is able to recover after breaking.

Supramolecular gels have several applications including sensing of biomolecules and ions (Pisoschi 2013; Prasad et al. 2018; Monton et al. 2012), light-harvesting systems (Fan et al. 2021), catalysis (Singh et al. 2017), optoelectronic devices (Cho et al. 2020; Yao et al. 2019), tissue engineering (Gaharwar et al. 2014; Jain and Roy 2019), targeted drug delivery (Mu et al. 2017), dyes and pollutant removal (Milli et al. 2016; Giuri et al. 2019a; Okesola and Smith 2016; Adhikari et al. 2009), and degradation (Guidetti et al. 2018) and may be implied as injectable gels (Zanna and Tomasini 2017).

In the last 15 years, the use of ultra-short peptides to form hydrogels has been studied by several research groups. To behave as LMWG, ultra-short peptides should have groups able to form weak interactions as hydrogen bonding, van der Waals interactions, π–π stacking, and electrostatic interactions; thus they usually contain aromatic amino acids and, more specifically, one or more Phe units (Tomasini and Castellucci 2013; Wychowaniec et al. 2020). One of the most popular triggers for hydrogel preparation is the pH change method. The dissolution of the gelator takes place at a pH suitable for its solubilisation; then, with the pH switch, the molecule solubility decreases and the gelation process starts. For acidic gelators and pH change method, GdL (glucono-δ-lactone) is the most used trigger. Its slow hydrolysis produces gluconic acid, thus allowing a controlled change in the pH of the solution and producing homogeneous and reproducible gels (Adams et al. 2009).

The unprotected dipeptide Phe-Phe, which is able to form several supramolecular structures, is surprisingly not able to form gels. However, this moiety is a recurring motif in peptide-based LMWGs, as π–π stacking seems to play a pivotal role in molecular self-assembly (Marchesan et al. 2015).

The smallest unprotected gelling unit has to include at least three amino acids (Marchesan et al. 2015). Marchesan et al. investigated the behaviour of gelators, where Phe-Phe is coupled with valine and leucine (Marchesan et al. 2012a). While the homochiral tripeptide L-Phe-L-Phe-L-Val is not able to form gels, D-Phe-L-Phe-L-Val and L-Phe-L-Phe-D-Val, containing an inverted chiral centre, produce gels at physiological pH after ultrasound sonication (Marchesan et al. 2014, 2012b). Ultra-sounds break the clusters of the gelator molecules dispersed in the medium, helping the dissolution; (Naota and Koori 2005) then a re-aggregation occurs to form a gel. In this case, ultrasounds act as promoter rather than the actual trigger, as these gels where prepared with the pH change method, dissolving the gelator at high pH and then adjusting the pH at 7.4 (Cringoli et al. 2020).

Moving to protected ultra-short peptides, Fmoc-Phe-Phe (where Fmoc is fluorenylmethyloxycarbonyl) is the first LMW peptide used as hydrogelator. Gazit et al. prepared a hydrogel, dissolving Fmoc-Phe-Phe in HFP and then adding water. The addition of water, that in this case is the trigger, causes a decrease in the solubility and leads to gel formation (Mahler et al. 2006). The behaviour and the properties of this strong hydrogelator were extensively studied by this and other groups (Smith et al. 2008; Tang et al. 2009; Liang et al. 2009; Ghosh et al. 2020).
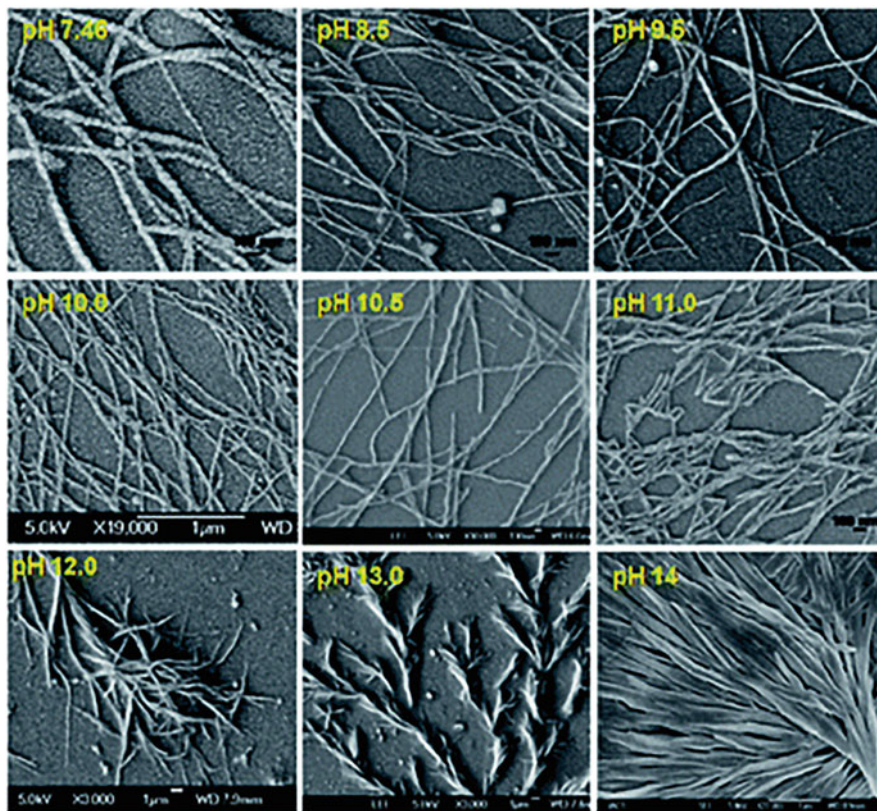
Fig. 4.8 Field emission SEM images of the dried hydrogels at different pH. Image adapted from (Nanda et al. 2013)

Starting from Fmoc-Phe-Phe, several gelators with similar structures were developed to observe which differences in the gelation ability would occur. For example, Banerjee et al. studied the protected amino acid Fmoc-Phe, removing the second Phe. This molecule can be considered as a super hydrogelator, as its critical gelation concentration (CGC) is 0.1% w/w (Roy and Banerjee 2011). Later on, the same group functionalised Phe with a pyrene derivative. The molecule Pyr-Phe (where Pyr is 3-(pyren-1-yl)butanoyl) formed gels in a concentration lower than 0.1% w/w in a wide range of pH (from 7.46 to 14) upon heating and cooling. The pH variation highly affects the shape of the fibres formed, ranging from thin and long at neutral pH to short, thick, and more compact at high pH (Fig. 4.8). The morphological structure affects the gels appearance, which is transparent at neutral pH and translucent at high pH, and influences their thixotropic behaviour (Nanda et al. 2013).

As the Fmoc protecting group is sensitive towards a basic environment, there are few limitations in its use for gelation with the pH change method. Moreover, the cytotoxicity associated with the use of Fmoc protected amino acids was reported

(Truong et al. 2015). For these reasons, there are a growing number of examples reporting the gelation ability of molecules bearing different protecting groups on the *N*-terminus. A representative example is 2-Nap (naphtalen-2-yloxy acetyl) that is stable in a wide range of pH.

2-Nap-Phe-Phe is a hydrogelator that can gel aqueous solutions under various conditions. Adams et al. extensively studied this molecule and found that it can form gels not only with pH change (Chen et al. 2010) but also with a solvent switch, starting from the gelator dissolved in DMSO (dimethylsulphoxide) and adding water (DMSO:H_2O in 1:9 ratio), and with the addition of calcium ions (Colquhoun et al. 2017).

The presence of divalent ions may also act as trigger (Zanna et al. 2017a). According to the methodology chosen, it is possible to obtain gels with different fibrous patterns. In this study, the gel formed with the solvent switch method (DMSO and water) has a spherulitic network. In contrast, the molecule dissolved in basic water tends to form worm-like micelles rather than being freely dispersed. The use of a divalent cation as trigger would act as a bridge between those micelles, while the use of protons would lead to an entangled fibrous network (Draper and Adams 2017).

The research on the gelling ability of peptides and pseudopeptides is rapidly expanding. In various studies, phenylalanine is substituted with similar scaffolds, like Tyr (tyrosine), Dopa (3,4-dihydroxyphenylalanine), or halogenated aromatic ring.

Tyr and Dopa offer the possibility to form additional H-bonds or to be functionalised with other groups that may improve the gelator gelling ability. One example is represented by Boc-L-Dopa(Bn)$_2$-OH (where Boc is *tert*-butyloxycarbonyl and Bn is benzyl), able to form gels both with pH change method and with the addition of calcium ions and to support the growth of inorganic crystal structures, like $CaCO_3$ (Giuri et al. 2019b). This process underlies the biomineralisation, by which living organisms can grow bones, teeth, shells, etc. (Lowenstam and Weiner 1989; van Driessche et al. 2017). Halogenation on the other hand offers the possibility to form a wide range of additional weak interactions, like halogen-π interactions, halogen bonds, or halogen-hydrogen bonds, depending on the size and polarisability of the halogen atom (Metrangolo 2008; Feng et al. 2016), and improve the effect of π–π stacking (Li et al. 2017; MacCormack et al. 2020).

Pseudo-peptides are often used in the design of a new gelator, as they are usually biocompatible and are not recognised by enzymes, thus are not cleaved in a biological system. We have explored the use of 4-carboxy-5-methyl-oxazolidin-2-one (Oxd) derived from threonine (Castellucci et al. 2011; Zanna et al. 2017b; Zanna et al. 2015). This rigid moiety induces a local constraint that may either strengthen the gel network or prevent the gel formation, depending on chirality. In fact, L-Dopa or L-Phe should be coupled with D-Oxd to obtain a gel, as if they are coupled with L-Oxd, no gel is formed. In these cases, diastereoisomers with DL configuration cause the formation of β-sheets structures, which end up into fibres and gels, while diastereoisomers with L-L configuration adopt a geometry in the range of PPII

(polyproline II), with the consequent inability of forming gels (Ravarino et al. 2021; Longhi et al. 2012).

The use of long alkyl chains in the design of a gelator is also considered, as their presence enhances the hydrophobic interactions that may improve the gelation ability. The amphiphilic behaviour helps the formation of superstructures like micelles and fibres, as the hydrophilic moieties interface water, while the hydrophobic ones interact with each other. For example, the use of pseudo-peptide-based bola-amphiphile gelators has been investigated and proved to form gels (Castellucci et al. 2013; Giuri et al. 2019c). In addition, Smith et al. reported the formation of gels using dendritic structures containing Lys (lysine) units (Hirst et al. 2003; Partridge et al. 2001).

4.4   Adhesives

Adhesives are widespread over living organisms. For example, mussels attach to rocks thanks to an adhesive protein (Waite and Tanzer 1980), spiders produce silk fibrils that contain proteins able to make sticky their net (Sahni et al. 2011), and geckos exploit an enormous number of protein-based threads (setae) under their pads to stick to surfaces (Autumn et al. 2000). In order to mimic nature, humans have synthesised different glues for a broad range of scope, spanning from buildings to biological issues. Most of them have a polymeric nature, and the use of ultra-short peptides in adhesive designing is a quite recent challenge.

Stickiness is a phenomenon arising from the balance and synergy between two forces, namely adhesion and cohesion (Yu et al. 1999). The first one is responsible for the interaction between the adhesive molecule and the surface, while the second one represents the intermolecular interaction of the adhesive molecules with each other. If a glue shows no adhesiveness, it may be for a lack of adhesion ("interfacial failure"), or a lack of cohesion ("cohesive failure") (Waite 2002).

One of most studied in the systems of adhesion is the byssus of mussels. The design of a new adhesive often draw inspiration from the chemical composition of the mussel foot proteins (mfps), the main responsible for the anchoring of mussels to rocks (Barbara 2002; Lee et al. 2011). These proteins contain a high molar percentage of L-Dopa, an uncommon amino acid found also in some plants and mushrooms. Since ultra-short peptides used as adhesives have predominantly L-Dopa in their features, we will briefly introduce this amino acid.

The side chain of L-Dopa is a catechol, a moiety able to give rise to several weak interactions like cation-π, π–π stacking, and hydrogen bonds. The ortho-position of the two hydroxyl groups makes L-Dopa also a good chelating agent for divalent cations like Ca^{2+}. As this side chain is able to create a broad range of weak bonds, it is widely believed that the presence of this amino acid is crucial for the adhesion of mussels on surfaces (Lee et al. 2011; Giuri et al. 2020; Mian and Khan 2017; Giuri et al. 2021). The catechol group is sensitive towards oxidation to produce 1,2-quinone. From a cohesive point of view, the catechol of L-Dopa can be
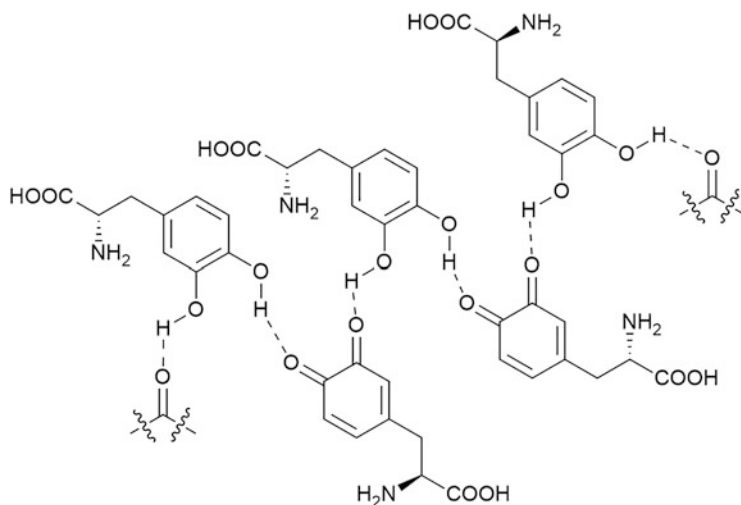
Fig. 4.9 Hydrogen bonds between the catechol and *ortho*-quinone of Dopa units. Image adapted from (Giuri et al. 2021)

considered as a Brönsted acid and can interact with its oxidised form of ortho-quinone, so that the two ortho-carbonyl groups act as Lewis bases as shown in Fig. 4.9 (Giuri et al. 2021). In fact, it is possible to tune the adhesion capability of a material containing L-Dopa by tuning its degree of oxidation.

The adhesive properties of these materials may be studied using different approaches. At a molecular level, single-molecule force microscopy (SMFM) (Neuman and Nagy 2008) is one of the most used techniques, while at a macroscopic level, traction test (North et al. 2017) and tack test (Giuri et al. 2020) are useful tools to determine the binding force between two surfaces.

A common strategy for designing adhesives is using L-Dopa as part of a repeating unit for the synthesis of oligomers (Li et al. 2020) or polymers (Yamamoto 1987; Tatehata et al. 2000). The first ultra-short peptide used as adhesive is Fmoc-Dopa$_2$-Lys and was reported in 2014 by Fichman et al. (Fichman et al. 2014). This protected tripeptide is able to form ordered fibrillary nanostructures with the macroscopic behaviour of a viscoelastic glue able to stick two plates of glass. In contrast, the protected dipeptide Fmoc-Dopa$_2$ showed no adhesive properties. The different behaviour may be ascribed to the amine on the lysine residue of Fmoc- Dopa$_2$-Lys that makes up for the lack of a Lewis base and bestows sticky properties to the peptide.

Considering the cooperation between the side chains of Dopa and Lys, Li et al. decided to compare oligopeptides of different chain length made of the repeating unit Lys-Dopa: Lys-Dopa, (Lys-Dopa)$_3$ and (Lys-Dopa)$_{10}$ (Li et al. 2020). The authors performed SMFS analysis to probe the adhesiveness of the peptides towards surfaces of TiO$_2$ (polar, negatively charged) and polystyrene (apolar, aromatic). All

the oligomers were adhesive towards both surfaces. While Lys-Dopa showed a modest force of 120 pN towards TiO_2, (Lys-Dopa)$_3$ showed a remarkable improvement, reaching 300 pN on the same surface, and (Lys-Dopa)$_{10}$ had a value of 250 pN, slightly lower compared to (Lys-Dopa)$_3$. This suggests that to a certain extent an increase in the chain length enhances the adhesiveness, but further elongation of the chain provides no further benefit. Peptides made of the repeating unit Lys-Phe of the same lengths were used as a comparison. These peptides were adhesive towards the polystyrene surface, while being only slightly adhesive towards the TiO_2 surface. These outcomes suggest that Dopa is a more versatile substrate than Phe for binding surfaces.

Our group reported another example of an ultra-short peptide possessing sticky properties (Giuri et al. 2020). The protected dipeptide Boc-(L-Dopa)$_2$-OMe showed macroscopic adhesiveness towards surfaces of glass and steel after the addition of an aqueous solution, while being completely non adhesive in the dry phase. We performed tack and traction tests on the films of the adhesive molecule and registered a force of 16 N when the film was wet with distilled water and a force of 47 N with a 1 M aqueous solution of $CaCl_2$. We also studied the adhesive properties of the protected amino acid Boc-L-Dopa(Boc)$_n$-OMe (n = 0, 1, 2). While Boc-L-Dopa-OMe was completely non-sticky both in dry and wet phase, the Boc protection dramatically improves the adhesiveness, reaching 82 N in pure water and 79 N in 1 M $CaCl_2$ for Boc-L-Dopa(Boc)$_2$-OMe, and 45 N in distilled water and 130 N in 1 M $CaCl_2$ for Boc-L-Dopa(Boc)-OMe. These results suggest that the presence of calcium ions leads to the formation of supramolecular structures that improve the adhesion ability.

The adhesive force values obtained with some polymeric substrates have similar results for both SMFM (Delparastan et al. 2019; Smith et al. 1999) and tack or traction tests (Shin et al. 2015; Clancy et al. 2016). Even though the use of ultra-short peptides in the field of adhesive is a recent topic, with these few examples they proved to be valid alternatives to polymeric adhesives.

4.5   Conclusions and Future Perspectives

In this chapter, that does not claim to be exhaustive, we reported an overview of the wide variety of materials that may be obtained by self-assembly of ultra-short peptides, where the definition ultra-short means peptides consisting of up to seven amino acids (Hauser et al. 2011; Seow and Hauser 2014; Makovitzki et al. 2006). The chemical diversity of the single amino acids is the key to understand why with this limited number of moieties it is possible to obtain a wide variety of materials that are "held together" by several noncovalent interactions including electrostatic (acidic and basic amino acids), hydrophobic, π-stacking (aromatic amino acids), hydrogen bonding (polar amino acids), as well as steric contributions. While individually these interactions are quite weak, collectively they can give rise to very

stable structures. Nevertheless, each of these interactions depends in different ways on environmental conditions such as ionic strength, pH, and temperature.

The interest in the behaviour of ultra-short peptides was initially stimulated by studies on the pathogenic processes that is triggered by Alzheimer's disease and, in particular, on the behaviour of the dipeptide Phe-Phe, that is the core recognition motif for the molecular self-assembly. Since the emergence of Phe-Phe as a self-assembling building block, many studies have been made to organise the Phe-Phe-based building blocks into various functional nanostructures such as nanotubes, spherical vesicles, nanofibrils, nanowires, and ordered molecular chains. Among all these categories, we chose to describe in some details the most representative nanomaterials. So, we focussed our attention on nanotubes, hydrogels, and adhesives that may be obtained by self-assembly of ultra-short peptides. We collected the papers of a good number of research groups from all around the world that clearly demonstrate that a wide *plethora* of nanomaterials may be obtained by carefully tuning the experimental conditions. Indeed, it is crucial to find the trigger that is more suitable to initiate the process of self-assembly, as the weak interactions involved depend in different ways on environmental conditions such as ionic strength, pH, and temperature.

There is still a lot of work to do in this area, as these nanomaterials may find further applications in many fields, also at the industrial scale. As Richard Feynman wrote more than 60 years ago, "There's plenty of room at the bottom." (Feynman 1959).

References

Adams DJ (2011) Dipeptide and tripeptide conjugates as low-molecular-weight hydrogelators. Macromol Biosci 11:160–173

Adams DJ, Topham PD (2010) Peptide conjugate hydrogelators. Soft Matter 6:3707–3721

Adams DJ, Butler MF, Frith WJ, Kirkland M, Mullen L, Sanderson P (2009) A new method for maintaining homogeneity during liquid–hydrogel transitions using low molecular weight hydrogelators. Soft Matter 5:1856–1862

Adhikari B, Palui G, Banerjee A (2009) Self-assembling tripeptide based hydrogels and their use in removal of dyes from waste-water. Soft Matter 5:3452–3460

Adler-Abramovich L, Reches M, Sedman VL, Allen S, Tendler SJB, Gazit E (2006) Thermal and chemical stability of diphenylalanine peptide nanotubes: implications for nanotechnological applications. Langmuir 22:1313–1320

Aizenberg J, Fratzl P (2009) Biological and biomimetic materials. Adv Mater 21:387–388

Amorín M, Castedo L, Granja JR (2003) New cyclic peptide assemblies with hydrophobic cavities: the structural and thermodynamic basis of a new class of peptide nanotubes. J Am Chem Soc 125:2844–2845

Amorín M, Castedo L, Granja JR (2005) Self-assembled peptide tubelets with 7 Å pores. Chem Eur J 11:6543–6551

Angelici G, Falini G, Hofmann H-J, Huster D, Monari M, Tomasini C (2008) A fiberlike peptide material stabilized by single intermolecular hydrogen bonds. Angew Chem Int Ed 47:8075–8078

Apostolopoulos V, Bojarska J, Chai TT, Elnagdy S, Kaczmarek K, Matsoukas J, New R, Parang K, Lopez OP, Parhiz H et al (2021) A global review on short peptides: frontiers and pesrspectives. Molecules (Basel, Switzerland) 26:1–45

Autumn K, Liang YA, Hsieh ST, Zesch W, Chan WP, Kenny TW, Fearing R, Full RJ (2000) Adhesive force of a single gecko foot-hair. Nature 405:681–685

Bai S, Pappas C, Debnath S, Frederix PWJM, Leckie J, Fleming S, Ulijn RV (2014) Stable emulsions formed by self-assembly of interfacial networks of dipeptide derivatives. ACS Nano 8:7005–7013

Barbara S (2002) Adhesion a. Biochemistry 1180:1172–1180

Bera S, Mondal S, Xue B, Shimon LJW, Cao Y, Gazit E (2019) Rigid helical-like assemblies from a self-aggregating tripeptide. Nat Mater 18:503–509

Binder WH, Smrzka OW (2006) Self-assembly of fibers and fibrils. Angew Chem Int Ed 45:7324–7328

Bong DT, Clark TD, Granja JR, Reza Ghadiri M (2001) Self-assembling organic nanotubes. Angew Chem Int Ed 40:988–1011

Cao X, Ding Q, Li Y, Gao A, Chang X (2018) Water-assisted formation of supramolecular self-assembly systems based on distyrylbenzene derivative. Chem Select 3:4720–4725

Carloni P, Andreoni W, Parrinello M (1997) Self-assembled peptide nanotubes from first principles. Phys Rev Lett 79:761–764

Castellucci N, Angelici G, Falini G, Monari M, Tomasini C (2011) L-Phe-D-Oxd: a privileged scaffold for the formation of supramolecular materials. Eur J Org Chem:3082–3088

Castellucci N, Sartor G, Calonghi N, Parolin C, Falini G, Tomasini C (2013) A peptidic hydrogel that may behave as a "trojan horse". Beilstein J Org Chem 9:417–424

Chapman R, Warr GG, Perrier S, Jolliffe KA (2013a) Water-soluble and PH-responsive polymeric nanotubes from cyclic peptide templates. Chem Eur J 19:1955–1961

Chapman R, Jolliffe KA, Perrier S (2013b) Multi-shell soft nanotubes from cyclic peptide templates. Adv Mater 25:1170–1172

Chen L, Revel S, Morris K, Adams DJ (2010) Energy transfer in self-assembled dipeptide hydrogels. Chem Commun 46:4267–4269

Chivers PRA, Smith DK (2019) Shaping and structuring supramolecular gels. Nat Rev Mater 4:463–478

Cho KG, Lee JI, Lee S, Hong K, Kang MS, Lee KH (2020) Light-emitting devices based on electrochemiluminescence gels. Adv Funct Mater 30:1907936

Clancy SK, Sodano A, Cunningham DJ, Huang SS, Zalicki PJ, Shin S, Ahn BK (2016) Marine bioinspired underwater contact adhesion. Biomacromolecules 17:1869–1874

Colquhoun C, Draper ER, Schweins R, Marcello M, Vadukul D, Serpell LC, Adams DJ (2017) Controlling the network type in self-assembled dipeptide hydrogels. Soft Matter 13:1914–1919

Cringoli MC, Romano C, Parisi E, Waddington LJ, Melchionna M, Semeraro S, De Zorzi R, Grönholm M, Marchesan S (2020) Bioadhesive supramolecular hydrogel from unprotected, short D,l-peptides with Phe-Phe and Leu-Asp-Val motifs. Chem Commun 56:3015–3018

Davidovich-Pinhas M (2019) Oil structuring using polysaccharides. Curr Opin Food Sci 27:29–35

Delparastan P, Malollari KG, Lee H, Messersmith PB (2019) Direct evidence for the polymeric nature of polydopamine. Angew Chem Int Ed 58:1077–1082

Demirel G, Malvadkar N, Demirel MC (2010) Control of protein adsorption onto core-shell tubular and vesicular structures of diphenylalanine/parylene. Langmuir 26:1460–1463

Draper ER, Adams DJ (2017) Low-molecular-weight gels: the state of the art. Chem 3:390–410

Du D, Wei X, Huang J, Tu Y (2021) Real-time monitoring of ROS secreted by Ana-1 mouse Macrophages by nanomaterial sensitized Electrochemiluminescence. J Electroanal Chem 889:115230

Estroff LA, Hamilton AD (2004) Water gelation by small organic molecules water gelation by small organic molecules. Chem Rev 104:1201–1218

Fan X, Teng CP, Yeo JCC, Li Z, Wang T, Chen H, Jiang L, Hou X, He C, Liu J (2021) Temperature and PH responsive light-harvesting system based on AIE-active microgel for cell imaging. Macromol Rapid Commun 42:1–8

Feng Y, Chen H, Liu Z-X, He Y-M, Fan Q-H (2016) A pronounced halogen effect on the organogelation properties of peripherally halogen functionalized poly(benzyl ether) dendrons. Chem Eur J 22:4980–4990

Fernandez-Lopez S, Kim HS, Choi EC, Delgado M, Granja JR, Khasanov A, Kraehenbuehl K, Long G, Weinberger DA, Wilcoxen KM et al (2001) Antibacterial agents based on the cyclic D, L-α-peptide architecture. Nature 412:452–455

Fichman G, Adler-Abramovich L, Manohar S, Mironi-Harpaz I, Guterman T, Seliktar D, Messersmith PB, Gazit E (2014) Seamless metallic coating and surface adhesion of self-assembled bioinspired nanostructures based on Di-(3,4-dihydroxy- l -phenylalanine) peptide motif. ACS Nano 8:7220–7228

Frederix PWJM, Scott GG, Abul-Haija YM, Kalafatovic D, Pappas CG, Javid N, Hunt NT, Ulijn RV, Tuttle T (2015) Exploring the sequence space for (Tri-)peptide self-assembly to design and discover new hydrogels. Nat Chem 7:30–37

Gaharwar AK, Peppas NA, Khademhosseini A (2014) Nanocomposite hydrogels for biomedical applications. Biotechnol Bioeng 111:441–453

García-Fandiño R, Amorín M, Castedo L, Granja JR (2012) Transmembrane ion transport by self-assembling α,γ-peptide nanotubes. Chem Sci 3:3280–3285

Ge J, Guo J, Yu X, Li Y, Ma Z (2021) Structural tunability on naphthalimide-based dendrimer gelators via glaser coupling interaction with tailored gelation solvent polarity and stimuli-responsive properties. Langmuir 37:2677–2682

General S, Antonietti M (2002) Supramolecular organization of oligopeptides, through complexation with surfactants. Angew Chem Int Ed 41:2957–2960

Ghosh M, Bera S, Schiffmann S, Shimon LJW, Adler-Abramovich L (2020) Collagen-inspired helical peptide coassembly forms a rigid hydrogel with twisted polyproline II architecture. ACS Nano 14:9990–10000

Giuri D, Zanna N, Tomasini C (2019a) Low molecular weight gelators based on functionalized L-dopa promote organogels formation. Gels 5:27

Giuri D, Jurković L, Fermani S, Kralj D, Falini G, Tomasini C (2019b) Supramolecular hydrogels with properties tunable by calcium ions: a bio-inspired chemical system. ACS Appl Bio Mater 2:5819–5828

Giuri D, Barbalinardo M, Zanna N, Paci P, Montalti M, Cavallini M, Valle F, Calvaresi M, Tomasini C (2019c) Tuning mechanical properties of pseudopeptide supramolecular hydrogels by graphene doping. Molecules 24:1–12

Giuri D, Jacob KA, Ravarino P, Tomasini C (2020) Boc-protection on L-DOPA: an easy way to promote underwater adhesion. Eur J Org Chem:7144–7150

Giuri D, Ravarino P, Tomasini C (2021) L -dopa in small peptides: an amazing functionality to form supramolecular materials. Org Biomol Chem 19:4622–4636

Guidetti G, Giuri D, Zanna N, Calvaresi M, Montalti M, Tomasini C (2018) Biocompatible and light-penetrating hydrogels for water decontamination. ACS Omega 3:8122–8128

Hamley IW (2021) Biocatalysts based on peptide and peptide conjugate nanostructures. Biomacromolecules 22:1835–1855

Hauser CAE, Deng R, Mishra A, Loo Y, Khoe U, Zhuang F, Cheong DW, Accardo A, Sullivan MB, Riekel C et al (2011) Natural tri- to hexapeptides self-assemble in water to amyloid β-type fiber aggregates by unexpected α-helical intermediate structures. Proc Natl Acad Sci U S A 108:1361–1366

Hirst AR, Smith DK, Feiters MC, Geurts HPM, Wright AC (2003) Two-component dendritic gels: easily tunable materials. J Am Chem Soc 125:9010–9011

Horne WS, Stout CD, Ghadiri MR (2003) A heterocyclic peptide nanotube. J Am Chem Soc 125:9372–9376

Huang R, Qi W, Su R, Zhao J, He Z (2011) Solvent and surface controlled self-assembly of diphenylalanine peptide: from microtubes to nanofibers. Soft Matter 7:6418–6421

Ivanov MS, Khomchenko VA, Salimian M, Nikitin T, Kopyl S, Buryakov AM, Mishina ED, Salehli F, Marques PAAP, Goncalves G et al (2018) Self-assembled diphenylalanine peptide microtubes covered by reduced graphene oxide/spiky nickel nanocomposite: an integrated nanobiomaterial for multifunctional applications. Mater Des 142:149–157

Jain R, Roy S (2019) Designing a bioactive scaffold from coassembled collagen-laminin short peptide hydrogels for controlling cell behaviour. RSC Adv 9:38745–38759

Jayawarna V, Ali M, Jowitt TA, Miller AF, Saiani A, Gough JE, Ulijn RV (2006) Nanostructured hydrogels for three-dimensional cell culture through self-assembly of fluorenylmethoxycarbonyl-dipeptides. Adv Mater 18:611–614

Khazanovich N, Granja JR, McRee DE, Milligan RA, Ghadiri MR (1994) Nanoscale tubular ensembles with specified internal diameters. Design of a self-assembled nanotube with a 13-Å pore. J Am Chem Soc 116:6011–6012

Knudtson CA, Dias JR (2019) Recent methods for diversification of bile acids and related steroids towards supramolecular. Steroids 151:108442

Kol N, Adler-Abramovich L, Barlam D, Shneck RZ, Gazit E, Rousso I (2005) Self-assembled peptide nanotubes are uniquely rigid bioinspired supramolecular structures. Nano Lett 5:1343–1346

Lee BP, Messersmith PB, Israelachvili JN, Waite JH (2011) Mussel-inspired adhesives and coatings. Annu Rev Mater Res 41:99–132

Lehn JM (2009) Towards complex matter: supramolecular chemistry and self-organization. Eur Rev 17:263–280

Li Q, Li R, Lan H, Lu Y, Li Y, Xiao S, Yi T (2017) Halogen effect on non-conventional organogel assisted by balanced π-π interaction. Chem Select 2:5421–5426

Li Y, Cheng J, Delparastan P, Wang H, Sigg SJ, DeFrates KG, Cao Y, Messersmith PB (2020) Molecular design principles of lysine-DOPA wet adhesion. Nat Commun 11:1–8

Liang G, Yang Z, Zhang R, Li L, Fan Y, Kuang Y, Gao Y, Wang T, Lu WW, Xu B (2009) Supramolecular hydrogel of a D-amino acid dipeptide for controlled drug release in vivo. Langmuir 25:8419–8422

Lipnick RL, Garbisch EW (1973) Conformational analysis of 2-methylbutane. J Am Chem Soc 95:6375–6379

Longhi G, Abbate S, Lebon F, Castellucci N, Sabatino P, Tomasini C (2012) Conformational studies of Phe-Rich foldamers by VCD spectroscopy and Ab initio calculations. J Org Chem 77:6033–6042

Lowenstam HA, Weiner S (1989) On biomineralization, 1st edn. Oxford University Press. ISBN 9780195049770

MacCormack AS, Busch VM, Japas ML, Giovanetti L, Di Salvo F, Di Chenna PH (2020) The effect of vicinal di-halo substituents on the organogelling properties of aromatic supramolecular gelators and their application as soft templates. New J Chem 44:8198–8208

Mahler A, Reches M, Rechter M, Cohen S, Gazit E (2006) Rigid, self-assembled hydrogel composed of a modified aromatic dipeptide. Adv Mater 18:1365–1370

Maity S, Nir S, Reches M (2014) Co-assembly of aromatic dipeptides into spherical structures that are similar in morphology to red and white blood cells. J Mater Chem B 2:2583–2591

Makovitzki A, Avrahami D, Shai Y (2006) Ultrashort antibacterial and antifungal lipopeptides. Proc Natl Acad Sci U S A 103:15997–16002

Marchesan S, Waddington L, Easton CD, Winkler DA, Goodall L, Forsythe J, Hartley PG (2012a) Unzipping the role of chirality in nanoscale self-assembly of tripeptide hydrogels. Nanoscale 4:6752–6760

Marchesan S, Easton CD, Kushkaki F, Waddington L, Hartley PG (2012b) Tripeptide self-assembled hydrogels: unexpected twists of chirality. Chem Commun 48:2195–2197

Marchesan S, Easton CD, Styan KE, Waddington LJ, Kushkaki F, Goodall L, McLean KM, Forsythe JS, Hartley PG (2014) Chirality effects at each amino acid position on tripeptide self-assembly into hydrogel biomaterials. Nanoscale 6:5172–5180

Marchesan S, Vargiu AV, Styan KE (2015) The Phe-Phe motif for peptide self-assembly in nanomedicine. Molecules 20:19775–19788

Matsumura S, Uemura S, Mihara H (2005) Construction of biotinylated peptide nanotubes for arranging proteins. Mol BioSyst 1:146–148

Metrangolo P, Resnati G (eds) (2008) Halogen bonding. Springer, Berlin, Heidelberg. ISBN 978-3-540-74329-3

Mian SA, Khan Y (2017) The adhesion mechanism of marine mussel foot protein: adsorption of L-dopa on α- and β-cristobalite silica using density functional theory. J Chem 2017:1–6

Milli L, Zanna N, Merlettini A, Di Giosia M, Calvaresi M, Focarete ML, Tomasini C (2016) Pseudopeptide-based hydrogels trapping methylene blue and eosin Y. Chem Eur J 22:12106–12112

Monton MRN, Forsberg EM, Brennan JD (2012) Tailoring sol-gel-derived silica materials for optical biosensing. Chem Mater 24:796–811

Moreira IP, Sasselli IR, Cannon DA, Hughes M, Lamprou DA, Tuttle T, Ulijn RV (2016) Enzymatically activated emulsions stabilised by interfacial nanofibre networks. Soft Matter 12:2623–2631

Morris J, Bietsch J, Bashaw K, Wang G (2021) Recently developed carbohydrate based gelators and their applications. Gels 7:1–61

Mu Y, Wu X, Pei D, Wu Z, Zhang C, Zhou D, Wan X (2017) Contribution of the polarity of mussel-inspired adhesives in the realization of strong underwater bonding. ACS Biomater Sci Eng 3:3133–3140

Nanda J, Biswas A, Banerjee A (2013) Single amino acid based thixotropic hydrogel formation and PH-dependent morphological change of gel nanofibers. Soft Matter 9:4198–4208

Naota T, Koori H (2005) Molecules that assemble by sound: an application to the instant gelation of stable organic fluids. J Am Chem Soc 127:9324–9325

Neuman KC, Nagy A (2008) Single-molecule force spectroscopy: optical tweezers, magnetic tweezers and atomic force microscopy. Nat Methods 5:491–505

North MA, Del Grosso CA, Wilker JJ (2017) High strength underwater bonding with polymer mimics of mussel adhesive proteins. ACS Appl Mater Interfaces 9:7866–7872

Okesola BO, Smith DK (2016) Applying low-molecular weight supramolecular gelators in an environmental setting-self-assembled gels as smart materials for pollutant removal. Chem Soc Rev 45:4226–4251

Partridge KS, Smith DK, Dykes GM, McGrail PT (2001) Supramolecular dendritic two-component gel. Chem Commun:319–320

Peppas NA, Bures P, Leobandung W, Ichikawa H (2000) Hydrogels in pharmaceutical formulations. Eur J Pharm Biopharm 50:27–46

Pisoschi AM (2013) Biosensors as bio-based materials in chemical analysis: a review. J Biobaased Mater Bioenergy 7:19–38

Prasad K, Mondal D, Sharma M, Freire MG, Mukesh C, Bhatt J (2018) Stimuli responsive ion gels based on polysaccharides and other polymers prepared using ionic liquids and deep eutectic solvents. Carbohydr Polym 180:328–336

Raeburn J, Mendoza-Cuenca C, Cattoz BN, Little M a, Terry AE, Zamith Cardoso A, Griffiths PC, Adams DJ (2015) The effect of solvent choice on the gelation and final hydrogel properties of Fmoc–diphenylalanine. Soft Matter 11:927–935

Ramasamy P, Guha S, Shibu ES, Sreeprasad TS, Bag S, Banerjee A, Pradeep T (2009) Size tuning of Au nanoparticles formed by electron beam irradiation of Au25 quantum clusters anchored within and outside of dipeptide nanotubes. J Mater Chem 19:8456–8462

Rao MR, Sun SS (2013) Supramolecular assemblies of amide-derived organogels featuring rigid π-conjugated phenylethynyl frameworks. Langmuir 29:15146–15158

Ravarino P, Giuri D, Faccio D, Tomasini C (2021) Designing a transparent and fluorine containing hydrogel. Gels 7:1–10

Reches M, Gazit E (2003) Casting metal nanowires within discrete self-assembled peptide nanotubes. Science 300:625–627

Reches M, Gazit E (2006) Controlled patterning of aligned self-assembled peptide nanotubes. Nat Nanotechnol 1:195–200

Reza Ghadiri M, Milligan RA, McRee DE, Khazanovich N (1994) Erratum: self-assembling organic nanotubes based on a cyclic peptide architecture (Nature (1993) 366 (324-327)). Nature 372:709

Ribeiro ACC, Souza GA, Pereira DH, Cordeiro DS, Miranda RS, Custódio R, Martins TD (2019) Phe-Phe Di-peptide nanostructure self-assembling modulated by luminescent additives. ACS Omega 4:606–619

Feynman RP (1959) Plenty of room at the bottom? Am Sci:1–7

Roy S, Banerjee A (2011) Amino acid based smart hydrogel: formation, characterization and fluorescence properties of silver nanoclusters within the hydrogel matrix. Soft Matter 7:5300–5308

Sahni V, Blackledge TA, Dhinojwala A (2011) A review on spider silk adhesion. J Adhes 87:595–614

Sanchez C, Arribart H, Guille MMG (2005) Biomimetism and Bioinspiration as tools for the design of innovative materials and systems. Nat Mater 4:277–288

Sangeetha NM, Maitra U (2005) Supramolecular gels: functions and uses. Chem Soc Rev 34:821

Sapra R, Verma RP, Maurya GP, Dhawan S, Babu J, Haridas V (2019) Designer peptide and protein dendrimers: a cross-sectional analysis. Chem Rev 119:11391–11441

Scott GG, McKnight PJ, Tuttle T, Ulijn RV (2016) Tripeptide emulsifiers. Adv Mater 28:1381–1386

Seow WY, Hauser CAE (2014) Short to ultrashort peptide hydrogels for biomedical uses. Mater Today 17:381–388

Shin SR, Bae H, Cha JM, Mun JY, Chen Y-C, Tekin H, Shin H, Farshchi S, Dokmeci MR, Tang S et al (2012) Carbon nanotube reinforced hybrid microgels as scaffold materials for cell encapsulation. ACS Nano 6:362–372

Shin J, Lee JS, Lee C, Park H-J, Yang K, Jin Y, Ryu JH, Hong KS, Moon S-H, Chung H-M et al (2015) Tissue adhesive catechol-modified hyaluronic acid hydrogel for effective, minimally invasive cell therapy. Adv Funct Mater 25:3814–3824

Singh N, Kumar M, Miravet JF, Ulijn RV, Escuder B (2017) Peptide-based molecular hydrogels as supramolecular protein mimics. Chem Eur J 23:981–993

Smith DK (2010) Supramolecular gels: building bridges. Nat Chem 2:162–163

Smith BL, Schäffer TE, Vlani M, Thompson JB, Frederick NA, Klndt J, Belcher A, Stucky GD, Morse DE, Hansma PK (1999) Molecular mechanistic origin of the toughness of natural adhesives, fibres and composites. Nature 399:761–763

Smith AM, Williams RJ, Tang C, Coppo P, Collins RF, Turner ML, Saiani A, Ulijn RV (2008) Fmoc-diphenylalanine self assembles to a hydrogel via a novel architecture based on π-π interlocked β-sheets. Adv Mater 20:37–41

Song Y, Challa SR, Medforth CJ, Qiu Y, Watt RK, Miller JE, Swol V, Shelnutt JA, Lafayette W, March A (2004) Synthesis of peptide-nanotube platinum-nanoparticle composites †. Chem Commun:1044–1045

Svobodová H, Noponen V, Kolehmainen E, Sievänen E (2012) Recent advances in steroidal supramolecular gels. RSC Adv 2:4985–5007

Tang C, Smith AM, Collins RF, Ulijn RV, Saiani A (2009) Fmoc-diphenylalanine self-assembly mechanism induces apparent PK a shifts. Langmuir 25:9447–9453

Tarvirdipour S, Huang X, Mihali V, Schoenenberger CA, Palivan CG (2020) Peptide-based nanoassemblies in gene therapy and diagnosis: paving the way for clinical application. Molecules:25

Tatehata H, Mochizuki A, Kawashima T, Yamashita S, Yamamoto H (2000) Model polypeptide of mussel adhesive protein. I. synthesis and adhesive studies of sequential polypeptides (X-Tyr-Lys)n and (Y-Lys)n. J Appl Polym Sci 76:929–937

Tomasic L, Lorenzi GP (1987) Some cyclic oligopeptide with S2n symmetry. Helv Chim Acta 70: 1012–1016

Tomasini C, Castellucci N (2013) Peptides and peptidomimetics that behave as low molecular weight gelators. Chem Soc Rev 42:156–172

Truong WT, Su Y, Gloria D, Braet F, Thordarson P (2015) Dissolution and degradation of Fmoc-diphenylalanine self-assembled gels results in necrosis at high concentrations in vitro. Biomater Sci 3:298–307

Tu S, Kim SH, Joseph J, Modarelli DA, Parquette JR (2011) Self-assembly of a donor-acceptor nanotube. a strategy to create bicontinuous arrays. J Am Chem Soc 133:19125–19130

van Driessche A, Kellermeier M, Benning LG, Gebauer D (2017) New perspectives on mineral nucleation and growth, 1st edn. Springer International Publishing. ISBN 978-3-319-45669-0

Vauthey S, Santoso S, Gong H, Watson N, Zhang S (2002) Molecular self-assembly of surfactant-like peptides to form nanotubes and nanovesicles. Proc Natl Acad Sci U S A 99:5355–5360

Waite JH (2002) Adhesion à La Moule. Integr Comp Biol 42:1172–1180

Waite JH, Tanzer ML (1980) The bioadhesive of Mytilus byssus: a protein containing L-DOPA. Top Catal 96:1554–1561

Wang J, Liu K, Xing R, Yan X (2016) Peptide self-assembly: thermodynamics and kinetics. Chem Soc Rev 45:5589–5604

Whitesides GM, Grzybowski B (2002) Self-assembly at all scales. Science 295:2418–2421

Wychowaniec JK, Patel R, Leach J, Mathomes R, Chhabria V, Patil-Sen Y, Hidalgo-Bastida A, Forbes RT, Hayes JM, Elsawy MA (2020) Aromatic stacking facilitated self-assembly of ultrashort ionic complementary peptide sequence: β-sheet nanofibers with remarkable gelation and interfacial properties. Biomacromolecules 21:2670–2680

Xu T, Zhao N, Ren F, Hourani R, Lee MT, Shu JY, Mao S, Helms BA (2011) Subnanometer Porous thin films by the co-assembly of nanotube subunits and block copolymers. ACS Nano 5:1376–1384

Yamamoto H (1987) Adhesive studies of synthetic polypeptides: a model for marine adhesive proteins. J Adhes Sci Technol 1:177–183

Yamanaka M (2013) Urea derivatives as low-molecular-weight gelators. J Incl Phenom Macrocycl Chem 77:33–48

Yan X, Zhu P, Li J (2010) Self-assembly and application of diphenylalanine-based nanostructures. Chem Soc Rev 39:1877–1890

Yan X, He Q, Wang K, Duan L, Cui Y, Li J (2007) Transition of cationic dipeptide nanotubes into vesicles and oligonucleotide delivery. Angew Chem Int Ed Engl 46:2431–2434

Yan X, Cui Y, He Q, Wang K, Li J, Mu W, Wang B, Ou-yang Z (2008) Reversible transitions between peptide nanotubes and vesicle-like structures including theoretical modeling studies. Chem Eur J 14:5974–5980

Yanlian Y, Ulung K, Xiumei W, Horii A, Yokoi H, Shuguang Z (2009) Designer self-assembling peptide nanomaterials. Nano Today 4:193–210

Yao Y, Zhang L, Orgiu E, Samorì P (2019) Unconventional nanofabrication for supramolecular electronics. Adv Mater 31:1–20

Yu M, Hwang J, Deming TJ (1999) Role of 1-3,4-dihydroxyphenylalanine in mussel adhesive proteins. J Am Chem Soc 121:5825–5826

Zanna N, Tomasini C (2017) Peptide-based physical gels endowed with thixotropic behaviour. Gels 3:39

Zanna N, Merlettini A, Tatulli G, Milli L, Focarete MLML, Tomasini C (2015) Hydrogelation induced by Fmoc-protected peptidomimetics. Langmuir 31:12240–12250

Zanna N, Focaroli S, Merlettini A, Gentilucci L, Teti G, Falconi M, Tomasini C (2017a) Thixo-tropic peptide-based physical hydrogels applied to three-dimensional cell culture. ACS Omega 2:2374–2381

Zanna N, Iaculli D, Tomasini C (2017b) The effect of L-DOPA hydroxyl groups on the formation of supramolecular hydrogels. Org Biomol Chem 15:5797–5804

Zhang S (2003) Fabrication of novel biomaterials through molecular self-assembly. Nat Biotechnol 21:1171–1178

Zhang S (2006) Another brick in the wall. Nat Nanotechnol 1:169–170

Zhang S, Holmes T, Lockshin C, Rich A (1993) Spontaneous assembly of a self-complementary oligopeptide to form a stable macroscopic membrane. Proc Natl Acad Sci U S A 90:3334–3338

Zhang S, Marini DM, Hwang W, Santoso S (2002) Design of nanostructured biological materials through self-assembly of peptides and proteins. Curr Opin Chem Biol 6:865–871

Zhang L, Li S, Squillaci MA, Zhong X, Yao Y, Orgiu E, Samorì P (2017) Supramolecular self-assembly in a sub-micrometer electrodic cavity: fabrication of heat-reversible π-gel memristor. J Am Chem Soc 139:14406–14411

Zou P, Chen WT, Sun T, Gao Y, Li LL, Wang H (2020) Recent advances: peptides and self-assembled peptide-nanosystems for antimicrobial therapy and diagnosis. Biomater Sci 8:4975–4996

Chapter 5
Peptide Amphiphile Nanomaterials

Priyam Das and Debapratim Das

Abstract Peptide amphiphiles (PAs) have emerged as an essential class of peptides, particularly in the bottom-up fabrication of innovative soft materials. They have potential in many vital applications across various fields of science and technology. A significant number of reports involving design, self-assembly, and applications of PAs have emerged over the last couple of decades. Thus, it is crucial to infer or analyze the outcomes of all these studies, which will help provide an overview of the work done and lead a guiding pathway to future studies in this area. This chapter discusses various classes of PAs, their applications, and a preliminary guideline on the design principles.

Keywords Peptide amphiphiles · Hydrogel · Self-aggregation · Bio-mdeical application · Nanomaterials · Hierarchical assembly

5.1   Introduction

Supramolecular assemblies of peptides offer useful biological functions and structural diversity to synthetic soft matter (Dasgupta et al. 2013; Levin et al. 2020). The possibility to integrate various biological functionalities within the same molecule is intriguing. Peptide assemblies can generate different nanostructures such as filaments, spheres, nanoparticles, networks, 2D sheets, tubes, and helices, to name a few. One subclass of self-assembling peptides is the peptide amphiphiles (PA) (Hendricks et al. 2017). Peptide amphiphiles possess both hydrophilic and hydrophobic segments within the same peptide molecule (Das and Das 2021; Dasgupta and Das 2019; Zhao et al. 2021). Like other small molecules, PA's assembly process is governed by the supramolecular forces like $\pi-\pi$ stacking, hydrogen bonding, hydrophobic interaction, etc. The presence of peptide segments and amide bonds in these molecules allows the formation of various secondary

P. Das · D. Das (✉)
Department of Chemistry, Indian Institute of Technology Guwahati, Guwahati, Assam, India
e-mail: ddas@iitg.ac.in

structures. Additionally, the hydrophobic segment provides hydrophobic interactions to allow self-assembly. Like other amphiphiles, in case of PAs, the hydrophobic-lipophilic balance (HLB) plays a crucial role in their aggregation pathway and dictates the resulting aggregate structure/morphology (Rosa et al. 2020; Yu et al. 1996). A minute change to the HLB can cause significant alteration in self-assembly path and function of the self-assembled systems (materials). The HLB depends on the sequence of the PA, and thus it is crucial to understand the design principle for PAs while planning for a targeted application. In this chapter, we discuss the classification, self-assembly processes, nanomaterials generated by PAs, and their applications.

5.2　Classification

Based on the chemical composition of the molecules, PAs can be classified into four broad categories. They are (a) amphiphilic PAs, (b) lipidated PAs, and (c) cyclic PAs, (d) supramolecular PAs (Fig. 5.1).
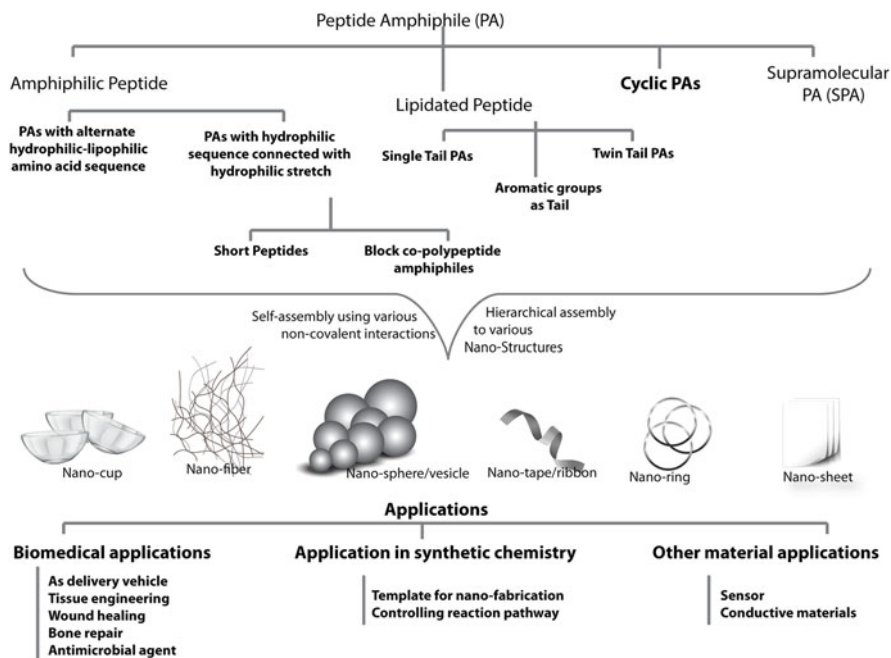

Fig. 5.1 Classification of peptide amphiphiles, different nanostructures formed by PAs, and their possible applications in various fields

5.2.1 Amphiphilic Peptides

Amphiphilic peptides fall under the category of all amino acid PAs. These peptides are composed of amino acids (natural or unnatural) only. However, amphiphilicity is generated due to the presence of both hydrophilic and hydrophobic amino acid residues. The positioning of these amino acids is crucial toward achieving the amphiphilic character and self-assembly propensity. The use of amphiphilic peptide sequences is common among the membrane proteins where two distinct surfaces are created within the folded structure. These proteins assimilate within the membrane using the hydrophobic surface, while the hydrophilic interior of the folded structure allows membrane transportation of hydrophilic molecules/signals. Structurally, many peptide-based antibiotics, toxins, and cell-penetrating and antimicrobial peptides are found to be all amino acid PAs in nature. These all amino acid PAs can further be categorized into two segments: (a) PAs with alternate hydrophobic-hydrophilic amino acid sequence and (b) PAs with hydrophilic sequence connected with hydrophilic stretch.
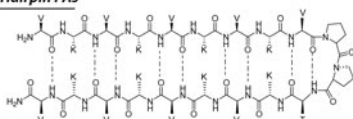
5.2.1.1 PAs with Alternate Hydrophilic-Hydrophobic Amino Acid Sequence

PAs with alternate hydrophilic-hydrophobic amino acids often tend to form β-sheet-like arrangements. In this way, they create two distinct faces, one hydrophobic and the other hydrophilic, like the membrane proteins mentioned earlier. This is the most common way of constructing all amino acid PAs. There are several such β-sheet-forming PAs in literature, for example, the series reported by Zhang et al. (1–3, Fig. 5.2) (Zhang et al. 1993). The amino acid repeats used in these peptides lead to

PAs with alternate hydrophobic-hydrophilic dyad

EAK8 :	H$_2$N-AEAEAKAK-COOH	1
EAK12 :	Ac-AEAEAKAKAEAE-CONH$_2$	2
EAK16 :	Ac-AEAEAKAKAEAEAKAK-CONH$_2$	3
KLD12:	Ac-KLDLKLDLKLDL-CONH$_2$	4
RADA16-I:	Ac-RADARADARADARADA-CONH$_2$	5
RADA16-II:	Ac-RARADADARARADADA-CONH$_2$	6
LK13:	LKLKLKLKLKLKL-NH$_2$	7

β-Hairpin PAs
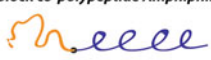
MAX1:	H$_2$N-VKVKVKVKV^{D}PPTKVKVKVKV-NH$_2$	8
TSS1:	VKVKVKVKV^{D}PPTKVKVKVK^{D}PPKVKVKVKV-NH$_2$	9
K15Q:	H$_2$N-VKVKVKVKV^{D}PPTKVQVKVKV-NH$_2$	10
IA-2:	H$_2$N-IKIKIKIKI^{D}PPTKIKIKIKI-NH$_2$	11
IC1-R:	H$_2$N-CKIKIKIKI^{D}PPTKIOIKIKC-NH$_2$	12

(O = Ornithine)

PAs with hydrophobic sequence connected to hydrophilic segment

PA	CMC (mM)	Morphology
A$_6$K (13)	2.28	nanotubes
A$_6$K$_2$(14)	7.93	vesicles
A$_6$K$_3$(15)	not detected	irregular aggregation
V$_6$K$_2$(16)	0.33	nanotubes
V$_6$K$_3$(17)	0.83	nanovesicles
V$_6$K$_4$(18)	4.65	irregular aggregation
L$_6$K$_2$(19)	0.046	Nanoribbons
L$_6$K$_3$(20)	0.25	Nanotubes
L$_6$K$_4$(21)	5.38	nanovesicles
L$_6$K$_5$(22)	not detected	irregular aggregation

Block co-polypeptide Amphiphiles

K$_m$L$_n$	23
K$_m$V$_n$	24
E$_m$L$_n$	25
K$_m$L$_n$K$_o$L$_n$K$_m$	26

(Hydrophilic amino acid)$_m$(Hydrophobic amino acid)$_n$

Fig. 5.2 Examples of different classes of peptide amphiphiles

the formation of β-sheet-like secondary structures. They self-assemble in an aqueous environment to form nanofibers. Hierarchical assembly of the nanofibers in a concentration-dependent fashion leads to a stable macroscopic membrane. Both EAK12 and EAK6 could form the membrane, but EAK8 failed to do so under similar conditions. Some other well-known all amino acid PAs with an alternate dyad of hydrophilic and hydrophobic residues are **4–7** (Geisler and Schneider 2012; Kisiday et al. 2002; Yokoi et al. 2005; Zhang and Altman 1999). It is to be noted that the list of all amino acid PAs mentioned in this chapter is some of the representative examples only, and the actual number developed so far is not limited to this list.

The pioneering works by Schneider et al. introduced another interesting group of PAs that primarily contain the repeat of an alternate hydrophilic-lipophilic dyad. However, these PAs result in β-hairpin structures due to a ^{D}Pro^{L}Pro (Pro = proline) sequence in the middle of the sequence (MAX1,**8**, Fig. 5.2) (Schneider et al. 2002). The peptides are highly soluble at low pH and could not adopt any particular secondary structure due to the electrostatic repulsion of protonated amine groups on Lys (Lysine) side chains. However, solubility decreases upon increasing pH of the medium as the deprotonation of amine groups allows them to form an antiparallel β-sheet structure. The ^{D}Pro^{L}Pro segment further stabilizes the secondary structure. It creates a Type II turn that facilitates the folding back and allows β-sheet formation. The folded molecules intermolecularly aggregated further to form hydrogels. Several minor alterations in the sequence show that the self-assembly can be controlled by other stimuli like temperature, ionic strength, light, metal ions, etc. Some representative examples (**9–12**) of β-hairpin PAs are shown in Fig. 5.2 (Larsen et al. 2009; Rughani et al. 2009).

5.2.1.2 PAs with Hydrophilic Sequence Connected with Hydrophobic Stretch

Another subclass of amphiphilic peptides is those where a hydrophilic sequence is attached with a hydrophobic segment. In these cases, the hydrophilic sequence acts like the polar head group of the amphiphile, while the hydrophobic stretch serves as the hydrophobic tail of the PA. Although these PAs are structurally similar to classical amphiphiles/surfactants, hydrogen bond donor and acceptors in the hydrophobic segment lead to distinctly different self-assembly mechanisms. A wide range of nanostructures is reported with these PAs including tubes, vesicles, micelles, and fibers, to name a few. A detailed study involving PAs (A_nK, $n = 3/6/9$) containing Lys as the head group and varied numbers of Ala (Alanine) as the hydrophobic tail showed the dependence of morphology on the tail length (Xu et al. 2009). The study showed that the structural transition from lamellar sheets (A_3K) to nanofibers/worm-like micelles (A_6K) to nanorods (A_7K) could be induced by enhancing the chain length of the tail. The structural transition with increasing hydrophobic tail demonstrates the prominent role of hydrophobic interaction between the side chains over the backbone hydrogen bonding and electrostatic repulsion between the Lys side chains. A systematic study on changes in the number and type of hydrophobic and

hydrophilic amino acids on the self-aggregation was reported by Liu et al. (Meng et al. 2012). A series of ten peptides (**13–22**) having the sequence X_6K_n (X = Ala, Val, or Leu; n = 1–5, Val = valine; Leu = leucine) were investigated. Interestingly, as the number of Lys increases, the critical micelle concentration (CMC) enhances. On the other hand, as the hydrophobicity of the tail is enhanced (by changing Ala to Val to Leu), keeping the head group unchanged, the CMC decreases. Both of these modifications in the PA sequence also result in the transformation of vesicles to nanotubes. It is important to note that head groups with a higher number of Lys residues (4 or 5) result in irregular aggregation in all cases. All these observations are in line with the molecular packing theory (Israelachvili 2011b) developed to describe surfactant structural transitions and indicate the critical role of HLB to control the self-assembly process.

5.2.1.3 Block co-Polypeptide Amphiphiles

This particular class strictly falls under the category of "PAs with hydrophilic sequence connected with hydrophilic stretch," but the size of these PAs makes them distinct. This particular class involves large peptide sequences where long stretches of hydrophobic sequences are connected with long hydrophilic sections (Deming 2005; Nowak et al. 2003). Each of these segments can be considered blocks of a block co-polymer (or co-polypeptide). PAs **23–25** are examples of such block co-polypeptide amphiphiles where highly water-soluble polyelectrolytes like poly (Lys) or poly(Glu) are attached to hydrophobic domains like poly(Leu) or poly(Val) (Glu = Glutamic acid) (Nowak et al. 2002). These co-polypeptides form thermally stable hydrogels at low concentrations in the aqueous medium. Since the PAs consist of polyelectrolytes, adding salt weakens the gels through screening polyelectrolyte charges. There could be more than two blocks (**26**), and the positioning of the hydrophilic and hydrophobic segments will affect the aggregation of the PA.

5.2.2 Lipidated Peptide Amphiphiles

Peptide sequences with hydrophilic character connected with a hydrocarbon chain are examples of lipidated PAs. Nature also utilizes lipidation of protein effectively. For example, signal transduction proteins like Ras superfamily proteins get post-translationally modified with one or more lipid groups. The lipidation instills amphiphilic character to the proteins and helps them anchor to the membrane (Das et al. 2012; Guo et al. 2008). Typically, for designer PAs, the hydrophobic tails are attached at the *N*-terminal of a hydrophilic sequence, presumably due to the synthesis ease. However, examples (**27**, Fig. 5.3) are present where the lipid groups are attached at the C-terminal (Ariga et al. 2000; Yamada et al. 1998).

Stupp's group reported a classic example of lipidated PA (**28**) (Hartgerink et al. 2001). The PA was designed to incorporate five distinct segments. The segments are
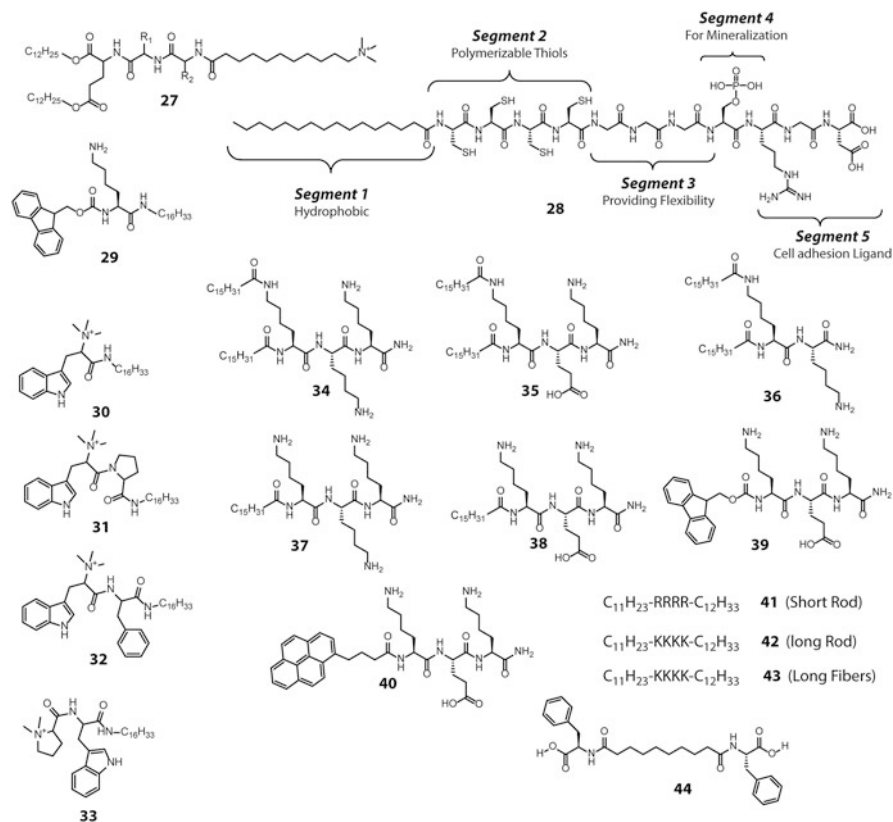
Fig. 5.3 Chemical structures of PAs with different hydrophobic tails

a lipid group (palmitoyl) at the *N*-terminal followed by a cross-linkable tetra-Cys (Cysteine) segment, a flexible segment consisting of three Gly (Glycine) residues, segment four contains phosphoserine, and the fifth and final segment comprising cell-adhesive RGD unit. The PA self-assembles into long nanofibers with the capacity to form a hydrogel that mimics the extracellular matrix (ECM). Moreover, the presence of phosphoserine allows nucleation of apatite crystals on the nanofiber surface.

Lipidated PAs can also be prepared with a single amino acid, di-, or tri-peptides as the polar head group. Though amphiphilic molecules with only one amino acid should not be considered PAs, they are generally included in this group as the amino acids, and amide linkages are involved in these structures. PA **29** is an example where Fmoc-Lys is connected with a hexadecyl group through amide linkage (Ahmed et al. 2013). It is important to note that the aqueous solubility of the PA can be achieved by the free side chain amine functionality. However, it is difficult to achieve sufficient hydrophilicity with single amino acids, and the tail length should be adjusted accordingly. Another way to increase hydrophilicity/solubility is by

incorporating permanently charged groups like quaternary ammonium. Das et al. reported a series of such PAs having one or two amino acids at the head group where the amine groups are quaternized (Das et al. 2006; Mitra et al. 2007; Mitra and Das 2008). Some representative examples are shown in Fig. 5.3 (**30–33**).

Lipidated PAs may have more than one hydrocarbon chain, and the number of chains plays a critical role in the aggregation pattern. A detailed study on the self-assembly of seven different lipidated PAs (**31–40**) has been reported by Dasgupta (Dasgupta 2016). Doubly lipidated PAs (**34–36**) form structures like twisted nanotapes or dense helical fibrils. On the other hand, non-lipidated or mono-lipidated PAs with the same head groups did not show any particular morphology. Doubly lipidated PAs can be of gemini amphiphile type as well. Gemini PAs (**41–43**) with two C_{12} chains containing $(Arg)_4$, $(Lys)_4$, or $(His)_4$ (Arg = Arginine; His = histidine) as spacers are reported by Wang et al. (Qi et al. 2020). PA **41** with Arg spacer assembles into short rods, while **42** and **43** formed long rods and long fibers, respectively. The dissociation of these self-assembled structures were found to be dependent on the polarity of the spacer group as **43** was found to be least prone to dissociate, while dissociation of short rods of **41** could be achieved easily. Another type of lipidated PA belongs to the bola amphiphile category. In these cases, two peptide sequences are connected by a single lipid group at two ends. One representative example of bola-PA is **44** that forms hydrogel consisting network of fibrillar morphology at physiological pH (pH 6.5–7.2) in presence of divalent metal salts ($MnCl_2$, $CoCl_2$, $CuSO_4$, and $NiCl_2$) on sonication.

Although not strictly lipidated, peptides with aromatic attachments serving as the hydrophobic segments can be considered as lipidated PAs. This subclass consists of a significant number of representations. For this group of PAs, the aromatic groups provide the hydrophobic character and serve as probable $\pi-\pi$ stacking unit that strengthens the self-assembly and often leads to higher-order aggregates like a hydrogel. A detailed review on aromatic peptide amphiphiles was authored by Ulijn and can be used as a ready reference while constructing such PAs (Fleming and Ulijn 2014).

Some of the Fmoc-protected amino acids tend to form self-assemblies in the aqueous medium. Fmoc-Tyr or Fmoc-Phe (Tyr = Tyrosine; Phe = Phenyl alanine) can form self-assembly that leads to hydrogelation (Sutton et al. 2009; Yang and Xu 2004). Fmoc-protected self-assembling short (di-, tri, tetra-) peptides (**45–47**, Fig. 5.4) are also reported on many occasions (Orbach et al. 2009; Smith et al. 2008). Additionally, naphthalene (**48–50**) (Yang et al. 2007), pyrene (**51**) (Pramanik et al. 2019a, b), Bhcmoc (**52**) (Ikeda et al. 2011) naphthalene diimide (NDI) (**53**) (Shao and Parquette 2010), perylene diimide (PDI) (**54**) (Ahmed et al. 2018; Ahmed et al. 2017), etc. can also serve the role of hydrophobicity provider. The aromatic group attachments are not limited to the terminal positions. These groups can be placed at the side chain of the amino acids (**53**) or used as a spacer to create bola-PAs (**54**). The aromatic capping plays a crucial role toward dictating the self-assembly outcome. In a recent work by Roy et al., a study of 12 short aromatic PAs showed that the aromatic capping has more pronounced effect than the amino-acid position in the sequence on the final self-assembled structure (Jain et al. 2019).
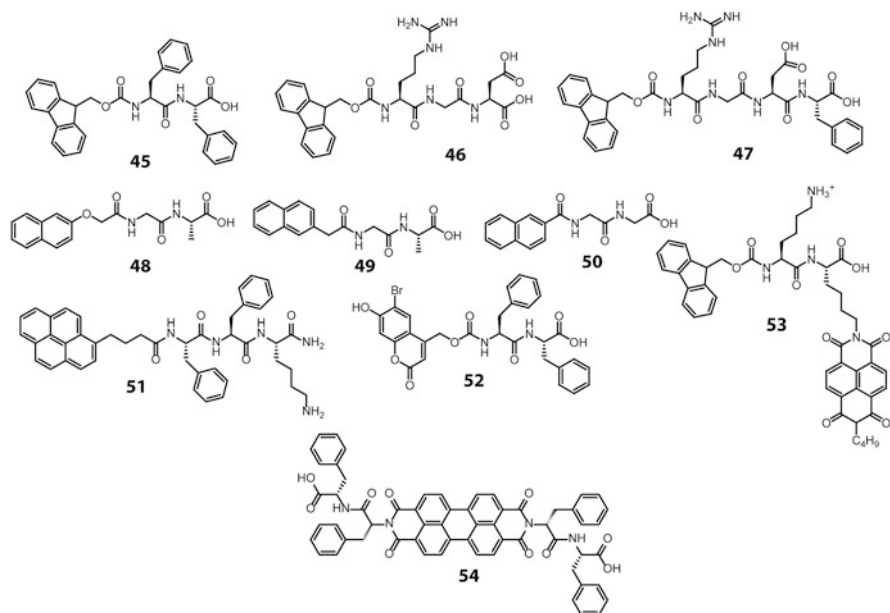
Fig. 5.4 Chemical structures of different aromatic PAs

5.2.3 Cyclic Peptide Amphiphiles

Another class of all PAs are made of cyclic peptides (cPAs). cPAs could be of all amino acid PA type involving hydrophilic and hydrophobic amino acids in the cyclic peptide sequence. There are three main types of such cPAs, cyclic D, L-α-peptides, cyclic β-peptides, and cyclic α − γ peptides (Chapman et al. 2012). Some representative examples of cPAs are shown in Fig. 5.5 (**55–57**) (Fletcher et al. 2007; Fujimura et al. 2007; Hourani et al. 2011). These peptides stack through intermolecular hydrogen bonding to form nanotubes. These nanotubes have key advantages over other tubular structures, including control over the internal diameter and the ability to control internal and external chemical functionality. Another type of cPAs is those where cyclic peptides are connected with lipid groups, and the peptide section acts as the hydrophilic segment of the amphiphile. For example, cPA **58** acts as a facial amphiphile and forms nanocapsule-like aggregates (Chung et al. 2010). Understandably, the cPAs are structurally distinct from other PAs. Consequently, their self-assembly paths are dictated more by the possibility to form the stacks through intermolecular hydrogen bonding. cPAs found application as antimicrobial agents, artificial ion-channel, and ion sensors, to name a few.
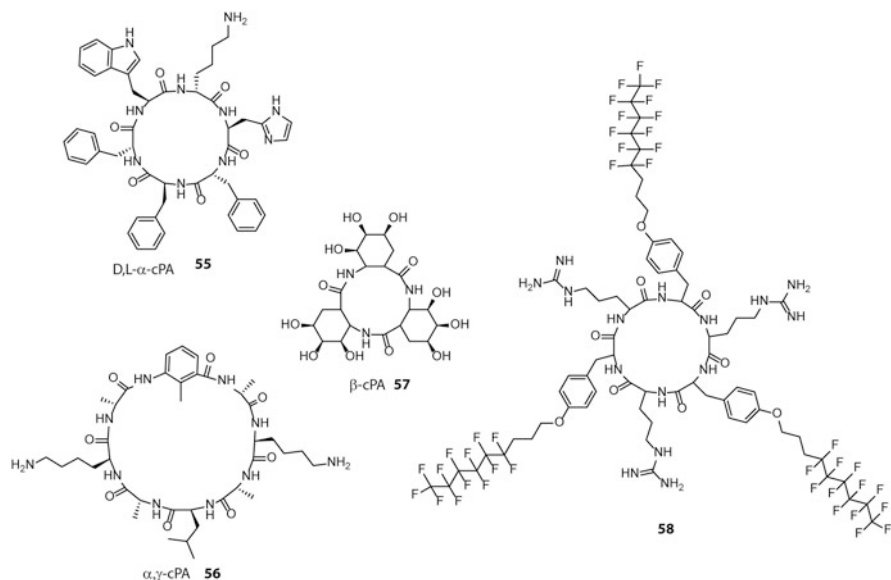
Fig. 5.5 Representative examples of cyclic PAs

5.2.4 Supramolecular Peptide Amphiphiles

A relatively new class of amphiphiles have emerged as an attractive alternative to traditional amphiphiles. Here, the head groups are connected with the tail through non-covalent interactions or dynamic covalent bonds (Zhang and Wang 2011). Different macrocyclic hosts like cyclodextrins (CD), calixarenes, crown ethers, pillararenes, and cucurbiturils (CB) are primarily used to construct such supramolecular amphiphiles. When the hydrophilic head group is composed of a peptide sequence, they are called supramolecular peptide amphiphiles (SPA).

These are called supramolecular peptide amphiphiles (SPA). It is important to mention that there are not many examples of SPAs in the literature yet. The concept of SPA construction can be elaborated with the example of CB-assisted SPA formation as shown in Fig. 5.6. Cucurbit[8]uril (CB[8]) has the unique ability to accommodate two guests within its hydrophobic cavity as shown in Fig. 5.6a (Das et al. 2019; Das and Scherman 2011). An electron-deficient moiety like viologen can form charge transfer complex with electron-rich group like naphthalene or pyrene within the CB[8] cavity through ternary complexation. Using this strategy, peptides functionalized with pyrene or naphthalene can be supramoleculary conjugated to form SPAs (**59**–**61**) (Dowari et al. 2019; Jiao et al. 2012; Mondal et al. 2015). Unlike other singly lipidated amphiphiles, these SPAs tend to form vesicles. Similarly, SPAs can be created using the host-guest chemistry of functionalized CD. Adamantyl group has strong affinity toward CDs. Kros et al. prepared an
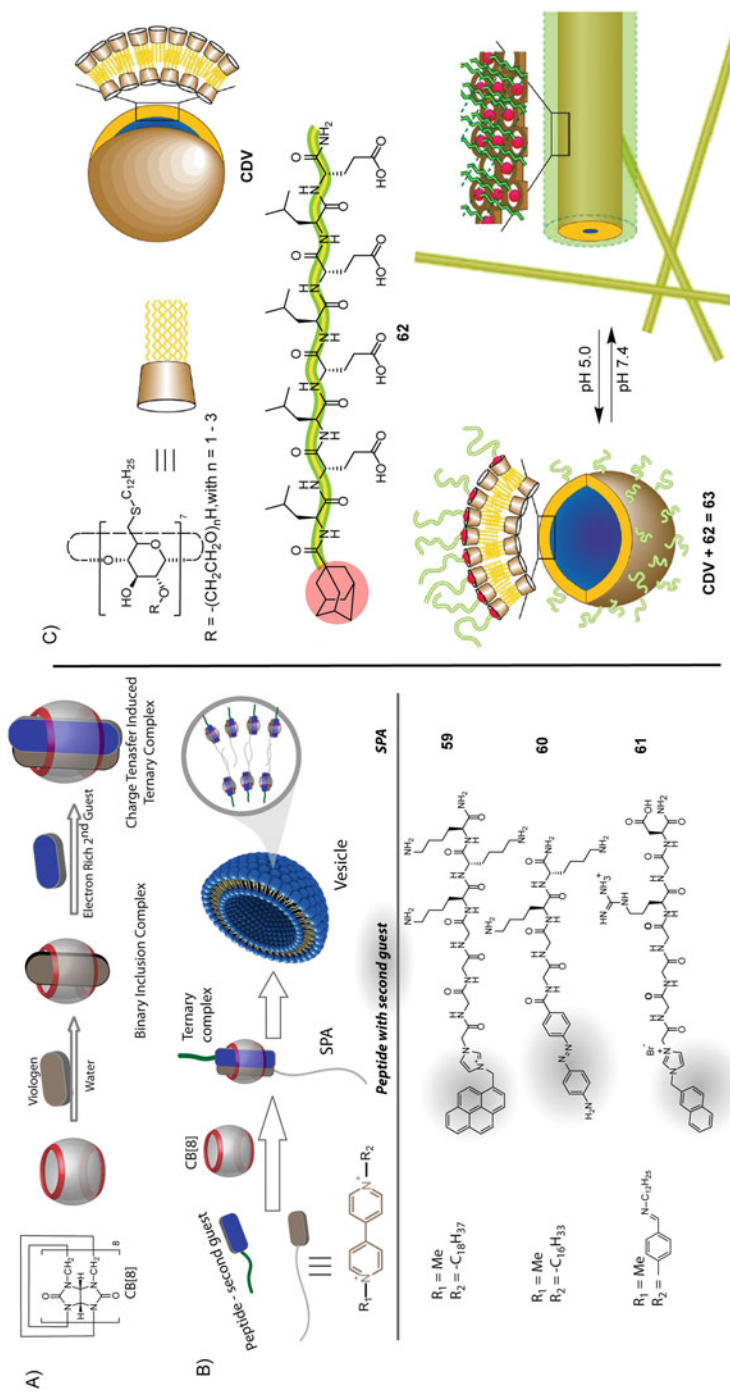
Fig. 5.6 Representative examples of supramolecular peptide amphiphiles. (**a**) Graphical presentation of ternary complexation by Cucurbit[8]uril through charge transfer complex between an electron-deficient first guest and an electron-rich second guest. (**b**) Graphical presentation and examples of CB[8]-assisted SPA formation. (**c**) Graphical presentation and example of lipid functionalized CD-assisted SPA formation. Parts of the figure are adapted with permission from reference (Versluis et al. 2009). Copyright 2009 American Chemical Society

adamantyl functionalized peptide (**62**) that forms complex with lipid functionalized cyclodextrin (CDV) to generate SPA **63** (Versluis et al. 2009). SPA **63** forms vesicular assembly under acidic pH while increasing the pH of the medium results into rod-like assembly. Similar SPAs can be constructed using other macrocyclic hosts like calixarenes, pillararenes, etc.

5.3 Self-Assembly and Nanostructures

5.3.1 Interactions Accountable for PA Self-Assembly

The self-assembly of PAs are dictated by various non-covalent interactions like hydrogen bonding, $\pi-\pi$ stacking, electrostatic, hydrophobic, van der Waals interactions, etc. Apparently, these forces, though individually, are scrutinized to be energetically insignificant and "weak" non-covalent forces; their measured, organized, and collective interplay can bring about a significant alterable variation in structure and activity. The fundamental rationale behind fabricating a PA-based nanomaterial lies in perceiving these non-covalent interactions and their targeted modification and clever manipulation. Several excellent reviews are available on the design principles of PA and controlling their self-assemblies (Dehsorkhi et al. 2014; Fleming and Ulijn 2014; Hamley 2011).

5.3.1.1 Hydrogen Bonding

Though they fall under the "weak interaction" category in the energy landscape, hydrogen bonds are crucial for biological macromolecules like DNA and proteins. They have energies of 10–40 kJ mol^{-1} (Israelachvili 2011a). Proteins and peptides are composed of amino acids that provide abundant hydrogen bonding sites. The most important is the hydrogen bond donor amide NH's and the carbonyl groups of the amide linkages, which serve as the hydrogen bond acceptors. Hydrogen bonds are dominantly involved in secondary structures in proteins and peptides. Hydrogen bonding is thus considered as the master-key interaction in protein and peptide folding. The PAs are no exception, and the hydrogen bonding in the peptide segment of any PA, in general, dictates the self-aggregation pattern. The high selectivity and directionality of hydrogen bonds in PAs can incite the formation of various one-dimensional (1D), 2D, and 3D nanostructures. For example, the β-hairpin formation by MAX1 (**8**) is majorly driven by the intramolecular hydrogen bonding between the two strands. Moreover, the turn created by the ^{D}Pro^{L}Pro segment is also an outcome of the intramolecular hydrogen bonding.

5.3.1.2 Hydrophobic Interaction

For any PA, the hydrophobic interaction is essential. Hydrophobic interactions are well known as one of the prime driving forces for amphiphilic systems. Nonpolar moieties (tail group) cannot interact favorably with surrounding water molecules. On the other hand, the head groups, being polar, can easily be dissolved in water. To accommodate themselves in the medium, the hydrophobic parts of these molecules try to aggregate and minimize their surface area in contact with water. Such arrangements lead to the formation of micelles, vesicles, etc. Hydrophobic interactions are stabilized due to favorable entropy and are not enthalpy-driven (Toksoz et al. 2010). In the presence of salt, due to charge screening, the effect of hydrophobic interactions can be significantly enhanced (Kabiri and Unsworth 2014). For lipidated PAs, the presence of hydrophobic tails provides a traditional surfactant-like structure and leads to the formation of micelles, and subsequent higher-order assemblies may result in other morphologies.

5.3.1.3 Electrostatic Interactions

Electrostatic interactions play a crucial role in PA self-assemblies. The Coulombic attractions between oppositely charged groups lead to the creation of ion-pair or electrostatic bonds. The energy associated with electrostatic interactions or ionic bonds falls in the range of $\sim$500 kJ mol^{-1} (Israelachvili 2011a). Electrostatic interactions are usually employed to induce structural specificity for charged peptides. Others have reviewed the critical role of electrostatic interactions on molecular self-assembly to form nanostructures (Faul and Antonietti 2003; Rehm and Schmuck 2010).

5.3.1.4 $\pi$$-$$\pi$ Stacking

The attractive, non-covalent interactions between aromatic rings are known as $\pi$$-$$\pi$ stacking (Hunter and Sanders 1990). The energy associated with such interactions is in the range of 8–12 kJmol^{-1}. The aromatic groups present in a PA provide stability to the self-aggregated state and allow the directional growth of the nanostructures through intermolecular $\pi$$-$$\pi$ stacking. As mentioned in Sect. 5.2.2, the introduction of aromatic residues in a PA can be done by using aromatic amino acids (Phe, Tyr or Trp; Trp = Tryptophan) or by incorporating different fused aromatic groups (**45**–**54**). It is worth mentioning that the effect of $\pi$$-$$\pi$ stacking depends on the medium as the interaction is much stronger and more dominant in toluene or other organic solvents than in water (Zhu et al. 2010).

5.3.1.5 Van der Waals Interactions

When two atoms come to extreme proximity, it induces charge fluxes, and as a result, a non-directional, non-specific instantaneous electrostatic attraction is generated. This attractive force is known as van der Waals interaction. The energy involved with each of these interactions is extremely low (4 kJmol^{-1}) (Pollard et al. 2017). However, when all such interactions present in the system are combined, the overall effect of van der Waals interaction becomes significant. Van der Waals forces are ubiquitous in self-assembled systems and PAs are no exception. These weak interactions are prevalent between the aliphatic tails of PAs and provide an important contribution to the self-assembly process of PAs.

5.3.1.6 Other Unusual Interactions

Though the abovementioned non-covalent interactions are majorly taken into account while designing PA-based assemblies, some other unconventional interactions can also play a role in the self-assembly process. Charge transfer (CT) interaction within organic molecules happens when an electron-deficient moiety and a π-electron cloud come close. The electron-rich π-ring partially donates its electron density to the electron-deficient group and stabilizes the complex. Though it is commonly observed in the case of self-assemblies of other types of organic molecules (Jalani et al. 2013; Wang et al. 2010), in case of PAs, one has to rationally introduce both electron-deficient and electron-rich groups to achieve CT interaction (Bartocci et al. 2018; Shin et al. 2003). Nevertheless, the presence of CT interactions in peptide self-assemblies is scarcely observed. Another uncommon supramolecular interaction is the cation–π interaction. This particular interaction is the result of closed-shell cations interacting with neutral π systems. Cation−π interactions are omnipresent in biological systems and have been utilized by several proteins to stabilize the tertiary or quaternary structures (Dougherty 2013; Li and Mooney 2016). For example, phosphatidylethanolamine (PE) and phosphatidylcholine (PC) interact with interfacial Trp (Tryptophan) via cation–π interactions. These unusual interactions can be introduced into the PA self-assemblies through proper design. One such example is shown in Fig. 5.7. PAs, **64** and **65**, form nanotapes through CT interaction between electron-rich pyrene and electron-deficient NDI groups of **64** and **65**, respectively, in the aqueous medium (Singha et al. 2019a). A combination of CT and cation–π interaction was used to construct sheet-like morphology and hydrogel using **51** and a cationic NDI molecule (Pramanik et al. 2019a).
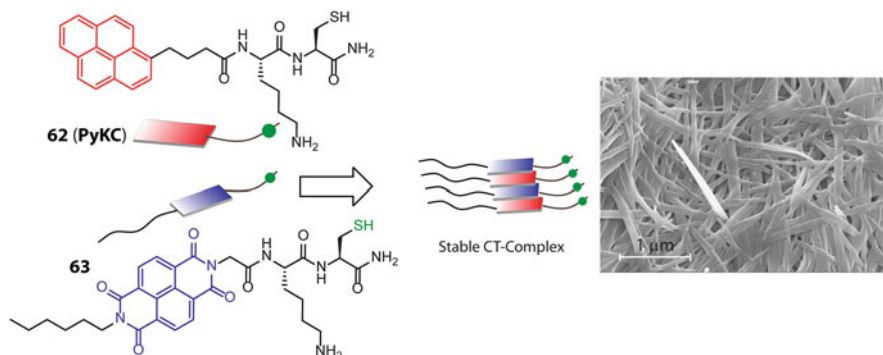
Fig. 5.7 Example of self-aggregation of two PAs through charge transfer interaction between pyrene and NDI groups. Adapted with permission from ref. Singha et al. (2019a). Copyright 2019 Royal Society of Chemistry

5.3.2 Nanoassemblies of PAs

The self-assembly of PAs is a hierarchical process. It is a concentration-dependent phenomenon. At a very low concentration, the molecules remain in monomeric state. Depending upon the sequence, the monomers may or may not form any secondary structure. For example, as the β-hairpin formation of MAX1 (**8**) is driven by intramolecular interactions between various segments of the molecule, the secondary conformation may be attained at this stage. However, if the attainment of the secondary structure depends on the interaction between two or more molecules, the secondary structure formation is not feasible at this low concentration. Nevertheless, as the concentration increases, the possibility of collision between molecules enhances. At this stage, two or more molecules assemble through non-covalent interactions to form smaller aggregates like dimer or trimer. This phenomenon can be called the nucleation process. Understandably, the secondary structures are also formed at this condition. With further increase in concentration, these smaller aggregates form relatively larger aggregates, and the aggregates elongate along the direction of the supramolecular forces. It may be in one, two, or even in three dimensions. The process continues with increasing concentration, and the aggregated structures get their final size and shape. Depending upon the surface functionalization of these aggregated structures, they remain solubilized in the medium or a phase separation may happen.

For PAs, one of the most common outcomes is gel formation. In the case of hydrogels, fibers are generally formed through elongation in one direction. With a higher concentration of PAs, the number of fibers in the system also increases, and they interact with each other and get interconnected to form the final network structures. The solvent molecules get trapped within the mesh of the network through cohesive forces. This results in immobilization of the solvents and the formation of gels. In the case of water as the solvent, the system is called hydrogel,
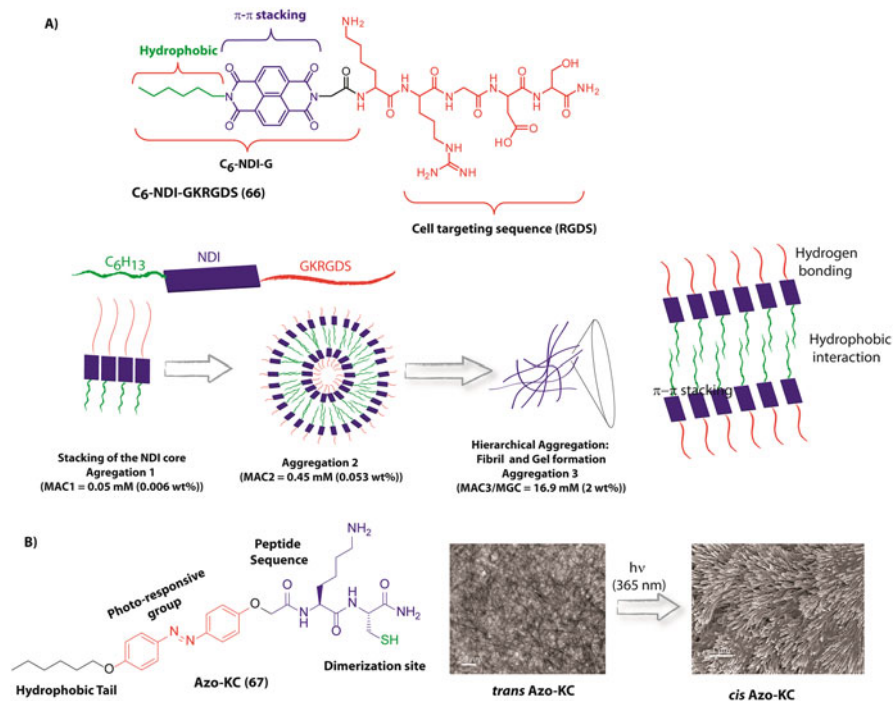
Fig. 5.8 (**a**) Stepwise aggregation of a lipidated PA. (**b**) Morphogenesis in response to light in case of an azo-functionalized lipidated PA. Parts of the figure adapted with permission from references (Das et al. 2020; Singha et al. 2017). Copyrights 2017 American Chemical Society and 2020 Royal Society of Chemistry

and the presence of any organic solvent in the system in principle generates organogel. It is worth mentioning that fibrous networks are not essential for the formation of gels; flake, sheet, and other types of morphologies are also found in PA-based gels.

The hierarchical assembly of PAs can be via multi-step where distinctly different types of aggregates are formed at various concentration levels. For example, C_6-NDI-GKRGDS (**66** Fig. 5.8a) forms very small aggregates (particle like) through the $\pi-\pi$ stacking between the NDI groups at a concentration above 0.05 mM (Singha et al. 2017). With the increase in concentration, the aggregation pattern changes to vesicle-like structures at and above 0.45 mM. At this stage, along with the $\pi-\pi$ stacking, hydrophobic interaction comes to prominence and stabilizes the bilayer structure of the vesicles. These vesicles further assemble to form fibers which eventually lead to forming a network for the hydrogel with a minimum gelation concentration (MGC) of 16.9 mM.

Though not very common, morphological transition from one nanostructure to another is also reported for PA-based gel systems (Panja and Adams 2019). As shown in Fig. 5.8b, the azo group containing PA (**67**, Azo-KC) forms hydrogel

showing a network of thin fibers (Das et al. 2020). As the hydrogel is irradiated with UV-light, *trans* to *cis* isomerization occurs in the azo group which changes the molecular arrangement within the gel state, and long rod-like morphology was observed. Moreover, the *trans-cis* isomerization also leads to syneresis as the hydrogel expels ~50% of the water of gelation and moves into a shrunken state.

Though nanofibers are the most common outcome of PA self-assemblies, several other nanostructures are reported, and a concise list of such morphologies is provided in Table 5.1.

5.3.3   Thermodynamic and Kinetics of PA Self-Assemblies

The synergistic effect of all the non-covalent interactions present in self-aggregating PAs determines the thermodynamic stability and minimum energy levels of the formed nanostructures (Fig. 5.9) (Wang et al. 2016a). However, the pattern of these non-covalent interactions can be modulated with various kinetic parameters such as temperature, pH, ionic strength, and solvents. In some cases, the assembled structures thus can be trapped in metastable states. Unless the kinetic parameters intervene, these metastable structures eventually grow into thermodynamically stable states. Thus, a competitive relationship between these two states (kinetic and thermodynamic) of assembly offers the possibility of transformation from thermodynamic to kinetic control. An understanding of kinetic control is necessary to create dynamic materials and out-of-equilibrium transient systems. The thermodynamic and kinetic control of PA self-assemblies and their final assembly structures are discussed in this section with the help of some selected examples. Meijer and Stupp studied the assembly pathway of a lipidated PA ($C_{16}V_3A_3E_3$) using solvents that either solubilize the PA (hexafluoropropanol, HFIP) or induce assembly (water). It was found that the assembly pathway could determine the supramolecular nanostructures and the assembly rate (Hendricks et al. 2017; Korevaar et al. 2014). With increasing HFIP concentration, smaller aggregates were formed, showing a lower extent of β-sheet character. Moreover, slower assembly kinetics was also associated with the increasing HFIP content. The study showed that 21% HFIP in water was the critical solvent composition that induced spontaneous nucleation of β-sheet containing fibers. These fibers did not disassemble with a further increase in HFIP content and thus are kinetically stable.

A similar PA ($C_{16}V_3A_3K_3$) was studied further to explore the energy landscape of its self-assembly pathway (Tantakitti et al. 2016). If we analyze the chemical structure of this PA, the aliphatic tail provides the hydrophobic interaction while the peptide sequence creates the head group. The major intermolecular forces that affect the assembly process are the hydrogen bonding among the β-sheet-forming segment V_3A_3 and the electrostatic repulsion between the positively charged Lys residues. The electrostatic repulsion works against the β-sheet formation as it prevents the molecules from coming close and forming hydrogen bonds. The repulsive force can be reduced by enhancing the medium's ionic strength, and such a situation

Table 5.1 List of various PAs discussed in this chapter, their self-assembled structures, and their reported applications

PA	Self-assembled structure formed	Application	Reference
2, 3	Network of interwoven fragments, stable macroscopic membrane	Tissue engineering	Liu et al. (2019); Zhang et al. (1993)
4	Well-ordered nanofibers, hydrogel	Cartilage tissue repair	Kisiday et al. (2002)
5	Nanofiber, hydrogel	Controlled release of functional proteins Tissue engineering	Koutsopoulos et al. (2009); Liu et al. (2013); Yokoi et al. (2005)
6	Interwoven fibers	–	Zhang and Altman (1999)
7	β-sheet-rich network of fibril, hydrogel	Antimicrobial	Geisler and Schneider (2012); Ju et al. (2020)
8–12	β-hairpin, nanofibers, hydrogel	Drug delivery, tissue engineering, antimicrobial activity	Kretsinger et al. (2005); Larsen et al. (2009); Rughani et al. (2009); Schneider et al. (2002)
23–26	Network, hydrogel	–	Nowak et al. (2002)
28	Cross-linked fibrous network, hydrogel	Biomineralization	Hartgerink et al. (2001)
29	Helical nanofibers, hydrogel	Synthesis of silica nanotube	Ahmed et al. (2013)
30	Helical nanofibers, hydrogel	–	Das et al. (2006)
31–33	Nanofibers, hydrogel	Synthesis of metal nanoparticles	Mitra et al. (2007); Mitra and Das (2008)
34–36	Twisted nanotapes to helical fibrils	Biomineralization	Dasgupta (2016)
44	Nanofiber, hydrogel	Dye adsorbing agent, water purifier, vitamin B12 carrier	Ray et al. (2007)
45	Nanofiber network, hydrogel	–	Smith et al. (2008)
46	Nanotube, hydrogel	–	Orbach et al. (2009)
47	Fibrous network, hydrogel	–	Orbach et al. (2009)
48	Helical nanofibers, hydrogel	–	Yang et al. (2007)
51	Fibrillar network, hydrogel	Picric acid sensing	Pramanik et al. (2019b)
52	Fibrillar network, hydrogel	Redox and photoresponsive material	Ikeda et al. (2011)
53	Nanofiber, hydrogel	Semiconducting material	Shao and Parquette (2010)

(continued)

Table 5.1 (continued)

PA	Self-assembled structure formed	Application	Reference
54	Nanoring (10% THF in water) Helical nanofiber (THF) Nanosphere (MeOH, HFIP, ACN, acetone) Nanofiber (CHCl$_3$)	Semiconducting material	Fletcher et al. (2007)
55	–	Active against MRSA and *E. coli* and the biofouling algae *Ulva linza* and *Navicula perminuta*	Hourani et al. (2011)
56	Nanotube	–	Hourani et al. (2011)
57	Columnar assembly	Preparation of protein nanotube	Fujimura et al. (2007)
58	Nanocapsule	Intracellular delivery	Chung et al. (2010)
59	Vesicles in SPA form	Drug delivery	Jiao et al. (2012)
60	Vesicles in SPA form	Switchable vesicle	Mondal et al. (2015)
61	Vesicles in SPA form	Transient vesicle	Dowari et al. (2019)
63	Vesicle (acidic pH) Rod (basic pH)	–	Versluis et al. (2009)
64	Tightly knitted fibrous network, hydrogel	Protect proteins from denaturing agents/effects	Singha et al. (2019c)
64 + 65	Nanoflakes, hydrogel	Organic methodology (asymmetric disulfide preparation)	Pramanik et al. (2019a)
66	Vesicle, nanofiber, hydrogel	Intracellular pH sensing	Singha et al. (2017)
67	Nanofibers, hydrogel	Syneresis, dye removal	Das et al. (2020)
68–70	Monolayer films prepared	Cell adhesion and proliferation	Pakalns et al. (1999)
71	Nanoparticles	Targeted accumulation and prolonged retention in heart tissue after myocardial infarction	Nguyen et al. (2015)
72 + 73	Nanofibers, composite hydrogel	Diabetic wound healing	Senturk et al. (2017)
74	Nanofibers, hydrogel	*p*-xylene sensing	Singha et al. (2019b)
75	Micelle	Artificial hydrolase	Nothling et al. (2020)
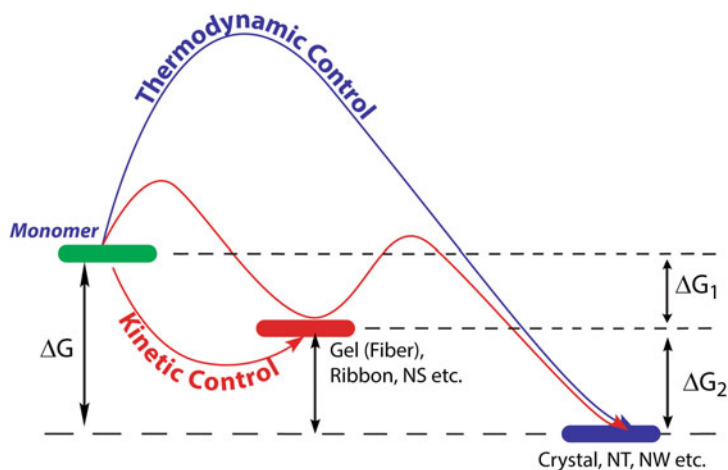
Fig. 5.9 Graphical presentation of the self-assembly processes under thermodynamic and kinetic paths. The final morphologies like nanotubes (NT) and crystal nanowire (NW) remain in the minimum free energy state under thermodynamic control (blue solid line). The structures can be trapped in a metastable state, including gel (fibers), nanosphere (NS), ribbon, and NW upon intervention of kinetic control-like pH, temperature, etc. (red solid line). These metastable structures can further grow into the thermodynamically favored state (red dashed line). The relative energies shown here are not accurate and may vary from system to system. All structures probably interconvert under certain kinetic controls. Adapted with permission from reference (Wang et al. 2016a). Copyright 2016 Royal Society of Chemistry

will favor the β-sheet formation. It was noticed that the PA behaved differently at the critical ionic strength (Ic) of 6 mM, independent of whether the ionic strength was caused by the PAs themselves or by the addition of salt. When the thermodynamic states are obtained by annealing the PA solution, below the I_c, monodispersed fibers of ~150 nm were obtained (Fig. 5.10a right). However, above the I_c, very long fibers were found exclusively (Fig. 5.10b left). The annealed samples can be perturbed away from their thermodynamic condition through the addition of salt or dilution. This leads to a change in the β-sheet character (Fig. 5.10b). Though no immediate change in the fiber structure was noticed, both fibers finally returned to the thermodynamic state. The long fibers were stable for days but, upon heating, converted to short fibers. This observation suggests a kinetically trapped state with an intermediate barrier to conversion. The short fibers grew into the thermodynamically stable long fibers over days suggesting a metastable state with a low barrier to conversion. Overall, this study defines two distinct energy landscapes dependent on the ionic strength of the solution, as depicted in Fig. 5.10c.

Quoting Stupp et al., "among the four major energy contributions, hydrogen-bonding, $\pi - \pi$, and hydrophobic interactions all tend to promote the aggregation of PA molecules, whereas electrostatic repulsion favors disassociation of PA molecules. The final properties of assemblies reflect a delicate balance of each energy contribution." (Cui et al. 2010b). The same group also obtained a "phase diagram" of
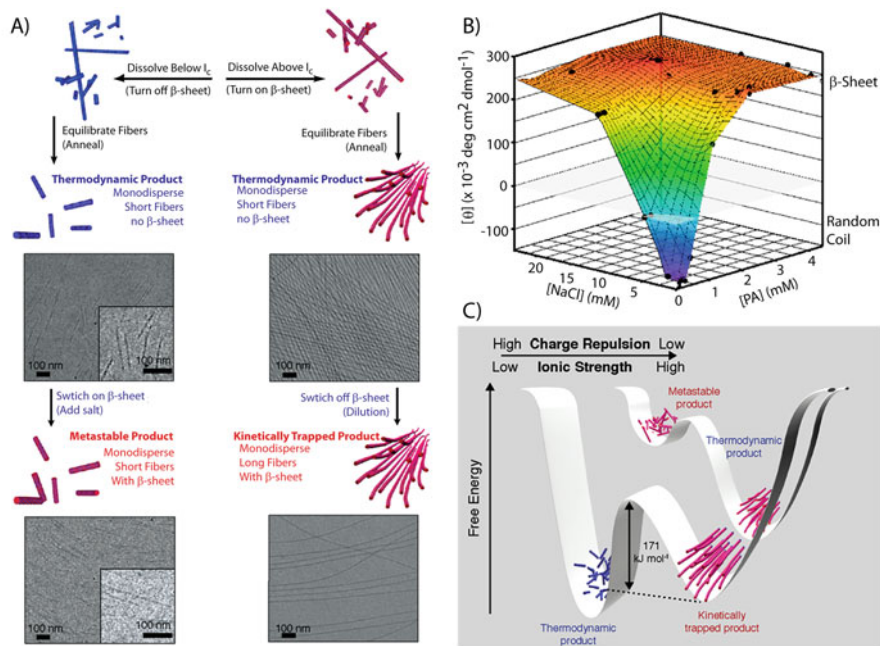
Fig. 5.10 (**a**) Schematic presentation and representative cryo-TEM micrographs of nanostructures obtained following assembly pathways initially below (left) and above (right) the Ic by first annealing to form the thermodynamically favored product and then adding salt (left) or diluting (right) to obtain the non-thermodynamic structures. (**b**) Map of CD signal at 202 nm plotted as a function of PA and salt concentrations. (**c**) Schematic representation of the free energy landscapes of PA assemblies below and above the critical ionic strength (front and back, respectively). Adapted with permission from reference Tantakitti et al. (2016). Copyright 2016 Nature Publishing Group

PA assembly process using molecular dynamics (MD) simulation (Cui et al. 2010a; Velichko et al. 2008). For this calculation, hydrogen bonding and hydrophobic interactions are considered. The analysis clearly shows that pure hydrophobic interaction of lipidated PAs leads to micelle-like aggregates, whereas pure hydrogen bonding interaction results in 1D β-sheets. However, the ultimate assembly kinetics may show the synergistic effect of these supramolecular interactions.

The effect of thermodynamic and kinetic parameters on the final structures of the PA assemblies can be highlighted with the example of a bola-amphiphile (**54**) that contains two PhePhe units connected by a PDI group in the middle (Ahmed et al. 2017). In this case, solvent polarity plays a crucial role in dictating the thermodynamic or kinetic pathway. Water is a bad solvent for **54** as the PA is insoluble water, while THF can be considered as a good solvent for the same. In THF, right-handed helical fibers were formed. On increasing the polarity of the medium to 10% THF in water, nanorings were obtained along with a switch in the helicity to left-handedness (Fig. 5.11). Analytical studies in combination with DFT calculations revealed that in both cases, the initial nucleation was kinetically controlled. However, in the case of
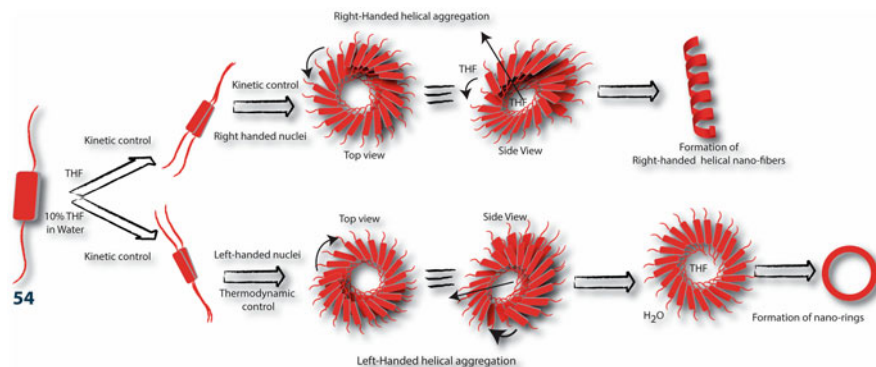
Fig. 5.11 Solvent polarity-driven kinetic and thermodynamic control of a PA self-assembly process. Nonpolar solvents lead to helical nanofibers through a kinetically controlled assembly process. Thermodynamic control of the aggregation pathway in case of polar solvent results in nanoring-like structures. Adapted with permission from reference (Ahmed et al. 2017). Copyright 2017 Nature Publishing Group

10% THF-water, the further aggregation process (elongation) is strictly governed by thermodynamic parameters. The differential solubility of the PA in these two solvents restricted the elongation of the nuclei into fibers after a critical length, and thermodynamic stability of the collapsed fibers was obtained via formation of ring-like morphology. On the other hand, the elongation of the nuclei followed the kinetic path in the case of THF, and the final helical fibrous morphology was observed. Further studies with **54** revealed a clear relation between the nanostructures and the solvent polarity. In nonpolar solvents ($CHCl_3$, THF), the PA tends to form fibrous aggregates, while in polar solvents like HFIP, MeOH, ACN, and acetone, spherical aggregates were formed (Ahmed et al. 2018).

5.3.4 Stimuli-Responsive Assemblies of PAs

Materials that change their properties in response to stimuli or environmental changes are extremely important for biomaterial applications. For example, hydrogels loaded with therapeutic molecules may release the cargo only when or where required in response to an overexpressed protein or local change in the pH at the infected tissue. The stimuli-responsive systems allow us to create newer and more effective soft materials, and their applications are not necessarily limited to the therapeutic purpose. PA-based systems can be made responsive by a simple manipulation in the sequence. In this section, a brief overview of stimuli-responsive PAs is provided with the help of some recently reported examples.

5.3.4.1 pH Responsive

pH-responsive systems are commonly used for targeted drug release to cancerous tissues/tumors in response to the slightly lower pH (~6.5) in the tissue microenvironment compared to healthy tissues. One of the most popular approaches to get pH-responsive systems is manipulating charged interaction between pH-sensitive amino acids such as Lys, Arg, His, Asp (Aspartic acid), and Glu in the PA backbone. For example, MAX1 (**8**) showed pH-induced sol-gel transitions (Schneider et al. 2002). Under the alkaline condition, owing to partial deprotonation of Lys, β-hairpin conformation is adopted by MAX1 that leads to the formation of an injectable hydrogel. When exposed to acidic medium, all the Lys residues get protonated resulting in unfolding of the β-hairpin and the gel disruption. Though the high pH (~9) required for hydrogelation of MAX1 makes it unsuitable for biological application, screening the charged Lys residues by increasing ionic strength decreases the gelation pH to physiological conditions (Kretsinger et al. 2005). Hydrogel of MAX1 in buffered (pH 7.4) saline solution was found to be cytocompatible and showed excellent cell adhesion and proliferation for fibroblast cells, making it a suitable candidate for drug delivery.

Entrapment of drug in the PA network often interferes with stimuli responsiveness, resulting in unsatisfactory release kinetics. To address this issue, Zhong et al. prepared a drug-reinforced hydrogelation strategy. Electrostatic interaction between the Asp residue of Nap-GFFYGRDH (Nap = Naphthalene) and the drug molecule, doxorubicin (DOX), lowers the MGC and strengthens the self-assembly as well as the pH responsiveness of the hydrogel (Mei et al. 2019). The sheer-thinning hydrogel showed a two-step release of the drug. The protonation of His at the acidic pH (6.5) around the tumor leads to partial disruption of the nanofibers. These nanofibers are later internalized into the cancer cells through integrin receptor-mediated endocytosis. The nanofibers are entirely disrupted by the even lower pH (5.5) at the endosome to release the drug.

(RATEA)$_4$ or RATEA16 is another example of pH-responsive PA, which forms elastic and thixotropic hydrogel (neutral pH) (Zhao et al. 2008). The charged residues of the PA can easily be regulated through the adjustment of the pH of the medium. At neutral condition, the hydrogen bonds among the peptide's antiparallel sheets, and electrostatic attraction between the Arg and Glu residues leads to the formation of the hydrogel. At acidic pH, charge neutralization results into dissolution of the hydrogel as repulsive interactions between the Arg residues dominate. pH-sensitive systems can also be created by utilizing acid labile groups like hydrazone, imine, oxime, amide, acetal and ketal, ether, and ortho-ester bonds. The self-assembled nanostructures formed by PAs containing any of these bonds can be disrupted with a subtle change in the pH. For example, 4-formylbenzoic acid (FBA) capped short peptides, FBA–GFFYGRGD and FBA–GFFYGRGE, were reported by Yang et al. (Ren et al. 2014). These peptides cannot form hydrogel under physiological condition, but the presence of an amine-functionalized drug, gemcitabine, spontaneously leads to the formation of Schiff base and hydrogel.

Enhanced hydrophobicity of the drug-conjugated peptides is responsible for self-aggregation. The hydrogels showed excellent pH-triggered cancer inhibitory activities on pancreatic cancer cells, and the imine linkage in both the conjugates did not attenuate the drug's efficacy.

5.3.4.2 Redox Responsive

Maintaining an optimal intracellular redox balance is important for the proper functioning of physiological processes like cell metabolism, proliferation, and differentiation. Reactive oxygen species (ROS) and antioxidants produced in normal cells help maintain this balance. However, cancer cells disturb the balance by regulating ROS generation due to the decreased metabolic rate and hypoxic environment. To counter the malicious effect of ROS, cancer cells produce excess amounts of reduced glutathione (GSH), an antioxidant. The higher level of GSH in malignant tumors opens up the possibility of creating therapeutic materials with redox-responsive character. GSH is an efficient disulfide bond breaker. Thus, systems containing disulfide linkages can be created where the self-assembly process can be controlled through the breakage of the disulfide linkages by GSH.

PyKC (**64**) is an example of GSH-responsive PA. Under neutral to basic conditions, the thiols of Cys residues get connected through disulfide linkages and form the PyKC dimer that self-assembles to form a very tightly knitted network of fibers and consequent hydrogel (Singha et al. 2019c). The hydrogel remains insoluble in water, buffers of pH 3–11, and various water-miscible organic solvents for more than a year. However, when treated with GSH, the hydrogel breaks down within a few minutes. Enzymes trapped inside this hydrogel showed strong resistance against various denaturing agents as they are shielded from all these agents as the hydrogel does not allow any solvent or solute exchange. In addition, the limited space inside the tight network does not allow the proteins to unfold in response to denaturing effects like heat. Once treated with GSH, the proteins came out of the entrapment and showed activity similar to the native proteins.

H_2O_2 is another redox-active agent found in biological systems. In certain cancers and cardiovascular diseases, enhanced production of H_2O_2 is observed. H_2O_2-responsive systems thus can be fruitful for efficient drug delivery at these sites. A selenide-containing PA hydrogelator is reported to self-assemble into a nano-fibrillar network at physiological pH (Miao et al. 2013). H_2O_2-mediated oxidation of selenide to the corresponding selenoxide affects the amphiphilicity of the product and results in a morphogenic transformation from nanofibers to micelles. Interestingly, the reversal of the morphology can be done by reducing the selenoxide with vitamin C. The reversible and interconvertible morphogenesis in response to biological redox could be useful for therapeutic applications.

5.3.4.3   Biocatalyst Responsive

Another important stimulus that can control the self-assembly of PAs is enzymes. A non-assembling precursor of a PA can be biocatalytically converted to a self-assembling PA. The process is called enzyme instructed self-assembly or EISA (Gao et al. 2020). For example, PA (Nap-FFGEY(H$_2$PO$_3$)-OH) prepared by Xu et al. remains in the solution state. Once injected subcutaneously, due to the presence of alkaline phosphatase, the phosphate group gets removed from the peptide to generate Nap-FFGEY-OH (Yang et al. 2006). This non-phosphorylated version of the PA is an efficient hydrogelator, and the hydrogel forms in situ under the skin. Interestingly, upon treatment with kinase enzyme, the PA again gets phosphorylated, leading to the sol state. A similar strategy has been applied to create a luminescent hydrogel where a non-gelling PA (Fmoc-FFY(H$_2$PO$_3$)-OH) is mixed with a non-fluorescent phosphorylated precursor of a fluorophore (Hai et al. 2017). When treated with ALP (Alkaline Phosphatase), the dephosphorylation process leads to the generation of the gelator PA (Fmoc-FFY-OH) and the fluorophore. The gelator PA self-assembles to form hydrogel, and the fluorophore gets trapped in the hydrogel network to develop a highly luminescent hydrogel. Using enzyme triggers, small precursor peptides can also be converted to a large self-assembling PA. A "dipeptide lego" (KL-ethyl ester) upon treatment with α-chymotrypsin forms mixture of oligomers with alternate K and L residues (KL)$_n$. This triggers rapid sol-gel transition in the system. Under alkaline condition, the resulting mixed chain oligomers self-assemble into β-sheets. These β-sheets further assemble through intermolecular hydrogen bonding to form physically entangled nano-fibrillar networks. A plethora of enzyme-responsive PAs has been reported till date (He et al. 2018; Thornton et al. 2013). Recent review articles can be consulted for further details (Du et al. 2015; Shy et al. 2019).

There are various other stimuli-responsive PAs reported in literature. Some of the commonly used triggers are temperature, light, metal ions, etc. (Falcone and Kraatz 2018; Zhang et al. 2020a, b).

5.4   Application-Specific Design and Execution Guideline

With the knowledge gathered over the last few decades in supramolecular assemblies and their mechanism, it is now possible to rationally design systems for specific applications. Understandably, PA-based systems' applications are in general aimed toward biomedical or therapeutic purposes. Thus, a stepwise strategy (Fig. 5.12) to design PAs for therapeutic application is outlined in this section.

The process of design begins with the understanding of the targeted application. For example, for tissue engineering, one has to design PA-based systems where the PAs possess sequences from the matrix protein to incorporate cell-adhesive properties. However, that is not the case for antimicrobial applications. In this case, the
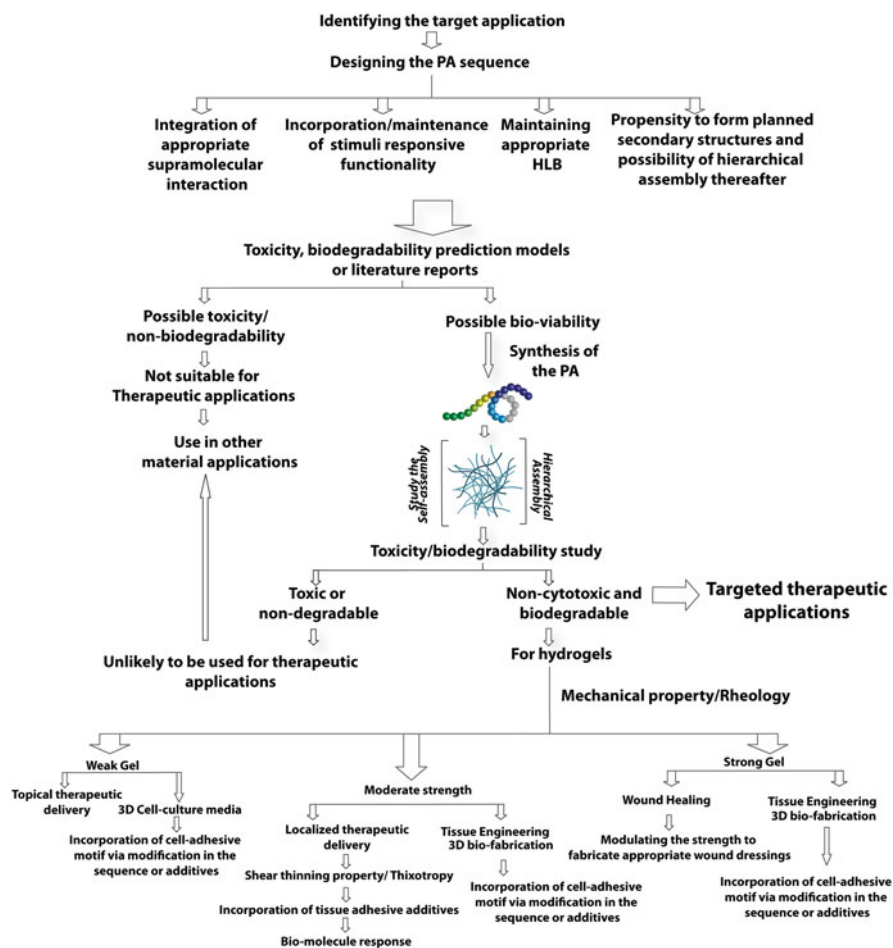
Fig. 5.12 Flow chart of design principles that can be followed to prepare PAs for targeted therapeutic applications

peptide segment should possess the ability to rupture the microbes' membrane. Thus, in general, incorporating several cationic residues like Arg or Lys is preferred. Based on this knowledge, PAs should be designed. While designing the PA, one needs to take care of a few more factors. First, appropriate HLB is incorporated by the attachment of hydrocarbon chain or hydrophobic amino acid residues. Next, to get a stronger assembly, appropriate supramolecular forces must be available in the PA structure. Again, it is important to consider what kind of assembly is required for the planned application. For drug delivery vehicles, the assembly could be of vesicular nature or a thixotropic hydrogel. Thus, to prepare a vesicle, understandably, lipidated PAs should be designed while, for thixotropic hydrogel, it could be of

any of the classes. Stimuli-responsiveness is one important criterion for most of these applications. The main question here is what are the stimuli for the planned application? Incorporating the responsive group or modulation in the peptide sequence depends on the stimuli. For GSH, the PA must possess disulfide linkages. On the other hand, light-responsive systems can be prepared by incorporating groups like Azo, nitroveratryl, etc. Self-assembly of PAs greatly depends on the secondary structure that the PA molecule adapts. Thus, one has to take care of the propensity to form planned secondary structures and the possibility of hierarchical assembly thereafter while designing the PA.

For any therapeutic application, the material used must be non-toxic and biocompatible. Thus, it is important to identify the possible toxicity of the designed PA. As prepared from amino acids, peptides are generally nontoxic. However, there are sequences like peptide toxins that show extreme toxicity. Moreover, unnatural amino acids and other groups are conjugated in designer PAs to incorporate various factors like stimuli-responsiveness, propensity to self-assembly, etc. Thus, one has to take care of the toxicity of the PA at the design stage. Though not guaranteed, this can be done using various software and online platforms available to identify the probable toxicity in a peptide sequence (Pavan and Worth 2008). Additionally, literature reports on the cytotoxicity of similar sequences as well as functional groups (which are incorporated) should also be consulted before further processing of the PAs. There are several ways to improve peptides' therapeutic index, and a detailed discussion on this issue can be found in the reference (Gupta et al. 2015).

Once the PAs are designed, they need to be prepared. Synthesis of PAs is done using solid-phase or solution-phase peptide synthesis protocols or a combination of both. The study of aggregation property is the next important step as it dictates the fate of the materials. An excellent document on self-aggregate preparation from peptides was published by Adams et al. (Wang et al. 2012). Choosing the right solvent (buffer), the mixing and incubation process is essential. A common practice is to dissolve the peptide in a buffer of pH where it is soluble and then adjust the pH of the system by the addition of acid or base to lower the solubility of the peptide. Due to the lessened solubility, the molecules tend to aggregate. However, it has been shown that a sudden change in pH leads to irregular aggregation, and the aggregation pattern might not be possible to reproduce (Adams et al. 2009). A slower change in the pH is thus preferred. For example, the introduction of glucono-δ-lactone (Gdl) in the system produces protons through slow hydrolysis in the background. Thus, the dissolved molecules (at higher pH) slowly get protonated, and consequently, aggregates are formed uniformly (Adams et al. 2009). Dissolving the molecules in buffer by heating and then allowing the solution to cool down to room temperature to induce aggregation is another common way. Another typical method to induce aggregation is to dissolve the material in small quantities of water miscible organic solvents (good solvent) followed by addition of buffer/water (bad solvent). As the solubility of the peptide in aqueous medium is low, the molecules start aggregating. The most common outcomes of this process are gel formation (Draper and Adams 2017). It is highly debatable whether these systems can be called hydrogels or not. On many occasions, these gels are projected as soft materials for therapeutic

applications. However, it is very unlikely that theses gels can be used for any in vivo applications unless the used organic solvent is biocompatible like ethanol. Other methods used to form the aggregates include dissolution in solvent and incubation for a long period, sonication, etc.

Analyses of these PAs and their aggregates for cytotoxicity and biocompatibility are essential at this stage. One common approach is to study the MTT (3-(4,5-dimethylthiazol-2-yl)-2,5-diphenyltetrazolium bromide) assay (Patravale et al. 2012) on different cell lines and check the viability with time and concentration. Though several methods are used for initial screening, MTT assay is the most prevalent choice owing to its ease of execution, cost-effectiveness, and relatively accurate results. The nontoxic materials can be utilized for biomedical applications, whereas the toxic materials can be routed for other applications (conductive material, template for nanofabrication, catalysis etc.).

Characterization of the aggregated structures/soft materials and the study of the aggregation mechanism are the essential next steps. Understanding the aggregation pattern and its formation is important to utilize them effectively for any application. The characterization may involve several spectroscopic and analytical tools based on the system. However, morphological characterization using electron microscopes (TEM, SEM, AFM, etc.) is essential to know the nanoscale structures formed by the PAs. In this regard, a common practice is to cast small portions (few microliters) of the solution or gel on a surface or TEM grid and dry it under ambient conditions. Because the aggregation is a concentration-dependent process, as the solvents evaporate, the effective concentration of PA in the droplet increases, which may lead to a different morphology from the actual structures formed initially (Adams 2018). The best solution for this problem is to use cryo technology (cryo-TEM), but that is not feasible all the time, mainly due to the non-availability of instruments. Thus, the described protocol is followed in most cases. The morphologies obtained are assumed to be the closest possible structures formed during the studied self-assembly. One alternative approach to tackle this situation could be instantly freezing the casted drops in liquid nitrogen followed by careful drying using lyophilizer (freeze dryer). This may eliminate the possible error. However, detailed analyses of systems using this protocol need to be carried out to confirm the same.

In case of gel formation, the mechanical characterization using rheology is essential to finalize the application of the aggregates. Typically, the *storage modulus* (G') and *loss modulus* (G") are recorded as functions of oscillatory frequency, oscillatory strain, and time (Yan and Pochan 2010). These parameters qualitatively represent the stiffness of gels. The linear viscoelastic regions, relaxation time scale, and gelation kinetics can be determined through these preliminary rheological measurements. Based on the mechanical stiffness, gels can be classified into three different categories, (a) weak gel (0.1–1 kPa), (b) moderately strong gel (8–17 kPa), and (c) strong gel (34 kPa) (Fig. 5.12) (Li et al. 2018). Though stiffness is not the only parameter to be looked at, the application can be selected based on these mechanical properties. For example, in wound healing dressings, rigid or semi-rigid gels are preferred to construct the dressing, while soft hydrogels are typically used for pain reliever gels. Similarly, as it has been reported earlier, stem cells

undergo stiffness-directed differentiation into neuronal, chondrogenic, and osteo-genic outcomes on soft, stiff, and rigid hydrogels, respectively; the appropriate hydrogel can be decided based on their stiffness (Alakpa Enateri et al. 2016; Engler et al. 2006). It is worth mentioning that the list of analyses for characterization of the aggregates of PAs does not end here. While applying for a particular purpose, several other studies may become essential. However, the mentioned techniques are pre-requisites before using these self-aggregated PA-based materials for any application. The flowchart provided in Fig. 5.12 can be considered as a basic guideline for this purpose.

5.5 Applications of PA Assemblies

5.5.1 Tissue Engineering

Tissue engineering is one of the latest scientific advancements in biomedical science in the last couple of decades. To regenerate tissues artificially, extracellular matrices (ECM) are created where cells are provided with an environment appropriate for regeneration, induction, and development of neo-tissues. Tissue engineering are directed by biodegradable scaffolds that mimic the natural state of the tissue by forming a three-dimensional surrounding, which is biocompatible and non-immunogenic and acts as artificial matrices to support and direct regeneration. PA self-assemblies offer excellent options to create these artificial scaffolds. Several detailed reviews on PA-based tissue engineering scaffolds are available in the literature (Ding et al. 2020; Yang et al. 2020).

For an artificial scaffold, it is important to provide adequate support for the cells to adhere properly. In nature, this is done by the extracellular proteins like laminin, bone sialoprotein, fibronectin, collagen, vitronectin, elastin, etc. (Zhu and Marchant 2011). A standard strategy is to use short peptide fragments from these ECM-proteins and attach them to the self-assembling sequences. These peptides are called cell-adhesive peptides (CAP). Tirrell and co-workers created some doubly lipidated PAs (68–67, Fig. 5.13) using linear RGD motifs (Pakalns et al. 1999). Melanoma and endothelial cells spread in a concentration-dependent fashion on Langmuir-Blodgett films of the looped PA (70). Unselective spreading was observed for the 68 (carboxyl-coupled), while no spreading was found in 69 (amino attached). Since then, many examples have surfaced where RGD or similar ECM-protein fragments are used to create PAs for tissue engineering purposes. Though not as popular as RGD sequence, other CAP sequences like VAPG (elastin); YIGSR, KQAGDV, and REDV (fibronectin); LGTIPG, IKVAV, PDGSR, LRE, LRGDN, and IKLLI (lamnin); and DGEA and GFOGER (Collagen) are also used to create peptide-based artificial ECM.

RADA16 peptides (5) are among the most studied PAs for 3D scaffold supporting cell differentiation. These ionic peptides are able to self-assemble spontaneously into cross-linked network structures that mimic ECM. For example, three different
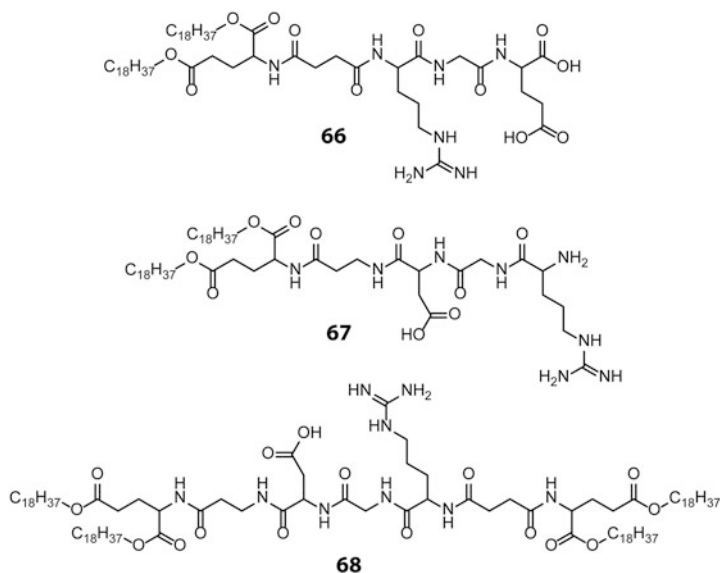
Fig. 5.13 Chemical structures of some RGD containing lipidated PAs used for cellular adhesion and proliferation studies

peptide hydrogels were used to create a 3D cell environment for human adipose stem cells through C-terminal functionalization of RADA16 peptide with biologically active peptide sequences (SKP, FHR, PRGD) (Liu et al. 2013). EAK16 (3) is another classic example of PAs that have been used for tissue engineering. EAK16 self-assembles through ionic interactions resulting into β-sheet formation, which grow further to form nanofibers and hydrogel. The D-version of the peptide D-EAK16 proved to be an effective artificial ECM for the proliferation of entrapped-SMMC7721 cells (Luo et al. 2013). Recently, several other modified EAK PAs have been reported that provided an excellent platform for cell-proliferation and tissue engineering (Liu et al. 2019). RADA, FEFEFKFK, and other short peptide self-assemblies (hydrogels) have successfully been used in bone tissue engineering (Castillo Diaz et al. 2016; Chowdhuri et al. 2021; Misawa et al. 2006).

5.5.2 As Delivery Vehicles

Delivery of therapeutic agents to the desired location inside the human body in a non-invasive mode is an uphill task. The therapeutic agents could be drugs, proteins, hormones, or genes. Nanocarriers with the potential to become internalized within the cells are desired. The purpose of these carriers is not only to protect the therapeutic agents but also to deliver at the right place to minimize side effects and

loss of the therapeutic agents in the process. PA-based systems appeared to be an excellent platform to achieve this targeted delivery of therapeutic agents.

The amphiphilic nature of PAs allows them to form membrane mimicking systems like micelles or vesicles that can entrap molecules otherwise insoluble in water. These vehicles can carry the entrapped drug to a specific location. The surfaces of the vehicles (nanocarriers) can be decorated with groups that selectively bind with the receptors present at the cell surface. The vehicle thus can locate the target cells/tissue and deliver the trapped therapeutics in response to stimuli present at the site or externally applied. In this section, we discuss some of the selected PA-based delivery vehicles.

Stupp et al. showed enhanced aqueous solubility of a hydrophobic chemotherapy agent, camptothecin (CPT), when a self-assembling PA ($C_{14}H_{29}CO$-$A_4G_3E_3$-COOH) nanofiber was used to encapsulate the drug (Soukasene et al. 2011). In vitro studies with human breast cancer cells using the nanofiber encapsulated CPT showed enhanced antitumor activity of the drug. Additionally, the treatment with CPT-encapsulated PA nanofibers showed significant inhibition to the tumor growth when treated in a mouse orthotopic model of human breast cancer.

Folate receptors are usually overexpressed in the epithelial or nonepithelial malignant tumor cells, and their folate binding ability has been exploited extensively to create targeted drug delivery vehicles. In a recent report, folate groups are grafted on a PA ($C_{15}H_{31}CO$-$V_3A_3K_3$)-based microparticles using the Lys linker to target the cells overexpressing folate receptors. The prepared microparticles contained a doxorubicin (DOX)-conjugated alginate as the core and a shell of the PA nanofibers decorated with folate groups at the surface. The system showed ~60fold higher cytotoxicity against MDA-MB-231 breast cancer cells than similar particles without the folate groups.

Enzymatically controlled self-aggregation and morphogenesis is a promising way to create therapeutic material-based delivery vehicles. The advantage here is that the self-aggregation happens inside the body in response to the enzymes present at site. A PA (71, Fig. 5.14) drug carrier capable of target accumulation and prolong retention in heart tissue was reported by Christman (Nguyen et al. 2015). Peptide sequences specific for the recognition of MMP-2 and MMP-9 were attached to a polymeric backbone that creates the PA. Nanoparticles formed by 71 respond to the upregulation of MMP-2 and MMP-9 in acute myocardial infarction. This creates a scaffold which retained in the tissue. Figure 5.14 shows that the carrier can differentiate MMP2 from MMP9 which results in morphogenesis from micellar nanoparticles to fibrous network-like scaffold. The results pave the way for a minimally invasive protocol to deliver a therapeutic scaffold to the acutely infarcted myocardium.

PA-based hydrogels can also be used as a delivery vehicle. A plethora of reports is available where PA-based hydrogels are shown to be efficient stimuli-responsive delivery vehicles. However, there are some fundamental issues which need to be addressed. (A) Hydrogel-based delivery vehicles are applicable only when they show injectability property. Understandably, a drug-loaded hydrogel cannot be introduced into the blood vessels. Thus, injectable hydrogels are also limited to
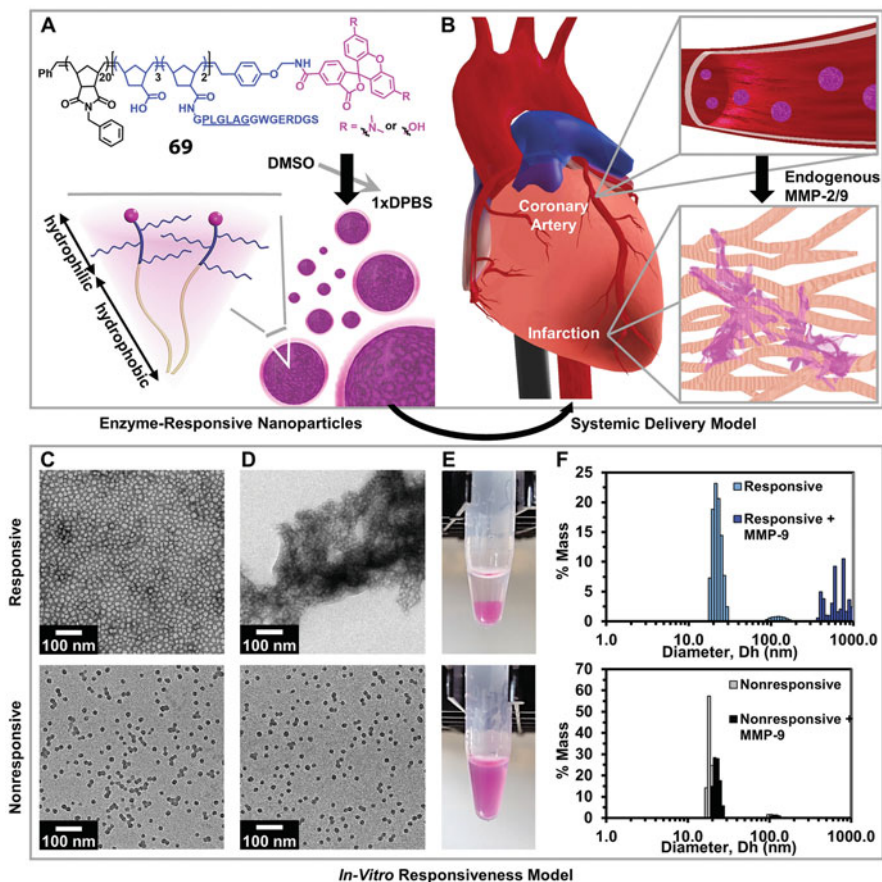
Fig. 5.14 Targeted, accumulated, and retained within an acute myocardial infarction. (**a**) Chemical structure of the dye-labeled brush peptide–polymer amphiphile (**71**) containing MMP-2- and MMP-9-specific recognition sequences. (**b**) Graphical representation of the PA nanoparticles freely circulating in the bloodstream upon systemic delivery. (**c**) Responsive (top) and non-responsive (bottom) nanoparticles are monodisperse micelles with a diameter of 15–20 nm, and (**d**) upon activation, only responsive nanoparticles form an aggregate-like scaffold. (**e**) The corresponding images of PA nanoparticle solutions following activation. (**f**) Dynamic light scattering of PA nanoparticles before and after MMP activation. They are adapted with permission from reference (Nguyen et al. 2015). Copyright 2015 WILEY-VCH Verlag GmbH& co

local delivery. Drug-loaded hydrogels are injected into the tumor, and the drugs are released in response to the stimuli present at the tumor site. However, enzymatically controlled hydrogelation of PA can be used for targeted delivery. In these cases, a precursor for the gelator can be injected, which forms a hydrogel upon enzymatic transformation to the gelator molecules. (B) Reports are available on hydrogel systems decorated with molecules that can bind with overexpressed receptors at tumor tissues. However, for hydrogel-based delivery systems, the targeting is not

essential as they are injected into the tumor. (C) Another important point is related to the commonly used in vitro drug delivery experiments reported on several occasions. In a typical experiment, buffers or the release medium are added on top of drug (or model dye)-loaded hydrogels prepared in a glass vial. The supernatant liquid is analyzed from time to time to find the cumulative release. However, these experiments are erroneous as only the top surface of the hydrogel remains in contact with the release medium and the diameter depends on the vial/container used. As the surface area of contact is not taken cared of, in general, the obtained released data do not represent the actual release profile. Nevertheless, such experiments certainly show the ability of the hydrogels to release the trapped molecules/drugs. There are reports where injectable PA-based hydrogels are successfully used as localized delivery vehicles. The case is exemplified with the help of one report by Jin et al. published recently. A well-studied PA hydrogelator (RADA)8 was conjugated with an extremely potent anticancer agent, Melittin, to prepare a conjugated peptide hydrogelator, Melittin-(RADA)8 (Jin et al. 2018). Thixotropic hydrogels can be prepared from this PA at physiological pH. DOX-loaded hydrogel was injected into B16-F10 tumor-bearing mice, and the presence of melittin dramatically increased the antitumor efficacy and immune responses and reduced the side effects. Dual delivery from the hydrogel causes a sustained antitumor effect along with an increased immunity, decreased immunosuppression, and activation of effector T cells.

5.5.3   Wound Healing

Another important application of PA self-assemblies is in the area of wound healing. It is an important biological process that involves the replacement of injured tissues, restraining the skin function, and maintaining internal homeostasis. To heal wounds, dressings are required that are moist and conducive to healing. PA-based hydrogels show potential for wound healing dressings, and several PAs have been tested for this purpose. Here, we discuss a few relevant and recent examples.

Burn wound is extremely challenging to cure. Hauser et al. have reported the superior effect of short peptide-based hydrogels as a dressing for burn wounds over the commercially available Mepitel®, a silicone-coated polyamide net (Loo et al. 2014). Dressings prepared using two non-toxic amphiphilic peptides (Ac-ILVAGK-NH_2 and Ac-LIVAGK-NH_2) were used as dressings. Excellent epithelial and dermal regeneration in the absence of exogenous growth factors was observed. 86.2% and 92.9% wound closures were seen, respectively, for these two peptides, whereas only 67.2% healing was observed for Mepitel®.

For diabetic patients, chronic wounds are common as diabetes involves endothelial dysfunction. For diabetic patients, these wounds may lead to the risk of limb amputation. Dressings mimicking ECM signals are helpful in the recovery of such diabetic wounds as they provide a conducive environment for blood vessel formation and are capable of modulating the immune system. A heparin-mimetic nanofiber forming composite hydrogel of two PAs (GAG-PA (72) and K-PA (73), Fig. 5.15)
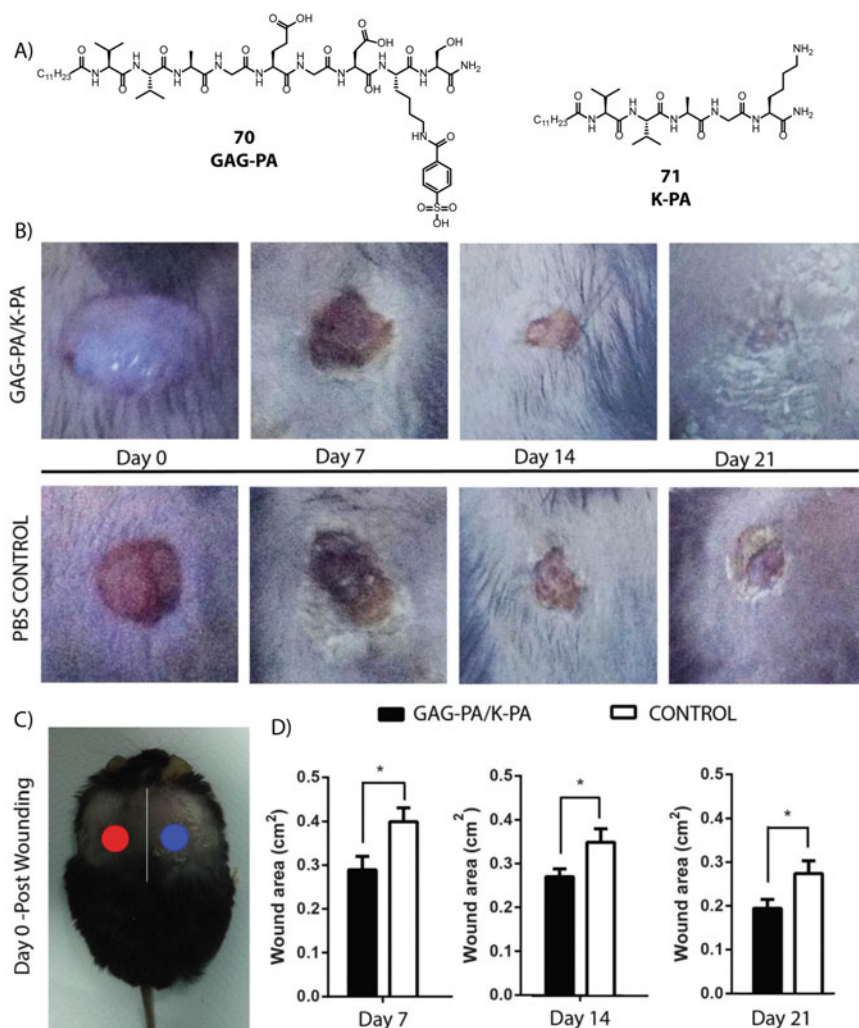
Fig. 5.15 Heparin-mimetic PA nanofiber treatment speeds up the recovery of diabetic wounds. (**a**) Chemical structures of the PAs used for diabetic chronic wound treatment. (**b**) Representative pictures showing the closure of wounds in **72/73** and PBS-treated animals on different days. (**c**) Two wounds (red and blue circle) were created through biopsy punches at the dorsal skin of db/db mice on day 0. (**d**) Wound area measurements of skin wounds treated with and without **72/73** nanofibers. Results show nanofiber-treated wounds close faster than control animals. Figure adapted with permission from reference (Senturk et al. 2017). Copyright 2017 Royal Chemical Society

was used by Tekiney et al. on full-thickness excisional in a diabetic mouse model (Senturk et al. 2017). The heparin-mimetic PA-gel supported tissue neovascularization and increased collagen deposition. The PA nanofibers also promote the expression of alpha-smooth muscle actin (α-SMA) and eliminate the

presence of interleukin-6 (IL-6) and tumor necrosis factor-alpha (TNF-α) in the wound site.

5.5.4 Antimicrobial PAs

The antimicrobial resistance against conventional antibiotics, the appearance of mutated multidrug-resistant microbes, and the delay in developing new classes of antibiotics resulted in the urgent progress of alternate classes of therapeutic molecules. To this end, antimicrobial peptides (AMPs) are a class of peptides/proteins present in nature that provide defense against microbial infection. AMPs are prospective alternative therapeutics in the future (Sarkar et al. 2021; Zou et al. 2020). Many AMPs have been identified and isolated from natural sources, tested for their efficacy, and modified rationally to get better and new synthetic AMPs. One major mode of destroying microbes by these AMPs involves rupturing/destroying the cell wall. In that respect, PAs are quite effective because of their membrane-binding ability owing to their amphiphilic nature. In this section, a few examples are presented to provide an idea about the PA-based AMPs.

Many AMPs carry positive charges (+2 − +9) due to the abundance of Lys and Arg residues in their sequences. The overall positive charge is an important parameter as it regulates the extent of binding to the negatively charged membranes through electrostatic interaction. Often these cationic AMPs fall under the class of PAs, and most of these PA-based AMPs function by membrane-disruptive pathway. For example, short triblock amphiphilic peptides like $K_nF_mK_n$, as reported by Huang et al., showed high potency against both gram-negative (*E. coli*) and gram-positive (*S. aureus*) bacteria and low cytotoxicity toward mammalian cells (Huang et al. 2020). Lipidated PAs are also commonly used as antimicrobial agents. Banerjee et al. reported a series of five different PAs with the general formula, H_2N-$(CH_2)_nCONH$-Phe-$CONHC_{12}$ ($n = 1–5$, C_{12} = dodecylamine) (Nandi et al. 2017). Hydrogels formed by the PAs with longer aliphatic chains showed higher membrane affinity and antibacterial property against both gram-positive and gram-negative bacteria (*B. subtilis*, *S. aureus*, and *E. coli*). Small amount of hemolysis was induced by these hydrogels at their minimal inhibitory concentration (MIC) for *E. coli* and *B. subtilis*.

The rigid hydrogel formed by MAX1 (**8**) in DMEM cell culture medium at pH 7.4 was reported to show antibacterial activity against both gram-positive and gram-negative bacteria. In these cases, the fibrils rich in β-sheet kill the bacteria by membranolytic mechanism (Salick et al. 2007). Another similar β-hairpin peptide MARGI was reported by the same group where two Lys residues were replaced by Arg residues at sixth and 17th positions of MAX1. MARGI was found to be more effective as an AMP (against methicillin-resistant *S. aureus*) than MAX-1, presumably due to the presence of Arg residues (Salick et al. 2009). β-hairpin peptides containing six Arg residues (VKVRVRVRVDPPTRVRVRVKV-NH$_2$) reported by Veiga et al. also showed distinct antibacterial activity against *E. coli* and *S. aureus*.

All these β-hairpin peptide-based hydrogels function through the membranolytic mechanism (Veiga et al. 2012).

Cyclic AMPs or cAMPs show superior affinity to the target receptors than their linear counterparts. The proteolytic susceptibility of linear peptides improves upon cyclization. Moreover, cyclization enhances the binding affinity of the AMPs with microbe membranes. Oh et al. reported a series of cyclic amphiphilic cell-penetrating peptides (CPP) in an extensive study (Oh et al. 2014). Among all 14 peptides studied, cyclic R_4W_4 was found the most efficient against methicillin-resistant *S. aureus* [MRSA, exhibiting a minimal inhibitory concentration (MIC) of 2.67 µg/mL]. Among lipidated cyclic peptides, C_{12}-KR_5, C_{16} -KR_5, and C_{12}-KR_6 exhibited very high potency against MRSA. PA **55** and similar D,L cAMPs were tested successfully for their activity against MRSA and *E. coli* and the biofouling algae *Ulva linza* and *Navicula perminuta* (Fletcher et al. 2007).

A core-shell nanoparticle was prepared by self-assembly of cholesterol-conjugated PA (Chol-G_3R_6TAT; TAT:YGRKKRRQRRR) that showed antimicrobial properties against a range of bacteria, yeasts, and fungi (Liu et al. 2009). The formation of the nanoparticles enhanced the antimicrobial effect considerably. The nanoparticles were able to efficiently inhibit the growth of these organisms with very low MIC, yet induced relatively low hemolysis. Moreover, the PA nanoparticles also show a high therapeutic index (50) against *S. aureus* infection and could suppress bacterial growth in the brain.

5.5.5 *Mineralization and Nanofabrication*

The process by which living organisms produce minerals is called biomineralization. This process is responsible for the hardening of existing tissues, and such tissues are called mineralized tissues. Biomineralization by living organisms is a common phenomenon, and over 60 different minerals have been identified in organisms (Weiner and Heinz 1989). Some of the commonly found minerals are silicates, carbonates, calcium phosphates, etc. These minerals are involved in the formation of structural features in these organisms like seashells, bones, etc. (Provot et al. 2021).

Mineralization on the synthetic template is a challenging task and can be considered as a subsection of tissue engineering. Stupp et al. pioneered the mineralization with their well-known peptide amphiphile (**28**) (Hartgerink et al. 2001). The discrete nanofibers formed by the PA, via a pH-controlled reversible mechanism, can be cross-linked through intermolecular disulfide linkage between the Cys residues. The cross-linking results in chemically robust fibers. When these cross-linked nanofibers were incubated in $CaCl_2$ and Na_2HPO_4, matured hydroxyapatite (HA) crystals completely covered the PA fibers. The mineralization is facilitated by the phosphate group present in the PA sequence. These mineralized nanofibers are similar to the lowest level of hierarchical organization of bone and can be applied for bone regeneration. Since then, several attempts have been made toward mineralization

of HA and utilization of the same for bone regeneration (Dasgupta 2016; Ghosh et al. 2017).

Recently, Mata et al. reported a supramolecular co-assembled hydrogel using synthetic nanoclay (Laponite, Lap) and peptide amphiphiles (PAs, PAH3) (Okesola et al. 2021). The PAH3 nanofibers electrostatically adsorbed and conformed to the surface of Lap nanodisks. Rheological analyses revealed the high stiffness and robust self-healing behavior of the co-assembled PAH3-Lap hydrogels. The three-dimensional matrix facilitated high-aspect-ratio HA nanorods' nucleation and hierarchical organization into well-defined spherical clusters. Importantly, these organic−inorganic PAH3-Lap hydrogels demonstrated efficient cell growth, stimulation of cell ingress, blood vessel infiltration, ECM production, and mineral deposition in a CAM (chorioallantoic membrane) model.

Polypeptide sequences with specific affinity to inorganics can be obtained in many possible ways. Phage display, in vivo combinatorial biology protocols, and cell-surface display are techniques used to identify biological ligands that show the specific binding affinity for various inorganic materials. A collagen mimicking 12-residue peptide (NPYHPTIPQSVH-GGGK-biotin: CLP12 peptide) was identified as a possible HA binding and nucleation motif using phage display (Chung et al. 2011). The CLP12 peptide was able to bind single-crystal HA. The HA-bound peptide was further used as a template for the nucleation and growth of crystalline HA minerals in a sequence- and composition-dependent manner. Similarly, block co-polypeptides like $K_{170}L_{30}$ have been used as templates for forming self-assembled calcium phosphate nanocomposites (Hu et al. 2009).

Magnetite nanocrystal mineralization was also achieved using lipidated PA nanofibers. The fibers formed by heating the His-containing PA ($C_{16}A_4G_3H_4$) were used to deposit magnetite crystals on the fiber surface. The nanofibers were formed even in acidic condition and thereby allowed the introduction of iron precursors ($FeCl_2$ and $FeCl_3$ in 1:2 ratio) to the preformed fiber suspensions. The pH was subsequently raised by exposing the suspension to ammonia vapors. The rise in pH leads to oxide formation without affecting the integrity of the nanofibers (Sone and Stupp 2011).

Fabrication of nanomaterials using the self-assembled PA nanostructures as template essentially follows the same strategy used for mineralization. For example, preparation of hollow silica nanotubes using PA nanofibers on several occasions (Yuwono and Hartgerink 2007). For example, helical nanofibers formed by PA **27** were used as a template for preparing hollow nanotubes. Tetraethoxysilane (TEOS) was deposited on the surface of the nanofibers which eventually get hydrolyzed by the amine groups present at the surface of the nanofibers and cover the nanofibers with silica. Removal of the template by calcination resulted in uniform single-walled hollow nanotubes (Fig. 5.16) (Ahmed et al. 2013). Silica nanotapes with striations were reported following a similar approach where the nanotapes formed by the $C_{16} − KTTKS$ peptide were used as a template (Dehsorkhi and Hamley 2014).

Syntheses of gold and silver nanoparticles of different shapes have been reported using simple single chain PA self-assemblies. In situ reduction of precursors within the hydrogel of Trp or Tyr containing peptide amphiphiles leads to the formation of
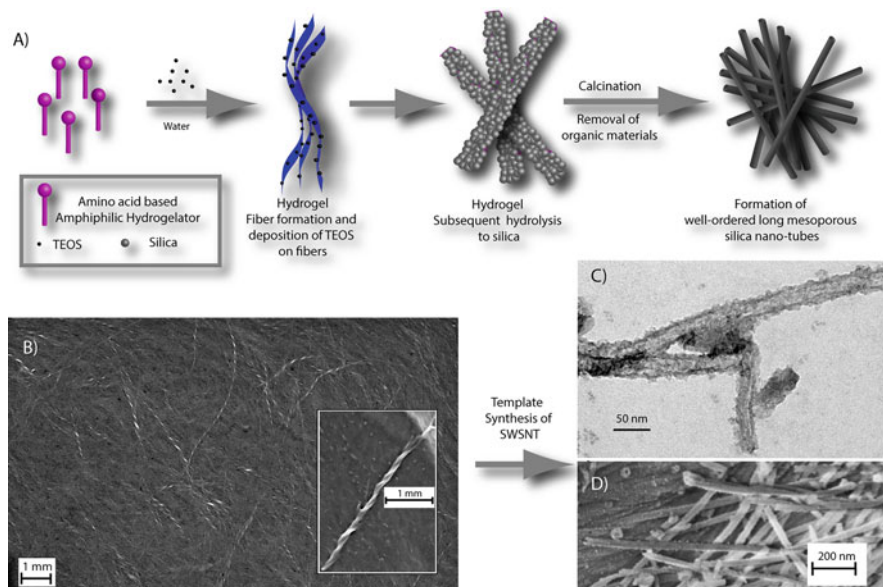
Fig. 5.16 Formation of hollow silica nanotubes (SNT) using PA nanofibers as template. (**a**) Schematic presentation of the SNT. (**b**) FESEM image of the helical nanofibers formed by the PA **27**. (**c**, **d**) TEM and FESEM images respectively of the SNTs formed. Adapted with permission from reference (Ahmed et al. 2013). Copyright 2013 American Chemical Society

the nanoparticles (Mitra and Das 2008). Gold nanocrystals with various shapes like octahedral, decahedral, wire, sheet, etc. were prepared with the help of different morphologies of the PA self-assemblies (Mitra and Das 2008).

5.5.6 Conductive Materials

The development of semiconducting materials is central to the modern electronics and optics industries. Conventional semiconducting materials are mainly inorganic and bear inherent limitations, especially in areas like interfacing with biological systems (Tao et al. 2017). Self-assembled nanostructures of small molecules are promising candidates for bioinspired semiconductors. The conducting property of organic semiconductors is governed by the semiconducting units' proper arrangement and orientation within the self-assembled systems. PA-semiconducting unit conjugates offer a suitable platform to manipulate the organization of these semiconducting units. The $\pi-\pi$ interactions and hydrogen bonding networks of PAs are highly ordered and directional in nature and thus allow the formation of quantum-confined structures. These ordered arrangements effectively decrease the band gaps of the semiconducting regions. The attached $\pi-$electron group should actively

contribute to the final morphology's stability and exhibit long-range interactions and conductivity. Hence, the final superstructure attained after hierarchical assembly dictates the quality and quantity of conduction.

The general strategy is to arylate a β-sheet-forming (or self-assembling) peptide sequence. Polythiophene bridged amphphilic peptide sequences and other polythiophene-based PAs have emerged as efficient semiconducting materials. Similar strategies have also been applied to oligo(*p*-phenylenevinylene) (OPV) p-type semiconductors. Appending the same with Gly-Ala repeat sequences ultimately resulted in conducting self-assembled nanostructures. Arylene monoimides and diimides too have prominent applications in organic electronic devices and materials due to their n-type semiconducting nature. Hence, ADI-conjugated PAs and their self-assembled materials can form the basis of many conductive nanostructures. The conductive properties of many ADI-conjugated PA-based self-assembled architectures have shown variation as a function of the different attainable morphologies.

In this respect, our group made an effort to relate the conducting ability with the morphology of the aggregated PAs. As shown in Fig. 5.11, PA **54** forms various nanostructures depending upon the solvent polarity. The system formed nanoring-like structure in a mixed solvent of 10% THF in water, as shown in Fig. 11 (Ahmed et al. 2017). In solvents with higher polarity (MeOH, HFIP, acetone, ACN, etc.), **54** tend to form spherical aggregates, while in nonpolar solvents (chloroform, THF), fibrous aggregates were formed (Ahmed et al. 2018). The nanorings were semiconducting, while the fibers from THF showed current rectifying behavior. The ac conductivities of these nanostructures showed differences at the low-frequency region. A dispersion of conductivity was observed for the nanospheres due to the possible polarization effect. With shrinking radii of curvature of the aggregation, the activation energy increases. It was observed that when the aggregates are small and closely packed, the long-range transport of charge carriers is less favorable.

These self-assembled semiconducting PAs can effectively be used to fabricate new devices. One such example is the PA, C_6-NDI-GKEK-$CONH_2$ (**74**, Fig. 5.17) (Singha et al. 2019b). This NDI containing lipidated PA self-assembled in aqueous medium to form hydrogel containing high aspect ratio fibers (length: >1 μm and diameter: ∼7–10 nm). The fibers showed moderate conductivity (conductance: 132 pS), which was further enhanced by doping carbon quantum dots (CQD) (conductance: 3840 pS). A composite hydrogel was thus prepared using a combination of **74**, CQD, and polyvinylalcohol (PVA, as a non-conducting bulk material). The presence of conducting PVA helped in providing the desired size and shape, and devices were prepared using the lyophilized powders of the hydrogel. These devices showed excellent sensing of *p*-Xylene selectively at room temperature.

5.5.7 Biomimics and Systems Chemistry

Chemists have time and again fallen back on nature for gaining inspiration for their targeted tasks. The ubiquity, ease, substrate, and task specificity, and selectivity
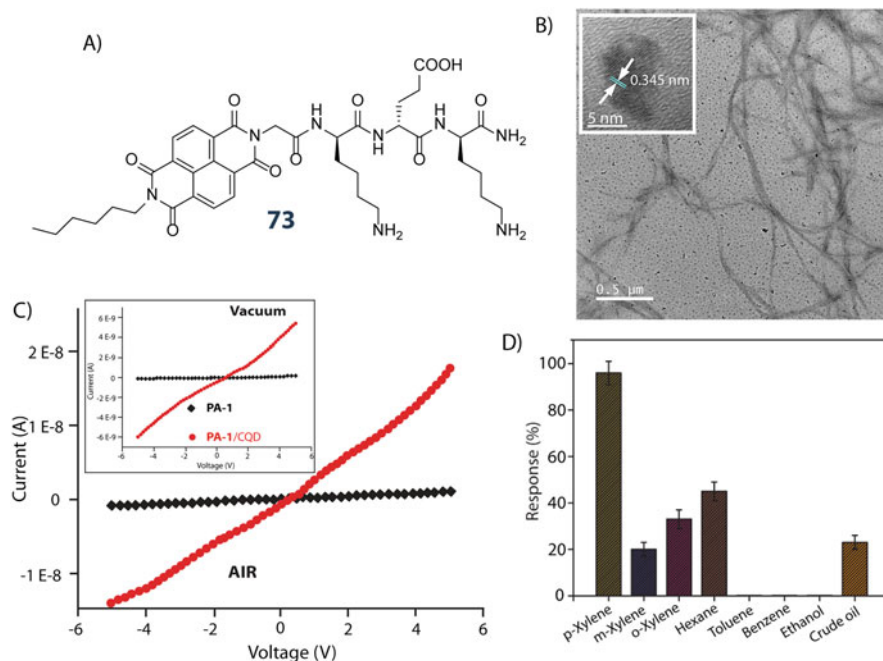
Fig. 5.17 Development of a selective *p*-xylene sensor using self-assembly of **74**. (**a**) Chemical structure of the PA. (**b**) FETEM image of the composite hydrogel (**74** + PVA + CQD) showing the fibers formed by the PA and the embedded CQDs. (**c**) IV profile of the composite hydrogels (**74** + PVA) with and without CQD in vacuum and in air. (**d**) Response of the device prepared from the composite hydrogel (**74**+ PVA + CQD) in the presence of various volatile organic compounds showing selective sensing of *p*-xylene. Adapted with permission from reference (Singha et al. 2019b). Copyright 2019 American Chemical Society

associated with enzymes acting as biocatalysts to perform an otherwise unfavorable chemical reaction have been a long-standing dream of scientists to be performed in laboratories. PAs and their corresponding materials have helped in the attainment of the same. Peptide-based enzyme mimics possess many unique advantages: (A) In line with natural enzymes, their catalytic role is an outcome of the side chains of amino acids; (B) amino acids are the primary building blocks of peptides, and the driving forces for their assembly are non-covalent interactions (e.g., hydrogen bonds, hydrophobic or electrostatic interactions, metal coordination), which bear resemblance with the fold of natural proteins; and (C) the supramolecular structures attained by non-covalent interactions usually generate a hydrophobic microenvironment facilitating the accumulation of substrates at the active site very similar like that in natural enzymes (Li et al. 2020).

Careful analysis and inference from the study of peptide sequences responsible for the activity of enzymes and the subsequent incorporation of the same into the development of a PA-based soft material have led to the realization of many peptide-
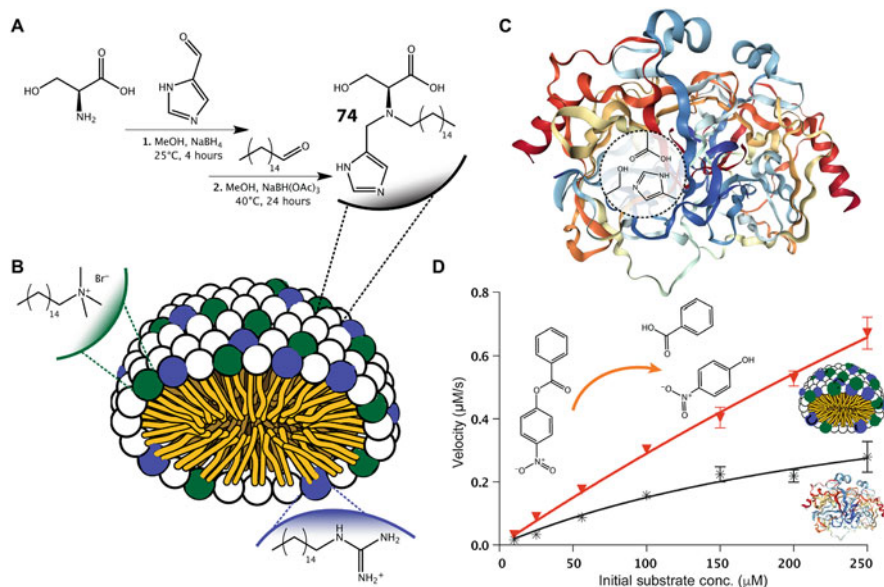
Fig. 5.18 Preparing artificial chymotrypsin using designer PA. (**a**) Synthetic route and chemical structure of the PA. (**b**) Self-assembly of **73** with co-surfactants, Guan-C$_{16}$, and CTAB, forming micelles decorated with the catalytic site and the possible hydrogen-bonding groups through guanidine functionality. (**c**) Active site of α-chymotrypsin showing the catalytic triad. (**d**) The catalysis profile for the hydrolysis of *p*-nitrophenyl benzoate for the co-assembly of **73**, Guan-C$_{16}$ and CTAB, and native α-chymotrypsin. Reproduced with permission from reference (Nothling et al. 2020). Copyright 2020 American Association for the Advancement of Science

based enzyme mimics. Even simple dipeptides can attain the biomimetic catalytic functions in their self-assembled forms (Chen et al. 2021). The construction of artificial enzymes using designer PAs can be explained with the help of hydrolases. Artificial hydrolases have been achieved on several occasions where the enzyme's catalytic site has been mimicked by rationally placing different amino acid residues on the head groups of PAs. The active site or catalytic pocket of a protein is a relatively small functional area that performs the catalytic process with the help of different constituent amino acids that form the active site. For hydrolases like chymotrypsin, the active site often contains His, Asp, and Ser in close spatial proximity. Proper arrangement of this catalytic triad at the surface of a hydrophobic aggregate may create the hydrolase mimic as the active site of hydrolases is hydrophobic in nature. A catalytic PA (**75**, Fig. 18) was prepared following this strategy (Nothling et al. 2020). The three functional groups of the triad (-OH, − imidazole, and -CO$_2$H) are positioned on a single surfactant molecule **75** (Fig. 5.18). The hydrogen bond donating arrangement of the oxyanion hole in the actual enzyme was created by imparting surfactant functionality to a guanidinium head group (hexadecylguanidium hydrochloride (Guan-C$_{16}$). Self-assembly of these amphiphiles in combination with cetyltrimethyammonium bromide (CTAB) in aqueous

medium forms micelle, which brings all the head groups nearby around a hydro-phobic nano environment and results in efficient hydrolysis of esters at a rate slightly higher than α-chymotrypsin. Similar strategies have been used on several occasions resulting in artificial enzymes of a different kind (Wang et al. 2016b; Zhang et al. 2016). In a very recent effort from our group, we have analyzed a series of PAs with different head group combinations (His, Ser, Asp, Arg) and tail length variation toward mimicking hydrolase activity (Dowari et al. 2022). The PA with the formula C_6-RDSH was found to be the most effective catalyst in its aggregated (micellar) form. Based on these findings, the PAs were grafted on silica nanoparticles to form a heterogeneous catalyst that can be reused for several cycles without any loss in activity and able to enantio-selectively hydrolyze esters.

Biocatalytic reaction networks often accumulate multiple cascade transforma-tions by localized confinement of enzymes and substrates. Often, a very trivial approach of appending a simple self-assembly promoting group to the functionally active peptide sequence gives an alternative and sometimes a very minimalistic approach of formulating an enzyme mimic, which might show complexities like cascade reactions. For example, recent reports on the short peptide-based cross β-amyloid nano-tubular hybrids exhibiting cascade reactions have come forward (Pal et al. 2021). The work demonstrated how a short peptide, Ac-HLVFFAL-CONH₂, self-assembles into nanotubes and utilizes a single substrate to show esterase-peroxidase tandem reaction with the assistance of bound hemin. The surface-exposed His is responsible for the esterase activity. Production of guaicol on hydrolytic cleavage of the ester substrate is further converted to tetraguaicol by hemin. The tetraguaicol formation from guaicol is a typical peroxidase like activity (Chatterjee et al. 2020). Another similar work on cascade reactions has also been established using similar self-assembled nanotubes formed from lipidated peptide amphiphile C_{10}-FFVK. The reaction network here emerged from breaking and making of C-C bonds in a tandem fashion forming an aldolase cascade reaction (Reja et al. 2020). The system also showed morphology-dependent catalytic rates indicative of the formation of the substrate pockets and even registered better activity in the presence of hydrogen-bonding donors, which is exploited by the aldolase. Additional attributes were substrate selectivity and templating certain adducts from a collection of adducts.

In the context of transient systems, our group has reported a transient SPA (**61**) utilizing the host-guest chemistry of CB[8]. The SPA forms vesicles reversibly that fostered pH clock regulated transient nature due to dynamic pH-responsive imine bonds (Pramanik and Das 2018) in the molecular structure (Dowari et al. 2019). In a recent report, using a similar approach, we have also reported a self-destructive transient nanozyme where the lifetime of the nanozyme can be controlled by varying the substrate (Das et al. 2022b). To further extend the work, we have recently shown the dual-feedback-assisted destruction of a transient nanozyme capable catalyzing esterase-peroxidase-like cascade reactions (Das et al. 2022a). Aided by fuel EDC, ester bonds are formed between C_{18}-COOH and *p*-nitrophenol (NP) molecules to give C_{18}H-NP, which further assemble and are the sites of cooperative catalysis for esterase activity owing to the presence of a dense, compact packing of His units in

close proximity of the ester units of the $C_{18}H$-NP molecules in the self-assembled morphology (Yang et al. 2021). On cleavage of ester bonds, the structural integrity is lost and then the dissipation occurs. The entire cycle is repetitive on further addition of fuel EDC. Temporal control on the electronic properties was also attained using transient polymerization of cross β-amyloid peptide sequences Ac-HLVFFAE-NH$_2$ and Ac-HLVFFAE-NP (Bal et al. 2020). These applications indulged in negative feedback responses to bring out the transient nature of the systems. To this end, Otto et al. have demonstrated multiple life-like complexifications and emergent characteristics like monomer exchange, nucleation, elongation, fragmentation, and replication in their process of transient self-assembly of cyclic disulfide-based peptide amphiphiles (Yang et al. 2021). Redox-responsive benzene-1,3-dithiol unit appended to the N-terminal end of GLKFK-COOH residues imparted the fuel-responsive characteristics of the PAs in this work which gives an insight into the preliminary footsteps aiming toward the realization of evolution process and attainment of artificial life.

5.6   Concluding Remarks

Significant advancement has been made in nanomaterials in the last few decades. The nanostructures obtained from PA self-assemblies have found several applications, including therapeutic, material science, organic chemistry, etc. In this chapter, we have tried to provide an overview of the various types of PAs that are available, their self-assembly mechanism, different nanostructures formed by these PAs, and their applications. Moreover, a general design guideline and usage pathway has been provided. Selected PAs and their applications are discussed to cover all classes of PAs and their applications. With the understanding and knowledge inferred from the voluminous work that has been done so far, it is now possible to design PAs to form specific nanostructure for a targeted application. We are hopeful that the discussion in this chapter will help to get the understanding and will be beneficial for the researchers.

References

Adams DJ (2018) Does drying affect gel networks? Gels 4(2):32

Adams DJ, Butler MF, Frith WJ, Kirkland M, Mullen L, Sanderson P (2009) A new method for maintaining homogeneity during liquid–hydrogel transitions using low molecular weight hydrogelators. Soft Matter 5(9):1856–1862

Ahmed S, Amba Sankar KN, Pramanik B, Mohanta K, Das D (2018) Solvent directed morphogenesis and electrical properties of a peptide–perylenediimide conjugate. Langmuir 34(28): 8355–8364

Ahmed S, Mondal JH, Behera N, Das D (2013) Self-assembly of peptide-amphiphile forming helical nanofibers and in situ template synthesis of uniform mesoporous Single Wall silica nanotubes. Langmuir 29(46):14274–14283

Ahmed S, Pramanik B, Sankar KNA, Srivastava A, Singha N, Dowari P, Srivastava A, Mohanta K, Debnath A, Das D (2017) Solvent assisted tuning of morphology of a peptide-perylenediimide conjugate: helical fibers to nano-rings and their differential semiconductivity. Sci Rep 7(1):9485

Alakpa Enateri V, Jayawarna V, Lampel A, Burgess Karl V, West Christopher C, Bakker Sanne CJ, Roy S, Javid N, Fleming S, Lamprou Dimitris A, Yang J, Miller A, Urquhart Andrew J, Frederix Pim WJM, Hunt Neil T, Péault B, Ulijn Rein V, Dalby Matthew J (2016) Tunable supramolecular hydrogels for selection of lineage-guiding metabolites in stem cell cultures. Chem 1: 298–319

Ariga K, Kikuchi J-i, Naito M, Koyama E, Yamada N (2000) Modulated supramolecular assemblies composed of tripeptide derivatives: formation of micrometer-scale rods, nanometer-size needles, and regular patterns with molecular-level flatness from the same compound. Langmuir 16(11):4929–4939

Bal S, Ghosh C, Ghosh T, Vijayaraghavan RK, Das D (2020) Non-equilibrium polymerization of cross-β amyloid peptides for temporal control of electronic properties. Angew Chem Int Ed 59(32):13506–13510

Bartocci S, Berrocal JA, Guarracino P, Grillaud M, Franco L, Mba M (2018) Peptide-driven charge-transfer Organogels built from synergetic hydrogen bonding and pyrene–Naphthalenediimide donor–acceptor interactions. Chem Eur J 24(12):2920–2928

Castillo Diaz LA, Elsawy M, Saiani A, Gough JE, Miller AF (2016) Osteogenic differentiation of human mesenchymal stem cells promotes mineralization within a biodegradable peptide hydrogel. J Tissue Eng 7:1–5

Chapman R, Danial M, Koh ML, Jolliffe KA, Perrier S (2012) Design and properties of functional nanotubes from the self-assembly of cyclic peptide templates. Chem Soc Rev 41(18): 6023–6041

Chatterjee A, Afrose SP, Ahmed S, Venugopal A, Das D (2020) Cross-β amyloid nanotubes for hydrolase–peroxidase cascade reactions. Chem Commun 56(57):7869–7872

Chen Y, Yang Y, Orr AA, Makam P, Redko B, Haimov E, Wang Y, Shimon LJW, Rencus-Lazar S, Ju M, Tamamis P, Dong H, Gazit E (2021) Self-assembled peptide nano-superstructure towards enzyme mimicking hydrolysis. Angew Chem Int Ed 60(31):17164–17170

Chowdhuri S, Ghosh M, Adler-Abramovich L, Das D (2021) The effects of a short self-assembling peptide on the physical and biological properties of biopolymer hydrogels. 13(10):1602

Chung EK, Lee E, Lim Y-b, Lee M (2010) Cyclic peptide facial amphiphile Preprogrammed to self-assemble into bioactive peptide capsules. Chem Eur J 16(18):5305–5309

Chung W-J, Kwon K-Y, Song J, Lee S-W (2011) Evolutionary screening of collagen-like peptides that nucleate hydroxyapatite crystals. Langmuir 27(12):7620–7628

Cui H, Webber MJ, Stupp SI (2010a) Self-assembly of peptide amphiphiles: from molecules to nanostructures to biomaterials. Pep Sci 94(1):1–18

Cui H, Webber MJ, Stupp SI (2010b) Self-assembly of peptide amphiphiles: from molecules to nanostructures to biomaterials. Biopolymers 94(1):1–18

Das BK, Pramanik B, Chowdhuri S, Scherman OA, Das D (2020) Light-triggered syneresis of a water insoluble peptide-hydrogel effectively removes small molecule waste contaminants. Chem Commun 56(23):3393–3396

Das D, Assaf KI, Nau WM (2019) Applications of cucurbiturils in medicinal chemistry and chemical biology. Front Chem 7:619

Das D, Dasgupta A, Roy S, Mitra RN, Debnath S, Das PK (2006) Water gelation of an amino acid-based amphiphile. Chem Eur J 12(19):5068–5074

Das D, Scherman OA (2011) Cucurbituril: at the Interface of small molecule host–guest chemistry and dynamic aggregates. Isr J Chem 51(5–6):537–550

Das D, Tnimov Z, Nguyen UTT, Thimmaiah G, Lo H, Abankwa D, Wu Y, Goody RS, Waldmann H, Alexandrov K (2012) Flexible and general synthesis of functionalized

phosphoisoprenoids for the study of prenylation in vivo and in vitro. Chembiochem 13(5):
674–683

Das S, Das D (2021) Rational design of peptide-based smart hydrogels for therapeutic applications.
Front Chem 9:770102

Das S, Das P, Dowari P, Das BK, Das D (2022a) Bi-directional feedback controlled transience in
cucurbituril based tandem nanozyme. J Colloid Interface Sci 614:172–180

Das S, Das T, Das P, Das D (2022b) Controlling the lifetime of cucurbit[8]uril based self-abolishing
nanozymes. Chem Sci

Dasgupta A (2016) Exploring architectures at the nanoscale: the interplay between hydrophobic
twin lipid chains and head groups of designer peptide amphiphiles in the self-assembly process
and application. Soft Matter 12(19):4352–4360

Dasgupta A, Das D (2019) Designer peptide amphiphiles: self-assembly to applications. Langmuir
35(33):10704–10724

Dasgupta A, Mondal JH, Das D (2013) Peptide hydrogels. RSC. Advances 3(24):9117–9149

Dehsorkhi A, Castelletto V, Hamley IW (2014) Self-assembling amphiphilic peptides. J Pep Sci
20(7):453–467

Dehsorkhi A, Hamley IW (2014) Silica templating of a self-assembling peptide amphiphile that
forms nanotapes. Soft Matter 10(11):1660–1664

Deming TJ (2005) Polypeptide hydrogels via a unique assembly mechanism. Soft Matter 1(1):
28–35

Ding X, Zhao H, Li Y, Lee AL, Li Z, Fu M, Li C, Yang YY, Yuan P (2020) Synthetic peptide
hydrogels as 3D scaffolds for tissue engineering. Ad Drug Deliv Rev 160:78–104

Dougherty DA (2013) The cation−π interaction. Acc Chem Res 46(4):885–893

Dowari P, Das S, Pramanik B, Das D (2019) pH clock instructed transient supramolecular peptide
amphiphile and its vesicular assembly. Chem Commun 55(94):14119–14122

Dowari P, Kumar Baroi M, Das T, Kanti Das B, Das S, Chowdhuri S, Garg A, Debnath A, Das D
(2022) Development of a hydrolase mimicking peptide amphiphile and its immobilization on
silica surface for stereoselective and enhanced catalysis. J Colloids Interface Sci 618:98–110

Draper ER, Adams DJ (2017) Low-molecular-weight gels: the state of the art. Chem 3(3):390–410

Du X, Zhou J, Shi J, Xu B (2015) Supramolecular hydrogelators and hydrogels: from soft matter to
molecular biomaterials. Chem Rev 115(24):13165–13307

Engler AJ, Sen S, Sweeney HL, Discher DE (2006) Matrix elasticity directs stem cell lineage
specification. Cell 126:677–689

Falcone N, Kraatz H-B (2018) Supramolecular assembly of peptide and metallopeptide gelators and
their stimuli-responsive properties in biomedical applications. Chem Eur J 24(54):14316–14328

Faul CFJ, Antonietti M (2003) Ionic self-assembly: facile synthesis of supramolecular materials.
Adv Mater 15(9):673–683

Fleming S, Ulijn RV (2014) Design of nanostructures based on aromatic peptide amphiphiles.
Chem Soc Rev 43(23):8150–8177

Fletcher JT, Finlay JA, Callow ME, Callow JA, Ghadiri MR (2007) A combinatorial approach to
the discovery of biocidal six-residue cyclic d,l-α-peptides against the bacteria methicillin-
resistant Staphylococcus aureus (MRSA) and E. coli and the biofouling algae Ulva linza and
Navicula perminuta. Chem Eur J 13(14):4008–4013

Fujimura F, Horikawa Y, Morita T, Sugiyama J, Kimura S (2007) Double assembly composed of
lectin association with columnar molecular assembly of cyclic tri-β-peptide having sugar units.
Biomacromolecules 8(2):611–616

Gao J, Zhan J, Yang Z (2020) Enzyme-instructed self-assembly (EISA) and hydrogelation of
peptides. Adv Mater 32(3):1805798

Geisler IM, Schneider JP (2012) Evolution-based design of an injectable hydrogel. Adv Funct
Mater 22(3):529–537

Ghosh M, Halperin-Sternfeld M, Grigoriants I, Lee J, Nam KT, Adler-Abramovich L (2017)
Arginine-presenting peptide hydrogels decorated with hydroxyapatite as biomimetic scaffolds
for bone regeneration. Biomacromolecules 18(11):3541–3550

Guo Z, Wu Y-W, Das D, Delon C, Cramer J, Yu S, Thuns S, Lupilova N, Waldmann H, Brunsveld L, Goody RS, Alexandrov K, Blankenfeldt W (2008) Structures of RabGGTase–substrate/product complexes provide insights into the evolution of protein prenylation. EMBO J 27(18):2444–2456

Gupta S, Kapoor P, Chaudhary K, Gautam A, Kumar R, Raghava GP (2015) Peptide toxicity prediction. Methods Mol Biol 1268:143–157

Hai Z, Li J, Wu J, Xu J, Liang G (2017) Alkaline phosphatase-triggered simultaneous hydrogelation and chemiluminescence. J Am Chem Soc 139(3):1041–1044

Hamley IW (2011) Self-assembly of amphiphilic peptides. Soft Matter 7(9):4122–4138

Hartgerink JD, Beniash E, Stupp SI (2001) Self-assembly and mineralization of peptide-amphiphile nanofibers. Science 294(5547):1684–1688

He H, Wang H, Zhou N, Yang D, Xu B (2018) Branched peptides for enzymatic supramolecular hydrogelation. Chem Commun 54(1):86–89

Hendricks MP, Sato K, Palmer LC, Stupp SI (2017) Supramolecular assembly of peptide amphiphiles. Acc Chem Res 50(10):2440–2448

Hourani R, Zhang C, van der Weegen R, Ruiz L, Li C, Keten S, Helms BA, Xu T (2011) Processable cyclic peptide nanotubes with tunable interiors. J Am Chem Soc 133(39):15296–15299

Hu Y-Y, Yusufoglu Y, Kanapathipillai M, Yang C-Y, Wu Y, Thiyagarajan P, Deming T, Akinc M, Schmidt-Rohr K, Mallapragada S (2009) Self-assembled calcium phosphate nanocomposites using block copolypeptide templates. Soft Matter 5(21):4311–4320

Huang T, Qian Y, Fu X, Huang S, Li Y, Zhou C (2020) De novo design of triblock amphiphilic short antimicrobial peptides. ACS Appl Biomater 2(9):3988–3992

Hunter CA, Sanders JKM (1990) The nature of .pi.-.pi. interactions. J Am Chem Soc 112(14):5525–5534

Ikeda M, Tanida T, Yoshii T, Hamachi I (2011) Rational molecular design of stimulus-responsive supramolecular hydrogels based on dipeptides. Adv Mater 23(25):2819–2822

Israelachvili J (2011a) Intermolecular and surface forces. Academic Press, San Diego

Israelachvili JN (2011b) 20 - soft and biological structures. In: Israelachvili JN (ed) Intermolecular and surface forces, 3rd edn. Academic Press, San Diego, pp 535–576

Jain R, Khandelwal G, Roy S (2019) Unraveling the design rules in ultrashort amyloid-based peptide assemblies toward shape-controlled synthesis of gold nanoparticles. Langmuir 35(17):5878–5889

Jalani K, Kumar M, George SJ (2013) Mixed donor–acceptor charge-transfer stacks formed via hierarchical self-assembly of a non-covalent amphiphilic foldamer. Chem Commun 49(45):5174–5176

Jiao D, Geng J, Loh XJ, Das D, Lee T-C, Scherman OA (2012) Supramolecular peptide amphiphile vesicles through host–guest complexation. Angew Chem Int Ed 51(38):9633–9637

Jin H, Wan C, Zou Z, Zhao G, Zhang L, Geng Y, Chen T, Huang A, Jiang F, Feng J-P, Lovell JF, Chen J, Wu G, Yang K (2018) Tumor ablation and therapeutic immunity induction by an injectable peptide hydrogel. ACS Nano 12(4):3295–3310

Ju X, Chen J, Zhou M, Zhu M, Li Z, Gao S, Ou J, Xu D, Wu M, Jiang S, Hu Y, Tian Y, Niu Z (2020) Combating pseudomonas aeruginosa biofilms by a chitosan-PEG-peptide conjugate via changes in assembled structure. ACS Appl Mater Interfaces 12(12):13731–13738

Kabiri M, Unsworth LD (2014) Application of isothermal titration calorimetry for characterizing thermodynamic parameters of biomolecular interactions: peptide self-assembly and protein adsorption case studies. Biomacromolecules 15(10):3463–3473

Kisiday J, Jin M, Kurz B, Hung H, Semino C, Zhang S, Grodzinsky AJ (2002) Self-assembling peptide hydrogel fosters chondrocyte extracellular matrix production and cell division: implications for cartilage tissue repair. Proc Natl Acad Sci 99(15):9996–10001

Korevaar PA, Newcomb CJ, Meijer EW, Stupp SI (2014) Pathway selection in peptide amphiphile assembly. J Am Chem Soc 136(24):8540–8543

Koutsopoulos S, Unsworth LD, Nagai Y, Zhang S (2009) Controlled release of functional proteins through designer self-assembling peptide nanofiber hydrogel scaffold. Proc Natl Acad Sci:2623–2628

Kretsinger JK, Haines LA, Ozbas B, Pochan DJ, Schneider JP (2005) Cytocompatibility of self-assembled beta-hairpin peptide hydrogel surfaces. Biomaterials 26(25):5177–5186

Larsen TH, Branco MC, Rajagopal K, Schneider JP, Furst EM (2009) Sequence-dependent gelation kinetics of β-hairpin peptide hydrogels. Macromolecules 42(21):8443–8450

Levin A, Hakala TA, Schnaider L, Bernardes GJL, Gazit E, Knowles TPJ (2020) Biomimetic peptide self-assembly for functional materials. Nat Rev Chem 4(11):615–634

Li J, Mooney DJ (2016) Designing hydrogels for controlled drug delivery. Nat Rev Mater 1(12): 16071

Li J, Zhu M, Wang M, Qi W, Su R, He Z (2020) Molecularly imprinted peptide-based enzyme mimics with enhanced activity and specificity. Soft Matter 16(30):7033–7039

Li X, Sun Q, Li Q, Kawazoe N, Chen G (2018) Functional hydrogels with Tunable structures and properties for tissue engineering applications. Front Chem 6:499

Liu L, Xu K, Wang H, Jeremy Tan PK, Fan W, Venkatraman SS, Li L, Yang Y-Y (2009) Self-assembled cationic peptide nanoparticles as an efficient antimicrobial agent. Nat Nanotechnol 4(7):457–463

Liu W, Wong-Noonan S, Pham NB, Pradhan I, Spigelmyer A, Funk R, Nedzesky J, Cohen H, Gawalt ES, Fan Y, Meng WS (2019) A genetically engineered Fc-binding amphiphilic polypeptide for congregating antibodies in vivo. Acta Biomater 88:211–223

Liu X, Wang X, Wang X, Ren H, He J, Qiao L, Cui F-Z (2013) Functionalized self-assembling peptide nanofiber hydrogels mimic stem cell niche to control human adipose stem cell behavior in vitro. Acta Biomater 9(6):6798–6805

Loo Y, Wong Y-C, Cai EZ, Ang C-H, Raju A, Lakshmanan A, Koh AG, Zhou HJ, Lim T-C, Moochhala SM, Hauser CAE (2014) Ultrashort peptide nanofibrous hydrogels for the acceleration of healing of burn wounds. Biomaterials 35:4805–4814

Luo Z, Yue Y, Zhang Y, Yuan X, Gong J, Wang L, He B, Liu Z, Sun Y, Liu J, Hu M, Zheng J (2013) Designer D-form self-assembling peptide nanofiber scaffolds for 3-dimensional cell cultures. Biomaterials 34:4902–4913

Mei L, Xu K, Zhai Z, He S, Zhu T, Zhong W (2019) Doxorubicin-reinforced supramolecular hydrogels of RGD-derived peptide conjugates for pH-responsive drug delivery. Org Biomol Chem 17(15):3853–3860

Meng Q, Kou Y, Ma X, Liang Y, Guo L, Ni C, Liu K (2012) Tunable self-assembled peptide amphiphile nanostructures. Langmuir 28(11):5017–5022

Miao X, Cao W, Zheng W, Wang J, Zhang X, Gao J, Yang C, Kong D, Xu H, Wang L, Yang Z (2013) Switchable catalytic activity: selenium-containing peptides with redox-controllable self-assembly properties. Angew Chem Int Ed 52:7781–7785

Misawa H, Kobayashi N, Soto-Gutierrez A, Chen Y, Yoshida A, Rivas-Carrillo JD, Navarro-Alvarez N, Tanaka K, Miki A, Takei J, Ueda T, Tanaka M, Endo H, Tanaka N, Ozaki T (2006) PuraMatrix™ facilitates bone regeneration in bone defects of calvaria in mice. Cell Transplant 15:903–910

Mitra RN, Das D, Roy S, Das PK (2007) Structure and properties of low molecular weight amphiphilic peptide hydrogelators. J Phys Chem B 111(51):14107–14113

Mitra RN, Das PK (2008) In situ preparation of gold nanoparticles of varying shape in molecular hydrogel of peptide amphiphiles. J Phys Chem C 112(22):8159–8166

Mondal JH, Ahmed S, Ghosh T, Das D (2015) Reversible deformation–formation of a multistimuli responsive vesicle by a supramolecular peptide amphiphile. Soft Matter 11(24):4912–4920

Nandi N, Gayen K, Ghosh S, Bhunia D, Kirkham S, Sen SK, Ghosh S, Hamley IW, Banerjee A (2017) Amphiphilic peptide-based supramolecular, noncytotoxic, stimuli-responsive hydrogels with antibacterial activity. Biomacromolecules 18(11):3621–3629

Nguyen MM, Carlini AS, Chien MP, Sonnenberg S, Luo C, Braden RL, Osborn KG, Li Y, Gianneschi NC, Christman KL (2015) Enzyme-responsive nanoparticles for targeted

accumulation and prolonged retention in heart tissue after myocardial infarction. Adv Mater 27(37):5547–5552

Nothling MD, Xiao Z, Hill NS, Blyth MT, Bhaskaran A, Sani M-A, Espinosa-Gomez A, Ngov K, White J, Buscher T, Separovic F, O'Mara ML, Coote ML, Connal LA (2020) A multifunctional surfactant catalyst inspired by hydrolases. Sci Adv 6(14):eaaz0404

Nowak AP, Breedveld V, Pakstis L, Ozbas B, Pine DJ, Pochan D, Deming TJ (2002) Rapidly recovering hydrogel scaffolds from self-assembling diblock copolypeptide amphiphiles. Nature 417(6887):424–428

Nowak AP, Breedveld V, Pine DJ, Deming TJ (2003) Unusual salt stability in highly charged Diblock co-polypeptide hydrogels. J Am Chem Soc 125(50):15666–15670

Oh D, Sun J, Nasrolahi Shirazi A, LaPlante KL, Rowley DC, Parang K (2014) Antibacterial activities of amphiphilic cyclic cell-penetrating peptides against multidrug-resistant pathogens. Mol Pharm 11(10):3528–3536

Okesola BO, Mendoza-Martinez AK, Cidonio G, Derkus B, Boccorh DK, Osuna de la Peña D, Elsharkawy S, Wu Y, Dawson JI, Wark AW, Knani D, Adams DJ, Oreffo ROC, Mata A (2021) De novo design of functional coassembling organic–inorganic hydrogels for hierarchical mineralization and neovascularization. ACS Nano 15:11202–11217

Orbach R, Adler-Abramovich L, Zigerson S, Mironi-Harpaz I, Seliktar D, Gazit E (2009) Self-assembled Fmoc-peptides as a platform for the formation of nanostructures and hydrogels. Biomacromolecules 10(9):2646–2651

Pakalns T, Haverstick LK, Fields GB, McCarthy JB, Mooradian LD, Tirrell M (1999) Cellular recognition of synthetic peptide amphiphiles in self-assembled monolayer films. Biomaterials 20(23):2265–2279

Pal S, Goswami S, Das D (2021) Cross β amyloid assemblies as complex catalytic machinery. Chem Commun 57(62):7597–7609

Panja S, Adams DJ (2019) Gel to gel transitions by dynamic self-assembly. Chem Commun 55(68): 10154–10157

Patravale V, Dandekar P, Jain R (2012) 4 - nanotoxicology: evaluating toxicity potential of drug-nanoparticles. In: Patravale V, Dandekar P, Jain R (eds) Nanoparticulate drug delivery. Woodhead Publishing, pp 123–155

Pavan M, Worth AP (2008) Review of estimation models for biodegradation. QSAR Comb Sci 27(1):32–40

Pollard TD, Earnshaw WC, Lippincott-Schwartz J, Johnson GT (2017) Chapter 4 - biophysical principles. Cell biology (third edition). Elsevier, pp 53–62

Pramanik B, Ahmed S, Singha N, Das BK, Dowari P, Das D (2019a) Unorthodox combination of cation−π and charge-transfer interactions within a donor–acceptor pair. Langmuir 35(2): 478–488

Pramanik B, Das D (2018) Aggregation-induced emission or hydrolysis by water? The case of Schiff bases in aqueous organic solvents. J Phys Chem C 122(6):3655–3661

Pramanik B, Singha N, Das D (2019b) Sol-, gel-, and paper-based detection of picric acid at femtogram level by a short peptide Gelator. ACS Appl Polym Mater 1(4):833–843

Provot S, Schipani E, Wu J, Kronenberg H (2021) Chapter 3 - development of the skeleton. In: Dempster DW, Cauley JA, Bouxsein ML, Cosman F (eds) Marcus and Feldman's osteoporosis (fifth edition). Academic Press, pp 39–73

Qi R, Zhang N, Zhang P, Zhao H, Liu J, Cui J, Xiang J, Han Y, Wang S, Wang Y (2020) Gemini peptide amphiphiles with broad-spectrum antimicrobial activity and potent antibiofilm capacity. ACS Appl Mater Interfaces 12(15):17220–17229

Ray S, Das AK, Banerjee A (2007) pH-responsive, bolaamphiphile-based smart metallo-hydrogels as potential dye-adsorbing agents, water purifier, and vitamin B12 carrier. Chem Mater 19(7): 1633–1639

Rehm TH, Schmuck C (2010) Ion-pair induced self-assembly in aqueous solvents. Chem Soc Rev 39(10):3597–3611

Reja A, Afrose SP, Das D (2020) Aldolase cascade facilitated by self-assembled nanotubes from short peptide amphiphiles. Angew Chem Int Ed 59(11):4329–4334

Ren C, Xu C, Li D, Ren H, Hao J, Yang Z (2014) Gemcitabine induced supramolecular hydrogelations of aldehyde-containing short peptides. RSC Adv 4:34729–34732

Rosa E, Diaferia C, Gallo E, Morelli G, Accardo A (2020) Stable formulations of peptide-based nanogels. Molecules 25(15):3455

Rughani RV, Salick DA, Lamm MS, Yucel T, Pochan DJ, Schneider JP (2009) Folding, self-assembly, and bulk material properties of a de novo designed three-stranded β-sheet hydrogel. Biomacromolecules 10(5):1295–1304

Salick DA, Kretsinger JK, Pochan DJ, Schneider JP (2007) Inherent antibacterial activity of a peptide-based β-hairpin hydrogel. J Am Chem Soc 129(47):14793–14799

Salick DA, Pochan DJ, Schneider JP (2009) Design of an Injectable β-hairpin peptide hydrogel that kills methicillin-resistant Staphylococcus aureus. Adv Mater 21(41):4120–4123

Sarkar T, Chetia M, Chatterjee S (2021) Antimicrobial peptides and proteins: from nature's reservoir to the laboratory and beyond. Front Chem 9:432

Schneider JP, Pochan DJ, Ozbas B, Rajagopal K, Pakstis L, Kretsinger J (2002) Responsive hydrogels from the intramolecular folding and self-assembly of a designed peptide. J Am Chem Soc 124(50):15030–15037

Senturk B, Demircan BM, Ozkan AD, Tohumeken S, Delibasi T, Guler MO, Tekinay AB (2017) Diabetic wound regeneration using heparin-mimetic peptide amphiphile gel in db/db mice. Biomater Sci 5(7):1293–1303

Shao H, Parquette JR (2010) A π-conjugated hydrogel based on an Fmoc-dipeptide naphthalene diimide semiconductor. Chem Commun 46(24):4285–4287

Shin Y-GK, Newton MD, Isied SS (2003) Distance dependence of electron transfer across peptides with different secondary structures: the role of peptide energetics and electronic coupling. J Am Chem Soc 125(13):3722–3732

Shy AN, Kim BJ, Xu B (2019) Enzymatic noncovalent synthesis of supramolecular soft matter for biomedical applications. Matter 1(5):1127–1147

Singha N, Das BK, Pramanik B, Das S, Das D (2019a) Freeze the dynamicity: charge transfer complexation assisted control over the reaction pathway. Chem Sci 10(43):10035–10039

Singha N, Gupta P, Pramanik B, Ahmed S, Dasgupta A, Ukil A, Das D (2017) Hydrogelation of a naphthalene Diimide appended peptide amphiphile and its application in cell imaging and intracellular pH sensing. Biomacromolecules 18(11):3630–3641

Singha N, Neogi S, Pramanik B, Das S, Dasgupta A, Ghosh R, Das D (2019b) Ultrafast, highly sensitive, and selective detection of p-xylene at room temperature by peptide-hydrogel-based composite material. ACS Appl Polym Mater 1(9):2267–2272

Singha N, Srivastava A, Pramanik B, Ahmed S, Dowari P, Chowdhuri S, Das BK, Debnath A, Das D (2019c) Unusual confinement properties of a water insoluble small peptide hydrogel. Chem Sci 10(23):5920–5928

Smith AM, Williams RJ, Tang C, Coppo P, Collins RF, Turner ML, Saiani A, Ulijn RV (2008) Fmoc-diphenylalanine self assembles to a hydrogel via a novel architecture based on π–π interlocked β-sheets. Adv Mater 20(1):37–41

Sone ED, Stupp SI (2011) Bioinspired magnetite mineralization of peptide−amphiphile nanofibers. Chem Matter 23(8):2005–2007

Soukasene S, Toft DJ, Moyer TJ, Lu H, Lee H-K, Standley SM, Cryns VL, Stupp SI (2011) Antitumor activity of peptide amphiphile nanofiber-encapsulated camptothecin. ACS Nano 5(11):9113–9121

Sutton S, Campbell NL, Cooper AI, Kirkland M, Frith WJ, Adams DJ (2009) Controlled release from modified amino acid hydrogels governed by molecular size or network dynamics. Langmuir 25(17):10285–10291

Tantakitti F, Boekhoven J, Wang X, Kazantsev RV, Yu T, Li J, Zhuang E, Zandi R, Ortony JH, Newcomb CJ, Palmer LC, Shekhawat GS, de la Cruz MO, Schatz GC, Stupp SI (2016) Energy landscapes and functions of supramolecular systems. Nat Mater 15(4):469–476

Tao K, Makam P, Aizen R, Gazit E (2017) Self-assembling peptide semiconductors. Science 358(6365):eaam9756

Thornton K, Abul-Haija YM, Hodson N, Ulijn RV (2013) Mechanistic insights into phosphatase triggered self-assembly including enhancement of biocatalytic conversion rate. Soft Matter 9(39):9430–9439

Toksoz S, Acar H, Guler MO (2010) Self-assembled one-dimensional soft nanostructures. Soft Matter 6(23):5839–5849

Veiga AS, Sinthuvanich C, Gaspar D, Franquelim HG, Castanho MARB, Schneider JP (2012) Arginine-rich self-assembling peptides as potent antibacterial gels. Biomaterials 33(35): 8907–8916

Velichko YS, Stupp SI, de la Cruz MO (2008) Molecular simulation study of peptide amphiphile self-assembly. J Phys Chem B 112(8):2326–2334

Versluis F, Tomatsu I, Kehr S, Fregonese C, Tepper AWJW, Stuart MCA, Ravoo BJ, Koning RI, Kros A (2009) Shape and release control of a peptide decorated vesicle through pH sensitive orthogonal supramolecular interactions. J Am Chem Soc 131(37):13186–13187

Wang C, Guo Y, Wang Z, Zhang X (2010) Superamphiphiles based on charge transfer complex: controllable hierarchical self-assembly of nanoribbons. Langmuir 26(18):14509–14511

Wang H, Yang Z, Adams DJ (2012) Controlling peptidebased hydrogelation. Mater Today 15(11): 500–507

Wang J, Liu K, Xing R, Yan X (2016a) Peptide self-assembly: thermodynamics and kinetics. Chem Soc Rev 45(20):5589–5604

Wang M, Lv Y, Liu X, Qi W, Su R, He Z (2016b) Enhancing the activity of peptide-based artificial hydrolase with catalytic ser/his/asp triad and molecular imprinting. ACS Appl Mater Interfaces 8(22):14133–14141

Weiner SL, Heinz A (1989) On biomineralization. Oxford University Press, Oxford

Xu H, Wang J, Han S, Wang J, Yu D, Zhang H, Xia D, Zhao X, Waigh TA, Lu JR (2009) Hydrophobic-region-induced transitions in self-assembled peptide nanostructures. Langmuir 25(7):4115–4123

Yamada N, Ariga K, Naito M, Matsubara K, Koyama E (1998) Regulation of β-sheet structures within amyloid-like β-sheet assemblage from tripeptide derivatives. J Am Chem Soc 120(47): 12192–12199

Yan C, Pochan DJ (2010) Rheological properties of peptide-based hydrogels for biomedical and other applications. Chem Soc Rev 39(9):3528–3540

Yang S, Schaeffer G, Mattia E, Markovitch O, Liu K, Hussain AS, Ottelé J, Sood A, Otto S (2021) Chemical fueling enables molecular complexification of self-replicators. Angew Chem Int Ed 60(20):11344–11349

Yang Z, Liang G, Ma M, Gao Y, Xu B (2007) Conjugates of naphthalene and dipeptides produce molecular hydrogelators with high efficiency of hydrogelation and superhelical nanofibers. J Mater Chem 17(9):850–854

Yang Z, Liang G, Wang L, Xu B (2006) Using a kinase/phosphatase switch to regulate a supramolecular hydrogel and forming the supramolecular hydrogel in vivo. J Am Chem Soc 128(9):3038–3043

Yang Z, Xu B (2004) A simple visual assay based on small molecule hydrogels for detecting inhibitors of enzymes. Chem Commun 21:2424–2425

Yang Z, Xu H, Zhao X (2020) Designer self-assembling peptide hydrogels to engineer 3D cell microenvironments for cell constructs formation and precise oncology remodeling in ovarian cancer. Adv Sci 7:1903718

Yokoi H, Kinoshita T, Zhang S (2005) Dynamic reassembly of peptide RADA16 nanofiber scaffold. Proc Natl Acad Sci 102(24):8414–8419

Yu Y-C, Berndt P, Tirrell M, Fields GB (1996) Self-assembling amphiphiles for construction of protein molecular architecture. J Am Chem Soc 118(50):12515–12520

Yuwono VM, Hartgerink JD (2007) Peptide amphiphile nanofibers template and catalyze silica nanotube formation. Langmuir 23(9):5033–5038

Zhang Q, He X, Han A, Tu Q, Fang G, Liu J, Wang S, Li H (2016) Artificial hydrolase based on carbon nanotubes conjugated with peptides. Nanoscale 8(38):16851–16856

Zhang S, Altman M (1999) Peptide self-assembly in functional polymer science and engineering. React Funct Polym 41(1):91–102

Zhang S, Holmes T, Lockshin C, Rich A (1993) Spontaneous assembly of a self-complementary oligopeptide to form a stable macroscopic membrane. Proc Natl Acad Sci U S A 90(8):3334–3338

Zhang W, Yu L, Ji T, Wang C (2020a) Tumor microenvironment–responsive peptide-based supramolecular drug delivery system. Front Chem 8:549

Zhang X, Wang C (2011) Supramolecular amphiphiles. Chem Soc Rev 40(1):94–101

Zhang Y-L, Chang R, Duan H-Z, Chen Y-X (2020b) Metal ion and light sequentially induced sol–gel–sol transition of a responsive peptide-hydrogel. Soft Matter 16(33):7652–7658

Zhao C, Chen H, Wang F, Zhang X (2021) Amphiphilic self-assembly peptides: rational strategies to design and delivery for drugs in biomedical applications. Colloids Surf B: Biointerfaces:112040

Zhao Y, Yokoi H, Tanaka M, Kinoshita T, Tan T (2008) Self-assembled pH-responsive hydrogels composed of the RATEA16 peptide. Biomacromolecules 9:1511–1518

Zhu J, Marchant RE (2011) Design properties of hydrogel tissue-engineering scaffolds. Expert Rev Med Devices 8:607–626

Zhu P, Yan X, Su Y, Yang Y, Li J (2010) Solvent-induced structural transition of self-assembled dipeptide: from Organogels to microcrystals. Chem Eur J 16(10):3176–3183

Zou P, Chen W-T, Sun T, Gao Y, Li L-L, Wang H (2020) Recent advances: peptides and self-assembled peptide-nanosystems for antimicrobial therapy and diagnosis. Biomater Sci 8(18):4975–4996

Chapter 6
Polypeptide-Based Multicomponent Materials: From Design to Applications

Burak Derkus and Babatunde O. Okesola

Abstract Polypeptides are of great interest to material scientists because of their functional versatility. The functionality of single-component polypeptide materials is ultimately limited by the physical and/or chemical nature of the molecular building blocks. Multicomponent materials that integrate a variety of chemical building blocks will facilitate the incorporation of greater molecular complexity, enhanced materials performance, and multifunctional properties in materials design. Multicomponent materials that integrate multiple polypeptides or polypeptides and synthetic polymers, nanoparticles, or biomolecules have been engineered for several useful applications including drug delivery, tissue engineering, biosensors, and template for biomineralization. In this chapter, we focus on the approaches for rational design and site-specific modification of polypeptides, which are critical for their effective interactions with the other components to create multicomponent materials for a wide range of applications.

Keywords Polypeptides · Recombinant technology · Multicomponent self-assembly · Biomaterials · Hydrogels · Supramolecular · Biomimetic · Organic–inorganic nanocomposites · Multifunctional materials · Bioconjugation · Biomedical applications

6.1 Introduction

In the last couple of decades, polypeptides have experienced a renaissance as powerful synthetic analogs of natural proteins in materials design (Sutherland et al. 2018). The increasing development in protein engineering has continued to

B. Derkus
Stem Cell Research Lab, Department of Chemistry, Faculty of Science, Ankara University, Ankara, Turkey

B. O. Okesola (✉)
School of Life Sciences, Faculty of Medicine and Health Sciences, University of Nottingham, Nottingham, United Kingdom
e-mail: babatunde.okesola@nottingham.ac.uk

provide insight into the protein sequence–structure–function relationship (Roberts et al. 2015). This understanding has provoked intense interest from the material science community to develop engineered polypeptides mimicking a domain of the native proteins known to drive a desirable property or functionality of the protein (Hollingshead et al. 2017; Balu et al. 2021). For example, repetitive structural motifs or functional fragments in proteins are increasingly used to build functional materials for a wide range of applications in bio- and nanotechnology (De La Rica and Matsui 2010). Specific advantage of synthetic polypeptide is that they provide simpler structures that enable easier structural modification as well as higher degree of control while retaining the intrinsic functionality of native proteins (Okesola and Mata 2018). The structural tunability of polypeptides thanks the chemical and structural diversity they offer which thanks the possibility to develop them into arrays of functional materials for applications in for examples, nanoelectronics, drug delivery, tissue engineering, and cell culture, among others (Rodríguez-Cabello et al. 2016; Werkmeister and Ramshaw 2012; Despanie et al. 2016).

Although there has been immense progress in designing materials with high precision using recombinant technology and self-assembly, the level of structural and functional complexities obtainable with single-component materials is incomparable to the functionality of native proteins. The natural protein machinery is an intricate assembly of multiple proteins that work together with exquisite specificity and coordination. This natural phenomenon has invigorated the vision of multicomponent materials based on multiple engineered polypeptides and their co-assemblies with nonpeptidic molecules and inorganics, which have well-defined functions that can be hybridized with predictable composite function. Co-assembly of polypeptides and the second components allows for rapid expansion of materials diversity, easy fabrication of multifunctional materials, and sustainable pathways to next-generation materials manufacture (Saha et al. 2020; Omenetto and Kaplan 2010).

The specific binding of native proteins to their ligands often results in complementarity in the emerging molecular architectures, surface chemistries, and functional properties. Similarly, in the design and co-assembly of polypeptides with their ligands, it is crucial to understand the nature of molecular recognition and co-assembly to optimize and tailor their properties and applications. The co-assembly of polypeptides with another component building blocks may originate from both chemical (e.g., hydrogen bonding, electrostatic interactions, polarity, and hydrophobic effects) and structural (size and conformation) recognition mechanisms as cleverly demonstrated in nature. For example, nature has exploit hydrophobic and electrostatic interactions to drive the supramolecular co-assembly of fatty acids and proteins to create the cell membrane (Fig. 6.1a) (Sych et al. 2018). Similarly, noncovalent interactions have been employed by nature to co-assemble RNA and proteins to create tobacco mosaic virus (Fig. 6.1b) (Greig and Philp 2001). Co-assembly of α- and β-heterodimers of tubulin proteins (Fig. 6.1c) mediated by noncovalent interactions underpins the formation of microtubule in the cells (Hohmann and Dehghani 2019). Careful and precise control of the ionic interactions
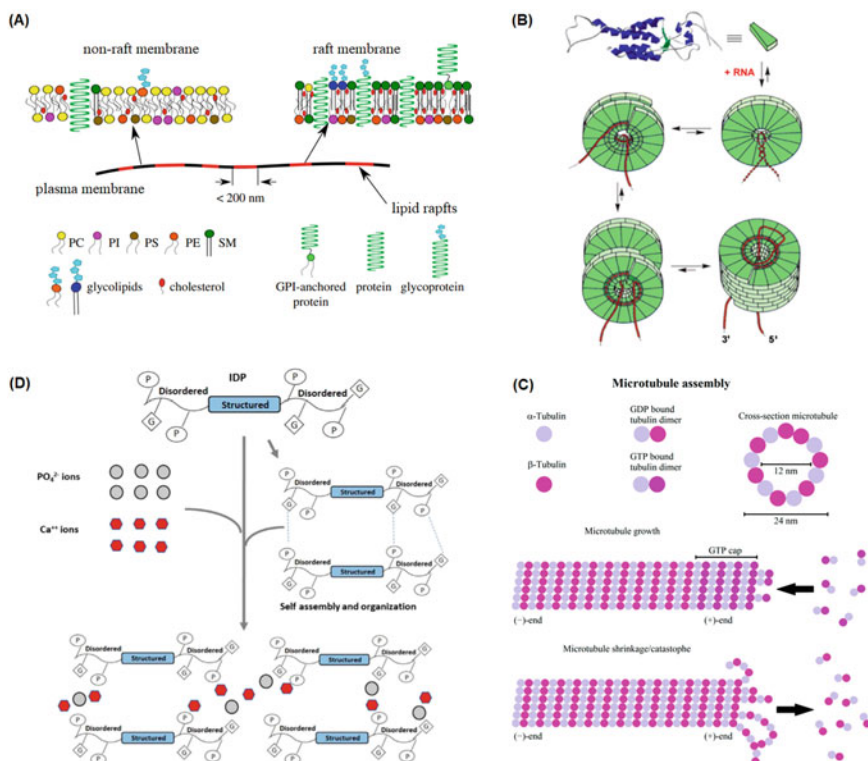
Fig. 6.1 Co-assembly in nature. (**a**) Co-assembly in nature. (**a**) Raft and non-raft types of native plasma membranes formation through assembly of multiple building blocks that mainly include extracellular proteins and lipids (sphingomyelin (SM), phosphatidylcholine (PC) lipids, while phosphatidylserine (PS), phosphatidylinositol (PI), and phosphatidyl ethanolamine (PE) lipids) via hydrophobic and electrostatic interactions. Reproduced with permission from Sych et al. (2018). Copyright © 2018 Royal Society Publishing. (**b**) Tobacco mosaic virus formation through supramolecular co-assembly of a negatively charged viral RNA with an oppositely charged polypeptides to form a double stick structure, which undergoes conformational changes and hierarchical organization to form a slipped double disk-like viral assembly. Reproduced with permission from Greig and Philip (2001). Copyright © 2001 Royal Society of Chemistry. (**c**) Schematic representation of the ionic interactions underpinning the dynamics of intrinsically disordered proteins to stabilize ion clusters to initiate and drive crystal deposition in hard tissue biomineralization. Reproduced with permission from Sharma et al. (2021). Copyright © 2021 Elsevier (**d**) Formation and dynamic instability of hollow microtubule through co-assembly of GTP-bound α-tubulin and β-tubulin via noncovalent interactions. This GDP/GTP-mediated tubulin co-assembly leads a hierarchical microstructure that contributes to the cell skeletal organization. Reproduced with permission from Hohmann and Dehghani (2019). Copyright © 2019 MDPI

between ionic species and proteins is the underlying driver for natural biomineralization (Fig. 6.1d) (Sharma et al. 2021).

Traditionally, the recognition motifs can be installed in polypeptides at the molecular level through chemical synthesis or genetic approaches. Under

appropriate conditions, the molecularly programmed information in the co-assembling subunits is then translated across multiple length scales into ordered macroscopic scale architectures. With careful engineering of this nanofabrication cascade, multicomponent materials able to display properties that are greater than the sum of their components can be envisioned. In the following section, an overview of the design of polypeptides and their intrinsic properties that can be harnessed to develop chimeric materials are provided. We exemplify the possibility to synergise intrinsic properties of multiple polypeptides, integrate the unique properties of synthetic polymers, nanoparticles, natural polymers, and peptidic small molecules with those of polypeptides using recently reported studies. The potential of this approach in creating innovative materials with highly useful properties is tremendous. The aim of this chapter is not to provide a comprehensive elucidation of polypeptides synthesis and conformational analysis but to highlight opportunities to rationally design next-generation of innovative materials with potential applications in bio- and nanotechnology.

6.2 Design Strategies for Engineered Polypeptides

In this section, we provide an overview of the technologies that can be used to engineer the repetitive sequences of polypeptides and highlight unique aspects of using these systems. We next discuss the mechanisms involved in structural engineering of polypeptides to drive effective intra- and intermolecular interactions between polypeptides and the second components.

The modular design of engineered polypeptides can be undertaken by first designing the putative peptide motifs derived from native proteins. Generally, the recombinant production of a polypeptide includes the following steps: (1) natural DNA sequence determination, (2) recombinant DNA design, (3) vector cloning, (4) host organism engineering and transformation, (5) culturing/protein production, and finally (6) protein purification (Salehi et al. 2020). Also, the use of computational modeling (Tarakanova et al. 2017; Prhashanna et al. 2019) and high-throughput combinatorial (Wang et al. 2014b; Qian et al. 2020) approaches have emerged as valuable strategies to design, predict properties of, and even manufacture polypeptide-based materials. Polypeptide modules including elastin-like (Nettles et al. 2010; Roberts et al. 2015), resilin-like (Elvin et al. 2005; Su et al. 2014; Balu et al. 2021), silk-like (Salehi et al. 2020), collagen-like (Strauss and Chmielewski 2017; Luo and Kiick 2013), abductin-like (Su et al. 2013), and mussel byssus-like (Horsch et al. 2018; Huang et al. 2019; Wei et al. 2016) domains that display properties reminiscent of the native proteins have been developed and characterized using modular gene assembly strategies, which provide genetic constructs encoding proteins with desirable consensus peptide blocks. For example, the recombinant polypeptide with consensus pentadecapeptide block (GGRPSDSYGAPGGGN) of native resilin can be chemically cross-linked into elastomeric hydrogel materials with native resilin-like resilience (Hu et al. 2019).

Similarly, structural blocks derived from nonrepetitive proteins such as viral capsids have been used to create artificial virus-like particles (Matsuura 2020). Recombinant peptide synthesis is increasingly evolving to expand the functionality of the conventional polypeptides by incorporating unnatural residues or modifications into the peptide backbones. These advances in polypeptides design will not only lead to new materials with unique reactivity, properties, and novel functionalities (Amiram et al. 2015) but also opportunity to integrate multiple polypeptides or polypeptides with other classes of functional systems to obtain new multicomponent materials with emergent properties.

6.2.1 Incorporating Unnatural Amino Acids

Although all proteins are made of twenty canonical amino acids, nature has cleverly incorporated rare amino acids, such as N-methyl glycine and L-selenocysteine, into proteins to obtain specific functions. The incorporation of unnatural amino acids (UAAs) with a chemically unique side chains or functionalities at a desirable location in polypeptide backbones is a powerful strategy to design polypeptides with unique structures, and to make site-specific covalent modification possible (Fig. 6.2a) (Mitra 2013; Martin et al. 2018; Lang and Chin 2014). Also, the introduction of UAAs into polypeptide backbones instead of the proteogenic analogs can add to the diversity of polypeptides and generate polypeptides with enhanced stability, new properties, and novel functionalities for innovative materials design (Saha et al. 2020). For example, Catherine et al. (2015) demonstrated the possibility to tune the thermal properties of elastin-like polypeptides (ELP) by replacing the cognate amino acid with isostructural unnatural amino acids including 4R-fluoroproline, 4S-fluoroproline, azetidine carboxylic acid, dehydroproline, and thiazolidine carboxylic acid. This study presents a cell-free protein synthesis approach that harnessed the promiscuity of aminoacyl tRNA synthetases to accept and process structurally similar amino acid analogs without cloning. This method of UAAs incorporation enables the design of unnatural biological machinery for an exclusive user-defined target for recombinant protein synthesis (Gao et al. 2019). Besides this cell-free approach, genetic incorporation of UAAs into proteins in bacteria, yeast, and mammalian cells has been widely demonstrated (Lang and Chin 2014; Liu et al. 2007b). Replacing a native amino acid in a polypeptide with a UAA such as p-benzoyl L-phenylalanine (Chin et al. 2002; Hino et al. 2005), 3′-azibutyl-N-carbamoyl-lysine (Chou et al. 2011), and p-azido-L-phenylalanine (Grunbeck et al. 2013) that can cross-link upon photo-irradiation can install molecular information that enables interactions with nearby complementary partners.

Costa et al. (2018) and co-workers developed thermo-responsive hydrogel particles with tunable sizes across multiple orders of magnitude, ranging from tens of nanometers to several microns by genetically encoding a photo-cross-linkable unnatural amino acid (UAA), p-azidophenylalanine (pAzF), into the ELP backbone. This structural modification was applied to two kinds of ELP backbones—one

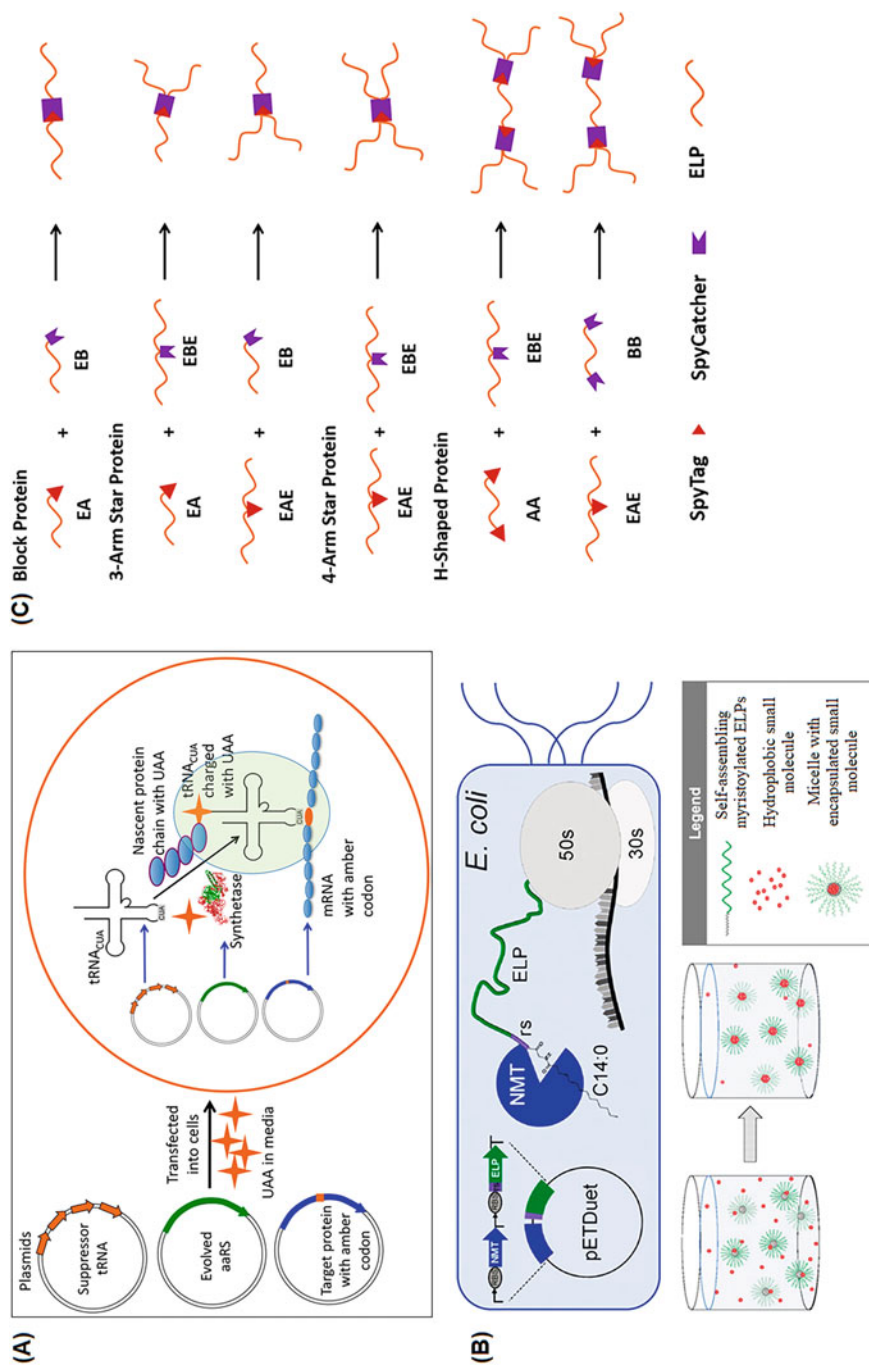**Fig. 6.2** (a) Schematic for unnatural amino acid incorporation into polypeptides using plasmids encoding the suppressor tRNACUA, the evolved amino acyltRNA synthetase (aaRS), and the target protein with the amber codon that are transfected into cells. Reproduced with Permission from Mitra (2013). Copyright

(PCE) composed of 80 pentameric repeats of VPGVG motif and the second (PCD) bearing a self-assembling amphiphilic diblock consisting VPGVG and VPGSG motifs. Biorthogonal approach was used to harness the intrinsic thermo-responsive nature of the ELP modules to create thermo-responsive gel particles and then stabilized the gel particles by photo-cross-linking of the pendant pAzF moiety via photolytic formation of the reactive nitrene. The biorthogonal strategy generates gel particles of different sizes spanning the mesoscale by tuning the ratio of PCE to PCD as well as their phase transition temperature (T_t), while integration with microfluidic devices enables the creation of microscale gel particles. This native biological machinery has been used to incorporate *p*AzF into suckerin-12 (S12), and thus facilitating controllable formation of nano-assembled architectures (Hershewe et al. 2020). Multisite insertion of UAAs into polypeptide backbones holds great promise in the fabrication of next-generation protein-based biomaterials, but this approach has not been well exploited in biomaterials design.

6.2.2 Posttranslational Modifications of Polypeptides

Posttranslational modifications (PTMs) of proteins are an orthogonal chemical approach that nature uses to modify proteins after expression, leading to the expansion of protein building blocks and increased proteomic diversity (Macek et al. 2019). PTMs can provide exciting opportunities for conceptually new types of polypeptide-based materials incorporating nonproteogenic moieties as well as increasing the chemical diversity of polypeptide-based nanotechnologies (Ramazi and Zahiri 2021). Although hydroxylation of tyrosine and proline has been mostly used as archetypal of natural PTMs to create genetically encoded recombinant materials that mimic mussel foot protein (Brennan et al. 2017) and collagen (Pinkas et al. 2011), there are numerous natural PTMs such as phosphorylation, glycosylation, ubiquitination, *S*-nitrosylation, methylation, lipidation, *N*-myristoylation, *N*-acylation, S-palmitoylation, *S*-prenylation, proteolysis, amongst others that have remained largely untapped in polypeptide-based materials design (Ramazi and Zahiri 2021).

Fig. 6.2 (continued) © 2013 Labome (www.labome.com). (**b**) Posttranslational strategy to functionalize ELPs with a myristoyl moiety to facilitate encapsulation of hydrophobic drugs. Reproduced with permission from Luginbuhl et al. (2017). Copyright © 2017 Wiley-VCH. (**c**) Topological diversification of ELPs using the SpyTag-SpyCatcher chemistry. The synthetic ELPs have unconventional nonlinear topologies including block, 3-arm, 4-arm and H-shaped configurations. This diversification occurs through binding of an ELP bearing the SpyTag to a second component bearing the SpyCatcher, leading to the formation of circular, tadpole, star, and H-shaped topologies. Adapted with permission from Zhang et al. 2013. Copyright © 2013 American Chemical Society

In 2017, Luginbuhl et al. (2017) demonstrated the possibility to posttranslationally functionalize ELPs with a myristoyl moiety. The new class of hybrid materials were synthesized by in situ conjugation of myristic acid through an N-myristoyltransferase (NMT) catalyzed reaction between the N-terminal glycine of the ELP backbone and the activated thioester of myristoyl-CoA (Fig. 6.2b). The myristoylated ELPs create genetically programmable spherical micelles and aggregates. The lipid cores of the self-assembled materials were harnessed to facilitate encapsulation and release of hydrophobic anticancer drug molecules doxorubicin and paclitaxel, which exhibit cytotoxic effect against cancer cell lines 4 T1 and PC3-luc. These materials also promote longer plasma circulation than the free drug molecules administered intravenously in mice. A similar module of myristoylated ELPs exhibits temperature-triggered hierarchical self-assembly across multiple length scales and varied morphologies, leading to the creation of novel responsive biohybrid materials (Mozhdehi et al. 2018). To increase the chemical diversity of lipidate ELPs, Mozhdehi et al. (2019) created cholesterol-modified analogs of the myristoylated ELPs using genetically encoded PTM. The authors demonstrated the possibility to use Hedgehog proteins (Hh) fusions to facilitate site-specific incorporation of cholesterol moiety at the C-terminus of an ELP. The incorporation of a single cholesterol group enables the self-assembly of cholesterol-ELP conjugates into micelles, rendering the resulting materials more biologically relevant. Put together, the two PTM approaches developed in the Chilkoti laboratory represent a landmark strategy to facilitate region- and site-selective incorporation of fatty acids.

6.2.3   Incorporation of Cross-Linking Moieties

Chemical cross-linking usually results in the formation of permanent and irreversible covalent bonds between chemically active functional groups in the polypeptide backbones. Substitution of the primary amine of the lysine residue in the polypeptide backbones has been used to incorporate a reactive site such as aldehydes, maleimide, acrylates, norbornene, and allyl along the polypeptide backbones for cross-linking or further functionalization. Direct cross-linking of polypeptides has been carried out in this manner to fabricate hydrogels (Lim et al. 2007; Mchale et al. 2005) or films (Nowatzki and Tirrell 2004) with enhanced properties. Photo-cross-linking has been performed via conjugation of photo-reactive moieties to the polypeptide backbones (Nagapudi et al. 2002; Farrell et al. 2005; Raphel et al. 2012). This strategy has been used to fabricate methacryloyl-substituted tropoelastin (MeTro) hydrogels with tunable elasticity and stiffness (Annabi et al. 2013) and high adhesive strength to effectively stop lung leakage in a rat model in the absence of sutures or staples (Annabi et al. 2017). Resilin-like polypeptides (RLP) functionalized with acrylamide moiety can be photo-cross-linked into hydrogels with tunable microstructures and macroscale mechanical properties (Garcia Garcia et al. 2021). The SpyTag and SpyCatcher system, which are split domains derived from the autocatalytic isopeptide bond-forming subunit from *Streptococcus pyrogenes* (Zakeri and

Howarth 2010; Zakeri et al. 2012), is an attractive platform to promote intermolecular interactions between molecular building blocks leading to the formation of innovative materials. When the polypeptides and other building blocks are functionalized with SpyTag and SpyCatcher moieties, interaction between these reactive partners can lead to covalent cross-linking of the building blocks via a specific aspartic acid on the SpyTag and a specific lysine residue on the SpyCatcher, and consequently creation of materials with controllable topology and enhanced stability (Fig. 6.2c) (Zhang et al. 2013; Hollingshead et al. 2017).

Beyond the possibility to use in situ cross-linking strategy to enhance the mechanical properties of single-component polypeptide-based materials, this phenomenon can be harnessed to drive the formation of multicomponent materials with complex properties and multifunctional applications. Therefore, in the subsequent sections, we will demonstrate how the incorporation of unnatural amino acids and cross-linking moieties into polypeptide backbones as well as the use of posttranslational modification has been used facilitate creation of polypeptide-based multicomponent materials.

6.3 Creating Multicomponent Materials with Polypeptides

Although each class of polypeptides has some unique features that make them suitable for specific applications, the possibility to hybridize multiple polypeptides during materials development offers huge opportunities not only to integrate the inherent properties of individual components but also harness new properties not inherent in the individual polypeptides. To develop multipolypeptide materials, both chemical (covalent) and physical (noncovalent) interactions have been used to integrate polypeptide building blocks including RLP, ELP, collagen-like polypeptides (CLP), and silk-like polypeptides (SLP).

As the natural resilin, RLP exhibit impressive mechanical properties including rubber-like elasticity, efficient energy storage, exceptional resilience, and fatigue life. The disordered conformation of RLPs underpins their capability to respond to multiple stimuli such as temperature, moisture, ions, and pH. Nevertheless, RLP-based materials are limited by low stiffness (Wang et al. 2021). Consequently, the intrinsic properties of RLP have been synergized with those of other polypeptides to create multicomponent materials with improved properties for multifunctional applications. For example, covalent cross-linking of RLP and collagen fibers mediated by poly(ethylene glycol) ether tetrasuccinimidyl glutarate generates a highly elastic scaffolds (Fig. 6.3a) (Sanami et al. 2015). While the stress and strain at break values of the scaffolds are several orders of magnitudes higher than values obtained for collagen alone scaffolds, the modulus values were significantly reduced. In addition, the incorporation of RLP did not compromise the inherent biological activities of collagen. This is a clear demonstration of how to maximize the potential of polypeptides in biomedical arena. Dual phase behavior, upper critical solution temperature (UCST, ~6 °C), and lower critical solution
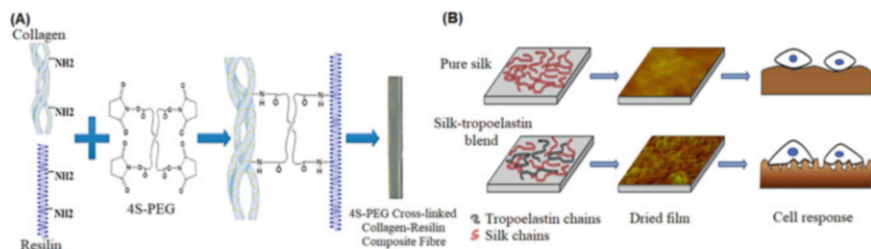
Fig. 6.3 (**a**) Rational design of highly elastic multicomponent materials based on covalent cross-linking between collagen and resilin-like polypeptide mediated by 4-arm poly (ethylene glycol) ether tetrasuccinimidyl glutarate as a cross-linker. Reproduced with permission from Sanami et al. (2015). Copyright © 2015 IOP Publishing Ltd. (**b**) Blending and drying of silk and tropoelastin create micro- and nanoscale porous 2D materials which promote better stem cell adhesion and proliferation than pure silk-based materials. Reproduced with permission from Hu et al. (2010). Copyright © 2021 Elsevier

temperature (LCST) (~70 °C) are unique properties of RLP. At these temperatures, RLP undergoes phase separation in solution, whereas it remains soluble in solution within this nonphysiological temperature range (Dutta et al. 2011). Any effort to reduce the LCST to a physiological temperature will constitute an attractive platform to tailor-made RLP for a wide range of biomedical applications including drug delivery and tissue engineering. In order to demonstrate the possibility to engineer the intrinsically disordered conformation of RLP, tune the LCST values and gain insight into the temperature-induced morphological changes of RLP by supramolecular co-assembly, Whittaker et al. (Whittaker et al. 2015) co-assembled RLP (Rec-1) with poly-L-proline (PP, a rigid model of polypeptide) or silk fibroin (SF, a model of hydrophobic rigid protein) via supramolecular interactions. Due to these interactions, the co-assembled polypeptides (RLP-PP or RLP-SF) acquired new ordered conformations as well as increased hydrophobicity, leading to LCST values comparable to the pure RLP. Such supramolecular engineering approach to tune the conformation of polypeptides has been used to lower the LCST values of ELPs via supramolecular co-assembly of ELPs of different molecular weights and amino acid sequences, as well as varying the mixing ratio of the ELPs (Fernández-Trillo et al. 2008; Ge et al. 2010). In contrast to the use of supramolecular co-assembly to integrate RLP and ELP, Chilkoti and co-workers developed RLP-ELP amphiphilic diblock copolymers that exhibit the ELP-like LCST and RLP-like UCST and self-assemble into spherical or cylindrical micelles (Weitzhandler et al. 2017). While the hydrophobic RLP constitute the core of the micelles and drives the self-assembly of the copolymers, the hydrophilic ELP represents a corona-forming domain that drives a transition from spherical to cylindrical morphology. The major findings of the study are (1) there is a minimum threshold length of the RLP block below which self-assembly does not occur regardless of the length of the ELP block, (2) the length of RLP block is a unique molecular parameter to independently tune copolymer self-assembly, and (3) increasing the hydrophobicity of the corona-forming ELP drives a morphological transition from spherical to cylindrical micelles. Such systems can

find application as nanoscale dual drug delivery vehicles in which case a hydrophobic drug is encapsulated in the hydrophobic core while hydrophilic drug is encapsulated in the hydrophobic corona of the polypeptide-based multicomponent nanostructures. Moving beyond engineering phase transition and morphological transformation of RLP, Li et al. (2013) developed RLPs bearing cell-binding and matrix metalloproteinase (MMP) domains. Chemical cross-linking of the mixtures of these RLPs produced hydrogels with elastic moduli in the range of 1–25 kPa and are suitable for 3D encapsulation of human mesenchymal stem cells (hMSCs) with excellent cell viability. Lv et al. (2010) developed a modular approach to design a novel multiblock polypeptide comprising a folded streptococcal-derived immunoglobulin-binding domain of protein G (GB1) interspersed with RLP sequences. The GB1-RLP conjugates recapitulate the complex molecular spring structure of titin and combine the unique mechanical properties of each component. The rubber-like complex biomaterial displayed Young's modulus value that is comparable to that of myofibrils (50–100 kPa).

Polypeptide conjugates comprising of thermo-responsive ELP and a triple-helix-forming CLP have been used to create multicomponent vesicles that integrate the thermo-responsiveness of ELP with the triple-helix formation of CLP (Luo and Kiick 2015). To enable covalent conjugation of the two components, a standard copper-catalyzed azide-alkyne cycloaddition reaction between alkyne-functionalized ELP and azide-functionalized CLP was carried out. At physiological temperature, the CLP domain exhibits a triple helix conformation which became unfolded at elevated temperature. Due to the anchoring effect of ELP coacervation, the CLP triple helical structure was stabilized at high temperature (57 °C), while anchoring effect of the hydrophilic CLP triple helix remarkably reduced the inverse phase transition temperature of the ELP-CLP conjugates. The distinct structural transformation of the individual components underpins the formation of a bilayer walls of the multicomponent vesicles, with collapsed ELP domains in the center and the CLP triple helical domains at both the interior and exterior surfaces. This approach offers a new platform to control the thermo-responsiveness of ELPs. Considering the bioactivity of CLP, the new multicomponent materials can find application as thermo-responsive scaffolds for tissue engineering applications.

The impressive mechanical properties of silk fibroin have stimulated its widespread applications in material design. Silk is a semicrystalline fibrous protein with a hydrophobic β-sheet-dominated structure capable of forming high packing density materials. This unique structure endows silk with high tensile strength and their toughness is similar or higher than many polymers including Kevlar fiber—one of the toughest known materials (Jin and Kaplan 2003; Hu et al. 2008). In light of this, silk has been compounded with other polypeptides to improve the mechanical properties of the resulting multicomponent materials. For example, Kaplan and co-workers developed multicomponent biomaterials that combine the elasticity of ELP and mechanical robustness of silk fibroin by simple blending the two proteins followed by casting on a glass dish to create biocompatible films with 68–97% resilience and elastic modulus between 2 and 9 MPa, depending on the ratio of the two polymers, while supporting stem cell viability. Similarly, multicomponent

systems comprising ELP and SLP have been used to stimulate the differentiation of stem cells into cardiac and bone cells (Hu et al. 2011). The composite biomaterials were obtained by temperature-controlled annealing, which amplifies the β-sheet conformation and thereby generates insoluble elastin/silk polypeptides composites. Materials with high concentration of ELP and surface roughness elicit osteogenic differentiation of human mesenchymal stem cells (hMSCs), whereas low surface roughness and high stiffness direct myogenic differentiation of C2C12 cells (Fig. 6.3b). Tirrell and co-workers harness the complementary interactions between the SpyTag and SpyCatcher to create hydrogels based on bioactive ELPs functionalized with the reactive partners (Sun et al. 2014). The resulting hydrogels are composed of "network of Spies" bearing cell-adhesion epitope, matrix metalloproteinase-1 cleavage sites, and full-length globular proteins (mCherry and leukemia inhibitory factor) and improved the pluripotency of encapsulated embryonic stem cells. This study clearly shows that this versatile strategy can be harnessed to design information-rich biomaterials to target complex tissue regeneration.

The desire to improve biomedical applications of silk has led to the development of silk-ELP polypeptides (SELPs), which combine the tandem repeats of silk-like domain from Bombyx mori silk heavy chains (GAGAGS) with ELP blocks (Nagarsekar et al. 2002; Hardy and Scheibel 2009; Hu et al. 2010). The first generation of SELPs generated biocompatible and irreversible gels at physiological temperature (Cappello et al. 1998). The gelation time for the gels can be decreased by increasing the number of silk blocks. Due to the intrinsic thermo-responsiveness of the ELP domain and tendency of SLP to self-assemble into insoluble tightly packed β-sheets, SELPs can undergo self-assembly into micellar nanostructures driven by both hydrophobic and hydrogen bonding interactions (Xia et al. 2011). While the hydrophobic SLP domains constitute the core of the nanostructures, the hydrophilic ELP domains form the corona. By applying heating–cooling cycling and controlling the ratio of SLP-to-ELP, the self-assembly can be controlled reversibly or irreversibly to induce morphological changes from nanoparticles to nanofibers.

Although two-component materials combining the intrinsic properties of individual polypeptides have been extensively investigated, the possibility to integrate more than two polypeptides will represent a useful strategy to develop biomaterials with ECM-like molecular complexity, tailored mechanical properties, and biological functions in an unprecedented manner. In 2011, Bracalello et al developed the first example of chimeric recombinant materials integrating the repetitive amino acid sequences derived from resilin, elastin, and collagen. The RLP-ELP-CLP chimera were genetically developed using the recursive directional ligation approach, which involves a stepwise combination of the repetitive sequences in tandem via recombinant DNA techniques. Aqueous solution of the multicomponent structure exhibits a circular dichroism (CD) fingerprint that is predominantly poly proline II left-handed helix (PPII), typical of collagen. On the other hand, in the presence of the less polar trifluoroethanol, the CD spectra is a mixture of β-turns and random coil that are reminiscent of the secondary structures of RLP and ELP, respectively, on their own right. Also, an aqueous solution of the chimeric systems undergoes morphological transition from a globular structure to aligned nanofibers with Young's modulus in

the range of 0.1–3 MPa in a time and temperature-dependent manner. Although the biomedical applicability of this system is yet to be explored, it could be a powerful platform to develop synthetic extracellular matrix whereby the effect of a complex mixtures of bioactive polypeptides on cellular behaviors can be dissected using high-throughput screening approaches such as materiomics (Groen et al. 2016).

6.4 Creating Multicomponent Materials Combining Polypeptides and Synthetic Polymers

6.4.1 Pros and Cons of Polypeptide-Based and Synthetic Polymer-Based Materials

Hybridizing polypeptides and synthetic polymers in a single material offers the unique opportunities to combine the best of both worlds. This approach represents an interesting strategy to synergise the properties of the two classes of materials and to overcome some of their inherent limitations (as shown in Table 6.1). A key feature of synthetic polymers is that they can display chemical functionality with which they

Table 6.1 Potential advantages and disadvantages of only polypeptide/protein-based, only synthetic polymer-based, and polypeptide/protein–polymer multicomponent biomaterials

Properties	Polypeptide/protein-based biomaterials	Synthetic polymer-based biomaterials	Hybrid polypeptide/protein-polymer biomaterials
Physical/mechanical	– Limited with lower and upper protein concentrations – Narrow mechanical tunability	– Mechanical properties can be tuned by increasing concentration or cross-linking intensity	– Mechanical properties can be tuned by adjusting component ratio
Biological	– Biocompatible – Might be toxic in high concentrations – Support cell adhesion – Potential immunogenic	– Vary in biocompatibility – Might be toxic in high concentrations – Do not support cell adhesion – Not immunogenic	– More biocompatible compared to only polymer-based group – Might be toxic in high concentrations – Support cell adhesion – Less immunogenic compared to only protein-based group
Chemical	– Open to enzymatic degradation – Form hierarchical structure	– Low enzymatic degradation – Form random structure	– Less enzymatic degradation compared to only protein-based group – Possible hierarchical structure formation
Cost	Higher	Lower	Medium

are designed to create materials with a diverse range of properties such as stimuli-responsiveness (Jochum and Theato 2013), conductivity (Nezakati et al. 2018), and having proper mechanical properties (Haq et al. 2017). Notwithstanding, most synthetic polymers are toxic to biological systems, and there is limited control over their nanoscale structure. Incorporating biological domain into a polymer backbone can impart the resulting materials with improved biocompatibility and allow interaction with biological systems, which are desirable for drug delivery and tissue engineering applications. Polypeptides are known to undergo self-assembly into stable hierarchical structures across multiple length scales driven by their intrinsic secondary structures. Incorporation of polypeptides into polymer structures can provide additional driving force, provided by the secondary structures, for the self-assembly of peptide–polymer conjugates, and thus results in a better control of the design of multicomponent materials and their properties.

6.4.2   Overarching Strategies for Designing Polypeptide—Synthetic Polymer Hybrids

Main approaches to obtain multicomponent hybrid materials based on the chemical conjugation of polypeptides and synthetic polymers fall into three categories: (i) Atom transfer radical polymerization (ATRP) (Rettig et al. 2004; Broyer et al. 2008), (ii) reversible addition fragmentation chain transfer (RAFT) polymerization (Liu et al. 2007a), (iii) R-amino acid N-carboxyanhydride (NCA) ring-opening polymerization (ROP) (Tardy et al. 2017), and click chemistry (Quadir et al. 2014), among others. These techniques facilitate the incorporation of polypeptides/proteins into polymer networks and offer the possibility to create tailor-made multicomponent biomaterials with predictable mechanical properties. The traditional ATRP method has been used to drive polypeptide-polymer conjugation. Using a combination of ATRP, ROP, and Click approaches, poly(n-butyl acrylate) (PBA) has been covalently conjugated with the highly hydrophobic and β-sheet forming poly(L-valine) to create PBA-b-poly(L-valine) with good control of molecular weight and composition (Sinaga et al. 2007). Polypeptide conjugates of various synthetic polymers including poly(ε-caprolactone) (PCL) (Gradišar et al. 2018), poly(lactic acid) (PLA) (Arimura et al. 2004), poly(pentadecalactone) (PPDC) (Tinajero-Díaz et al. 2019), and poly(lactic-co-glycolic acid) (PLGA) (Hong et al. 2014) have been obtained using ROP reactions. Polymerization of poly[N-(2-hydroxypropyl)-methacrylamide)] (poly[HPMA]) with poly(L-lysine) (PLL) to form block copolymers of polypeptide/synthetic polymers has been achieved by combining NCA and RAFT polymerization approaches (Tappertzhofen et al. 2015).

6.4.3 Designing Inducible Systems Via Polypeptide–Synthetic Polymer Conjugation

Creation of dynamic or inducible materials based on the interactions between polypeptides and synthetic polymers remains an attractive strategy to mimic the dynamic nature of the biological systems and therefore constitute a useful tool in bioengineering. The possibility to engineer morphological transformation in polypeptide-polymer hybrid systems by a variety of stimuli has been extensively demonstrated. For example, Gao et al. (2011) developed a thermo-responsive dumbbell-like polymer conjugate via ATRP-mediated in situ growth of poly(oligo(ethylene glycol) methyl ether methacrylate) (poly (OEGMA)) from the first and third blocks of a triblock ELP (tELP). The attachment of poly(OEGMA) to the tELP significantly increases the hydrophobicity of the conjugate, leading to a significant increase in the inverse phase transition temperature of the conjugate. While oscillatory rheological profile of the tELP-poly(OEGMA) conjugate shows a temperature-dependent evolution of an elastic network leading to the formation of gel-like materials at ≥ 70 °C, pure tELP shows a viscous component-dominated structure that could not result in gel-like materials across a broad range of temperatures. An in vitro enzymatic degradation assay on the tELP-poly(OEGMA) conjugate shows that the presence of tELP can promote a timely degradation of the material in the presence of collagenase. This study showcased the synergistic benefits of both components whereby the synthetic polymer provides the physico-mechanical properties and the polypeptide confers biological functionality, bridging together the world of synthetic polymer and polypeptides for an effective performance of biomaterials. To investigate the self-assembly propensity and stimulus responsiveness of ELP-PEG conjugates, alkyne-azide cycloaddition reaction was used to conjugate ELP and PEG blocks functionalized with azide and cyclooctyne moieties, respectively (Van Eldijk et al. 2014). Following the formation of amphiphilic ELP-PEG block copolymers, the introduction of sodium chloride (NaCl) into the system triggers self-assembly into micelles having a hydrophobic ELP core and hydrophilic PEG corona. Encapsulation of 1-anilinonaphthalene-8-sulfonic acid, a hydrophobic fluorescent dye that fluoresces in hydrophobic environment, in the cores of the micelles was used to demonstrate the potential applicability of the micelle as a drug delivery vehicle. Also, ring opening metathesis polymerization (ROMP) was used to prepare thermo-responsive random copolymers of ELP monomers and oligo(ethylene glycol)-based monomers (Conrad and Grubbs 2009).

6.4.4 Opportunities for Multicomponent Polypeptide/Protein-Synthetic Polymer Biomaterials in Bioengineering Applications

The synergistic combination of polypeptides and synthetic polymers may produce new biomaterials that possess novel properties and functionalities for biomedical applications. Manipulation of mechanical properties and cellular behaviors can be
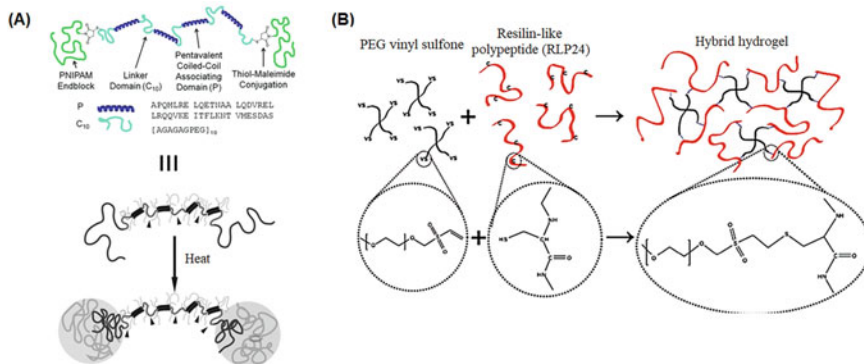
Fig. 6.4 (**a**) Molecular design of a thermo-responsive polypeptide-synthetic polymer conjugate composed of PNIPAM (green chains) and coiled coil polypeptide (blue chains). The self-assembled protein-polymer triblock copolymers are able to respond to heat induction, that drives emerging shear-thinning and mechanically robust (up to five-fold) hydrogels. Adapted with permission from Glassman et al. (2013). Copyright © 2013 Wiley-VCH. (**b**) Covalent interaction between RLP and PEG vinyl sulfone that forms hybrid hydrogels. The hybrid hydrogels were obtained through a Michael-type addition reaction between RLP cysteine residues and vinyl sulfones of an end-functionalized multiarm star PEG. Reproduced with permission from McGann et al. (2013). Copyright © 2013 Wiley-VCH

achieved by conjugating the two distinct class of materials. Glassman et al. (2013) used physical interactions in both thermo-responsive poly(N-isopropylacrylamide) (PNIPAM) and an engineered polypeptide networks of a triblock polymer-polypeptide copolymer to create double-network hydrogels with reversible energy dissipation, enabling both toughness and fatigue resistance (Fig. 6.4a). The thermo-responsive block copolymer self-assembled to form a second reinforcing network within a single-network shear thinning gel initially formed via coiled-coil aggregation of the polypeptide domain. The thermo-responsive reinforcement approach reduces the high temperature creep compliance of the hydrogels by over four orders of magnitude, decreases the erosion rate by at least a factor of five, and increases the yield stress by up to a factor of seven. These multicomponent hydrogels and the sequential method used to fabricate them can be an attractive strategy to precisely control the interaction of an implantable scaffold with a target tissue environment while delivering therapeutics and cells for regenerative purposes. Also, the thermo-responsive properties of multicomponent hydrogels can render them extremely useful in cell-sheet engineering applications (Swierczewska et al. 2008). Chemical conjugation of collagen polypeptide with PEG diacrylate enables creation of hybrid hydrogels able to stimulate cell-manipulated cross-linking and production of native ECMs by encapsulated chondrocytes with prolong retention of collagen I within the hydrogels (Lee et al. 2006).

McGann et al. (2013) developed cysteine-containing RLPs that can be cross-linked with vinyl sulfone-functionalized four-arm PEG via Michael-type addition

reaction (Fig. 6.4b). This approach enables the integration of chain architecture of PEG with inherent biological functionality of RLP, leading to the creation of self-supporting hydrogels with elastic moduli ranging from 7 to 12 kPa. Human aortic adventitial fibroblast cells encapsulated in the hydrogels show high viability and a spread morphology, suggesting the potential of this novel hydrogels in cardiovascular applications. Similarly, McGann et al. (2016) used photoinitiated thiol-ene reactions to cross-link norbornene-functionalized RLP and multiarm PEG thiols to create elastic multicomponent hydrogels at concentrations of RLP much more below the concentration required to prepare RLP only hydrogels, suggesting that incorporation of PEG domain confers additional structural organization. The cross-linking approach enables encapsulation of mesenchymal stem cells during hydrogel preparation without compromising cell viability. The micromechanical environment in multicomponent hydrogels can influence cellular function and as such understanding the micromechanics of multicomponent hydrogels will enhance the design of biomaterials for tissue engineering. Considering this, Lau et al used small-strain oscillatory shear rheometry, compression dynamic mechanical analysis, small-strain microindentation, and large-strain indentation puncture to investigate the influence of microstructure of multicomponent hydrogels prepared with acrylamide-functionalized RLP and 4-arm PEG acrylate on bulk and local micromechanical properties of the hydrogels (Lau et al. 2020). Cyclic loading–unloading microindentation of the RLP-PEG hydrogels revealed high resilience value (85%), and the failure initiation is controllable by the RLP-rich domain.

Liquid–liquid phase separation (LLPS) is a well-known approach to create heterogeneous microstructures through coalescence of two dissimilar polymer blends, proteins and polysaccharides into dense phase that resembles liquid droplets (Alberti et al. 2019). This approach has emerged as a fascinating strategy to fabricate multicomponent nanostructures based on supramolecular interactions between polypeptides and synthetic polymers. LLPS of aqueous solutions of RLPs and 4-arm PEG-NH_2 was used to create tunable microstructures, which were further captured via a Mannich-type reaction mediated by tris(hydroxymethyl phosphine) (THP) (Lau et al. 2017). Multicomponent hydrogels with controllable micromechanical properties were created through this reaction. In a follow-up study by the authors, photo-induced cross-linking was used to capture microstructures created by LLPS of aqueous solutions of RLP-4 AC and PEG-4 AC and generate multicomponent hydrogels with chemically, morphologically, and mechanically distinct phases (Lau et al. 2018).

6.5 Creating Multicomponent Materials Combining Polypeptides and Nanoparticles

Material platforms that exploit the functionalities of polypeptides and nanoparticles (NPs) as well as their hybridization offer an exciting possibility for the engineering of advanced materials with high spatiotemporal control and multiple functionality.

This concept has rapidly expanded the scope of nanotechnology from NPs synthesis and characterization toward hierarchical organization of NPs such as inorganics and carbon nanomaterials into higher order structures. Another opportunity for engineering polypeptide-NPs composite materials stems from the growing recognition that the disordered regions of proteins play a pivotal role in their dynamic properties (Okesola and Mata 2018). The possibility to control the disorder–order transition in polypeptides through the interaction with NPs would represent a major step forward in harnessing new properties from polypeptide-based materials.

The possibility to encode polypeptides with molecular recognition motifs for selective interaction with NPs pave the way to integrate the intrinsic magnetism, optical properties, electrical conductivity, adhesiveness, and spatial distribution of NPs with the inherent phase transition behaviors, structural conformation, self-assembly, and biological functionalities of polypeptides in polypeptides-NPs hybrid structures for applications in drug delivery (Mitchell et al. 2021), photodynamic therapy (Lucky et al. 2015), immunotherapy (Irvine et al. 2015), tissue engineering (Fang et al. 2020), optics and photonics, catalysis (Gao et al. 2021), nanoelectronics (Murray 2008), and biosensing and bioimaging (Derkus 2016).

6.5.1 Multicomponent Materials Based on Polypeptides and Carbon Nanoparticles

The emergence of carbon nanomaterials has provided a great opportunity for the development of functional hybrid materials. Carbon nanomaterials including one dimensional (1D) carbon nanotubes and two-dimensional (2D) graphene derivatives are known for their valuable optical, mechanical, electronic, and thermal properties (Zhu et al. 2010; Novoselov et al. 2012; Daneshvar et al. 2021). Due to these properties, carbon nanomaterials constitute an integral part of materials in nanomedicine, optoelectronics and biotechnological applications (Janssen and Nelson 2013; Maiti et al. 2019). The possibility to integrate the distinct properties of carbon NPs with those of the polypeptides present an incredible opportunity to develop multifunctional and multicomponent materials for high-tech applications. Integration of ELP with carbon NPs to create functional hybrid materials has attracted increasing attention in the past decades.

Wang et al. (2013) reported the elegant design of ELP-graphene oxide (rGO) hybrid hydrogel actuators that undergo rapid and tunable motions including finger-like flexing and crawling controllable by light position, intensity, and path (Fig. 6.5a). Taking advantage of the modular nature of ELP, the authors incorporated graphene-binding peptide motifs in the ELP backbone. Due to this binding motif, rGO noncovalently co-assembled with the ELP to create ELP-rGO composite nanoparticles, which undergoes thermal- and near-infrared light-induced aggregation due to the inverse phase transition of ELP and photothermal heating of rGO. This study and others (Guo et al. 2019) show how the best of both world of carbon nanomaterials and polypeptides can be synergized to develop dynamic, responsive,
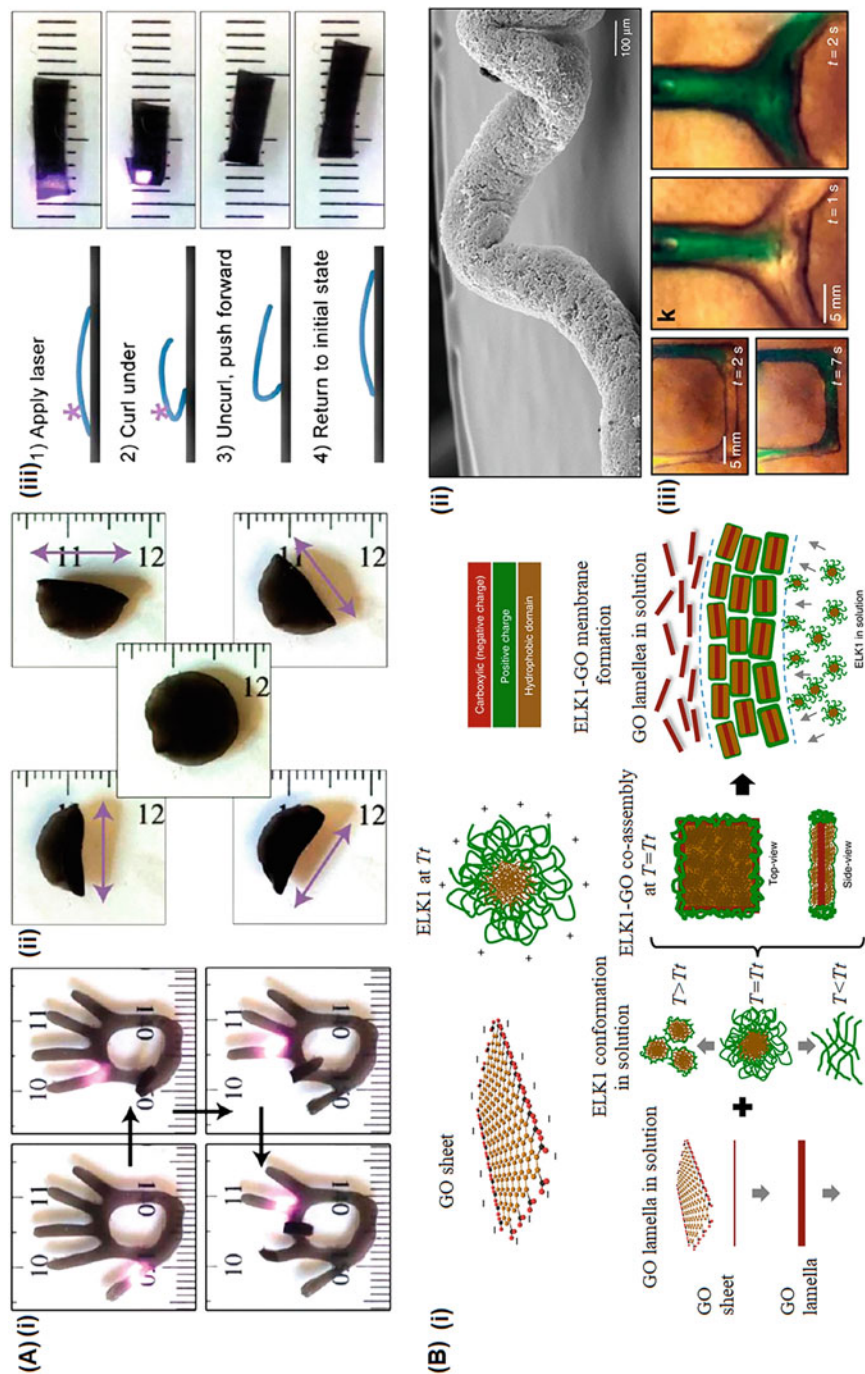
Fig. 6.5 (**a**) Controlled motion of anisotropic GO-ELP multicomponent hydrogels created through the interaction of a~50 pentapeptide long ELP with rGO in the presence of water vapor. Laser was used to (i) bend and unbend fingers of hand-shaped hydrogels, (ii) facilitate direction-dependent folding of a circular

and functional materials with potential applications in soft robotics (Lee et al. 2020; Son and Yoon 2020). In a follow-up study, the authors confirmed that the stimuli-responsive GO-binding ELP can be used to dynamically modulate the aggregation of GO under low and high ionic strength to enable GO dispersion in organic solvents (Wang et al. 2014a). Hybrid ELP-GO composite materials prepared with an ELP functionalized with the cell-binding RGD motif also showed improved cell adhesion, which suggests that the ELP-GO composite materials can be useful for various biomedical applications (Li et al. 2017a).

The possibility to create ELP-based materials that can control the interplay between order and disorder conformations through supramolecular interactions with GO was demonstrated by Wu et al. (2020) (Fig. 6.5b). Diffusion reaction process was used to fabricate hierarchically organized and capillary-like ELP-GO materials that exhibit high stability, biocompatibility, and capacity to withstand flow. Because of the high stability of these innovative materials, they can be 3D printed into high fidelity perfusible and biocompatible device with tunable permeability and potential applications in microfluidics and organ-on-a-chip platforms (Wu et al. 2021).

RLP is another class of intrinsically disordered proteins that has dramatically changed the structure–function paradigm of composite materials (Balu et al. 2021). The excellent surface chemistry of GO has been harnessed to facilitate the directed self-assembly of RLP. Recently, Hu et al fabricated multifunctional RLP_{64}-graphene composite hydrogels via carbodiimide/N-hydroxysuccinimide-mediated strategy (Hu et al. 2019). The hydrogels display high adhesion strength (24 kPa), electrical conductivity (0.9 S/m), and improved stiffness and toughness. These multifunctional properties make the composite hydrogels ideal candidates for biosensors and bioelectronics applications. In another study by Balu et al. (2020), GO was incorporated into a photo-cross-linkable Rec1 to create hydrogels with improved hydrophobicity, resilience, amorphous domain, and biocompatibility relative to the pristine Rec1 hydrogels, showing the interplay of GO and RLP to create functional materials for biomedical engineering applications.

Hybridization of carbon nanoparticles with silk to create nanocomposite materials represents an innovative strategy to create multifunctional materials with enhance properties. Multicomponent materials composed of silk and carbon nanotubes have been utilized to develop flexible supercapacitors (Yang et al. 2020), flexible biocatalytic fuel cells (Tseng et al. 2016), and wearable triboelectric generators (Su and Kim 2020). Combining silk with GO can also be used to improve the biological properties of the resulting composite biomaterials. Uniform deposition of GO on silk

Fig. 6.5 (continued) hydrogel, and (iii) induce hydrogel curling. Reproduced with permission from Wang et al. (2013). Copyright © 2013 American Chemical Society. (**b**) (i) Supramolecular co-assembly of GO and cationic ELPs driven by a diffusion-reaction mechanism and disorder-to-order transition at the inversed phase transition temperature (T_t) of the ELPs create (ii) mechanically stable multicomponent tubular materials with capillary-like fluidic microstructures (iii) that can withstand fluid flow. Adapted with permission from Wu et al. (2020). Copyright © 2020 Nature Publishing Group

followed by in situ reduction of GO resulted in composite materials with nanofibrous architectures and improved conductivity and capability to promote cardiac tissue formation (Zhao et al. 2018; Zhao et al. 2020).

6.5.2 Multicomponent Materials Based on Polypeptides and Inorganic Nanoparticles

Nature is replete with diverse examples of organic–inorganic composite materials composed of stiff nanoscale inorganics and soft biomolecules (e.g., proteins, peptides, and polysaccharides) (Dunlop and Fratzl 2010; Gupta et al. 2005; Ji and Gao 2010). It is not just the combination but the hierarchical spatial organization of both the organic and inorganic constituents that gives rise to the remarkable stiffness and toughness of bone, teeth, nacre, and crustacean exoskeletons (Rho et al. 1998; Fratzl and Weinkamer 2007). This revelation has led to the development of high-performance synthetic analogs (Elsharkawy and Mata 2018).

Due to the modular nature of ELPs, they have been designed to incorporate motifs such as the statherin-derived peptide DDDEEKFLRRIGRFG to nucleate and promote apatite mineralization (Elsharkawy et al. 2016; Li et al. 2014; Tejeda-Montes et al. 2014; Tejeda-Montes et al. 2012). Li et al. (2017b) developed ELP nanofibers that promote intrafibrillar mineralization of hydroxyapatite in a manner that is similar to natural collagen nanofiber-guided biomineralization phenomenon. This ELP nanofiber-guided biomineralization event was attributed to the spatial confinement created by the acquired β-spiral conformation of the nanofibers. Mata and co-workers have extensively investigated how the disorder–order transition of ELP can be harnessed to direct apatite mineralization using both in vitro (Tejeda-Montes et al. 2012; Shuturminska et al. 2017) and in vivo (Tejeda-Montes et al. 2014) models. By systematic modulation of disorder–order transition of an ELP-based materials, Elsharkawy et al. developed a self-assembled membrane that can nucleate calcium phosphate and facilitate hierarchical growth and stabilization of hydroxyapatite crystals (Elsharkawy et al. 2018). The ELP-hydroxyapatite composite materials can be grown over large uneven surfaces of native tissues, exhibit acid resistant and high stiffness similar to those of the dental enamel. Combination of the conformational transformation of ELP and nanotopography can control the alignment and spatiotemporal orientation of apatite nanocrystals (Deng et al. 2021).

SLP can assemble with organic and inorganic structures at different levels. The modification of SLP with specific binding motifs for hydroxyapatite has been demonstrated by Huang et al. (Huang et al. 2007). The incubation of β-sheet-rich recombinant chimeric polypeptides films based on dragline spidroin and dentin matrix protein 1 in the simulated body fluid promoted the growth of hydroxyapatite crystals on the film surface. Similarly, genetically engineered chimeric polypeptides composed of SLP and silaffin-derived peptide (known as R5 peptides of *Cylindrotheca fusiformis* that is responsible for silica mineralization) have been reported to promote self-assembly and biomineralization of silica (Mieszawska et al. 2010). The presence of silica in the

SLP-R5 peptide hybrid films influenced osteogenic gene expression in hMSCs. These results indicate the potential use of these new silk–silica hybrid systems for bone regeneration. Also, SLP produced from recombinant minispidroins promotes homogenous formation of thick layer of crystalline calcium phosphate on the surface of SLP nanofiber following the incubation in modified simulated body fluid (Yang et al. 2010). The hybrid SLP-inorganic nanoparticles supported the growth of hMSCs, suggesting their potential applications in tissue engineering applications. Magnetosomes, which are natural magnetic nanoparticles synthesized by magnetotactic bacteria via biomineralization, are known for their exceptional magnetic properties that make them innovative NPs for nanotechnological applications (Yan et al. 2017). Genetically fused multicomponent polypeptides based on SLP and magnetosome membrane proteins enable the design of materials that enhanced magnetite biomineralization and caused the formation of a proteinaceous capsule, which increased the colloidal stability of isolated particles (Mickoleit et al. 2018). The genetically encoded hybrid composite materials can be used to design innovative nanotechnology platforms.

Apart from biomineralization, polypeptides have been explored as templates for the synthesis of inorganic metallic nanoparticles. For example, ELPs incorporating silver-binding motifs were designed and used to reduce chloroaurate ($[AuCl_4]_3^-$) to form gold nanoparticles or silver (Ag^+) ions to silver nanoparticles under physiological conditions (Anh et al. 2013). The aggregated or cross-linked spun-coated thin films of ELP-Ag composites possess antibacterial properties, indicating promising use as antibacterial biomedical implants. The ability of RLPs to interact with and stabilize inorganic NPs has stimulated their widespread use in nanomaterials engineering. Mayavan et al. (2011) demonstrated the use of the fluorescent *Rec1-resilin* as soft molecular template and capping agent for gold nanoparticles (AuNPs) via noncovalent interactions, leading to the formation of fluorophore-modified AuNPs with unique photophysical properties for potential applications in sensing devices. In contrast to the use of external reducing agent, Balu et al demonstrated a one-pot green synthesis of highly stable, fluorescent, and water-dispersible gold nanoclusters (AuNCs) harnessing the multifunctional properties of Rec1-resilin as both ligand, directing agent, template, and reducing agent (Balu et al. 2015), thus, rendering AuNCs as ideal fluorophores for bio-imaging, optoelectronics, catalysis, and biomedical engineering. In another study, the authors used *Rec1-resilin* to direct and stabilize platinum nanoparticles (PtNPs) to create colloidal fuel cell catalyst with the capability to enhance the performance of electrocatalytic fuel cell (Balu et al. 2019).

6.6 Creating Multicomponent Materials Combining Polypeptides and Other Molecules

The co-assembly of small- and macro-molecules with polypeptides has offered the possibility to create multicomponent materials with increasing levels of control including not only morphological organisation but also chemical gradients, hierarchical organization, and dynamic properties.

Peptide amphiphiles (PA), which are a class of self-assembling peptides with propensity to self-assemble into cylindrical nanofibers in an aqueous environment, have been explored as molecular manipulator to drive the spatiotemporal organization of polypeptides across multiple length scales. Inostroza-Brito et al. (2015) reported the formation of a highly ordered membranous architecture arising at the liquid–liquid interface between a solution of a positively charged PA and another of a negatively charged ELP (Fig. 6.5b). This polypeptide comprised four domains based on the pentameric sequence VPGXG (with X being isoleucine (I), valine (V), or glutamic acid (E)) derived from natural elastin while also included a fifth domain with the cell adhesion RGDS motif derived from fibronectin. When a small volume of PA solution is immersed in a large volume of an ELP solution, a dynamic interfacial assembly spontaneously develops and a closed membrane is formed, entrapping the PA solution inside it and leaving the ELP component outside (Fig. 6.6a). Shortly after the formation of the structure and upon contact with a surface, the membrane opens, adheres, and seals to the surface, creating a tubular structure. Small-angle X-rays scattering (SAXS) and scanning electron microscopy (SEM) have demonstrated that the co-assembly process in this case is determined primarily by the conformational changes of the ELP triggered by co-assembly with PA molecules. This work demonstrates that by slightly modifying the PA sequence, it is possible to access different co-assembling processes, which in turn generate different hierarchical structures and consequently biomaterial properties. The most remarkable assets of this ELP-PA system are its capability to access nonequilibrium for substantial periods of time as well as to enable growth and morphogenesis into vascular-like tubular structures that can serve as scaffolds for tissue engineering without the use of molds or templates.

One of the major limitations of PA-ELP multicomponent materials is their poor mechanical properties and instability in high ionic strength media. Covalent co-assembly holds great promise for the fabrication of hydrogels with controllable nanostructure, versatile chemical composition, and enhanced mechanical properties given its relative simplicity, high efficiency, and bond stability. Considering this, Okesola et al. (2020) designed multicomponent hydrogels based on photo-induced chemical interactions between an acrylamide-functionalized RLP and a thiolated PA ($C_{15}H_{31}$-CONH-V3A3E3CY) (Fig. 6.6b). The multicomponent hydrogels exhibit tunable conformation, nanostructures, high extensibility, and self-healing properties. By controlling the concentration of PAs co-assembled with the RLP, the authors were able to engineer the nanostructure of the materials from nano-beads (pure RLP) to beaded string (low PA concentration) and nanofibers (high PA concentration). These properties make the PA-RLP hydrogels ideal candidates for biomedical applications including tissue engineering and sustained drug release systems.

The possibility to create multicomponent materials composed of polysaccharides and polypeptides for a wide range of biomedical applications has attracted increased attention. For example, King et al. (2019) developed cytocompatible and elastomeric multicomponent hydrogels based on materials thiol-ene interactions between acrylamide-functionalized RLP (RLP-AM) and thiolated hyaluronic acid (HA-SH). The mechanical properties of the multicomponent hydrogels resembled
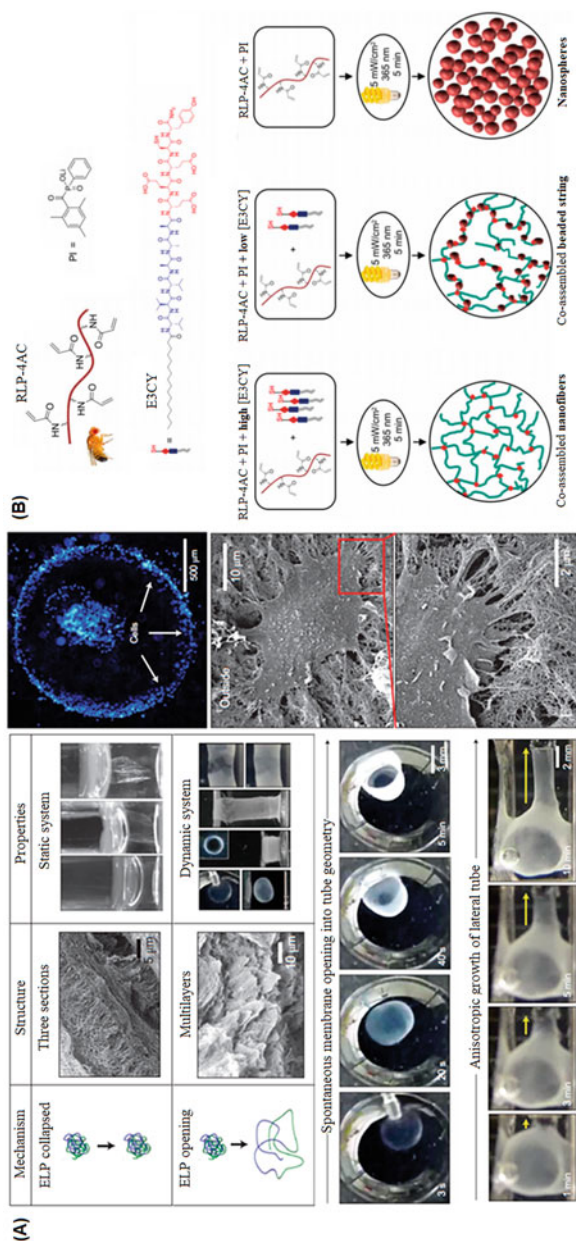
Fig. 6.6 (a) Supramolecular co-assembly of a cationic PA (PAK3) to control structure and conformation of an anionic ELP to spontaneously create membrane-like hydrogels with tunable architectures and significant biocompatibility. The emerged robust membrane exhibits a controlled assembly and disassembly, adhesion and sealing to surfaces, self-healing, and induced morphogenesis in spatiotemporal manner. Umbilical vein endothelial cells displayed an effective cell adhesion and spreading across the tubular structure. Reproduced with permission from Inostroza-Brito et al. (2015). Copyright © 2012 Nature Publishing Group. (**b**) Schematic for controllable nanostructures of multicomponent hydrogels based on thiol-ene photoclicked reaction between acrylic acid-modified RLP (RLP-4 AC) and thiolated PAs (E3Y). Reproduced with permission from Okesola et al. (2020). Copyright © 2020 Royal Society of Chemistry

native vocal fold tissue. Histological analysis revealed that the multicomponent hydrogels elicit only mild inflammation in vocal fold lamina propria with demonstrated safety in the airway for up to 3 weeks. These findings suggest that RLP-AM/HA-SH multicomponent hydrogels are highly promising materials for vocal fold tissue engineering. Similarly, photo-cross-linking of ELP and methacrylated HA (MeHA) gave rise to the formation of elastic multicomponent hydrogels with high tissue adhesive strength. Incorporation of zinc oxide (ZnO) nanoparticles into the hydrogels led to the creation of multicomponent organic–inorganic composite hydrogels with excellent antimicrobial properties against methicillin-resistant *Staphylococcus aureus* (MRSA). In addition, the composite hydrogels promote in vitro cell growth, spreading, and proliferation without eliciting any significant inflammatory response in vivo, suggesting that the hydrogels can be used as adhesive and antimicrobial biomaterials for tissue engineering applications (Shirzaei Sani et al. 2018).

6.7 Conclusion and Outlook

In this chapter, we presented an overview of different routes toward the creation of multicomponent materials from multiple polypeptides or via the interactions of polypeptides with other components including synthetic polymers, nanoparticles, and other molecular building blocks to take advantage of the best properties of each component. By rational design and site-specific modification of the polypeptides via the incorporation of unnatural amino acids, cross-linking moieties, or posttranslational modifications of the polypeptide backbones, the direct manipulation of polypeptides at the molecular level to form macro-scale 3D multicomponent superstructures can be achieved through interactions with other components. These design strategies were discussed alongside the possibility to harness new and multifunctional properties from the resulting multicomponent materials. The design and self-assembly of polypeptides have not only become an exciting field for multidisciplinary research but also opening new opportunities for a limitless variety of multicomponent materials to address the multifunctional materials discovery issues.

Despite impressive progress in recent years, to proceed from poor mechanical properties to robust materials with mechanical properties suitable for real-life applications, further substantial efforts are still required to explore the molecular design of polypeptides and their reacting partners to provide synergistic effects including strength and directionality that can modulate the resulting multicomponent materials in a predictable manner. This is particularly important for load-bearing applications including bone tissue engineering and microfluidic devices. In addition, the combination of two or more functional polypeptides and a second component could customize the functional complexity of the next generation of assorted building blocks and consequently create exciting novel multicomponent biomaterials. In this way, new advanced functionalities, which each single constituent component could

not produce individually, can appear from the collective and synergistic behavior of multicomponent materials. Furthermore, the sophisticated structural architecture of multicomponent materials and the intrinsic functionalities of the building blocks should be considered to achieve optimal design strategy and materials performance.

In summary, the broader opportunities for the design and functions of multicomponent materials that result from combining polypeptides and multiple types of building blocks are subject to a high level of control across various length scales and predictability of materials performance, thus enabling new discoveries and pushing the boundaries of complex material design.

References

Alberti S, Gladfelter A, Mittag T (2019) Considerations and challenges in studying liquid-liquid phase separation and biomolecular condensates. Cell 176:419–434

Amiram M, Haimovich AD, Fan C, Wang Y-S, Aerni H-R, Ntai I, Moonan DW, Ma NJ, Rovner AJ, Hong SH, Kelleher NL, Goodman AL, Jewett MC, Söll D, Rinehart J, Isaacs FJ (2015) Evolution of translation machinery in recoded bacteria enables multi-site incorporation of nonstandard amino acids. Nat Biotechnol 33:1272–1279

Anh TTH, Xing M, Le DHT, Sugawara-narutaki A, Fong E (2013) Elastin-based silver-binding proteins with antibacterial capabilities. Nanomedicine 8:567–575

Annabi N, Mithieux SM, Zorlutuna P, Camci-unal G, Weiss AS, Khademhosseini A (2013) Engineered cell-laden human protein-based elastomer. Biomaterials 34:5496–5505

Annabi N, Zhang Y-N, Assmann A, Sani ES, Cheng G, Lassaletta AD, Vegh A, Dehghani B, Ruiz-esparza GU, Wang X, Gangadharan S, Weiss AS, Khademhosseini A (2017) Engineering a highly elastic human protein–based sealant for surgical applications. Sci Transl Med 9:eaai7466

Arimura H, Ohya Y, Ouchi T (2004) The formation of biodegradable polymeric micelles from newly synthesized poly(aspartic acid)-block-polylactide AB-type Diblock copolymers. Macromol Rapid Commun 25:743–747

Balu R, Bourgeois L, Elvin CM, Hill AJ, Choudhury NR, Dutta NK (2015) A multi-responsive intrinsically disordered protein (IDP)-directed green synthesis of fluorescent gold nanoclusters. J Mater Chem B 3:6580–6586

Balu R, Choudhury NR, Mata JP, De Campo L, Rehm C, Hill AJ, Dutta NK (2019) Evolution of the interfacial structure of a catalyst ink with the quality of the dispersing solvent: a contrast variation small-angle and ultrasmall-angle neutron scattering investigation. ACS Appl Mater Interfaces 11:9934–9946

Balu R, Dorishetty P, Mata JP, Hill AJ, Dutta NK, Choudhury NR (2020) Tuning the hierarchical structure and resilience of resilin-like polypeptide hydrogels using graphene oxide. ACS Appl Bio Mater 3:8688–8697

Balu R, Dutta NK, Dutta AK, Choudhury NR (2021) Resilin-mimetics as a smart biomaterial platform for biomedical applications. Nat Commun 12:149

Bracalello A, Santopietro V, Vassalli M, Marletta G, Del Gaudio R, Bochicchio B, Pepe A (2011) Design and production of a chimeric resilin-, elastin-, and collagen-like engineered polypeptide. Biomacromolecules 12:2957–2965

Brennan MJ, Kilbride BF, Wilker JJ, Liu JC (2017) A bioinspired elastin-based protein for a cytocompatible underwater adhesive. Biomaterials 124:116–125

Broyer RM, Quaker GM, Maynard HD (2008) Designed amino acid ATRP initiators for the synthesis of biohybrid materials. J Am Chem Soc 130:1041–1047

Cappello J, Crissman JW, Crissman M, Ferrari FA, Textor G, Wallis O, Whitledge JR, Zhou X, Burman D, Aukerman L, Stedronsky ER (1998) In-situ self-assembling protein polymer gel systems for administration, delivery, and release of drugs. J Control Release 53:105–117

Catherine C, Oh SJ, Lee K-H, Min S-E, Won J-I, Yun H, Kim D-M (2015) Engineering thermal properties of elastin-like polypeptides by incorporation of unnatural amino acids in a cell-free protein synthesis system. Biotechnol Bioprocess Eng 20:417–422

Chin JW, Martin AB, King DS, Wang L, Schultz PG (2002) Addition of a photocrosslinking amino acid to the genetic code of *Escherichia coli*. Proc Natl Acad Sci 99:11020

Chou C, Uprety R, Davis L, Chin JW, Deiters A (2011) Genetically encoding an aliphatic diazirine for protein photocrosslinking. Chem Sci 2:480–483

Conrad RM, Grubbs RH (2009) Tunable, temperature-responsive polynorbornenes with side chains based on an elastin peptide sequence. Angew Chem Int Ed 48:8328–8330

Costa SA, Simon JR, Amiram M, Tang L, Zauscher S, Brustad EM, Isaacs FJ, Chilkoti A (2018) Photo-crosslinkable unnatural amino acids enable facile synthesis of thermoresponsive nano- to microgels of intrinsically disordered polypeptides. Adv Mater 30:1704878

Daneshvar F, Chen H, Noh K, Sue H-J (2021) Critical challenges and advances in the carbon nanotube–metal Interface for next-generation electronics. Nanoscale Adv 3:942–962

De La Rica R, Matsui H (2010) Applications of peptide and protein-based materials in bionanotechnology. Chem Soc Rev 39:3499–3509

Deng X, Hasan A, Elsharkawy S, Tejeda-montes E, Tarakina NV, Greco G, Nikulina E, Stormonth-Darling JM, Convery N, Rodriguez-Cabello JC, Boyde A, Gadegaard N, Pugno NM, AL-Jawad M, Mata A (2021) Topographically guided hierarchical mineralization. Mater Today Bio:100119

Derkus B (2016) Applying the miniaturization technologies for biosensor design. Biosens Bioelectron 79:901–913

Despanie J, Dhandhukia JP, Hamm-Alvarez SF, Mackay JA (2016) Elastin-like polypeptides: therapeutic applications for an emerging class of nanomedicines. J Control Release 240:93–108

Dunlop JWC, Fratzl P (2010) Biological composites. Annu Rev Mater Res 40:1–24

Dutta NK, Truong MY, Mayavan S, Roy Choudhury N, Elvin CM, Kim M, Knott R, Nairn KM, Hill AJ (2011) A genetically engineered protein responsive to multiple stimuli. Angew Chem Int Ed 50:4428–4431

Elsharkawy S, AL-Jawad M, Pantano MF, Tejeda-montes E, Mehta K, Jamal H, Agarwal S, Shuturminska K, Rice A, Tarakina NV, Wilson RM, Bushby AJ, Alonso M, Rodriguez-Cabello JC, Barbieri E, Del Río Hernández A, Stevens MM, Pugno NM, Anderson P, Mata A (2018) Protein disorder-order interplay to guide the growth of hierarchical mineralized structures. Nat Commun 9:2145–2145

Elsharkawy S, Mata A (2018) Hierarchical biomineralization: from nature's designs to synthetic materials for regenerative medicine and dentistry. Adv Healthc Mater 7:1800178

Elsharkawy S, Tejeda-Montes E, AL-Jawad M, Mata A (2016) Preferential nucleation and crystal growth on microfabricated topography. Mater Today 19:478–480

Elvin CM, Carr AG, Huson MG, Maxwell JM, Pearson RD, Vuocolo T, Liyou NE, Wong DCC, Merritt DJ, Dixon NE (2005) Synthesis and properties of crosslinked recombinant pro-resilin. Nature 437:999–1002

Fang J, Hsueh Y-Y, Soto J, Sun W, Wang J, Gu Z, Khademhosseini A, Li S (2020) Engineering biomaterials with micro/nanotechnologies for cell reprogramming. ACS Nano 14:1296–1318

Farrell IS, Toroney R, Hazen JL, Mehl RA, Chin JW (2005) Photo-crosslinking interacting proteins with a genetically encoded benzophenone. Nat Methods 2:377–384

Fernández-Trillo F, Van Hest JCM, Thies JC, Michon T, Weberskirch R, Cameron NR (2008) Fine-tuning the transition temperature of a stimuli-responsive polymer by a simple blending procedure. Chem Commun:2230–2232

Fratzl P, Weinkamer R (2007) Nature's hierarchical materials. Prog Mater Sci 52:1263–1334

Gao C, Lyu F, Yin Y (2021) Encapsulated metal nanoparticles for catalysis. Chem Rev 121:834–881

Gao W, Cho E, Liu Y, Lu Y (2019) Advances and challenges in cell-free incorporation of unnatural amino acids into proteins. Front Pharmacol 10

Gao W, Xu D, Lim DW, Craig SL, Chilkoti A (2011) In situ growth of a thermoresponsive polymer from a genetically engineered elastin-like polypeptide. Polym Chem 2:1561–1566

Garcia Garcia C, Patkar SS, Jovic N, Mittal J, Kiick KL (2021) Alteration of microstructure in biopolymeric hydrogels via compositional modification of resilin-like polypeptides. ACS Biomater Sci Eng

Ge X, Hoare T, Filipe CDM (2010) Protein-based aqueous−multiphasic systems. Langmuir 26:4087–4094

Glassman MJ, Chan J, Olsen BD (2013) Reinforcement of shear thinning protein hydrogels by responsive block copolymer self-assembly. Adv Funct Mater 23:1182–1193

Gradišar Š, Žagar E, Pahovnik D (2018) Hybrid block copolymers of polyesters/polycarbonates and polypeptides synthesized via one-pot sequential ring-opening polymerization. Polym Chem 9:4764–4771

Greig LM, Philp D (2001) Applying biological principles to the assembly and selection of synthetic superstructures. Chem Soc Rev 30:287–302

Groen N, Guvendiren M, Rabitz H, Welsh WJ, Kohn J, De Boer J (2016) Stepping into the omics era: opportunities and challenges for biomaterials science and engineering. Acta Biomater 34:133–142

Grunbeck A, Huber T, Sakmar TP (2013) Chapter fourteen—mapping a ligand binding site using genetically encoded photoactivatable crosslinkers. In: Conn PM (ed) Methods in enzymology. Academic Press

Guo L, Hao Y-W, Yang P, Li P-L, Sun N, Feng X-W, Zhao J, Chen C-A, Song J-F (2019) Fast fabrication of graphene oxide/reduced graphene oxide hybrid hydrogels for thermosensitive smart actuator utilizing laser irradiation. Mater Lett 237:245–248

Gupta HS, Wagermaier W, Zickler GA, Raz-ben Aroush D, Funari SS, Roschger P, Wagner HD, Fratzl P (2005) Nanoscale deformation mechanisms in bone. Nano Lett 5:2108–2111

Haq MA, Su Y, Wang D (2017) Mechanical properties of PNIPAM based hydrogels: a review. Mater Sci Eng C 70:842–855

Hardy JG, Scheibel TR (2009) Silk-inspired polymers and proteins. Biochem Soc Trans 37:677–681

Hershewe JM, Wiseman WD, Kath JE, Buck CC, Gupta MK, Dennis PB, Naik RR, Jewett MC (2020) Characterizing and controlling nanoscale self-assembly of Suckerin-12. ACS Synth Biol 9:3388–3399

Hino N, Okazaki Y, Kobayashi T, Hayashi A, Sakamoto K, Yokoyama S (2005) Protein photo-crosslinking in mammalian cells by site-specific incorporation of a photoreactive amino acid. Nat Methods 2:201–206

Hohmann T, Dehghani F (2019) The cytoskeleton—a complex interacting meshwork. Cell 8

Hollingshead S, Lin C-Y, Liu JC (2017) Designing smart materials with recombinant proteins. Macromol Biosci 17:1600554

Hong W, Chen D, Jia L, Gu J, Hu H, Zhao X, Qiao M (2014) Thermo- and pH-responsive copolymers based on PLGA-PEG-PLGA and poly(l-histidine): synthesis and in vitro characterization of copolymer micelles. Acta Biomater 10:1259–1271

Horsch J, Wilke P, Pretzler M, Seuss M, Melnyk I, Remmler D, Fery A, Rompel A, Börner HG (2018) Polymerizing like mussels do: toward synthetic mussel foot proteins and resistant glues. Angew Chem Int Ed 57:15728–15732

Hu X, Kaplan D, Cebe P (2008) Dynamic protein−water relationships during β-sheet formation. Macromolecules 41:3939–3948

Hu X, Park S-H, Gil ES, Xia X-X, Weiss AS, Kaplan DL (2011) The influence of elasticity and surface roughness on myogenic and osteogenic-differentiation of cells on silk-elastin biomaterials. Biomaterials 32:8979–8989

Hu X, Wang X, Rnjak J, Weiss AS, Kaplan DL (2010) Biomaterials derived from silk–Tropoelastin protein systems. Biomaterials 31:8121–8131

Hu X, Xia X-X, Huang S-C, Qian Z-G (2019) Development of adhesive and conductive resilin-based hydrogels for wearable sensors. Biomacromolecules 20:3283–3293

Huang J, Liu S, Zhang C, Wang X, Pu J, Ba F, Xue S, Ye H, Zhao T, Li K, Wang Y, Zhang J, Wang L, Fan C, Lu TK, Zhong C (2019) Programmable and printable Bacillus subtilis biofilms as engineered living materials. Nat Chem Biol 15:34–41

Huang J, Wong C, George A, Kaplan DL (2007) The effect of genetically engineered spider silk-dentin matrix protein 1 chimeric protein on hydroxyapatite nucleation. Biomaterials 28:2358–2367

Inostroza-Brito KE, Collin E, Siton-Mendelson O, Smith KH, Monge-Marcet A, Ferreira DS, Rodríguez RP, Alonso M, Rodríguez-Cabello JC, Reis RL, Sagués F, Botto L, Bitton R, Azevedo HS, Mata A (2015) Co-assembly, spatiotemporal control and morphogenesis of a hybrid protein–peptide system. Nat Chem 7:897–904

Irvine DJ, Hanson MC, Rakhra K, Tokatlian T (2015) Synthetic nanoparticles for vaccines and immunotherapy. Chem Rev 115:11109–11146

Janssen RAJ, Nelson J (2013) Factors limiting device efficiency in organic photovoltaics. Adv Mater 25:1847–1858

Ji B, Gao H (2010) Mechanical principles of biological nanocomposites. Annu Rev Mater Res 40:77–100

Jin H-J, Kaplan DL (2003) Mechanism of silk processing in insects and spiders. Nature 424:1057–1061

Jochum FD, Theato P (2013) Temperature- and light-responsive smart polymer materials. Chem Soc Rev 42:7468–7483

King RE, Lau HK, Zhang H, Sidhu I, Christensen MB, Fowler EW, Li L, Jia X, Kiick KL, Thibeault SL (2019) Biocompatibility and viscoelastic properties of injectable resilin-like polypeptide and hyaluronan hybrid hydrogels in rabbit vocal folds. Regen Eng Transl Med 5:373–386

Lang K, Chin JW (2014) Cellular incorporation of unnatural amino acids and bioorthogonal labeling of proteins. Chem Rev 114:4764–4806

Lau HK, Li L, Jurusik AK, Sabanayagam CR, Kiick KL (2017) Aqueous liquid–liquid phase separation of resilin-like polypeptide/polyethylene glycol solutions for the formation of microstructured hydrogels. ACS Biomater Sci Eng 3:757–766

Lau HK, Paul A, Sidhu I, Li L, Sabanayagam CR, Parekh SH, Kiick KL (2018) Microstructured elastomer-PEG hydrogels via kinetic capture of aqueous liquid–liquid phase separation. Adv Sci 5:1701010

Lau HK, Rattan S, Fu H, Garcia CG, Barber DM, Kiick KL, Crosby AJ (2020) Micromechanical properties of microstructured elastomeric hydrogels. Macromol Biosci 20:1900360

Lee HJ, Lee J-S, Chansakul T, Yu C, Elisseeff JH, Yu SM (2006) Collagen mimetic peptide-conjugated photopolymerizable PEG hydrogel. Biomaterials 27:5268–5276

Lee Y, Song WJ, Sun JY (2020) Hydrogel soft robotics. Mater Today Phys 15:100258

Li D, Liu T, Yu X, Wu D, Su Z (2017a) Fabrication of graphene–biomacromolecule hybrid materials for tissue engineering application. Polym Chem 8:4309–4321

Li L, Tong Z, Jia X, Kiick KL (2013) Resilin-like polypeptide hydrogels engineered for versatile biological function. Soft Matter 9:665–673

Li Y, Chen X, Ribeiro AJ, Jensen ED, Holmberg KV, Rodriguez-Cabello JC, Aparicio C (2014) Hybrid Nanotopographical surfaces obtained by biomimetic mineralization of Statherin-inspired elastin-like recombinamers. Adv Healthc Mater 3:1638–1647

Li Y, Rodriguez-Cabello JC, Aparicio C (2017b) Intrafibrillar mineralization of self-assembled elastin-like Recombinamer fibrils. ACS Appl Mater Interfaces 9:5838–5846

Lim DW, Nettles DL, Setton LA, Chilkoti A (2007) Rapid cross-linking of elastin-like polypeptides with (hydroxymethyl)phosphines in aqueous solution. Biomacromolecules 8:1463–1470

Liu J, Bulmus V, Herlambang DL, Barner-Kowollik C, Stenzel MH, Davis TP (2007a) In situ formation of protein–polymer conjugates through reversible addition fragmentation chain transfer polymerization. Angew Chem Int Ed 46:3099–3103

Liu W, Brock A, Chen S, Chen S, Schultz PG (2007b) Genetic incorporation of unnatural amino acids into proteins in mammalian cells. Nat Methods 4:239–244

Lucky SS, Soo KC, Zhang Y (2015) Nanoparticles in photodynamic therapy. Chem Rev 115:1990–2042

Luginbuhl KM, Mozhdehi D, Dzuricky M, Yousefpour P, Huang FC, Mayne NR, Buehne KL, Chilkoti A (2017) Recombinant synthesis of hybrid lipid–peptide polymer fusions that self-assemble and encapsulate hydrophobic drugs. Angew Chem Int Ed 56:13979–13984

Luo T, Kiick KL (2013) Collagen-like peptides and peptide–polymer conjugates in the design of assembled materials. Eur Polym J 49:2998–3009

Luo T, Kiick KL (2015) Noncovalent modulation of the inverse temperature transition and self-assembly of elastin-b-collagen-like peptide bioconjugates. J Am Chem Soc 137:15362–15365

Lv S, Dudek DM, Cao Y, Balamurali MM, Gosline J, Li H (2010) Designed biomaterials to mimic the mechanical properties of muscles. Nature 465:69–73

Macek B, Forchhammer K, Hardouin J, Weber-Ban E, Grangeasse C, Mijakovic I (2019) Protein post-translational modifications in bacteria. Nat Rev Microbiol 17:651–664

Maiti D, Tong X, Mou X, Yang K (2019) Carbon-based nanomaterials for biomedical applications: a recent study. Front Pharmacol 9

Martin RW, Des Soye BJ, Kwon Y-C, Kay J, Davis RG, Thomas PM, Majewska NI, Chen CX, Marcum RD, Weiss MG, Stoddart AE, Amiram M, Ranji Charna AK, Patel JR, Isaacs FJ, Kelleher NL, Hong SH, Jewett MC (2018) Cell-free protein synthesis from genomically recoded bacteria enables multisite incorporation of noncanonical amino acids. Nat Commun 9:1203

Matsuura K (2020) Dressing up artificial viral capsids self-assembled from C-terminal-modified β-annulus peptides. Polym J 52:1035–1041

Mayavan S, Dutta NK, Choudhury NR, Kim M, Elvin CM, Hill AJ (2011) Self-organization, interfacial interaction and photophysical properties of gold nanoparticle complexes derived from resilin-mimetic fluorescent protein Rec1-resilin. Biomaterials 32:2786–2796

Mcgann CL, Dumm RE, Jurusik AK, Sidhu I, Kiick KL (2016) Thiol-ene photocrosslinking of cytocompatible resilin-like polypeptide-PEG hydrogels. Macromol Biosci 16:129–138

Mcgann CL, Levenson EA, Kiick KL (2013) Resilin-based hybrid hydrogels for cardiovascular tissue engineering. Macromol Chem Phys 214:203–213

Mchale MK, Setton LA, Chilkoti A (2005) Synthesis and in vitro evaluation of enzymatically cross-linked elastin-like polypeptide gels for cartilaginous tissue repair. Tissue Eng 11:1768–1779

Mickoleit F, Borkner CB, Toro-Nahuelpan M, Herold HM, Maier DS, Plitzko JM, Scheibel T, Schüler D (2018) In vivo coating of bacterial magnetic nanoparticles by magnetosome expression of spider silk-inspired peptides. Biomacromolecules 19:962–972

Mieszawska AJ, Nadkarni LD, Perry CC, Kaplan DL (2010) Nanoscale control of silica particle formation via silk−silica fusion proteins for bone regeneration. Chem Mater 22:5780–5785

Mitchell MJ, Billingsley MM, Haley RM, Wechsler ME, Peppas NA, Langer R (2021) Engineering precision nanoparticles for drug delivery. Nat Rev Drug Discov 20:101–124

Mitra N (2013) Incorporating unnatural amino acids into recombinant proteins in living cells. Mater Methods 3:204

Mozhdehi D, Luginbuhl KM, Dzuricky M, Costa SA, Xiong S, Huang FC, Lewis MM, Zelenetz SR, Colby CD, Chilkoti A (2019) Genetically encoded cholesterol-modified polypeptides. J Am Chem Soc 141:945–951

Mozhdehi D, Luginbuhl KM, Simon JR, Dzuricky M, Berger R, Varol HS, Huang FC, Buehne KL, Mayne NR, Weitzhandler I, Bonn M, Parekh SH, Chilkoti A (2018) Genetically encoded lipid–polypeptide Hbrid biomaterials that exhibit temperature-triggered hierarchical self-assembly. Nat Chem 10:496–505

Murray RW (2008) Nanoelectrochemistry: metal nanoparticles, nanoelectrodes, and nanopores. Chem Rev 108:2688–2720

Nagapudi K, Brinkman WT, Leisen JE, Huang L, Mcmillan RA, Apkarian RP, Conticello VP, Chaikof EL (2002) Photomediated solid-state cross-linking of an elastin−mimetic recombinant protein polymer. Macromolecules 35:1730–1737

Nagarsekar A, Crissman J, Crissman M, Ferrari F, Cappello J, Ghandehari H (2002) Genetic synthesis and characterization of pH- and temperature-sensitive silk-elastin-like protein block copolymers. J Biomed Mater Res 62:195–203

Nettles DL, Chilkoti A, Setton LA (2010) Applications of elastin-like polypeptides in tissue engineering. Adv Drug Deliv Rev 62:1479–1485

Nezakati T, Seifalian A, Tan A, Seifalian AM (2018) Conductive polymers: opportunities and challenges in biomedical applications. Chem Rev 118:6766–6843

Novoselov KS, Fal′ko VI, Colombo L, Gellert PR, Schwab MG, Kim K (2012) A roadmap for graphene. Nature 490:192–200

Nowatzki PJ, Tirrell DA (2004) Physical properties of artificial extracellular matrix protein films prepared by isocyanate crosslinking. Biomaterials 25:1261–1267

Okesola BO, Lau HK, Derkus B, Boccorh DK, Wu Y, Wark AW, Kiick KL, Mata A (2020) Covalent co-assembly between resilin-like polypeptide and peptide amphiphile into hydrogels with controlled nanostructure and improved mechanical properties. Biomater Sci

Okesola BO, Mata A (2018) Multicomponent self-assembly as a tool to harness new properties from peptides and proteins in material design. Chem Soc Rev 47:3721–3736

Omenetto FG, Kaplan DL (2010) New opportunities for an ancient material. Science 329:528

Pinkas DM, Ding S, Raines RT, Barron AE (2011) Tunable, post-translational hydroxylation of collagen domains in Escherichia coli. ACS Chem Biol 6:320–324

Prhashanna A, Taylor PA, Qin J, Kiick KL, Jayaraman A (2019) Effect of peptide sequence on the LCST-like transition of elastin-like peptides and elastin-like peptide–collagen-like peptide conjugates: simulations and experiments. Biomacromolecules 20:1178–1189

Qian Z-G, Pan F, Xia X-X (2020) Synthetic biology for protein-based materials. Curr Opin Biotechnol 65:197–204

Quadir MA, Martin M, Hammond PT (2014) Clickable synthetic polypeptides—routes to new highly adaptive biomaterials. Chem Mater 26:461–476

Ramazi S, Zahiri J (2021) Post-translational modifications in proteins: resources, tools and prediction methods. Database 2021

Raphel J, Parisi-Amon A, Heilshorn SC (2012) Photoreactive elastin-like proteins for use as versatile bioactive materials and surface coatings. J Mater Chem 22:19429–19437

Rettig H, Krause E, Börner HG (2004) Atom transfer radical polymerization with polypeptide initiators: a general approach to block copolymers of sequence-defined polypeptides and synthetic polymers. Macromol Rapid Commun 25:1251–1256

Rho J-Y, Kuhn-Spearing L, Zioupos P (1998) Mechanical properties and the hierarchical structure of bone. Med Eng Phys 20:92–102

Roberts S, Dzuricky M, Chilkoti A (2015) Elastin-like polypeptides as models of intrinsically disordered proteins. FEBS Lett 589:2477–2486

Rodríguez-Cabello JC, Arias FJ, Rodrigo MA, Girotti A (2016) Elastin-like polypeptides in drug delivery. Adv Drug Deliv Rev 97:85–100

Saha S, Banskota S, Roberts S, Kirmani N, Chilkoti A (2020) Engineering the architecture of elastin-like polypeptides: from Unimers to hierarchical self-assembly. Adv Ther 3:1900164

Salehi S, Koeck K, Scheibel T (2020) Spider silk for tissue engineering applications. Molecules 25

Sanami M, Shtein Z, Sweeney I, Sorushanova A, Rivkin A, Miraftab M, Shoseyov O, O'Dowd C, Mullen AM, Pandit A, Zeugolis DI (2015) Biophysical and biological characterisation of collagen/resilin-like protein composite fibres. Biomed Mater 10:065005

Sharma V, Srinivasan A, Nikolajeff F, Kumar S (2021) Biomineralization process in hard tissues: the interaction complexity within protein and inorganic counterparts. Acta Biomater 120:20–37

Shirzaei Sani E, Portillo-Lara R, Spencer A, Yu W, Geilich BM, Noshadi I, Webster TJ, Annabi N (2018) Engineering adhesive and antimicrobial hyaluronic acid/elastin-like polypeptide hybrid hydrogels for tissue engineering applications. ACS Biomater Sci Eng 4:2528–2540

Shuturminska K, Tarakina NV, Azevedo HS, Bushby AJ, Mata A, Anderson P, AL-Jawad M (2017) Elastin-like protein, with Statherin derived peptide, controls fluorapatite formation and morphology. Front Physiol 8

Sinaga A, Ravi P, Hatton TA, Tam KC (2007) Synthesis of poly(acrylic acid)-block-poly(L-valine) hybrid through combined atom transfer radical polymerization, click chemistry, and nickel-catalyzed ring opening polymerization methods. J Polym Sci A Polym Chem 45:2646–2656

Son H, Yoon C (2020) Advances in stimuli-responsive soft robots with integrated hybrid materials. Actuators 9

Strauss K, Chmielewski J (2017) Advances in the design and higher-order assembly of collagen mimetic peptides for regenerative medicine. Curr Opin Biotechnol 46:34–41

Su M, Kim B (2020) Silk fibroin-carbon nanotube composites based fiber substrated wearable triboelectric nanogenerator. ACS Appl Nano Mater 3:9759–9770

Su RSC, Kim Y, Liu JC (2014) Resilin: protein-based elastomeric biomaterials. Acta Biomater 10:1601–1611

Su RSC, Renner JN, Liu JC (2013) Synthesis and characterization of recombinant Abductin-based proteins. Biomacromolecules 14:4301–4308

Sun F, Zhang W-B, Mahdavi A, Arnold FH, TirrelL DA (2014) Synthesis of bioactive protein hydrogels by genetically encoded SpyTag-SpyCatcher chemistry. Proc Natl Acad Sci 111:11269

Sutherland TD, Huson MG, Rapson TD (2018) Rational design of new materials using recombinant structural proteins: current state and future challenges. J Struct Biol 201:76–83

Swierczewska M, Hajicharalambous CS, Janorkar AV, Megeed Z, Yarmush ML, Rajagopalan P (2008) Cellular response to nanoscale elastin-like polypeptide polyelectrolyte multilayers. Acta Biomater 4:827–837

Sych T, Mély Y, Römer W (2018) Lipid self-assembly and lectin-induced reorganization of the plasma membrane. Philos Trans R Soc B Biol Sci 373:20170117

Tappertzhofen K, Weiser F, Montermann E, Reske-Kunz A, Bros M, Zentel R (2015) Poly-l-lysine–poly[HPMA] block copolymers obtained by RAFT polymerization as polyplex-transfection reagents with minimal toxicity. Macromol Biosci 15:1159–1173

Tarakanova A, Huang W, Weiss AS, Kaplan DL, Buehler MJ (2017) Computational smart polymer design based on elastin protein mutability. Biomaterials 127:49–60

Tardy A, Nicolas J, Gigmes D, Lefay C, Guillaneuf Y (2017) Radical ring-opening polymerization: scope, limitations, and application to (bio)degradable materials. Chem Rev 117:1319–1406

Tejeda-Montes E, Klymov A, Nejadnik MR, Alonso M, Rodriguez-cabello JC, Walboomers XF, Mata A (2014) Mineralization and bone regeneration using a bioactive elastin-like recombinamer membrane. Biomaterials 35:8339–8347

Tejeda-Montes E, Smith KH, Poch M, López-Bosque MJ, Martín L, Alonso M, Engel E, Mata A (2012) Engineering membrane scaffolds with both physical and biomolecular Signaling. Acta Biomater 8:998–1009

Tinajero-Díaz E, Martínez De Ilarduya A, Muñoz-Guerra S (2019) Synthesis and properties of Diblock copolymers of ω-Pentadecalactone and α-amino acids. Eur Polym J 116:169–179

Tseng P, Perotto G, Napier B, Riahi P, Li W, Shirman E, Kaplan DL, Zenyuk IV, Omenetto FG (2016) Silk fibroin-carbon nanotube composite electrodes for flexible biocatalytic fuel cells. Adv Electron Mater 2:1600190

Van Eldijk MB, Smits FCM, Vermue N, Debets MF, Schoffelen S, Van Hest JCM (2014) Synthesis and self-assembly of well-defined elastin-like polypeptide–poly(ethylene glycol) conjugates. Biomacromolecules 15:2751–2759

Wang B, Patkar SS, Kiick KL (2021) Application of thermoresponsive intrinsically disordered protein polymers in nanostructured and microstructured materials. Macromol Biosci n/a:2100129

Wang E, Desai MS, Heo K, Lee S-W (2014a) Graphene-based materials functionalized with elastin-like polypeptides. Langmuir 30:2223–2229

Wang E, Desai MS, Lee S-W (2013) Light-controlled graphene-elastin composite hydrogel actuators. Nano Lett 13:2826–2830

Wang Q, Xia X, Huang W, Lin Y, Xu Q, Kaplan DL (2014b) High throughput screening of dynamic silk-elastin-like protein biomaterials. Adv Funct Mater 24:4303–4310

Wei W, Petrone L, Tan Y, Cai H, Israelachvili JN, Miserez A, Waite JH (2016) An underwater surface-drying peptide inspired by a mussel adhesive protein. Adv Funct Mater 26:3496–3507

Weitzhandler I, Dzuricky M, Hoffmann I, Garcia Quiroz F, Gradzielski M, Chilkoti A (2017) Micellar self-assembly of recombinant resilin−/elastin-like block copolypeptides. Biomacromolecules 18:2419–2426

Werkmeister JA, Ramshaw JAM (2012) Recombinant protein scaffolds for tissue engineering. Biomed Mater 7:012002

Whittaker JL, Dutta NK, Knott R, Mcphee G, Voelcker NH, Elvin C, Hill A, Choudhury NR (2015) Tunable Thermoresponsiveness of resilin via Coassembly with rigid biopolymers. Langmuir 31: 8882–8891

Wu Y, Fortunato GM, Okesola BO, Brocchetti FLPD, Suntornnond R, Connelly J, De Maria C, Rodriguez-Cabello JC, Vozzi G, Wang W, Mata A (2021) An interfacial self-assembling bioink for the manufacturing of capillary-like structures with tuneable and anisotropic permeability. Biofabrication 13:035027

Wu Y, Okesola BO, Xu J, Korotkin I, Berardo A, Corridori I, Di Brocchetti FLP, Kanczler J, Feng J, Li W, Shi Y, Farafonov V, Wang Y, Thompson RF, Titirici M-M, Nerukh D, Karabasov S, Oreffo ROC, Carlos Rodriguez-Cabello J, Vozzi G, Azevedo HS, Pugno NM, Wang W, Mata A (2020) Disordered protein-graphene oxide co-assembly and supramolecular biofabrication of functional fluidic devices. Nat Commun 11:1182

Xia X-X, Xu Q, Hu X, Qin G, Kaplan DL (2011) Tunable self-assembly of genetically engineered silk–elastin-like protein polymers. Biomacromolecules 12:3844–3850

Yan L, Da H, Zhang S, López VM, Wang W (2017) Bacterial magnetosome and its potential application. Microbiol Res 203:19–28

Yang L, Hedhammar M, Blom T, Leifer K, Johansson J, Habibovic P, Van Blitterswijk CA (2010) Biomimetic calcium phosphate coatings on recombinant spider silk fibres. Biomed Mater 5: 045002

Yang M, Zeng X, Zhang X, Yang Z (2020) 3D silk fibroin/carbon nanotube array composite matrix for flexible solid-state supercapacitors. New J Chem 44:6575–6582

Zakeri B, Fierer JO, Celik E, Chittock EC, Schwarz-Linek U, Moy VT, Howarth M (2012) Peptide tag forming a rapid covalent bond to a protein, through engineering a bacterial adhesin. Proc Natl Acad Sci 109:E690

Zakeri B, Howarth M (2010) Spontaneous intermolecular amide bond formation between side chains for irreversible peptide targeting. J Am Chem Soc 132:4526–4527

Zhang W-B, Sun F, Tirrell DA, Arnold FH (2013) Controlling macromolecular topology with genetically encoded SpyTag–SpyCatcher chemistry. J Am Chem Soc 135:13988–13997

Zhao G, Qing H, Huang G, Genin GM, Lu TJ, Luo Z, Xu F, Zhang X (2018) Reduced graphene oxide functionalized nanofibrous silk fibroin matrices for engineering excitable tissues. NPG Asia Mater 10:982–994

Zhao G, Zhang X, Li B, Huang G, Xu F, Zhang X (2020) Solvent-free fabrication of carbon nanotube/silk fibroin electrospun matrices for enhancing cardiomyocyte functionalities. ACS Biomater Sci Eng 6:1630–1640

Zhu Y, Murali S, Cai W, Li X, Suk JW, Potts JR, Ruoff RS (2010) Graphene and graphene oxide: synthesis, properties, and applications. Adv Mater 22:3906–3924

Chapter 7
Chirality in Peptide Self-Assembly and Aggregation

Francine E. Yanchik-Slade, Julian E. von Hofe, and Bradley L. Nilsson

Abstract Peptide self-assembly is relevant to the formation of functional and dysfunctional biological structures and has also been used in the fabrication of designed biomaterials. Chirality is a critical feature of evolved biological systems. As such, chirality has also been explored as a structural variable in self-assembled peptide and protein systems. These studies have involved a comparison of the self-assembly properties of single-enantiomer peptides as well as the assembly properties observed in mixtures of mirror image L- and D-peptides. Peptide mixtures of opposite chirality have been shown to self-associate with peptides of like chirality and to coassemble with the enantiomeric peptides, depending on the peptide sequence. The purpose of this chapter is to explore the effect that chirality has on the assembly of a variety of protein/peptide systems, including β-sheet, α-helical, collagen, and heterochiral hybrid peptides composed of both L- and D-amino acids. These studies have offered insight into fundamental protein/peptide interfacial interactions and have provided novel next-generation biomaterials.

Keywords Peptide self-assembly · Chirality · β-sheet · α-helix · Heterochiral peptide · Coassembly

7.1 Introduction

Chirality is an inherent feature of the building blocks of biological systems, including amino acids, nucleosides/nucleotides, and carbohydrates (Blackmond 2010). Chirality is a term used to describe the symmetry properties of molecules. Some molecules, referred to as enantiomers, can exist in one of two three-dimensional configurations that are nonsuperimposable mirror images of the other (Fig. 7.1). Enantiomers have identical physical and chemical characteristics, although they may interact with other chiral molecules in distinct ways. Proteins in nature are composed

---

F. E. Yanchik-Slade · J. E. von Hofe · B. L. Nilsson (✉)
Department of Chemistry, University of Rochester, Rochester, NY, USA
e-mail: bradley.nilsson@rochester.edu

229

Fig. 7.1 Chemical structures of the L- and D-enantiomers of the amino acid alanine. The letters *S* and *R* designate the absolute stereochemical configuration of the L- and D-alanine enantiomers, respectively

of L-amino acids, which define the overall chirality of folded proteins. The structure and function of a protein are intrinsically related to its chirality (Frenkel-Pinter et al. 2020). For example, it has been demonstrated that HIV-1 protease composed entirely of L-amino acids recognizes and cleaves its L-peptide substrate, but fails to interact with the D-substrate enantiomer (Milton et al. 1992). Conversely, the enantiomeric HIV-1 protease composed of D-amino acids specifically recognizes the D-substrate.

Chirality has been exploited to influence the assembly of peptides and proteins. For example, structural biologists and chemists have found that racemic mixtures of proteins, that is, mixtures of equal ratios of enantiomeric proteins of L- and D-amino acids, often display unique crystallization properties relative to the single enantiomers (Yeates and Kent 2012; Yan et al. 2017). This has enabled the use of "racemic protein crystallography" to facilitate the elucidation of structures of proteins that have been resistant to crystallization as single enantiomers (Mandal et al. 2016; Wehner et al. 2020; Bredikhin et al. 2020). Chirality has also been used to influence the noncovalent assembly of peptides and proteins into one-dimensional fibrils (Raskatov et al. 2021a; Zheng et al. 2021). The chirality of the constituent peptides can dramatically alter the properties of these self-assembled materials. For example, polymers of lysine adopt α-helical structures in homochiral solutions but assume β-sheet structures as racemic mixtures of L and D mirror image polymers (Fuhrhop et al. 1987). Evidence is building for the coassembly of mixtures of mirror image peptides into structures composed of both L- and D-peptides in the context of β-sheet assemblies (Raskatov et al. 2021a). On the other hand, self-replicating systems in which homochiral peptides are used as templates for the assembly of peptides from mixtures of heterochiral peptide fragments have shown a preference for the propagation of peptides that match the chirality of the template (Chung and Nowick 2004; Saghatelian et al. 2001). The interrogation of the assembly properties of peptides in mixtures with varying chirality is thus emerging as a topic of great research interest.

In this chapter, we will discuss the influence of chirality on the assembly of peptide nanomaterials in the context of fibrous assemblies. First, work that has explored the assembly behavior of homochiral and heterochiral peptide mixtures in β-sheet systems will be presented. Next, efforts to understand molecular interactions in heterochiral helical peptides will be discussed. Finally, research focused on the assembly characteristics of heterochiral peptides composed of both L and D peptides will be examined. This chapter will highlight the impact of chirality on the design of next-generation supramolecular biomaterials and in the design of

agents to perturb aberrant self-assembly in the biological context (Zheng et al. 2021). While the development of D-peptides to interact with L-proteins for biomedical applications has emerged as a field of research that probes interactions between materials of differing chirality, a detailed discussion of this topic is beyond the scope of this chapter (Schumacher et al. 1996; Funke and Willbold 2009).

7.2   Pleated and Rippled β-Sheets

A diverse range of peptides and proteins have been shown to self-assemble into β-sheet fibrils. These assemblies are a common feature of amyloid protein-folding disorders (Chiti and Dobson 2017). Material scientists have also engineered self-assembled β-sheet fibrils as next-generation biomaterials (Raskatov et al. 2021a; Zheng et al. 2021). β-Sheet nanofiber assemblies adopt a "cross-β" structure in which the backbone amide groups of the constituent β-strands are oriented parallel to the fibril axis, which enables the formation of an intermolecular hydrogen bond network (Fitzpatrick et al. 2013; Lutter et al. 2021). The side-chain groups of the constituent β-strands are thus oriented perpendicular to the fiber axis where they can participate in both intrasheet and intersheet hydrophobic, aromatic, and charge interactions that influence the stability of the fiber. The cross-β motif is common to amyloid assemblies and related designed biomaterials.

Pauling and Corey reported an early structural characterization of the β-sheet motif in 1951 (Pauling and Corey 1951). They interrogated the structure of fibrous proteins that were assigned the "β-keratin" structure found in silk fibroin, feather keratin, and connective tissue in an attempt to find structural configurations consistent with the X-ray diffraction patterns obtained from these materials. They concluded that a structure they referred to as a "pleated sheet" most closely aligned with the available data. The pleated β-sheet is among the most common structures found in nature (Cheng et al. 2013). As shown in Fig. 7.2a, b, peptides within pleated β-sheets can be aligned in antiparallel or parallel orientations. These orientations differ in the hydrogen bond pattern that exists between neighboring peptides within the sheets, but both orientations exhibit aligned side-chain arrangements that give rise to the pleated appearance of these β-sheet structures.

Shortly after their report on the structure of pleated β-sheets, Pauling and Corey postulated an alternative β-sheet form that could arise from mixtures of enantiomeric mirror image peptides (Pauling and Corey 1953a). Specifically, they predicted that mixtures of L- and D-β-strand peptides would form β-sheets in which the L- and D-peptides would align in an alternating L/D arrangement (Fig. 7.2c, d). They coined the term "rippled β-sheet" to describe these novel β-sheets based on the rippled appearance the putative sheets would exhibit as a function of the staggered side-chain arrangement (Fig. 7.2c, d). Since the prediction of the rippled β-sheet motif in 1953, little work was done to confirm the existence of this structure prior to 2008 (Raskatov et al. 2021a). Lotz and coworkers drew the conclusion that polyglycine I adopted an antiparallel rippled β-sheet structure based on a theoretical analysis of
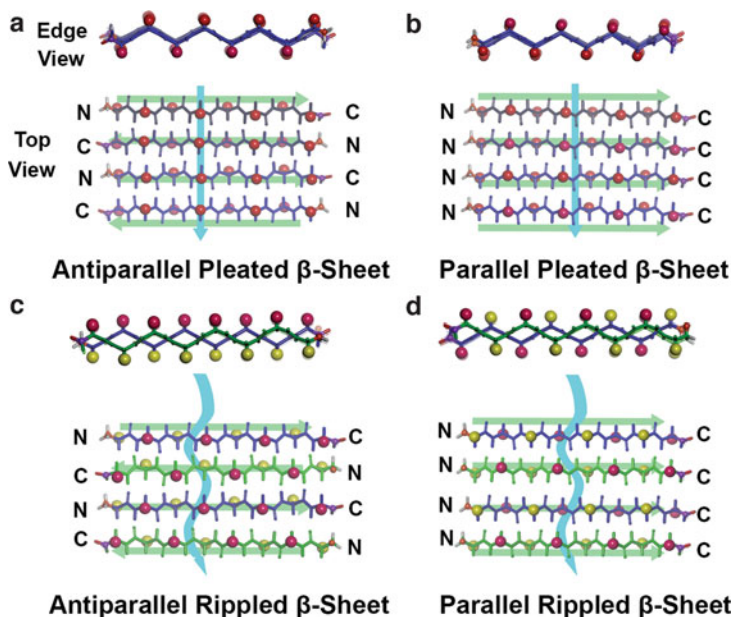
Fig. 7.2 Schematic representations of β-sheet structures. (**a**) An antiparallel pleated β-sheet shown from the leading edge (top panel) and from the top face (bottom panel). The constituent peptides are oriented in alternating arrangements, with the N-terminus alternating from the left to the right in the peptides shown in the bottom panel from top to bottom. The side-chain groups of neighboring strands are aligned between neighboring strands as indicated by the arrow in the bottom panel. This aligned arrangement gives rise to the pleated appearance. (**b**) A parallel pleated β-sheet shown from the leading edge (top panel) and from the top face (bottom panel). The constituent peptides are oriented with the N-terminus of each of the constituent peptides at the left edge as shown in the bottom panel from top to bottom. (**c**) An antiparallel rippled β-sheet composed of alternating L- and D-peptides, with the L-peptides shown in blue (side chains are red spheres) and the D-peptides shown in green (side chains are yellow spheres) shown from the leading edge (top panel) and from the top face (bottom panel). The constituent peptides are oriented in alternating arrangements, with the N-terminus alternating from the left to the right in the peptides shown in the bottom panel from top to bottom. The side-chain groups of neighboring cross-strand amino acids occupy the opposite face of the sheet as shown in the top panel. The side-chain groups on the same face of the rippled sheet adopt a staggered arrangement as indicated by the arrow in the bottom panel. This side-chain alignment gives rise to the rippled appearance. (**d**) A parallel rippled β-sheet composed of alternating L- and D-peptides, with the L-peptides shown in blue (side chains are red spheres) and the D-peptides shown in green (side chains are yellow spheres) shown from the leading edge (top panel) and from the top face (bottom panel)

electron diffraction data (Lotz 1974; Colonna-Cesari et al. 1974). The rippled structure of the polyglycine I system was later supported by the analysis of vibrational spectroscopic data by Moore and Krimm (Bandekar and Krimm 1979).

Büldt and coworkers reported another system that potentially adopts the rippled β-sheet structure (Fuhrhop et al. 1987). They found that solutions of polymers of L- or D-lysine (poly-L-Lys or poly-D-Lys, respectively) with polydisperse lengths adopted α-helical conformations. These solutions of single enantiomers of

poly-Lys remained homogenous and clear when stored under nitrogen at room temperature. However, a colorless precipitate was formed within a few minutes when equimolar amounts of poly-L-Lys and poly-D-Lys were mixed. They proposed that an antiparallel pleated β-sheet was the most likely form of the racemic aggregate based on scattering reflections. It is likely in this case that the proposed pleated sheet structure was misassigned and the actual structure was, in actuality, a rippled β-sheet.

In 2011, Schneider and coworkers conducted a study in which racemic mixtures of self-assembling β-hairpin peptides were found to have unique properties relative to the single-enantiomer assemblies (Nagy et al. 2011). They had previously developed the MAX1 peptide (VKVKVKVKV^{D}PPTKVKVKVKV-NH$_2$, where ^{D}P is D-proline), which undergoes folding into a β-hairpin followed by rapid self-assembly into nanofibrils at sufficient solution ionic strength (Schneider et al. 2002). The fibrils of MAX1 entangle to form a hydrogel network that has been applied to a range of biomaterial applications (Rajagopal et al. 2009; Yan et al. 2010). They found that mixtures of MAX1 and the enantiomeric D-peptide, DMAX1, formed hydrogels with distinct viscoelastic character compared to the self-assembled networks formed by only MAX1 or DMAX1 (Nagy et al. 2011). Specifically, the viscoelasticity increased in mixtures of MAX1 and DMAX1. The most rigid hydrogels were observed at equimolar ratios of the mirror-image peptides. The racemic mixture exhibited fibrils that were distinctive in morphology from the self-assembled L- or D-nanofibrils. Schneider and coworkers performed a series of experiments that confirmed that MAX1 and DMAX1 coassemble into fibrils that contain both peptides. In this report, it was not clear that these mixtures possessed rippled β-sheet structure, but the initial data were suggestive of this motif.

Schneider and Tycko subsequently performed a structural analysis of MAX1/DMAX1 cofibrils to better understand the spatial relationship of the L- and D-peptides within the coassembled material and to ascertain whether the structure possessed elements consistent with the Pauling and Corey rippled β-sheet (Nagy-Smith et al. 2017). Solid-state NMR spectroscopy (ssNMR), small-angle neutron scattering (SANS), Fourier transform infrared spectroscopy (FTIR), and computational modeling were used to assess relative orientations and distance constraints between L- and D-peptides in this system and to build a model of the coassembled materials (Fig. 7.3). Structural analysis of homochiral assemblies had previously shown that MAX1 folded into a β-hairpin conformation that assembled into pleated β-sheet bilayer nanofibrils (Fig. 7.3d) (Nagy-Smith et al. 2015). They demonstrated using FRET experiments in which the L- and D-peptides were modified with donor and acceptor molecules that the L/D mixtures formed fibrils that contained both the L- and D-peptides. Solid-state NMR experiments in which selected amino acids in MAX1 and DMAX1 were labeled with ^{13}C stable isotopes enabled the determination of specific through-space interactions and the measurement of distances between atomic labels. The selection of commercially available labeled D-amino acids is limited, which allowed them to use only labeled D-proline (Fig. 7.3a) in DMAX1. Nonetheless, these ssNMR experiments provided interstrand β-sheet distance measurements that were consistent with an *anti* orientation of alternating
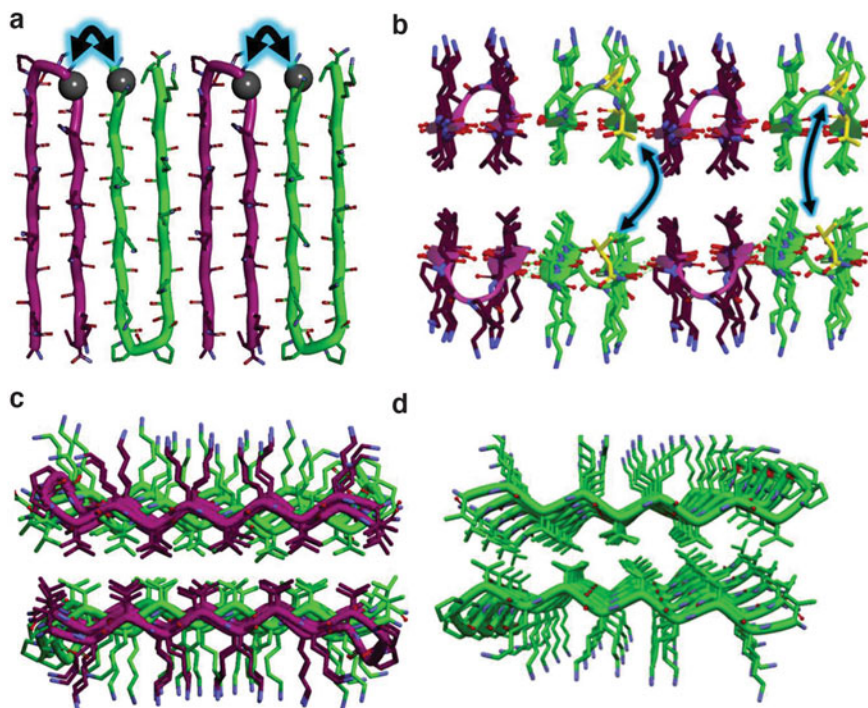
Fig. 7.3 Structural models of racemic β-hairpin fibrils of L- and D- MAX1, with L-MAX1 peptides shown in green and D-MAX1 shown in purple (Nagy-Smith et al. 2017). (**a**) In this schematic is shown the LMAX1-NMR1 peptide in green with valine-1 (gray sphere) having uniform ^{13}C and ^{15}N stable isotope labels (**V**KVKVKVKV^{D}PPTKVKVKVKV-NH$_2$, labeled V1 bold and underlined) and the DMAX1-NMR peptide in purple with D-proline-11 (gray sphere) having uniform ^{13}C and ^{15}N stable isotope labels (*VKVKVKVKV*^{L}P*^{D}**PT**KVKVKVKV*-NH$_2$, labeled ^{D}P11 bold and underlined). The arrow indicates a distance correlation measured with PITHIRDS-CT ssNMR experiments, with a measured distance of approximately 6.5 Å between the labels. This indicates an alternating arrangement of the L- and D-peptides with an *anti* configuration in which the β-turns alternate along the fibril axis as shown. (**b**) Possible enantiomer pairing across the bilyer based on ssNMR correlations. The MAX1-NMR2 peptide (green) is shown with uniformly ^{13}C/^{15}N labeled proline-11, threonine-12, and valine-20 residues (VKVKVKVKV^{D}P**PT**KVKVKVKV**V**-NH$_2$, labeled P11, T12, and V20 bold and underlined). The arrows indicate weak cross-peaks between T12-V20 and P11-V20, consistent with the cross-bilayer pairing shown. It should be noted that these interactions were not definitive and other cross-bilayer arrangements cannot be ruled out based on these experiments. (**c**) A model of a rippled β-sheet arrangement of MAX1/DMAX1 fibrils that is consistent with the available spectroscopic data. (**d**) A model of MAX1 pleated β-sheet fibrils consistent with the available data. This figure was adapted with permission from (Nagy-Smith et al. 2017). Copyright 2017 American Chemical Society

MAX1 and DMAX1 within the β-sheet structure (Fig. 7.3a). This structure is a hybrid that possesses pleated β-sheet character within the intramolecular sheet formed within the β-hairpin and rippled β-sheet structure at the interfacial contacts between MAX1 and DMAX1. In addition, a label pattern was chosen for MAX1

Fig. 7.4 TEM images of assemblies of the KFE8 peptide (Ac-(FKFE)$_2$-NH$_2$). (**a**) Left-handed helical ribbons formed from self-assembly of L-KFE8. (**b**) Right-handed helical ribbons formed from self-assembl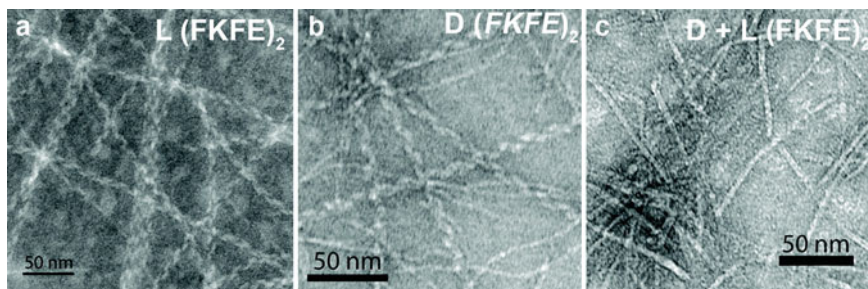y of D-FKE8. (**c**) Fibrils formed by coassembly of L-KFE8 and D-KFE8. These fibrils lack the helical character observed from the corresponding self-assembled materials, exhibiting distinctive flat nanoribbon morphology. Adapted with permission from (Swanekamp et al. 2012). Copyright 2012 American Chemical Society

(Fig. 7.3b) that allowed analysis of the cross-sheet orientation of peptides between the two laminated β-sheets. These experiments were not unambiguous but suggested that peptides were self-paired with like enantiomers across the β-sheet structure (Fig. 7.3b). These structural analyses were among the first to provide direct evidence confirming the Pauling and Corey rippled β-sheet.

Concurrent with this work in the Schneider group, Nilsson and coworkers conducted studies that suggested the formation of rippled β-sheet materials from mixtures of mirror image amphipathic peptides (Swanekamp et al. 2012). Specifically, they characterized assembly of mirror image L- and D- Ac-(FKFE)$_2$-NH$_2$ (KFE8) peptides to determine whether enantiomeric peptides would self-sort into L- and D-mirror image fibrils or coassemble into rippled β-sheets (Swanekamp et al. 2012). The nanofibrils formed from L-KFE8 adopt a left-handed helical nanoribbon morphology and the enantiomer, D-KFE8, self-assembles into mirror image right-handed helical nanoribbons (Fig. 7.4a, b). When equimolar amounts of L- and D-KFE8 were mixed, they did not form helical nanoribbons, but instead formed tape-like nanofibrils that lacked any helical character (Fig. 7.4c). This change in morphology was suggestive of coassembly. A series of spectroscopic studies, including FRET analysis in which L- and D-KFE8, were labeled with donor and quencher molecules, respectively, and isotope-edited FTIR experiments provided evidence consistent with rippled β-sheet formation. Isothermal titration calorimetry indicated that coassembly of L- and D-KFE8 had an enthalpic advantage relative to self-assembly of L-KFE8 of ~9 kcal/mol^{-1} (Swanekamp et al. 2012). Presumably, this energetic advantage could be attributed to the unique β-sheet packing structure of rippled β-sheets relative to pleated β-sheets. Later analysis of the putative rippled β-sheet fibrils formed from the KFE8 peptide demonstrated that these materials had an increased resistance to proteolytic degradation compared to the corresponding pleated β-sheet materials (Swanekamp et al. 2014).

These studies by Schneider and Nilsson both utilized amphipathic peptides with sequence patterns of alternating hydrophobic and hydrophilic amino acids. In an effort to understand whether peptides with other sequence patterns might undergo mirror image coassembly, Nilsson and coworkers interrogated another self-assembling peptide, the Aβ 16–22 fragment (Aβ(16–22), Ac-KLVFFAE-NH$_2$) (Urban et al. 2019). MAX1 and KFE8 assemblies have characteristic bilayer structures that impart high water solubility. In contrast, Aβ(16–22) fibrils precipitate from solution upon assembly. It was found that mixtures of L- and D-Aβ(16–22) became turbid immediately upon mixing, with precipitation being observed shortly thereafter. The L- and D-Aβ(16–22) self-assembled solutions required days before turbidity was observed, indicating that the kinetics of L/D coassembly is much more rapid in this system than self-assembly of the isolated enantiomers. In addition, self-assembled L- and D-Aβ(16–22) formed twisted fibrils (Fig. 7.5a, b), while the L/D mixture formed distinct nanosheet pseudocrystals (Fig. 7.5c). A similar set of spectroscopic analyses as those used for the KFE8 system were used along with ssNMR to confirm a structure consistent with rippled β-sheet formation. Solid-state NMR analysis was applied to measure distances between ^{13}C and ^{19}F labels in the L- and D-peptides respectively, and the measured distances were consistent with predictive models of the putative pleated and rippled β-sheet assemblies (Fig. 7.5d, e). Sedimentation analysis showed ~2 kcal mol^{-1} enthalpic advantage for coassembly of the L/D mixture compared to self-assembly of either the L- or D-enantiomers. This work provided evidence consistent with rippled β-sheet formation from mixtures of L- and D-peptides with sequence patterns other than alternating hydrophobic/hydrophilic amino acids.

Raskatov and coworkers have also explored rippled β-sheet formation in the context of the Alzheimer's disease amyloid-β (Aβ) peptide (Dutta et al. 2017). Specifically, they studied racemic mixtures of Aβ40 and Aβ42. They noticed a dramatic change in morphology between self-assembled enantiopure L- or D-peptides, which were twisted fibrils, and the mixed racemic L/D systems, which formed flat, untwisted fibrils (Dutta et al. 2017). Self-assembly of the single enantiomers proceeded with a pronounced lag phase, which was eliminated in mixtures of enantiomers. Raskatov and coworkers also reported that the racemic mixtures of L/D Aβ were significantly less toxic compared to their enantiopure components, a phenomenon referred to as chiral inactivation (Raskatov 2017; Raskatov and Teplow 2017). In subsequent work, Raskatov and Tycko exploited ssNMR and computational analysis to provide evidence consistent with rippled β-sheet formation in the mirror-image racemic mixtures of L- and D-Aβ40 (Raskatov et al. 2021b). To gain further insight into both chiral inactivation and the formation of rippled β-sheets, density functional theory (DFT) quantum-chemical calculations were performed on the Aβ fragment peptide, LVFFA (Aβ(17–21)) (Dutta et al. 2019; Raskatov 2020). In this work, it was found that the LVFFA:D-LVFFA rippled dimers were thermodynamically more stable than the LVFFA:LVFFA homochiral dimers. This work indicates that the possible sequence scope of rippled β-sheet formation may be exceptionally broad, and that the formation of rippled β-sheets may be exploited to perturb aggregation pathways in protein misfolding disorders.
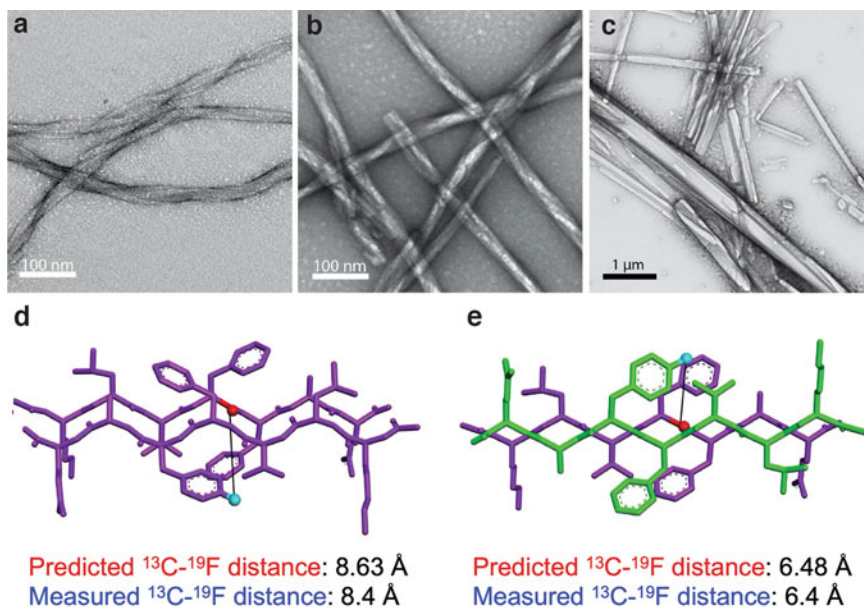
Fig. 7.5 (**a**) TEM image of twisted fibrils formed by L-Aβ(16–22). (**b**) TEM image of twisted fibrils formed by D-Aβ(16–22). (**c**) Pseudocrystalline nanosheets formed by equimolar mixtures of L- and D-Aβ(16–22). (**d**) A schematic showing the proposed pleated β-sheet alignment in L-Aβ(16–22) fibrils based on measured ssNMR distances between ^{13}C (red sphere) and ^{19}F (cyan sphere) labels. (**e**) A schematic showing the proposed rippled β-sheet alignment in L/D-Aβ(16–22) assemblies based on measured ssNMR distances between ^{13}C (red sphere) and ^{19}F (cyan sphere) labels. Adapted with permission from (Urban et al. 1983). Copyright The Authors, some rights reserved; exclusive licensee MDPI. Distributed under a Creative Commons Attribution License 4.0 (CCBY)

The work of Raskatov, Schneider, and Nilsson seemingly confirms the Pauling and Corey prediction of rippled β-sheet formation from mixtures of mirror image β-sheet peptides (Raskatov et al. 2021a). However, significant questions remain. First, it should be noted that despite the evidence cited in the previous sections, no high-resolution structures that confirm the rippled β-sheet architecture at near-atomic resolution have yet been reported. Until this type of structural confirmation is available, we must consider that other conformations that are not strictly rippled β-sheet may account for the observations above. Second, the fundamental molecular basis for the observed kinetic and thermodynamic advantages observed for coassembly of mirror image peptides is still unclear. Significant effort is needed to gain this insight. Finally, further insight into the emergent properties of rippled β-sheets as materials is needed. Efforts to elucidate the material and biological properties of rippled β-sheets will enable the application of these multicomponent materials as next-generation biomaterials (Raymond and Nilsson 2018; Distaffen et al. 2021).
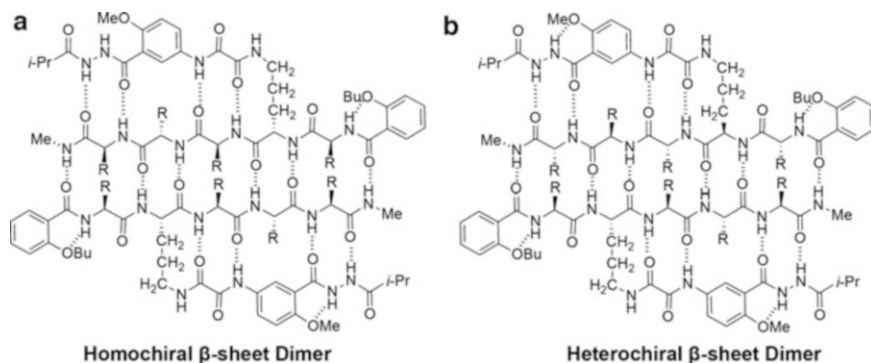
Fig. 7.6 (**a**) Chemical structure of a homochiral β-sheet dimer formed by Nowick's templated β-sheet system. Both peptides in these structures are composed of L-amino acids and the resulting dimer structure is expected to be a pleated β-sheet. The R groups are mixtures of Val, Ala, Leu, or Ile. (**b**) Chemical structure of a heterochiral β-sheet dimer formed by Nowick's templated β-sheet system. The bottom peptide in these structures is composed of L-amino acids while the top structure is composed of D-amino acids. This dimer is expected to adopt a rippled β-sheet structure. As in panel (**a**), the R groups are mixtures of Val, Ala, Leu, or Ile

Not all mixtures of enantiomeric peptides have shown a preference for rippled β-sheet formation. Nowick and coworkers have conducted studies on pleated versus rippled β-sheet formation using a constrained templated β-sheet dimer system (Chung and Nowick 2004). In order to conduct these studies, Nowick et al. prepared a system that is designed to be limited to dimer formation based on a templated β-sheet structure with a Lys side chain linked to a hydrazide group that blocks the back face from intermolecular interactions (Fig. 7.6). This design is based on prior work with templated β-sheets from the Nowick lab (Nowick 2008). They prepared a series of these templated tetrapeptides in both L- and D-stereochemical configurations and studied the preference for homochiral dimerization (presumed pleated β-sheet arrangement) or heterochiral dimerization (rippled β-sheet arrangement) using NMR. The anilide and hydrazide groups provide unambiguously distinct peaks in the dimer structures in which the homochiral and heterochiral pairing become diastereomeric. Upon analyzing various mixtures of the L- and D-templated peptides, they concluded that there was a preference for homochiral (pleated sheet) assembly over heterochiral (rippled sheet) assembly for each of their systems. The energetic preference for homochiral association was 3.1–4.2 kcal mol^{-1}, with an energetic benefit of 0.6–0.8 kcal mol^{-1} per interacting residue (Chung and Nowick 2004). This suggests an apparent preference for pleated β-sheet versus rippled β-sheet formation in this system. It is difficult to understand how generalizable this finding might be since the constraint of the templated heterocylic structure may also introduce limitations into how the peptides can interact at the interface. Nonetheless, this work is a critical element in the data that must be considered when discussing the Pauling and Corey rippled β-sheet motif.

Gellman and coworkers have also reported the use of a templated β-hairpin system to assess preference for homochiral or heterochiral peptide association consistent with either pleated or rippled β-sheet folding (Liu and Gellman 2021). In this study, β-hairpins based on the tryptophan zipper (Trpzip) model were designed in which the Aib-Gly turn motif was flanked by either L/L strands or L/D strands. The L/L pairing was expected to give a pleated β-sheet folded hairpin, while the L/D pairing was predicted to give a rippled β-sheet hairpin. In this system, evidence for homochiral β-hairpin folding was observed by the presence of cross-strand NMR NOE interactions between side-chain groups. In contrast, no folding was observed for heterochiral folding in the mixed stereochemical L/D peptides. This work seems to suggest that, in this system, pleated sheet formation is more favorable than rippled sheet formation. The authors acknowledge that these results are not necessarily in conflict with evidence for rippled β-sheet formation in other systems (Raskatov et al. 2021a) since the templated Aib-Gly turn motif may limit the packing configuration available in the hairpin system. This work further illustrates the importance of context in assessing formation of rippled or pleated sheets in mixed enantiomer systems.

Several additional systems have been used to explore the preference for homochiral self-sorting versus heterochiral coassembly (Torbeev et al. 2016; Wang et al. 2016). Hilvert analyzed chiral recognition between enantiomeric systems using β2-microglobulin (β2m) as a model (Torbeev et al. 2016). They used both the full-length, 99-residue β2m and the 20–41 fragment of β2m ([20–41]β2m) prepared as a disulfide-constrained 44-residue covalent dimer. They found that the 44 residue dimers of L-[20–41]β2m and D-[20–41]β2m precipitated as homochiral fibers due to self-sorting of the enantiomeric dimers into all-L and all-D mirror image assemblies. The presence of the D-enantiomers of full-length β2m in solutions of L-β2m resulted in morphologically unique fibrils that could be transformed into the typical long straight rods observed from single enantiomer assemblies when the L-component of the coassembled material was removed by proteolytic degradation. This led them to conclude that the L- and D-mixed assemblies must be resolved into L- and D-domains. They also found that the presence of D-β2m had an inhibitory effect on the self-assembly of L-β2m. These observations can be compared to previous work done by Goto and coworkers using nondimerized L-[20–41]β2m and D-[20–41]β2m (Wadai et al. 2005). Goto found that these peptides in isolation formed fibrils of opposite handedness, but that mixtures of these peptides formed fibrils in which the L- and D-content was not readily apparent. They also found that L-fibrils seeded only assembly of L-monomers and that D-fibrils seeded only assembly of D-monomers. They thus concluded that cross-enantiomer interactions must be disfavored, suggesting that the Pauling-Corey rippled β-sheet is not favored in this system.

Craik and coworkers studied the interactions of enantiomers of the β-sheet antimicrobial defensin peptides in the context of structural analysis of crystals of these peptides (Wang et al. 2016). Three peptides, baboon θ-defensin (BTD-2), protegrin-1 (PG-1), and polyphemusin-1 (PM-1), were assessed. Each of these peptides is an 18-amino acid sequence stabilized in a heterocyclic β-hairpin formed
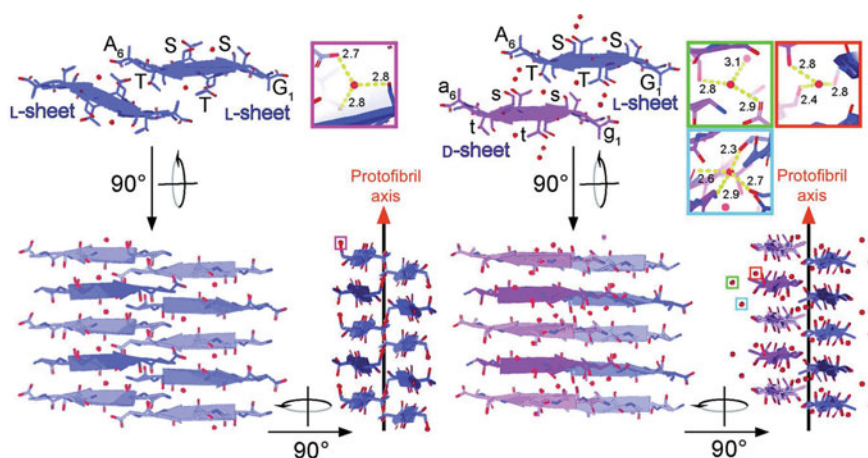
Fig. 7.7 (**a**) Representation of the structure of crystals of the single enantiomer GSTSTA sequence (all-L amino acids) derived from the InaZ ice-nucleation protein. This structure was obtained via cryo-EM MicroED analysis and features paired antiparallel pleated β-sheets that have amyloid-like characteristics. (**b**) Structure of crystals of the mixed enantiomer GSTSTA (equimolar mixture of L- and D-peptides) obtained via cryo-EM MicroED analysis. In this structure, the L- and D-enantiomers assemble into antiparallel pleated β-sheets that pair with the sheet of opposite chirality in an amyloid-like assembly. Reproduced with permission from (Zee et al. 2019)

by two disulfide bonds (PG-1 and PM-1) or three disulfide bonds and an N to C amide bond cyclization for BTD-2. Crystallization of mixtures of enantiomers of these peptides resulted in racemic crystals in which amyloid-like homochiral protofibrils of either all-L or all-D peptides assembled and packed against the mirror image fibrils of opposite chirality. This demonstration of racemic crystallization illustrates other possible ways that peptides of opposite chirality might interact other than rippled β-sheet assemblies. It is not clear how these processes are influenced by the conditions of crystallization or by constraint of the peptides.

Zee et al. conducted structural analyses of assemblies of a peptide fragment from the ice nucleation protein, InaZ (Zee et al. 2019). In these studies, they crystallized the GSTSTA segment from a homochiral solution and from a mixture of L- and D-enantiomers of the peptide. They found that these peptide solutions crystallized into packing architectures that were pleated β-sheet assemblies that shared many characteristics of self-assembled amyloid systems. They determined the structure of these assemblies at high resolution (0.9 Å) using cryo-EM MicroED methods. They found that the crystals of L-GSTSTA featured the peptide assembled into antiparallel β-sheets with pairs of sheets laminated into two-sheet layers (Fig. 7.7a). Interestingly, the mixed L/D-GSTSTA crystals gave a packing structure in which the enantiomers self-sorted into all-L and all-D pleated β-sheets that were organized in pairs of L-sheets and D-sheets within the protofibril structure (Fig. 7.7b). This is a fascinating illustration of another possible interaction mode for β-sheet peptides of opposite chirality in the context of self-assembled supramolecular materials.

Collectively, this work demonstrates the incredible scope of possibilities for polymorphic assembly of β-sheet peptides of opposite chirality. First postulated in 1953, the Pauling and Corey rippled β-sheet is only one possibility for how enantiomeric peptides may interact in the context of supramolecular materials. The studies reported herein provides evidence for rippled β-sheets in some systems, but also indicate that self-sorting of enantiomers may be preferred in other systems, particularly those with structural constraints. In yet other systems enantiomers might assemble into L- and D-pleated sheets that then interact selectively in the context of a self-assembled structure. Clearly, there are abundant questions and opportunities presented at the current moment in this emerging area of research.

7.3 Helical Peptides

Peptides that adopt α-helical structure have also been developed as the basis for supramolecular self-assembling materials (Beesley and Woolfson 2019). Pauling and Corey described two possible arrangements of polypeptides into a helical structure with either 3.7 or 5.1 residues per turn (Pauling et al. 1951). Based on their calculations for hydrogen bonding distances, they predicted that a helix with 3.7 residues per turn was most similar to the structures of α-keratin, α-myosin, and other fibrous proteins. Shortly thereafter, Pauling and Corey refined their structural analysis of α-keratin to include multiple α-helices interacting in a coiled-coil structure (Pauling and Corey 1953b). Crick further examined the role that helix handedness, or sense, plays in coiled-coil structures (Crick 1953). Crick suggested that heterochiral coiled coils should be accessible to pairs of right- and left-handed helices (Crick 1953).

Gellman and coworkers performed a structural analysis of racemic α-helical peptide mixtures to interrogate possible heterochiral interactions between α-helical peptides of opposite handedness (Mortenson et al. 2015). They specifically analyzed a transmembrane segment of the influenza M2 ion channel (Mortenson et al. 2015). The M2-transmembrane (M2-TM) peptide contains a single membrane-spanning α-helix that has been characterized crystallographically and has been shown to adopt a four-helix coiled-coil structure (Acharya et al. 2010). Gellman and coworkers applied the methods of racemic crystallography (Yan et al. 2017; Mandal et al. 2016; Kent 2018; Mandal et al. 2012; Kreutzer et al. 2020) to the M2-TM peptide and were able to gain high-resolution structural data that describes how L- and D-α-helix enantiomers interact. The L- and D-M2-TM peptides were crystallized in the presence of a racemic mixture of the detergents octyl-D-glucoside (D-OG) and octyl-L-glucoside (L-OG). The racemic M2-TM/OG crystal forms a distinctive crystal from the homochiral tetrameric assembly that was seen in all L-peptide crystals (Acharya et al. 2010; Stouffer et al. 2008). The racemic crystal obtained from L/D-M2-TM with L/D-OG contained a unit cell with one molecule of L-M2-TM and one molecule of D-M2-TM (Fig. 7.8a). The most intimate peptide interactions are between heterochiral helices with three distinct interfaces. They found that the heterochiral
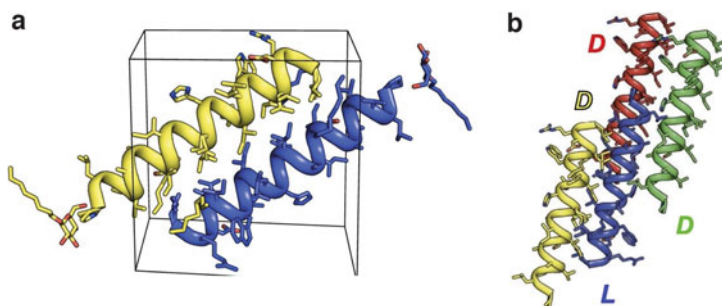
Fig. 7.8 (**a**) The unit cell of the racemic M2-TM/OG crystals with the L-M2-TM peptide shown in blue, the D-M2-TM peptide shown in yellow, D-OG shown in blue, and L-OG shown in yellow, showing the three distinct heterochiral interfaces. (**b**) A section of the structure of the racemic M2-TM/OG crystals that displays the three heterochiral interfaces within the crystal, with one L-M2-TM molecule shown (blue) and three D-M2-TM molecules shown (yellow, green, red). Reproduced with permission from (Mortenson et al. 2015)

interactions followed both a heptad, 7-residue, repeat and hendecad, 11-residue, repeat sequence pattern. The presence of the hendecad sequence motif shows a distinct geometry compared to the heptad pattern that is normally seen in α-helical assemblies, indicating that heterochiral interactions are distinctive from those found in homochiral coiled coils.

Gellman and coworkers subsequently explored structures of additional heterochiral coiled-coils based on variations of the M2-TM sequence (Kreitler et al. 2019). As described in the previous paragraph, the heterochiral coiled coils of L- and D-M2-TM were found to contain an 11-residue hendecad repeat (3,4,4 spacing) which is distinct from the 7-residue heptad repeat found commonly in homochiral coiled coils (Mortenson et al. 2015). To test the generality of a hendecad motif in heterochiral coiled-coils, they prepared M2-TM variants in which amino acid substitutions were made that would minimize steric interactions at the heterochiral interface. Crystal structures from these variants were consistent with the hendecad (11-residue) sequence motif being the most compatible form for heterochiral assemblies. This packing mode allows for the greatest number of stabilizing knob-in-hole interactions to occur between peptides of opposite chirality. This work has provided critical insight into the use of chirality to create novel peptide assemblies that promise to serve as design rules for next-generation materials derived from α-helical peptides.

Collagen is known to assemble into a distinct helical structure (Shoulders and Raines 2009; Bella 2016). The natural collagen mimetic sequence, $(_LP_LPG)_{10}$, assembles into a right-handed triple helix supercoil, $[(_LP_LPG)_{10}]_3$; this supercoil has a left-handed surface ridge feature defined by the edges of the proline groups (Xu et al. 2013). Conversely, the enantiomeric peptide, $(_DP_DPG)_{10}$ forms left-handed $[(_DP_DPG)_{10}]_3$ triple helices with a right-handed handed ridge. The constrained proline rings in these helices make heterochiral coassembly of $(_LP_LPG)_{10}$ and

($_D$P$_D$PG)$_{10}$ peptides into triple helices due to the highly hindered proline backbone conformations that would be required. However, Nanda and coworkers discovered that mixtures of [($_L$P$_L$PG)$_{10}$]$_3$ and [($_D$P$_D$PG)$_{10}$]$_3$ triple helices have unique properties that suggest heterochiral interactions between the triple helices (Xu et al. 2013). Solutions of the enantiopure collagen triple helices were found to be highly soluble. However, equimolar mixtures of [($_L$P$_L$PG)$_{10}$]$_3$ and [($_D$P$_D$PG)$_{10}$]$_3$ rapidly precipitated. Precipitation was accompanied by the appearance of unique sheetlike structures in microscopic images. Any changes in the ratio of [($_L$P$_L$PG)$_{10}$]$_3$ to [($_D$P$_D$PG)$_{10}$]$_3$ resulted in an elongation of precipitation time and a decrease in the amount of precipitate formation. Computational studies showed favorable packing of L and D helices. This work indicates that chirality in supramolecular structures can also be exploited to promote selective heterochiral interactions in the design of materials with novel properties.

7.4 Cyclic Heterochiral Peptide Assemblies

In the previous sections, we have discussed the heterochiral interactions between peptides in which the peptides are composed entirely of L- or D-amino acids. Heterochiral peptides, which possess both L- and D-amino acids within their primary sequence, have also been shown to have interesting properties relative to corresponding homochiral systems. The effect of changing the chirality at one or more amino acid positions within a peptide has been shown to have a drastic impact on the assembly of the peptide and its resulting structure. In this section, we describe efforts that have been made to exploit heterochiral primary sequences in the development of novel materials.

Ghadiri et al. reported an early example of self-assembling heterochiral peptides (Ghadiri et al. 1993). In this work, Ghadiri et al. designed a cyclic peptide with alternating D and L amino acids (D-Ala, L-Gln, see Fig. 7.9a). In this configuration, the side-chain groups are all extended at the periphery of the heterocycle and the amide NH and carbonyl groups are able to form intermolecular hydrogen bonds in the context of a self-assembled material (Fig. 7.9b). As expected, this cyclic peptide was found to assemble into fibrillar nanotube structures hundreds of nm in length with internal diameters of 7–8 Å. The heterochiral structure of the constituent cyclic peptide is critical for efficient self-assembly. This example of self-assembling heterochiral peptides is a powerful illustration of the use of chirality in the design of supramolecular materials.

Montenegro and coworkers have exploited this cyclic, alternating D/L amino acid template in the design of a system in which the resulting one-dimensional fibrils further assemble into two-dimensional sheets (Insua and Montenegro 2020). Their 8-residue cyclic peptide (cyclic-D-Leu-L-Trp-D-Leu-L-His-D-Glu-L-Gln-D-His-L-Glu) was designed with three distinct domains to aid in the self-assembly process; (1) a hydrophobic tripeptide of (D-Leu-L-Trp-D-Leu), (2) two hydrophilic ionizable domains to enable assembly remodeling by pH or temperature changes, and (3) a
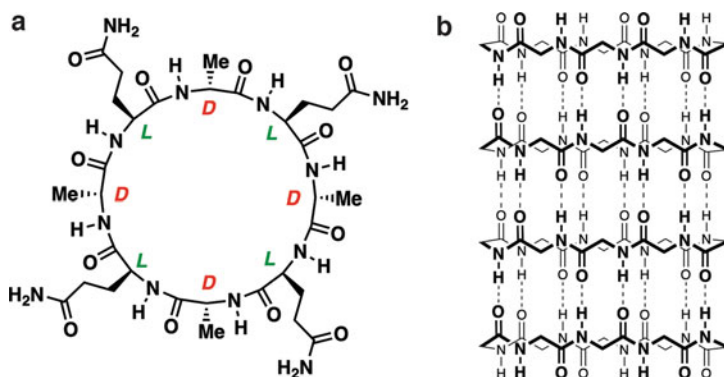
Fig. 7.9 (**a**) Chemical structure of heterochiral cyclic octomer of alternating D-Ala and L-Gln. (**b**) Schematic of a self-assembled nanotube of cyclic peptides from panel A. Hydrogen bonds are shown as dotted lines. Side-chain groups are omitted for clarity

neutral glutamine residue opposite to the tryptophan in the hydrophobic domain. This cyclic peptide (CP_X) self-assembled into a 1D nanotube in 20 mM Na_2HPO_4 buffer, pH 7.4. When the CP_X nanotubes were heated at 80 °C for 1.5 h and cooled to room temperature, the formation of transparent and flexible nanosheets was observed. The resulting nanosheets were disrupted into nanotubes when sonicated, with nanosheet reformation observed over time. The L-Trp residue was believed to orient the amino acids within the 1D tubes by formation of aromatic Trp-stacks along the length of the tube. This aligns the other amino acids as well, resulting in distinct hydrophobic and hydrophilic surfaces that are aligned along the entire length of each tube. It was hypothesized that intertube interdigitation of surface Leu side chains stabilizes the tube tube network that defines the two-dimensional sheets. This hypothesis was interrogated in later work in which the impact of changing the central hydrophobic and hydrophilic residues was assessed (Diaz et al. 2020). Collectively, these studies illustrate the use of heterochiral cyclic peptides in the design of next-generation materials that undergo hierarchical self-assembly.

7.5   Linear Heterochiral Peptide Assemblies

As described previously, the KFE8 peptide (Ac-$(FKFE)_2$-NH_2) has been used as a self-assembly model in the exploration of rippled β-sheet assembly from enantiomeric peptides (Swanekamp et al. 2012). Rudra and coworkers have explored the self-assembly properties of heterochiral variants of KFE8 (Clover et al. 2020). Specifically, they characterized the effects of mixing the FKFE repeats within this sequence with D-amino acids (D-fkfe). The peptides examined in this study included LL (Ac-FKFEFKFE-NH_2), DD (Ac-fkfefkfe-NH_2), LD (Ac-FKFEfkfe-NH_2), and DL (Ac-fkfeFKFE-NH_2). The LL and DD peptides self-assembled into characteristic

helical nanofibrils that have been reported previously (Swanekamp et al. 2012). The LD and DL peptides were found to self-assemble into morphologically unique twisted sheets (Fig. 7.10). Hydrogels of the block heterochiral LD and DL peptides displayed a weaker storage modulus in comparison to the homochiral LL and DD peptide (Nagy et al. 2011; Swanekamp et al. 2012). Interestingly, models of self-assembled LD and DL peptides suggest that antiparallel β-sheet formation provides cross-strand packing interactions between L- and D-fragments with structures consistent with rippled β-sheets. No high-resolution structural characterization is provided in this study to confirm rippled β-sheet formation, but these heterochiral peptides warrant further study.

Low-molecular-weight peptides (di- and tripeptides) have been broadly used as self-assembling hydrogel biomaterials (Draper and Adams 2017; Li et al. 2021; Ryan and Nilsson 2012). Marchesan and coworkers have examined heterochiral tripeptides as supramolecular self-assembling hydrogels (Marchesan et al. 2015; Marchesan et al. 2014). They based their studies on peptide sequences that contain a diphenylalanine (Phe-Phe) motif that has been shown to readily self-assemble (Guo et al. 2016). In early work, they used Phe-Phe-Val and Val-Phe-Phe tripeptides as models determine the impact of amino acid stereochemical configuration on self-assembly and hydrogelation propensity (Marchesan et al. 2015; Marchesan et al. 2014). It was found that efficient self-assembly and hydrogelation was retained only when a single amino acid at position one or three was changed from L to D, the compositions that led to stable hydrogels were the DLL/LDD configurations. Any

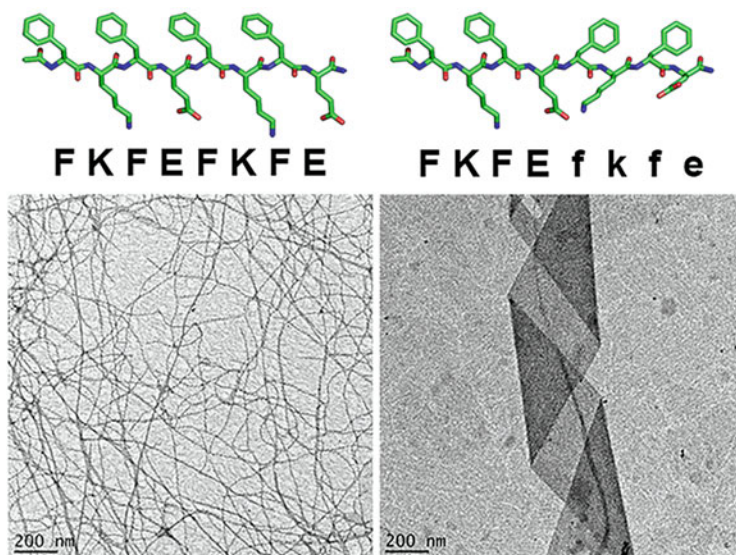**Fig. 7.10** TEM images of assemblies of the LL (Ac-(FKFE)-NH$_2$) and DL (Ac-FKFEfkfe-NH$_2$) peptides (D-amino acids are shown in lower case letters). Reproduced with permission from (Clover et al. 2020). Copyright 2020 American Chemical Society

stereochemical alteration at position two abrogated self-assembly of the resultant peptide. In later work, Marchesan and coworkers expanded these studies to alter the identity of the amino acid at position two to understand whether any D-amino acid might be tolerated in this position (Garcia et al. 2018). Specifically, they used L-Phe-D-Xaa-L-Phe where D-Xaa is an aliphatic D-amino acid (Ala, Val, Nva, Ile, Leu, and Nle). In contrast to their previous work, the addition of a D-amino acid at position two did not inhibit self-assembly when non-Phe D-amino acid residues were in position two. Interestingly, none of the homochiral peptides produced hydrogels. Marchesan and coworkers also explored the self-assembly and hydrogelation of Pro-Phe-Phe tripeptides as a function of the stereochemical configuration of the amino acids at each position (Garcia et al. 2021). The combination of proline with the diphenylalanine motif is an interesting decision due to the fact that proline has been shown to perturb or "break" β-sheet secondary structure in self-assembling peptides (Guo et al. 2016; Estrada and Soto 2007). It was found that the self-assembly properties of Pro-Phe-Phe tripeptides were dependent on the stereochemical sequence configures. Pro-Phe-Phe tripeptides with DLL/LDD stereochemical configurations (pro-Phe-Phe or Pro-phe-phe, where lower case amino acids are D-configurations) readily self-assembled and formed highly viscoelastic hydrogels, whereas LDL/DLD and LLL/DDD stereochemical patterned peptides did not. The morphologies of assemblies varied depending on the stereochemical sequence pattern. Homochiral peptides (LLL/DDD) primarily formed amorphous aggregates (Fig. 7.11a). The LDL/DLD-patterned tripeptides formed nanoparticles approximately 8 nm in diameter (Fig. 7.11c). Nanosphere formation was confirmed through all-atom MD simulations where 7 nm nanoparticles that were dimers and trimers of the peptide were formed. The DLL/LDD and LLD/DDL tripeptides assembled into nanofibrils and nanotapes (Fig. 7.11b, d, respectively).

Marchesan and coworkers have also explored the impact of chirality on the self-assembly and hydrogelation of diphenylalanine (FF) (Kralj et al. 2020). Specifically, they studied D-Phe-L-Phe dipeptides in which the side chain of the D-Phe residue was halogenated. Halogenation of the Phe side chain has been shown to influence the self-assembly and emergent properties of peptides that contain these residues. D-4-Iodo-Phe and D-2, 3, and 4-fluoro-Phe were included along with D-Phe in the D-amino acid position in these D-Phe-L-Phe dipeptides. All D-Phe-L-Phe dipeptides, including those with D-amino acids with halogenated side chains, were found to self-assemble and form hydrogel networks. The hydrogels were generally stable, although those formed from D-3F-Phe-L-Phe and D-4F-Phe-L-Phe were less stable over extended incubation periods. The hydrogels were thermoreversible and a change in fibril morphology was observed after thermoreversion. The structure of the homochiral (L-Phe-L-Phe) and heterochiral (D-Phe-L-Phe) assemblies was interrogated using single-crystal X-ray diffraction. The L-Phe-L-Phe dipeptide stacked into arrangements in which the Phe side chains engaged in intramolecular edge-to-face interactions, while the D-Phe-L-Phe dipeptides were oriented into face-to-face intramolecular stacks. The D-Phe-L-Phe dipeptides with fluorinated side chains were found to form similar packing arrangements to the nonhalogenated dipeptide. In contrast, the bulk of the iodine atom in D-4I-Phe-L-Phe prevented this packing
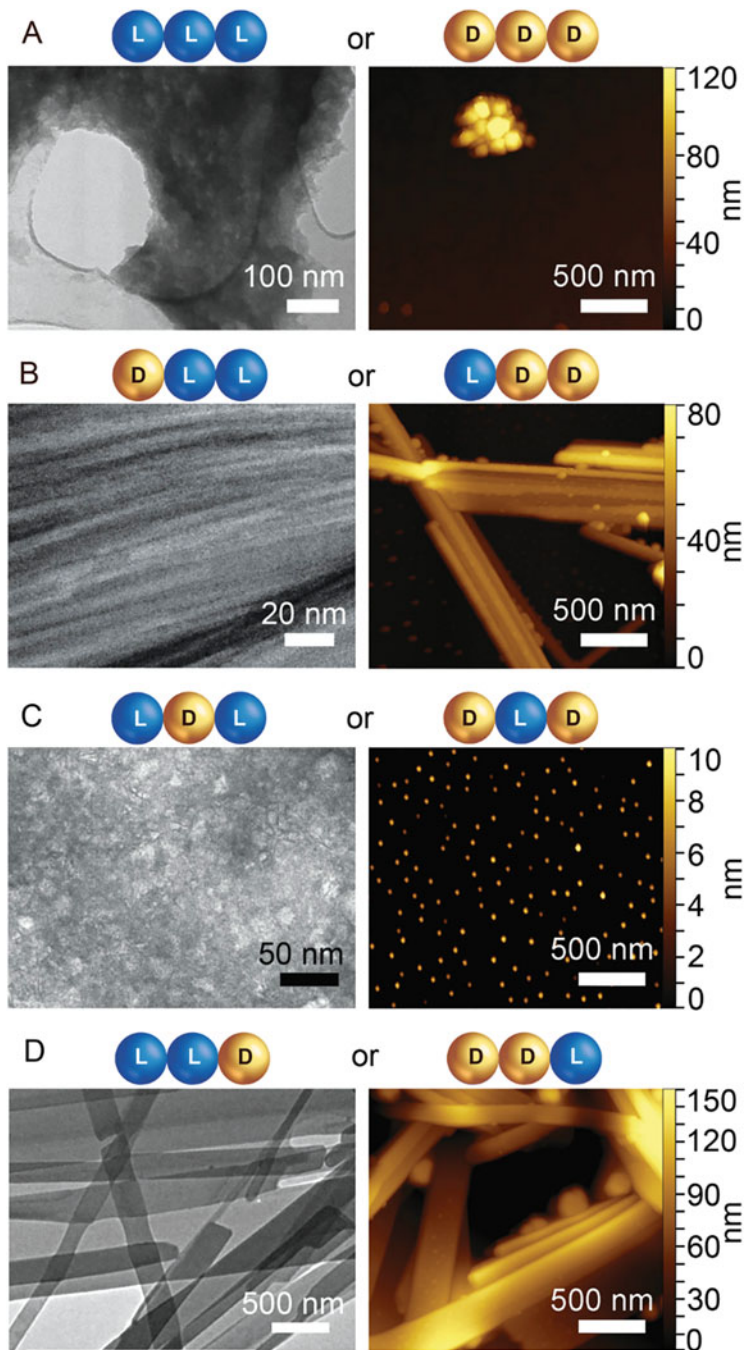
Fig. 7.11 TEM (left) and AFM (right) images of nanostructures formed by Pro-Phe-Phe (PFF) tripeptides in which the amino acid stereochemical configuration (L or D) was altered by position. The stereochemical L/D amino acid sequence pattern of the PFF tripeptides is indicated above each

interaction and limited this peptide to assembly into unique morphologies with distinct properties. D-4I-Phe-L-Phe assembled into well-defined hydrophobic and hydrophilic layers with no halogen bonding seen with the iodine. D-4I-Phe-L-Phe and D-Phe-L-Phe hydrogels provided matrices that supported the growth of fibroblasts, although the low optical transparency of D-4I-Phe-L-Phe hydrogels impeded efficient imaging of cells. The fluorinated dipeptide hydrogels proved to lack stability in tissue culture media, reducing their utility for cell culture applications. The formation of heterochiral dipeptide systems increases hydrophobicity of the resulting compound (Garcia et al. 2021; Bellotto et al. 2022). This work has contributed to a deeper understanding of the relationship between structure and function in hydrogel systems and demonstrates the promise of heterochiral systems as next-generation biomaterials.

Heterochiral peptides have also been used to perturb the handedness of the resulting self-assembled fibrils. For example, Xu and coworkers examined I_3K and its enantiomer and diastereomers to characterize the relationship between the peptide stereochemical patterns and the handedness of the assemblies (Wang et al. 2017). $^{L}I_3^{L}K$ and $^{D}I_3^{D}K$ formed left- and right-handed helices respectively. The $^{D}I_3^{L}K$ diastereomer formed left-handed fibrils and the enantiomeric $^{L}I_3^{D}K$ fibrils were right-handed, as would be expected. To further investigate the role of the hydrophobic amino acids in the peptide they added either L-*allo*-Ile or D-*allo*-Ile, which provide differing stereochemistry at C_β while maintaining the stereochemistry at C_α. Addition of L-*allo*-Ile in the peptide $^{La}I_3^{L}K$ resulted in left-handed fibrils as was observed in $^{L}I_3^{L}K$ and $^{D}I_3^{L}K$ assemblies. The handedness was inverted when D-*allo*-Ile was incorporated into $^{Da}I_3^{D}K$, which provided right-handed fibrils. Molecular dynamics analysis of $^{L}I_3^{L}K$, $^{D}I_3^{D}K$, $^{La}I_3^{L}K$, $^{Da}I_3^{D}K$, $^{D}I_3^{L}K$, and $^{L}I_3^{D}K$ peptides confirmed the handedness observed experimentally. This work highlights how molecular chirality affects the morphology of self-assembled materials in these heterochiral systems.

Fig. 7.11 (continued) panel. L-amino acids are shown as blue spheres and D-amino acids are shown as gold spheres (Garcia et al. 2021). (**a**) Aggregates formed by homochiral tripeptides (PFF or pff, upper case amino acids are L-configurations and lower case amino acids are D-configurations). (**b**) Nanofibril assemblies formed by DLL or LDD sequence patterns (pFF or Pff). (**c**) Nanoparticle assemblies formed by LDL or DLD assemblies (PfF or pFf). (**d**) Nanotape assemblies formed by LLD or DLL assemblies (PFf or pFF). Reproduced with permission from (Garcia et al. 2021). Copyright 2021 American Chemical Society

7.6 Inhibition of Amyloid Toxicity

Principles of heterochiral design have been used in the development of agents that modify the functional toxicity of pathological amyloid assemblies. As described in Sect. 8.2, Raskatov and coworkers have observed that assemblies of mixed L/D Aβ were less cytotoxic compared to homochiral assemblies (Dutta et al. 2017; Raskatov 2017; Raskatov and Teplow 2017). There are other examples of chiral inactivation using D-peptides or heterochiral peptides to prevent the formation of toxic amyloidogenic assemblies. Marchesan and coworkers also demonstrated that the nonassembling LDL/DLD patterned peptides described in Sect. 8.5 inhibited the formation of toxic Aβ$_{1-42}$ assemblies (Garcia et al. 2021). Gazit and coworkers used a heterochiral D-Trp-Aib dipeptide to inhibit the formation of toxic amyloid-β globulomers (Frydman-Marom et al. 2009). The dipeptide, D-Trp-Aib, was chosen for the combination of an indole ring to interact with the aromatic Phe-Phe region of Aβ and α-aminoisobutyric acid (Aib) for its β-breaker potential. The dipeptide had an affinity for Aβ$_{1-42}$ of ~300 nM and was shown to stabilize nontoxic oligomer structures and prevent their evolution into more toxic assemblies. Alzheimer's disease mouse models showed increased cognitive ability when treated with the D-Trp-Aib dipeptide. Phenylketonuria (PKU) is an amyloid disorder in which the self-assembly of phenylalanine results in the formation of toxic amyloid assemblies (Singh et al. 2014). Thakur and coworkers analyzed the interactions of L-Phe and D-Phe in the context of PKU. They observed that L-Phe is capable of self-assembling at a wide range of concentrations (300 μM – 300 mM) and transitions into a gel at higher concentrations (300 mM). When D-Phe was added at the initial stages of assembly, the formation of nanoflakes over nanofibers was observed along with the lack of hydrogel formation. A more negative Gibbs free energy was observed for the L/D-Phe mixtures, indicating increased stability of the coassembled nanoflakes over the self-assembled nanofibers. This data suggests that D-Phe is a potential therapeutic for PKU. These examples highlight the potential usefulness of heterochiral assemblies in the inhibition of toxic fibril formation.

7.7 Conclusion and Future Perspectives

The impact of chirality on peptide self-assembly processes has been a topic of supposition for over 60 years (Pauling and Corey 1953a; Crick 1953). Recent work to correlate stereochemical effects with self-assembly or coassembly of peptide systems has begun to provide deeper insight into the range of polymorphism that is possible in these complex systems. For example, there is evidence that β-sheet peptides of opposite chirality coassemble into L/D patterned rippled β-sheets, self-sort into L- and D-pleated β-sheets, or form L- and D-pleated β-sheets that pair into L/D bilayers. The fundamental basis for these various polymorphic possibilities is still poorly understood. Many of these systems lack high-resolution structures to confirm

precise orientations of stereoisomeric peptides within the assembled materials. This emerging area of research thus presents many intriguing questions for further study. Research that bridges significant gaps in understanding regarding the effects of chirality on intermolecular interactions in self-assembly processes will facilitate the development of stereodiverse peptide assemblies as next-generation biomaterials.

References

Acharya R, Carnevale V, Fiorin G, Levine BG, Polishchuk AL, Balannik V et al (2010) Structure and mechanism of proton transport through the transmembrane tetrameric M2 protein bundle of the influenza a virus. Proc Natl Acad Sci U S A 107(34):15075–15080

Bandekar J, Krimm S (1979) Vibrational analysis of peptides, polypeptides, and proteins: characteristic amide bands of beta-turns. Proc Natl Acad Sci U S A 76(2):774–777

Beesley JL, Woolfson DN (2019) The de novo design of alpha-helical peptides for supramolecular self-assembly. Curr Opin Biotechnol 58:175–182

Bella J (2016) Collagen structure: new tricks from a very old dog. Biochem J 473(8):1001–1025

Bellotto O, Kralj S, Melchionna M, Pengo P, Kisovec M, Podobnik M et al (2022) Self-assembly of unprotected dipeptides into hydrogels: water-channels make the difference. Chembiochem 23(2):e202100518

Blackmond DG (2010) The origin of biological homochirality. CSH Perspect Biol 2(5):a002147

Bredikhin AA, Zakharychev DV, Bredikhina ZA, Kurenkov AV, Samigullina AI, Gubaidullin AT (2020) Stereoselective crystallization of chiral 3,4-Dimethylphenyl glycerol ether complicated by plurality of crystalline modifications. Crystals 10(3):201

Cheng PN, Pham JD, Nowick JS (2013) The supramolecular chemistry of beta-sheets. J Am Chem Soc 135(15):5477–5492

Chiti F, Dobson CM (2017) Protein Misfolding, amyloid formation, and human disease: a summary of Progress over the last decade. Annu Rev Biochem 86:27–68

Chung DM, Nowick JS (2004) Enantioselective molecular recognition between beta-sheets. J Am Chem Soc 126(10):3062–3063

Clover TM, O'Neill CL, Appavu R, Lokhande G, Gaharwar AK, Posey AE et al (2020) Self-assembly of block Heterochiral peptides into helical tapes. J Am Chem Soc 142(47): 19809–19813

Colonna-Cesari F, Premilat S, Lotz B (1974) Structure of polyglycine I: a comparison of the antiparallel pleated and antiparallel rippled sheets. J Mol Biol 87(2):181–191

Crick FHC (1953) The packing of α-helices: simple coiled-coils. Acta Crystallogr 6(8):689–697

Diaz S, Insua I, Bhak G, Montenegro J (2020) Sequence decoding of 1D to 2D self-assembling cyclic peptides. Chemistry 26(64):14765–14770

Distaffen HE, Jones CW, Abraham BL, Nilsson BL (2021) Multivalent display of chemical signals on self-assembled peptide scaffolds. Pept Sci 113(2):e24224

Draper ER, Adams DJ (2017) Low-molecular-weight gels: the state of the art. Chem 3(3):390–410

Dutta S, Finn TS, Kuhn AJ, Abrams B, Raskatov JA (2019) Chirality dependence of amyloid beta cellular uptake and a new mechanistic perspective. Chembiochem 20(8):1023–1026

Dutta S, Foley AR, Warner CJA, Zhang X, Rolandi M, Abrams B et al (2017) Suppression of oligomer formation and formation of non-toxic fibrils upon addition of Mirror-image Abeta42 to the natural l-enantiomer. Angew Chem Int Edit 56(38):11506–11510

Estrada LD, Soto C (2007) Disrupting beta-amyloid aggregation for Alzheimer disease treatment. Curr Top Med Chem 7(1):115–126

Fitzpatrick AW, Debelouchina GT, Bayro MJ, Clare DK, Caporini MA, Bajaj VS et al (2013) Atomic structure and hierarchical assembly of a cross-beta amyloid fibril. Proc Natl Acad Sci U S A 110(14):5468–5473

Frenkel-Pinter M, Samanta M, Ashkenasy G, Leman LJ (2020) Prebiotic peptides: molecular hubs in the origin of life. Chem Rev 120(11):4707–4765

Frydman-Marom A, Rechter M, Shefler I, Bram Y, Shalev DE, Gazit E (2009) Cognitive-performance recovery of Alzheimer's disease model mice by modulation of early soluble amyloidal assemblies. Angew Chem Int Edit 48(11):1981–1986

Fuhrhop J-H, Krull M, Büldt G (1987) Precipitates with β-pleated sheet structure by mixing aqueous solutions of helical poly(D-lysine) and poly(L-lysine). Angew Chem Int Edit 26(7): 699–700

Funke SA, Willbold D (2009) Mirror image phage display--a method to generate D-peptide ligands for use in diagnostic or therapeutical applications. Mol BioSyst 5(8):783–786

Garcia AM, Iglesias D, Parisi E, Styan KE, Waddington LJ, Deganutti C et al (2018) Chirality effects on peptide self-assembly unraveled from molecules to materials. Chem 4(8):1862–1876

Garcia AM, Melchionna M, Bellotto O, Kralj S, Semeraro S, Parisi E et al (2021) Nanoscale assembly of functional peptides with divergent programming elements. ACS Nano 15(2): 3015–3025

Ghadiri MR, Granja JR, Milligan RA, McRee DE, Khazanovich N (1993) Self-assembling organic nanotubes based on a cyclic peptide architecture. Nature 366(6453):324–327

Guo C, Arnon ZA, Qi R, Zhang Q, Adler-Abramovich L, Gazit E et al (2016) Expanding the Nanoarchitectural diversity through aromatic Di- and tri-peptide Coassembly: nanostructures and molecular mechanisms. ACS Nano 10(9):8316–8324

Insua I, Montenegro J (2020) 1D to 2D self assembly of cyclic peptides. J Am Chem Soc 142(1): 300–307

Kent SB (2018) Racemic & quasi-racemic protein crystallography enabled by chemical protein synthesis. Curr Opin Chem Biol 46:1–9

Kralj S, Bellotto O, Parisi E, Garcia AM, Iglesias D, Semeraro S et al (2020) Heterochirality and halogenation control Phe-Phe hierarchical assembly. ACS Nano 14:16951

Kreitler DF, Yao Z, Steinkruger JD, Mortenson DE, Huang L, Mittal R et al (2019) A Hendecad motif is preferred for Heterochiral coiled-coil formation. J Am Chem Soc 141(4):1583–1592

Kreutzer AG, Samdin TD, Guaglianone G, Spencer RK, Nowick JS (2020) X-ray crystallography reveals parallel and antiparallel beta-sheet dimers of a beta-hairpin derived from Abeta16-36 that assemble to form different tetramers. ACS Chem Neurosci 11(15):2340–2347

Li L, Xie L, Zheng R, Sun R (2021) Self-assembly dipeptide hydrogel: the structures and properties. Front Chem 9:739791

Liu X, Gellman SH (2021) Comparisons of beta-hairpin propensity among peptides with Homochiral or Heterochiral strands. Chembiochem 22(18):2772–2776

Lotz B (1974) Crystal structure of polyglycine I. J Mol Biol 87(2):169–180

Lutter L, Aubrey LD, Xue WF (2021) On the structural diversity and individuality of polymorphic amyloid protein assemblies. J Mol Biol 433(20):167124

Mandal K, Dhayalan B, Avital-Shmilovici M, Tokmakoff A, Kent SB (2016) Crystallization of Enantiomerically pure proteins from quasi-racemic mixtures: structure determination by X-ray diffraction of isotope-labeled Ester insulin and human insulin. Chembiochem 17(5):421–425

Mandal K, Uppalapati M, Ault-Riche D, Kenney J, Lowitz J, Sidhu SS et al (2012) Chemical synthesis and X-ray structure of a heterochiral {D-protein antagonist plus vascular endothelial growth factor} protein complex by racemic crystallography. Proc Natl Acad Sci U S A 109(37): 14779–14784

Marchesan S, Easton CD, Styan KE, Waddington LJ, Kushkaki F, Goodall L et al (2014) Chirality effects at each amino acid position on tripeptide self-assembly into hydrogel biomaterials. Nanoscale 6(10):5172–5180

Marchesan S, Styan KE, Easton CD, Waddington L, Vargiu AV (2015) Higher and lower supramolecular orders for the design of self-assembled heterochiral tripeptide hydrogel bio-materials. J Mater Chem B 3(41):8123–8132

Milton RC, Milton SC, Kent SB (1992) Total chemical synthesis of a D-enzyme: the enantiomers of HIV-1 protease show reciprocal chiral substrate specificity [corrected]. Science 256(5062): 1445–1448

Mortenson DE, Steinkruger JD, Kreitler DF, Perroni DV, Sorenson GP, Huang L et al (2015) High-resolution structures of a heterochiral coiled coil. Proc Natl Acad Sci U S A 112(43): 13144–13149

Nagy KJ, Giano MC, Jin A, Pochan DJ, Schneider JP (2011) Enhanced mechanical rigidity of hydrogels formed from enantiomeric peptide assemblies. J Am Chem Soc 133(38): 14975–14977

Nagy-Smith K, Beltramo PJ, Moore E, Tycko R, Furst EM, Schneider JP (2017) Molecular, local, and network-level basis for the enhanced stiffness of hydrogel networks formed from Coassembled racemic peptides: predictions from Pauling and Corey. ACS Cent Sci 3(6): 586–597

Nagy-Smith K, Moore E, Schneider J, Tycko R (2015) Molecular structure of monomorphic peptide fibrils within a kinetically trapped hydrogel network. Proc Natl Acad Sci U S A 112(32):9816–9821

Nowick JS (2008) Exploring beta-sheet structure and interactions with chemical model systems. Acc Chem Res 41(10):1319–1330

Pauling L, Corey RB (1951) The pleated sheet, a new layer configuration of polypeptide chains. Proc Natl Acad Sci U S A 37(5):251–256

Pauling L, Corey RB (1953a) Two rippled-sheet configurations of polypeptide chains, and a note about the pleated sheets. Proc Natl Acad Sci U S A 39(4):253–256

Pauling L, Corey RB (1953b) Compound helical configurations of polypeptide chains: structure of proteins of the alpha-keratin type. Nature 171(4341):59–61

Pauling L, Corey RB, Branson HR (1951) The structure of proteins; two hydrogen-bonded helical configurations of the polypeptide chain. Proc Natl Acad Sci U S A 37(4):205–211

Rajagopal K, Lamm MS, Haines-Butterick LA, Pochan DJ, Schneider JP (2009) Tuning the pH responsiveness of beta-hairpin peptide folding, self-assembly, and hydrogel material formation. Biomacromolecules 10(9):2619–2625

Raskatov JA (2017) Chiral inactivation: an old phenomenon with a new twist. Chemistry 23(67): 16920–16923

Raskatov JA (2020) Conformational selection as the driving force of amyloid beta chiral inactivation. Chembiochem 21(20):2945–2949

Raskatov JA, Foley AR, Louis JM, Yau WM, Tycko R (2021b) Constraints on the structure of fibrils formed by a racemic mixture of amyloid-beta peptides from solid-state NMR, electron microscopy, and theory. J Am Chem Soc 143(33):13299–13313

Raskatov JA, Schneider JP, Nilsson BL (2021a) Defining the landscape of the Pauling-Corey rippled sheet: an orphaned motif finding new homes. Acc Chem Res 54(10):2488–2501

Raskatov JA, Teplow DB (2017) Using chirality to probe the conformational dynamics and assembly of intrinsically disordered amyloid proteins. Sci Rep 7(1):12433

Raymond DM, Nilsson BL (2018) Multicomponent peptide assemblies. Chem Soc Rev 47(10): 3659–3720

Ryan DM, Nilsson BL (2012) Self-assembled amino acids and dipeptides as noncovalent hydrogels for tissue engineering. Polym Chem 3(1):18–33

Saghatelian A, Yokobayashi Y, Soltani K, Ghadiri MR (2001) A chiroselective peptide replicator. Nature 409(6822):797–801

Schneider JP, Pochan DJ, Ozbas B, Rajagopal K, Pakstis L, Kretsinger J (2002) Responsive hydrogels from the intramolecular folding and self-assembly of a designed peptide. J Am Chem Soc 124(50):15030–15037

Schumacher TN, Mayr LM, Minor DL Jr, Milhollen MA, Burgess MW, Kim PS (1996) Identification of D-peptide ligands through mirror-image phage display. Science 271(5257):1854–1857

Shoulders MD, Raines RT (2009) Collagen structure and stability. Annu Rev Biochem 78:929–958

Singh V, Rai RK, Arora A, Sinha N, Thakur AK (2014) Therapeutic implication of L-phenylalanine aggregation mechanism and its modulation by D-phenylalanine in phenylketonuria. Sci Rep 4(4):3875

Stouffer AL, Acharya R, Salom D, Levine AS, Di Costanzo L, Soto CS et al (2008) Structural basis for the function and inhibition of an influenza virus proton channel. Nature 451(7178):596–599

Swanekamp RJ, DiMaio JT, Bowerman CJ, Nilsson BL (2012) Coassembly of enantiomeric amphipathic peptides into amyloid-inspired rippled beta-sheet fibrils. J Am Chem Soc 134(12):5556–5559

Swanekamp RJ, Welch JJ, Nilsson BL (2014) Proteolytic stability of amphipathic peptide hydrogels composed of self-assembled pleated beta-sheet or coassembled rippled beta-sheet fibrils. Chem Commun (Camb) 50(70):10133–10136

Torbeev V, Grogg M, Ruiz J, Boehringer R, Schirer A, Hellwig P et al (2016) Chiral recognition in amyloid fiber growth. J Pept Sci 22(5):290–304

Urban JM, Ho J, Piester G, Fu R, Nilsson BL (2019) Rippled beta-sheet formation by an amyloid-beta fragment indicates expanded scope of sequence space for enantiomeric beta-sheet peptide Coassembly. Molecules 24(10):1983

Wadai H, Yamaguchi K, Takahashi S, Kanno T, Kawai T, Naiki H et al (2005) Stereospecific amyloid-like fibril formation by a peptide fragment of beta2-microglobulin. Biochemistry 44(1):157–164

Wang CK, King GJ, Conibear AC, Ramos MC, Chaousis S, Henriques ST et al (2016) Mirror images of antimicrobial peptides provide reflections on their functions and Amyloidogenic properties. J Am Chem Soc 138(17):5706–5713

Wang M, Zhou P, Wang J, Zhao Y, Ma H, Lu JR et al (2017) Left or right: how does amino acid chirality affect the handedness of nanostructures self-assembled from short amphiphilic peptides? J Am Chem Soc 139(11):4185–4194

Wehner M, Rohr MIS, Stepanenko V, Wurthner F (2020) Control of self-assembly pathways toward conglomerate and racemic supramolecular polymers. Nat Commun 11(1):5460

Xu F, Khan IJ, McGuinness K, Parmar AS, Silva T, Murthy NS et al (2013) Self-assembly of left- and right-handed molecular screws. J Am Chem Soc 135(50):18762–18765

Yan B, Ye L, Xu W, Liu L (2017) Recent advances in racemic protein crystallography. Bioorg Med Chem 25(18):4953–4965

Yan C, Altunbas A, Yucel T, Nagarkar RP, Schneider JP, Pochan DJ (2010) Injectable solid hydrogel: mechanism of shear-thinning and immediate recovery of injectable beta-hairpin peptide hydrogels. Soft Matter 6(20):5143–5156

Yeates TO, Kent SB (2012) Racemic protein crystallography. Annu Rev Biophys 41:41–61

Zee CT, Glynn C, Gallagher-Jones M, Miao J, Santiago CG, Cascio D et al (2019) Homochiral and racemic MicroED structures of a peptide repeat from the ice-nucleation protein InaZ. IUCrJ 6 (Pt 2):197–205

Zheng Y, Mao K, Chen S, Zhu H (2021) Chirality effects in peptide assembly structures. Front Bioeng Biotechnol 9:703004

Chapter 8
Characterization of Peptide-Based Nanomaterials

Check for updates

Charlotte J. C. Edwards-Gayle and Jacek K. Wychowaniec

Abstract In this chapter, we will thoroughly discuss characterization techniques used to elucidate the exact structure and define properties of peptide-based nanomaterials. In particular we divide methods into:

1. Quality control performance (mass spectroscopy and high-performance liquid chromatography.
2. Spectroscopy (Fourier transform infrared spectroscopy, Raman spectroscopy, circular and linear dichroism, nuclear magnetic resonance and fluorescence spectroscopy).
3. Microscopy (scanning and transmission electron microscopies, atomic force microscopy, optical and polarized light microscopy).
4. Scattering (small angle X-ray and neutron scattering, X-ray diffraction).
5. Bulk structures (mainly hydrogels) rheological characterization.

The methodology is described for molecular structures, self-assembled nanostructures and aggregates, as well as hybrid, composite and/or conjugated nanomaterials and their bulk forms. Both common, as well as more exotic versions of all methods are presented in the context of peptide-based nanomaterials. Where utilized, examples of combinatorial use of techniques are demonstrated. Representative studies accompany the discussion and usefulness of all presented methods.

Keywords Peptides · Hydrogels · Characterization methods · Spectroscopy · Microscopy · Scattering · Rheology

Charlotte J. C. Edwards-Gayle and Jacek K. Wychowaniec contributed equally to this chapter.

C. J. C. Edwards-Gayle
Diamond Light Source, Harwell Science and Innovation Campus, Didcot, UK

J. K. Wychowaniec (✉)
School of Chemistry, University College Dublin, Dublin, Ireland

AO Research Institute Davos, Davos, Switzerland
e-mail: jacek.wychowaniec@aofoundation.org

8.1 Introduction

In this chapter, we will thoroughly discuss characterization techniques used to elucidate exact structure and define properties of peptide-based nanomaterials. We will start by describing techniques necessary to elucidate peptide purity and confirm its molecular structure. Next, we will focus on methods to determine the interactions and factors affecting self-assembly, focussing on chemical titrations, charge stabilization and the role of thermodynamics. We will then move on describing spectroscopic methods that determine the exact secondary structure of peptide-based nanomaterials, and thus enable identification of main self-assembly factors driving the peptides into well-defined structures and nanomaterials. After that, we will describe current microscopy techniques and how they can help us visualise the peptide structures, as well as discuss how microscopy (electron, atomic force and optical) can help determine structural features, time-dependent phenomena and supplementary properties that are key for applications. This will be further complemented with scattering techniques, including small angle scattering methods and X-ray diffraction (wide-angle X-ray scattering), used to describe peptide-based nanomaterials across multiple length scales, from atomic spacing, up to larger (~500 nm) constructs. Lastly, we will discuss methods of characterizing various bulk materials, such as rheological and mechanical testing of peptide-based hydrogels. Throughout all chapters, we will be discussing various combined approaches that can elucidate the performance of peptide-based nanomaterials, e.g. under external stimuli, such as shear. Finally, we will finish with a short guide on how to choose characterization techniques for different materials, as well with a prospective view of the potential development of the analytical and characterization techniques for use in this field.

8.2 Peptide Quality Control

It is essential before performing any characterization of peptide-based nanomaterials discussed later in this chapter to first confirm the purity of the peptide. Purity is an important aspect affecting multiple measurements and can change the assembling properties of the nanomaterial. Thus, particular care and attention must be taken when purifying peptides and peptide conjugates. In this section, we will discuss two of the most commonly used techniques to measure peptide purity and peptide molecular structure, and touch on how these methods can also be utilized beyond quality control for characterizing peptide-based nanomaterials. With this, we would like to point out that peptides are most often synthesized using variations of solid phase peptide synthesis platform (SPPS) (Amblard et al. 2006; Elsawy et al. 2012, 2013), and either research groups perform it themselves (to obtain smaller amounts <1 g), or larger companies provide their services, for small up to bulk amounts. Due to cleavage and purification conditions, peptides are mainly obtained in the presence

of trifluoroacetic acid (TFA) and, for cationic peptides, as trifluoroacetate (TF-acetate) salts (Roux et al. 2008). With this in mind, one has to note that original TFA salt can also be replaced using multiple procedures, with most often used HCl as counter-ions (Roux et al. 2008; Andrushchenko et al. 2007a). It is of utmost importance to realize that the effective mass of used peptide for research is different due to the amount of salt contributing to the overall mass, and thus will affect all physicochemical peptide-based nanomaterials properties that depend on the effective peptide concentration (e.g. shifts in critical gelation concentrations or interactions with various other systems). Furthermore, the presence of various salts will differently impact biological applications, with excessive TFA salts shown to impair the proliferation of cells (Cornish et al. 1999). Thus, the purity of synthesized peptides, and type of the counter ion are initial key characteristics requiring pre-defined establishment prior to the development of peptide-based nanomaterials. The two most commonly used techniques confirming the peptide structure are mass spectroscopy (MS) and high-performance liquid chromatography (HPLC).

MS is a spectroscopic technique that measures the mass-to-charge ratio (m/z) of induced ions. Samples are vaporized and then ionized by an ion source to create positively charged ions, accelerated down a mass analyzer and are then measured by a detector. This produces a mass spectrum, which is a plot of ion abundance vs. m/z. There are three main types of MS used to analyze peptides. These are: electrospray ionization (ESI), atmospheric-pressure chemical ionization (APCI) and matrix-assisted laser desorption/ionization (MALDI). Whilst all methods are acceptable to use, it is important to consider some of the advantages and drawbacks to each of the methods which may make certain types better to use for different peptide lengths.

ESI has no inherent size limit of molecule (Chen et al. 1995; Smith et al. 1994), and can be coupled to other techniques such as HPLC. However, it can be hindered by high salt concentrations. APCI can have higher salt concentrations, but labile compounds can be thermally decomposed due to heat. MALDI has increased sensitivity (being able to provide data from sub-femtomolar concentrations) over the other two techniques and has a high tolerance of salt and buffers (Lay Jr 2001), but there is more noise below 500 Da making analysis of smaller molecules more difficult (Glish and Vachet 2003). MS allows screening and analysis of multiple peptides extracted from a given sample (Alyousef et al. 2019), but also to fully confirm the desired peptide that has been synthesized/obtained (Elsawy et al. 2012, 2013; Wychowaniec et al. 2020a). Effectively, peaks in mass spectrum can be correlated to the molecular weights of peptides and peptide fragments. The largest fragment of a peptide is called the "parent" ion, where only one electron has been knocked off, and no fragmentation or bond breaking has occurred. This peak correlates to the overall molecular weight of the peptide. It is possible to identify the peptide sequence through examining the molecular weight of the fragments (Zhang et al. 2010a; Coon et al. 2005; Hunt et al. 1986). It is also possible to determine peptide abundance based on the area of peaks, and see impurities in the sample through unexpected molecular weights of fractions (Zhang et al. 2010b). Various algorithms and tools have been developed for fast identification of peptides in a high throughput (Bartels 1990; Halligan et al. 2005). However, one thing to note

is that MS does not distinguish the enantiomers, as two enantiomers do not differ in mass. HPLC, a chromatographic technique used for separation of materials via columns, is used to identify purity of samples, including identification of amino acid-specific peptides and their enantiomers (Yoshida 2004; Dołowy and Pyka 2014). In fact, HPLC is such a versatile platform, that it can be coupled together with other techniques, including MS (Geiser et al. 2008; Qian et al. 2021).

For proteins and peptides, reversed-phase HPLC (RP-HPLC) is most often used, based on principle of hydrophobicity, stemming from the high symmetry in the dipolar water structure surrounding molecules, thus enabling more efficient separation than in a typical polar column (Guilbaud et al. 2013). Purity of peptides is calculated based on the main peptide peak detected at a given retention time, compared to the overall area of all peaks. For example, based on the area of the main FFHFFHKKGRGD (P12) peptide peak at 10.8 min retention time, over all remaining other peaks (impurities), a purity of 96.46% has been estimated (Song et al. 2020). In other work, Gao et al. estimated purity of four self-assembling peptides over 95% in each case, demonstrating highly pure materials for fabrication of tuneable hydrogels (Fig. 8.1). An exemplar method is provided in description of Fig. 8.1 to aid the development of purification methods. One thing to bear in mind is to avoid oversaturation of the intensity signal, i.e. by using appropriate concentrations, typically recommended with maximum up to 1 mg mL^{-1} peptide concentration. Peptide retention signals larger than 2000 a.u. in intensity may lead to inaccurate calculations of purity, thus impacting the validity of further experiments.

HPLC can also be used to define degradation or formation of products of enzymatic reactions in peptide-based nanomaterials (Guilbaud et al. 2013; Burgess et al. 2018). For example, Geiser and co-workers demonstrated the use of two complementary monoliths located in injecting capillaries system for RP-HPLC, for protein/peptide digestion and pre-concentration ability, respectively (Geiser et al. 2008). Both monoliths were prepared from co-polymers leading to distinct porous structures, one of which was capable of covalently bonding to a Pepsin enzyme (that digests peptides and proteins) and other capable of concentrating digested peptide fragments for MS-HPLC combined analysis. The authors used a few proteins including myoglobin, albumin and haemoglobin as a proof-of-principle study to demonstrate the digestion and successful injection of concentration proteins, with repeatability of the method for at least 20 successful digestions. In another study by Burgess et al., RP-HPLC was used to define the time-dependent enzymatic degradation of peptide-based hydrogels (Burgess et al. 2018). The percentage of non-degraded peptide was calculated using the following equation:

$$\%_{\text{Non – degraded peptide}} = \frac{\text{AUPt}}{\text{AUPc}} * 100\% \tag{8.1}$$

where AUPt and AUPc are the areas under the RP-HPLC peaks, for the sample treated (e.g. by enzyme) and the untreated control sample, respectively.

Overall, we note that both MS and HPLC are not only useful, but often required techniques for determining the quality of the peptide. Furthermore, HPLC can be
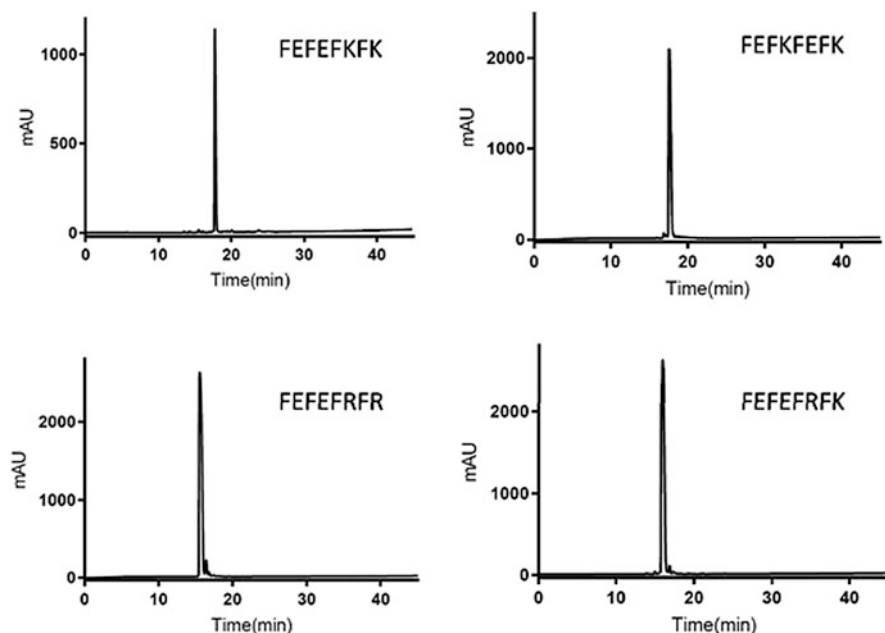
Fig. 8.1 HPLC traces of the four exemplar self-assembling peptides. (Method: The 1 mg mL^{-1} peptide solutions in 1% trifluoroacetic acid (TFA) in water/acetonitrile (50/50 V/V) were injected on the RP-HPLC column Phenomenex Jupiter 4μ Proteo column 90 A° (250 mm × 4.66 mm) equipped with UV detector ($\lambda = 220$ nm). An elution gradient was used with a flow rate of 1 ml/min that went from 90% solvent A (0.05% TFA in H$_2$O)/10% solvent B (0.05% TFA in CH$_3$CN) to 30% solvent A/70% solvent B in 45 min). Reprinted (adapted) with permission from (Gao et al. 2017). Copyright © 2017 American Chemical Society

used to define degradation products of synthesized/used peptide-based nanomaterials, a tool very useful particularly for applications in regenerative medicine and tissue engineering.

8.3   Establishing Interactions in Peptide-Based Nanomaterials

8.3.1   Phase Diagrams and Titrations

The self-assembly and formation of nanomaterials from peptides is intrinsically dependent on the designed peptide-based sequence and driven by the exact choice of amino acids. Particularly of interest are amino acids that contain both basic (NH$_3$$^+$/NH$_2$) and acidic (COOH/COO$^-$) side chain groups (Table 8.1), which can be deprotonated as a function of pH, and as a result carry a charge. Lysine, arginine and histidine amino acids all contain NH$_2$ side chain groups and as a result can

Amino acid	Theoretical pK_a
NH_3^+/NH_2 side chain	
Lysine	10.53
Arginine	12.84
Histidine	6.00
COOH/COO$^-$ side chain	
Aspartic acid	3.65
Glutamic acid	4.32

contribute positive charge to overall peptide sequence. On the other hand, aspartic acid and glutamic acid both contain COOH side chain groups, and can contribute negative charge to overall peptide sequence. The overall charge carried by a peptide can be calculated using the following equation:

$$Z = \sum_i N_i \frac{10^{pK_{a_i}}}{10^{pH} + 10^{pK_{a_i}}} - \sum_j N_j \frac{10^{pH}}{10^{pH} + 10^{pK_{a_j}}} \qquad (8.2)$$

where $N_{i/j}$ are the numbers and $pK_{a\ i/j}$ the pK_a values of the basic $(i - pK_a > 7)$ and acidic $(j - pK_a < 7)$ groups present, respectively (Nelson et al. 2017). The ionic groups present on the peptides are carboxylic acid (COOH/COO$^-$) at the C-terminus, with theoretical pK_a values ranging from 1.71 to 2.38, depending on which amino acid the C-terminus group is attached to (Nelson et al. 2017; Barrett 1985). Similarly, N-terminus amine (NH_3^+/NH_2) theoretical pK_a value is dependent on which amino acid the groups is attached to, and ranges from 8.18 to 10.60 (Nelson et al. 2017; Barrett 1985). As mentioned, all charged amino acids (Table 8.1) should be taken into account for calculating overall peptide charge status.

Overall charge status has been shown to play a key role in the self-assembly and gelation properties of designed peptides-based nanomaterials (Roberts et al. 2012; Caplan et al. 2000; Aggeli et al. 2003). Previously it has been shown that titrations can shift apparent pK_a values of the side chain amino acids groups (Wychowaniec et al. 2020a; Tang et al. 2009), as well as terminal side groups (Grimsley et al. 2009), due to the occurrence of self-assembly, folding and chemical environment. The apparent shifts of pK_a values can be measured experimentally via acid-base titrations (Wychowaniec et al. 2020a), or using automated isothermal titration calorimetry (ITC) (Nakamura and Kidokoro 2004). This is particularly good start for any peptide-based nanomaterials that can yield overall charge status compared to the theoretical one and that can be related to the overall physical properties such as fibrillization or hydrogelation. For example, Wychowaniec et al. used base titrations to compare charge profile of self-assembling FEFKFEFK (F8) peptide to the modified version with added two lysine amino acids on both ends: KFEFKFEFKK (KF8K, Fig. 8.2a–b). The specifically found apparent pK_a value of lysine was assigned to the more polar surrounding environment in KF8K peptide sequence and was related to the overall propensity for bulk hydrogelation, where phase of the sample was presented as a function of peptide concentration and pH (Fig. 8.2c–d).

Fig. 8.2 (**a**) Theoretical charge carried by each peptide vs pH (dotted lines indicate the theoretical pKa of the different ionic groups present on the peptides); (**b**) molar ratio of added NaOH to peptide vs pH (shadowed regions indicate the protonation/deprotonation transition regions of the different ionic groups); (**c**, **d**) concentration vs pH phase diagrams describing the samples' physical appearance/state. Reproduced under a Creative Commons Attribution License (CC-BY) from (Wychowaniec et al. 2020a)

8.3.2 Characterizing Peptide Interactions: Thermodynamics

8.3.2.1 Isothermal Titration Calorimetry

Isothermal titration calorimetry (ITC) can be thoroughly used to investigate the nature of biomolecular interactions in self-assembling peptides. This is based on the fact that thermodynamic parameters (enthalpy−entropy compensation) describing self-assembly can be measured, and related to the macromolecular crowding, aggregation and assembly of molecules (Kabiri and Unsworth 2014). Kabiri and Unsworth have described this in detail and presented case study of ITC on self-assembling peptides, concluding that hydrophobic forces, electrostatics and H-bonding are three most crucial types of interactions driving assembly of peptide-based systems (Kabiri and Unsworth 2014). Noteworthy, most often experimental self-assembling peptide systems are accompanied by series of simulations elucidating exact assembly mechanisms (Garcia et al. 2021; Kralj et al. 2020). These however are out of the scope of the current chapter and can be found described in another chapter of the current book.

8.3.2.2 Differential Scanning Calorimetry

Differential scanning calorimetry (DSC) is a thermal method used to characterize the stability of a protein or peptide by measuring its thermal denaturation (Graziano et al. 1996). DSC has several variations that correlate to different sample types that can be measured. In standard DSC, samples tend to be measured in DSC pans, and are solid or gel like samples. Micro and nano-DSC tend to measure solutions (Edwards-Gayle et al. 2019; Maslovskis et al. 2011). It is commonly used to measure transition temperature of denaturation of proteins from a folded to unfolded state, or transitions between secondary structures upon external stimuli (Scholtz et al. 1991). In the field of peptides, an example of how it has been used is through the characterization of peptide Lanreotide nanotubes (Valéry et al. 2004). DSC enabled a thorough investigation on the effect of temperature and concentration on the self-assembling behaviour of nanotube formation, determining the phase diagram of these conditions, allowing tuneability of the system (Valéry et al. 2004). DSC can also be used to understand energy landscape of interactions, e.g. energy of H-bonding between peptide–peptide (N_1–$H_1 \cdots O_2 = C_2$) and peptide–water hydrogen bonds. Borvskina and co-workers used DSC to analyze collagen type I and model collagen polypeptide poly(GPP) (Boryskina et al. 2007). Together with other techniques (Fourier transform infrared spectroscopy and quartz piezogravimetry), they found an average of 3–4 H_2O molecules formed an internal hydration shell around each GPP unit, overall leading to reorganization of the triple helix and contributing to H-bonding between peptide chains, strengthening the conformation of the peptide backbone (Boryskina et al. 2007). It is also common to use DSC to measure the effects of peptide interaction with other systems, for example lipid membranes models (Edwards-Gayle et al. 2019; Klajnert et al. 2006a; Malanovic and Lohner 2016; Andrushchenko et al. 2007b), and detection of peptide–polymer interactions (Maslovskis et al. 2011), extensive discussion of which is outside the scope of this chapter.

8.4 Spectroscopy

In this section, the use of spectroscopic characterization methods, including Fourier transform infrared spectroscopy (FTIR), Raman spectroscopy, circular and linear dichroism (CD and LD), nuclear magnetic resonance (NMR) spectroscopy and fluorescence spectroscopy will be described.

8.4.1 Fourier Transform Infrared Spectroscopy

Fourier transform infrared spectroscopy (FTIR) is one of the most utilized spectroscopic techniques describing peptides. FTIR has excellent sensitivity to chemical composition and molecule architecture, giving particularly invaluable information rapidly.

Andreas Barth thoroughly described the utilization of infrared spectroscopy in peptide and protein research paving the way for facile identification of multiple bands (Barth 2007). Described IR bands can be assigned to both side chains of amino acids and secondary structure formation, with latter being mostly utilized to characterize assembly of peptide-based nanomaterials (Barth 2007). Peptide and protein IR spectra consist of three distinctive amide regions, called amide I, II and III bands. Amide I band is centred near 1650 cm^{-1}, in the range 1600–1700, amide II resides in the range 1470–1570 cm^{-1}, and amide III in the range 1250–1350 cm^{-1}. Amide I bands, which arise mainly from the C–O stretching vibration, come from the structural peptide backbone. One should be aware that certain amino acid side chains (Table 8.2) have band positions in this region, so caution must be taken when assigning the secondary structure of peptides containing these amino acids. It is recommended to use a secondary technique such as circular dichroism to determine the secondary structure of peptides containing these amino acids.

Different amino acids have different propensities for secondary structure formation (Fig. 8.3). These values were calculated computationally by Chen and co-workers (Chou and Fasman 1974). Assignment of secondary structures is one of the most useful tools, with typical values quoted in Table 8.3, for α-helix, β-sheet, turns and disordered states (Barth 2007; Barth and Zscherp 2002).

Table 8.2 Amino acid side chain vibrations that are close to or within the amide I band, where ν is stretching vibration, ν_s is symmetric stretching vibration, ν_{as} is asymmetric bond vibration, δ is in plane bending vibration

Amino acid	Chain vibration	Band position in H_2O/cm^{-1}	Band position in D_2O/cm^{-1}
Asn	ν(C=O)	1677–1678	1649
	δ(NH$_2$)	1612–1622	N/A
Arg	ν_{as}(CN$_3$H$_5{}^+$)	1672–1673	1608
	ν_s(CN$_3$H$_5{}^+$)	1633–1636	1586
Gln	ν(C=O)	1668–1687	1635–1654
	δ(NH$_2$)	1586–1610	1163
HisH$_2{}^+$	ν(C=C)	1631	1600
Lys	δ_{as}(NH$_3{}^+$)	1626–1629	1201
Tyr-OH	ν(CC) δ(CH)	1614–1621	1612–1618
Tyr-O$^-$	ν(CC)	1594–1602	1590–1591
	ν(CC)	1599–1602	1603
Trp	ν(CC)ν(C=C)	1622	1618

References to the peaks were taken from (Chirgadze et al. 1975; Venyaminov and Kalnin 1990; Rahmelow et al. 1998). Table in part adapted with permissions from (Barth 2000). Copyright © 2000 Elsevier

	Strong β-sheet former			Strong α-helix former	
	Met	M		Glu	D
	Val	V		Ala	A
	Ile	I		Leu	L
	Cys	C		His	H
	Tyr	Y		Met	M
Weak β-sheet former	Phe	F	Weak α-helix former	Gln	N
	Gln	N		Trp	W
	Leu	L		Val	V
	Thr	T		Phe	F
	Trp	W	Indifferent	Lys	K
Indifferent	Ala	A		Ile	I
	Arg	R		Asp	E
	Gly	G		Thr	T
	Asp	E		Ser	S
	Lys	K		Arg	R
	Ser	S		Cys	C
Weak β-sheet Breaker	His	H	Weak α-helix Breaker	Asn	N
	Asn	N		Tyr	Y
	Pro	P		Pro	P
Strong β-sheet Breaker	Glu	D	Strong α-helix Breaker	Gly	G

Fig. 8.3 The propensity of each amino acid for forming different secondary structures

Table 8.3 Assignment of amide I band positions to secondary structure

	Band position in H_2O/cm^{-1}		Band position in D_2O/cm^{-1}	
Secondary structure	Average	Extremes	Average	Extremes
α-Helix	1654	1648–1657	1652	1642–1660
β-Sheet	1633	1623–1641	1630	1615–1638
	1684	1674–1695	1679	1672–1694
Turns	1672	1662–1686	1671	1653–1691
Disordered	1654	1642–1657	1645	1639–1654

The table is adapted with permissions from (Barth 2007). Copyright © 2007 Elsevier

For example, Ridgley et al. used FTIR over time to elucidate not only the peptide self-assembly rules in amyloid structures across nanometre up to micrometre length scale, but also by monitoring aggregation over time they identified specific amino acids implication in the formation and evolution of β-sheet structures in peptide mixtures (Ridgley et al. 2013). This can be correlated back to the occurring intermolecular and intramolecular peptide–peptide interactions and provide necessary information to infer the observed structural changes.

One important thing to note is that typical FTIR spectra are never of singular secondary structure and thereby are accumulations of individual contributions from

Fig. 8.4 Infrared spectrum in the amide I region of the aqueous solution of concanavalin A. The upper and lower figures represent the curve fitted, and the second derivative spectrum, respectively. Reproduced under a Creative Commons Attribution License (CC-BY) from Sadat and Joye (2020)

multiple structural components, as well as chemical signatures (Ridgley et al. 2013). With that respect, one most commonly used method is that of spectra deconvolution in the amide I region into sum of all peaks assigned for all individual secondary structure components (peaked at wavelengths guided by Table 8.3). For example, deconvolution of FTIR spectrum of concanavalin A is presented in Fig. 8.4, showing distinct regions contributing to the overall signal (Sadat and Joye 2020). Typically, the second derivative of the amide I spectral region is taken without filtering to identify the individual amide I components (Fig. 8.4), peaking around relevant secondary structure wavenumbers (as per Table 8.3). Various software packages including OMNIC or OriginPro can be used to match Fourier deconvolution to series of Gaussian or Lorentzian distributions to maximize the outcome; with latter software allowing facile and rapid identifications of secondary regions. The area of each peak is typically representative of the molar concentration of that particular secondary structure (Kong and Yu 2007). One thing to realize then, is that peptides of different lengths (i.e. having different numbers of peptide bonds in backbone) should only be compared after appropriate normalization is taken into account, in that case of the area of amide II region (Wychowaniec et al. 2020a).

Due to the ease of use of FTIR and availability of the technique, it is frequently used to characterize peptide-based systems as a function of concentration, pH, chemical additives such as salts or enzymes, or other external stimuli. Evolution of spectra can also be recorded as a function of time including both short time scales, through minutes and hours, up to days and weeks. This can give indication of temporal changes in samples, e.g. to describe their time-dependent degradation (Quilès et al. 2016).

8.4.2 Raman Spectroscopy

Raman spectroscopy is a less known and utilized technique characterizing peptide-based nanomaterials, although it still allows viewing chemical and structural, including mechanical, features of peptide-based systems. For example, Tuma summarized the use of Raman spectroscopy, quoting its ability to resolve some crystallographic structures with higher resolution than X-ray diffraction (XRD) (Tuma 2005). Raman spectroscopy measurements are useful in defining amino acid composition and assigning backbone spectra. Moreover, it is intrinsically sensitive to aromatic amino acids, thus allowing easier band assignments, which can lead to greater understanding of molecular interactions between aromatic acids and external chemicals/applied stimuli (Tuma 2005; Hernández et al. 2013). Water is characterized by a weak Raman scattering, therefore is a well suitable solvent for studying water-based peptide nanomaterials (Keiderling 2020).

Like all spectroscopic techniques, Raman spectroscopy allows reliable assignments of amino acids (composition) or structural features (secondary structure) based on the previously established band positions and intensities. Notably, Zhu et al. provided one of the most comprehensive Raman bands assignments for majority of amino acids, both as powders and as solutions (Zhu et al. 2011). In fact, the provided band assignments by Zhu and co-workers should be a starting point for all those performing Raman spectroscopy on peptide-based nanomaterials. We also refer readers to multiple well-established reviews in the field (Ridgley et al. 2013; Tuma 2005; Hernández et al. 2013). One obvious limitation of the studies and reviews provided is the fact that more complex structures and inter-amino acid interactions can occur, which make unravelling Raman spectra a more complex task.

In Table 8.4, we show most common structural and amide features on peptide-based systems. We note that secondary structure assignments in Raman spectroscopy are alike those displayed in FTIR, except for the β-sheet band, which typically appears shifted centred between 1665 and 1670 cm^{-1} (Table 8.4) (Pelton and McLean 2000; Böcker et al. 2007; Rabolt et al. 1977; Williams and Dunker 1981).

Table 8.4 Assignment of common structural, amide and vibrational modes in Raman spectroscopy

Assignment	Average Raman shift (cm^{-1})
Amide I: β-sheet	1665
Amide I: α-helix	1650
υ(C=C): Aromatic stretch on tyrosine (Y)	1614
υ(C=C): Aromatic stretch on phenylalanine	1610, 1207, 1031 and 1003
δ(CH$_2$): CH$_2$ deformation on A, I, L, V side groups	1475
δ(CH$_3$): CH$_3$ deformation on A, I, L, V side groups	1410
Amide III: C–N stretch, υ(CN) and N–H bend, δ(NH), on Q, K side groups	1230–1280
υ(CN): C–N stretch of Q, K side group	1100

Peak references were adapted from (Ridgley et al. 2013; Rygula et al. 2013; Pelton and McLean 2000)

Fig. 8.5 Structural features of self-assembling amphiphilic ultrashort peptides. (**a**) Chemical structures of the individual three tetrapeptides. (**b**) Raman spectra of IIFK (left), IIZK (middle) and IZZK (right). Reprinted (adapted) with permission from (Susapto et al. 2021). Copyright © 2021 American Chemical Society

Like for all materials, one has to note the sensitivity and differences of some structural features and amino acids, depending on the used laser wavelength in Raman spectroscopy (Rygula et al. 2013). In fact, Rygula and co-workers summarized the dependence of secondary structures of multiple proteins, including collagens, β-sheet proteins, pepsins, elastases and many more, on laser excitation wavenumber (Rygula et al. 2013). The authors carefully selected a few classes of proteins based on their secondary structure, i.e. including those with highest propensity for: (1) α-helices, (2) β-sheet, (3) mixed structures (α/β, α + β) and various hemoproteins. Based on those, they provided comprehensible table of individual amino acids as well as secondary structures present, which we highly recommend as a good reference for assigning spectra of peptide-based nanomaterials (Rygula et al. 2013). Similarly to FTIR, decomposition of amide I region can also be performed from Raman spectra. For example, Susapto et al. used Raman spectroscopy on three tetra peptides forming bio-inks to unravel their exact secondary structure fractions by deconvolution (Fig. 8.5) (Susapto et al. 2021). Susapto and co-workers showed that for all the three studied tetrapeptides the deconvoluted β-turns peaked at 1664 and 1680 cm^{-1} Raman shift (Fig. 8.5), as mentioned, in the range originally anticipated (Pelton and McLean 2000; Böcker et al. 2007; Rabolt et al. 1977; Williams and Dunker 1981). Furthermore, the extracted full width at half-maximum (FWHM) of the Ac-IIFK-NH$_2$ peptide was smaller than those containing cyclohexylalanine, which indicated more ordered Ac-IIFK-NH$_2$

self-assembly and packing. Thus, detailed analysis of secondary structures of peptide-based nanomaterials is not only possible, but also can reveal hitherto unobserved interactions or structures.

Sloan-Dennison et al. (Sloan-Dennison et al. 2021), using Raman spectroscopy mapping, recently demonstrated difficulty of interpreting Raman spectra based on self-assembling KYY peptide fibres. In particular, they show that two distinct fibrillar forms can be obtained during the drying procedure, with one of the polymorphs easier to identify in spectra compared to the other one. Whilst the Y amide marker bands at 852 and 828 cm^{-1} were present in both fibrillar forms with similar intensities, thus indicating similar secondary structure (i.e. the same stacking of aromatic Y rings), the bands at 1614 and 1661 cm^{-1} varied considerably between the two forms (Fig. 8.6). Along with other identified differences, particularly in lysine residues side chain band, Sloan-Dennison and co-workers elucidated two forms of conformational interactions driving assembly. On one hand, this work shows the difficulty of using Raman spectroscopy, however on the other hand, it shows this technique allows rapid mapping and elucidating spatial and molecular differences in peptide-based materials.

One of the early work that utilised an amended version of Raman spectroscopy, namely Raman Optical Activity (ROA), had already shown that differentiation of disordered and α-helical structures may be possible, in both amide I and III regions (Keiderling 2020; Hecht et al. 1999). A particularly useful experimental ROA parameter is the dimensionless circular intensity difference (CID), defined as: (Barron and Buckingham 1971)

$$\Delta_{\mathrm{CID}} = \frac{(I_{\mathrm{R}} - I_{\mathrm{L}})}{(I_{\mathrm{R}} + I_{\mathrm{L}})} \tag{8.3}$$

where I_{R} and I_{L} are the intensities of right- and left-circularly polarized components of Raman scattered light, respectively (Smith et al. 2009). For example, this way, poly-Lysine was distinguished from poly-glutamic acids (Hecht et al. 1999). These days ROA is frequently utilized to study multiple phenomena, such as structures of condensed phases of peptide-based nanomaterials (Keiderling 2020), or achiral elements in a chiral environment (Smith et al. 2009). This way ROA is a sensitive technique offering insights into chiral and otherwise undistinguishable molecular structures.

Interestingly, the sensitivity of Raman spectroscopy to aromatic amino acids, such as phenylalanine, offers unprecedented opportunities to tag various molecules by it and study molecular binding mechanisms or degradation (Sahoo et al. 2016). Sahoo and co-workers demonstrated that unique capability on peptide-functionalized surfaces detecting enzymatic hydrolysis as a function of time. They showed that Raman spectroscopy can be used to monitor thin peptide films and feedback in real time the degradation and exact amino acid compositions of the degraded fragments. Since Raman spectroscopy is a non-destructive (e.g. on tissue) technique, it offers opportunities to be used in multiple biomedical settings,

Fig. 8.6 (**a**) White light image of KYY fibre area mapped. (**b**) False colour image of map created using 1661 cm^{-1} peak. (**c**) False colour image of map created using 1614 cm^{-1} peak. (**d**) False colour image created from principal component analysis (PCA) analysis using the loading plot of principal component 1 (red) and the loadings plot of principle component 2 (cyan). (**e–h**) show repeat analysis. (**i**) Normalized spectrum of form 1 (blue) and form 2 (blue). KYY fibres mapped with a centred scan at 1130 cm^{-1}, a 1 s acquisition time and 5×5 μm step size, 532 nm laser excitation and 2.5 mW laser. Reproduced under a Creative Commons Attribution License (CC-BY) from (Sloan-Dennison et al. 2021)

studying, e.g. real-time degradation of implanted peptide-based nanomaterials in vitro or in vivo.

Finally, we note that Raman spectroscopy can also be used to study mechanical properties, such as Young's modulus, based on molecularly recognized vibrational modes. Zelenovskiy and co-workers demonstrated that high stiffness (i.e. Young's modulus) of FF nanotubes (reported using other techniques as 19–27 GPa (Kol et al. 2005; Niu et al. 2007)) stems from lattice vibrations (Zelenovskiy et al. 2016). Particularly important was contribution of water inside FF nanotube core, which

appeared to uniquely bring the Young's modulus value of FF at least magnitude higher compared to other peptide-based nanostructures (Smith et al. 2006).

8.4.3 Circular Dichroism

Circular dichroism (CD) is a technique used to characterize the secondary structures of chiral molecules, by passing plane polarized light through them (Greenfield 2006; Beychok 1966). Plane polarized light is made up of equal circularly polarized components. One rotates clockwise (or right-handed), whilst the other anti-clockwise (left-handed). CD measures the difference between the absorption of these two components, similar to ROA described in the previous section (Keiderling 2020). Thus, if a sample is either not chiral meaning there is no absorption or if a sample is racemic (i.e. containing equal quantities of two chiral enantiomers), then there will be equal amounts of left and right absorption overall resulting in zero difference in absorption (Beychok 1966).

Amino acids (apart from Glycine) are chiral molecules, and thus all contribute to a CD spectrum. This means that they have unequal absorption of left and right-handed circularly polarized light, which produces a non-zero CD signal. Far UV CD spectrum (typically between 180 and 260 nm) can be used to determine secondary structure conformations of peptides, and used to estimate the fraction of each contribution, typically by deconvolution process, which we will describe below. When performing CD, several factors must be considered to ensure correct sample preparation. Absorption must be below 1 to obtain an accurate spectrum, suggesting concentration, path length or buffer composition must be appropriately checked. We also note that salt concentrations severely affect the absorption levels and thus need to be adjusted. Sample purity must be high, at least 95% determined by an alternative technique (similarly to what we discussed in initial sections of quality control). Buffers must be without any optically active components. Oxygen absorbs light below 200 nm, so it's best to degas buffers/samples before use or use glass filtered distilled water. Often systems running <200 nm require large amounts of N_2 gas flushing.

The difference in absorption, ΔA, is written as the difference between left (A_L) and right (A_R) handed-circularly polarized light:

$$\Delta A = A_L - A_R \tag{8.4}$$

CD is often reported in molar ellipticity which can be calculated using the equation below:

$$[\theta] = \frac{\theta}{C \times L} \tag{8.5}$$

Fig. 8.7 Circular Dichroism (CD) scan showing the different secondary structures you can form, including α-helix (characterized by positive peak at 193 nm, and negative peaks at 208 and 222 nm) (Holzwarth and Doty 1965), β-sheet (characterized by a negative peak around 218 nm (Greenfield and Fasman 1969)) and unordered structures characterized by a negative peak at 190 nm (Venyaminov et al. 1993) and a slight increase at around 230 nm)

where $[\theta]$ is molar ellipticity in deg cm^2 dmol^{-1}, θ = ellipticity in mdeg (mo), L = pathlength in cm and C = molar concentration.

Secondary structure can be characterized by distinctive profiles (Fig. 8.7) and the percentages of each secondary structure can be calculated using various software packages, details of which can be found in the review article by Greenfield et al. (Greenfield 2006).

CD spectroscopy is particularly useful tool to study transition or gelation of materials, and their interactions with other molecules. One example of such work was carried out on peptide MAX1, a 20-amino acid peptide composed of alternating valine and lysine residues (Fichman and Schneider 2021). CD spectroscopy was used to unravel the secondary structure landscape of MAX1 peptide, as well as in the presence and absence of dopamine monomers capable of forming secondary polymer network (Fig. 8.8a). Firstly, CD was used to study the rate of β-sheet formation in MAX1 gel as a function of time (Fig. 8.8b), both in the presence and absence of dopamine monomers. This was done by presenting the characteristics of molar ellipticity for β-sheet taken at 216 nm ($[\theta]_{216\ nm}$) as a function of time. Then, they used CD to record spectra of MAX1 peptide, again, in the presence and absence of dopamine, as a function of temperature (Fig. 8.8c–d), and finally presented as the $[\theta]_{216\ nm}$ as a function of temperature for both water (non-gelling) and buffer (gelling) conditions (Fig. 8.8e). Overall, CD spectroscopy is a versatile tool that can be used to study the self-assembly process as a function of time, temperature, as well as in the presence or absence of other molecules, being applicable to a wide range of scenarios for peptide-based nanomaterials.

Fig. 8.8 Secondary structural analysis of the MAX1-dopamine gel system using circular dichroism (CD) spectroscopy. (**a**) CD spectra at 37°C were collected for 1 wt.% MAX1 in water (blue triangles) and in buffer, in the absence or presence of dopamine (black squares and red circles, respectively). Data collection was initiated after 20 min of sample equilibration at 37 °C. (**b**) Rate of β-sheet formation of MAX1 in the absence or presence of dopamine. The evolution of β-sheet is monitored by recording $[\theta]_{216 \text{ nm}}$ as a function of time for 1 wt.% peptide solution at 37°C, starting 5 min after peptide assembly is initiated by the addition of buffer (pH 7.4). (**c, d**) Temperature-dependent wavelength CD spectra of 1 wt.% MAX1 in buffer, in the absence or presence of dopamine (**c, d**, respectively). (**e**) The evolution of β-sheet as a function of temperature is presented for MAX1 in water (blue triangles) and in buffer, in the absence or presence of dopamine (black squares and red circles, respectively). Reproduced under a Creative Commons Attribution License (CC-BY) from (Fichman and Schneider 2021)

8.4.4 Linear Dichroism

One has to be careful when performing CD measurements of peptide, due to their natural propensity for alignment along the flow during loading (Wychowaniec et al. 2020a; Hamley et al. 2017). In this case, the structure of peptides can be measured using linear dichroism (LD) spectroscopy. This technique uses parallel polarized light to measure the difference in absorbance of molecular groups through a detector with a polarizer arranged parallel and perpendicular to that of the light source (Norden et al. 2010). This arrangement allows detection of chemical groups aligned to the polarizer which commonly occurs in long structures, such as fibres aligned through flow (Hicks et al. 2010). For example, by measuring the sample with the quartz plate placed vertically and then rotated through regular intervals (e.g. 15 or 30°), it should be possible to see what groups are aligned and their orientation to the fibre axis. For a β-sheet structure with the strands perpendicular to the fibre axis, a cross β-structure, it would be expected that with the sample orientated so that the fibre axis is vertical (0°) there would be negative peak around 198 nm and for the fibre axis orientated horizontal (90°) there would be a positive peak at a slightly (approx. 5 nm) higher wavelength.

8.4.5 Nuclear Magnetic Resonance Spectroscopy

Nuclear magnetic resonance (NMR) spectroscopy is a technique that uses the magnetic spin properties of specific nuclei within a molecule to identify atoms which are close together in space (Williamson and Waltho 1992). Since hydrogen exchange occurs in all biological macromolecules, NMR is a powerful method allowing studies of both structural and dynamic properties of macromolecules (Dempsey 2001). Only certain specific nuclei have magnetic spin properties. Most relevant for biological samples include ^{1}H, ^{13}C, ^{15}N and ^{31}P. Isotopes such as oxygen, ^{16}O and ^{12}C are inactive in NMR spectroscopy, thus cannot be detected. When these molecules are placed into a magnetic field, they absorb electromagnetic radiation. It is common to enrich samples with NMR active isotopes to assist in simplifying the NMR data to identify particular chemical groups (Howard 1998). From NMR spectrum it is possible to determine peptide purity and correct peptide sequence from 1D methods, as well as solve the secondary and tertiary structures through using more advanced two-dimensional (2D) methods.

There are several effects that are important for solving structures of proteins and peptides using NMR. One of the most important effects is the nuclear Overhauser effect (NOE), which arises from two nuclei close in space relaxing back down to the basal state. In 1D spectrum, this presents as a change in intensity of signals of the two corresponding nuclei. In 2D NMR, this experiment is known as NOSEY. Further information on how to interpret this data can be found in the relevant cited article (Williamson and Waltho 1992). In summary, it is common to back calculate the

expected NOEs based on the protein sequence to compare to the experimental values, which can then be used to go through refinements to determine the structure (Boelens et al. 1989). One issue for determining peptide secondary structure using this method is that peptides can have high motion, and several intramolecular structures, that are dynamic. This can cause bias, particularly if a minor conformation has short NOE distances, as the NOE signal will be much larger than other species. In combination with analyzing NOE'S, J-coupling constants are dependent on the angle between protons. Between these two methods of analysis, it is possible to determine peptide and protein structure. One example is in combination with Small angle X-ray scattering (SAXS), peptide C16-KTTKS was found to form spherical micelles which could be confirmed by NMR (Miravet et al. 2013).

1D NMR spectroscopy in/solution is a very useful tool for confirming covalent conjugations, e.g. of peptides to other polymers (Dempsey 2001). Golunova et al. conjugated a bone-sialoprotein-derived peptide TYRAY to amidated alginate with the use of Cu-catalyzed azide-alkyne cycloaddition (Golunova et al. 2021). Multiple reaction pathways were tested and NMR analysis allowed understanding the exact final chemical structures, yield and level of amide group substitution with a TYRAY peptide. In particular, ^{1}H NMR spectrum was recorded of conjugated sodium alginate in D_2O at 50 °C (which allowed easier solubilisation of the construct), and compared to the control sodium alginate measured in the same conditions. Level of substitution was calculated using equation:

$$L_{\text{substitution}} = \frac{I_S/N_H}{2.56\,I_G} * 100\% \tag{8.6}$$

where I_S is the area under the specific signal, N_H is the number of hydrogen atoms related to the specific signal and I_G is the area under the hydrogen signal, in this particular case at C1 of the guluronic acid (at 5.1 ppm). Furthermore, the substitution is normalized to the signal of all alginate units, calculated based on the fact that α-l-guluronic acid (G) to β-D-mannuronic acid (M) ratio is 1.56. Whence, the intensity of all alginate units (G + M) was calculated to be $2.56 \cdot I_G$. The equation can be easily adjusted to other type of reactions involving peptides or substitutions of particular groups on peptide-based macromolecules (Singha et al. 2011; van Dijk-Wolthuis et al. 1999; Birchall et al. 2001). NMR techniques have also been utilized to calculate diffusion constants of individual amino acids and peptide-based nanomaterials (Germann et al. 2007; Buffy et al. 2005). Since both protein and peptide-based nanomaterials key properties lie in dimensions and the degree of folding, measurements of self-diffusion coefficients D that determine the hydrodynamic dimensions are very useful. Dudás and Bodor recently derived empirical variations of D as a function of protein/peptides' molecular mass M that distinguish folded, intrinsically disordered and urea-denatured biomolecules (Dudás and Bodor 2019). The authors further established an easy set of guidance and analytical tools to also study the aggregation of peptide-based nanomaterials, and corrected all measurements for viscosity values of original solutions.

Two-dimensional nuclear magnetic resonance spectroscopy (2D NMR) can also be applied to study more complex systems. Some 2D NMR methods include correlation spectroscopy (COSY) and total correlation spectroscopy (TOCSY), which create correlations between geminal and vicinal protons (in COSY) or all protons within a given spin system (in TOCSY). For example, these two methods were used to unravel the 3D structure of two similar 13 residue-long peptides derived from frog skin, temporin-SHa and temporin-SHc, which both are antimicrobial, but exhibit different membrane-damaging properties (Abbassi et al. 2008).

Other NMR methods include solid-state NMR, which allows studies of exact molecular structures formed by peptide-based nanomaterials. For example, secondary structure of a mutant prion protein involved in neuronal regulation was unravelled (Laws et al. 2001). Interactions of peptides with lipid membranes (Bechinger and Salnikov 2012), or within bilayer membranes (Salnikov et al. 2019; Bechinger 1999) have also been studied. In general, NMR methods are vast and offer a large pool of analytical probing of peptide-based nanomaterials, from molecular structure, diffusion coefficients, up to macromolecular structures and 3D-formed structures. However, the methods require specialized algorithms and correlations and are rarely the first choice for studying peptide-based nanomaterials, except for quality control confirmation of successful reactions. Nevertheless, we anticipate rapid evolution of this field, partially driven by arising machine learning for improved algorithms. For more details, we refer the readers to the recently published sister book chapter on this topic (Hamley and Castelletto 2021).

8.4.6 Fluorescence Spectroscopy Assays

Fluorescence spectroscopy can be used to determine the critical aggregation concentration (cac) of a peptide solution, and give some information on the likely secondary or tertiary structure the peptide has formed. Fluorescence spectroscopy works through excitation of electrons into a higher energy state, called the singlet state. Once excited, the electrons will relax back down to the ground state. As they relax, photons of light are released, usually with shifted energy as compared to the energy of photons used for excitation. This is known as Stoke's shift. A beam of light at a specific wavelength is passed through the sample, and light is absorbed (excitation spectrum) or emitted (emission spectrum). Fluorescence is directly proportional to absorbance, as shown by the Beer-Lambert Law:

$$A = \varepsilon c L \qquad (8.7)$$

where A is absorbance, ε is the molar extinction coefficient, L is the path length, and c is the solute (peptide) concentration.

Compounds that fluoresce are known as fluorophores and usually contain aromatic groups (Yasuda 2019). Peptide sequences with intrinsic aromatic amino acids, such as tryptophan, phenylalanine and tyrosine can have their aggregation measured

by just exciting the peptide at the correct wavelength across a concentration series. Commonly used fluorescence probes such as 8-Anilinonaphthalene-1-sulphonic acid (ANS), pyrene and pyrene carboxylic acid generally have an increase in fluorescence when exposed to a hydrophobic environment, making them very sensitive to hydrophobic collapse. Since 1959, fluorescent dye Thioflavin-T (ThT) has become a gold standard for selective staining and identification, firstly of amyloid fibrils and subsequently of β-sheet fibres, both in vitro and in vivo (Biancalana and Koide 2010). ThT has increased fluorescence when bound to an amyloid β-sheet fibril structure. ThT is thought to bind to fibril-like β-sheets along the surface side chain grooves, parallel to the long β-sheet fibre axis with remarkable affinity, often due to strong electrostatic attraction (Biancalana and Koide 2010; Arad et al. 2020). This affinity provides unprecedented tool for imaging and diagnostics of processes involving β-sheet like nanomaterials. A typical sudden increase in ThT fluorescence is observed, which can be used to monitor the progression of fibrillization in time, as a function of pH (Fig. 8.9a–b). The use of commonly used molecular probes for fluorescence measurements is summarized in Table 8.5.
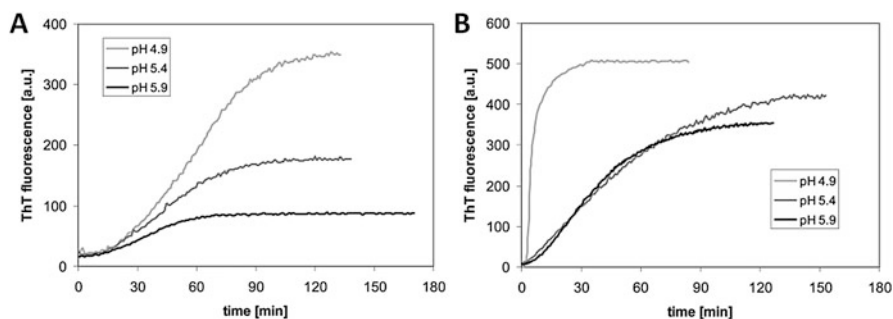
Fig. 8.9 Changes in fluorescence of ThT during the aggregation processes of (**a**) prion peptide 185–208 and (**b**) Aβ 1-28. Reprinted (adapted) with permission from (Klajnert et al. 2006b). Copyright © 2006, American Chemical Society

Table 8.5 Most commonly used molecular probes for measurements of aggregation/self-assembly

Molecular probe	Type of affinity structure binding	References
Thioflavine-T (ThT)	β-Sheet/amyloid fibres	Edwards-Gayle et al. (2019), Wychowaniec et al. (2020b), Castelletto et al. (2019a)
ANS ((8-anilinonaphthalene-1-sulphonic acid)	Any structure[a]	Edwards-Gayle et al. (2019), Edwards-Gayle et al. (2020), Lindgren et al. (2005), Castelletto et al. (2019b)
Pyrene/pyrene carboxylic acid	Any structure	Castelletto et al. (2019a), Hutchinson et al. (2019a), Hamley et al. (2016), Hutchinson et al. (2018), Kwon et al. (1993), Li et al. (2020)

[a]May have problems with this if pH of the peptide is changed

8.5   Microscopy

The ability to visualize objects on nanometre scale remains one of the most important characterization techniques. Although direct information of sizes, morphologies, structure, and topology can be obtained, it is important to realize that the most accessible techniques (discussed below), give information of a 2D impression of the object in comparison to its native 3D conformation in aqueous solution. Furthermore, these kinds of measurements are heavily relying on the preparation method, thus are intrinsically partially biased. Furthermore, researchers tend to image particular parts of the grids, thus being intrinsically biased towards seeing sample closest to their expectations. Having said that, they are the first line of imaging that allows formation of proper 3D structures using advanced techniques, such as small angle X-ray scattering in native aqueous solution, which requires modelling that can aid from microscopically derived relevant size and structural ranges. This will be discussed later in detail in Sect. 8.6.

8.5.1   Transmission and Scanning Electron Microscopies

Transition Electron Microscopy (TEM) is a high-resolution imaging technique, where an electron beam is passed through a sample with a different density. Electrons have a significantly shorter wavelength than visible light, allowing for up to 1000 times higher resolution images, enabling the nanostructure of peptide nanomaterials to be resolved (Touve et al. 2019). Scanning electron microscopy (SEM) produces images by scanning the surface of a sample with a focused beam. This gives useful information about the surface topography of peptide nanomaterials, in particular those forming hydrogels (Wychowaniec et al. 2020b). One has to note that the resolution of SEM is lower (~30 nm) than that of TEM (~0.2 nm).

For both techniques, an electron beam is emitted from a negatively charged electron gun, the most common being lanthanum hexaboride (LaB_6) source or a tungsten filament cathode. These electrons are then accelerated through a series of anodes, at high voltage and under vacuum. For SEM the voltage ranges from 0.2 to 40 keV and for TEM it is higher at 60–200 keV. Both instruments have a series of lenses that focus the beam, predominantly these are condenser, projector and objective lenses. Apertures can also be used to decrease beam intensity and filter out electrons scattered at high angles. High-angle electron scattering can lead to spherical and/or chromatic aberrations, and diffraction. For TEM, samples must be below 100 μm in thickness whereas thickness is not an issue for SEM (Efimov et al. 2007; Graham and Orenstein 2007).

Firstly, for peptides, which are mainly built from low atomic number elements, a heavier contrast agent that strongly binds is typically required (De Carlo and Harris 2011). De Carlo and Harris summarized advanced in the use of macromolecule

staining, including peptides and proteins (De Carlo and Harris 2011). Although there are several negative staining molecules, uranyl acetate solution still remains a gold standard for staining peptide-based nanomaterials (Anthony et al. 2014). The negative staining contrast in TEM micrographs formed due to its exclusion from the dense ordered peptide structures, providing dark highlights along the edges of the peptide structure (Anthony et al. 2014; Childers et al. 2010). For SEM, since peptide-based samples are generally non-conductive, they are coated with a thin layer of gold (Ag) (or other conductive metal) in order for the samples to be visible under the microscope (Heu et al. 2019).

Due to changes in peptide morphology through the drying process, as dehydration can have a large impact on self-assembled structure, TEM and SEM can be limited to these changes. Cryo-TEM and cryo-SEM, which allow for the peptide solutions/hydrogels to be frozen in situ are very powerful techniques for determining peptide self-assembled structure, as it overcomes the issue with drying (Sharp et al. 2012; Merg et al. 2019; Mehta et al. 2008). Various combined methods can also be used to achieve 3D images of the samples, provided a sufficiently small thickness of sample of up to 200 nm is retained, can be performed (Schaffer et al. 2017).

Next, it is important to realize that for macrostructures, such as hydrogel, which are built from individual nano-sized peptide building blocks, sample preparation requires dilution and agitation to disentangle the fibrous network and allow observation of the isolated nano-objects, such as, e.g. nanofibres (Wychowaniec et al. 2020a; Elsawy et al. 2016; Ding et al. 2013; Ligorio et al. 2019). This process is particularly appealing for studying peptide-based nanostructures, with the resulting TEM images demonstrating apparent (typically dehydrated) sizes, pitches, turning points and overall network topologies for assembled systems (Gao et al. 2017). Rather than true 3D structure of peptide-based nanomaterial in aqueous solution/or of hydrated networks, TEM indirectly enables estimation of inter-objects interactions and "adhesion" strength (Gao et al. 2017; Wychowaniec et al. 2020a; Anderson et al. 2009; Gras et al. 2008).

For example, in recent work, Fichman and Schneider used TEM as an aid to investigate changes upon fibrillization from self-assembling peptides in the presence of a secondary dopamine-polymerized network (Fig. 8.10) (Fichman and Schneider 2021). TEM allowed the establishment of the thickness distribution of fibres, with peak thickness shifting from around 3 to 4 nm upon incubation with dopamine. For hydrated peptide-built networks (resembling hydrogels), in addition to above mention information, quantification based on a number of images can be performed for identification of *entanglements* (fibres crossing on top of each other); *branches* (one fibre splitting into two "daughter" fibres); *bundles* (multiple fibres coming together to form a larger fibre bundle). It is worth noting that *entanglement*s are present in any fibrillar network, whereas branching or bundles depends on the level of peptide miss-assembly and fibre edge interactions (Wychowaniec et al. 2020a; Branco et al. 2009; Rughani et al. 2009).

For sufficiently large peptide-based nanomaterial (>30 nm or more) SEM can also be used. For example, Goktas and co-workers used SEM to image nanofibrous self-assembled peptide amphiphile (PA) and poly(ethylene glycol) (PEG) composite
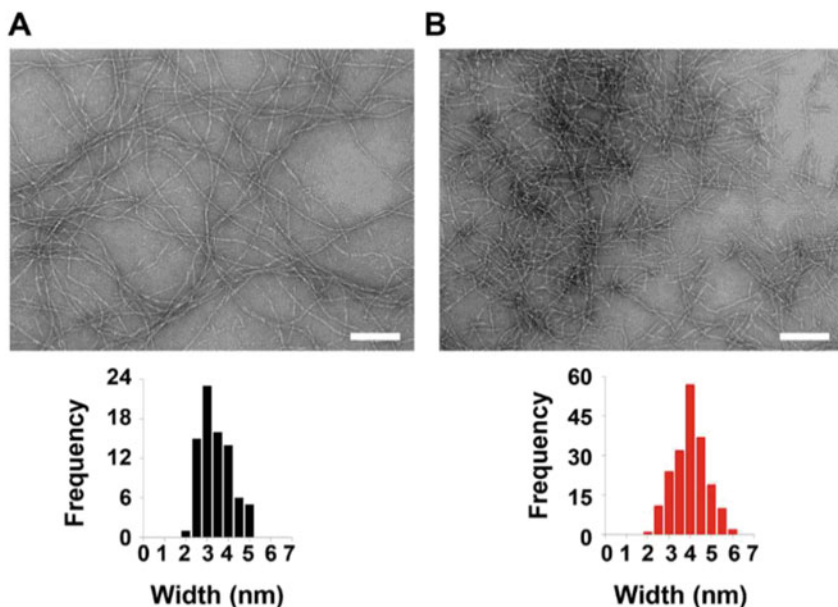
Fig. 8.10 Representative TEM micrographs showing fibrils isolated from 1 wt.% fibrillar gel networks 3 days after gelation is triggered in the absence or presence of 10 mM Dopamine (**a** and **b**, respectively). Scale bar = 100 nm. Widths of individual fibrils of each sample were determined using ImageJ software, by measuring the width of fibrils from 3 separate micrographs, representing different locations of the fibrils on the grid, $n = 193$ and $n = 80$ for the gel with/without dopamine, respectively. Reproduced under a Creative Commons Attribution License (CC-BY) from (Fichman and Schneider 2021)

hydrogel system (Fig. 8.11a) (Goktas et al. 2015). Clearly visible fibrillar networks were identified for the composite systems, showing the role the used peptide amphiphiles, Lauryl-VVAGEEE (E3-PA), Lauryl-VVAGERGD (RGD-PA) and Lauryl-VVAGEGDGEA-Am (DGEA-PA), play in forming topological networks with higher mesh size compared to purely chemically crosslinked synthetic poly (ethylene glycol dimethacrylate) (PEGDMA) (Fig. 8.11a) (Goktas et al. 2015). On the other hand, SEM is most useful in establishing pore sizes of freeze-dried hydrogels (Fig. 8.11b), as well as changes in their morphologies due to degradation or external factors (e.g. due to injection) (Wychowaniec et al. 2020b; Berillo et al. 2012; Zhu et al. 2018; Soto Morales et al. 2021). One has to note that pore sizes and structures established this way are always affected by the preparation technique, thus not reflecting true hydrated structures. Quite often, environmental SEM (ESEM) technique is also used, where the examination of pore structures of hydrogels is performed under saturated water vapour environment, thus enabling closer to a better environment evaluation of pores, with minimal drying (Chawla et al. 2011).
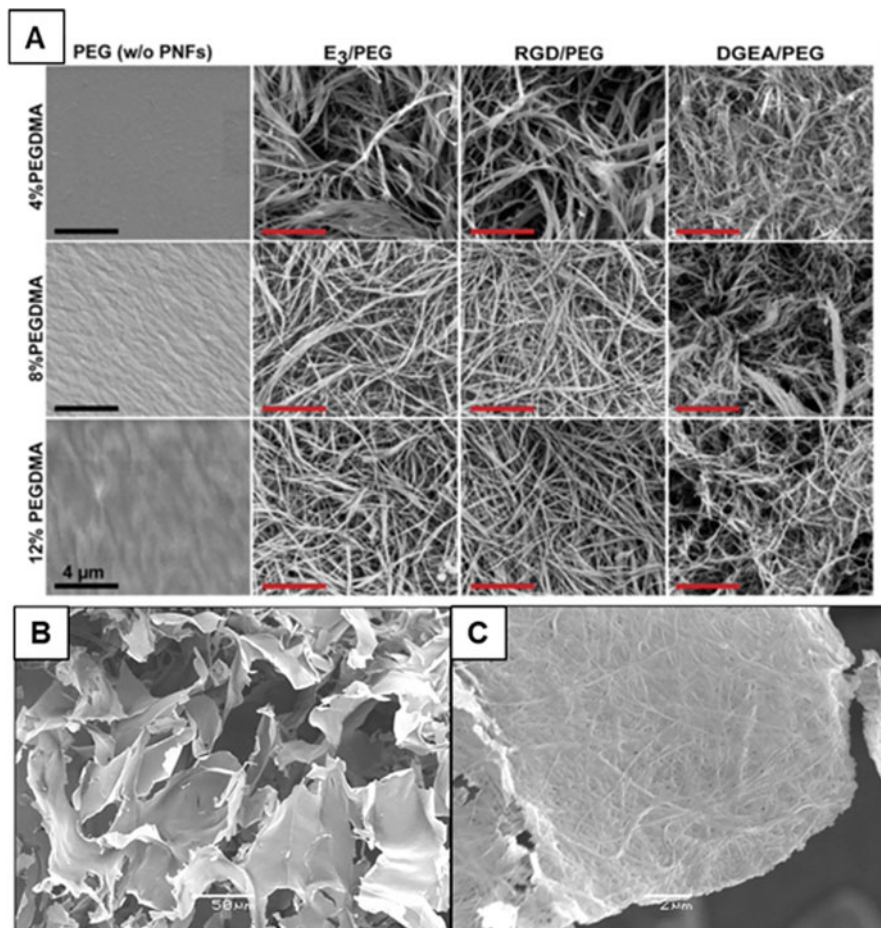
Fig. 8.11 (**a**) Scanning electron microscopy (SEM) images of PEG (w/o PA nanofibres, PNFs) and PA/PEG composite substrates (scale bars: 4 μm). Reprinted (adapted) with permission from (Goktas et al. 2015). Copyright © 2015 American Chemical Society. (**b**–**c**) SEM images show a porous cryogel from 15 mM Fmoc–FF after freeze-drying at (**b**) low magnification and (**c**) at high magnification prepared in the presence of 0.1 M K_2SO_4. Reprinted (adapted) with permission from (Berillo et al. 2012). Copyright © 2012 Elsevier

8.5.2 Atomic Force Microscopy

Atomic force microscopy (AFM) is a versatile method for imaging two-dimensional topography of materials in a versatile way, including dry and wet samples (Jalili and Laxminarayana 2004; Alessandrini and Facci 2005). The two basic AFM modes allow imaging in so-called "contact" and "tapping" modes, where the probe either scans over the surface of deposited material or taps above the surface at a given rate, thus allowing visualization of topography (Dufrêne et al. 2017). Over the past three

decades, AFM has evolved and multiple variations and improvements of the method have been utilized, including multi-frequency modes for high-speed nanomechanical mapping (Garcia and Herruzo 2012; Wychowaniec et al. 2021a), high-speed AFM combined with fluorescence imaging (Uchihashi et al. 2016), tip modifications for more tailored interactions, e.g. with carbon nanotubes (Wilson and Macpherson 2009), as well as many more, allowing simultaneous view of mechanical (Dokukin and Sokolov 2012), magnetic (Yamamoto et al. 1997) and electrical properties (Jalili and Laxminarayana 2004) of materials at the same time as topographical view.

Sample preparation in AFM is crucial. Although imaging dry samples, as well as liquid based is possible, the more common approach still remains a dry state. In this approach, a sample concentration is determinant, with preliminary screening almost always necessary. Here, peptide-based nanomaterials can be drop-casted and overnight dried, or spin-coated, onto a substrate. The choice of substrate is also important. Typical substrates include SiO_2, mica or highly oriented pyrolytic graphite (HOPG). For peptide-based nanomaterials, choice of substrate has to be carefully thought out, with flatness and charge being important factors to consider. Most commonly, due to atomic flatness, mica is used; however, its charge is often driving electrostatic interactions that can mask the true structure of the deposited sample. Poly-lysine coatings can also be used to reverse the charge on mica from negative to positive, allowing negatively charged samples to stick better.

Adamcik and Mezzenga reviewed the use of atomic force microscopy in the context of amyloid fibrils (Adamcik and Mezzenga 2012). In particular, they summarized the possibilities of the AFM techniques, including elucidation of the exact structure from topographical maps and obtained height (Fig. 8.12), demonstrating the possibilities of seeing twisted ribbons, helical ribbons and nanotubes. Previously, Adamcik et al. have also shown the possibility of using high-end statistical analysis on AFM images to unravel exact structures of protofilaments on left-handed twisted peptide fibrils (Adamcik et al. 2010), which paved the way for the more common use of statistical tools in AFM for establishing fibrillar structures. Jurado et al. have also utilized AFM to show the fibrillation pathways for rigid apoferritin protein amyloid fibrils (Jurado et al. 2021). Authors showed fibrillization was dependent on the concentration of apoferritin and pH of solution, showing multiple AFM images after incubation of samples for 9 h and confirming the obtained fibrillation pathways using complementary TEM technique. In fact, many groups have used AFM to unravel the propensity for self-assembly, e.g. by controlling amino acid sequence of N-acetylated tri-β3-peptides (Seoudi et al. 2015a, b).

AFM can also be used as an effective method for mapping interactions between proteins, peptides and other materials (Ligorio et al. 2019, 2021; Wychowaniec et al. 2018). For example, interactions between a selection of 2D material fillers and various peptide materials can be visualized using AFM, overall contributing to seeing the effective balance of hydrophobic or electrostatic interactions, based on the visual adhesion and distance of peptide nanofibres to the graphene-based materials (Wychowaniec et al. 2018).

AFM is famously used to establish mechanical properties on nanoscale. Nanoindentation (Rubin et al. 2015), force-curve analysis from conventional and
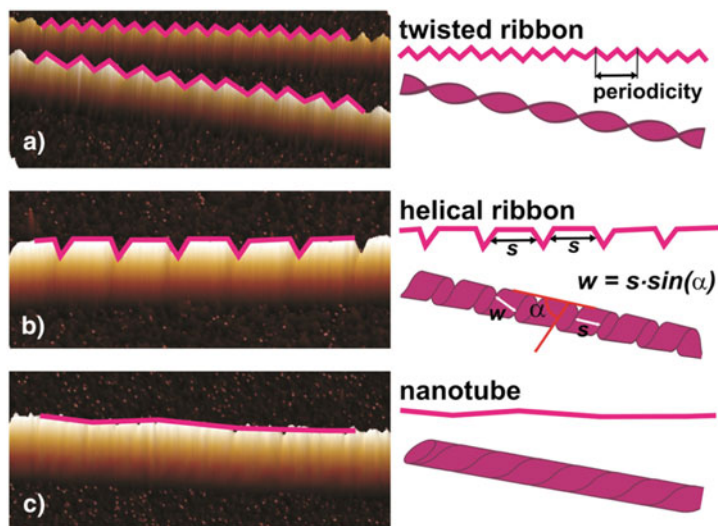
Fig. 8.12 The height profiles of different morphological structures assembled from the heptapeptide CH₃CONH-βAβAKLVFF-CONH₂. (**a**) 3D AFM image of twisted ribbons with corresponding height profiles (left part). The scheme of twisted ribbon and the estimation of periodicity of twisted fibrils using the height profile which has a sharp "zig-zag" shape (right part). (**b**) 3D AFM image of helical ribbon with corresponding height profile (left part). The scheme of helical ribbon and the estimation of the width of helical ribbons using the height profile with a plateau of width s, where s is related to the real width of the ribbon w by $w = s \cdot \sin(\alpha)$, α being the tilt angle of the helical ribbon edges with respect to the fibril axis (right part). (**c**) 3D AFM image of nanotube-like structure with corresponding height profile (left part). The scheme of nanotube and the corresponding height profile with a flat shape (right part). Reprinted (adapted) with permission from (Adamcik and Mezzenga 2012). Copyright © 2012 Elsevier

peak-force atomic force microscopy (AFM) (Adamcik and Mezzenga 2012; Guo and Akhremitchev 2006; Liao et al. 2016), torsional harmonics atomic force microscopy (TH-AFM) (Passeri et al. 2015), and bimodal atomic force microscopy (Benaglia et al. 2019), have all been used in addition to computational simulation methods (Paparcone et al. 2010; Paul et al. 2016) to measure and estimate peptide fibre Young's moduli. For example, Dong et al. used AFM-based spectroscopy to measure Young's modulus of mature amyloid fibrils formed from the 29-residues amphipathic peptide hormone glucagon (Dong et al. 2008). Authors measured force–distance curves of glucagon fibrils taken with the 0.01 N m⁻¹ silicon nitride cantilever probe, but also single molecules force spectroscopy (SMFS), by picking up molecules and looking at the force extension during the event. Combined measurements confirmed a reversible elastic behaviour of the fibrils, but also the fact that H-bonding across backbone of fibrils contributed mostly to the Young's moduli and that the force is equivalently distributed across all bonds. More recently, Christoff-Tempesta and co-workers showed the self-assembly of Kevlar-inspired aramid amphiphile nanoribbons and established using statistical AFM analysis that they have a Young's modulus of 1.7 GPa and a tensile strength of 1.9 GPa

(Christoff-Tempesta et al. 2021), overall showing extremely robust and small fibres of about 20 µm in thickness, outperforming multiple so far known materials including silk, amyloids, actin and ligaments, amongst others.

Interestingly, in other measurements on Fmoc-FF peptide, contact mode AFM and piezoelectric force microscopy (PFM) measurements revealed enhanced piezo-electric response (Ryan et al. 2015). PFM is a modified technique of AFM, where an electric voltage is applied to the surface via a conducting tip, allowing phase imaging of conductive and piezo-responsive samples. Analysis by Ryan et al. unravelled that the piezoelectric response results from the non-central symmetry (tilted) nature of the formed β-sheet fibres. Strong piezoelectric response using PFM has also been shown in other peptide-based nanomaterials (Kholkin et al. 2010). This opened up a way for various peptide-based nanomaterials acting as biocompatible actuators, motor and various molecular machines, but also more common utilization of AFM-based techniques for studying various processes in these kinds of materials (Bdikin et al. 2012; Nguyen et al. 2015, 2016; Bystrov et al. 2012).

8.5.3   *Light Microscopy*

Optical microscopy that came as the first microscopy technique is a versatile tool allowing visualization of multiple specimens. By virtue of using light, unlike electrons, the imaging resolution is limited by a diffraction limit to visible light wavelengths. However, recent approaches in fluorophores and fluorescent switches allowed developments of high-resolution optical microscopies, dropping resolutions down to ten nanometres. In particular, similarly to biological specimens, in peptide-based nanomaterials immunochemical staining offers easy microscopic evaluation. Various modes of optical microscopy allowed the evaluation of features of peptide-based nanomaterials, including phase contrast optical microscopy (Domingues et al. 2020), polarized light imaging (Zhang et al. 2010c) and confocal microscopy (Mammadov et al. 2012).

Ye and co-workers designed nanometre-sized (~4.7 nm in diameter) positively charged fluorescent rapid photoswitches from conjugated polymers that had a large propensity for binding to β-amyloid peptide fibrils (Ye et al. 2019). The developed photoswitches allowed the use of high-resolution (~20 nm) optical microscopy, enabling rapid evaluation of the dosage-dependent inhibition effect of polymer conjugates on the Aβ1−40 fibrillation process at 0, 4, 8 and 12 h.

Polarized light microscopy, which used cross-polarized light, is one of the most commonly used techniques for unravelling alignment of nanomaterials, including, in particular, peptides that have a tendency to form liquid crystal phases (Pomerantz et al. 2006, 2008; Rüter et al. 2020). In particular, Zhang et al. demonstrated that charged amphiphilic molecules self-assembly into well-defined lamellar plague structures with fibrous textures that break upon cooling into large arrays of aligned nanofibres and strongly birefringent solutions (Fig. 8.13) (Zhang et al. 2010c). One peptide amphiphilic molecule C_{16}-$V_3A_3E_3$(COOH), formed a β-sheet hydrogel, that
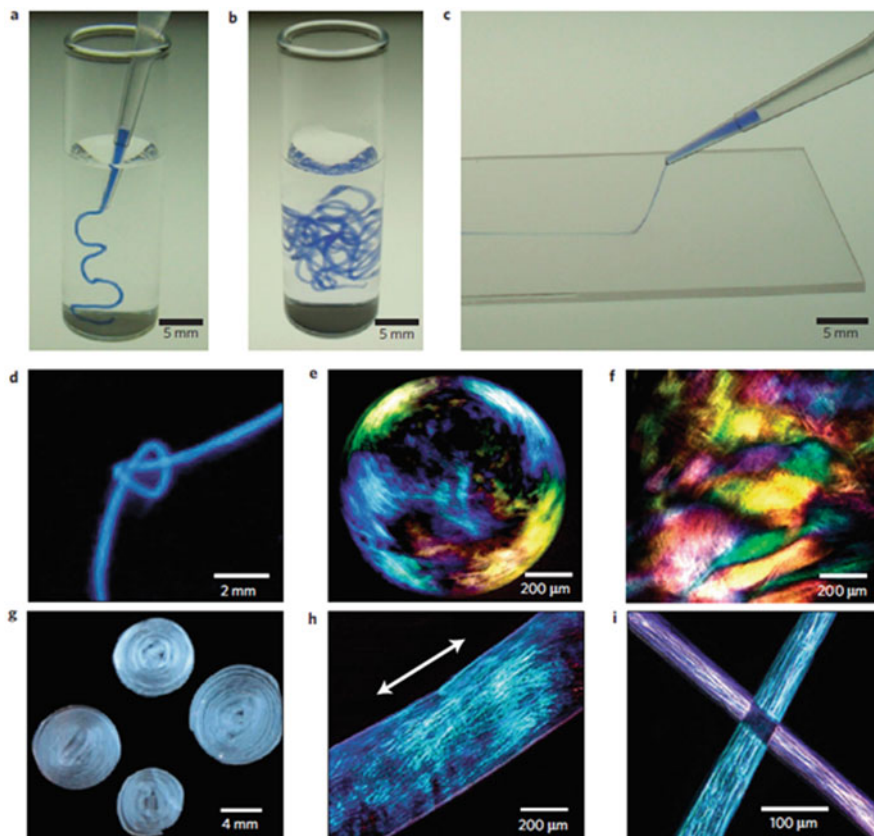
Fig. 8.13 Strings and gels with long-range internal alignment. (**a**, **b**) A peptide amphiphile solution coloured with trypan blue injected into phosphate-buffered saline after heat treatment. (**c**) The same solution dragged through a thin layer of aqueous $CaCl_2$ to form a noodle-like string. (**d**) A knot made with peptide amphiphile string. (**e**) Birefringence of a bubble gel observed between cross polarizers suggesting the presence of macroscopically aligned domains. (**f**) Similar domains in a gel film. (**g**) Peptide amphiphile noodle spirals prepared on a spin coater. (**h**) Birefringence of a single string suggesting alignment along the string axis. (**i**) Light extinction between cross polarizers at the cross point of two noodles demonstrating uniform alignment in each. Reprinted (adapted) with permission from (Zhang et al. 2010c). Copyright © 2010, Nature Publishing Group

could be injected into a salt containing solution to make a noodle form (Fig. 8.13a). Using polarized optical microscopy, authors revealed that heat-formed noodle gel contained large birefringent domains, whereas one prepared from unheated solution was completely isotropic. The liquid crystal domains were shown from all material's cross-sections, and across all length scales (Fig. 8.13), particularly with uniform birefringence along the length of the noodle string (Fig. 8.13h-i).

One method which combines rotational rheology (which will be discussed in depth later in Sect. 8.7) and optical birefringence-based techniques and allows a full view of a sample during rheological measurements using various geometries and

different states of polarized light is known as shear-induced polarized light imaging (SIPLI) (Mykhaylyk et al. 2012, 2016; Mykhaylyk 2010). In this technique, briefly, the polarized light imaging device is coupled to a rotational stress-controlled rheometer, that has a parallel-plate setup. The bottom plate is transparent and the top is a reflective plate (polished steel mirror), allowing reflected polarized light images to be recorded during shear (Mykhaylyk et al. 2016). The method has recently been used to image the alignment state of the self-assembling β-sheet peptide-based hydrogels (Wychowaniec et al. 2020a). Two peptides were studied that varied by the outer content of Lysine residues, FEFKFEFK (F8) and KFEFKFEFK (KF8K), but had a similar capacity to form β-sheet-rich fibres (Wychowaniec et al. 2020a). On the other hand, hydrophobic fibre−fibre associative interactions were decreased in the case of KF8K, resulting in a reduced tendency for fibres to associate/aggregate laterally and form large fibre bundles, and consequently network cross-links. This effect resulted in the formation of hydrogels with lower storage modulus but faster dynamics. SIPLI helped unravelling the difference on macroscopic scale under shear, where KF8K fibres were observed to align only under high shear and at high concentration, whilst F8 hydrogel fibres were found to align rapidly at low shear and low concentrations.

Finally, we note that Mammadov and co-workers provided a comprehensive review of the microscopic characterization of peptide-based nanomaterials (Mammadov et al. 2012). For more detailed sample preparation methods, we refer the readers to that review.

8.6 Scattering

8.6.1 Small Angle Scattering

Small angle X-ray scattering (SAXS) is a powerful method to study the structural properties of materials at the nanoscale. It is a non-destructive and accurate method that requires little sample preparation. Originally developed in the 1930s to study metal alloys (La Guinier 1939), it has been shown to be useful for many other purposes including structure and orientation of polymers, colloids and biological macromolecules, such as peptides (Guilbaud and Saiani 2011; Shriky et al. 2020; Wychowaniec et al. 2021b). There have been two milestones that have increased the popularity of the technique. The first was in the 1970s, with the appearance of intense synchrotron sources. The second, in the 1990s, was associated with computational advances and methods allowing for high-throughput SAXS (Blanchet and Svergun 2013). Recent progress in instrumentation and analysis methods has led to an increasing number of applications of this technique for biomacromolecule studies in the solution state, allowing, for example self-assembly to be studied in solution or in hydrogels (Wychowaniec et al. 2020a; Guilbaud and Saiani 2011; Blanchet and Svergun 2013).

SAXS measurements on solutions are typically performed when molecules are randomly orientated. It is still possible to obtain information on magnitudes of the

interatomic distances, and the overall form factor or shape of the self-assembled nanomaterial. SAXS can be used to assess oligomeric states in peptide or protein aggregation, chemical equilibria and reaction kinetics, temperature profiles, self-assembly, co-assembly, complexation and other interactions (Edwards-Gayle et al. 2019; Castelletto et al. 2019b; Singh 2013; Vestergaard et al. 2007; Valéry et al. 2003; Mandal et al. 2014).

SAXS has an advantage over other techniques such as crystallization or XRD (which will be described later) as energetically favourable conformation for crystallization/the conformation of the peptide after drying is often different from how the peptide would behave in solution (Hutchinson et al. 2019b; Griebenow and Klibanov 1995). SAXS is a powerful technique to study self-assembly in solution or in hydrogel formation. Scattering is isotropic, and photons are collected on a 2D detector (Fig. 8.14a). To overcome this, the image is radially averaged to obtain scattering intensities, as a function of the momentum of transfer or wavevector, q:
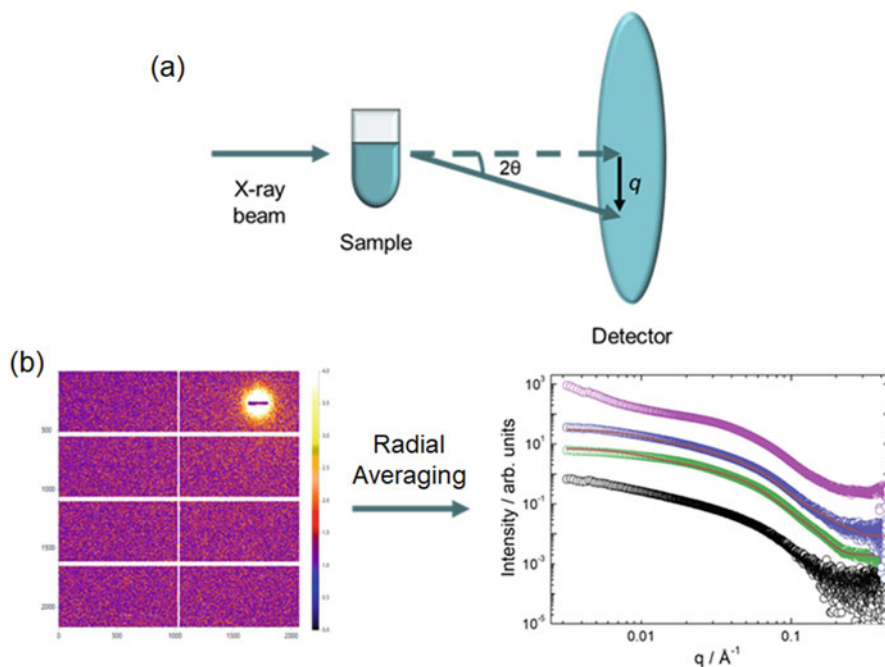
Fig. 8.14 A basic schematic of a SAXS experiment. (**a**) When a monochromatic beam hits the sample, photons are scattered at different angles. The scattered photons are collected by a 2D detector and the data is radially averaged to obtain a scattering curve. The overall q-range (which dictates the size of structure that can be measured) is determined by camera length. For a SANS experiment, the X-ray beam is replaced by a neutron beam, but the same principles apply. Example of an (**b**) SAXS detector image and (**c**) example 1D SAXS data after radially averaging the data, showing several concentrations of a peptide amphiphile that forms a mixture of spherical micelles and short fibres

$$q = \frac{4\pi \, \sin \theta}{\lambda} \tag{8.8}$$

where λ is equal to the wavelength of the incident beam, θ is half the angle of incidence (angle between incident beam and scattered radiation). A typical scattering curve will have intensity plotted against q in nm^{-1} or Å dependent on instrumentation (Fig. 8.14b). The q-range is determined by instrument setup, particularly the distance of the detector to the sample and beam energy.

During an experiment, scattering of the dissolved particles and that from the pure solvent are separately collected. The scattering of the pure solvent is subtracted from that of dissolved particles. The difference in signal is proportional to the concentration of the solution, and to the difference in electron density between particle Pp and solvent Ps. For biological molecules, including peptides, the density of the particle is only slightly higher than that of the corresponding aqueous buffer, meaning that the useful subtracted signal may be small (Guilbaud and Saiani 2011; Blanchet and Svergun 2013).

For a monodisperse system, consisting of non-interacting identical particles, the scattering intensity from a single particle averaged over all orientations is proportional to the background-corrected intensity $I(q)$, as such that:

$$I(q) = I(q)_\Omega = A(q)A^*(q)_\Omega \tag{8.9}$$

where the scattering amplitude, $A(q)$ is a Fourier transformation of excess scattering length density, and Ω is the solid angle in the reciprocal space of the scattering. Guinier analysis, developed in the 1930s is still the most straightforward way to determine the radius of gyration (R_g) and forward scattering $I(q)$ (Wychowaniec et al. 2020a; Gelain et al. 2012). The radius of gyration, is a model-independent size parameter, that can eventually be used to calculate the particle dimensions if a model is found. The Guinier approximation for a monodisperse system is:

$$I(q) = I(0). \exp\left(- \frac{1}{3} \, R_g^2 q^2\right) \tag{8.10}$$

This approximation is valid for the range $q.R_g < 1.3$ (Blanchet and Svergun 2013). In practice R_g and $I(0)$ are determined through a Guinier plot, a plot of $\ln[I(s)]$ against q^2. The slope is equal to R_g, and the intersection with the ordinate is the forward scattering intensity. A linear Guinier plot is a good indicator of sample quality and monodispersity (Wychowaniec et al. 2020a; Blanchet and Svergun 2013). However, for differently shaped materials, complimentary techniques should be used, for example imaging techniques and other scattering techniques discussed later (Wychowaniec et al. 2020a; Trewhella et al. 2017). Non-linear Guinier plots can be due to a number of reasons, for example polydispersity, improper background subtraction and inter-particle interactions (Singh 2013). As the Guinier region is influenced by interactions, non-specific aggregation can result in a sharp increase at low angles and overestimation of both R_g and $I(0)$. Although this effect is not ideal, it

does have some uses, for example finding crystallization conditions of a peptide (Blanchet and Svergun 2013; Singh 2013). In general, it is rare that a sample is truly monodisperse, except for the case of proteins. Polydisperse samples can still be measured using techniques such as size-exclusions SAXS (SEC-SAXS), which separates fractions within a sample before running them into the beamline (O'Brien et al. 2018; Cowieson et al. 2020; Ryan et al. 2018). It can also be used to detect different aggregation states. SEC-SAXS is a well-established technique for proteins, which may in the future be able to be applied more to peptide self-assembled systems with the correct column selection and buffer conditions.

The Guinier approximate provides a way to access $I(0)$. Overall the Guinier method provides size information, data quality, interactions and oligomeric state. Today, it can be calculated automatically by computer programmes (Blanchet and Svergun 2013). Every particle produces a form factor (an interference pattern describing every wave that is scattered by every atom inside the particle) that is characteristic of its structure. Overall size is determined primarily by the slope at low q, the final slope at high q bears the surface information (Porod's region). Shape and internal distribution information are determined through the oscillating part of the middle section of the SAXS curve (Fig. 8.15) (Blanchet and Svergun 2013; Singh 2013). Rough classifications into globular, cylindrical and lamella shapes can be done by investigating the power law form factor at small angles (Singh 2013). On a double logarithmic scale, an initial slope of q^0 indicates globular objects, q^{-1} indicates cylindrical shape and q^{-2} equates to lamellae objects (Fig. 8.15a) (Singh 2013). When q values exceed this, the objects are too large for the resolution limit and only the Porod region (region observed that gives information about structure surface, towards q_{max}) is observed (Singh 2013). A Porod decay of between -2 and -3 is considered to be a mass fractal, a structure containing cross-linking or branching resembling a 3D network, where closer to values of -3 indicate increased clustering. A Porod decay of between -3 and -4 is considered to be a surface fractal which gives information on the roughness or smoothness of the particle. q^{-3} decay indicates a rough surface, whereas q^{-4} corresponds to a smooth surface (Cherny et al. 2019; Anitas 2018).

A second method to examine the form factor is to plot the paired-distance distribution function of a peptide solution (Singh 2013). The paired-distribution function is a Fourier transform of the small angle scattering data. From the $P(r)$ you obtain information about the maximum particle dimension in the sample (D_{max}) as well as some form factor information (Fig. 8.15b) and information on the particle's electron density (whether it has a hollow core or a filled core) (Fig. 8.15c) (Singh 2013).

For self-assembled structures, it is possible to model them using form factor fitting (Guilbaud and Saiani 2011; Hamley 2008). This is based on using the shape of the SAXS data to select and fit the data to different shaped models by adjusting various parameters. Programmes such as SasView, Igor Pro and SASfit can be used to model structures using this method. Through this, it has been possible to model spherical and cylindrical micelle structures (Miravet et al. 2013; Guilbaud and Saiani 2011; Hutchinson et al. 2019b; Shi et al. 2017), bilayers (Cenker et al. 2011), fibres
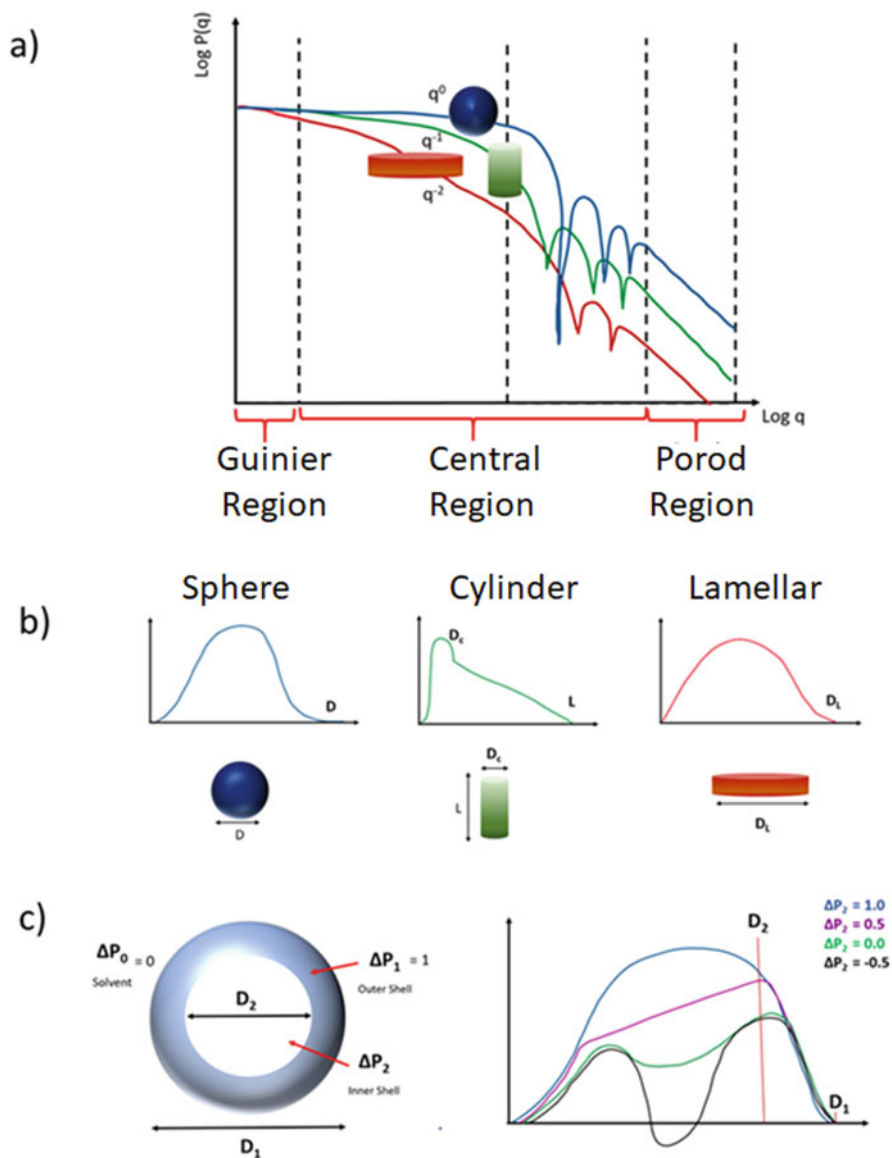
Fig. 8.15 Obtaining the form factor of the particle. (a) by plotting the data on a double logarithmic scale, it is possible to obtain some information on whether the particle is spherical, cylindrical or lamellar, $P(r)$ distribution can be used to obtain information equally on the shape through (b) the general shape of the curve can indicate structure, and (c) oscillation in the curve can give information on the particle's electron density

(Wychowaniec et al. 2020a, b; Shi et al. 2017; Castelletto et al. 2017; Boothroyd et al. 2013), and nanotube assemblies (Bressler et al. 2015; Lu et al. 2007; Krysmann et al. 2008; Narayanan et al. 2021).

Another method of investigating overall shape is to do a Fourier transform, and the resulting curve $P(r)$ is the "pair-distribution distance function". This produces a histogram of distances found inside the particle. This gives an initial idea of the shape (Blanchet and Svergun 2013). From here, it is possible to perform model calculations to determine relative positioning and orientations. They involve repeated calculations of pair-distribution distance functions, and comparisons with experimental curves. Ab initio modelling, such as a dummy bead modelling algorithm can be used to build models for particles of different shapes based on beads. Rigid-body modelling requires all atomic points (although this can be overcome by combination with ab initio techniques) (Elsawy et al. 2012). There are many computer programmes available that can perform modelling functions including the ATSAS package for academic users (Vestergaard et al. 2007; Konarev et al. 2006).

SAXS can also be used in conjugation with multiple other methods in situ, particularly to look at the changes under the influence of external stimuli, such as shear using rheometry (called Rheo-SAXS) (Hamley et al. 2017; Wychowaniec et al. 2021b) and peristatic pumps to induce flow (Flow-SAXS) (Wychowaniec et al. 2020a). In particular, Cinader and Burghardt developed a mathematical framework for describing the alignment of samples (e.g. liquid crystals) in the form of orientation parameters alongside orientation angles and corresponding orientation vectors (Cinader and Burghardt 1998). 2D SAXS scattering patterns can be recorded (e.g. during shear) (Wychowaniec et al. 2021b) and the tilt angle of the overall anisotropic scattering ($\Phi = 0 \rightarrow 2\pi$) can be calculated using those procedures developed by Cinader and Burghardt, by deriving an orientation angle and orientation parameter from a weighted average of the second moment tensor of the scattering pattern (from the eigenvectors and difference in eigenvalues, respectively) (Burghardt et al. 1999). Easier approaches for rapidly defining degree of alignment of peptides under shear or flow can also be used, such as a simple ratio of the meridian (y) over the equatorial axis (x) lengths of the 2D SAXS patterns observed for given peptides (Wychowaniec et al. 2020a).

8.6.2   Small Angle Neutron Scattering (SANS)

Small angle neutron scattering (SANS) is similar to SAXS, with similar concepts to the above section being very relevant for the technique. There are some important marked differences that will now briefly be discussed. As the name suggests, SANS involves the scattering of neutrons as opposed to X-rays. For X-rays, the scattering length density (SLD) increases with the number of electrons in the sample. However,

for neutrons, these changes are more irregular. One of the largest benefits is that the average scattering length density (SLD) of lipids, proteins and nucleic acids are very different. Moreover, the difference between the SLDs of H_2O and D_2O are vastly different (Jacrot 1976; Stuhrmann 1974; Svergun et al. 2013). This opens up the possibility to match-out certain components of your sample so they become "invisible" to the neutrons. Contrast matching experiments have been very powerful in examining peptide self-assembly. One example of contrast matching SANS in conjunction with SAXS to determine the packing of pre-gelled aggregates and gelled particles from low molecular weight gels based on phenylalanine (Draper et al. 2020). It is also possible to examine peptide interaction with other molecules, for example lipids (Nielsen et al. 2018).

8.6.3   X-Ray Powder Diffraction/Wide Angle X-Ray Scattering

X-ray powder diffraction (XRD) and wide-angle X-ray scattering (WAXS) are analogous techniques which can be used to assess smaller d-spacing distances in peptide samples, and lead to atomic level resolution of samples (Graewert and Svergun 2013). WAXS is similar to SAXS, but with closer sample-detector distances, which means a shorter camera length (Singh 2013; Nozue et al. 2007). It is possible at many synchrotrons to measure both SAXS and WAXS simultaneously. The main difference between WAXS and XRD is angle dependence. Generally for WAXS, the material is randomly orientated, all angles are collected at once, and generally it is used to characterize non-crystalline or semi-crystalline materials (Nozue et al. 2007). XRD samples tend to be crystalline, and have angle dependence, where sample data are collected at different orientations. This leads to the ability to assess unit cells and crystal structure. For example, Marchesan group used single crystal XRD to confirm nanotube peptide formation from heterochiral and halogenated FF peptide analogues (Kralj et al. 2020), as well as tripeptides containing FF motifs (Garcia et al. 2021).

One advantage of WAXS over XRD is the ability to measure the sample in the solution state (Hiew et al. 2019), as samples must be dried for XRD. As discussed in previous sections, drying can affect the sample's self-assembled state (Hutchinson et al. 2019b; Griebenow and Klibanov 1995). Due to the atomic level detail of these techniques, it is possible to probe peptide secondary structure (Hiew et al. 2019; Sanii et al. 2014; Hamley et al. 2013; Khakshoor et al. 2010). It is also possible to collect WANS (wide angle neutron scattering) data (Loong et al. 2017), which is similar in concept to WAXS but with the principles discussed above in the SANS section applied.

8.6.4 Dynamic Light Scattering (DLS) and Zeta Potential

Dynamic light scattering (DLS) is a technique where laser light is shined onto a sample, and the light is scattered by particles that undergo Brownian motion. This is then detected in the direction of the scattering angle. The resultant spectrum contains relaxation time, which, in turn, provides insights into rotational, internal and translational motions of suspended molecules. This depends on the shape and size of the particles, as well as inter-particle interactions. There are many useful reviews on the theory of dynamic light scattering, for a more comprehensive theoretical understanding please see the referenced papers (Stetefeld et al. 2016; Rimai et al. 1970; Jamieson et al. 1972; Harvey 1973; Harding and Jumel 1998; Bloomfield 1981). Due to intrinsic algorithms approximating particles as spheres, it has been very useful in the study of proteins, nucleic acids and viruses, giving information on size and aggregation properties. DLS often requires minimal sample preparation, and large sample volumes which are normally dilute.

For peptide research, DLS has been used to observe the slow formation of peptide fibres over time (Aggeli et al. 2001). Peptide K24, which assembles into β-sheet tapes and further assembles into hydrogels was examined using FTIR, SAXS, Rheology and DLS (Aggeli et al. 2001). Through studying several concentrations over time, DLS confirmed that the tapes behave as semi-flexible elongated chains, of a persistent length (Aggeli et al. 2001). Other applications include studying peptide complexes (Papish et al. 2002) and peptide aggregation (Hawe et al. 2011; Thunecke et al. 1998).

Zeta potential is a technique that measures the magnitude of either charge or electrostatic interactions between particles that repulse/attract each other. These interactions are important to determine causes of self-assembly, dispersion or flocculation, which can lead to the design of improved mixed nanomaterial solutions. In peptide research zeta potential has been used to confirm the charge of peptide sequences alongside titration (Hutchinson et al. 2018), examine the effects of different solution environments on peptide charge state to explain secondary structure changes (He et al. 2021), and examine interactions of peptides with other molecules, for example membrane models (Bogdanova et al. 2020), or nano-fillers, such as 2D materials (Wychowaniec et al. 2018).

8.7 Rheology: Characterization of Viscoelasticity and Printability

Rheology studies flow behaviour of materials, spanning through liquids and viscoelastic solids, including many peptide-based nanomaterials and biomaterials. Various rheological setups can be used with varying geometries, including plate-plate, cone-plate and various coaxial cylindrical or double gaps (Macosko 1994). Each

type of geometry provides unique capabilities for studying rheological phenomena and properties and structures of materials undergoing flow.

Plate-plate geometries are most often used for hydrogels and soft solids in *oscillatory* mode, to study materials' deformation and stiffness. Most common oscillatory rheological tests include amplitude sweep (that defines materials' so-called linear viscoelastic region LVR), and frequency sweep. In those tests, the storage shear moduli (G′) and loss shear moduli (G″) are measured as a function of strain, or frequency, respectively. If storage modulus is larger than loss modulus, then the material is typically said to be a soft hydrogel, noting that magnitude of that ratio (known as tanδ), defines the degree of a solid-like structure. These types of rheological tests accompany all frequently formed peptide-based hydrogels and are the first line of study of their physical properties (Yan and Pochan 2010). For example, oscillatory rheology was used on hydrogels formed from self-assembling FEFKFEFK (F8) and KFEFKFEFKK (KF8K) peptides at 26.8 mM concentration (Fig. 8.16) (Wychowaniec et al. 2020a). Figure 8.16a represents a typical amplitude sweep for the two studied peptides, F8 and KF8K. As can be seen, linear storage
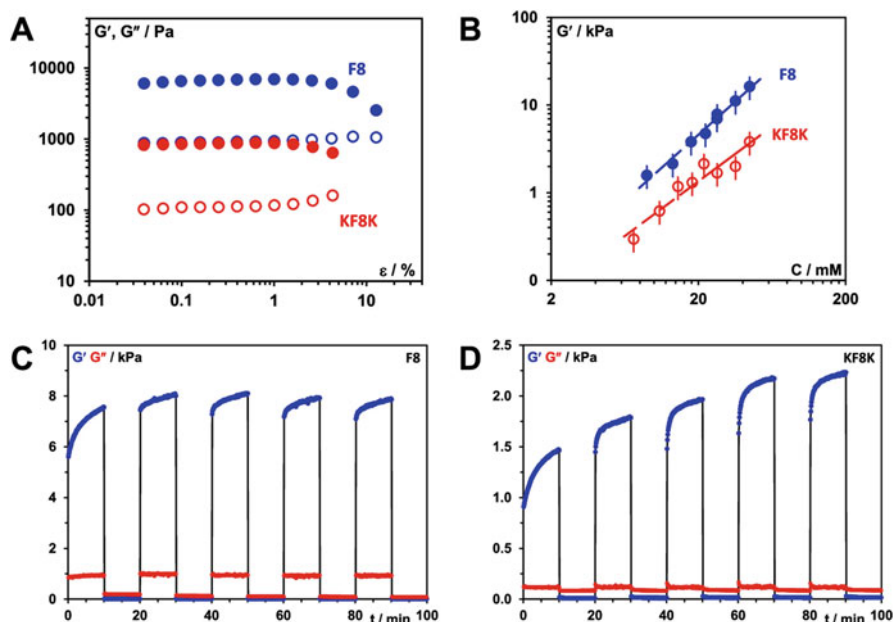
Fig. 8.16 (**a**) Storage (G′—closed symbols) and loss (G″—open symbols) shear moduli vs strain (ε) curves were obtained at 1 Hz frequency for F8 and KF8K hydrogels prepared at 26.8 mM concentration. (**b**) Storage modulus (G′) vs. peptide concentration (**c**) plots were obtained for F8 and KF8K hydrogels measured at 0.2% strain and 1 Hz frequency. (**c**, **d**) Shear thinning and recovery behaviour of F8 and KF8K hydrogels prepared at 26.8 mM peptide concentration. Experiments were performed at 1 Hz and shear strain of 0.2 and 100% were applied alternatingly in 10 min intervals. Reproduced under a Creative Commons Attribution (CC-BY) from (Wychowaniec et al. 2020a)

modulus and loss modulus are recorded until a breaking point, thereby defining clear viscoelastic region at strain values lower than $\varepsilon \approx 2\%$ and $\varepsilon \approx 1\%$, for F8 and KF8K, respectively. On the other hand, frequency sweeps are commonly used to look at the type of materials behaviour (Newtonian vs. non-Newtonian), but also to allow comparison of stiffness of materials, for hydrogels defined as the storage modulus value at 1 Hz measured in the LVR strain range. This can be done for example as a function of peptide concentration (Fig. 8.16b).

Multiple theories linking structures of polymeric-based materials to the rheological properties were developed. In particular, Guenet has provided a comprehensive description of polymer-based materials and their rheological behaviour, and pointed out at the possibility of using rheology as a means to study types of topology from materials (Guenet 2000, 2016). For example, one of the used theories described by Guenet is that of Marques and Jones, who linked rheological storage modulus as a function of concentration to the types of networks (Wychowaniec et al. 2020a; Gao et al. 2017; Guenet 2000). Two types of elastic networks can form, those related to enthalpic elasticity, or those based on entropic elasticity. The derived expressions are:

1. For enthalpic elasticity dominated networks:

$$G' \propto C^{\frac{(3+D_f)}{(3-D_f)}} \tag{8.11}$$

2. For entropic elasticity dominated networks:

$$G' \propto C^{\frac{3}{(3-D_f)}} \tag{8.12}$$

where D_f is the fractal dimension of the fibre long axis and is defined as: $= L^{\frac{1}{D_f}}$, where S is the end-to-end distance of the fibre and L is its contour length. For rigid straight fibrer, $D_f = 1$, leading to power laws of 2 and 1.5 for enthalpic and entropic elasticity dominated networks, respectively. Therefore, rheological measurements as a function of concentration may indirectly give insights into types of networks forming from peptides, and whether the self-assembled peptide fibres are of rigid, semi-flexible, or fully flexible nature.

Recently, peptide-based hydrogels have been used as inks for extrusion-based 3D printing (Raphael et al. 2017; Chiesa et al. 2020). Due to the large interest in using hydrogels as next-generation bio-inks for 3D printing cell scaffolding and organ printing (He et al. 2016), multiple research groups recently attempted to summarize required physical and chemical factors affecting inks during printing (Schwab et al. 2020; Paxton et al. 2017; Lee et al. 2020; Gillispie et al. 2020). To achieve the best performance and quality of printed scaffolds, viscoelastic properties, namely rheological characteristics must be matched. These include shear thinning, i.e. reduction of viscosity upon increased shear rate, and shear-recovery, i.e. ability to self-heal/return to an original state of high fidelity (Schwab et al. 2020; Paxton et al. 2017).

Figure 8.16c–d represents exemplar use of oscillatory rheology for assessing shear thinning and shear recovery of F8 and KF8K hydrogels, that under increased strain of $\varepsilon = 100\%$ turned to liquid (were shear thinning, mimicking 3D printing procedure) and recovered upon restoration of low strain value of $\varepsilon = 0.2\%$. As can be seen, different types of materials exhibit different recovery rates, which is related to their molecular structure, type of network topology and cross-links (Yan et al. 2010).

Another option for assessing printability of peptide-based hydrogels and materials is using cone-plate geometry in rotational mode and probe viscosity as a function of shear rate. This method would require viscosity of peptide-based materials to be above a certain threshold, allowing the torque measurements on the rheometer to be accurate. If viscosity is below the threshold, double gap cylindrical geometry should be used, which allows measurements of viscosities as low as water. For example, Ruter and co-workers measured shear flow curves for the set of hydrogels made of short rigid rod-like peptides A_8K and $A_{10}K$ (where subscript defines number of A residues), and obtained the perfect shear-thinning system with $\eta = \dot{\gamma}^{-1}$ over the whole range of shear rates investigated (Rüter et al. 2020). In those tests, slope of the shear thinning can be used to define the flow behaviour of materials. In fact, multiple rheological models and parameters can be used to describe such flows, but for comprehensive discussions we refer users to the rheological textbooks (Macosko 1994).

Finally, we note that rheological measurements need to be performed and interpreted with care due to the possibility of multiple errors coming into play. Sathaye et al. pointed out at the possibility of hydrogel fracture using combined rheology with confocal microscopy (Sathaye et al. 2015). Various processes can mask the real rheological processes and combinatorial techniques may be required to unravel those, such as previously described rheo-SIPLI (Wychowaniec et al. 2020a). Another issue is probing rheological properties of consistently more complex structures, including 3D printed multi-layered structures. Fuentes-Caparrós et al. recently tackled this issue by comparing plate-plate rheology to vane-type rheology on 3D printed hydrogels with different layers (Fuentes-Caparrós et al. 2021). In particular, they point out to the fact that rheological properties of hydrogels vary after printing, and vane geometry allows probing those changes, based on an exemplar set of Fmoc-FF gels.

8.8 Conclusions

In Table 8.6, we present a summary of the discussed techniques and their main uses for peptide-based nanomaterials and thereof made macrostructures and hydrogels. The derived table can serve as a guide for starting to look for available methods to characterize peptide-based nanomaterials. Multiple methods were discussed, spanning from quality control, via molecular structures and imaging, up to functional properties. We note that whilst we discussed the most common techniques and some of their arising combinations, the field of methodology and analytical methods is

Table 8.6 Summary of discussed characterization methods and their main utilization for peptide-based nanomaterials and thereof made structures

(1) Quality control

Method	Mass spec	HPLC
Use	Peptide molecular weight; confirms structure	Peptide purity; measures degradation or formation of peptide-based materials

(2) Spectroscopy

Method	FTIR	Raman spectroscopy	CD dichroism	LD dichroism	NMR spectroscopy	Fluorescence
Use	Molecular vibrations, secondary structures, confirms chemical reactions, and can be measured as a function of temp, time, or additives	Molecular vibrations, secondary structures, confirms chemical reactions, can be measured as a function of temp, time, or additives	Secondary structures, can be measured as a function of temp, time, or additives	Linearly aligned strictures, can be measured as a function of temp, time, or additives	Molecular structure, confirms chemical reactions, diffusion coefficients, can be measured as a function of temp, time, or additives. Can measure secondary structure through J-coupling/TOCSEY and tertiary structure through NOSEY/COSEY	Confirms aggregation concentration of peptides and formation of particular secondary structures

(3) Microscopy

Method	SEM/Cryo-SEM	TEM/Cryo-TEM	AFM	Polarized light microscopy
Use	Can visualize structures larger than 30 nm, used for visualizing pores/larger structures/surfaces of peptide nanomaterials	Can visualize nanostructures	Can visualize nanostructures and measure nanomechanical (elastic), magnetic, electric, piezoelectric properties on nanoscale	Can visualize alignment and liquid crystal phases

(4) Scattering

Method	SANS	SAXS	XRD/ WAXS	DLS	Zeta potential
Use	Can measure low-resolution 3D structures, and contrast match out specific components in solution with correct buffer matching conditions	Can measure low-resolution shapes of 3D structures	Can measure high-resolution nm length distances to obtain unit cell data/confirm secondary structure information	Can be used to obtain size of molecules and observe aggregation over time	Can be used to examine repulsion/attraction of molecules which can explain self-assembly

(5) Bulk-structure characterization

Method	Oscillatory rheology	Rotational rheology
Use	Can measure storage and loss modulus as a function of strain and frequency; used to define LVR and stiffness. Allows indirect information about topology of formed networks. Can measure recovery	Allows measurements of shear thinning (flow curve) and recovery. Measures viscosity and allows understanding properties of materials for printability

constantly evolving. We expect enormous growth in the field where machine learning and artificial intelligence can contribute, particularly in improving analytical algorithms leading to more accurate measurements and approximations of true systems. The representative studies collect the major possibilities of discussed methods and may be used as a guide towards those who begin to design and characterize peptide-based nanomaterials.

Notes The authors declare no competing financial interest.

References

Abbassi F et al (2008) Solution structure and model membrane interactions of Temporins-SH, antimicrobial peptides from amphibian skin. A NMR spectroscopy and differential scanning calorimetry study. Biochemistry 47:10513–10525

Adamcik J, Mezzenga R (2012) Study of amyloid fibrils via atomic force microscopy. Curr Opin Colloid Interface Sci 17:369–376

Adamcik J et al (2010) Understanding amyloid aggregation by statistical analysis of atomic force microscopy images. Nat Nanotechnol 5:423–428

Aggeli A et al (2001) Structure and dynamics of self-assembling β-sheet peptide tapes by dynamic light scattering. Biomacromolecules 2:378–388

Aggeli A, Bell M, Boden N, Carrick LM, Strong AE (2003) Self-assembling peptide polyelectrolyte beta-sheet complexes form nematic hydrogels. Angew Chem Int Ed 42:5603–5606

Alessandrini A, Facci P (2005) AFM: a versatile tool in biophysics. Meas Sci Technol 16:R65–R92

Alyousef AA et al (2019) Screening & analysis of anionic peptides from Foeniculum vulgare Mill by mass spectroscopy. Saudi J Biol Sci 26:660–664

Amblard M, Fehrentz JA, Martinez J, Subra G (2006) Methods and protocols of modern solid phase peptide synthesis. Mol Biotechnol 33:239–254

Anderson JM, Andukuri A, Lim DJ, Jun H-W (2009) Modulating the gelation properties of self-assembling peptide amphiphiles. ACS Nano 3:3447–3454

Andrushchenko VV, Vogel HJ, Prenner EJ (2007a) Optimization of the hydrochloric acid concentration used for trifluoroacetate removal from synthetic peptides. J Pept Sci 13:37–43

Andrushchenko VV, Vogel HJ, Prenner EJ (2007b) Interactions of tryptophan-rich cathelicidin antimicrobial peptides with model membranes studied by differential scanning calorimetry. Biochim Biophys Acta (BBA) - Biomem 1768:2447–2458

Anitas EM (2018) Small-angle scattering from mass and surface fractals. In: Complexity in biological and physical systems-bifurcations, solitons and fractals, pp 169–189

Anthony NR, Berland KM, Mehta AK, Lynn DG, Seth Childers W (2014) In: Uversky VN, Lyubchenko YL (eds) Bio-nanoimaging. Academic Press, pp 27–36

Arad E, Green H, Jelinek R, Rapaport H (2020) Revisiting thioflavin T (ThT) fluorescence as a marker of protein fibrillation – the prominent role of electrostatic interactions. J Colloid Interface Sci 573:87–95

Barrett GC (1985) Chemistry and biochemistry of the amino acids. Chapman and Hall

Barron LD, Buckingham AD (1971) Rayleigh and Raman scattering from optically active molecules. Mol Phys 20:1111–1119

Bartels C (1990) Fast algorithm for peptide sequencing by mass spectroscopy. Biomed Environ Mass Spectrom 19:363–368

Barth A (2000) The infrared absorption of amino acid side chains. Progress Biophys Mol Biol 74: 141–173

Barth A (2007) Infrared spectroscopy of proteins. Biochim Biophys Acta, Rev Bioenerg 1767: 1073–1101

Barth A, Zscherp C (2002) What vibrations tell us about proteins. Q Rev Biophys 35:369–430

Bdikin I et al (2012) Polarization switching and patterning in self-assembled peptide tubular structures. J Appl Phys 111:074104

Bechinger B (1999) The structure, dynamics and orientation of antimicrobial peptides in membranes by multidimensional solid-state NMR spectroscopy. Biochim Biophys Acta (BBA) - Biomem 1462:157–183

Bechinger B, Salnikov ES (2012) The membrane interactions of antimicrobial peptides revealed by solid-state NMR spectroscopy. Chem Phys Lipids 165:282–301

Benaglia S, Amo CA, Garcia R (2019) Fast, quantitative and high resolution mapping of viscoelastic properties with bimodal AFM. Nanoscale 11:15289–15297

Berillo D, Mattiasson B, Galaev IY, Kirsebom H (2012) Formation of macroporous self-assembled hydrogels through cryogelation of Fmoc–Phe–Phe. J Colloid Interface Sci 368:226–230

Beychok S (1966) Circular dichroism of biological macromolecules. Science 154:1288

Biancalana M, Koide S (2010) Molecular mechanism of Thioflavin-T binding to amyloid fibrils. Biochim Biophys Acta (BBA) - Proteins Proteom 1804:1405–1412

Birchall AC, Bush SM, North M (2001) Copolymerization of peptide derived monomers and methyl methacrylate. Polymer 42:375–389

Blanchet CE, Svergun DI (2013) Small-angle X-ray scattering on biological macromolecules and nanocomposites in solution. Annu Rev Phys Chem 64:37–54

Bloomfield VA (1981) Quasi-elastic light scattering applications in biochemistry and biology. Annu Rev Biophys Bioeng 10:421–450

Böcker U et al (2007) Revealing covariance structures in Fourier transform infrared and Raman microspectroscopy spectra: a study on pork muscle fiber tissue subjected to different processing parameters. Appl Spectrosc 61:1032–1039

Boelens R, Koning TMG, van der Marel GA, van Boom JH, Kaptein R (1989) Iterative procedure for structure determination from proton-proton NOEs using a full relaxation matrix approach. Application to a DNA octamer. J Magn Reson 1969(82):290–308

Bogdanova LR, Valiullina YA, Faizullin DA, Kurbanov RK, Ermakova EA (2020) Spectroscopic, zeta potential and molecular dynamics studies of the interaction of antimicrobial peptides with model bacterial membrane. Spectrochim Acta A Mol Biomol Spectrosc 242:118785

Boothroyd S, Miller AF, Saiani A (2013) From fibres to networks using self-assembling peptides. Faraday Discuss 166:195–207

Boryskina OP, Bolbukh TV, Semenov MA, Gasan AI, Maleev VY (2007) Energies of peptide–peptide and peptide–water hydrogen bonds in collagen: evidences from infrared spectroscopy, quartz piezogravimetry and differential scanning calorimetry. J Mol Struct 827:1–10

Branco MC, Nettesheim F, Pochan DJ, Schneider JP, Wagner NJ (2009) Fast dynamics of semiflexible chain networks of self-assembled peptides. Biomacromolecules 10:1374–1380

Bressler I, Kohlbrecher J, Thunemann AF (2015) SASfit: a tool for small-angle scattering data analysis using a library of analytical expressions. J Appl Crystallogr 48:1587–1598

Buffy JJ, Waring AJ, Hong M (2005) Determination of peptide oligomerization in lipid bilayers using 19F spin diffusion NMR. J Am Chem Soc 127:4477–4483

Burgess KA et al (2018) RNA extraction from self-assembling peptide hydrogels to allow qPCR analysis of encapsulated cells. PLoS One 13:e0197517

Burghardt WR, Ugaz VM, Cinader DK (1999) In: Scattering from polymers. ACS Symposium Series Ch. 24. American Chemical Society, vol 739, pp 374–389

Bystrov VS et al (2012) In: Ciofani G, Menciassi A (eds) Piezoelectric nanomaterials for biomedical applications. Springer, Berlin, pp 187–211

Caplan MR, Moore PN, Zhang SG, Kamm RD, Lauffenburger DA (2000) Self-assembly of a beta-sheet protein governed by relief of electrostatic repulsion relative to van der Waals attraction. Biomacromolecules 1:627–631

Castelletto V et al (2017) Self-assembly and anti-amyloid cytotoxicity activity of amyloid beta peptide derivatives. Sci Rep 7:43637

Castelletto V et al (2019a) Self-assembly, tunable hydrogel properties, and selective anti-cancer activity of a carnosine-derived lipidated peptide. ACS Appl Mater Interfaces 11:33573–33580

Castelletto V et al (2019b) Peptide-stabilized emulsions and gels from an arginine-rich surfactant-like peptide with antimicrobial activity. ACS Appl Mater Interfaces 11:9893–9903

Cenker ÇÇ, Bucak S, Olsson U (2011) Nanotubes and bilayers in a model peptide system. Soft Matter 7:4868–4875

Chawla K, Yu TB, Liao SW, Guan Z (2011) Biodegradable and biocompatible synthetic saccharide−peptide hydrogels for three-dimensional stem cell culture. Biomacromolecules 12:560–567

Chen R et al (1995) Trapping, detection, and mass determination of coliphage T4 DNA ions by electrospray ionization Fourier transform ion cyclotron resonance mass spectrometry. Anal Chem 67:1159–1163

Cherny AY, Anitas EM, Osipov VA, Kuklin AI (2019) The structure of deterministic mass and surface fractals: theory and methods of analyzing small-angle scattering data. Phys Chem Chem Phys 21:12748–12762

Chiesa I et al (2020) Modeling the three-dimensional bioprinting process of β-sheet self-assembling peptide hydrogel scaffolds. Front Med Technol 2:4

Childers WS, Mehta AK, Ni R, Taylor JV, Lynn DG (2010) Peptides organized as bilayer membranes. Angew Chem Int Ed 49:4104–4107

Chirgadze YN, Fedorov OV, Trushina NP (1975) Estimation of amino acid residue side-chain absorption in the infrared spectra of protein solutions in heavy water. Biopolymers 14:679–694

Chou PY, Fasman GD (1974) Prediction of protein conformation. Biochemistry 13:222–245

Christoff-Tempesta T et al (2021) Self-assembly of aramid amphiphiles into ultra-stable nanoribbons and aligned nanoribbon threads. Nat Nanotechnol 16:447–454

Cinader DK, Burghardt WR (1998) Mixed orientation state induced by expansion flow of a thermotropic liquid-crystalline polymer. Macromolecules 31:9099–9102

Coon JJ, Syka JEP, Shabanowitz J, Hunt DF (2005) Tandem mass spectrometry for peptide and protein sequence analysis. BioTechniques 38:519–523

Cornish J et al (1999) Trifluoroacetate, a contaminant in purified proteins, inhibits proliferation of osteoblasts and chondrocytes. Am J Physiol-Endocrinol Metab 277:E779–E783

Cowieson NP et al (2020) Beamline B21: high-throughput small-angle X-ray scattering at diamond light source. J Synchrotron Radiat 27:1438–1446

De Carlo S, Harris JR (2011) Negative staining and cryo-negative staining of macromolecules and viruses for TEM. Micron 42:117–131

Dempsey CE (2001) Hydrogen exchange in peptides and proteins using NMR spectroscopy. Prog Nucl Magn Reson Spectrosc 39:135–170

Ding Y, Li Y, Qin M, Cao Y, Wang W (2013) Photo-cross-linking approach to engineering small tyrosine-containing peptide hydrogels with enhanced mechanical stability. Langmuir 29:13299–13306

Dokukin ME, Sokolov I (2012) Quantitative mapping of the elastic modulus of soft materials with HarmoniX and PeakForce QNM AFM modes. Langmuir 28:16060–16071

Dołowy M, Pyka A (2014) Application of TLC, HPLC and GC methods to the study of amino acid and peptide enantiomers: a review. Biomed Chromatogr 28:84–101

Domingues TM, Perez KR, Riske KA (2020) Revealing the mode of action of halictine antimicrobial peptides: a comprehensive study with model membranes. Langmuir 36:5145–5155

Dong M et al (2008) AFM-based force spectroscopy measurements of mature amyloid fibrils of the peptide glucagon. Nanotechnology 19:384013

Draper ER et al (2020) Using small-angle scattering and contrast matching to understand molecular packing in low molecular weight gels. Matter 2:764–778

Dudás EF, Bodor A (2019) Quantitative, diffusion NMR based analytical tool to distinguish folded, disordered, and denatured biomolecules. Anal Chem 91:4929–4933

Dufrêne YF et al (2017) Imaging modes of atomic force microscopy for application in molecular and cell biology. Nat Nanotechnol 12:295–307

Edwards-Gayle CJC et al (2019) Self-assembly, antimicrobial activity, and membrane interactions of arginine-capped peptide bola-amphiphiles. ACS Appl Bio Mater 2:2208–2218

Edwards-Gayle CJC et al (2020) Selective antibacterial activity and lipid membrane interactions of arginine-rich amphiphilic peptides. ACS Appl Bio Mater 3:1165–1175

Efimov AE, Tonevitsky AG, Dittrich M, Matsko NB (2007) Atomic force microscope (AFM) combined with the ultramicrotome: a novel device for the serial section tomography and AFM/TEM complementary structural analysis of biological and polymer samples. J Microsc 226:207–216

Elsawy MA, Hewage C, Walker B (2012) Racemisation of N-Fmoc phenylglycine under mild microwave-SPPS and conventional stepwise SPPS conditions: attempts to develop strategies for overcoming this. J Pept Sci 18:302–311

Elsawy MA, Martin L, Tikhonova IG, Walker B (2013) Solid phase synthesis of Smac/DIABLO-derived peptides using a 'safety-catch' resin: identification of potent XIAP BIR3 antagonists. Bioorg Med Chem 21:5004–5011

Elsawy MA et al (2016) Modification of beta-sheet forming peptide hydrophobic face: effect on self-assembly and gelation. Langmuir 32:4917–4923

Fichman G, Schneider JP (2021) Dopamine self-polymerization as a simple and powerful tool to modulate the viscoelastic mechanical properties of peptide-based gels. Molecules (Basel, Switzerland) 26:1363

Fuentes-Caparrós AM et al (2021) Mechanical characterization of multilayered hydrogels: a rheological study for 3D-printed systems. Biomacromolecules 22:1625–1638

Gao J, Tang C, Smith AM, Miller AF, Saiani A (2017) Controlling self-assembling peptide hydrogel properties through network topology. Biomacromolecules 18(3):826–834

Garcia R, Herruzo ET (2012) The emergence of multifrequency force microscopy. Nat Nanotechnol 7:217–226

Garcia AM et al (2021) Nanoscale assembly of functional peptides with divergent programming elements. ACS Nano 15:3015–3025

Geiser L, Eeltink S, Svec F, Fréchet JMJ (2008) In-line system containing porous polymer mono-liths for protein digestion with immobilized pepsin, peptide preconcentration and nano-liquid chromatography separation coupled to electrospray ionization mass spectroscopy. J Chromatogr A 1188:88–96

Gelain F et al (2012) New bioactive motifs and their use in functionalized self-assembling peptides for NSC differentiation and neural tissue engineering. Nanoscale 4:2946–2957

Germann MW, Turner T, Allison SA (2007) Translational diffusion constants of the amino acids: measurement by NMR and their use in modeling the transport of peptides. Chem A Eur J 111:1452–1455

Gillispie G et al (2020) Assessment methodologies for extrusion-based bioink printability. Biofabrication 12:022003

Glish GL, Vachet RW (2003) The basics of mass spectrometry in the twenty-first century. Nat Rev Drug Discov 2:140–150

Goktas M et al (2015) Self-assembled peptide amphiphile nanofibers and PEG composite hydrogels as tunable ECM mimetic microenvironment. Biomacromolecules 16:1247–1258

Golunova A et al (2021) Direct and indirect biomimetic peptide modification of alginate: efficiency, side reactions, and cell response. Int J Mol Sci 22

Graewert MA, Svergun DI (2013) Impact and progress in small and wide angle X-ray scattering (SAXS and WAXS). Curr Opin Struct Biol 23:748–754

Graham L, Orenstein JM (2007) Processing tissue and cells for transmission electron microscopy in diagnostic pathology and research. Nat Protoc 2:2439–2450

Gras SL et al (2008) Functionalised amyloid fibrils for roles in cell adhesion. Biomaterials 29:1553–1562

Graziano G, Catanzano F, Giancola C, Barone G (1996) DSC study of the thermal stability of S-protein and S-peptide/S-protein complexes. Biochemistry 35:13386–13392

Greenfield NJ (2006) Using circular dichroism spectra to estimate protein secondary structure. Nat Protoc 1:2876–2890

Greenfield NJ, Fasman GD (1969) Computed circular dichroism spectra for the evaluation of protein conformation. Biochemistry 8:4108–4116

Griebenow K, Klibanov AM (1995) Lyophilization-induced reversible changes in the secondary structure of proteins. Proc Natl Acad Sci 92:10969

Grimsley GR, Scholtz JM, Pace CN (2009) A summary of the measured pK values of the ionizable groups in folded proteins. Protein Sci 18:247–251

Guenet JM (2000) Structure versus rheological properties in fibrillar thermoreversible gels from polymers and biopolymers. J Rheol 44:947–960

Guenet J-M (2016) Organogels: thermodynamics, structure, solvent role, and properties

Guilbaud J-B, Saiani A (2011) Using small angle scattering (SAS) to structurally characterise peptide and protein self-assembled materials. Chem Soc Rev 40:1200–1210

Guilbaud JB, Rochas C, Miller AF, Saiani A (2013) Effect of enzyme concentration of the morphology and properties of enzymatically triggered peptide hydrogels. Biomacromolecules 14:1403–1411

Guo S, Akhremitchev BB (2006) Packing density and structural heterogeneity of insulin amyloid fibrils measured by AFM nanoindentation. Biomacromolecules 7:1630–1636

Halligan BD, Ruotti V, Twigger SN, Greene AS (2005) DeNovoID: a web-based tool for identifying peptides from sequence and mass tags deduced from de novo peptide sequencing by mass spectroscopy. Nucleic Acids Res 33:W376–W381

Hamley IW (2008) Form factor of helical ribbons. Macromolecules 41:8948–8950

Hamley IW, Castelletto V (2021) In: Peptide-based biomaterials. The Royal Society of Chemistry, pp 19–46

Hamley IW et al (2013) Self-assembly of a model amphiphilic oligopeptide incorporating an arginine headgroup. Soft Matter 9:4794–4801

Hamley IW et al (2016) Nanosheet formation by an anionic surfactant-like peptide and modulation of self-assembly through ionic complexation. Langmuir 32:10387–10393

Hamley IW et al (2017) Shear alignment of bola-amphiphilic arginine-coated peptide nanotubes. Biomacromolecules 18:141–149

Harding SE, Jumel K (1998) Light scattering. Curr Protoc Protein Sci 11:7.8.1–7.8.14

Harvey JD (1973) Diffusion coefficients and hydrodynamic radii of three spherical RNA viruses by laser light scattering. Virology 56:365–368

Hawe A, Hulse WL, Jiskoot W, Forbes RT (2011) Taylor dispersion analysis compared to dynamic light scattering for the size analysis of therapeutic peptides and proteins and their aggregates. Pharm Res 28:2302–2310

He Y et al (2016) Research on the printability of hydrogels in 3D bioprinting. Sci Rep 6:29977

He L, Ying L, Jingting X, Chen C, Shuntang G (2021) Changes in the secondary structures and zeta potential of soybean peptide and its calcium complexes in different solution environments. Food Funct 12:5967–5974

Hecht L, Laurence DB, Blanch EW, Bell AF, Day LA (1999) Raman optical activity instrument for studies of biopolymer structure and dynamics. J Raman Spectrosc 30:815–825

Hernández B, Pflüger F, Kruglik SG, Ghomi M (2013) Characteristic Raman lines of phenylalanine analyzed by a multiconformational approach. J Raman Spectrosc 44:827–833

Heu R, Shahbazmohamadi S, Yorston J, Capeder P (2019) Target material selection for sputter coating of SEM samples. Microscopy Today 27:32–36

Hicks MR, Kowałski J, Rodger A (2010) LD spectroscopy of natural and synthetic biomaterials. Chem Soc Rev 39:3380–3393

Hiew SH et al (2019) A short peptide hydrogel with high stiffness induced by 310-helices to β-sheet transition in water. Adv Sci 6:1901173

Holzwarth G, Doty P (1965) The ultraviolet circular dichroism of polypeptides1. J Am Chem Soc 87:218–228

Howard MJ (1998) Protein NMR spectroscopy. Curr Biol 8:R331–R333

Hunt DF, Yates JR, Shabanowitz J, Winston S, Hauer CR (1986) Protein sequencing by tandem mass spectrometry. Proc Natl Acad Sci 83:6233

Hutchinson JA et al (2018) The effect of lipidation on the self-assembly of the gut-derived peptide hormone PYY3–36. Bioconjug Chem 29:2296–2308

Hutchinson JA et al (2019a) Melanin production by tyrosinase activity on a tyrosine-rich peptide fragment and pH-dependent self-assembly of its lipidated analogue. Org Biomol Chem 17: 4543–4553

Hutchinson JA et al (2019b) Self-assembly of lipopeptides containing short peptide fragments derived from the gastrointestinal hormone PYY3–36: from micelles to amyloid fibrils. J Phys Chem B 123:614–621

Jacrot B (1976) The study of biological structures by neutron scattering from solution. Rep Prog Phys 39:911–953

Jalili N, Laxminarayana K (2004) A review of atomic force microscopy imaging systems: application to molecular metrology and biological sciences. Mechatronics 14:907–945

Jamieson AM, Downs CE, Walton AG (1972) Studies of elastin coacervation by quasielastic light scattering. Biochim Biophys Acta (BBA) – Protein Struct 271:34–47

Jurado R et al (2021) Understanding the formation of apoferritin amyloid fibrils. Biomacromolecules 22(5):2057–2066

Kabiri M, Unsworth LD (2014) Application of isothermal titration calorimetry for characterizing thermodynamic parameters of biomolecular interactions: peptide self-assembly and protein adsorption case studies. Biomacromolecules 15:3463–3473

Keiderling TA (2020) Structure of condensed phase peptides: insights from vibrational circular dichroism and Raman optical activity techniques. Chem Rev 120:3381–3419

Khakshoor O et al (2010) X-ray crystallographic structure of an artificial β-sheet dimer. J Am Chem Soc 132:11622–11628

Kholkin A, Amdursky N, Bdikin I, Gazit E, Rosenman G (2010) Strong piezoelectricity in bioinspired peptide nanotubes. ACS Nano 4:610–614

Klajnert B, Janiszewska J, Urbanczyk-Lipkowska Z, Bryszewska M, Epand RM (2006a) DSC studies on interactions between low molecular mass peptide dendrimers and model lipid membranes. Int J Pharm 327:145–152

Klajnert B, Cladera J, Bryszewska M (2006b) Molecular interactions of dendrimers with amyloid peptides: pH dependence. Biomacromolecules 7:2186–2191

Kol N et al (2005) Self-assembled peptide nanotubes are uniquely rigid bioinspired supramolecular structures. Nano Lett 5:1343–1346

Konarev PV, Petoukhov MV, Volkov VV, Svergun DI (2006) ATSAS 2.1, a program package for small-angle scattering data analysis. J Appl Crystallogr 39:277–286

Kong J, Yu S (2007) Fourier transform infrared spectroscopic analysis of protein secondary structures. Acta Biochim Biophys Sin 39:549–559

Kralj S et al (2020) Heterochirality and halogenation control Phe-Phe hierarchical assembly. ACS Nano 14:16951–16961

Krysmann MJ et al (2008) Self-assembly of peptide nanotubes in an organic solvent. Langmuir 24: 8158–8162

Kwon G et al (1993) Micelles based on AB block copolymers of poly(ethylene oxide) and poly(. beta.-benzyl L-aspartate). Langmuir 9:945–949

La Guinier A (1939) Diffraction des rayons X aux très petits angles: application à l'étude de phénomènes ultramicroscopiques. Ann Phys 11:161–237

Laws DD et al (2001) Solid-state NMR studies of the secondary structure of a mutant prion protein fragment of 55 residues that induces neurodegeneration. Proc Natl Acad Sci 98:11686

Lay JO Jr (2001) MALDI-TOF mass spectrometry of bacteria*. Mass Spectrom Rev 20:172–194

Lee SC, Gillispie G, Prim P, Lee SJ (2020) Physical and chemical factors influencing the printability of hydrogel-based extrusion bioinks. Chem Rev 120:10834–10886

Li H, Hu D, Liang F, Huang X, Zhu Q (2020) Influence factors on the critical micelle concentration determination using pyrene as a probe and a simple method of preparing samples. R Soc Open Sci 7:192092

Liao H-S et al (2016) Self-assembly mechanisms of nanofibers from peptide amphiphiles in solution and on substrate surfaces. Nanoscale 8:14814–14820

Ligorio C et al (2019) Graphene oxide containing self-assembling peptide hybrid hydrogels as a potential 3D injectable cell delivery platform for intervertebral disc repair applications. Acta Biomater 92:92–103

Ligorio C et al (2021) TGF-β3-loaded graphene oxide - self-assembling peptide hybrid hydrogels as functional 3D scaffolds for the regeneration of the nucleus pulposus. Acta Biomater 127:116–130

Lindgren M, Sörgjerd K, Hammarström P (2005) Detection and characterization of aggregates, prefibrillar amyloidogenic oligomers, and protofibrils using fluorescence spectroscopy. Biophys J 88:4200–4212

Loong CK, Scherillo A, Festa G (2017) In: Kardjilov N, Festa G (eds) Neutron methods for archaeology and cultural heritage. Springer International Publishing, pp 183–207

Lu K et al (2007) Macroscale assembly of peptide nanotubes. Chem Commun 2729–2731

Macosko CW (1994) Rheology: principles, measurements, and applications

Malanovic N, Lohner K (2016) Gram-positive bacterial cell envelopes: the impact on the activity of antimicrobial peptides. Biochim Biophys Acta (BBA) - Biomem 1858:936–946

Mammadov R, Tekinay AB, Dana A, Guler MO (2012) Microscopic characterization of peptide nanostructures. Micron 43:69–84

Mandal D, Nasrolahi Shirazi A, Parang K (2014) Self-assembly of peptides to nanostructures. Org Biomol Chem 12:3544–3561

Maslovskis A, Tirelli N, Saiani A, Miller AF (2011) Peptide-PNIPAAm conjugate based hydrogels: synthesis and characterisation. Soft Matter 7:6025–6033

Mehta AK et al (2008) Facial symmetry in protein self-assembly. J Am Chem Soc 130:9829–9835

Merg AD et al (2019) 2D crystal engineering of nanosheets assembled from helical peptide building blocks. Angew Chem Int Ed 58:13507–13512

Miravet JF et al (2013) Self-assembly of a peptide amphiphile: transition from nanotape fibrils to micelles. Soft Matter 9:3558–3564

Mykhaylyk OO (2010) Time-resolved polarized light imaging of sheared materials: application to polymer crystallization. Soft Matter 6:4430–4440

Mykhaylyk OO, Parnell AJ, Pryke A, Fairclough JPA (2012) Direct imaging of the orientational dynamics of block copolymer lamellar phase subjected to shear flow. Macromolecules 45:5260–5272

Mykhaylyk OO, Warren NJ, Parnell AJ, Pfeifer G, Laeuger J (2016) Applications of shear-induced polarized light imaging (SIPLI) technique for mechano-optical rheology of polymers and soft matter materials. J Polym Sci Part B-Polym Phys 54:2151–2170

Nakamura S, Kidokoro S-I (2004) Isothermal acid-titration calorimetry for evaluating the pH dependence of protein stability. Biophys Chem 109:229–249

Narayanan T, Rüter A, Olsson U (2021) SAXS/WAXS investigation of amyloid-β(16-22) peptide nanotubes. Front Bioeng Biotechnol 9:199

Nelson DL, Lehninger AL, Cox MM (2017) Lehninger principles of biochemistry, 7th edn, Basingstoke

Nguyen V, Jenkins K, Yang R (2015) Epitaxial growth of vertically aligned piezoelectric diphenylalanine peptide microrods with uniform polarization. Nano Energy 17:323–329

Nguyen V, Zhu R, Jenkins K, Yang R (2016) Self-assembly of diphenylalanine peptide with controlled polarization for power generation. Nat Commun 7:13566

Nielsen JE, Bjørnestad VA, Lund R (2018) Resolving the structural interactions between antimicrobial peptides and lipid membranes using small-angle scattering methods: the case of indolicidin. Soft Matter 14:8750–8763

Niu L, Chen X, Allen S, Tendler SJB (2007) Using the bending beam model to estimate the elasticity of diphenylalanine nanotubes. Langmuir 23:7443–7446

Norden B, Rodger A, Dafforn T (2010) Linear dichroism and circular dichroism: a textbook on polarized light spectroscopy

Nozue Y, Shinohara Y, Amemiya Y (2007) Application of microbeam small- and wide-angle X-ray scattering to polymeric material characterization. Polym J 39:1221–1237

O'Brien DP et al (2018) SEC-SAXS and HDX-MS: a powerful combination. The case of the calcium-binding domain of a bacterial toxin. Biotechnol Appl Biochem 65:62–68

Paparcone R, Keten S, Buehler MJ (2010) Atomistic simulation of nanomechanical properties of Alzheimer's Aβ(1–40) amyloid fibrils under compressive and tensile loading. J Biomech 43:1196–1201

Papish AL, Tari LW, Vogel HJ (2002) Dynamic light scattering study of calmodulin–target peptide complexes. Biophys J 83:1455–1464

Passeri D, Tamburri E, Terranova ML, Rossi M (2015) Polyaniline–nanodiamond fibers resulting from the self-assembly of nano-fibrils: a nanomechanical study. Nanoscale 7:14358–14367

Paul TJ et al (2016) Structural and mechanical properties of amyloid beta fibrils: a combined experimental and theoretical approach. J Phys Chem Lett 7:2758–2764

Paxton N et al (2017) Proposal to assess printability of bioinks for extrusion-based bioprinting and evaluation of rheological properties governing bioprintability. Biofabrication 9:044107

Pelton JT, McLean LR (2000) Spectroscopic methods for analysis of protein secondary structure. Anal Biochem 277:167–176

Pomerantz WC, Abbott NL, Gellman SH (2006) Lyotropic liquid crystals from designed helical β-peptides. J Am Chem Soc 128:8730–8731

Pomerantz WC et al (2008) Nanofibers and lyotropic liquid crystals from a class of self-assembling β-peptides. Angew Chem Int Ed 47:1241–1244

Qian C, Niu B, Jimenez RB, Wang J, Albarghouthi M (2021) Fully automated peptide mapping multi-attribute method by liquid chromatography–mass spectrometry with robotic liquid handling system. J Pharm Biomed Anal 198:113988

Quilès F, Saadi S, Francius G, Bacharouche J, Humbert F (2016) In situ and real time investigation of the evolution of a Pseudomonas fluorescens nascent biofilm in the presence of an antimicrobial peptide. Biochim Biophys Acta (BBA) - Biomem 1858:75–84

Rabolt JF, Moore WH, Krimm S (1977) Vibrational analysis of peptides, polypeptides, and proteins. 3. α-poly(L-alanine). Macromolecules 10:1065–1074

Rahmelow K, Hübner W, Ackermann T (1998) Infrared absorbances of protein side chains. Anal Biochem 257:1–11

Raphael B et al (2017) 3D cell bioprinting of self-assembling peptide-based hydrogels. Mater Lett 190:103–106

Ridgley DM, Claunch EC, Barone JR (2013) Characterization of large amyloid fibers and tapes with Fourier transform infrared (FT-IR) and Raman spectroscopy. Appl Spectrosc 67:1417–1426

Rimai L, Hickmott JT, Cole T, Carew EB (1970) Quasi-elastic light scattering by diffusional fluctuations in RNase solutions. Biophys J 10:20–37

Roberts D, Rochas C, Saiani A, Miller AF (2012) Effect of peptide and guest charge on the structural, mechanical and release properties of beta-sheet forming peptides. Langmuir 28:16196–16206

Roux S et al (2008) Elimination and exchange of trifluoroacetate counter-ion from cationic peptides: a critical evaluation of different approaches. J Pept Sci 14:354–359

Rubin DJ et al (2015) Structural, nanomechanical, and computational characterization of d,l-cyclic peptide assemblies. ACS Nano 9:3360–3368

Rughani RV et al (2009) Folding, self-assembly, and bulk material properties of a De novo designed three-stranded beta-sheet hydrogel. Biomacromolecules 10:1295–1304

Rüter A, Kuczera S, Gentile L, Olsson U (2020) Arrested dynamics in a model peptide hydrogel system. Soft Matter 16:2642–2651

Ryan K et al (2015) Nanoscale piezoelectric properties of self-assembled Fmoc-FF peptide fibrous networks. ACS Appl Mater Interfaces 7:12702–12707

Ryan TM et al (2018) An optimized SEC-SAXS system enabling high X-ray dose for rapid SAXS assessment with correlated UV measurements for biomolecular structure analysis. J Appl Crystallogr 51:97–111

Rygula A et al (2013) Raman spectroscopy of proteins: a review. J Raman Spectrosc 44:1061–1076

Sadat A, Joye IJ (2020) Peak fitting applied to Fourier transform infrared and Raman spectroscopic analysis of proteins. Appl Sci 10

Sahoo JK et al (2016) Analysis of enzyme-responsive peptide surfaces by Raman spectroscopy. Chem Commun 52:4698–4701

Salnikov ES, Aisenbrey C, Anantharamaiah GM, Bechinger B (2019) Solid-state NMR structural investigations of peptide-based nanodiscs and of transmembrane helices in bicellar arrangements. Chem Phys Lipids 219:58–71

Sanii B, Martinez-Avila O, Simpliciano C, Zuckermann RN, Habelitz S (2014) Matching 4.7-Å XRD spacing in amelogenin nanoribbons and enamel matrix. J Dent Res 93:918–922

Sathaye S et al (2015) Rheology of peptide- and protein-based physical hydrogels: are everyday measurements just scratching the surface? Wiley Interdisc Rev-Nanomed Nanobiotechnol 7:34–68

Schaffer M et al (2017) Optimized cryo-focused ion beam sample preparation aimed at in situ structural studies of membrane proteins. J Struct Biol 197:73–82

Scholtz JM et al (1991) Calorimetric determination of the enthalpy change for the alpha-helix to coil transition of an alanine peptide in water. Proc Natl Acad Sci 88:2854

Schwab A et al (2020) Printability and shape fidelity of bioinks in 3D bioprinting. Chem Rev 120(19):11028–11055

Seoudi RS et al (2015a) Amino acid sequence controls the self-assembled superstructure morphology of N-acetylated tri-β3-peptides. Pure Appl Chem 87:1021–1028

Seoudi RS et al (2015b) Supramolecular self-assembly of 14-helical nanorods with tunable linear and dendritic hierarchical morphologies. New J Chem 39:3280–3287

Sharp TH et al (2012) Cryo-transmission electron microscopy structure of a gigadalton peptide fiber of de novo design. Proc Natl Acad Sci 109:13266

Shi Y et al (2017) Enzymatic activation of cell-penetrating peptides in self-assembled nanostructures triggers fibre-to-micelle morphological transition. Chem Commun 53:7037–7040

Shriky B et al (2020) Pluronic F127 thermosensitive injectable smart hydrogels for controlled drug delivery system development. J Colloid Interface Sci 565:119–130

Singh HSY (2013) (Anton Paar: Graz)

Singha NK, Gibson MI, Koiry BP, Danial M, Klok H-A (2011) Side-chain peptide-synthetic polymer conjugates via tandem "Ester-amide/thiol–Ene" post-polymerization modification of poly(pentafluorophenyl methacrylate) obtained using ATRP. Biomacromolecules 12:2908–2913

Sloan-Dennison S et al (2021) Elucidation of the structure of supramolecular polymorphs in peptide nanofibres using Raman spectroscopy. J Raman Spectrosc 52:1108–1114

Smith RD, Cheng X, Brace JE, Hofstadler SA, Anderson GA (1994) Trapping, detection and reaction of very large single molecular ions by mass spectrometry. Nature 369:137–139

Smith JF, Knowles TPJ, Dobson CM, MacPhee CE, Welland ME (2006) Characterization of the nanoscale properties of individual amyloid fibrils. Proc Natl Acad Sci 103:15806

Smith AM, Collins RF, Ulijn RV, Blanch E (2009) Raman optical activity of an achiral element in a chiral environment. J Raman Spectrosc 40:1093–1095

Song P et al (2020) Preparation, characterization, and in vitro evaluation of amphiphilic peptide P12 and P12-DOX nanomicelles as antitumor drug carriers. Nanomater Nanotechnol 10: 1847980420911519

Soto Morales B et al (2021) Injectable nanofibrillar hydrogels based on charge-complementary peptide co-assemblies. Biomater Sci 9:2494–2507

Stetefeld J, McKenna SA, Patel TR (2016) Dynamic light scattering: a practical guide and applications in biomedical sciences. Biophys Rev 8:409–427

Stuhrmann H (1974) Neutron small-angle scattering of biological macromolecules in solution. J Appl Crystallogr 7:173–178

Susapto HH et al (2021) Ultrashort peptide bioinks support automated printing of large-scale constructs assuring long-term survival of printed tissue constructs. Nano Lett 21:2719–2729

Svergun DI, Koch MH, Timmins PA, May RP (2013) Small angle X-ray and neutron scattering from solutions of biological macromolecules, vol 19. Oxford University Press

Tang C, Smith AM, Collins RF, Ulijn RV, Saiani A (2009) Fmoc-diphenylalanine self-assembly mechanism induces apparent pK(a) shifts. Langmuir 25:9447–9453

Thunecke M et al (1998) Aggregation of Aβ Alzheimer's disease-related peptide studied by dynamic light scattering. J Pept Res 52:509–517

Touve MA, Carlini AS, Gianneschi NC (2019) Self-assembling peptides imaged by correlated liquid cell transmission electron microscopy and MALDI-imaging mass spectrometry. Nat Commun 10:4837

Trewhella J et al (2017) 2017 publication guidelines for structural modelling of small-angle scattering data from biomolecules in solution: an update. Acta Crystallogr Sect D 73:710–728

Tuma R (2005) Raman spectroscopy of proteins: from peptides to large assemblies. J Raman Spectrosc 36:307–319

Uchihashi T, Watanabe H, Fukuda S, Shibata M, Ando T (2016) Functional extension of high-speed AFM for wider biological applications. Ultramicroscopy 160:182–196

Valéry C et al (2003) Biomimetic organization: octapeptide self-assembly into nanotubes of viral capsid-like dimension. Proc Natl Acad Sci 100:10258

Valéry C et al (2004) Self-association process of a peptide in solution: from β-sheet filaments to large embedded nanotubes. Biophys J 86:2484–2501

van Dijk-Wolthuis WNE et al (1999) A versatile method for the conjugation of proteins and peptides to poly[2-(dimethylamino)ethyl methacrylate]. Bioconjug Chem 10:687–692

Venyaminov SY, Kalnin NN (1990) Quantitative IR spectrophotometry of peptide compounds in water (H2O) solutions. I. Spectral parameters of amino acid residue absorption bands. Biopolymers 30:1243–1257

Venyaminov SY, Baikalov IA, Shen ZM, Wu CSC, Yang JT (1993) Circular dichroic analysis of denatured proteins: inclusion of denatured proteins in the reference set. Anal Biochem 214:17–24

Vestergaard B et al (2007) A helical structural nucleus is the primary elongating unit of insulin amyloid fibrils. PLoS Biol 5:e134

Williams RW, Dunker AK (1981) Determination of the secondary structure of proteins from the amide I band of the laser Raman spectrum. J Mol Biol 152:783–813

Williamson MP, Waltho JP (1992) Peptide structure from NMR. Chem Soc Rev 21:227–236

Wilson NR, Macpherson JV (2009) Carbon nanotube tips for atomic force microscopy. Nat Nanotechnol 4:483–491

Wychowaniec JK et al (2018) Designing peptide/graphene hybrid hydrogels through fine-tuning of molecular interactions. Biomacromolecules 19:2731

Wychowaniec JK et al (2020a) Role of sheet-edge interactions in β-sheet self-assembling peptide hydrogels. Biomacromolecules 21:2285–2297

Wychowaniec JK et al (2020b) Aromatic stacking facilitated self-assembly of ultrashort ionic complementary peptide sequence: β-sheet nanofibers with remarkable gelation and interfacial properties. Biomacromolecules 21:2670–2680

Wychowaniec JK, Moffat J, Saiani A (2021a) Quantitative nanomechanical properties evaluation of a family of β-sheet peptide fibres using rapid bimodal AFM. J Mech Behav Biomed Mater 124: 104776

Wychowaniec JK et al (2021b) Elastic flow instabilities and macroscopic textures in graphene oxide lyotropic liquid crystals. Npj 2D Mater Appl 5:11

Yamamoto S-I, Ishida T, Mizutani W, Tokumoto H, Yamada H (1997) Identification of materials using direct force modulation technique with magnetic AFM cantilever. Jpn J Appl Phys 36: 3868–3871

Yan C, Pochan DJ (2010) Rheological properties of peptide-based hydrogels for biomedical and other applications. Chem Soc Rev 39:3528–3540

Yan C et al (2010) Injectable solid hydrogel: mechanism of shear-thinning and immediate recovery of injectable beta-hairpin peptide hydrogels. Soft Matter 6:5143–5156

Yasuda R (2019) In: Alfano RR, Shi L (eds) Neurophotonics and biomedical spectroscopy. Elsevier, pp 53–64

Ye Z, Wei L, Li Y, Xiao L (2019) Efficient modulation of β-amyloid peptide fibrillation with polymer nanoparticles revealed by super-resolution optical microscopy. Anal Chem 91:8582–8590

Yoshida T (2004) Peptide separation by hydrophilic-interaction chromatography: a review. J Biochem Biophys Methods 60:265–280

Zelenovskiy P, Kornev I, Vasilev S, Kholkin A (2016) On the origin of the great rigidity of self-assembled diphenylalanine nanotubes. Phys Chem Chem Phys 18:29681–29685

Zhang G, Annan RS, Carr SA, Neubert TA (2010a) Overview of peptide and protein analysis by mass spectrometry. Curr Protoc Protein Sci 62:16.11.11–16.11.30

Zhang G et al (2010b) In: Fenyö D (ed) Computational biology. Humana Press, pp 211–222

Zhang S et al (2010c) A self-assembly pathway to aligned monodomain gels. Nat Mater 9:594–601

Zhu G, Zhu X, Fan Q, Wan X (2011) Raman spectra of amino acids and their aqueous solutions. Spectrochim Acta A Mol Biomol Spectrosc 78:1187–1195

Zhu J et al (2018) Biodegradable and pH sensitive peptide based hydrogel as controlled release system for antibacterial wound dressing application. Molecules 23

Chapter 9
In Silico Prediction of Peptide Self-assembly into Nanostructures

Attilio Vittorio Vargiu, Giuliano Malloci, and Silvia Marchesan

Abstract Self-assembling peptides bear tremendous potential in the fields of material sciences, nanoscience, and medicine. In contrary to the popular building blocks used in supramolecular chemistry, which exploit rigid molecular structures with defined geometry, peptides are highly flexible. This feature renders the prediction of their most stable conformations and self-assembly ability, as well as an understanding of the mechanism behind aggregation, more challenging for experimental techniques. In this context, in silico techniques have progressed at a fast pace to provide highly valuable tools to study, predict, and visualize peptides' behavior and their dynamics to assist with their design. In this chapter, we will provide an overview of popular computational techniques used to investigate the self-assembly of peptides and peptide-containing molecules. Together with the applications, we will briefly discuss the pros and cons of these methodologies and conclude with a perspective on the future directions that this exciting field can lead to.

Keywords Self-assembly · Peptides · Peptide amphiphiles · Nanostructures · Chirality · Molecular modeling · Molecular dynamics · Coarse grain · Machine learning

9.1 Introduction

In the past decades, peptide-based systems have gained particular interest as building blocks of a large variety of disparate self-assemblies, with applications ranging from material science to medicine (Cui et al. 2010; Ung and Winkler 2011; Mandal et al. 2014; Panda and Chauhan 2014; Marchesan et al. 2015b; Frederix et al. 2018; Zhao

A. V. Vargiu (✉) · G. Malloci
Physics Department, University of Cagliari, Cittadella Universitaria, Monserrato, Italy
e-mail: vargiu@dsf.unica.it

S. Marchesan
Chemical and Pharmaceutical Sciences Department, University of Trieste, Trieste, Italy

INSTM, University of Trieste, Trieste, Italy
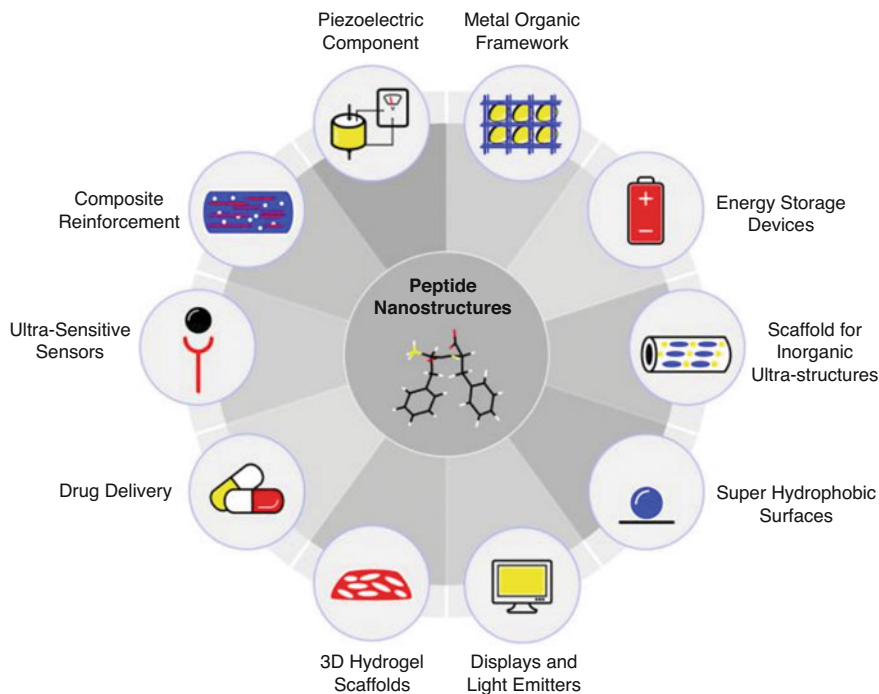
Fig. 9.1 Schematic view of some applications of peptide-based nanostructures. Reproduced from Adler-Abramovich and Gazit (2014) with permission from the Royal Society of Chemistry

et al. 2018; Chakraborty and Gazit 2018; Lee et al. 2019; Chen and Zou 2019; Gupta et al. 2020; Cringoli et al. 2021) (Fig. 9.1). Compared to other molecules, peptides bring the advantage of being biocompatible, biodegradable, bioactive when composed by three or more amino acids, easy to synthetize (particularly if short), and able to form varied supramolecular structures with only small variations in the individual monomers. Unfortunately, characterizing the properties of these materials remains challenging, which limits the drafting of quantitative (molecular) structure–property relationships in the context of properties extending beyond the nanoscale. As in many research fields involving biomolecules, the main issues arise from the multidimensional and shallow potential energy surface associated with the interaction among flexible molecules, promoting local disorder and continuous entropy/enthalpy interchange.

Due to the sparse nature of the nanostructures formed in solution, experimental methods employed to study self-assembly, which include light absorption, circular dichroism, nuclear magnetic resonance, and diffraction techniques, often cannot resolve conformations of individual building blocks. As a result, researchers need to employ different complementary experimental techniques and combine the various pieces of information obtained from each experiment to gain an overall picture of intermolecular interactions (Frederix et al. 2018). However, the entropic

contribution to the process is often neglected due to the (ensemble) averaged properties measured experimentally, and this can potentially lead to misleading interpretative models. The early stages of aggregation, crucial in defining the resulting nanostructures and thus their properties, could occur within a few nanoseconds (ns), which implies they are virtually unobservable by most experimental techniques. Finally, the models employed to interpret raw experimental data are often tailored on macromolecular systems that are largely different from peptides and their derivatives (for instance, circular dichroism data are often interpreted by comparison to models that are strictly valid for proteins).

Molecular simulations, by collecting atomic/molecular-level snapshots of every modelable system including peptides and their derivatives, provide an invaluable complementary tool to understand the physics and the chemistry behind self-assembly mechanisms. The large number of building blocks needed to form nanostructures and the many degrees of freedom involved in packing small molecules together have long limited the scope of simulations in this field (Colombo et al. 2007; Tuttle 2015; Manandhar et al. 2017; Yuan et al. 2017; Frederix et al. 2018; Katyal et al. 2020). Fortunately, the recent advances in computational hardware [dedicated machines such as Anton (Shaw et al. 2014)] and software [particularly the coding on GPUs (Harvey and De Fabritiis 2009; Salomon-Ferrer et al. 2013; Kutzner et al. 2019; Phillips et al. 2020)], as well as the development of simulations protocols (Bottaro and Lindorff-Larsen 2018; Huggins et al. 2019; Yang et al. 2019; Noé et al. 2020; Brooks et al. 2021; Glielmo et al. 2021), have enabled significant progress. Computational studies contribute nowadays to unveil key elements from the early steps of the self-assembly to the macroscopic properties of the resulting structures. Furthermore, they provide useful insights for the design of new materials with tailored functions and features.

Several reviews recapitulated, from different perspectives, the research performed over the last decades on self-assembling nanomaterials, including peptides and peptide-containing molecules among others (Colombo et al. 2007; Cui et al. 2010; Hamley 2011; Adler-Abramovich and Gazit 2014; Mandal et al. 2014; Panda and Chauhan 2014; Fichman and Gazit 2014; Tuttle 2015; Marchesan et al. 2015b; Wang et al. 2016; Manandhar et al. 2017; Yuan et al. 2017; Frederix et al. 2018; Zhao et al. 2018; Chakraborty and Gazit 2018; Lee et al. 2019; Chen and Zou 2019; Katyal et al. 2020; Zheng et al. 2021). In this chapter, we made an effort to provide an updated survey of computational investigations performed on natural peptides, as well as on capped or esterified materials to produce peptide amphiphiles (PA—composed by a peptide and generally a lipid moiety), aromatic peptide amphiphiles (APA), branched peptides, and other derivatives.

Selected studies are collected into three main sections based on the model/algorithm employed to investigate self-assembly. The first two sections are dedicated to all-atom and coarse-grained molecular dynamics (MD) simulations, which still represent the method of choice according to the literature. A third section reports investigations performed using other approaches, including quantum-mechanical calculations and machine-learning methods; particularly the latter is gaining momentum in these years. Note that, given the huge literature on this subject, we will limit

our survey to studies aimed at deciphering the molecular architectures of peptide-based nanostructures as well as the mechanisms underlying their formation. Studies addressing physico-chemical properties of peptides or peptide-containing molecules and inferring self-assembly propensities in an indirect manner will not be reported. Also, in this chapter we will omit studies describing the interactions between peptides and surfaces and/or inorganic materials, or nucleic acids.

9.2 All-Atom MD Simulations

All-atom calculations allow to follow the dynamics of biomolecules at high (atomic) spatial resolution, generally capturing via accurate force-fields many essential interactions, such as van der Waals, electrostatics, and H-bonding (Brooks et al. 2021). They have been extensively employed to unveil key factors driving the self-assembly process of natural and capped peptides, as well as of peptide-based molecules (Cui et al. 2010; Mandal et al. 2014; Panda and Chauhan 2014; Tuttle 2015; Marchesan et al. 2015b; Wang et al. 2016; Manandhar et al. 2017; Yuan et al. 2017; Frederix et al. 2018; Zheng et al. 2021). To cope with the relatively long simulation time needed to mimic aggregation of many molecules in aqueous solution, some of the first computational studies represented the solvent as a continuum medium described by an effective dielectric constant (implicit solvent).

Tamamis et al. (2009a) employed this strategy to explore the self-assembly of diphenylalanine (FF) and triphenylalanine (FFF) peptides. By means of MD simulations, they confirmed experimental findings showing that FF self-assembles into discrete and well-ordered nanotubes and showed for the first time the formation of plate-like nanostructures with β-sheet content by the FFF peptides. Furthermore, analysis of the energetics of self-assembly allowed rationalizing the higher network propensities and increased aggregate stabilities of FFF with respect to FF. The same authors employed implicit solvent MD simulations to study the self-assembly of two amyloidogenic octapeptides derived from the adenovirus fiber shaft (Tamamis et al. 2009b). Simulations revealed that both peptides can readily form intermolecular β-sheets stabilized by extensive interactions involving the C-terminal moieties. Analysis of structural and energetic properties of these sheets enabled the identification of suitable positions for rational modification of peptide building blocks.

Due to the key role of the solvent in the self-assembly process, most of the studies performed in the past decade described this component explicitly. This implied a careful study design strategy to provide useful insights despite the higher computational costs. Many studies focused on minimal models, such as the FF dipeptide, which is very important both as prototype of amyloidogenic molecules and in technological applications (Marchesan et al. 2015b). Jeon et al. (2013) performed MD simulations of zwitterionic and uncharged models of this peptide to investigate the assembly mechanism into nanotubes and shed light on the forces underlying their stability. They found that, while electrostatic interactions steer zwitterions into more ordered dimeric and trimeric assemblies, hydrophobic interactions determine the

structures of larger oligomers. The authors concluded that the amphiphilic nature of FF is key to understanding its self-assembly and that the early precursors to nanotube structures likely undergo substantial hydrophobic clustering.

Kelly et al. (2015) studied the effect of a constant electric field on the self-assembly of FF peptides. Both neutral and charged systems ranging from a single unit up to 64 molecules were considered. Simulations revealed that even relatively weak fields are able to accelerate ordered response of individual peptides, primarily through the alignment of their molecular dipole moments. Overall, electric fields increase the self-assembly propensity of FF peptides into ordered nanomaterials. This observation is particularly relevant to fully exploit the fascinating properties of their assemblies, including piezoelectricity (Kholkin et al. 2010) and ferroelectricity (Gan et al. 2013). Their combination with other (carbon) nanomaterials displaying conductivity and unique electronic properties is well set to develop a new generation of innovative hybrids or composites with applications in various biomedical areas (Rozhin et al. 2021).

Replica-exchange MD simulations (Sugita and Okamoto 1999) of the self-assembly of FF and dialanine (AA) dipeptides in water and methanol were performed by Rissanou et al. (2013) to assess the impact of solvent on the process. In agreement with experiments, FF self-assembling was largely hindered in the organic solvent due to the lack of attractive interactions between pairs of molecules, as it happens in water solution. In addition, while increasing the temperature led to smaller aggregates in water, structures formed in methanol were almost unaffected by this parameter. A similar tendency was observed for the less hydrophobic AA, although the solvent has a substantially smaller impact than for FF.

Gazit and coworkers took advantage of co-assembly of amyloid-derived dipeptides (namely, fluorenyl-methoxycarbonyl-diphenylalanine—FmocFF) and bipyridine derivatives to promote transformation of self-assemblies from stable β-sheet-rich structures into adaptable secondary structural fibrils (Ji et al. 2020). Density functional theory (DFT) calculations and MD simulations, performed to investigate the molecular mechanism of co-assembly and structural transition, suggest intermolecular H-bonding as the predominant driving force of the formation of new molecular arrangements. Detailed visualization of the molecular mechanisms associated with conformational switches is crucial to understand complex phenomena, such as amyloid fluorescence, which still bears many unanswered questions, but already holds great promise for bioimaging applications (Lapshina et al. 2019).

Sun et al. (2015a) investigated the driving forces underlying self-assembly of dipeptide sodium salts derived from alanine. Simulations showed that the dipeptides can organize into helical fibrils and that a bilayer structure is the basic unit in the nanostructure. Analysis of the modeled assemblies allowed to rationalize the formation of helical nanofibers, whereby alkyl chains, aggregating toward the center of the nanostructure, are partially exposed to the bulk water and contribute to stabilize the structure in a polar solvent.

A comparative experimental and computational study of self-assembly and gelation of Fmoc-conjugated alanine-lactic acid (Fmoc-Ala-Lac) and the analog Fmoc-Ala-Ala was presented by Eckes et al. (2014). MD simulations allowed

to explain the molecular determinants underlying the different sizes, morphologies, and mechanical properties of the supramolecular assemblies formed by the two capped peptides. This study underlined how the network of amide-amide H-bonds is key not only for the stability of the assembly, but rather in determining the nature of the higher-order aggregation of intermediate fibrils. Melting temperature and potential of mean force calculations indicated that both the intra- and inter-fibril interactions are stronger in Fmoc-Ala-Lac than in Fmoc-Ala-Ala assemblies. The overall difference in fibril amphiphilicity was thus suggested to be responsible for the higher order assembly of the nanostructures detected in experiments. An interesting comparison of the hierarchical self-assembly processes of three selected octapeptides with the same amino acid composition but different sequences was performed by Zhou et al. (2016). Simulations provided useful insights on how the competition between electrostatic and hydrophobic interactions shapes the interstrand packing modes, as well as on how the balance between intra- and inter-β-sheet interactions affect their twisting and stacking and the resulting mesoscopic structures.

Muthusivarajan et al. (2020) investigated the role of alkylated residues in the assembly of the tetrapeptide YXKX (X = alkylated tyrosine). Alkylation was employed to obtain two distinct sides (hydrophobic vs. hydrophilic) relative to the peptide backbone. MD simulations revealed that this tetrapeptide self-assembled into a nanosphere structure, with hydrophilic residues occupying the surface of the assembly and alkyl chains constraining its size and shape. Furthermore, simulations unveiled how tyrosine alkylation boosts the self-assembly process via a strong hydrophobic effect and by forming a hydrophobic core to reduce exposure to the solvent.

Several studies focused on a wide variety of peptide-based molecules, such as peptide amphiphiles (PAs). Lee et al. (2011) shown that PAs formed by a hydrophobic alkyl chain attached to the N-terminus of the sequence SLSLAAAEIKVAV can assemble into stable cylindrical nanofibers excluding water molecules from their interior, filled by alkyl tails (Fig. 9.2). Of note, several patches of the PAs molecules assume often a β-sheet structure, consistently with circular dichroism results. Lai et al. (2017) employed extensive all-atom MD simulations to describe the spontaneous structural transformation of PAs from a planar assembly to a twisted aggregate or to a helical ribbon. Importantly, the atomic-level description of self-assembly dynamics pinpointed how the oxidation of a single Met residue in each PA leads to a change from bilayer to monolayer assemblies with significantly different ribbon properties. Further analysis of the secondary structure content showed how the extent of β-sheet and polyproline II-like structures formation is linked to helix formation. The twist angle and the helical diameter of the ribbon resulting from the simulations closely matched the experimental data, demonstrating the capability of MD simulations to predict PAs self-assembly into nanochiral structures.

Chirality as a feature to shape the morphology in the self-assembly of peptides and their derivatives has been one of the most intriguing parameters being exploited in the field. The first notable example with regard to the alternation of D- and L-residues in cyclic peptides to allow for their stacking into supramolecular
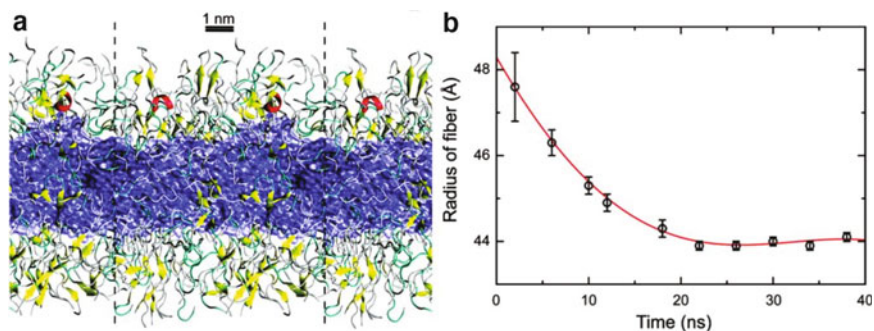
Fig. 9.2 (**a**) Conformation assumed at the end of the MD simulation by self-assembling PAs studied in Lee et al. (2011). The hydrophobic core is represented by a blue surface: α-helixes, β-sheets, turns, and coils are colored, respectively, red, yellow, cyan, and gray. Periodic boundaries along the axis of the fiber are shown by dotted lines. (**b**) Radius of the fiber as a function of simulation time. Adapted with permission from Lee et al. (2011). Copyright 2011 American Chemical Society

nanotubes as described by Ghadiri et al. (1993). However, even a single stereoconfiguration change (i.e., by substituting one L-amino acid with its D-enantiomer) can have dramatic effects on the self-organization of linear peptides, as first described by Marchesan et al. (2012a, b). Amphipathic segregation between hydrophilic and hydrophobic components is key to stabilize the resulting supramolecular structures (Vargiu et al. 2016). Given the atomistic detail of the difference between L- and D- amino acids, all-atom MD simulations are required to unveil the supramolecular amplification of fine molecular differences between stereoisomers as they self-assemble from the nanoscale to the macroscale (Garcia et al. 2018). In this manner, it was possible to rationalize the effects of the position of the D-amino acid in a tripeptide to attain a higher (LDD or DLL peptides) or lower (LDL or DLD isomers) level of supramolecular order, thus yielding hydrogels at physiological pH with tunable properties (e.g., stiffness, melting temperature, etc.) (Marchesan et al. 2015a). When the sequence encodes for conflicting instructions, as in PFF that unites the β-breaker P with self-assembling FF, then positioning of the D-amino acid becomes a strategic tool to resolve the inherent encoded tension toward the formation of short- (LDL or DLD), medium- (LLD or DDL), or long-range (DLL or LDD) assemblies (Garcia et al. 2021) (Fig. 9.3). The resulting functional structures can find diverse applications, such as supramolecular organo-catalysis when assembly prevails (Sinibaldi et al. 2021) or pathological amyloid fibrillization inhibition in the opposite case (Garcia et al. 2021). To further elucidate the reasons behind the different behavior of homochiral and heterochiral peptides, in (Garcia et al. 2018) the different assembly propensities of homo and heterochiral tripeptides was investigated in continuo from molecular level to macroscopic hydrogels. Extensive all-atom MD simulations unveiled how the occurrence of amphiphilic structures, stable in polar solvents, is uniquely enabled by the stereochemistry of heterochiral peptides. Simulations showed that the presence of F at both peptide termini allows
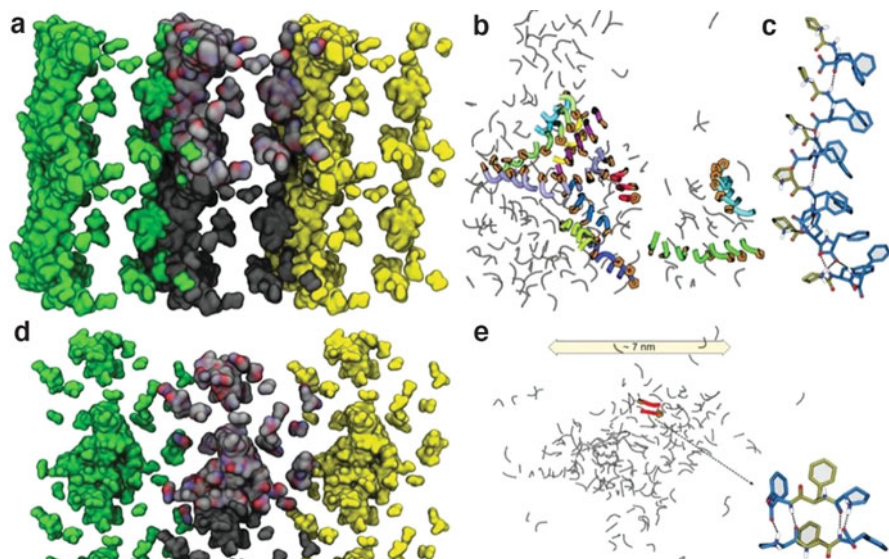
Fig. 9.3 Representative assemblies of ^{D}PFF (**a–c**) and P^{D}FF (**d–e**) as extracted from multiple all-atom MD simulations. The surface colored by atom type (C, N, and O in gray, blue, and red, respectively) is the one in the primary simulation box. The one in dark gray extends along the x direction, while yellow and green surfaces represent adjacent images. (**a–c**) ^{D}PFF peptides associated into parallel stacks forming fibrils (colored ribbons with Pro in orange), while P^{D}FF (**d–e**) self-associated into scattered nanoparticles containing mainly antiparallel dimeric and trimeric stacks. Reprinted from Garcia et al. (2021)

interdigitation between stacks (held together by an ordered H-bond pattern between amides and by salt bridges between the charged NH_3^+ and COO^- termini) into supramolecular zippers excluding water molecules.

Wang et al. (2017) designed three pairs of enantiomeric PAs (containing $^LI_3{}^LK$, $^LI_3{}^DK$ and $^DI_3{}^LK$, and $^{La}I_3{}^LK$ and $^{Da}I_3{}^DK$) and assessed how aminoacid chirality affects the morphology of self-assembled nanofibrils through the combined use of atomic force, circular dichroism, scanning electron microscopies, and MD simulations. Simulations delineated the handedness development from molecular chirality to supramolecular level by showing that all peptides formed β-sheets, which exhibited a propensity to twist in a left-handed or right-handed direction, depending on the stereoconfiguration of the C-terminal residue (i.e., L- or D-amino acid, respectively). Along the same line, Clover et al. (2020) designed heterochiral analogs of the model PA KFE8 (Ac-FKFEFKFE-NH$_2$), composed of two FKFE repeat motifs with opposite chirality, showing how they assemble into helical tapes with dimensions greatly exceeding those of their fibrillar homochiral counterparts. Simulations revealed that the energy-minimized heterochiral fibril structure consists of peptides featuring an ~160° rotation about the "LD" plane; the kink at the interface between L- and D-blocks leads to the assembly of flat monolayers displaying alternating stacks of hydrophobic and charged groups.

Chirality and pH were the parameters considered by Guler and coworkers (Hatip Koc et al. 2017) to control the hierarchical self-assembly of histidine-functionalized PAs containing D or L amino acids. MD simulations were employed as a complement to several experimental studies to address the effects of the stereochemistry and amino acid sequence of the PA on the supramolecular organization. Pure [L]PAs turned out to form more H-bonds than mixtures of L and D PAs. However, while the H-bonding capacity decreases as the relative amount of [D]PA increases, a peak is found for systems composed of only [D]PAs. An investigation of the self-assembly mechanism of enantiomers of the aromatic amino acids phenylalanine and tryptophan, highlighting a critical role of chirality in dictating macroscopic features of the assemblies, was performed by Gazit and coworkers (Bera et al. 2020). In particular, MD simulations on patches of crystal structures of [L]Phe, [L/D]Trp, and racemic [LD]Trp mixtures revealed that homochiral crystals might grow along one dimension (that of the aromatic zipper formed between adjacent aminoacid side chains), while mixed [L/D]Trp assumed an overall flat morphology since their possible twists are compensated by the presence of both enantiomers. As a result, crystals of [LD]Trp racemic mixtures might grow in 2D or 3D.

9.3 Coarse-Grain Simulations

With respect to all-atom MD, coarse-grain (CG) approaches offer a clear advantage in terms of enhanced sampling of the conformational space and of the size of the simulated systems (Yuan et al. 2017; Frederix et al. 2018). In this section, we review a selection of studies employing CG approaches to decipher the molecular determinants for different supramolecular structures obtained by self-assembling of peptides and peptide derivatives. Among the latter, the class of molecules that has received by far more attention is that of PAs. We first describe studies performed with the popular MARTINI model (Monticelli et al. 2008), which is the most widely used force field for simulating self-assembly of biological molecules. Next, we describe studies based on ad hoc modifications to this force field. Finally, we provide some examples of alternative approaches either based on different coarse-graining or hybrid schemes.

Tuttle's lab pioneered the use of MARTINI-based CG MD simulations to understand the self-assembling of short peptides (Tuttle 2015). About 10 years ago, these authors developed a protocol for the rapid screen of all 400 possible dipeptide combinations in order to predict their aggregation propensity (AP) in aqueous solution (Frederix et al. 2011). An AP score was introduced as the ratio of the solvent-accessible surface area (SASA) of the peptides in the initial (structurally relaxed) conformation of the simulation box to the SASA of the final configuration. The larger the ratio, the higher the degree of aggregation. Most dipeptides featured AP values close to 1, indicating no propensity to aggregate; as expected, F and W were particularly good in promoting self-assembly (Fig. 9.4a). Dipeptide pairs selected by applying this protocol were in good agreement with previous literature;
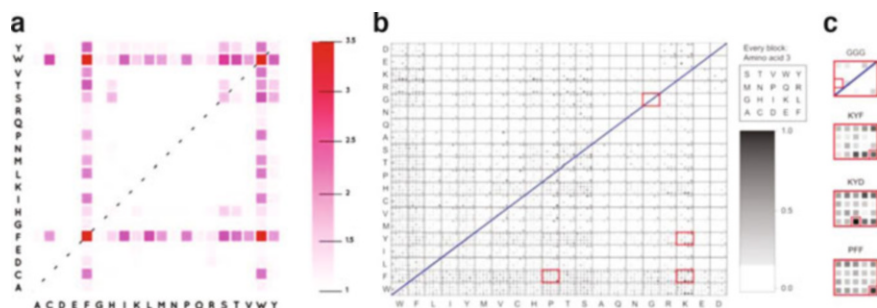
Fig. 9.4 Two-dimensional grids reporting the aggregation propensity scores for dipeptides (**a**) and tripeptides (**b**, values normalized to 1). Horizontal and vertical axes show the amino acid one-letter codes for the first (N-terminus) and second (C-terminus) amino acid, respectively. In (**b**) the third amino acid is represented by the position of the colored square at the locations indicated in the legend on the right. A darker shade indicates a larger degree of aggregation. (**c**) Zooming of the highlighted areas showing the four peptide entries highlighted by red rectangles in (**b**). Adapted with permission from Frederix et al. (2011, 2015). Further permission related to the material excerpted in (**a**) should be directed to the ACS

among these, the FF system was subjected to extended CG simulations that proved to be able to reproduce salient features of its nanoscale assemblies, providing insight into the self-assembly process.

The FF motif has since long attracted interest being the smaller building block to elucidate the self-assembly of short peptides and their analogs into supramolecular structures and hydrogels with broad applications (Marchesan et al. 2015b). Guo et al. (2012) investigated for the first time the self-assembly mechanism of hundreds of FF peptides at different concentrations, showing that they could spontaneously associate into spherical vesicles and nanotubes, as reported by experiments (Song et al. 2004; Görbitz 2006). Moreover, their simulations allowed to discover additional nanoarchitectures such as planar bilayers and vesicle-like structures with alternative shapes including toroid, ellipsoid, discoid, and pot-shaped assemblies, the exact shape depending on the ratio between peptide-peptide and peptide–solvent interactions. The use of different concentrations shaded light on the impact of this parameter on the assembly pathway, which involves vesicle or vesicle/bilayer fusion or formation of a bilayer that bends and self-seals at low or high concentrations, respectively. The study was complemented by all-atom MD simulations of a spherical vesicle back-mapped from the CG MD trajectory, showing a preference towards T-shaped arrangement between two adjacent aromatic rings in the ordered nanostructures. Later, the same lab investigated the self-assembly dynamics of FFF tripeptides (Guo et al. 2014), predicting the formation of nm-sized nanospheres and nanorods containing a relevant fraction of β-sheet-like structures that are larger in size compared to those formed by FF dipeptides. Dissection of the intermolecular forces into main and side-chain contributions (a typical analysis coming at no additional cost with simulations) highlighted how the subtle interplay between

these interactions leads to different nanostructures formed by FF and FFF assemblies.

Brown et al. (2018) examined carboxybenzyl-protected diphenylalanine (Cbz-FF) as a minimal model to further understand the self-assembly process of triaromatic peptides. Consistently with experimental results, CG MD simulations lead to the formation of either fibers or spheres depending on the solvent model. The self-assembly process resembles that reported for FFF peptides (apart for the absence of toroidal structures, possibly attributed to the size and time limits of the simulations), suggesting that Cbz-FF may be employed as a minimal member of the tri-aromatic peptide family.

A comprehensive study on the self-assembly of tripeptides was conducted by Frederix et al. (2015), who expanded their previous investigation (Frederix et al. 2011) to screen for self-assembly propensities of all the 8000 possible tripeptides deriving from the permutation of the 20 natural aminoacids (Fig. 9.4b, c). The work correlated hydrophobicity with self-assembly propensity and highlighted how subtle differences in molecular properties have a huge impact on supramolecular order. In all of the gel-forming peptides, the predicted supramolecular structure corresponded to nanofibers. Computational findings were compared to experiments, providing a platform to derive a set of design rules for self-assembling sequences and to discover the first tripeptides forming hydrogels at neutral pH. The same labs exploited a computational/experimental approach to report the first example of unprotected tripeptides able to self-assemble in biphasic systems to stabilize oil/water emulsions (Scott et al. 2016). Depending on the peptide sequence and charge, emulsions are stabilized by the formation of either standard surfactant-like droplets (D-containing tripeptides) or through the assembly of a spherical network of nanofibers (K-containing tripeptides). Noteworthy, peptides assembling into fibril networks have a superior stabilizing action compared to the traditional surfactant model. In a very recent work, the same lab employed CG simulations to demonstrate the possibility to identify specific sequences of tetrapeptides endowed with surface activity values that enable their use as emulsifiers (Scott et al. 2022). These compounds have the advantage of being easily degradable and less toxic as compared to classical substances. Simulations were used within a rational design approach to consecutively reduce the molecular search space from more than 83,500 initial candidates considered in the screen to only four ones that were studied experimentally. The results of the experimental study performed on these four tetrapeptides validated the overall computational predictions and highlighted the potential of the screening methodology developed by the authors to be applied to a range of different molecular systems.

Moitra et al. performed multiple CG MD simulations of the tripeptide KFG, whose absence has been associated with the onset of many neurodegenerative diseases (Moitra et al. 2017). The authors showed that the self-assembly and morphology of KFG aggregates are largely dependent on the concentration: while vesicles are mostly formed at low concentrations, nanotubes are the main morphology at high ones. Furthermore, this study predicted the onset of rectangular blocks at higher concentration, a finding further confirmed by experiments.

Sasselli et al. (2017) investigated the molecular mechanism for variations in self-assembling tendencies for mixtures of peptides (co-assembly), detected experimentally by Ulijn and coworkers using dynamic peptide libraries (Pappas et al. 2016). In their experiments, Pappas et al. exposed unprotected dipeptides to a nonspecific protease because of the competing aggregation and amide hydrolysis (thermodynamically favored over condensation, in aqueous solvent) reactions, this setup promoted the self-assembly of the most stable aggregates. While homogenous solutions of F and L dipeptides resulted in self-assembly aggregates of hexameric peptides, mixing them with thermolysin drastically reduced the yield. Simulations of assembly of F and L di-, tetra-, and hexa-peptides, as well as of the co-assembly of F_6 and L_2 peptides, revealed a destructive co-assembly effect that can explain the low yield seen in experiments. Moreover, this work points out the importance of considering disruptive assembly processes when working with peptide libraries because such phenomenon could blur the self-assembling tendencies of the molecules of interest.

Similarly, Guo et al. (2016) performed hundreds of simulations to explore the occurrence of possibly new morphologies during the co-assembly of FF and FFF peptides as a function of their relative concentration. New noncanonical topologies, such as toroidal nanostructures, poorly sampled during the self-assembly of either peptide, were clearly detected in the FF-FFF co-assembly simulations, a finding validated by scanning electron microscopy (Fig. 9.5). A much wider set of nanomorphologies, including hollow and solid assemblies, was seen in co-assembly. Simulations were able to catch the dynamics of the transformation between these two types of structures and to show that the hollow-solid structural transition is dominated by the interaction between di- and tri-peptides, while the competition between FF–water and FFF–water interactions drives nanotoroid formation.

Moreira et al. (2019) further explored CG MD simulations of tripeptide-dipeptide co-assembly to develop an in silico screening protocol for the detection of systems forming hydrogels (or more stable emulsions) via association into nanofibers. In this case, investigations were performed both in water and in oil/water mixtures. Of note, the authors identified some promising dipeptides that, together with H-aspartyl-phenylalanyl-phenylalanine-OH (DFF), act as hydrogelators or emulsifiers with superior characteristics compared to DFF alone. Interestingly, the inclusion of a cationic amino acid at the N-terminus enhanced fiber formation when co-assembling with DFF in aqueous system, which is reminiscent of the findings in (Scott et al. 2016).

Tang et al. (2020) performed a systematic investigation of the co-assembly of FF with all remaining dipeptides, which further confirmed how such a strategy could be employed to expand the morphological diversity of peptide nanoarchitectures. Indeed, the mixing FF with several peptides resulted in structures (including vesicles, single and multicavity assemblies, planar sheets) that are rarely observed in the self-assembly of other dipeptides, a signature of enhanced aggregation propensity and significantly expanded structural diversity.
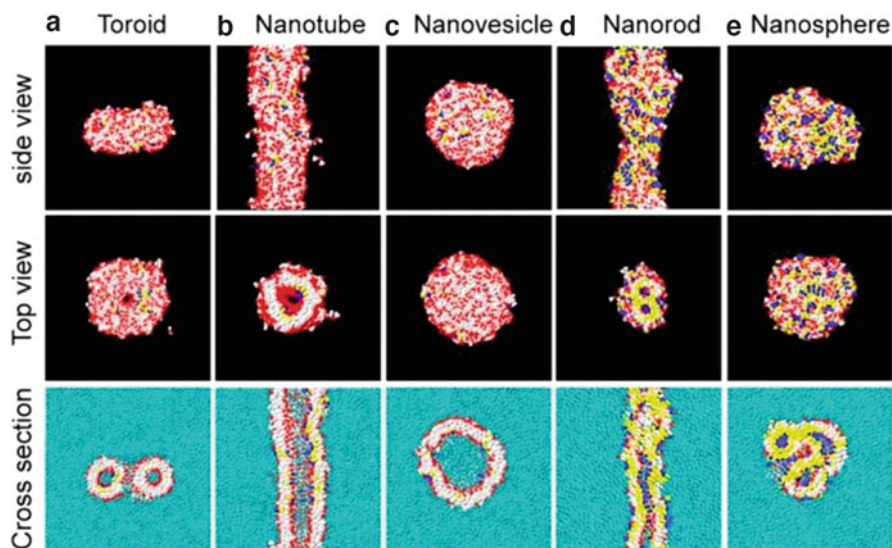
Fig. 9.5 Different nanostructures formed during the coassembly of FF and FFF peptides. Side, top, and cross-section views of nanostructures including (**a**) toroids, (**b**) nanotubes, (**c**) spherical nanovesicles, (**d**) solid nanorods, and (**e**) solid nanospheres. The FF main chain, FF side chain, FFF main chain, FFF side chain, and the water molecule CG beads are colored red, white, blue, yellow, and cyan, respectively. Adapted with permission from Guo et al. (2016). Copyright 2016 American Chemical Society

Despite the key insights into the mechanism of self-assembly obtained by employing the MARTINI force field, it is worth noticing that (a) this model has known shortcomings in the prediction of local conformational preferences due to preassigning of the secondary structure and (b) interactions mediated by H-bonds are not considered by construction. Such a uniform treatment of the data set may become inaccurate when dealing with subtle details and/or local structure/conformation effects playing a significant role in aggregate formation. With these limitations in mind, Jain et al. (2019) optimized a MARTINI model to explain the striking different aggregation dynamics and morphologies of the closely related pentapeptides FLPLF and FLGLF. They introduced information on local peptide behavior extracted from previous all-atom simulations, apply supportive dihedral angles, adjust some bead types to finely tune solvent/peptide interactions, and introduce an additional bond between two peptides to mimic a dimer. Similarly, Emamyari et al. performed atomistic simulations of long and flexible peptides of the EAK16 family to infer about secondary structure assignments to be used in subsequent MARTINI-based CG simulations (Emamyari et al. 2015). By combining all-atom simulations of single- and double-chain systems to CG simulations of self-assembly the authors were able to reproduce and rationalize the preference of two peptides of the EAK16 family toward fibrillary or globular structures, respectively.

Lee et al. further exploited the computational advantages of CG simulations with the MARTINI force field (Monticelli et al. 2008) to detect interconversion between different supramolecular structures (Lee et al. 2012). They assigned three different secondary structures to the CG models of the peptides in the ratio observed in previous atomistic simulations of the same systems (Lee et al. 2011). Using such an approach, multiple extended simulations of hundreds of PA molecules in water solvent were performed to reveal the spontaneous formation of fibers of almost 10 nm in diameter mediated by the fusion of spherical micelles into a three-dimensional network. The process is driven by van der Waals interactions leading to the exclusion of water molecules from within the hydrophobic core of the fiber. Sun et al. (2015b) assigned, respectively, coil and β-sheet secondary structures to MARTINI-based CG models of amphiphilic heptapeptides A_6K and V_6K based on atomistic replica exchange MD simulations (the structural outcomes of which agreed with experimental measures performed in aqueous solution). Of note, ordered β-sheet-rich conformations of amphiphilic peptides were observed for the first time in this work. Subsequent CG MD simulations of hundreds of peptides indicated two different self-assembly processes for A_6K and V_6K, the former assembling into monolayer lamellas and the latter into plate-like structures.

Wang et al. (2020) also used the MARTINI force field with an ad hoc modification of energetic parameters to investigate the properties of supramolecular structures formed by a set of APA tetramers with the general structure K_SXEK_S, where K_S, X and E stand for S-aroylthiooxime modified lysine, glutamic acid or citrulline, and glutamic acid, respectively. Simulations at low and high salt concentrations resulted in the formation of nanoribbons and nanohelices, respectively, a result matching experimental observation. Furthermore, they suggested that due to the closer packing of carboxylate beads in the nanohelices than in the nanoribbons, the former could better transport ions; experiments confirmed indeed a dramatic increase of the ionic conductivity under high salt conditions in their nanohelix form. These studies illustrate the importance of carefully parametrize CG models to reproduce the chemical and structural properties of specific systems.

Mazza et al. employed CG MD simulations with a modified version of MARTINI to rationalize the enhanced delivery of the model peptide dalargin to the brain following chemical modification with the amphipathic moiety palmitoyl (Mazza et al. 2013). The blood–brain barrier normally hinders delivery of dalargin to the central nervous system. Simulations showed that functionalization with palmitoyl induces self-assembly into nanofibers (resulting from the association of small clusters formed during the early stages of the simulation) featuring the peptide chains wrapped tightly around the nanofiber core. This key property has the double advantage of preventing in vivo degradation of these peptides as well as their dissolution in the plasma.

Liang et al. (2016) adopted an alternative approach, whereby all-atom MD simulations were used to unveil the details of the nanostructures formed along CG MD. They show that the Alzheimer's β-amyloid tetrapeptide core VFFA preferentially assembles into nanospheres, while its variants FFFA and KFFA evolve, respectively, into bilayer membranes and nanorods architectures. Furthermore,
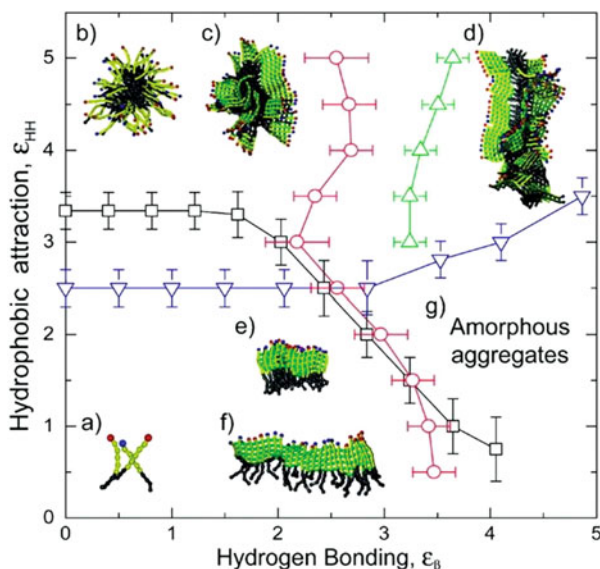
Fig. 9.6 Schematic phase diagram of PA assemblies obtained with a simplified CG model as a function of the H-bonding energy, ε_β, and the hydrophobic interaction between units, ε_{HH}. Relevant assemblies in the phase diagram include (**a**) free molecules, (**b**) spherical micelles, (**c**) micelles with β-sheets on the outside forming the corona, (**d**) long cylindrical fibers, (**e**) stacks of parallel β-sheets, (**f**) single β-sheets, and (**g**) the amorphous aggregate phase. Adapted with permission from ref. Velichko et al. (2008). Further permission related to the material excerpted should be directed to the ACS

simulations highlighted a propensity of VFFA toward extended β-sheet like structures, pointing to the importance of this tetrapeptide in Aβ aggregation and as a possible target for the inhibition of the amyloid fibrillation process.

Out of the MARTINI framework, several groups employed alternative CG models to investigate self-assembly of peptides and their derivatives. In their seminal investigations on PAs self-assembly, Velichko et al. developed a CG model describing the interaction between molecules in terms of hydrophobic interactions and H-bonding (Velichko et al. 2008). Despite its simplicity (absence of electrostatic interactions between epitope head groups or with salt ions; secondary structure of the assembly controlled by two dihedral angles that are fixed at the beginning of the simulation; absence of solvent), the model coupled to mixed Monte Carlo (MC)-stochastic dynamics simulations (Chandler 1978) demonstrated how (in addition to the molecular structure, temperature and concentration) the interplay of hydrophobic interactions between alkyl tails and H-bonds between peptide blocks shapes the assemblies' morphology from spherical micelles (when hydrophobic interactions prevail) to long cylindrical fibers to stacks of β-sheets (mainly driven by the occurrence of a stable H-bond network) (Fig. 9.6). The authors further suggested that micellization occurs through a closed association pathway that involves a dominant nucleation mechanism above a critical micellization temperature and/or

concentration. In contrast, H-bond-driven association follows an open association scenario in which step-by-step aggregation leads to a broad distribution of 1D β-sheets.

Villa et al. (2009) developed a specific CG model to perform MD simulations of FF mimicking an aqueous environment. They followed a bottom-up approach, in which bonded and non-bonded terms were derived by minimizing the differences in the conformational sampling and intermolecular interactions between CG and all-atom simulations. In this way, the authors mapped solvent effects into bead–bead nonbonded interactions, providing a computationally very efficient (solvent-free) model to simulate the self-assembly process.

Fu et al. developed a CG force field to simulate the spontaneous self-assembly of the peptide amphiphile palmitoyl-$V_3A_3E_3$ into nanofiber-based hydrogel under physiological-like conditions (Fu et al. 2014). Hydrophobic interactions turned out to be mainly responsible for the formation of cylindrical nanostructures containing either β-sheets or random coils. The authors further investigated the impact of the solvent conditions on the most likely self-assembly morphologies, showing that in addition to cylindrical nanofibers, also open networks of β-sheets and elongated micelles can be formed as stable nanostructures depending on the relative strength of the hydrophobic interactions (Fu et al. 2015). By analyzing the kinetic mechanism of assembly, the authors detected the presence of multiple transient intermediate structures depending on the properties of the solvent. Fu et al. developed also the ePRIME CG model (Fu et al. 2013), which allows for spontaneous formation of H-bonds and secondary structures, and coupled it to discontinuous molecular dynamics (Alder and Wainwright 1959) simulations to investigate the self-assembly of PAs as a function of the electrostatics and temperature, deriving a phase diagram in this bidimensional space. The authors hypothesized a three-steps self-assembling process leading to the formation of cylindrical nanofibers at optimal conditions and identified alternative kinetic mechanisms resulting in a wide variety of morphologies as the electrostatics and the temperature vary. The study provides an example of in silico investigation of morphological transitions in self-assembly of peptides in response to external stimuli. Later, the same authors applied this protocol to understand how small differences in aminoacid sequence of PAs induce subtle alterations in the propensity to form β-sheet-like structures (Fu and Nguyen 2015), which in turn correlate and explain different mechanical properties observed in experiments.

Mansbach and Ferguson (2018) proposed a CG patchy particle model to investigate the mechanism of pH-triggered assembly of DXXX−Π–XXXD oligopeptides into β-sheet-like aggregates with optical and electronic functionality. The morphological predictions of the model are consistent with experimental measurements. Moreover, by enabling unprecedented simulations of the self-assembly of 10,000 molecules over hundreds of nanometers and hundreds of microseconds, the model was crucial to identify parameter regimes favoring assembly and to map these regimes to candidate peptides for experimental synthesis and testing. The authors proposed to apply their protocol to the computational screening of peptides assembling into nanostructures with specific optoelectronic properties.

9.4   Alternative Approaches

In this section, we describe studies on self-assembly that are based on alternative approaches, such as quantum mechanics (QM), molecular theory, elastic models, MC methods, and hybrid atomistic/CG schemes. The latter approach were exploited by Xiong et al. (2019), who in an effort to overcome the limitations of both atomistic and CG approaches, employed the hybrid-resolution model PACE (Han et al. 2010) to simulate the self-assembly of hundreds to thousands terminally capped FF peptides for microseconds. In PACE, the solvent is modeled using the MARTINI force field, while the solute is described at an atomistic level to capture important details such as H-bonds and peptide conformations. Extensive simulations enabled the authors to observe spontaneous assembly of peptides into doubled-layered patches further curving up into hollow vesicles and tubes. Moreover, PACE simulations revealed that only a few specific conformations are geometrically compatible with the assembled structures, among which is predominant a crystal-like structure rarely observed in simulations of single peptides in water solution but allowing an energetically favorable and ordered packing of FFs (Fig. 9.7). Remarkably, the reconfiguration of agglomerating peptides might allow escaping trapped states,
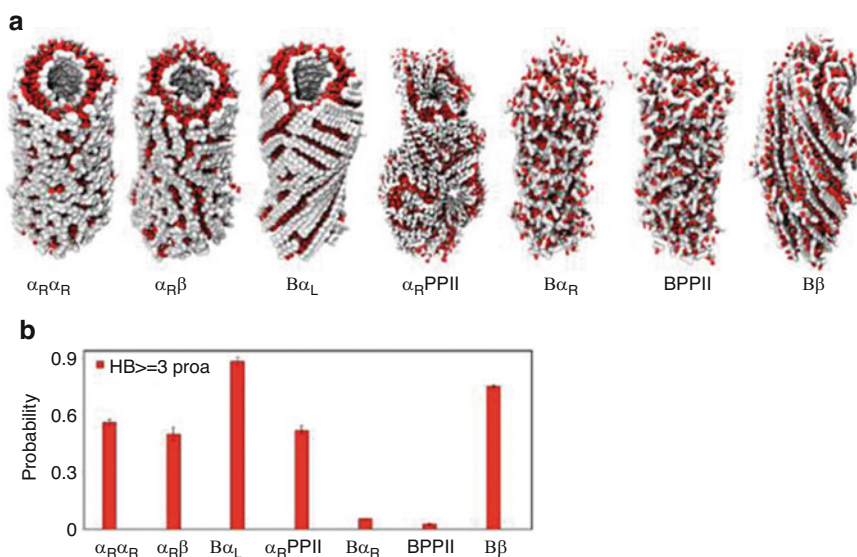
Fig. 9.7 (**a**) Representative structures of the major capped-FF conformations (top) and corresponding assembled supramolecular structures (bottom) when peptides were constrained to each of these conformations in self-assembly simulations. Backbones and side chains are shown as white and red ellipsoids, respectively. The crystal-like conformation is labeled Bα_L. (**b**) Probability of finding peptides involved in continuous H-bond chains (formed through repeated parallel stacking of at least three peptides) when they were fixed to different conformations. Adapted with permission from Xiong et al. (2019). Further permission related to the material excerpted should be directed to the ACS

thus facilitating either the formation of stable assembled structures or the transformation of the assemblies between different structures.

A different approach was sought by Deng et al. (Deng and Wang 2021), who developed a multiscale protocol by combining elastic theory with atomistic enhanced-sampling MD simulations to predict the β-sheet morphology of self-assembled short peptides. Using this method, the authors demonstrated a dependency of the aggregate morphology on the ratio of intersheet to intrasheet interaction. Meli et al. (2008) investigated the early stages of peptide aggregation using a mixed simulation scheme in which putative morphologies of the assemblies are identified by CG MC simulations, while all-atom MD simulations are used to analyze in detail possible pathways for the stabilization of oligomers. Simulations of the peptide GNNQQNY unveiled a hierarchical mechanism of assembly via the formation of stable parallel β-sheet dimers and identified in the formation of polar zipper motifs a key feature for the stabilization of initial oligomers.

Zaldivar et al. (2018) took advantage of a molecular theory to investigate the self-assembly of short amphiphiles blocks bearing a head-tail or head-linker-tail structure. By systematically exploring the effects of the molecular architecture and of the solvent-blocks affinity, the authors were able to reproduce micelle to fiber to lamella transitions by increasing the lengths of the tail/linker blocks or by decreasing the solvent-block affinity, both findings being in qualitative agreement with experiments.

Gazit and coworkers investigated the effect of metal ions on the inhibition of the self-assembly of the amyloid-like β-sheet dipeptide Fmoc-FF by means of experimental techniques complemented with DFT calculations (Ji et al. 2019). QM-based models make possible the investigation of phenomena, such as those involving metal bonding, for which the explicit inclusion of electronic degrees of freedom is crucial. In this case, calculations were employed to unravel the coordination environments of different metal ions within the Fmoc-FF-M^{n+} complexes undergoing self-assembly. This enabled rationalizing the structural transformations from an amyloid-like β-sheet into superhelix or random coil seen in experiments and prompted for a role of metal ions in inhibiting amyloid formation.

Elsawy and coworkers employed both MD and semiempirical QM simulations to demonstrate how a minimal structural modification in the nonassembling ultrashort ionic self-complementary tetrapeptide FEFK (Phe4), namely the replacement of phenylalanine (F) by phenylglycine (Phg), remarkably enhanced the stability of self-assembly into β-sheet nanofibers and induced hydrogelation (Wychowaniec et al. 2020). This was attributed to the prone-to-stacking orientation assumed by the aromatic rings in the PhgEPhgK peptide. Simulations were used to predict the contribution of specific non-covalent interactions (π-stacking of aromatic side chains and H-bonding between the backbone amides along the nanofiber axis) in stabilizing self-assembly of the shortest reported sequence of this class.

Far away from QM calculations in the time/length scale accessible by computational methods, dissipative particle dynamics simulations were employed by Sun et al. (2019) to assess the co-assembly capacity of different small molecules with the rhein-diphenylalanine peptide, which spontaneously assembles into spherical
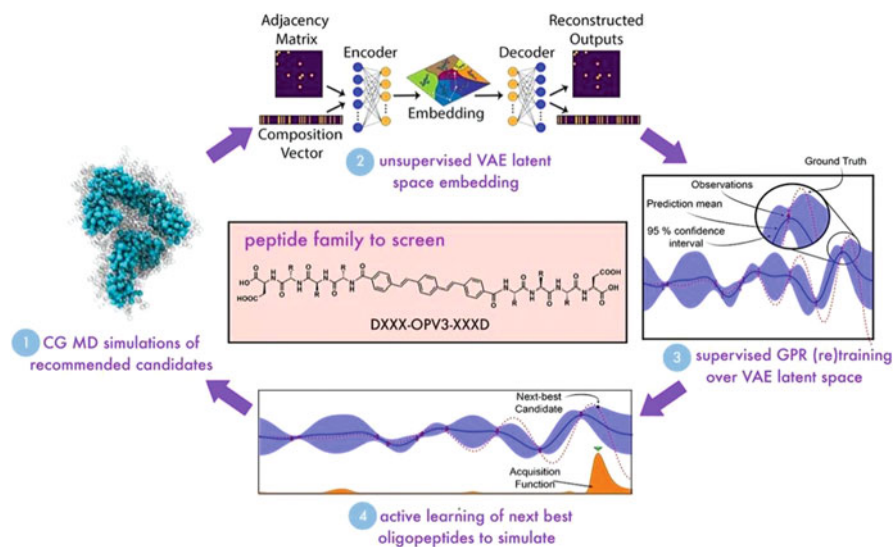
Fig. 9.8 Computational cycle for the discovery of optimally self-assembling DXXX-OPV3-XXXD peptides. Reprinted with permission from Shmilovich et al. (2020). Further permission related to the material excerpted should be directed to the ACS

nanocarriers. The protocol allowed to identify compounds with high capacity to be absorbed by the nanocarrier; subsequent in vivo experiments targeting tumor sites confirmed that these molecule-loaded nanoassemblies can improve drug biodistribution and antitumor efficacy compared to standard delivery methods.

MC simulations using a lattice model were performed by Song et al. (2004) to investigate concentration-dependent nanoarchitectures formed during self-assembly of $^DF^DF$ dipeptides in aqueous solution. A transition from unilamellar vesicles, to nanotubes, to porous and nonporous multilamellar structures with water in between the layers, and to porous bi-continuous phases are predicted at increasing concentrations. The former two morphologies were also detected by scanning electron microscopy. About 10 years later, Mu and Yu (2014) also employed MC simulations coupled to a CG model to perform a systematic investigation of the influence of hydrophobic interaction strength and temperature on the self-assembly of hydrophobic hexapeptides. Noteworthy, by varying these two parameters, the authors identified optimal values enabling the formation of ordered fibrillar nanostructures.

Ferguson and co-workers (Shmilovich et al. 2020) coupled Bayesian optimization with CG MD simulations to efficiently screen for DXXX-OPV3-XXXD oligopeptides (D: Asp; OPV3: oligophenylenevinylene oligomer (1,4-distyrylbenzene); X: natural aminoacid) able to assemble into pseudo-1D nanoaggregates featuring a good stacking of the electronically active π-cores (Fig. 9.8). Bayesian optimization works by traversing the chemical space exploiting information on all prior measurements to choose the "next-best" measurement to conduct. By direct simulation of only 2.3% of the 8000 possible tripeptide

sequences, the authors identify hit self-assembling molecules and new design rules governing this process, providing a platform that in principle could be applied to other peptide-based and peptide-like systems.

van Teijlingen and Tuttle (2021) employed active learning using a limited set of molecular descriptors and CG MD simulations to extend their search for peptides with high propensity to aggregation to sequences longer than three aminoacids. The authors developed a multistep approach: first, a limited set of molecular descriptors was estimated from the peptide sequences to perform a low-resolution screening of candidates with desirable target properties; next, a more computationally expensive approach was implemented by feeding the active learning algorithm with a larger number of molecular descriptors and the addition of data extracted from CG MD simulations performed on a few top-ranking peptides. By reducing the number of simulations to be performed by one/two orders of magnitude, the protocol led to a huge acceleration in the discovery process.

9.5 Conclusions and Perspectives

Developments in the field of peptide self-assembly promise to have a huge impact in the advancement of high-tech industry (e.g., natural fibrils mimicking mechanical properties of steel or silk), nanomedicine (e.g. designed nanostructures for in vivo recognition of markers or analytes), and biotechnology (e.g., controlled fabrication of 3D architectures working as analytical sensors and devices) (Colombo et al. 2007; Cui et al. 2010; Ung and Winkler 2011; Adler-Abramovich and Gazit 2014; Mandal et al. 2014; Panda and Chauhan 2014; Marchesan et al. 2015b; Wang et al. 2016; Frederix et al. 2018; Zhao et al. 2018; Lee et al. 2019; Chen and Zou 2019; Gupta et al. 2020; Cringoli et al. 2021). Importantly, peptide-based applications could extend beyond research niches to consumer goods due to the low cost of peptide synthesis at large scales. Furthermore, in the near future, they could include materials that possess not only unique passive physico-chemical properties but also active and functional ones, such as the ability to self-healing, respond to stimuli of different nature, and catalyze reactions.

Successful realization of these scenarios requires a deep knowledge of the intimate relationship between physico-chemical features of building blocks and the mechanical, thermodynamic, kinetic, optical, and electronic properties of their assemblies. Unfortunately, the prediction of the behavior of peptide self-assembly has been often based mainly on empirical observations. In an effort to gain a better understanding of the properties of these materials, in silico studies demonstrated their ability to elucidate the molecular factors underlying the self-assembly process and to establish qualitative and quantitative relationships between constituent peptides and their assembled supramolecular structures. Clearly, thoroughly sampling the conformational space associated to the self-assembly of a huge number of peptides remains probably the biggest challenge for any kind of computational technique (Colombo et al. 2007; Frederix et al. 2018). Fortunately, the tremendous

developments in both the hardware and software (GPU-computing and dedicated machines, to give two examples) and the computational algorithms are all boosting the exploration of self-assembly beyond the early stages of aggregation. These algorithms include new implementations of theoretical models, enhanced-sampling algorithms, and multiscale protocols allowing faster and more exhaustive conformational sampling, as well as study of out-of-equilibrium aggregates. Machine-learning algorithms provide a powerful way to expand the scope of computational studies, particularly if coupled with molecular simulations in active learning approaches. In addition to the sampling problem, more realistic models of the molecules under study, as well as of their reciprocal interactions and with the solvent, are desirable to catch the subtle determinants leading to divergent macro-structures from the assembly of very similar molecules. Optimization of force fields able to reproduce key features related to self-assembly, or exploitation of suitable properties to target the conformational distribution sampled during simulations, represent possible routes to improve the accuracy of computational modeling (Bochicchio and Pavan 2017; Frederix et al. 2018).

The next years hold promise to enable reproducing and predicting the overall morphologies arising from assembly of thousands of peptides, as well as identifying the manifold of kinetic pathways connecting them. Combining the information gathered from in silico studies with the knowledge obtained from experiments will enable us to unveil the mechanism governing the self-assembly of peptides. This in turn will pave the way for the design of materials with targeted assembled structures and properties, as well as new drugs to effectively provide new theranostics for applications spanning from cancer to amyloidosis.

References

Adler-Abramovich L, Gazit E (2014) The physical properties of supramolecular peptide assemblies: from building block association to technological applications. Chem Soc Rev 43:6881–6893

Alder BJ, Wainwright TE (1959) Studies in molecular dynamics. I. General method. J Chem Phys 31:459–466

Bera S, Xue B, Rehak P et al (2020) Self-assembly of aromatic amino acid enantiomers into supramolecular materials of high rigidity. ACS Nano 14:1694–1706

Bochicchio D, Pavan GM (2017) From cooperative self-assembly to water-soluble supramolecular polymers using coarse-grained simulations. ACS Nano 11:1000–1011

Bottaro S, Lindorff-Larsen K (2018) Biophysical experiments and biomolecular simulations: a perfect match? Science 361:355–360

Brooks CL, Case DA, Plimpton S et al (2021) Classical molecular dynamics. J Chem Phys 154: 100401

Brown N, Lei J, Zhan C et al (2018) Structural polymorphism in a self-assembled tri-aromatic peptide system. ACS Nano 12:3253–3262

Chakraborty P, Gazit E (2018) Amino acid based self-assembled nanostructures: complex structures from remarkably simple building blocks. ChemNanoMat 4:730–740

Chandler D (1978) Statistical mechanics of isomerization dynamics in liquids and the transition state approximation. J Chem Phys 68:2959

Chen J, Zou X (2019) Self-assemble peptide biomaterials and their biomedical applications. Bioact Mater 4:120–131

Clover TM, O'Neill CL, Appavu R et al (2020) Self-assembly of block heterochiral peptides into helical tapes. J Am Chem Soc 142:19809–19813

Colombo G, Soto P, Gazit E (2007) Peptide self-assembly at the nanoscale: a challenging target for computational and experimental biotechnology. Trends Biotechnol 25:211–218

Cringoli MC, Fornasiero P, Marchesan S (2021) Chapter 10. Minimalistic peptide self-assembly into supramolecular biomaterials. In: Azevedo HS, Mano JF, Borges J (eds) Soft matter series. Royal Society of Chemistry, Cambridge, pp 236–263

Cui H, Webber MJ, Stupp SI (2010) Self-assembly of peptide amphiphiles: from molecules to nanostructures to biomaterials. Biopolymers 94:1–18

Deng L, Wang Y (2021) Multiscale computational prediction of β-sheet peptide self-assembly morphology. Mol Simul 47:428–438

Eckes KM, Mu X, Ruehle MA et al (2014) β sheets not required: combined experimental and computational Studies of self-assembly and gelation of the ester-containing analogue of an Fmoc-dipeptide hydrogelator. Langmuir 30:5287–5296

Emamyari S, Kargar F, Sheikh-hasani V et al (2015) Mechanisms of the self-assembly of EAK16-family peptides into fibrillar and globular structures: molecular dynamics simulations from nano- to micro-seconds. Eur Biophys J 44:263–276

Fichman G, Gazit E (2014) Self-assembly of short peptides to form hydrogels: design of building blocks, physical properties and technological applications. Acta Biomater 10:1671–1682

Frederix PWJM, Ulijn RV, Hunt NT, Tuttle T (2011) Virtual screening for dipeptide aggregation: toward predictive tools for peptide self-assembly. J Phys Chem Lett 2:2380–2384

Frederix PWJM, Scott GG, Abul-Haija YM et al (2015) Exploring the sequence space for (tri-) peptide self-assembly to design and discover new hydrogels. Nat Chem 7:30–37

Frederix PWJM, Patmanidis I, Marrink SJ (2018) Molecular simulations of self-assembling bio-inspired supramolecular systems and their connection to experiments. Chem Soc Rev 47:3470–3489

Fu IW, Nguyen HD (2015) Sequence-dependent structural stability of self-assembled cylindrical nanofibers by peptide amphiphiles. Biomacromolecules 16:2209–2219

Fu IW, Markegard CB, Chu BK, Nguyen HD (2013) The role of electrostatics and temperature on morphological transitions of hydrogel nanostructures self-assembled by peptide amphiphiles via molecular dynamics simulations. Adv Healthc Mater 2:1388–1400

Fu IW, Markegard CB, Chu BK, Nguyen HD (2014) Role of hydrophobicity on self-assembly by peptide amphiphiles via molecular dynamics simulations. Langmuir 30:7745–7754

Fu IW, Markegard CB, Nguyen HD (2015) Solvent effects on kinetic mechanisms of self-assembly by peptide amphiphiles via molecular dynamics simulations. Langmuir 31:315–324

Gan Z, Wu X, Zhu X, Shen J (2013) Light-induced ferroelectricity in bioinspired self-assembled diphenylalanine nanotubes/microtubes. Angew Chem Int Ed 52:2055–2059

Garcia AM, Iglesias D, Parisi E et al (2018) Chirality effects on peptide self-assembly unraveled from molecules to materials. Chem 4:1862–1876

Garcia AM, Melchionna M, Bellotto O et al (2021) Nanoscale assembly of functional peptides with divergent programming elements. ACS Nano 15:3015–3025

Ghadiri MR, Granja JR, Milligan RA et al (1993) Self-assembling organic nanotubes based on a cyclic peptide architecture. Nature 366:324–327

Glielmo A, Husic BE, Rodriguez A et al (2021) Unsupervised learning methods for molecular simulation data. Chem Rev 121:9722–9758

Görbitz CH (2006) The structure of nanotubes formed by diphenylalanine, the core recognition motif of Alzheimer's β-amyloid polypeptide. Chem Commun (22):2332–2334

Guo C, Luo Y, Zhou R, Wei G (2012) Probing the self-assembly mechanism of diphenylalanine-based peptide nanovesicles and nanotubes. ACS Nano 6:3907–3918

Guo C, Luo Y, Zhou R, Wei G (2014) Triphenylalanine peptides self-assemble into nanospheres and nanorods that are different from the nanovesicles and nanotubes formed by diphenylalanine peptides. Nanoscale 6:2800

Guo C, Arnon ZA, Qi R et al (2016) Expanding the nanoarchitectural diversity through aromatic di- and tri-peptide coassembly: nanostructures and molecular mechanisms. ACS Nano 10:8316–8324

Gupta S, Singh I, Sharma AK, Kumar P (2020) Ultrashort peptide self-assembly: front-runners to transport drug and gene cargos. Front Bioeng Biotechnol 8:504

Hamley IW (2011) Self-assembly of amphiphilic peptides. Soft Matter 7:4122

Han W, Wan C-K, Jiang F, Wu Y-D (2010) PACE force field for protein simulations. 1. Full parameterization of version 1 and verification. J Chem Theory Comput 6:3373–3389

Harvey MJ, De Fabritiis G (2009) An implementation of the smooth particle mesh Ewald method on GPU hardware. J Chem Theory Comput 5:2371–2377

Hatip Koc M, Cinar Ciftci G, Baday S et al (2017) Hierarchical self-assembly of histidine-functionalized peptide amphiphiles into supramolecular chiral nanostructures. Langmuir 33:7947–7956

Huggins DJ, Biggin PC, Dämgen MA et al (2019) Biomolecular simulations: from dynamics and mechanisms to computational assays of biological activity. WIREs Comput Mol Sci 9:e1393

Jain AN, Cleves AE, Gao Q et al (2019) Complex macrocycle exploration: parallel, heuristic, and constraint-based conformer generation using ForceGen. J Comput Aided Mol Des 33:531–558

Jeon J, Mills CE, Shell MS (2013) Molecular insights into diphenylalanine nanotube assembly: all-atom simulations of oligomerization. J Phys Chem B 117:3935–3943

Ji W, Yuan C, Zilberzwige-Tal S et al (2019) Metal-ion modulated structural transformation of amyloid-like dipeptide supramolecular self-assembly. ACS Nano 13:7300–7309

Ji W, Yuan C, Chakraborty P et al (2020) Coassembly-induced transformation of dipeptide amyloid-like structures into stimuli-responsive supramolecular materials. ACS Nano 14:7181–7190

Katyal P, Mahmoudinobar F, Montclare JK (2020) Recent trends in peptide and protein-based hydrogels. Curr Opin Struct Biol 63:97–105

Kelly CM, Northey T, Ryan K et al (2015) Conformational dynamics and aggregation behavior of piezoelectric diphenylalanine peptides in an external electric field. Biophys Chem 196:16–24

Kholkin A, Amdursky N, Bdikin I et al (2010) Strong piezoelectricity in bioinspired peptide nanotubes. ACS Nano 4:610–614

Kutzner C, Páll S, Fechner M et al (2019) More bang for your buck: improved use of GPU nodes for GROMACS 2018. J Comput Chem arXiv:190305918. [physics, q-bio]

Lai C-T, Rosi NL, Schatz GC (2017) All-atom molecular dynamics simulations of peptide amphiphile assemblies that spontaneously form twisted and helical ribbon structures. J Phys Chem Lett 8:2170–2174

Lapshina N, Shishkin II, Nandi R et al (2019) Bioinspired amyloid nanodots with visible fluorescence. Adv Opt Mater 7:1801400

Lee O-S, Stupp SI, Schatz GC (2011) Atomistic molecular dynamics simulations of peptide amphiphile self-assembly into cylindrical nanofibers. J Am Chem Soc 133:3677–3683

Lee O-S, Cho V, Schatz GC (2012) Modeling the self-assembly of peptide amphiphiles into fibers using coarse-grained molecular dynamics. Nano Lett 12:4907–4913

Lee S, Trinh THT, Yoo M et al (2019) Self-assembling peptides and their application in the treatment of diseases. IJMS 20:5850

Liang L, Wang L-W, Shen J-W (2016) The self-assembly mechanism of tetra-peptides from the motif of β-amyloid peptides: a combined coarse-grained and all-atom molecular dynamics simulation. RSC Adv 6:100072–100078

Manandhar A, Kang M, Chakraborty K et al (2017) Molecular simulations of peptide amphiphiles. Org Biomol Chem 15:7993–8005

Mandal D, Nasrolahi Shirazi A, Parang K (2014) Self-assembly of peptides to nanostructures. Org Biomol Chem 12:3544–3561

Mansbach RA, Ferguson AL (2018) Patchy particle model of the hierarchical self-assembly of π-conjugated optoelectronic peptides. J Phys Chem B 122:10219–10236

Marchesan S, Easton CD, Kushkaki F et al (2012a) Tripeptide self-assembled hydrogels: unexpected twists of chirality. Chem Commun 48:2195–2197

Marchesan S, Waddington L, Easton CD et al (2012b) Unzipping the role of chirality in nanoscale self-assembly of tripeptide hydrogels. Nanoscale 4:6752

Marchesan S, Styan KE, Easton CD et al (2015a) Higher and lower supramolecular orders for the design of self-assembled heterochiral tripeptide hydrogel biomaterials. J Mater Chem B 3:8123–8132

Marchesan S, Vargiu A, Styan K (2015b) The Phe-Phe motif for peptide self-assembly in nanomedicine. Molecules 20:19775–19788

Mazza M, Notman R, Anwar J et al (2013) Nanofiber-based delivery of therapeutic peptides to the brain. ACS Nano 7:1016–1026

Meli M, Morra G, Colombo G (2008) Investigating the mechanism of peptide aggregation: insights from mixed Monte Carlo-molecular dynamics simulations. Biophys J 94:4414–4426

Moitra P, Subramanian Y, Bhattacharya S (2017) Concentration dependent self-assembly of TrK-NGF receptor derived tripeptide: new insights from experiment and computer simulations. J Phys Chem B 121:815–824

Monticelli L, Kandasamy SK, Periole X et al (2008) The MARTINI coarse-grained force field: extension to proteins. J Chem Theory Comput 4:819–834

Moreira IP, Scott GG, Ulijn RV, Tuttle T (2019) Computational prediction of tripeptide-dipeptide co-assembly. Mol Phys 117:1151–1163

Mu Y, Yu M (2014) Effects of hydrophobic interaction strength on the self-assembled structures of model peptides. Soft Matter 10:4956–4965

Muthusivarajan R, Allen WJ, Pehere AD et al (2020) Role of alkylated residues in the tetrapeptide self-assembly—a molecular dynamics study. J Comput Chem 41:2634–2640

Noé F, Tkatchenko A, Müller K-R, Clementi C (2020) Machine learning for molecular simulation. Annu Rev Phys Chem 71:361–390

Panda JJ, Chauhan VS (2014) Short peptide based self-assembled nanostructures: implications in drug delivery and tissue engineering. Polym Chem 5:4431–4449

Pappas CG, Shafi R, Sasselli IR et al (2016) Dynamic peptide libraries for the discovery of supramolecular nanomaterials. Nat Nanotech 11:960–967

Phillips JC, Hardy DJ, Maia JDC et al (2020) Scalable molecular dynamics on CPU and GPU architectures with NAMD. J Chem Phys 153:044130

Rissanou AN, Georgilis E, Kasotakis E et al (2013) Effect of solvent on the self-assembly of dialanine and diphenylalanine peptides. J Phys Chem B 117:3962–3975

Rozhin P, Charitidis C, Marchesan S (2021) Self-assembling peptides and carbon nanomaterials join forces for innovative biomedical applications. Molecules 26:4084

Salomon-Ferrer R, Götz AW, Poole D et al (2013) Routine microsecond molecular dynamics simulations with AMBER on GPUs. 2. explicit solvent particle mesh Ewald. J Chem Theory Comput 9:3878–3888

Sasselli IR, Moreira IP, Ulijn RV, Tuttle T (2017) Molecular dynamics simulations reveal disruptive self-assembly in dynamic peptide libraries. Org Biomol Chem 15:6541–6547

Scott GG, McKnight PJ, Tuttle T, Ulijn RV (2016) Tripeptide emulsifiers. Adv Mater 28:1381–1386

Scott GG, Börner T, Leser ME et al (2022) Directed discovery of tetrapeptide emulsifiers. Front Chem 10:822868

Shaw DE, Grossman JP, Bank JA et al (2014) Anton 2: raising the bar for performance and programmability in a special-purpose molecular dynamics supercomputer. In: SC14: international conference for high performance computing, networking, storage and analysis. IEEE, New Orleans, LA, pp 41–53

Shmilovich K, Mansbach RA, Sidky H et al (2020) Discovery of self-assembling π-conjugated peptides by active learning-directed coarse-grained molecular simulation. J Phys Chem B 124: 3873–3891

Sinibaldi A, Della Penna F, Ponzetti M et al (2021) Asymmetric organocatalysis accelerated via self-assembled minimal structures. Eur J Org Chem 2021:5403–5406

Song Y, Challa SR, Medforth CJ et al (2004) Synthesis of peptide-nanotube platinum-nanoparticle composites. Chem Commun (9):1044–1045

Sugita Y, Okamoto Y (1999) Replica-exchange molecular dynamics method for protein folding. Chem Phys Lett 314:141–151

Sun J, Zhang H, Guo K, Yuan S (2015a) Self-assembly of dipeptide sodium salts derived from alanine: a molecular dynamics study. RSC Adv 5:102182–102190

Sun Y, Qian Z, Guo C, Wei G (2015b) Amphiphilic peptides A_6K and V_6K display distinct oligomeric structures and self-assembly dynamics: a combined all-atom and coarse-grained simulation study. Biomacromolecules 16:2940–2949

Sun M, Zhang X, Gao Z et al (2019) Probing a dipeptide-based supramolecular assembly as an efficient camptothecin delivering carrier for cancer therapy: computational simulations and experimental validations. Nanoscale 11:3864–3876

Tamamis P, Adler-Abramovich L, Reches M et al (2009a) Self-assembly of phenylalanine oligopeptides: insights from experiments and simulations. Biophys J 96:5020–5029

Tamamis P, Kasotakis E, Mitraki A, Archontis G (2009b) Amyloid-like self-assembly of peptide sequences from the adenovirus fiber shaft: insights from molecular dynamics simulations. J Phys Chem B 113:15639–15647

Tang Y, Yao Y, Wei G (2020) Expanding the structural diversity of peptide assemblies by coassembling dipeptides with diphenylalanine. Nanoscale 12:3038–3049

Tuttle T (2015) Computational approaches to understanding the self-assembly of peptide-based nanostructures. Isr J Chem 55:724–734

Ung P, Winkler DA (2011) Tripeptide motifs in biology: targets for peptidomimetic design. J Med Chem 54:1111–1125

van Teijlingen A, Tuttle T (2021) Beyond tripeptides two-step active machine learning for very large data sets. J Chem Theory Comput 17:3221–3232

Vargiu AV, Iglesias D, Styan KE et al (2016) Design of a hydrophobic tripeptide that self-assembles into amphiphilic superstructures forming a hydrogel biomaterial. Chem Commun 52:5912–5915

Velichko YS, Stupp SI, de la Cruz MO (2008) Molecular simulation study of peptide amphiphile self-assembly. J Phys Chem B 112:2326–2334

Villa A, Peter C, van der Vegt NFA (2009) Self-assembling dipeptides: conformational sampling in solvent-free coarse-grained simulation. Phys Chem Chem Phys 11:2077

Wang J, Liu K, Xing R, Yan X (2016) Peptide self-assembly: thermodynamics and kinetics. Chem Soc Rev 45:5589–5604

Wang M, Zhou P, Wang J et al (2017) Left or right: how does amino acid chirality affect the handedness of nanostructures self-assembled from short amphiphilic peptides? J Am Chem Soc 139:4185–4194

Wang J, Peng C, Yu Y et al (2020) Exploring conformational change of adenylate kinase by replica exchange molecular dynamic simulation. Biophys J 118:1009–1018

Wychowaniec JK, Patel R, Leach J et al (2020) Aromatic stacking facilitated self-assembly of ultrashort ionic complementary peptide sequence: β-sheet nanofibers with remarkable gelation and interfacial properties. Biomacromolecules 21:2670–2680

Xiong Q, Jiang Y, Cai X et al (2019) Conformation dependence of diphenylalanine self-assembly structures and dynamics: insights from hybrid-resolution simulations. ACS Nano 13:4455–4468

Yang YI, Shao Q, Zhang J et al (2019) Enhanced sampling in molecular dynamics. J Chem Phys 151:070902

Yuan C, Li S, Zou Q et al (2017) Multiscale simulations for understanding the evolution and mechanism of hierarchical peptide self-assembly. Phys Chem Chem Phys 19:23614–23631

Zaldivar G, Samad MB, Conda-Sheridan M, Tagliazucchi M (2018) Self-assembly of model short triblock amphiphiles in dilute solution. Soft Matter 14:3171–3181

Zhao Y, Yang W, Chen C et al (2018) Rational design and self-assembly of short amphiphilic peptides and applications. Curr Opin Colloid Interface Sci 35:112–123

Zheng Y, Mao K, Chen S, Zhu H (2021) Chirality effects in peptide assembly structures. Front Bioeng Biotechnol 9:703004

Zhou P, Deng L, Wang Y et al (2016) Different nanostructures caused by competition of intra- and inter-β-sheet interactions in hierarchical self-assembly of short peptides. J Colloid Interface Sci 464:219–228

Chapter 10
Advanced Manufacturing of Peptide Nanomaterials

Essyrose Mathew, Edward Weaver, Raúl Cazoria-Luna, Emilia Utomo, Eneko Larrañeta, and Dimitrios A. Lamprou

Abstract This chapter aims to cover recent advanced research in peptide nanomaterials. Peptide research is gaining more interest as the knowledge around their role in pathophysiology becomes better understood. Peptides are highly specific, can have low toxicity and be easily scaled up for manufacture; however, they are prone to enzymatic degradation within the body and are poorly permeable through biological membranes, which can inhibit efficient and targeted delivery in the body. New manufacturing techniques are being explored to improve the stability of peptide formulations and the bioavailability of these formulations in the body. This chapter will cover three main manufacturing techniques: microfluidics, exploring the encapsulation and incorporation of the peptide into the nanoparticle shell as well as diagnostic uses; electrospinning and incorporation of proteins and peptides for drug delivery and other biomedical applications; and additive manufacturing and varying 3D printing techniques that can be combined with peptide formulations for effective drug delivery.

Keywords Nanomaterials · Drug delivery · Peptide · Microfluidics · Electrospinning · Additive manufacturing

10.1 Introduction

Peptides are considered building blocks of proteins in the human body. These peptides are essential for immune function, new tissue generation, skin and hormone regulation as well as cellular signalling (Pentlavalli et al. 2020). Peptides and their derivatives are highly versatile in nature due to the array of amino acid building blocks available. The structure of peptides can be modified to create self-assembling systems that are made up of amino acid building blocks, which spontaneously organise via intermolecular interactions into highly defined nanostructures in

E. Mathew · E. Weaver · R. Cazoria-Luna · E. Utomo · E. Larrañeta · D. A. Lamprou (✉)
School of Pharmacy, Queen's University Belfast, Belfast, UK
e-mail: d.lamprou@qub.ac.uk

response to physiological stimuli, e.g. temperature, enzymes, pH and ionic strength (Laverty 2018). The self-assembly process is key for fabricating cell-penetrating peptides, as it can play a vital role in allowing drugs to move across the cell membrane and transporting genes into the nucleus. Peptides can be synthesised using the solid-phase synthesis method, which is a well-established method providing high yields. Peptides possess high chemical versatility, which is due to the ability to change the amino acid R-group and allows for specific functionalities of peptides. These peptides can also be further functionalised easily by the addition of drugs, antibodies, enzymes and other compounds (Pentlavalli et al. 2020). A range of peptide architectures is present, including tapes, sheets, spheres tubes and fibres (Zelzer and Ulijn 2010). These different architectures can be created by modifying the amino acid sequence of the peptides.

Peptides provide a promising approach to the treatment of disease as they provide a bridge between naturally occurring biologics and chemically synthesised drugs. This allows peptides to be highly selective to drug targets, resulting in improved therapeutic efficacy and limiting adverse effects (Laverty 2018). However, the widespread use of peptide nanomaterials throughout medicine has been limited due to their high manufacturing cost and low bioavailability. This chapter aims to explore some of the novel manufacturing techniques of peptide nanomaterials for drug delivery, focusing on the areas of microfluidics, electrospinning and additive manufacturing.

10.2 Role of Microfluidics in Peptide Research

When peptide molecules are exposed to internal human environments, they are subject to massive decomposition due to inhospitable conditions and a vast array of proteases that are present, leading to a severely decreased bioavailability. Formulation of the peptides into a vesicle such as nanoparticles (NPs) would not only help circumvent this obstacle but could also provide the opportunity to provide a region-specific targeted therapy of the peptide(s) used. The potential of peptide therapy is limitless; it could give rise to crucial future chemotherapeutic treatments including monoclonal antibodies (MABs) that are sought after current therapies. Moreover, with future research, it could also be expanded to an oral formulation to decrease the invasiveness of administration.

The use of peptides in nanostructures can be classified into three categories:

1. Full encapsulation—The peptide will act as the active pharmaceutical ingredient (API) in the medicine and is encapsulated in a non-peptide material, such as in a lipid (e.g. liposomes) or polymers (e.g. PLGA, chitosan).
2. Peptide incorporation—The peptide is utilised as a part of the NP shell alongside another non-peptide material; the peptide could provide suitable epitopes for targeted delivery of an encapsulated API (Chan and Tay 2019).

3. Full peptide nanostructure—The nanostructure shell consists purely of the peptide chain.

Peptides, by nature, are large, complex molecules with various side-chain interactions, which often proves to be the major challenge during synthesis into a medicinal formulation. It has previously been observed that attempts to synthesise peptides into NPs without any additional apparatus have led to an infeasibly high distribution of the NPs (Chan and Tay 2019), which is an issue for the medical efficacy, as well as running into issues with NP morphology and size.

The microfluidics (MFs) process was developed in the 1980s (Lin et al. 2011) and has since gained much attention due to its extremely promising properties, such as end-product uniformity and the level of control that can be implemented during the procedure. The procedure has been gaining exponential traction due to properties that will be explained below. MFs have previously been used to encapsulate compounds into nano- or microparticles; however, the research into encapsulating biological molecules and peptides is incredibly sparse.

The usage of MFs during NP synthesis has been documented to assist with controlling particle size, shape and distribution (Zhang et al. 2016). These three properties are essential for determining the particle's pharmacokinetic properties, such as absorption and stability. MFs offer a more efficient and controlled synthesis of NPs and could prove to be more environmentally friendly due to the reduction of unwanted by-product synthesis and the possibility for solvent recycling (Yap et al. 2017). There is also the potential to convert the synthesis into a favourable continuous process compared to the classic batch manufacturing method used for general NP synthesis. A continuous process is far more advantageous, as it adheres to a more time and cost-efficient schedule (Jamkhande et al. 2019).

The synthesis of NPs using MFs consists of combining two variable-rate flows of liquids into a highly controlled, low-volume environment and conceiving NPs with concentrated distribution and usable sizes. The apparatus offers the means to alter various parameters during the process, which can provide rise to different outcomes for the final nanomaterial. Investigating total flow rate (TFR) is one of the main factors to consider during MFs, as it dictates the ratio and speed the fluids meet; however, there are so many other factors such as channel size, angle of flow, temperature, etc., to consider (KianvashRad et al. 2019), which must all be factored in when synthesising the optimal formulation. The actual MF chip (Fig. 10.1) is frequently synthesised from polydimethylsiloxane (PDMS), which is a recently developed polymer favoured in MFs due to the relative cost of synthesis compared to its predecessors, and its favourable properties such as high biocompatibility and low autofluorescence (Raj and Chakraborty 2020). The main drawback with this material when incorporating peptides into synthesis is the level of hydrophobicity, if this factor is left unaccounted for, it can lead to deposition within the MF channels and hence blockage.

There are multiple ways of synthesising the MF chip, for example, photolithography, micro-thermoforming, micro-injection moulding or 3D printing (3DP) (Van Den Driesche et al. 2018; Wei et al. 2017). Each method has its advantages and

Fig. 10.1 Basic microfluidic chip layout used for many synthetic methods when combining materials; it is possible to connect chips in series if a multi-step procedure is required
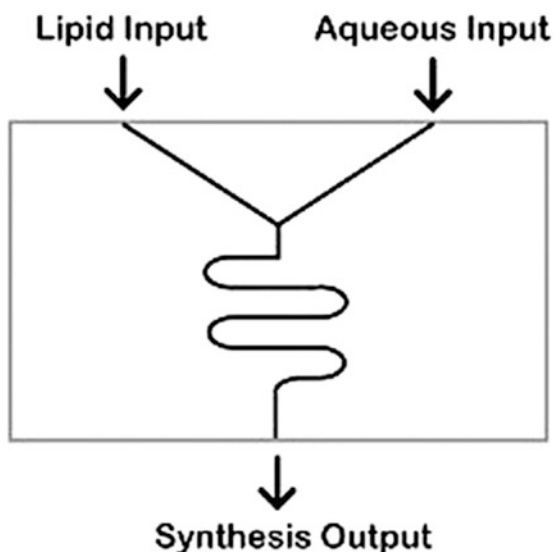
disadvantages; however, a field of great interest recently has been in 3DP [often referred to as additive manufacturing (AM)]. The AM field, in particular, has been researched extensively because of the multiple options available for printing, depending on what materials are being used. Specifically for printing MF devices, inkjet, stereolithography (SLA), fused deposition modelling (FDM) and two-photon polymerisation (TPP) (Waheed et al. 2016) have been used. 3D printed MF chips ensure that the chip has fortified connection ports to prevent rupture, allow for simple detector integration and, by the nature of their additive synthesis, also reduce material waste during construction (Chen et al. 2016), as well as provide an alternate source for the laboratory to obtain viable MF chips. If an identical chip can be printed within the research facility using low-cost polymeric materials, both supply chain issues and budget impact are minimised. By the use of 3DP, virtually any MF structure can be synthesised (although this is limited by the printer's resolution and materials), depending on the chip's needs; this allows a vast array of structures to be assayed to determine the optimal tubular structure for a molecule's synthesis. The constriction of space, coupled with a constant flow of materials past "chaos" points within the MF system, can ensure the self-assembly of NPs within the system (Kastner et al. 2015).

One massive advantage of using MFs is that the process can be performed at room temperature or in any controlled environment, which is especially significant for proteins due to temperature-associated denaturation.

10.2.1 Peptide Incorporation into NP Shell

The presence of peptides in an active NP shell is only possible by exploiting unnatural D-amino acid-based peptides, as the presence of natural peptides within the body triggers swift degradation by the multitude of proteases present. The unnatural D-amino acid-based peptides are not degraded this way and remain viable molecules (Chan and Tay 2019).

Multiple options are available when peptides are incorporated into the NP shell structure depicted in Fig. 10.2b. The first formulation consists of a shell fabricated solely from a peptide chain. The other option involves coupling the peptide chain with a non-peptide to form the external NP shell. One of the biggest advantages of peptide incorporation is that it allows for targeted NP delivery, as the active groups on the peptides can be chosen to complement interactive forces at a desired region (Spicer et al. 2018).

Peptide NP self-assembly can be employed using MFs, but it appears to be a very sensitive process, as the assembly does not occur properly if parameters such as TFR are subcritical or supercritical (Chan and Tay 2019). A similar trial using cyclo-diphenylalanine subunits to form peptide nanotubes found the same results that the TFR had a considerable effect upon the success of nanostructure formation (Arnon et al. 2016). It appears from this study that nanotube formation was hindered by the crystalline structure of the monomers being added, but it was suggested that without MFs, the process of peptide self-assembly would be far less successful. Nanofibrils created via this method could be employed as well as a healing mechanism, to relieve injury (Charmet et al. 2018) (Fig. 10.3).

By functionalising NPs with peptides, it has the potential to enhance the base pharmaceutical characteristics of an NP, for example, addition of hexahistidine (HIS6) chains in the NP shell improves the affinity of the NP towards certain metals, such as zinc or cadmium (Spicer et al. 2018; Ruiyi et al. 2017). Peptide–nanoparticle complexes already exist; however, a major drawback to their use is how difficult they are to synthesise. Various techniques of immobilising peptides, such as the use

● - Peptide Molecule

⌒ - Non-peptide Material
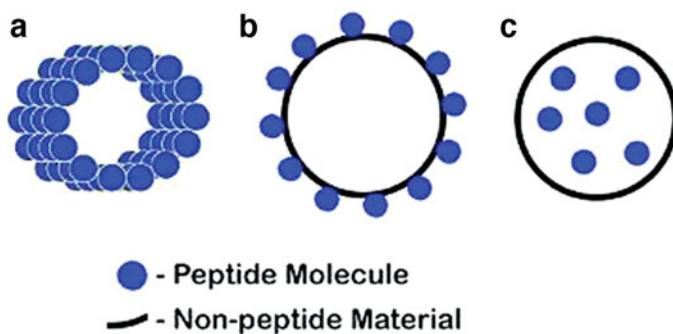
Fig. 10.2 Graphical representation of (**a**) Full peptide nanostructure (**b**) Peptide incorporation and (**c**) Full encapsulation
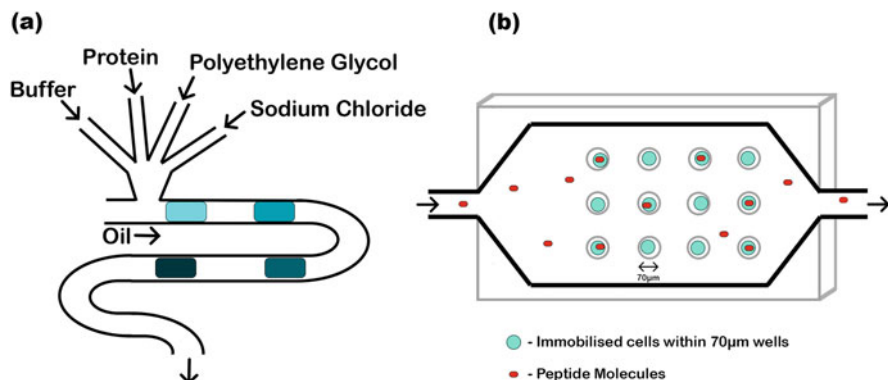
Fig. 10.3 (**a**) Simplified diagram of organ-on-a-chip by Charmet et al. (2018), displaying components used in a simulated in vivo assay (Charmet et al. 2018). (**b**) Microfluidic chip design by Safa et al. (2019) for cell trapping within 70 μm microwells to allow analysis of cell uptake of CPP (Safa et al. 2019)

of solid-binding peptides (Care et al. 2015) or Fmoc solid-phase addition (Di Pietro et al. 2016) onto the NP shell, have been shown to increase the local concentration of API (Xiao et al. 2016); however, it is frequently mentioned upon review that the process is expensive and lacks the capacity to be scaled up to an industrial level. Based on the evidence supporting the efficacy of MFs, it is strongly theorised could be employed to assist with this synthesis of these NPs (Spicer et al. 2018).

Research surrounding gold NPs has recently been of high interest, and one particular study attempted to attach peptide molecules, using MFs, onto a gold nanoparticle for specific delivery to amyloid plaques in the brain to treat Alzheimer's (Hassan et al. 2018). The study had success at molecule synthesis and determined that microfluidics offered means of producing a highly repeatable process, which is always favourable. The peptide epitopes present allow for region-specific delivery and are designed to allow the sufficient endosomal escape of the API to enact a therapeutic effect. The peptide-modified gold NP was previously available before microfluidics; however, it required an inefficient multi-step synthesis pathway, suggesting that MFs are the key to the future synthesis of the molecule. Another interesting use of peptide incorporation is ultra-short peptide (USP) chains within an NP shell to act as carriers for curcumin, which is another highly researched material currently (Ni et al. 2020). Once again, MFs are successfully employed to help manage the morphology and size of the NPs.

One of the main usages for peptide NPs is an imaging agent, as NPs offer advantageous properties for in vivo imaging compared to other imaging technologies and biotechnologies, most notably a better signal-to-noise ratio and a higher spectral resolution (Spicer et al. 2018). Release studies do not necessarily need to be performed for imagining NPs, as an endosomal escape is not a concern for the particle's role (Spicer et al. 2018). The presence of peptides within the NP can only further improve the specificity of the imaging, owing to the unique interactions of the

peptide moieties. MFs have the perfect opportunity to improve knowledge around this area of science, owing to the ease of performing multiple assaying within a limited time [allowing for efficient high-throughput screening (HTS)]. Positron emission tomography (PET) imaging using an MF-synthesised peptide imaging agent [fludeoxyglucose (F-FDG)] has already been shown to be successful (Liu et al. 2013). MF synthesis allowed simpler purification (due to reducing the multistep process required previously) and ameliorated heat and mass transfer, improving the yield of the process. The labelled peptides also had a preferential clearance time from the blood and target tissue compared to their non-peptide counterparts, increasing the safety profile of the imaging agent (Liu et al. 2013).

10.2.2 Peptide Encapsulation Within NP Shell

Polymers and lipids, whether synthetic or natural, are the most researched materials used for constructing the external shell of NPs for drug delivery applications. The choice of NP material when encapsulating cargo is very important, owing to individual interactions between the chosen materials. This is even more important for formulations involving peptides because the individual amino acid side chains present many potential problems or opportunities within the formulation. The use of poly(lactic-co-glycolic acid) (PLGA), as well as various lipids [e.g. DSPC (1,2-distearoyl-glycero-3-phosphocholine) or PC (phosphatidylcholine)], have been applied extensively to encapsulate materials into nano-sized structures. MFs have been employed using PLGA as the NP shell to encapsulate inorganic substances such as ibuprofen and doxorubicin (Rezvantalab and Keshavarz Moraveji 2019), but once again, its use with peptides is extremely limited. This may be due to peptides often complicating synthesis pathways (e.g. pH considerations, peptide geometry, mechanical properties, porosity), or it could be due to limitations of the MF system, such as negative interactions with the MF chip's environments (e.g. chip materials or pressure).

Incorporation of cholesterol into liposome preparations is essential to increase the stability of the NPs but can affect the encapsulation efficiency of the target material (Briuglia et al. 2015). The liposomes are amphiphilic in nature, so they can encapsulate both hydrophilic molecules, within the aqueous interior, or hydrophobic, within the lipid membrane (Spicer et al. 2018). Their amphiphilic property makes lipids ideal carriers for an assortment of materials.

Encapsulating the peptide would see the peptide within the NP being the API substance in the formulation depicted in Fig. 10.2c, so matters such as drug release profile and stability are essential to the medicine's activity. Encapsulation of proteins into microcapsules (similar to NPs but on a microscale, often in droplet form) using MFs recorded extremely high encapsulation efficiencies (84%) when encapsulating bovine serum albumin (BSA) (Pessi et al. 2014). This process is less challenging, in terms of encapsulation, due to the relative abundance of space within the microcapsules compared to NPs.

Due to the physical size of peptides, encapsulation within an NP is often challenging, as the resulting formulation consists of dispersed, non-uniform-sized NPs (Herrera Estrada and Champion 2015). Studies conducted previously have investigated BSA, ovalbumin (OVA) and insulin encapsulated into liposomes [consisting of PC, dipalmitoylphospatidylcholine (DMPC) and DSPC] using MFs to assist the process (Forbes et al. 2019). This study showed a relatively efficient encapsulation rate (circa 30%), as well as very promising particle size and polydispersity index (PDI) values, showing true promise to the process of MFs.

10.2.3   Other Uses of MFs in Peptide Research

MFs are not only used for synthetic means; it is often used as a diagnostic medium. Due to the ability to control the environment within the chip, a so-called "organ-on-a-chip" has been created to investigate protein interactions within a simulated environment (Charmet et al. 2018). Such studies can determine optimal conditions for protein manipulation and characterisation, providing a far simpler option than in vivo studies. Technologies such as this have already received patents, for example, the patent obtained by Fathollahi et al. allows simulation protein digestion using an MF device (Fathollahi et al. 2015). As mentioned previously, it is common practice for MF devices to integrate detectors within their structure. The detectors can be calibrated to monitor peptide progression throughout the MF system, recording the degradation pathway that is undergone.

One of the most ambitious studies involving MFs and peptides consisted of the co-delivery of a peptide (glucagon-like peptide-1) as well as a DPP-4 inhibitor peptide as a single formulation aimed for oral delivery. The encapsulation agents were PLGA, chitosan (also a promising encapsulating polymer) and hydroxypropylmethylcellulose acetylsuccinate (HPMC-AS). This project was ambitious for many reasons as it attempted to tackle the lack of oral peptide therapies available and employ a multi-level encapsulation formulation within an MF environment. The resultant molecule fell into the microparticles range with a diameter of roughly 60 μm, and expressed incredibly low PDI values (ranging between 0.08 and 0.34, depending on the NP composition) due to utilising the MF devices (Araújo et al. 2015).

As an example of high-throughput screening, MFs have been used to analyse the efficacy of cell-penetrating peptides (CPPs) on a molecular level. Using a multifaceted droplet trapping array within the MF chip structure, labelled CPP molecules were injected into the MF system to categorise the penetrating capacity of four separate peptides (Safa et al. 2019); by analysing the results of experiments such as this, it could unlock the key for delivering crucial APIs such as siRNA or enzyme inhibitors to targeted locations.

The MF environment has been capitalised to imitate peptide self-assembly to form supramolecular microfibres. These peptide microfibres could imitate naturally occurring storage and transport networks found within the body. If scaled up, it

could help solve the problem of artificial growth and repair (Méndez-Ardoy et al. 2020).

It is clear to see how many uses MFs already have within the scientific community and how it is allowing researchers to improve the standard of many of the procedures that are performed.

10.3 Applications of Protein and Peptide Electrospun Nanofibres

10.3.1 Fundamentals of Electrospinning

Nanofibres (NFs) are nanosystems that are morphologically described as structures with two similar dimensions and a third one considerably larger. NFs can be obtained from a wide range of materials and possess properties such as large surface area and the possibility of surface functionalisation and improved mechanical performance (Rasouli et al. 2019). Different methods have been used for the manufacturing of NFs (Table 10.1).

The most commonly used technique nowadays is electrospinning (ES). ES consists of three basic parts, a syringe with a metal nozzle, a high-voltage supplier and a collector (Fig. 10.4). A polymer solution or melt is forced to flow at a constant rate through the syringe using a pump. After connecting a high voltage to the end of the nozzle, the hemispherical surface of the liquid drop extends in a conical form, the Taylor cone. The value at which the repulsive electrostatic force overcomes the surface tension of the liquid must be reached to form a liquid jet, which will be solvent-dried and collected in a ground collector (Pelipenko et al. 2015).

The NFs size and morphology are conditioned by several parameters that can be classified as follows (Yıldız et al. 2020):

1. Solution parameters: polymer properties (e.g. concentration, viscosity, molecular weight) and polymers ratio for blends, and solvent properties (e.g. conductivity or surface tension) (Choi et al. 2015).
2. Process parameters: applied voltage, flow rate or capillary–collector distance. These must be finely adjusted based on the characteristics of the polymer or blend solution or melt (Choi et al. 2016). The collector plate must also be carefully selected to obtain the desired alignment for the NFs (Yıldız et al. 2020).
3. Ambient parameters: such as temperature and relative humidity (Pelipenko et al. 2013).

ES allows obtaining nanostructured NFs with low cost and high performance in the short times required to obtain the final product, which makes ES a versatile, scalable and reliable method (Yıldız et al. 2020; Khadka and Haynie 2012). The technique makes obtaining both two-dimensional and three-dimensional structures possible, and the latter have received great interest for scaffold manufacturing (Bucci

Table 10.1 Summary of the most used techniques for nanofibres manufacturing and their main advantages and disadvantages, according to several authors (Yıldız et al. 2020; Pelipenko et al. 2015; Garg et al. 2015)

Technique	Advantages	Disadvantages
Drawing	Inexpensive; Easy; Easily modified	Time consuming; Not for all polymers; Very low single fibers; Poor shape
Template synthesis	Wide range of possible materials, including semiconductors and carbon; Possible to manage fibre diameter	Time consuming; Laboratory scale; Not one by one continuous nanofibre
Phase separation	Inexpensive; Easy; One by one and mass productions possible	Time consuming; Not for all polymers; Laboratory scale; Lack of structural stability; Difficult to maintain porosity
Self-assembly	Simple; Easy; One by one and mass production possible	Time consuming; Laboratory scale; Not control over the fibres dimensions; Not for all polymers
Fibre mesh	Large surface area; High cell attachment; Rapid diffusion of nutrients	Lack of structural stability; Difficult to maintain porosity; Not for all polymers; Low loading ability
Fibre-bonding	Easy; Inexpensive; High surface area; Control over pore size	Poor mechanical integrity; Residual organic solvents; Poor structural stability; Difficult to maintain porosity
Melt blown	Smooth surface texture; Large surface area; Low fibre diameter.	Roping; Shot Fly
Electrospinning	Easy; Inexpensive; Versatile; High entrapment efficiency; Control over pore geometry (size and distribution); High surface area; Wide range of bioactive material can be encapsulated; High permeability; Usually in form of non-woven web: possible alignment	Not all polymers; Not applicable for cell seeding or cell infiltration
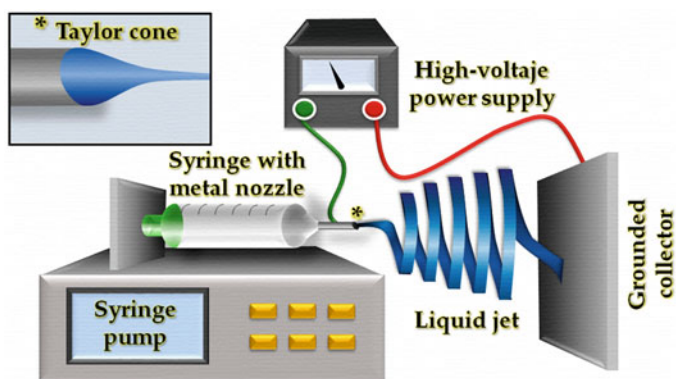
Fig. 10.4 Scheme of the electrospinning system

et al. 2021). Besides, this technique may allow the manufacturing of NFs from materials that do not naturally assemble into fibre-shaped structures (Nuansing et al. 2013). Compared to other methods of manufacturing NFs, those obtained by ES have several advantages, like a larger surface area, higher permeability, the possibility to hold electrical charges and higher porosity, being possible to adjust pore size and distribution and surface properties by thoroughly selecting the parameters of the process (Yıldız et al. 2020).

10.3.2 Proteins and Peptides in Electrospinning

Protein and peptide-based NFs possess some useful features that have attracted interest for their use in many fields (e.g., drug delivery, tissue engineering, biosensors or the food industry). As proteins and peptides are the basic building blocks of living organisms, they are non-cytotoxic and exhibit high biocompatibility. They can mimic the endogenous extracellular matrix (ECM), providing a stabilizing and protecting the environment for different cell types. They are also biodegradable, so it is possible, for example, to remove protein-based grafts without surgical intervention. Isoelectric properties of peptides and proteins may enhance the loading of drugs that are difficult to load in synthetic polymer NFs. Moreover, these NFs can mimic various tissues and organs, a really useful feature for tissue engineering (Yıldız et al. 2020; Dror et al. 2008).

ES has the advantage of enhancing and even inducing the assembly of materials into NFs, including those that do not naturally assemble into NFs, which also applies to peptides and proteins. Nevertheless, the ES of peptides and proteins can be changeling as they lack the viscoelastic properties of traditionally used polymers, which is essential for stable ES. However, peptides and proteins have been shown to be able to form electrospun NFs, blended with other polymers but also in their absence if the parameters have appropriately adjusted (Nuansing et al. 2013; Dror et al. 2008). In order for this to be achievable, some conditions must be studied with the aim of preserving the structure of proteins and peptides during ES, as they are easily degraded and/or denaturalised. Temperature, pH or the use of organic solvents are some examples of such conditions, and the process must be monitored and controlled to avoid undesired modifications in the peptide structure (Yıldız et al. 2020).

Different approaches exist to obtaining protein and peptide-based electrospun NFs (Fig. 10.5). One approach consists of including the peptide or protein in the solution, alone or blended with other polymers before ES, thus obtaining directly electrospun peptide or protein-based NFs. Another approach is modifying the NF-forming polymer by grafting proteins or peptides onto its functional groups, before or after ES, thus obtaining protein-functionalised NFs (Yıldız et al. 2020; Khadka and Haynie 2012; Bucci et al. 2021). Using proteins or peptides for direct electrospinning usually causes the proteins to release from the NFs after administration. The same happens if proteins or peptides are used to functionalise NFs by
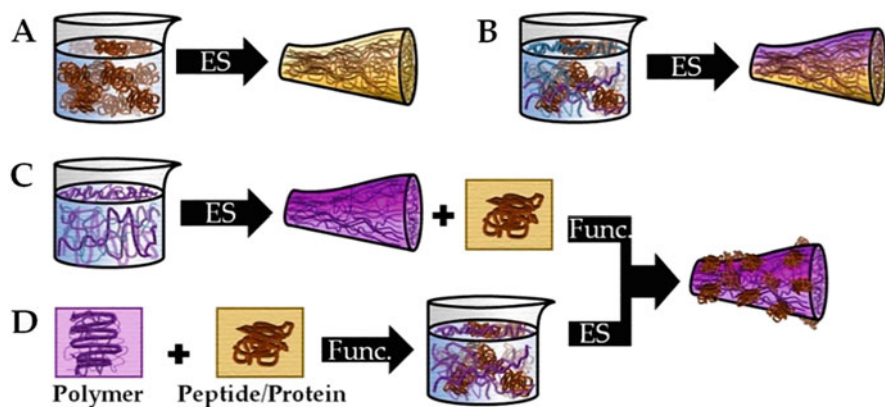
Fig. 10.5 Different approaches to obtain electrospun protein-based fibres: electrospinning (ES) of a protein or peptide solution (**a**); ES of a polymer/protein blend (**b**); ES of a polymer solution prior to functionalisation of the resulting fibre with a protein or peptide (**c**) and functionalisation of a polymer with a protein or peptide and then, ES to obtain a protein-functionalised fibre (**d**)

physical adsorption. This can be an advantage in protein delivery systems but a drawback in tissue engineering, as the scaffold could disintegrate. On the contrary, covalent linking of the peptide molecule to the polymer allows for obtaining more robust materials, keeping the protein trapped in the NF and improving the properties of the native polymer (Bucci et al. 2021). To this end, chemical reactions occur in accessible (or terminal) amino acids through either the acid or the amino group. Likewise, reactions can also occur through accessible amino acid side chains (Archibong et al. 2016).

The proteins used for ES can be classified into three large groups (Yıldız et al. 2020):

1. Plant-derived proteins are usually available in large amounts and are inexpensive. They are also biocompatible and biodegradable as they are part of the diet. The main drawback of using plant-derived proteins is the need to use various crosslinking agents. Some examples are zein, pea protein, soy protein or gluten (Akhmetova and Heinz 2021).

2. Animal-derived proteins are also readily available and inexpensive, although less than plant-derived proteins. Their convenient construction makes them interesting candidates for ES, and, due to their chemical cues, they play an important role in controlling cell behaviour. However, they exhibit higher immunogenic potential than plant-derived proteins, sometimes causing animal-borne diseases. Some examples are collagen, casein, silk fibroin, haemoglobin, fibrinogen, lactoferrin, bovine serum albumin, elastin, gelatin and keratin (Babitha et al. 2017).

3. Synthetic peptides are nowadays emerging to overcome some of the drawbacks of naturally occurring peptides. Among their advantages, they can be manufactured by selecting the composition sequence of amino acids. This may lead to new unique and diverse peptides with a wide range of properties.

10.3.3 Applications of Protein and Peptides in Electrospinning

Protein and peptide-based electrospun NFs are promising tools for various biomedical applications (Fig. 10.6), such as tissue engineering and drug delivery systems (e.g. vaginal, rectal, transmucosal or oral) (Yıldız et al. 2020). These materials can also be applied for other biomedical (e.g. biosensors and sutures) and non-biomedical applications (e.g. filtration devices or textile and food industry), among others (Khadka and Haynie 2012; Wen et al. 2017).

10.3.3.1 Drug Delivery

Peptides and proteins are considered the most functional molecules in the organism; they participate in most of the body's processes: as catalysts in biochemical reactions, modulating cell proliferation or regulating metabolic or signalling pathways. A wide variety of diseases is the consequence of a protein deficiency or dysfunction, such as cancer, inflammatory processes or metabolic disorders. Furthermore, due to their complex structure, they have the advantage of being highly selective with the site of action, which reduces adverse effects. For this reason, interest in proteins as therapeutic agents is growing. However, the administration of proteins is problematic since the large size of the molecules and the presence of ionisable groups hinders their absorption through membranes, leading to low bioavailability. Therefore, it is necessary to use the parenteral route, which is frequently rejected by the patient. In addition, aggressive media, such as gastric fluid, lead to the alteration of proteins by denaturalisation, misfolding or aggregation, which can reduce their effectiveness or make them toxic (Moreira et al. 2020).

In the recent years, the use of nanotechnology to produce drug delivery systems has aroused great interest in the field of health science, and nanosystems have allowed for solving traditional problems such as low solubility and bioavailability of drugs and have led to efficient targeting of drugs to the disease site. For this reason, NFs can be used as drug delivery systems for proteins and peptides and can greatly improve the efficacy of said substances since the NFs can encapsulate and protect them from harsh environments, thus increasing their stability. Furthermore, proteins can be efficiently targeted to the site of action, increasing their
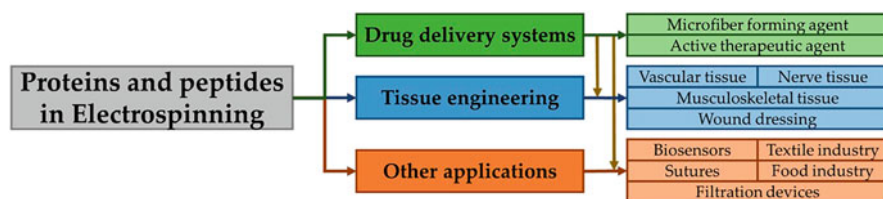
Fig. 10.6 Scheme of the applications of protein and peptide-based electrospun nanofibres
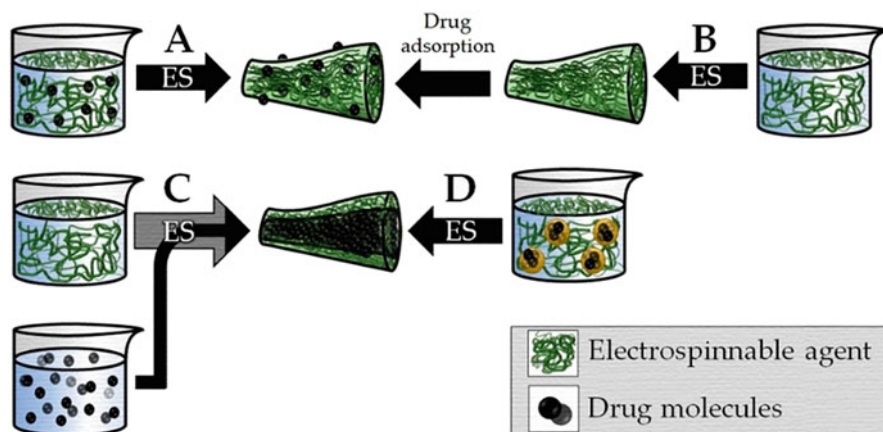
Fig. 10.7 Different approaches to obtain protein-based drug delivery systems: electrospinning (ES) of a solution containing the fibre-forming agent and the drug (**a**), ES of the fibre-forming agent and then, functionalization through drug adsorption (**b**), coaxial ES with the drug in the core and the fibre-forming agent in the sheath (**c**) and ES of an emulsion containing the drug in the internal phase and the fibre-forming agent in the external phase (**d**)

bioavailability. Some examples include the delivery of lysozyme or insulin from mucoadhesive buccal electrospun patches (Lancina III et al. 2017; Edmans et al. 2020) or the oral administration of capsules containing electrospun NFs loaded with melatonin (Vlachou et al. 2019). In the same field, peptides and proteins have been explored as excipients for obtaining NFs for drug delivery systems. Among the advantages of proteins for this purpose, it is important to highlight their high biocompatibility, high cell adhesion and high drug-loading capacity compared to synthetic polymeric NFs (Yıldız et al. 2020).

Drugs can be loaded into NFs in different ways due to the versatility of the ES method (Fig. 10.7), and the method selected to load the drug into the NF strongly conditions release kinetics, which can be very advantageous to obtain formulations with carefully selected release profiles. The simplest option is blending ES, in which the drug is solved or dispersed in the polymer solution or melt, then used to produce loaded NFs. In order to ensure the even distribution of the drug in the NF matrix, crosslinkers are generally required. However, the drug can also be loaded onto previously prepared NFs via physical absorption, covalent binding or other surface-treatment methods. Other innovative loading methods include coaxial ES, based on the use of concentric needles: the solution for the nucleus is forced to pass through the inner nozzle, while the one for the sheath is forced to pass through the outer nozzle. The solution used for the shell must be spinnable, but the core does not have to be. This produces a concentric flow of the solutions that, after electrospinning, produces of coaxial NFs. This means that using coaxial ES, the drug can be encapsulated within a hollow polymer or protein NF. The same structure can also be obtained through emulsion ES, but instead of a polymer solution, an emulsion is directly electrospun, with the electrospinnable agent dissolved in the

external phase and the drug in the internal phase (Ye et al. 2019; Han and Steckl 2019).

10.3.3.2 Tissue Engineering

In tissue engineering, it is especially important that the materials provide an environment similar to what cells would find in the original tissue. The natural ECM provides a suitable structure and contains the chemical and mechanical signals necessary for the development of cells, including differentiation, morphogenesis and homeostasis. The composition of the matrix is variable depending on the tissue, but it can be mimicked by peptide or protein NFs to achieve cell adhesion, differentiation or growth of a specific type of cell. The cellular response will therefore depend on the protein composition of the NFs, but also on their physical characteristics such as hydrophobicity, surface charge, porosity, roughness and the presence of functional surface elements. The spatial arrangement of the fibres in 2D or 3D structures also conditions the cellular response (Arslan et al. 2014). The most explored protein in this area is undoubtedly collagen. Nevertheless, other proteins have been and are being studied, such as fibrinogen or silk fibroin, among others (Khadka and Haynie 2012). Tissue engineering scaffolds may also act as drug delivery systems of therapeutic proteins, improving their performance in the graft area. Among the proteins to be delivered from tissue engineering scaffolds, it is worth highlighting growth factors delivery, which has been widely used in tissue engineering as they promote cell growth, differentiation and migration. These factors, if administered directly, suffer from low stability and short half-life, and overexposure to them may lead to harmful side effects, such as cancer development. The research therefore focuses on obtaining drug-delivery devices for tissue engineering capable of preserving their bioactivity while providing controlled release after the graft implantation. Besides, if different growth factors are combined in the same graft, they will perform distinct functions and improve the function of the graft (Moreira et al. 2020). The main applications of electrospun proteins in tissue engineering are the following:

1. Scaffolds for vascular tissue engineering: NFs based on proteins are emerging for vascular tissue engineering due to their ability to stimulate the differentiation and proliferation of structurally organised tissues, facilitating the rapid restoration of the endothelium at the intervention site (Cheraghi and Pooria 2019). Although synthetic vascular prostheses have been vastly used for replacing large calibre arteries, they fall in replacing small calibre vessels, causing thrombosis or blockage caused by plaque deposition. In this scenario, using protein-based grafts obtained through ES can be a good choice, as they can mimic the natural vessels. In this field, Zhang et al. developed small bilayer caliber vascular scaffolds obtained by knitting collagen. They mimicked the natural lumen of the vessels by adding an electrospun-collagen layer, and their results demonstrated good mechanical properties and superior biological performance (Zhang et al. 2018).

2. Scaffolds for nerve tissue engineering: in large injuries peripheral nerve regeneration and functional recovery usually fail. The most common treatment method is the use of autografts, but the requirement for a second surgery and the lack of available donor nerves fuel the search for better alternatives. It has been stated that this deficient nerve regeneration is due to a poor formation of the ECM, which could be solved by pre-filling the nerve channels with ECM proteins, but also to the lack of neurotrophic factors in the distal nerve section, responsible for providing an adequate microenvironment for regeneration. It has been proposed to deliver neurotrophic factors to the injury site, which may promote myelination of nerve fibres and proliferation of Schwann cells. With this aim, electrospun scaffolds containing proteins (such as collagen) mimicking the ECM and/or delivering neurotrophic factors have been proposed as grafts for nerve tissue regeneration in large injuries (Prabhakaran et al. 2013; Chew et al. 2007).

3. Scaffolds for musculoskeletal tissue engineering: Including bone, cartilage, ligament and skeletal muscle tissue engineering. Since the ideal matrix must reproduce the form and function of the natural ECM, electrospun proteins are considered an excellent option, as NFs can also be oriented at will, with various porosities and functionalisation options (Khadka and Haynie 2012). For instance, decellularised ECM has been blended with polycaprolactone (PCL) to obtain scaffolds of aligned electrospun muscle-mimicking NFs, which supported satellite cell growth, myogenic protein expression and also myokine production (Patel et al. 2019).

4. Wound dressing scaffolds: The wound healing process depends on the patient's physiology and the infections that can delay re-epithelialisation. Electrospun wound dressings have many properties suitable for accelerating wound healing, such as good physical and mechanical protection, high surface area, and correct gas exchange. In addition, if made with proteins, they are cytocompatible and biodegradable and mimic the structure of the native ECM. Finally, antimicrobial substances can be added to prevent possible infections (Akhmetova and Heinz 2021); it is important to highlight the use of antimicrobial peptides, which are molecules expressed by multicellular organisms to regulate the immune response against infections. These mediators are essential in wound healing and have attracted interest for their inclusion in wound dressings, and may be especially beneficial against antibiotic-resistant bacterial strains (Amariei et al. 2018).

10.3.3.3   Other Applications

Biosensors contain biological detectors (usually enzymes), sensitive components for a concrete analyte. The high surface area of NFs can be used to obtain materials functionalised with these substances, allowing the detection of different analytes. The most studied biosensors for biomedical purposes are glucose biosensors through the immobilisation of glucose-oxidase in, for example, silk fibroin or polyvinylalcohol/β-cyclodextrin polymer NFs (Khadka and Haynie 2012; Kim and Kim 2020). Other applications include biosensors for chlorophenol monitoring, a

substance that supposes a significant environmental risk. These biosensors were prepared by functionalizing polyvinyl alcohol (PVA) electrospun NFs with *Trametes versicolor* laccase, and showed a good immobilisation of the enzyme, with good sensibility against chlorophenols (Liu et al. 2011).

The functionalisation of sutures is also a promising field for peptides in ES. Surgical site infections occur in wounds produced by invasive surgery, affecting 2–5% of patients in the United States, and can even lead to death. With this backdrop, Chen et al. developed sutures functionalised with the peptide pam3CSK4 and 25-hydroxyvitamin D3. The sutures were prepared by coaxial ES, the sheath containing 25-hydroxyvitamin-D3 and poly(ε-caprolactone) and the core containing pam3CSk4 and pluronic F-127. These sutures led to an increase in the production of the antimicrobial peptide cathelicidin, which could reduce the incidence of surgical site infections (Chen et al. 2017). Ye et al. proposed other sutures, containing Heparin to promote local blood supply in Achilles tendon reconstruction. These sutures contained heparin and poly-L-lactic-acid in the sheath and polyamide in the core and showed to induce the expression of growth factors TGF-β1 and VEGF, improving healing and regeneration compared to non-functional sutures (Ye et al. 2018).

Other applications of protein-based electrospun NFs have been proposed. David et al. developed monolithic electrospun membranes and filtration devices containing keratin and polyamide to treat wastewaters (David et al. 2020). Neu et al. manufactured electrospun films containing Zein/ethylcellulose NFs loaded with cinnamaldehyde essential oil. These films could be useful for developing water-resistant packages and prolong the shelf-life of *Agaricus bisporus* (Niu et al. 2020). Although a field yet to be explored, smart textiles obtained by ES technology have been previously described in order to obtain eco-friendly next-generation textiles with novel functionalities, such as solar harvesting, improved mechanical properties, and self-cleaning (Ding 2017). The functionalisation of these systems with proteins and peptides could lead to a greater improvement in the properties.

10.4   Role of Additive Manufacturing in Peptide Research

Additive manufacturing, or 3D Printing, is a promising manufacturing set of technologies for producing medical devices and drug delivery systems (Ventola 2014; Mathew et al. 2019a, 2020; Larrañeta et al. 2020; Farmer et al. 2020). This technology was first introduced by Charles Hull in the 1980s (Ventola 2014). It was during the early 2000s when medical applications of 3D printing started to be reported. These applications were focused on the preparation of custom prosthetics and dental implants (Park et al. 2019). Nowadays, 3D printing technology has been widely explored to fabricate dental and orthopaedic prostheses, pharmaceutical dosage forms and drug delivery systems, such as tablet and drug-eluting implants (Ali et al. 2020). The term additive manufacturing defines the process of fabrication involving layer-by-layer sequential deposition of materials (Mathew et al. 2020). In

order to print 3D objects, a computer-aided design (CAD) model is required. The main advantage of additive manufacturing technology is its flexibility in terms of the shape and size of the objects that can be produced and the wide variety of materials that can be used. These factors allow to prepare individualised dosage forms adapted to patient's needs (Ali et al. 2020). Additive manufacturing is not a single technique but a family of manufacturing technologies. The main technologies that are used for biomedical applications are: fused deposition modelling (FDM), stereolithography (SLA), selective laser sintering (SLS), digital light processing (DLP) and semi-solid extrusion (EXT) (Mathew et al. 2020; Shahrubudin et al. 2019). These technologies have been previously used for protein peptide delivery. The following sections will describe the main characteristics of these types of 3D printing and their applications in the protein/peptide delivery field.

10.4.1 Fused Deposition Modelling

FDM was first developed in 1991 and has become one of the most common types of 3D printing techniques. The reasons behind this are its low cost, acceptable print quality and its ability to print products using a wide variety of materials (Mathew et al. 2020; Alhnan et al. 2016). These materials are thermoplastic polymers produced using hot melt extrusion. In this way, drugs or active molecules can be pre-loaded into the filaments prior to the 3D printing process. As a consequence, the thermostability of the drug cargo needs to be assessed in order to avoid any degradation during the extrusion (Warsi et al. 2018). During the printing process, filaments are extruded and deposited layer by layer through a heated nozzle to obtain a 3D object (Fig. 10.8a). Another advantage offered by FDM is the possibility to print using more than one material as some FDM machines are equipped with two
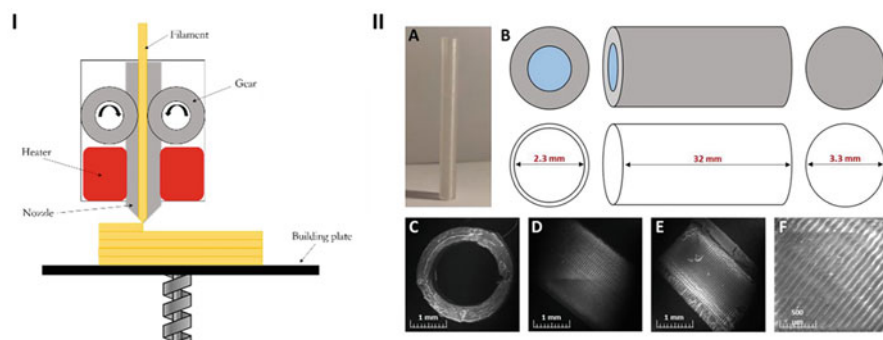

Fig. 10.8 Schematic of a FDM 3D printer (**a**). Characteristics of the FDM-printed PLA implant for the delivery of single-domain antibodies (**b**). Photograph of the implant (A) and implant design and dimensions (B). SEM images of the implant's open end (C), outer surface (D), and inner surface (E, F). Reproduced with permission from Nicolas et al. (2020)

nozzles (Shahrubudin et al. 2019). However, mass production using this technique could be challenging as it needs a longer time to prepare objects (Mathew et al. 2020; Stewart et al. 2018). Commonly used polymers in FDM for biomedical applications are poly(lactic acid) (PLA), thermoplastic polyurethane (TPU), poly(propylene) (PP), poly(vinyl alcohol) (PVA) or poly(ether ether ketone) (PEEK) among many others (Zhang et al. 2020). However, there are reports of other types of polymers used for this purpose such as pharmaceutical excipients (Shaqour et al. 2020).

Several studies have reported using FDM techniques to prepare solid dosage forms, medical devices or implantable drug delivery systems (Farmer et al. 2020; Xu et al. 2019; Goyanes et al. 2015; Stewart et al. 2020a, b; Domínguez-Robles et al. 2019, 2020; Mathew et al. 2019b; Martin et al. 2021). However, including therapeutic proteins and or peptides within a drug delivery system prepared using FDM is challenging. The main limitation is the high temperature required to prepare 3D objects using this technique. The native structure of proteins and peptides will be affected by these temperatures. It has been reported that the denaturation of proteins at temperatures higher than 80 °C is considered irreversible (Matsuura et al. 2015). Therefore, this significantly limits the number of thermoplastics that can be directly combined with proteins and peptides. In order to use FDM to prepare protein/peptide-loaded drug delivery systems, biomolecules should be loaded separately after completing the 3D printing of the drug delivery system. These systems are normally reservoir-type drug delivery systems. A few examples of this type of system can be found in the literature. Stewart et al. reported the use of FDM to prepare reservoir type implantable devices using PLA. In this work, two small drug models were tested (methylene blue and ibuprofen). However, this system can be applied for protein or peptide delivery as the cargo was loaded after the printing process (Stewart et al. 2018, 2020a). Following a similar approach, Nicolas et al. developed a reservoir type implantable device using PLA that was subsequently loaded with single-domain antibodies (Nicolas et al. 2020) (Fig. 10.8b). This approach was followed as this type of antibodies reversibly unfolds at higher temperatures. Additionally, the use of FDM for the preparation of reservoir-type oral dosage forms has been reported (Melocchi et al. 2015; Linares Blasco et al. 2019) by several authors. In order to optimise the loading process, Linares et al. used a special type of 3D printer equipped with an FDM printing head and an EXT system. In this way, the drug-containing formulation was added with the EXT system to avoid exposure to high temperatures (Linares Blasco et al. 2019).

10.4.2   Stereolithography and Digital Light Processing

This type of 3D printing technology was first commercialised in 1988 by Charless Hull, called SLA-250 (Ventola 2014). SLA process is based on photopolymerisation. The material used to prepare 3D printable objects are resins containing photo-sensitive polymers that solidify after being irradiated with light of specific wavelengths (Fig. 10.9a). Initially, the build-plate moves towards the
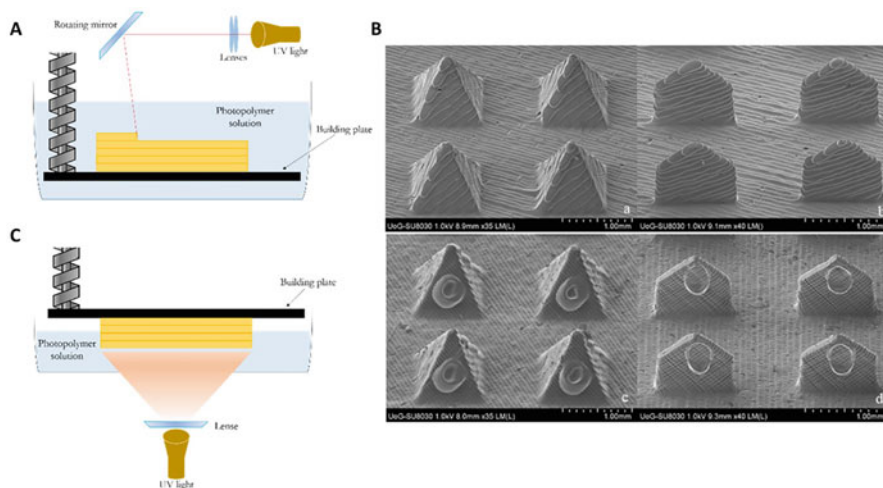
Fig. 10.9 Schematic of SLA 3D printer (**a**). SEM image of two types of microneedles produced using SLA printer. Pristine microneedles (**a**, **b**) and coated with an insulin formulation (**c**, **d**). Schematic of DLP 3D printer (**c**). Reproduced with permission from Economidou et al. (2019)

surface of the liquid photopolymer. Afterwards, the plate is lowered according to the defined layer height while the laser is applied. This process continues until the object is fully formed (Park et al. 2019). The final product obtained is subsequently treated to complete the photopolymerisation of the object, improve its mechanical integrity and remove unreacted monomers/initiators (Warsi et al. 2018). SLA is equipped with digitally controlled mirrors that direct the light to defined spots to start the photopolymerisation reaction. Liquid photopolymer resins contain normally low-molecular weight polyacrylates or epoxy macromers (Alhnan et al. 2016). In order to load drugs or other active compounds, these molecules are dissolved/dispersed in the resin polymer prior to the printing process. The main advantage of SLA is the ability to produce objects with high accuracy and resolution. Additionally, this technique does not involve high temperatures, which are preferable for thermolabile drugs or biomolecules, such as proteins and peptides (Park et al. 2019; Alhnan et al. 2016). However, the use of certain types of photoinitiators can cause potential toxicity issues. However, researchers have developed new alternatives to avoid this issue (Bagheri and Jin 2019).

SLA is frequently utilised in the preparation of solid oral dosage forms (Healy et al. 2019; Robles-Martinez et al. 2019) and drug-loaded medical devices (Xu et al. 2021; Asikainen et al. 2019). These systems contain small drug molecules rather than biomolecules. In order to include peptides or proteins within the printed object, these compounds should be mixed with the monomers and initiators. This can potentially lead to the denaturation of the protein. In order to achieve protein/peptide delivery by using SLA, researchers prepare drug delivery systems using this technique prior to loading the protein/peptide cargo. A good example of this is the use of

SLA to prepare microneedles. Microneedles are minimally invasive devices capable of bypassing the outermost layer of the skin to enhance drug delivery (Larraneta et al. 2016; Donnelly and Larrañeta 2018; Hutton et al. 2018; Larrañeta et al. 2016). These devices can be used to deliver proteins and peptides through the skin. SLA has been previously used by Economidou et al. to prepare microneedle patches for intradermal insulin delivery (Economidou et al. 2019). Solid microneedle arrays were prepared using a commercially available resin and subsequently coated with an insulin solution (Fig. 10.9b). The system was successfully applied in vivo using a diabetic mice model. The animals treated with the insulin-containing patches showed good hypoglycaemia control and lower glucose levels compared to subcutaneous insulin injections. In order to improve these results, Economidou et al. developed a microelectromechanical system equipped with hollow microneedles prepared using SLA for insulin delivery (Economidou et al. 2021). In this work, microneedle arrays were hollow in order to be able to inject insulin in a painless way. The combination of hollow microneedles with an electrical pump allows a higher degree of control over insulin dosing. This system was successfully evaluated using an animal model showing better results in terms of glycaemic control over subcutaneous injections.

In addition to use SLA for printing protein/peptide devices, some studies have used SLA to prepare scaffolds containing growth factors for bone regeneration dispersed into photopolymerisable resins (Lee et al. 2011). Growth factors were previously encapsulated into PLGA microparticles and subsequently dispersed into the resin. The resulting scaffolds were prepared using poly(propylene fumarate). These studies suggested that the growth factors loaded into the resulting scaffolds were not only not affected by the resin, but they were able to stimulate bone formation in a preclinical rat model (Lee et al. 2011).

Finally, SLA can be used to prepare scaffolds that can be subsequently loaded with cells. These cells will be producing and secreting active peptides/proteins. Kang et al. developed scaffolds prepared with a commercial resin (Ormocomp®) that were loaded with a mixture of cells and alginate gel (Kang et al. 2014). The scaffold was prepared and subsequently the cell/alginate mixture was injected into the internal space of the scaffold framework. These scaffolds were designed to treat Parkinson's disease as the loaded cells could produce and release dopamine. The study showed that the device could provide dopamine release for up to 8 weeks.

Besides SLA, DLP is an alternative 3D printing technology using photopolymerisation. The main principle of DLP is similar to SLA (Shahrubudin et al. 2019). Instead of using a laser as the source of light, DLP employs a conventional light source, such as an arc lamp with a liquid crystal display panel (Fig. 10.9c) (Park et al. 2019; Shahrubudin et al. 2019). This technology allows simultaneous irradiation of a single layer allowing the curing of polymers at once. This system results in faster fabrication processes than SLA, which cures the polymers point-to-point moving the laser beam. Besides, this technique is also able to produce high-resolution objects (Park et al. 2019).

DLP technique was utilised to prepare solid oral dosage form (Madzarevic et al. 2019). However, some alternative studies focused on the delivery of peptides/

proteins using DLP printing can be found in the literature. Lim et al. prepared microneedles loaded with an anti-wrinkle small peptide (acetyl-hexapeptide 3) using DLP 3D printing. In this case, the peptide was directly included in the resin (Lim et al. 2021). The peptide was stable within the resin that contained two biocompatible polymers (polyethylene glycol diacrylate and vinyl pyrrolidone). The versatility of 3D printing allowed the authors to prepare microneedles arrays adapted to the face of the patients.

10.4.3 Selective Laser Sintering (SLS)

SLS technology is quite similar to SLA as both require the use of a laser in the printing process. Instead of using liquid resin, SLS used powder material such as metals, ceramics, composites and polymers (polyamides, polystyrenes, and polycarbonates) (Shahrubudin et al. 2019; Alhnan et al. 2016). The layers of powder are fused together to form a 3D object through a laser-based sintering process (Fig. 10.10a). The sintered powder forms part of the final object while the unsintered powder has to be removed at the end of the printing process (Alhnan et al. 2016). This technique is widely used for tissue engineering and non-medical manufacturing industries (Warsi et al. 2018). The first research on the application of SLS 3D printing technology in the pharmaceutical field was carried out by Awad et al. (2019). In this study, mono-drug and multi-drugs pellets were able to be prepared using paracetamol and ibuprofen as model drugs (Awad et al. 2019). The applications of SLS for drug delivery purposes are mainly limited to small drug molecules. The delivery of proteins or peptides using this technology remains relatively unexplored. SLS relies on thermal processing using a laser, accordingly this can be problematic for biomolecules, as it has been described before. However, a few studies have reported methods to achieve protein loading into SLS-printed objects. These methods commonly rely on coating previously printed objects. Vaithilingam
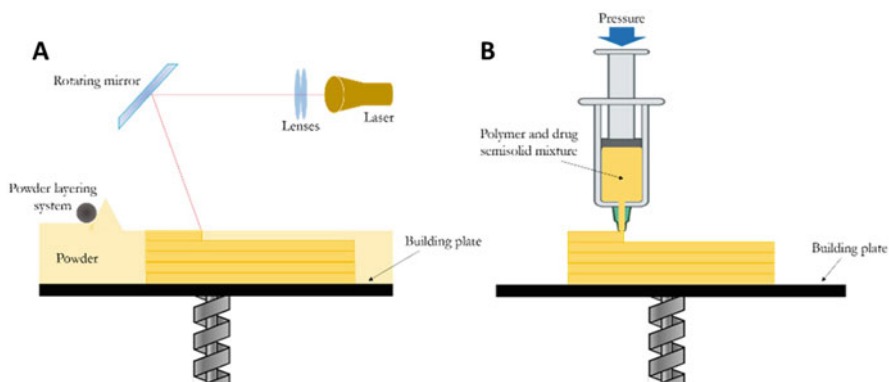
Fig. 10.10 Schematic of SLS (**a**) and EXT (**b**) printing

et al. described a methodology to coat proteins into Ti_6Al_4V metallic implants by using phosphonic acid-based self-assembled monolayers (Vaithilingam et al. 2015). Amphiphilic compounds containing head and tail groups are used to prepare these monolayers.

10.4.4 Semi-solid Extrusion (EXT)

Semi-solid extrusion is a nozzle-based deposition 3D printing technology. The starting material used in this process is a viscous (semi-solid) mixture, either paste or gel. EXT systems can use thermoplastic materials as they are equipped with heating systems. The materials used for printing are commonly known as "inks". These "inks" can be made of a wide variety of materials ranging from aqueous gels containing cells/biomolecules, ceramic slurries or mixtures of drugs with thermoplastics. The "inks" are placed in a syringe and further extruded by applying pneumatic pressure creating objects by adding layers of material (Park et al. 2019) (Fig. 10.10b). In order to form 3D objects, inks have to solidify after being deposited. For this purpose, gel-type materials are commonly used for EXT. These gels can be either physical gels or chemical gels. Physical gels are formed by non-covalent interactions (Economidou et al. 2021; Larrañeta and Isasi 2012; Larrañeta et al. 2014; Permana et al. 2021), while chemical gels (or covalent gels) are formed when the hydrogel structure is covalently cross-linked (Larrañeta et al. 2018a, b; Tekko et al. 2020). Chemical crosslinking can be easily achieved by using photocurable polymers in the gel and irradiating the 3D object during the printing process (GhavamiNejad et al. 2020). Therefore, the "inks" plays a critical part in the printing process. EXT is a suitable alternative to print products containing thermosensitive drugs (Warsi et al. 2018).

This type of 3D printing is commonly used in bioprinting. For this particular application, the "inks" are called "bioinks" as they are loaded with cells and biomolecules. These solutions form gels during the printing process. EXT is a highly versatile technique allowing to print a wide variety of objects such as solid dosage forms, medical devices and scaffolds for tissue engineering (Alhnan et al. 2016; Seoane-Viaño et al. 2021). However, this 3D printing technique presents some limitations. The resolution of the object obtained is lower than other 3D printing techniques considering the size of the typical nozzle is 0.4–0.8 mm. Moreover, shrinking and deformation may occur during the drying process. Also, printed objects may collapse if the previous layer has not completely dried and therefore is not able to sustain the successive layers.

The use of EXT for protein/peptide delivery has been reported by using several approaches. One of the common approaches is to load biomolecules in previously printed 3D objects using a coating procedure. Kim et al. followed this procedure to load bone morphogenic protein-2 into PCL/PLGA scaffolds functionalised with a heparin-dopamine conjugate (Kim et al. 2014). Bone morphogenic protein-2 is an FDA-approved biomolecule used for anterior lumbar interbody fusion. Scaffolds
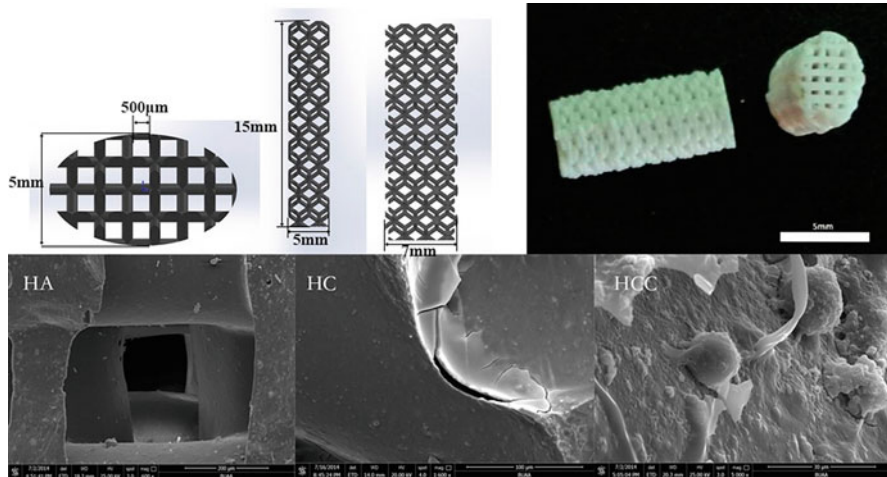
Fig. 10.11 Design and SEM images of hydroxyapatite scaffolds. The SEM pictures correspond to non-coated scaffolds (HA), scaffolds coated with collagen (HC) and scaffolds coated with micro-particles containing bone morphegnic protein-2 (HCC). Reproduced with permission from Wang et al. (2016)

prepared using EXT printing loaded with this protein could providing sustained releases of this biomolecule for up to 1 month. Additionally, it was reported that the resulting scaffolds stimulated bone formation and mineralisation when applied in vivo into rat femurs. Alternatively, Kang et al. followed a similar procedure to load bone morphogenic protein-2 into 3D printed scaffolds (PCL/PLGA) by using a dip-coating method using a hydrogel coating formulation (fibrin and hyaluronic acid) (Kang et al. 2011). However, the release profiles were shorter than the ones described previously (up to a few days vs. 1 month). An alternative to prevent quick burst releases from biomolecules loaded on the surface of 3D-printed objects is to load the protein/peptide cargo inside micro/nanoparticles (Wang et al. 2016). Wang et al. developed 3D printed hydroxyapatite scaffolds coated with bone morphogenic protein-2 encapsulated into hyaluronic acid/collagen microspheres (Fig. 10.11). They achieved the release of this protein during periods of time of up to 21 days (Wang et al. 2016). Similarly, Lee et al. incorporated two different types of growth factors encapsulated into PLGA microspheres for cartilage regeneration (Park et al. 2016). For this purpose, a porous PCL scaffold was prepared and microparticle suspensions were added subsequently into the microchannels of PCL scaffolds. These scaffolds could release these growth factors at a different rate over periods of up to 40 days. Moreover, these scaffolds were implanted into the knees of an animal model (sheep). These scaffolds could promote the regeneration of the cartilaginous matrix of the meniscus.

Encapsulating proteins inside micro/nanoparticles can protect the biomolecule cargo from external stresses that can appear during the 3D printing process. Tarafder et al. described a method to incorporate growth factor encapsulated into PLGA

microspheres inside PCL microfibres (Tarafder et al. 2016). Microspheres were incorporated inside the scaffold as they were mixed with PCL powder before printing. The printing process was carried out by melting PCL (120 °C). PLGA did not melt at that temperature.

Finally, another way of achieving protein/peptide delivery from EXT 3D-printed objects is by encapsulating cells within the 3D structure. These cells should be capable of producing and releasing biomolecules. Several authors have followed this approach to develop functional 3D-printed scaffolds/implants. A good example of this approach was developed by Kim et al. (2019). In this work, pancreatic tissue-derived bioink was developed and applied to EXT printing. Moreover, the bioink was capable of secreting insulin as a response to external glucose concentration.

10.5   Conclusion and Future Directions

Concerning peptides, it has been shown that MFs offer the opportunity to improve many aspects of synthesis, but there are still gaps in our knowledge surrounding the subject, simply due to a lack of research. It appears that MFs not only produce a more efficacious and repeatable product, it can do this while being more economically and resource-wise efficient. It has been shown multiple times how much more control can be added to a process by MFs, frequently leading to a superior product and, as discussed, there are numerous applications for MFs and their potential to be scaled up to an industrial level making it an important field of research to be exploited. The current knowledge of the specific interactions between peptides and the MF process (e.g. deposition, peptide-solvent reactions) must be developed more, as this plays a key role in determining the feasibility of the overall process.

There is room for evidence-lead creativity when designing aspects such as the MF chip design as this could prove key to optimising the use of the chip; depending on its use; however, it is safe to say that current applications are having high levels of success. An exciting trait surrounding MFs is their capacity to be scaled up by the addition of multiple chips in parallel, once an optimal process is established, allowing the development of molecules on an industrial level.

Nanofibres obtained by electrospinning have proven to be very useful and versatile tools for multiple applications thanks to features such as their high surface area, excellent mechanical properties, tunable porosity, and capacity to load drugs or the possibility of adjusting properties to the needs thanks to the versatility of the manufacturing technique. Peptides and proteins, on the other hand, have many promising advantages, such as high availability and biocompatibility, and the ability to mimic the natural extracellular matrix or their involvement in most physiological and physiopathological processes. However, more research is required since proteins are difficult to electrospin. Nonetheless, the results to date are very promising in multiple fields, such as drug delivery and tissue engineering. However, protein-based electrospun nanofibres have also proven useful for other industries, such as the food, textile or environmental industries. This gives an idea of the number of

different applications that can be given to these materials and, therefore, of the potential they present.

Concerning 3D printing, EXT presents the most research around the topic of peptides and 3D printing, although EXT provided lower resolution capabilities in comparison to the other 3D printing methods mentioned and are more prone to deformation post printing. Many of the current studies using EXT involve printing of a base structure and then adding a peptide solution or coating the printed product in a peptide solution post-printing. Peptides can be directly printed by encapsulating them in a polymer prior to printing. Overall, a majority of current research on 3D printing and peptide delivery shows the 3D printing of a base structure with post-printing process such as coating or extrusion of peptide formulation on the printed structure, as the main methods for peptide addition. In future, increased focus on the direct printing of peptides into the 3D structure would be beneficial so that production times can be reduced and simplified, especially using the techniques of SLA and DLP where direct inclusion of peptides within the resin has been proven.

In view of the results obtained to date, the need to advance in the research of peptide nanomaterials is evident, since most of the investigations are in the initial phase of development. It is therefore necessary to corroborate that the benefits of these materials will be effective at the time of their application and not only in preliminary investigations. These novel methods of peptide nanomaterial manufacture show a promising future for the widened advocation of peptide research in medicine.

References

Akhmetova A, Heinz A (2021) Electrospinning proteins for wound healing purposes: opportunities and challenges. Pharmaceutics 13(1):4

Alhnan MA, Okwuosa TC, Sadia M et al (2016) Emergence of 3D printed dosage forms: opportunities and challenges. Pharm Res 33(8):1817–1832

Ali A, Ahmad U, Akhtar J (2020) 3D printing in pharmaceutical sector: an overview. Pharmaceutical Formulation Design-Recent Practices

Amariei G, Kokol V, Boltes K et al (2018) Incorporation of antimicrobial peptides on electrospun nanofibres for biomedical applications. RSC Adv 8(49):28013–28023

Araújo F, Shrestha N, Shahbazi MA et al (2015) Microfluidic assembly of a multifunctional tailorable composite system designed for site specific combined oral delivery of peptide drugs. ACS Nano 9(8):8291–8302

Archibong E, Foster A, Caldwell K et al (2016) Synthesis, characterization, and electrospinning of novel polyaniline–peptide polymers. Appl Mater Today 4:78–82

Arnon ZA, Vitalis A, Levin A et al (2016) Dynamic microfluidic control of supramolecular peptide self-assembly. Nat Commun 7(1):13190

Arslan E, Garip IC, Gulseren G et al (2014) Bioactive supramolecular peptide nanofibers for regenerative medicine. Adv Healthcare Mater 3(9):1357–1376

Asikainen S, van Bochove B, Seppälä JV (2019) Drug-releasing biopolymeric structures manufactured via stereolithography. Biomed Phys Eng Exp 5(2):025008

Awad A, Fina F, Trenfield SJ et al (2019) 3D printed pellets (miniprintlets): a novel, multi-drug, controlled release platform technology. Pharmaceutics 11(4):148

Babitha S, Rachita L, Karthikeyan K et al (2017) Electrospun protein nanofibers in healthcare: a review. Int J Pharm 523(1):52–90

Bagheri A, Jin J (2019) Photopolymerization in 3D printing. ACS Appl Polymer Mater 1(4): 593–611

Briuglia ML, Rotella C, McFarlane A et al (2015) Influence of cholesterol on liposome stability and on in vitro drug release. Drug Deliv Transl Res 5(3):231–242

Bucci R, Vaghi F, Erba E et al (2021) Peptide grafting strategies before and after electrospinning of nanofibers. Acta Biomater 122:82–100

Care A, Bergquist PL, Sunna A (2015) Solid-binding peptides: smart tools for nanobiotechnology. Trends Biotechnol 33(5):259–268

Chan KH, Tay JJJ (2019) Advancement of peptide nanobiotechnology via emerging microfluidic technology. Micromachines 10(10):627

Charmet J, Arosio P, Knowles TPJ (2018) Microfluidics for protein biophysics. J Mol Biol 430(5): 565–580

Chen C, Mehl BT, Munshi AS et al (2016) 3D-printed microfluidic devices: fabrication, advantages and limitations—a mini review. Anal Methods 8(31):6005–6012

Chen S, Ge L, Gombart AF et al (2017) Nanofiber-based sutures induce endogenous antimicrobial peptide. Nanomedicine 12(21):2597–2609

Cheraghi M, Pooria A (2019) A review: nanofibrous scaffold in possible prevention and treatment of coronary artery disease. Biotechnol Appl Biochem 66(4):478–483

Chew SY, Mi R, Hoke A et al (2007) Aligned protein–polymer composite fibers enhance nerve regeneration: a potential tissue-engineering platform. Adv Funct Mater 17(8):1288–1296

Choi JS, Kim HS, Yoo HS (2015) Electrospinning strategies of drug-incorporated nanofibrous mats for wound recovery. Drug Deliv Transl Res 5(2):137–145

Choi J-H, Lee J, Oh B-K (2016) Nanomaterial-based in vitro analytical system for diagnosis and therapy in microfluidic device. BioChip J 10(4):331–345

David PS, Karunanithi A, Fathima NN (2020) Improved filtration for dye removal using keratin–polyamide blend nanofibrous membranes. Environ Sci Pollut Res 27(36):45629–45638

Di Pietro P, Zaccaro L, Comegna D et al (2016) Silver nanoparticles functionalized with a fluorescent cyclic RGD peptide: a versatile integrin targeting platform for cells and bacteria. RSC Adv 6(113):112381–112392

Ding B (2017) Electrospinning, fibers and textiles: a new driving force for global development. e-Polymers 17(3):209–210

Domínguez-Robles J, Martin NK, Fong ML et al (2019) Antioxidant PLA composites containing lignin for 3d printing applications: a potential material for healthcare applications. Pharmaceutics 11(4):165

Domínguez-Robles J, Mancinelli C, Mancuso E et al (2020) 3D printing of drug-loaded thermo-plastic polyurethane meshes: a potential material for soft tissue reinforcement in vaginal surgery. Pharmaceutics 12(1):63

Donnelly RF, Larrañeta E (2018) Microarray patches: potentially useful delivery systems for long-acting nanosuspensions. Drug Discov Today 23(5):1026–1033

Dror Y, Ziv T, Makarov V et al (2008) Nanofibers made of globular proteins. Biomacromolecules 9(10):2749–2754

Economidou SN, Pere CPP, Reid A et al (2019) 3D printed microneedle patches using stereolithography (SLA) for intradermal insulin delivery. Mater Sci Eng C 102:743–755

Economidou SN, Uddin MJ, Marques MJ et al (2021) A novel 3D printed hollow microneedle microelectromechanical system for controlled, personalized transdermal drug delivery. Addit Manuf 38:101815

Edmans JG, Murdoch C, Santocildes-Romero ME et al (2020) Incorporation of lysozyme into a mucoadhesive electrospun patch for rapid protein delivery to the oral mucosa. Mater Sci Eng C 112:110917

Farmer Z-L, Domínguez-Robles J, Mancinelli C et al (2020) Urogynecological surgical mesh implants: new trends in materials, manufacturing and therapeutic approaches. Int J Pharm 585:119512

Fathollahi B, Farinas JA, Chow AW et al (2015) Method and apparatus for performing peptide digestion on a microfluidic device. Google Patents

Forbes N, Hussain MT, Briuglia ML et al (2019) Rapid and scale-independent microfluidic manufacture of liposomes entrapping protein incorporating in-line purification and at-line size monitoring. Int J Pharm 556:68–81

Garg T, Rath G, Goyal AK (2015) Biomaterials-based nanofiber scaffold: targeted and controlled carrier for cell and drug delivery. J Drug Target 23(3):202–221

GhavamiNejad A, Ashammakhi N, Wu XY et al (2020) Crosslinking strategies for 3D bioprinting of polymeric hydrogels. Small 16(35):2002931

Goyanes A, Chang H, Sedough D et al (2015) Fabrication of controlled-release budesonide tablets via desktop (FDM) 3D printing. Int J Pharm 496(2):414–420

Han D, Steckl AJ (2019) Coaxial electrospinning formation of complex polymer fibers and their applications. ChemPlusChem 84(10):1453–1497

Hassan N, Cordero ML, Sierpe R et al (2018) Peptide functionalized magneto-plasmonic nanoparticles obtained by microfluidics for inhibition of β-amyloid aggregation. J Mater Chem B 6(31):5091–5099

Healy AV, Fuenmayor E, Doran P et al (2019) Additive manufacturing of personalized pharmaceutical dosage forms via stereolithography. Pharmaceutics 11(12):645

Herrera Estrada LP, Champion JA (2015) Protein nanoparticles for therapeutic protein delivery. Biomater Sci 3(6):787–799

Hutton AR, Quinn HL, McCague PJ et al (2018) Transdermal delivery of vitamin K using dissolving microneedles for the prevention of vitamin K deficiency bleeding. Int J Pharm 541(1-2):56–63

Jamkhande PG, Ghule NW, Bamer AH et al (2019) Metal nanoparticles synthesis: an overview on methods of preparation, advantages and disadvantages, and applications. J Drug Deliv Sci Technol 53:101174

Kang S-W, Kim J-S, Park K-S et al (2011) Surface modification with fibrin/hyaluronic acid hydrogel on solid-free form-based scaffolds followed by BMP-2 loading to enhance bone regeneration. Bone 48(2):298–306

Kang KS, Lee S-I, Hong JM et al (2014) Hybrid scaffold composed of hydrogel/3D-framework and its application as a dopamine delivery system. J Control Release 175:10–16

Kastner E, Verma V, Lowry D et al (2015) Microfluidic-controlled manufacture of liposomes for the solubilisation of a poorly water soluble drug. Int J Pharm 485(1–2):122–130

Khadka DB, Haynie DT (2012) Protein-and peptide-based electrospun nanofibers in medical biomaterials. Nanomedicine 8(8):1242–1262

KianvashRad N, Barkhordari E, Mostafavi SH et al (2019) Optimizing microfluidic preparation parameters of nanosuspension to evaluate stability in nanoprecipitation of stable-iodine (127I). SN Appl Sci 1(9):1054

Kim GJ, Kim KO (2020) Novel glucose-responsive of the transparent nanofiber hydrogel patches as a wearable biosensor via electrospinning. Sci Rep 10(1):1–12

Kim T-H, Yun Y-P, Park Y-E et al (2014) In vitro and in vivo evaluation of bone formation using solid freeform fabrication-based bone morphogenic protein-2 releasing PCL/PLGA scaffolds. Biomed Mater 9(2):025008

Kim J, Shim IK, Hwang DG et al (2019) 3D cell printing of islet-laden pancreatic tissue-derived extracellular matrix bioink constructs for enhancing pancreatic functions. J Mater Chem B 7(10):1773–1781

Lancina MG III, Shankar RK, Yang H (2017) Chitosan nanofibers for transbuccal insulin delivery. J Biomed Mater Res A 105(5):1252–1259

Larrañeta E, Isasi JR (2012) Self-assembled supramolecular gels of reverse poloxamers and cyclodextrins. Langmuir 28(34):12457–12462

Larrañeta E, Martínez-Ohárriz C, Vélaz I et al (2014) In vitro release from reverse poloxamine/α-cyclodextrin matrices: modelling and comparison of dissolution profiles. J Pharm Sci 103(1):197–206

Larraneta E, Lutton RE, Woolfson AD et al (2016) Microneedle arrays as transdermal and intradermal drug delivery systems: materials science, manufacture and commercial development. Mater Sci Eng R Rep 104:1–32

Larrañeta E, Stewart S, Fallows SJ et al (2016) A facile system to evaluate in vitro drug release from dissolving microneedle arrays. Int J Pharm 497(1–2):62–69

Larrañeta E, Barturen L, Ervine M et al (2018a) Hydrogels based on poly (methyl vinyl ether-co-maleic acid) and Tween 85 for sustained delivery of hydrophobic drugs. Int J Pharm 538(1–2): 147–158

Larrañeta E, Stewart S, Ervine M et al (2018b) Hydrogels for hydrophobic drug delivery. Classification, synthesis and applications. J Funct Biomater 9(1):13

Larrañeta E, Dominguez-Robles J, Lamprou DA (2020) Additive manufacturing can assist in the fight against COVID-19 and other pandemics and impact on the global supply chain. 3D Print Addit Manuf 7(3):100–103

Laverty G (2018) Peptide nanomaterials as future antimicrobial technologies. Future Microbiol 13: 5–7

Lee JW, Kang KS, Lee SH et al (2011) Bone regeneration using a microstereolithography-produced customized poly (propylene fumarate)/diethyl fumarate photopolymer 3D scaffold incorporating BMP-2 loaded PLGA microspheres. Biomaterials 32(3):744–752

Lim SH, Kathuria H, Amir MHB et al (2021) High resolution photopolymer for 3D printing of personalised microneedle for transdermal delivery of anti-wrinkle small peptide. J Control Release 329:907–918

Lin C-C, Tseng C-C, Chuang T-K et al (2011) Urine analysis in microfluidic devices. Analyst 136(13):2669–2688

Linares Blasco V, Casas Delgado M, Caraballo Rodríguez I (2019) Printfills: 3D printed systems combining Fused Deposition Modeling and Injection Volume Filling. Application to colon-specific drug delivery. Eur J Pharm Biopharm 134:138–143

Liu J, Niu J, Yin L et al (2011) In situ encapsulation of laccase in nanofibers by electrospinning for development of enzyme biosensors for chlorophenol monitoring. Analyst 136(22):4802–4808

Liu Y, Tian M, Zhang H (2013) Microfluidics for synthesis of peptide-based PET tracers. Biomed Res Int 2013:1–8

Madzarevic M, Medarevic D, Vulovic A et al (2019) Optimization and prediction of ibuprofen release from 3D DLP printlets using artificial neural networks. Pharmaceutics 11(10):544

Martin NK, Domínguez-Robles J, Stewart SA et al (2021) Fused deposition modelling for the development of drug loaded cardiovascular prosthesis. Int J Pharm 595:120243

Mathew E, Domínguez-Robles J, Larrañeta E et al (2019a) Fused deposition modelling as a potential tool for antimicrobial dialysis catheters manufacturing: new trends vs. conventional approaches. Coatings 9(8):515

Mathew E, Domínguez-Robles J, Stewart SA et al (2019b) Fused deposition modeling as an effective tool for anti-infective dialysis catheter fabrication. ACS Biomater Sci Eng 5(11): 6300–6310

Mathew E, Pitzanti G, Larrañeta E et al (2020) 3D printing of pharmaceuticals and drug delivery devices. Multidisciplinary Digital Publishing Institute

Matsuura Y, Takehira M, Joti Y et al (2015) Thermodynamics of protein denaturation at temperatures over 100 C: CutA1 mutant proteins substituted with hydrophobic and charged residues. Sci Rep 5(1):1–9

Melocchi A, Parietti F, Loreti G et al (2015) 3D printing by fused deposition modeling (FDM) of a swellable/erodible capsular device for oral pulsatile release of drugs. J Drug Deliv Sci Technol 30:360–367

Méndez-Ardoy A, Bayón-Fernández A, Yu Z et al (2020) Spatially controlled supramolecular polymerization of peptide nanotubes by microfluidics. Angew Chem Int Ed 59(17):6902–6908

Moreira A, Lawson D, Onyekuru L et al (2020) Protein encapsulation by electrospinning and electrospraying. J Control Release 329:1172–1197

Ni M, Tresset G, Iliescu C et al (2020) Ultrashort peptide theranostic nanoparticles by microfluidic-assisted rapid solvent exchange. IEEE Trans NanoBiosci 19(4):627–632

Nicolas A, Dejoux A, Poirier C et al (2020) Contribution of intrinsic fluorescence to the design of a new 3D-printed implant for releasing SDABS. Pharmaceutics 12(10):921

Niu B, Zhan L, Shao P et al (2020) Electrospinning of zein-ethyl cellulose hybrid nanofibers with improved water resistance for food preservation. Int J Biol Macromol 142:592–599

Nuansing W, Frauchiger D, Huth F et al (2013) Electrospinning of peptide and protein fibres: approaching the molecular scale. Faraday Discuss 166:209–221

Park JY, Gao G, Jang J et al (2016) 3D printed structures for delivery of biomolecules and cells: tissue repair and regeneration. J Mater Chem B 4(47):7521–7539

Park BJ, Choi HJ, Moon SJ et al (2019) Pharmaceutical applications of 3D printing technology: current understanding and future perspectives. J Pharm Investig 49(6):575–585

Patel KH, Dunn AJ, Talovic M et al (2019) Aligned nanofibers of decellularized muscle ECM support myogenic activity in primary satellite cells in vitro. Biomed Mater 14(3):035010

Pelipenko J, Kristl J, Janković B et al (2013) The impact of relative humidity during electrospinning on the morphology and mechanical properties of nanofibers. Int J Pharm 456(1):125–134

Pelipenko J, Kocbek P, Kristl J (2015) Critical attributes of nanofibers: preparation, drug loading, and tissue regeneration. Int J Pharm 484(1–2):57–74

Pentlavalli S, Coulter S, Laverty G (2020) Peptide nanomaterials for drug delivery applications. Curr Protein Pept Sci 21(4):401–412

Permana AD, Utomo E, Pratama MR et al (2021) Bioadhesive-thermosensitive in situ vaginal gel of the gel flake-solid dispersion of itraconazole for enhanced antifungal activity in the treatment of vaginal candidiasis. ACS Appl Mater Interfaces 13(15):18128–18141

Pessi J, Santos HA, Miroshnyk I et al (2014) Microfluidics-assisted engineering of polymeric microcapsules with high encapsulation efficiency for protein drug delivery. Int J Pharm 472(1–2):82–87

Prabhakaran MP, Vatankhah E, Ramakrishna S (2013) Electrospun aligned PHBV/collagen nanofibers as substrates for nerve tissue engineering. Biotechnol Bioeng 110(10):2775–2784

Raj MK, Chakraborty S (2020) PDMS microfluidics: a mini review. J Appl Polym Sci 137(27): 48958

Rasouli R, Barhoum A, Bechelany M et al (2019) Nanofibers for biomedical and healthcare applications. Macromol Biosci 19(2):1800256

Rezvantalab S, Keshavarz Moraveji M (2019) Microfluidic assisted synthesis of PLGA drug delivery systems. RSC Adv 9(4):2055–2072

Robles-Martinez P, Xu X, Trenfield SJ et al (2019) 3D printing of a multi-layered polypill containing six drugs using a novel stereolithographic method. Pharmaceutics 11(6):274

Ruiyi L, Zaijun L, Junkang L (2017) Histidine-functionalized carbon-based dot-Zinc(II) nanoparticles as a novel stabilizer for Pickering emulsion synthesis of polystyrene microspheres. J Colloid Interface Sci 493:24–31

Safa N, Vaithiyanathan M, Sombolestani S et al (2019) Population-based analysis of cell-penetrating peptide uptake using a microfluidic droplet trapping array. Anal Bioanal Chem 411(12):2729–2741

Seoane-Viaño I, Januskaite P, Alvarez-Lorenzo C et al (2021) Semi-solid extrusion 3D printing in drug delivery and biomedicine: personalised solutions for healthcare challenges. J Control Release 332:367–389

Shahrubudin N, Lee TC, Ramlan R (2019) An overview on 3D printing technology: technological, materials, and applications. Proc Manuf 35:1286–1296

Shaqour B, Samaro A, Verleije B et al (2020) Production of drug delivery systems using fused filament fabrication: a systematic review. Pharmaceutics 12(6):517

Spicer CD, Jumeaux C, Gupta B et al (2018) Peptide and protein nanoparticle conjugates: versatile platforms for biomedical applications. Chem Soc Rev 47(10):3574–3620

Stewart SA, Domínguez-Robles J, Donnelly RF et al (2018) Implantable polymeric drug delivery devices: classification, manufacture, materials, and clinical applications. Polymers 10(12):1379

Stewart SA, Domínguez-Robles J, McIlorum VJ et al (2020a) Development of a biodegradable subcutaneous implant for prolonged drug delivery using 3D printing. Pharmaceutics 12(2):105

Stewart SA, Domínguez-Robles J, McIlorum VJ et al (2020b) Poly (caprolactone)-based coatings on 3D-printed biodegradable implants: a novel strategy to prolong delivery of hydrophilic drugs. Mol Pharm 17(9):3487–3500

Tarafder S, Koch A, Jun Y et al (2016) Micro-precise spatiotemporal delivery system embedded in 3D printing for complex tissue regeneration. Biofabrication 8(2):025003

Tekko IA, Chen G, Domínguez-Robles J et al (2020) Development and characterisation of novel poly (vinyl alcohol)/poly (vinyl pyrrolidone)-based hydrogel-forming microneedle arrays for enhanced and sustained transdermal delivery of methotrexate. Int J Pharm 586:119580

Vaithilingam J, Kilsby S, Goodridge RD et al (2015) Functionalisation of Ti6Al4V components fabricated using selective laser melting with a bioactive compound. Mater Sci Eng C 46:52–61

Van Den Driesche S, Lucklum F, Bunge F et al (2018) 3D printing solutions for microfluidic chip-to-world connections. Micromachines 9(2):71

Ventola CL (2014) Medical applications for 3D printing: current and projected uses. Pharm Therap 39(10):704

Vlachou M, Kikionis S, Siamidi A et al (2019) Fabrication and characterization of electrospun nanofibers for the modified release of the chronobiotic hormone melatonin. Current Drug Deliv 16(1):79–85

Waheed S, Cabot JM, Macdonald NP et al (2016) 3D printed microfluidic devices: enablers and barriers. Lab Chip 16(11):1993–2013

Wang H, Wu G, Zhang J et al (2016) Osteogenic effect of controlled released rhBMP-2 in 3D printed porous hydroxyapatite scaffold. Colloids Surf B: Biointerfaces 141:491–498

Warsi MH, Yusuf M, Al Robaian M et al (2018) 3D printing methods for pharmaceutical manufacturing: opportunity and challenges. Curr Pharm Des 24(42):4949–4956

Wei D, Sun J, Bolderson J et al (2017) Continuous fabrication and assembly of spatial cell-laden fibers for a tissue-like construct via a photolithographic-based microfluidic chip. ACS Appl Mater Interfaces 9(17):14606–14617

Wen P, Wen Y, Huang X et al (2017) Preparation and characterization of protein-loaded electrospun fiber mat and its release kinetics. J Agric Food Chem 65(23):4786–4796

Xiao D, Hu JJ, Zhu JY et al (2016) A redox-responsive mesoporous silica nanoparticle with a therapeutic peptide shell for tumor targeting synergistic therapy. Nanoscale 8(37):16702–16709

Xu X, Zhao J, Wang M et al (2019) 3D printed polyvinyl alcohol tablets with multiple release profiles. Sci Rep 9(1):1–8

Xu X, Goyanes A, Trenfield SJ et al (2021) Stereolithography (SLA) 3D printing of a bladder device for intravesical drug delivery. Mater Sci Eng C 120:111773

Yap SK, Wong WK, Ng NXY et al (2017) Three-phase microfluidic reactor networks—design, modeling and application to scaled-out nanoparticle-catalyzed hydrogenations with online catalyst recovery and recycle. Chem Eng Sci 169:117–127

Ye YJ, Zhou YQ, Jing ZY et al (2018) Electrospun heparin-loaded core–shell nanofiber sutures for achilles tendon regeneration in vivo. Macromol Biosci 18(7):1800041

Ye K, Kuang H, You Z et al (2019) Electrospun nanofibers for tissue engineering with drug loading and release. Pharmaceutics 11(4):182

Yıldız A, Kara AA, Acartürk F (2020) Peptide-protein based nanofibers in pharmaceutical and biomedical applications. Int J Biol Macromol 148:1084–1097

Zelzer M, Ulijn RV (2010) Next-generation peptide nanomaterials: molecular networks, interfaces and supramolecular functionality. Chem Soc Rev 39(9):3351–3357

Zhang J, Yan S, Yuan D et al (2016) Fundamentals and applications of inertial microfluidics: a review. Lab Chip 16(1):10–34

Zhang B, Korolj A, Lai BFL et al (2018) Advances in organ-on-a-chip engineering. Nat Rev Mater 3(8):257–278

Zhang P, Wang Z, Li J et al (2020) From materials to devices using fused deposition modeling: a state-of-art review. Nanotechnol Rev 9(1):1594–1609

Chapter 11
Self-assembling Peptide Hydrogels as Extracellular Matrix-Mimicking Scaffolds for Tissue Regeneration in Chronic-Degenerative Diseases

Luis A. Castillo-Díaz, Juan A. Ruiz-Pacheco, Isaac O. Pérez-Martínez, and Araida Hidalgo-Bastida

Abstract Over the past decades, scientists have aimed to overcome the limitations of current approaches to recover the integrity and functionality of tissues severely damaged by trauma or disease. Therefore, strategies that mimic the architecture and biological functions of the extracellular matrix (ECM) in vitro represent a promising route to direct the processes involved in the maintenance of such tissues. The extracellular matrix is a complex three-dimensional niche where several types of cells and biomolecules interact with each other to orchestrate the specific functions of each tissue.

Within the field of nanomaterials, bioinspired self-assembling peptide hydrogels constructed from a bottom-up approach form hierarchical structures used to carry out cutting-edge research in vitro and in vivo for a better understanding of cell biology and the potential development of the novel and more accurate treatments for repairing tissues.

L. A. Castillo-Díaz (✉)
Departamento de Medicina y Ciencias de la Salud, Universidad de Sonora, Hermosillo, Sonora, México
e-mail: luis.castillo@unison.mx

J. A. Ruiz-Pacheco
Consejo Nacional de Humanidades, Ciencias y Tecnologías (CONAHCYT), Ciudad de México, México
e-mail: jaruiz@conahcyt.mx

I. O. Pérez-Martínez
Sección de Neurobiología de las Sensaciones y Movimientos Oro-faciales, Facultad de Estudios Superiores Iztacala, Universidad Nacional Autónoma de México, Estado de México, México
e-mail: isaac.perez@unam.mx

A. Hidalgo-Bastida
Centre for Bioscience, Centre for Advanced Materials and Surface Engineering, Centre for Musculoskeletal Science and Sport Medicine, Manchester Metropolitan University, Manchester, UK
e-mail: a.hidalgo@mmu.ac.uk

367

In this chapter, we discuss the state of the art of rationale design, and the development and use of self-assembling peptide hydrogels to improve and optimize strategies intended to tackle chronic diseases affecting bone, cartilage, heart, pancreas, and nerve tissues.

Keywords Peptide · Hydrogel · Cell · Matrix · Tissue · Regeneration · Medicine

11.1 Introduction

Cell biology research has been carried out using standard cell cultures in vitro, which, although valuable, very often do not reflect the biology in vivo. This is more noticeable when non-human cells and macromolecules are used, which frequently leads to misinterpretations of observed outcomes, thus delaying the transference of technology (Jensen and Teng 2020).

Since the discovery of significant differences between monolayer and three-dimensional (3D) cell cultures in vitro (Wang et al. 2002; Weaver et al. 2002), natural materials, such as collagens (Samadian et al. 2019), hyaluronic acid (Almeida et al. 2018), fibrin (Nellenbach et al. 2020), chitosan (Saekhor et al. 2019), alginate (Guillaume et al. 2014), decellularized scaffolds (Belviso et al. 2020), and synthetic materials, such as poly(ethylene glycol) dimethacrylate, poly (hydroxyethyl methacrylate), poly (lactic acid) hydrogels (Nicolas et al. 2020), have been exploited in an attempt to mimic the extracellular matrix (ECM) in cell culture, tissue engineering, and regenerative medicine applications (Tibbitt and Anseth 2009).

The ECM is a dynamic and complex fibrillar network that provides structural support to tissues and regulates cell biology (Alberts et al. 2002; Mecham 2011). Cells sense the microarchitecture, macromolecules, and mechanics of the ECM, which eventually triggers various cellular activities, such as adhesion, growth, spreading, differentiation, proliferation, migration, synthesis of macromolecules, and apoptosis (Petreaca and Martins-Green 2014).

Self-assembling peptide hydrogels (SAPHs) represent one of the most prominent ECM analogs in the field. In the early 90's, Shuguang Zhang reported that an ionic-complementary repeated segment of a yeast protein called Zuotin was self-assembled in an aqueous solution and formed a well-defined nanofibrillar network that supported the formation of a hydrogel resembling the nanoarchitecture of the ECM (Zhang et al. 1993).

SAPHs biotechnology exploits a bottom-up approach, where amino acids act as building blocks to form hierarchical secondary structures (Caplan et al. 2002; Ulijn and Smith 2008). The most popular SAPHs are short aromatics (Jayawarna et al. 2006; Gelain et al. 2006), β-sheet tapes (Zhang et al. 1993; Aggeli et al. 2001), α-helix coiled coils (Woolfson 2017; Gribbon et al. 2008), β-hairpin (Schneider et al. 2002; Ozbas et al. 2004), and amphiphile compounds (Niece et al. 2003; Cui et al. 2010). Overall, SAPHs applications include cell culture (Hellmund et al. 2021; Wang et al. 2020), encapsulation and controlled delivery of mammalian cells

(Szkolar et al. 2014; Castillo Diaz et al. 2014), growth factors (Huang et al. 2019; Stendahl et al. 2008), and drugs (Roy et al. 2020; Fu et al. 2018) in an attempt to face chronic-degenerative diseases. According to the World Health Organization, such diseases have a significant worldwide impact (World Health Organization 2005a), including musculoskeletal disorders (bone and cartilage disorders) (Castillo Diaz et al. 2014, 2016; Firth et al. 2006; Krishnan and Grodzinsky 2018) and diseases affecting heart, vessels (Burgess et al. 2021; Ichihara et al. 2018), nerves, (Yoshimatsu et al. 2020; Lu et al. 2018), and pancreas (Fu et al. 2018; Yoon et al. 2015). This greatly affects the economy and quality of life of people suffering from them (World Health Organization 2005b).

SAPHs have succeeded in improving bone tissue biology when affected by osteoporosis by acting as vehicles of stem cells (SCs), which can be subsequently delivered into affected sites and by inducing osteointegration and mineralization (Compston et al. 2019; Nuti et al. 2019; Murai et al. 2021). Likewise, SAPHs are able to mimic the functions of hormones, such as estradiol to prevent osteoporosis (Wang et al. 2012). Previous research showed that an ionic-complementary peptide gel is effective in inducing the osteogenic differentiation of osteoblasts and mesenchymal stem cells (MSCs) in vitro (Castillo Diaz et al. 2014, 2016).

Self-assembling peptide hydrogels are also widely use to regenerate infarcted cardiac tissue when combined with SCs (Guo et al. 2010; Puig-Sanvicens et al. 2015), as well as biomolecules derived from progenitor cells and growth factors, reducing infarcted cardiac tissue in vivo (Han et al. 2019).

With regard to nerve tissue, SAPHs can protect and deliver neuroprotective molecules (Lu et al. 2018, 2019; Altunbas et al. 2011) and precursor SCs (Wang et al. 2015; Wiseman et al. 2020) to recover neural cells affected by neurodegenerative disorders (NDs), such as Parkinson's disease (PD), Alzheimer's disease (AD) (Palhano et al. 2013; Cui et al. 2016), and spinal cord injury (SCI) (Cigognini et al. 2014; Hassannejad et al. 2019; Bordoni et al. 2020).

Finally, the encapsulation of pancreatic islets in SAPHs and their subsequent delivery into affected sites are being explored to address the limitations related to islet grafting in type I diabetes therapy (Hwang et al. 2017; Lim et al. 2011; Uzunalli et al. 2015). Moreover, SAPHs act as depots and smart releasers of insulin and other hypoglycemic agents as a potential alternative treatment to prevent type II diabetes mellitus (TIIDM) (Fu et al. 2018; Lammi et al. 2018).

In this chapter, we discuss the current progress of SAPHs as versatile 3D scaffolds to encapsulate and transfer mammalian cells, relevant macromolecules, and drugs to improve current approaches intended to tackle chronic-degenerative diseases that have an increasing worldwide burden (World Health Organization 2005a, b).

11.2   The ECM: A Key Regulator of Tissues' Biology

The ECM is a sophisticated 3D cross-linked network hosting cells and a wide myriad of macromolecules, such as glycosaminoglycans (GAGs) and proteins (Table 11.1). The ECM separates tissues from each other and supports their biological functions (Alberts et al. 2002; Mecham 2011; Mouw et al. 2014). The basement membrane and interstitial ECM are mainly formed of collagens and non-collagen glycoproteins, as shown in Table 11.1 (Mecham 2011).

The type of macromolecules, stiffness, topography, fiber size, and porosity of the ECM vary according to the particular function of each tissue, which has a significant impact on cell behavior (Walma and Yamada 2020).

Thus, once cells sense any stimuli from the ECM through their membrane receptors (integrins), various cellular functions are triggered (Alberts et al. 2002; Hubbell 2007). These include changes in morphology, adhesion, mechanotransduction, survival, proliferation, differentiation, migration, and synthesis of molecules (Alberts et al. 2002; Mecham 2011). Consequently, the bidirectional interaction between macromolecules of the ECM and cells tightly orchestrates the biological function of tissues (Hubbell 2007).

Table 11.1 Components of ECM and their roles

Basement Membrane		Interstitial ECM	
Molecules	Major functions	Molecules	Major functions
Non-fibrillar collagens IV, VI, VIII	Fix basal lamina to stratified epithelium of connective tissue	Fibrillar collagens I–III, V, XI	Support to the ECM. Cell adhesion and signaling
Heparan sulfate proteoglycans: perlecan, agrin	Hydration and bearing compressive stress. Encapsulation and diffusion of macromolecules	Fibrillar-associated collagens IX, XII	Join fibrils with each other and to other ECM components. Bearing traction stress
Chondroitin sulfate proteoglycans: aggrecan, neurocan, versican, brevican	Cellular adhesion, growth, migration	Fibronectin	Bind growth factors. Cell migration, and differentiation
Small leaking-rich repeat proteoglycans: decorin, biglycan, lumican	Assembly of fibrillar collagens	Elastin, tenascin	Recovery of tissue conformation after deformation. Restriction of the extension of the elastic network
Laminins, nidogens, perlecans, entactin	Cell adhesion, proliferation, migration, and differentiation	Growth factors, cytokines, chemokines, enzymes	Cell growth, proliferation migration, apoptosis

Alberts et al. (2002), Mouw et al. (2014), Walma and Yamada (2020), and Gough et al. (2012)

11.3   Functionalization of SAPHs to Direct Cell Biology

Nowadays, scientists take advantage of SAPHs technology, which is based on the naturally occurring "bottom-up" approach where amino acids with distinct chemistry form supramolecular structures, such as β-sheet tapes (Zhang et al. 1993; Aggeli et al. 2001), α-helix coiled coils (Woolfson 2017), β-hairpin (Schneider et al. 2002), amphiphiles (Niece et al. 2003; Cui et al. 2010), or short aromatic (Smith et al. 2008).

The possible combinations of amino acids for the rational design of polypeptides capable of forming fibrillar networks supporting the formation of SAPHs are wide (Aggeli et al. 2001; Woolfson 2017; Schneider et al. 2002; Smith et al. 2008). This makes SAPHs versatile and attractive materials for biomedical applications (Li et al. 2019; Gelain et al. 2021).

One major challenge during the development of SAPHs is designing peptide chains that inherently can offer inductive biological cues to regulate specific cellular responses in a well-controlled manner since most synthetic nanomaterials inherently lack inductive moieties. Such a limitation is solved through the functionalization of SAPHs with ECM cues that are associated with collagens, fibronectin, or laminins of the ECM (Table 11.2) (Gelain et al. 2006; Wang et al. 2020; Jung et al. 2011).

This remarkable approach represents a step forward in the field making SAPHs attractive analogs of the ECM in vitro. Furthermore, this strategy avoids the use of whole proteins (highly susceptible to enzymatic degradation) to induce cell activity and facilitates the replacement of animal models, which carry ethical concerns and do not necessarily resemble the physiology of human tissues (Gough et al. 2012; Shekaran and Garcia 2011).

Table 11.2 Peptides based on ECM proteins

Biofunctional moiety	ECM protein	Major function	Cellular integrin recognition
RGDS, PHSRN, REDV, LDV	Fibronectin type II	Cell adhesion, growth, survival, proliferation, differentiation, migration. Wound healing. Bind collagens, fibrins, GAGs	$\alpha_1\beta_1$, $\alpha_2\beta_1$, $\alpha_5\beta_1$, $\alpha_v\beta_1$, $\alpha_v\beta_3$, $\alpha IIb\beta_3$
RGDS	Collagens, laminin, vitronectin		
GFOGER, DGEA, RGDT	Collagens I, II, and III		
IKVAV, YIGSR, PDSGR, RGDN	Laminins	Cell anchorage and spreading	$\alpha_1\beta_1$, $\alpha_2\beta_1$, $\alpha_3\beta_1$, $\alpha_6\beta_1$, $\alpha_7\beta_1$

Gough et al. (2012), Hubbell (2007), Jung et al. (2011), Shekaran and Garcia (2011), and Najafi et al. (2021)

Single letters in the text of the first column of the table represent single-letter amino acids' nomenclature

11.4 Musculoskeletal Tissue Diseases

Musculoskeletal diseases impair mobility and dexterity, and reduces the quality of life of people worldwide. These diseases affect mainly bone and cartilage tissues. Etiological factors include aging, fractures, sprains, and intense strains (World Health Organization 2021a).

11.4.1 Bone Diseases

Bone diseases are caused by imbalances in the mineralization activity of connective tissue. Subtle changes in bone remodeling can alter its microarchitecture and density. Incidence and demographic prevalence depend on environmental factors, which include genetics, age, type of diet, and sedentarism. The most common bone diseases include Osteogenesis Imperfecta (OI), Osteoporosis, Paget's disease, bone cancer, and inflammatory bone diseases (Rodan and Martin 2000). Standard therapies for bone diseases include surgery for resection, correction, or reconstruction (autografts-patients or allografts-cadaveric tissue), drugs (bisphosphonates to inhibit the osteo-clastic activity, recombinant antibodies, and hormones), and physiotherapy (Marom et al. 2020; Madhuri et al. 2021).

Recently, regenerative medicine has used biomaterials either as physical scaffolds to home SCs to remodel the affected site, or to deliver SCs therapies maximizing the clinical benefit. In addition, some congenital bone diseases, such as OI, are ideal candidates for genetic therapy, but these are still at the experimental stage (Ralston and Gaston 2019).

Bone Diseases: SAPHs for Osteogenesis Imperfecta
Osteogenesis imperfecta is a rare congenital disease which affects 1 in 15,000–20,000 individuals worldwide. It is mostly triggered by a defect on *COL1A1/2* gene, causing decreased bone mass and bone fragility and presenting clinically in childhood with a higher fracture rate and reduced growth. Based on the severity of this collagen disorder severity, OI can also affect ligaments, muscles, teeth, hearing, and blood vessels (Ralston and Gaston 2019; Etich et al. 2020).

In addition to the orthopedic treatments mentioned, cellular therapy is a relevant approach for OI. This includes transplantation of adult Human Leukocyte Antigen (HLA)-matched MSCs into pediatric patients or of fetal MSCs in utero. Cell therapy for OI has demonstrated an improvement in patients' growth velocity and in the microarchitecture of the bone, including increased production of collagen I (Madhuri et al. 2021; Gotherstrom and Walther-Jallow 2020). Nevertheless, initial clinical trials indicate a short-term effect of a single dose; hence, reiterative infusions are needed to support long-term linear growth and mineral content (Madhuri et al. 2021; Infante et al. 2021). As such, SAPHs mimickers of the bone ECM greatly improve homing and remodeling, as they provide the right ECM niche for patient's/donor's
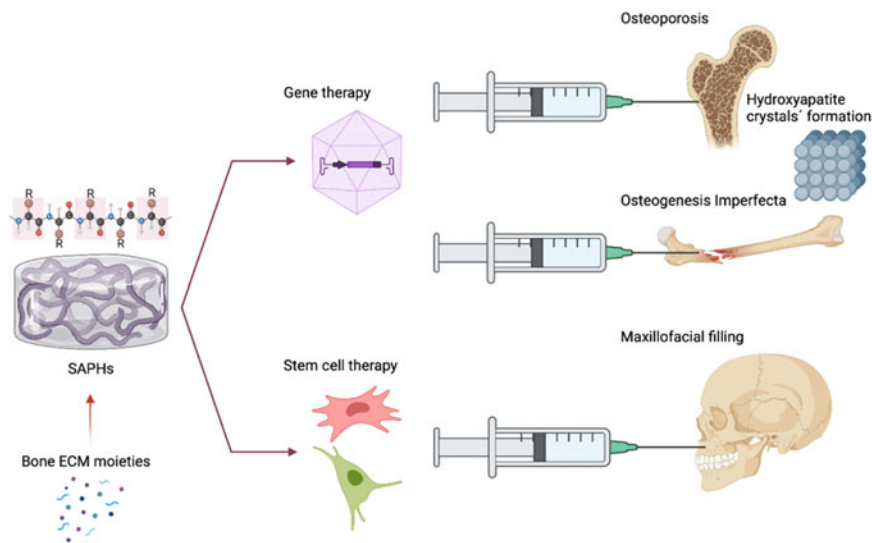
Fig. 11.1 Representation of SAPHs as 3D scaffolds for cell induction and tissue fillers for bone diseases

SCs, offering many alternatives, depending on combinations with other active molecules (Fig. 11.1).

Regulation of cell therapy products, or Advanced Therapy Medicinal Products (ATMPs), means strict procedures are in place for manufacturing for clinical use. Although not included in these, "reconstitution" prior to administration is a key step which relies on the delivery vehicle. Currently, cells are directly delivered in tissues (heart, pancreas, bone), electrolyte solutions (Ringer lactate) (Infante et al. 2021), or patient's sera. For this goal, SAPHs could improve the short-term efficacy related to such an approach, by encapsulating SCs on site, increasing their "seeding" efficiency and thus their clinical benefit.

As mentioned, peptides used in SAPHs can be designed to include sequences recognized by cell receptors for specific roles, including osteo-differentiation. These peptides mimic the native ECM in bone (collagen I, fibronectin, laminin) or bone morphogenetic proteins (BMPs) for osteoconductive properties. ECM-derived peptides sequences, such as RGD, PSHRN, SVVYGLR, DGEA, RRETAWA, and RADA-16 (Ac-RADARADARADARADA-CONH$_2$), are recognized by several integrins in bone cells, enabling them to support adhesion, proliferation, migration, osteo-integration, and mineralization, including nucleation of hydroxyapatite formation (Fig. 11.1) (Najafi et al. 2021; Ando et al. 2018; Saha et al. 2019). These can be used as stand-alone or combined for enhanced activity, such as KFE-RGD to improve matrix stiffness and promote bone regeneration (Hogrebe et al. 2018).

Bone Diseases: SAPHs for Osteoporosis

Osteoporosis is a systemic skeletal disease characterized by loss of bone mass and altered bone microarchitecture, which eventually may lead to an increased risk of fractures. Osteoporosis is the most common bone disease with a significant prevalence in over 55-year-old female and over 65-year-old male individuals, partly related to polymorphisms of *COLIA1*, *ER*, and *VDR* genes (Compston et al. 2019; Nuti et al. 2019). Screening based on bone mineral density (BMD) during adulthood has been successful in some countries for early diagnosis, enabling effective management by patients to reduce the risk of fractures, especially hip and vertebrae. Once diagnosed, the current management tools for osteoporosis include antiresorptive drugs (bisphosphonates), anabolic drugs (teriparatide), hormone replacement therapy, monoclonal antibodies, and/or changes in lifestyle (exercise and nutrition) (Compston et al. 2019; Nuti et al. 2019; Sozen et al. 2017).

Novel biomaterials and cell-based therapies are being developed to improve the clinical outcome of osteoporotic patients. Murai et al. have suggested a biomaterial approach to bone diseases using SAPHs as scaffolds to support calcium carbonate mineralization. In this research, the sequence Ac-(VHVEVS)$_3$-CONH$_2$ self-assembled to form a hydrogel able to improve CaCO$_3$ mineralization (Fig. 11.1) (Murai et al. 2021). Another example of SAPHs supporting mineralization in bone disease is their use to improve the therapeutic efficiency of drugs; peptides, such as GGGD, coupled with silica nanoparticles, can be used as injectable vehicles to deliver calcitonin (CT). This has been evaluated in animal models showing an increased half-life of CT, enhancing trabeculation, and improving the biomechanical properties of the remodeled bone (Yu et al. 2019).

As already mentioned, peptide sequences look at providing biochemical cues, such as the osteogenic factor lactoferrin. Recent work from Pal et al. assessed the efficacy of SAPHs based on RKVRGPPVSCIKRDSPIQ to support bone healing in animal models. This research confirmed that this peptide hydrogel has substantial osteogenic activity to stimulate osteoblasts and bone morphogenetic protein 2 (BMP-2) production, making it an ideal candidate as a peptide drug for bone disease as well as trauma treatments (Pal et al. 2021).

Specific anti-osteoporosis strategies also include self-assembly peptides, as in the case of an oral treatment for osteoporosis based on 11 alpha-hydroxyandrost-1,4-diene-3-one paired with RGDS, RGDV, and RGDF. This approach has not only been shown to outperform estradiol in the prevention of osteoporosis but also presented no side effects, differing from estradiol which induced endometrial hyperplasia and thromboses in a rodent model (Wang et al. 2012).

Mesenchymal stem cell therapy is also considered a promising treatment for osteoporosis. SCs quantity and regenerative profile decrease with age. Given that osteoporosis is mainly prevalent in late adulthood, MSCs transplantation has the potential to restore MSCs numbers, improving bone remodeling through their proliferation and differentiation activity, regardless of their origins (bone marrow, adipose derived, or umbilical cord derived) (Macias et al. 2020). Results indicate that SCs can also increase osteoblastic differentiation to increase bone density, and osteoclast activation, with clinical trials running now in phase II (Jiang et al. 2021;

Arjmand et al. 2020). Nevertheless, maintaining MSCs viability and function after transplantation remain a challenge that needs to be addressed to optimize SCs therapy. In this regard, an octapeptide hydrogel (KFERGD) functionalizaed with RGD have also shown increased MSCs osteogenic profile by increasing the matrix stiffness in vitro (3 kPa), which depends on RGD concentration) (Fig. 11.1) (Hogrebe et al. 2018).

11.4.2   Cartilage Diseases

One major disease affecting cartilage is Osteoarthritis (OA), which affects synovial joints and is characterized by fibrillation of the cartilage surface, formation of clefts, loss of cartilage volume, and severe damage of the cartilage ECM. The etiology of OA is not yet fully understood. However, this pathology frequently appears after trauma or aging (Krishnan and Grodzinsky 2018).

Today, the standard medical treatment for OA is based on anti-inflammatory drugs to reduce pain and partially recover the function of joints. This therapy is often accompanied by a physiotherapeutic approach. In late stages of OA, surgery is an option that replaces the damaged joint. However, joint replacement very often fails in the long term. Regenerative medicine represents a promising alternative for individuals suffering from OA (Kloppenburg and Berenbaum 2020).

Cartilage Diseases: SAPHs for Osteoarthritis
Osteoarthritis represents the most common type of arthritis and affects hundreds of million people globally. This pathology impairs the structure and function of hyaline cartilage found in joints, such as knees, hands, hips, and shoulders. Since hyaline cartilage is an innervated and avascular tissue, its physiological healing and regeneration are poor or null. At late stages, OA causes degeneration of cartilage, which eventually leads to a significant reduction of the joint space and subchondral bone thickness. This is accompanied by inflammation and pain (Krishnan and Grodzinsky 2018).

Some external factors associated with OA include congenital abnormalities related to the structure of cartilage, aging, obesity, and trauma. Acute trauma leads to cell death and loss of cartilage aggrecans. This is because inflammatory cytokines, such as TNF-α, IL-1, and IL-6, stimulate the activity of proteases, metalloproteinases, and aggrecanases, leading to the degradation of the cartilage ECM. Thus, the mechanical strength of cartilage is significantly compromised, making it susceptible to degradation after mechanical stress (Krishnan and Grodzinsky 2018).

While non-steroidal anti-inflammatory drugs, along with neurotrophin antibody, and dexamethasone can resolve OA pain, they do not stop its progression or cure the disease (Krishnan and Grodzinsky 2018).

In recent years, avidin, a positively charged protein, has been used as a carrier of dexamethasone to progressively release the anti-inflammatory drug into damaged

articulations of rabbits (Bajpayee et al. 2017). Likewise, to maximize the viability of OA drugs, researchers designed carbon nanotubes carriers modified with polyethylene glycol (PEG) shells. This nanotechnology showed the ability to reach murine chondrocytes in joints with damaged cartilage within 2 months without eliciting or worsening inflammation (Sacchetti et al. 2014). However, further studies must eliminate any toxicity derived from the internalization of nanotubes, as well as to evaluate its efficacy to encapsulate and deliver OA medical formulations in vivo.

Within novel approaches to treat OA, SAPHs are being used as lubricants of bovine knees ex situ to extend the life span of OA medications and induce cellular activity (Bell et al. 2006). The feasibility of this approach is based on the capability of SAPHs to promote the growth of human and animal stem cells, and chondrocytes in vitro (Mujeeb et al. 2013; Jayawarna et al. 2009; Kopesky et al. 2010; Kisiday et al. 2002), as well as to potentially repair cartilage in vivo (Miller et al. 2010; Kim et al. 2014). Therefore, a cellular therapy combined with peptide gels to induce the healing of damaged joints represents a promising option to induce hyaline cartilage regeneration during OA.

Recently, Dufour et al. showed that the peptide gel Ac-IEIKIEIKIEIKI-NH_2 (IEIK13) encapsulating autologous articular chondrocytes, previously stimulated with BMP-2, insulin, and triiodothyronine (T3), restored the thickness (3.5 mm) of cartilage defects in a primate femoral condyle model after 3 months of treatment. Previously, researchers showed that IEIK13 induced the production of cartilage from human and monkey chondrocytes in vitro. Interestingly, the formation of GAGs, and collagens was observed after gel transfer with and without cells. This suggests that the IEIK13 gel could induce the recruitment and physiological function of local chondrocytes in monkeys. The advantage of using SAPHs, like IEIK13, for cartilage repairing is that they are highly hydrated materials with high absorption capability. SAPHs also efficiently integrate into tissues and allow cellular migration. It should be noted that a significant limitation of this investigation is the small number of animals used. Only three animals were treated with the IEIK13 gel, from which only two showed a clear cartilage defect recovery (Dufour et al. 2021). Thus, forthcoming investigations in vivo might shed light on the efficacy of this peptide gel before clinical trials can be conducted.

To induce hyaline cartilage repairing, the peptide gel (KLDL)$_3$-$CONH_2$ (KLD-12) functionalized with N-peptide (LPP), where the latter is known to orchestrate cell proliferation and the synthesis of ECM by chondrocytes, formed a gel called KLPP. This gel recorded a soft tensile strength of ca. 500 Pa., which induced the migration of both rabbit chondrocytes and bone marrow mesenchymal stem cells (BMSCs) after seeded on KLPP for 7 days in vitro. Once the KLPP peptide solution was transferred into damaged rabbit joints, it was allowed to complete gelation for 15–30 min in situ, and the gel progressively integrated with host cartilage without eliciting an inflammatory reaction. Interestingly, cartilage reparation showed a semi-transparent appearance resembling physiological hyaline cartilage over 10 days of treatment with the gel. Likewise, treatment with KLPP recorded high scores of cartilage repairing (measurements based on the international Cartilage Repair Society) as histological evaluations showed in comparison to KLD-12 gel. However,

some limitations of this study include the number of animals used and that the cartilage defect model was limited to a thin layer of cartilage, which may not resemble human hyaline cartilage defect conditions (Lv et al. 2020).

Previously, KLD-12 was used to encapsulate murine BMSCs, which inherently possess an anti-inflammatory effect that may help decrease inflammation, chondrocyte hypertrophy, and apoptosis in hyaline cartilage. After KLD-12 with BMSCs was intra-articularly injected in a rat knee model, OA progression decreased after 6 weeks. This outcome was supported by no detection of the apoptotic marker capase-9, and the metalloproteinase-9 (MMP-9) in treated animals. Moreover, proteoglycan synthesis from chondrocytes could be detected histologically in the articular cavity of OA knee joints treated with KLD-12 encapsulating BMSCs in comparison to treatment with only BMSCs. The authors suggest that KLD-12 plays a key role in allowing chondrocytes to synthetize proteoglycans in the treated site. This highlights the capability of SAPHs to act as 3D vehicles providing protection to cells from harsh environments, as well as to allow cell adhesion, migration, and differentiation. As for most of the research discussed here, there were limitations to these studies. In this case, the use of animal cells, the short number of animals used, and the need for using autologous cells should be addressed in order to translate these approaches into clinical trials (Kim et al. 2014).

To provide more peptide gel alternatives to address OA, three peptide gels P_{11}-4, P_{11}-8, and P_{11}-12 were separately combined with chondroitin sulfate with the goals of investigating their ability to assemble and evaluating the effect that such a glycosaminoglycan has on the mechanical strength of gels. Both P_{11}-4 and P_{11}-8 were able to assemble into β-sheet secondary structures with a dense entangled fibril network and offering a higher mechanical strength, when combined with chondroitin sulfate at the highest ratio (1:64) and under Na^+ solution at the highest concentration (230 mM). This outcome may be due to the ionic-strength held between the glutamine-based residues of P_{11}-4 and P_{11}-8 gels, and the presence of salt. This contrasted with a poor capability of the serine-based peptide gel P_{11}-12 to self-assemble, which could not elucidate an ionic-strength enough to form stable gels under the presence of chondroitin sulfate and salt. Thus, P_{11}-4 and P_{11}-8 gels might be promising alternatives to retain GAGs and to be applied to OA treatment after their self-assembling and glycan concentration formulations can be standardized to elucidate a positive cartilage regeneration in vitro or in vivo (Barco et al. 2018).

11.5   Cardiovascular Diseases

Cardiovascular diseases (CVDs) comprise strokes and heart attacks, which cause the death of 17.9 million people annually. The gold standard to address CVDs include pharmacotherapy and surgery (Moller et al. 2006; Nesto and Kowalchuk 1987). Alternatively, acellular and cellular therapeutics are considered to treat acute myocardial infarct (AMI) (Moller et al. 2006; Nesto and Kowalchuk 1987). However,

poor retention and viability of cardiac tissue inducers when transferred remain unsolved (Schachinger et al. 2006; Wollert et al. 2004; Schuleri et al. 2008; Orlic et al. 2001). In this regard, SAPHs emerge as an alternative biological depot to encapsulate cardiac cells and molecules to improve current CVD therapeutics (Rivas et al. 2019).

11.5.1 Cardiovascular Diseases: SAPHs as Cardiac Molecules Depots for Heart Attack

The formation of fibrotic tissue during AMI is a major concern in cardiology (Boopathy et al. 2015). The injectable amphiphile GTAGLIGQ peptide (PGN) hydrogel was shown to induce cell attachment, and its functionalization with the cardioprotective GHRPS was shown to promote the survival of murine myoblasts in vitro. After gel disassociation, the release of exosomes derived from human umbilical cord MSCs induces the expression of Transforming Growth Factor-beta (TGF-β), which favors angiogenesis, diminishes inflammation, and forms fibrotic tissue (Han et al. 2019).

Another acellular strategy involves the encapsulation and release of both platelet-derived growth factor (PDGF) and fibroblast growth factor (FGF) in RADA-16 gel, which is formed by fibrils of 10–20 nm in diameter and of 2.5–5 nm in length. RADA-16, combined with growth factors, prevents myocardial fibrosis, induces angiogenesis, and reduces apoptosis of cardiomyocytes in a myocardial infarction model in animals. Thus, cardiac protection is facilitated through vascularization and inhibition of fibrosis (Kim et al. 2011).

Research is also exploring the suitability of RADA-16 gel to encapusulate and progresively release non-selective adrenergic receptor blockers, such as quinine and pindolol. This strategy might improve the effectiveness of cardiac medications and reduce dosages for cardiac tissue therapeutics (Briuglia et al. 2014).

Likewise, the use of functionalized RADA-16 hydrogel with CDDYYYGFGCNKFCRPR, a peptide mimicker of the Notch1 (as an inducer of cell proliferation, maturation, and apoptosis), significantly decreases fibrosis, stimulates angiogenesis, and favors the recruitment of SCs in a rat infarcted model (Fig. 11.2) (Boopathy et al. 2015).

11.5.2 Cardiovascular Diseases: SAPHs as Cellular Depots for Heart Attack

The incorporation of genetically modified murine MSCs in ^{D}FEFKDFEFKYRG^{D} gel has been explored to induce the production of hepatocyte growth factor (HGF) to diminish scars in a rat infarcted myocardial model. Accordingly, after gel treatment,
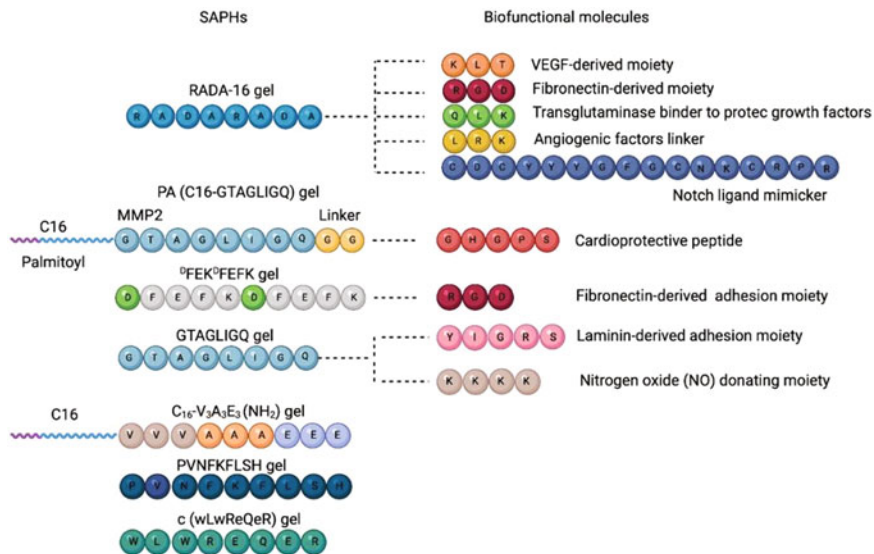
Fig. 11.2 Representation of functionalized SAPHs for CVDs

cell adhesion, viability, and cardiac differentiation improves cardiac tissue repairing and functions (Wu et al. 2017).

Similarly, the transfer of MSCs encapsulated in RADA-16 into murine hearts subjected to coronary artery ligation significantly decreases ventricular dilatation and interstitial collagen deposition. Moreover, treated cardiac tissue expresses anti-inflammatory molecules, which makes RADA-16 a potential candidate to improve cardiac cells transfer into damaged tissue (Ichihara et al. 2018).

The discussed outcome is in good agreement with previous research showing that RADA-16 functionalized with RGD and KLT promotes the retention of murine bone marrow MSCs, induces angiogenesis, and reduces infarcted areas in vivo (Fig. 11.2) (Li et al. 2017). Further evidence strongly suggests the suitability of RADA-16 to facilitate the retention of cardiac SCs under anoxic and low glucose conditions in vitro (Guo et al. 2010).

An attractive goal is the development of bioactive patches carrying cells to remodel cardiac tissue in a more effective manner. In this regard, human induced pluripotent stem cells (hiPSCs) seeded in RADA-16 survived and differentiated into a cardiac cellular lineage as evidenced by the expression of cardiac markers in vitro (Puig-Sanvicens et al. 2015).

Similarly, progenitor cells derived from adipose tissue of patients undergoing cardiac surgery encapsulated in RADA-16 induced the regeneration of damaged cardiac tissue in a murine myocardial infarction model, as evidenced by improvement in cell viability and blood vessel formation (Soler-Botija et al. 2014).

Previously, a biotinylated RADA-16 was designed to conjugate streptavidin and biotinylated-IGF-1, to retain human IGF-1 and allowed its subsequent delivery.

After injection of RADA-16/IGF-1 into a rat heart attack model, systolic function improved, and the expression of cardiac troponin was enhanced in murine cardiomyocytes (Davis et al. 2006).

Overall, the outcomes discussed suggest that RADA-16 could act as a suitable depot of progenitor cells to improve the current strategies that use cardiac cell transfer to address CVDs.

11.5.3   Cardiovascular Diseases: SAPHs as Cell-Load Depots for Other Cardiovascular Diseases Disorders

Preventing or reversing vascular damage is another important challenge in medicine. It has been shown that RADA-16 functionalized with QLK and LRK induced the formation of vascular tissue on chicken chorioallantoic membranes. It is believed that QLK is critical to protect HGF and vascular endothelial growth factor (VEGF) from hydrolysis, while LRK is capable to bind and retain HGF and VEGF in gel. Thus, human umbilical vein endothelial cells were able to form capillary-like tubular structures in vitro (Huang et al. 2019).

The amphiphilic peptide C_{16}-$V_3A_3E_3(NH_2)$ gel has been designed to mimic the tubular shape of coronary arteries on a macro scale. To achieve this, gelation of the amphiphilic peptide solution containing human smooth muscle cells was induced through the injection of the peptide solution into a shear flow chamber containing saline solution. Once gelation was induced, the peptide hydrogel with cells was subjected to contractional and rotational motion to emulate blood flow, stimuli that induced cell survival, growth, endothelial contraction, and cell migration toward the surface of the tubular gel over 4 days of culture (Fig. 11.2). Thus, gelation in situ of SAPHs could represents a good strategy to transfer human mature cells to form vessel-like structures and support cell functions for repairing in patients with heart disease in the near future (McClendon and Stupp 2012).

Similarly, to promote endothelialization for CVDs, the GTAGLIGQ gel was functionalized with YIGSR and KKKKK, which are laminin-derived adhesion and nitrogen oxide (NO) donating moieties, respectively. The peptide also incorporated an MMP-2-mediated cleavage site to promote enzymatic degradation of the gel and the subsequent release of both short peptide moieties (Fig. 11.2). When hydrogel was used to coat silicone-based cell culture chambers supplied with NO, adhesion, and proliferation of endothelial cells were enhanced because of the NO released from the gel. It is known that NO is a key mediator of vascular homeostasis and induces endothelial cell proliferation (Kushwaha et al. 2010).

Finally, research has been conducted to modulates the morphology and activity of high-density lipoproteins (HDL). To achieve this, the cyclic peptide c(wLwReQeR) treated with human plasma, was designed to mimic the functions of Apo-1, a key protein involved in the formation of HDL, and that has atheroprotective and anti-inflammatory effects. Thus, the c(wLwReQeR) peptide combined with human

plasma could remodel the formation of human and murine HDL, as it increased the concentration of lipid-poor pre-beta HDL in vitro, which can arrest cholesterol and promotes its efflux from murine macrophages (Zhao et al. 2017). Likewise, the transfer of c(wLwReQeR) peptide into an acute inflammation model in vivo, induced the formation of lipid-poor HDL, which subsequently exerted an anti-inflammatory effect without any side effects. Thus, this strategy arises as an alternative to face cardiovascular diseases, such as stroke, coronary heart disease and other cardiovascular diseases related to the modulation of HDL (Zhao et al. 2017).

11.6 SAPHs for Principal Neurodegenerative Disorders

Neurodegenerative disorders are on the rise as a result of the increase in the world's elderly population, causing severe cognitive deficits, disability, morbidity, and mortality (Erkkinen et al. 2018). The main sign of NDs is a significant loss of neuronal cell population in a disease-specific way; NDs include PD and AD, as well as SCI, among others (Bordoni et al. 2020).

To understand not only their symptomatic presentation but also the exact cause of such neurodegenerative diseases, the development of new therapeutic approaches is required. In this sense, outstanding contributions have been made using SAPHs due to their ability to mimic the ECM environment (Li et al. 2019). In this section, the role of SAPHs as novel therapeutics for the treatment of major NDs will be discussed.

11.6.1 Neurodegenerative Disorders: SAPHs for Alzheimer's Disease

Alzheimer's disease is the principal cause of dementia; it is a progressive ND characterized by loss of memory and other cognitive abilities (GBD 2016 Dementia Collaborators 2019). The precise etiology of AD still remains unclear; however, distorted fibers of Tau proteins inside neurons, inflammation, oxidative stress, and cerebrovascular alterations are possible causes of this pathology (Du et al. 2018). Presently, the most accepted cause of AD is the accumulation of amyloid-β (Aβ) peptides in the brain, which induces severe inflammation and ultimately leads to neuronal degeneration and dementia (Kinney et al. 2018; Grodzicki and Dziendzikowska 2020).

Curcumin, an antioxidant and neuroprotective compound, is a potent inhibitor of Aβ aggregation (Thapa et al. 2016). Therefore, using SAPHs' technology as a carrier and delivery system for curcumin is being explored, as shown with the β-hairpin VKVKV^{D}PPTKVKVKVKVKVKV-NH$_2$ (MAX8) hydrogel. Hydrogelation of MAX8 and homogeneous encapsulation of curcumin has been successfully achieved under physiological conditions, and the release of curcumin from gel facilitates the

survival and distribution of cell medulloblastoma cultured on cell culture plates (Altunbas et al. 2011).

The aforementioned outcome is in good agreement with that reported for epigallocatechin-3-gallate (EGCG) and curcumin hyaluronic acid (HA)-based gels to effectively inhibit Aβ aggregation (Palhano et al. 2013), when both molecules are used together, and synergic inhibition of Aβ peptides accumulation is achieved (Jiang et al. 2018).

One promising strategy for AD treatment is the transfer of neural SCs to improve cognition and synaptic growth in vivo (Ager et al. 2015). Nevertheless, local inflammation in AD is hostile, which impairs the retention and viability of grafted cells (Porayette et al. 2009). Countering this, RADA-16 hydrogel functionalized with YIGSR promotes notable benefits for neural cells, since apoptosis and Aβ aggregation decrease when neural cells are seeded in RADA-16-YIGSR in vitro. In addition, the transfer of cell-loaded RADA-16-YIGSR into rodents improves their memory behavioral tasks and enhances neuronal survival and differentiation even under an inflammatory microenvironment. Furthermore, the rates of Aβ aggregation and apoptosis in the hippocampus (CA1 region) significantly decrease. Thus, this treatment can restore synaptic function and anti-inflammatory response in vivo, making RADA-16 a promising neuroprotective vehicle for the potential clinical transplantation of neural cells for AD treatment (Cui et al. 2016).

It has been proposed that human mutant genes for AD alter the capillary vessel architecture in the brain, a sign called "amyloid angiopathy" (Lee et al. 2005). Many shreds of evidence suggest that neurovascular dysfunction contributes to cognitive decline and neurodegeneration, supporting the comorbidity between AD and cerebrovascular disease (Zlokovic 2005). It is clear that VEGF plays as a critical role in brain angiogenesis (Greenberg and Jin 2005); however, evidence shows that it also participates in the development of neurodegeneration (Storkebaum and Carmeliet 2004). AD patients have shown changes in the rates of VEGF in cerebrospinal fluid (Tarkowski et al. 2002), as well as in serum (Mateo et al. 2007). Accordingly, two functionalized peptides RAD/KLT and RAD/RGI were, respectively, blended to mimic VEGF and brain-derived neurotrophic factor (BDNF) bioactivity, respectively, to bridge peripheral nerve gaps in rats. Once the gel successfully supported a culture of endothelial and neural cells in vitro, it was used to fill up chitosan tubes and then transferred to bridge the ends of excised sciatic nerve in rats. This strategy induced axonal regeneration and motor functional recovery in the treated sites (Lu et al. 2019), making it a promising alternative after clinical trials for AD treatment.

11.6.2 Neurodegenerative Disorders: SAPHs for Parkinson's Disease

Globally, Parkinson's disease affects about 1% of adults over the age of 60, decreasing their quality of life due to the development of severe disorders in movements and

the sensory system. This condition is also characterized by selective loss of dopa-minergic neurons in the substantia nigra (Porayette et al. 2009). A considerable dopamine depletion has been reported in the striatum by 6-hydroxydopamine in the substantia nigra in vivo (Sachs and Jonsson 1975). Therefore, the implantation of SAPHs, for a controlled release of dopamine in vivo arises as a significant strategy for treatment of PD.

Recently, iPSCs were compromised into dopaminergic neurons in RADA-16 gel, as evidenced by the expression of the neural markers Tuj1, MAP2, TH, and FOXA2 in vitro. When cells in gel are transferred in vivo, motor and behavioral recovery functions are regained (Francis et al. 2020). This outcome supports previous inves-tigation showing dopaminergic reprograming of murine embryonic SCs and iPSCs in RADA-16 under basic fibroblast growth factor (bFGF) stimulation (Ni et al. 2013).

Another appealing strategy to address PD is the release of neurotrophic factors, such as glial cell-derived neurotrophic factor (GDNF), neurotrophic nerve growth factor (NGF), and BDNF, into damaged brain tissue (Allen et al. 2013). A recent study explored the role of the RGD-functionalized peptide hydrogel Ac-b A (C_{14}) β-kβ AOH, in which a C_{14} hydrophobic alkyl chain is attached to the first residue. The peptide gel allows the encapsulation and release of BNDF, which eventually facilitates the migration of murine neural cells once the hydrogel is implanted into the subventricular zone of transgenic mice NestinCreER^{T2}. This investigation dem-onstrates that SAPHs can repair brain lesions that require SCs migration (Motamed et al. 2019), which is encouraging for the development of novel approaches to diminish oral dopamine dosage.

11.6.3 NDs: SAPHs for Spinal Cord Injury

Spinal cord injury is a neurological disorder that causes neural circuitry dysfunction (Rofi'i et al. 2019), In SCI, harmful immunological reactions are developed, which lead to a harsh microenvironment that impairs the physiological repairing of glial scares and the spinal cord (Bradbury and Burnside 2019). Chondroitin sulfate pro-teoglycans (CSPGs) are abundant at glial scar sites during SCI and are known to inhibit axonal regeneration (Mukherjee et al. 2020). The peptide gels NH_2-FAQRVPPGGGLDLKLDLKLDLK-CONH$_2$ (called FAQ) and Ac-CGGLKLKLKLKLKLKGGC-CONH$_2$ (called CK) containing chondroitinase ABC (ChABC) can re-connect broken nerve tissue in a chronic SCI model, where neural regeneration and the recovery of behavioral signs are recovered after gel treatment in animals with neurological disorders (Fig. 11.3) (Bordoni et al. 2020). Such an outcome seems to be due to the progressive release of the neuroregenerative ChABC, molecule that impairs the activity of CSPGs in vitro and in vivo. This ultimately leads to the reduction of glial scares, as well as the recovery of hindlimb locomotor function in animals, an outcome that is supported by the presence of GAP43 (protein involved in branching neurons) (Raspa et al. 2021).
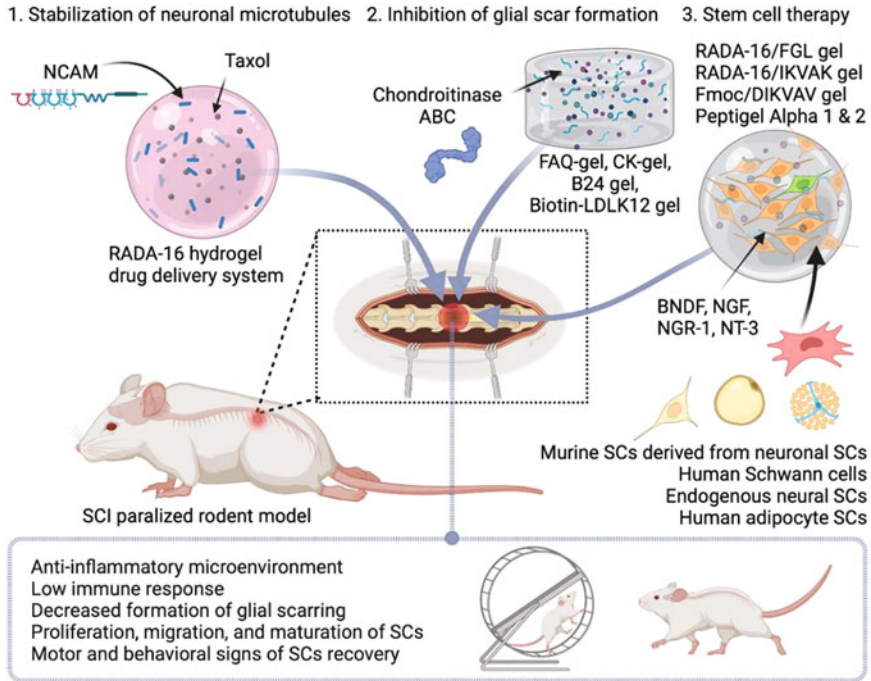
Fig. 11.3 Representation of current strategies for the treatment of SCI in vivo and in vitro using SAPHs

In additional research, two SAPHs known as B24 and biotin-LDLK12, induce a significant attenuation of hematoma after being transferred into lesioned spinal cord of rats. Moreover, such gels increased axonal regeneration in vivo after 22 days. In particular, the gelation of B24 peptide solution functionalized with bone marrow peptide 1 (BMHP1), an inducer of stem cell differentiation, was shown to be more effective than gels already formed when transferred into a damaged spinal cord tissue in vivo. According to the authors, this outcome may be due to a better diffusion and subsequently gelation of peptide solutions when transferred into the treated tissue, facilitating the action of BMHP1 (Fig. 11.3) (Cigognini et al. 2014).

Recently, it also has been reported that the transference into a SCI model of adult human neural SCs cultured in RADA-16 hydrogel enhances cell survival and differentiation, which is followed by a reduction in volume of neural lesions and enhanced neurological functions in a rat SCI (Abdolahi et al. 2021).

The use of the chemotherapy agent Taxol has been shown to stabilize neuronal microtubules (Yang and Horwitz 2017) and promote neural regeneration when blended with RADA-16 (Baas and Ahmad 2013; Hellal et al. 2011). The release of Taxol from the functionalized RADA-16 with EVYVVAENQQGKSKA, a neural

cell adhesion molecule (NCAM), induces neurite preservation and extension in vitro (Fig. 11.3). Additionally, glial scarring and inflammation were shown to decrease after gel transfer into a thoracic SCI model. However, further investigations are needed to finely tune drug release from gels to overcome the current clinical side effects of neurogenerative drugs (Xiao et al. 2020).

Previous research reported the suitability of RADA-16 as an ECM analog to promote the proliferation and migration of murine spinal cord-derived neural SCs (Wang et al. 2015). RADA-16 also supported the culture of human Schwann cells, which after implantation in vivo, reduced astrogliosis and increased cell infiltration at the injury site of a rat SCI model (Fig. 11.3) (Moradi et al. 2012).

A current SCI-related disorder is the formation of classical post-SCI cavities, which limit the recuperation of spinal cordon after injury. To treat such a condition, RADA-16, functionalized with IKVAV and RGD to carry neurotrophic factor (CNTF), BNDF, and NGF, is capable of bridging SCI cavities in rats. The hydrogel also facilitates the proliferation, differentiation, maturation, and myelination of endogenous neural SCs, which form news interconnections in severe cases of SCI in vivo (Fig. 11.3) (Liu et al. 2020).

Likewise, the amphiphile IKVAV-CH3(CH2)14CO-AAAAGGGEIKVAV hydrogel provides sustained release of BNDF in severe rat SCI. Remarkably, BNDF maintained its bioactivity for 21 days, promoting axon preservation and long-term gliosis reduction, elucidating a minimal inflammatory response in treated animals (Hassannejad et al. 2019).

A Fmoc peptide (Fmoc FF) gel (Zhou et al. 2009) functionalized with DIKVAV (Fmoc-DIKVAV) loaded with murine viable and non-viable mesenchymal precursor cells was shown to heal injured murine spinal cord. Animals treated with functionalized gel exhibited axonal regeneration, which according to researchers, might be derived from cellular infiltration and axonal regrowth facilitated by the peptide gel (Fig. 11.3). Although this outcome seems promising to promote axonal regeneration, further research is needed to finely tune the rate of ECM moieties incorporated in gel to facilitate its eventual use for clinical SCI treatment (Wiseman et al. 2020).

Most recently, two octapeptide hydrogels commercially known as PeptiGel-Alpha 1 and PeptiGel-Alpha 2 supported the culture and neurotrophic compromise of human adipocyte SCs (hdASCs). Both peptide hydrogels allowed the survival of hdASCs and neuronal extensions, as well as the expression of neurotrophic markers, such as BNDF, NGF, neuregulin 1 (NRG-1), and neurotrophin 3 (NT-3) after 1 day of culture without the incorporation of any biological stimuli (Fig. 11.3) (Faroni et al. 2019). This investigation suggests the feasibility of such peptide gels as a potential treatment for peripheral nerve injuries after following appropriate clinical evaluations.

11.7 Pancreatic Diseases

Diabetes mellitus (DM) is a metabolic disease characterized by hyperglycemia, which causes severe damage to various organs and tissues and the death of 1.6 million people each year (World Health Organization 2021b). Type I diabetes DM (TIDM) is characterized by low or null production of insulin, whereas in TIIDM, there is insulin resistance or little production of it (World Health Organization 2021b). The gold standard for tackling DM includes lifestyle changes and medication. However, patients suffering from TIDM may be subject to pancreatic islet grafting followed by immunotherapy (World Health Organization 2021c).

11.7.1 Pancreatic Diseases: SAPHs as Vehicles for Islet Transplant

Improving the retention, survival, and function of pancreatic islet grafts remains as major goal in medicine, since the viability of such grafts limits insulin dependence of treated patients. This has encouraged scientists to seek for alternatives to protect islets from harsh environments after transfer (Reyes-Martinez et al. 2019; Castillo-Diaz et al. 2020; Rickels and Robertson 2019).

In this context, the 3D nanoarchitecture of SAPHs has shown to be suitable for protecting and enhancing the survival of islets (Lim et al. 2011; Zhao et al. 2010), β-cells (Hwang et al. 2017; Liu et al. 2015; Khan et al. 2012; Beenken-Rothkopf et al. 2013), and pancreatic molecules (Hwang et al. 2017; Lim et al. 2011; Liu et al. 2015; Khan et al. 2012; Beenken-Rothkopf et al. 2013; Chow et al. 2010) for grafting applications (Stendahl et al. 2008; Uzunalli et al. 2015; Liu et al. 2016).

An example of this is the amphiphile gel GTAGLIGQRGDS (*Nanomatrix*), which is supported by fibers of 8–10 nm in diameter that offers pore sizes of 100–300 nm large enough to allow the diffusion of cellular nutrients and insulin. This hydrogel functionalized with RGD induces pancreatic cell anchorage and survival (Fig. 11.4) (Hwang et al. 2017; Lim et al. 2011). Both murine (Lim et al. 2011) and human islets (Hwang et al. 2017) cultured in *Nanomatrix* synthesize insulin under glucose stimulation and inflammatory environments for long time period (Hwang et al. 2017; Lim et al. 2011), making this gel an appealing ECM analogous to protect pancreatic grafts to face TIDM.

An interesting approach focused on the functionalization of two amphiphilic *Nanomatrix* gels with molecules involved in pancreatic cell survival. The first gel was functionalized with the laminin-derived adhesive ligand YIGSR, which in turn was linked to the MMP-2 degradable site (GTAGLIGQ) to favor cell migration. The second amphiphilic gel incorporated the pentapeptide KKKKK as a nitric oxide (NO) donor, since it is believed that NO can induce cellular viability and insulin production. However, the role of NO in biological models remains controversial. In this case, the combination of both hydrogels significantly favored the survival of
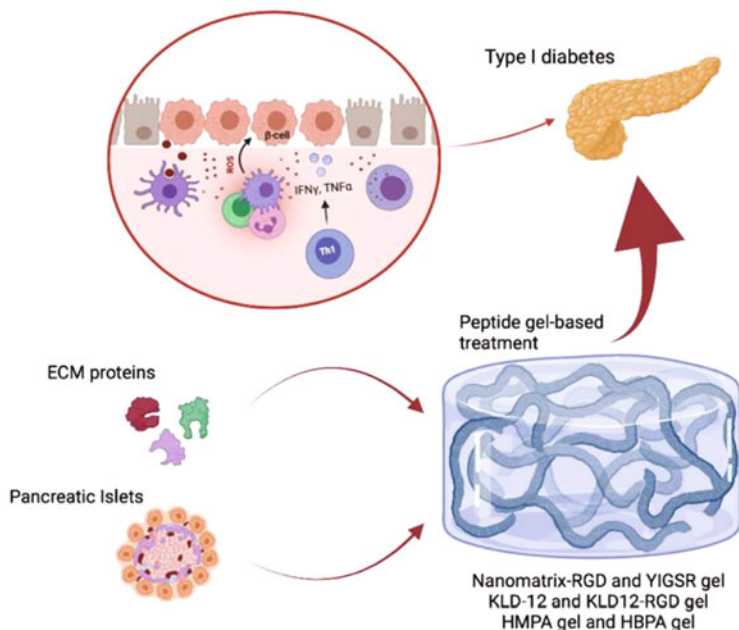
Fig. 11.4 Representation of functionalized SAPHs supporting the encapsulation of pancreatic molecules and mammalian cells to improve islet transplant

murine β-cells and stimulated insulin production along with the expression of *Ins1* and *Pdx* genes coding for insulin in vitro (Fig. 11.4) (Lim et al. 2014). Nevertheless, additional research must be conducted to clearly support the positive role that NO release from peptide gels has to induce the survival of pancreatic cells and ultimately the production of insulin production in vivo.

Similarly, arginine has been incorporated into the peptide sequence of KLD-12 to favor the formation of a cationic hydrogel electrostatically capable of binding HGF, which is known to have an anti-inflammatory effect. KLD-12-HGF succeeded to improve the survival and function of rat insulin producing cells cultured in 3D. Furthermore, once rat β-cells resuspended in KLD-12-HGF solution were transferred into rat kidneys, hydrogelation was held and cells increased the production of insulin as HGF was progressively released from KLD-12 gel under inflammatory conditions for 7 days in vivo. In addition, β-cell apoptosis, T lymphocyte infiltration, and inflammatory-related pathways were inhibited after hydrogel treatment (Liu et al. 2016). This outcome highlights the suitability of SAPHs as protective carriers of cells to improve islet grafting. The functionalization of KLD-12 with RGD and GEFYFDLRLKGDK (from collagen IV) also improves the viability, proliferation, and insulin production of murine β-cells when cultured in 3D (Fig. 11.4), corroborating the suitability of SAPHS as promising ECM analogs for pancreatic regeneration applications (Liu et al. 2015).

Angiogenesis is key to maintain the integrity of tissues and facilitate the success of islet transplant. In this sense, SAPHs mimicking the function of heparin (an angiogenic inducer), such as the heparin mimetic amphiphile (HM-PA) hydrogel (Lauryl-VVAGEGD (K-pbs) S-Am), promote the viability of murine islets and insulin production in vitro under stimulation with VEGF and bFGF. Remarkably, the transfer of islets in HM-PA gels into diabetic mice, restores euglycemia to levels that are comparable with healthy mice in up to 28 days (Uzunalli et al. 2015). This research exemplifies the versatility of peptide hydrogels to inherently offer ECM-like biofunctionality once ECM ligands are incorporated into them. However, as for most research discussed here, forthcoming investigations must be conducted to standardize the concentrations of biological ligands linked to peptide gels to direct regenerative biological functions without inducing non-desirable physiological responses.

In a similar approach, the peptide (HBPA) (LRKKLGKA) forms a self-assembled hydrogel once it binds heparin. This hydrogel is formed by nanofibers of 6–7.5 nm in diameter and from 6–7.5 nm to 1 μm in length (Chow et al. 2010; Rajangam et al. 2006). The hydrogel can retain and deliver angiogenic growth factors (VEGF and bFGF). This promotes the survival and the production of insulin by murine islets cultured in gel in vitro (Fig. 11.4). According to researchers, both growth factors are crucial to induce neovascularization of islets inside the HBPA hydrogel (Chow et al. 2010). Previously, the release of VEGF and bFGF from the HBPA hydrogel increased the density of blood vessels after transfer in vivo. Moreover, the encapsulation of both growth factors supported islet grafting and promoted normoglycemia in diabetic mice (Stendahl et al. 2008).

Finally, a self-assembled glucagon-like peptide 1 (GLP-1) hydrogel formed by cylindrical nanofibers (ca. 10 nm diameter) can mimic the function of GLP-1 to induce insulin production when murine β-cells are cultured in the gel in vitro. Insulin production is induced after glucose stimulation like it occurs in vivo and is similar to the performance of clinically used GLP-1 analogous exendin-4. More interestingly, this outcome is achieved under an inflammatory environment (Khan et al. 2012).

The investigations discussed to put in perspective the feasibility of SAPHs as promising 3D depots to protect pancreatic cells (Beenken-Rothkopf et al. 2013) under inflammatory environments, which is encouraging for the improvement of current islet grafting techniques (Fig. 11.4). However, further research is needed to discard any toxicity or immunogenic reactions derived from such approaches.

11.7.2 Pancreatic Diseases: SAPHs for Hyperglycemia and Wound Healing

Nowadays, there is a push to find novel strategies to prevent and revert hyperglycemia to increase the efficacy of hypoglycemic drugs and decrease the number of doses.
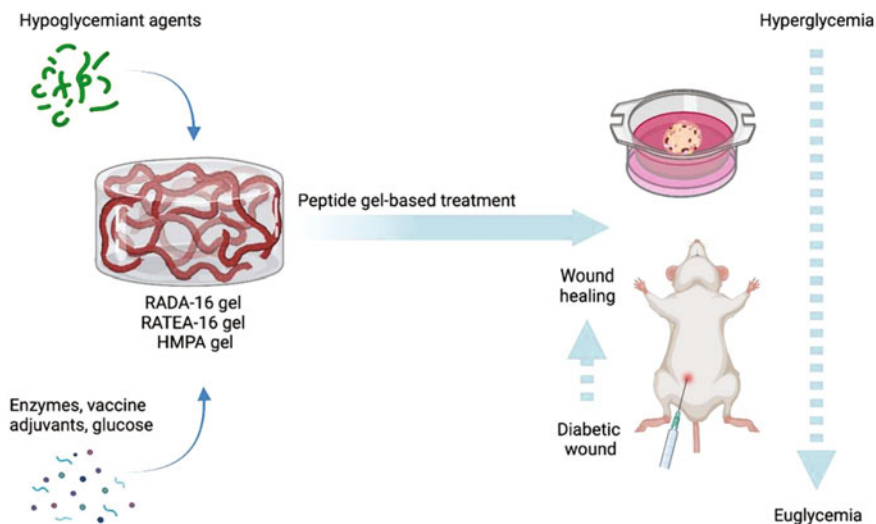
Fig. 11.5 Representation of functionalized SAPHs to act as 3D scaffolds to induce wound healing in vivo and restore euglycemia in vitro and in vivo

A recent investigation explored the suitability of the encapsulation of the hypoglycemic agents: hempseed hydrolysates and sitagliptin, the latter a commercial dipeptidyl peptidase IV (DDPIV) in RADA-16 gel. The results of this research showed that hempseed hydrolysates are efficiently protected from DDPIV degradation when encapsulated in gel (Fig. 11.5). In addition, RADA-16/hempseed induces synergistic activity along with sitagliptin to inhibit the activity of DDPIV in vitro (Lammi et al. 2018).

The pH-sensitive RATEA-16 peptide assembles into a β-sheet secondary structure to form a gel that supports the release of insulin in a glucose-dependent manner. The release of insulin from RATEA-16 is held at low pH, where the gel disassembles because of the conversion of glucose into gluconic acid through enzymatic reactions carried out by catalase, and glucose oxidase is also encapsulated in the gel. Importantly, the release of insulin from RATEA-16 induced euglycemia for up to 12 h in vitro and up to 8 days in diabetic rats (Fig. 11.5) (Fu et al. 2018).

In another interesting approach, RADA-16 hydrogel was used to develop an antidiabetic vaccine to prevent hyperglycemia. Both granulocyte macrophage colony-stimulating factor (GM-GSF) and CpG ODN 1826 (CpG), acting as adjuvants, were encapsulated in RADA-16 along with poly(lactide-co-glycolide) (PLGA) microparticles loaded with insulin. After subcutaneous administration of RADA-16 into non-obese diabetic mice, TIDM protection is achieved with a 40% effectivity up to 28 days (Fig. 11.5). It is believed that such an outcome after gel treatment is significantly due to the action from CpG, which stimulates the production of the anti-inflammatory interleukin-10 (Yoon et al. 2015).

Last but not least, wound healing is a DM-related medical condition characterized by chronic inflammation and impairment of angiogenesis. Untreated diabetic wounds can lead to ulcers, which may cause the loss of extremities at late stages. Recently, it was found that angiogenesis, wound closure, and re-epithelialization can be induced through the application of an HMPA hydrogel in diabetic mice (Fig. 11.5). This peptide gel is made by merging two amphiphile peptides: Lauryl-VVAGEGDK (pbs)S-am and Lauryl-VVAGK-Am, which carry negative (-3) and positive charges ($+1$), respectively. Following topical gel treatment, inflammation decreased up to 21 days in treated animals. It is believed that angiogenesis induction is facilitated by the capability of the hydrogel to electrostatically bind VEGF and subsequently deliver it into treated wounds (Senturk et al. 2017).

11.8 Conclusion and Future Perspectives

There is no doubt that SAPHs offer a suitable niche not only to deliver functional biomolecules and cells to treat several chronic diseases but also to trap them once gelation is induced, optimizing seeding efficiency. Nonetheless, there are shortcomings to address, such as mechanical properties, degradation profiles, stability, and sterilization.

SAPHs mechanical properties are not comparable to those of hard tissues, such as bone, which might be a challenge if these are used on load-bearing sites. Also, SAPHs stability depends greatly on pH needed for various types of cells to survive, especially under harsh conditions during disease.

When translating this technology into the clinic, we must consider manufacturing aspects, such as peptide synthesis cost, shelf-life, sterilization issues, and the standardization of the rate of biological ECM ligands or proteins included in them. Yet, SAPHs have unique advantages due to their versatility in functionalizing them to improve properties, such as biocompatibility, tunability (biological inducers and mechanics), and antimicrobial activity. In addition, they are not derived from an animal source. Given these benefits, in the long term, SAPHs might greatly facilitate current clinical treatments to address chronic diseases discussed here.

References

Abdolahi S, Aligholi H, Khodakaram-Tafti A, Khaleghi Ghadiri M, Stummer W, Gorji A (2021) Improvement of rat spinal cord injury following lentiviral vector-transduced neural stem/

progenitor cells derived from human epileptic brain tissue transplantation with a self-assembling peptide scaffold. Mol Neurobiol 58(6):2481–2493

Ager RR, Davis JL, Agazaryan A, Benavente F, Poon WW, LaFerla FM et al (2015) Human neural stem cells improve cognition and promote synaptic growth in two complementary transgenic models of Alzheimer's disease and neuronal loss. Hippocampus 25(7):813–826

Aggeli A, Nyrkova IA, Bell M, Harding R, Carrick L, McLeish TC et al (2001) Hierarchical self-assembly of chiral rod-like molecules as a model for peptide beta -sheet tapes, ribbons, fibrils, and fibers. Proc Natl Acad Sci U S A 98(21):11857–11862

Alberts B, Johnson A, Lewis J, Walter P, Raff M, Roberts K (2002) Molecular biology of the cell, 4th edn: international student edition. Routledge, London

Allen SJ, Watson JJ, Shoemark DK, Barua NU, Patel NK (2013) GDNF, NGF and BDNF as therapeutic options for neurodegeneration. Pharmacol Ther 138(2):155–175

Almeida LDF, Babo PS, Silva CR, Rodrigues MT, Hebling J, Reis RL et al (2018) Hyaluronic acid hydrogels incorporating platelet lysate enhance human pulp cell proliferation and differentiation. J Mater Sci Mater Med. 29(6):88

Altunbas A, Lee SJ, Rajasekaran SA, Schneider JP, Pochan DJ (2011) Encapsulation of curcumin in self-assembling peptide hydrogels as injectable drug delivery vehicles. Biomaterials 32(25):5906–5914

Ando K, Imagama S, Kobayashi K, Ito K, Tsushima M, Morozumi M et al (2018) Feasibility and effects of a self-assembling peptide as a scaffold in bone healing: an in vivo study in rabbit lumbar posterolateral fusion and tibial intramedullary models. J Orthop Res 36(12):3285–3293

Arjmand B, Sarvari M, Alavi-Moghadam S, Payab M, Goodarzi P, Gilany K et al (2020) Prospect of stem cell therapy and regenerative medicine in osteoporosis. Front Endocrinol (Lausanne) 11:430

Baas PW, Ahmad FJ (2013) Beyond taxol: microtubule-based treatment of disease and injury of the nervous system. Brain 136(Pt 10):2937–2951

Bajpayee AG, De la Vega RE, Scheu M, Varady NH, Yannatos IA, Brown LA et al (2017) Sustained intra-cartilage delivery of low dose dexamethasone using a cationic carrier for treatment of post traumatic osteoarthritis. Eur Cell Mater 34:341–364

Barco A, Ingham E, Fisher J, Fermor H, Davies RPW (2018) On the design and efficacy assessment of self-assembling peptide-based hydrogel-glycosaminoglycan mixtures for potential repair of early stage cartilage degeneration. J Pept Sci 24(8-9):e3114

Beenken-Rothkopf LN, Karfeld-Sulzer LS, Davis NE, Forster R, Barron AE, Fontaine MJ (2013) The incorporation of extracellular matrix proteins in protein polymer hydrogels to improve encapsulated beta-cell function. Ann Clin Lab Sci 43(2):111–121

Bell CJ, Carrick LM, Katta J, Jin Z, Ingham E, Aggeli A et al (2006) Self-assembling peptides as injectable lubricants for osteoarthritis. J Biomed Mater Res A 78(2):236–246

Belviso I, Romano V, Sacco AM, Ricci G, Massai D, Cammarota M et al (2020) Decellularized human dermal matrix as a biological scaffold for cardiac repair and regeneration. Front Bioeng Biotechnol 8:229

Boopathy AV, Martinez MD, Smith AW, Brown ME, Garcia AJ, Davis ME (2015) Intramyocardial delivery of notch ligand-containing hydrogels improves cardiac function and angiogenesis following infarction. Tissue Eng Part A 21(17–18):2315–2322

Bordoni M, Scarian E, Rey F, Gagliardi S, Carelli S, Pansarasa O et al (2020) Biomaterials in neurodegenerative disorders: a promising therapeutic approach. Int J Mol Sci 21(9):3243

Bradbury EJ, Burnside ER (2019) Moving beyond the glial scar for spinal cord repair. Nat Commun 10(1):3879

Briuglia ML, Urquhart AJ, Lamprou DA (2014) Sustained and controlled release of lipophilic drugs from a self-assembling amphiphilic peptide hydrogel. Int J Pharm 474(1–2):103–111

Burgess KA, Frati C, Meade K, Gao J, Castillo Diaz L, Madeddu D et al (2021) Functionalised peptide hydrogel for the delivery of cardiac progenitor cells. Mater Sci Eng C Mater Biol Appl 119:111539

Caplan MR, Schwartzfarb EM, Zhang S, Kamm RD, Lauffenburger DA (2002) Control of self-assembling oligopeptide matrix formation through systematic variation of amino acid sequence. Biomaterials 23(1):219–227

Castillo Diaz LA, Saiani A, Gough JE, Miller AF (2014) Human osteoblasts within soft peptide hydrogels promote mineralisation in vitro. J Tissue Eng 5:2041731414539344

Castillo Diaz LA, Elsawy M, Saiani A, Gough JE, Miller AF (2016) Osteogenic differentiation of human mesenchymal stem cells promotes mineralization within a biodegradable peptide hydrogel. J Tissue Eng 7:2041731416649789

Castillo-Diaz LA, Ruiz-Pacheco JA, Elsawy MA, Reyes-Martinez JE, Enriquez-Rodriguez AI (2020) Self-assembling peptides as an emerging platform for the treatment of metabolic syndrome. Int J Nanomedicine 15:10349–10370

Chow LW, Wang LJ, Kaufman DB, Stupp SI (2010) Self-assembling nanostructures to deliver angiogenic factors to pancreatic islets. Biomaterials 31(24):6154–6161

Cigognini D, Silva D, Paloppi S, Gelain F (2014) Evaluation of mechanical properties and therapeutic effect of injectable self-assembling hydrogels for spinal cord injury. J Biomed Nanotechnol 10(2):309–323

Compston JE, McClung MR, Leslie WD (2019) Osteoporosis. Lancet 393(10169):364–376

Cui H, Webber MJ, Stupp SI (2010) Self-assembly of peptide amphiphiles: from molecules to nanostructures to biomaterials. Biopolymers 94(1):1–18

Cui GH, Shao SJ, Yang JJ, Liu JR, Guo HD (2016) Designer self-assemble peptides maximize the therapeutic benefits of neural stem cell transplantation for Alzheimer's disease via enhancing neuron differentiation and paracrine action. Mol Neurobiol 53(2):1108–1123

Davis ME, Hsieh PC, Takahashi T, Song Q, Zhang S, Kamm RD et al (2006) Local myocardial insulin-like growth factor 1 (IGF-1) delivery with biotinylated peptide nanofibers improves cell therapy for myocardial infarction. Proc Natl Acad Sci U S A 103(21):8155–8160

Du X, Wang X, Geng M (2018) Alzheimer's disease hypothesis and related therapies. Transl Neurodegener 7:2

Dufour A, Lafont JE, Buffier M, Verset M, Cohendet A, Contamin H et al (2021) Repair of full-thickness articular cartilage defects using IEIK13 self-assembling peptide hydrogel in a non-human primate model. Sci Rep 11(1):4560

Erkkinen MG, Kim MO, Geschwind MD (2018) Clinical neurology and epidemiology of the major neurodegenerative diseases. Cold Spring Harb Perspect Biol 10(4):a033118

Etich J, Lessmeier L, Rehberg M, Sill H, Zaucke F, Netzer C et al (2020) Osteogenesis imperfecta-pathophysiology and therapeutic options. Mol Cell Pediatr 7(1):9

Faroni A, Workman VL, Saiani A, Reid AJ (2019) Self-assembling peptide hydrogel matrices improve the neurotrophic potential of human adipose-derived stem cells. Adv Healthcare Mater 8(17):1900410

Firth A, Aggeli A, Burke JL, Yang X, Kirkham J (2006) Biomimetic self-assembling peptides as injectable scaffolds for hard tissue engineering. Nanomedicine (Lond) 1(2):189–199

Francis NL, Zhao N, Calvelli HR, Saini A, Gifford JJ, Wagner GC et al (2020) Peptide-based scaffolds for the culture and transplantation of human dopaminergic neurons. Tissue Eng Part A. 26(3–4):193–205

Fu M, Zhang C, Dai Y, Li X, Pan M, Huang W et al (2018) Injectable self-assembled peptide hydrogels for glucose-mediated insulin delivery. Biomater Sci 6(6):1480–1491

GBD 2016 Dementia Collaborators (2019) Global, regional, and national burden of Alzheimer's disease and other dementias, 1990–2016: a systematic analysis for the Global Burden of Disease Study 2016. Lancet Neurol 18(1):88–106

Gelain F, Bottai D, Vescovi A, Zhang S (2006) Designer self-assembling peptide nanofiber scaffolds for adult mouse neural stem cell 3-dimensional cultures. PLoS One 1:e119

Gelain F, Luo Z, Rioult M, Zhang S (2021) Self-assembling peptide scaffolds in the clinic. NPJ Regen Med 6(1):9

Gotherstrom C, Walther-Jallow L (2020) Stem cell therapy as a treatment for osteogenesis imperfecta. Curr Osteoporos Rep 18(4):337–343

Gough JE, Saiani A, Miller AF (2012) Peptide hydrogels: mimicking the extracellular matrix. Bioinspir Biomim Nanobiomater 1(1):4–12

Greenberg DA, Jin K (2005) From angiogenesis to neuropathology. Nature 438(7070):954–959

Gribbon C, Channon KJ, Zhang W, Banwell EF, Bromley EH, Chaudhuri JB et al (2008) MagicWand: a single, designed peptide that assembles to stable, ordered alpha-helical fibers. Biochemistry 47(39):10365–10371

Grodzicki W, Dziendzikowska K (2020) The role of selected bioactive compounds in the prevention of Alzheimer's disease. Antioxidants (Basel) 9(3):229

Guillaume O, Daly A, Lennon K, Gansau J, Buckley SF, Buckley CT (2014) Shape-memory porous alginate scaffolds for regeneration of the annulus fibrosus: effect of TGF-beta3 supplementation and oxygen culture conditions. Acta Biomater 10(5):1985–1995

Guo HD, Cui GH, Wang HJ, Tan YZ (2010) Transplantation of marrow-derived cardiac stem cells carried in designer self-assembling peptide nanofibers improves cardiac function after myocardial infarction. Biochem Biophys Res Commun 399(1):42–48

Han C, Zhou J, Liang C, Liu B, Pan X, Zhang Y et al (2019) Human umbilical cord mesenchymal stem cell derived exosomes encapsulated in functional peptide hydrogels promote cardiac repair. Biomater Sci 7(7):2920–2933

Hassannejad Z, Zadegan SA, Vaccaro AR, Rahimi-Movaghar V, Sabzevari O (2019) Biofunctionalized peptide-based hydrogel as an injectable scaffold for BDNF delivery can improve regeneration after spinal cord injury. Injury 50(2):278–285

Hellal F, Hurtado A, Ruschel J, Flynn KC, Laskowski CJ, Umlauf M et al (2011) Microtubule stabilization reduces scarring and causes axon regeneration after spinal cord injury. Science 331(6019):928–931

Hellmund KS, von Lospichl B, Böttcher C, Ludwig K, Keiderling U, Noirez L et al (2021) Functionalized peptide hydrogels as tunable extracellular matrix mimics for biological applications. Pept Sci 113(2):e24201

Hogrebe NJ, Reinhardt JW, Tram NK, Debski AC, Agarwal G, Reilly MA et al (2018) Independent control of matrix adhesiveness and stiffness within a 3D self-assembling peptide hydrogel. Acta Biomater 70:110–119

Huang LC, Wang HC, Chen LH, Ho CY, Hsieh PH, Huang MY et al (2019) Bioinspired self-assembling peptide hydrogel with proteoglycan-assisted growth factor delivery for therapeutic angiogenesis. Theranostics 9(23):7072–7087

Hubbell JA (2007) Chapter 21—Matrix effects. In: Lanza R, Langer R, Vacanti J (eds) Principles of tissue engineering, 3rd edn. Academic Press, Burlington, pp 297–308

Hwang PTJ, Shah DK, Garcia JA, Alexander GC, Lim DJ, Cui W et al (2017) Encapsulation of human islets using a biomimetic self-assembled nanomatrix gel for protection against cellular inflammatory responses. ACS Biomater Sci Eng 3(9):2110–2119

Ichihara Y, Kaneko M, Yamahara K, Koulouroudias M, Sato N, Uppal R et al (2018) Self-assembling peptide hydrogel enables instant epicardial coating of the heart with mesenchymal stromal cells for the treatment of heart failure. Biomaterials 154:12–23

Infante A, Gener B, Vazquez M, Olivares N, Arrieta A, Grau G et al (2021) Reiterative infusions of MSCs improve pediatric osteogenesis imperfecta eliciting a pro-osteogenic paracrine response: TERCELOI clinical trial. Clin Transl Med 11(1):e265

Jayawarna V, Ali M, Jowitt TA, Miller AF, Saiani A, Gough JE et al (2006) Nanostructured hydrogels for three-dimensional cell culture through self-assembly of fluorenylmethoxycarbonyl–dipeptides. Adv Mater 18(5):611–614

Jayawarna V, Richardson SM, Hirst AR, Hodson NW, Saiani A, Gough JE et al (2009) Introducing chemical functionality in Fmoc-peptide gels for cell culture. Acta Biomater 5(3):934–943

Jensen C, Teng Y (2020) Is it time to start transitioning from 2D to 3D cell culture? Front Mol Biosci 7:33

Jiang Z, Dong X, Yan X, Liu Y, Zhang L, Sun Y (2018) Nanogels of dual inhibitor-modified hyaluronic acid function as a potent inhibitor of amyloid beta-protein aggregation and cytotoxicity. Sci Rep 8(1):3505

Jiang Y, Zhang P, Zhang X, Lv L, Zhou Y (2021) Advances in mesenchymal stem cell transplantation for the treatment of osteoporosis. Cell Prolif 54(1):e12956

Jung JP, Moyano JV, Collier JH (2011) Multifactorial optimization of endothelial cell growth using modular synthetic extracellular matrices. Integr Biol (Camb) 3(3):185–196

Khan S, Sur S, Newcomb CJ, Appelt EA, Stupp SI (2012) Self-assembling glucagon-like peptide 1-mimetic peptide amphiphiles for enhanced activity and proliferation of insulin-secreting cells. Acta Biomater 8(5):1685–1692

Kim JH, Jung Y, Kim SH, Sun K, Choi J, Kim HC et al (2011) The enhancement of mature vessel formation and cardiac function in infarcted hearts using dual growth factor delivery with self-assembling peptides. Biomaterials 32(26):6080–6088

Kim JE, Lee SM, Kim SH, Tatman P, Gee AO, Kim DH et al (2014) Effect of self-assembled peptide-mesenchymal stem cell complex on the progression of osteoarthritis in a rat model. Int J Nanomedicine 9(Suppl 1):141–157

Kinney JW, Bemiller SM, Murtishaw AS, Leisgang AM, Salazar AM, Lamb BT (2018) Inflammation as a central mechanism in Alzheimer's disease. Alzheimers Dement (N Y) 4:575–590

Kisiday J, Jin M, Kurz B, Hung H, Semino C, Zhang S et al (2002) Self-assembling peptide hydrogel fosters chondrocyte extracellular matrix production and cell division: implications for cartilage tissue repair. Proc Natl Acad Sci U S A 99(15):9996–10001

Kloppenburg M, Berenbaum F (2020) Osteoarthritis year in review 2019: epidemiology and therapy. Osteoarthr Cartil 28(3):242–248

Kopesky PW, Vanderploeg EJ, Sandy JS, Kurz B, Grodzinsky AJ (2010) Self-assembling peptide hydrogels modulate in vitro chondrogenesis of bovine bone marrow stromal cells. Tissue Eng Part A 16(2):465–477

Krishnan Y, Grodzinsky AJ (2018) Cartilage diseases. Matrix Biol. 71–72:51–69

Kushwaha M, Anderson JM, Bosworth CA, Andukuri A, Minor WP, Lancaster JR Jr et al (2010) A nitric oxide releasing, self assembled peptide amphiphile matrix that mimics native endothelium for coating implantable cardiovascular devices. Biomaterials 31(7):1502–1508

Lammi C, Bollati C, Gelain F, Arnoldi A, Pugliese R (2018) Enhancement of the stability and anti-DPPIV activity of hempseed hydrolysates through self-assembling peptide-Based hydrogels. Front Chem 6:670

Lee GD, Aruna JH, Barrett PM, Lei DL, Ingram DK, Mouton PR (2005) Stereological analysis of microvascular parameters in a double transgenic model of Alzheimer's disease. Brain Res Bull 65(4):317–322

Li X, Chen YY, Wang XM, Gao K, Gao YZ, Cao J et al (2017) Image-guided stem cells with functionalized self-assembling peptide nanofibers for treatment of acute myocardial infarction in a mouse model. Am J Transl Res 9(8):3723–3731

Li J, Xing R, Bai S, Yan X (2019) Recent advances of self-assembling peptide-based hydrogels for biomedical applications. Soft Matter 15(8):1704–1715

Lim DJ, Antipenko SV, Anderson JM, Jaimes KF, Viera L, Stephen BR et al (2011) Enhanced rat islet function and survival in vitro using a biomimetic self-assembled nanomatrix gel. Tissue Eng Part A 17(3–4):399–406

Lim DJ, Andukuri A, Vines JB, Rahman SM, Hwang PT, Kim J et al (2014) Enhanced MIN-6 beta cell survival and function on a nitric oxide-releasing peptide amphiphile nanomatrix. Int J Nanomedicine 9(Suppl 1):13–21

Liu J, Liu S, Chen Y, Zhao X, Lu Y, Cheng J (2015) Functionalized self-assembling peptide improves INS-1 beta-cell function and proliferation via the integrin/FAK/ERK/cyclin pathway. Int J Nanomedicine 10:3519–3531

Liu S, Zhang L, Cheng J, Lu Y, Liu J (2016) Sustained release of hepatocyte growth factor by cationic self-assembling peptide/heparin hybrid hydrogel improves beta-cell survival and function through modulating inflammatory response. Int J Nanomedicine 11:4875–4890

Liu H, Xu X, Tu Y, Chen K, Song L, Zhai J et al (2020) Engineering microenvironment for endogenous neural regeneration after spinal cord injury by reassembling extracellular matrix. ACS Appl Mater Interfaces 12(15):17207–17219

Lu C, Wang Y, Yang S, Wang C, Sun X, Lu J et al (2018) Bioactive self-assembling peptide hydrogels functionalized with brain-derived neurotrophic factor and nerve growth factor mimicking peptides synergistically promote peripheral nerve regeneration. ACS Biomater Sci Eng 4(8):2994–3005

Lu J, Yan X, Sun X, Shen X, Yin H, Wang C et al (2019) Synergistic effects of dual-presenting VEGF- and BDNF-mimetic peptide epitopes from self-assembling peptide hydrogels on peripheral nerve regeneration. Nanoscale 11(42):19943–19958

Lv X, Sun C, Hu B, Chen S, Wang Z, Wu Q et al (2020) Simultaneous recruitment of stem cells and chondrocytes induced by a functionalized self-assembling peptide hydrogel improves endogenous cartilage regeneration. Front Cell Dev Biol 8:864

Macias I, Alcorta-Sevillano N, Rodriguez CI, Infante A (2020) Osteoporosis and the potential of cell-based therapeutic strategies. Int J Mol Sci 21(5):1801400

Madhuri V, Ramesh S, Raymond R, Selina A, Loganathan L (2021) Translational research in osteogenesis imperfecta and cell therapy. Proceedings 72(1):3

Marom R, Rabenhorst BM, Morello R (2020) Osteogenesis imperfecta: an update on clinical features and therapies. Eur J Endocrinol 183(4):R95–r106

Mateo I, Llorca J, Infante J, Rodriguez-Rodriguez E, Fernandez-Viadero C, Pena N et al (2007) Low serum VEGF levels are associated with Alzheimer's disease. Acta Neurol Scand 116(1): 56–58

McClendon MT, Stupp SI (2012) Tubular hydrogels of circumferentially aligned nanofibers to encapsulate and orient vascular cells. Biomaterials 33(23):5713–5722

Mecham RP (2011) The extracellular matrix: an overview. Springer, Berlin

Miller RE, Grodzinsky AJ, Vanderploeg EJ, Lee C, Ferris DJ, Barrett MF et al (2010) Effect of self-assembling peptide, chondrogenic factors, and bone marrow-derived stromal cells on osteochondral repair. Osteoarthr Cartil 18(12):1608–1619

Moller JE, Pellikka PA, Hillis GS, Oh JK (2006) Prognostic importance of diastolic function and filling pressure in patients with acute myocardial infarction. Circulation 114(5):438–444

Moradi F, Bahktiari M, Joghataei MT, Nobakht M, Soleimani M, Hasanzadeh G et al (2012) BD PuraMatrix peptide hydrogel as a culture system for human fetal Schwann cells in spinal cord regeneration. J Neurosci Res 90(12):2335–2348

Motamed S, Del Borgo MP, Zhou K, Kulkarni K, Crack PJ, Merson TD et al (2019) Migration and differentiation of neural stem cells diverted from the subventricular zone by an injectable self-assembling β-peptide hydrogel. Front Bioeng Biotechnol 7:315

Mouw JK, Ou G, Weaver VM (2014) Extracellular matrix assembly: a multiscale deconstruction. Nat Rev Mol Cell Biol 15(12):771–785

Mujeeb A, Miller AF, Saiani A, Gough JE (2013) Self-assembled octapeptide scaffolds for in vitro chondrocyte culture. Acta Biomater 9(1):4609–4617

Mukherjee N, Nandi S, Garg S, Ghosh S, Ghosh S, Samat R et al (2020) Targeting chondroitin sulfate proteoglycans: an emerging therapeutic strategy to treat CNS injury. ACS Chem Neurosci 11(3):231–232

Murai K, Funamizu Y, Ogura T, Nishio K (2021) Bioinspired mineralization of calcium carbonate in peptide hydrogel acting as a multifunctional three-dimensional template. J Asian Ceram Soc 9:1–11

Najafi H, Jafari M, Farahavar G, Abolmaali SS, Azarpira N, Borandeh S et al (2021) Recent advances in design and applications of biomimetic self-assembled peptide hydrogels for hard tissue regeneration. Biodes Manuf 4:1–22

Nellenbach K, Nandi S, Peeler C, Kyu A, Brown AC (2020) Neonatal fibrin scaffolds promote enhanced cell adhesion, migration, and wound healing in vivo compared to adult fibrin scaffolds. Cell Mol Bioeng 13(5):393–404

Nesto RW, Kowalchuk GJ (1987) The ischemic cascade: temporal sequence of hemodynamic, electrocardiographic and symptomatic expressions of ischemia. Am J Cardiol 59(7):23c–30c

Ni N, Hu Y, Ren H, Luo C, Li P, Wan JB et al (2013) Self-assembling peptide nanofiber scaffolds enhance dopaminergic differentiation of mouse pluripotent stem cells in 3-dimensional culture. PLoS One 8(12):e84504

Nicolas J, Magli S, Rabbachin L, Sampaolesi S, Nicotra F, Russo L (2020) 3D extracellular matrix mimics: fundamental concepts and role of materials chemistry to influence stem Cell fate. Biomacromolecules 21(6):1968–1994

Niece KL, Hartgerink JD, Donners JJ, Stupp SI (2003) Self-assembly combining two bioactive peptide-amphiphile molecules into nanofibers by electrostatic attraction. J Am Chem Soc 125(24):7146–7147

Nuti R, Brandi ML, Checchia G, Di Munno O, Dominguez L, Falaschi P et al (2019) Guidelines for the management of osteoporosis and fragility fractures. Intern Emerg Med 14(1):85–102

Orlic D, Kajstura J, Chimenti S, Bodine DM, Leri A, Anversa P (2001) Transplanted adult bone marrow cells repair myocardial infarcts in mice. Ann N Y Acad Sci 938:221–229. discussion 9–30

Ozbas B, Kretsinger J, Rajagopal K, Schneider JP, Pochan DJ (2004) Salt-triggered peptide folding and consequent self-assembly into hydrogels with tunable modulus. Macromolecules 37(19): 7331–7337

Pal S, Sayeed M, Kumar A, Verma DP, Harioudh MK, Verma NK et al (2021) Self-assembling nano-globular peptide from human lactoferrin acts as a systemic enhancer of bone regeneration: a novel peptide for orthopedic application. ACS Appl Mater Interfaces 13(15):17300–17315

Palhano FL, Lee J, Grimster NP, Kelly JW (2013) Toward the molecular mechanism(s) by which EGCG treatment remodels mature amyloid fibrils. J Am Chem Soc 135(20):7503–7510

Petreaca M, Martins-Green M (2014) Chapter 9—The dynamics of cell-ECM interactions, with implications for tissue engineering. In: Lanza R, Langer R, Vacanti J (eds) Principles of tissue engineering, 4th edn. Academic Press, Boston, pp 161–187

Porayette P, Gallego MJ, Kaltcheva MM, Bowen RL, Vadakkadath Meethal S, Atwood CS (2009) Differential processing of amyloid-beta precursor protein directs human embryonic stem cell proliferation and differentiation into neuronal precursor cells. J Biol Chem 284(35): 23806–23817

Puig-Sanvicens VA, Semino CE, Zur Nieden NI (2015) Cardiac differentiation potential of human induced pluripotent stem cells in a 3D self-assembling peptide scaffold. Differentiation 90(4–5): 101–110

Rajangam K, Behanna HA, Hui MJ, Han X, Hulvat JF, Lomasney JW et al (2006) Heparin binding nanostructures to promote growth of blood vessels. Nano Lett 6(9):2086–2090

Ralston SH, Gaston MS (2019) Management of osteogenesis imperfecta. Front Endocrinol (Lausanne) 10:924

Raspa A, Carminati L, Pugliese R, Fontana F, Gelain F (2021) Self-assembling peptide hydrogels for the stabilization and sustained release of active Chondroitinase ABC in vitro and in spinal cord injuries. J Control Release 330:1208–1219

Reyes-Martinez JE, Ruiz-Pacheco JA, Flores-Valdez MA, Elsawy MA, Vallejo-Cardona AA, Castillo-Diaz LA (2019) Advanced hydrogels for treatment of diabetes. J Tissue Eng Regen Med 13(8):1375–1393

Rickels MR, Robertson RP (2019) Pancreatic islet transplantation in humans: recent progress and future directions. Endocr Rev 40(2):631–668

Rivas M, Del Valle LJ, Aleman C, Puiggali J (2019) Peptide self-assembly into hydrogels for biomedical applications related to hydroxyapatite. Gels 5(1):14

Rodan GA, Martin TJ (2000) Therapeutic approaches to bone diseases. Science 289(5484): 1508–1514

Rofi'i A, Maria R, Masfuri (2019) Quality of life after spinal cord injury: an overview. Enferm Clin 29(Suppl 2):1–4

Roy K, Pandit G, Chetia M, Sarkar AK, Chowdhuri S, Bidkar AP et al (2020) Peptide hydrogels as platforms for sustained release of antimicrobial and antitumor drugs and proteins. ACS Appl Bio Mater 3(9):6251–6262

Sacchetti C, Liu-Bryan R, Magrini A, Rosato N, Bottini N, Bottini M (2014) Polyethylene-glycol-modified single-walled carbon nanotubes for intra-articular delivery to chondrocytes. ACS Nano 8(12):12280–12291

Sachs C, Jonsson G (1975) Mechanisms of action of 6-hydroxydopamine. Biochem Pharmacol 24(1):1–8

Saekhor K, Udomsinprasert W, Honsawek S, Tachaboonyakiat W (2019) Preparation of an injectable modified chitosan-based hydrogel approaching for bone tissue engineering. Int J Biol Macromol 123:167–173

Saha S, Yang XB, Wijayathunga N, Harris S, Feichtinger GA, Davies RPW et al (2019) A biomimetic self-assembling peptide promotes bone regeneration in vivo: a rat cranial defect study. Bone 127:602–611

Samadian H, Vaez A, Ehterami A, Salehi M, Farzamfar S, Sahrapeyma H et al (2019) Sciatic nerve regeneration by using collagen type I hydrogel containing naringin. J Mater Sci Mater Med 30(9):107

Schachinger V, Erbs S, Elsasser A, Haberbosch W, Hambrecht R, Holschermann H et al (2006) Intracoronary bone marrow-derived progenitor cells in acute myocardial infarction. N Engl J Med 355(12):1210–1221

Schneider JP, Pochan DJ, Ozbas B, Rajagopal K, Pakstis L, Kretsinger J (2002) Responsive hydrogels from the intramolecular folding and self-assembly of a designed peptide. J Am Chem Soc 124(50):15030–15037

Schuleri KH, Amado LC, Boyle AJ, Centola M, Saliaris AP, Gutman MR et al (2008) Early improvement in cardiac tissue perfusion due to mesenchymal stem cells. Am J Physiol Heart Circ Physiol 294(5):H2002–H2011

Senturk B, Demircan BM, Ozkan AD, Tohumeken S, Delibasi T, Guler MO et al (2017) Diabetic wound regeneration using heparin-mimetic peptide amphiphile gel in db/db mice. Biomater Sci 5(7):1293–1303

Shekaran A, Garcia AJ (2011) Nanoscale engineering of extracellular matrix-mimetic bioadhesive surfaces and implants for tissue engineering. Biochim Biophys Acta 1810(3):350–360

Smith AM, Williams RJ, Tang C, Coppo P, Collins RF, Turner ML et al (2008) Fmoc-diphenylalanine self assembles to a hydrogel via a novel architecture based on π–π interlocked β-sheets. Adv Mater 20(1):37–41

Soler-Botija C, Bagó JR, Llucià-Valldeperas A, Vallés-Lluch A, Castells-Sala C, Martínez-Ramos C et al (2014) Engineered 3D bioimplants using elastomeric scaffold, self-assembling peptide hydrogel, and adipose tissue-derived progenitor cells for cardiac regeneration. Am J Transl Res 6(3):291–301

Sozen T, Ozisik L, Basaran NC (2017) An overview and management of osteoporosis. Eur J Rheumatol 4(1):46–56

Stendahl JC, Wang LJ, Chow LW, Kaufman DB, Stupp SI (2008) Growth factor delivery from self-assembling nanofibers to facilitate islet transplantation. Transplantation 86(3):478–481

Storkebaum E, Carmeliet P (2004) VEGF: a critical player in neurodegeneration. J Clin Invest 113(1):14–18

Szkolar L, Guilbaud JB, Miller AF, Gough JE, Saiani A (2014) Enzymatically triggered peptide hydrogels for 3D cell encapsulation and culture. J Pept Sci 20(7):578–584

Tarkowski E, Issa R, Sjögren M, Wallin A, Blennow K, Tarkowski A et al (2002) Increased intrathecal levels of the angiogenic factors VEGF and TGF-β in Alzheimer's disease and vascular dementia. Neurobiol Aging 23(2):237–243

Thapa A, Jett SD, Chi EY (2016) Curcumin attenuates amyloid-beta aggregate toxicity and modulates amyloid-beta aggregation pathway. ACS Chem Neurosci 7(1):56–68

Tibbitt MW, Anseth KS (2009) Hydrogels as extracellular matrix mimics for 3D cell culture. Biotechnol Bioeng 103(4):655–663

Ulijn RV, Smith AM (2008) Designing peptide based nanomaterials. Chem Soc Rev 37(4):664–675

Uzunalli G, Tumtas Y, Delibasi T, Yasa O, Mercan S, Guler MO et al (2015) Improving pancreatic islet in vitro functionality and transplantation efficiency by using heparin mimetic peptide nanofiber gels. Acta Biomater 22:8–18

Walma DAC, Yamada KM (2020) The extracellular matrix in development. Development 147(10): dev175596

Wang F, Hansen RK, Radisky D, Yoneda T, Barcellos-Hoff MH, Petersen OW et al (2002) Phenotypic reversion or death of cancer cells by altering signaling pathways in three-dimensional contexts. J Natl Cancer Inst 94(19):1494–1503

Wang Y, Wu J, Kang G, Zhao M, Gui L, Li N et al (2012) Novel nano-materials, RGD-tetrapeptide-modified 17β-amino-11α-hydroxyandrost-1,4-diene-3-one: synthesis, self-assembly based nano-images and in vivo anti-osteoporosis evaluation. J Mater Chem 22(11):4652–4659

Wang J, Zheng J, Zheng Q, Wu Y, Wu B, Huang S et al (2015) FGL-functionalized self-assembling nanofiber hydrogel as a scaffold for spinal cord-derived neural stem cells. Mater Sci Eng C Mater Biol Appl 46:140–147

Wang Y, Zhang W, Gong C, Liu B, Li Y, Wang L et al (2020) Recent advances in the fabrication, functionalization, and bioapplications of peptide hydrogels. Soft Matter 16(44):10029–10045

Weaver VM, Lelièvre S, Lakins JN, Chrenek MA, Jones JC, Giancotti F et al (2002) beta4 integrin-dependent formation of polarized three-dimensional architecture confers resistance to apoptosis in normal and malignant mammary epithelium. Cancer Cell 2(3):205–216

Wiseman TM, Baron-Heeris D, Houwers IGJ, Keenan R, Williams RJ, Nisbet DR et al (2020) Peptide hydrogel scaffold for mesenchymal precursor cells implanted to injured adult rat spinal cord. Tissue Eng Part A. 27(15–16):993–1007

Wollert KC, Meyer GP, Lotz J, Ringes-Lichtenberg S, Lippolt P, Breidenbach C et al (2004) Intracoronary autologous bone-marrow cell transfer after myocardial infarction: the BOOST randomised controlled clinical trial. Lancet 364(9429):141–148

Woolfson DN (2017) Coiled-coil design: updated and upgraded. Subcell Biochem 82:35–61

World Health Organization (2005a) Chronic diseases and their common risck factors. World Health Organization, Geneva

World Health Organization (2005b) Preventing chronic diseases a vital investment. World Health Organization, Geneva

World Health Organization (2021a) Musculoskeletal conditions. World Health Organization, Geneva

World Health Organization (2021b) Diabetes overview. World Health Organization, Geneva

World Health Organization (2021c) Diabetes treatment. World Health Organization, Geneva

Wu Z, Chen G, Zhang J, Hua Y, Li J, Liu B et al (2017) Treatment of myocardial infarction with gene-modified mesenchymal stem cells in a small molecular hydrogel. Sci Rep 7(1):15826

Xiao Z, Yao Y, Wang Z, Tian Q, Wang J, Gu L et al (2020) Local delivery of taxol from FGL-functionalized self-assembling peptide nanofiber scaffold promotes recovery after spinal cord injury. Front Cell Dev Biol 8:820

Yang CH, Horwitz SB (2017) Taxol((R)): the first microtubule stabilizing agent. Int J Mol Sci 18(8):1733

Yoon YM, Lewis JS, Carstens MR, Campbell-Thompson M, Wasserfall CH, Atkinson MA et al (2015) A combination hydrogel microparticle-based vaccine prevents type 1 diabetes in non-obese diabetic mice. Sci Rep 5:13155

Yoshimatsu M, Nakamura R, Kishimoto Y, Yurie H, Hayashi Y, Kaba S et al (2020) Recurrent laryngeal nerve regeneration using a self-assembling peptide hydrogel. Laryngoscope 130(10): 2420–2427

Yu P, Chen Y, Wang Y, Liu Y, Zhang P, Guo Q et al (2019) Pentapeptide-decorated silica nanoparticles loading salmon calcitonin for in vivo osteoporosis treatment with sustained hypocalcemic effect. Mater Today Chem 14:100189

Zhang S, Holmes T, Lockshin C, Rich A (1993) Spontaneous assembly of a self-complementary oligopeptide to form a stable macroscopic membrane. Proc Natl Acad Sci U S A 90(8): 3334–3338

Zhao M, Song C, Zhang W, Hou Y, Huang R, Song Y et al (2010) The three-dimensional nanofiber scaffold culture condition improves viability and function of islets. J Biomed Mater Res A 94(3):667–672

Zhao Y, Leman LJ, Search DJ, Garcia RA, Gordon DA, Maryanoff BE et al (2017) Self-assembling cyclic d,l-alpha-peptides as modulators of plasma HDL function. A supramolecular approach toward antiatherosclerotic agents. ACS Cent Sci 3(6):639–646

Zhou M, Smith AM, Das AK, Hodson NW, Collins RF, Ulijn RV et al (2009) Self-assembled peptide-based hydrogels as scaffolds for anchorage-dependent cells. Biomaterials 30(13):2523–2530

Zlokovic BV (2005) Neurovascular mechanisms of Alzheimer's neurodegeneration. Trends Neurosci 28(4):202–208

Chapter 12
Peptide Nanostructured Materials as Drug Delivery Carriers

Ottavia Bellotto and Silvia Marchesan

Abstract Peptides are ideal building blocks for biomaterials and nanostructures aimed at advanced drug delivery, with hydrogels playing an elected role for their ability to mimic natural soft tissues and provide a matrix for the sustained release of therapeutic cargo. In this chapter, we discuss the advantages and innovation potential of using peptide-based vehicles for drug delivery; we then describe recent examples in the literature where peptide nanostructures or hydrogels were designed for this type of application, using non-covalent or covalent approaches to load the therapeutics. Finally, we conclude with a perspective on the future of this exciting field that is moving towards life-like materials to address the unsolved challenges in clinical applications.

Keywords Peptides · Nanostructures · Drug delivery · Nanomaterials · Hydrogels

Abbreviations

5-FU	5-Fluorouracil
Boc	*tert*-Butyloxycarbonyl
Cbz	Benzyloxycarbonyl
CD	Circular dichroism
CDPs	Cyclodipeptides
CNM	Carbon nanomaterials
CNTs	Carbon nanotubes
CPT	Camptothecin
DAP	Diaminopropane
DBC	N,N'-dibenzoyl-L-cystine
DKPs	2,5-diketopiperazines
Dox	Doxorubicin

O. Bellotto · S. Marchesan (✉)
Department of Chemical and Pharmaceutical Sciences, University of Trieste, Trieste, Italy
e-mail: smarchesan@units.it

ER   Encapsulation ratio
Fmoc   Fluorenylmethyloxycarbonyl
GO   Graphene oxide
MMP-7   Matrix metallopeptidase 7
MMP-9   Matrix metallopeptidase 9
MTT   3-(4,5-dimethylthiazol-2-yl)-2,5-diphenyl tetrazolium bromide
Nap   Naphthalene
Nle   Norleucine
NPs   Nanoparticles
OMet   Methoxy
OVA   Ovalbumin
PBS   Phosphate-buffered saline
PEG   Polyethylene glycol
Phg   Phenylglycine
PTX   Paclitaxel
SA   Salicylic acid
TEM   Transmission electron microscopy

12.1 Introduction

12.1.1 Nanomaterials for Nanomedicine

In recent years, nanomedicine has shown great promise for biomedical research, thanks to the progress made on the understanding and development of nanosized materials that were envisaged for the diagnosis and treatment of several diseases. The advanced performance that can be provided by nanomaterials renders them highly attractive in many aspects of medicine, including bioimaging, targeted drug delivery with low invasiveness, early disease diagnosis, and tissue engineering (Marchesan and Prato 2013).

To overcome common pitfalls that can be encountered when working with nanomaterials (e.g. low targeting limit, high renal clearance, systemic toxicity, lack of biocompatibility, immunogenicity), developments have been made for the design of the so-called "*smart*" or "*intelligent*" materials. The term "smart" implies that they are able to respond to environmental changes or external stimuli, for instance, through variations in their properties and, consequently, their function. Such triggers are usually classified into three categories: chemical (such as solvent polarity, pH, ionic strength), physical (such as light, temperature, magnetic and sonic triggers), and biological ones (for instance, enzymes or other biomolecules) (Shah et al. 2018). Intelligent materials can exert a variety of actions in response, ranging from targeting and motion to self-regulation and sensing (Zhang et al. 2019). Usually, the reversibility of the response depends on the inherent nature of the material and a variety of reversible and non-reversible transitions can be engineered

to finely tailor the properties of the final systems (Vázquez-González and Willner 2020). Their specificity and their ability to respond to stimuli inherently present in biological systems means a net gain of new properties in a localized environment with low invasiveness, especially for in vivo applications. To this end, particularly attractive are bioresponsive materials that interact with the components of physiological or pathological environments for controlled drug release, theranostics, biomedical devices, and tissue engineering (Lu et al. 2016).

The nanomaterials' landscape is very wide and diverse, ranging from nanoparticles (NPs) of different chemical natures (e.g. inorganic, lipid, and polymeric) and carbon nanomaterials (e.g. graphene-based materials, fullerenes, etc.) to those with different internal structures, such as liposomes, dendrimers, and nanogels (Yan et al. 2019). In particular, nanoparticles have attracted growing interest especially when combined with therapeutic agents thanks to their great versatility. By changing the size, shape, structure, morphology, and surface properties, it is possible to obtain diverse nanocarriers that are able to release drugs in a more specific manner to the target site, compared to traditional vehicles used in medicine (Radwan et al. 2020). To this end, the bio–nano interface, that is, the interactions of biological components with the surface of nanomaterials play a key role in determining their performance and fate in vivo (Cortez-jugo et al. 2021). The nanosized features of these particles combined with the enhanced permeability and retention (EPR) effect on the vascular system in disease states, such as the permeable tumour sites, have been long studied to attain a high level of local concentration of drugs in the pathological tissue, with a reduction of side effects thanks to lower concentrations at the other physiological sites (Maeda 2021).

However, a number of barriers have limited the effective translation of novel therapies from animal models to patients (Bhattacharjee and Brayden 2021). These include challenges in the production scale-up, regulation hurdles, and adverse effects. Furthermore, human tumours are far more heterogeneous than those represented by animal models. In this regard, personalized (nano)medicine (Fig. 12.1) has brought new hope for the correct profiling of the pathological state for each individual towards the adoption of ad hoc therapy for enhanced therapeutic success (Luque-Michel et al. 2017). In particular, personalized and tumour-specific cancer vaccines represent a hot area of research that is well set to make a qualitative leap in the way we treat cancer (Hu et al. 2018).

12.1.2 Nanomaterials with Peptides for Medicine

Peptides and nanomaterials have been combined together in many different ways to innovate in medicine. On one hand, nanoparticles may prevent the degradation of biological drugs, such as peptides and proteins, thus leading to an improvement in stability and pharmacological effect of these therapeutics, which bear high potential especially in regenerative medicine. These aspects may greatly change the way to detect and treat diseases to make progress in biomedicine (Garbayo et al. 2020). On

Fig. 12.1 Schematic illustration of nanomedicine development approach based on patient-personalized protein coronas on bioactive nanoparticles. Reproduced with permission from Ren et al. (2019), Copyright © 2019 American Chemical Society
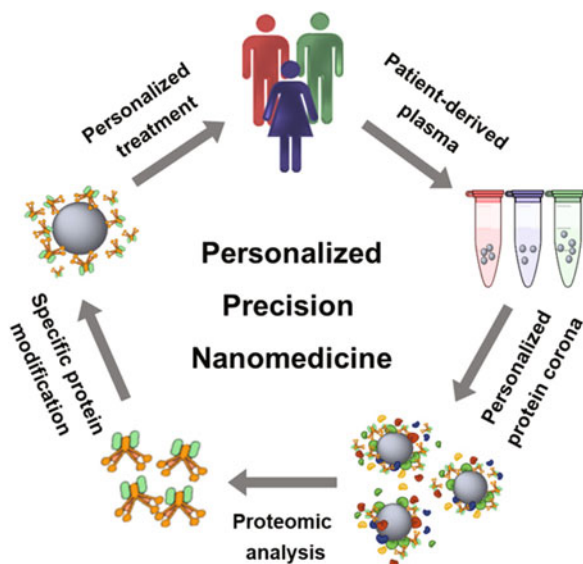
the other hand, peptides have been largely used to organize and assemble nanoparticles into composite and hybrid materials through specific chemical interactions (Walsh and Knecht 2017). Furthermore, self-assembling peptides have been used also to template the nucleation and growth of nanoparticles through a green approach without the use of organic solvents or harsh chemicals, and nanoparticles may even be stabilized within the resulting peptide-based hydrogel matrix that prevents nanoparticle aggregation (Bellotto et al. 2021).

Bioinspired peptides can self-organize in vivo not only to exert a therapeutic effect but also to release drugs or allow for imaging, even in combined advanced theranostic applications. To this end, it is useful to operate a modular design, for instance, through the combination of different amino acid sequences with specific functions, such as targeting, self-assembling, and drug releasing (Fig. 12.2). Depending on the chemical structure of the components, a variety of nanomorphologies can be attained, ranging from nanoparticles and nanotubes to nanofibres (Hainline et al. 2018), which can also entrap large amounts of water to yield macroscopic, yet nanostructured, hydrogels. The latter have been designed also to respond to biological stimuli (Li et al. 2019), such as enzymes, which can convert precursors into gelling agents or hydrolyse peptide-based building blocks to release drugs, through the so-called enzyme-instructed self-assembly approach. Clearly, if the target enzyme that can reconfigure the material's building blocks is overexpressed in a pathological tissue, then the approach allows for selective targeting to exert the biomedical function, be it therapeutic, for imaging, or both (Gao et al. 2020).
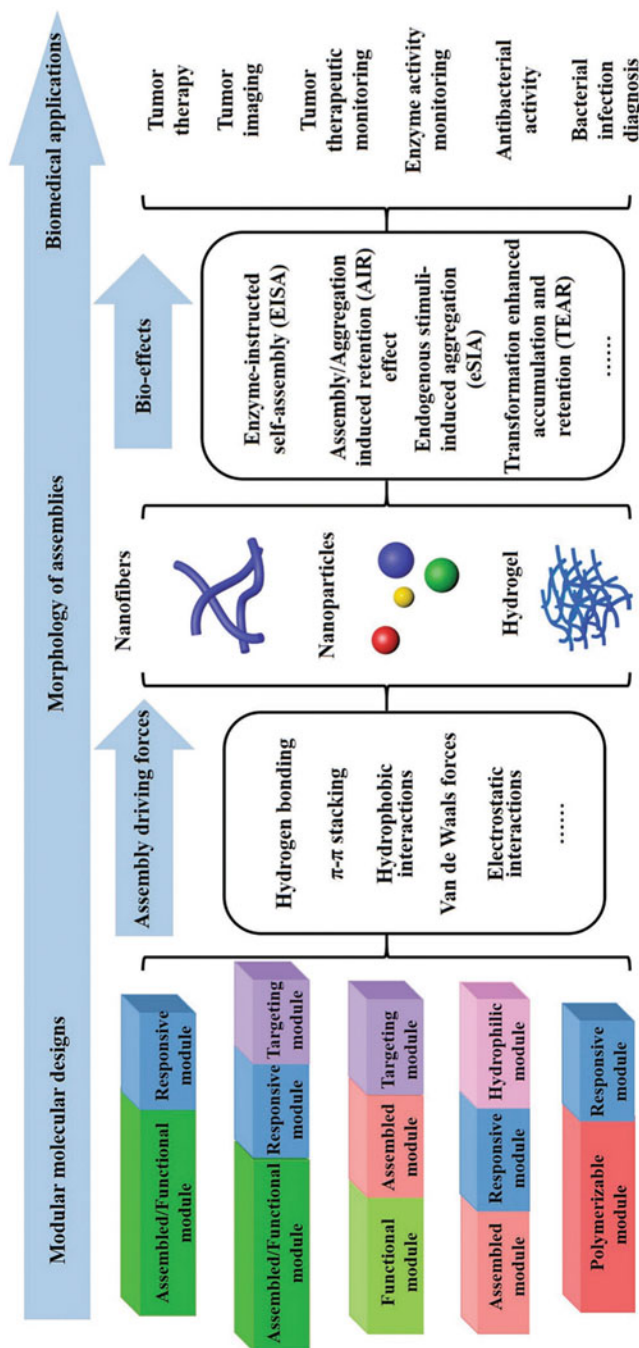
Fig. 12.2 Schematic representation of peptide-based nanomaterials with a modular design for self-assembly into functional structures for biomedical use. Reproduced with permission from Li et al. (2019), Copyright © 2018 WILEY-VCH Verlag GmbH & Co. KGaA, Weinheim

12.1.3   Bioinspiration for Self-Assembling Nanomaterials

Nature is certainly a generous source of inspiration for the design of functional supramolecular nanocomposites (Lossada et al. 2020). Molecular assembly is a dynamic and versatile process, typically driven by non-covalent interactions. These include hydrogen bonding, van der Waals forces, electrostatic interactions, hydrophobicity, and stacking effects. Although these interactions may be weak when considered alone, once they are combined together they can give rise to supramolecular architectures that display advantageous features, such as reversibility, responsiveness, and tuneable characteristics (Zhou et al. 2017). Many examples of molecular self-assembly, especially in protein systems, are worth to note. They include the following: (1) the assembly of silk by spiders, (2) the assembly of collagen and keratin into ligaments and hair, (3) in cells, the individual chaperone proteins assembly into a sophisticated ring structure to sort out, fold, and refold proteins, and (4) the seashell biomineralization (Zhang 2002). Another well-known process of protein self-assembly that has inspired scientists for biomimicry regards viral capsids, and bioinspired protein assembly into cages finds many potential applications in the biomedical field, including drug delivery (Bhaskar and Lim 2017). Ad hoc modification of bioinspired building blocks can open the way to new geometries for large protein capsules (Fig. 12.3) (Stupka and Heddle 2020).

However, producing and handling large proteins bears many technical challenges and can rise concerns for uses in vivo, such as immunogenicity and stability against enzymatic degradation. Nowadays, there is thus a great interest in small molecules, such as organic compounds, nuclei acid motifs, saccharides, and peptides, that are able to self-assemble into distinct nanostructures and supramolecular architectures with diverse properties (Du et al. 2015). In particular, the inherent propensity of amyloid peptides to naturally self-organize into nanostructures is widespread and has been a great source of inspiration to design functional nanomaterials for a variety of applications (Wei et al. 2017).

There are also many other classes of peptides that provide useful building blocks for nanomaterials design as described in other chapters of this book. The self-assembly process is now considered a promising approach, which is bioinspired and aims to biomimicry, to achieve revolutionary advances in the design, fabrication, and synthesis of functional biomaterials for technological and therapeutic applications. It has recently emerged as a new approach in chemical synthesis, polymer science, materials, and engineering. It provides a means for the bottom-up fabrication of various materials to tailor novel physicochemical and functional properties that arise from the assembly of the simplest molecular building blocks.
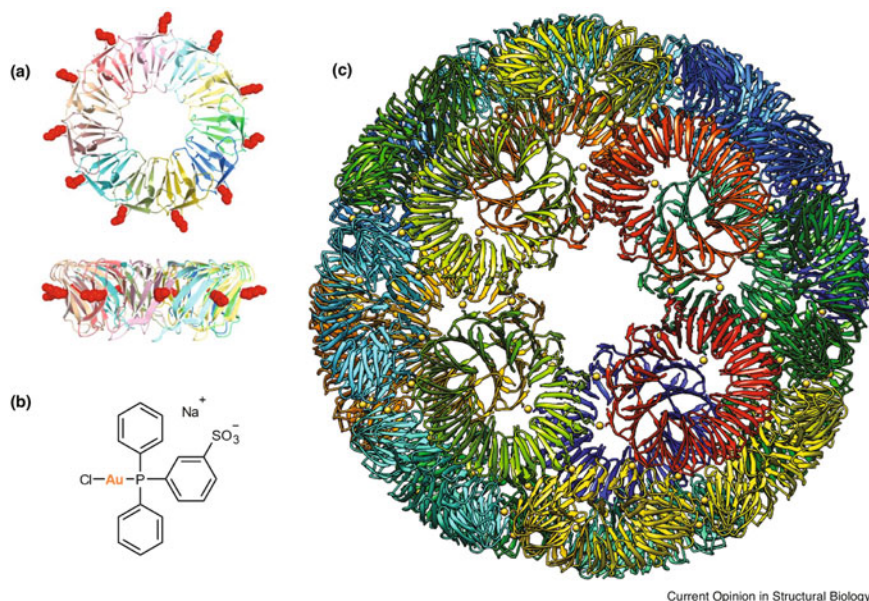
Fig. 12.3 Artificial protein cage. (**a**) The crystal structure of the TRAP ring protein (PDB 4v4f) with 11 monomers shown in different colours. Red spheres indicate Lys35 that was mutated to Cys. (**b**) Monosulfonyl triphenylphosphine gold(I) (orange) used to bind Cys residues and form a cage. (**c**) TRAP cage consisting of 24 TRAP rings with each ring connected to five neighbours via S-Au-S bonds involving opposing Cys side chains. Each TRAP ring is shown in a different colour with gold (I) ions as yellow spheres. Reproduced from Stupka and Heddle (2020) under a Creative Commons license

12.2 Proteins and Peptides as Building Blocks for Self-Assembled Biomaterials

12.2.1 From Natural Self-Assembling Proteins to Peptides

In nature, proteins play an elective role as building blocks to attain functional structures and materials, thanks to their large chemical diversity. Through years of intense research, several functions have been decoded into corresponding short motifs that can consist of simple sequences of just a few amino acids, exerting specific functions ranging from targeting to bioactivity and belonging to several peptide classes (Fig. 12.4) (Hamley 2017). It is thus not surprising that peptides have since enjoyed popularity as building blocks of supramolecular materials, thanks to their great diversity, inherent biocompatibility and biodegradability, and the possibility to attain structural and functional complexity from very simple building blocks (Levin et al. 2020). Their ability to deliver powerful and selective biological messages to cells is very important for possible biological applications. Likewise, their inherent biocompatibility and biodegradability means the possibility to work in
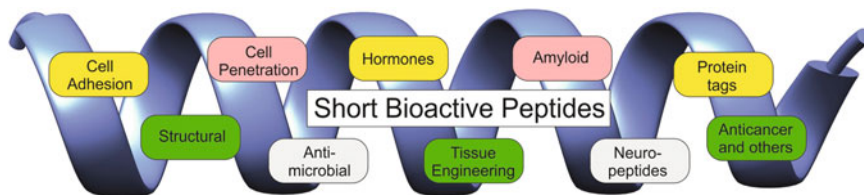
Fig. 12.4 Bioactive short motifs belonging to several classes have been recently reviewed. Reproduced with permission from Hamley (2017), Copyright © 2017 American Chemical Society

environmentally friendly conditions, thus facilitating the use of green solvents, such as water, with consequent lower impact on the environment (Rubert Pérez et al. 2015).

Peptides can be attained through the very easy and modular solid-phase synthesis, although costs can rise exponentially as the number of amino acids in the desired product increases, and especially for the scale-up on large amounts. However, short motifs can be obtained also through liquid-phase methods, which are significantly cheaper, and whose chemistry is also well-established. Depending on the amino acid sequence, they can present a great chemical diversity, which can be further amplified through the introduction of non-proteogenic amino acids (Ding et al. 2020). Although peptide and proteins are weakly resistant to enzymatic activity, a higher degree of proteolytic protection can be pursued through several chemical approaches aimed at the modification of the original chemical structure. Some examples are cyclization, introduction of D-residues, methylation of the α-C, methylation of the amidic N, and introduction of β^3 residues. Among them, a change in chirality has been shown to be a very efficient strategy for this purpose (Werner et al. 2016).

Overall, the versatility of peptides and proteins, alongside notable physicochemical properties, offers an ideal playground to employ them in the design of new technological tools, bulk nanomaterials, or adaptive nanostructures. Peptides are able to gather into diverse nanomorphologies, including fibres, spheres, rods, tubes, vesicles, and particles supported by their device and self-assembly conditions. Different hydrogen-bonding pattern interactions stabilize the secondary structures elements, among which α-helices and β-sheets have been predominantly used in peptide materials (Wang et al. 2016a). Combination of multiple peptide components into the assemblies allows to further expand the versatility of these systems (Raymond and Nilsson 2018). One of the main challenges is the identification of the smallest and cheapest components with enhanced performance to allow for their self-assembly into complex structures in a controlled manner. Within the peptide landscape, reductionist approaches became popular towards the identification of the shortest self-assembling peptides for biomaterials (Gazit 2019). Indeed, this interesting strategy allows to minimize the synthesis and purification steps and to reduce the costs of production for practical applications.

12.2.2 Minimalistic Peptides as Building Blocks for Supramolecular Biomaterials

Already in 2003, Reches and Gazit identified the dipeptide diphenylalanine (Phe-Phe) as a powerful minimalistic self-assembling motif belonging to the amyloid beta peptide sequence (Reches and Gazit 2003). Actually, even the amino acid Phe was shown to self-assemble on its own into ordered fibrillar structures with amyloid-like properties (Adler-Abramovich et al. 2012). Besides, with increasing knowledge about supramolecular self-assembly, much more attention has been devoted to the capacity of other single amino acids as building blocks, both natural and synthetic, for their arrangement into supramolecular structures (Chakraborty and Gazit 2018). There is a large scope to study minimalistic short sequences (especially di- and tripeptides) as bioactive building blocks for biomaterials. Whereas the presence of polyaromatic N-capping groups (i.e. Fmoc, Nap, Cbz, etc.), that drive self-assembly in water, is usually required, safety concerns exist on the biological fate of such N-caps in vivo (Truong et al. 2015). To this end, simpler aromatic analogues whose nature can assist hydrophobic-driven self-organization with desirable biocompatibility in vivo or in vitro would be preferable alternatives (Martin and Thordarson 2020). In this context, it is worth mentioning the case of a single amino acid derivative, the N-(4-nitrobenzoyl)-Phe, which is able to self-assemble into supramolecular hydrogels in phosphate-buffered saline solutions and displays a mild antimicrobial activity and promising mammalian cell biocompatibility in vitro (Garcia et al. 2020).

The substitution of these N-capping groups with another hydrophobic amino acid (e.g. D-Phe (Kralj et al. 2020), Leu (Bellotto et al. 2020), Ile (De Groot et al. 2007, Bellotto et al. 2022), etc.) could be a preferable strategy that yields dipeptides able to form hydrogels in phosphate buffer with potentially enhanced stability endowed by an appropriate choice of amino acid chirality, for instance. Furthermore, unexpected advantages may arise, as shown for heterochiral D-Phe-L-Phe (Kralj et al. 2020), which maintains the ability of the homochiral Phe-Phe to self-assemble into nanotubes, yet it displays an intramolecular interaction between the Phe side chains that replaces intermolecular interactions involved in hierarchical bundling (Fig. 12.5). As a result, heterochiral Phe-Phe assembles into highly homogenous four-nm-wide nanotubes that yield a stable and clear hydrogel with promising biocompatibility in vitro. Further investigations are needed, especially to unveil the relation between the chemical structure and supramolecular behaviour of these systems.

The literature is rich of gelling tripeptides and tetrapeptides, of which the vast majority exploit polyaromatic N-caps (Du et al. 2015) and especially the Fmoc group (Tao et al. 2016). Other design strategies include heterochirality (Garcia et al. 2018) and amphipathic sequences (Frederix et al. 2015). As the sequence elongates, interesting functionalities can be attained, for instance, hydrolase mimicry for D-Ser-D-His-L-Phe-L-Phe (Kurbasic et al. 2021) and emulsifying properties for

Fig. 12.5 Single-crystal XRD structures of homochiral Phe-Phe (**1**) (Görbitz 2001) (silver) and heterochiral Phe-Phe (**2**) (cyan) peptide nanotubes. (**a**) Side view of stacked peptides revealed opposite screw sense for **1** (silver) and **2** (cyan), dictated by the chirality of the N-terminal amino acids. (**b**) Top view of nanotube inner cavities defined by the projection six peptide molecules arranged head-to-tail for both **1** (silver) and **2** (cyan), but only in **2** the two Phe side chains do interact face to face intramolecularly. (**c**) Top view of the nanotubes identified by the projection of 18 peptide molecules for **1** (silver) showed hierarchical bundling stabilized by aromatic zippers; instead, a space-fill view of heterochiral **2** (cyan) revealed the outer diameter of a double layer of peptide molecules to agree with the four-nm-diameter of fibrils measured by TEM. Reproduced from Kralj et al. (2020) under a Creative Commons license
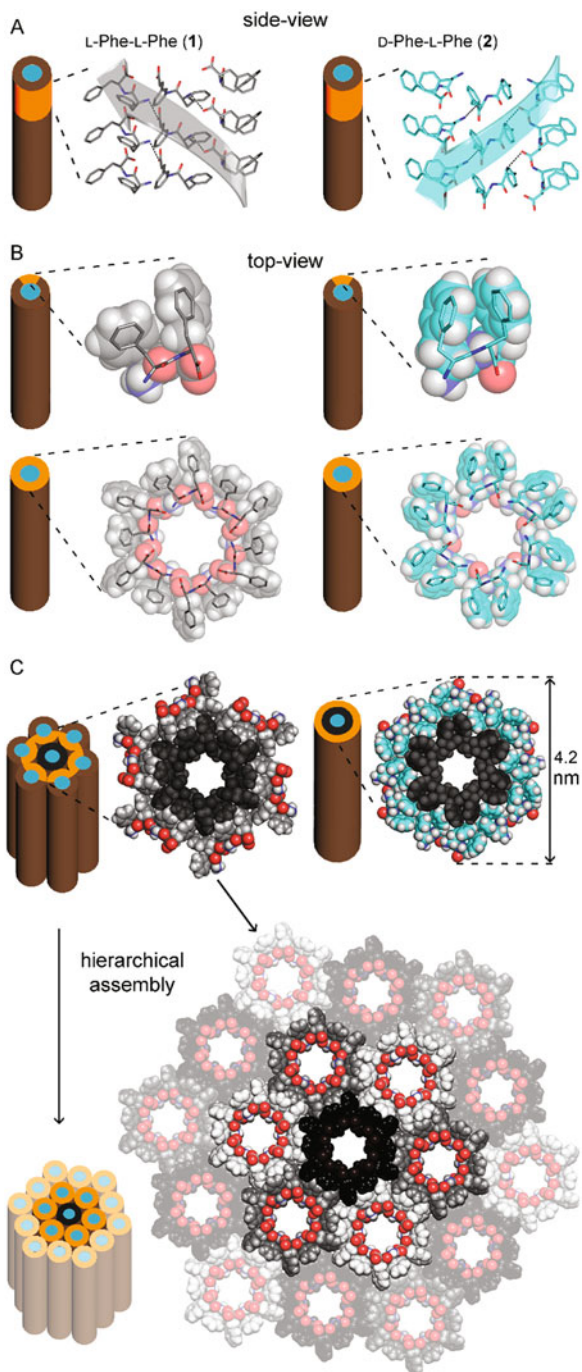
Phg-Glu-Phg-Lys that could be potentially useful for the delivery of both hydrophilic and hydrophobic drugs (Wychowaniec et al. 2020).

Besides linear short di- or tripeptides, the literature has recently witnessed the increasing importance of their cyclic derivatives, cyclodipeptides (CDPs), or 2,5-diketopiperazines (DKPs) (Borthwick 2012). They exhibit a pronounced resistance to enzymatic hydrolysis as well as a higher stability against harsh conditions, relative to their linear dipeptide counterparts. In virtue of their several advantages, such as biodegradability, ease of scale-up and synthesis, and the propensity to self-assemble into gels, they offer an innovative platform for the design of peptide-based biomaterials (Scarel and Marchesan 2021) and, generally, nanomaterials for several other applications (Manchineella and Govindaraju 2016).

It is thus not surprising that there is an active research towards the design of short peptides and their derivatives, containing structural motifs required to induce self-assembly and bottom-up fabrication of nanostructures with specific properties. So far, these peptide-based supramolecular materials offer unique advantages over other classes of molecules and have exhibited a great potential for a wide range of biomedical applications, ranging from immunotherapy and biosensing to the development of scaffolds for tissue engineering and theranostic tools, and drug delivery vehicles (Yadav et al. 2020).

12.2.3 Modern Peptide Therapeutics

New structural and functional properties, such as self-healing, shape memory, mechanical strength, and bioactivity, can be easily introduced in peptide-based materials through chemical modifications, by further broadening their scope as nanosized systems for nanomedicine (Chen and Zou 2019). For instance, while traditional formulations with peptide and protein therapeutics required parenteral administration that can be a deterrent for patient compliance, recent progresses have allowed for the development of oral peptide therapeutics (Drucker 2020). Antimicrobial peptides represent a promising avenue to address the current crisis of spreading resistance against common antibiotics (Lazzaro et al. 2020) and a link was made between this class and self-assembling amyloids, thus opening the door to the development of smart antimicrobials, whose activity can be switched on/off with assembly/disassembly cycles (Kurbasic et al. 2020). Peptide-based vaccines are another class that is enjoying intense research efforts, in this case to prevent, rather than treat, a variety of chronic diseases (Malonis et al. 2020) with benefits coming also from self-assembling peptide components (Zeigler et al. 2019). Current challenges in the new frontiers in this area that go well-beyond self-assembly towards "living" materials that operate out of equilibrium have been recently discussed, with the aim to achieve fine control over the creation of hierarchical nanostructured architectures that feature many attractive properties of living systems (Ariga et al. 2020).

12.3 Peptide Nanostructures for Drug Delivery

By virtue of their properties and useful advantages, self-assembling peptide-based biomaterials have been considered excellent candidates for several kinds of applications in biomedicine. Nowadays, drug delivery is probably one of the main fields in which such systems have found promising applications, especially in place of other nanomaterials (i.e. inorganic nanoparticles, liposomes, polymers, etc.) that may be difficult to functionalize or that may arise safety concerns in living systems (Panda and Chauhan 2014). However, great progress has been made in the successful conjugation of nanoparticles and peptides for biomedical use, including drug delivery (Spicer et al. 2018). Among the well-defined peptide-based assemblies, nanostructured hydrogels have a great importance as soft materials to be used as drug delivery vehicles. Thanks to their three-dimensional (3D) network, they are able to swell and retain a large amount of water and acquire physicochemical properties similar to the natural soft tissues. The porous structure of the hydrogel thus allows drug loading into the matrix and they can be designed for *on-demand* cargo release using specific triggering factors (i.e. temperature, pH, ionic strength, etc.) at the target site (Panda and Chauhan 2014). This allows for a precise control over the amount of drug and its release rate in a site-specific way. In general, this could have numerous advantages over conventional therapeutics' release, such as enhanced bioavailability of the drug and decreased systemic side effects in the body, thus improving the patient's well-being (Mayr et al. 2018).

Sometimes short peptide hydrogels can suffer from limited mechanical properties that could be potentially overcome by the inclusion of other components, such as metal ions (Xia et al. 2017) or nanomaterials, inside the system. In light of their physicochemical properties, nanocarbons have demonstrated to be ideal candidates to obtain hydrogels with enhanced viscoelastic properties or acquired self-healing ability, for instance, in the presence of graphene oxide (GO) or carbon nanotubes (CNTs), respectively (Iglesias et al. 2018). Furthermore, inclusion of inorganic nanoparticles on peptide assemblies can open the way to a diverse set of additional functions that span form enzyme mimicry to imaging and therapy (Pigliacelli et al. 2020).

Besides hydrogels, peptide-based nanoparticles or nanovesicles can also be developed as delivery agents to load several cargos, from therapeutics and bioactive molecules (i.e. DNA, water-insoluble drugs, tagged molecules for imaging) to enzymes for biosensing purpose and genes. Furthermore, these self-assembled soft materials can be used as scaffolds for stem cell therapy (Huang et al. 2017) and also, through high-affinity binding, to control protein drug release (Abune and Wang 2021). Overall, self-assembled peptide structures stand out as promising smart materials as drug delivery systems and worldwide research in this area in very active to translate their use into the clinical practice. The choice of the gelator with specific properties to entrap the cargo molecules and control their release in a desirable manner is one of the main challenges to be faced for future medicine for the upcoming years.
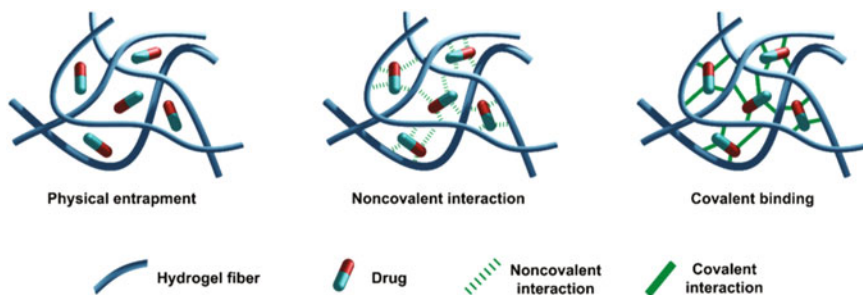
Fig. 12.6 Different modes for drug entrapment into hydrogels. Reproduced from Caporale et al. (2021)

The way the drug is loaded into the matrix has a great influence on controlling the release kinetics. This can be carried out through different strategies, classified as follows: (1) physical entrapment, in which no chemical interactions occur between the vehicles and the cargo; (2) hydrogel–drug non-covalent interactions; and (3) drug covalent binding with the molecular carrier (Fig. 12.6). The choice of the delivery method for a given therapeutic application is aimed at maximizing the drug efficacy and patient's compliance. The way in which the hydrogel releases the drug is often crucial for desirable therapeutic outcomes, which require optimal duration of drug availability (long or short term) and its release profile (sustained or *on demand*), depending on the specific pathological target. Each delivery method will be examined/explained in detail in the next sections with very recent examples taken from literature, since the topic was already covered in 2017 (Iglesias and Marchesan 2017). Although the emphasis will be on peptide nanostructured hydrogels that have been largely studied, a few examples will be described pertaining to nanosized discrete morphologies as vehicles.

12.3.1 Physical Entrapment of Drugs

In hydrogels containing the cargo molecule encapsulated by physical interactions, the release of the molecule is due to a physical change in the structure of the gel matrix, such as degradation, de-swelling, and mechanical deformation. This is one of the simplest methods to encapsulate a cargo within the vehicle, yet it can be combined with selective triggers to control drug release, such as the cancer-overexpressed MMP-9-mediated cleavage to enable micelle-to-fibre transition for a self-assembling peptide and control the release of antitumoural drug doxorubicin (Dox) (Kalafatovic et al. 2014), resulting in tumour growth inhibition in vivo (Kalafatovic et al. 2016).

In a recent study, the well-known peptide hydrogelator Fmoc-Phe-Phe has been chosen to develop hydrogels or nanogels for the delivery of Dox to improve its clinical use, which is affected by its dose-limiting toxicity. Nanogel formulations

combine in the same structure the hydrate inherent network of the hydrogel with the nanosize dimension that is ideal for systemic, oral, and pulmonary administration compared to macroscopic hydrogels, which are more suitable for transepithelial drug delivery and in situ gelation of implants. Fmoc-Phe-Phe has been used alone or in combination with (Phe-Tyr)$_3$ hexapeptide or its PEGylated analogue PEG$_8$-(Phe-Tyr)$_3$ to prepare these delivery systems that showed the decreased mechanical strength and slower gelation kinetics due to the presence of PEG, as revealed by rheological measurements. The hydrogels were obtained by following the "solvent-switch method", while the "top-down method" was used for nanoparticle preparation (Gallo et al. 2021).

Briefly, in the first method, a stock solution of the peptide component, alone or in a combination, was prepared in dimethyl sulfoxide and then diluted with distilled water under stirring to obtain the hydrogel. The nanogels instead were obtained by preparing a gel disk into a silicone mould, then homogenized in water solution with the addition of surfactants, such as Tween, and final sonication. The loading of the drug in the hydrogels or nanogels was easily achieved by following the same procedures reported above and by adding in each of them the Dox in aqueous solution. Dox-filled hydrogels with both the gelator and its PEGylated analogue were more homogeneous than Dox-filled Fmoc-Phe-Phe hydrogels, and no synersis occurred after 10 days. Thanks to this advantage, such systems revealed the possibility to control in a precise manner the release of water-soluble drugs entrapped in the systems. Confocal images of Dox-filled hydrogels in their xerogel form showed the intricate network of fibrils in which the drug was entrapped with a high-loading content and a calculated encapsulation ratio (ER) of 100%, with ER defined as the weight percentage of drug encapsulated in the hydrogels and the drug used in the protocol. The peptide composition was found to influence the drug release over time and the time required for the gelation process (in the range of 20–40 min). Compared to Dox-filled hydrogels, a lower drug-loading content and a lower amount of released drug (20–40%) after 72 h were observed in the case of Dox-filled nanogels. In cytotoxicity assays on a breast cancer cell line, the Dox-loaded systems significantly reduced cell viability after 24 h (49–57%) and 72 h (7–25%) of incubation, while hydrogel and nanogels vehicles alone showed high cell viability (>95%). Besides, a different cell localization for Dox delivered through hydrogels or nanogels was observed in comparison to the free drug, suggesting an alternative and efficient mechanism of internalization for the drug. Overall, in vitro cell assays revealed the potential of such peptide-based systems as promising tools for the delivery of Dox inside tumour cells with a high efficiency (Gallo et al. 2021).

A pH-sensitive amphiphilic drug delivery peptide was also designed for the release of the anticancer drug Dox in response to the acidic tumour microenvironment, based on the amphipathic peptide sequence Ac-LLLLLLKKKGRGDS-NH$_2$. The presence of the RGD motif, able to bind specific receptor overexpressed on the tumour cell surface, enhanced the target selectivity of the peptide nanocarrier system to the tumour site. TEM and SEM showed that the monomer self-assembled into ordered spherical NPs under neutral conditions with a concentration of 0.5 mM, while nanofibres and nanoband-like structures were observed for higher

concentrations. These NPs were able to entrap the hydrophobic Dox. In acidic microenvironment, Dox-NPs swelled and burst, and rapidly released the drug. A higher drug accumulation on tumour cells was observed by flow cytometry and fluorescence techniques in comparison to mammalian cells (Gong et al. 2021).

Appropriate choice of amino acid stereoconfiguration is a strategic tool to fine-tune linear peptide assembly (Marchesan et al. 2012) and control the vehicle biodegradation rate (Marchesan et al. 2015). However, it is not always straightforward to anticipate the performance of such systems, despite the fact that design rules are finally starting to emerge (Garcia et al. 2018). Initially, a popular approach consisted in simply preparing the D-mirror image of a self-assembling L-peptide, so that it displayed analogous self-assembling propensity into a vehicle for drug delivery, and also increased resistance against enzymatic degradation. However, the fact that D-peptides are not easily processed by enzymes can lead to undesired adverse effects. For instance, this was the case for the amphipathic hydrogelator Phe-Glu-Phe-Gln-Phe-Lys-NH$_2$ that was developed as delivery system for the controlled release of opioid drugs after subcutaneous injections. It was then further modified on the peptide side chain as well as on its C- and N-termini, and prepared as a D-mirror image to improve its gelation and in vivo stability for clinical purposes. Stability studies in human plasma at 37 °C confirmed the resistance to enzymatic hydrolysis of the sequence with D-amino acids, with not-determinable half-life. Transmission electron microscopy (TEM) images showed entangled fibres in both hydrogels useful for the entrapment and controlled release of drugs. In this case, morphine and naloxone (an opioid antagonist) were chosen as opiate drug candidates, and in vitro release studies revealed the same release for both hydrogels. The release consisted in a rapid burst effect (20%) in the first hours followed by a sustained release over 3 days with a recovery rate of about 90%. The fast initial release rate was due to both the porosity of the hydrogel structure and the weak forces that entrapped the drug. This release profile could be desirable for clinical purposes (i.e. chronic pain) that require an immediate pain relief followed by a prolonged therapeutic effect. Viability experiments performed on mouse fibroblast cells revealed that only the L-hydrogelator was not cytotoxic; for this reason, only this compound was selected for subsequent in vivo studies. Experiments revealed high stability and absence of side effects of the hydrogel after subcutaneous injection and a high drug-loading capacity (up to ca. 77%) of the peptide–hydrogel system to obtain an efficient antinociceptive effect after 24 h without significant alterations in the behaviour of mice during treatment (Martin et al. 2016).

Therefore, it can be advisable instead to choose a combination of both D- and L-amino acids at specific positions of the peptide sequence to yield a heterochiral hydrogelator with tuneable lifetime. For instance, in the case of the self-assembling peptide Boc-Phe-Phe-Phe, four thixotropic gels were obtained from different stereo-isomers (LLL, DLL, DDD, and LDD), and all were able to entrap and release the drug doxorubicin, although with different kinetics. The gels formed by DDD and LDD showed a more efficient release in a shorter time (76% after 79 h) compared to the ones formed by LLL and DLL stereoisomers (65% after 52 h). Due to the greater delivery efficacy and the best proteolytic stability among all of them, the gel made

from the LDD isomer was shown to be the most promising candidate as delivery carrier for the anticancer drug. Cytotoxicity assays for this gel on a breast cancer cell line confirmed the lack of cytotoxicity for the self-assembling peptide vehicle alone and an enhanced cytotoxicity profile for the Dox-loaded gel, relative to the free drug (Basu et al. 2016).

Different cationic Fmoc-Phe derivatives were employed to achieve a sustained and localized delivery of an anti-inflammatory drug for the treatment of pain. The modification at the C-terminus with a diaminopropane (DAP) group and the fluorination of the benzyl ring of Phe significantly enhanced the self-assembly potential of such systems that spontaneously gelled upon addition of physiologically relevant sodium chloride concentrations. The hydrogels had shown to efficiently entrap the non-steroidal anti-inflammatory drug diclofenac during the self-assembly process, and their viscoelastic properties appeared ideal for delivery by injection, as revealed by rheological measurements. In vivo drug release studies showed an immediate pain relief after the initial injection, followed by a sustained profile for nearly 2 weeks, compared to the diclofenac control whose therapeutic effect lasted less than a day (Raymond et al. 2019).

An amino acid derivative, N,N'-dibenzoyl-L-cystine (DBC), has been used to develop a stimuli-responsive supramolecular hydrogel as the carrier of salicylic acid (SA). The transition sol-gel occurred by decreasing the pH below 3.5, and the hydrogel showed a stability for over a month. By adding NaOH to the hydrogel (pH >9.4), it returned easily to the sol state. The DBC hydrogel could also be transformed into a solution upon heating, and reform upon cooling down to room temperature. The self-assembly of DBC molecules was facilitated by strong intermolecular hydrogen bonds between amides and carboxylic acid as well as hydrogen bonds among water molecules, and π–π stacking interactions amid aromatic rings. Thanks to thermoreversibility and pH responsiveness, along with suitable mechanical properties, the DBC hydrogel displayed ideal properties for the controlled drug release. To entrap the drug into the hydrogel matrix, first a certain amount of DBC and SA were dissolved in ethanol with continuous stirring, and then the addition of PBS with a suitable pH triggered the gelation process. The release studies showed a release ratio of 58% at high concentrations, both for SA (200 mg L^{-1}) and DBC (3.0 g L^{-1}) in PBS (pH 4), and it revealed the influence of several parameters (e.g. DBS and SA concentration, PBS pH) on the drug release rate (Zhong et al. 2019).

In another study, a pH-sensitive peptide drug delivery system was developed as suitable carrier for the anticancer drug Paclitaxel (PTX) after intratumoural injection (Raza et al. 2019). Here, the octapeptide FEFEFRFK (FER-8) was selected to obtain a stable hydrogel under physiological conditions (pH 7.4), in which the PTX was loaded efficiently (9 mg/mL) without compromising the hydrogel stability. The hydrophobic nature of the peptide was due to the Phe residues which led to β-sheet structural organization and drove the self-assembly. After tumour injection, the acidic conditions of the cancer microenvironment led to the disassembly of the PTX-loaded FER-8 and a gel to sol transition occurred. This change in pH allowed for the drug delivery from the hydrogel at tumour cell site with a sustained release for

almost 1 week. At microscopic level, TEM analysis confirmed the correlation between the hydrogel stability and pH conditions: a uniform network of fibres with an average size of either 500 nm or less than 200 nm was found for neutral and acidic pH values, respectively. In vitro studies showed the ability of the doped hydrogel to increase the amount of the drug inside the tumour cells and inhibit the tumour cell growth relative to the free drug. Furthermore, an enhancement in drug accumulation was observed also inside the tumour of mice models with a sustained retention time of the drug (96 h) inside the tumour after administration.

Besides tumours, another pathological target is damaged nerve tissue, which is notoriously challenging to repair. Nanofibrous materials stand out for their ability to positively interact with neurons to promote their growth and reconnectivity (Marchesan et al. 2017). In particular, self-assembling amphiphilic peptides have been successfully employed for the loading and release of chondroitinase ABC, which is a lyase that degrades the gliotic scar, and thus has attracted researchers' attention in the area of regeneration after spinal cord injury (Raspa et al. 2021). Furthermore, a similar type of peptidic scaffold has been applied also for osteogenesis and angiogenesis for bone regeneration, through the co-delivery of growth factors (Zhang et al. 2022).

12.3.2 *Non-covalent Drug Interactions*

Non-covalent interactions provide several advantages for the development of self-assembled structures as drug delivery systems; for example, they can favour drug loading and allow for carrier-mediated transport and selectivity for cellular uptake (Mishra and Panda 2019). Although these interactions are fairly weak, the involvement of the drug in the supramolecular structure could offer the opportunity to tailor its structural, nanomorphological and spectroscopic properties as well as the release kinetics that could differ from the ones achieved through simply a physical entrapment. To this end, short, self-assembling sequences are highly attractive as delivery agents; for instance, they are capable of engaging in various weak interactions, such as H-bonds, ionic bonds, π–π stacking, and van der Waals interactions to fine-tune drug delivery kinetics (Theodoroula et al. 2022).

For instance, a peptide-based supramolecular hydrogel was tested as the carrier for the protein ovalbumin (OVA) to achieve a promising vaccine adjuvant (Wang et al. 2016b). OVA was chosen as a model protein to study the immune response, because it is already and widely used as vaccine adjuvant. The peptide Nap-Gly-Phe-Phe-pTyr-OMe or its D-enantiomer was used to form co-assembled fibres and hydrogels with the protein, whose presence did not influence the viscoelastic properties of hydrogels, as revealed by rheology. TEM analysis showed homogeneous fibril populations, either with or without OVA, with slightly bigger sizes in the former case, thus suggesting the co-assembly of peptide and protein. Both co-assembled hydrogels had a good biocompatibility versus immune cell lines and could strongly induce antibody production and cytokine secretion whose levels were

measured by ELISA assay. Overall, the D-hydrogel with OVA showed to be a more promising vaccine adjuvant than its L-analogue, in terms of efficiently raising the immune response in a mice model.

The heterochiral tripeptide D-Leu-L-Phe-L-Phe is a well-established low-molecular weight gelator in phosphate buffer at physiological pH and has demonstrated to offer interesting properties for the co-assembly with drugs, whereby the drugs take part to the supramolecular structures. When the structure disassembly occurs, the cargo is slowly released, thus allowing for a sustained release over time. In literature, several examples have been reported for the loading and release of drugs with the tripeptide D-Leu-L-Phe-L-Phe, based on non-covalent interactions. Earlier studies on the antibiotic ciprofloxacin revealed supramolecular interactions between the peptide vehicle and the drug that allowed for a sustained release over days, as a well as a high loading for this notoriously poorly soluble drug (Marchesan et al. 2013).

Years later, experiments with either one of two anti-inflammatory drugs, i.e. ketoprofen or naproxen, were undertaken in an attempt to preliminarily delineate drug structural features for successful co-assembly with the peptide (Kurbasic et al. 2017). The tripeptide was first dissolved in alkaline phosphate buffer and ketoprofen or naproxen were added as sodium salts to the solution. Thus, the drugs were mixed with the peptide prior to assembly to favour their subsequent incorporation into the supramolecular structure. A comparison of the rheological measurements of the peptide assemblies with or without the drugs revealed a lowered resistance against applied stress for the hydrogel containing either drug, which was ascribed to fewer connections between fibrils relative to the tripeptide alone. TEM analysis showed that fibrils formed by the peptide alone (9.8 ± 1.4 nm wide) became thinner upon the co-assembly with either drug (i.e. 7.3 ± 1.0 nm for the peptide plus ketoprofen, and 8.3 ± 2.2 nm for the peptide with naproxen). Thinner fibrils could justify the lower stiffness registered for the co-assembled system. No changes in peptide conformation were observed upon addition of either drug, as probed by circular dichroism (CD) analysis. Drug release studies revealed different kinetics for the two-anti-inflammatory drugs. In the case of naproxen, a high percentage of the drug (around 70%) was released within the first 72 h; meanwhile, the release of ketoprofen occurred completely in just 24 h. These data suggested different interactions between the two anti-inflammatory drugs with the tripeptide, more efficient for the naproxen, presumably due to the presence of the more extended aromatic unit of naphthalene in its chemical structure that could favour aromatic and hydrophobic interactions.

Different was the case for the same peptide gelator when combined with a more hydrophilic drug, i.e. the anticancer 5-fluoruracil (5-FU) (Parisi et al. 2019). This is a well-known antineoplastic drug with a chemical structure different from the previous examples that usually suffers from a short biological half-life. The presence of 5-FU in the hydrogel did not significant influence the kinetics of hydrogelation, which was very rapid with a plateau reached within 10 min, whereas the stress sweep analysis showed a slightly lower resistance for the peptide–hydrogel upon drug inclusion. The latter data suggested a lower level of physical cross-linking in the co-assembled fibrillar network relative to the hydrogel alone. During the release studies the
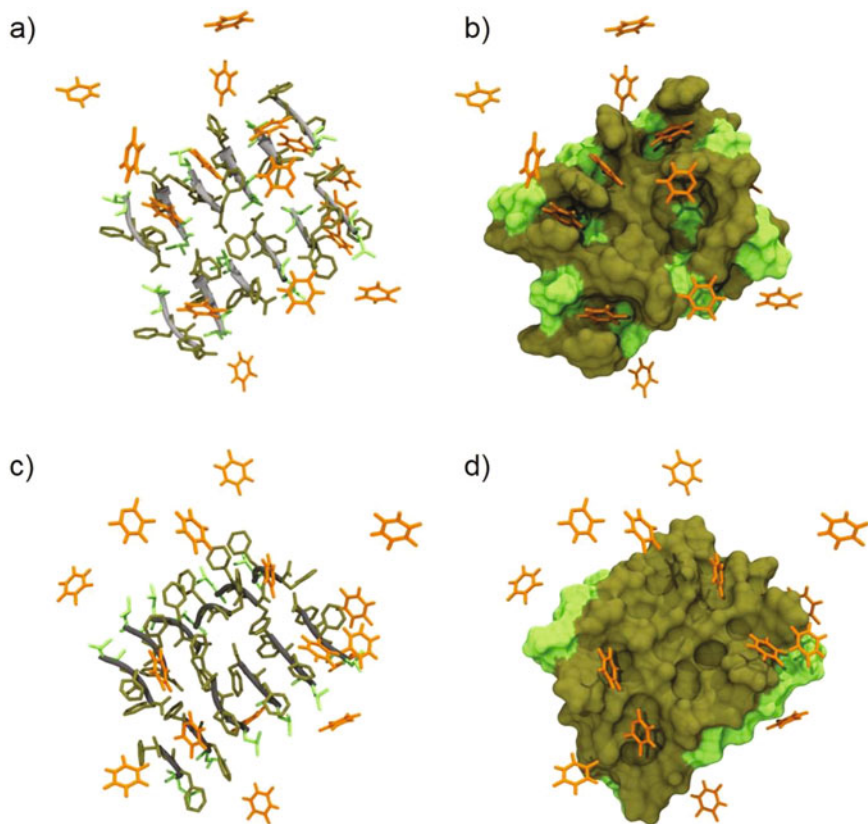
Fig. 12.7 All-atom molecular dynamics snapshots (left) and corresponding molecular surface (right) of D-Leu-L-Phe-L-Phe stacks in the presence of 5-FU. (**a**–**b**) and (**c**–**d**) images refer to antiparallel and parallel β-sheets, respectively. The peptide backbone is depicted in grey and the Leu/Phe side chains are depicted in light and dark green, respectively. 5-FU molecules are represented as orange sticks. Water and ions are not shown for clarity. Reproduced from Parisi et al. (2019)

hydrogel integrity was preserved without any visible swelling or syneresis, but the very fast kinetics of drug release suggested just a limited and transient interaction between the 5-FU and the peptide, mediated by hydrogen bonding as revealed by in silico studies (Fig. 12.7). As a result, most of the drug was released during the first hour, almost half of the loaded drug in the first half-hour. Overall, it is clear that the delineation of drug chemical structure requirements to ensure successful participation in the peptide supramolecular structure for sustained release is rather challenging, and far more examples are needed to allow for a systematic study in this direction.

The cationic LL37 peptide is an efficient antimicrobial agent belongs to the cathelicidin family to treat pulmonary infections related to the presence of the *Pseudomonas aeruginosa* (PA) bacteria. However, concerns exist over its biosafety,

low bioavailability, and fast clearance in vivo that limit its clinical use. In this recent work, it has been reported the efficient encapsulation of LL37 into NPs as a promising strategy to address these shortcomings and improve the antimicrobial effect of the peptide. To this end, the cationic LL37 peptide was entrapped through electrostatic interactions inside an albumin-based nanodrug delivery system to synthetize LL37 NPs. The NP system shielded the cargo from the external environment, increasing its availability in vivo. A sustained release of LL37 over more than 48 h was attained, with a prolonged antimicrobial activity by increasing incubation time. LL37 NPs showed to exert an anti-inflammatory effect both in vitro, by significantly reducing the levels of cytokines, such as TNF-α and IL-6, secreted by peritoneal macrophages after PA infection, and in vivo in a murine model of acute PA lung infection (Yang et al. 2021).

One of the risk factors for vision loss is the corneal neovascularization (CNV), which can be inhibited by the drug Cabozantinib (a tyrosine kinase inhibitor). A sustained delivery system was based on cationic polypeptide NPs displaying mucoadhesive properties and that carried the lipophilic drug Cabozantinib (Cabo-NPs). The inclusion of the drug occurred during the formation of the NPs in aqueous solution. After the penetration through the hydrophilic tear, the cationic delivery system adhered to the mucosal surface of the cornea by leading to a sustained release of the drug over time and enhancement of its bioavailability. Inhibition of angiogenesis by the Cabo-NPs was observed after in vitro angiogenesis studies in which a significant inhibitory effect on cell migration and tube formation was observed. Furthermore, the delivery system Cabo-NPs showed a good biocompatibility both in mouse corneas and in corneal epithelial cells (Han et al. 2020).

Another study described an enzyme-triggered self-assembled peptide nanostructure for cancer therapy, based on the surfactant-like peptide Nap-FFGPLGLARKRK with three functional motifs in the sequence: (1) Nap-FF to drive the self-assembly, (2) the enzyme-cleavable motif -GPLGLA, and (3) the positive segment -RKRK to promote the interaction with cell membranes. The peptide was able to self-assemble into long fibrils and its hydrophobic properties were ideal to entrap high amount of the drug Dox. At tumour sites, the overexpressed MMP-7 degraded the fibrils into thinner ones and the following disassembly led to a sustained release of the drug with an efficient and selective antitumoural activity on cancer cells. At normal cell sites, the drug-loaded peptide nanostructures retained their integrity and no drug release was observed. In vivo studies confirmed the potential applicability of such delivery systems for cancer therapy. A visible suppression inhibition of cell growth and metastasis was observed in mice models without prominent side effects of Dox (Cao et al. 2019). Dox is expected to be in cationic form at physiological pH; thus, its release can be controlled also via electrostatic and cation–pi interactions (Elsawy et al. 2022). Furthermore, enhanced drug uptake by tumour cells can be attained by using a self-assembled peptide vehicle that disassembles at mildly acidic pH (Li et al. 2022). Electrostatic interactions between opposite charges have been exploited also for the complexation of mercaptoundecahydrododecaborate with the self-assembling peptide A6K. In this manner, successful uptake by human glioma cells

was demonstrated for applications in boron neutron capture tumour therapy (Michiue et al. 2021).

Stimuli-responsive systems triggered by the tumour microenvironment hold great promises for a selective delivery and release of tumour therapeutics. A multifunctional peptide (P51) was able to self-assemble into spherical NPs (50 nm) and entrap the drug Pirarubicin (THP) through electrostatic and hydrophobic interactions. The multiple functions of the P51-THP NPs were related to the presence inside the peptide sequence of the specific ligand motif (RGD) for tumour membrane protein and three tumour-microenvironment-sensitive release triggers (i.e. acid environment, reducing agents, and selective enzymes). A marked increase of the drug release was observed when all the three triggers were present. Both in vitro and in vivo studies demonstrated the efficiency of such systems to enhance selective drug delivery and antitumour effect by showing a reduced systemic cytotoxicity (Jiang et al. 2019).

Another work reported the use of peptide-based nanomaterials as carrier for tumour imaging and treatment (Yang et al. 2017). The peptide sequence consisted in four motifs: (1) an hydrophobic bis-pyrene (BP) group, (2) the sequence peptide Lys-Leu-Val-Phe-Phe (KLVFF) for beta-sheet-like fibre formation, (3) a hydrophilic moiety polyethylene glycol (PEG) chain, and iv) a pH-responsive motif of six histidine residues (H_6). The peptide BP-KLVFF-H_6-PEG self-assembled into nanoparticles in PBS at pH 7.4 with a green fluorescence emission related to the BP aggregation. After intravenous injection into tumour-bearing mice models, a change in the NP morphology occurred due to an alteration in the hydrophilic/hydrophobic balance related to the acidity of the tumour microenvironment (pH ~ 6.5). Thus, the NPs transformed into nanofibres that covered the tumour for a long time (up to 96 h). This structure was able to interact and capture a variety of small molecules, such as nile red, indocyanine green photothermal agent, and the chemotherapeutic Dox, leading to their accumulation inside the tumour site. This phenomenon allowed for an improvement in the imaging, photothermal therapy, and chemotherapy, respectively.

12.3.3 Covalent Drug Binding

Another strategy to develop a drug delivery system involves covalent interactions between a self-assembled gelator and a drug to achieve a sustained, long-term, and controlled drug release. Such covalent binding can lead to a change in the inherent properties of the hydrogel (i.e. ionization state, functionalization of C- and N-termini, solubility) and in the gelator self-assembling propensity. Furthermore, the solubility and biocompatibility of the supramolecular system have to be taken into account for biomedical purposes. The chemical conjugation can be achieved through modification of peptide side chains and/or the peptide termini (C- or N-termini), whereas the drug release occurs after the hydrolysis of covalent bonds triggered by several stimuli (i.e. pH, enzymes, etc.). Besides, targeting moduli and
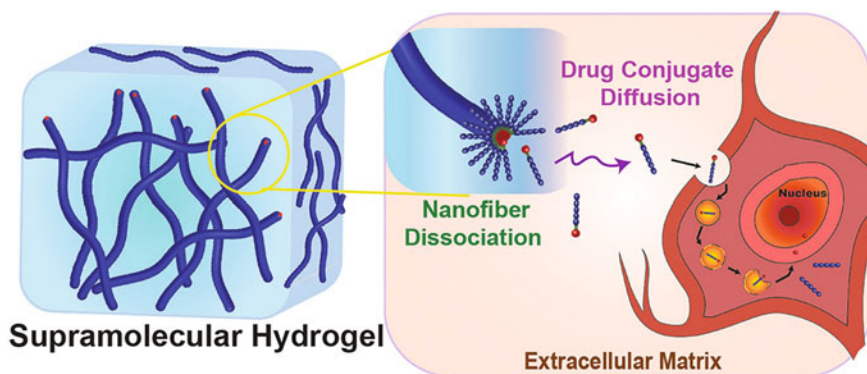
Fig. 12.8 Supramolecular hydrogel from the self-assembly of a drug-peptide amphiphile conjugate is internalized into cells for the delivery of chemotherapeutics. Reproduced with permission from Chakroun et al. (2019), Copyright © 2019, American Chemical Society

enzymatically cleavable moduli can be introduced to ensure further control over self-assembly and intracellular drug delivery (An et al. 2021).

A recent study has described the conjugation of the anticancer paclitaxel (PTX) with an amphiphilic short peptide through several strategies (Chakroun et al. 2019). The crafted PTX-peptide conjugates were able to spontaneously form injectable hydrogels with a controlled release. Four different PTX prodrug hydrogelators were designed and they shared some functional structural motifs: a biodegradable linker, 4-(pyridin-2-yl-disulfanyl)butyrate (buSS) for the conjugation of PTX to the bioactive RGDR peptide sequence, a VVV segment, and a GG spacer. The PTX was chosen due to its efficacy as anticancer drug able to induce cancer cell apoptosis by interfering with the microtubule stabilization. The RGDR sequence was chosen to enhance a tissue penetration effect of the prodrug conjugate. The VVV segment was designed to promote intermolecular hydrogen bonding among the conjugates, and the GG spacer to improve the drug solubility. After cell internalization of the prodrug conjugate, the high concentration of glutathione would reduce the disulphide linker, thus allowing for the release of the free drug PTX (Fig. 12.8). TEM images revealed that all the four PTX prodrug hydrogelators self-assembled into filamentous nanostructures. A two-phase release mechanism of the drug was proposed: (1) in the first phase, immediately after PBS addition onto the gel, local gel swelling and network disruption occurred. Due to a difference in osmolarity, the monomeric conjugate started to diffuse into the PBS, while the water of the medium started to deeply penetrate into the filamentous network, thus leading to its disruption; (2) the second phase consisted in the drug release after filament dissociation into monomers. In all cases, a long-term linear profile was observed, which was slowed down by incorporation of an alkyl group in the structure or accelerated in the presence of several amino acids with opposite charges. When tested on two different cancer cell lines, the PTX prodrug gelator preserved the cytotoxic activity, which was negligible in the case of the peptide alone, thus confirming its good biocompatibility for clinical

scope. Furthermore, all PTX conjugates promoted the tumour inhibition in spheroid models by reducing the tumour volume over 2 weeks similarly to the free drug PTX.

Camptothecin was used as hydrophobic chemotherapeutic agent covalently linked to a hydrophilic peptide to develop new self-assembling amphiphilic prodrugs (Cheetham et al. 2017). In this study the drug was conjugated to three different peptide sequences: all of them were identical for the same peptide backbone –"-C"GVQIVYKK ("C" indicates a cysteine-containing segment) derived from the Tau protein but different for the number of cysteine residues inside the sequence (mCys-Tau, dCys-Tau and qCys-Tau). A reduction-sensitive disulfylbutyrate linker (-buSS-) was chosen to link the drug with each peptide to form the prodrug conjugates (mCPT-buSS-Tau, dCPT-buSS-Tau, and qCPT-buSS-Tau). The linker was designed to allow for the release of the free drug after the reduction in the intracellular environment. The two lysine (Lys) residues promoted the solubility of the systems, and by simply changing the design of the peptide, the loading of the drug could be precisely controlled (one, two, or four drug molecules per conjugate). All the peptide-based prodrug self-assembled into nanofibrous structures under physiological conditions. In vitro studies confirmed the cytotoxicity effect of the prodrug systems and a potential biocompatibility for the peptide alone.

12.4 Conclusions and Future Perspectives

Over the last few decades, a great progress has been made in the understanding of peptides' supramolecular behaviour for the design of advanced vehicles for drug delivery (Eskandari et al. 2017). The great chemical diversity, biocompatibility, and ease of preparation of peptides has enabled the development of various types of hydrogels, nanostructures, and nanomaterials. Research efforts worldwide have proceeded in the direction of stimuli-responsive delivery systems, so that drugs could be released selectively at the pathological site, thus reducing systemic side effects. In this chapter we have described systems that respond to physicochemical or biological stimuli, usually exploiting peptides' ability to interact with other bio-molecules (e.g. enzymes) and to undergo chemical changes at physiologically relevant conditions (e.g. ionizable ionisable or redox-active amino acids).

The concomitant development of peptide chemistry has also enabled the attainment of peptide-based drug delivery vehicles with prolonged lifetime, to overcome the notorious peptides' rapid biodegradation in vivo. As we witness a renaissance of peptide therapeutics and active vehicles for drugs, there is scope to advance the field towards life-like systems that display the ability to evolve and adapt as needed (Ariga et al. 2020), to address the hardest challenges in the clinic that still have not found viable solutions, for instance, through multi-stage autonomous development in adaptation to the evolution of the pathological process to treat.

An additional strategic avenue consists of creating synergy by combining peptides with other types of nanostructures that exploit the unique properties of working at the nanoscale, for instance, to attain multi-responsive systems. Recent examples

have appeared in this direction, for instance, to attain NPs (Ruan et al. 2019) or magnetogels for drug release induced by local hyperthermia (Veloso et al. 2021). Indeed, this type of approach is promising to treat solid tumours (Seynhaeve et al. 2020), by exploiting the properties of magnetic NPs, and especially the highly biocompatible superparamagnetic iron oxide NPs (SPIONs) (Kralj et al. 2017). SPIONs can be even biosynthesized in living organisms into anisotropic nanochains, which could potentially lead to further innovation in medicine thanks to their unique magneto-responsive mechanical effects (Kralj and Marchesan 2021).

Other types of physical stimuli that could, in line of principle, be operated by surgeons and clinicians directly at the pathological site include ultrasounds (Pappas et al. 2015a, b) and laser irradiation for photothermal drug release (Moorcroft et al. 2020). Inclusion of imaging agents would then allow for theranostic applications on tumours, as demonstrated recently through an NP system for NIR laser-induced drug release, photoacoustic imaging, and synergistic chemotherapy and phototherapy, leading to a 50% complete cure rate in a subcutaneous melanoma model (Cong et al. 2020). Clearly such complex multicomponent systems require a multidisciplinary team as further opportunities for innovation can be found through collaborative joint efforts from scientists with expertise in different fields, spanning from physics and materials science to nanotechnology, chemistry, and medicine. In particular, the active involvement of clinicians will be key to facilitate the new therapeutic solutions reaching patients.

References

Abune L, Wang Y (2021) Affinity hydrogels for protein delivery. Trends Pharmacol Sci 42:300–312

Adler-Abramovich L, Vaks L, Carny O et al (2012) Phenylalanine assembly into toxic fibrils suggests amyloid etiology in phenylketonuria. Nat Chem Biol 8:701–706

An HW, Mamuti M, Wang X et al (2021) Rationally designed modular drug delivery platform based on intracellular peptide self-assembly. Exp Dermatol 1:20210153

Ariga K, Jia X, Song J et al (2020) Nanoarchitectonics beyond self-assembly: challenges to create bio-like hierarchic organization. Angew Chem Int Ed 59:15424–15446

Basu K, Baral A, Basak S et al (2016) Peptide based hydrogels for cancer drug release: modulation of stiffness, drug release and proteolytic stability of hydrogels by incorporating d-amino acid residue(s). Chem Commun 52:5045–5048

Bellotto O, Kralj S, De Zorzi R et al (2020) Supramolecular hydrogels from unprotected dipeptides: a comparative study on stereoisomers and structural isomers. Soft Matter 16:10151–10157

Bellotto O, Cringoli MC, Perathoner S et al (2021) Peptide gelators to template inorganic nanoparticle formation. Gels 7:14

Bellotto O, Kralj S, Melchionna M et al (2022) Self-assembly of unprotected dipeptides into hydrogels: water-channels make the difference. Chembiochem 23:e202100518

Bhaskar S, Lim S (2017) Engineering protein nanocages as carriers for biomedical applications. NPG Asia Mater 9:e371

Bhattacharjee S, Brayden DJ (2021) Addressing the challenges to increase the efficiency of translating nanomedicine formulations to patients. Expert Opin Drug Discov 16:235–254

Borthwick AD (2012) 2,5-Diketopiperazines:synthesis, reactions, medicinal chemistry, and bioactive natural products. Chem Rev 112:3641–3716

Cao M, Lu S, Wang N et al (2019) Enzyme-triggered morphological transition of peptide nanostructures for tumor-targeted drug delivery and enhanced cancer therapy. ACS Appl Mater Interfaces 11:16357–16366

Caporale A, Adorinni S, Lamba D, Saviano M (2021) Peptide-protein interactions: from drug design to supramolecular biomaterials. Molecules 26:1219

Chakraborty P, Gazit E (2018) Amino acid based self-assembled nanostructures: complex structures from remarkably simple building blocks. ChemNanoMat 4:730–740

Chakroun RW, Wang F, Lin R et al (2019) Fine-tuning the linear release rate of paclitaxel-bearing supramolecular filament hydrogels through molecular engineering. ACS Nano 13:7780–7790

Cheetham AG, Lin Y, Lin R, Cui H (2017) Molecular design and synthesis of self-assembling camptothecin drug amphiphiles. Acta Pharmacol Sin 38:874–884

Chen J, Zou X (2019) Self-assemble peptide biomaterials and their biomedical applications. Bioact Mater 4:120–131

Cong Z, Zhang L, Ma SQ et al (2020) Size-transformable Hyaluronan stacked self-assembling peptide nanoparticles for improved transcellular tumor penetration and photo-chemo combination therapy. ACS Nano 14:1958–1970

Cortez-jugo C, Czuba-wojnilowicz E, Tan A, Caruso F (2021) A focus on " bio " in bio – nanoscience: the impact of biological factors on nanomaterial interactions. Adv Healthc Mater 10:2100574

De Groot NS, Parella T, Aviles FX et al (2007) Ile-Phe dipeptide self-assembly: clues to amyloid formation. Biophys J 92:1732–1741

Ding Y, Ting JP, Liu J et al (2020) Impact of non-proteinogenic amino acids in the discovery and development of peptide therapeutics. Amino Acids 52:1207–1226

Drucker DJ (2020) Advances in oral peptide therapeutics. Nat Rev Drug Discov 19:277–289

Du X, Zhou J, Shi J, Xu B (2015) Supramolecular hydrogelators and hydrogels: from soft matter to molecular biomaterials. Chem Rev 115:13165–13307

Elsawy MA, Wychowaniec JK, Castillo Diaz La, et al (2022) Controlling doxorubicin release from a peptide hydrogel through fine-tuning of drug–peptide fiber interactions. Biomacromolecules 23(6):2624–2634

Eskandari S, Guerin T, Toth I, Stephenson RJ (2017) Recent advances in self-assembled peptides: implications for targeted drug delivery and vaccine engineering. Adv Drug Deliv Rev 110–111: 169–187

Frederix PWJM, Scott GG, Abul-Haija YM et al (2015) Exploring the sequence space for (tri-) peptide self-assembly to design and discover new hydrogels. Nat Chem 7:30–37

Gallo E, Diaferia C, Rosa E et al (2021) Peptide-based hydrogels and nanogels for delivery of doxorubicin. Int J Nanomedicine 16:1617–1630

Gao J, Zhan J, Yang Z (2020) Enzyme-instructed self-assembly (EISA) and hydrogelation of peptides. Adv Mater 32:1805798

Garbayo E, Pascual-Gil S, Rodríguez-Nogales C et al (2020) Nanomedicine and drug delivery systems in cancer and regenerative medicine. WIREs Nanomed Nanobiotechnol 12:e1637

Garcia AM, Iglesias D, Parisi E et al (2018) Chirality effects on peptide self-assembly unraveled from molecules to materials. Chem 4:1862–1876

Garcia AM, Lavendomme R, Kralj S et al (2020) Self-assembly of an amino acid derivative into an antimicrobial hydrogel biomaterial. Chem Eur J 26:1880–1886

Gazit E (2019) Reductionist approach in peptide-based nanotechnology. Annu Rev Biochem 87: 533–553

Gong Z, Liu X, Zhou B et al (2021) Tumor acidic microenvironment-induced drug release of RGD peptide nanoparticles for cellular uptake and cancer therapy. Coll Surf B, Biointerfaces 202: 111673

Görbitz CH (2001) Nanotube formation by hydrophobic dipeptides. Chem Eur J 7:5153–5159

Hainline KM, Fries CN, Collier JH (2018) Progress toward the clinical translation of bioinspired peptide and protein assemblies. Adv Healthc Mater 7:1700930

Hamley IW (2017) Small bioactive peptides for biomaterials design and therapeutics. Chem Rev 117:14015–14041

Han H, Yin Q, Tang X et al (2020) Development of mucoadhesive cationic polypeptide micelles for sustained cabozantinib release and inhibition of corneal neovascularization. J Mater Chem B 8: 5143–5154

Hu Z, Ott PA, Wu CJ (2018) Towards personalized, tumour-specific, therapeutic vaccines for cancer. Nat Rev Immunol 18:168–182

Huang Q, Zou Y, Arno MC et al (2017) Hydrogel scaffolds for differentiation of adipose-derived stem cells. Chem Soc Rev 46:6255–6275

Iglesias D, Marchesan S (2017) Short peptide self-assembled nanostructures for therapeutics innovative delivery. In: Nanostructures for novel therapy, pp 227–250. Elsevier

Iglesias D, Melle-Franco M, Kurbasic M et al (2018) Oxidized nanocarbons-tripeptide supramolecular hydrogels: shape matters! ACS Nano 12:5530–5538

Jiang X, Fan X, Xu W et al (2019) Self-assembled peptide nanoparticles responsive to multiple tumor microenvironment triggers provide highly efficient targeted delivery and release of antitumor drug. J Control Release 316:196–207

Kalafatovic D, Nobis M, Javid N et al (2014) MMP-9 triggered micelle-to-fibre transitions for slow release of doxorubicin. Biomater Sci 3:246–249

Kalafatovic D, Nobis M, Son J et al (2016) MMP-9 triggered self-assembly of doxorubicin nanofiber depots halts tumor growth. Biomaterials 98:192–202

Kralj S, Marchesan S (2021) Bioinspired magnetic nanochains for medicine. Pharmaceutics 13: 1262

Kralj S, Potrc T, Kocbek P, et al (2017) Magnetically responsive nanocarriers for drug delivery. Curr Med Chem 24:454–469

Kralj S, Bellotto O, Parisi E et al (2020) Heterochirality and halogenation control phe-phe hierarchical assembly. ACS Nano 14:16951–16961

Kurbasic M, Romano C, Garcia A et al (2017) Assembly of a tripeptide and anti-inflammatory drugs into supramolecular hydrogels for sustained release. Gels 3:29

Kurbasic M, Parisi E, Garcia AM, Marchesan S (2020) Self-assembling, ultrashort peptide gels as antimicrobial biomaterials. Curr Top Med Chem 20:1300–1309

Kurbasic M, Garcia AM, Viada S et al (2021) Heterochiral tetrapeptide self-assembly into hydrogel biomaterials for hydrolase mimicry. J Pep Sci 28:e3304

Lazzaro BP, Zasloff M, Rolff J (2020) Antimicrobial peptides: application informed by evolution. Science (80-) 368:eaau5480

Levin A, Hakala TA, Schnaider L et al (2020) Biomimetic peptide self-assembly for functional materials. Nat Rev Chem 4:615–634

Li LL, Qiao ZY, Wang L, Wang H (2019) Programmable construction of peptide-based materials in living subjects: from modular design and morphological control to theranostics. Adv Mater 31: 1804971

Li J, Wang Z, Han H et al (2022) Short and simple peptide-based pH-sensitive hydrogel for antitumor drug delivery. Chin Chem Lett 33:1936–1940

Lossada F, Hoenders D, Guo J et al (2020) Self-assembled bioinspired nanocomposites. Acc Chem Res 53:2622–2635

Lu Y, Aimetti AA, Langer R, Gu Z (2016) Bioresponsive materials. Nat Rev Mater 2:16075

Luque-Michel E, Imbuluzqueta E, Sebastián V, Blanco-Prieto MJ (2017) Clinical advances of nanocarrier-based cancer therapy and diagnostics. Expert Opin Drug Deliv 14:75–92

Maeda H (2021) The 35th anniversary of the discovery of EPR effect: a new wave of nanomedicines for tumor-targeted drug delivery-personal remarks and future prospects. J Pers Med 11:229

Malonis RJ, Lai JR, Vergnolle O (2020) Peptide-based vaccines: current progress and future challenges. Chem Rev 120:3210–3229

Manchineella S, Govindaraju T (2016) Molecular self-assembly of cyclic dipeptide derivatives and their applications. ChemPlusChem 82:88–106

Marchesan S, Prato M (2013) Nanomaterials for (Nano)medicine. ACS Med Chem Lett 4:147–149

Marchesan S, Easton CD, Kushkaki F et al (2012) Tripeptide self-assembled hydrogels:unexpected twist of chirality. Chem Commun 48:2195–2197

Marchesan S, Qu Y, Waddington LJ et al (2013) Self-assembly of ciprofloxacin and a tripeptide into an antimicrobial nanostructured hydrogel. Biomaterials 34:3678–3687

Marchesan S, Styan KE, Easton CD et al (2015) Higher and lower supramolecular orders for the design of self-assembled heterochiral tripeptide hydrogel biomaterials. J Mater Chem B 3:8123–8132

Marchesan S, Ballerini L, Prato M (2017) Nanomaterials for stimulating nerve growth. Science 356: 1010–1011

Martin AD, Thordarson P (2020) Beyond Fmoc: a review of aromatic peptide capping groups. J Mater Chem B 8:863–877

Martin C, Oyen E, Mangelschots J et al (2016) Injectable peptide hydrogels for controlled-release of opioids. MedChemComm 7:542–549

Mayr J, Saldías C, Díaz Díaz D (2018) Release of small bioactive molecules from physical gels. Chem Soc Rev 47:1484–1515

Michiue H, Kitamatsu M, Fukunaga A et al (2021) Self-assembling A6K peptide nanotubes as a mercaptoundecahydrododecaborate (BSH) delivery system for boron neutron capture therapy (BNCT). J Control Release 330:788–796

Mishra J, Panda JJ (2019) Short peptide-based smart targeted cancer nanotherapeutics: a glimmer of hope. Ther Deliv 10:135–138

Moorcroft SCT, Roach L, Jayne DG et al (2020) Nanoparticle-loaded hydrogel for the light-activated release and photothermal enhancement of antimicrobial peptides. ACS Appl Mater Interfaces 12:24544–24554

Panda JJ, Chauhan VS (2014) Short peptide based self-assembled nanostructures: implications in drug delivery and tissue engineering. Polym Chem 5:4418–4436

Pappas CG, Frederix PWJM, Mutasa T et al (2015a) Alignment of nanostructured tripeptide gels by directional ultrasonication. Chem Commun 51:8465–8468

Pappas CG, Mutasa T, Frederix PWJM et al (2015b) Transient supramolecular reconfiguration of peptide nanostructures using ultrasound. Mater Horiz 2:198–202

Parisi E, Garcia AM, Marson D et al (2019) Supramolecular tripeptide hydrogel assembly with 5-fluorouracil. Gels 5:5

Pigliacelli C, Sánchez-Fernández R, García MD et al (2020) Self-assembled peptide-inorganic nanoparticle superstructures: from component design to applications. Chem Commun 56:8000–8014

Radwan SAA, El-Maadawy WH, Yousry C et al (2020) Zein/phospholipid composite nanoparticles for successful delivery of Gallic acid into aHSCs: influence of size, surface charge, and vitamin a coupling. Int J Nanomedicine 15:7995–8018

Raspa A, Carminati L, Pugliese R et al (2021) Self-assembling peptide hydrogels for the stabilization and sustained release of active chondroitinase ABC in vitro and in spinal cord injuries. J Control Release 330:1208–1219

Raymond DM, Nilsson BL (2018) Multicomponent peptide assemblies. Chem Soc Rev 47:3659–3720

Raymond DM, Abraham BL, Fujita T et al (2019) Low-molecular-weight supramolecular hydrogels for sustained and localized in vivo drug delivery. ACS Appl Bio Mater 2:2116–2124

Raza F, Zhu Y, Chen L et al (2019) Paclitaxel-loaded pH responsive hydrogel based on self-assembled peptides for tumor targeting. Biomater Sci 7:2023–2036

Reches M, Gazit E (2003) Casting metal nanowires within discrete self-assembled peptide nanotubes. Science (80-) 300:625–627

Ren J, Cai R, Wang J et al (2019) Precision nanomedicine development based on specific opsonization of human cancer patient-personalized protein coronas. Nano Lett 19:4692–4701

Ruan L, Chen W, Wang R et al (2019) Magnetically stimulated drug release using nanoparticles capped by self-assembling peptides. ACS Appl Mater Interfaces 11:43835–43842

Rubert Pérez CM, Stephanopoulos N, Sur S et al (2015) The powerful functions of peptide-based bioactive matrices for regenerative medicine. Ann Biomed Eng 43:501–514

Scarel M, Marchesan S (2021) Diketopiperazine gels: new horizons from the self-assembly of cyclic dipeptides. Molecules 26:3376

Seynhaeve ALB, Amin M, Haemmerich D et al (2020) Hyperthermia and smart drug delivery systems for solid tumor therapy. Adv Drug Deliv Rev 163–164:125–144

Shah A, Malik MS, Khan GS et al (2018) Stimuli-responsive peptide-based biomaterials as drug delivery systems. Chem Eng J 353:559–583

Spicer CD, Jumeaux C, Gupta B, Stevens MM (2018) Peptide and protein nanoparticle conjugates: versatile platforms for biomedical applications. Chem Soc Rev 47:3574–3620

Stupka I, Heddle JG (2020) Artificial protein cages – inspiration, construction, and observation. Curr Opin Struct Biol 64:66–73

Tao K, Levin A, Adler-Abramovich L et al (2016) Fmoc-modified amino acids and short peptides: simple bio-inspired building blocks for the fabrication of functional materials. Chem Soc Rev 45:3935–3953

Theodoroula NF, Karavasili C, Vlasiou MC et al (2022) NGIWY-amide: a bioinspired ultrashort self-assembled peptide Gelator for local drug delivery applications. Pharmaceutics 14:133

Truong WT, Su Y, Gloria D et al (2015) Dissolution and degradation of Fmoc-diphenylalanine self-assembled gels results in necrosis at high concentrations in vitro. Biomater Sci 3:298–307

Vázquez-González M, Willner I (2020) Stimuli-responsive biomolecule-based hydrogels and their applications. Angew Chem Int Ed 59:15342–15377

Veloso SRS, Silva JFG, Hilliou L et al (2021) Impact of citrate and lipid-functionalized magnetic nanoparticles in dehydropeptide supramolecular magnetogels: properties, design and drug release. Nano 11:16

Walsh TR, Knecht MR (2017) Biointerface structural effects on the properties and applications of bioinspired peptide-based nanomaterials. Chem Rev 117:12641–12704

Wang J, Liu K, Xing R, Yan X (2016a) Peptide self-assembly: thermodynamics and kinetics. Chem Soc Rev 45:5589–5604

Wang H, Luo Z, Wang Y et al (2016b) Enzyme-catalyzed formation of supramolecular hydrogels as promising vaccine adjuvants. Adv Funct Mater 26:1822–1829

Wei G, Su Z, Reynolds NP et al (2017) Self-assembling peptide and protein amyloids: from structure to tailored function in nanotechnology. Chem Soc Rev 46:4661–4708

Werner HM, Cabalteja CC, Horne WS (2016) Peptide backbone composition and protease susceptibility: impact of modification type, position, and tandem substitution. Chembiochem 17:712–718

Wychowaniec JK, Patel R, Leach J et al (2020) Aromatic stacking facilitated self-assembly of ultrashort ionic complementary peptide sequence: β-sheet nanofibers with remarkable gelation and interfacial properties. Biomacromolecules 21:2670–2680

Xia Y, Xue B, Qin M et al (2017) Printable fluorescent hydrogels based on self-assembling peptides. Sci Rep 7:1–10

Yadav N, Chauhan MK, Chauhan VS (2020) Short to ultrashort peptide-based hydrogels as a platform for biomedical applications. Biomater Sci 8:84–100

Yan L, Zhao F, Wang J et al (2019) A safe-by-design strategy towards safer nanomaterials in nanomedicines. Adv Mater 31:1805391

Yang PP, Luo Q, Bin QG et al (2017) Host materials transformable in tumor microenvironment for homing theranostics. Adv Mater 29:1605869

Yang L, Liu Y, Wang N et al (2021) Albumin-based LL37 peptide nanoparticles as a sustained release system against Pseudomonas aeruginosa lung infection. ACS Biomater Sci Eng 7:1817–1826

Zeigler DF, Gage E, Roque R, Clegg CH (2019) Epitope targeting with self-assembled peptide vaccines. npj Vaccines 4:30

Zhang S (2002) Emerging biological materials through molecular self-assembly. Biotechnol Adv 20:321–339

Zhang X, Chen L, Lim KH et al (2019) The pathway to intelligence: using stimuli-responsive materials as building blocks for constructing smart and functional systems. Adv Mater 31: 1804540

Zhang R, Liu Y, Qi Y et al (2022) Self-assembled peptide hydrogel scaffolds with VEGF and BMP-2 enhanced in vitro angiogenesis and osteogenesis. Oral Dis 28:723–733

Zhong J, Fu H, Jia X et al (2019) A pH-/thermo-responsive hydrogel formed from *N,N'*-dibenzoyl-L-cystine: properties, self-assembly structure and release behavior of SA. RSC Adv 9:11824–11832

Zhou J, Li J, Du X, Xu B (2017) Supramolecular biofunctional materials. Biomaterials 129:1–27

Chapter 13
Peptide and Protein Emulsifiers

Mohamed A. N. Soliman, Abdulwahhab Khedr, and Mohamed A. Elsawy

Abstract There has recently been a growing attention towards peptide and protein molecules as potential bioemulsifiers for the stabilization of foams and emulsions, thanks to their innate tendency towards interfacial adsorption. Additionally, peptides and proteins are biodegradable and biocompatible, making them less toxic if compared to traditional emulsifiers. This chapter provides a comprehensive overview of the different classes of peptide, protein and mixed protein–polysaccharide emulsifiers and discusses the emulsification mechanisms of these systems. In essence, peptide-mediated emulsification can occur either via traditional surfactant-like mechanism, where amphiphilic molecular peptide chains adsorb at the biphasic interface forming 'spherical micelles', or through peptide self-assembly into higher secondary structure (α-helices or β-sheets) with the formation of amphiphilic nanofibrous structures adsorbing at the interface. Moreover, peptides can self-assemble in the continuous aqueous phase forming nanofibrous network of viscous hydrogels that enhance system stability. On the other hand, emulsion stabilization by proteins is mainly achieved through either electrostatic repulsion or steric stabilization. The various characterization techniques for emulsification and interfacial stabilization will be visited throughout this chapter, focusing on structural, mesoscopic and macroscopic characterization of these systems.

M. A. N. Soliman
Leicester School of Pharmacy, Leicester Institute for Pharmaceutical Innovation, De Montfort University, Leicester, UK

Department of Pharmaceutics and Industrial Pharmacy, Faculty of Pharmacy, Cairo University, Cairo, Egypt

A. Khedr
Leicester School of Pharmacy, Leicester Institute for Pharmaceutical Innovation, De Montfort University, Leicester, UK

Department of Pharmaceutics and Industrial Pharmacy, Faculty of Pharmacy, Zagazig University, Zagazig, Egypt

M. A. Elsawy (✉)
Leicester School of Pharmacy, Leicester Institute for Pharmaceutical Innovation, De Montfort University, Leicester, UK
e-mail: mohamed.elsawy@dmu.ac.uk

13.1 Introduction

Emulsifiers have been widely developed and exploited in many industries, such as wastewater treatment, improved oil recovery, food and beverages, detergents, cosmetics as well as coating industries, in addition to their utilization in chemical catalysis and cell assays (Moreira et al. 2017; Dexter et al. 2006; Lv et al. 2019; Dexter 2010; Bai et al. 2014; Platzman et al. 2013). Importantly, they have been used in various pharmaceutical formulations for drug encapsulation and controlled drug delivery (Dexter et al. 2006; Nishida et al. 2017; Windbergs et al. 2013; Naseef et al. 2018). Emulsifiers are required for controlling the characteristics of fluid–fluid interface, which is highly crucial for stabilization of foam and emulsion-based formulations (Dexter et al. 2006; Dexter 2010; Wilde 2000). Long-term stabilization remains as a pivotal challenge for these industries when developing such colloidal systems, which are instinctively thermodynamically unstable and vulnerable to phase separation (Li et al. 2016). Therefore, there is a crucial need for the development of emulsifiers that can enhance long-term stabilization while being biocompatible, non-toxic, sustainable and environment friendly (Li et al. 2016).

In essence, emulsifiers are a distinctive group of surfactants that can efficiently adsorb at different interfaces, particularly air–liquid and liquid–liquid, reducing interfacial tension and thus allowing for the dispersion of immiscible phases and formation of kinetically stable colloidal systems (Bouyer et al. 2012; Lee 2008; Mondal et al. 2017). According to Myers, emulsifiers can be classified into four main classes, based on their interfacial adsorption and emulsification mechanisms (Myers 1999). The first class includes non-surfactant ionic compounds capable of interfacial adsorption at drop surface resulting in electrostatic repulsions between close droplets, thereby stabilizing emulsions against coalescence. However, these ionic compounds neither impact the interfacial tension nor contribute to the emulsification steps. The second category comprises small non-surfactant colloidal solids, such as clay or silica, forming Pickering emulsions, as they adhere to droplet surface generating a physical barrier between globules that delays or prohibits coalescence. The third group encompasses the typical monomeric surfactant amphiphiles. They are composed of a charged/hydrophilic head conjugated to a hydrophobic tail. According to the inherent charge of the head part, they can be subdivided into anionic, cationic, zwitterionic or non-ionic molecules (Lee 2008; Caballero et al. 2003). At the interface, they adsorb and self-assemble, directing the hydrophilic head to the aqueous phase, whereas the hydrophobic tail towards the oil or gas phase forming protective layer preventing breakdown and lowering interfacial tension between phases, and consequently stabilizing the system (Petsev 2004). Finally, the fourth class contains polymer surfactants that impart steric and/or electrostatic stabilization to the system besides their interfacial tension diminishing capacity. They can also form cohesive interfacial films which inhibit the rupture of thin layers

of emulsifier surrounding the droplets or bubbles, which is the last stage in coalescence (Dexter et al. 2006; van Aken 2004). Moreover, they improve emulsion stability through enhancing elasticity and viscosity of the interface or by changing the bulk viscosity of the systems.

It can be noticed that interfacial adsorption and self-assembly is a common characteristic among the four classes of emulsifiers. Interfacial self-assembly is governed by mutual interactions between the emulsifier units and the interface itself. These interactions can also affect intermolecular forces between assembled emulsifier units and thus make the interfacial assembly significantly different from bulk self-assembly (Lee 2008). Better understanding of interfacial self-assembly processes can inform the rational design of emulsifier units that are capable of self-assembly at interfaces creating interfacial nanoarchitectures which can inhibit coalescence and coarsening (Scott et al. 2016).

Besides the molecular nature of emulsifiers, emulsions can be classified, according to the proportion and distribution of aqueous to oil phase in the system, into either simple or double emulsions. Simple emulsion may be either oil in water (O/W) when the oil is the dispersed phase and water constitutes the continuous phase or water in oil (W/O) which is the reverse state. Double emulsions are W/O/W or O/W/O systems offering merits over simple emulsions for encapsulation of therapeutic molecules and their controlled release due to the enveloped internal framework (Okochi and Nakano 2000; Hanson et al. 2008). The type of emulsion created, either O/W or W/O, depends on various intrinsic parameters including physicochemical properties of the emulsifier used, temperature and composition of the system. These parameters could affect the competition between coalescence tendency and emulsified droplet stabilization. In general, the highly stabilized phase will constitute the dispersed droplets, while the other phase coalesces forming the continuous phase (Lee 2008). Extrinsic manufacturing parameters can also affect emulsion order, such as the type of energy used (stirring), the way and time of its application as well as the order of ingredients mixing. Based on globular size and thermodynamic behaviour, emulsions can be classified into microemulsions (10–100 nm, thermodynamically stable), nanoemulsions (100–400 nm, kinetically stable) and macroemulsions (>400 nm, kinetically stable) (McClements 2012; Callender et al. 2017). The miniaturized size of nanoemulsions/microemulsions droplets shows several privileges over macroemulsions involving improved optical clarity, enhancement of drug cargo bioavailability and long-term formulation stability, which are all key attributes for drug delivery vehicle (Table 13.1) (Yang et al. 2017).

Although traditional emulsifiers are well suited for formation and stabilization of foams and emulsions, many of these emulsifiers are neither biodegradable nor biocompatible (Scott et al. 2016). Additionally, some have potential toxicity towards human health and the environment (Bouyer et al. 2012; Mondal et al. 2017; Rebello et al. 2014). Other limitations include impaired stabilization under environmental stresses, such as elevated temperatures, extreme pH ranges and high salt concentrations, as well as the insufficient long-term stability and not being amenable for structural modifications, all hindering their practical use in various industries

Table 13.1 Emulsion types and their properties

Emulsion	Type	Droplet size	Appearance	Energy input	Stability
Macroemulsion	Simple (O/W and W/O) and double (W/O/W and O/W/O) emulsions	>400 nm	Opaque turbid system	Required	Kinetic
Nanoemulsion		100–400 nm	Blue-white to semi-opaque system		
Microemulsion	Type I: Biphasic O/W Type II: Biphasic W/O Type III: Triphasic bicontinuous Type IV: Monophasic	10–100 nm	Single phase transparent system	Not required	Thermodynamic

(Adjonu et al. 2014; Fowler et al. 2011; Minkenberg et al. 2009; Lotfallah et al. 2015). Peptides and proteins came in the forefront as potential alternative emulsifiers that can overcome these limitations, thanks to the innate surface activity, biocompatibility and physicochemical tunability.

In this chapter, we will shed the light on recent advances in formulation of emulsions and foams using peptide, protein and mixed protein/polysaccharide emulsifiers. The various mechanisms of emulsification and interfacial stabilization will be discussed in terms of their structural and mesoscopic characteristics and their stabilization efficiency for longer term and under drastic conditions.

13.2 Peptide Emulsifiers

Peptide molecules possess the inherent characteristics of proteins, such as the biodegradability, biocompatibility and safety with additional advantages of low production costs with high purity and low batch-to-batch variations (Moreira et al. 2017; Li et al. 2016; Wibowo et al. 2017). In addition, exploitation of the amino acid chemical toolbox provides infinite possibilities of various chemical designs, enabling physicochemical tunability of peptide emulsifiers, for instance, tailoring hydrophilic and lipophilic properties and controlling the non-covalent electrostatic or hydrophobic interactions between molecules, which are essential for controlling interfacial self-assembly (Wibowo et al. 2017). Peptides can rapidly adsorb to interfaces at lower concentrations compared to proteins, facilitating droplet or bubble formation which is the most critical step for emulsion or foam formation, respectively. This is normally followed by interfacial adsorption into rigid cohesive
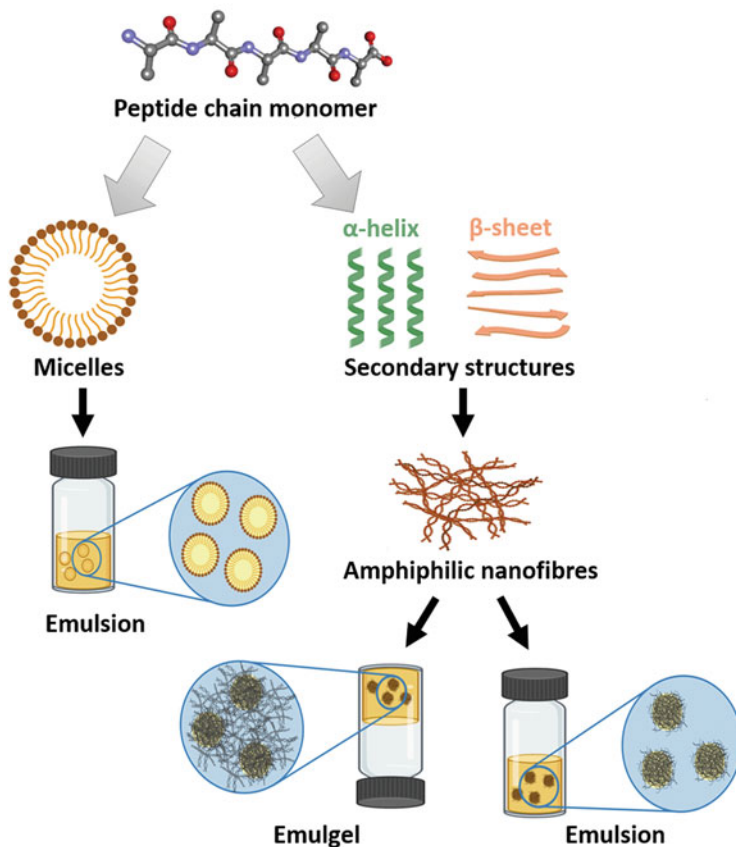
Fig. 13.1 The possible mechanisms of interfacial arrangement of peptide emulsifiers at the droplet interface through either micelle formation or self-assembly into nanofibrous structures, forming emulsions or emulgels

structures surrounding the droplets or bubbles maintaining their attachment and stabilization of these system (Scott et al. 2016).

Interfacial adsorption of peptide molecules can lead to the formation of micellar structures, akin to conventional surfactant, where the hydrophilic heads are solubilized in aqueous phase and the hydrophobic tail projecting to the organic or gas phase (Fig. 13.1). Interfacial self-assembly into higher secondary structure (α-helices or β-sheets) could also happen, forming amphiphilic nanofibrous structure at the interface (Fig. 13.1). Additionally, self-assembly into nanofibrous network in the bulk aqueous phase could occur, leading to hydrogel formation, which increases the system's viscosity and hinders emulsion coalescence or foam collapse, a system known as 'emulgel' (Fig. 13.1).

Based on their chemical structures, peptide emulsifiers can be classified into short aromatic, α-helix, β-sheet and surfactant-like peptides. In this section we will present

these different classes and will discuss their interfacial adsorption mechanisms in more details.

13.2.1   Short Aromatic Peptide Emulsifiers

Short synthetic peptides were developed to self-assemble into a variety of higher nanostructures, as discussed in Chap. 4: short peptide and peptidomimetic nanomaterials. Interestingly, short aromatic peptides have been designed to self-assemble into amphiphilic nanofibrous structures which exhibit interfacial activity. For instance, the Ulijn group reported the ability of amphiphilic dipeptides, which are N-capped with aromatic moieties, to self-assemble into nanofibrous networks at organic/aqueous interfaces (Fig. 13.2a) (Bai et al. 2014). Unlike traditional emulsifiers, which work via adsorption of the molecular amphiphile at the biphasic interface forming micellar structures, these short aromatic peptides form interfacial nanofibrous stabilization matrices (Figs. 13.1 and 13.2a). The 9-fluorenylmethoxycarbonyl tyrosine-leucine (Fmoc-YL) is one example of these short aromatic peptide emulsifiers, which was successfully used to stabilize chloroform-in-water emulsion by hand shaking for few seconds at 80 °C (Table 13.2). Interfacial self-assembly of Fmoc-YL into a less ordered β-sheet-like assemblies occurred via interchain hydrogen bonding (H-bonding) between peptide backbone amides as well as aromatic π stacking of Fmoc capping groups, forming amphiphilic nanofibrous structures, which entangle into interfacial network film stabilizing the suspended chloroform droplets within the aqueous continuous phase (Figs. 13.1, 13.2a, g and i). The Fmoc-YL-based emulsion exhibited greater stability (months) at room temperature than the commercial emulsifier sodium dodecyl sulphate (SDS), with the latter showing phase separation within 2 weeks. In addition, better thermal stability as well as resistance to salting out were achieved with Fmoc-YL in comparison to SDS emulsifier.

On-demand demulsification of Fmoc-YL systems was made possible using thermolysin protease enzyme, which digested the interfacial peptidic film under mild physiological conditions. Fmoc-YL also showed to be a successful emulsifier for other organic phases, such as hexadecane and mineral oil. Replacement of L residue in Fmoc-YL with A or S also produced peptide emulsifiers that formed chloroform-in-water emulsions. However, these changes significantly affected the emulsion characteristics, such as globular size and critical emulsion concentration. In case of Fmoc-YA, reduction of sequence hydrophobicity arising from replacing L by A did not influence β-sheet nanofibres formation in water. However, introduction of S impaired the peptide tendency to self-assemble into nanofibrous structures; consequently, higher critical emulsion concentration and emulsion globular size were observed for Fmoc-YS compared to both Fmoc-YL and Fmoc-YA (Table 13.2 and Fig. 13.2a–c). In essence, increasing both hydrophobicity and H-bonding interactions enhanced interfacial adsorption and lowered the emulsion droplet sizes as well as critical emulsion concentrations. To increase sequence
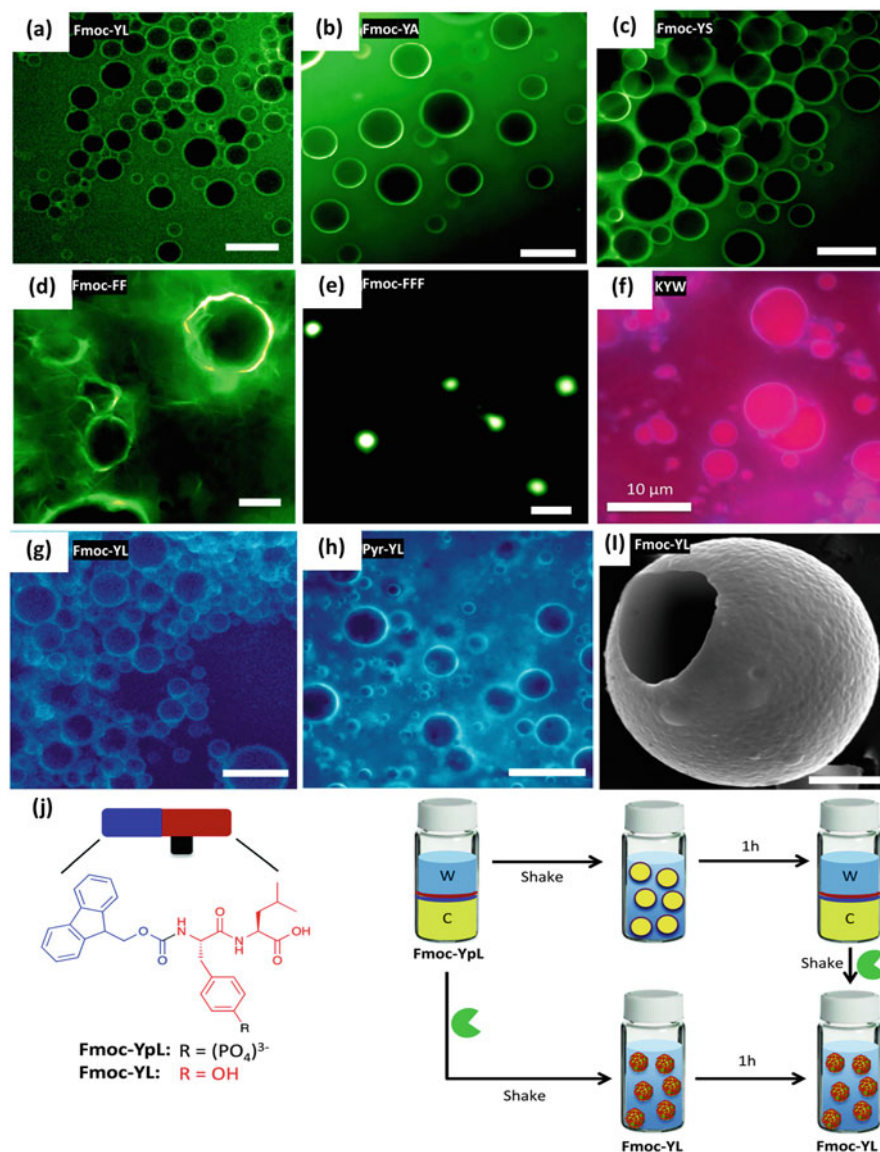
Fig. 13.2 Fluorescent microscope images of chloroform-in-water emulsion droplets stabilized by (**a**) Fmoc-YL, (**b**) Fmoc-YA, (**c**) Fmoc-YS, (**d**) Fmoc-FF networks containing fluorescence iso-thiocyanate (FITC) in water phase, (**e**) water-in-chloroform emulsion droplets stabilized by Fmoc-FFF containing FITC in water phase and (**f**) Fluorescence microscopy of KYW chloroform-in-water emulsion droplets with overlay of Sudan II and Thioflavin T (ThT) staining, (**g**) Fmoc-YL and (**h**) Pyrene-YL emulsions. Scale bar is 50 μm except for KYW (10 μm). (**i**) SEM micrograph of air-dried Fmoc-YL microcapsules at chloroform/water interface. Scale bar is 2 μm. Adapted from (Bai et al. 2014), with copyrights permission from the American Chemical Society and (Scott et al. 2016), with copyrights permission from John Wiley and Sons. (**j**) left. Chemical structure of Fmoc-YpL and Fmoc-YL, Right, Schematic representation of the Fmoc-YpL before and after alkaline phosphatase dephosphorylation in a biphasic system, showing Fmoc-YL stabilized emulsions,

lipophilicity, Fmoc was replaced by pyrene or YL by FF, where the Fmoc-FF and Pyr-YL successfully created chloroform-in-water emulsions (Fig. 13.2d, h). Further increase in lipophilicity resulted in inverted emulsion (water-in-chloroform), when using the highly hydrophobic tripeptide Fmoc-FFF as emulsifier (Fig. 13.2e and Table 13.2).

Ulijn and co-workers have also introduced biocatalytic-controlled interfacial self-assembly of phosphorylated Fmoc-YL (Fmoc-YpL) at chloroform/water interface using a phosphatase enzyme (Fig. 13.2j and Table 13.2) (Moreira et al. 2016), inspired by Xu's group strategy who first demonstrated that enzymatic dephosphorylation of Fmoc-tyrosine phosphate (Fmoc-Yp), using alkaline phosphatase, triggered self-assembly of the product Fmoc-Y into supramolecular hydrogel (Yang et al. 2004). Ulijn and co-workers demonstrated that the parallel arrangement of fluorenyl groups of Fmoc-YpL led to the formation of micelles, which when dephosphorylated by alkaline phosphatase into Fmoc-YL rearranged into fibrous structures at the organic/aqueous interface (Fig. 13.2j). The phosphorylated precursor Fmoc-YpL behaved as an amphiphile with surfactant-like adsorption, where the hydrophobic Fmoc tail projected to organic phase while the hydrophilic YpL chain head to water with low emulsion stabilization, with phase separation occurring within 1 h. Upon enzymatic dephosphorylation into Fmoc-YL, interfacial self-assembly into nanofibrous network was achieved via non-covalent interactions, as explained above, forming a very stable emulsion with no phase separation observed for months. The same group showed the possible conversion of a phase separated biphasic oil/water mixture containing Fmoc-YpL stored for up to 1 month into emulsion catalysed by enzymatic dephosphorylation. However, slower emulsification rate was observed compared to the immediate activation approach, with the formed emulsion exhibiting less stability and larger droplet size. This is attributed to the slower dephosphorylation of Fmoc-YpL leading to less ordered H-bonding, hence impairing the interfacial self-assembled fibrous network. Molecular dynamic simulation suggested the absence of permanent H-bonding between Fmoc-YpL monomers, while the dephosphorylated form showed Fmoc/L and Y/L H-bonding that agreed with FTIR results. Results of this study confirmed the importance of interfacial self-assembly of nanofibres for emulsion stabilization rather than individual peptide monomers (Fig. 13.1) (Moreira et al. 2016).

Although the Fmoc-capped dipeptides exhibit good surface activity, which was shown to be better than commercial emulsifiers in many cases, its potential translation to emulsifiers in food, pharmaceutical and cosmetic industries was withheld as the molecular design is based on the non-biological Fmoc group, which could potentially impair the biocompatibility of these materials. To overcome this limitation, Ulijn and co-workers developed unprotected tripeptide emulsifiers, with a peptide sequence design of two successive aromatic residues (Ar) flanked with a

Fig. 13.2 (continued) while Fmoc-YpL acted like a conventional surfactant and system separated into two phases after 1 h. Adapted from (Moreira et al. 2016), with copyrights permission from Royal Society of Chemistry

Table 13.2 Classes of peptide emulsifiers and their application

Class of emulsifier	Sequence of peptide	Emulsion/Foam type	References
Short aromatic peptides	Fmoc-YL	Chloroform-in-water emulsion Hexadecane-in-water emulsion Mineral oil-in-water emulsion	Bai et al. (2014)
	Fmoc-YA, Fmoc-YS, Pyr-YL, Fmoc-FF	Chloroform-in-water emulsion	
	Fmoc-FFF	Water-in-chloroform emulsion	
	Dephosphorylated Fmoc-YpL	Chloroform-in-water emulsion	Moreira et al. (2016)
	FFD, DFF, KFF, KYW, KYF	Rapeseed oil-in-water emulsion and oleic acid-in-water emulsion	Scott et al. (2016), Dragulska et al. (2018)
	Dephosphorylated KYpF	O/W emulgel	Moreira et al. (2017)
	Fc-FFD, Fc-FFH, Fc-FFS, Fc-FFF	Ethyl acetate-in-water emulsion	Yang et al. (2017)
	Nap-FF, BrNapFF, 2Nap-FF	Wet foams Isopropyl myristate, dodecane and silicon oil-in-water emulsions	Li et al. (2016), Aviño et al. (2017), Li et al. (2014)
Alpha helices forming peptides	SHR-FLLF, SHR-FLELF, SHR-FLKLF	Silicon oil-in-water emulsion	Mondal et al. (2017)
	AM1	Foam Toluene-in-water emulsion	Dexter et al. (2006) Dexter and Middelberg (2007), Middelberg et al. (2008)
	Lac21E	Foam	Middelberg et al. (2008)
	AFD4	Foam	Dexter and Middelberg (2007)
	AM-S	Foam	Wibowo et al. (2017)
	C8-AM	Miglyol 812 oil-in-water nanoemulsion	Wang et al. (2017)
	SurSi	Miglyol 812 oil-in-water nanoemulsion and silica nanocapsules	Wibowo et al. (2014), Hui et al. (2016)
	DAMP1, DAMP4 and their mixture	Foam	Middelberg and Dimitrijev-Dwyer (2011), Dwyer et al. (2013)
	SP16	Foam	Zhao et al. (2017)
	PBLG ($n = 12$ and 32)	Dichloromethane-in-water microemulsion	Morikawa et al. (2005)

Table 13.2 (continued)

Class of emulsifier	Sequence of peptide	Emulsion/Foam type	References
		Dichloromethane/methanol-in-water microemulsion	
	$K_x(rac-L)_y$, $R_{40}(rac-L)_{10}$, $E_{40}(rac-L)_{10}$, $K_{60}(rac-V)_{20}$, $K_{60}(rac-A)_{20}$	W/O/W emulsion	Hanson et al. (2008)
	$K_{60}L_{20}$	O/W emulsion	Hanson et al. (2008)
β-Sheets forming peptides	B-14, B-15, B-16, B-17	Dodecane-in-water emulsion	Dexter (2010)
	Q11	W/O emulsion	Tian et al. (2011)
	A_9R	O/W emulsion	Castelletto et al. (2019)
	Phg4	Chloroform-in-water emulsion Melissa oil-in-water emulgel	Wychowaniec et al. (2020)
Miscellaneous peptides	GAP	Isopropyl myristate oil-in-water emulsion	Lotfallah et al. (2015)
	C_{13}-KR	Medium chain triglyceride oil-in-water emulsion	Lv et al. (2019)
	NH_2-lauroylGGGH/ 1,4-phthalaldehyde mixture	O/W emulsion	Nishida et al. (2017)

charged residue ($X^{+/-}$) either from the N- or C-terminus (i.e. $X^{+/-}$-Ar-Ar or Ar-Ar-$X^{+/-}$) (Scott et al. 2016). Two types of tripeptide emulsifiers were developed, the anionic (such as FFD and DFF), which formed bilayer-like assemblies at the oil/water interface, and the cationic (such as KFF, KYW and KYF), which formed interfacial nanofibrous networks that highly stabilized the rapeseed oil-based emulsions compared to the anionic type (Table 13.2). Interestingly, the cationic tripeptides self-assembled in both aqueous and biphasic media through H-bonding into β-stranded fibres, while the anionic tripeptides only showed interfacial self-assembly upon introduction of oil to the aqueous phase, where peptide chains stack into parallel orientation at the oil/water interface with lateral H-bonding interactions. The nanofibre forming peptide emulsifier KYF possessed superior thermal stability with no phase separation observed for the formed O/W emulsion at 80 °C, while KYW and KFF showed thermal stability only up to 50 °C and 40 °C, respectively, due to the breakdown of fibrous structure. Based on this, KYF was exploited as an emulsifier to formulate O/W nanoemulsion that can entrap oleic acid-platinum II conjugate for treatment of ovarian cancer (Dragulska et al. 2018). A nanoprecipitation method was employed by a dropwise addition of organic phase (oleic acid-platinum II conjugate in isopropanol) to aqueous phase (KYF dissolved in water at 37 °C and pH 7) with stirring overnight to prepare the nanoemulsion. The

miniaturized droplet size (240 nm) enabled its ability for extravasation and passive targeting of tumours with long-term stability upon storage for months. This strategy can be employed to encapsulate and deliver other active moieties.

Besides nanoemulsion formation, Moreira et al. demonstrated the ability of the phosphorylated tripeptide analogue KYpF to act as on-demand emulsifier that stabilizes O/W emulsion and emulgel upon treatment with alkaline phosphatase (Table 13.2) (Moreira et al. 2017). Complete dephosphorylation occurred 24 hours after incubation with phosphatase enabling the transformation of a biphasic system containing few micelles of KYpF at the interface (40 mM) into an O/W emulsion at low enzyme concentration and O/W emulgel at high enzyme concentration where both were stabilized by the dephosphorylated KYF. Emulsion stabilization was achieved via creation of β-sheet nanostructures at the oil droplet surfaces lowering interfacial tension, while emulgel additionally has crosslinked β-sheet nanofibres in the aqueous phase that enhanced the continuous phase viscosity. Enzyme concentration was found to be a crucial factor in controlling the emulsifying capacity of the peptide, as it affects the rate of self-assembly and densities of fibrous networks at the interface hindering coalescence. Increasing enzyme concentration led to faster dephosphorylation, higher levels of π–π stacking, more organized H-bonding between backbone amide of peptide chains, and overall better self-assembly and control of emulgel properties. The lowest enzyme concentration tested (0.07 μM) did not form emulgel but stabilized the emulsion through short un-entangled thick fibres (14 nm width), while increased entanglement and dense thin fibres (3 nm) appeared with the highest concentration (6.6 μM), stabilizing the system for more than 1 week. On the other hand, there was no evidence of secondary structure formation of KYpF in the absence of enzyme. The failure of KYpF assembly was ascribed to the hydration of phosphate ions in water rather than the repulsion between the anionic groups, so modifying the peptide hydrophilicity can affect self-assembly. The best catalyst concentration of the enzyme was 3.3 μM that produced sharper peaks at 1620 and 1560 cm^{-1} in FTIR. Interestingly, the biocatalytic emulsion formation was thermo-reversible displaying switchability between demulsification and re-emulsification upon heating to 50–60 °C then cooling overnight, respectively. This study also showed that controlled biocatalytic activation of KYpF gave more ordered structures than the use of KYF peptide per se, with less entangled slightly thicker fibres (~4.6 nm) formed.

Another triggering approach for self-assembly of the diphenylalanine-based tripeptide emulsifiers FFX (where X is a hydrophilic residue, such as S, F, D or H) that failed to form nanofibres at the oil/water interface (Scott et al. 2016), involved the conjugation of the organometallic moiety ferrocene (Fc) to the tripeptide sequence (Table 13.2) (Yang et al. 2017). The biocompatible moiety increased peptides hydrophobicity as well as steric bulk and imparted redox power to the peptide system. Taking FFH as example, the peptide failed to stabilize emulsion formation; however, the amphiphilic Fc-FFH conjugate monomers gathered at the ethyl acetate/phosphate buffer (pH 7.2) interface into thin shells (Yang et al. 2017). This orientation stabilized the fabricated nanoemulsion, which is composed of hollow nanovesicles (100–200 nm), for more than 4 months at ambient conditions

and exhibited high thermostability at 70 °C. This perfect stabilization efficiency was due to an enthalpy-controlled equilibrium among the association energy within the self-assembled peptide structure and the interfacial free energy between the peptide monomers and solvent. Other Fc-FFX sequences also successfully stabilized the nanoemulsions (Yang et al. 2017). Interestingly, tailoring the nanoemulsion droplet size, its physical appearance and its redox, as well as catalytic activity, was performed through adjusting the ratio of solvents, temperature, oxidation state of Fc group and the sequence of tripeptide. Moreover, oxidation of the ferrocene peptide-based nanoemulsion led to emergence of small micellar structures that can be employed as drug delivery vehicle. Increasing the water to organic solvent ratio led to conversion of emulsion size from microscale to nanoscale with transparent appearance. Rising the temperature of the systems to 70 °C did not cause phase separation, but only increased droplet size was observed. However, upon cooling below 25 °C, Fc-FFH emulsion showed transition into hydrogel due to reduction of monomers' aqueous solubility after cooling and increasing the association energy, which led to change of peptide conformation. Fc-FFH monomers reorganized themselves or dissociated from the interface followed by their assembly into twisted β-sheet fibres and then nanostructured hydrogels, where the FTIR of nanoemulsion showed an unstructured system (Peak at 1654 cm^{-1}), while hydrogel had a characteristic β-sheet peak at 1629 cm^{-1}. It has also been reported that His-based peptides can perform like an artificial hydrolase enzyme (Garcia et al. 2017; Wang et al. 2016; Huang et al. 2013; Guler and Stupp 2007). Based on this, Yang et al. found that Fc-FFH nanoemulsion was able to hydrolyse *p*-nitrophenyl butyrate (PNPB) into PNP, so Fc-FFH nanoemulsion also acted as an ideal artificial hydrolase enzyme with better storage stability than enzymes (Yang et al. 2017).

Other N-capped short aromatic peptides showed to stabilize foam systems, where Li et al. reported that naphthyl derivatives of the short aromatic dipeptide FF (NapFF and BrNapFF) self-assemble into thin interfacial films of β-sheet fibrous structure at the air/water interface using drop-casting technique (Table 13.2 and Fig. 13.3a–c) (Li et al. 2014). The peptide was dispersed in alkaline solvent (pH >10) where wormlike micellar structure formed followed by its dropwise addition onto a low pH solvent, leading to formation of woven strands of β-sheets configuration. The creation of interfacial self-assembled film required high peptide concentration (>0.35 wt%) besides quick protonation of peptide achieved by adjusting the subphase pH to be less than the pKa of the dipeptides, which was 3.5 and 2 for NapFF and BrNapFF, respectively. The β-sheet strands were in nanoscale width (40 nm) and when carboxylate group become protonated, bundled together to generate elastic fibres of 800 nm in thickness. They displayed an episodic wrinkle when compressed in a Langmuir trough conferring stabilization of large air bubbles for numerous days, with no coalescence or Ostwald ripening was observed. On the other hand, BrNapAV failed to build interfacial films at any concentration and different pH values although it exhibited β-sheet arrangement at high pH. This might be ascribed to the type of micelles (spherical micelles) formed at high pH differed from that formed with NapFF and BrNapFF (wormlike micelles) or the lower hydrophobicity of BrNapAV.
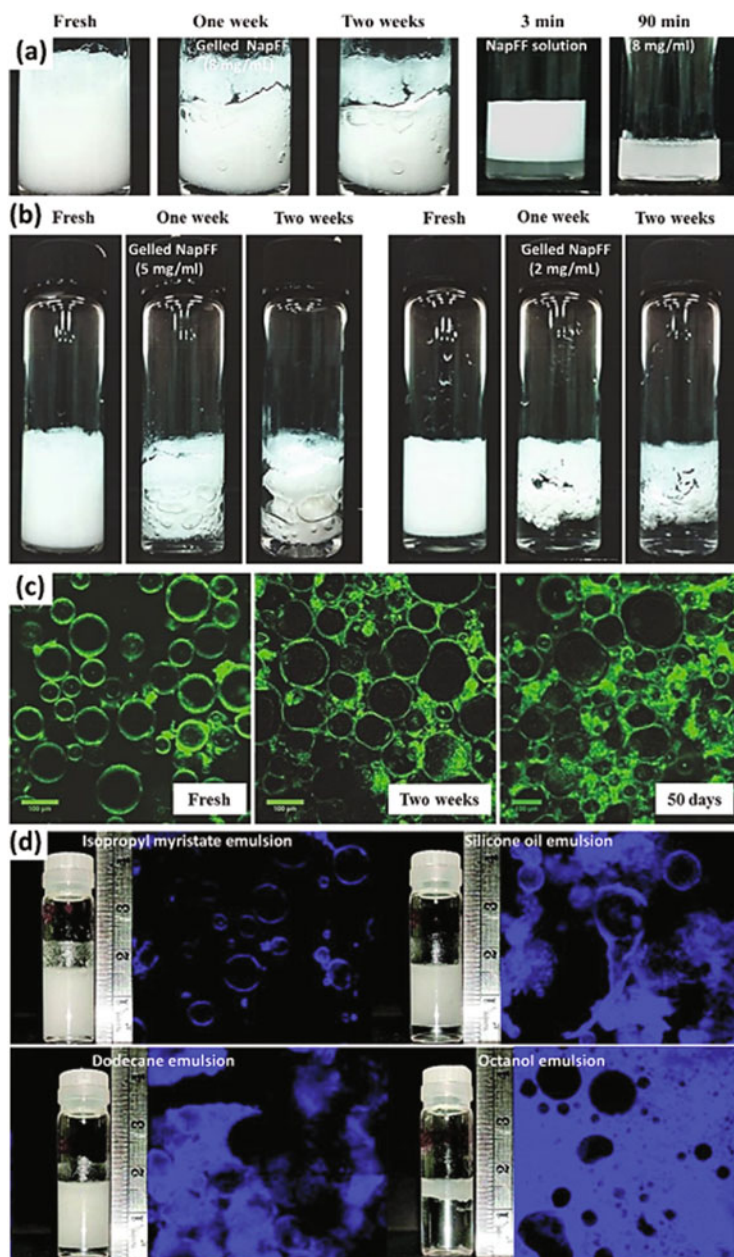
Fig. 13.3 Stabilization of foam using different NapFF concentrations, (**a**) 8 mg/mL, left, after adding CaCl₂, Right, without CaCl₂. (**b**) 5 and 2 mg/mL. (**c**) Confocal images of the air bubbles in foam showing non-spherical shapes upon bubbles distortion. Adapted from (Li et al. 2016), with copyrights permission from John Wiley and Sons. (**d**) Characteristics of four emulsions stabilized by 2 mM 2NapFF at 50 °C and the dipeptide were dyed with Nile blue in the confocal images. Adapted from (Aviño et al. 2017), with copyrights permission from Royal Society of Chemistry

The same group used the hydrophobic dipeptide NapFF (0.8 wt%) to formulate self-assembled viscoelastic hydrogel in presence of Ca^{2+} ions that can generate wet foams and stabilize them for more than 2 weeks (Table 13.2 and Fig. 13.3a) (Li et al. 2016). Due to interchain H-bonding, hydrophobicity of NapFF as well as external stimulation by cationic metals, the aromatic dipeptide self-assembled at the air/water interface into β-sheet oriented fibrous network films and stabilize the foam bubbles. The formed fibre (200 nm width) at the air/water interface (Li et al. 2016) was found to be thicker than fibres obtained from the drop casting method (40 nm width) (Li et al. 2014). In addition, the extra dipeptide moieties self-assembled in the bulk continuous phase forming a 3D structured hydrogel with high storage modulus (Li et al. 2016). Such viscoelastic hydrogel could arrest the migration of bubbles, and hence delay bubble size growth, as well as lower the liquid drainage out of the system pointing out the great stabilization of the formed foam. However, upon foam cessation, part of the aqueous phase separated from the hydrogel (Fig. 13.3a). On the other hand, the NapFF solution that was not treated with Ca^{2+} ions did not form a gel and so produced a very weak foam that ceased in less than 2 h (Fig. 13.3a) (Li et al. 2016).

Interestingly, system stabilization was shown to be concentration dependent, which might be enhanced by increasing the dipeptide concentration. For instance, 0.2 wt% NapFF formed thin fibres that collapsed in 7 days, while 0.5 wt% led to better stabilization where water leakage out of the system, reduction in foam volume and phase separation happened within 2 weeks (Fig. 13.3b, c) (Li et al. 2016). However, increasing peptide concentration to 0.8 wt% formed stable wet foam hydrogel system for more than 2 weeks (Fig. 13.3a) (Li et al. 2016). Moreover, the type of metal cation affected foam stabilization, where divalent cations can develop stiffer hydrogels than monovalent ones (Li et al. 2016; Chen et al. 2011a). In the view of this, it was found that foam induced by $CaCl_2$ addition was more stable (no coalescence) than $MgSO_4/MgCl_2$ followed by KCl that showed higher bubbles coarsening rate due to the absence of crosslinked fibres and presence of thin fibres 10 nm (Li et al. 2016).

Aviño et al. used extremely low concentration of 2NapFF (0.1 wt%) with two different $MgSO_4$ concentrations (18 and 142 mM) to induce self-assembled hydrogel for stabilizing foam and emulsions of different oils (Table 13.2) (Aviño et al. 2017). Micellar structure was formed after dissolving the peptide at high pH (11 ± 0.5) that converted to hydrogel after adding salt. The fibrous structure formed at the air/water interface upon adding salt to low dipeptide concentration was very loose that failed to hinder bubbles ripening leading to a weakly stabilized foam (Aviño et al. 2017). At low salt concentration, better foam quality was formed compared to higher salt concentrations, but both foams collapsed only after 2 h due to the preferential interfacial adsorption of the nanofibres leading to the weakness of the hydrogel in the bulk phase. A different behaviour was observed at the oil/water interface, where significantly more stable long-standing emulsions were produced with both $MgSO_4$ salt concentrations upon testing three different oils, isopropyl myristate, dodecane and silicone oils, while only octanol failed to be emulsified due to peptide accumulation in the oil and poor wetting of the interface

(Fig. 13.3d). The isopropyl myristate-based emulsion was the optimum formulation with no obvious creaming due to the formed interfacial film that greatly stabilized the system. However, in case of silicone and dodecane oil-based emulsions, stabilization was only attributed to hydrogel formation in the continuous phase, as well as wetting properties of peptide at the interface. To that end, it could be concluded that gelation of naphthyl derivatives of short aromatic peptides is possible by dissolving the peptide in an alkaline medium then adding salts or lowering the pH.

13.2.2 α-Helix Peptide Emulsifiers

Bioinspired short amphiphilic peptide sequences that have tendency to acquire α-helical structures at organic/aqueous interfaces have been widely studied for their surface activity and emulsification capacity. For instance, the surface activity, conformational rigidity and helical propensity of the fungal structural hydrophobin proteins inspired the development of a library of short biotriggered helical emulsifiers, by Gazit and co-workers (Mondal et al. 2017). The helical heptad amphipathic peptides showed to stabilize silicon oil-based O/W emulsions. The design was based on the incorporation of the helical-forming non-proteinogenic amino acid, α-aminoisobutyric acid (Aib), at positions (*i*, *i* + 3), which enabled the formation of supramolecular helical structure both in aqueous phase and at oil/water interface (Fig. 13.4a). The parent peptide of this library was designed by modifying the previously reported helix-forming peptide, SHR-FF peptide (Ser-Aib-Phe-Ser-Aib-Phe-Aib) (Mondal et al. 2015), into SHR-FLLF (*Phe*-Aib-*Leu*-Ala-Aib-*Leu*-Phe) (Table 13.2). The terminal Phe groups of one strand allowed the π–π stacking with another adjacent one, while Leu inclusion offered zipper conformation via hydrophobic bonding in addition to increasing hydrophobicity by adding alanine instead of serine (Fig. 13.4a) (Mondal et al. 2017). Such structural modulation favoured the self-assembly into highly ordered supramolecular aggregates of helices, forming cylindrical micelles-like nanofibres (Fig. 13.4a) (Mondal et al. 2017). It was postulated the presence of 2 asymmetric structural units: (A) right-handed α-helix and
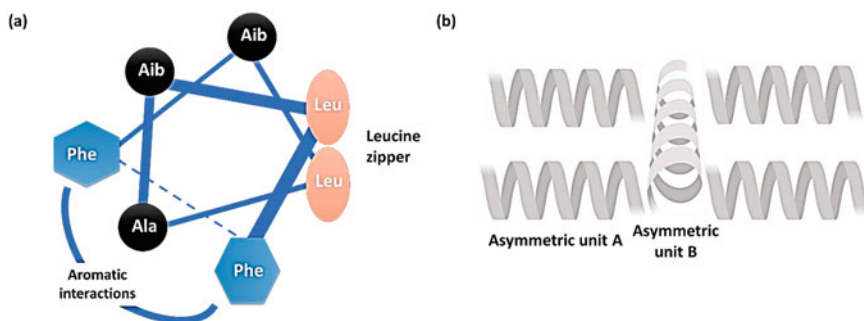

Fig. 13.4 (**a**) Helical wheel representation and (**b**) perpendicular packing pattern of SHR-FLLF

(B) 3_{10}-helix, due to intrahelical H-bonding, with perpendicular orientation of unit A to B triggering hydrophobic and π stacking interactions forming knob-into-hole arrays (Fig. 13.4b) (Mondal et al. 2017). This arrangement created a helical hydrophobic column with dual hydrophilic terminals similar to bolaamphiphiles. SHR-FLLF showed to act as a biosurfactant at concentrations of 5, 10 and 15 mg/mL (critical assembly concentration, CAC = 2.8 mg/mL), emulsifying silicone oil in water (pH <2) forming O/W emulsions. The lowest peptide concentration (5 mg/mL) demonstrated stability for >1 week which was comparable to the commercial anionic surfactant sodium dodecyl sulphate (SDS), whereas higher concentrations (10 and 15 mg/mL) showed at least 2-month stability and some formulations did not show any signs of phase separation for up to 8 months. SHR-FLLF-based emulsions displayed highly charged droplets with similar emulsion properties to SDS due to the helical arrangement at the interface, in addition to interfacial self-assembly ensuring its strong surface activity. Additionally, emulsions formed at 10 and 15 mg/mL peptide concentrations demonstrated viscoelastic characteristics preventing phase separation, due to high viscosity of the formulations. The Tween 20-emulsified system showed larger droplet size than the SHR-FLLF peptide-based emulsions, leading to creaming and phase separation in 48 h. The replacement of alanine with a charged amino acid either glutamic acid or lysine (SHR-FLELF and SHR-FLKLF) was examined, which aimed to break the bolaamphiphilic behaviour while retaining helical propensity. Both charged analogues acquired the α- and 3_{10} helical structures in water, where SHR-FLELF self-organized forming a micellar arrangement, while SHR-FLKLF stayed in unaggregated form. Consequently, SHR-FLKLF (5 and 7.5 mg/mL) stabilized the emulsion for less than a week, while the SHR-FLELF-based emulsion showed longer stability (>2 months at concentrations of 7.5 and 10 mg/mL) with viscoelastic shear-thinning behaviour.

A bioinspired switchable amphiphilic helical peptide emulsifier, Lac21, was also designed by the Middelberg's group, which mimic the bacterial Lac repressor DNA-binding protein (Dexter et al. 2006). The Lac21 amphiphilic peptide (Ac-MKQLADSLMQLARQVSRLESA-CONH$_2$) is a hydrophilic heptad repeating motif *abcdefg* containing hydrophobic amino acids at the *a* and *d* positions spaced by alternating 3 and 4 amino acid residues of the bacterial Lac repressor protein sequence, with acetylated and amidated C- and N-terminals, respectively, to prevent interpeptide charge–charge interactions (Fig. 13.5) (Dexter et al. 2006). Lac21 did not form organized structure in water; however, it could adsorb and adopt a supercoiled α-helix structure at organic/aqueous and air/aqueous interfaces in a monomeric free "detergent" state reducing interfacial tension, in a similar behaviour to low molecular weight surfactants (Fig. 13.5) (Dexter et al. 2006). Despite the interfacial adsorption and helical structure formation, Lac21 failed to stabilize foams and emulsions as it lacks the ability to form interfacial cohesive film, although it is derived from protein that could form interfacial films. Interestingly though, Lac21 peptide was used as a parent sequence for the design of a library of peptides exhibiting robust intermolecular crosslinking at the interface generating stable cohesive interfacial films.
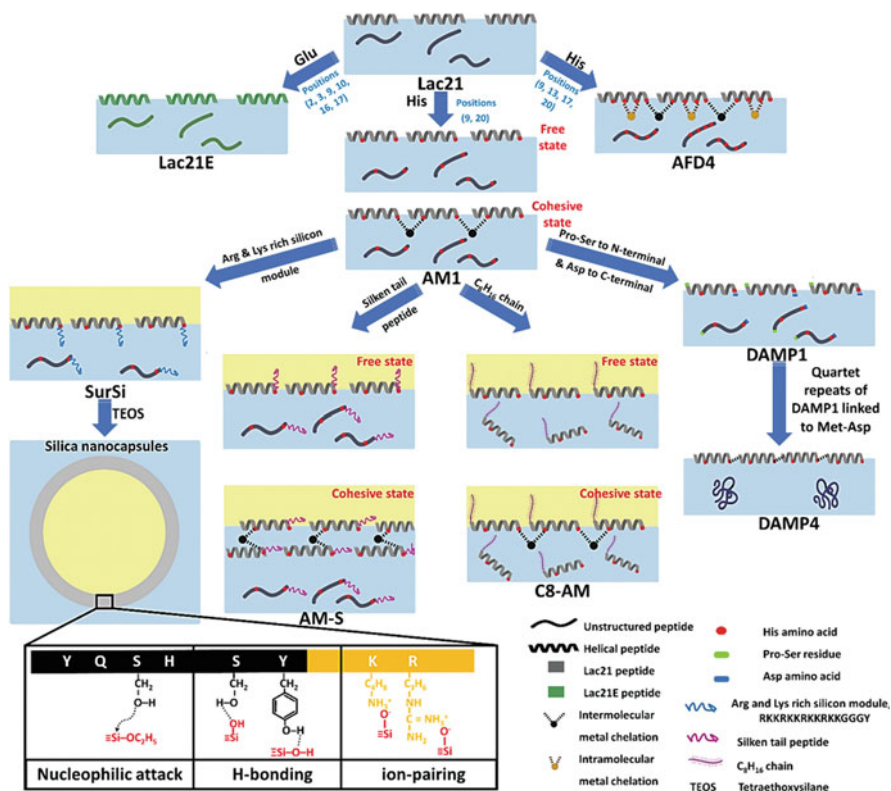
Fig. 13.5 Self-assembly of α-helix-forming peptides (Lac21 and its derivatives) in bulk phase and at interface

One example of these peptides is the 21-residue peptide AM1, which is a Lac21 sequence mutated with histidine (H) residues at positions 9 and 20 (Ac-MKQLADSL*H*QLARQVSRLE*H*A-CONH$_2$). AM1 showed to form and stabilize foams as well as 20%v/v toluene/water emulsions upon changing the composition of the continuous aqueous media using metal cations and by tuning pH to 7.4 (Table 13.2) (Dexter et al. 2006). This peptide adsorbed at fluid–fluid interface acquiring α-helical structure in a detergent mobile state where the hydrophobic moieties were directed towards the interface exhibiting interfacial tension lowering property like Lac21 (Fig. 13.5) (Dexter et al. 2006). However, the interfacial tension reduction due to AM1 occurred more rapidly than Lac21, which is attributed to the less organized structure of AM1 (random coil monomers) in bulk phase due to replacing the high helix-forming methionine (M) at position 9 in Lac21 with low helix-forming H residue. Such modification decreased the energy barrier against the adsorption of AM1 and led to its arrangement in α-helical structure at the interface. Interestingly, the H residues at positions 9 and 20 were oriented towards the bulk hydrophilic phase (Fig. 13.5) (Dexter et al. 2006). These residues bind to

metal ions (100 μM Zn^{2+}) at neutral pH allowing intermolecular crosslinking of the peptides located at the interface without metal binding in the bulk (Fig. 13.5) (Dexter et al. 2006). The interfacial assembly of AM1 developed a monolayer of a cohesive mechanically rigid film with elasticity modulus 121 mN/m comparable to the protein's interfacial film, and no major effect on the lowered interfacial tension was recorded after metals. Additionally, the great spacing between the H residues in same sequence prohibited the intramolecular crosslinking using metal ions.

Treating of the AM1-based system with chelating agent (EDTA) or protonation of H residues by acidification to pH 3.6 did not change the interfacial tension but reversed the film state into the starting loose form (elasticity modulus <30 mN/m) in seconds due to abortion of crosslinking leading to emulsion break down and foam collapse. Adding excess metal ions or neutralizing the medium pH could return the interfacial peptides into their coherent film again and stabilize the system. AM1 stabilized the foam for about 10 min which collapsed within 1 min after acidification or metal sequestration by EDTA (Dexter et al. 2006). Such switchable behaviour of AM1 allowed a novel and easy demulsification technique for clean oil and water recovery without residues in any phases, which is better than other energy consuming and ineffective approaches. In another study, Dexter and Middelberg compared the effect of various metals on the strength of the formed interfacial film, where Zn^{2+} was the best crosslinker followed by Ni^{2+} and then CO^{2+}, while Ca^{2+} and La^{3+} failed to create interfacial bridges, implying the different binding behaviour of metals that can influence film formation and the characteristics of formed films (Table 13.2) (Dexter and Middelberg 2007).

Middelberg et al. also compared between Lac21E (Ac-M*EE*LADSL*EE*LARQV*EE*LESA-NH$_2$) and AM1 for foam stabilization (Table 13.2) (Middelberg et al. 2008). Lac21E formed a strong elastic interfacial layer of organized connected α-helices at pH 3 (close to isoelectric point 3.95) with lowered interfacial tension (ON state), followed by interfacial disassembly and dissociation from the interface into the bulk medium upon neutralizing the pH to 7.4 due to acquiring a high negative charge and loss of interfacial activity and elasticity (OFF state) that was reversed again by reacidification. So, Lac21E stabilized foams for 5 min at pH 3 but collapsed within 1 min at pH 7. The film formed by Lac21E was stronger than AM1 due to greater accumulation of Lac21E at the interface.

Another Lac21 peptide analogue reported by Dexter and Middelberg is AFD4 (Ac-MKQLADS L*H*QLA*H*KVS*H*LEH*A-CONH$_2$), in which 4 H residues are present at positions (i, i + 3) and (i, i + 4) to endorse intramolecular crosslinking with 'metal clip'via sequential α-helical peptide turns to further stabilize the helix, in addition to the interfacial intermolecular bridging (Fig. 13.5 and Table 13.2) (Dexter and Middelberg 2007). Unlike Lac21 and AM1, AFD4 caused a more rapid decline in interfacial tension in the absence of metal ions, since substitution of R with H residue at position 13 widely destabilized the helical form in the bulk phase besides the electrostatic repulsion between cationic amino acids. Addition of metal ions to AFD4-based systems was found to reduce surface tension at a slower rate due to the slower adsorption kinetics after crosslinking in the bulk phase into higher helical

structure (Fig. 13.5) (Dexter and Middelberg 2007). AFD4 yielded tougher cohesive films at the interface after metal incorporation than AM1 at same environmental conditions, which demonstrated to be as strong as the lysozyme and β-lactoglobulin films. The effect of metal ion type on AFD4 film strength was similar to AM1, where Zn^{2+} constructed the strongest intermolecular bridge, whereas Ni^{2+} allowed the most stable helix. Like AM1, AFD4 film could be simply switched to detergent state using EDTA or acidification. Foam stabilization property was studied for the three peptides (Dexter and Middelberg 2007), where Lac21 showed to reduce interfacial tension without bubble stabilization both in the presence and absence of metal ions. While AM1 failed in the absence of metal ions to stabilize foam with low foam height after 25 min (3 mm), which slightly increased after metal addition. Same behaviour was observed for AFD4, but the metal addition significantly increased the foam height to 50–53 mm after 25 min and the AFD4-Zn^{2+} systems stabilized the foam for more than 1 h without collapse.

Wibowo et al. introduced the helix-forming peptide AM-S, which is a modified analogue of the peptide bioemulsifier AM1, by conjugating a silken tail peptide inspired from *Bombyx mori* silkworm fibroin, which is composed of eight hydrophobic amino acid sequence of alternating G and A using *PS* residues as linkers (Ac-MKQLADS LHQLARQ VSRLEHA-*PS-GAGAGAGY-CONH₂*) (Fig. 13.5 and Table 13.2) (Wibowo et al. 2017). AM-S combined the AM1 features of facial amphiphilicity, interfacial activity as well as crosslinking ability in the presence of metal ions, in addition to improved air/water interfacial adsorption capability of silken tail, thus maintaining optimum rate of interfacial adsorption and enhancing interfacial stability. The P and S residues of the linker sequence provided free rotation of strands. As discussed earlier for AM1, AM-S peptide also exhibited a random coil structure in aqueous phase with quick diffusion to the interface lowering the interfacial tension to 52 mN/m using 10 μM peptide, which was not changed by introducing $ZnCl_2$. AM-S created interfacial multilayers of self-associated α-helical conformation rather than the monolayers produced by AM1 due to the hydrophobic bonding between molecules after the silk tail addition (Fig. 13.5). Interestingly, the thickness of AM-S/Zn^{2+} films was higher than AM1 one because of the peptide multiple layering, so greatly resisted desorption from the interface upon compression and stabilized the dense foams containing miniaturized bubbles (Wibowo et al. 2017). However, AM-S interfacial adsorption kinetics was slower than AM1 owing to its increased molecular weight by silk tail. Both AM1 and AM-S could not stabilize the foam, which collapsed within 2 min while they expressed film stability in the presence of $ZnCl_2$ due to film elasticity without increase in bubble size.

Wang and co-workers constructed another derivative of AM1, C8-AM, which is AM1 peptide sequence capped from N-terminus by a C8 hydrocarbon chain, which is a hydrophobic functionality for enhancing its interfacial anchoring propensity (Table 13.2) (Wang et al. 2017). In comparison to AM-S, C8-AM acquired an α-helical conformation in bulk phase rather than the random coiling of AM-S, where the latter only assembled at the interface and did not form micelles in bulk, but only soluble dimers to tetramers. C8-AM (20 μM) adsorbed at oil/water interface

at a slower rate than AM-S, due to its ordered helical structure in bulk in addition to the hydrophobic interaction between C8 chains. In the absence of Zn^{2+}, C8-AM reduced interfacial tension to 8.4 mN/m within 400 s compared to 17 mN/m in case of AM-S. In the presence of Zn^{2+}, C8-AM crosslinking happened via H residues forming a cohesive interfacial film (Fig. 13.5). After treatment with EDTA, C8-AM-based emulsion was disrupted after 6 hours while AM-S emulsion broke down within 20 min due to the robust binding of C8 groups to the interface even after interrupting the metal ions-mediated crosslinking. Interestingly, C8-AM created 2% Miglyol 812-based O/W nanoemulsion of smaller globular size (147 nm) than AM-S (180 nm) after sonication, where a concentration of 100 μM of C8-AM was enough to stabilize the system for 3 weeks, whereas higher concentration of AM-S (400 μM) was required to achieve equivalent stabilization. Unlike AM-S, C8-AM did not show flexible reversibility at the interface due to rigid binding of C8 hydrophobic group to the interface.

Middelberg and co-workers deigned a novel bifunctional peptide SurSi (Ac-MKQLAHSVSRLEHA-*RKKRKKRKKRKKGGGY-CONH₂*), by conjugating the R- and K-rich peptide segment, Si module (RKKRKKRKKRKKGGGY), to AM1 (Wibowo et al. 2014). Hui et al. made further study on SurSi, which revealed the ability of this peptide to stabilize nanoemulsion at 400 μM concentration for at least 2 weeks (Table 13.2) (Hui et al. 2016). Furthermore, the ability of coating oil droplets by silica shell was investigated, in order to formulate stable oil-filled nanocapsules near neutral pH at ambient conditions with no harmful ingredients showing sustained release property for the entrapped drugs (Wibowo et al. 2014). AM1 peptide could not perform this function where precipitation of silica occurred in continuous phase not at the interface, forming irregular aggregates. On the other hand, SurSi successfully created the nanocapsule, as the dual functionalized peptide combined the surface active AM1-derived moiety responsible for nanoemulsion formation with the R- and K-rich Si module, which developed biosilicification at oil/water interface (Fig. 13.5). The modulated AM1 moiety contained solely the first and last heptads of the parent AM1, while D at position 7 in the first heptad was replaced with H to retain the metal binding capacity for crosslinking at the interface to enable the formation of cohesive films. The use of 2 heptads only instead of 3 was to enhance interfacial adsorption, as there is an inverse relation between the peptide molecular weight and the square of interfacial adsorption rate (Middelberg et al. 2000).

SurSi interfacial activity and surface coverage were very low at neutral pH as compared to AM1, due to the delayed diffusion to the interface resulting from the strong repulsive forces between peptide chains (theoretical charge = 13.44), leading to large spacing between the strands and hence lack of interfacial film formation even upon adding Zn^{2+}. However, neutralizing the charge through increasing the pH could enhance the adsorption kinetics and interfacial activity of SurSi. Indeed, SurSi peptide successfully emulsified Miglyol 812 oil containing oil-soluble moiety (fipronil) in water at neutral pH 7.5, forming nanoemulsion of droplet size 66.5 nm, which was larger in size, lower in zeta potential and less stable than AM1-based emulsion. Increasing the peptide concentration had a positive effect

on reducing the droplet size of emulsion (Hui et al. 2016). The addition of tetraethoxysilane (TEOS) to the system produced silica nanocapsules after 20 h via different mechanisms (Fig. 13.5). It was suggested that E, Y, S and H residues hydrolysed TEOS via nucleophilic attack on silicon atom resulting in silanolate anion and silanol (Wibowo et al. 2014). Furthermore, silanolate anions developed electrostatic attraction with the cationic residues K and R, in addition to the H-bonding between silanol, as well as with hydroxyl groups of Y and S. Silanolate anion and silanol acted as nuclei inducing further silica precipitation. The thickness of nanocapsules shell could be amplified by elevating pH to increase the levels of silanolate, reaction time and levels of TEOS (silica species precursor) to slow the release rate of entrapped compounds.

Middelberg and Dwyer crosslinked four AM1 peptides via DPS short peptide linker to enhance folding propensity, developing a soluble and stable protein emulsifier DAMP4 [MD(PSMKQLADSLHQLARQ-VSRLEHAD)$_4$] (Table 13.2) (Middelberg and Dimitrijev-Dwyer 2011). The D anionic residue induced repulsive forces between strands and P would terminate helix formation, whereas S residue supported the free rotation. The cationic K residue was deprotonated at pH 8.5, so DAMP4 acquired a single negative charge and stabilized the foams created, while decreasing pH by 1 unit (pH 7.4) expedited the foam collapse due to neutralization of the charge, though there was no change of its effect on interfacial tension at both pH values. Destabilization effect of divalent cation Ca^{2+} on the foam formed at pH 8.5 was higher than that of the monovalent Na^+, due to greater charge screening effect of Ca^{2+}. Interestingly, the use of kosmotropic electrolyte such as Na_2SO_4 salt was able to share the intrinsic surface hydration layer of DAMP4 and support the foam stability at pH 7.4 where DAMP4 net charge was zero. Na_2SO_4 salt allowed the electrostatic interaction of SO_4^{2-} ion to the basic residues of DAMP4 (R and K), resulting in amplified repulsive force 'hard-sphere repulsion', as well as highly oriented robust hydration film and better foam stability (Middelberg and Dimitrijev-Dwyer 2011; Parsons and Ninham 2010; Tavares et al. 2004; Besseling 1997). On the other hand, the chaotropic salt (NaSCN) does not have a tightly held hydration layer and debilitate the hydration layer of DAMP4 (Middelberg and Dimitrijev-Dwyer 2011; Gao et al. 2009).

In a further study, Dwyer and co-workers investigated the influence of molecular size of peptides and proteins and their bulk structure on their respective interfacial activities, by comparing the long well-organized protein DAMP4 to its simple unorganized peptidic precursor DAMP1 as well as studying their mixture (Table 13.2) (Dwyer et al. 2013). DAMP1 was a slightly modified form of AM1 via adding P and S residues to the N-terminus and a D residue to the C-terminal (PSMKQLADS-LHQLARQVSRLEHAD), while DAMP4 was the quadriad form of DAMP1 with the inclusion of a M and D to N-terminus [MD(PSMKQLADS-LHQLARQ-VSRLEHAD)$_4$]. The unstructured DAMP1 adsorbed quickly to the air/water interface as monomers of α-helices whereas DAMP4, as mentioned before, formed a robust package of 4 helices, so it was slowly attracted to the interface after unfolding into a chain of engaged DAMP1 forming interfacial monolayers and recording greater interfacial elasticity (Fig. 13.5). Both the peptide and protein

quantities were identical at bulk and interface indicating that adsorption energy was affected by the chemical structure only rather than the size which only influenced the adsorption rate. Strikingly, a faster interfacial tension drops upon mixing DAMP1 and DAMP4 compared to individual components, implying augmentation effect of the mixture surface activity.

Inspired by DAMP4 molecular design, Zhao et al. developed the anionic protein emulsifier SP16 [MD(*P-S*-ANSVAESLANLAESVSELVSNA-*D*)₄] to create and tailor foams, which can be controlled by pH and ionic strength (Table 13.2) (Zhao et al. 2017). SP16 is composed of four repeats of one peptide sequence linked by an acid cleavable sequence DP followed by S residue as a spacer. The hydrophobic part of the structure maintained the 4-helix bundle conformation, implying heat resistance property besides the hydrophilic and hydrophobic faces created by the orientation of amino acids which guaranteed the surface activity of SP16. Being anionic in nature, SP16 had a very low isoelectric point (pI) of 2.98, leading to the high pH responsiveness of the folded structure and hence the foaming properties. Minor foam formation was achieved at the pI, but altering the pH above or below pI by 1 pH point led to folding of SP16 into helix bundle followed by quick interfacial adsorption, as well as reduction of interfacial tension with enough charge to stabilize foam formation. Increasing the pH to 6 and above, negatively charged the protein hindering its folding, consequently decreased interfacial adsorption propensity and disrupted the orientation of hydrophilic and hydrophobic residues at the interface as well as surface activity, though charge screening by NaCl recovered the foaming activity. Interestingly, at pH 5, SP16 was able to fold into helix bundle in the bulk; however, due to its high negative charge there was a delay in interfacial adsorption behaviour leading to weak foam formation, unless NaCl was added.

Besides the hydrophobin and Lac analogous peptides, other designs of α-helical peptide emulsifiers were reported. For instance, anionic poly(γ-benzyl L-glutamate)ₙ polypeptides (PBLG) were developed by Morikawa and co-workers, with different polymerization numbers (1a, $n = 12$ and 1b, $n = 32$) (Table 13.2) (Morikawa et al. 2005). PBLGs could self-associate into α-helical robust rods and form O/W microemulsion (CH_2Cl_2/water = 1:2 or CH_2Cl_2/methanol/water = 1:1:1, v/v), which were used as templates for formulation of stable hollow microcapsules upon evaporation of the volatile organic phase, a system that could be used to deliver both hydrophilic and lipophilic drugs. Only 68% of the shorter oligopeptide 1a formed α-helices in the emulsion (with the appearance of some β-sheet structure after air drying), while the longer one 1b had 97% of α-helix conformation confirming that longer sequences provided more helical propensity. The amphiphilic polypeptide was adsorbed to the organic/aqueous interface and upon evaporation more monomers were attracted to the interface forming small multilayered microcapsules of assembled peptides (1–5 μm) containing aqueous phase in the core. These microcapsules were able to entrap a hydrophobic molecule (pyrene) via binding to the shell. The dichloromethane emulsion showed aqueous layers separation after 5 min and the emulsion layer contained droplets of 5–60 μm in size. Adding methanol to the system decreased the droplet size within 3 min to <10 μm and enabled longer stabilization for 24 h before separation of aqueous layers.
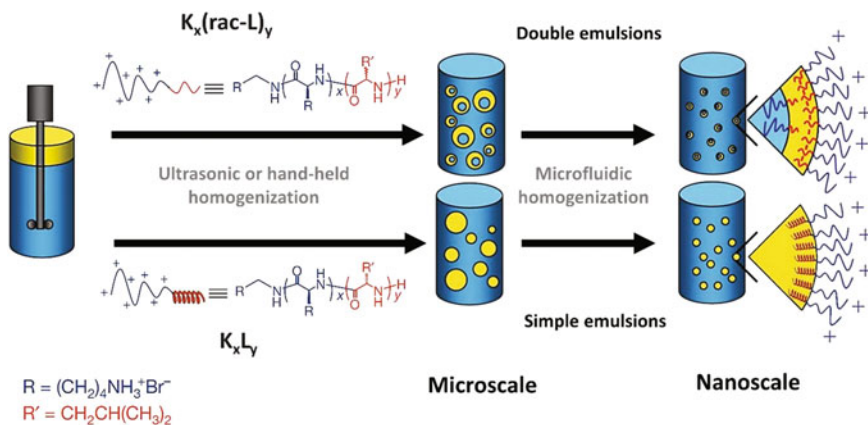
Fig. 13.6 Emulsification technique to generate both simple and double emulsions by block copolypeptide surfactants. Adapted from (Hanson et al. 2008), with copyrights permission from Springer Nature

Amphiphilic diblock copolypeptide emulsifiers were also developed by Hanson et al., with N-terminus hydrophilic block formed of cationic poly-L-lysine sequence (20–100 residues) conjugated to a hydrophobic racemic leucine (rac-L) sequence (5–30 residues) from the C-terminus (Fig. 13.6) (Hanson et al. 2008). The surfactant-like design imbued the polypeptide with surface activity and interfacial stabilization ability owing to the amphiphilicity and intermolecular H-bonding. These emulsifiers $K_{20}(rac-L)_{10}$, $K_{40}(rac-L)_{10}$, $K_{40}(rac-L)_{20}$, $K_{40}(rac-L)_{30}$, $K_{60}(rac-L)_{20}$ and $K_{100}(rac-L)_{10}$ could develop W/O/W double emulsions (Table 13.2 and Fig. 13.6) via easy homogenization and microfluidic techniques without the aid of other emulsifiers, as well as providing long-term stabilization for the formed emulsions (>9 months), while the less hydrophobic emulsifiers (5 residues of rac-L) stabilized the system for 12 months with bigger droplet size. The use of hand operated homogenization or ultrasonic mixing yielded microemulsion which was converted to nanoemulsion after microfluidic homogenization (Fig. 13.6). The flexibility of orientation of rac-L chain in diblock copolypeptide enhanced its solubility in oil with minimal interchain H-bonding and packing and hence weakly stabilized the inner water globules in the external oil phase. However, on the outer oil/water interface, intense packing of the rac-L in oily phase resulted in strong crosslinking by H-bonding that inhibited the conversion into a simple emulsion and stabilization of the double emulsion without inclusion of other additives. Interestingly, the $R_{40}(rac-L)_{10}$, $E_{40}(rac-L)_{10}$, $K_{60}(rac-V)_{20}$ and $K_{60}(rac-A)_{20}$ also stabilized double emulsions due to structure similarity to $K_x(rac-L)_y$, with the flexibility of design versatility (Table 13.2 and Fig. 13.6). On the other hand, the $K_{60}L_{20}$ emulsifier only produced simple O/W emulsions owing to the low solvation of the homochiral L-leucine part in oil phase upon acquisition of α-helical structure, while the hydrophilicity of the homopolypeptide block K_{60} favoured rapid phase separation

(Table 13.2 and Fig. 13.6). Thus, for this type of emulsifiers, the interfacial helical propensity impaired surface activity rather than enhancing it.

13.2.3 β-Sheets Peptide Emulsifiers

β-sheet forming peptides have been widely studied for the development of amyloid-like nanofibrous structures for the formation of hydrogels in aqueous media (Wychowaniec et al. 2020; Gazit 2007; Aggeli et al. 2001; Zhang et al. 1994). In addition to hydrogelation properties, amphiphilic β-sheet forming peptides have been shown to possess interfacial activity (Fig. 13.7a). Dexter was the first to introduce amphiphilic β-strand peptides as emulsifying agent that adsorbed from bulk to the interface (Dexter 2010). Inspired by the β-sheet forming amphiphilic sequence design of the Tirrell group that form monolayer at the air/water interface (Rapaport et al. 2000), Dexter developed the following four short nonapeptides B-14 (Ac-PDFDFDFDP-CONH$_2$), B-15 (Ac-PHFHFHFHP-CONH$_2$), B-16 (Ac-PEFEFEFEP-CONH$_2$), and B-17 (Ac-PKFKFKFKP-CONH$_2$) of alternating hydrophobic residues (P or F) with same charged residues, which are either anionic (E, D) or cationic (K or H), to hinder any possible electrostatic crosslinking of the β-sheets in bulk phase and aid in the interfacial adsorption (Table 13.2 and Fig. 13.7b) (Dexter 2010). These peptides showed surface activity at different pH values in a similar manner to traditional ionic emulsifiers, but with good biocompatibility and biodegradability. When the peptide was uncharged by adjusting the pH of B-14 and B-16 to acidic or B-15 and B-17 to basic, it acquired β-hairpin conformation rather than β-sheet in bulk phase, owing to the aromatic interaction of F residues at positions 3 and 7. Formation of strong rigid film of peptide aggregates at the interface is mediated by H-bonding and hydrophobic interactions, forming emulsion with large droplet size ~1500 ± 100 nm except for B-17 (~400 nm) due to the reduced zeta potential which allowed coalescence to happen (Fig. 13.7b). Increasing zeta potential through pH change led to formation of polyproline II-form helices in bulk and decreased the interfacial spreading with better emulsification due to electrostatic repulsion, so intermediate charging of peptide was the optimum. Based on this, B-14 to B-17 could stabilize emulsions at different pH ranges; however, they were more successful as ionic emulsifiers than film forming emulsifiers. The kinetics of B-14 and B-16 peptides adsorption were similar at all pH ranges, while decreasing charges of B-15 and B-17 slowed their adsorption rate due to aggregation in aqueous solution.

Another β-sheet forming peptide is the fibrillized short peptide Q11 (Ac-QQKFQFQFEQQ-Am), which was reported by Tian et al. to self-assemble at oil/water interface (Table 13.2) (Tian et al. 2011). Interfacial self-assembly of Q11 is triggered by the addition of Dulbecco's phosphate buffer saline to stabilize W/O emulsion via formation of microgel spheres surrounding the internal aqueous phase
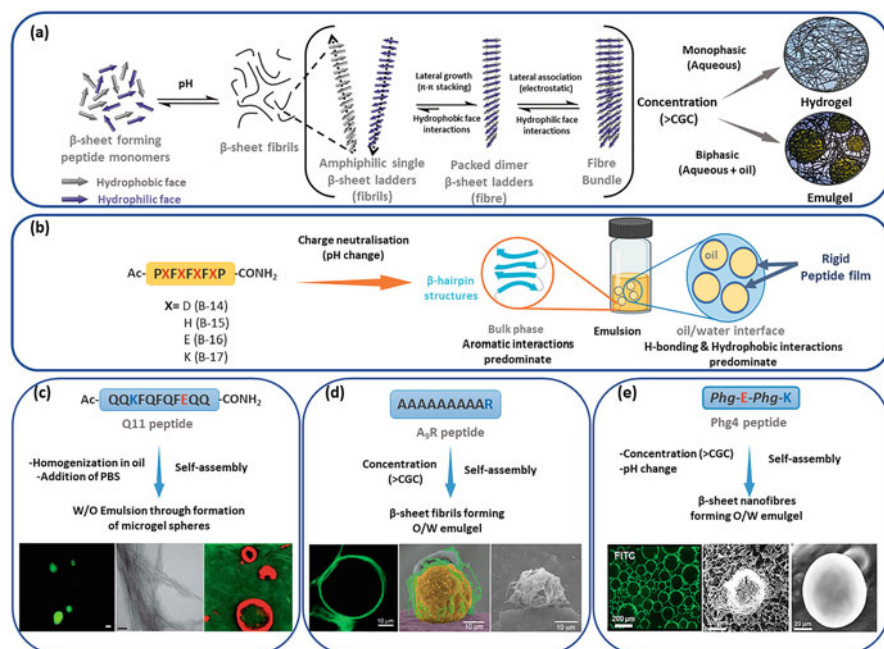
Fig. 13.7 (**a**) Schematic presentation of the general self-assembly mechanism of β-sheet forming peptides into amphiphilic β-sheet nanofibres, forming hydrogels in aqueous media and emulsions/emulgels in biphasic media. Adapted from (Wychowaniec et al. 2020), with copyrights permission from the American Chemical Society published under Creative Commons Attribution 4.0 International license. (**b**–**e**) Examples of β-sheet forming peptide emulsifiers, (**b**) Amphiphilic β-strand forming peptides; B-14, B-15, B-16 and B-17, which self-assemble at oil/water interface into rigid peptide films, stabilizing emulsion formation. Adapted from (Dexter 2010), with copyrights permission from the American Chemical Society. (**c**) Self-assembly of Q11 peptide at oil/water interface, forming W/O emulsion through formation of microgel spheres surrounding the aqueous media, Left: Fluorescent nitrobenzoxadiazole (NBD)-containing microgels produced with a paddle-type stirrer, Middle: TEM of the microgel fibrous structure (scale bar 100 nm), Right: Laser scanning confocal microscopy of Congo red-stained microgels. Adapted from (Tian et al. 2011), with copyrights permission from Royal Society of Chemistry. (**d**) Self-assembly of A₉R peptide into hydrogel in water and O/W emulsion. Left: Laser scanning confocal microscopy, Middle and Right: cryo-SEM of 0.05 wt% A₉R emulsion. Adapted from (Castelletto et al. 2019), with copyrights permission from the American Chemical Society. (**e**) Self-assembly of Phg4 peptide into β-sheet nanofibres, forming hydrogel and O/W emulgel, Left: Fluorescence microscopy of Phg4 O/W emulsion (stained with FITC), Middle: SEM of Phg4 vacuum-dried O/W emulgel, Right: SEM of Phg4 air-dried O/W emulgel. Adapted from (Wychowaniec et al. 2020), with copyrights permission from the American Chemical Society published under Creative Commons Attribution 4.0 International license

(Fig. 13.7c). It was possible to control the microgel size and size distribution using characteristics of speed and type of blade mixer, as well as further shear steps beyond the gelation. Interestingly, NIH 3T3 fibroblasts and C3H10T½ mouse pluripotent stem cells were encapsulated within the microgel spheres with acceptable

biocompatibility during the emulsion preparation process, by dispersing the cells within the peptide aqueous solution before addition of buffer for emulsification.

Surfactant-like β-sheet forming peptides were also designed to act as emulsifiers, where Castelletto and co-workers introduced the surfactant-like A_9R peptide which formed hydrogel in water and stabilized O/W Pickering emulsions, in a similar way to proteins (Table 13.2) (Castelletto et al. 2019). Unlike traditional surfactants, A_9R did not from interfacial monolayers, but rather the emulsion droplets were wrapped by a network of self-assembled β-sheet fibrils (25 nm diameter) of A_9R when exceeding the critical aggregation concentration (0.05–0.07%) without the need for pH tuning due to the strong packing of A residues in the core and surface exposure of the R residue to aqueous phase (Fig. 13.7d). The emulsion was stable by A_9R emulsifier for 3 days instead of 1 day only in absence of the peptide. On-demand demulsification was achieved by the addition of the proteolytic enzyme elastase, which could be exploited for site-specific release of entrapped drugs. In addition, A_9R showed a remarkable antimicrobial action towards G-ve bacteria including *P. aeruginosa* and *E. coli*.

Ionic self-complementary peptides are characterized by alternation of a hydrophobic residue with counter charge residues and are the most used sequences for the formation of β-sheet assembled structures. Elsawy and co-workers were the first to develop the shortest ionic self-complementary tetrapeptide Phg4 (PhgEPhgK, where Phg is phenylglycine), which can self-assemble into thermodynamically stable β-sheet nanofibres (diameter ~ 7–11 nm) that are not only capable of hydrogel formation in monophasic aqueous medium but can also stabilize O/W emulsions in biphasic media (Table 13.2) (Wychowaniec et al. 2020). Emulsification was pH and concentration dependent, where surface activity was only achieved at the assembly pH range (4.5–8) and concentration (>2%W/V). Electron microscopy (both SEM and TEM) showed the adsorption of peptide nanofibres at the oil/water interface forming nanofibrillar microspheres (~50–200 μm) encapsulating oil droplets within the nanofibrous network of the continuous phase (Fig. 13.7e). These structural features stabilized the formation of viscoelastic emulgels, which showed to be shear thinning and thixotropic. Emulsification was pH switchable, as emulgel formation only happened at self-assembly pH range (4.5–8), where the overall charge of the peptide chain is neutral favouring both assembly and interfacial adsorption. While outside this pH range, phase separation occurred owing to the repulsion of charged peptide chains and failure to self-assemble into the emulsifier β-sheet nanofibre form. Phg4 successfully formed O/W emulgels with chloroform and melissa oil as the organic phase at a range of oil:water ratios and peptide concentrations. The peptide emulsifier stabilized melissa emulgels for longer than 5 weeks and showed to withstand harsh environmental conditions (heating at 60 °C for 3 hours and salting out for 1 week) with no signs of phase separation, which was superior to commercial emulsifiers, such as cetrimide, SDS and tween 80.

13.2.4   Miscellaneous Surfactant-Like Peptides

In addition to peptide emulsifiers that assemble into well-defined secondary structures, there has been endeavours for molecular engineering of peptides that mimic surfactant structures. One example of these emulsifiers is the synthetic pseudopeptide gemini amphiphile (GAP), which was reported by Lotfallah et al. (Lotfallah et al. 2015). GAP was designed to have a hydrophilic head of valine-derived pseudopeptide exposed to aqueous phase with 2 hydrophobic tails that solubilize in oil phase by van der Waals force with variable critical aggregation concentration (4–25 mM) depending on the ionic strength and pH of the system (Fig. 13.8). Amphiphilic GAP thus self-associates at oil/water interface forming hollow microspheres (1–5 mm in diameter), therefore stabilizing O/W emulsion containing <1% of isopropyl myristate oil, after strong mixing by magnetic stirrer for 30–90 min (Table 13.2 and Fig. 13.8). The formed emulsion displayed a superior stability against exposure to strong acids, heating at 45 °C for 4 months, mechanical stress (centrifugation for 30 min at 3000 rpm with good system recovery if centrifuged for longer time) and long-term storage. However, proteolysis with thermolysin enzyme or alkalinisation to pH 12 led to disassembly and phase separation. It was suggested that surface activity of GAP required total or partial protonation of its amino groups to stabilize the emulsion droplets, so it could be exploited as a carrier for delivery of anionic nucleic acids. The system can also be used for the encapsulation of a variety of hydrophobic compounds, which was demonstrated by the successful encapsulation of the fluorescent hydrophobic model compounds N,N-diethyldansylamide and 9,10-dimethylanthracene.

Lipopeptides also showed to exhibit good surface activity thanks to the amphiphilicity of the molecular design. The lipodipeptide emulsifier, C_{13}-KR, was purposely designed by Lv et al. to stabilize emulsions in acidic environment, where its surface activity was compared to whey protein isolate and Tween 80 (Table 13.2) (Lv et al. 2019). The peptide-based emulsion showed the smallest droplet size (<1 μm) and the largest surface charge (100 mV), electrostatic repulsion and creaming stability, compared to the emulsions formed by the other two emulsifiers.
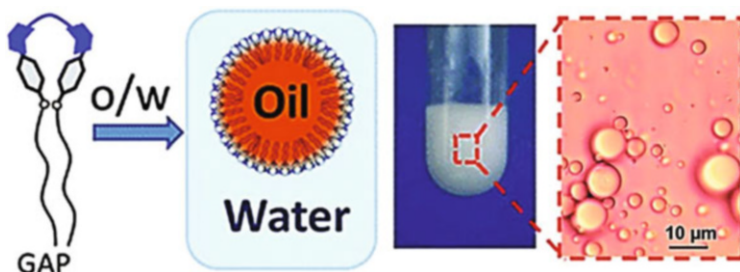

Fig. 13.8 Diagram of GAP self-assembling to form an O/W emulsion with macroscopic and microscopic images of the formed emulsion. Adapted from (Lotfallah et al. 2015), with copyrights permission from Royal Society of Chemistry

The low molecular weight and high surface charge of C_{13}-KR offered a fast interfacial adsorption rate (400 Hz). Besides, the enhanced surface activity due to the good interfacial anchoring of the hydrocarbon chain decreased droplet size of the emulsion, with further size reduction achieved by either increasing the peptide concentration or prolongation of sonication time. Formation of stable highly elastic films at the interface in addition to the good surface activity enhanced storage stability. In addition, the high zeta potential of the C_{13}-KR stabilized droplets, conferring resistance to salting out and thermal aggregation.

Another lipopeptide emulsifier and gelator was formed via Schiff's base formation upon mixing the precursors A, hydrophilic peptide NH_2-lauroylGGGH, and B, lipophilic 1,4-phthalaldehyde, at ambient temperature with molar ratio of A:B 2:1 (Table 13.2) (Nishida et al. 2017). The product was a mixture of ABA and AB that self-assembled into nanofibres (30–100 nm) entangled into thicker bundles at pH 7.4 without heating. Entangled nanofibres stabilized emulsions in biphasic media and formed hydrogel in aqueous medium within short period, 1 and 15 min, respectively. The hydrogel storage modulus was higher than its loss modulus after 3 min of precursors blending and progressively increased by time confirming the self-assembly and gelation process. Gel–sol transition occurred by heating to 75 °C or changing the pH to low or high values due to protonation or hydrolysis of the Schiff's base. Fabrication of emulsion was triggered by homogenizing 4 parts by volume of aqueous phase containing A with 1 part of organic phase containing B with the amount of precursor A was double B quantity. Homogenization for 1 min yielded thinner nanofibril bundles of ABA and AB (30–40 nm thickness) at the interface only, to produce globules of 22.4 μm diameter, without gelation in the bulk phase. This system was not formed upon the use of single precursor only and this was confirmed by confocal laser scanning microscopy. Acidification of the system with HCl or heating to 80 °C led to disassembly of the interfacial nanofibres and droplets fusion into larger size. The formed emulsion droplets were employed as stimuli-sensitive microreactors to regulate a click reaction of an alkyne with an azide by entrapping each reactant in separate oil droplets of the emulsion stabilized by the nanofibres and then initiating the reaction on demand when disassembly induced by external stimulus (heating or acidification).

13.3   Protein Emulsifiers

Proteins have been widely used as emulsifying and foaming agent in food industry (Wilde et al. 2004; McClements 2004). They are readily available, natural and non-toxic; moreover, they can produce and stabilize emulsions with desirable physicochemical properties. Proteins adsorb to the interface and allow droplet dispersion through reduction of interfacial tension while hindering droplet coalescence via either steric stabilization or electrostatic repulsion of the formed protective layer (Fig. 13.9) (McClements 2004; Walstra 2003). In this section, we will expand
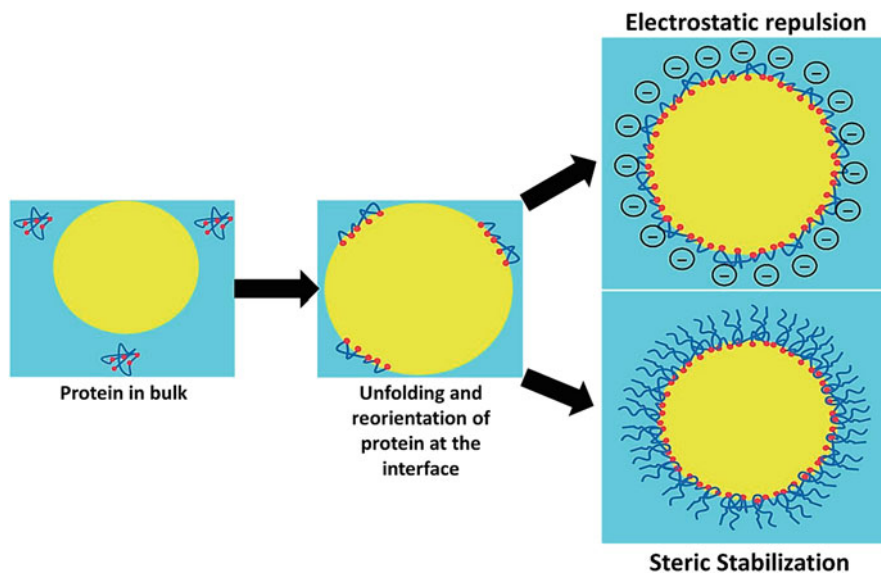
Fig. 13.9 The possible emulsion stabilization mechanisms using proteins by electrostatic repulsion or steric stabilization

more on the main protein emulsifiers, which have been commonly used in industry, such as milk proteins, hydrophobins, gelatin and pea proteins.

13.3.1 Milk Protein Emulsifiers

Milk proteins are mainly divided into two families, caseins and whey proteins.

13.3.1.1 Caseins

Caseins, belonging to phosphoproteins, are known to be the principal protein constituents in milk (80%) (Tomadoni et al. 2020). Caseins include four major flexible proteins, namely, α_{s1}-, α_{s2}-, β- and κ-casein. They are unstructured negatively charged proteins that do not form α-helices or β-sheets due to the numerous P residues in their sequence as well as absence of disulphide bonds (Bouyer et al. 2012; Tomadoni et al. 2020; Sarkar and Singh 2016). Caseins acquire self-assembled micellar forms upon binding to calcium phosphate in milk that interconnect via non-covalent bindings (Dickinson 2006). α_{s1} and β caseins are highly efficient emulsifiers that have good tendency to adsorb at oil/water interface and reduce interfacial tension as a result of their amphiphilicity (Table 13.3) (Bouyer

Table 13.3 Classification of the protein emulsifiers and their uses

Name of protein	Use	References
α$_{s1}$ and β caseins	O/W emulsion	Bouyer et al. (2012)
Whey proteins (-β-lactoglobulin, α-lactalbumin and lactoferrin)	Food emulsions	Sedaghat Doost et al. (2019), Teo et al. (2016), Ng et al. (2017), Zhu et al. (2018), Fioramonti et al. (2015)
Hydrophobins	Foams and O/W emulsions	Paukkonen et al. (2017), Tchuenbou-Magaia et al. (2009), Green et al. (2013), Cox et al. (2007), Cox et al. (2009)
Gelatin	O/W emulsion Foam	Surh et al. (2006), Zarai et al. (2016)
Pea proteins (vicilin and legumin)	Emulsion	Burger and Zhang (2019), Liang and Tang (2014), Ducel et al. (2004), Sridharan et al. (2020)

et al. 2012). β-casein exhibited tail-like anchoring behaviour to the interface via its terminal part, while α$_{s1}$ casein attached to the interface in a loop-like orientation through the mid-part of its sequence (Fig. 13.10).

β-casein showed better emulsification properties, more reduction of interfacial tension and higher preferential interfacial adsorption with thicker film formation than α$_{s1}$ (Sarkar and Singh 2016). β-casein can also prevent the coalescence of globules for long time via two mechanisms: firstly steric as well as electrostatic repulsive forces through extended saturated monolayer film of 10 nm width as reported by Dickinson and Davies (1999) as well as Fang and Dalgleish (1998) and secondly the viscoelastic behaviour of the adsorbed protein film at the interface as illustrated by Bantchev and Schwartz (2003) and Gau et al. (1994) (Fig. 13.9). Despite its prominent surface activity, casein-based emulsions can easily flocculate when treated with calcium ions, due to screening of the protein's negative charge and thinning of its interfacial film (Dalgleish 1997; Agboola and Dalgleish 1995).

Sodium caseinate is the commonly used form as emulsifier which is the sodium salt of mixture of all casein proteins, as it is not possible to use individual types of casein because of the high purification cost of individual components (Bouyer et al. 2012; Sarkar and Singh 2016). Sodium caseinate is produced by reducing the pH of skimmed milk to 4.6 to precipitate the casein followed by solubilization using sodium salts at neutral pH and finally drying. Stabilization of the sodium caseinate-based O/W emulsions is affected by protein concentration, molecular orientation in the bulk phase and the components of protein interfacial film (Sarkar and Singh 2016).

The enzymatic hydrolysis of β-casein yielded 2 peptide sequences: a hydrophilic peptide (β-CN, f1–25) of 25 amino acids and a hydrophobic one (β-CN, f193–209) of 17 amino acids (Lee et al. 1987). These peptides showed poor emulsification properties at neutral pH, which was ascribed to the short length of these hydrolysates. However, surface activity improved at extreme pH (below 4 and above 8) in
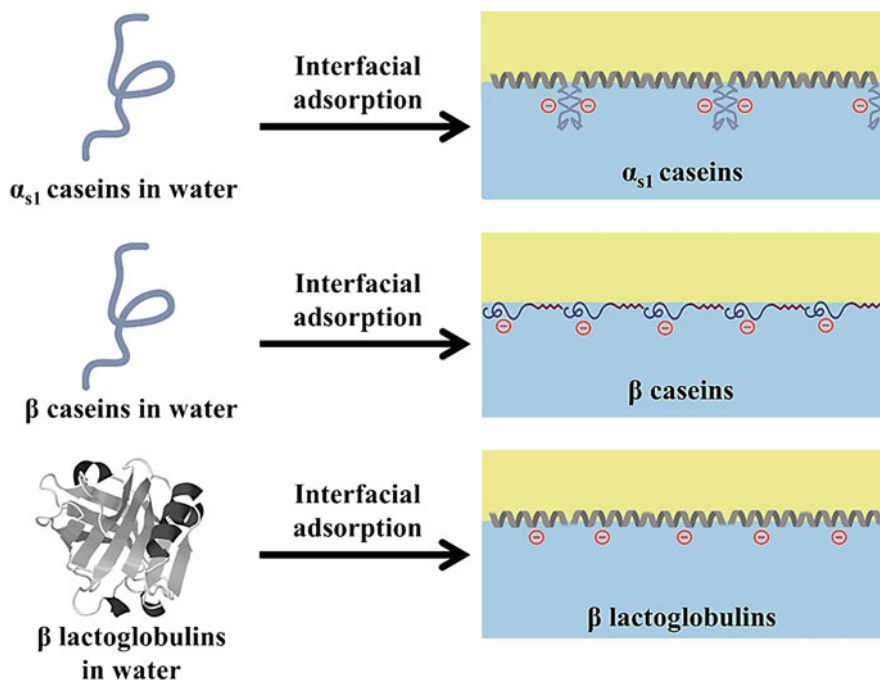
Fig. 13.10 Milk proteins interfacial adsorption where α_{s1} and β caseins acquire random coil structure in solution that adsorb to the emulsion interface and then β caseins exhibit tail-like anchoring behaviour to the interface via its terminal part, while α_{s1} casein attached to the interface in a loop-like orientation through the mid-part of its sequence. Moreover, the folded structure of β-lactoglobulin in water shows interconnected antiparallel β-sheets and flanked α-helices that rearranges upon adsorption to the interface. Adapted from (Dickinson 1998), with copyrights permission from Royal Society of Chemistry and (Zhai et al. 2011), reference with copyrights permission from the American Society of Chemistry

case of the β-CN, f193–209 sequence and at acidic pH for β-CN, f1–25 peptide. These casein-derived peptides showed formation of thick films around the oil droplets suggesting the possible association of peptides at the interface.

13.3.1.2 Whey Proteins

Milk whey proteins are primarily composed of 80% β-lactoglobulin and 15% α-lactalbumin with minor proteins of lactoferrin, serum albumin and immunoglobulins (Bouyer et al. 2012; Tomadoni et al. 2020). Unlike caseins, they have secondary, tertiary and quaternary structures connected by disulphide bridges, therefore not as flexible as casein (Bouyer et al. 2012). β-lactoglobulin and α-lactalbumin hold ideal emulsification characteristics and were utilized successfully to stabilize food emulsions; however, both possessed a slight lower stability than casein-based

emulsion in similar environment (Tcholakova et al. 2006; Dickinson 1997; Hunt and Dalgleish 1994; Dalgleish 1995). β-lactoglobulin, a dense folded protein, is constituted of 162 amino acid sequence containing 2 disulphide bridges as well as 1 free thiol moiety. Its folded structure shows interconnected antiparallel β-sheets and flanked α-helices (Fig. 13.10) (Sarkar and Singh 2016). After interfacial adsorption, partial unfolding is initiated with intermolecular binding of β-sheets through their free sulfhydryl groups to form disulphide bridges between molecules and develops a compact interfacial layer of 2 nm width irreversibly fortified upon storage with the increment of polymerization degree (Dickinson 1998; Dalgleish 2004). β-lactoglobulin is able to stabilize emulsions at neutral medium due to the protein negative charge that promoted electrostatic repulsion between emulsion globules besides reduction of interfacial tension (Kim et al. 2002; Wüstneck et al. 1999; Paulsson and Dejmek 1992). However, like most proteins, β-lactoglobulin is thermolabile, where it unfolds at 70 °C, resulting in protein aggregation and droplet coalescence (Kim et al. 2002; Ye 2010).

The second abundant whey protein, α-lactalbumin, is a calcium metalloprotein held together via 4 intrachain disulphide bridges without free thiol groups, unlike β-lactoglobulin (Sarkar and Singh 2016). α-lactalbumin possesses more C residues and less P moieties than β-lactoglobulin (Ng-Kwai-Hang 2003). In addition, α-lactalbumin thermally degrades at lower temperature (66 °C) than β-lactoglobulin without aggregation due to the absence of free thiols (Sarkar and Singh 2016; Considine et al. 2007). Dickinson et al. studied the competitive interfacial adsorption between both proteins and suggested the irreversible adsorption of the firstly added protein, which predominated the interface and could not be displaced by the secondly added one (Dickinson et al. 1989).

Lactoferrin is another whey protein component present in a minor level, composed of 700 amino acids capable of binding to iron and exhibits a high positive zeta potential (+50 mV) at neutral pH. It can therefore form stable emulsions of cationic droplets at a wider pH range (3–7), unlike caseinates and β-lactoglobulin that can stabilize emulsion at neutral pH only where their pI ranged between 4.5 and 5.5 (Baker and Baker 2005; Ye and Singh 2006). Wahlgren et al. reported the possibility of electrostatic attraction between the anionic β-lactoglobulin and the cationic lactoferrin (Wahlgren et al. 1993). Based on this, Ye and Singh developed stable O/W emulsions with thick films of multilayered binary protein mixture at neutral pH (Ye and Singh 2007). Although the net charge of the protein mixture is zero, the dense multilayers offered robust steric hindrance that prevented coalescence of the emulsion droplets.

The marketed forms of whey protein emulsifiers are whey protein concentrate (WPCs) (25–80% protein) and whey protein isolate (WPIs) (>90% protein) extensively utilized in food industries (Sarkar and Singh 2016). WPI has been also utilized to develop O/W emulsions using simple stirring methods (Table 13.3) (Sedaghat Doost et al. 2019; Teo et al. 2016; Ng et al. 2017; Zhu et al. 2018; Fioramonti et al. 2015).

To summarize, milk proteins are considered the most widely used bioemulsifier in food industry being a natural amphiphile, generally regarded as safe (GRAS),

i.e. biocompatible, non-toxic, biodegradable, offer great nutritional value and have antioxidant properties and easily sourced from milk, hence sustainable (Ha and Lee 2020; He et al. 2011). However, they suffer from batch-to-batch variabilities and immunogenicity where cow's milk is one of the eight main food categories causing 90% of food allergies (Nutten et al. 2020; Broersen 2020).

13.3.2 Hydrophobins

Hydrophobins are a group of globular fungal proteins that are believed to behave like small molecule emulsifiers. As a result of their high amphiphilicity, as well as rapid interfacial adsorption due to their relatively small sizes, hydrophobins showed the greatest surface activity between all types of protein emulsifiers (Paukkonen et al. 2017; Berger and Sallada 2019). They can be classified according to their self-assembled conformation, hydropathy patterns and solubility into two types: class I as SC3 that yields insoluble rodlets with amyloid orientation solely soluble in strong acids, and class II, like HFBI and HFBII, which acquire highly organized 2D interfacial monolayers. Class II also are widely soluble in organic solvents and detergents and easily solubilized in water even at high concentration (100 mg/mL) (Paukkonen et al. 2017; Berger and Sallada 2019). Hydrophobins possess 4 disulphide bridges in their tertiary structure and show intermolecular interactions which allow self-association as amphipathic elastic monolayer films at oil/water and air/water interfaces. Hence, they decrease interfacial tension and can change the behaviour of surfaces from lipophilic nature to hydrophilic and vice versa (Paukkonen et al. 2017; Paananen et al. 2013). Therefore, hydrophobins are suitable for formulation of foams and O/W emulsions with long-term stability up to 4 months at ambient storage conditions (Table 13.3) (Paukkonen et al. 2017; Tchuenbou-Magaia et al. 2009; Green et al. 2013; Cox et al. 2007, 2009) and are considered as non-toxic and non-immunogenic pharmaceutical excipients (Aimanianda et al. 2009; Ebbole 1997).

13.3.3 Gelatin

Gelatin is a high-molecular weight protein obtained by hydrolysis of animal collagen via boiling at acidic pH to yield Type A gelatin or basic pH to produce Type B gelatin (Bouyer et al. 2012; Taherian et al. 2011). The difference in their preparation method led to differences in their physicochemical properties where pI of Type A gelation is ranged from 7 to 9, whereas Type B gelatin is 4.8 to 5.1 (Djagny et al. 2001). Such variation in characteristic was attributed to that basic hydrolysis of collagen had converted N and Q into D and E that yielded Type B gelatin (Veis 1964).

Gelatin proteins showed to have some surface activity. Both low- and high-molecular weight fish gelatin demonstrated to stabilize 20% corn oil in water as O/W emulsion at ≥4% w/w total gelatin concentration as reported by Surh and co-workers (Table 13.3) (Surh et al. 2006). However, large oil droplets (>10 μm) were observed in the emulsion due to low surface activity of gelatin, which could lead to coalescence. Low-molecular weight fish gelatin produced greater fractions of large droplets than high-molecular weight one; however, emulsions formed by the earlier were more stable against creaming. Emulsions stabilized by fish gelatin showed resistance to phase separation at pH range between 3 and 8, heating for 30 min at 90 °C and NaCl salt up to 250 mM.

Land snails-derived gelatin also possessed interfacial activity. Zarai et al. studied the emulsifying properties of this gelatin and suggested the possibility to act a bioemulsifier, since it demonstrated to stabilize olive O/W emulsions at total gelatin concentrations of 0.5–4% w/v (Table 13.3) (Zarai et al. 2016). At high gelatin levels, a crosslinked 3D matrix was formed in the bulk phase, which, in addition to its interfacial adsorption, help trapping the oil globules inside the hydrogel network forming a strong emulgel. Land snails-derived gelatin produced emulsions with higher stability than other gelatins from different origins (smooth hound, zebra blenny, barbel and grey triggerfish), could be attributed to the differences in composition, protein conformation and properties. Snail gelatin also produced dense stable foams at high concentrations 1–4%w/v due to the formation of interfacial thick gelatin films, but markedly collapsed after 1 hour of mixing (Zarai et al. 2016).

13.3.4   Pea Proteins

Pea proteins include two main constituents: vicilin, a 7S storage globulin, and legumin, a 11S storage globulin (Gueguen et al. 1988). Legumin protein consists of linked subunits via non-covalent binding in a hexameric structure, while vicilin protein shows a trimeric conformation (Bouyer et al. 2012; Burger and Zhang 2019). The ratio between legumin and vicilin, as well as their structures, differs depending on the production technique and species, consequently variation of their functions. In general, vicilin possessed higher surface activity and emulsion stabilization efficiency than legumin (Burger and Zhang 2019). Pea proteins successfully produced emulsions through interfacial adsorption that occurred in two stages. Firstly, protein migration from aqueous phase and anchoring to the oil/water interface via the exposed hydrophobic part of the molecule. Secondly, protein reorientation occurred to position the hydrophilic parts towards the aqueous phase and solubilize the lipophilic areas in the organic phase forming a viscoelastic rigid interfacial layer that stabilized the system by steric effect and electrostatic repulsions (Burger and Zhang 2019; Sridharan et al. 2020). In essence, pea proteins are capable of reducing interfacial tension (Ducel et al. 2004) and stabilize emulsion formation at low pH both by Pickering mechanism and hydrogelation (Table 13.3) (Liang and Tang 2014). However, pea proteins emulsions could not withstand changing salts

concentration, where increasing NaCl concentration of 50 to 200 mM enlarged the emulsion droplet from 6 to 14.05 μm and the medium pH should be away from its pI (4.5) where the extreme pH values (pH 3 and 8) were preferred to allow the charging of protein molecules, so it was necessary to add another emulsifier, such as pectin, to stabilize emulsions and prevent phase separation in harsh conditions (Gharsallaoui et al. 2010a, b; Ettoumi et al. 2016; Ladjal-Ettoumi et al. 2016).

13.4 Protein–Polysaccharide Mixed Emulsifiers

On one hand, proteins are characterized by the quick interfacial adsorption and film formation that prohibits emulsion coalescence, though stability can always be impaired either by changing pH near to pI or by salting out (Ozturk and McClements 2016; Yang et al. 2019). On the other hand, polysaccharides can develop highly stable emulsions but using extremely high polymer levels (Chen et al. 2011b; Kharat et al. 2018). Therefore, combining both proteins and polysaccharides via covalent conjugation, electrostatic attractions or by physical mixing combines the attributes of both components, fast interfacial adsorption of protein in addition to the viscosity increment and steric hindrance of polysaccharides, thus creating highly stable emulsions (de Oliveira et al. 2016; Setiowati et al. 2020). In this section we will discuss protein–polysaccharide mixed emulsifiers formed by covalent conjugation and non-covalent interaction.

13.4.1 Protein–Polysaccharide Covalent Conjugates

Controlled Maillard reaction was used to conjugate amino groups of protein with the carbonyl functionalities of polysaccharides to yield composites having higher emulsifying power than either polysaccharides or proteins alone, such as sodium caseinate/maltodextrin (O'Regan and Mulvihill 2010), β-lactoglobulin/dextran (Wooster and Augustin 2006) and whey protein isolate/maltodextrin (Akhtar and Dickinson 2007). These complexes also offered resistance to undesirable environmental conditions, such as freezing, heating or great ionic strength (Bouyer et al. 2012; Setiowati et al. 2020). For instance, O'Regan and Mulvihill previously showed the augmented stability of emulsion formulated using sodium caseinate maltodextrin for 7 days at 45 °C in comparison to sodium caseinate (O'Regan and Mulvihill 2010). Setiowati and co-workers also demonstrated that chemical conjugation of whey protein isolate to low methoxy pectin resulted in a conjugate of superior interfacial activity and emulsion stabilization than the electrostatic complex (Diah Setiowati et al. 2019; Setiowati et al. 2017).

Zhang et al. showed the effect of glycosylation of soy protein isolates with maltodextrin using Maillard reaction on the emulsification of fish oil compared with soy protein isolate/maltodextrin mixture where smaller droplet size, lower
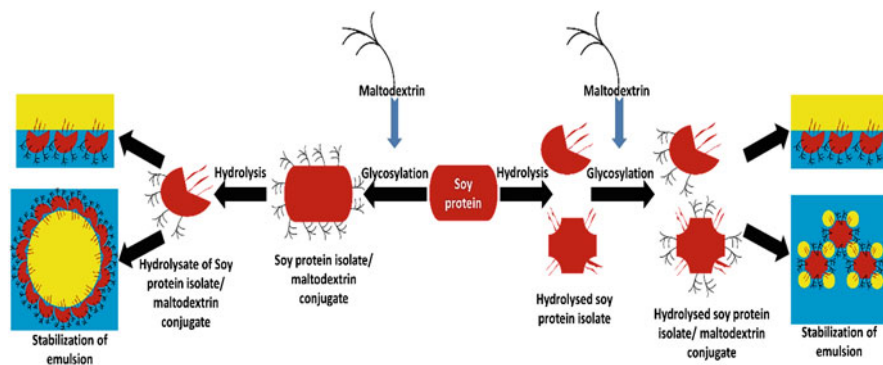
Fig. 13.11 O/W emulsion stabilization through conjugation between the hydrolysed soy protein and maltodextrin or hydrolysis of the conjugated soy protein and maltodextrin using Maillard reaction. Adapted from (Zhang et al. 2015), and (Zhang et al. 2014), with copyrights permission from Elsevier

polydispersity index and improved physical stability (3-week storage) were observed with both hydrolysate of soy protein isolate/maltodextrin conjugate and hydrolysed soy protein isolate/maltodextrin conjugate-based O/W emulsions (Fig. 13.11) (Zhang et al. 2014, 2015).

13.4.2 Protein–Polysaccharide Physical Mixtures

Electrostatic interactions between counter charge polysaccharides and proteins at the interface were claimed to boost the emulsion stability (Li et al. 2019). There are two main reported methods for mixing emulsifiers, where one method involved one pot mixing of the two components to prepare the complex necessary for emulsion production (Yang et al. 2019; Lutz et al. 2009; Laplante et al. 2006; Yildiz et al. 2018). However, the other method is layer by layer electrostatic deposition, where initially a primary protein-based emulsion was developed followed by incorporating the polysaccharide to the system that interacted at droplet interface with the protein to form a second coat around droplets (Khalloufi et al. 2009). These deposition steps could be repeated several times to produce multicoats stabilizing the emulsion.

Initial emulsification with protein is essential, as protein emulsifiers exhibit fast stabilization kinetics and reduction of interfacial tension. The protein–polysaccharide mixed emulsifiers showed greater resistance to environmental conditions including dehydration, high salt concentrations and temperature changes. For example, coalescence of casein-based emulsion near the pI of casein was substantially hindered by adding octenyl succinic anhydride modified starch (OSAS) and this blend demonstrated higher oxidative stability than OSAS-based emulsion (Yang et al. 2019).

Another physical mixing approach, not involving electrostatic interaction, depends on addition of a protein emulsifier to the biphasic system for interfacial adsorption and formation of small globules of the internal phase. This is followed by the introduction of the polysaccharide component as a viscosity modifying agent, which enhances the viscosity of the continuous aqueous phase via thickened networks and hampers droplet movement, thus preventing creaming/sedimentation of the internal phase droplets. Several mixtures were prepared by the viscosity enhancement method, such as whey protein isolate/xanthan gum (Sun and Gunasekaran 2009), sodium caseinate/locust bean gum (Perrechil and Cunha 2010), sodium caseinate/xanthan gum (Moschakis et al. 2005) and whey protein isolate/flaxseed gum (Khalloufi et al. 2008).

13.5 Summary

Short peptides are emerging new class of bioemulsifiers that have been shown to stabilize different foams and emulsions and have proven to be superior to traditional commercial emulsifiers in long-term stabilization of these colloidal systems. Besides, peptides are similar to proteins in being safe, biodegradable, biocompatible and of low toxicity to human health and environment, thus overcoming the common limitations of the currently used traditional emulsifiers. On the top of these, the physicochemical properties of peptide emulsifiers can be finely tuned by the rational chemical design of the amino acid sequence, providing a plethora of design options for controlling their behaviour at the organic/aqueous and gas/aqueous interfaces. In general, peptide-based emulsification was reported to occur either via micelle-like structure formation, akin to conventional emulsifier, or through self-assembly into amphiphilic nanofibrous structure at the interface and in bulk continuous phase. Proteins have also been widely used in food industry to stabilize emulsions, through steric stabilization and/or electrostatic repulsion. However, proteins have some limitations, mainly due to the possible batch-to-batch variation, chemical and physical instability as well as potential immunogenicity. Protein–polysaccharide mixed emulsifiers have also been introduced but have shown to be less efficient in stabilizing emulsions and foams when compared to peptides and proteins. In brief, peptides and proteins are important emerging subclasses of bioemulsifier armamentarium, though there is still a lot of work to be done for their wide utilization in industry, when it comes to large-scale production of these molecules, as well as tackling stability issues during storage and manufacturing.

References

Adjonu R, Doran G, Torley P, Agboola S (2014) Whey protein peptides as components of nanoemulsions: a review of emulsifying and biological functionalities. J Food Eng 122:15–27

Agboola SO, Dalgleish DG (1995) Calcium-induced destabilization of oil-in-water emulsions stabilized by caseinate or by β-lactoglobulin. J Food Sci 60:399–404

Aggeli A, Nyrkova IA, Bell M, Harding R, Carrick L, McLeish TC, Semenov AN, Boden N (2001) Hierarchical self-assembly of chiral rod-like molecules as a model for peptide β-sheet tapes, ribbons, fibrils, and fibers. Proc Natl Acad Sci 98:11857–11862

Aimanianda V, Bayry J, Bozza S, Kniemeyer O, Perruccio K, Elluru SR, Clavaud C, Paris S, Brakhage AA, Kaveri SV (2009) Surface hydrophobin prevents immune recognition of airborne fungal spores. Nature 460:1117–1121

Akhtar M, Dickinson E (2007) Whey protein-maltodextrin conjugates as emulsifying agents: an alternative to gum Arabic. Food Hydrocoll 21:607–616

Aviño F, Matheson AB, Adams DJ, Clegg PS (2017) Stabilizing bubble and droplet interfaces using dipeptide hydrogels. Org Biomol Chem 15:6342–6348

Bai S, Pappas C, Debnath S, Frederix PW, Leckie J, Fleming S, Ulijn RV (2014) Stable emulsions formed by self-assembly of interfacial networks of dipeptide derivatives. ACS Nano 8:7005–7013

Baker EN, Baker HM (2005) Lactoferrin. Cell Mol Life Sci 62:2531

Bantchev GB, Schwartz DK (2003) Surface shear rheology of β-casein layers at the air/solution interface: formation of a two-dimensional physical gel. Langmuir 19:2673–2682

Berger BW, Sallada ND (2019) Hydrophobins: multifunctional biosurfactants for interface engineering. J Biol Eng 13:10

Besseling N (1997) Theory of hydration forces between surfaces. Langmuir 13:2113–2122

Bouyer E, Mekhloufi G, Rosilio V, Grossiord J, Agnely F (2012) Proteins, polysaccharides, and their complexes used as stabilizers for emulsions: alternatives to synthetic surfactants in the pharmaceutical field? Int J Pharm 436:359–378

Broersen K (2020) Milk processing affects structure, bioavailability and immunogenicity of β-lactoglobulin. Foods 9:874

Burger TG, Zhang Y (2019) Recent progress in the utilization of pea protein as an emulsifier for food applications. Trends Food Sci Technol 86:25

Caballero B, Trugo LC, Finglas PM (2003) Encyclopedia of food sciences and nutrition, 2nd edn. Academic

Callender SP, Mathews JA, Kobernyk K, Wettig SD (2017) Microemulsion utility in pharmaceuticals: implications for multi-drug delivery. Int J Pharm 526:425–442

Castelletto V, Edwards-Gayle CJ, Hamley IW, Barrett G, Seitsonen J, Ruokolainen J (2019) Peptide-stabilized emulsions and gels from an arginine-rich surfactant-like peptide with antimicrobial activity. ACS Appl Mater Interfaces 11:9893–9903

Chen L, Pont G, Morris K, Lotze G, Squires A, Serpell LC, Adams DJ (2011a) Salt-induced hydrogelation of functionalised-dipeptides at high pH. Chem Commun 47:12071–12073

Chen B, Li H, Ding Y, Rao J (2011b) Improvement of physicochemical stabilities of emulsions containing oil droplets coated by non-globular protein-beet pectin complex membranes. Food Res Int 44:1468–1475

Considine T, Patel HA, Anema SG, Singh H, Creamer LK (2007) Interactions of milk proteins during heat and high hydrostatic pressure treatments-a review. Innovative Food Sci Emerg Technol 8:1–23

Cox AR, Cagnol F, Russell AB, Izzard MJ (2007) Surface properties of class II hydrophobins from Trichoderma reesei and influence on bubble stability. Langmuir 23:7995–8002

Cox AR, Aldred DL, Russell AB (2009) Exceptional stability of food foams using class II hydrophobin HFBII. Food Hydrocoll 23:366–376

Dalgleish D (1995) Structures and properties of adsorbed layers in emulsions containing milk proteins. In: Structures and properties of adsorbed layers in emulsions containing milk proteins. Food Macromolecules and Colloids, pp 23–33

Dalgleish DG (1997) Adsorption of protein and the stability of emulsions. Trends Food Sci Technol 8:1–6

Dalgleish DG (2004) Food emulsions: their structures and properties. Food Emulsions 4

de Oliveira FC, Coimbra JS, dos Reis EB, de Oliveira ADG, Zuñiga EEGR (2016) Food protein-polysaccharide conjugates obtained via the Maillard reaction: a review. Crit Rev Food Sci Nutr 56:1108–1125

Dexter AF (2010) Interfacial and emulsifying properties of designed β-strand peptides. Langmuir 26:17997–18007

Dexter AF, Middelberg AP (2007) Switchable peptide surfactants with designed metal binding capacity. J Phys Chem C 111:10484–10492

Dexter AF, Malcolm AS, Middelberg AP (2006) Reversible active switching of the mechanical properties of a peptide film at a fluid–fluid interface. Nat Mater 5:502–506

Diah Setiowati A, Rwigamba A, Van der Meeren P (2019) The influence of degree of methoxylation on the emulsifying and heat stabilizing activity of whey protein-pectin conjugates. Food Hydrocoll 96:54–64

Dickinson E (1997) Properties of emulsions stabilized with milk proteins: overview of some recent developments. J Dairy Sci 80:2607–2619

Dickinson E (1998) Proteins at interfaces and in emulsions stability, rheology and interactions. J Chem Soc Faraday Trans 94:1657–1669

Dickinson E (2006) Colloid science of mixed ingredients. Soft Matter 2:642–652

Dickinson E, Davies E (1999) Influence of ionic calcium on stability of sodium caseinate emulsions. Colloids Surf B: Biointerfaces 12:203–212

Dickinson E, Rolfe SE, Dalgleish DG (1989) Competitive adsorption in oil-in-water emulsions containing α-lactalbumin and β-lactoglobulin. Food Hydrocoll 3:193–203

Djagny KB, Wang Z, Xu S (2001) Gelatin: a valuable protein for food and pharmaceutical industries. Crit Rev Food Sci Nutr 41:481–492

Dragulska SA, Chen Y, Wlodarczyk MT, Poursharifi M, Dottino P, Ulijn RV, Martignetti JA, Mieszawska AJ (2018) Tripeptide-stabilized oil-in-water nanoemulsion of an oleic acids–Platinum (II) conjugate as an anticancer nanomedicine. Bioconjug Chem 29:2514–2519

Ducel V, Richard J, Popineau Y, Boury F (2004) Adsorption kinetics and rheological interfacial properties of plant proteins at the oil-water Interface. Biomacromolecules 5:2088–2093

Dwyer MD, He L, James M, Nelson A, Middelberg AP (2013) Insights into the role of protein molecule size and structure on interfacial properties using designed sequences. J R Soc Interface 10:20120987

Ebbole DJ (1997) Hydrophobins and fungal infection of plants and animals. Trends Microbiol 5:405–408

Ettoumi YL, Chibane M, Romero A (2016) Emulsifying properties of legume proteins at acidic conditions: effect of protein concentration and ionic strength, LWT-food. Sci Technol 66:260–266

Fang Y, Dalgleish DG (1998) The conformation of α-lactalbumin as a function of pH, heat treatment and adsorption at hydrophobic surfaces studied by FTIR. Food Hydrocoll 12:121–126

Fioramonti SA, Arzeni C, Pilosof AMR, Rubiolo AC, Santiago LG (2015) Influence of freezing temperature and maltodextrin concentration on stability of linseed oil-in-water multilayer emulsions. J Food Eng 156:31–38

Fowler CI, Muchemu CM, Miller RE, Phan L, O'Neill C, Jessop PG, Cunningham MF (2011) Emulsion polymerization of styrene and methyl methacrylate using cationic switchable surfactants. Macromolecules 44:2501–2509

Gao B, Wyttenbach T, Bowers MT (2009) Protonated arginine and protonated lysine: hydration and its effect on the stability of salt-bridge structures. J Phys Chem B 113:9995–10000

Garcia AM, Kurbasic M, Kralj S, Melchionna M, Marchesan S (2017) A biocatalytic and thermoreversible hydrogel from a histidine-containing tripeptide. Chem Commun 53:8110–8113

Gau CS, Yu H, Zografi G (1994) Surface viscoelasticity of β-casein monolayers at the air/water interface by electrocapillary wave diffraction. J Colloid Interface Sci 162:214–221

Gazit E (2007) Self assembly of short aromatic peptides into amyloid fibrils and related nanostructures. Prion 1:32–35

Gharsallaoui A, Saurel R, Chambin O, Cases E, Voilley A, Cayot P (2010a) Utilisation of pectin coating to enhance spray-dry stability of pea protein-stabilised oil-in-water emulsions. Food Chem 122:447–454

Gharsallaoui A, Yamauchi K, Chambin O, Cases E, Saurel R (2010b) Effect of high methoxyl pectin on pea protein in aqueous solution and at oil/water interface. Carbohydr Polym 80:817–827

Green AJ, Littlejohn KA, Hooley P, Cox PW (2013) Formation and stability of food foams and aerated emulsions: hydrophobins as novel functional ingredients. Curr Opin Colloid Interface Sci 18:292–301

Gueguen J, Chevalier M, And JB, Schaeffer F (1988) Dissociation and aggregation of pea legumin induced by pH and ionic strength. J Sci Food Agric 44:167–182

Guler MO, Stupp SI (2007) A self-assembled nanofiber catalyst for ester hydrolysis. J Am Chem Soc 129:12082–12083

Ha H, Lee W (2020) Milk protein-stabilized emulsion delivery system and its application to foods. J Dairy Sci Biotechnol 38:189–196

Hanson JA, Chang CB, Graves SM, Li Z, Mason TG, Deming TJ (2008) Nanoscale double emulsions stabilized by single-component block copolypeptides. Nature 455:85–88

He W, Tan Y, Tian Z, Chen L, Hu F, Wu W (2011) Food protein-stabilized nanoemulsions as potential delivery systems for poorly water-soluble drugs: preparation, in vitro characterization, and pharmacokinetics in rats. Int J Nanomedicine 6:521

Huang Z, Guan S, Wang Y, Shi G, Cao L, Gao Y, Dong Z, Xu J, Luo Q, Liu J (2013) Self-assembly of amphiphilic peptides into bio-functionalized nanotubes: a novel hydrolase model. J Mater Chem B 1:2297–2304

Hui Y, Wibowo D, Zhao C (2016) Insights into the role of biomineralizing peptide surfactants on making nanoemulsion-templated silica nanocapsules. Langmuir 32:822–830

Hunt JA, Dalgleish DG (1994) Adsorption behaviour of whey protein isolate and caseinate in soya oil-in-water emulsions. Food Hydrocoll 8:175–187

Khalloufi S, Alexander M, Goff HD, Corredig M (2008) Physicochemical properties of whey protein isolate stabilized oil-in-water emulsions when mixed with flaxseed gum at neutral pH. Food Res Int 41:964–972

Khalloufi S, Corredig M, Goff HD, Alexander M (2009) Flaxseed gums and their adsorption on whey protein-stabilized oil-in-water emulsions. Food Hydrocoll 23:611–618

Kharat M, Zhang G, McClements DJ (2018) Stability of curcumin in oil-in-water emulsions: impact of emulsifier type and concentration on chemical degradation. Food Res Int 111:178–186

Kim H, Decker EA, McClements DJ (2002) Role of postadsorption conformation changes of β-lactoglobulin on its ability to stabilize oil droplets against flocculation during heating at neutral pH. Langmuir 18:7577–7583

Ladjal-Ettoumi Y, Boudries H, Chibane M, Romero A (2016) Pea, chickpea and lentil protein isolates: physicochemical characterization and emulsifying properties. Food Biophysics 11:43–51

Laplante S, Turgeon SL, Paquin P (2006) Emulsion-stabilizing properties of chitosan in the presence of whey protein isolate: effect of the mixture ratio, ionic strength and pH. Carbohydr Polym 65:479–487

Lee YS (2008) Self-assembly and nanotechnology: a force balance approach. Wiley

Lee SW, Shimizu M, Kaminogawa S, Yamauchi K (1987) Emulsifying properties of peptides obtained from the hydrolyzates of β-casein. Agric Biol Chem 51:161–166

Li T, Kalloudis M, Cardoso AZ, Adams DJ, Clegg PS (2014) Drop-casting hydrogels at a liquid interface: the case of hydrophobic dipeptides. Langmuir 30:13854–13860

Li T, Nudelman F, Tavacoli JW, Vass H, Adams DJ, Lips A, Clegg PS (2016) Long-lived foams stabilized by a hydrophobic dipeptide hydrogel. Adv Mater Interfaces 3:1500601

Li Q, Wang Z, Dai C, Wang Y, Chen W, Ju X, Yuan J, He R (2019) Physical stability and microstructure of rapeseed protein isolate/gum Arabic stabilized emulsions at alkaline pH. Food Hydrocoll 88:50–57

Liang H, Tang C (2014) Pea protein exhibits a novel Pickering stabilization for oil-in-water emulsions at pH 3.0, vol 58. LWT-Food Sci Technol, pp 463–469

Lotfallah AH, Burguete MI, Alfonso I, Luis SV (2015) Highly stable oil-in-water emulsions with a gemini amphiphilic pseudopeptide. RSC Adv 5:36890–36893

Lutz R, Aserin A, Wicker L, Garti N (2009) Double emulsions stabilized by a charged complex of modified pectin and whey protein isolate. Colloids Surf B: Biointerfaces 72:121–127

Lv W, Hu T, Taha A, Wang Z, Xu X, Pan S, Hu H (2019) Lipo-dipeptide as an emulsifier: performance and possible mechanism. J Agric Food Chem 67:6377–6386

McClements DJ (2004) Protein-stabilized emulsions. Curr Opin Colloid Interface Sci 9:305–313

McClements DJ (2012) Nanoemulsions versus microemulsions: terminology, differences, and similarities. Soft Matter 8:1719–1729

Middelberg AP, Dimitrijev-Dwyer M (2011) A designed biosurfactant protein for switchable foam control. ChemPhysChem 12:1426–1429

Middelberg AP, Radke CJ, Blanch HW (2000) Peptide interfacial adsorption is kinetically limited by the thermodynamic stability of self association. Proc Natl Acad Sci 97:5054–5059

Middelberg AP, He L, Dexter AF, Shen H, Holt SA, Thomas RK (2008) The interfacial structure and Young's modulus of peptide films having switchable mechanical properties. J R Soc Interface 5:47–54

Minkenberg CB, Florusse L, Eelkema R, Koper GJ, van Esch JH (2009) Triggered self-assembly of simple dynamic covalent surfactants. J Am Chem Soc 131:11274–11275

Mondal S, Adler-Abramovich L, Lampel A, Bram Y, Lipstman S, Gazit E (2015) Formation of functional super-helical assemblies by constrained single heptad repeat. Nat Commun 6:1–8

Mondal S, Varenik M, Bloch DN, Atsmon-Raz Y, Jacoby G, Adler-Abramovich L, Shimon LJ, Beck R, Miller Y, Regev O, Gazit E (2017) A minimal length rigid helical peptide motif allows rational design of modular surfactants. Nat Commun 8:14018

Moreira IP, Sasselli IR, Cannon DA, Hughes M, Lamprou DA, Tuttle T, Ulijn RV (2016) Enzymatically activated emulsions stabilised by interfacial nanofibre networks. Soft Matter 12:2623–2631

Moreira IP, Piskorz TK, van Esch JH, Tuttle T, Ulijn RV (2017) Biocatalytic self-assembly of tripeptide gels and emulsions. Langmuir 33:4986–4995

Morikawa M, Yoshihara M, Endo T, Kimizuka N (2005) α-helical polypeptide microcapsules formed by emulsion-templated self-assembly. Chem–A Eur J 11:1574–1578

Moschakis T, Murray BS, Dickinson E (2005) Microstructural evolution of viscoelastic emulsions stabilised by sodium caseinate and xanthan gum. J Colloid Interface Sci 284:714–728

Myers D (1999) Surfaces, interfaces, and colloids, 2nd edn. Wiley, New York

Naseef MA, Ibrahim HK, Nour SAE (2018) Solid form of lipid-based self-nanoemulsifying drug delivery systems for minimization of diacerein adverse effects: development and bioequivalence evaluation in albino rabbits. AAPS PharmSciTech 19:3097–3109

Ng S, Nyam K, Lai O, Nehdi IA, Chong G, Tan C (2017) Development of a palm olein oil-in-water (o/w) emulsion stabilized by a whey protein isolate nanofibrils-alginate complex. LWT Food Sci Technol 82:311–317

Ng-Kwai-Hang KF (2003) Milk proteins heterogeneity. fractionation and isolation. Encyclopedia of Dairy Sciences 1881–1894

Nishida Y, Tanaka A, Yamamoto S, Tominaga Y, Kunikata N, Mizuhata M, Maruyama T (2017) In situ synthesis of a supramolecular hydrogelator at an oil/water Interface for stabilization and stimuli-induced fusion of microdroplets. Angew Chem 129:9538–9542

Nutten S, Schuh S, Dutter T, Heine RG, Kuslys M (2020) Design, quality, safety and efficacy of extensively hydrolyzed formula for management of cow's milk protein allergy: what are the challenges? Adv Food Nutr Res 93:147–204

O'Regan J, Mulvihill DM (2010) Sodium caseinate-maltodextrin conjugate stabilized double emulsions: encapsulation and stability. Food Res Int 43:224–231

Okochi H, Nakano M (2000) Preparation and evaluation of w/o/w type emulsions containing vancomycin. Adv Drug Deliv Rev 45:5–26

Ozturk B, McClements DJ (2016) Progress in natural emulsifiers for utilization in food emulsions, current opinion in food. Science 7:1–6

Paananen A, Ercili-Cura D, Saloheimo M, Lantto R, Linder MB (2013) Directing enzymatic cross-linking activity to the air-water interface by a fusion protein approach. Soft Matter 9:1612–1619

Parsons DF, Ninham BW (2010) Charge reversal of surfaces in divalent electrolytes: the role of ionic dispersion interactions. Langmuir 26:6430–6436

Paukkonen H, Ukkonen A, Szilvay G, Yliperttula M, Laaksonen T (2017) Hydrophobin-nanofibrillated cellulose stabilized emulsions for encapsulation and release of BCS class II drugs. Eur J Pharm Sci 100:238–248

Paulsson M, Dejmek P (1992) Surface film pressure of β-lactoglobulin, α-lactalbumin and bovine serum albumin at the air/water interface studied by Wilhelmy plate and drop volume. J Colloid Interface Sci 150:394–403

Perrechil FA, Cunha RL (2010) Oil-in-water emulsions stabilized by sodium caseinate: influence of pH, high-pressure homogenization and locust bean gum addition. J Food Eng 97:441–448

Petsev DN (2004) Emulsions: structure, stability and interactions. Elsevier

Platzman I, Janiesch J, Spatz JP (2013) Synthesis of nanostructured and biofunctionalized water-in-oil droplets as tools for homing T cells. J Am Chem Soc 135:3339–3342

Rapaport H, Kjaer K, Jensen TR, Leiserowitz L, Tirrell DA (2000) Two-dimensional order in β-sheet peptide monolayers. J Am Chem Soc 122:12523–12529

Rebello S, Asok AK, Mundayoor S, Jisha MS (2014) Surfactants: toxicity, remediation and green surfactants. Environ Chem Lett 12:275–287

Sarkar A, Singh H (2016) Emulsions and foams stabilised by milk proteins. In: Emulsions and foams stabilised by milk proteins. Advanced Dairy Chemistry, Springer, pp 133–153

Scott GG, McKnight PJ, Tuttle T, Ulijn RV (2016) Tripeptide emulsifiers. Adv Mater 28:1381–1386

Sedaghat Doost A, Nikbakht Nasrabadi M, Kassozi V, Dewettinck K, Stevens CV, Van der Meeren P (2019) Pickering stabilization of thymol through green emulsification using soluble fraction of almond gum – whey protein isolate nano-complexes. Food Hydrocoll 88:218–227

Setiowati AD, Saeedi S, Wijaya W, Van der Meeren P (2017) Improved heat stability of whey protein isolate stabilized emulsions via dry heat treatment of WPI and low methoxyl pectin: effect of pectin concentration, pH, and ionic strength. Food Hydrocoll 63:716–726

Setiowati AD, Wijaya W, Van der Meeren P (2020) Whey protein-polysaccharide conjugates obtained via dry heat treatment to improve the heat stability of whey protein stabilized emulsions. Trends Food Sci Technol 98:150

Sridharan S, Meinders MB, Bitter JH, Nikiforidis CV (2020) On the emulsifying properties of self-assembled pea protein particles. Langmuir 36:12221–12229

Sun C, Gunasekaran S (2009) Effects of protein concentration and oil-phase volume fraction on the stability and rheology of menhaden oil-in-water emulsions stabilized by whey protein isolate with xanthan gum. Food Hydrocoll 23:165–174

Surh J, Decker EA, McClements DJ (2006) Properties and stability of oil-in-water emulsions stabilized by fish gelatin. Food Hydrocoll 20:596–606

Taherian AR, Britten M, Sabik H, Fustier P (2011) Ability of whey protein isolate and/or fish gelatin to inhibit physical separation and lipid oxidation in fish oil-in-water beverage emulsion. Food Hydrocoll 25:868–878

Tavares FW, Bratko D, Blanch HW, Prausnitz JM (2004) Ion-specific effects in the colloid−colloid or protein− protein potential of mean force: role of salt− macroion van der Waals interactions. J Phys Chem B 108:9228–9235

Tcholakova S, Denkov ND, Ivanov IB, Campbell B (2006) Coalescence stability of emulsions containing globular milk proteins. Adv Colloid Interf Sci 123:259–293

Tchuenbou-Magaia FL, Norton IT, Cox PW (2009) Hydrophobins stabilised air-filled emulsions for the food industry. Food Hydrocoll 23:1877–1885

Teo A, Dimartino S, Lee SJ, Goh KKT, Wen J, Oey I, Ko S, Kwak H (2016) Interfacial structures of whey protein isolate (WPI) and lactoferrin on hydrophobic surfaces in a model system monitored by quartz crystal microbalance with dissipation (QCM-D) and their formation on nanoemulsions. Food Hydrocoll 56:150–160

Tian YF, Devgun JM, Collier JH (2011) Fibrillized peptide microgels for cell encapsulation and 3D cell culture. Soft Matter 7:6005–6011

Tomadoni B, Capello C, Valencia GA, Gutiérrez TJ (2020) Self-assembled proteins for food applications: a review. Trends Food Sci Technol 101:1

van Aken GA (2004) Coalescence mechanisms in protein-stabilized emulsions. Food Emulsions 299:325

Veis A (1964) The macromolecular chemistry of gelatin. Academic, New York

Wahlgren MC, Arnebrant T, Paulsson MA (1993) The adsorption from solutions of β-lactoglobulin mixed with lactoferrin or lysozyme onto silica and methylated silica surfaces. J Colloid Interface Sci 158:46–53

Walstra P (2003) Physical chemistry of foods. Marcel Decker, New York

Wang M, Lv Y, Liu X, Qi W, Su R, He Z (2016) Enhancing the activity of peptide-based artificial hydrolase with catalytic Ser/His/Asp triad and molecular imprinting. ACS Appl Mater Interfaces 8:14133–14141

Wang H, Wibowo D, Shao Z, Middelberg AP, Zhao C (2017) Design of modular peptide surfactants and their surface activity. Langmuir 33:7957–7967

Wibowo D, Zhao C, Middelberg AP (2014) Emulsion-templated silica nanocapsules formed using bio-inspired silicification. Chem Commun 50:11325–11328

Wibowo D, Wang H, Shao Z, Middelberg AP, Zhao C (2017) Interfacial films formed by a biosurfactant modularized with a silken tail. J Phys Chem C 121:14658–14667

Wilde PJ (2000) Interfaces: their role in foam and emulsion behaviour. Curr Opin Colloid Interface Sci 5:176–181

Wilde P, Mackie A, Husband F, Gunning P, Morris V (2004) Proteins and emulsifiers at liquid interfaces. Adv Colloid Interf Sci 108:63–71

Windbergs M, Zhao Y, Heyman J, Weitz DA (2013) Biodegradable core–shell carriers for simultaneous encapsulation of synergistic actives. J Am Chem Soc 135:7933–7937

Wooster TJ, Augustin MA (2006) β-Lactoglobulin-dextran Maillard conjugates: their effect on interfacial thickness and emulsion stability. J Colloid Interface Sci 303:564–572

Wüstneck R, Moser B, Muschiolik G (1999) Interfacial dilational behaviour of adsorbed β-lactoglobulin layers at the different fluid interfaces. Colloids Surf B: Biointerfaces 15:263–273

Wychowaniec JK, Patel R, Leach J, Mathomes R, Chhabria V, Patil-Sen Y, Hidalgo-Bastida A, Forbes RT, Hayes JM, Elsawy MA (2020) Aromatic stacking facilitated self-assembly of ultrashort ionic complementary peptide sequence: β-sheet nanofibres with remarkable gelation and interfacial properties. Biomacromolecules 21:2670

Yang Z, Gu H, Fu D, Gao P, Lam JK, Xu B (2004) Enzymatic formation of supramolecular hydrogels, Adv Mater 16:1440–1444

Yang X, Wang Y, Qi W, Su R, He Z (2017) Bioorganometallic ferrocene-tripeptide nanoemulsions. Nanoscale 9:15323–15331

Yang L, Qin X, Kan J, Liu X, Zhong J (2019) Improving the physical and oxidative stability of emulsions using mixed emulsifiers: casein-octenyl succinic anhydride modified starch combinations. Nano 9:1018

Ye A (2010) Surface protein composition and concentration of whey protein isolate-stabilized oil-in-water emulsions: effect of heat treatment. Colloids Surf B: Biointerfaces 78:24–29

Ye A, Singh H (2006) Adsorption behaviour of lactoferrin in oil-in-water emulsions as influenced by interactions with β-lactoglobulin. J Colloid Interface Sci 295:249–254

Ye A, Singh H (2007) Formation of multilayers at the interface of oil-in-water emulsion via interactions between lactoferrin and β-lactoglobulin. Food Biophys 2:125–132

Yildiz G, Ding J, Andrade J, Engeseth NJ, Feng H (2018) Effect of plant protein-polysaccharide complexes produced by mano-thermo-sonication and pH-shifting on the structure and stability of oil-in-water emulsions. Innovative Food Sci Emerg Technol 47:317–325

Zarai Z, Balti R, Sila A, Ali YB, Gargouri Y (2016) Helix aspersa gelatin as an emulsifier and emulsion stabilizer: functional properties and effects on pancreatic lipolysis. Food Funct 7:326–336

Zhai J, Wooster TJ, Hoffmann SV, Lee T, Augustin MA, Aguilar M (2011) Structural rearrangement of β-lactoglobulin at different oil–water interfaces and its effect on emulsion stability. Langmuir 27:9227–9236

Zhang S, Lockshin C, Cook R, Rich A (1994) Unusually stable β-sheet formation in an ionic self-complementary oligopeptide, biopolymers. Original Res Biomol 34:663–672

Zhang Y, Tan C, Abbas S, Eric K, Zhang X, Xia S, Jia C (2014) The effect of soy protein structural modification on emulsion properties and oxidative stability of fish oil microcapsules. Colloids Surf B: Biointerfaces 120:63–70

Zhang Y, Tan C, Abbas S, Eric K, Xia S, Zhang X (2015) Modified SPI improves the emulsion properties and oxidative stability of fish oil microcapsules. Food Hydrocoll 51:108–117

Zhao C, Dwyer MD, Yu L, Middelberg AP (2017) From folding to function: design of a new switchable biosurfactant protein. ChemPhysChem 18:488–492

Zhu Y, Chen X, McClements DJ, Zou L, Liu W (2018) pH-, ion- and temperature-dependent emulsion gels: fabricated by addition of whey protein to gliadin-nanoparticle coated lipid droplets. Food Hydrocoll 77:870–878

Chapter 14
Antimicrobial Peptide Nanomaterials

Sophie M. Coulter and Garry Laverty

Abstract Antimicrobial peptides exist throughout nature and are produced by multicellular organisms as a defence mechanism against pathogenic microbes. Multi-drug-resistant bacteria pose a serious threat to public health. In the increasing absence of new antibiotic agents, there is a need for the development of novel strategies to target bacterial infections. One such strategy receiving great interest is that of the field of antimicrobial peptide nanomaterials. Peptides represent an attractive approach owing to their unique chemical versatility, potential for structural and functional modification and capacity to self-assemble into a variety of nanostructures. Ultrashort sequences are particularly interesting in the development of novel antimicrobials since they are ultimately more cost-effective to upscale and require reduced manufacturing times. A variety of ultrashort sequences also demonstrate a propensity to self-assemble into nanotube and hydrogel structures that themselves can provide an inherently antimicrobial material and/or delivery vehicle. Despite widespread research, few peptide nanostructures have made it to market, and this is due to recurring issues with stability and longevity within clinical applications. To surmount such issues, there has been increasing focus on peptidomimetics, which displays increased residence times and resistance to degradation by proteolytic enzymes in vivo, with successful implementation likely to result in the growth of the peptide therapeutic market.

Keywords Antimicrobial · Peptide · Self-assembly · Nanomaterial · Nanotube · Hydrogel · Peptidomimetic

S. M. Coulter · G. Laverty (✉)
Biofunctional Nanomaterials Group, School of Pharmacy, Queen's University Belfast, Medical Biology Centre, Belfast, Ireland
e-mail: garry.laverty@qub.ac.uk

475

14.1 Introduction

Antimicrobial resistance is a complex and multi-faceted issue that is considered an urgent public health threat (Evans and Lewis 2020). The increasing incidence of bacterial resistance, in addition to the lack of new antimicrobial therapeutics being approved, has left the global population in a precarious position and heightened the interest of researchers towards the development of novel antimicrobial agents. One such approach is the use of peptides that are considered a promising alternative to small drug molecules in the development of novel antimicrobial therapeutics. Short, naturally occurring, cationic amphiphilic peptides that display antimicrobial and/or immunomodulatory activities exist across virtually every domain of life and act as an important component of the innate immune defences (Hancock and Sahl 2006). Indeed, there are numerous examples of naturally occurring cationic peptides that display antimicrobial activity such as α- and β-defensins isolated from the phagocytic and epithelial cells of numerous mammals, including human LL-37 and the frog-derived peptide brevinine (Devine and Hancock 2002). In addition to their inherent antimicrobial activity, antimicrobial peptides have been shown to bind and neutralize endotoxins (lipopolysaccharide) released from Gram-negative bacteria which are linked to an exacerbated and severe host inflammatory response (Piotrowska et al. 2017). The licensed antimicrobial peptide daptomycin that has been observed to self-assemble into micelles with unordered secondary structures (Kirkham et al. 2016), serves as an important reminder of the clinical promise of peptides as a source of clinical therapies and in addressing the significant problem of antimicrobial resistance (Taylor and Palmer 2016).

Taking inspiration from nature, there has been an increasing interest in the development of synthetic peptide sequences which harness and exploit these inherent antimicrobial properties in the race to develop novel therapeutics. There are 20 naturally occurring amino acids encoded by DNA, each composed of carboxylic acid and amine moieties, with variation occurring at the R-group attached to the α-carbon (Zhao et al. 2008). These 20 amino acids alone represent a wealth of opportunities for the synthesis of an assortment of different peptide structures with varying properties. Through careful consideration of the properties conferred by the R-group, it is possible to tailor the desired properties according to the amino acids incorporated thereby harnessing a so-called 'bottom-up' approach to functional design (McCloskey et al. 2014). For example, the incorporation of aliphatic residues such as alanine or leucine within the sequence can be used to provide a general hydrophobic environment. Aromatic residues such as phenylalanine and tyrosine are involved in π-π stacking and hydrophilic uncharged residues such as serine and asparagine can partake in hydrogen bonding interactions (Ulijn and Smith 2008). This vast structural versatility combined with the inherent biocompatibility, biodegradability and tailored immunogenicity often displayed by peptide sequences renders them an interesting and attractive approach to the development of innovative antimicrobial systems (Guler et al. 2006; Laverty et al. 2014).

14.2 General Mechanisms of Antimicrobial Peptide Action

Unlike conventional antibiotics, which often have very defined and specific molecular targets, host cationic peptides display varying, complex and very rapid mechanisms of action that make it difficult for microorganisms to form an effective defence, thereby reducing the rate of development of antimicrobial resistance. For example, antimicrobial peptides may act at multiple intracellular (enzymes, protein folding and cell wall synthesis) and extracellular (membrane) sites. This means pathogens would be required to alter multiple pathways and phenotypic traits in order to develop resistance which far reduces the likelihood, or at least the rate, of development when compared to conventional antibiotics with a single specific target site (Laverty et al. 2011; Laverty 2018). Importantly, antimicrobial peptides are often potent and display antimicrobial activity at micromolar concentrations or less.

Cationic and amphipathic peptides represent the largest class of antimicrobial peptides, typically varying in net positive charge between +2 and +9, often because of the presence of arginine and lysine residues (Hancock et al. 1995; Chan et al. 2006; Ramesh et al. 2016; Piotrowska et al. 2017). The amphiphilicity of antimicrobial peptides facilitates targeting of cell membranes, particularly bacterial membranes which possess an overall negative charge due to the presence of acidic hydroxylated phospholipids (Yeaman and Yount 2003). Areas of dense anionic charge exist within the membranes of both Gram-positive and Gram-negative bacteria enabling cationic peptides to selectively target bacterial membranes and exert their bactericidal effect (Arouri et al. 2009; Laverty et al. 2011). Despite the exact mechanism of antimicrobial peptide action remaining unknown, it is thought that they can act directly on the cell membrane to disrupt the phospholipid bilayer causing a loss of integrity or function by four recognized mechanisms: the aggregate, toroidal pore, barrel-stave and carpet models (Brogden 2005), as outlined in Table 14.1 and displayed in Fig. 14.1. Membrane lysis, however, is not a prerequisite

Table 14.1 The four recognized mechanisms by which antimicrobial peptides disrupt bacterial phospholipid bilayers (Brogden 2005; Laverty et al. 2011)

Model	Mechanism
(A) Aggregate	Peptides span the phospholipid bilayer as disordered aggregates and form complexes between themselves and membrane lipids
(B) Torroidal pore	A similar mechanism to the aggregate model only more organized. Peptides orientate themselves perpendicular to the plane of the phospholipid bilayer to create a pore possessing a hydrophobic core (blue) and a hydrophilic exterior (red) which facilitates the entry of further peptide
(C) Barrel-stave	Peptides insert themselves perpendicular to the plane of the lipid bilayer to form 'staves' in a 'barrel-shaped' cluster. The hydrophilic regions (red) of the peptide face the lumen of the membrane-spanning pore that is created while the hydrophobic regions (blue) of the peptide interact with the bilayer
(D) Carpet	Peptide monomers aggregate parallel to the phospholipid bilayer coating it like a carpet and at a threshold concentration this is thought to result in a detergent-like effect creating both micelles and membrane pores
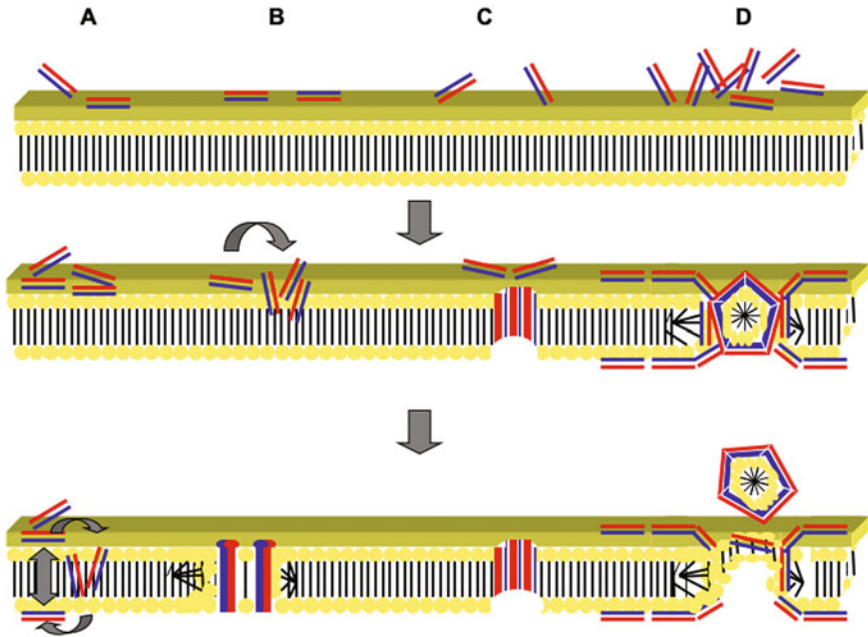
Fig. 14.1 Peptide targeting of bacterial membranes by (A), toroidal pore (B), barrel stave (C) and carpet models (D). Key: red = hydrophilic amino acid residues; blue = hydrophobic amino acid residues, yellow: hydrophilic head groups bacterial cell membrane i.e. phosphate groups, brown = lipophilic groups i.e. fatty acid chain, of bacterial cell membrane. (Adapted with permission from Laverty et al. 2011, which is licensed under the Creative Commons Attribution 3.0 Unported License)

to bacterial cell death, as observed within the proline-rich natural antimicrobial peptide indolicidin (Falla et al. 1996). Membrane permeation is observed with indolicidin but cidal activity is mediated by the inhibition of DNA, RNA and protein synthesis.

Irrespective of the mechanism by which the membrane is disrupted, an important consideration is that a pathogen would have to alter its entire cell membrane architecture in order to develop resistance to this type of destruction. This therefore renders the likelihood of resistance developing much less likely than conventional antibiotics. Indeed, Liu and colleagues developed several cationic oligomers which displayed broad-spectrum membrane lytic activity for which the bacteria failed to develop resistance to, even after multiple exposures to sub-lethal doses of the oligomers (Liu et al. 2014). There have been various investigations into the rational design of synthetic antimicrobial peptides, for example, Strøm and colleagues described the minimum content of charge, bulk, and lipophilicity necessary to confer antimicrobial activity against a range of clinically relevant Gram-positive and Gram-negative microorganisms (Strom et al. 2003). They proposed that to demonstrate activity against Gram-positive microorganisms, such as staphylococci, a minimum of two units of charge and two units of hydrophobic bulk were necessary within a

peptide sequence, while for Gram-negative microorganisms, an additional unit of hydrophobic bulk was necessary. Additionally, they reported that the order of residues within the sequence was not critical to activity but rather the overall number of charged species and the net content of bulk. This work has encouraged researchers, including our own group, to focus on developing synthetic peptide and peptidomimetic sequences which contain the minimum pharmacophore necessary to confer antimicrobial activity, since this will ultimately confer savings in terms of time and reduce costs to upscale. Work by Xu et al. investigated the development of a design strategy capable of producing a peptide sequence which could confer the ideal balance of minimal cytotoxicity, enhanced stability, potent cell penetration and effective antimicrobial activity with potential therapeutic application in intracellular microbial infections and systemic infections alike (Xu et al. 2015). Various approaches have been adopted in order to identify novel antimicrobial sequences and structural patterns associated with antimicrobial activity. These include the following: relying on the modification of known antimicrobial sequences to identify which amino acids and positions are important for antimicrobial activity with limited computational input; rigorous biophysical modelling to understand peptide activity by examining structures in various environments or by modelling at the atomic level; and the use of virtual screening in which numerical methods are used to determine quantifiable properties of peptides, such as charge and hydrophobicity, and these are related to biological activities using structure–activity relationships (Fjell et al. 2012). Irrespective of the methods employed, the successful design of ultrashort peptide sequences which display antimicrobial activity will advance their application in clinically relevant settings. Interestingly, the properties that govern the antimicrobial activity of a peptide sequence, such as the hydrophobic: hydrophilic balance and charge, are typically closely related to the self-assembly process (Laverty 2018). Many antimicrobial peptide systems therefore also display some type of self-assembly, which is important for either their delivery or mechanism of action as an antimicrobial.

14.3   Self-Assembly

The process of self-assembly is ubiquitous throughout nature. Self-assembling molecules such as peptides, proteins, nucleic acids and lipids, the central building blocks of life assemble to enable the development of higher ordered structures such as cell membranes and the extracellular matrix (Schnaider et al. 2017). The ability to self-assemble can be exploited in the development of novel synthetic peptide sequences with the potential for a range of medical applications, including as antimicrobials, as scaffolds for tissue engineering and for drug delivery applications. A major benefit of using such peptide-based assembly systems is that they negate the need for conventional drug delivery vehicles. These often rely on synthetic polymers which can result in bioaccumulation due to a lack of biodegradability, leading to toxicity issues (Habibi et al. 2016). Indeed, peptide-based systems are typically
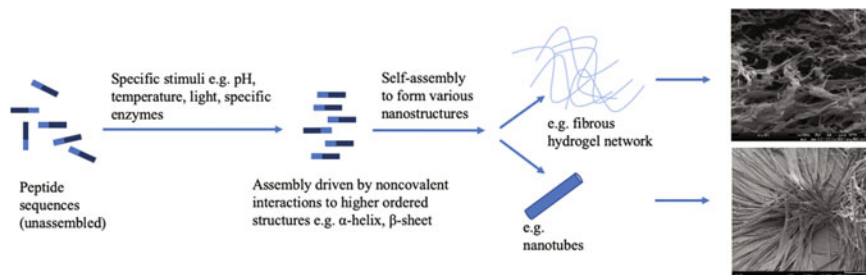
Fig. 14.2 The self-assembly of peptide monomers in response to various environmental and physiological stimuli triggers resulting in assembly via non-covalent interactions to form higher ordered structures, such as hydrogels and nanotubes. Key: blue = hydrophobic residues; black = hydrophilic residues

regarded as being fully biocompatible owing to their primary structure being constructed of simple amino acid building blocks, which also renders them biodegradable and it is expected that they should not elicit undesired immunogenic responses. Peptide-based self-assembly is reliant on various non-covalent interactions including hydrogen bonding, electrostatic interactions, aromatic−aromatic interactions, van der Waals forces, π-π stacking and hydrophobic interactions, each of which in isolation is considered rather weak. However, collectively they exert strong molecular forces to facilitate the formation of higher ordered structures (Sun et al. 2016). As shown in Fig. 14.2, various higher ordered architectures can present with linear peptides often forming nanofibers, nanoribbons, nanotubes or vesicles; cyclic peptides stacking to form nanotubes and branched peptides may form micelles or vesicles (Hu et al. 2020). Each of these types of self-assembling system has been developed and investigated in the race to formulate novel antimicrobial agents with a special interest in the use of nanotubes and nanofibers that can form hydrogels. For example, Gontsarik et al. designed and characterized an amphiphilic, pH-responsive antimicrobial nanomaterial based on the self-assembly of oleic acid with the human peptide cathelicidin LL-37 (Gontsarik et al. 2019). The development of this self-assembling nanocarrier system was postulated to enable more targeted delivery while reducing side effects and improving biostability. They found that the nanocarrier structure itself was pH sensitive and formed cylindrical micelles at pH 7 while at pH 5, aggregates of branched threadlike micelles form thus enabling targeted delivery of antimicrobials at acidic pH.

Perhaps of particular interest is the fact that peptide self-assembly can be triggered and indeed altered in response to very specific environmental stimuli, thus offering the potential for tuneable assembly and antimicrobial activity under desirable conditions. For example, assembly in response to acidic wound environments (Pfalzgraff et al. 2018), or under the alkaline conditions generated by the metabolism of urea to ammonia by urease-producing bacteria such as *Proteus mirabilis* (Panja and Adams 2019; Cross et al. 2020). The self-assembly of various peptide sequences into higher ordered structures has been reported in response to chemical, physical

and environmental triggers including pH and ionic strength (Liu et al. 2013), ultrasound (Yu et al. 2010), temperature (Rughani et al. 2009), light (Haines et al. 2005) and specific enzymes (Hughes et al. 2013; He et al. 2018b). The various triggers for self-assembly highlight the wealth of research opportunities available to tailor the assembly process to desired functional and therapeutic requirements.

Ultrashort aromatic dipeptide gelators, often consisting of two phenylalanine (F) residues conjugated to a highly aromatic molecule such as naphthalene/naphthanoyl (Nap) or fluoren-9-methyloxycarbonyl (Fmoc), are receiving increased clinical interest as antimicrobial agents (Lombardi et al. 2019a). Nap-FF-OH (Laverty et al. 2014) and Fmoc-FF-OH (Reches and Gazit 2003; McCloskey et al. 2017) have been shown to self-assemble to form secondary structures and possess inherent antimicrobial activity making them ideal structures for the development of antimicrobial systems. Schnaider and colleagues demonstrated that diphenylalanine nano-assemblies could completely inhibit the growth of Gram-negative *Escherichia coli* by triggering the upregulation of stress response regulons, inducing substantial disruption to bacterial cell morphology, and eventually resulting in membrane permeation and depolarization (Schnaider et al. 2017). These ultrashort sequences are considered to represent the minimum pharmacophore necessary to achieve antimicrobial activity and can as such be used as a platform to develop more potent self-assembled nanosystems (Lombardi et al. 2019a).

For all antimicrobial peptides, especially those that form nanoarchitectures, there is an increased emphasis on establishing whether self-assembly is succinctly linked to antimicrobial efficacy and spectrum of activity (Cross et al. 2021). Recently Shen and colleagues studied a peptide with the ability to self-assemble into nanofibers, FF8 (KRRFFRRK), alongside a non-assembling GG8 (KRRGGRRK) control sequence where phenylalanine was switched with glycine (Shen et al. 2020). Interestingly FF8 was found to self-assemble into β-sheet-derived nanofibers in response to: (1) anionic model membranes that mimic those found in bacteria or (2) alkaline pH >9.4. GG8 was not able to self-assemble and demonstrated reduced antibacterial activity relative to FF8 (GG8 MIC vs. *E. coli*: 819.2 μM, FF8: 25.6 μM). The formation of FF8 peptide nanofibers disrupts the lipid membrane of bacteria by a process similar to the carpet model (Fig. 14.1D). As FF8 is also responsive to alkaline pH, it may also be useful as a pH-triggered approach in the long-term prevention of urinary catheter infection (Milo et al. 2021). This is especially promising given FF8 was shown to be more effective against Gram-negative bacteria implicated in urinary catheter infections i.e. *E. coli* than Gram-positives (*Staphylococcus aureus*).

14.4 Nanotubes

Peptide nanotubes are receiving increasing attention for chemical, engineering and drug delivery applications owing to their high aspect ratio (length-to-diameter), their ability to provide enhanced transport and delivery of drugs in vivo and their high

surface area, enabling greater encapsulation efficiency than other nanoparticles e.g. nanospheres (Gazit 2007; Gratton et al. 2008; Barua et al. 2013). These characteristics contribute to improved cellular interactions and the potential to reduce required doses for therapeutic efficacy, thereby reducing side effects. Peptide nanotubes have been extensively studied for their inherent antibacterial properties owing to their ability to interact with cellular membranes, causing depolarization and subsequent cell destruction (Schnaider et al. 2017). The interaction of these supra-molecular structures with biological membranes is highly dependent on the amino acid composition of the nanotube itself and the chemical properties of the residue side chains that orientate themselves towards the outer portion of the tube and are therefore in contact with the components of the cell membrane (Dartois et al. 2005).

Extensive studies have been performed on alternating D- and L-α-octapeptide sequences capable of undergoing cyclization and subsequent stacking via hydrogen bonding to form nanotubular assemblies that possess antimicrobial activity (Rho et al. 2019). Fernandez-Lopez et al. found that these structures could selectively target and self-assemble in the phospholipid bilayer of both Gram-positive and negative bacterial membranes to increase membrane permeability and exert a cidal action (Fernandez-Lopez et al. 2001). They suggested that the carpet model (Fig. 14.1D) most likely represented the method by which the nanotubes inserted themselves within the cell membrane with hydrophobic side chains inserted into the lipid components of the membrane and the hydrophilic residues remaining exposed to the hydrophilic components of the cell membrane. This was confirmed by quantitative atomic force microscopy and Fourier Transform infrared spectroscopy measurements, indicating that the nanotubes were oriented at a $70 \pm 5°$ tilt angle from the membrane normal, consistent with the carpet-like mode of action (Oren and Shai 1998). Work by Dartois and colleagues further investigated short cyclic peptides composed of alternating D- and L-α-amino acids focussing on their in vivo tolerability and efficacy in murine models of infection (Dartois et al. 2005). Upon intravenous administration of test sequences, equal efficacy against methicillin-sensitive and -resistant *S. aureus* was observed. More rapid kill was achieved compared to conventional antibiotic controls of vancomycin or oxacillin, consistent with the proposed mode of action of cyclic peptide nanotube structures that interact with the membrane as a whole rather than individual enzymatic processes of the cell.

Our group recently reported the development of phenylalanine–phenylalanine (FF) nanotubes with the capacity to selectively eradicate bacterial biofilms (Porter et al. 2018). After heating, these ultrashort motifs can spontaneously self-assemble in solution to form nanotubes as a result of intermolecular π–π interactions between neighbouring phenyl groups, hydrophobic interactions and hydrogen bonding with the surrounding solvent (Jeon et al. 2013). Three variants based on the FF motif were chosen, NH_2–FF–COOH, NH_2–ff–COOH and NH_2–FF–NH_2 and the nanotubes were tested against planktonic and more resistant biofilm forms of clinically relevant Gram-positive and -negative pathogens. NH_2–FF–COOH demonstrated the most potent activity against both forms of bacteria, with greater than a three Log_{10} CFU/mL viable biofilm reduction (>99.9%) at 5 mg/mL and total biofilm kill at 10 mg/mL against *S. aureus* after 24-h exposure. Interestingly, scanning electron

microscopy of the biofilm after treatment confirmed that NH_2–FF–COOH was able to disrupt the peptidoglycan cell wall and cytoplasmic lipid membrane of *S. aureus* resulting in cell lysis and death in line with previously proposed membrane mechanisms of action of antimicrobial peptide nanotubes.

Another approach of interest is to use synthetic, non-peptide-based, nanotubes loaded with antimicrobial peptides to achieve antimicrobial action. Recently, Chen et al. reported the use of a titanium implant containing titania nanotubes loaded with HHC-36 antimicrobial peptide to achieve localized delivery in an effort to achieve on-demand storage and release of antimicrobials (Chen et al. 2020). The nanotubes incorporated a pH-responsive molecular gate composed of poly(methacrylic acid) which swelled under normal physiological pH (7.4) thereby trapping the antimicrobial peptides within the hollow nanotube core. Upon exposure to acidic pH, in the case of bacterial infection (pH $\leq$ 6.0), the molecular gate collapsed enabling burst release of antimicrobial peptide and targeted antimicrobial action. The antimicrobial peptide HHC-36 (KRWWKWWRR-NH_2) has been shown to display broad-spectrum antimicrobial activity in addition to biocompatibility (Kazemzadeh-Narbat et al. 2013). The Chen group reported the bactericidal activity of the antimicrobial peptide-loaded titania nanotubes against four clinically relevant pathogens, *S. aureus*, *E. coli*, *P. aeruginosa* and methicillin-resistant *S. aureus* (MRSA). They also demonstrated a favourable cytotoxicity profile in the presence of human bone mesenchymal stem cells (hBMSCs). The group went on to demonstrate in vivo bactericidal activity and biocompatibility in a bone-defect model in rabbits.

14.5 Hydrogel-Forming Nanostructures

Another type of self-assembling system that has received considerable interest is the development of peptide hydrogels with inherent antimicrobial activity. This is owing to the additional benefits such as the ability to act as a three-dimensional support for cell culture (Discher et al. 2005; Salick et al. 2007) and a high water content, providing a moist environment suitable for applications such as infected wound healing (Pfalzgraff et al. 2018). Any hydrogel system, including those created via peptide self-assembly, consists of a three-dimensional self-supporting viscoelastic network with water entrapped within the interstices, thereby imparting rigidity to the system (Menger and Caran 2000). In the case of peptide-based hydrogelators, the process of self-assembly via non-covalent interactions generates a network of entangled fibres capable of entrapping water in order to form a gel.

Various methods have been employed to utilize peptide-based hydrogels as antimicrobial agents, including incorporating known antimicrobial peptides within synthetic hydrogels, conjugating self-assembling peptide motifs to antimicrobial peptides to achieve gelation and finding peptide sequences which can form hydrogels and possess inherent antimicrobial activity (Ng et al. 2014). Liu and colleagues developed two antimicrobial peptides, connected via a central tetrapeptide linker, in order to achieve self-assembly and antimicrobial action (Liu

et al. 2013). The sequence had the capacity to self-assemble into a β-sheet structure and form a hydrogel in response to the external stimuli pH, ionic strength or heat and demonstrated inhibition of the growth of planktonic *E. coli*. Sarkar et al. reported the design of a set of modular cationic amphiphilic self-assembling peptides with a common self-assembling core and positively charged domains at the termini (Sarkar et al. 2019). These sequences are a type of multidomain peptide, a subset of self-assembling peptides, outlined more fully below (Sect. 14.5.3). They varied the number of lysine residues and therefore the degree of cationic charge in order to generate and investigate antimicrobial hydrogelators. They found that sequences could self-assemble into robust hydrogels, acting as potent disruptors of bacterial cell membranes. They could be syringe aspirated and injected onto or into a particular administration site e.g. wound.

Our group studied the use of ultrashort sequences, such as Fmoc-based and naphthalene-conjugated peptides, capable of forming hydrogels to eradicate established biofilms. These have potential applications in the field of wound dressings or as novel coatings for the surface of medical devices (Laverty et al. 2014; McCloskey et al. 2017). Naphthalene-conjugated ultrashort sequences were made to self-assemble in response to a pH trigger, with the terminal carboxylic acid moiety deprotonated under alkaline conditions enabling full dissolution and re-protonated upon pH titration back to physiological pH, resulting in reduced solubility and the formation of a homogenous hydrogel. These sequences demonstrated antimicrobial activity in the presence of Gram-positive and Gram-negative species biofilms, with a 2.0% w/v NapFFKK–OH hydrogel shown to reduce a viable *Staphylococcus epidermidis* biofilm by 94%. Further research on Fmoc-based gelators demonstrated that Fmoc-peptides (FmocFF–OH, FmocFFKK–OH, FmocFFFKK–OH, FmocFFOO–OH) had the capacity to form surfactant-like soft gels at concentrations of 1% w/v and above via glucono-δ-lactone-mediated pH induction. Most of the Fmoc-peptides investigated demonstrated selective action against established biofilms of both Gram-positive and Gram-negative pathogens. We have also harnessed the presence of aromatic moieties within non-steroidal anti-inflammatory drugs to provide the aromatic bulk necessary for gelation, while also conferring therapeutic activity to inherently antimicrobial peptide sequences (McCloskey et al. 2016). These dual function hydrogels also have potential applications in the field of wound healing, where the hydrogel provides the moist environment favourable for healing, in addition to antimicrobial and anti-inflammatory action, especially important in chronic wound therapies. Such gelators were found to display broad-spectrum antimicrobial activity in addition to cyclooxygenase-2 (COX-2) inhibition, indicating potential anti-inflammatory action.

Another interesting approach being adopted is the use of intracellular enzymatic hydrolysis of peptides to trigger self-assembly, in order to form peptide hydrogels within cells, resulting in cellular disruption and ultimately bacterial cell death (Ng et al. 2014). The Xu group reported peptide gelator precursors capable of entering *E. coli* cells via simple diffusion with subsequent phosphatase induced hydrogelation resulting in a change in the viscosity of the cytoplasm, therefore stressing bacterial cell and ultimately resulting in cell death upon accumulation of

the gelator (Yang et al. 2007). This technique was reliant on the overexpression of phosphatase within *E. coli* cells and the group therefore suggested targeted antimicrobial action could be achieved in future clinical applications with healthy mammalian cells remaining unaffected. Hughes and colleagues used a similar approach to the Xu group to investigate if the treatment of *E. coli* with different aromatic peptide amphiphiles would result in varying antimicrobial properties (Hughes et al. 2013). They found that numerous Fmoc-based ultrashort gelators could be used to achieve intracellular gelation and subsequent bacterial cell death and that the response was insignificantly different regardless of the chemical structure of aromatic peptide amphiphiles. There are several other peptide systems that have demonstrated an ability to combine self-assembly into supramolecular hydrogels and/or nanoarchitectures with antimicrobial properties. Within this chapter, these are outlined below under the following classes: surfactant-like peptides; peptide amphiphiles; multidomain peptides and β-hairpin peptides. The dominant characteristic they share which determines both self-assembly and antimicrobial activity is amphiphilicity. It is the organisation of this property i.e. chemical structure/sequence and its constituent units, that varies between each class. We have summarised the most commonly studied antimicrobial peptide nanomaterials in Table 14.2.

14.5.1 Surfactant-Like Peptides

Similar to ultrashort variants, the antibacterial activity of surfactant-like peptides depends primarily upon electrostatic interactions with anionic bacterial cell membranes. Surfactant-like peptides are composed of a charged amino acid head group e.g. lysine, arginine, aspartic acid, attached to a hydrophobic region of several amino acids e.g. alanine. They include the A_nK_m, A_nR, RA_nR peptide sequences (where $n = 3, 6, 9$, $m = 1, 2$) studied by the groups of Xu, Lu, (Xu et al. 2009) Hamley and Castelletto (Dehsorkhi et al. 2013). Surfactant-like peptides have the propensity to self-assemble into a variety of nanostructures including nanosheets, nanotapes, nanorods, worm-like micelles and nanofibers. The nature of hydrophobic regions determines the supramolecular structures formed and their antibacterial efficacy, as it governs their ability to disrupt bacterial membranes (Chen et al. 2010). As the hydrophobic region increases in size i.e. increased the number of alanine residues, the antibacterial efficacy improves alongside an increase in the size and shape of formed nanostructures. A_3K creates unstable membrane-like nanosheets, A_6K assembles into long nanofibers and worm-like micelles, while A_9K creates short nanorods (Xu et al. 2009). The Xu and Lu groups extended this work to include two lysine residues and twelve alanines ($A_{12}K$ and A_9K_2) (Chen et al. 2012). $A_{12}K$ also formed short nanorods but the increase in alanine units resulted in a reduction in antibacterial activity relative to A_9K. $A_{12}K$ was deemed too hydrophobic, above the threshold of hydrophobicity acceptable for its optimal hydrophobic: hydrophilic balance and membrane-disrupting power (Laverty et al. 2011). For A_9K_2, an increase in charge provided by two lysines did not lead to a resultant increase in

Table 14.2 Examples of peptide sequences studied as potential antimicrobial nanostructures and their corresponding properties

Peptide name and/or sequence	Trigger for self-assembly	Secondary structure formed	Self-assembled nanostructure	Antimicrobial efficacy	Hemo/cell cytotoxicity	References
Daptomycin	Both in the presence and absence of CaCl$_2$. Critical aggregation concentration = 0.12 mM	Unordered	Micelles	Not tested in micelle form	Not tested in micelle form	Kirkham et al. (2016)
Nap-FF-OH	pH triggered (high to low) ~0.5% w/v	β-Sheet	Nanofibers forming hydrogels	Broad-spectrum. >60% bio-film reduction vs. S. aureus, S. epidermidis, E. coli, P. aeruginosa at 2.0% w/v gel	>85% viability at 0.5% w/v gel vs. L929 fibroblasts. ~45% viability at 2% w/v gel (alamarBlue assay)	Laverty et al. (2014)
Nap-FFY(p)-OH	Enzyme (phosphatase) ~0.025–0.05% w/v	β-Sheet	Nanofibers forming hydrogels	IC$_{50}$ E. coli (with phosphatase plasmid + isopropyl β-D-1-thiogalactopyranoside [IPTG]) = 20 μg/mL, E. coli without plasmid and IPTG) = >2000 μg/mL	Not tested	Yang et al. (2007)
Fmoc-FY(p)-OH	Enzyme (phosphatase) ~10 mg/mL	β-Sheet	Nanofibers forming hydrogels	E. coli MC-1000 (overexpresses phosphatase + inosine) at 13 mg/20 mL = 34.9% cell death (live/dead assay)	Not tested	Hughes et al. (2013)
Nap-FFKK-OH	pH triggered (high to low), ~1.0% w/v	β-Sheet	Nanofibers forming hydrogels	Broad-spectrum. >87% bio-film reduction vs. S. aureus, S. epidermidis, E. coli, P. aeruginosa at 2% w/v gel.	~40% viability at 0.5–2% w/v gel vs. L929 fibroblasts.	Laverty et al. (2014)
Fmoc-FF-OH	pH triggered (high to low), 0.5% w/v, glucono-δ-lactone pH induction	β-Sheet	Nanofibers forming hydrogels	Broad-spectrum, >75% bio-film reduction vs. S. aureus, S. epidermidis, E. coli, P. aeruginosa at 0.5–2% w/v gel	>60% viability at 0.5–2% w/v gel vs. L929 fibroblasts	McCloskey et al. (2017)

Fmoc-FFKK-OH	pH triggered (high to low), 1% w/v, glucono-δ-lactone pH induction	β-Sheet	Nanofibers forming hydrogels	Broad-spectrum, 82% bio-film reduction vs. S. aureus and E. coli at 2% w/v gel	>65% viability at 0.5–2% w/v gel vs. L929 fibroblasts	McCloskey et al. (2017)
Naproxen-FFKK-OH	pH triggered (high to low), 0.4% w/v	β-Sheet	Nanofibers forming hydrogels	Broad-spectrum, >5.5 Log_{10} CFU/mL reduction in S. aureus, S. epidermidis at 2% w/v gel. >4 Log_{10} CFU/mL reduction in. E. coli and P. aeruginosa at 2% w/v gel	At 500 μM = 97% viability (live/dead), 95% viability (alamarBlue) vs. L929 fibroblasts	McCloskey et al. (2016)
FF8 (KRRFFRRK)	Anionic membranes e.g. bacterial, and pH 9.4	β-Sheet in response to anionic vesicles mimicking bacterial membranes. Antiparallel 30%, random coil 30% (pH 7.4). Antiparallel 41%, random coil: 21% (pH 9.4), 200 μM minimum concentration tested	Nanofibers (no hydrogel)	MIC: E. coli = 25.6 μM, S. aureus = 625 μM	40% viability HeLa cells at 15 mM, (MTT assay), >100% 0.8 mM	Shen et al. (2020)
FF-OH	Heated to 90 °C and cooled (1 mg/ml)	Primarily β-sheet + unordered	Nanotubes	25 μg/ml reduced E. coli by 7.1 Log_{10} CFU/ml. MIC: R. radiobacter = 250 μg/ml, S. epidermidis = 250 μg/ml, L. monocytogenes = 125 μg/ml, E. coli = 125 μg/ml. 3 Log_{10} CFU/mL viable biofilm reduction (>99.9%) at 5 mg/mL and total biofilm kill at 10 mg/mL against S. aureus after 24 h exposure. 3 Log_{10} CFU/mL reduction 10 mg/mL E. coli and P. aeruginosa biofilms	>95% cell viability with 250 μg/ml in HEK293 and HaCaT cells	Schnaider et al. (2017), Porter et al. (2018)

Table 14.2 (continued)

Peptide name and/or sequence	Trigger for self-assembly	Secondary structure formed	Self-assembled nanostructure	Antimicrobial efficacy	Hemo/cell cytotoxicity	References
ASCP1 [(KIGAKI)$_3$-TpPG-(KIGAKI)$_3$-NH$_2$]	pH and ionic strength, Tris–HCl buffer (pH 8.8, 170 mmol/L NaCl)	β-Hairpin/antiparallel β-sheet	Hydrogel	15 mg/mL hydrogel leads to >3 Log$_{10}$ CFU/mL reduction $E.\ coli$ after 36 h incubation	Not studied	Liu et al. (2013)
ASCP2 [(KIGAKI)$_3$-TPPG-(KIGAKI)$_3$-NH$_2$]	pH and ionic strength attempted	Non-ordered, random coil	Micelles	Not studied	Not studied	Liu et al. (2013)
Surfactant-like peptides						
A$_3$K	pH, dissolution in water at 3 mM. Then pH reduced to 6.0. Critical aggregation concentration: 0.01 to 10 mM studied, not distinct.	β-Sheet	Nanosheets	No significant reduction in $E.\ coli$ and $S.\ aureus$ (0.2 mg/mL)	Not studied	Xu et al. (2009), Chen et al. (2010)
A$_6$K	pH, dissolution in water at 3 mM. Then pH reduced to 6.0. Critical aggregation concentration = ~0.2 mM	β-Sheet	Long nanofibers and worm-like micelles	35% and 45% reductions for $E.\ coli$ and $S.\ aureus$ (0.2 mg/mL)	Not studied	Xu et al. (2009), Chen et al. (2010)
A$_9$K	pH, dissolution in water at 3 mM then pH reduced to 6.0. Critical aggregation concentration = ~0.015 mM	β-Sheet	Nanorods	80% reduction $E.\ coli$; 70% reduction $S.\ aureus$ (0.1 mg/mL)	No significant haemolysis ≤0.1 mg/mL, ~55% at 0.5 mg/mL. NIH 3 T3 cells cell viability >90% at 0.005–0.1 mg/mL, 40% viability HeLa (tumour) cells (MTT assay)	Xu et al. (2009), Chen et al. (2010), Chen et al. (2012)
A$_{12}$K	Dissolved in pure water, assembled in response to anionic model membranes. Critical aggregation concentration = 0.005 mg/mL	β-Sheet (in response to model bacterial membranes)	Nanorods	Reduction in antibacterial activity relative to A$_9$K. 0.2 mg/mL A$_{12}$K could only achieve about 30% CFU reduction in $E.\ coli$ and $B.\ subtilis$, while A$_9$K achieved over 80% CFU reduction in $E.\ coli$ and $B.\ subtilis$ (1 h incubation)	Haemolysis ≤0.1 mg/mL, = <3%. NIH 3 T3 cells cell viability >90% at 0.005–0.1 mg/mL, ~75% viability HeLa (tumour) cells (MTT assay)	Chen et al. (2012)

Peptide	Self-assembly	Conformation	Nanostructure	Antibacterial activity	Cytotoxicity	References
A$_9$K$_2$	Dissolved in pure water, assembled in response to anionic model membranes. Critical aggregation concentration = 0.13 mg/mL	α-Helix (in response to model bacterial membranes)		~70% CFU reduction in *E. coli* (1 h incubation)	Haemolysis ≤0.1 mg/mL, = <3%. NIH 3 T3 cells cell viability >90% at 0.005–0.1 mg/mL, ~65% viability HeLa (tumour) cells (MTT assay)	Chen et al. (2012)
A$_6$R	Assembled in response to anionic model membranes. Critical aggregation concentration = 1.4% w/v	α-Helix	Nanotapes and nanotubes	Broad-spectrum antibacterial activity against Gram-positive *S. aureus listeria monocytogenes*, and Gram-negative *E. coli*. 75–85% reduction *E. coli* and *S. aureus* within 1 h (5 mg/mL). > 5 Log_{10} reduction *L. monocytogenes* and *E. coli*. > 3 Log_{10} reduction *S. aureus* (all 0.5% w/v)	Cell viability >50% at ≥0.5% w/v ECACC human skin fibroblast, non-significant ≥0.01% w/v (MTT assay)	Dehsorkhi et al. (2013), Hamley et al. (2013a), Castelletto et al. (2018)
CH$_3$CONH-A$_6$R (capped A$_6$R)	Assembled in response to anionic model membranes, 0.5% w/v studied	β-Sheet	Nanofibers forming hydrogels	Selective activity against the gram-positive *L. monocytogenes* = 4.7 Log_{10} reduction in CFU/ml (0.05% w/v)	Cell viability > ~55% at ≤0.5% w/v ECACC human skin fibroblast, non-significant ≤0.01% w/v (MTT assay)	Castelletto et al. (2018)
A$_9$R	Critical aggregation concentration = 0.5% w/v. forms hydrogel in water without pH adjustment	β-Sheet	Nanofibers forming hydrogels	Selective for Gram-negative *P. aeruginosa*, 4 Log_{10} reduction in CFU/ml (0.05% w/v)	Cell viability = ~60% at 0.5% w/v, ~80% at 0.005% w/v ECACC human skin fibroblast, non-significant ≤0.01% w/v (MTT assay)	Castelletto et al. (2019b)
RA$_6$R	No self-assembly in water	Absent	Soluble	Active against Gram-negative bacteria *P. aeruginosa*	Cell viability > ~55% at ≤0.5% w/v ECACC human skin fibroblast, non-significant ≤0.01% w/v (MTT assay)	Edwards-Gayle et al. (2019)
RA$_9$R	Assembles in water. Critical aggregation concentration = 0.18% w/v	Polyproline II (collagen-like) conformation up to 1% w/v, >1% w/v = β-sheet	Nanofibers (+ hydrogel) self-standing gel at ≥10% w/v	No significant antibacterial efficacy ≤0.1% w/v in *E. coli*, *S. aureus*, *P. aeruginosa*, *P. syringae*	≤0.1% w/v = >~70% cell viability ECACC human skin fibroblast (MTT assay)	Edwards-Gayle et al. (2019)

Table 14.2 (continued)

Peptide name and/or sequence	Trigger for self-assembly	Secondary structure formed	Self-assembled nanostructure	Antimicrobial efficacy	Hemo/cell cytotoxicity	References
RA$_3$R	Assembles with model anionic membranes	Polyproline II secondary structure	Nanovesicles	Selective for *L. monocytogenes* bacteria, 5.6 Log$_{10}$ reduction in CFU/mL (0.25% w/v, 1 h)	Cell viability ~35% at 0.5% w/v, ~80% at 0.005% w/v ECACC human skin fibroblast (MTT assay)	Castelletto et al. (2019a)
R$_3$F$_3$	Assembles in water. Critical aggregation concentration = 0.32% w/v	Antiparallel β-sheets	Twisted tapes	Active against *P. aeruginosa*, 3.2 Log$_{10}$ reduction in CFU/mL (0.05% w/v, 24 h). No significant reduction *E. coli* or *S. aureus*	161br human skin fibroblasts: IC$_{50}$ = 4.31 mM (4 mg/mL or 0.4% w/v	Edwards-Gayle et al. (2020)
R$_4$F$_4$	Assembles in water. Critical aggregation concentration = 0.22% w/v	Antiparallel β-sheets	Nanosheets	Active against *Pseudomonas* species, including biofilm forms. Complete kill = ~9 Log$_{10}$ reduction CFU/mL (0.05% w/v, 24 h). Biofilm reduced 37% for *P. aeruginosa* strain PA01 and 33% for strain ATCC-12600 (crystal violet assay). No significant reduction *E. coli* or *S. aureus*	161br human skin fibroblasts: IC$_{50}$ = 2.15 mM (or 2.64 mg/mL or 0.264% w/v)	Edwards-Gayle et al. (2020)
Peptide amphiphiles						
CH$_3$(CH$_2$)$_7$CO-KKK	200 µM studied in double-distilled water	Undefined	Micelle-like	Broad-spectrum antimicrobial. MICs: *E. coli* = 1.56 µM, *P. aeruginosa* = 12.5 µM, *E. cloacae* = 3.1 µM, *A. baumannii* = 12.5 µM, *S. aureus* = 3.1 µM, *E. faecalis* = 6.2 µM, *C. albicans* = 6.2 µM, *A. fumigatus* = 3.1 µM	<~10% haemolysis ≤100 µM	Makovitzki et al. (2008)

CH$_3$(CH$_2$)$_5$CO-OOWW-NH$_2$	Soluble in water ~2 mg/mL	Undefined	Undefined	Broad-spectrum including biofilms. MIC: S. epidermidis = 1.95 µg/mL, S. aureus = 0.95 µg/mL, MRSA = 1.95 µg/mL, P. aeruginosa = 1.95 µg/mL, E. coli = 7.81 µg/mL, C. tropicalis = 1.95 µg/mL	≤31.25 µg/mL >90% cell viability HaCaT cells (MTT assay)	Laverty et al. (2010)
CH$_3$(CH$_2$)$_7$CO-V$_4$K$_4$G (AKKARA)$_2$	Assemble in deionized water. Critical micelle concentration = 45 µM	β-Sheets	Nanorods (no hydrogels)	Broad-spectrum activity vs. Gram-positive and Gram-negative bacteria. Gram-negative efficacy lost below critical micelle concentration (45 µM). At 80 µM 2 Log$_{10}$ CFU/mL reduction in S. aureus and MRSA. At 60 µM 5 Log$_{10}$ CFU/mL reduction in E. coli and P. aeruginosa	≤60 µM >80% cell viability human dermal fibroblasts (MTS assay)	Chang et al. (2017)
CH$_3$(CH$_2$)$_{15}$CO-GR$_7$RGDS	Assembled in deionized water	Not defined	Nanoparticle	Active vs. Gram-positive staphylococci at 4 µM	≤12 µM no significant toxicity, ~100% kill at 160 µM, human dermal fibroblasts (MTS assay)	Mi et al. (2017)
PAF26 (Ac-RKKWFW-NH$_2$)	pH triggered (to 7.5 using NaOH). 40 mg/mL tested	β-Sheet	Nanofibers (+ hydrogel)	Effective against C. albicans (2 cm), S. aureus (1.35 cm), and E. coli (2.01 cm) 40 mg/mL tested agar diffusion	Not tested	Cao et al. (2019)
K$_2$F$_2$	pH triggered (to 7.5 using NaOH). 40 mg/mL tested	β-Sheet	Straight nanofibers (+ hydrogel)	Active against C. albicans, S. aureus, and E. coli but agar diffusion rings smaller than those for PAF26	Not tested	Cao et al. (2021)
K$_4$F$_4$	pH triggered (to 7.5 using NaOH). 40 mg/mL tested	Unordered coils	Bent nanofibers (+ hydrogel)	No evident inhibition rings against C. albicans, S. aureus, and E. coli	Not tested	Cao et al. (2021)

Table 14.2 (continued)

Peptide name and/or sequence	Trigger for self-assembly	Secondary structure formed	Self-assembled nanostructure	Antimicrobial efficacy	Hemo/cell cytotoxicity	References
R_2F_2	pH triggered (to 7.5 using NaOH). 40 mg/mL tested	β-Sheet	Straight nanofibers (+ hydrogel)	Active against *C. albicans*, *S. aureus*, and *E. coli* but agar diffusion rings smaller than those for PAF26	Not tested	Cao et al. (2021)
R_4F_4	pH triggered (to 10 using NaOH). 40 mg/mL tested	Unordered coils	Bent nanofibers (+ hydrogel)	Not tested as pH value ~10, deemed antimicrobial itself	Not tested	Cao et al. (2021)
WMR2PA=$C_{19}H_{38}O_2$-WMR (NH$_2$-WGIR$_2$ILKYG KRSA$_6$K(C$_{19}$)-CONH$_2$)	Suspended in water and sonicated ~15 mins. Critical aggregation concentration = 5 µM	Coexistence of α-helix (dominant) and β-sheet	Nanofibers	Active against biofilms of *P. aeruginosa* and *C. albicans* (both >80% eradication 50 µM, 48 h, crystal violet and XTT assays)	>70% cell viability Vero cells ≤100 µM 24 h (MTT assay)	Lombardi et al. (2019b)
Cholesterol-G$_3$R$_6$-TAT (Cholesterol-G$_3$R$_6$-YGRK$_2$R$_2$Q$_3$)	Dissolved dimethyl sulphoxide, dialysed against deionized water, then freeze-dried	β-Sheet	Nanoparticles	Active against fungi and bacteria. MICs: *S. aureus* (8.1 µM), MRSA (11.4 µM), *B. subtilis* (10.7 µM), *E. faecalis* (11.4 µM), vancomycin-resistant *Enterococcus* (4.1 µM), *S. haemolyticus* (2.0 µM), *C. albicans* 1 (13.0 µM), *C. albicans* (10.8 µM), *C. tropicalis* (13.0 µM), *C. neoformans* (8.1 µM), *S. chartarum* (11.0 µM)	In vivo: did not elevate alanine transaminase (ALT), aspartate transaminase (AST), total bilirubin, direct bilirubin, creatinine and urea nitrogen levels of meningitis rabbit model	Liu et al. (2009)
C_{16}-WILA$_2$G$_3$K$_9$-TAT	Formed in water	Not defined	Nanoparticles	Broad-spectrum including *S. aureus*. MIC: MRSA (40 µM), *S. aureus* (34 µM), *B. subtilis* (27 µM), *E. coli* (27 µM), *P. aeruginosa* (27 µM)	Haemolysis: 25 mg/L = 6%, 50 mg/L = 19% haemolysis	He et al. (2018a)

	Preparation/conditions	Secondary structure	Morphology	Antimicrobial activity	Cytotoxicity	Reference
Surfactin	Milli-Q water, sonicated at ~50 °C for 5–10 min	Lacks definition	Spherical nanomicelles	Not tested	Not tested	Hamley et al. (2013b)
Mycosubtilin	Milli-Q water, sonicated at ~50 °C for 5–10 min	Lamellar ordering with some α-helical content	Extended nanotape	Not tested	Not tested	Hamley et al. (2013b)
Plipastatin	Milli-Q water, sonicated at ~50 °C for 5–10 min	Lacks definition	Spherical nanomicelles	Not tested	Not tested	Hamley et al. (2013b)
Multidomain peptides						
MDP-1 (WK$_2$(QL)$_6$K$_2$)	Aqueous buffer. Critical aggregation concentration = 0.87 μM	Stable β-sheet	Nanofibers	Least effective MDP. MIC: E. coli (>80 μM), P. aeruginosa (>80 μM), S. aureus (>80 μM), S. epidermidis (>80 μM)	Bone marrow-derived monocytes, >1 μM significantly reduced, due to reduction of free monomers? (LDH assay)	Dong et al. (2007), Xu et al. (2015)
MDP-2 (WK$_3$(QL)$_6$K$_2$)	Aqueous buffer. Critical aggregation concentration = 1.24 μM	Unstable β-sheet, 41.4% β-sheets, 40% random coils, 18.6% α-helix	Nanofibers	MIC: E. coli (20 μM), P. aeruginosa (20 μM), S. aureus (10 μM), S. epidermidis (5 μM)	Bone marrow-derived monocytes, >1 μM significantly reduced, due to reduction of free monomers? (LDH assay)	Dong et al. (2007), Xu et al. (2015)
MDP-3 (K$_3$W(QL)$_6$K$_2$)	Aqueous buffer. Critical aggregation concentration = 1.37 μM	β-Sheet	Nanofibers	MIC: E. coli (80 μM), P. aeruginosa (80 μM), S. aureus (20 μM), S. epidermidis (10 μM)	Bone marrow-derived monocytes, >1 μM significantly reduced, due to reduction of free monomers? (LDH assay)	Dong et al. (2007), Xu et al. (2015)
K$_2$W(QL)$_6$K$_2$,	Water (4% w/v tested)	β-Sheet	Nanofibers (+ hydrogel)	MIC (in solution) S. aureus (>160 μM)	Haemolysis: <5% at ≤2% w/v (1 h)	Jiang et al. (2015)
WK$_2$(QL)$_6$K$_2$	Water (4% w/v tested)	β-Sheet	Nanofibers (+ hydrogel)	MIC (in solution) S. aureus (160 μM)	Haemolysis: <5% at ≤2% w/v (1 h)	Jiang et al. (2015)
D-W362 (wk$_3$(QL)$_6$k$_2$,	Tris buffer (20 mM, pH 7.4). Critical aggregation concentration = 7.3 μM	β-Sheet	Nanofibers (+ hydrogel)	MIC: E. coli (20 μM)	Not tested	Xu et al. (2018)

(continued)

Table 14.2 (continued)

Peptide name and/or sequence	Trigger for self-assembly	Secondary structure formed	Self-assembled nanostructure	Antimicrobial efficacy	Hemo/cell cytotoxicity	References
SAANs: (QL)$_6$-Mellitin and (QL)$_6$K co-assembly	1:1 (V/V) water and acetonitrile	β-Sheet	Nanofibers (+ hydrogel)	Increased selectivity for bacteria over mammalian cells compared to melittin alone. MIC: *E. coli*, free melittin (2.5 μM), SAANs (Mel-10%) (>80 [81 μM], SAANs (Mel-30%) (10 [3.3] μM), SAANs (Mel-50%) (10 [5] μM)	NIH/3 T3 mouse fibroblasts: 80% cell viability ≤40 μM, 70% at 80 μM (nuclear-specific dye, Hoechst assay)	Chen et al. (2019b)
WH$_5$(QL)$_6$K$_2$	Formulated in Tris buffer (pH 7.4, 20 mM) or MES buffer (pH 5.7, 20 mM). Critical aggregation concentration at pH 7.4 = 8.6 μM	pH 7.4 = β-sheet, pH 5.7 = highly disordered random coil	Nanofibers	Not tested	Not tested	Chen et al. (2019a)
WH$_7$(QL)$_6$K$_2$	Formulated in Tris buffer (pH 7.4, 20 mM) or MES buffer (pH 5.7, 20 mM). Critical aggregation concentration at pH 7.4 = 6.6 μM	pH 7.4 = β-sheet, pH 5.7 = highly disordered random coil	Nanofibers	Not tested	Not tested	Chen et al. (2019a)
WH$_9$(QL)$_6$K$_2$	pH responsive antibacterial (to acidic pH). Formulated in Tris buffer (pH 7.4, 20 mM) or MES buffer (pH 5.7, 20 mM). Critical aggregation concentration at pH 7.4 = 9.1 μM	pH 7.4 = β-sheet, pH 5.7 = highly disordered random coil	Nanofibers	MIC: Aerobic conditions = *B. fragilis* (5 μM), *E. coli* (10 μM), *S. aureus* (5 μM). Anaerobic conditions = *E. coli* (10 μM at pH 5.7, >40 μM at pH 7.4)	NIH/3 T3 cells: >80% cell viability ≤40 μM, 70% at 80 μM	Chen et al. (2019a)
O$_5$(SL)$_6$O$_5$ O=hydroxyproline	10 mg/mL forms hydrogel in water	β-Sheet in the amphiphilic (SL)$_6$ core, hydroxyproline = polyproline II helix	Nanofibers (+ hydrogel)	Not tested	Supports growth of NIH-3 T3 fibroblast cells. ~80% viability 5 days at 1% w/v	Lopez-Silva et al. (2019)

β-Hairpin peptides

MAX1 (H$_2$N-VKVKVKVK VKVpPTKV KVKVKV-CONH$_2$)	Ionic strength/salts	β-Hairpin	Nanofibers (+ hydrogel)	Broad-spectrum of pathogens: Gram-positive *S. epidermidis, S. aureus,* and *Streptococcus pyogenes* = able to inhibit the proliferation of up to 2×10^9 CFU/dm^2 for 48 h. MRSA = up to 2×10^7 CFU/dm^2. Gram-negative *Klebsiella pneumoniae* and *E. coli* = able to inhibit up to 2×10^8 CFU/dm^2	NIH -3 T3 murine fibroblasts selectively survive on 2% w/v peptide with *A. xylosoxidans* + *S. maltophilia* co-culture (visually assessed). Non-haemolytic at 2% w/v	Schneider et al. (2002), Salick et al. (2007), Salick et al. (2009)
MAX2 (H$_2$N-VKVKVKVKVKVᴰP PTKVKTKVKV -CONH$_2$)	Thermo-responsive, T$_{gel}$ ~ 40 °C	β-Hairpin	Nanofibers (+ hydrogel)	Not tested	Not tested	Pochan et al. (2003)
MAX3 (H$_2$N-VKVKVKVKT KVᴰPPTKVKTKVKV -CONH$_2$)	Thermo-responsive, T$_{gel}$ ~ 60 °C	β-Hairpin	Nanofibers (+ hydrogel)	Not tested	Not tested	Pochan et al. (2003)
MAX7 (H$_2$N-VKVKVKVK VKVpPTKVKCKVKV -CONH$_2$)	Not tested	β-Hairpin	Nanofibers (+ hydrogel)	Not tested	Not tested	Haines et al. (2005)
MAX7CNB (H$_2$N-VKVKVK VKVpPTKVKXKVKV -CONH$_2$), including α-carboxy-2-nitrobenzyl protected cysteine (labelled X)	UV responsive (λ 260–360 nm ≥ 2%w/v)	β-Hairpin	Nanofibers (+ hydrogel)	Not tested	NIH-3 T3: 2% w/v gel non-toxic (live/dead assay)	Haines et al. (2005)

(continued)

Table 14.2 (continued)

Peptide name and/or sequence	Trigger for self-assembly	Secondary structure formed	Self-assembled nanostructure	Antimicrobial efficacy	Hemo/cell cytotoxicity	References
MARG1 (H$_2$N-VKVKVR VKVpPTKVKVRVKV -CONH$_2$)	Ionic strength/salts	β-Hairpin	Nanofibers (+ hydrogel)	Active against methicillin resistant S. aureus. Unlike MAX1, it is able to inhibit the proliferation of up to 2×10^8 CFU/dm^2	Not tested	Salick et al. (2009)
PEP2R (H$_2$N-VKVKVK VRV^{D}PPTRVKVKVKV -CONH$_2$)	Ionic strength/salts	β-Hairpin	Nanofibers (+ hydrogel)	At ≥0.5% w/v = selective Gram-positive S. aureus. 2% w/v = 0% inhibition E. coli	Low haemolysis at 2% w/v (1 h)	Veiga et al. (2012)
PEP4R (H$_2$N-VKVKVR VRV^{D}PPTRVRVKVKV- CONH$_2$)	Ionic strength/salts	β-Hairpin	Nanofibers (+ hydrogel)	Broad-spectrum activity. E. coli, S. aureus, P. aeruginosa ≥ 0.5% w/v	Low haemolysis at 2% w/v (1 h)	
PEP6R (H$_2$N-VKVRVR VRV^{D}PPTRVRVRVKV -CONH$_2$)	Ionic strength/salts	β-Hairpin	Nanofibers (+ hydrogel)	Most effective PEPnR. Broad-spectrum activity. E. coli, S. aureus, P. aeruginosa ≥ 0.5% w/v	Low haemolysis at 2% w/v (1 h)	Veiga et al. (2012)
PEP8R (VRVRVRV RV^{D}PPTRVRVRVRV -CONH$_2$)	Ionic strength/salts, critical gelation concentration~0.5% w/v	β-Hairpin	Nanofibers (+ hydrogel)	Inhibits 10^5 CFU/dm^2 E. coli, S. aureus at ≥0.5% w/v (live/dead)	Increased mammalian cell toxicity relative to other PEPnR peptides. Haemolysis ~25% at 2% w/v (1 h)	Veiga et al. (2012)
Peptidomimetics						
Boc-D-Phe-γ^4-L-Phe-PEA	3 and 5 mg in DMSO (50 µL), which was then transferred to deionized water (50 µL)	β-Sheet like and random coils	Nanofibers (+ hydrogel)	Broad-spectrum antibacterial activity. 3% w/v gel = 59% inhibition vs. E. coli, 65% vs. B. subtilis, 51% vs. P. aeruginosa, and 40% vs. S. aureus after 18 h	NIH 3 T3 cells: Cell viability >80% at 3 and 5% w/v peptide gel (MTT and LDH assays)	Malhotra et al. (2018)
Boc-L-Phe-γ^4-L-Phe-PEA	Deionized water (50 µL) was added dropwise to the peptide solution in DMSO (50 µL)	CD spectra = random-coil, disordered conformation. FTIR = turn-like structures	Nanofibers (+ hydrogel)	Broad-spectrum antibacterial activity. 3% w/v gel = 66% inhibition vs. E. coli, 67% vs. B. subtilis, 71% vs. P. aeruginosa, 60% vs. S. aureus after 18 h	NIH 3 T3 cells: Cell viability >80% at 3 and 5% w/v peptide gel (MTT and LDH assays)	Malhotra et al. (2018)

bacterial membrane interactions and antibacterial activity. This was attributed to A_9K_2 forming an α-helix secondary structure in response to model bacterial membranes, whereas A_9K and $A_{12}K$ form β-sheet structures, hypothesized to be more antibacterial in this case (Chen et al. 2012). It was suggested that the predominant hydrophobic interactions within β-sheets enabled the formation of more stable peptide nanostructures in bacterial membranes, when compared with α-helices, formed primarily by intramolecular hydrogen bonding. These β-sheet, peptide-dominant, nanostructures disrupt bacterial phospholipid bilayers more effectively as the ordered aggregates described primarily in Fig. 14.1B and C.

The replacement of lysine with arginine, for example A_6R, also affects the supramolecular structure formed. A_6R forms nanotapes and nanotubes, as opposed to the nanofibers and worm-like micelles observed in the lysine variant A_6K (Dehsorkhi et al. 2013; Hamley et al. 2013a; Castelletto et al. 2018). A_6R nanotapes, derived from α-helices, demonstrate broad-spectrum antibacterial activity against Gram-positive *S. aureus*, *Listeria monocytogenes* and Gram-negative *E. coli* (Dehsorkhi et al. 2013). Capping A_6R with CH_3CONH, forming $CH_3CONH\text{-}A_6R$, enables the creation of peptide nanofibers derived from β-sheets, possessing more selective activity against the Gram-positive *L. monocytogenes* (Castelletto et al. 2018). A_9R possessed sufficient β-sheet formation to drive hydrogel-forming ability alongside antibacterial activity. This was demonstrated to be more selective for Gram-negative *P. aeruginosa* than Gram-positive pathogens (Castelletto et al. 2019b). The addition of an extra arginine at each peptide terminal, forming RA_6R and RA_9R (Edwards-Gayle et al. 2019), provided sufficient charge to RA_6R that it did not self-assemble in water due to its high solubility but it was active against Gram-negative *P. aeruginosa*. RA_9R was able to form ordered β-sheet nanofibers due to sufficient hydrophobicity provided by nine central alanine residues. However, it possessed relatively little antibacterial activity. In a separate study by the Castelletto and Hamley groups, RA_3R formed nanovesicles selective for *L. monocytogenes* bacteria vs. *E. coli*, *S. aureus* and mammalian skin fibroblast cells (Castelletto et al. 2019a). More recently short peptide sequences containing hydrophobic phenylalanines (F) and cationic arginines (R), R_3F_3 and R_4F_4, were studied (Edwards-Gayle et al. 2020). Despite subtle differences in their primary structures, R_3F_3 formed twisted tapes and R_4F_4 nanosheets, each assumed to be derived from antiparallel β-sheets. Both R_3F_3 and R_4F_4 were active against *Pseudomonas* species, with R_4F_4 demonstrating antibiofilm activity. The observations outlined for surfactant-like peptides demonstrate the commonly complicated and unpredictable correlation among peptide charge, hydrophobicity, nanostructure formation and antimicrobial activity that exists throughout the antimicrobial peptide field, but especially within short, low molecular weight motifs.

14.5.2   Peptide Amphiphiles

Peptide amphiphiles share structural similarities to surfactant-like peptides; however, their hydrophobic character tends to be provided by a lipophilic, most

commonly alkyl tail of 8–16 carbons in length, rather than a sequence of amino acid residues. Therefore, they may also be classified as forms of lipopeptide. Some of the most promising early studies in this area were conducted by the Shai group (Makovitzki et al. 2007). Their $CH_3(CH_2)_nCO$-KXK lipopeptide motif (where X = A, L, G or K) was particularly potent, possessing broad-spectrum antimicrobial activity when palmitic acid was conjugated to a KKK peptide sequence (Makovitzki et al. 2008). The substitution of L-enantiomers with D-forms had no significant impact on in vitro efficacy, although it is feasible, this may improve in vivo biostability against proteolytic enzymes. This study was followed by our own work, whereby the unnatural amino acid ornithine (O) was included in an ultrashort amphiphilic lipopeptide sequence $CH_3(CH_2)_nCO$–OOWW–NH_2, where $n = 6$–18. $CH_3(CH_2)_5CO$–OOWW–NH_2 was particularly potent, demonstrating broad-spectrum activity against planktonic and biofilm forms of bacteria and fungi implicated in nosocomial infection (Laverty et al. 2010). The assembled nature and secondary structure of these sequences have not been fully elucidated. Due to their soluble nature, it is unlikely they form any defined nanostructures.

The Webster group has been involved in several interesting studies involving peptide amphiphiles. They utilized a $CH_3(CH_2)_7CO$–V_4K_4G peptide amphiphile and attached a heparin-binding motif $(AKKARA)_2$ to improve binding to bacteria cell membranes (Chang et al. 2017). $CH_3(CH_2)_7CO$–$V_4K_4G(AKKARA)_2$ self-assembled into β-sheet-forming nanorods. While unable to form hydrogels, assembled nanorods demonstrated broad-spectrum activity against both Gram-positive and Gram-negative bacteria. Efficacy against Gram-negative pathogens was lost when $CH_3(CH_2)_7CO$–$V_4K_4G(AKKARA)_2$ was tested below its critical micelle concentration (45 μM), in its non-assembled form. Interestingly binding to lipopolysaccharide, a major component of the outer membrane of Gram-negative bacteria, was shown to be significantly increased in its nanorod form, suggesting lipopolysaccharide may be a key target in the antibacterial efficacy of assembled forms of peptides. The Webster group was also able to form an arginine-rich amphiphilic self-assembled peptide nanoparticle $CH_3(CH_2)_{15}CO$–GR_7RGDS with activity against Gram-positive staphylococci (Mi et al. 2017). Cationic arginine improved bacterial membrane interactions, with the attached lipophilic sequence driving self-assembly. The arginine-glycine-aspartic acid-serine (RGDS) was employed as a common cell recognition motif. The authors stated this motif improved interactions with mammalian cells and competitively reduced bacterial adherence to the adhesive protein fibronectin. Fibronectin is utilized by bacteria to facilitate attachment and drive biofilm formation. It is commonly found on the surfaces of healthy cells and also the host conditioning film laid down upon implanted medical devices (Laverty et al. 2015).

The Cao group recently studied an amphipathic antimicrobial hexapeptide PAF26 (Ac-RKKWFW-NH_2) and variations on this sequence. PAF26 was able to self-assemble into an injectable hydrogel formed from β-sheets, again with potential use in wound-healing applications due to its effectiveness against *Candida albicans*, *S. aureus* and *E. coli* (Cao et al. 2019). A follow-on study by the group (Cao et al. 2021), focussing on four PAF26 derivatives K_2F_2, K_4F_4, R_2F_2 and R_4F_4, found that

while all derivatives formed nanofibers, peptides with more hydrophobic and cationic residues i.e. K_4F_4 and R_4F_4, had unordered coiled secondary structures, leading to the formation of bent nanofibers. Peptides K_2F_2 and R_2F_2, with a reduced number of hydrophobic and cationic residues, formed more ordered β-sheets with straight nanofibers. K_4F_4 demonstrated reduced efficacy against *C. albicans*, *S. aureus* and *E. coli*. This was attributed to increased crosslinks between K_4F_4 molecules, meaning K_4F_4 could not diffuse as readily from formed hydrogels in order to generate antimicrobial activity.

Peptide amphiphiles can also result from shortening or modifying naturally occurring antimicrobial peptides. WMR (WGIRRILKYGKRS-NH$_2$), a variant of the marine peptide myxinidin, was able to self-assemble into antimicrobial nanofibers upon the covalent attachment of a hydrophobic, aliphatic $C_{19}H_{38}O_2$ sequence (Lombardi et al. 2019b). This peptide amphiphile possessed activity not only against biofilm forms of the Gram-negative bacteria *P. aeruginosa* but also fungal biofilms of *C. albicans*. Liu and colleagues developed amphiphilic peptide nanoparticles from a modified form of the transcriptional activator TAT protein of human immunodeficiency virus type-1 (HIV-1) (Liu et al. 2009). TAT is a promising peptide for enhancing intracellular delivery of therapeutic cargo due to its strong cell-surface binding (Wadia et al. 2004; Fu et al. 2015). The TAT (YGRK$_2$R$_2$Q$_3$) peptide was attached to a short amphiphilic sequence containing lipophilic cholesterol, a tri-glycine spacer and six arginines, forming cholesterol-G_3R_6-YGRK$_2$R$_2$Q$_3$ (cholesterol-G_3R_6-TAT) micelles. These nanoparticles were proven to target a range of fungi and bacteria, including those implicated in meningitis, due to an increase in the peptide's density of localized cationic charge. The authors hypothesized that these nanoparticles were capable of crossing the blood–brain barrier by adsorptive endocytosis due to the presence of TAT on the nanoparticle surface. Overcoming the blood–brain barrier is a major challenge in addressing infections of the central nervous system. Follow-on work by He et al, studied the attachment of TAT to the cationic peptide PA-28, creating C_{16}-WILA$_2$G$_3$K$_9$-TAT (He et al. 2018a). This also self-assembled into nanoparticles of ~150 nm size with broad-spectrum antibacterial activity, including the ability to cross blood–brain barrier to reduce *S. aureus* brain infection in rat models. In a separate work, the Hamley group characterized the self-assembled nanostructures of the three amphiphilic lipopeptides surfactin, mycosubtilin and plipastatin derived from *Bacillus subtilis* (Hamley et al. 2013b). This is of interest in the wider production of new antimicrobial therapies, given the use of bacteria as vectors in the fermentation of proteins and peptide manufacture. These amphiphilic peptides were also capable of self-assembling into a variety of nanostructures Plipastatin and surfactin formed spherical nanomicelles of 2 nm diameter but mycosubtilin formed a very different extended nanotape structure, most likely from β-sheet formation. The differences were attributed to significant changes in the peptide headgroup and alkyl chain branching of mycosubtilin that alerted its surfactant packing parameter (ratio of the areas hydrophobic: hydrophilic portions of the molecule) relative to plipastatin and surfactin.

A different subset of peptide amphiphiles consist of an alternating sequence of cationic, hydrophobic and anionic amino acids. The RADA16 peptide is perhaps the

best-known example, whereby arginine (R), alanine (A) and aspartic acid (D) provide the cationic, hydrophobic and anionic character, respectively. RADA16's intermolecular interactions are sufficiently strong to enable it to self-assemble and form hydrogel that have been widely studied within regenerative medicine and a haemostatic dressing (Wang et al. 2019). To our knowledge, its antimicrobial activity has not been tested.

14.5.3 Multidomain Peptides

The antimicrobial activity and self-assembling properties of multidomain peptides (MDP) are due to a central amphiphilic unit (designated B) surrounded by two separate charged end groups (labelled A) within an ABA structure. Examples include $K_n(QL)_6K_2$, $WH_n(QL)_6K_2$, $K_nW(QL)_6K_2$, $K_n(SL)_6K_n$ and $H_3(QL)_6K_2$. Research in this field has been driven by the Dong and Hartgerink groups. They developed and established the antibacterial properties of MDP-1 ($WK_2(QL)_6K_2$), MDP-2 ($WK_3(QL)_6K_2$) and MDP-3 ($K_3W(QL)_6K_2$) (Dong et al. 2007; Xu et al. 2015). MDP-1 demonstrated improved broad-spectrum antibacterial activity compared to MDP-2 and MDP-3, despite sharing the same overall charge, due to its ability to fully form stable β-sheet nanofibers. They have also suggested a link between improved antibacterial efficacy, bacterial selectivity vs. mammalian cells and the formation of self-assembled supramolecular structures derived from β-sheets, including hydrogels (Jiang et al. 2015; Xu et al. 2018). Modifications to the original MDP sequences, $K_2W(QL)_6K_2$, $WK_2(QL)_6K_2$ and D-W362 ($wk_3(QL)_6k_2$), enabled hydrogel formation due to the presence of more densely packed β-sheet nanofibers. It was hypothesized that these inferred antibacterial activity by entrapping bacteria, reducing their mobility and increasing their exposure to areas of dense localized charge. Attaching the naturally occurring antimicrobial peptide melittin to $(QL)_6$ and formulating it 1:1 with $(QL)_6K$ created a $(QL)_6$-Mel and $(QL)_6K$ β-sheet nanofiber co-assembly with reduced toxicity and increased selectivity for bacteria over mammalian cells compared to melittin alone. This was attributed to changes in melittin's confirmation, notably reduced hydrophobic interactions with mammalian cell membranes, when presented on the MDP nanofiber surface (Chen et al. 2019b). Improved hemocompatibility, important for biomaterial applications, can be achieved by covalent conjugation of polyethylene glycol (PEGylation) but only to MDPs that fully form β-sheet nanofiber architectures (Xu et al. 2016). Further work by the Dong group enabled pH responsiveness to be introduced to MDP motifs via substitution of lysine residues with histidine, forming $WH_5(QL)_6K_2$, $WH_7(QL)_6K_2$ and $WH_9(QL)_6K_2$ (Chen et al. 2019a). Acidic pH is a valid trigger for some infections given its link to the host's immune response to infection (phagocytosis) and fermentation in anaerobic bacteria. $WH_9(QL)_6K_2$ was particularly effective. At acidic pH, below the pK_a of histidine, peptides become positively charged. This results in electrostatic repulsion between MDPs, effectively destabilizing formed nanofibers and releasing MDPs which kill *Bacteroides fragilis,*

E. coli and *S. aureus* under anaerobic conditions. Antibacterial activity was demonstrated to be pH dependent. The Hartgerink group studied an alternative MDP whereby glutamine (Q) in the central amphiphilic unit i.e. B, was replaced with serine (S), forming $(SL)_6$. End groups were also varied, composed of several hydroxyproline residues designated O_n, creating an $O_n(SL)_6O_n$ ($n = 1–6$) structure (Lopez-Silva et al. 2019). Only $O_5(SL)_6O_5$ formed a hydrogel, achieving an optimal balance of fibre length, rigidity and solubility, supporting the growth of fibroblast cells. The MDPs SL: $K_2(SL)_6K_2$ and SLac: $K(SL)_2(SLRG)(SL)_3K(GRGDS)$ have been similarly studied by the group for a range of biomedical applications, most notably cytokine delivery (Kumar et al. 2015) and tissue engineering applications (Galler et al. 2010). Their antimicrobial activity has so far not been tested.

14.5.4   β-Hairpin Peptides

The β-hairpin class of hydrogel-forming antimicrobial peptides elucidated by Schneider and Pochan is among the most seminal work in this field (Schneider et al. 2002). They are composed of two alternating peptide sequences of eight alternating amino acids, joined by a central L-valine-D-proline-L-proline-L-threonine (VpPT) motif (Salick et al. 2007; Salick et al. 2009). This central sequence forms a type II' β-turn under specific conditions, for example, increased ionic strength i.e. in cell media containing salts, resulting in an amphiphilic β-hairpin that can result in hydrogel formation if intermolecular interactions are sufficiently strong. The concept of harnessing repeating hydrophobic and cationic units to provide antimicrobial activity is well established for other classes of antimicrobial peptides. For example, within the $(RW)_n$ group of peptides, where although no true secondary structure could be elucidated, the impact of chain length was deemed important to bacterial selectivity and efficacy with $(RW)_3$ optimal (Liu et al. 2007). The original MAX1 peptide is composed of alternating valine and cationic lysine residues (H_2N-VKVKVKVKVpPTKVKVKVKV-$CONH_2$) and demonstrated activity against a broad-spectrum of pathogens implicated in hospital infections, including Gram-positive *S. epidermidis*, *S. aureus* and *Streptococcus pyogenes* and Gram-negative *Klebsiella pneumoniae* and *E. coli* (Salick et al. 2007). MAX1 was capable of selectively inhibiting bacterial growth in co-cultures of NIH3T3 fibroblasts and *Achromobacter xylosoxidans* and *Stenotrophomonas maltophilia* bacteria. The presence of cationic residues again proved to be important for the disruption of bacterial membranes by a mechanism of 'contact killing'.

This work has resulted in several variants of MAX1, primarily MARG1 and PEPnR, whereby the cationic amino acid is varied and valine is retained. MARG1 contains six lysine and two arginine residues and is active against MRSA (Salick et al. 2009). MARG1 gels are shear-thinning, enabling delivery and gel recovery by syringe, for improved ease of administration to infected skin and tissue sites. PEPnR represents a sequential increase in the number of lysine to arginine substitutions e.g. PEP6R refers to a 20 amino acid containing peptide whereby arginine replaces

six lysine residues (H$_2$N-VKVRVRVRV^{D}PPTRVRVRVKV-CONH$_2$) (Veiga et al. 2012). PEP4R, PEP6R and PEP8R all demonstrated similar broad-spectrum activity; however, PEP2R was only active against Gram-positive *S. aureus*, indicating at least four arginines were required to extend the activity to Gram-negatives. Increased mammalian cell toxicity was observed with PEP8R, suggesting PEP6R provided optimal characteristics especially since it also possessed the highest gel strength. Several other changes have been made to the MAX1 motif mainly to alter its gel trigger (ionic strength, salt), widening its range of use in biomedical applications. These include improved thermo-responsiveness by substitution of some valine residues with the less hydrophobic amino acid threonine, creating MAX2 (H$_2$N-VKVKVKVKV^{D}PPTKVKTKVKV-CONH$_2$) and MAX3 (H$_2$N-VKVKVKTKV^{D}PPTKVKTKVKV-CONH$_2$) (Pochan et al. 2003). The exact temperature at which self-assembly was triggered (T$_{gel}$) increased with a decrease in hydrophobic character. MAX2 demonstrated a T$_{gel}$ ∼ 40 °C, 20 °C less than MAX3 (T$_{gel}$ ∼ 60 °C). A MAX peptide whereby hydrogel formation is triggered by UV irradiation was also developed by including a α-carboxy-2-nitrobenzyl protected cysteine (labelled X) in a MAX7 sequence (H$_2$N-VKVKVKVKVpPTKVKCKVKV-CONH$_2$). This created a photocaged peptide MAX7CNB (H$_2$N-VKVKVKVKVpPTKVKXKVKV-CONH$_2$) that self-assembles into a hydrogel at 2% w/v upon irradiation between λ 260 and 360 nm (Haines et al. 2005). Whether light can act as an antimicrobial trigger for such a peptide system would be an interesting hypothesis for future study and could be harnessed as a tool for biomaterial development e.g. ocular materials/contact lenses.

14.6   Increasing In Vivo Longevity

Despite the plethora of research into the area of self-assembling peptides displaying antimicrobial action and indeed the positive results attained in initial studies, there have been a few peptide-based therapeutics to reach the clinic. Polymyxins, a series of cationic lipopeptides, are likely the most notable peptide-based therapeutic to reach patients (Landman et al. 2008). Several avenues of research have focussed on extending their spectrum of activity to Gram-positives, reducing potential for toxicity and improving their larger-scale manufacturer and ease of synthesis (Grau-Campistany et al. 2016; Huwaitat et al. 2021). Similarly natural peptides such as human cathelicidin LL-37 serve as a starting template for improved synthetic variants e.g. OP-145 (Malanovic et al. 2015). While natural form L-α-amino acids have served as a prosperous starting block for peptide-related research, they suffer from several limitations as systemic or localized therapeutics. These include the following: limited bioavailability; low stability and rapid proteolytic degradation and clearance systemically (Gentilucci et al. 2006). Indeed, Thapa and colleagues highlighted that 'bare' antimicrobial peptides have limited activity following topical application owing to their susceptibility to environmental (hydrolysis, oxidation, photolysis) and wound (pH, proteolysis) related conditions (Thapa et al. 2020). The

formulation of antimicrobial peptides into more robust systems or modification of the primary sequence is therefore essential to enhance stability, prolong delivery and optimize effectiveness. In order to overcome these problems, there has been an increasing focus on the development of non-native sequences which retain all the advantages of parent peptide sequences, while overcoming rapid proteolytic degradation. The stability of promising synthetic sequences is typically improved by cyclization or insertion of non-proteinogenic building blocks, including D-amino acids, peptoids (N-substituted glycines) and other peptidomimetics such as α-peptide/β-peptides (Molchanova et al. 2017; Lone et al. 2019). Approaches to achieve stability typically rely on post-synthetic modification of traditional sequences or the synthesis of modified sequences that recapitulate the desirable properties while enhancing stability. Post-synthetic modification approaches include the protection of the carboxy or amino terminus and cyclization, which is often successful at inhibiting degradation by carboxy- and aminopeptidases in vivo (Henninot et al. 2018). The introduction of isosteric groups during synthesis has resulted in various peptidomimetic classes that involve either partially or totally replacing peptide backbones with non-natural oligomeric units (Liskamp et al. 2011). Some of these approaches are outlined below.

14.6.1 D-α-Form Amino Acids

In D-α-form amino acids, the corresponding enantiomers of native L-counterparts are relatively simple to synthesize and share identical chemical and physical properties to their parent L-α-form but differ in the direction in which they rotate plane-polarized light (Feng and Xu 2016). A simple modification such as this is often sufficient to improve stability and enhance residence times since D-α-form amino acids rarely act as the substrates for endogenous proteolytic enzymes. For example, Lone and colleagues developed an antimicrobial octapeptide sequence composed entirely of D-α-monomers with clinically significant activity demonstrated against *Acinetobacter baumannii*, *E. coli*, *P. aeruginosa* and *S. aureus*. It was postulated to have enhanced resistance to degradation owing to the use of non-native residues (Lone et al. 2019). Bactenecin is a 12-amino acid cyclic cationic antimicrobial peptide that contains one intramolecular disulphide bond. Sim et al. synthesized various bactenecin analogues by several approaches, including amino acid substitution, use of the D-enantiomeric forms, and lipidation to overcome low bioavailability under physiological conditions (Sim et al. 2019). Their results revealed that a fatty acid-acylated D-form of cyclic bactenecin was most effective against Gram-positive and Gram-negative bacteria, including some drug-resistant bacteria such as MRSA, multi-drug resistant *P. aeruginosa* and *A. baumannii* and suggested that the structure may serve as an effective template for the design of novel therapeutic lipopeptide antibiotics. Zhong et al. attached fatty acid chains of various lengths to the side chains of D-α-monomers within peptide sequences (Zhong et al. 2020). The sequences exhibited excellent in vitro protease stability and antimicrobial activity

against multi-drug-resistant bacteria, such as MRSA, with fatty acid chains of 8–12 carbons in length presenting preferable antimicrobial selectivity and antibiofilm activity. They suggested the likely mechanism of action to result from membrane permeabilization by typical non-receptor mediated mechanisms but also suggested some intracellular activity by identifying an affinity for the sequences to bind to bacterial genomic DNA. The authors highlighted the low tendency to develop bacterial resistance in the presence of repeated sub-therapeutic doses and went on to prove their in vivo antimicrobial potency.

14.6.2 Other Peptidomimetics

Various peptide analogues have been developed through the introduction of unusual residues such as β-amino acids, γ-amino acids and δ-amino acids. Substitutions of α-amino acids with β-forms elongate the peptide backbone by one carbon (–CH_2) with a further additional carbon (two) being added in the case of γ and three for δ. Consequently, the bulky R-group attached to the carbon in these analogues often exhibits higher rotational freedom, thereby enhancing flexibility and thermodynamic stability (Trabocchi and Guarna 2005). Malhotra and colleagues reported a broad-spectrum antibacterial activity of proteolytically stable self-assembled α/γ-hybrid peptide gels (Malhotra et al. 2018). The sequences Boc-D-Phe-γ⁴-L-Phe-PEA and Boc-L-Phe-γ⁴-L-Phe-PEA displayed resistance against the proteolytic enzymes proteinase K, pepsin and chymotrypsin with the sequence containing D-Phe displaying greater resistance owing to reduced recognition. Mechanistic studies into the exact mechanism of antimicrobial action indicated bacterial cell entrapment within the hydrogel matrix, interaction with the cell membrane and subsequent cell lysis. Dewangan et al. reported the synthesis of an α/β-diastereomeric peptidomimetic based on an α-helical template which was resistant to enzymatic degradation by trypsin and proteinase K while displaying antimicrobial action (Dewangan et al. 2018). A broad-spectrum antimicrobial activity was observed in vitro against pathogens including MRSA and methicillin-resistant *S. epidermidis* (MRSE) and in an in vivo murine model using MRSA.

14.6.3 Peptoids

Peptoids are oligomers of *N*-substituted glycines in which the side chain is appended to the amide nitrogen rather than the α-carbon as in a typical peptide sequence. This renders the backbone achiral and flexible while bestowing resistance to degradation by endogenous proteases (Simon et al. 1992; Saini 2017). The loss of the amide hydrogen in the peptoid sequence means that the ability to form hydrogen bonds within the secondary sequence is lost meaning they are generally stabilized by backbone and steric constraints (Armand et al. 1997). The Zuckermann group has,

however, proven the self-assembly of peptoid structures to form stable nanosheets in water despite the loss of hydrogen bonding capacity (Nam et al. 2010; Kudirka et al. 2011). Chongsiriwatana et al. investigated the development of peptoids that could mimic the structure, function and mechanism of parent helical antimicrobial peptide sequences (Chongsiriwatana et al. 2008). They found that such peptoid sequences demonstrated a similar antimicrobial activity as the parent compound in the presence of a range of clinically relevant pathogens and attributed this to similar levels of hydrophobicity and net cationic charge. The group went investigated the mechanism of bacterial killing by peptoid systems and found that peptoids and other antimicrobial peptide sequences could trigger extensive, rapid non-specific aggregation of intracellular biomacromolecules resulting in microbial death (Chongsiriwatana et al. 2017). They suggested that bacterial death was not achieved solely as a result of membrane disruption as previously thought but rather that the peptoid and indeed other antimicrobial peptide sequences could penetrate cells causing intracellular polyanions, vital to many cellular processes, to flocculate. This disrupts spatial organization, diffusion and accessibility of cytoplasmic components with these changes thought to be sufficient to halt growth and, in many cases, kill bacteria altogether. This suggested mechanism, like that of membrane disruption, is unlikely to result in the development of rapid bacterial resistance since there is no a specific intracellular target, with intracellular polyanions likely to be conserved as they are crucial to cell functioning.

There have been reports of pure peptoid formulations with the capacity to self-assemble, for example, as reported in work by the Zuckermann group. More often it is necessary to include a peptide portion within the sequence to enable self-assembly to proceed. Self-assembly of the sequence itself is often an important consideration in the development of novel antimicrobial nanomaterials as this will dictate the mode of delivery and often the duration of action. Wu et al. investigated the formation of molecular hydrogels using pure peptoid sequences in spite of the lack of hydrogen bonding capacity (Wu et al. 2012). They were unsuccessful but formed hydrogels by developing peptoid–peptide conjugates based on tetra-phenylalanine ((Phe)$_4$), a known gelation motif, with the corresponding peptoid monomers used ((NPhe)$_4$). The peptoid sequence was coupled to various bioactive tripeptides, using glycine as a linker in each case. Frederiksen and colleagues investigated the development of peptide–peptoid hybrid oligomers and explored how the peptoid chain length, hydrophobicity and cationic nature affected antibacterial activity (Frederiksen et al. 2019). As a general trend, they found that increased cationic side chain length resulted in reduced hydrophobicity since the amino functionalities were more accessible to the surroundings i.e. there was a lower shielding effect. The peptidomimetics were tested against a range of Gram-positive and Gram-negative microorganisms with varying results. Interestingly all tested analogues were active against *E. coli* with the two least hydrophobic structures having reducing activity indicating that there may be a hydrophobicity threshold necessary for activity against *E. coli*. Aside from this, there emerged no clear design rules regarding sequence optimization for antimicrobial activity with only slight increase in potency observed with increasing hydrophobicity reported suggesting that the development of novel

antimicrobial systems using peptoid-peptide hybrids continues to be a largely serendipitous process. Molecular modelling does, however, continue to play a role in the development of novel antimicrobials as evidenced by Czyzewski and colleagues who reported a successful QSAR model based on 27 diverse peptoid sequences that could accurately correlate antimicrobial peptoid structure with antimicrobial activity (Czyzewski et al. 2016). The in vitro antibacterial activity of these peptoids was compared to two clinically relevant antimicrobial peptides and four broad-spectrum antibiotics. Several peptoids exhibited enhanced potency with respect to their comparators against pathogenic and multi-drug-resistant bacteria. Interestingly the use of a lipopolysaccharide assay demonstrated that peptoids are capable of interacting with the polyanionic component of Gram-negative bacterial cell walls to a similar extent as parent peptides indicating that they may indeed represent a viable novel approach to the development of biologically stable antimicrobial nanomaterials.

14.7   Conclusions and Future Perspectives

It has been estimated that without significant intervention, the global death toll as a result of antimicrobial resistance will reach ten million by 2050 (Ghosh et al. 2019). The fight against antimicrobial resistance is therefore constant and the discovery of novel antimicrobial agents is critical. The research presented in this chapter highlights a paradigm shift in the field of novel antimicrobials away from the development of new small drug entities and towards the development of innovative nanomaterial strategies. Antimicrobial peptide-based nanomaterials are well placed to meet this need due to their rapid, broad-spectrum activity in addition to their low tendency for resistance development. Despite the significant promise they herald, there are a few antimicrobial peptide products on the market currently. In order to advance the field of antimicrobial peptide nanomaterials and propel these agents towards clinical approval, several hurdles will need to be addressed and surmounted. Of critical importance will be overcoming issues with rapid degradation which are beginning to be addressed by the various peptidomimetic strategies being researched, as discussed. The use and development of combinatorial libraries and computational systems for peptide sequence analysis may encourage the exposure of new peptides with inherent antimicrobial activity and be used to enhance the activity of already existing bioactive molecules via synthetic modifications (Giuliani and Rinaldi 2011). In addition to this, improvement and refinement of synthetic techniques which are more amenable to upscale producing sequences in adequate quantities and of high purity will be needed if such materials are to receive enthusiastic support from industrial manufacturers. The focus on ultrashort sequences is, however, promising since these materials will offer reduced time and costs associated with manufacture.

   Most studies undertaken to date to assess the biocompatibility and/or cytotoxicity of peptide nanomaterials towards human or animal cells focus on in vitro cell culture

assay. While in vitro studies yield important information and offer a series of advantages including the ability to test directly on human cells; high sensitivity of cultured cells to toxic agents; the capacity to investigate specific interactions at a cellular level and the ability to perform a range of experiments under the same conditions. There are, however, disadvantages to using such techniques including the relatively short culture times governed by the finite lifespan of cultured cells and the vast simplification of the in vitro system compared to that of an in vivo scenario (Pizzoferrato et al. 1994). Nonetheless, these initial studies are still considered a crucial starting point in defining biocompatibility and cytotoxicity often proving to be time-saving and cost-effective in the long run by reducing the likelihood of toxic materials passing on to further investigations and in vivo modelling and ultimately failing at a later stage. Robust in vivo modelling systems that accurately and closely replicate human infection will be required in order to reduce failures at the clinical trial stage.

Research continues to bloom surrounding the field of antimicrobial resistance with peptides being used for increasingly innovative techniques. Kuru et al. recently reported the use of a fluorescently labelled D-α-amino acid-based peptidoglycan sequence capable of inserting itself within the bacterial peptidoglycan layer during cell membrane synthesis (Kuru et al. 2019). This provides a powerful method for observing morphological changes within the cell membrane and since it is a common target for antimicrobial therapeutics could prove a valuable tool in understanding the role of peptidoglycan in overall bacterial cell morphology therefore enabling the development of targeted novel antimicrobials to treat drug-resistant infections. The numerous examples of approaches to develop novel antimicrobial peptide-based therapeutics is encouraging and cements their place within the race to overcome antimicrobial resistance, reaffirming the hope that they will reach the clinic as novel therapeutics.

References

Armand P, Kirshenbaum K, Falicov A, Dunbrack RL, Dill KA, Zuckermann RN, Cohen FE (1997) Chiral N-substituted glycines can form stable helical conformations. Fold Des 2:369–375

Arouri A, Dathe M, Blume A (2009) Peptide induced demixing in PG/PE lipid mixtures: A mechanism for the specificity of antimicrobial peptides towards bacterial membranes? Biochimica et Biophysica Acta (BBA) - Biomembranes 1788:650–659

Barua S, Yoo J-W, Kolhar P, Wakankar A, Gokarn YR, Mitragotri S (2013) Particle shape enhances specificity of antibody-displaying nanoparticles. Proc Natl Acad Sci U S A 110:3270–3275

Brogden KA (2005) Antimicrobial peptides: pore formers or metabolic inhibitors in bacteria? Nat Rev Microbiol 3:238–250

Cao F, Mei L, Zhu G, Song M, Zhang X (2019) An injectable molecular hydrogel assembled by antimicrobial peptide PAF26 for antimicrobial application. RSC Adv 9:30803–30808

Cao F, Ma G, Song M, Zhu G, Mei L, Qin Q (2021) Evaluating the effects of hydrophobic and cationic residues on antimicrobial peptide self-assembly. Soft Matter 17:4445–4451

Castelletto V, Barnes RH, Karatzas K-A, Edwards-Gayle CJC, Greco F, Hamley IW, Rambo R, Seitsonen J, Ruokolainen J (2018) Arginine-containing surfactant-like peptides: interaction with lipid membranes and antimicrobial activity. Biomacromolecules 19:2782–2794

Castelletto V, Barnes RH, Karatzas K-A, Edwards-Gayle CJC, Greco F, Hamley IW, Seitsonen J, Ruokolainen J (2019a) Restructuring of lipid membranes by an arginine-capped peptide bolaamphiphile. Langmuir 35:1302–1311

Castelletto V, Edwards-Gayle CJC, Hamley IW, Barrett G, Seitsonen J, Ruokolainen J (2019b) Peptide-stabilized emulsions and gels from an arginine-rich surfactant-like peptide with antimicrobial activity. ACS Appl Mater Interfaces 11:9893–9903

Chan DI, Prenner EJ, Vogel HJ (2006) Tryptophan- and arginine-rich antimicrobial peptides: structures and mechanisms of action. Biochimica et Biophysica Acta (BBA) - Biomembranes 1758:1184–1202

Chang R, Subramanian K, Wang M, Webster TJ (2017) Enhanced antibacterial properties of self-assembling peptide amphiphiles functionalized with heparin-binding cardin-motifs. ACS Appl Mater Interfaces 9:22350–22360

Chen C, Pan F, Zhang S, Hu J, Cao M, Wang J, Xu H, Zhao X, Lu JR (2010) Antibacterial activities of short designer peptides: a link between propensity for nanostructuring and capacity for membrane destabilization. Biomacromolecules 11:402–411

Chen C, Hu J, Zhang S, Zhou P, Zhao X, Xu H, Zhao X, Yaseen M, Lu JR (2012) Molecular mechanisms of antibacterial and antitumor actions of designed surfactant-like peptides. Biomaterials 33:592–603

Chen W, Li S, Renick P, Yang S, Pandy N, Boutte C, Nguyen KT, Tang L, Dong H (2019a) Bacterial acidity-triggered antimicrobial activity of self-assembling peptide nanofibers. J Mater Chem B 7:2915–2919

Chen W, Yang S, Li S, Lang JC, Mao C, Kroll P, Tang L, Dong H (2019b) Self-assembled peptide nanofibers display natural antimicrobial peptides to selectively kill bacteria without compromising cytocompatibility. ACS Appl Mater Interfaces 11:28681–28689

Chen J, Shi X, Zhu Y, Chen Y, Gao M, Gao H, Liu L, Wang L, Mao C, Wang Y (2020) On-demand storage and release of antimicrobial peptides using Pandora's box-like nanotubes gated with a bacterial infection-responsive polymer. Theranostics 10:109–122

Chongsiriwatana NP, Patch JA, Czyzewski AM, Dohm MT, Ivankin A, Gidalevitz D, Zuckermann RN, Barron AE (2008) Peptoids that mimic the structure, function, and mechanism of helical antimicrobial peptides. Proc Natl Acad Sci U S A 105:2794–2799

Chongsiriwatana NP, Lin JS, Kapoor R, Wetzler M, Rea JAC, Didwania MK, Contag CH, Barron AE (2017) Intracellular biomass flocculation as a key mechanism of rapid bacterial killing by cationic, amphipathic antimicrobial peptides and peptoids. Sci Rep 7:16718

Cross ER, Coulter SM, Fuentes-Caparrós AM, Mcaulay K, Schweins R, Laverty G, Adams DJ (2020) Tuning the antimicrobial activity of low molecular weight hydrogels using dopamine autoxidation. Chem Commun 56:8135–8138

Cross ER, Coulter SM, Pentlavalli S, Laverty G (2021) Unravelling the antimicrobial activity of peptide hydrogel systems: current and future perspectives. Soft Matter 17:8001–8021

Czyzewski AM, Jenssen H, Fjell CD, Waldbrook M, Chongsiriwatana NP, Yuen E, Hancock REW, Barron AE (2016) In vivo, in vitro, and in silico characterization of peptoids as antimicrobial agents. PLoS One 11:e0135961

Dartois V, Sanchez-Quesada J, Cabezas E, Chi E, Dubbelde C, Dunn C, Granja J, Gritzen C, Weinberger D, Ghadiri MR, Parr TR, JR. (2005) Systemic antibacterial activity of novel synthetic cyclic peptides. Antimicrob Agents Chemother 49:3302–3310

Dehsorkhi A, Castelletto V, Hamley IW, Seitsonen J, Ruokolainen J (2013) Interaction between a cationic surfactant-like peptide and lipid vesicles and its relationship to antimicrobial activity. Langmuir 29:14246–14253

Devine DA, Hancock RE (2002) Cationic peptides: distribution and mechanisms of resistance. Curr Pharm Des 8:703–714

Dewangan RP, Bisht GS, Singh VP, Yar MS, Pasha S (2018) Design and synthesis of cell selective α/β-diastereomeric peptidomimetic with potent in vivo antibacterial activity against methicillin resistant *S. aureus*. Bioorg Chem 76:538–547

Discher DE, Janmey P, Wang YL (2005) Tissue cells feel and respond to the stiffness of their substrate. Science 310:1139–1143

Dong H, Paramonov SE, Aulisa L, Bakota EL, Hartgerink JD (2007) Self-assembly of multidomain peptides: balancing molecular frustration controls conformation and nanostructure. J Am Chem Soc 129:12468–12472

Edwards-Gayle CJC, Castelletto V, Hamley IW, Barrett G, Greco F, Hermida-Merino D, Rambo RP, Seitsonen J, Ruokolainen J (2019) Self-assembly, antimicrobial activity, and membrane interactions of arginine-capped peptide bola-amphiphiles. ACS Appl Bio Mater 2:2208–2218

Edwards-Gayle CJC, Barrett G, Roy S, Castelletto V, Seitsonen J, Ruokolainen J, Hamley IW (2020) Selective antibacterial activity and lipid membrane interactions of arginine-rich amphiphilic peptides. ACS Appl Bio Mater 3:1165–1175

Evans CD, Lewis JWS (2020) Collaborative antimicrobial stewardship in the health department. Infect Dis Clin N Am 34:145–160

Falla TJ, Karunaratne DN, Hancock RE (1996) Mode of action of the antimicrobial peptide indolicidin. J Biol Chem 271:19298–19303

Feng Z, Xu B (2016) Inspiration from the mirror: D-amino acid containing peptides in biomedical approaches. Biomol Concepts 7:179–187

Fernandez-Lopez S, Kim HS, Choi EC, Delgado M, Granja JR, Khasanov A, Kraehenbuehl K, Long G, Weinberger DA, Wilcoxen KM, Ghadiri MR (2001) Antibacterial agents based on the cyclic D,L-alpha-peptide architecture. Nature 412:452–455

Fjell CD, Hiss JA, Hancock REW, Schneider G (2012) Designing antimicrobial peptides: form follows function. Nat Rev Drug Discov 11:37–51

Frederiksen N, Hansen PR, Björkling F, Franzyk H (2019) Peptide/peptoid hybrid oligomers: the influence of hydrophobicity and relative side-chain length on antibacterial activity and cell selectivity. Molecules 24

Fu H, Shi K, Hu G, Yang Y, Kuang Q, Lu L, Zhang L, Chen W, Dong M, Chen Y, He Q (2015) Tumor-targeted paclitaxel delivery and enhanced penetration using TAT-decorated liposomes comprising redox-responsive poly(ethylene glycol). J Pharm Sci 104:1160–1173

Galler KM, Aulisa L, Regan KR, D'souza RN, Hartgerink JD (2010) Self-assembling multidomain peptide hydrogels: designed susceptibility to enzymatic cleavage allows enhanced cell migration and spreading. J Am Chem Soc 132:3217–3223

Gazit E (2007) Self-assembled peptide nanostructures: the design of molecular building blocks and their technological utilization. Chem Soc Rev 36:1263–1269

Gentilucci L, Tolomelli A, Squassabia F (2006) Peptides and peptidomimetics in medicine, surgery and biotechnology. Curr Med Chem 13:2449–2466

Ghosh C, Sarkar P, Issa R, Haldar J (2019) Alternatives to conventional antibiotics in the era of antimicrobial resistance. Trends Microbiol 27:323–338

Giuliani A, Rinaldi AC (2011) Beyond natural antimicrobial peptides: multimeric peptides and other peptidomimetic approaches. Cell Mol Life Sci 68:2255–2266

Gontsarik M, Yaghmur A, Ren Q, Maniura-Weber K, Salentinig S (2019) From structure to function: pH-switchable antimicrobial nano-self-assemblies. ACS Appl Mater Interfaces 11:2821–2829

Gratton SEA, Ropp PA, Pohlhaus PD, Luft JC, Madden VJ, Napier ME, Desimone JM (2008) The effect of particle design on cellular internalization pathways. Proc Natl Acad Sci U S A 105:11613–11618

Grau-Campistany A, Manresa Á, Pujol M, Rabanal F, Cajal Y (2016) Tryptophan-containing lipopeptide antibiotics derived from polymyxin B with activity against Gram-positive and Gram-negative bacteria. Biochimica et Biophysica Acta (BBA) - Biomembranes 1858:333–343

Guler MO, Hsu L, Soukasene S, Harrington DA, Hulvat JF, Stupp SI (2006) Presentation of RGDS epitopes on self-assembled nanofibers of branched peptide amphiphiles. Biomacromolecules 7: 1855–1863

Habibi N, Kamaly N, Memic A, Shafiee H (2016) Self-assembled peptide-based nanostructures: smart nanomaterials toward targeted drug delivery. Nano Today 11:41–60

Haines LA, Rajagopal K, Ozbas B, Salick DA, Pochan DJ, Schneider JP (2005) Light-activated hydrogel formation via the triggered folding and self-assembly of a designed peptide. J Am Chem Soc 127:17025–17029

Hamley IW, Dehsorkhi A, Castelletto V (2013a) Self-assembled arginine-coated peptide nanosheets in water. Chem Commun 49:1850–1852

Hamley IW, Dehsorkhi A, Jauregi P, Seitsonen J, Ruokolainen J, Coutte F, Chataigné G, Jacques P (2013b) Self-assembly of three bacterially-derived bioactive lipopeptides. Soft Matter 9:9572–9578

Hancock REW, Sahl H-G (2006) Antimicrobial and host-defense peptides as new anti-infective therapeutic strategies. Nat Biotechnol 24:1551–1557

Hancock RE, Falla T, Brown M (1995) Cationic bactericidal peptides. Adv Microb Physiol 37:135–175

He B, Ma S, Peng G, He D (2018a) TAT-modified self-assembled cationic peptide nanoparticles as an efficient antibacterial agent. Nanomedicine 14:365–372

He H, Wang H, Zhou N, Yang D, Xu B (2018b) Branched peptides for enzymatic supramolecular hydrogelation. Chem Commun 54:86–89

Henninot A, Collins JC, Nuss JM (2018) The current state of peptide drug discovery: back to the future? J Med Chem 61:1382–1414

Hu X, Liao M, Gong H, Zhang L, Cox H, Waigh TA, Lu JR (2020) Recent advances in short peptide self-assembly: from rational design to novel applications. Curr Opin Colloid Interface Sci 45:1–13

Hughes M, Debnath S, Knapp CW, Ulijn RV (2013) Antimicrobial properties of enzymatically triggered self-assembling aromatic peptide amphiphiles. Biomater Sci 1:1138–1142

Huwaitat RC, Porter SL, Pentlavalli S, Laverty G (2021) Antibacterial and antibiofilm efficacy of synthetic polymyxin-mimetic lipopeptides. Pept Sci 113

Jeon J, Mills CE, Shell MS (2013) Molecular insights into diphenylalanine nanotube assembly: all-atom simulations of oligomerization. J Phys Chem B 117:3935–3943

Jiang L, Xu D, Sellati TJ, Dong H (2015) Self-assembly of cationic multidomain peptide hydrogels: supramolecular nanostructure and rheological properties dictate antimicrobial activity. Nanoscale 7:19160–19169

Kazemzadeh-Narbat M, Lai BF, Ding C, Kizhakkedathu JN, Hancock RE, Wang R (2013) Multilayered coating on titanium for controlled release of antimicrobial peptides for the prevention of implant-associated infections. Biomaterials 34:5969–5977

Kirkham S, Castelletto V, Hamley IW, Inoue K, Rambo R, Reza M, Ruokolainen J (2016) Self-assembly of the cyclic lipopeptide daptomycin: spherical micelle formation does not depend on the presence of calcium chloride. ChemPhysChem 17:2118–2122

Kudirka R, Tran H, Sanii B, Nam KT, Choi PH, Venkateswaran N, Chen R, Whitelam S, Zuckermann RN (2011) Folding of a single-chain, information-rich polypeptoid sequence into a highly ordered nanosheet. Biopolymers 96:586–595

Kumar VA, Taylor NL, Shi S, Wickremasinghe NC, D'souza RN, Hartgerink JD (2015) Self-assembling multidomain peptides tailor biological responses through biphasic release. Biomaterials 52:71–78

Kuru E, Radkov A, Meng X, Egan A, Alvarez L, Dowson A, Booher G, Breukink E, Roper DI, Cava F, Vollmer W, Brun Y, Vannieuwenhze MS (2019) Mechanisms of incorporation for D-amino acid probes that target peptidoglycan biosynthesis. ACS Chem Biol 14:2745–2756

Landman D, Georgescu C, Martin DA, Quale J (2008) Polymyxins revisited. Clin Microbiol Rev 21:449–465

Laverty G (2018) Antimicrobial peptides as hydrogels for tissue regeneration and repair. In: Barbosa MAMMCL (ed) Peptides and proteins as biomaterials for tissue regeneration and repair. Elsevier

Laverty G, Mclaughlin M, Shaw C, Gorman SP, Gilmore BF (2010) Antimicrobial activity of short, synthetic cationic lipopeptides. Chem Biol Drug Des 75:563–569

Laverty G, Gorman SP, Gilmore BF (2011) The potential of antimicrobial peptides as biocides. Int J Mol Sci 12:6566–6596

Laverty G, McCloskey AP, Gilmore BF, Jones DS, Zhou J, Xu B (2014) Ultrashort cationic naphthalene-derived self-assembled peptides as antimicrobial nanomaterials. Biomacromolecules 15:3429–3439

Laverty G, Gorman SP, Gilmore BF (2015) Biofilms and implant-associated infections. In: Barnes L, Cooper IR (eds) Biomaterials and medical device-associated infections, 1st edn. Woodhead Publishing, Waltham, MA

Liskamp RM, Rijkers DT, Kruijtzer JA, Kemmink J (2011) Peptides and proteins as a continuing exciting source of inspiration for peptidomimetics. Chembiochem 12:1626–1653

Liu Z, Brady A, Young A, Rasimick B, Chen K, Zhou C, Kallenbach NR (2007) Length effects in antimicrobial peptides of the $(RW)_n$ series. Antimicrob Agents Chemother 51:597–603

Liu L, Xu K, Wang H, Tan PK, Fan W, Venkatraman SS, Li L, Yang YY (2009) Self-assembled cationic peptide nanoparticles as an efficient antimicrobial agent. Nat Nanotechnol 4:457–463

Liu Y, Yang Y, Wang C, Zhao X (2013) Stimuli-responsive self-assembling peptides made from antibacterial peptides. Nanoscale 5:6413–6421

Liu SQ, Venkataraman S, Ong ZY, Chan JM, Yang C, Hedrick JL, Yang YY (2014) Overcoming multidrug resistance in microbials using nanostructures self-assembled from cationic bent-core oligomers. Small 10:4130–4135

Lombardi L, Falanga A, Del Genio V, Galdiero S (2019a) A new hope: self-assembling peptides with antimicrobial activity. Pharmaceutics 11:166

Lombardi L, Shi Y, Falanga A, Galdiero E, De Alteriis E, Franci G, Chourpa I, Azevedo HS, Galdiero S (2019b) Enhancing the potency of antimicrobial peptides through molecular engineering and self-assembly. Biomacromolecules 20:1362–1374

Lone A, Thomsen TT, Nielsen JE, Thulstrup PW, Klitgaard RN, Løbner-Olesen A, Lund R, Jenssen H, Hansen PR (2019) Structure-activity study of an all-D antimicrobial octapeptide D2D. Molecules 24

Lopez-Silva TL, Leach DG, Li IC, Wang X, Hartgerink JD (2019) Self-assembling multidomain peptides: design and characterization of neutral peptide-based materials with pH and ionic strength independent self-assembly. ACS Biomater Sci Eng 5:977–985

Makovitzki A, Viterbo A, Brotman Y, Chet I, Shai Y (2007) Inhibition of fungal and bacterial plant pathogens *in vitro* and *in planta* with ultrashort cationic lipopeptides. Appl Environ Microbiol 73:6629–6636

Makovitzki A, Baram J, Shai Y (2008) Antimicrobial lipopolypeptides composed of palmitoyl Di- and tricationic peptides: *in vitro* and *in vivo* activities, self-assembly to nanostructures, and a plausible mode of action. Biochemistry 47:10630–10636

Malanovic N, Leber R, Schmuck M, Kriechbaum M, Cordfunke RA, Drijfhout JW, De Breij A, Nibbering PH, Kolb D, Lohner K (2015) Phospholipid-driven differences determine the action of the synthetic antimicrobial peptide OP-145 on Gram-positive bacterial and mammalian membrane model systems. Biochimica et Biophysica Acta (BBA) - Biomembranes 1848:2437–2447

Malhotra K, Shankar S, Rai R, Singh Y (2018) Broad-spectrum antibacterial activity of proteolytically stable self-assembled αγ-hybrid peptide gels. Biomacromolecules 19:782–792

McCloskey AP, Gilmore BF, Laverty G (2014) Evolution of antimicrobial peptides to self-assembled peptides for biomaterial applications. Pathogens 3:791–821

McCloskey AP, Gilmore SM, Zhou J, Draper ER, Porter S, Gilmore BF, Xu B, Laverty G (2016) Self-assembling ultrashort NSAID-peptide nanosponges: multifunctional antimicrobial and anti-inflammatory materials. RSC Adv 6:114738–114749

McCloskey AP, Draper ER, Gilmore BF, Laverty G (2017) Ultrashort self-assembling Fmoc-peptide gelators for anti-infective biomaterial applications. J Pept Sci 23:131–140

Menger FM, Caran KL (2000) Anatomy of a gel. Amino acid derivatives that rigidify water at submillimolar concentrations. J Am Chem Soc 122:11679–11691

Mi G, Shi D, Herchek W, Webster TJ (2017) Self-assembled arginine-rich peptides as effective antimicrobial agents. J Biomed Mater Res A 105:1046–1054

Milo S, Heylen RA, Glancy J, Williams GT, Patenall BL, Hathaway HJ, Thet NT, Allinson SL, Laabei M, Jenkins ATA (2021) A small-molecular inhibitor against *Proteus mirabilis* urease to treat catheter-associated urinary tract infections. Sci Rep 11:3726

Molchanova N, Hansen PR, Franzyk H (2017) Advances in development of antimicrobial peptidomimetics as potential drugs. Molecules 22

Nam KT, Shelby SA, Choi PH, Marciel AB, Chen R, Tan L, Chu TK, Mesch RA, Lee B-C, Connolly MD, Kisielowski C, Zuckermann RN (2010) Free-floating ultrathin two-dimensional crystals from sequence-specific peptoid polymers. Nat Mater 9:454–460

Ng VW, Chan JM, Sardon H, Ono RJ, García JM, Yang YY, Hedrick JL (2014) Antimicrobial hydrogels: a new weapon in the arsenal against multidrug-resistant infections. Adv Drug Deliv Rev 78:46–62

Oren Z, Shai Y (1998) Mode of action of linear amphipathic alpha-helical antimicrobial peptides. Biopolymers 47:451–463

Panja S, Adams DJ (2019) Maintaining homogeneity during a sol–gel transition by an autocatalytic enzyme reaction. Chem Commun 55:47–50

Pfalzgraff A, Brandenburg K, Weindl G (2018) Antimicrobial peptides and their therapeutic potential for bacterial skin infections and wounds. Front Pharmacol 9:281

Piotrowska U, Sobczak M, Oledzka E (2017) Current state of a dual behaviour of antimicrobial peptides-therapeutic agents and promising delivery vectors. Chem Biol Drug Des 90:1079–1093

Pizzoferrato A, Ciapetti G, Stea S, Cenni E, Arciola CR, Granchi D, Savarino L (1994) Cell culture methods for testing biocompatibility. Clin Mater 15:173–190

Pochan DJ, Schneider JP, Kretsinger J, Ozbas B, Rajagopal K, Haines L (2003) Thermally reversible hydrogels via intramolecular folding and consequent self-assembly of a *de novo* designed peptide. J Am Chem Soc 125:11802–11803

Porter SL, Coulter SM, Pentlavalli S, Thompson TP, Laverty G (2018) Self-assembling diphenylalanine peptide nanotubes selectively eradicate bacterial biofilm infection. Acta Biomater 77:96–105

Ramesh S, Govender T, Kruger HG, De La Torre BG, Albericio F (2016) Short AntiMicrobial peptides (SAMPs) as a class of extraordinary promising therapeutic agents. J Pept Sci 22:438–451

Reches M, Gazit E (2003) Casting metal nanowires within discrete self-assembled peptide nanotubes. Science 300:625–627

Rho JY, Cox H, Mansfield EDH, Ellacott SH, Peltier R, Brendel JC, Hartlieb M, Waigh TA, Perrier S (2019) Dual self-assembly of supramolecular peptide nanotubes to provide stabilisation in water. Nat Commun 10:4708

Rughani RV, Salick DA, Lamm MS, Yucel T, Pochan DJ, Schneider JP (2009) Folding, self-assembly, and bulk material properties of a *de novo* designed three-stranded β-sheet hydrogel. Biomacromolecules 10:1295–1304

Saini AV (2017) Peptoids: tomorrow's therapeutics. In: Ficai DG, A. (eds) Nanostructures for novel therapy. Elsevier

Salick DA, Kretsinger JK, Pochan DJ, Schneider JP (2007) Inherent antibacterial activity of a peptide-based beta-hairpin hydrogel. J Am Chem Soc 129:14793–14799

Salick DA, Pochan DJ, Schneider JP (2009) Design of an injectable β-hairpin peptide hydrogel that kills methicillin-resistant *Staphylococcus aureus*. Adv Mater 21:4120–4123

Sarkar B, Siddiqui Z, Nguyen PK, Dube N, Fu W, Park S, Jaisinghani S, Paul R, Kozuch SD, Deng D, Iglesias-Montoro P, Li M, Sabatino D, Perlin DS, Zhang W, Mondal J, Kumar VA

(2019) Membrane-disrupting nanofibrous peptide hydrogels. ACS Biomater Sci Eng 5:4657–4670

Schnaider L, Brahmachari S, Schmidt NW, Mensa B, Shaham-NIV S, Bychenko D, Adler-Abramovich L, Shimon LJW, Kolusheva S, Degrado WF, Gazit E (2017) Self-assembling dipeptide antibacterial nanostructures with membrane disrupting activity. Nat Commun 8:1365-017-01447-x

Schneider JP, Pochan DJ, Ozbas B, Rajagopal K, Pakstis L, Kretsinger J (2002) Responsive hydrogels from the intramolecular folding and self-assembly of a designed peptide. J Am Chem Soc 124:15030–15037

Shen Z, Guo Z, Zhou L, Wang Y, Zhang J, Hu J, Zhang Y (2020) Biomembrane induced in situ self-assembly of peptide with enhanced antimicrobial activity. Biomater Sci 8:2031–2039

Sim JY, Kim S, Lee J, Lim H, Kim HH, Park ZY, Kim JI (2019) A significantly enhanced antibacterial spectrum of D-enantiomeric lipopeptide bactenecin. Biochem Biophys Res Commun 514:497–502

Simon RJ, Kania RS, Zuckermann RN, Huebner VD, Jewell DA, Banville S, Ng S, Wang L, Rosenberg S, Marlowe CK (1992) Peptoids: a modular approach to drug discovery. Proc Natl Acad Sci U S A 89:9367–9371

Strom MB, Haug BE, Skar ML, Stensen W, Stiberg T, Svendsen JS (2003) The pharmacophore of short cationic antibacterial peptides. J Med Chem 46:1567–1570

Sun L, Zheng C, Webster TJ (2016) Self-assembled peptide nanomaterials for biomedical applications: promises and pitfalls. Int J Nanomedicine 12:73–86

Taylor SD, Palmer M (2016) The action mechanism of daptomycin. Bioorg Med Chem 24:6253–6268

Thapa RK, Diep DB, Tønnesen HH (2020) Topical antimicrobial peptide formulations for wound healing: current developments and future prospects. Acta Biomater 103:52–67

Trabocchi AG, Guarna A (2005) γ- and δ-amino acids: synthetic strategies and relevant applications. Curr Org Chem 9

Ulijn RV, Smith AM (2008) Designing peptide based nanomaterials. Chem Soc Rev 37:664–675

Veiga AS, Sinthuvanich C, Gaspar D, Franquelim HG, Castanho MARB, Schneider JP (2012) Arginine-rich self-assembling peptides as potent antibacterial gels. Biomaterials 33:8907–8916

Wadia JS, Stan RV, Dowdy SF (2004) Transducible TAT-HA fusogenic peptide enhances escape of TAT-fusion proteins after lipid raft macropinocytosis. Nat Med 10:310–315

Wang R, Wang Z, Guo Y, Li H, Chen Z (2019) Design of a RADA16-based self-assembling peptide nanofiber scaffold for biomedical applications. J Biomater Sci Polym Ed 30:713–736

Wu Z, Tan M, Chen X, Yang Z, Wang L (2012) Molecular hydrogelators of peptoid–peptide conjugates with superior stability against enzyme digestion. Nanoscale 4:3644–3646

Xu H, Wang J, Han S, Wang J, Yu D, Zhang H, Xia D, Zhao X, Waigh TA, Lu JR (2009) Hydrophobic-region-induced transitions in self-assembled peptide nanostructures. Langmuir 25:4115–4123

Xu D, Jiang L, Singh A, Dustin D, Yang M, Liu L, Lund R, Sellati TJ, Dong H (2015) Designed supramolecular filamentous peptides: balance of nanostructure, cytotoxicity and antimicrobial activity. Chem Commun 51:1289–1292

Xu D, Ran Q, Xiang Y, Jiang L, Smith BM, Bou-Abdallah F, Lund R, Li Z, Dong H (2016) Toward hemocompatible self-assembling antimicrobial nanofibers: understanding the synergistic effect of supramolecular structure and PEGylation on hemocompatibility. RSC Adv 6:15911–15919

Xu D, Chen W, Tobin-Miyaji YJ, Sturge CR, Yang S, Elmore B, Singh A, Pybus C, Greenberg DE, Sellati TJ, Qiang W, Dong H (2018) Fabrication and microscopic and spectroscopic characterization of cytocompatible self-assembling antimicrobial nanofibers. ACS Infect Dis 4:1327–1335

Yang Z, Liang G, Guo Z, Guo Z, Xu B (2007) Intracellular hydrogelation of small molecules inhibits bacterial growth. Angew Chem 46:8216–8219

Yeaman MR, Yount NY (2003) Mechanisms of antimicrobial peptide action and resistance. Pharmacol Rev 55:27–55

Yu X, Liu Q, Wu J, Zhang M, Cao X, Zhang S, Wang Q, Chen L, Yi T (2010) Sonication-triggered instantaneous gel-to-gel transformation. Chemistry 16:9099–9106

Zhao X, Pan F, Lu JR (2008) Recent development of peptide self-assembly. Prog Nat Sci 18:653–660

Zhong C, Zhu N, Zhu Y, Liu T, Gou S, Xie J, Yao J, Ni J (2020) Antimicrobial peptides conjugated with fatty acids on the side chain of D-amino acid promises antimicrobial potency against multidrug-resistant bacteria. Eur J Pharm Sci 141:105123

Chapter 15
Multifunctional Peptide Biointerfaces

King Hang Aaron Lau and Asma Mukhtar

Abstract In creating useful devices for biomedical and other applications that come into contact with biological fluids, it is of great interest to mimic the multifaceted control of complex biomolecular and cell interactions observed in nature. On the molecular level, all such interactions involve surfaces and interfaces. In biology, this is often a cell membrane interface. In devices, this is the surface or interface of an artificial material, be it a nanoparticle or the surface of a biomaterial or biosensor. Multifunctional biointerfaces aim to provide simultaneous modulation of several biological signals. This chapter highlights the use of both linear and multi-armed peptide designs specifically conceived for such multifunctional surface applications. As shown by the studies reviewed, this dedicated strategy has met with considerable success, not least because even relatively short oligopeptide sequences, including cell-instructive and antimicrobial motifs, are being shown to be capable of diverse and robust bioactivities. Moreover, these sequences (and related peptidomimetics) may be rationally combined and conveniently synthesized by standardized solid phase peptide synthesis. In addition, research into multifunctional peptide biointerfaces has been greatly aided by advances in simple and facile surface immobilization chemistries (e.g. SAMs and DOPA/polydopamine), as well as the realization that proteins possess native "antifouling" properties that can be mimicked by simple and mostly zwitterionic residue compositions to suppress non-specific interactions and enhance biorecognition binding. Overall, functionalization of biointerfaces with multifunctional peptides stands out as a powerful strategy to engineer protein-mimetic bioactivity on artificial materials and device surfaces, and great scope remains for the development of applications based on even more

K. H. A. Lau (✉)
Department of Pure and Applied Chemistry, University of Strathclyde, Glasgow, UK
e-mail: aaron.lau@strath.ac.uk

A. Mukhtar
Department of Pure and Applied Chemistry, University of Strathclyde, Glasgow, UK

Department of Chemistry and Chemical Engineering, Lahore University of Management Sciences, Lahore, Pakistan

diverse peptide architectures as well as an expanded range of protein-mimetic biorecognition and multifunctionality.

Keywords Biomaterial · Biosensing · Peptoid · Antifouling · RGD · Cell-surface interactions · Solid phase peptide synthesis · Zwitterionic polymers

15.1 Introduction

Biointerfaces can be most broadly defined as surfaces designed to interact with a biomolecule or a biologically living system. In this manner, the term has been used to include a wide range of research and applications, from biosensing and nanomedicine to even protein affinity purification as well as anti-biofouling of industrial and healthcare surfaces. The biointerfacial interaction may be resulting from the native surface property of a material (e.g. hydrophobicity, charge, roughness, etc.) or, in more sophisticated instances, be imparted by surface nano-patterns, nanostructures/topography or specialized (bio)chemistries that elicit specific biomolecular and cellular responses (Mas-Moruno et al. 2019). Indeed all peptide nanomaterials, self-assembled hydrogels, tissue engineering scaffolds, etc., must interact with biomolecules and living cells in the biological and therapeutic environments through surface contacts, at least initially (Amit et al. 2018). What distinguishes biointerfacial research may be the additional concept of surface functionalization or modification, whereby the surface is considered separately and often added as a distinct coating to the native surface of the material or nanostructure (Jurczak et al. 2020).

This review will highlight the exquisite potential of rationally designed oligopeptide molecular layers in precisely controlling biointerfacial interactions that may ultimately benefit biosensing, cell culture and other biomaterial applications. As highly functional and versatile biomolecules, peptides have been used to tailor biointerfaces through two main approaches. The first, more conventional approach is the surface coupling of sequences that directly induce a desired biomolecular response, e.g. functionalizing surfaces with the Arg-Gly-Asp (RGD) cell-adhesive peptide motif originally found in many extracellular matrix (ECM) proteins (Ruoslahti and Pierschbacher 1987; Hersel et al. 2003). The second is the more ambitious and novel preparation of bioinspired surfaces that exhibit various aspects of protein function. While proteins are widely recognized for their roles in biorecognition binding, the often-unappreciated dimension underlying these specific interactions is their equally important property of screening non-specific interactions (i.e. their non-aggregation and antifouling abilities). Thus, proteins are intrinsically multifunctional. Moreover, with regard to enabling surface functionalization, a peptide biointerfacial design must also possess chemical functionalities for surface attachment.

This current interest in bioinspired, multifunctional peptides for biointerfacial applications is the focus of this chapter. After a brief discussion on the main advantages of multifunctional peptide designs in comparison with other approaches

to preparing biointerfaces, the first topic discussed is the research of "antifouling" peptides that resist non-specific interactions with proteins and/or cells. This section traces first the historical development of early peptide biointerfaces from the early search of "biocompatible" biomaterial surfaces, and it underscores second the protein-mimetic aspects of discovered antifouling peptide sequences realized only in the past decade. Two key contributions are highlighted—zwitterionic protein-mimetic peptides (Nowinski et al. 2012; White et al. 2012) and peptide-mimetic poly (N-substituted glycine) "peptoid" brushes (Statz et al. 2005; Lau 2014). The bifunctional nature of these early designs (i.e. surface binding plus antifouling) also illustrate the critical roles that the facile surface chemistries such as self-assembled monomers (SAMs) (Chen et al. 1997) and DOPA/polydopamine (Dalsin et al. 2003; Lee et al. 2007) play in developing biointerfaces.

The second main area discussed in this chapter is the explicit development of peptide constructs with more than one biofunctionality beyond antifouling. These include not only "simple" linear constructs where a bioactive motif may be coupled to the terminus of an antifouling surface design, but also more recent concepts such as branched peptide construct exhibiting different functionalities that have been enabled by increasingly sophisticated and mature techniques in solid phase peptide synthesis (Behrendt et al. 2016). Simply put, multifunctional coatings are desirable because the biological environment is complex and biointerfaces would ideally need to address multiple interaction partners to deliver the desired performance (e.g. cell adhesion and vascularization, osseointegration and resistance to bacteria, antifouling and biorecognition/sensing, etc.) (Raphel et al. 2016; Pagel and Beck-Sickinger 2017).

15.2   Advantages of Multifunctional Peptide Biointerfaces

The principal and obvious advantage of utilizing peptides as the platform for creating biointerfacial designs is the biochemical versatility of peptides as sequence-specific biomolecules. As illustrated in the next sections, many short motifs already elicit highly specific and robust biological responses, so the use of proteins, including the attendant use of animals or high(er) cost biotechnology means of production, is no longer required. Moreover, combining multiple functionalities in one peptide construct guarantees that different functionalities are co-immobilized on the surface. The covalent peptide linkages between multiple sequence motifs especially prevent the random loss of one or another biofunctionality, which is a major concern in mixed surfaces generated through non-covalent interactions (Pagel and Beck-Sickinger 2017). Scientifically, this co-immobilization guarantees uniform distribution of the motifs on the molecular scale, and the spatial separation may also be precisely controlled by sequence design, which together greatly enables more sophisticated control of biointerfacial interactions, e.g. multi-ligand control of cell-surface responses.

Furthermore, there are major experimental and practical advantages. Since olig-omeric lengths are used in many biointerfacial designs, peptide designs may rely on solid phase peptide synthesis (SPPS) to conveniently generate sets of polyfunctional designs, including the preparation of "knock-out" control sequences that may have functional segments removed or residues scrambled to directly test hypothesized mechanisms of each intended sequence functionality. "Fusing" different functional motifs in one construct also brings with it ease of surface characterization since the signature of any of the residues present in the multifunctional sequence can be used to characterize the surface chemistry, while sequence identity is readily confirmed by conventional (solution phase) chemical characterization (e.g. mass spectrometry). The use of peptides also brings with it more convenient (and lower cost) storage than proteins. Incorporating surface coupling chemical groups within the (multi)-functional peptide design opens up the possibilities of pre-sterilization and (long-term) storage before immobilization of the active construct on the material surface for actual application. On this last point, as discussed in Sects. 15.3.2 and 15.3.3 below, many biointerfacial peptide constructs incorporate cysteines or mussel-inspired "DOPA" residues to enable convenient one-step surface coupling.

In addition, since SPPS protocols are essentially standardized (Behrendt et al. 2016) and the shorter oligopeptides can be prepared manually without the use of automated synthesizers, peptide biointerfaces are highly accessible even for researchers without formal chemical training or significant investment in equipment (Hansen and Oddo 2015; Al Musaimi et al. 2020). In terms of commercialization, the use of SPPS also brings with it a cost advantage compared with proteins production. More importantly, an increasing number of commercial companies also provide custom synthesis at ever-decreasing prices, akin to the situation with oligonucleo-tides. Therefore, the scope of peptide designs is becoming limited only by scientific imagination.

15.3   Origins of Modern Peptide Biointerfaces

15.3.1   The Fundamental Role of Antifouling Surfaces

Biofouling is the addition of undesired biomolecules or cells on a surface. The search for biointerfaces that prevent non-specific protein adsorption began several decades ago when it was recognized that these adsorbed proteins mediated cell-surface interactions and other immunological, thrombotic or inflammatory responses (Vroman 1962; Prime and Whitesides 1991; Szleifer 1997). Such "antifouling" surfaces that resist both protein adsorption and cell attachment are still a central concern. They are critical to reducing background signals of biosensors (hence increasing sensitivity and specificity) (Russo et al. 2021), controlling the protein corona formed around nanoparticles (hence enhancing targeting, preventing opsonization and enabling theranostics) (Lara et al. 2018; Mohammad-Beigi et al.

2020; Wheeler et al. 2021) and preventing non-specific masking of surface-immobilized ligands (hence realizing biorecognition for cell culture and tissue engineering biomaterials) (Chen et al. 2021c).

Poly(ethylene glycol) (PEG) has until recently been recognized as the "gold standard" antifouling surface chemistry since it has excellent short-term performance suitable for biosensing and cell patterning applications (Prime and Whitesides 1991; Unsworth et al. 2005). However, significant effort has been devoted to investigating alternatives because PEG can exhibit complement activity (Toda et al. 2010) and loss of therapeutic efficacy after repeated administration when used to protect nanomedicine (Zhang et al. 2016; Yuan et al. 2020) and in general has not shown long-term antifouling performance (Lau et al. 2015; Maan et al. 2020). In this respect, the chemical versatility of peptides offers considerable potential to tailor surface interactions that can prevent non-specific biomolecular interactions—to in fact mimic the fact that proteins do not aggregate and are able to engage in specific biorecognition in complex in vivo environments. Accordingly, recent reports demonstrate the importance of these peptide-based coatings for applications ranging from biomedical implants to biosensors (Vaisocherová et al. 2015 functionalizable coatings biosensing, Sakala and Reches 2018; Saxena et al. 2020; Wang et al. 2021b multifunctional biomolecule nanostructures for cancer therapy).

15.3.2 Self-Assembled Monolayers (SAMs) and Thiol–Gold Surface Functionalization

The Whitesides group opened the door to the widespread use of thiol SAMs on gold for biointerfacial studies when they reported control of the amount of protein adsorption on SAMs chemically functionalized with oligo ethylene glycol (OEG) units at the top, surface terminal group of each SAM molecule (Prime and Whitesides 1991) (Fig. 15.1a). This initial antifouling study soon led to their joint pioneering work with Ingber et al. on patterning proteins and cells (Singhvi et al. 1994) and on engineering cell shape and function (Chen et al. 1997) (Fig. 15.1b, c). Moreover, the Whitesides group also followed up with a pioneering survey of the antifouling performance of SAMs modified with diverse surface chemical groups (Ostuni et al. 2001a, b).

In particular, this survey gave an early hint to the potential of peptide surface designs, when they found that terminations of glycine, sarcosine (a "peptoid"; see below) and a zwitterionic design (see further below) were as antifouling, if not more so, than OEG. With the obvious choice of installing cysteine—the amino acid residue with an alkyl-thiol sidechain—at the end of a peptide sequence for thiol–gold coupling, many researchers have since investigated peptide-SAMs for antifouling (and other) biointerfacial applications. The cysteine thiol could also be used to chemically couple with other solid substrate surfaces, e.g. reactions with amine groups generated on polyaniline (PANI) conducting polymer electrodes useful for
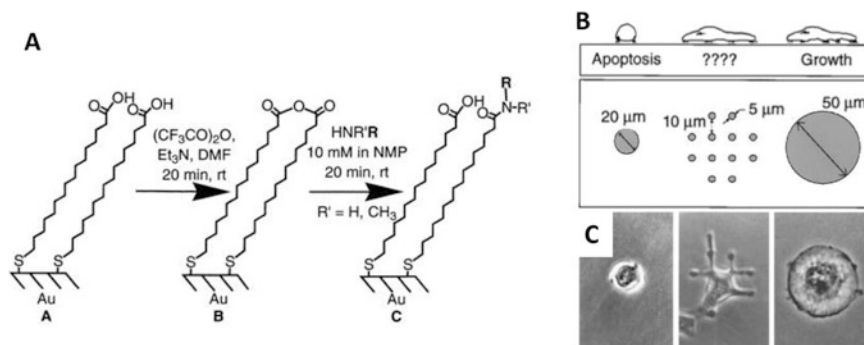
Fig. 15.1 (**a**) Basic chemical design of the Whitesides group's SAM platform that may be functionalized by a variety of "R" groups, including antifouling ethylene glycol, amino acid designs (e.g. glycine, sarcosine) and zwitterions. (**b**) Schematic showing surface designs with antifouling SAMs surrounding micro-contact printed patterns of adhesive patches. (**c**) Micrographs of preferential cells attachment on the printed patterns and demonstration of geometric control of cell fate. Adapted with permission from Ostuni et al. (2001a) and Chen et al. (1997). Copyright 2001 American Chemical Society (**a**), and 1997 The American Association for the Advancement of Science (**b**, **c**)

point-of-care (POC) electrochemical biosensing (Liu et al. 2021). However, the thiol–gold surface coupling is of particular importance because of its reliable and facile one-step solution preparation and the fact that many biointerfaces can have a gold surface, including not just sensor electrodes but also surface plasmon sensors and gold nanoparticles for nanomedicine.

15.3.3 Polysarcosine Peptoid Antifouling and the DOPA Universal Surface Adhesive

Sarcosine (*N*-methyl glycine) is a structural isomer of alanine, a glycine transporter inhibitor (Cioffi et al. 2010) and an intermediate in the metabolism of choline and creatine (Smith-Palmer 2019). Chemically, it is also the simplest example of N-substituted glycine "peptoids", a class of synthetic structural isomers of peptides for which the only difference is a one-atom shift in the attachment position of the functional sidechain to the α-nitrogen along the backbone (Fig. 15.2a). This non-natural molecular structure results in virtually complete resistance against enzymatic degradation by proteases that are abundant in vivo. This is an attractive feature drawing increasing attention to the use of peptoids for therapeutics and long-term biomedical applications (Lau 2014; Knight et al. 2015). The sidechain shift also removes backbone chirality and hydrogen-bond (H-bond) donors, both principal features deduced in Whitesides' survey to prevent non-specific intermolecular interactions (Ostuni et al. 2001a).
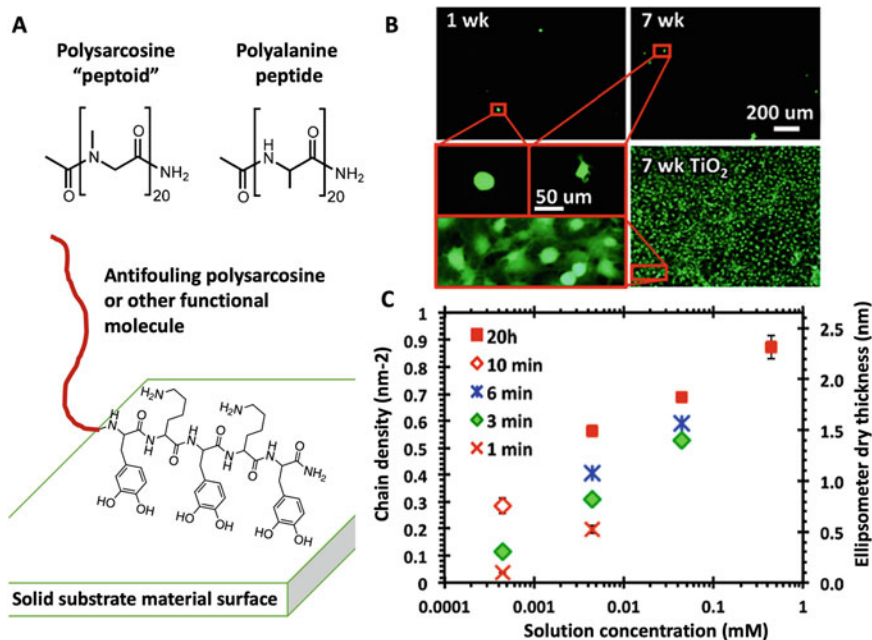
Fig. 15.2 (a) Chemical structures of the "peptoid" polysarcosine, its natural analogue polyalanine and the DOPA surface grafting motif (DOPA-Lys-DOPA-Lys-DOPA used by Lau and Messersmith et al. for antifouling studies is shown). (b) The NIH-3 T3 fibroblast cells attached on a polysarcosine-coated surface was very low throughout the 7-week test period, while a confluent layer (coverage = 1) was achieved on the uncoated TiO_2 control surface after 7 days. Although some cells were observed on the polysarcosine surface, their morphologies were rounded, exhibiting few filopodia, and were poorly attached. In contrast, cells on the TiO_2 control spread very well. (c) The degree of immobilized surface density possible with the DOPA motif. The peptide chain-grafted density is shown on the left axis and the corresponding thickness as measured by ellipsometry is shown on the right axis. Adapted with permission from Lau et al. (2012b). © 2012 American Chemical Society (b and c)

Experimentally, Lau and Messersmith first demonstrated the excellent hydration of surface-immobilized 10- to 20-mer long polysarcosine chains, as opposed to the hydrophobic polyalanine peptide analogue, and up to 7 weeks' "long-term" suppression of cell fouling (Lau et al. 2012b) (Fig. 15.2a, b). Other groups have since exploited polysarcosine for a range of applications (Gangloff et al. 2015), including as "stealth" coatings of nanoparticles for targeted therapies (Zhu et al. 2017a; Birke et al. 2018), and there is intense interest in using polysarcosine as a practical replacement of PEG in nanomedicine and therapeutic protein conjugation (Hu et al. 2018; Bleher et al. 2019; Viricel et al. 2019).

In the area of biointerfaces, the polysarcosine antifouling study by Lau et al. also highlighted the use of "universal" DOPA/polydopamine surface binding (Fig. 15.2a) previously introduced by the Messersmith group (Dalsin et al. 2004; Lee et al. 2007) and now widely applied (Ryu et al. 2018). DOPA stands for the amino acid 3,4-dihydroxyphenylalanine, which is post-translation modified from tyrosine, and

its application to molecular adhesion was inspired by its unusual abundance in proteins secreted by marine mussels, where it often appears next to lysine residues, to enable wet adhesion on virtually any surface (Waite and Tanzer 1981). The directly inspired DOPA-Lys motif has been used by Lau and Messersmith in a series of antifouling studies (Lau et al. 2015, 2012a, b; Ryu et al. 2014, 2018; Cheung and Lau 2019; Pan et al. 2020). At the same time, the abstracted incorporation of single DOPA residues, or simply just the dihydroxyphenyl (i.e. catechol) sidechain group in peptide and other functional polymer constructs, is also effective (Pagel et al. 2016; Ryu et al. 2018; Martin-Gomez et al. 2021b). Like the case of thiol SAMs, DOPA/polydopamine's popularity can also be attributed to its commercial availability as well as the reliability and ease of catechol-mediated one-step solution preparation to enable surface binding. Uniquely, the density of functionalization using DOPA/polydopamine may be controlled by easily accessible parameters such as solution concentration, time and temperature, to suit a wide range of applications (Fig. 15.2c).

15.3.4 Protein Mimicry and Zwitterionic Glu-Lys (EK) Peptides

In their influential studies of zwitterionic polymers, the Jiang group observed that polymers with balanced mixtures of positively and negatively charged moieties generally exhibited very low degrees of fouling (Jiang and Cao 2010 advanced materials). Indeed, taking advantage of combinatorial peptide discovery using solid phase peptide synthesis (SPPS), they were able to confirm that a number of net neutral alternating peptide sequences characterized by consecutive Glu (E)-Lys (K) dimer pairs were able to greatly reduce protein adsorption (e.g. EKEKEKEK) (Keefe et al. 2013). Since this first report, the "EK peptides" have been demonstrated in various applications, especially in the field of nanomedicine (Zhao et al. 2017; Yuan et al. 2020) and biosensing (see below).

The antifouling properties of EK sequences are actually protein-mimetic. Functioning proteins are natively non-fouling—they do not aggregate and are able to engage in specific binding even in complex biological fluidics. In a bioinformatics analysis of protein *surface* amino acid composition, the Jiang group found that K and E residues were especially abundant on the exterior of extracellular proteins and the interior binding surfaces of molecular chaperones (White et al. 2012). The latter class of proteins are large complexes that assist in folding and assembly of other macromolecular structures, which must resist non-specific interactions. Indeed, chaperones in a thermophilic organism were found to exhibit 52% K–E surface content. Moreover, the polar, uncharged serine (S) and asparagine (N) residues were also found to be abundant on protein surfaces, and their abundance was hypothesized to contribute to protein hydration and to solubility in the complex biological milieu. Along this direction, a serine-rich SGKGSSGSST peptide had also been uncovered

to exhibit excellent antifouling properties (Chelmowski et al. 2008). Furthermore, a D-peptide analogue of this sequence was also demonstrated (Beyer et al. 2020) to reproduce peptoid's resistance against enzymatic degradation and suitability for long-term biointerfacial applications.

It has further been proposed that a potential advantage of mixed charge antifouling designs comprised of acid and base chemical groups, compared with chemically inert like polysarcosine, is the possibility of additional modifications through the chemically functional groups (Vaisocherova et al. 2009; Mi et al. 2010). While this may be true of synthetic polymer analogues, adding extra residues to an antifouling peptide is arguably just as convenient. On the other hand, Lau et al. were able to show that zwitterionic peptoids could better suppress protein adsorption than uncharged designs over an acidic pH range studied from pH 5 to 7.4 (Lau et al. 2015). Therefore zwitterionic (peptoid) sequences could be advantageous in biomedical applications related to biomedically important acidic environments, including lysosomes (for drug delivery) and cancer tumours.

15.4 Multifunctional Peptides for Surface Functionalization

15.4.1 Direct Application of Bioactive Peptides

Bioactive peptide sequences may be coupled on surfaces as independent units to enable a desired response (e.g. RGD for cell adhesion) without an explicit biointerfacial focus. Some prime application areas include biosensing (e.g. see Vaisocherová et al. 2015 functionalizable coatings biosensing and sections below), cell adhesion (e.g. Fischer et al. 2020; Zhu et al. 2021), functional peptide self-assemblies (e.g. Goncalves et al. 2017; Amit et al. 2018), antimicrobial surfaces (Costa et al. 2011; Andrea et al. 2018; He et al. 2018, Xiao et al. 2018; Hasan et al. 2020) and functional nanoparticles for nanomedicine and theranostics (e.g. Peng et al. 2016; Liu et al. 2020; Rai and Ferreira 2021; Wang et al. 2021b multifunctional biomolecule nanostructures for cancer therapy). High molecular weight polymers or synthetic proteins with functional amino acid residues or peptide motifs incorporated along the backbone or as sidechains have also been demonstrated (Fan Zhang, 2020 #2250; Gao, 2020 #2258; Godoy-Gallardo, 2015; Kizhakkedathu, 2011 biomaterials). The reader is referred to the aforementioned references for these often monofunctional, direct applications of peptide sequences that do not utilize dedicated peptide designs to tailor the structure or to enhance functionality of the biointerfacial.
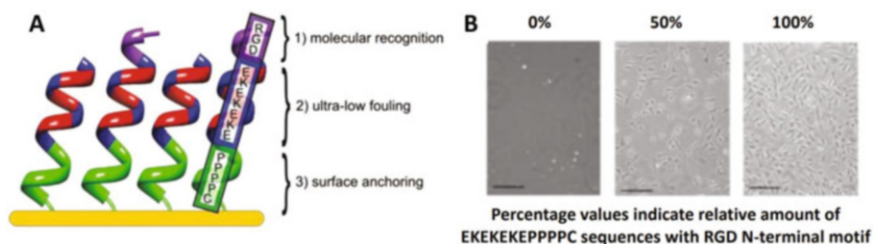
Fig. 15.3 (**a**) Schematic showing the mixture of multifunctional linear EKEKEKEPPPPC and RGDEKEKEKEPPPPC sequences immobilized via the terminal Cys on a gold surface. (**b**) Optical micrographs showing the extents of NIH-3 T3 fibroblast cell-surface coverage obtained with different mixing ratio of peptides with and without RGD. Adapted with permission from Nowinski et al. (2012). © 2012 American Chemical Society

15.4.2 Linear SAM Designs

As an archetypical sample (Fig. 15.3a), the Jiang group added to their "EK" zwitterionic sequence a surface immobilization and structuring motif composed of a C-terminal cysteine (C) and a tetra-proline (P) linker (i.e. PPPPC), and an N-terminal RGD, to derive a sequence that can self-assemble on a gold surface and simultaneously enable resistance against non-specific protein adsorption and specific integrin-mediated cell adhesion (Nowinski et al. 2012). While the cysteine thiol enabled gold surface coupling, the presence of PPPP was shown to engender a more ordered secondary structure that enabled higher packing density of the chemisorbed chains and reduced non-specific protein adsorption. Moreover, the cell coverage could be controlled by mixing different ratios of sequences with and without the RGD during surface preparation (Fig. 15.3b). Thus, this report illustrated how a highly functional biointerface may be enabled by a combination of convenient surface immobilization (mixed SAMs) and convenient preparation of linear oligopeptide sequences.

Linear sequences are the most facile to generate and many three-part designs like the above "RGD-EK" self-assembling peptide have been demonstrated (the antifouling peptides described in Sect. 15.3. may be conceptualized as two-part designs). For example, the Luo group has variously used EK or the aspartic acid-based DK analogue as the central antifouling segment and attached different terminal biomolecular motifs to enable biosensing applications. For a prostate cancer diagnostic application, they coupled the sequence HSSKLQK to a CPPPP-DKDKDKD segment to enable recognition and cleaving by the prostate-specific antigen (PSA) protein and hence PSA sensing (Ding et al. 2019). As a variation on the theme, Luo et al. have also investigated immobilization of HWRGWVA, an immunoglobulin G (IgG)-recognizing peptide identified from a combinatorial library (Yang et al. 2005). This was linked to another antifouling sequence (NQNQNQNQ) to enable IgG quantification with a remarkable 0.26 ng mL^{-1} limit of detection in neat serum

and patient blood samples (Liu et al. 2018). (The full sequence was CPPPPNQNQNQNQDHWRGWVA; both C- and N-terminal Cys should be equivalent for surface coupling.) Elsewhere, the Messersmith group had earlier combined an antimicrobial 12-mer with an antifouling peptoid linked to the aforementioned DOPA-Lys surface anchor group to enable both surface antifouling and antimicrobial properties (Statz et al. 2008).

Analogous to the surface terminal modification of SAMs discussed above, the antifouling peptide platform also enables convenient immobilization of non-peptidic biomolecules, e.g. DNA/RNA and antibodies, especially for biosensing applications. For example, screening of chromosomal abnormalities was demonstrated by immobilizing an aptamer to the N-terminus of EKEKEKEK-PPPPC to enable detection of the biomarker alpha fetoprotein (AFP) (Liu et al. 2021). Interestingly, in this instance, the surface with the lowest non-specific fouling and hence highest sensitivity was obtained by immobilizing a mixture of aptamer-coupled EKEKEKEK-PPPPC peptide with a shorter purely antifouling EKEKEK-PPPPC—a remarkable limit of detection (LOD) of 0.59 fg mL^{-1} was obtained, lower than that of many reported sensing platforms. Aptamer immobilization on antifouling (peptide) layers is a generally applicable strategy for protein marker detection (Oberhaus et al. 2020 immobilization gold electrochemical detection of proteins). Furthermore, immobilization of miRNA (Wang et al. 2017; Wang et al. 2021a MicroRNA PANI zwitterionic peptide), DNA (Wang et al. 2020a, b CPPPPNQNQNQNQ PEDOT BRCA1) and antibodies (Han et al. 2020; Oberhaus et al. 2020) has been demonstrated on various antifouling sequences, e.g. KAEAKAEA and KQEQEQEQ, in addition to the aforementioned EK, QN, DK, as well as SGKGSSGSST sequences.

At the same time, the versatility of peptide solid phase synthesis also enables facile incorporation of further functionalities even just along a linear chain. For example, an SDSD or AEAE motif for promoting poly(3,4-ethylenedioxythiophene) (PEDOT) electropolymerization may be inserted between PPPP and the C-terminal cysteine in the self-assembly segment (Wang et al. 2020a, b). The PEDOT-conducting polymer matrix formed around the base of the peptide chains would not only improve the stability of the assembled peptide layer but the acidic peptide motif also acted as a PEDOT dopant to enhance conductivity and electrochemical biosensing performance. Overall, a number of biosensing and other applications have been enabled by the further functionalization of peptide antifouling surface assembled layers (Bolduc et al. 2011, Xu et al. 2019, Jiang et al. 2020, Chen et al. 2021c).

15.4.3   Non-linear Multifunctional Peptide Surface Designs

A number of research groups have been developing increasingly sophisticated multifunctional designs that take advantage of the possibilities offered by solid
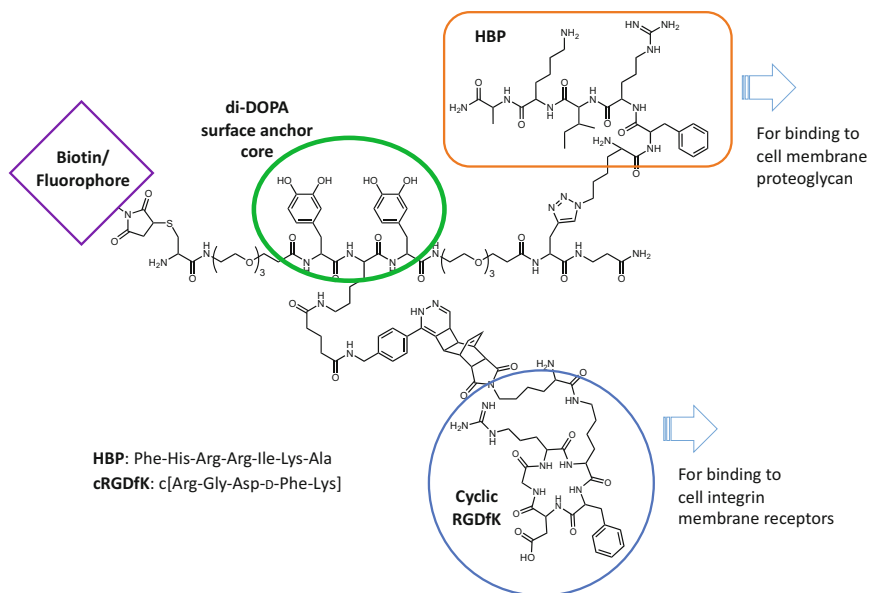
Fig. 15.4 Multifunctional peptide design introduced by Beck-Sickinger et al. (Pagel et al. 2016) with the di-DOPA core for surface attachment (green), cRGDfK (blue) and HBP (orange) units for cell binding, and additional possible groups such as biotin or a fluorophore. Coupling to the functional units is through Cys, Lys and Pra sidechains

phase peptide synthesis. First, there is an impetus to shift from co-immobilization of mixed sequences to combining multiple functionalities in one construct to enable one-step immobilization and to simplify sample surface characterization—this viewpoint is already well illustrated in the examples given in Sect. 15.4.2. More recently, there is a progression from linear towards multi-armed or branched designs. In fact, the many preceding examples of multifunctional linear designs could be viewed as special, albeit broadly useful, cases for which it is advantageous to "bury" one of the functional segments (e.g. antifouling and conductive electrode polymerization motifs) under the terminal bioactive sequences. While these linear designs may trace a history to the early work in thiol-SAMs (Sect. 15.3.2), the increasingly common technical competence in SPPS, combined with the maturing methods of orthogonal sidechain protection and post-synthesis chemical conjugation, is also contributing to the drive towards designs that display multiple peptide motifs laterally from each other.

In a tour de force demonstration of multi-armed peptide designs, the Beck-Sickinger group developed a peptide construct with five functional elements (Pagel et al. 2016). As shown in Fig. 15.4, a core sequence Cys-EG$_3$-DOPA-Lys-DOPA-EG$_3$-Pra-βAla was synthesized to offer a double DOPA motif for surface immobilization, three chemical coupling sidechains (Cys thiol, Lys amine and the non-natural propargylglycine—Pra alkyne) for biofunctionalization and triethylene glycol (EG$_3$) linkers near both termini of the sequence for antifouling cell repellency.

Specifically, the biotin was used to bind (labelled) streptavidin to verify surface immobilization by fluorescence microscopy, and a cyclic RGD^{D}FK (cRGD) and a heparin-binding FHRRIKA motif were simultaneously attached to investigate whether RGD-sensitive integrin-mediated cell-surface adhesion may be further supported by proteoglycan interactions (via heparin).

To enable this design and to illustrate the possibilities offered by combining solid phase synthesis and orthogonal chemistry, FHRRIKA was coupled to Pra using copper (I)-catalysed azide–alkyne cyclo-addition "click" reaction, cRGD was coupled to the central Lys, derivatized with a tetrazine group, via Diels–Alder reaction, biotin was coupled to the N-terminal Cys via regular thiol-maleimide reaction, and all reactions were accomplished on solid phase resin together with the inclusion of the DOPA, EG$_3$ and Cys groups. In experiments with osteoblast-like cells (SaOS-2), cRGD and FHRRIKA were shown to be necessary for proper cell adhesion and the presence of both motifs enabled the highest levels of actin cytoskeleton formation and focal contacts. Control experiments with heparinase I to degrade heparan sulphate of the transmembrane proteoglycans also resulted in a decrease in cell spreading. In comparison, "simpler" surfaces with statistical mixtures of immobilized RGD and FHRRIKA reported in the literature led to inconsistent results.

Following up on this work, the same multi-armed peptide platform was used to investigate the functionalization of polymeric biomedical implant materials and the potential of using FHRRIKA to capture (angiogenic) cytokines and enhance implant-tissue integration. First of all, it was found that the DOPA moieties could successfully enable surface immobilization on hydrophilized polycaprolactone-co-lactide, a common resorbable implant material, as well as on more conventional glass and polystyrene substrates (Clauder et al. 2020b). It was also shown that the FHRRIKA motif could bind with deliberately introduced heparin that in turn was able to capture heparin-binding angiogenic factors VEGF, FGF-2 and CXCL12 onto the functionalized surface. In particular, CXCL12 is a chemokine pro-angiogenic factor that also guides the recruitment of hematopoietic stem and progenitor cells. Overall, the peptide-functionalized surfaces complexed with CXCL12 or VEGF greatly enhanced HUVEC adhesion and survival under both static and fluidic conditions anticipated in cardiovascular implant applications. In a second study, a construct with heparin mimetic sulphated hyaluronic acids to substitute the FHRRIKA motif was also prepared (Clauder et al. 2020a). This examined whether direct cytokine capture with the biomimetic glycan could also be effective in affecting migration of immortalized T lymphocytes (Jurkat cells) as an indication of the potential for mediating issues of chronic inflammation around implants. However, only the original indirect cytokine capturing based on FHRRIKA in this study resulted in high-enough cytokine loading that exceeded the threshold for a migration response.

While the above multifunctional design is exceptionally elegant, a simpler, synthetically more convenient design could still be advantageous in controlling biointerfacial responses. In this vein, Mas-Moruno et al. (2014) had earlier demonstrated a Y-shaped design to pair the cell adhesion peptide motifs RGDS and
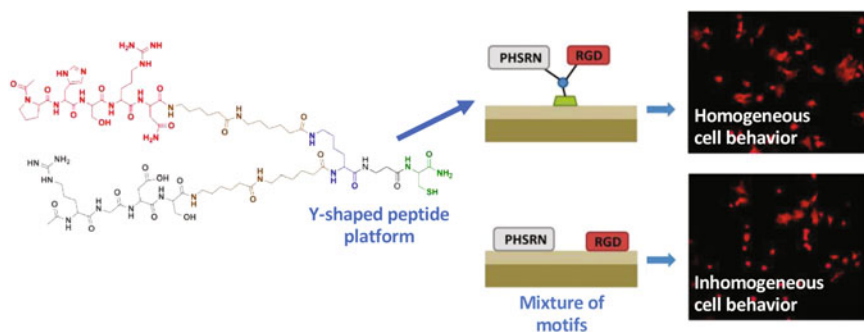
Fig. 15.5 Y-shaped peptide platform reported by Mas-Moruno et al. (2014) co-presenting PHSRN (residues in red) and RGD (dark green) using a central Lys residue as the branch point. Only the Y-shaped peptide produced homogeneous cell behaviour (right panels). Adapted with permission. © 2014 American Chemical Society

PHSRN by utilizing a central Lys residue, with its two amines (i.e. the backbone and sidechain amines), as a branch point (Fig. 15.5). (Such peptide architectures are also alternatively referred as "fusion peptide" by other groups (Chen et al. 2021b).) Surface immobilization was then enabled by a cysteine residue at the C-terminus of the Lys stem. With only one branch point, the two adhesion motifs may be synthesized one after the other by selective deprotection of each of the Lys amines followed by routine SPPS. Using also an in vitro model of osteoblast-like SaOS-2 cells, the researchers were able to demonstrate improved cell spreading and proliferation using the Y-shaped design compared to controls using only RGDS or PHSRN single peptides, or using a 1:1 mixture of separately immobilized motifs. Importantly, more uniform spreading morphologies between individual cells could be observed when using the Y-shaped co-immobilization peptide, whereas mixed immobilization resulted in heterogeneous spreading, which the researchers attributed to uniform presentation (i.e. enforced pairing) of the RGDS and PHSRN motifs leading to a synergetic effect in activating ($\alpha5\beta1$) integrin binding.

In more recent studies, the researchers also paired RGD with a KRSR proteoglycan binding motif (Hoyos-Nogues et al. 2019) as well as with an osteogenic DWIVA motif derived from bone morphogenetic protein-2 (BMP-2) (Oliver-Cervelló et al. 2021). Like the aforementioned FHRRIKA, KRSR is a heparin-binding peptide and is in fact a consensus motif found in five different bone-related adhesive proteins (fibronectin, vitronectin, bone sialoprotein, thrombospondin and osteopontin). Correspondingly, co-immobilization using the Y-shaped peptide design enhanced mineralization observed in the SaOS-2 cell model compared to RGD or KRSR alone, which was hypothesized to arise from an effective crosstalk between integrins and cell-membrane proteoglycans. In the case of the RGD-DWIVA pair, an impetus for this design is to avoid the direct clinical use of the BMP-2 protein, due to potential immunogenic issues with whole proteins. Indeed, the Y-shaped peptide design was able to uniquely improve the adhesion of C2C12 cells, a mouse myoblast line, inhibit myotube formation and activate BMP-dependent signalling via the p38 protein
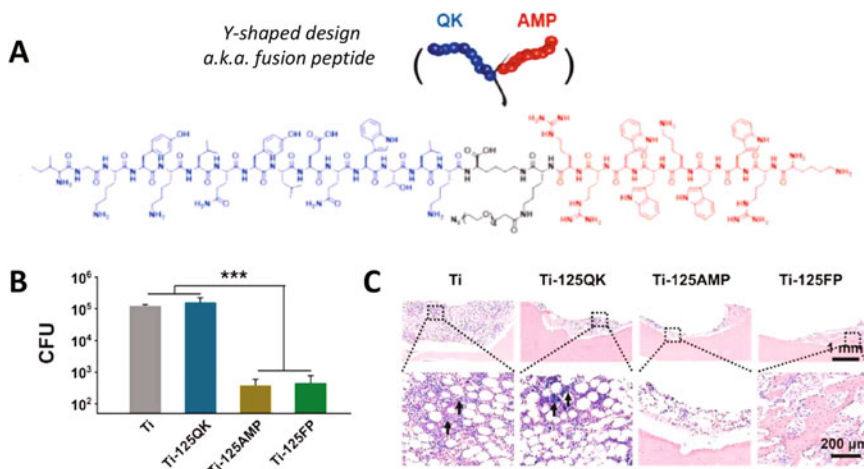
Fig. 15.6 (**a**) Co-presentation of an angiogenic "QK" sequence (IGKYKLNYLNNWTLK) with a cationic antimicrobial peptide (AMP) sequence (KRWWJWWRR) joined by a central surface immobilization unit in a Y-shaped, or "fusion peptide" design, as reported by Chen et al. (2021a). (**b**) In vivo antimicrobial activity of implants against *Staphylococcus aureus* by the agar plate method ($n = 3$; Ti is blank TiO_2 substrate; the labels 125QK, 125AMP and 125FP denote functionalized with QK only, with AMP only and with the fusion peptide). *** denotes $p < 0.001$. (**c**) H&E staining of decalcified bone sections after 7 days of implantation. The high-magnification images were taken from the black rectangles. The black arrow indicated the inflammatory cells. Adapted with permission from Chen et al. (2021a). Copyright © 2021 Elsevier Ltd.

pathway, which were all effects not observed with soluble DWIVA, with either only one of the two ligands or with a mixture of both motifs. These results demonstrated the potential of simultaneously engaging integrin and other cell adhesion pathways via molecular-based biointerfaces.

In addition to the synergistic presentation of cell adhesion factors, another obvious opportunity for multifunctional peptide biointerfaces is in pairing antimicrobial peptides (AMPs) with cell adhesion peptide motifs. For example, biomedical implants can suffer from poor tissue integration and healing due to bacterial infection, so combining osseointegrative signalling and antimicrobial activity should offer a more functional implant (Raphel et al. 2016). In a recent report, the Wang group demonstrated a Y-shaped peptide design (Fig. 15.6) fusing a cationic antimicrobial peptide (HHC36: KRWWJWWRR) with an angiogenic "QK" sequence (IGKYKLNYLNNWTLK) that could simultaneously enhance cellular proliferation and, in an in vivo assay bone-defect model, kill 99.63% of *Staphylococcus aureus* bacteria (Chen et al. 2021a). This 26-residue "fusion peptide" sequence with an additional azide-EG_4 linker is significantly longer than previously reported multifunctional peptide designs, demonstrating that even large constructs may be suitable for biointerfacial designs. In fact, the QK sequence is the helical region (17–25) of the human vascular endothelial growth factor (VEGF) protein but its ability to induce angiogenesis had previously not been consistently shown until this

report. With the Y-shaped design, expression of the angiogenesis-related genes/ proteins (VEGF and VEGFR-2) in HUVECs and osteogenesis-related genes/proteins (ALP, COL-1, RUNX-2, OPN and OCN) in hBMSCs was all up-regulated in vitro, and cell proliferation was also enhanced. It was also shown that the antimicrobial activities against *S. aureus*, *Escherichia coli*, *Pseudomonas aeruginosa* and methicillin-resistant *S. aureus* were all stronger with the fusion design than with control experiments using mixed peptides. Overall, the enhancements observed are suggestive of the ability of multifunctional peptide designs to inherently provide a degree of steric separation between copies of each type of immobilized ligand and hence enhance binding.

Mas-Moruno et al. had also earlier demonstrated co-immobilization of AMPs with cell-adhesive sequences (Hoyos-Nogues et al. 2017; Martin-Gomez et al. 2021a). They combined the lactoferrin-derived LF1–11 AMP (GRRRSVQWCAV) with RGD to obtain statistically significant improvements in the adhesion, proliferation and mineralization of cells and reduced bacterial colonization. This was shown for cell culture of both SaOS-2 osteoblast-like cells and human bone marrow mesenchymal stem cells (MSCs), and antibacterial activities against *Streptococcus sanguinis* and *S. aureus*. The combination with SaOS-2 could be indicative of a dental osseointegration application. In experiments with MSCs, the researchers also trialled selected lengths of flexible oligoethylene glycol (OEG) linkers inserted between the surface anchor (di-DOPA) unit and the LF1–11 and RGD motifs. They demonstrated that the best combination of AMP activity and cell adhesion was to use relatively equal arm lengths in the Y-shaped design—no linker for LF1–11 and OEG_4 or OEG_8 for (cyclic) RGD (Martin-Gomez et al. 2021a). Thus, this study showed that the surface activity of multifunctional peptides may be further enhanced by optimization of the spatial presentation (i.e., separation control) of their designs. This is a process similar to enhancing activity of peptide therapeutics by optimization of their multimerization.

As logical extensions of the examples discussed above, the Y-shaped design may also be applied to antifouling and other biorecognition sequences to enable, e.g., biosensing. For example, the Luo group, following on from their linear designs (see Sect. 15.4.2), paired the EKEKEKE antifouling sequence with IgG binding HWRGWV sequence, one motif on each arm, to enable electrochemical biosensing in human serum and blood samples (Chen et al. 2021b). The 0.032 ng mL^{-1} limit of detection achieved for IgG detection was an order of magnitude lower than the 0.26 ng mL^{-1} achieved with the earlier linear design, although this could also have been influenced by the choice of electrode material (PANI vs. AuNP-PEDOT).

15.5 Conclusions

The studies reviewed in this chapter demonstrate that peptides constitute a versatile platform to convey multiple biointerfacial functionalities in a (bio)chemically defined manner, which enables both the delineation of cell–surface interaction

mechanisms and applications ranging from biosensing to biomaterials. The broad underlying theme of this research is protein mimicry, and researchers have implicitly or explicitly attempted to transplant both the biorecognition and antifouling features of proteins onto a surface, not only by co-immobilizing suitable peptide sequence motifs but also by precisely structuring their spatial relationships on the molecular/nanoscale. Although antifouling already has a long history of study, it is evident that it remains a central practical consideration in engineering biointerfaces capable of specific biorecognition, as seen in, e.g., the very low biosensing limits of detection demonstrated. Moreover, the sophisticated presentation of peptide motifs regulating cell adhesion is a prime demonstration of ECM mimicry.

On reflection, it is remarkable that the relatively short oligopeptide motifs surveyed (mostly 3–15 residues long) can already deliver such robust biochemical signalling. Moreover, these studies also demonstrate that rationally combining disparate functional motifs not found in nature can be a successful approach. In this regard, the molecular design strategy presented, of covalently combining different sequences, adding branch points and tailoring linkers of different lengths, is greatly aided by the versatility and convenience of solid phase peptide synthesis and related orthogonal chemistry techniques that are increasingly available "off the shelf". Overall, multifunctional peptide biointerfacial designs possess a number of intrinsic advantages, as outlined in Sect. 15.2 and also demonstrated in the rest of the chapter. These include their robust capabilities to direct biomolecular and cell interactions on material surfaces, convenience in designing experiments with precise controls, and hence delineating mechanisms, and relative convenience in surface characterization and storage.

Looking ahead, the great scope for further advancements in multifunctional peptide biointerfaces can be illustrated by a couple of "out of the box" designs. The first relates to biomimetic demonstrations of the nuclear (nano)pore complexes (NPC) that selectively control transport of all proteins and polynucleotides through the cell nuclear membrane and which are controlled by a family of nucleoporin proteins found in them (Knockenhauer and Schwartz 2016; Hampoelz et al. 2019). The nanopore (and hydrogel) demonstrations have so far been based on high molecular weight chains produced by protein expression (Frey et al. 2006; Jovanovic-Talisman et al. 2009; Kowalczyk et al. 2011; Schleicher et al. 2014; Kim et al. 2015; Schmidt and Görlich 2015; Pathirathna et al. 2019), due to the complex functionalities of the nucleoporins that have to be mimicked, from biorecognition to antifouling and reversible crosslinking. Nonetheless, NPCs may represent another beacon for the possibilities of designing (oligo)peptide biointerfaces presenting multiple and coordinated functionalities abstracted from proteins. The other system is the peptoid nanosheet (PNS), assembled from 20–40 residue long peptoid sequences assembled in a de novo secondary structure (coined "Σ-strand"), that constitutes lipid bilayer-like membranes 3 nm thick and many microns wide. The decoration of these sheets with single species of functional peptide, peptoid and oligosaccharide biorecognition sequences by both covalent coupling and non-covalent insertions have been demonstrated (Robertson et al. 2014; Zhu et al. 2017b; Battigelli et al. 2018; Gao et al. 2020; Kim et al. 2020).

Together with the wide lateral span of these membranes, PNS represents the potential multifunctionality and diverse molecular architectures that synthetic peptide biointerfaces can achieve.

References

Al Musaimi O, de la Torre BG, Albericio F (2020) Greening Fmoc/tBu solid-phase peptide synthesis. Green Chem 22:996–1018

Amit M, Yuran S, Gazit E, Reches M, Ashkenasy N (2018) Tailor-made functional peptide self-assembling nanostructures. Adv Mater 30:13

Andrea A, Molchanova N, Jenssen H (2018) Antibiofilm peptides and peptidomimetics with focus on surface immobilization. Biomol Ther 8:27

Battigelli A, Kim JH, Dehigaspitiya DC, Proulx C, Robertson EJ, Murray DJ, Rad B, Kirshenbaum K, Zuckermann RN (2018) Glycosylated peptoid nanosheets as a multivalent scaffold for protein recognition. ACS Nano 12:2455–2465

Behrendt R, White P, Offer J (2016) Advances in Fmoc solid-phase peptide synthesis. J Pept Sci 22: 4–27

Beyer CD, Reback ML, Heinen N, Thavalingam S, Rosenhahn A, Metzler-Nolte N (2020) Low fouling peptides with an all (D) amino acid sequence provide enhanced stability against proteolytic degradation while maintaining low antifouling properties. Langmuir 36:10996–11004

Birke A, Ling J, Barz M (2018) Polysarcosine-containing copolymers: synthesis, characterization, self-assembly, and applications. Prog Polym Sci 81:163–208

Bleher S, Buck J, Muhl C, Sieber S, Barnert S, Witzigmann D, Huwyler J, Barz M, Süss R (2019) Poly(sarcosine) surface modification imparts stealth-like properties to liposomes. Small 15: 1904716

Bolduc OR, Lambert-Lanteigne P, Colin DY, Zhao SS, Proulx C, Boeglin D, Lubell WD, Pelletier JN, Féthière J, Ong H, Masson J-F (2011) Modified peptide monolayer binding His-tagged biomolecules for small ligand screening with SPR biosensors. Analyst 136:3142–3148

Chelmowski R, Köster SD, Kerstan A, Prekelt A, Grunwald C, Winkler T, Metzler-Nolte N, Terfort A, Wöll C (2008) Peptide-based SAMs that resist the adsorption of proteins. J Am Chem Soc 130:14952–14953

Chen CS, Mrksich M, Huang S, Whitesides GM, Ingber DE (1997) Geometric control of cell life and death. Science 276:1425–1428

Chen JJ, Hu GS, Li TJ, Chen YH, Gao M, Li QT, Hao LJ, Jia YG, Wang L, Wang YJ (2021a) Fusion peptide engineered "statically-versatile" titanium implant simultaneously enhancing anti-infection, vascularization and osseointegration. Biomaterials 264:15

Chen M, Song Z, Han R, Li Y, Luo XL (2021b) Low fouling electrochemical biosensors based on designed Y-shaped peptides with antifouling and recognizing branches for the detection of IgG in human serum. Biosens Bioelectron 178:7

Chen Q, Zhang D, Gu J, Zhang H, Wu X, Cao C, Zhang X, Liu R (2021c) The impact of antifouling layers in fabricating bioactive surfaces. Acta Biomater 126:45–62

Cheung DL, Lau KHA (2019) Atomistic study of zwitterionic peptoid antifouling brushes. Langmuir 35:1483–1494

Cioffi CL, Liu S, Wolf MA (2010) Recent developments in glycine transporter-1 inhibitors. In: Macor JE (ed) Annual reports in medicinal chemistry, vol 45. Academic, pp 19–35

Clauder F, Moller S, Kohling S, Bellmann-Sickert K, Rademann J, Schnabelrauch M, Beck-Sickinger AG (2020a) Peptide-mediated surface coatings for the release of wound-healing cytokines. J Tissue Eng Regen Med 14:1738–1748

Clauder F, Zitzmann FD, Friebe S, Mayr SG, Robitzki AA, Beck-Sickinger AG (2020b) Multifunctional coatings combining bioactive peptides and affinity-based cytokine delivery for enhanced integration of degradable vascular grafts. Biomater Sci 8:1734–1747

Costa F, Carvalho IF, Montelaro RC, Gomes P, Martins MCL (2011) Covalent immobilization of antimicrobial peptides (AMPs) onto biomaterial surfaces. Acta Biomater 7:1431–1440

Dalsin JL, Hu B-H, Lee BP, Messersmith PB (2003) Mussel adhesive protein mimetic polymers for the preparation of nonfouling surfaces. J Am Chem Soc 125:4253–4258

Dalsin JL, Lin L, Tosatti S, Vörös J, Textor M, Messersmith PB (2004) Protein resistance of titanium oxide surfaces modified by biologically inspired mPEG−DOPA. Langmuir 21:640–646

Ding CF, Wang XY, Luo XL (2019) Dual-mode electrochemical assay of prostate-specific antigen based on antifouling peptides functionalized with electrochemical probes and internal references. Anal Chem 91:15846–15852

Fischer NG, He JH, Aparicio C (2020) Surface immobilization chemistry of a laminin-derived peptide affects keratinocyte activity. Coatings 10:14

Frey S, Richter RP, Görlich D (2006) FG-rich repeats of nuclear pore proteins form a three-dimensional meshwork with hydrogel-like properties. Science 314:815–817

Gangloff N, Ulbricht J, Lorson T, Schlaad H, Luxenhofer R (2015) Peptoids and polypeptoids at the frontier of supra-and macromolecular engineering. Chem Rev 116:1753–1802

Gao H, Liu M, Zhao Z, Yang C, Zhu L, Cai Y, Yang Y, Hu Z (2020) Diagnosis of mild cognitive impairment and Alzheimer's disease by the plasma and serum amyloid-beta 42 assay through highly sensitive peptoid nanosheet sensor. ACS Appl Mater Interfaces 12:9693–9700

Goncalves DPN, Rodriguez RD, Kurth T, Bray LJ, Binner M, Jungnickel C, Gur FN, Poser SW, Schmidt TL, Zahn DRT, Androutsellis-Theotokis A, Schlierf M, Werner C (2017) Enhanced targeting of invasive glioblastoma cells by peptide-functionalized gold nanorods in hydrogel-based 3D cultures. Acta Biomater 58:12–25

Hampoelz B, Andres-Pons A, Kastritis P, Beck M (2019) Structure and assembly of the nuclear pore complex. Annu Rev Biophys 48:515–536

Han R, Wang G, Xu Z, Zhang L, Li Q, Han Y, Luo X (2020) Designed antifouling peptides planted in conducting polymers through controlled partial doping for electrochemical detection of biomarkers in human serum. Biosens Bioelectron 164:112317

Hansen PR, Oddo A (2015) Fmoc solid-phase peptide synthesis. Peptide antibodies: methods and protocols. Springer, New York, pp 33–50

Hasan A, Lee K, Tewari K, Pandey LM, Messersmith PB, Faulds K, Maclean M, Lau KHA (2020) Surface design for immobilization of an antimicrobial peptide mimic for efficient anti-biofouling. Chem Eur J 26:5789–5793

He J, Chen J, Hu G, Wang L, Zheng J, Zhan J, Zhu Y, Zhong C, Shi X, Liu S, Wang Y, Ren L (2018) Immobilization of an antimicrobial peptide on silicon surface with stable activity by click chemistry. J Mater Chem B 6:68–74

Hersel U, Dahmen C, Kessler H (2003) RGD modified polymers: biomaterials for stimulated cell adhesion and beyond. Biomaterials 24:4385–4415

Hoyos-Nogues M, Velasco F, Ginebra MP, Manero JM, Gil FJ, Mas-Moruno C (2017) Regenerating bone via multifunctional coatings: the blending of cell integration and bacterial inhibition properties on the surface of biomaterials. ACS Appl Mater Interfaces 9:21618–21630

Hoyos-Nogues M, Falgueras-Batlle E, Ginebra MP, Manero JM, Gil J, Mas-Moruno C (2019) A dual molecular biointerface combining RGD and KRSR sequences improves osteoblastic functions by synergizing integrin and cell-membrane proteoglycan binding. Int J Mol Sci 20:13

Hu Y, Hou Y, Wang H, Lu H (2018) Polysarcosine as an alternative to PEG for therapeutic protein conjugation. Bioconjug Chem 29:2232–2238

Jiang SY, Cao ZQ (2010) Ultralow-fouling, functionalizable, and hydrolyzable zwitterionic materials and their derivatives for biological applications. Adv Mater 22:920–932

Jiang C, Wang G, Hein R, Liu N, Luo X, Davis JJ (2020) Antifouling strategies for selective in vitro and in vivo sensing. Chem Rev 120:3852–3889

Jovanovic-Talisman T, Tetenbaum-Novatt J, McKenney AS, Zilman A, Peters R, Rout MP, Chait BT (2009) Artificial nanopores that mimic the transport selectivity of the nuclear pore complex. Nature 457:1023–1027

Jurczak P, Witkowska J, Rodziewicz-Motowidlo S, Lach S (2020) Proteins, peptides and peptidomimetics as active agents in implant surface functionalization. Adv Colloid Interf Sci 276:21

Keefe AJ, Caldwell KB, Nowinski AK, White AD, Thakkar A, Jiang S (2013) Screening nonspecific interactions of peptides without background interference. Biomaterials 34:1871–1877

Kim M, Chen WG, Kang JW, Glassman MJ, Ribbeck K, Olsen BD (2015) Artificially engineered protein hydrogels adapted from the nucleoporin Nsp1 for selective biomolecular transport. Adv Mater 27:4207–4212

Kim JH, Grzincic EM, Yun L, Spencer RK, Kline MA, Zuckermann RN (2020) Lipid-anchor display on peptoid nanosheets via co-assembly for multivalent pathogen recognition. Soft Matter 16:907–913

Knight AS, Zhou EY, Francis MB, Zuckermann RN (2015) Sequence programmable peptoid polymers for diverse materials applications. Adv Mater 27:5665–5691

Knockenhauer KE, Schwartz TU (2016) The nuclear pore complex as a flexible and dynamic gate. Cell 164:1162–1171

Kowalczyk SW, Kapinos L, Blosser TR, Magalhaes T, van Nies P, Lim RYH, Dekker C (2011) Single-molecule transport across an individual biomimetic nuclear pore complex. Nat Nanotechnol 6:433–438

Lara S, Perez-Potti A, Herda LM, Adumeau L, Dawson KA, Yan Y (2018) Differential recognition of nanoparticle protein Corona and modified low-density lipoprotein by macrophage receptor with collagenous structure. ACS Nano 12:4930–4937

Lau KHA (2014) Peptoids for biomaterials science. Biomater Sci 2:627–633

Lau KHA, Ren C, Park SH, Szleifer I, Messersmith PB (2012a) An experimental–theoretical analysis of protein adsorption on peptidomimetic polymer brushes. Langmuir 28:2288–2298

Lau KHA, Ren C, Sileika TS, Park SH, Szleifer I, Messersmith PB (2012b) Surface-grafted polysarcosine as a peptoid antifouling polymer brush. Langmuir 28:16099–16107

Lau KHA, Sileika TS, Park SH, Sousa AML, Burch P, Szleifer I, Messersmith PB (2015) Molecular design of antifouling polymer brushes using sequence-specific peptoids. Adv Mater Interf 2:1400225

Lee H, Dellatore SM, Miller WM, Messersmith PB (2007) Mussel-inspired surface chemistry for multifunctional coatings. Science 318:426–430

Liu NZ, Hui N, Davis JJ, Luo XL (2018) Low fouling protein detection in complex biological media supported by a designed multifunctional peptide. Acs Sensors 3:1210–1216

Liu XH, Zhang QW, Knoll WG, Liedberg B, Wang Y (2020) Rational design of functional peptide-gold hybrid nanomaterials for molecular interactions. Adv Mater 32:37

Liu NZ, Fan XJ, Hou HQ, Gao FX, Luo XL (2021) Electrochemical sensing interfaces based on hierarchically architectured zwitterionic peptides for ultralow fouling detection of alpha fetoprotein in serum. Anal Chim Acta 1146:17–23

Maan AMC, Hofman AH, de Vos WM, Kamperman M (2020) Recent developments and practical feasibility of polymer-based antifouling coatings. Adv Funct Mater 2000936

Martin-Gomez H, Oliver-Cervello L, Buxadera-Palomero J, Ginebra MP, Mas-Moruno C (2021a) Chemically diverse multifunctional peptide platforms with antimicrobial and cell adhesive properties. Chembiochem 22:839–844

Martin-Gomez H, Oliver-Cervello L, Sanchez-Campillo I, Marchan V, Ginebra MP, Mas-Moruno C (2021b) A versatile click chemistry-based approach for functionalizing biomaterials of diverse nature with bioactive peptides. Chem Commun 57:982–985

Mas-Moruno C, Fraioli R, Albericio F, Manero JM, Gil FJ (2014) Novel peptide-based platform for the dual presentation of biologically active peptide motifs on biomaterials. ACS Appl Mater Interfaces 6:6525–6536

Mas-Moruno C, Su B, Dalby MJ (2019) Multifunctional coatings and Nanotopographies: toward cell instructive and antibacterial implants. Adv Healthc Mater 8:26

Mi L, Bernards MT, Cheng G, Yu Q, Jiang S (2010) pH responsive properties of non-fouling mixed-charge polymer brushes based on quaternary amine and carboxylic acid monomers. Biomaterials 31:2919–2925

Mohammad-Beigi H, Hayashi Y, Zeuthen CM, Eskandari H, Scavenius C, Juul-Madsen K, Vorup-Jensen T, Enghild JJ, Sutherland DS (2020) Mapping and identification of soft corona proteins at nanoparticles and their impact on cellular association. Nat Commun 11:4535

Nowinski AK, Sun F, White AD, Keefe AJ, Jiang SY (2012) Sequence, structure, and function of peptide self-assembled monolayers. J Am Chem Soc 134:6000–6005

Oberhaus FV, Frense D, Beckmann D (2020) Immobilization techniques for aptamers on gold electrodes for the electrochemical detection of proteins: a review. Biosensors 10:45

Oliver-Cervello L, Martin-Gomez H, Reyes L, Noureddine F, Cavalcanti-Adam EA, Ginebra MP, Mas-Moruno C (2021) An engineered biomimetic peptide regulates cell behavior by synergistic integrin and growth factor signaling. Adv Healthc Mater 10:10

Ostuni E, Chapman RG, Holmlin RE, Takayama S, Whitesides GM (2001a) A survey of structure–property relationships of surfaces that resist the adsorption of protein. Langmuir 17:5605–5620

Ostuni E, Chapman RG, Liang MN, Meluleni G, Pier G, Ingber DE, Whitesides GM (2001b) Self-assembled monolayers that resist the adsorption of proteins and the adhesion of bacterial and mammalian cells. Langmuir 17:6336–6343

Pagel M, Beck-Sickinger AG (2017) Multifunctional biomaterial coatings: synthetic challenges and biological activity. Biol Chem 398:3–22

Pagel M, Hassert R, John T, Braun K, Wiessler M, Abel B, Beck-Sickinger AG (2016) Multifunctional coating improves cell adhesion on titanium by using cooperatively acting peptides. Angewandte Chemie-International Edition 55:4826–4830

Pan F, Aaron Lau KH, Messersmith PB, Lu JR, Zhao X (2020) Interfacial assembly inspired by marine mussels and antifouling effects of polypeptoids: a neutron reflection study. Langmuir 36:12309–12318

Pathirathna P, Balla RJ, Meng G, Wei Z, Amemiya S (2019) Nanoscale electrostatic gating of molecular transport through nuclear pore complexes as probed by scanning electrochemical microscopy. Chem Sci 10:7929–7936

Peng LH, Huang YF, Zhang CZ, Niu J, Chen Y, Chu Y, Jiang ZH, Gao JQ, Mao ZW (2016) Integration of antimicrobial peptides with gold nanoparticles as unique non-viral vectors for gene delivery to mesenchymal stem cells with antibacterial activity. Biomaterials 103:137–149

Prime KL, Whitesides GM (1991) Self-assembled organic monolayers - model systems for studying adsorption of proteins at surfaces. Science 252:1164–1167

Rai A, Ferreira L (2021) Biomedical applications of the peptide decorated gold nanoparticles. Crit Rev Biotechnol 41:186–215

Raphel J, Holodniy M, Goodman SB, Heilshorn SC (2016) Multifunctional coatings to simultaneously promote osseointegration and prevent infection of orthopaedic implants. Biomaterials 84:301–314

Robertson EJ, Olivier GK, Qian M, Proulx C, Zuckermann RN, Richmond GL (2014) Assembly and molecular order of two-dimensional peptoid nanosheets through the oil-water interface. Proc Natl Acad Sci USA 111:13284–13289

Ruoslahti E, Pierschbacher M (1987) New perspectives in cell adhesion: RGD and integrins. Science 238:491–497

Russo MJ, Han MY, Desroches PE, Manasa CS, Dennaoui J, Quigley AF, Kapsa RMI, Moulton SE, Guijt RM, Greene GW, Silva SM (2021) Antifouling strategies for electrochemical biosensing: mechanisms and performance toward point of care based diagnostic applications. Acs Sensors 6:1482–1507

Ryu JY, Song IT, Lau KHA, Messersmith PB, Yoon T-Y, Lee H (2014) New antifouling platform characterized by single-molecule imaging. ACS Appl Mater Interfaces 6:3553–3558

Ryu JH, Messersmith PB, Lee H (2018) Polydopamine surface chemistry: a decade of discovery. ACS Appl Mater Interfaces 10:7523–7540

Sakala GP, Reches M (2018) Peptide-based approaches to fight biofouling. Adv Mater Interfaces 5: 26

Saxena V, Merrilees MGL, Lau KHA (2020) In: Chandra P, Pandey LM (eds) Antifouling peptoid biointerfaces. Biointerface engineering: prospects in medical diagnostics and drug delivery. Springer, Singapore, pp 55–73

Schleicher KD, Dettmer SL, Kapinos LE, Pagliara S, Keyser UF, Jeney S, Lim RYH (2014) Selective transport control on molecular velcro made from intrinsically disordered proteins. Nat Nanotechnol 9:525–530

Schmidt HB, Görlich D (2015) Nup98 FG domains from diverse species spontaneously phase-separate into particles with nuclear pore-like permselectivity. elife 4:e04251

Singhvi R, Kumar A, Lopez G, Stephanopoulos G, Wang D, Whitesides G, Ingber D (1994) Engineering cell shape and function. Science 264:696–698

Smith-Palmer T (2019) Clinical analysis | sarcosine, creatine, and creatinine☆. In: Worsfold P, Poole C, Townshend A, Miró M (eds) Encyclopedia of analytical science, 3rd edn. Academic, Oxford, pp 163–172

Statz AR, Meagher RJ, Barron AE, Messersmith PB (2005) New peptidomimetic polymers for antifouling surfaces. J Am Chem Soc 127:7972–7973

Statz AR, Park JP, Chongsiriwatana NP, Barron AE, Messersmith PB (2008) Surface-immobilised antimicrobial peptoids. Biofouling 24:439–448

Szleifer I (1997) Protein adsorption on surfaces with grafted polymers: a theoretical approach. Biophys J 72:595–612

Toda M, Arima Y, Iwata H (2010) Complement activation on degraded polyethylene glycol-covered surface. Acta Biomater 6:2642–2649

Unsworth LD, Sheardown H, Brash JL (2005) Polyethylene oxide surfaces of variable chain density by chemisorption of PEO-thiol on gold: adsorption of proteins from plasma studied by radiolabelling and immunoblotting. Biomaterials 26:5927–5933

Vaisocherova H, Zhang Z, Yang W, Cao ZQ, Cheng G, Taylor AD, Piliarik M, Homola J, Jiang SY (2009) Functionalizable surface platform with reduced nonspecific protein adsorption from full blood plasma-material selection and protein immobilization optimization. Biosens Bioelectron 24:1924–1930

Vaisocherová H, Brynda E, Homola J (2015) Functionalizable low-fouling coatings for label-free biosensing in complex biological media: advances and applications. Anal Bioanal Chem 407: 3927–3953

Viricel W, Fournet G, Beaumel S, Perrial E, Papot S, Dumontet C, Joseph B (2019) Monodisperse polysarcosine-based highly-loaded antibody-drug conjugates. Chem Sci 10:4048–4053

Vroman L (1962) Effect of absorbed proteins on the wettability of hydrophilic and hydrophobic solids. Nature 196:476–477

Waite HJ, Tanzer ML (1981) Polyphenolic substance of Mytilus edulis: novel adhesive containing L-Dopa and hydroxyproline. Science 212:1038–1040

Wang GX, Han R, Su XL, Li YN, Xu GY, Luo XL (2017) Zwitterionic peptide anchored to conducting polymer PEDOT for the development of antifouling and ultrasensitive electrochemical DNA sensor. Biosens Bioelectron 92:396–401

Wang GX, Han R, Li Q, Han YF, Luo XL (2020a) Electrochemical biosensors capable of detecting biomarkers in human serum with unique long-term antifouling abilities based on designed multifunctional peptides. Anal Chem 92:7186–7193

Wang J, Wang D, Hui N (2020b) A low fouling electrochemical biosensor based on the zwitterionic polypeptide doped conducting polymer PEDOT for breast cancer marker BRCA1 detection. Bioelectrochemistry 136:107595

Wang D, Wang J, Song Z, Hui N (2021a) Highly selective and antifouling electrochemical biosensors for sensitive MicroRNA assaying based on conducting polymer polyaniline functionalized with zwitterionic peptide. Anal Bioanal Chem 413:543–553

Wang J, Li Y, Nie G (2021b) Multifunctional biomolecule nanostructures for cancer therapy. Nat Rev Mater

Wheeler KE, Chetwynd AJ, Fahy KM, Hong BS, Tochihuitl JA, Foster LA, Lynch I (2021) Environmental dimensions of the protein corona. Nat Nanotechnol 16:617–629

White AD, Nowinski AK, Huang W, Keefe AJ, Sun F, Jiang S (2012) Decoding nonspecific interactions from nature. Chem Sci 3:3488–3494

Xiao M, Jasensky J, Gerszberg J, Chen J, Tian J, Lin T, Lu T, Lahann J, Chen Z (2018) Chemically immobilized antimicrobial peptide on polymer and self-assembled monolayer substrates. Langmuir 34:12889–12896

Xu C, Wu F, Yu P, Mao L (2019) In vivo electrochemical sensors for neurochemicals: recent update. ACS Sens 4:3102–3118

Yang H, Gurgel PV, Carbonell RG (2005) Hexamer peptide affinity resins that bind the fc region of human immunoglobulin G. J Pept Res 66:120–137

Yuan ZF, Li BW, Niu LQ, Tang CJ, McMullen P, Jain P, He YW, Jiang SY (2020) Zwitterionic peptide cloak mimics protein surfaces for protein protection. Angewandte Chemie-International Edition 59:22378–22381

Zhang P, Sun F, Liu SJ, Jiang SY (2016) Anti-PEG antibodies in the clinic: current issues and beyond PEGylation. J Control Release 244:184–193

Zhao J, Qin ZH, Wu JN, Li LJ, Jin Q, Ji J (2017) Zwitterionic stealth peptide-protected gold nanoparticles enable long circulation without the accelerated blood clearance phenomenon. Biomater Sci 6:200–206

Zhu H, Chen Y, Yan F-J, Chen J, Tao X-F, Ling J, Yang B, He Q-J, Mao Z-W (2017a) Polysarcosine brush stabilized gold nanorods for in vivo near-infrared photothermal tumor therapy. Acta Biomater 50:534–545

Zhu L, Zhao Z, Cheng P, He Z, Cheng Z, Peng J, Wang H, Wang C, Yang Y, Hu Z (2017b) AntibodyMimetic peptoid nanosheet for label-free serum-based diagnosis of Alzheimer's Disease. Adv Mater 29:1700057

Zhu ML, Zhang KY, Feng L, Lin SE, Pan Q, Bian LM, Li G (2021) Surface decoration of development-inspired synthetic N-cadherin motif via Ac-BP promotes osseointegration of metal implants. Bioactive Mater 6:1353–1364

Chapter 16
Peptide Bionanomaterials Global Market: The Future of Emerging Industry

Ayeesha Mujeeb and Aline F. Miller

Abstract Over the years, the rising popularity of peptides has led to a paradigm shift in the focus of biotechnology and pharmaceutical industry from traditional molecular-based interventions to the development of multifaceted nanomaterial-based interventions. The 'bench-to-bedside' approach has enabled researchers to work with a variety of peptide-based bionanomaterials for applications in tissue engineering, regenerative medicine, drug delivery, biosensing and 3D printing, paving the way for clinical translation. Owing to the very nature of peptide molecular building blocks that form the basis of self-assembled biomaterials, the final materials exhibit extraordinary properties, such as biocompatibility, flexibility in design, reproducibility and stability, which help expedite their translation into different application domains within biomedicine. In this chapter, we highlight the clinical need for translation of peptide nanomaterials, outline current priority application areas and discuss how these are currently bridging gaps between academic and industrial research to support product development, scale up and adoption of technology. The chapter also outlines the substantial growth in global market size of peptide-based biomaterial products. Many examples of peptide nanomaterials include hydrogels as scaffolds and wound dressing materials; 3D printed nanostructures; and nanotubes as drug delivery vehicles and components for reconstruction of soft tissues and 3D cell culture.

Keywords Peptide · Bionanomaterials · Hydrogels · Tissue engineering · Regenerative medicine · Drug delivery · 3D printing · Biomaterial global market

A. Mujeeb (✉)
Atta-ur-Rahman School of Applied Biosciences, National University of Sciences and Technology, Islamabad, Pakistan
e-mail: ayeeshamujeeb@asab.nust.edu.pk

A. F. Miller
Department of Chemical Engineering, Manchester Institute of Biotechnology, University of Manchester, Manchester, UK

16.1   Introduction

The global biomaterials market was estimated to be worth US$135.4 billion in 2021 and is expected to register at a compound annual growth rate (CAGR) of 15.4% from 2022 to 2030 (Global Market Size and Share Report 2022). Interestingly, the global hydrogel market was estimated to be worth US$22.45 billion in 2021 (16.54% of the total biomaterials market in 2021) and is expected to reach a value of US$37.98 billion by 2030, growing at a CAGR of 6% during the forecast period from 2022 to 2030 (Precedence Research 2022). Some of the factors contributing towards the growth in the global hydrogel market include clinical need due to an ageing population in healthcare; advances in cell and fundamental biology as researchers can now do in-depth biological studies in pursuit of new tissue-engineered constructs, delivery systems and diagnostics; and many pharmaceutical and biotech companies are committed to the principles of 3Rs (animal reduction, refinement to minimise pain and replacement of animals to be used). Two-dimensional (2D) cell models do not provide physiologically relevant data; therefore there is a big push to transfer to three-dimensional (3D) models, for which typically a self-supporting 3D scaffold is required to help control and direct cell behaviour.

The global hydrogel market is segmented into three types of raw materials: natural, synthetic and hybrid hydrogels. Natural materials are naturally occurring; synthetic materials are man-made; and hybrid materials are composites consisting of natural and synthetic building blocks. The highest share of the hydrogel market is contributed by synthetic hydrogels because of their advantage over naturally extracted materials that frequently undergo conventional extraction protocols, are difficult to handle and reproducibility is compromised because of varying properties such as water content, mechanical strength and elasticity (Kibungu et al. 2021). In comparison, due to improved consistency and the ability to modify properties of synthetic peptides, attention is being drawn to fabricate function-oriented bionanomaterials that are clinically viable. To serve this purpose, considerable efforts have been directed towards the design of peptide-based hydrogel bionanomaterials, because of their favourable characteristics such as easy formation, functionalisation, biodegradability, scalability and high biocompatibility for different biological applications (Das and Das 2021; Li et al. 2022a; Wang et al. 2022). Owing to these properties, synthetic peptide hydrogels are progressively dominating the market since 2018, and their need is expected to rise due to the demand for complying with the 3Rs and working with more physiologically relevant 3D models. Consequently, this is driving the companies and government bodies to invest in the development of synthetic peptide-based strategies and different delivery methods and techniques.

Herein, we will review the current status of peptide bionanomaterials for different biomedical applications and study their market reach within the pharma and biotech industry, discuss some of the challenges faced and focus on the future direction of peptides as nanomaterials for clinical translation.

16.2 Peptides as Bionanomaterials

To date, stem cell therapy, regenerative medicine and tissue engineering segments dominate the biomaterials market (Grandview Research 2022). The growth (15.4% CGAR from 2022 to 2030) (Grandview Research 2022) can be strongly attributed to the growing implementation of biomaterial innovation and technology for reconstruction surgeries, drug delivery, tissue repair and regeneration; and the need for more physiologically relevant disease models for both cell biology understanding and toxicity testing. No longer is 2D able to predict drug behaviour, and the need for 3D environments is important, especially for the growth of organoids in this regard. One of the most important goals of translational research is to develop bionanomaterials that can be fabricated in the lab, and used in the clinic, and ultimately be scaled up so they may be adopted as viable treatment solutions for the current unmet clinical need. As peptides are readily degraded in the human body, their delivery via scaffolds, injectables and sprayables is still under investigation (Qi et al. 2018; Sharma et al. 2021; Bernhard and Tibbitt 2021; Elsawy et al. 2022). In particular, modern-day analytical techniques—purification methods, which greatly affect the purity, percentage yield and performance—facilitate the discovery of novel peptides with great therapeutic potential. Peptides have exceptional attributes, such as much easier and cost-effective synthesis, higher mechanical stability, excellent tissue penetration and less immunogenicity, in comparison to lipids and carbohydrates (Apostolopoulos et al. 2021).

Peptides when dissolved in water form stable hydrogels under physiological conditions, for example, change in pH, temperature or peptide concentration, by the process of molecular self-assembly, a spontaneous organisation of nanostructures that involves non-covalent interactions, including hydrogen bonding, electrostatic interactions, hydrophobic interactions and π–π interactions (Bowerman et al. 2011; Mujeeb et al. 2013; Wychowaniec et al. 2020). Due to these physical interactions, the nanofibres stack together to form mesh of fibres, which in turn give rise to macroscopic structures of synthetic peptide hydrogels that can be precisely controlled and tuned for function. The microstructures include nanofibres, nanosheets, nanospheres, nanotubes and nanowires. In this chapter, we focus on nanofibrous hydrogels as bionanomaterials. The effect on function by changes in structure, for example, nanotapes, nanospheres and nanotubes (Vauthey et al. 2002; Edwards-Gayle and Hamley 2017), can also be effectively predicted by machine learning algorithms, which allow us to precisely design these nanomaterials for different biomedical applications (Li et al. 2019). For example, self-assembled peptide nanospheres have been generated from L,L-cyclic peptides using hydrophobic and hydrophilic amino acid residues that formed vehicles for intracellular delivery of VEGF siRNA and VEGF antisense oligonucleotide (Panigrahi et al. 2022). In another study, self-assembled cyclic peptide nanotubes have shown to function as synthetic integral transmembrane channels. Manipulating the sequence of cyclic peptides enables the control of the outer and inner surfaces of the nanotubes, thus affecting the permeability to different molecules such as water and
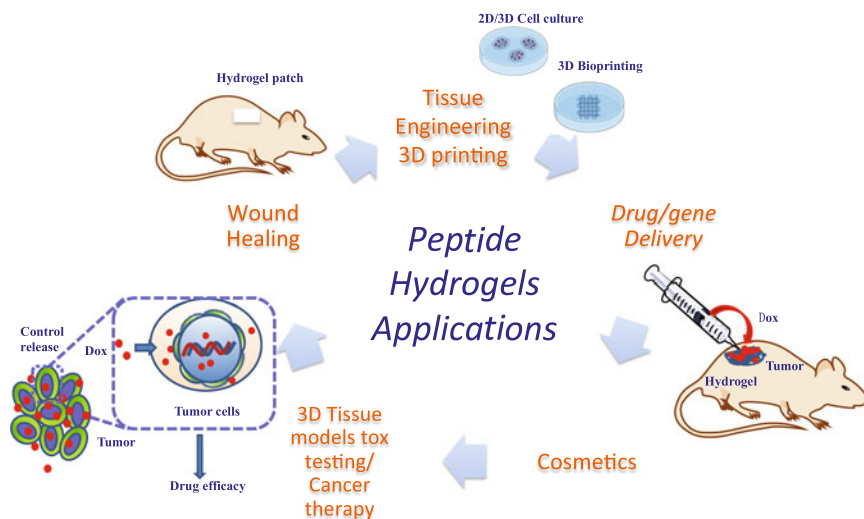
Fig. 16.1 A schematic showing peptide hydrogels as bionanomaterials for tissue engineering, 3D bioprinting, drug and gene delivery, cosmetics, 3D tissue models for toxicity testing and cancer therapy and wound healing applications

ions. Such dynamic structures have demonstrated their potential to serve as drug or diagnostic agent carrier systems (Blanco-González et al. 2021; Calvelo et al. 2021), where the application potential has arisen from the structure and properties of the self-assembled material.

Peptide-based hydrogels consisting of meshes of nanofibres are particularly fascinating because of their unique transparency, biocompatibility, biodegradability and bioactivity with structures that mimic the natural proteins and extra-cellular matrix (Mujeeb et al. 2013; Liu et al. 2019). The nanofibrous networks in hydrogels can house drugs, which give them controlled drug release properties under various stimuli, and have been shown, for example, to participate in the treatment of breast cancer recurrence in vivo as an injectable system (Qi et al. 2018). Hydrogels can regulate physiological functions in vivo and are readily modified and functionalised through side-chain and backbone modification to satisfy specific applications (Song et al. 2017). As a result, structural optimisation of peptides is easier and gives rise to the formation of different nanostructures that hold great promise in biomedical applications including tissue engineering, 3D bioprinting, drug and gene vehicles (Gupta et al. 2020), cancer therapy, wound healing and cosmetics (Fig. 16.1).

16.3 Market Segments Based on Applications

16.3.1 Tissue Engineering and 3D Printing

Most peptide-related research is beginning to progress towards the clinic (Gelain et al. 2021; Correa et al. 2021). Hydrogels using peptides as their building block are being employed in tissue engineering applications and used as space-filling agents, delivery vehicles for bioactive substances or 3D scaffolds that organise cells and present stimuli to encourage the development of new extra-cellular matrices. Many studies are progressing from the fundamental material design to design for specific application and are being tested for application within animal studies, and their potential is proven. The challenge is to take the work to the next phase: into preclinical and phase 1 to phase 3 clinical trials. For example, RADA16 peptide system is currently used in clinical application of blood clotting for wound repair and regeneration (Sankar et al. 2021). For an ideal scaffold, biochemical and biophysical cues need to be incorporated in order to mimic natural tissues such as stiffness, roughness and porous features, which serve as biomechanical signals to influence cellular functions in terms of cell proliferation and laying down relevant matrices (Pashuck and Stevens 2012). Additionally, fabricated peptide bionanomaterials can form a varying range of structures such as nanofibres, nanotubes, nanofilms and wires, which make them excellent candidates for replacing damaged tissues or organs (Webber et al. 2010; Hosoyama et al. 2019; Bermúdez et al. 2021). The potential applications of peptide hydrogels in the clinic also include heart valve repair and regeneration, cartilage tissue engineering and drug delivery systems for cancer therapy (Sankar et al. 2021; Dufour et al. 2021; British Heart Foundation 2022). Progress in peptide systems suggests it will most likely reach the clinic in the next 5–20 years (Gelain et al. 2021; Correa et al. 2021; Pashuck and Stevens 2012).

Vascular tissue engineering is one of the leading applications in tissue engineering. The global vascular graft market size was valued at US\$4.9 million in 2020 and is projected to reach US\$8.13 million by 2030, registering a CAGR of 4.9% from 2021 to 2030 (Cardiovascular Surgery 2022). Advances in engineering vascular tissues, stemming from an increasing understanding of tissue homeostasis and subsequent matrix turnover, are a consequence of rigorous research activities, influential clinical studies and dedicated funding bodies. Several in vivo studies have shown that vascular tissues in the body can effectively interact with synthetic 3D nanostructures for repair. Recently, researchers developed a jigsaw-shaped self-assembling peptide hydrogel, which revealed its potential to regenerate damaged brain tissue. The work involved the incorporation of vascular endothelial growth factor (VEGF) into hydrogels, and the controlled release was assessed in many cells. The team then showed that a single injection of the JigSAP peptide with VEGF-JigSAP improved blood vessel formation and protected nerve cells from dying of stoke in a mouse model (Yaguchi et al. 2021). The British Heart Foundation funded a study that revealed the advantages of using biodegradable injectable peptide-based hydrogel to repair damaged tissues caused by a heart attack. In collaboration,

Manchester BIOGEL Ltd., the British Heart Foundation and researchers at the University of Manchester are involved in conducting in vivo studies to assess whether the heart cells can develop new muscle tissues and restore the heart's ability to pump efficiently (British Heart Foundation 2022).

Despite efforts such as these, regeneration of mature tissues in the clinic remains a significant scientific challenge. Translation to create mature extra-cellular matrices containing all the relevant biochemical and biophysical cues for tissue maturation may take another decade. For example, cartilage tissue comprises several biologic and chemical building blocks controlling the maturation processes involved. Mature cartilage once damaged has a low ability to self-heal, leading to the use of medical interventions to promote tissue repair and regeneration. Currently, many different repair-enhancing therapies are being employed including biomaterials to aid cell proliferation, differentiation and neo-tissue formation (Williams et al. 2008); chondroprotective agents to stimulate chondrogenesis and synthesis of collagen and proteoglycans (Johnson et al. 2012); and surgical methods (Redman et al. 2005; Brittberg 2008). However, these approaches face the challenge of regenerating cartilage with a mature extra-cellular matrix, layered architectures leading to integration with the subchondral bone and surrounding cartilage and high mechanical strength to meet long-term clinical needs (ranging between 12 and 24 months) (Place et al. 2009).

In this regard, 3D printed nanostructures for tissue engineering applications have shown great potential as scaffolds due to their ability to withstand mechanical stresses; provide high reproducibility and control over the constructs; and subsequent long-term stability for tissue growth. Between the years 2022 and 2027, the global 3D bioprinting market size is expected to develop at a CAGR of 21.2% and value US$1724 million by 2027 (Markets and Markets 2021). In 2021, 3D bioprinting based on the use of synthetic bioinks to print complex living tissues on substrates accounted for 36%. Several applications such as cancer therapies, bone and cartilage regeneration, skin tissue formation and organ modelling have significant developments in the 3D bioprinting field. Artificial intelligence (AI) is rapidly developing and reshaping the 3D bioprinting industry to build tissues from a digital 3D model using a combination of cells, growth factors and biomaterials. Bioprinting is expected to show the highest growth due to its reliability and increasing demand. Advanced Biomatrix, 3D Systems, Bespoke Innovations and BD Biosciences are among the major players in the global 3D bioprinting market space (Market Data Forecast 2022). Cellink and RegenHU develop 3D bioprinting technologies (Table 16.1), which enable researchers to print human organs and 3D tissue models. Their bioinks mixed with living cells print functional tissues to regenerate and repair damaged tissues, opening potential doors to peptide hydrogels as bioinks.

In 2019, research findings from Rice University by Jordan Miller and co-workers featured a proof of principle, a scale model of a lung-mimicking air sac with airways and blood vessels that provide oxygen to red blood cells. The group designed a 'stereolithography apparatus for tissue engineering' (SLATE). The system uses additive manufacturing to make soft hydrogels one layer at a time (Zhu et al. 2021).

Table 16.1 Selected commercial products in different market segments based on application

Product name	Company name	Application	References
Cervidil®	Ferring Pharmaceuticals Inc.	Drug delivery	Cervidil.com
Evarrest®	Omrix Biopharmaceuticals Ltd (Johnson & Johnson)	Blood clotting and wound healing	Jnjmedtech.com
Peptide Vinci 02™	Ashland	Dermal repair and regeneration	Ashland.com
Bioinks	Cellink	Tissue engineering and 3D bioprinting	Cellink.com
Nano emulsion	Hanacure	Anti-ageing	Hanacure.com
PuraMatrix™	Corning Inc. Life sciences	Tissue engineering	Corning.com
PeptiGel®	Manchester BIOGEL	Tissue engineering, 3D bioprinting	Manchesterbiogel.com

In 2020, exciting research by Adam Feinberg and his team from Carnegie Mellon University revealed the development of the first full-sized human heart model using the new 'freeform reversible embedding of suspended hydrogels' (FRESH) technique. FRESH 3D printing works by taking multiple MRI scans of a patient's heart and then using it as a digital model for FRESH 3D printing. The printer injects a bioink into a soft hydrogel, as a support system for the object as it prints. At the end of the procedure, by providing heat the hydrogel melts, leaving only the 3D-printed object behind (Lee et al. 2019).

To facilitate innovative projects, companies like UpNano launched a new NanoOne Bio 3D bioprinting system in 2021, which is capable of printing 3D tissue structures at the nanoscale level. The company partnered with Ghent University-originated biomaterial company called Bio INX®, to design a hydrogel bioink for their new system (UpNano). Bio INX®'s new ink called Hydrobio INX© U200 is a water-soluble gelatin-based hydrogel. Once embedded into the bioink, nutrients can be provided to cells directly into the NanoOne Bio, where they are printed within a 3D scaffold (UpNano 2021).

In 2022, Latteri and his team from the University of Virginia were awarded the National Science Foundation (NSF) CAREER Award to develop advanced biomaterials. Their work focuses on designing peptide hydrogels that combine synthetic polymers to replicate the complex features of human tissues. These materials can be used by other researchers in cell culture studies and 3D bioprinting (Gray et al. 2022). Kumar and colleagues at the Rutgers School of Dental Medicine have proposed a non-invasive alternative to root canal: restoring the lost tissue in the tooth cavity by inducing the body to regenerate it. The team has created an injectable peptide hydrogel RADA16-I to recruit a patient's own dental pulp stem cells directly to the disinfected cavity after a root canal. Composed of biocompatible amino acid peptides that aggregate into fibres, the hydrogel VEGF directs the growth of blood vessels and amino acids to direct tissue growth, as well as a scaffold structure to support it (Mu et al. 2020).

All these fascinating proof-of-concept studies, collaborations between academia and industry and the interactions between physicians and pharmaceutical companies reveal the broad scope of hydrogels as biomaterials and bioinks, thus creating a market niche for peptide-based biomaterials for further exploitation.

16.3.2 Drug Delivery

Insights show that the global sales of hydrogel-based drug delivery systems in 2021 were held at US$6.7 billion. With an 8.8% CAGR, the projected market growth between the years 2022 and 2032 is expected to be seen (Future Market Insights 2022). Figures reveal an increase of 7.7% CAGR in the market share of hydrogel-based drug delivery systems from 2017 to 2021, and the demand for such systems is on the rise driven by the 3Rs. Reports suggest that North America holds the largest hydrogel-based drug delivery systems market, accounting for a market size of US$2.9 billion in 2021 (Future Market Insights 2022). Clinical trials using these systems have shown promising results, thus leading pharmaceutical companies to invest large sums in R&D. According to a 2019 NCBI report, hydrogels were tested in 223 clinical trials for medical and diagnostic purposes. The key players operating in hydrogel-based drug delivery systems market include GALDERMA, Blairex Laboratories, Ocular Therapeutix, Ferring Pharmaceuticals Inc., Johnson & Johnson, Akorn, Incorporated, Bausch and Lomb and Tolmar Pharmaceuticals. For example, Cervidil® developed by Ferring Pharmaceuticals Inc. is the first pharmacological treatment for cervical ripening, approved by the Ministry of Health, Labour and Welfare (MHLW) in 2020 (Table 16.1). It is a hydrogel vaginal insert to deliver prostaglandin E2 into the cervix. The system contains the active substance dinoprostone used for the initiation of cervical ripening in women from 37 completed weeks of gestation (Ferring Pharmaceuticals 2020). The clearance of Ferring's drug from MHLW reflects rapid development in hydrogel technology and its growing applications in diverse cultures.

Difficulties in translating peptide systems (not in combination with polymeric materials) to the clinic has been seen, primarily due to parameters such as mesh size and aggregation, surface charge, morphology, drug release and interaction patterns with body fluids, thus defining their biological fate as drug carriers. Many examples in literature show that controlling these parameters at the design stage may result in the formation of much stable hydrogels, where reproducibility is not compromised, which ultimately becomes one of the biggest barriers between academic research and clinical studies. Peptide hydrogels are widely employed in the development of subcutaneous drug delivery systems because they are mucoadhesive, biocompatible, biodegradable, injectable and easy to deliver. To achieve the sustained release of anticancer drugs, many hydrogels have recently been designed. Previously, nanofibers of D-peptides generated via enzymatic dephosphorylation were also investigated for the controlled release of the anticancer drug taxol and of a fluorophore (e.g. 4-nitro-2,1,3-benzoxadiazole) used as imaging agents in vivo

(Li et al. 2013). Animal studies using Phe-Phe (FF) peptide-based nanofibers have shown to serve as vehicles of hydrophobic drugs, like hydroxycamphothecin (HCPT), for cancer therapy (Tesauro et al. 2019). Likewise, an injectable hexapeptide was tested for localised chemotherapy. Guangjun and co-workers revealed that peptide-based nanocarrier injected at the tumour site by co-assembly of tailor-made hexapeptide and doxorubicin provided targeted delivery and allowed sustained release of the encapsulated drug molecules leading to high therapeutic efficacy against tumour recurrence (Qi et al. 2018).

Additionally, a study demonstrated that a peptide for ocular delivery was conjugated with poly(lactic-co-glycolic acid) (PLGA)–polyethylene glycol (PEG) nanoparticles (NPs) to improve ocular drug availability. Flubiprofen was used as an example of an anti-inflammatory drug. PLGA-PEG-POD NPs exhibited greater entrapment of the drug and sustained release was observed in vivo. This was possible because the positive charge on the surface of NPs conjugated with positively charged peptide facilitated penetration into the corneal epithelium, leading to prevention of ocular inflammation (Vasconcelos et al. 2015).

We see many excellent examples of peptide-based drug delivery systems in the lab; however, translation remains a challenge due to controlled delivery and controlled rate of the desired drug concentration, targeted delivery, decreased toxicity and scalability. Considering the depth and breadth of the on-going research, it is highly anticipated that researchers will be able to achieve this in the next 5–10 years.

16.3.3   Antibacterial Peptides for Wound Healing

According to Grandview Research, the global antimicrobial peptide (AMP) market was valued at US$1.06 billion in 2015 (Grandview Research 2022), and the global market for antimicrobial peptides in particular is anticipated to grow at a CAGR of 7.5% between 2017 and 2030. North America dominated the market in 2021 with a revenue share of over 45.0% (Grandview Research 2022). Asia Pacific antimicrobial peptide (AMP) market was valued at US$0.18 billion in 2016 and is expected to show a potential market growth. Rising R&D investments to develop novel antimicrobial peptides (AMPs) in countries such as Australia, Japan, Singapore and South Korea is likely to contribute to the growth of the market in the region.

Wound healing is a complex biological process, and in recent years efforts are directed to fabricate antibacterial hydrogels with unique properties to assist in the process of repair and regeneration, and simultaneously reduce inflammation and infections.

Researchers developed a technique to use melittin, created from the venom of the European honeybee, to reduce biofilm formation by the bacteria *Pseudomonas aeruginosa* in mouse wounds (Maiden et al. 2019). Antibacterial treatments alone do not work effectively due to the resistant nature of biofilms; however, AMPs' (containing 12–50 amino acid residues) delivery system showed remarkable effectiveness against several different biofilms (Luo and Song 2021). AMPs interact with

the bacteria and disrupt the bacterial cell wall, thus effectively killing the bacteria. Zhu and colleagues produced an AMP-based hydrogel that is sensitive to environmental acidity. Under low pH conditions, the gel disintegrates to release antibacterial agents and functions as an inert wound dressing under normal conditions (Liu et al. 2022; Cross et al. 2021). Recently, Zhang and co-workers designed an amphipathic AMP (Ac-KHHQKLVFFAK-NH$_2$; KKd-11) that consists of D-amino acid residues. KKd-11 self-assembled to form a stable hydrogel with a profound antimicrobial ability, in comparison to the hydrogel formed by Ac-KHHQKLVFFAK-NH$_2$ containing L-amino acid residues (KK-11). Additionally, KKd-11 inhibited the formation of biofilms and effectively damaged mature biofilms, demonstrating D-peptide hydrogels have great potential in the treatment of biofilm-induced infections (Guo et al. 2021), and may serve as an excellent candidate for wound repair.

Antibacterial AMP-hydrogel patches were developed at Sweden's Chalmers University of Technology led by Martin Andersson, who established the company Amferia. In 2020, Amferia received US$650, 000 to commercialise wound patches, wound-healing granules and medical device coatings (World Bio Market Insights 2022). Findings suggest that AMP-hydrogel has a 99% killing efficiency against multiple gram-negative- and gram-positive-resistant bacterial strains including methicillin-resistant *Staphylococcus aureus* (MRSA), *Escherichia Coli,* and *Pseudomonas aeruginosa* (Amferia AB 2019). It has also been proven to be non-toxic to mammalian cells.

Wound sealants provide a humid environment for wound repair. The global surgical sealants and adhesives market size was valued at US$1.82 billion in 2021 and is expected to expand at a CAGR of 11.4% from 2022 to 2030 (Grandview Research 2022). In North America, increasing R&D in tissue glue manufacturing and bio-adhesive sealants is also projected to contribute to the growth of the tissue sealants and tissue adhesive market share (Future Market Insights 2022). Advanced hydrogel-based tissue repair treatments include Evarrest® (Omrix Biopharmaceuticals, Ltd.), a sterile sealant matrix designed by Johnson and Johnson that is bio-absorbable (Table 16.1). Upon contact with the damaged tissue, the thrombin is activated and converts fibrinogen into fibrin; the stable blood clot that is produced sticks to the patch and integrates within the tissue to stop bleeding. After about 8 weeks, that patch disintegrates into the body and assimilates without requiring any removal. If used in combination with AMPs or RADA16 peptide systems, the effectiveness of wound repair may be enhanced.

Peptide hydrogels with inherent antibacterial properties inhibit bacterial growth and also assist in the repair process in surrounding cells. However, in the current scenario, peptide antibacterial hydrogels suffer from poor stability due to the presence of proteolytic enzymes at the wound site. There is a need to design and develop peptide hydrogels with improved stability against proteolytic enzymes.

16.3.4   Cosmetics

The UN projections suggest that the world's population is expected to reach an enormous 8.5 billion in 2030 (UN.org 2022) and thus, ultimately the cosmetic industry will boom with increased sales due to increased population, with the focus on advancements in formulations and age-tech products. Nutricosmetics along with cosmeceuticals are also an important application of peptide-based hydrogels. Small peptides or short polypeptides are water soluble and can be easily incorporated into several cosmetic formulations (Mitura et al. 2020).

Ashland™, a nutracosmetic brand focusing on age tech designed Peptide q10™ which is a bioengineered anti-ageing peptide designed to help boost the synthesis of coenzyme q10 and enhance the skin's natural antioxidant defence mechanism. Applications include creams, lotions, hydrogels, face masks and many more. Another peptide designed is Peptide Vinci 02™ is biofunctional a peptide designed to promote skin regeneration (Table 16.1); has also been clinically proven to help give the appearance of plump lips (Ashland™).

Nano emulsion, a moisturising lotion designed by Hanacure® received the Harper's bazaar win for the best anti-ageing product in 2019. It is a multi-peptide nano emulsion designed to deliver a high concentration of peptides, squalane, sodium hyaluronate, and mushroom extract; subsequently developed for optimised absorption (Hanacure®) (Table 16.1). Recently in 2021, a research study by Han et al. showed lipid-coated nanoliposomes could improve the absorption of collagen obtained from *Asterias pectinifera*, a starfish. The peptides extracted from *Asterias pectinifera* were of lower molecular weight and had higher encapsulation efficiency than those extracted from animals which are the traditional source of collagen for cosmeceuticals (Salvioni et al. 2021). Moreover, the elastic nanoliposome containing the collagen peptide has shown to reduce MMP-1 expression caused by UV radiations. Therefore, the combination of *Asterias pectinifera*-derived collagen peptides and elastic nanoliposomes may be a promising formulation for anti-ageing cosmetics (Han et al. 2021).

Overall, the studies on peptide hydrogels for cosmeceuticals suggest that nanoformulation may improve antioxidant activity, even when incorporated into semisolid formulations. Since many commercial products incorporate more than one antioxidants. Future investigations may be directed towards the development of more complex nanocarriers containing multiple antioxidants.

16.4   COVID-19 Impact on the Biomaterials Market

The coronavirus first emerged as a threat in late 2019 and by the first quarter of 2020, the pandemic outbreak had already massively impacted businesses and the economy due to quarantine and social distancing protocols. The nanotechnology market was one of the hardest hit; it also had an impact on bionanomaterials (Research and

Markets 2022). For instance, aesthetic procedures, which mainly constitute cosmetic surgeries and non-essential dental procedures, were delayed due to the pandemic. Moreover, From March to June 2020, the health system in different countries experienced a significant decline in surgical volumes compared with the same period during the previous year. The pandemic had a major impact on the United States, Japan, and China economies, as well as many major European countries. Since most of these countries are major manufacturers of biomaterials in particular peptide-based products, the pandemic and nationwide lockdowns caused a decline in sales (Markets and Markets 2022). This, in turn, affected the overall bionanomaterials market. The global transplantation market was valued at US$5.47 billion in 2020 and the COVID pandemic resulted in a huge decline of 52.5% in 2020 as compared to the growth in 2017–2019 (Fortune Business Insights 2021). According to a Report Linker report, the global implantable biomaterials market was valued to grow from US$103.9 billion in 2020 to US$114.35 billion in 2021 (at a CAGR of 10.1%). The growth seen was due to the companies resuming operations after the impact of COVID-19. By 2025, the market is expected to reach US$161.22 billion at a CAGR of 9% (Report Linker 2021).

16.5   Market Comparisons

In this section, we highlight the different markets and segments, where peptide hydrogels as bionanomaterials may be used. The global transplantation market size was estimated at US$12.4 billion in 2021 and is expected to reach US$15.05 billion in 2022 (Markets and Markets 2022). The global cancer therapeutics market size was valued at US$166.5 billion in 2021. The peptide therapeutics market was valued at approximately US$28,510.60 million in 2020, and it is expected to grow with a CAGR of 9.66% (Research and Markets 2022). In contrast, the global market for nanobiotechnology is estimated to grow from US$38.5 billion in 2021 to US$68.4 billion by 2026, at a CAGR of 12.2% for the period 2021–2026 (Research and Markets 2021). The global hydrogel market was valued at US$22.1 billion in 2019 and is projected to reach US$31.4 billion by 2027, growing at a CAGR of 6.7%. The global 3D cell culture market is projected to be US$2.6 billion by 2027 from US$1.3 billion in 2022, at a CAGR of 15.6% between 2022 and 2027 (Markets and Markets 2022). Growth in all the above-mentioned segments (Fig. 16.2) is mainly driven by the increasing focus on developing alternatives to animal testing, growing focus on personalised medicine, increasing incidence of chronic diseases and the direction of funding from medical research councils and other government bodies for R&D and clinical research. This paves the way for developing peptide hydrogels as bionanomaterials for the transplantation and cancer therapeutics segments. The bottleneck of peptide hydrogel application is mostly due to acceptance of pre-clinical data and lack of data available from clinical trials. In the next 5 years or more, these challenges may be addressed, allowing peptide hydrogels to penetrate
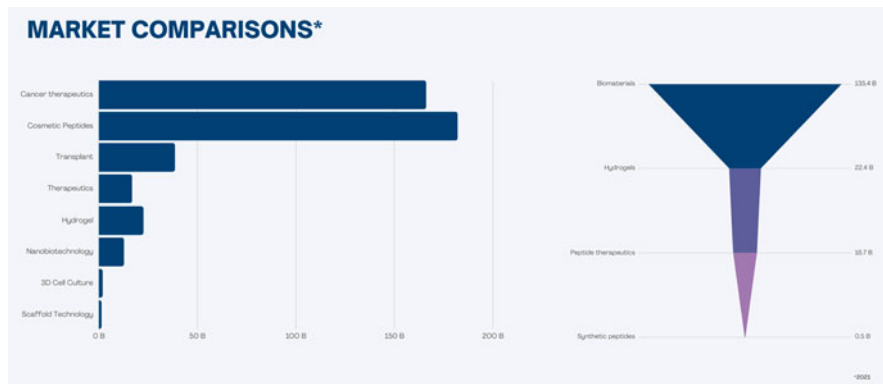
Fig. 16.2 An overview of the market size of each segment. The bar chart represents cosmetic peptides to control the market share in 2021, whereas the funnel graph correlates to the stages in the sales process and shows the potential revenue for each segment

into different market segments, especially 3D printing and transplantation (Fig. 16.2).

16.6 The Future for Peptide Bionanomaterials

Considerable technological advancements in soft bionanomaterials development have bridged the gaps between academia and industry, giving new business the platform to excel in the arena of peptide hydrogel design and technology. For instance, Corning® PuraMatrix™ is a synthetic peptide-based hydrogel matrix used to create well-defined 3D microenvironments for a variety of cell culture works (Corning Inc. Life sciences) (Table 16.1). PuraMatrix™ consists of synthetic amino acid residues (1% w/v) and 99% water. Under physiological conditions, the peptide self-assembles into nanofibrous networks resulting in the formation of hydrogels. The hydrogel has been shown to promote the differentiation of hepatocyte progenitor cells, hippocampal neurons and endothelial cells. Other potential applications include stem cell proliferation, tumour cell migration and invasion (Gelain et al. 2021; Correa et al. 2021).

PeptiGel®, from Manchester BIOGEL Ltd., is one other commercial peptide hydrogel (Table 16.1) that is available with additional fibronectin, laminin and/or collagen functionality as needed through the incorporation of -RGD, -IKVAV/ YIGSR and -GFOGER, respectively. Their peptide hydrogels are designed for use as scaffolds for 3D cell culture, bioprinting and organoid growth for drug discovery (Burgess et al. 2021; Clough et al. 2021; Lachowski et al. 2021; Faroni et al. 2019).

In light of these advances and given these evidences, we anticipate a bright future for self-assembling peptide bionanomaterials (Li et al. 2022b). Although extensive

studies have been done on peptide hydrogels, they are paving their way to clinical trials. The 3D bioprinting of peptide hydrogels is flourishing thanks to the emergence of microfluidics-based 3D cell culture, rapidly emerging economies and the developments in regenerative medicine like age-tech and cosmetic implants. Adopting safe-by-design and quality-by-design approaches at the design stage has shown to accelerate the translational pathway, enabling compliance with the 3Rs (replacement, reduction and refinement). By incorporating GMP manufacturing, large-scale batches of peptide bionanomaterials are produced, which in turn reduce in vivo preclinical costs leading to translation and accurate prediction of their therapeutic outcomes in clinical subjects.

References

Amferia AB (2019)

Apostolopoulos V, Bojarska J, Chai TT, Elnagdy S, Kaczmarek K, Matsoukas J, New R, Parang K, Lopez OP, Parhiz H, Perera CO (2021) A global review on short peptides: frontiers and perspectives. Molecules 26(2):430

Ashland™

Bermúdez M, Hoz L, Montoya G, Nidome M, Pérez-Soria A, Romo E, Soto-Barreras U, Garnica-Palazuelos J, Aguilar-Medina M, Ramos-Payán R, Villegas-Mercado C (2021) Bioactive synthetic peptides for oral tissues regeneration. Front Mater 8:655495

Bernhard S, Tibbitt MW (2021) Supramolecular engineering of hydrogels for drug delivery. Adv Drug Deliv Rev 171:240–256

Blanco-González A, Calvelo M, Garrido PF, Amorín M, Granja JR, Piñeiro Á, Garcia-Fandino R (2021) Transmembrane self-assembled cyclic peptide nanotubes based on α-residues and cyclic δ-amino acids: a computational study. Front Chem 9:530

Bowerman CJ, Liyanage W, Federation AJ, Nilsson BL (2011) Tuning β-sheet peptide self-assembly and hydrogelation behavior by modification of sequence hydrophobicity and aromaticity. Biomacromolecules 12(7):2735–2745

British Heart Foundation (2022)

Brittberg M (2008) Autologous chondrocyte implantation – technique and long-term follow-up. Injury 39(Suppl. 1):40–49

Burgess KA, Frati C, Meade K, Gao J, Diaz LC, Madeddu D, Graiani G, Cavalli S, Miller AF, Oceandy D, Quaini F (2021) Functionalised peptide hydrogel for the delivery of cardiac progenitor cells. Mater Sci Eng C 119:111539

Calvelo M, Lynch CI, Granja JR, Sansom MS, Garcia-Fandiño R (2021) Effect of water models on transmembrane self-assembled cyclic peptide nanotubes. ACS Nano 15(4):7053–7064

Cardiovascular Surgery (2022)

Clough HC, O'Brien M, Zhu X, Miller AF, Saiani A, Tsigkou O (2021) Neutrally charged self-assembling peptide hydrogel recapitulates in vitro mechanisms of breast cancer progression. Mater Sci Eng C 127:112200

Correa S, Grosskopf AK, Lopez Hernandez H, Chan D, Yu AC, Stapleton LM, Appel EA (2021) Translational applications of hydrogels. Chem Rev 121(18):11385–11457

Cross ER, Coulter SM, Pentlavalli S, Lavety G (2021) Unravelling the antimicrobial activity of peptide hydrogel systems: current and future perspectives. Soft Matter 17(35):8001–8021

Das S, Das D (2021) Rational design of peptide-based smart hydrogels for therapeutic applications. Front Chem 9:9

Dufour A, Lafont JE, Buffier M, Verset M, Cohendet A, Contamin H, Confais J, Sankar S, Rioult M, Perrier-Groult E, Mallein-Gerin F (2021) Repair of full-thickness articular cartilage defects using IEIK13 self-assembling peptide hydrogel in a non-human primate model. Sci Rep 11(1):1–7

Edwards-Gayle CJ, Hamley IW (2017) Self-assembly of bioactive peptides, peptide conjugates, and peptide mimetic materials. Org Biomol Chem 15(28):5867–5876

Elsawy MA, Wychowaniec JK, Castillo Díaz LA, Smith AM, Miller AF, Saiani A (2022) Controlling doxorubicin release from a peptide hydrogel through fine-tuning of drug–peptide fiber interactions. Biomacromolecules

Faroni A, Workman VL, Saiani A, Reid AJ (2019) Self-assembling peptide hydrogel matrices improve the neurotrophic potential of human adipose-derived stem cells. Adv Healthc Mater 8(17):1900410

Ferring Pharmaceuticals (2020)

Fortune Business Insights (2021)

Future Market Insights (2022)

Gelain F, Luo Z, Rioult M, Zhang S (2021) Self-assembling peptide scaffolds in the clinic. Npj Regen Med 6(1):1–8

Global Market Size and Share Report 2022–2030. Grandview Research Inc.

Grandview Research (2022)

Gray VP, Amelung CD, Duti IJ, Laudermilch EG, Letteri RA, Lampe KJ (2022) Biomaterials via peptide assembly: design, characterization, and application in tissue engineering. Acta Biomater 140:43–75

Guo Z, Song Y, Wang Y, Tan T, Ji Y, Zhang G, Hu J, Zhang Y (2021) Macrochirality of self-assembled and co-assembled supramolecular structures of a pair of enantiomeric peptides. Front Mol Biosci 8:700964

Gupta S, Singh I, Sharma AK, Kumar P (2020) Ultrashort peptide self-assembly: front-runners to transport drug and gene cargos. Front Bioeng Biotechnol 8:504

Han SB, Won B, Yang SC, Kim DH (2021) Asterias pectinifera derived collagen peptide-encapsulating elastic nanoliposomes for the cosmetic application. J Ind Eng Chem 98:289–297

Hanacure®

Hosoyama K, Lazurko C, Muñoz M, McTiernan CD, Alarcon EI (2019) Peptide-based functional biomaterials for soft-tissue repair. Front Bioeng Biotechnol 7:205

Johnson K, Zhu S, Tremblay MS, Payette JN, Wang J, Bouchez LC, Meeusen S, Althage A, Cho CY, Wu X, Schultz PG (2012) A stem cell–based approach to cartilage repair. Science 336(6082):717–721

Kibungu C, Kondiah PP, Kumar P, Choonara YE (2021) This review recent advances in chitosan and alginate-based hydrogels for wound healing application. Front Mater 8:681960

Lachowski D, Matellan C, Cortes E, Saiani A, Miller AF, del Río Hernández AE (2021) Self-assembling polypeptide hydrogels as a platform to recapitulate the tumor microenvironment. Cancers 13(13):3286

Lee AR, Hudson AR, Shiwarski DJ, Tashman JW, Hinton TJ, Yerneni S, Bliley JM, Campbell PG, Feinberg AW (2019) 3D bioprinting of collagen to rebuild components of the human heart. Science 365(6452):482–487

Li J, Gao Y, Kuang Y, Shi J, Du X, Zhou J, Wang H, Yang Z, Xu B (2013) Dephosphorylation of D-peptide derivatives to form biofunctional, supramolecular nanofibers/hydrogels and their potential applications for intracellular imaging and intratumoral chemotherapy. J Am Chem Soc 135(26):9907–9914

Li F, Han J, Cao T, Lam W, Fan B, Tang W, Chen S, Fok KL, Li L (2019) Design of self-assembly dipeptide hydrogels and machine learning via their chemical features. Proc Natl Acad Sci 116(23):11259–11264

Li Z, Zhu Y, Matson JB (2022a) pH-responsive self-assembling peptide-based biomaterials: designs and applications ACS applied bio materials

Li T, Lu XM, Zhang MR, Hu K, Li Z (2022b) Peptide-based nanomaterials: self-assembly, properties and applications. Bioactive Mater 11:268–282

Liu C, Zhang Q, Zhu S, Liu H, Chen J (2019) Preparation and applications of peptide-based injectable hydrogels. RSC Adv 9(48):28299–28311

Liu J, Jiang W, Xu Q, Zheng Y (2022) Progress in antibacterial hydrogel dressing gels. 8(8):503

Luo Y, Song Y (2021) Mechanism of antimicrobial peptides: antimicrobial, anti-inflammatory and Antibiofilm activities. Int J Mol Sci 22(21):11401

Maiden MM, Zachos MP, Waters CM (2019) Hydrogels embedded with melittin and tobramycin are effective against Pseudomonas aeruginosa biofilms in an animal wound model. Front Microbiol 10:1348

Market Data Forecast (2022)

Markets and Markets (2021)

Markets and Markets (2022)

Mitura S, Sionkowska A, Jaiswal A (2020) Biopolymers for hydrogels in cosmetics. J Mater Sci Mater Med 31(6):1–4

Mu X, Shi L, Pan S, He L, Niu Y, Wang X (2020) A customized self-assembling peptide hydrogel-wrapped stem cell factor targeting pulp regeneration rich in vascular-like structures. ACS Omega 5(27):16568–16574

Mujeeb A, Miller AF, Saiani A, Gough JE (2013) Self-assembled octapeptide scaffolds for in vitro chondrocyte culture. Acta Biomater 9(1):4609–4617

Panigrahi B, Singh RK, Suryakant U, Mishra S, Potnis AA, Jena AB, Kerry RG, Rajaram H, Ghosh SK, Mandal D (2022) Cyclic peptides nanospheres: a '2-in-1' self-assembled delivery system for targeting nucleus and cytoplasm. Eur J Pharm Sci 171:106125

Pashuck ET, Stevens MM (2012) Designing regenerative biomaterial therapies for the clinic. Sci Transl Med 4(160):160sr4

Place ES, Evans ND, Stevens MM (2009) Complexity in biomaterials for tissue engineering. Nat Mater 8:457–470

Precedence Research (2022)

Qi Y, Min H, Mujeeb A, Zhang Y, Han X, Zhao X, Anderson GJ, Zhao Y, Nie G (2018) Injectable hexapeptide hydrogel for localized chemotherapy prevents breast cancer recurrence. ACS Appl Mater Interfaces 10(8):6972–6981

Redman SN, Oldfield SF, Archer CW (2005) Current strategies for articular cartilage repair Europe. Cells Mater 9:23–32

Report Linker (2021)

Research and Markets (2021)

Research and Markets (2022)

Salvioni L, Morelli L, Ochoa E, Labra M, Fiandra L, Palugan L, Prosperi D, Colombo M (2021) The emerging role of nanotechnology in skincare. Adv Colloid Interf Sci 293:102437

Sankar S, O'Neill K, Bagot D'Arc M, Rebeca F, Buffier M, Aleksi E, Fan M, Matsuda N, Gil ES, Spirio L (2021) Clinical use of the self-assembling peptide RADA16: a review of current and future trends in biomedicine. Front Bioeng Biotechnol 9:679525

Sharma P, Pal VK, Roy S (2021) An overview of latest advances in exploring bioactive peptide hydrogels for neural tissue engineering. Biomater Sci 9(11):3911–3938

Song Z, Chen X, You X, Huang K, Dhinakar A, Gu Z, Wu J (2017) Self-assembly of peptide amphiphiles for drug delivery: the role of peptide primary and secondary structures. Biomater Sci 5(12):2369–2380

Tesauro D, Accardo A, Diaferia C, Milano V, Guillon J, Ronga L, Rossi F (2019) Peptide-based drug-delivery systems in biotechnological applications: recent advances and perspectives. Molecules 24(2):351

UN.org (2022)

UpNano (2021)

Vasconcelos A, Vega E, Pérez Y, Gómara MJ, García ML, Haro I (2015) Conjugation of cell-penetrating peptides with poly (lactic-co-glycolic acid)-polyethylene glycol nanoparticles improves ocular drug delivery. Int J Nanomedicine 10:609

Vauthey S, Santoso S, Gong H, Watson N, Zhang S (2002) Molecular self-assembly of surfactant-like peptides to form nanotubes and nanovesicles. Proc Natl Acad Sci 99(8):5355–5360

Wang Y, Li X, Yuan J, Wang X, Tao K, Yan J (2022) A bionic self-assembly hydrogel constructed by peptides with favorable biosecurity, rapid hemostasis and antibacterial property for wound healing. Front Bioeng Biotechnol 10:901534

Webber MJ, Kessler JA, Stupp SI (2010) Emerging peptide nanomedicine to regenerate tissues and organs. J Intern Med 267(1):71–88

Williams GM, Klisch SM, Sah RL (2008) Bioengineering cartilage growth, maturation, and form. Pediatr Res 63(5):527

World Bio Market Insights (2022)

Wychowaniec JK, Patel R, Leach J, Mathomes R, Chhabria V, Patil-Sen Y, Hidalgo-Bastida A, Forbes RT, Hayes JM, Elsawy MA (2020) Aromatic stacking facilitated self-assembly of ultrashort ionic complementary peptide sequence: β-sheet nanofibers with remarkable gelation and interfacial properties. Biomacromolecules 21(7):2670–2680

Yaguchi A, Oshikawa M, Watanabe G, Hiramatsu H, Uchida N, Hara C, Kaneko N, Sawamoto K, Muraoka T, Ajioka I (2021) Efficient protein incorporation and release by a jigsaw-shaped self-assembling peptide hydrogel for injured brain regeneration. Nat Commun 12(1):1–2

Zhu Y, Sazer D, Miller JS, Warmflash A (2021) Rapid fabrication of hydrogel micropatterns by projection stereolithography for studying self-organized developmental patterning. PLoS One 16(6):e0245634